

AD-752 551

LIGHTNING AND STATIC ELECTRICITY  
CONFERENCE, 12-15 DECEMBER 1972

Air Force Avionics Laboratory  
Wright-Patterson Air Force Base, Ohio

December 1972

DISTRIBUTED BY:

**NTIS**

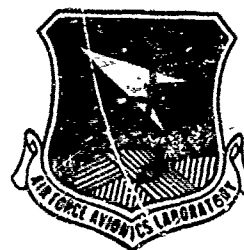
National Technical Information Service  
U. S. DEPARTMENT OF COMMERCE  
5285 Port Royal Road, Springfield Va. 22151

AFAL-TR-72-325

AD 752551

**1972  
LIGHTNING  
AND  
STATIC ELECTRICITY  
CONFERENCE**

12-15 DECEMBER 1972



*IN COOPERATION WITH  
SAE COMMITTEE AE-4 ON ELECTROMAGNETIC COMPATIBILITY*

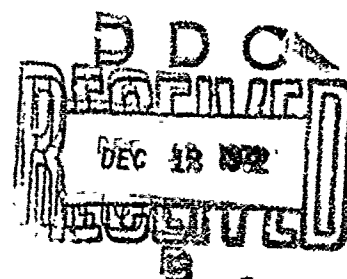
*AND*

**AIR FORCE AVIONICS LABORATORY  
AIR FORCE SYSTEMS COMMAND  
WRIGHT-PATTERSON AIR FORCE BASE, OHIO**

Reproduced by  
**NATIONAL TECHNICAL  
INFORMATION SERVICE**  
U.S. Department of Commerce  
Springfield, MA 01104

**This document has been approved for public release  
and sale; its distribution is unlimited.**

DECEMBER 1972





# NOTICE

When Government drawings, specifications, or other data are used for any purpose other than in connection with a definitely related Government procurement operation, the United States Government thereby incurs no responsibility nor any obligation whatsoever; and the fact that the government may have formulated, furnished, or in any way supplied the said drawings, specifications, or other data, is not to be regarded by implication or otherwise as in any manner licensing the holder or any other person or corporation, or conveying any rights or permission to manufacture, use, or sell any patented invention that may in any way be related thereto.

ACCESSION for	
NTIS	Write Section <input checked="" type="checkbox"/>
DDC	Buff Section <input type="checkbox"/>
UNANNOUNCED	<input type="checkbox"/>
JUSTIFICATION .....	
BY .....	
DISTRIBUTION/AVAILABILITY CODES	
ASL	AVAIL. REG/SP SPECIAL
A	

Copies of this report should not be returned unless return is required by security considerations, contractual obligations, or notice on a specific document.

Security Classification

## DOCUMENT CONTROL DATA - R &amp; D

(Security classification of title, body of abstract and indexing annotation must be entered when the overall report is classified)

## 1. ORIGINATING ACTIVITY (Corporate author)

Air Force Avionics Laboratory and the SAE Committee  
AE-4 on Electromagnetic Compatibility

## 2a. REPORT SECURITY CLASSIFICATION

UNCLASSIFIED

## 2b. GROUP

## 3. REPORT TITLE

1972 LIGHTNING AND STATIC ELECTRICITY CONFERENCE, 12-15 December

## 4. DESCRIPTIVE NOTES (Type of report and inclusive dates)

## 5. AUTHOR(S) (First name, middle initial, last name)

## 6. REPORT DATE

December 1972

## 7a. TOTAL NO. OF PAGES

694

## 7b. NO. OF REFS

## 8a. CONTRACT OR GRANT NO.

## b. PROJECT NO.

## c.

## d.

## 9a. ORIGINATOR'S REPORT NUMBER(S)

AFAL-TR-72-325

## 9b. OTHER REPORT NO(S) (Any other numbers that may be assigned this report)

## 10. DISTRIBUTION STATEMENT

This document has been approved for public release and sale; its distribution is unlimited.

## 11. SUPPLEMENTARY NOTES

## 12. SPONSORING MILITARY ACTIVITY

Air Force Avionics Laboratory  
Wright-Patterson Air Force Base OH 45433

## 13. ABSTRACT

This document contains the text of unclassified papers presented at the 1972 Conference on Lightning and Static Electricity, held 12-15 December 1972. The papers document the discussion of the theoretical aspects of both lightning and atmospheric electrification. In addition, the practical control of adverse effects is addressed relative to aerospace vehicles and installations. Sessions include fundamental aspects, missiles and spacecraft, aircraft, advanced composites, fuels, and lightning simulation.

IA

DD FORM 1 NOV 65 1473

UNCLASSIFIED

Security Classification

UNCLASSIFIED  
Security Classification

14. KEY WORDS	LINK A		LINK B		LINK C	
	ROLE	WT	ROLE	WT	ROLE	WT
Lightning Hazards						
Static Electricity						
Electromagnetic Interference						
Aerospace Vehicle Safety						
Missiles						
Space Craft						
Aircraft						
Advanced Composites						
Fuels						
Lightning Simulation						
Atmospheric Electrification						
Flight Safety						
Ib						

UNCLASSIFIED

Security Classification

**LIGHTNING  
AND  
STATIC ELECTRICITY  
CONFERENCE**

12-15 DECEMBER 1972

This document has been approved for public release  
and sale; its distribution is unlimited.

IC

## FOREWORD

The Air Force Avionics Laboratory (AFSC) and the Society of Automotive Engineers jointly sponsored the "1972 Lightning and Static Electricity Conference" on 12 - 15 December 1972 in Las Vegas, Nevada. This report presents the proceedings of the conference. Mr. C. R. Austin, Air Force Avionics Laboratory was the Conference Organizer.

Research described herein represents the efforts of numerous persons in many organizations. The Air Force Avionics Laboratory and the Society of Automotive Engineers desires to express gratitude and appreciation to the following for their contributions in the conduct of this Conference and preparation of the proceedings:

Members of the General Committee, the Program Planning Committee, and AE-4 Electromagnetic Compatibility Committee of SAE and the conference co-chairmen, Messrs. C. Seth and J. Moe, Messrs. J. M. Kelly, Tom Wolff, C. R. Austin, and Mrs. Pam Hutmier who spent many hours assisting in organizing the Conference and preparing material.

Publication of this proceeding does not constitute Air Force or Society of Automotive Engineers approval of the findings or conclusions. The proceedings are published only for the exchange and stimulation of ideas, and to highlight the state-of-the-art.

*Bernard H List*

BERNARD H. LIST  
Chief Scientist  
AF Avionics Laboratory

## CHAIRMEN'S MESSAGE

Prior to 1968, a need existed for an international forum concerning the natural phenomena of Lightning and Static Electricity. Technical communication and exchange of information was restricted to minimal coverage in conjunction with other symposia. Accordingly, a Conference on Lightning and Static Electricity was held to establish technical communication within the area and highlight the state-of-the-art. The Conference was co-sponsored by the Air Force and the Society of Automotive Engineers (SAE) Committee AE-4 on Electromagnetic Compatibility. Again in 1970, the need for continuing communication became apparent, and another Conference was held which was also co-sponsored by the Air Force and SAE Committee AE-4.

This year, the Air Force and SAE Committee AE-4 have again teamed to present this third biennial Conference on Lightning and Static Electricity. It is the hope of the Chairmen that the Conference will highlight the state-of-the-art while providing a forum for technical interchange. This type of communication among the experts in the field will create a general "awareness" of atmospheric electricity problems. The Proceedings include extensive technical information and will serve as a valuable reference for many years.

Preliminary plans are underway for another conference in 1974. The current chairmen will act as a focal point until the conference officers are designated. One objective of the next conference will be to obtain additional participation from other nations so that the International aspects of these common problems are highlighted.

Your Chairmen wish to acknowledge the extensive efforts and contributions made by so many on behalf of the Conference. Particularly, we extend our thanks to the Conference Session Organizers, Messrs. M. P. Amason, Dr. J. G. Breland, R. W. Ellison, J. B. Godwin, Dr. J. E. Nanevich, R. A. Peterson, J. A. Plumer, J. D. Robb, H. S. Schwartz and G. L. Weinstock. Also, we acknowledge the special efforts of Miss Janice Howe and Mr. H. J. Hunter in the preparation of the Conference Proceedings. Special thanks are extended to the Chairman of SAE Committee AE-4, Mr. W. D. McKerchar and the Chairman of EIA Committee G-46, Mr. E. S. Hughes, for their help and assistance. Also, we extend a special vote of thanks to our consultants, Messrs. C. R. Austin, H. M. Bartman, S. Caine, W. L. Evans, J. J. Fisher, Dr. D. R. Fitzgerald and S. Skolnik for their valuable advice and guidance.

*J L Moe*  
J. L. MOE  
FOR INDUSTRY

*C E Seth*  
C. E. SETH  
FOR GOVERNMENT

# ABSTRACT

This document contains the text of unclassified papers presented at the 1972 Conference on Lightning and Static Electricity, held 12-15 December 1972. The papers document the discussion of the theoretical aspects of both lightning and atmospheric electrification. In addition, the practical control of adverse effects is addressed relative to aerospace vehicles and installations. Sessions include fundamental aspects, missiles and spacecraft, aircraft, advanced composites, fuels, and lightning simulation.

# LIGHTNING AND STATIC ELECTRICITY CONFERENCE

## GENERAL CHAIRMEN

J.L. Moe  
For Industry

C.E. Seth  
For Government

## SECRETARY

Miss Janice R. Howe

## EXECUTIVE STEERING COMMITTEE

M.P. Amason  
C.R. Austin  
Dr. J.G. Breland  
R.W. Ellison  
J.B. Godwin

E.S. Hughes  
J.L. Moe  
Dr. J.E. Nanevich  
R.A. Peterson  
J.A. Plumer

J.D. Robb  
H.S. Schwartz  
C.E. Seth  
G.L. Weinstock  
T.W. Wolff

## FINANCIAL & ARRANGEMENTS

J.L. Moe

T.W. Wolff

## SPECIAL ARRANGEMENTS, SECURITY, & HOUSING

J.M. Kelly

## FINANCIAL ADMINISTRATOR

C.R. Austin

## DEMONSTRATIONS

K.A. Moore

C.E. Seth

## DOCUMENTATION AND PROCEEDINGS

H.J. Hunter

## SAE LIAISON

A.G. Salem

## SAE COMMITTEE AE-4

W.D. McKerchar  
Chairman

J.L. Moe  
Vice-Chairman

D.M. Hish  
Secretary

## EIA COMMITTEE G-46 LIAISON

E.S. Hughes  
Chairman

## NAVY LIAISON

S. Caine

J.J. Fisher

## CONSULTANTS

H.M. Bartman  
W.L. Evans

Dr. D.R. Fitzgerald  
S. Skolnik



## P R O G R A M

### INTRODUCTION

Tuesday Morning

- Welcome and Opening Remarks
  - J. L. Mce, General Dynamics Corporation
    - .. Conference Chairman for Industry
  - C. E. Seth, U.S. Air Force
    - .. Conference Chairman for Government
- Introduction of the Keynote Speaker
  - Col. M. M. Bonner, Commander, USAF Avionics Laboratory
- Keynote Address
  - Dr. Bernard List, Chief Scientist, USAF Avionics Laboratory

### SESSION I

#### FUNDAMENTAL ASPECTS OF LIGHTNING

Tuesday Morning

- Introduction of the Session
  - M. P. Amason, McDonnell Douglas Corporation
    - .. Session Chairman and Organizer
- Atmospheric Electricity
- Movie: "Atmospheric Electricity"
  - Professor Bernard Vonnegut, Department of Atmospheric Science, State University of New York at Albany
- Instrumentation and Measurements Associated with Lightning Strikes
  - Professor M. Brook and Professor C. Moore
    - New Mexico Institute of Mining and Technology
- Spark Simulation of Natural Lightning
  - Professor Martin A. Uman, Department of Electrical Engineering, University of Florida

### SESSION II

#### FUNDAMENTAL ASPECTS OF STATIC ELECTRICITY

Tuesday Afternoon

- Introduction of the Session
  - Dr. Joseph E. Nanevich, Stanford Research Institute
    - .. Session Chairman and Organizer
- Ice Crystal Electrification
  - Professor G. A. Dawson, Institute of Atmospheric Physics, The University of Arizona
- Processes of Frictional Electrification
  - Professor Ion I. Inculet, Faculty of Engineering Science, The University of Western Ontario, Canada

- Effects of Static Electrification on Systems
  - Robert W. Ellison, Martin Marietta Aerospace, Denver Division
- Techniques for the Study of Noise Generation and Coupling
  - E. F. Vance, Stanford Research Institute
- Structure of Lightning Noise - Especially Above HF
  - Dr. N. Cianos, Dr. G. N. Oetzel, and Dr. E. T. Pierce  
Stanford Research Institute

### SESSION III      ELECTRIFICATION - OPERATIONAL PROBLEMS

Tuesday Afternoon

- Introduction of the Session
  - Dr. J. G. Breland, Captain, U.S. Air Force, F. J. Seiler Research Laboratory, AFSC
  - Session Chairman and Organizer
- Static Electricity Problems - VLF/LORAN Systems
  - John B. Chown and Dr. Joseph E. Nanevich  
Stanford Research Institute
- ILS/VOR Navigation and Approach Errors From Precipitation Static Interference  
Part 1 - Basic Concepts
  - J. D. Robb, Lightning and Transients Research Institute
- ILS/VOR Navigation and Approach Errors  
Part 2 - Experimental Investigations
  - Robert L. Truax, The Truax Company
- Conductive Polymeric Coatings for Combined Anti Static Properties and Erosion Resistance
  - George F. Schmitt, Jr., Air Force Materials Laboratory
- A Review of Air Force Experience With Static Electricity Problems on Aircraft Windshields
  - Robert E. Wittman, Air Force Materials Laboratory
- Windshield Static Electrification Problems - Commercial Aircraft Experience and Protection Parameters
  - M. M. Newman, J. D. Robb, and J. R. Stahmann  
Lightning and Transients Research Institute
- Windshield Related Problems - A Manufacturer's View
  - F. H. Gillery, Senior Scientist, Pittsburgh Plate Glass Industries, Inc.
- Windshield Related Electrostatic Problems - Electrification Studies on the 747
  - Rowan O. Brick, The Boeing Company, Commercial Airplane Group

### SESSION IV      MISSILES AND SPACECRAFT

Wednesday Morning

- Introduction of the Session
  - Robert W. Ellison, Martin Marietta Aerospace, Denver Division
  - Session Chairman and Organizer

- Results of Titan III Flight Electrostatic Experiments
  - Dr. Joseph E. Nanevich, Stanford Research Institute
- Static Electricity in the Apollo and Skylab Spacecraft
  - Dr. Andrew E. Potter, Jr. and B. R. Baker  
NASA Manned Spacecraft Center
- The Role of Electrostatics in Skylab Contaminant Behavior
  - H. E. Beaver and R. W. Ellison  
Martin Marietta Aerospace, Denver Division
- Electrostatic Potentials Developed by ATS-5
  - Dr. Sherman E. DeForest, University of California, San Diego
- Electrostatic Charges Acquired by Spacecraft and Their Possible Effects on Instruments
  - Dr. Elden C. Whipple, Jr., National Oceanic and Atmospheric Administration

SESSION V      AIRCRAFT I

Wednesday Afternoon

- Introduction of the Session
  - G. L. Weinstock, McDonnell Douglas Corporation
  - Session Chairman and Organizer
- Triggered Lightning and Its Application to Rockets and Aircraft
  - Dr. Edward T. Pierce, Stanford Research Institute
- Engineering Aspects of Lightning Environments
  - Dr. N. Cianos and Dr. E. T. Pierce  
Stanford Research Institute
- Aircraft Initiation of Lightning
  - Dr. J. F. Shaeffer, McDonnell Douglas Corporation
- General Aviation Lightning Effects and Protection
  - J. A. Plumer, General Electric Company, Corporate Research and Development
- Aircraft Lightning Protection Design Considerations
  - M. P. Amason, G. J. Cassell, J. T. Kung, J. A. LaManna, W. W. McCloud  
McDonnell Douglas Corporation
- B-1 Lightning and Electrification Program
  - Harry Z. Wilson, North American Rockwell
  - John D. Robb, Lightning and Transients Research Institute
- Experimental Investigation of Problems Associated with Discharging Hovering Helicopters
  - Dr. J. E. Nanevich and D. G. Douglas  
Stanford Research Institute
  - S. Blair Poteate, U.S. Army Material Research and Development Laboratory
  - B. J. Solak, Boeing Company, Vertol Division
- Data from the Airlines Lightning Strike Reporting Project
  - J. A. Plumer, General Electric Company, Corporate Research and Development

SESSION VI      ADVANCED COMPOSITES, MATERIALS, AND STRUCTURES      Thursday Morning

- Introduction of the Session
  - H. S. Schwartz, U.S. Air Force Materials Laboratory
  - Session Chairman and Organizer
- Current Flow Phenomena in Boron and Graphite Fiber Reinforced Composites Exposed to Simulated Lightning
  - John L. Perry, Philco-Ford Corporation
  - Kenneth J. Lloyd, General Electric Company
- Electromagnetic Shielding Properties of Composite Materials
  - F. A. Fisher, General Electric Company, Corporate Research and Development
- New Developments in Lightning Protective Coatings for Advanced Structural Composites
  - Dr. John Quinlivan, The Boeing Company
  - Mr. J. H. Weaver, Air Force Materials Laboratory
- Dielectric Shielding Lightning Protection for Composite Aircraft Structures
  - J. T. Kung and M. P. Amason
  - McDonnell Douglas Corporation
- Lightning Protection for Aircraft Sandwich Structures with Boron/Epoxy Composite Skins
  - Geroge Lubin and Sam Dastin
  - Grumman Aerospace Corporation

SESSION VII      ELECTROSTATICS IN AVIATION FUEL SYSTEMS      Thursday Afternoon

- Introduction of the Session
  - J. B. Godwin, U.S. Air Force, Directorate of Aerospace Fuels
  - Session Chairman and Organizer
- Principles of Electrostatics in Aircraft Fuel Systems
  - Dr. Joseph T. Leonard, Naval Research Laboratory
- Static Electricity Accident Reports - American Petroleum Institute
  - W. L. Bulkley, American Oil Company
- Electrification Study - A Multi Purpose Single Element Test Rig Approach
  - R. P. Foster, Gulf Research and Development Company
- Ten Years' of Experience with Anti/Static Additives in Aviation Turbine Fuel
  - J. G. Kirtley, Shell International Petroleum Company, London
- Electrostatics at Airports - Coordinating Research Council
  - P. P. Campbell, United Airlines
- Protective System Measurements for Aviation Fuel Handling
  - W. G. Dukek, ESSO Research and Development
- Future Trends in Jet Fuel
  - A. V. Churchill, Air Force Aero Propulsion Laboratory

SESSION VIII AIRCRAFT II

Friday Morning

- Introduction of the Session
  - R. A. Peterson, The Boeing Company
  - Session Chairman and Organizer
- Lightning Protection Techniques for Large Canopies on High Speed Aircraft
  - Robert Aston, R. Gorton, and G. L. Weinstock
  - McDonnell Douglas Corporation
- Lightning and Electromagnetic Compatibility Analyses - A Joint Study on Lightning Effects for the B-1 Program
  - E. S. Hughes, North American Rockwell, B-1 Division
  - Coordinator
  - J. D. Robb, Lightning and Transients Research Institute
  - W. R. Johnson, TRW Systems
  - J. A. Plumer, General Electric Company, Corporate Research and Development
- Control Surface and Door Hinge Bonding Effectiveness in Modern Aircraft
  - James R. Stahmann, Lightning and Transients Research Institute
- A Test Technique for Measurement of Lightning-Induced Voltages in Aircraft Electrical Circuitry
  - Lawrence C. Walko, General Electric Company, Corporate Research and Development
  - Paul T. Hacker, Aerospace Safety Research and Data Institute, National Aeronautics and Space Administration, Lewis Research Center
- Lightning Protection Approaches For Helicopters
  - J. D. Robb and J. R. Stahmann
  - Lightning and Transients Research Institute
- Helicopter Cargo Handling - Electrostatic Considerations
  - B. J. Solak, The Boeing Company
  - J. E. Nanevich, Stanford Research Institute
  - G. J. Wilson, The Boeing Company
  - C. H. King, The Boeing Company, Commercial Aircraft Group

SESSION IX WORKSHOP: LIGHTNING SIMULATION, TESTING,  
AND MIL-B-5087B

Friday Afternoon

- Introduction of the Session
  - J. D. Robb, Lightning and Transients Research Institute
  - J. A. Plumer, General Electric Company, Corporate Research and Development
  - Session Chairmen and Organizers

.....PANEL MEMBERS.....

INDUSTRY

• M. P. Amason  
McDonnell Douglas Corporation

• F. P. Holder  
Lockheed Georgia

GOVERNMENT

• R. Auburn  
Federal Aviation Agency

• P. T. Hacker  
NASA, Lewis

#### INDUSTRY (CONTD)

• A. D. Schneider  
The Boeing Company

• N. Z. Scott  
Lockheed California

• A. G. Zimbalatti  
Grumman Aerospace Corporation

#### GOVERNMENT (CONTD)

• C. Mudd  
U.S. Army Aviation Systems Command

• B. L. Perry  
British Air Registry Board  
United Kingdom

• E. Rivera  
Naval Air Systems Command

C. E. Seth  
United States Air Force

#### INDEPENDENT LIGHTNING LABORATORIES

• D. W. Clifford  
McDonnell Douglas Corporation

• F. A. Fisher  
General Electric High Voltage  
Laboratory

• J. Phillpott  
Culham - United Kingdom

• J. R. Stahmann  
Lightning & Transients Research  
Institute

#### CONFERENCE ADJOURNMENT

- Closing Remarks
  - J. L. Moe
    - .. Chairman for Industry
  - C. E. Seth
    - .. Chairman for Government

# TABLE OF CONTENTS

	PAGE
FOREWARD	ii
CHAIRMEN'S MESSAGE	iii
CONFERENCE ABSTRACT	iv
CONFERENCE COMMITTEE ORGANIZATION	v
CONFERENCE PROGRAM	vi
 SESSION I      FUNDAMENTAL ASPECTS OF LIGHTNING	 1
● Introduction of the Session	2
M.P. Amason, McDonnell Douglas Corporation	
.. Session Chairman and Organizer	
● Atmospheric Electricity	3
Professor Bernard Vonnegut, Department of Atmospheric	
Science, State University of New York at Albany	
● Spark Simulation of Natural Lightning	5
Professor Martin A. Uman, Department of Electrical	
Engineering, University of Florida	
 SESSION II      FUNDAMENTAL ASPECTS OF STATIC ELECTRICITY	 14
● Introduction of the Session	15
Dr. Joseph E. Nanevich, Stanford Research Institute	
.. Session Chairman and Organizer	
● Ice Crystal Electrification	18
Professor G. A. Dawson, Institute of Atmospheric	
Physics, The University of Arizona	
● Processes of Frictional Electrification	21
Professor Ion I. Inculet, Faculty of Engineering	
Science, The University of Western Ontario, Canada	
● Effects of Static Electrification on Systems	28
Robert W. Ellison, Martin Marietta Aerospace,	
Denver Division	
● Techniques for the Study of Noise Generation and	
Coupling	34
E. F. Vance, Stanford Research Institute	
● Structure of Lightning Noise - Especially Above HF	50
Dr. N. Cianos, Dr. G. N. Oetzel, and Dr. E. T. Pierce	
Stanford Research Institute	

# TABLE OF CONTENTS (CONT'D)

SESSION III	ELECTRIFICATION - OPERATIONAL PROBLEMS	57
●	Introduction of the Session Dr. J. G. Breland, Captain, U.S. Air Force, F. J. Seiler Research Laboratory, AFSC .. Session Chairman and Organizer	58
●	Static Electricity Problems - VLF/LORAN Systems John B. Chown and Dr. Joseph E. Nanevitz Stanford Research Institute	59
●	ILS/VOR Navigation and Approach Errors From Precipitation Static Interference Part I - Basic Concepts J. D. Robb, Lightning and Transients Research Institute	71
●	ILS/VOR Navigation and Approach Errors Part 2 - Experimental Investigations Robert L. Truax, The Truax Company	79
●	Conductive Polymeric Coatings for Combined Anti- Static Properties and Erosion Resistance George F. Schmitt, Jr., Air Force Materials Laboratory	88
●	A Review of Air Force Experience With Static Electricity Problems on Aircraft Windshields Robert E. Wittman, Air Force Materials Laboratory	97
●	Windshield Static Electrification Problems - Commercial Aircraft Experience and Protection Parameters M. M. Newman, J. D. Robb, and J. R. Stahmann Lightning and Transients Research Institute	98
●	Windshield Related Problems - A Manufacturer's View (Abstract) F. H. Gillery, Senior Scientist, Pittsburgh Plate Glass Industries, Inc.	102
●	Windshield Related Electrostatic Problems - Electrification Studies on the 747 Rowan O. Brick, The Boeing Company, Commercial Airplane Group	103
SESSION IV	MISSILES AND SPACECRAFT	104
●	Introduction of the Session Robert W. Ellison, Martin Marietta Aerospace, Denver Division .. Session Chairman and Organizer	105



# TABLE OF CONTENTS (CONT'D)

## SESSION IV (CONT'D)

- Results of Titan III Flight Electrostatic Experiments 106  
Dr. Joseph E. Nanevich, Stanford Research Institute
- Static Discharge in the Apollo and Skylab Spacecraft 132  
Dr. Andrew E. Potter, Jr. and B. R. Baker  
NASA Manned Spacecraft Center
- The Role of Electrostatics in Skylab Contaminant Behavior 141  
H. E. Beaver and R. W. Ellison, Martin Marietta Aerospace, Denver Division
- Electrostatic Potentials Developed by ATS-5 150  
Dr. Sherman E. DeForest, University of California, San Diego
- Electrostatic Charges Acquired by Spacecraft and Their Possible Effects on Instruments 166  
Dr. Elden C. Whipple, Jr., National Oceanic and Atmospheric Administration

- |           |  |     |
|-----------|--|-----|
| SESSION V | AIRCRAFT I   | 178 |
| ●         | Introduction of the Session  | 179 |
|           | G. L. Weinstock, McDonnell Douglas Corporation                             |     |
|           | .. Session Chairman and Organizer  |     |
| ●         | Triggered Lightning and Its Application to Rockets and Aircraft            | 180 |
|           | Dr. Edward T. Pierce, Stanford Research Institute                          |     |
| ●         | Engineering Aspects of Lightning Environments                              | 189 |
|           | Dr. W. Cianos and Dr. E. T. Pierce   |     |
|           | Stanford Research Institute  |     |
| ●         | Aircraft Initiation of Lightning   | 192 |
|           | Dr. J. F. Shaeffer, McDonnell Douglas Corporation                          |     |
| ●         | General Aviation Lightning Effects and Protection                          | 201 |
|           | J. A. Plumer, General Electric Company, Corporate Research and Development |     |
| ●         | Aircraft Lightning Protection Design Considerations                        | 214 |
|           | M. P. Amason, G. J. Casell, J. T. Kung, J. A. LaManna,                     |     |
|           | W. W. McCloud  |     |
|           | McDonnell Douglas Corporation  |     |
| ●         | B-1 Lightning and Electrification Program                                  | 242 |
|           | Harry Z. Wilson, North American Rockwell                                   |     |
|           | J. D. Robb, Lightning and Transients Research Institute                    |     |

# TABLE OF CONTENTS (CONT'D)

## SESSION V (CONT'D)

- Experimental Investigation of Problems Associated with Discharging Hovering Helicopters 251  
Dr. J. E. Nanevich and D. G. Douglas, Stanford Research Institute  
S. Blair Poteate, U.S. Army Material Research and Development Laboratory  
B. J. Solak, The Boeing Company, Vertol Division
- Data from the Airlines Lightning Strike Reporting Project 282  
J. A. Plumer, General Electric Company, Corporate Research and Development

## SESSION VI ADVANCED COMPOSITES, MATERIALS, AND STRUCTURES 290

- Introduction of the Session 291  
H. S. Schwartz, U.S. Air Force Materials Laboratory  
.. Session Chairman and Organizer
- Current Flow Phenomena in Boron and Graphite Fiber Reinforced Composites Exposed to Simulated Lightning 294  
John L. Perry, Philco-Ford Corporation  
Kenneth J. Lloyd, General Electric Company
- Electromagnetic Shielding Properties of Composite Materials 306  
F. A. Fisher, General Electric Company, Corporate Research and Development
- New Developments in Lightning Protective Coatings for Advanced Structural Composites 315  
Dr. John Quinlivan, The Boeing Company  
Mr. J. H. Weaver, Air Force Materials Laboratory
- Dielectric Shielding Lightning Protection for Composite Aircraft Structures 337  
J. T. Kung and M. P. Amason, McDonnell Douglas Corporation
- Lightning Protection for Aircraft Sandwich Structures With Boron/Epoxy Composite Skins 359  
Geroge Lubin and Sam Dastin, Grumman Aerospace Corporation

## SESSION VII ELECTROSTATICS IN AVIATION FUEL SYSTEMS 413

- Introduction of the Session 414  
J. B. Gcdwin, U.S. Air Force, Directorate of Aerospace Fuels  
.. Session Chairman and Organizer

# TABLE OF CONTENTS (CONT'L)

## SESSION VII (CONTD)

- Principles of Electrostatics in Aircraft Fuel Systems 415  
Dr. Joseph T. Leonard, Naval Research Laboratory
- Ten Years' Experience of Anti-Static Additives in Aviation Fuels 449  
A. Lewis, Shell Research Limited and J. G. Kirtley, Shell International Petroleum Company Limited
- Protective System Measures For Aviation Fuel Handling 476  
W. G. Dukek and K. C. Bachman  
Esso Research and Engineering Company

## SESSION VIII AIRCRAFT II 505

- Introduction of the Session 506  
R. A. Peterson, The Boeing Company  
.. Session Chairman and Organizer
- Lightning Protection Techniques for Large Canopies on High Speed Aircraft 507  
Robert Aston, R. Gorton, and G. L. Weinstock, McDonnell Douglas Corporation
- Lightning and Electromagnetic Compatibility Analyses - A Joint Study on Lightning Effects for the B-1 Program 512  
E. S. Hughes, North American Rockwell, B-1 Division Coordinator  
J. D. Robb, Lightning and Transients Research Institute  
W. R. Johnson, TRW Systems  
J. A. Plumer, General Electric Company, Corporate Research and Development
- Control Surface and Door Hinge Bonding Effectiveness in Modern Aircraft 527  
James R. Stahmann, Lightning and Transients Research Institute
- A Test Technique for Measurement of Lightning-Induced Voltages in Aircraft Electrical Circuitry 535  
Lawrence C. Walko, General Electric Company, Corporate Research and Development  
Paul T. Hacker, Aerospace Safety Research and Data Institute, National Aeronautics and Space Administration, Lewis Research Center
- Lightning Protection Approaches for Helicopters 563  
J. D. Robb and J. R. Stahmann, Lightning and Transients Research Institute

# TABLE OF CONTENTS (CONT'D)

## SESSION VIII (CONT'D)

- Helicopter Cargo Handling - Electrostatic Considerations 579
  - E. J. Solak, The Boeing Company
  - J. E. Nanevich, Stanford Research Institute
  - G. J. Wilson, The Boeing Company
  - C. H. King, The Boeing Company, Commercial Aircraft Group

## SESSION IX      WORKSHOP: LIGHTNING SIMULATION, TESTING, AND MIL-B-5087B 592

- Introduction of the Session 593
  - J. D. Robb, Lightning and Transients Research Institute
  - J. A. Plumer, General Electric Company, Corporate Research and Development
  - Session Chairmen and Organizers
- British Civil Airworthiness Requirements For Electrical Bonding and Lightning Discharge Protection in Relation to Specification MIL-B-5087 595
  - B. L. Perry, UK Civil Aviation Authority, Airworthiness Division
- Factors Affecting Puncture of Aluminum Alloy by Simulated Lightning 607
  - John Phillpott, UK Atomic Energy Authority, Culham Laboratory, U.K.
- Comments on MIL-B-5087B(2), Bonding, Electrical, and Lightning Protection, for Aerospace Systems 613
  - Floyd P. Holder, Lockheed-Georgia Company
- Lightning Simulation and Testing in Relation to Specification MIL-B-5087 616
  - R. H. Evans, UK Ministry of Defence
  - J. Phillpott, UK Atomic Energy Authority

## SESSION X      SUPPLEMENTARY PAPERS 621

- Aerosol Discharge System for Heavy Lift Helicopters 622
  - Dr. Rudolf G. Buser, Helmuth M. Kaunzinger, and Hans E. Inslerman, US Army Electronics Command, Fort Monmouth, New Jersey
- A Passive Discharge System for the Electrically Charged Hovering Helicopter 634
  - G. J. Born and E. J. Durbin, Instrumentation and Control Laboratory Department of Aerospace & Mechanical Sciences, Princeton University

SESSION I

FUNDAMENTAL ASPECTS OF LIGHTNING

M.P. AMASON, CHAIRMAN & ORGANIZER

MCDONNELL DOUGLAS CORPORATION

## FUNDAMENTAL ASPECTS OF LIGHTNING

Chairman and Organizer — M. P. Amosson

Douglas Aircraft Company  
McDonnell Douglas Corporation  
Long Beach, California

The Fundamental Aspects of Lightning Session is organized with the objective of presenting discussions of the basic elements of natural lightning strike phenomena with special emphasis placed on the conditions that are of importance to the design of lightning protection for aerospace vehicles.

A motion picture\* of the thunderstorm with its associated electrical and lightning phenomena and the related research activities will first be presented by Professor B. Vonnegut of the State University of New York at Albany. The lightning prestrike activities, such as the cloud electrification phenomena and the propagation of lightning stepped leaders, will be discussed. This will provide a general over-all view of the operational environment and the aerospace vehicle's involvement with the lightning strike.

The electrical current and field characteristics of lightning strikes are of major concern to the aerospace designers. It is generally accepted that most of the lightning damage to the aerospace vehicles are related to the electrical aspects of lightning strikes, such as the peak current flow, the rate of rise of the current and the charge transfer. A better understanding of these characteristics will enable the designers to establish more realistic design criteria for lightning protection. The instrumentation and measurements associated with defining electrical current and field characteristics of various types of lightning strikes will be discussed by Professors M. Brook and C. Moore of the New Mexico Institute of Mining and Technology.\*\*

Most of the lightning protection research and development work in the aerospace industry has been carried out using laboratory spark simulation techniques. In the past, there has been concern with certain simulation methods in view of the differences found between test results and in-service data. The understanding of the characteristics of natural and simulated lightning strikes and the differences between them will assist in the interpretation of data collected in the laboratory. The laboratory spark simulation of natural lightning strikes will be analyzed by Professor M. A. Uman of the University of Florida.

An impressive amount of information related to natural lightning strike characteristics has been obtained during the past few years. This information has been used as a guide line for the current lightning protection research and development work. Many factors are still unknown, especially those associated with the prestrike and the cloud-to-cloud and intra-cloud lightning stroke phenomena, which may affect certain lightning protection design features. Research efforts should continue until all phases of the natural lightning strike to aircraft phenomena can be understood. If required, improved laboratory simulation techniques should be devised and better lightning protection techniques for aerospace vehicles developed.

\* Movie film "Atmospheric Electricity," by the American Meteorological Society, Film No. 1841, Modern Learning Aids, 1212 Avenue of the Americas, New York, N.Y., 10036.

\*\* Copies of this paper will be distributed at the Conference.

## Atmospheric Electricity

Bernard Vonnegut  
State University of New York at Albany

A general picture of thunderstorm and associated electrical phenomena is provided by a motion picture entitled, "Atmospheric Electricity". This film, prepared by the Educational Development Center under the direction of the American Meteorological Society and the sponsorship of the National Science Foundation, provides a rather elementary and nontechnical introduction to the electrical processes taking place in the atmosphere.

To introduce the concept of electricity in the atmosphere several familiar charge separation mechanisms are illustrated--the electrification experienced when walking across a rug and the contact electrification of the belt passing over a pulley of a Van de Graaff high voltage generator.

The important concept that electrical forces are produced between separated electric charges is illustrated by the electrical attraction exhibited between two high voltage electrodes and the coalescence of water drops suspended in an electric field in a nonconducting oil.

The fact that significant electrification is present in the atmosphere even during fine weather in the complete absence of clouds is illustrated by duplication of early experiments in which charge is shown to flow when a wire attached to an arrow is projected into the air or when a wire is supported by a kite or balloon. The results of studies of atmospheric electricity during fair weather, which indicate that the solid earth carries a charge of about a million coulombs of negative charge while the lower atmosphere carries an equal positive charge, are illustrated. The consequent potential difference of several hundred kilovolts that exists between the earth and the upper atmosphere and the global conduction current of several kiloamperes flowing continuously from the atmosphere to the earth is also illustrated.

Some of the many sources of atmospheric electrification are shown, such as the production of charge by bursting bubbles, the blowing of snow and dust, as well as waterfalls and erupting volcanoes. Although these processes undoubtedly contribute in important ways to atmospheric electrification, it is generally agreed that the dominant source of atmospheric charge is

provided by thunderstorms, perhaps a thousand in number, continuously occurring somewhere over the surface of the earth. Studies being carried out by scientists to determine the nature of thunderstorm electrification and its origin are illustrated with scenes taken in New Mexico showing various research activities. An animated sequence, prepared with the help of Professor Marx Brook, illustrates how a lightning discharge develops under the influence of the electrical stresses produced by the thunderstorm cloud.

The still unsolved and critical problem of how clouds generate strong electric fields is illustrated by descriptions of two varieties of electrification mechanisms, the first caused by the falling of electrified precipitation, and the second caused by the transport of charged particles in updrafts and downdrafts.

The phenomenon of point discharge, in which elevated points, such as trees and buildings beneath thunderstorms, produce ionization and emit electrical charge is illustrated by a duplication of Schonland's experiment, in which a current is shown to flow from an electrically isolated tree.

Some of the apparatus and techniques used to study thunderstorms are illustrated with scenes showing Professor Moore and his colleagues carrying out studies of thunderstorms from the summit of a mountain in New Mexico.

Data obtained with electrical measuring apparatus, photography and radar show that electrification appears early in the life of the thunderstorm and that increases in electrification coincide with rapid growth in the height of the cloud. Radar data indicating that lightning is sometimes followed by the formation of a heavy gush of rain suggest that electrical processes may be playing a role in accelerating droplet coalescence.

Laboratory experiments are shown which indicate that electricity may play a role in speeding the formation of rain and also perhaps in supplying energy to tornadoes.

Despite many recent advances in our knowledge of atmospheric electrification, it still is too fragmentary and inadequate to provide a sound scientific basis for answering many of the practical questions that arise in our modern

technology. At the present time, most studies of thunderstorm electricity have been confined to measurements made of garden variety thunderstorms occurring over land masses in the temperate zone. It is conceivable, in fact probable, that the electrical characteristics of storms occurring over the water and in other geographical locations may differ in important respects from those that have been studied. For the most part, the storms that have been studied are of an intermediate size extending to altitudes of approximately 10 kilometers. Very little data has been obtained on the very intense giant electrical storms that extend to altitudes of 20 kilometers and that produce lightning at rates an order of magnitude or more larger than usual storms. Few measurements have been made of the sometimes strong electrification known to occur in large-scale winter storms and the intense "lake effect storms" that occur in the fall over the warmer waters of the Great Lakes.

We do not yet have the key pieces of information in strongly electrified storms of any kind necessary to a satisfactory understanding of the electrical charge generating process. We don't know the nature and origin of the charged particles responsible for electrification, nor do we understand the convective circulation of the storm that determines the movement and accumulation of these charge carriers. Although it has not been possible to obtain this information thus far and although the job will certainly not be easy, it now appears that the job can be done. With our modern technology of aircraft, electrical instruments, radar and computers, we are at last capable of securing this information and putting our understanding of cloud electrification on a sound basis.



## Spark Simulation of Natural Lightning

Martin A. Uman  
Department of Electrical Engineering  
University of Florida  
Gainesville, Florida 32601

### ABSTRACT

Laboratory sparks are often considered to be miniature lightning and, as such, are sometimes used to simulate the effects of natural lightning on aerospace vehicles. This testing is generally concerned with the vulnerability of electrical systems, mechanical parts, and fuel systems to lightning as well as a determination of the likely lightning points-of-strike.

Very little is known about the characteristics of the intracloud, intercloud, and cloud-to-air discharge which aerospace vehicles generally encounter. Cloud-to-ground discharges, which are occasionally encountered and about which considerably more is known, appear to be more severe. Most lightning-simulation studies attempt to reproduce the properties of cloud-to-ground lightning.

The characteristics of natural lightning which are of most interest relative to aerospace vehicle protection are (1) the initial breakdown processes, (2) the current and energy transferred from the lightning channel to the vehicle, (3) the electric and magnetic fields generated by a direct or close strike, and (4) the shock wave produced by the expanding lightning channel. Sparks cannot be used to simulate (1) adequately although they can give some idea of likely points-of-strike. Sparks or voltage and current generators can be used to simulate (2) to a reasonable degree. Sparks cannot be used to simulate (3), and it is unlikely that a large enough voltage and current generator is practical to simulate (4).

LIGHTNING IS A TRANSIENT high-current electric discharge whose path length is generally measured in kilometers [1].\* Lightning occurs when some region of the atmosphere, usually part of a thundercloud, attains an electric charge sufficiently large that the electric field associated with the charge causes electrical breakdown of the air. The region of the thundercloud charge which feeds the typical cloud-to-ground lightning discharge is of the order of kilometers in diameter and, before lightning occurs, consists primarily of charged and uncharged ice and water particles with a total net negative charge of tens to hundred of coulombs.

Long laboratory sparks are often considered to be miniature lightning and are used to simulate lightning. Long sparks are used in model tests to determine lightning's probable point of strike. Long sparks are used to test the vulnerability of fuel systems and electronic equipment of commercial and military aircraft and aerospace vehicles to lightning.

The validity of lightning testing using long sparks is sometimes questionable since, as we shall see, lightning and long sparks differ in many of their characteristics. The physical properties of the long laboratory sparks created by impulse breakdown by the Westinghouse 6.4 MV impulse generator located at Trafford, Pa., have been the subject of a number of studies [2]-[6]. Most sparks studied were 4-m in length, although 2.5-m and 5-m sparks have received some study. Since the properties of long laboratory sparks are, to a considerable extent, dependent upon the generator and associated electrical circuits which produce the sparks, we will, in this paper, confine our discussion primarily to those laboratory sparks created by the Westinghouse Trafford generator.

In the present comparison of lightning with laboratory sparks we consider only those lightning discharges which take place between cloud and ground; that is, we choose not to discuss intracloud, intercloud, or cloud-to-air discharges. We do this for three reasons: (1) Much more is known about cloud-to-ground lightning than about any other type of lightning because the cloud-to-ground discharge is usually visible and hence is amenable to optical measurements (e.g., photography, spectroscopy); (2) Cloud-to-ground lightning is thought to exhibit higher values of current than cloud discharges and hence in that sense is more severe; and (3) Most lightning simulation studies attempt to reproduce the properties of cloud-to-ground lightning.

We will compare the following properties of lightning and long laboratory sparks: (1) the initial breakdown; (2) electrical properties including current and energy; (3) the electric and magnetic fields generated; and (4) the shock wave.

### THE INITIAL BREAKDOWN

A drawing of a streak camera photograph of the luminous features of a cloud-to-ground lightning discharge is shown in Fig. 1. A streak camera photograph is obtained with a camera composed basically of a stationary lens and a strip of photographic film that is moved horizontally at constant velocity across the image plane. Each cloud-to-ground lightning discharge is made up of one or more intermittent partial discharges. A total lightning discharge (whose time duration is of the order

\*Numbers in brackets designate references at end of paper.

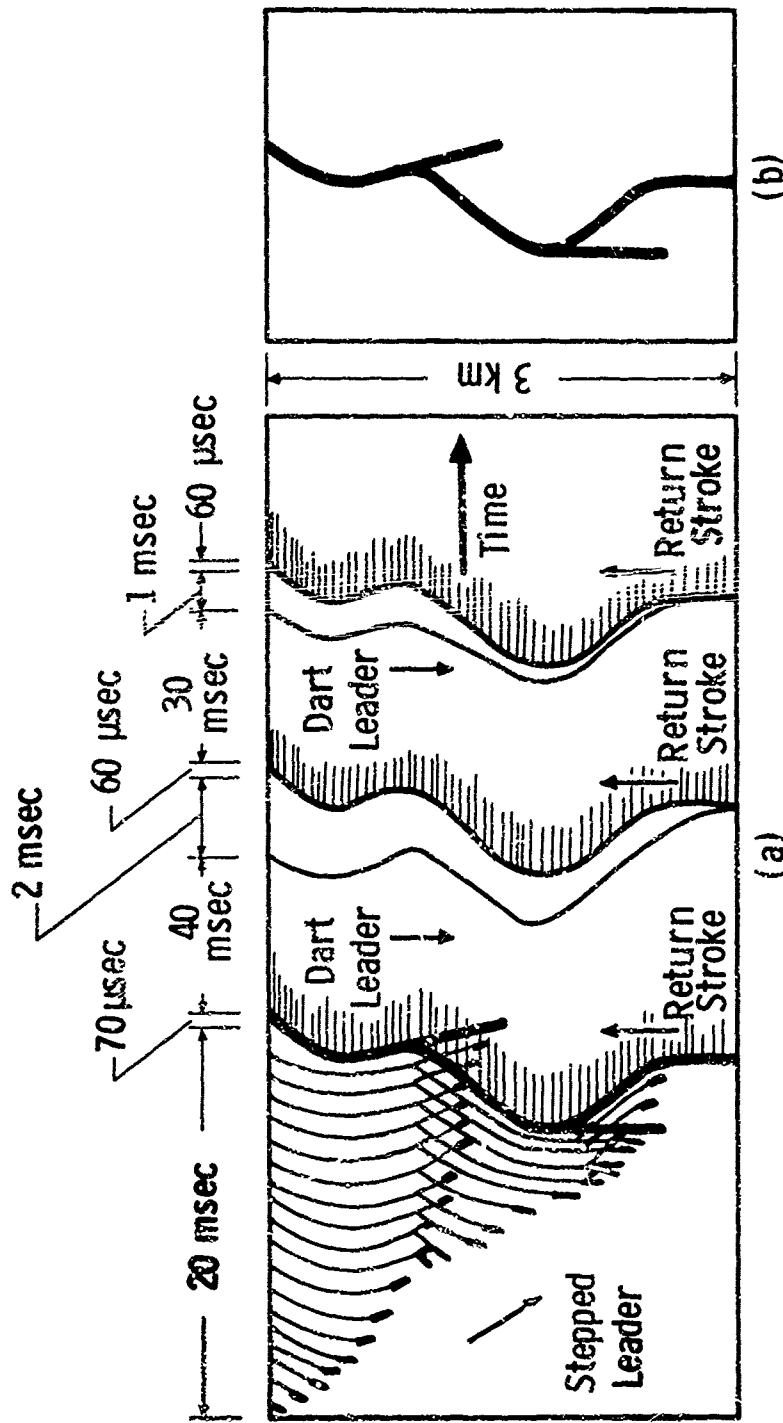


Fig. 1 (a) The luminous features of a lightning flash as would be recorded by a camera with fixed lens and moving film. Increasing time is to the right. For clarity the time scale has been distorted. (b) The same lightning flash as recorded by a camera with stationary film.

of a half second) is called a flash; each component discharge (whose luminous phase is measured in hundreds of microseconds) is called a stroke. There are usually three or four strokes per flash, the strokes typically being separated by about 40 ms. Each lightning stroke begins with a weakly luminous pre-discharge, the leader process, which propagates from cloud to ground and which is followed immediately by a very luminous return stroke. The return stroke propagates from ground to cloud.

The cloud-to-ground pre-discharge preceding the first return stroke in a flash is called the stepped leader. The stepped leader appears to move downward in luminous steps of typically 50-m length with a pause time between steps of about 50  $\mu$ s. During the pause time the stepped-leader channel is not luminous, or, more properly, is not luminous enough to be recorded on photographic film using standard streak-camera techniques. Each leader step becomes bright and observable in a time less than a microsecond. In Fig. 1 the 50-m steps appear as darkened tips on the faintly luminous channel which extends upward into the cloud. The typical average velocity of the stepped leader during its trip to the ground is  $1.5 \times 10^5$  m/s. From electric field measurements made during the stepped leader process, it has been determined that a typical stepped leader has of the order of 5 C of negative charge distributed over its length when it is near ground. The average currents which must flow in the stepped leader to deposit this amount of charge in tens of milliseconds of travel time to ground are of the order of  $10^2$  A. Peak currents in leader steps are of the order of  $10^3$  A [7]. Undoubtedly, there are electrical and luminous phenomena occurring in the stepped leader on a time and distance scale much smaller than have been observed.

When the stepped leader has lowered a charged column of high negative potential to near the ground, the resulting high electric field at the ground is sufficient to cause upward-moving discharges to be launched from the ground or from objects on the ground toward the leader tip. When one of these discharges contacts the leader, the bottom of the leader is effectively connected to ground potential while the remainder of the leader is at negative potential and is negatively charged. The situation is somewhat similar to a transmission line charged to a constant potential with a short circuit applied at its end. The leader channel acts like a transmission line (nonlinear) supporting a very luminous return stroke. The return-stroke wavefront, an ionizing wavefront of high electric field intensity, carries ground potential up the path forged previously by the stepped leader. The return-stroke wavefront propagates at a velocity of typically one-third to one-tenth the speed of light, making the round trip between cloud-to-base and

ground in a time of the order of 70  $\mu$ s. The region between the return-stroke wavefront and ground is traversed by large currents. The net negative charge deposited on the leader channel is effectively lowered to earth through the highly conducting channel beneath the return-stroke wavefront.

After the stroke current has ceased to flow, the lightning flash may be ended. On the other hand, if additional charge is made available to the top of the channel, the flash may contain additional strokes. (The flash is then termed a multiple-stroke flash.) If additional charge is made available to the decaying return-stroke channel in a time less than about 100 ms, a continuous or dart leader will traverse that return-stroke channel, increasing its degree of ionization, depositing charge along the channel, and carrying the cloud potential earthward once more. The dart leader thus sets the stage for the second (or any subsequent) return stroke. The dart leader appears to be a luminous section of channel about 50 m in length which travels smoothly earthward at about  $2 \times 10^6$  m/s, an order of magnitude faster than the average velocity of the stepped leader. Schematic drawings of streak-camera photographs of dart leaders are shown in Fig. 1. If the current in the previous return stroke has ceased to flow for several hundreds of milliseconds, any subsequent stroke will be preceded by a stepped leader whose path is different from that of the decayed channel.

As we have seen, cloud-to-ground lightning is initiated by a stepped leader. Exactly how the stepped leader forms and how it manages to funnel negative charge previously stored in a relatively large volume of cloud into a relatively narrow leader channel is not understood. There has been a great deal of speculation about how the stepped leader gets started and how it propagates (with most attention being given to the reasons for the steps). Unfortunately, however, no quantitative theory of the stepped leader is available nor is there any consensus agreement that any one of the qualitative theories is adequate. Thus our knowledge of the lightning breakdown process is primarily observational. Unfortunately, much the same state of affairs exists relative to our understanding of long laboratory sparks. Worse yet, while lightning occurring at different locations around the world appears to have about the same characteristics, sparks studied by different investigators appear to have very different characteristics.

The luminous features of the breakdown process leading to the 4-m sparks produced by the Westinghouse Trafford generator have been studied using a TRW image converter camera at a distance of about 20 m from the spark [5]. The voltage applied across the rod-plane gap would have been a standard 1.5 x 40 wave (1.5  $\mu$ s to peak and 40  $\mu$ s to half value) with a

crest value of approximately  $3.3 \times 10^6$  V in the absence of gap breakdown and corona load. For a negative rod and grounded plane this voltage is about 20 percent above that required for breakdown.

No luminous processes are recorded by the image converter camera until about 3 or 4  $\mu$ s after the application of the negative voltage to the rod. At that time a secondary streamer (the terminology advocated by Loeb [8]) or leader (in analogy to the lightning leader) emerges from the rod and propagates continuously toward the plane at about  $2 \times 10^6$  m/s. As it propagates, it becomes brighter. Before the downward-moving leader has crossed half of the gap, one or more upward-moving leaders are initiated from the plane. The downward-moving leader and one of the upward-moving leaders meet, usually just below mid-gap, and a bright luminosity or return stroke (in analogy to lightning) is propagated from the junction both upward and downward toward the two electrodes at about  $3 \times 10^7$  m/s. The return stroke is initiated about 5  $\mu$ s after the application of the voltage. The junction of the downward and upward-moving leaders is frequently characterized by a region of multiple channels.

The image-converter photographs showed no primary streamers (Loeb's terminology [8]) or impulse corona (the notation used in most of the earlier literature [9,10] prior to the leader's appearance as had been observed by Saxe and Meek [9], Park and Cones [10], Kritzinger [11], and others for gaps about 1 m or smaller. The image tube threshold was probably not low enough to record the impulse corona was, however, found in electrical current and photoelectric measurements.

From a general point of view, the luminous breakdown modes of the long spark between a negative rod and a grounded plane and of lightning are similar. Both discharges are initiated by a downward-propagating negatively charged leader which can be relatively easily photographed. The leader is met by an upward-going discharge, and this meeting is followed by a return stroke. Undoubtedly, undetected luminous processes (primary streamers, impulse corona) precede the observed lightning stepped leader as they do the spark leader. On the other hand, the lightning stepped leader and the spark leader appear to be quite different. The spark leader has a velocity about an order of magnitude greater than the average velocity of the lightning stepped leader. The spark leader moves continuously (at least within the time and spatial resolution of the measurements), while the lightning leader moves discontinuously in steps whose characteristic length is many tens of meters. The characteristic length of one leader step is about the length of the longest laboratory spark that at present can be created. It should be pointed out, however, that spark leaders produced by  $1.5 \times 40$ - $\mu$ s impulse voltages

have a velocity which is dependent on the impulse generator circuit impedances and, further, that spark leaders may apparently be made to step if the circuit impedances are properly adjusted [9,12]. In addition, spark leaders produced by applied gap voltages which rise to peak in a time of the order of 100  $\mu$ s (so-called "switching surge" voltages) have been reported to step although it is not known whether this stepping is a characteristic of the breakdown or of the circuit impedances [12]. It is not known whether the mechanism for the stepping of laboratory spark leaders is related to the mechanism for the stepping of the lightning leader.

The lightning or laboratory-spark strike point is determined by which upward-going discharge contacts the downward-moving leader. The most significant upward-moving discharge is generated in the region of highest electric field. The electric field is determined by (1) the charge on the electrodes and on the leader and (2) the space charge in the inter-electrode gap. Adequate spark simulation of lightning strike-points depends on the similarity of the lightning and spark situation just prior to the strike. Since conducting surfaces of small radius of curvature greatly enhance the ambient electric field, it would be expected that both lightning and laboratory sparks would strike these surfaces. Thus spark simulation of strike points is physically reasonable. Errors, however, could be made if the space charge field is appreciable and if there are significant differences in the space charge configurations in the spark and lightning cases. More space charge would be expected in the lightning case since the discharge takes longer to develop and strong ambient electric fields are usually present before the discharge.

#### ELECTRICAL PROPERTIES

We begin this section by estimating the electrical energy available to produce lightning. If we imagine the negative-charge region of the thundercloud to be the upper electrode of a capacitor and the ground to be the lower electrode, the available energy is  $QV/2$  where  $Q$  is the charge initially stored in the cloud and then brought to earth during the discharge and  $V$  is the potential difference between the charge region and ground. The charge  $Q$  is of the order of tens of coulombs. A charge of this magnitude contained in a sphere of radius 1 km, whose center was a few kilometers above ground, would produce a potential difference between the surface of the charge-containing volume and ground of the order of  $10^8$  V. The resultant electrical energy stored is of the order of  $10^9$  J. It follows that for a typical multiple-stroke flash of a few kilometers length, the energy available per stroke per meter of channel is roughly  $10^5$  J/m.

The return stroke current measured at ground consists of the current contribution

due to the upward-propagating discharge followed by the current due to the return stroke. Lightning current waveforms at ground for first and subsequent strokes are shown in Fig. 2 [13,14]. The time from detection of measurable current to peak current for first strokes is generally about 10  $\mu$ s and for subsequent strokes is 1  $\mu$ s or less. Current rates-of-rise in excess of 80 kA/ $\mu$ s have been measured. Peak return-stroke currents are generally 10 to 20 kA, but a few reliable values in excess of 100 kA have been obtained. The lightning current is usually less than 10<sup>4</sup>A after about 100  $\mu$ s and generally has a total duration of a few milliseconds unless a "continuing current" flows. Continuing currents of the order of 10<sup>2</sup>A may flow for tens or even hundreds of milliseconds. First return strokes have larger peak currents than subsequent strokes. On the average, first return strokes discharge to earth of the order of 5 C of charge, subsequent strokes of the order of 1 C.

Return stroke currents flowing in lightning channels above ground have recently been determined [15] from measurements of the electric fields generated by lightning. In this study, both first and subsequent stroke currents reached peak in about 1  $\mu$ s. From a small sample of 98 strokes in 21 flashes there were several peak currents in the 100 kA range. The fastest observed current rate of rise was near 200 kA/ $\mu$ s. Channel currents almost always were found to have much sharper peaks than currents measured in grounded towers or tall buildings.

Marx circuit generators can be used to produce lightning-like current rise-times and peak values. Whether the same generator can produce lightning-like current decay-times and continuing currents is mainly a property of the initial energy stored in the generator. In general, laboratory generators cannot, and additional current sources are used for charge transfers exceeding about 1C. The typical lightning input energy per unit length of channel, 10<sup>5</sup>J/m, is over an order of magnitude greater than the Westinghouse spark input energy per unit length, 5 x 10<sup>3</sup>J/m. That the lightning energy input is much greater also follows from the fact that thunder is composed of lower frequencies than the noise from the sparks as we shall discuss later. The Westinghouse spark current and charge transfer closely resemble the current and charge transfer of a weak lightning subsequent stroke. It may well be that the values of electric field and peak power dissipation in the spark and lightning channels are not very much different; that the main contributor to the input energy differences are the different magnitudes and time scales of the currents and charges.

Lightning damage to aerospace vehicles due to thermal effects of mechanical stress is generally related to the value of current

flowing at and near the damage point. Simulation of these effects by current generators is therefore reasonable.

#### ELECTRIC AND MAGNETIC FIELDS

The electric and magnetic fields from close lightning can induce deleterious voltages and currents in electronic circuits. An example of these fields at 3 km height from a straight, vertical return stroke of average current a distance of 10 m (essentially a direct hit) and 100 m away is given in Fig. 3. Electric fields approaching 10<sup>6</sup> V/m which vary on a microsecond time-scale are apparently present in the event of a direct hit. Relatively large voltages will inevitably be picked-up in any unshielded electronic circuitry. The magnetic field at ten meters is such that a loop of 1 m<sup>2</sup> area will have about 500 V generated around it. Electric and magnetic fields from more distant lightning should be similar to the electric fields given in [15] and [16].

A laboratory spark carrying a lightning-like current will not produce the waveforms shown in Fig. 3. The fields from the laboratory spark will be due to a complete current loop including the generator as well as the spark. The close lightning fields are strongly dependent on the return stroke velocity, and the fact that the wavefront is propagating. In the laboratory spark the return stroke phase has ended during the early parts of the current waveform. It is probably possible to tailor a voltage source to be applied between two large parallel planes (the object to be tested would be placed between the planes) so that it would produce electric fields similar to those of Fig. 3. The magnetic field could be generated from an independent current source.

#### THE SHOCK WAVE

When energy is pumped into the leader channel by the return stroke current and electric field, the radially expanding return stroke channel acts as a piston creating an outward propagating shock wave. If the shock wave is generated by a given straight section of channel, it should be a cylindrical shock until it is further away from the channel section than the length of that section. Beyond that point, the shock wave might be expected to make a transition to more of a spherical shock wave and eventually to a sound wave. Since the lightning channel is very tortuous, it is reasonable to expect, to a first approximation, that thunder from distant lightning is the superposition of many sound waves [17].

No reliable pressure measurements have been made within a few meters of a lightning channel, but there is a considerable body of

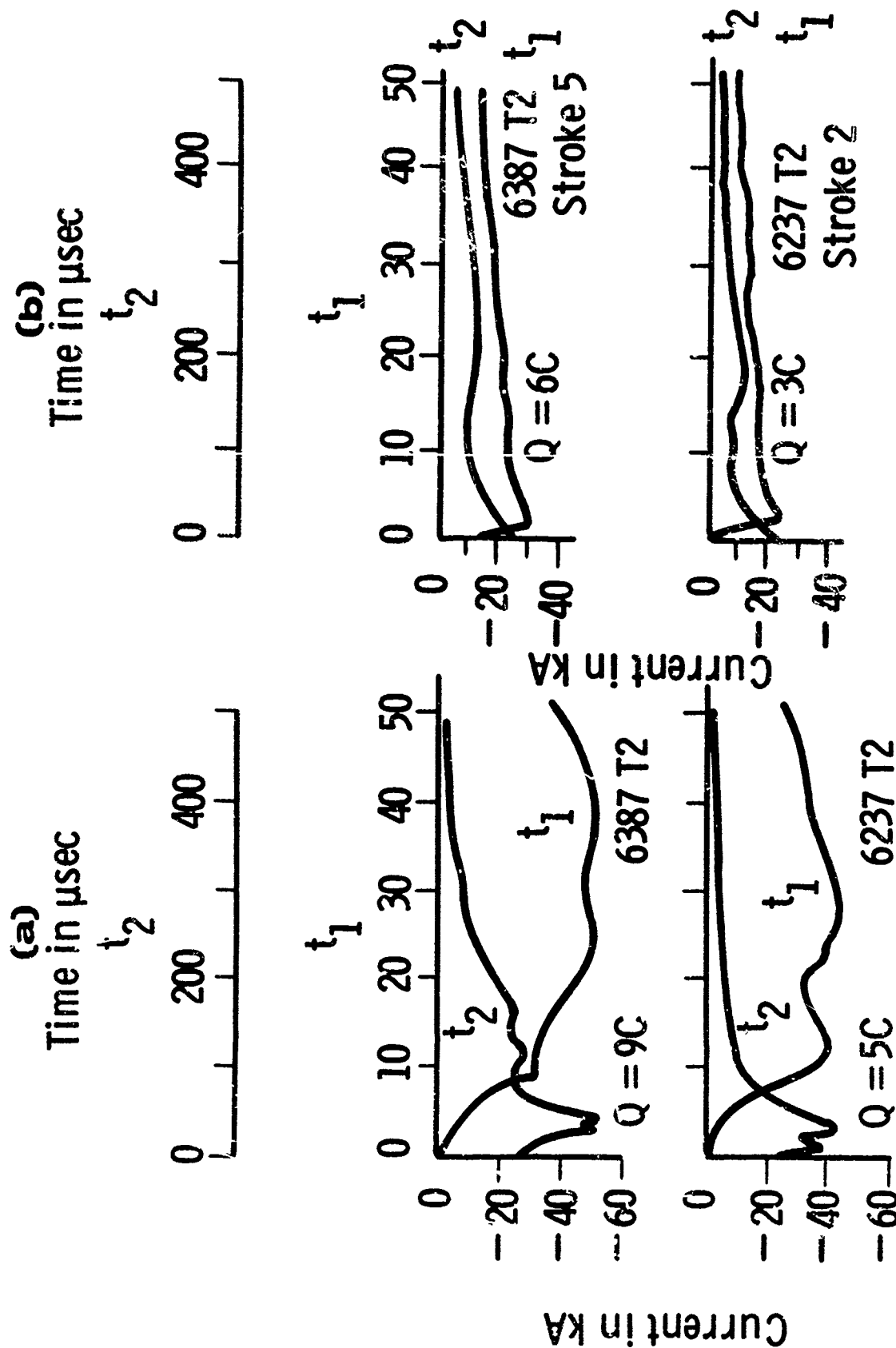


Fig. 2. Current vs. time for representative lightning strokes with peak currents greater than or equal to 10 kA 13,14. For each stroke, data are presented on two time scales:  $t_1$ , fast;  $t_2$ , slow. (a) Two first strokes. (b) Two subsequent strokes. Charge  $Q$  is the time integral of current of 1 ms. Current measured in tower on top of Mount San Salvatore, Lugano, Switzerland.

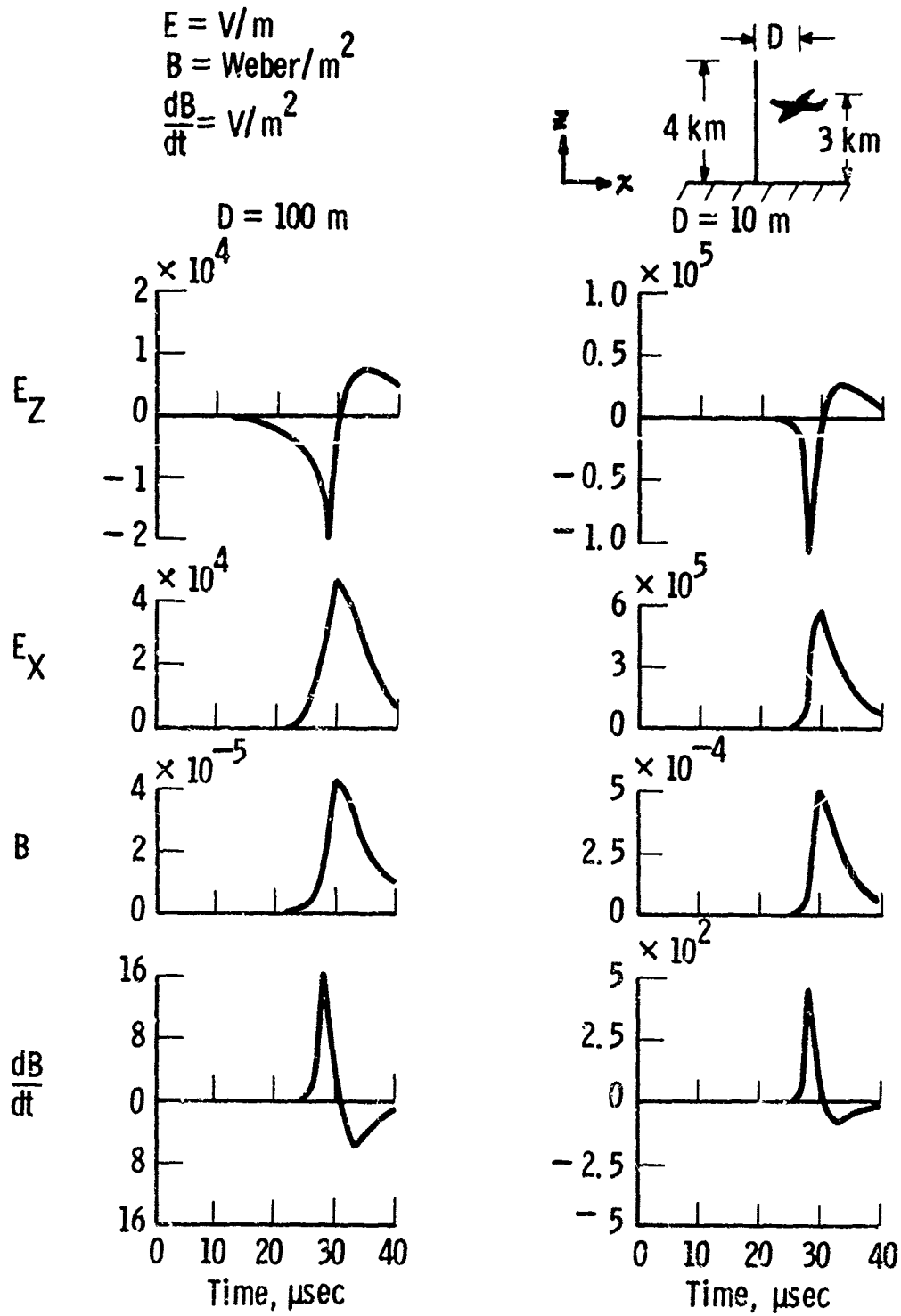


Fig. 3. The electric and magnetic fields near a typical lightning return stroke.

theory available predicting the shock overpressures and waveshapes to be expected for a given energy input to the shock wave [18,24]. Since the energy input to the shock wave determines the shock waveshape, it also determines the acoustic frequency spectrum. Thus the thunder frequency spectrum is a measure of the energy input to the shock wave. It is customary to assume that the bulk of the electrical energy input to a lightning channel ends up in the shock wave. (Only a small fraction of the input energy to the long spark escapes the discharge channel as radiation or is stored in the channel as heat [5,6], so that this assumption would appear reasonable.) With some assumptions about the form of the transition from cylindrical to spherical shock waves and the use of available theory, Few [25] has derived the following formula describing the relation between the peak frequency  $f$  of the thunder acoustic spectrum the energy input per unit length to the channel  $W$  in Joules and the ambient pressure  $P$  in Newtons/m<sup>2</sup>

$$f = 0.63 C \left(\frac{P}{W}\right)^{1/2} \quad (1)$$

where  $C$  is the speed of sound in m/s. For a frequency spectrum peak in the range 20 to 100 Hz [25], the energy input per unit length computed from (1) is in the range  $3 \times 10^5$  to  $8 \times 10^6$  J/m, values somewhat larger than our previous estimate of  $10^5$  J/m.

On the other hand, Plooster's [22-24] calculations show an input energy to the channel of about  $10^4$  J/m or less, at least an order of magnitude lower than our estimate. The expected overpressure for an energy input of  $10^5$  J/m is about 1 atmosphere a meter or so from the channel and 10 to 100 atmospheres a few centimeters from the channel. The overpressure scales linearly with energy input as long as the overpressure considerably exceeds unity.

Shock waves observed close to the Westinghouse spark are of the N-wave type [6]. Farther away from the spark than about a channel length, multiple shock waves are usually observed. Apparently, different sections of the tortuous spark channel produce individual shock waves as has been hypothesized to be the case for the tortuous lightning channel.

Equation (1) has been tested on the long spark and works reasonably well for measurements made about 20 m from the channel, a frequency spectrum peak of about 1400 Hz being measured at about 20 m for an energy input of  $5 \times 10^3$  J/m [3,6]. The spark shock wave, however, lengthens as a function of distance from the source [6]. Unfortunately, no measurements have been made beyond 20 m. The effect of the lengthening of the shock wave is to make the constant in (1) distance dependent; it must become smaller with increase in distance from the channel. The result is that use

of (1) for distant thunder may well produce an overestimate of the actual lightning energy input, as would appear to be the case from the high values of energy computed.

For the long spark there are some quantitative discrepancies between the measured shock overpressures and waveshapes close to the channel and the theoretical values [6]. A detailed discussion of the possible reasons for these discrepancies has been given in [6] and in [23].

In any event, it is probable that both lightning and long spark acoustic radiation are primarily functions of the electrical energy input to the lightning or spark channels and the shape of the channels. It follows that both the spark and lightning acoustic parameters probably scale as the same function of the energy input, and thus that spark generators cannot generate lightning-like shock waves unless they can deliver about  $10^5$  J/m to the spark channel.

## CONCLUSIONS

Lightning simulation using spark generators is not exact and in some aspects (e.g. electromagnetic radiation, shock wave) is very poor. On the other hand, lightning currents can be well simulated and strike-point determinations made with some degree of confidence. Lightning simulation using sparks is necessary and valuable. It is important, however, to keep in mind the limitations of this type of testing.

## ACKNOWLEDGEMENTS

This work was supported in part by the National Science Foundation (GA-31976) and by the Atmospheric Sciences Program of the Office of Naval Research (N00014-68-A-0173-0018).

## REFERENCES

1. Bibliography to any data or discussion relative to lightning not specifically referenced in this paper can be found in M. A. Uman, *Lightning*. New York: McGraw Hill, 1969. In general if the data or discussion are the result of the work of any investigators, no specific references will be presented here. If the data or discussion represent the work of only one or two investigators or are not considered in lightning, references will be given.
2. R. E. Orville, M. A. Uman, and A. M. Sletten, "Temperature and Electron Density in Long Air Sparks," *J. Appl. Phys.*, vol. 38, Feb. 1967, pp. 895-896.
3. G. A. Dawson, C. N. Richards, E. F. Krider, and M. A. Uman "Acoustic Output of a Long Spark," *J. Geophys. Res.*, Vol. 73, Jan. 15, 1968, pp. 815-816.
4. E. P. Krider, G. A. Dawson and M. A. Uman, "Peak Power and Energy Dissipation in a Single-Stroke Lightning Flash," *J. Geophys. Res.*



- vol. 73, May 15, 1968, pp. 3335-3339.
5. M.A. Uman, R.E. Orville, A.M. Sletten, and E.P. Krider, "Four-meter Sparks in Air," J. Appl. Phys., vol. 39, Oct. 1968, pp. 5162-5168.
6. M.A. Uman, A.H. Cookson, and J. B. Mooreland, "Shock Wave from a Four-Meter Spark," J. Appl. Phys., vol. 41, June 1970, pp. 3148-3155.
7. M.A. Uman and D.K. McLain, "Radiation Field and Current of the Lightning Stepped Leader," J. Geophys. Res., vol. 75, Feb. 20, 1970, pp. 1058-1066.
8. L.B. Loeb, "Ionizing Waves of Potential Gradient," Science, vol. 148, June 11, 1965, pp. 1417-1726.
9. R.F. Saxe and J.M. Meek, "The Initiation Mechanism of Long Sparks in Point-plane Gaps," Proc. Inst. Elec. Engr., vol. 102, part C, Apr. 1955, pp. 221-230.
10. J.H. Park and H.N. Cones, "Surge Voltage Breakdown of Air in a Nonuniform Field," J. Res. Natl. Bur. Stand., vol. 56, Apr. 1956, pp. 201-222.
11. J.J. Kritzinger, "The Breakdown Mechanism of Long Sparks in Air," Ph.D. dissertation, University of Witwatersrand, Johannesburg, South Africa, 1962; "The Relation Between Impulse Corona and Breakdown," Proc. 6th Int. Conf. Ionization Phenomena in Gases, vol. II, 1963, pp. 295-299; "Impulse Corona and the Pre-breakdown Mechanism of Long Sparks," Nature, vol. 197, Mar. 23, 1963, pp. 1165-1166.
12. I.S. Stekolnikov and A.V. Shkilev, "Investigation of Negative Spark Mechanisms," Sov. Phys.-Dokl., vol. 8, Feb. 1964, pp. 829-833; "The Development of a Long Spark and Lightning," Tr. Energet. Inst. (Moscow), 1966, pp. 97-110. Available from Defense Doc. Center as ASTIA Doc. AD 675456.
13. K. Berger, "Novel Observations on Lightning Discharges: Results of Research on Mount San Salvatore," J. Franklin Inst., vol. 283, June 1967, pp. 478-525.
14. K. Berger and E. Vogelsanger, "Messungen und Resultate der Blitzforschung der Jahre 1955-1963 auf dem Monte San Salvatore," Bull. SEV, vol. 56, 1965, pp. 2-22.
15. M.A. Uman and D.K. McLain, "Lightning Criteria Relative to Space Shuttles: Currents and Electric Field Intensity in Florida Lightning," Westinghouse Research Laboratories Report No. 72-9C3-LISTU-RI to NASA Marshall Space Flight Center, Alabama 35812, June 30, 1972.
16. R.J. Fisher and M.A. Uman, "Measured Electric Field Risetimes for First and Subsequent Lightning Return Strokes," J. Geophys. Res., vol. 77, January 1972, pp. 399-406.
17. A.A. Few, H.B. Garrett, M.A. Uman, and L.E. Salanave, "Comments on letter by W. W. Troutman 'Numerical Calculation of the Pressure Pulse from a Lightning Stroke'," J. Geophys. Res., vol. 75, July 20, 1970, pp. 4192-4195.
18. D.L. Jones, G.G. Goyer, and M.N. Plooster, "Shock Wave from a Lightning Discharge," J. Geophys. Res., vol. 73, May 15, 1968, pp. 3121-3127.
19. M.N. Plooster, "Shock Waves from Line Sources," National Center for Atmospheric Research, Boulder, Colo., Tech. Note NCAR-TN-37, 1968.
20. H.L. Brode, "The Blast Wave in Air Resulting from a High Temperature, High Pressure Sphere of Air," The Rani Corporation Santa Monica, Calif., Res. Memo RM-1825-AEC, 1956.
21. W.W. Troutman, "Numerical Calculation of the Pressure Pulse from a Lightning Stroke," J. Geophys. Res., vol. 74, Aug. 20, 1969, pp. 4595-4596.
22. M.N. Plooster, "Shock Waves from Line Sources. Numerical Solutions and Experimental Measurements," Phys. Fluids, vol. 13, Nov. 1970, pp. 2665-2675.
23. M.N. Plooster, "Numerical Simulation of Spark Discharges in Air," Phys. Fluids, vol. 14, Oct. 1971, pp. 2111-2123.
24. M.N. Plooster, "Numerical Model of the Return Stroke of the Lightning Discharge," Phys. Fluids, vol. 14, Oct. 1971, pp. 2124-2133.
25. A. A. Few, "Power Spectrum of Thunder," J. Geophys. Res., vol. 74, Dec. 20, 1969, pp. 6926-6934.

SESSION II

FUNDAMENTAL ASPECTS OF STATIC ELECTRICITY

DR. J.E. NANEVICZ, CHAIRMAN & ORGANIZER

STNAFORD RESEARCH INSTITUTE

## FUNDAMENTAL ASPECTS OF STATIC ELECTRICITY (Introduction to Session)

Joseph E. Nanevich  
Stanford Research Institute

VARIOUS CONSIDERATIONS went into the planning of this session. First, it was observed that this conference has a strong aerospace orientation so that the topics covered should ultimately be relatable to problems or techniques of interest to the aerospace community. On the other hand, it was observed that if we restrict our consideration strictly to work carried out in our own community, we run the risk of becoming parochial in our thinking, and of overlooking important applicable work being carried out by scientists in other areas. (In reviewing the proceedings from the previous conferences in this series, one is struck by the fact that the authors were almost exclusively active in the aerospace field.) Accordingly, the first two papers in this session "Ice Crystal Electrification" and "Processes of Frictional Electrification" are being presented by university professors whose interests range from atmospheric electricity and its generation to the electrostatic beneficiation of mineral ores in mining. Their two papers are concerned with static electrification processes in general. They discuss the physical mechanisms involved in the charge separation process, and indicate our degree of understanding of static electrification. A reasonable familiarity with electrification processes and the state of our understanding of them is essential to effective functioning in the area of static electricity. One is constantly faced with situations in which the presence of electrostatic charging must be recognized and analyzed, and either enhanced or eliminated. To hope to achieve these goals, one must be familiar with the fundamental processes involved. Of equal or perhaps greater importance is acquiring the ability to recognize situations where one must accept the electrification and adjust matters so that one can live with it.

Although we are all familiar with many of the manifestations of static electrification (most of them troublesome) such as the spark one gets after walking across a dry rug, they take a wide variety of forms and occur with unexpected frequency in systems. Often the electrostatic processes or the possibility of such processes are not recognized until one or more system malfunctions have occurred. Since these malfunctions can have catastrophic consequences, it is important to be aware of possible electrostatic effects so that steps can be taken for their circumvention early in the system design

and development program. The third paper, "Effects of Static Electrification on Systems", provides a wide ranging review of electrostatic incidents and their causes. The incidents discussed range from events with which one normally associates static electricity to unusual and surprising manifestations of electrification. The locales considered include the earth, space, and even the moon. The devious ways in which electrification manifested itself, and its ubiquitous nature are of particular interest in that they indicate the care that must be taken to consider all aspects of static electrification in system design. An important feature of this paper is its extensive bibliography which permits one to secure additional details regarding the incidents described.

One of the ways in which static electrification manifests itself is in the generation and coupling of noise into systems. In the past, considerable work has been done to characterize precipitation static noise sources and to measure the noise coupling to systems. Most of this work was done over 10 years ago using state-of-the-art instrumentation and analytical tools. Recently, in connection with EMP studies, the problem of analyzing transient pulse generation and coupling has received considerable attention. Sophisticated measurement systems have been developed, and powerful analytical tools have evolved. The fourth paper, "Techniques for the Study of Noise Generation and Coupling" describes some of these new techniques and indicates how they can be used (in somewhat more modest form) to study static noise generation and coupling. The paper considers analytical methods in considerable detail, and points out the trade-offs between time domain and frequency domain analysis. In particular, the pitfalls of trying to take shortcuts with either approach are discussed. It is concluded that a proper analysis requires a certain amount of effort and that operating in one or the other of the domains does not significantly alter the total effort required. The paper also discusses powerful experimental modelling techniques that are now possible with the advent of sampling oscilloscopes and subnanosecond pulse generators. These techniques should have wide application in the study of transient signal coupling.

At first glance it might seem that the fifth paper, "Structure of Lightning Noise--

Especially above HF" is out of place in this session, and that it should be in a session devoted to lightning. Actually its inclusion here is in keeping with the convention followed at the two previous conferences in this series. The lightning sessions have concentrated largely on the consequences of high stroke currents flowing in a system, while the static electricity sessions have concerned themselves with the more subtle noise sources. The paper reports an experimental work carried out by the authors and others to study the frequency structure of the noise radiated by lightning. This noise can couple into systems in an analogous manner to the EMP coupling. The work is also significant here in that it suggests techniques for the rapid, precise location of the VHF impulses from lightning and therefore of the associated lightning channels - even within a cloud. The ability to locate and identify these VHF pulses has important possibilities in the study of lightning itself and also in the development of light-weight lightning avoidance systems.

The sixth and final paper "Equations of Ion Motion" considers the problem of getting charges to move in air. It is important to recognize that the charges always exist as ions, and that their motion is controlled by collisions between the ions and air molecules. Since the motion of ions under these conditions is very slow, they form enormous space charge sheaths around discharge points, and limit the current that can be discharged. Recognition of these facts of ion motion is essential to the intelligent design of discharging systems.

In reviewing the papers in this session, one is struck by the fact that none deal with useful applications of static electricity. This was not done deliberately, but stems from the fact that, until recently, very few systems used static electricity deliberately. The situation is gradually changing (Xerox in the United States, and rotating static machines for generation of high voltage in Europe), and at the next conference it might be desirable to deliberately seek out at least one paper on useful applications of static electricity to get us thinking positively. After fighting static electricity and its effects all this time we don't want to miss some positive applications.

Also, in reviewing the papers in this session and in the conference in general, it is apparent that all the authors are from North America; whereas in the past we have included papers from Europe. This restriction of authors is not deliberate, and undoubtedly stems from the fact that there was so much lightning and static electricity work going on here during the past two years that the session organizers filled

their sessions immediately without considering less familiar activity in Europe. This is unfortunate because we have benefitted in the past from the exchange of information with European engineers.

In summary, the following observations appear appropriate regarding the area of static electricity. R. Ellison's paper shows the wide variety of ways in which static electricity has affected systems in the past. We should expect, therefore, that new effects will manifest themselves in the future. These will have to be tracked down and "fixed" for them developed. Accordingly, we should be prepared for continuing activity involving systems designers working with specialists in static electricity. As new effects are unearthed, it will also be necessary to develop new analytical and experimental techniques to further our understanding of the basic processes involved. At the same time, considerable effort will have to be devoted to the development of new hardware and fabrication techniques to cope with the new effects. A good example of a "new effect" is the aircraft windshield charging problem discussed in the next session. It has been known for years that windshields become charged and that the development of a tough, transparent, conductive coating would be desirable. In the past, however, it has been possible to live with the problem. Now, with the advent of larger windshields and for other reasons, the problem can no longer be tolerated. Work is now underway to devise acceptable ways of discharging the outer surfaces of windshields.

Not only is the impact of static electricity on systems likely to continue, it may be expected to increase. The increasing sophistication and miniaturization of aerospace systems has also rendered them increasingly susceptible to static electricity. This increased basic susceptibility will probably continue to grow. For example, solid-state devices are now used almost exclusively in newly developed electronic systems. Because these systems operate at lower energy levels than vacuum tube counterparts, they are more prone to upset. The active components in these systems can be damaged or destroyed by much lower energy levels than vacuum tubes. Field effect transistors are particularly susceptible in this regard.

Reducing susceptibility by discontinuing the use of sensitive components in these systems is not a tenable approach: their elimination would mean that the desired system could not be built. The use of solid-state devices also allows much more complex systems within a given weight and volume. This means that digital computers and control systems are feasible,

and, indeed, attractive. Unfortunately, a single noise pulse coupled into a computer logic system at a critical time can cause the computer to malfunction.

The papers of Prof. Dawson and Prof. Inculet indicate that our understanding of basic electrification processes is far from complete. In fact, Prof. Inculet's observation that, "We have now progressed to the point that, under rigidly controlled conditions, we can predict the polarity of the charging.", indicates that much basic work remains to be done. In this area, it is important for our purposes that a reasonable balance be maintained between extremely "clean" experiments which are satisfying to the physicist, but provide little practical guidance to the systems designer, and overly specialized "dirty" experiments which apply only to a single situation.

Finally, it appears that there are areas in which the application of newly-developed concepts and techniques should be pursued. For example, the Cianos-Oetzel-Pierce (C-O-P) lightning locator could be operated on an aircraft in conjunction with the weather radar system to compare the radar returns from storm cells producing lightning with the returns from passive cells. This would undoubtedly give us new insights into the problem of lightning avoidance. The C-O-P location system could be used in a more basic experiment to identify the temporal and spatial sequence of the VHF radiators around and within a thundercloud, and thereby to delineate the development of lightning channels in a manner which up to now has been entirely impossible.

We may observe in closing, therefore, that there are a sufficient number of challenging avenues to explore that activity in the area of static electricity can continue at its present pace and assure us of new and interesting topics for papers two years from now.

## Ice Crystal Electrification

G. A. Dawson  
Institute of Atmospheric Physics  
The University of Arizona

### ABSTRACT

A review is given of some of the more important processes whereby ice crystals and particles in the atmosphere can become charged. It is pointed out that the relative importance of these charging mechanisms is apparently quite different for hydrometeors and aircraft, but the possible application of some of the mechanisms to aircraft charging is discussed.

THE MOST INTERESTING ASPECT of electrification studies involving ice and water (e.g., those concerned with cumulus cloud electrification) is not that charge separation can readily occur, but that charge can be separated in so many different ways. In this paper we shall review the major mechanisms whereby ice particles in the atmosphere can become electrified, restricting ourselves to those processes that could in some way be involved in the problem of aircraft electrification. It should, however, be stressed that it is very difficult to assign with any real certainty a relative importance to the various charging mechanisms either in the cloud or aircraft environment, even though results are available for laboratory conditions.

### THERMOELECTRIC EFFECTS

The thermoelectric effect is a very powerful charging mechanism, and may easily be dominant in the atmosphere. Whenever two surfaces of ice of similar impurity-content at different temperatures come into temporary contact, charge transfer occurs and a potential difference is developed between the surfaces. The process was originally explained in terms of the different mobilities of  $H^+$  and  $OH^-$ ; now it is considered that lattice defects ( $OH_3^+$ ,  $(OH)^-$  and Bjerrum L and D orientational defects (vacant and doubly occupied hydrogen bonds, respectively) are responsible. The mobility of  $(OH_3)^+$  is greater than that of  $(OH)^-$ , and the mobility of the L defect is greater than that of the D defect. Furthermore, the number of each rapidly increases with temperature. Large numbers of defects are produced in the warmer ice and migrate towards the colder ice, becoming annihilated on the way. The positive defects move faster so the warm ice is left negatively charged and the colder ice positively charged, until the internal field produces equilibrium. The actual potential difference developed depends on a number of factors, but a frequently quoted value is about  $2mV/^\circ C$ . Ionic impurities

(e.g., NaCl) increase mobilities by a factor of about 2 (i.e., if warmer ice is doped with NaCl, charge transfer is increased; if colder ice is doped, charging is decreased).

Several other factors can affect the amount of charge transferred, e.g., contact time and the presence of air bubbles in the ice. Both have to do with thermal conduction across the ice surfaces. If contact time is too long, temperature gradients are decreased and charge transfer reduced. Optimum contact time is calculated to be about 10 msec; it has been observed, for low velocity collisions, to be about 3 msec. This effect is partly offset by the presence of air bubbles in the ice (cloudy ice), which apparently act to reduce the thermal conductivity. The influence of impact velocity is not clear. At low velocities (up to about 45 mph), charging has been observed to increase with increasing speed. I am not aware of work at much higher speeds. The various thermoelectric crystal charging mechanisms differ only in the specific way in which the initial temperature difference is produced.

Asymmetric Rubbing Contact - Whenever two ice surfaces rub against each other in such a way that the frictionally produced heat is not deposited with equal density on the two surfaces, one gets warmer than the other and electrification results. The most obvious example in the laboratory is that of two rods of ice where one is drawn across the other, and heating is localized on one rod and spread over the other.

In the air, the situation can become much more complicated. It is not always clear which surface will receive the greater density of heat, and therefore become negative. For example, in one experiment (1)\*, ice crystals were caused to collide with a shiny simulated hailstone. The hailstone became positively charged (low density of heat), i.e., the crystals rubbed around part of the hailstone, having a small area of contact on the crystal and a large area on the stone. When the hailstone was roughened by letting it first rime (i.e., pick up and freeze) supercooled water droplets, the sign of charging was reversed. The hailstone now became negative, the magnitude of the charge was much larger than before and increased with roughness. The ice crystals could, in this case, be conceived as rubbing only the high spots on the rimed pellet. There must have been an intermediate roughness for which the charging was zero. In this study the form of ice crystal was not

\* Numbers in parentheses designate References at end of paper.

given. In a similar but more detailed experiment (2), an ice sphere moving through a natural cloud or snowfall became highly charged only when ice was present in the cloud. When the cloud was completely glaciated and the temperature below  $-4^{\circ}\text{C}$ , the ice sphere became negatively charged. At temperatures above  $-4^{\circ}\text{C}$ , the sign of the charge was the same as that on the particles in the air. So in this type of charging, the microscopic details of the ice collision processes determine the sign of the resulting charge.

**Thermal Lag** - In rapid downdrafts or updrafts or regions of rapid temperature change, ice crystals of different size (which can collide) will in general have slightly different temperatures because of their different heat capacities. Similarly the breakup of fragile crystal dendrites in blowing snow can produce electrification whose sign depends on whether the breakup occurs in a downdraft or an updraft. If a downdraft, the air and splinters are warmer than the body of the crystal, so the ejected splinters are generally negatively charged. In an updraft, the air and splinters are cooler than the crystals, and so positive splinters result.

**Latent Heat** - Probably the most important source of temperature difference between ice particles in a cloud is the latent heat of freezing of supercooled cloud drops with which the crystals collide. If the rate of acquisition of supercooled water and the rate of heat transfer to the air are different for differently sized ice particles (as in general they are), considerable temperature differences can result. Subsequent collisions between these ice particles can lead to substantial charging, with the smaller particles in general becoming positively charged and the larger particles negatively charged. The classic experiments on this mechanism were performed by Reynolds, Brook and Gourley (3) in 1957. They rotated an ice pellet in a cold box containing a cloud of either ice crystals, supercooled water, or a mixture of both. Substantial charging was found only in this latter case. (Note in this case, the riming causes both a temperature difference and also appreciable surface roughness.) The magnitude of the charging depends, of course, on the relative number of ice crystals and supercooled drops in the cloud.

#### FREEZING POTENTIALS

Rain and cloud drops are dilute solutions of salts, and when dilute solutions freeze, they produce freezing potentials, i.e., the ice becomes charged (usually negatively) with respect to the water (4). The mechanism is the preferential incorporation of some of the anions (negative ions) of the salt into the ice lattice. The only exception is the action of ammonium salts ( $\text{NH}_4^+$ ) which makes the ice strongly positive. The potentials developed across the ice/water interface depend on

freezing rate and solution concentration, but are typically  $\approx 30\text{V}$  for a  $10^{-4}\text{M}$  NaCl solution, one or two hundred for a similar ammonium solution. The maximum occurs at a concentration of about  $10^{-6}\text{M}$ . Typical salt concentrations in continental rainwater are  $10^{-6} - 10^{-4}\text{M}$ , and at the coast up to  $10^{-3}\text{M}$ . This seems to be a very potent charging mechanism.

#### RIMING

There is a considerable amount of evidence that surfaces undergoing riming with large enough supercooled drops become highly charged by a mechanism which has never been fully explained. All experimenters except one found the riming surface to become strongly negatively charged. A mechanism has been offered which depends on the freezing of the impinging drops from the outside, building up pressure inside the drop and resulting in shattering and the production of a large number of ice splinters. The theory and the experiment on which it was based have since been strongly criticized, particularly as regards the number of splinters produced. The experiments need to be repeated under more controlled conditions. Nevertheless it appears that, splinters or no, riming always produces charging of the rimed surface, including aircraft. All evidence on the effects of impurities, e.g., salts or  $\text{CO}_2$ , indicate that this electrification mechanism is not the same as that discussed above under "FREEZING POTENTIALS."

#### EVAPORATING OR MELTING ICE

Some slight charging of evaporating ice has been explained by (crudely speaking) the evaporation of aggregates containing defects from the surface. Much more important is the charging accompanying ice melting (the Dinger-Gunn effect) (5). Bubbles frozen into the ice due to the decrease of air solubility on freezing are freed upon melting and burst at the surface. This is a well-known water charging process.

#### APPLICATION TO AIRCRAFT ELECTRIFICATION

It is interesting that the conditions that accompany the most vigorous cloud electrification are apparently not the same as those conducive to rapid aircraft electrification. Aircraft charging, it seems, is greatest in the presence of dry crystals of ice and snow; for clouds, the greatest efficiency is associated with the presence of both phases, ice and water. However, some experiments (2) have found maximum hailstone charging in completely glaciated clouds colder than  $-4^{\circ}\text{C}$ .

With supercooled or partially glaciated

clouds, one might expect contributions to aircraft charging from all the processes described above, plus charged particle sweep-up and frictional electrification. The work of Imanitov, Nanavicz, Gunn, Couch, and others suggests that the latter dominates.

With dry crystals, apart from frictional electrification, only thermoelectric effects due to asymmetric rubbing and thermal lag could produce charging. For high-speed aircraft, the Thermal Lag or Blowing Snow mechanism deserves a little attention. The temperature rise of the air at the leading edge of an airplane approaching Mach 1 should be about 50°C (80°F) at about 25,000 to 30,000 feet. This is a much higher temperature difference — air to ice crystal — than has been used in experiments on blowing snow electrification where appreciable charging was produced. If the temperature rise of the air causes a heating of fragile splinters of ice (with respect to the body of the crystal) of, say, 5°C before they are broken off by the air accelerations, experiments indicate that charges of at least  $10^{-16}$  Coulomb per splinter could be produced. The rate of charging of an aircraft under these conditions, however, may not be much greater than a few tens of microamps.

#### ACKNOWLEDGMENTS

This research was supported by the Atmospheric Sciences Section, National Science Foundation, and the Atmospheric Sciences Program of the Office of Naval Research.

#### REFERENCES

1. J. Latham and A. H. Miller, "The Role of Ice Specimen Geometry and Impact Velocity in the Reynolds-Brook Theory of Thunderstorm Electrification." *J. Atmos. Sci.*, Vol. 22, 505, 1965.
2. P. V. Hobbs and D. A. Burrows, "The Electrification of an Ice Sphere Moving Through Natural Clouds." *J. Atmos. Sci.*, Vol. 23, 757, 1966.
3. S. E. Reynolds, M. Brook, and M. F. Gourley, "Thunderstorm Charge Separation." *J. Meteorol.*, Vol. 14, 426, 1957.
4. E. J. Workman and S. E. Reynolds, "Electrical Phenomena Occurring during the Freezing of Dilute Aqueous Solutions and their Possible Relationship to Thunderstorm Electricity." *Phys. Rev.*, Vol. 78, 254, 1950.
5. J. E. Dinger and R. Gunn, "Electrical Effects Associated With a Change of State of Water." *Terr. Mag. Atmos. Elect.*, Vol. 51, 477, 1946.



## Processes in Frictional Electrification

Ion I. Inculet  
Faculty of Engineering Science  
The University of Western Ontario

### ABSTRACT

Frictional electrification, defined as the electric charges which remain on the surface after the separation of solid-to-solid contacts, involves at least two physical phenomena which are equally important in determining the electrification. The phenomena are the electronic charge transfer across the interface at the point of contact of the two materials and the electronic charge backflow which takes place as the two solids are separated. Under rigidly controlled conditions, the present status of knowledge of electron transfer between materials of different work functions permits the prediction of the polarity of the static electrification. The magnitude of the charge transfer which remains on the surface after separation is still far from being predictable. Engineering applications involving electrification can only be based on experimental results of a sufficiently large number of tests as well as on the proven ability to maintain or reproduce the surface and ambient conditions under which the original experiments were carried out. According to the application, the wanted or unwanted electrification due to solid-to-solid contact is generated under various external ambients or fields. The combined effects of such influences often have a very pronounced effect on the final charges. The paper reviews some of the recent fundamental work on humidity, temperature and electric field influences on solid-to-solid contact electrification and under what practical applications the electric field plays a predominant role.

### FRICTIONAL ELECTRIFICATION

A standard terminology for static electrification phenomena, and not excluding the basic word electrostatics, has been long overdue. Frictional electrification is described in literature under at least two other terms, such as tribo-electrification and contact electrification. This paper presents some of the practical and theoretical knowledge which may be useful in controlling the electrical charge which remains on the contact surfaces after the separation of two solids. The two solids may be a combination of conductors, semi-conductors and insulators. Any rubbing or friction of the two surfaces which is implied by the term "frictional" should be interpreted as merely providing a larger area of contact. Additional effects of rubbing, such as altering or damaging of the surface, transient high temperature spots, etc. are far from being understood in the overall process and hence must be minimized

in any experimental set-up attempting to investigate the phenomenon.

Frictional electrification defined as above involves two physical phenomena equally important to the net result: (1) electrification of the interface, and (2) charge backflow. For the theoretical aspects of the first phenomenon, as applied to clean surfaces, the reader is directed to solid state physics. However, the considerable progress made by the solid state science and engineering, covering the electrification of clean solid interfaces, stops there. It is of hardly any practical interest to the solid state engineer to investigate what happens or how to control the amount of electric charge which may remain on the contact surface if we were to break a transistor or a diode in two along an interface. As to the second phenomenon, the charge backflow which ultimately determines what is left on the surfaces after the separation, the knowledge is very scant. The hardly explored field is waiting for applied electrostatics investigators.

While the solid state vast body of knowledge is limited to certain classes of materials and clean surfaces, the frictional electrification and its applications generally deals with complex materials and surfaces influenced and/or contaminated by various ambients. Humidity, temperature, dust, gaseous pollutants, external electric fields, etc. could have a considerable influence on both polarity and charge magnitude. As little as a mono-molecular layer of adsorbed gas may sufficiently change the work function of a solid material to reverse the polarity of the electrification.

### ELECTRIFICATION OF CLEAN SURFACES IN CONTROLLED AMBIENTS

It was relatively recently, 1967, that the solid state electron transfer theory applied to static electrification found experimental proof. Practically simultaneous experiments in England (1)\* and Canada (2) produced adequate correlations between the work function of the materials in contact and charge transfer. To achieve these correlations, the surfaces of the materials had to be clean and the ambients, generally vacuum, well controlled. One investigator (2) introduced electric sputtering as the last step in the cleaning procedure for the metallic surface prior to the

\*Numbers in parentheses designate References at end of paper.

frictional electrification experiment. The experiment (2) studied the frictional electrification of a series of metals arranged in the order of increasing work function values, contacting borosilicate pyrex glass 7740. The electric charges developed on the metals varied from a maximum positive value for zirconium, the experimental metal with the lowest work function value, to a minimum negative charge for the platinum, the experimental metal with the highest work function value. Consequently, there exists a theoretical work function value which will give zero electrification when contacting the pyrex glass. This was interpreted as the "work function" value of the pyrex glass itself.

In a more general way, if one plots as in Figure 1 the frictional electrification (C) of several materials of known work function ( $\phi$ ) in contact with a specific material of unknown work function, the intersection at zero electrification gives the work function value of the material. The relative magnitude of the charges does not matter in this method, and the Coulomb scale was omitted in Figure 1. Perhaps it is just as well as the predictability of the amount of charge is still very uncertain. Thus the work function theory gives a good tool to analyze and predict the polarity of the charge on clean surfaces and controlled ambients. Based on the same theory, experimenters (3) and (4) have determined "frictional" work function values for materials such as polyvinylchloride, polyimide, polycarbonate, polystyrene, nylon 66, polyethylene, polypropylene, teflon, etc.

SURFACE STATES theory in addition to the work function of a material is an emerging theory for the understanding of the more complex frictional electrification phenomena. The symmetry surrounding an atom in a crystal lattice ends abruptly at the surface. In addition, one cannot avoid the surface from contamination with foreign atoms and/or adsorbed gases. The result is that the energy bands configurations which exist in the interior of the material are no longer valid for the surface where separate energy bands may appear. The energy levels of these new bands may lie in the forbidden gap of the material; although the crystal may be an insulator, the surface state may allow some electrical conduction. The electrification of polymers (5) has been of recent interest in the support of this theory.

CHARGE BACKFLOW, the second phenomenon in electrification, is perhaps the most important to control in any application. The amount of charge which flows back may be an order of magnitude, or more, larger than the charge which remains. It is believed that the charge backflow depends on several parameters, such as the materials in contact, the surface preparation, the geometry of the contact, the speed of separation, the temperature, the ambient gas, etc. One must realize that while the contact appears to take place between two inert solids, it is in fact a molecular or atomic

phenomenon. Any surface changes due to the impact or adsorbed molecules and impurities by the surface of contact are likely to change the amount of charge flowing back, and it is practically impossible to give an accurate description of the real surface in contact or what happens to the various atoms during the separation.

#### ELECTRIFICATION IN AIR

The experiments with clean surfaces, simple elements and controlled environments to maintain the surfaces clean, such as vacuum, have helped apply some of the solid state theoretical explanations to the frictional electrification phenomena. When dealing with complex materials in normal ambients, any prediction as to the polarity or amount of charge cannot be but guess work. However, if the number of experiments is sufficiently large to be statistically valid and at the same time the reproducibility of the materials and of the ambient conditions can be maintained, practical applications may be designed on the basis of such obtained values. A good example of reliable data for frictional electrification in air is that obtained from electrification in fluidized beds. The very large number of collisions between the different materials which are mixed in a fluidized bed, ensures a statistically valid result. The process is successfully used in mineral ore separation. For example, in the iron ore beneficiation, where a mixture of  $\text{Fe}_2\text{O}_3$  and silica particles are present, the great majority of the  $\text{Fe}_2\text{O}_3$  particles will charge positively whereas the silica negatively.

Referring to Figure 2, one sees that in the electrostatic beneficiation of ores in a fluidized bed, the point of contact between two particles may be traversed by the electric field in various directions as seen at A, B and C. Of particular interest are cases A and C. If the electric field plays a predominant role, such as in inductive induction, the frictional electrification of one polarity for a specific component can no longer be achieved. The particles will charge alternately positively and negatively with a resultant cancellation of most of the charge.

The fluidized bed electrification requires a rigid control of the humidity, temperature and electric fields in the bed. The same applies to the control of any electrification process in air. The three parameters have been recently analyzed experimentally by two investigators working on different projects. One (4) doing fundamental work on frictional electrification based on rolling contacts, and the other (6) on electrostatic beneficiation of iron ores in fluidized beds.

THE TEMPERATURE influence on the frictional electrification under various electric fields is exemplified in Figure 3. As shown in the figure, positive fields are assumed to be those directed from the pyrex to the stainless

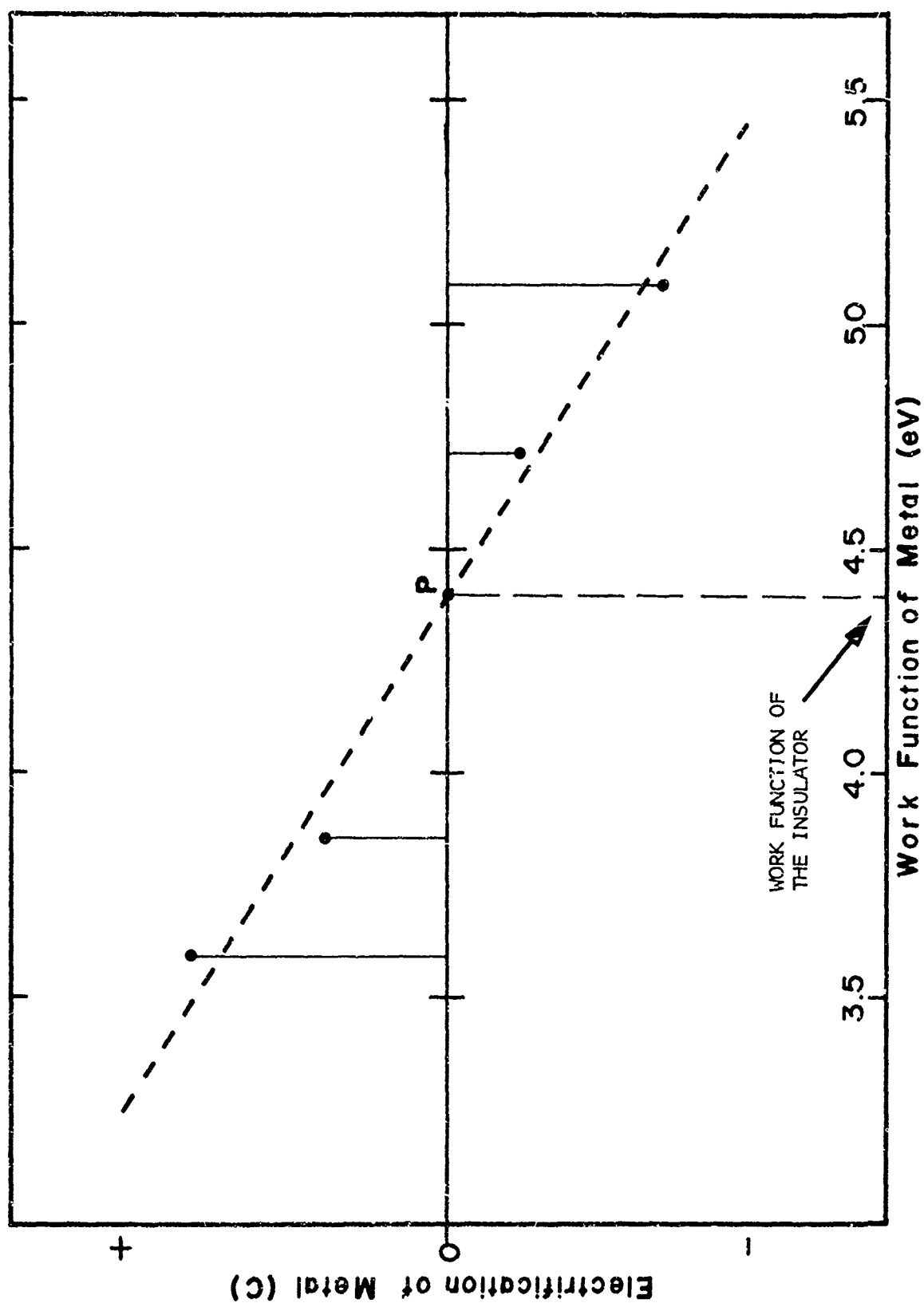


Fig. 1 - Frictional electrification of a work function series of metals in contact with an insulator.

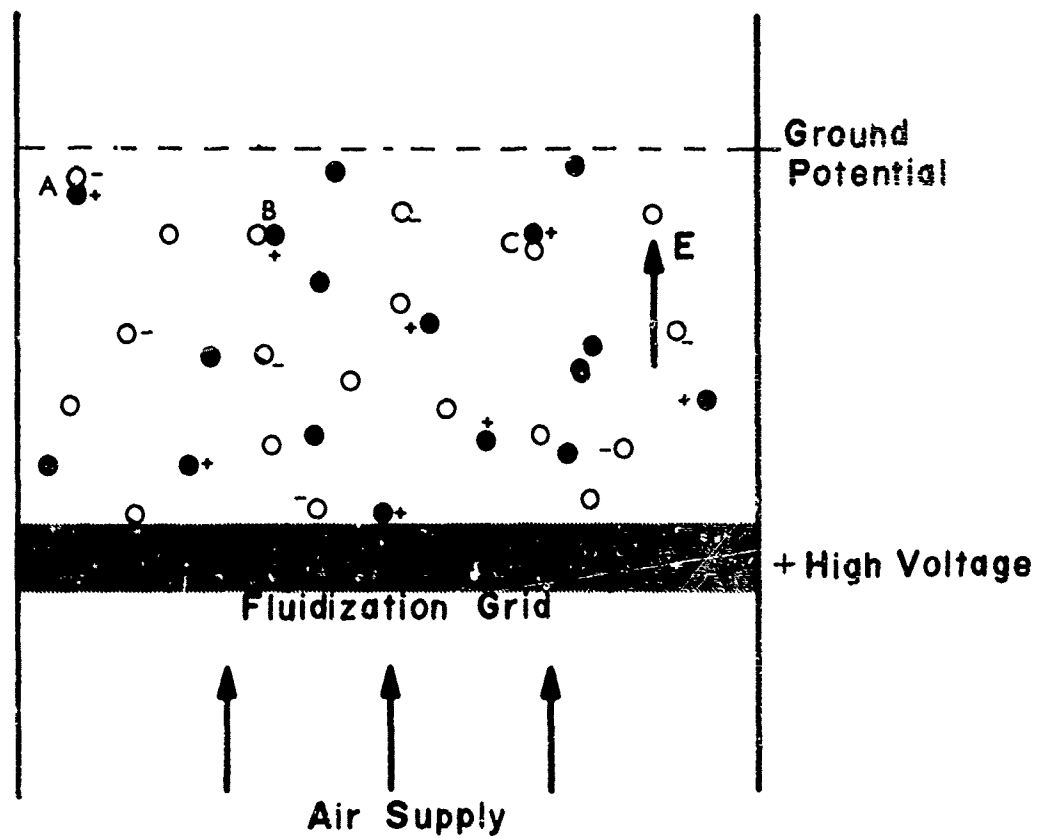


Fig. 2 - Frictional electrification of two different materials in a fluidized bed traversed by an electric field.

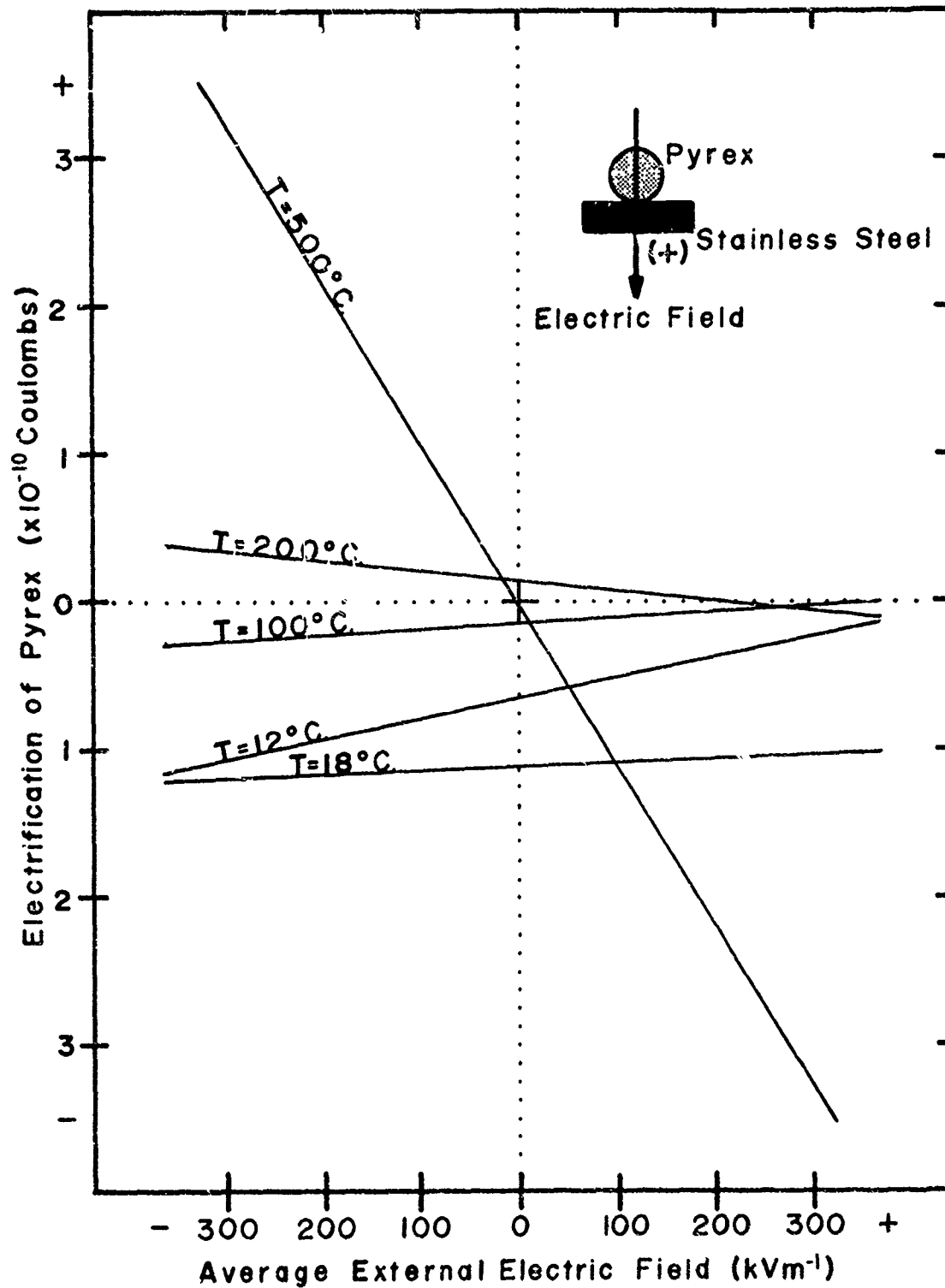


Fig. 3 - Temperature and external electric field influence on the electrification of pyrex glass in contact with stainless steel (Greason, 1972).

steel, and negative fields those in the opposite direction. At normal ambient temperatures the frictional electrification of the pyrex stays fairly constant and is negative over the range of fields measured. As the temperature is increased to 100°C or 200°C the electric charges which develop are considerably smaller but continue to remain relatively constant over the electric field range. Finally, at the much more elevated temperature, 500°C, the charge versus field characteristic becomes a straight line with a very pronounced slope. For negative fields the electric charges on the pyrex are positive, and for positive fields the reverse takes place. The phenomenon is an interesting transition from frictional electrification to what some investigators call conductive induction charging. At the higher temperatures the pyrex glass becomes more conductive and the field dependent conductive induction becomes the predominant phenomenon.

THE RELATIVE HUMIDITY of the air in which frictional electrification takes place is also of considerable importance and some of the recent results (4) are shown in Figure 4. Somewhat similar to the temperature effects, low relative humidities give constant electrification of the pyrex over the range of fields studied. As the humidity increases one observes a pronounced shift in the charge versus electric field characteristic indicating conductive induction electrification. The higher the humidity the greater the negative slope of the curve.

Both the temperature and the humidity affect the conductivity of the pyrex as evidenced by the conductive induction electrification. However the processes are entirely different. While the increase in temperature decreases the volume resistivity of the pyrex, as seen in Table 1, the increase in relative humidity very likely produces a surface conduction through the various impurities present.

Table 1 Pyrex 7740 Glass					
Temperature °C	0	50	100	150	200
Resistivity ohm-cm	$10^{15}$	$10^{13}$	$10^{12}$	$10^{10}$	$10^9$

#### CONCLUSIONS

Frictional electrification comprises two phenomena - interface charging and charge backflow after the contact separation. While the electrification of the interface of simple elements under controlled conditions may be adequately explained and predicted by means of the solid state theory of work function and surface states density, the charge backflow is still far from being fully understood and often

represents the greatest portion of the electric charge which one must control for an engineering application.

Experiments in air require a very rigid control of temperature, humidity and external electric fields, and any design data must be based on a number of experiments which is sufficiently large to be statistically valid.

#### REFERENCES

1. D.K. Davies, "The Generation and Dissipation of Static Charge on Dielectrics in a Vacuum", Proceedings, 2nd Conference on Static Electrification, Institute of Physics, Conference Series No.4, pp.29-36, 1967.
2. I.I. Inculet and E.P. Wituschek, "Electrification by Friction in a  $3 \times 10^{-7}$  Torr Vacuum", Proceedings, 2nd Conference on Static Electrification, Institute of Physics, Conference Series No.4, pp.37-43, 1967.
3. D.K. Davies, "Charge Generation on Solids", Proceedings, 1st International Conference on Static Electricity, European Federation of Chemical Engineering, pp.10-21, 1970.
4. W.D. Greason, "Effect of Electric Fields and Temperature on the Electrification of Metals in Contact with Insulators and Semiconductors", University of Western Ontario, Canada, Ph.D. Thesis, 1972.
5. H. Krupp, "Physical Models of the Static Electrification of Solids", Proceedings, 3rd Conference on Static Electrification, Institute of Physics, Conference Series No.11, pp.1-15, 1971.
6. S. Bauer, "Electrostatic Beneficiation of Iron Ores in Fluidized Beds", University of Western Ontario, Canada, M.E.Sc. Thesis, 1972.

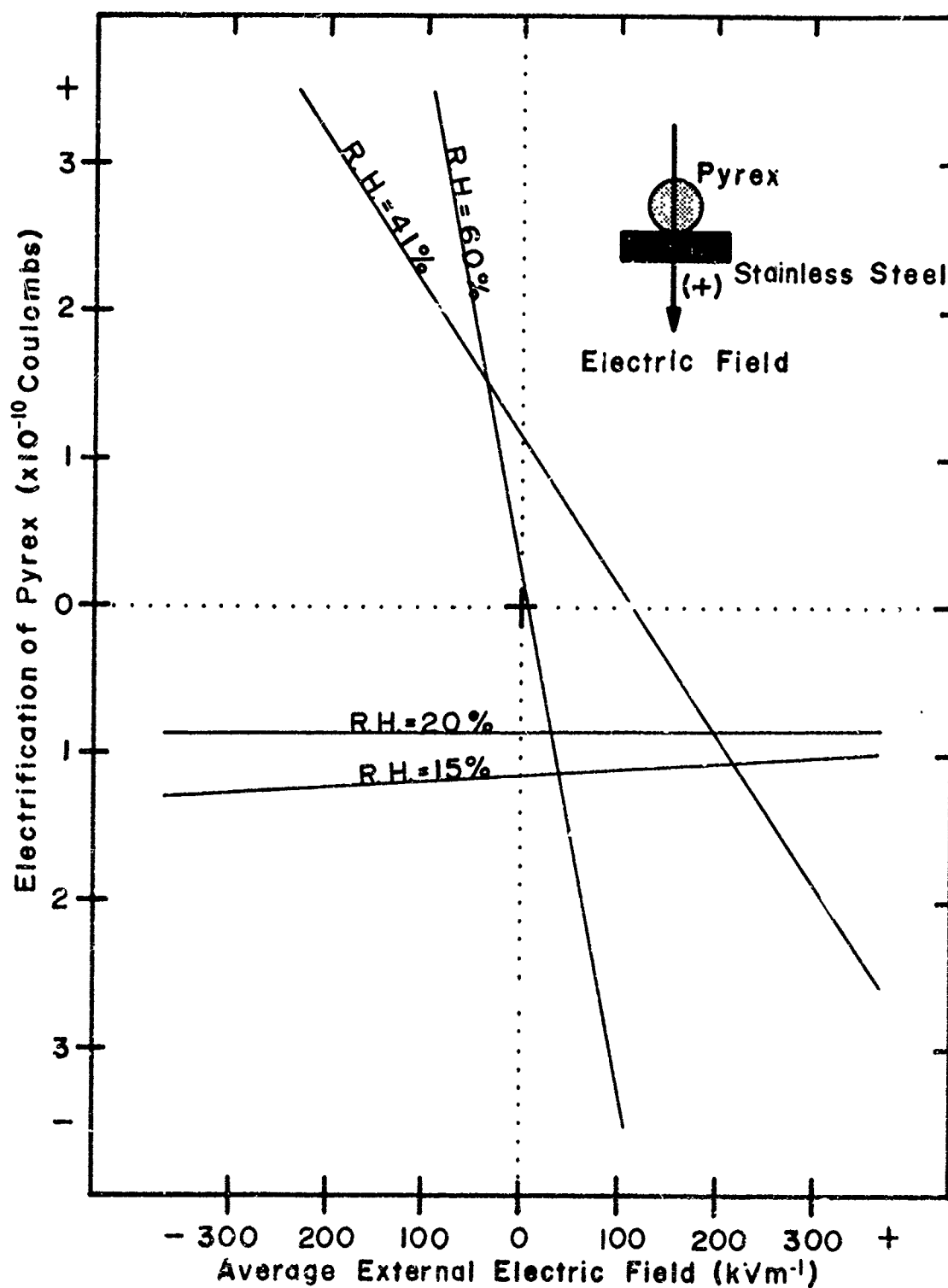


Fig. 4 - Relative humidity and external electric field influence on the electrification of pyrex gl. ss in contact with stainless steel (Greason, 1972).

## The Effects of Static Electrification on Systems

Robert W. Ellison  
Martin Marietta Aerospace

### ABSTRACT

Static electrification has become increasingly important because of its effects on systems. Biological shock, fires, premature ignition of electroexplosive devices, mechanical effects, and radio interference were the kinds of effects; the systems affected were man, the propulsion system, the ordnance system, the hydraulic system, and the complete range of avionics systems. In recent years, static electricity has also been found to interfere with computers, telemetry, tracking and guidance systems, the sensors employed to acquire scientific data, and thermal control systems.

Historically, system effects have been produced when the static electricity discharged. Most recently, it has been found that the mere presence of static electricity--in the absence of discharges--can interfere with science instruments and thermal control systems, and can potentially affect contamination control systems as well. By considering some of the effects of voltage potentials we can gain an overview of the developing discipline of static electrification and apply this knowledge to control the effects of static electrification on aerospace systems.\*

STATIC ELECTRIFICATION has been implicated in all phases and modes of flight. Biological shocks, fires, premature ignition of squibs, and mechanical effects were all experienced in early flights with kites, balloons, and dirigibles. Today, these and other effects are encountered with helicopters, aircraft, artillery shells, missiles, satellites, spacecraft, and lunar surface equipment.

Historically, the system effects occurred when the accumulated static electricity discharged. However, recent studies have shown that the mere presence of static electricity can also have serious consequences.

### BIOLOGICAL SHOCK

Biological shock was first noted with kites flown in thunderstorms, and was later experienced by crews filling and launching balloons and releasing and docking dirigibles. Substantial shocks have also been felt by personnel who touched helicopters operating on or near the ground, or who came into contact with a cable from a hovering craft during cargo and personnel transfer. The shock hazard to Apollo astronauts was

recently investigated when sparks were observed during simulated, ground-based operations such as donning suits and handling equipment in the spacecraft.

Controlling Biological Shock - Controlling biological shock is now a general practice, and usually consists of minimizing the hazard rather than protecting the man. In lightning research using balloons, the winches are remotely controlled and are well grounded and, when it is not necessary to apply kilovolt potentials to the balloon payload, insulating cables are used. Similarly aircraft regulations call for all planes to be provided with static dischargers. The charging problem with helicopters is so severe that active discharger systems are also employed, at least on military helicopters required to operate in bad weather or over dusty terrain.

The guideline for assessing the hazard for biological shock is the energy of the available discharge, which is computed from the capacity of the source and the measured potential acquired. An energy below 0.0004 joule (4000 ergs) is generally considered acceptable.

### IGNITION OF COMBUSTIBLES

The Hindenberg fire is an example of the catastrophe that can result from the ignition of combustibles by static electricity. A similar discharge was responsible for the ignition of a Z-248 rocket engine assembled into an orbital observatory satellite at Kennedy Space Center. A subsequent investigation showed that a triboelectric charge created by the movement of a plastic (dust-protecting) sheet initiated a squib firing circuit and lit off a solid-propellant rocket.

In the early 1960s ordnance devices associated with the payloads on balloons were frequently initiated by discharges of static electricity, and static electricity was also responsible for the destruction of two Surveyor spacecraft test articles during drop tests from aircraft in the 1960s. The discharge of static electricity at separation of the test article initiated the ordnance for the descent systems.

The sinking of three tankers during 1969 by static electricity discharges that ignited combustible vapors during cleaning was reported at previous conferences, as were cases involving the ignition of aircraft fuels during flight and during ground fueling. The possibility that static electricity might ignite combustibles aboard the Apollo spacecraft in an oxygen atmosphere has also been investigated and will be reported during this conference.

Controlling the Ignition of Combustibles - The catastrophic explosion and fire at a Royal Dutch Shell refinery at Pernis in 1954 was the proximate cause of much of the research on the physics and control of

\*This work was sponsored by the National Aeronautics and Space Administration.



liquid fuel ignition by static electricity. The aircraft industry is indebted to two early researchers, Klingenberg and van der Minne, for the development of anti-static additives used in automotive and aircraft fuels.

The sponsors of this conference have pioneered in controlling the hazard through specifications for the grounding of equipment and for controlling the potential propagation of incipient flames.

The possibility that static electricity might initiate ordnance devices was recognized in the 1950s and 1960s. As a result, specifications established a requirement for "1-watt, 1-amp, no-fire devices" and further required shorting devices for flight circuitry and during transportation. In some cases, a dielectric insulation was also required to eliminate pin-to-case modes of initiation. In another case, where it was found that RF or static electricity could cause the firing via a bridgewire-to-bridgewire mode, the second bridgewire was eliminated.

#### MECHANICAL EFFECTS

The Lunar Excursion Module was equipped with a Teflon fabric belt and a motor-driven winch to hoist rocks collected by the astronauts. In simulated operations the belt was found to charge to 5000 volts and to attract powdered minerals. On the lunar surface, lunar dust has been seen to jump from the surface and to stick indefinitely to vertical surfaces covered with thermal control paints. In another controlled experiment, lunar dust was observed to collect on optical and paint samples according to the electrostatic field lines. These three examples show how mechanical effects can be produced by the mere presence of static electricity. These effects, if they should occur on operational lunar surface sensors, would seriously degrade the performance of the thermal control system or the optics of the sensor.

Liquids flowing in tubes are also known to produce severe electrification. Certain fuels, hydraulic fluids, and inert coolants have been found to charge hoses or insulated fittings to as high as 60 kv. When the electric stress exceeds the dielectric strength of the hose or insulator, the hose is punctured and leaks. Alternatively, the energy may be discharged and affect avionics systems, with or without concurrent punctures.

Finally, some investigators have suggested that electrostatically-induced mechanical forces may inhibit the proper deployment of parachutes made from the newer, highly insulating and/or highly triboelectric fabrics. And electrostatics has been suspected in problems with rigidity of reeled magnetic tapes.

Controlling mechanical effects - Most attempts to minimize the mechanical effects

of electrical discharges rely on reducing the resistivity of the materials involved. A value of  $10^9$  ohms or ohms per square or ohm-cm is widely used as the maximum permissible level. In the case of hoses, conductive liners are provided whenever the resistivity of the basic material cannot be reduced by additives. All parts conductive and grounded is a required standard practice.

#### RF INTERFERENCE

Radio frequency interference has been encountered since the first flights of early aircraft in bad weather. Precipitation-static is well understood today and has become the subject of specifications that control both the charging of the source and the susceptibility of radio equipment. Nevertheless, P-static control remains an active discipline as the evolution toward more complex, more sensitive avionics systems continues to uncover new modes of interference. Phase-lock systems, FM systems, radio-guidance systems, and navigation aids are all affected by static electrification discharges through different interference modes. Much recent attention has been directed toward quantifying the acceptable interference level in terms more appropriate for systems than the simple signal power/noise power parameter. Expressions for the bit rate error and the probability of a loss of phase lock, and techniques to reject unreasonable data have been developed.

#### LOGIC ERRORS

Logic errors caused by a single discharge of static electricity have been encountered when using computers for guidance, navigation, and sequencing and in logic-based programs for telemetry and data acquisition systems. This type of interference is quite a different matter than RF interference and P-static. Airborne and ground computers, widely used for radio-controlled guidance and commands, are extremely susceptible to a single discharge of very low-energy static electricity.

During early test flights, two Minuteman missiles were lost when a discharge affected the guidance computer more than once before the last single bit error terminated the flight.

Single discharges of static also occurred on two separate Titan III flights in the late 1960s. In the first flight, a computer instruction was altered and the computer jumped into a backup flight mode. There were ten other modes it could have entered, any of which would have terminated the flight. On the next flight, steering data were altered and the missile turned off path; the guidance error introduced by the electrical discharge was eventually corrected. During an extensive ground test program that ensued, it was discovered that

a spark energy as low as 565 ergs (0.0000565 joule) was sufficient to upset the computer. For comparison, an operating room is considered ether-safe at 40,000 ergs, and safe for the most sensitive anesthetics at 4000 ergs.

Other computers of quite different and more advanced design were tested during a subsequent program. Despite the fact that these designs included isolators and filters on input-output lines, we still found that some circuits were susceptible to as little as a few thousand ergs in a single spark. In one case, there is a period of 187 microseconds during certain logic operations in which the susceptibility is an order-of-magnitude more severe than it is at other times.

A similar situation has been encountered with data multiplexing systems. In one particular case, one of the wires is susceptible to a few hundred ergs in a discharge, and to an energy as low as 1 millivolt at a 100-kc rate. This wire is the midpoint connection between a balanced bipolar power supply and the differential (operational) amplifiers used to amplify all samples of data.

Finally, a very simple operational amplifier, used in an ordnance circuit monitor to ensure that there are no stray signals, has been found to be susceptible to a single static electricity discharge of 0.1 joule applied in the positive sense, but susceptible to as little energy as 500 ergs applied identically, except in the negative sense.

**Controlling Logic Errors** - Incorporating filters and isolators in all input/output lines of logic-based avionics has not proved feasible. The single, most effective means of reducing logic errors is to incorporate protection in the software. There is no excuse today for flying logic programs in which picking up or dropping a single bit will result in serious consequences. It has proven feasible and practical to reprogram even operational systems in the strategic inventory so that:

(1) Any single unreasonable input - for example, an acceleration signal of 100 m/sec<sup>2</sup> - is rejected. Reasonableness tests are available for angular, as well as translational, guidance and steering signals.

(2) Any single-bit error in a critical instruction or address must be matched by another word before the instruction is passed or the addressee is connected.

(3) No single-bit error is indefinitely enlarged by indefinite integration.

This means of protection against static electricity-induced errors is also fully effective against conducted transient interference (electromagnetic incompatibility).

Since the capacities of logic-based avionics and computers are limited and costly to expand, software protection will ordinarily be combined with hardware protection, such as filters and isolators.

## SCIENCE SYSTEM INTERFERENCE

The deposition of dust and space debris on critical surfaces of instruments, meteorological satellites, and military payloads employing optical instruments has recently been encountered. Ever since Mariner 3, a few dust specks have appeared and remained on the TV vidicon face plate. In fact, the object of one experiment carried on Apollo 11 was to study the electrostatic behavior and attenuation of lunar dust on three different types of solar cells. When the Lunar Module lifted off to rendezvous with the Command Module, the output of the bare, exposed silicon cell was not affected, but those of the second cell (thin quartz cover) and third cell (thick quartz cover) were reduced by 7% and 18%, respectively. Lunar dust has been seen to stand almost vertically against lunar gravity and even to jump to vertical thermal control surfaces. This is best explained as an electrostatic phenomenon.

Tests with liquids dumped into simulated space environments show that a substantial fraction of the resultant ice particles are highly charged, and it is known that spacecraft carry a small charge that is driven toward higher voltages by the dumping of liquids.

The seriousness of the electrostatic retention and electrostatically controlled deposition of particles emitted by spacecraft is unknown. If further work should confirm that the electrostatic charges are as large as preliminary studies indicate, there could be important effects of static electrification on spacecraft thermal control systems, astronaut viewing windows, solar power systems, and on the capability of scientific instruments to acquire the primary data. However, the designs of future spacecraft reduce, and in some cases eliminate, the contaminant sources, and despite a potential for problems with electrostatic aggravation, contamination effects should not degrade spacecraft systems.

The outstanding example of static electrification on science subsystems has, of course, involved corona effects, but this is a matter addressed primarily by designers working with systems definitions of the environment and will be left to the corona and corona control experts.

In summary, Table 1 depicts the six kinds of effects static electrification has had on aerospace systems. Note that effects have been encountered in all modes of flight, and that all subsystems of current flight vehicles have experienced one or more of the six effects on one or more occasions--either when conditions were peculiarly wrong, so that the magnitude of electrification was larger than usual, when the environment was less protective than usual, or when the new subsystem was more sensitive than the preceding subsystem.

Table 1 - Systems Affected by Static Electrification

SYSTEM	PARACHUTE	LIGHTER-THAN-AIR	FIXED WING	ROTARY WING	BOOSTERS	ORBITAL SATELLITES	MANNED SPACECRAFT	PLANETARY SCIENCE	SYMPTOM
MAN/BIOLOGICAL SHOCK	X	X	X	X			X		BIOLOGICAL SHOCK
ORDNANCE	X		X	X	X	OXO	X	X	IGNITION/DUDDING
PROPULSION PROPELLANT		HINTENBERG ●	●	●	●		X		INFLIGHT FIRE/EXPLOSION, FIRES DURING FUELING
PLUMBING & HOSES			X		●	TIH	X		HOSE PUNCTURED
HYDRAULICS & HOSES			X	X	X				HOSE PUNCTURED
THERMAL CONTROL ACTIVE COOLANT PASSIVE					●	TIH	ALSEP ● SAMSO	X	HOSE PUNCTURED α/c RATIO DEGRADED BY DEPOSIT OF CONTAMI- NANTS
AVIONICS COMMUNICATIONS, Rf INTERFERENCE		X	X	X	OA0	STAR	X TRACKER	X	INITIATING MEASURE TO QUAN- TIFY LOSS OF ABILITY TO COMMUNICATE
GUIDANCE/NAVIGATION			X	X	X	X	X(?)		COMPUTER UPSET/PHASE UNLOCK
COMMAND/TRACKING DIGITAL DEVICES/ COMPUTERS			X	?	X	?	X	X	LOSS OF SYNC, DATA
TELEMETRY		X	X	X	X	X	X	X	COMPUTER UPSET
SCIENTIFIC PACKAGE SENSORS					SATURN XII X TIH SV	X X	X	TBD	MEASUREMENT ALTERED PERFORMANCE DEGRADED
HOUSEKEEPING SUB- SYSTEM						X		X	OVERHEATING BY VIRTUE OF CONTAMINANT DEPOSITS

**LEGEND:**

- X AFFECTED  
● MAJOR KNOWN INCIDENTS

**GENERAL REFERENCES ON STATIC ELECTRICITY PHENOMENA**

1. R. E. Baier, et al., "Adhesion: Mechanisms that Assist or Impede It," Science, Vol 162, No. 1360, 1968.
2. B. V. Derjaguin and V. P. Smilga, "Electronic Theory of Adhesion," Journal of Applied Physics, Vol 38, No. 12, p. 4609, November 1967. For more complete version of theory see B. V. Derjaguin and V. P. Smilga, "Electronic Theory of Adhesion in Adhesion Fundamentals and Practice - A Report of an International Conference Held at the University of Nottingham, England, 20-22 September 1966," The University Press, Aberdeen, Scotland, 1969. Available through Gordon & Breach Science Publishers, Inc., New York.

3. W. R. Harper, "Contact and Frictional Electrification," Oxford, 1967.
4. A. Klingenberg and J. L. van der Merine, "Electrostatics in the Petroleum Industry," Elsevier, 1958, and Van Nostrand, 1958.
5. Proceedings, Lightning and Static Electricity Conference, Sponsored by the Air Force Avionics Laboratory and the Society of Automotive Engineers, San Diego, California, 9-11 December 1970.
6. Proceedings, Lightning and Static Electricity Conference, 3-5 December, 1968. Technical Report AFAL-TR-68-290, Part II, Air Force Avionics Laboratory, Air Force Systems Command, Wright-Patterson AFB, Ohio, May 1969.

# REFERENCES ON SPECIFIC PHENOMENA

1. L. Cheng and S. L. Soo, "Charging of Dust Particles by Impact." *Journal of Applied Physics*, Vol 41, No. 2, p. 585, 1970.
2. K. P. Chopra, "Thermionic and Photoelectric Screening of Objects Moving in an Ionized Medium," Presented at the International Symposium on Space Vehicles in an Ionized Medium, Warsaw, Poland, 10 September 1964.
3. R. W. Ellison, "Non-Ohmic Properties of Electrostatic Materials." Presented to the American Association for the Advancement of Science, El Paso, Texas, April 1968.
4. R. W. Ellison, "Non-Ohmic Behavior of Fluorocarbon Coolants." Presented at the Lightning and Static Electricity Conference, Miami, Florida, December 1968.
5. F. M. Ernsberger, "Mechanism of Frictional Electrification of Dielectric Liquids." *Journal of Applied Physics*, Vol 27, No. 4, 1956.
6. D. R. Fitzgerald and H. R. Byers, "Aircraft Electrostatic Measurement Instrumentation and Observations of Cloud Electrification." Technical Report AFCL-TR-62-805. Department of the Geophysical Sciences, University of Chicago, Illinois.
7. K. J. Hinners and D. A. Brown, "Gemini Electrical Potential Analysis." Technical Report LMSC-A014291. Lockheed Missiles and Space Company, Sunnyvale, California, 22 January 1963.
8. I. M. Imyanitov, G. L. Gdalevich, and Ya. M. Shvarts, "Measurements of the Electrostatic Field on the Surfaces of Geophysical Rockets Moving Through the Upper Atmosphere."
9. Benjamin Y. H. Liu and Hsu-Chi Yeh, "On the Theory of Charging of Aerosol Particles in an Electric Field." *Journal of Applied Physics*, Vol 39, No. 3, 15 February 1968.
10. J. Nichol, V. Siminski, and H. G. Wolfhard, "Ionization in Rocket Flames." Thiokol Chemical Corporation.
11. D. Pinatti and S. Mascarenhas, "Electrical Current Produced during the Solidification of Water." *Journal of Applied Physics*, May 1967.
12. W. R. Smith and F. A. Grosse, "Vapor Condensation in a Shock Tube - Electrostatic Effects in Sec-Butyl Alcohol and Carbon Tetrachloride." *The American Physical Society*, p. 281.
13. E. C. Whipple, Jr., "The Equilibrium Electric Potential of a Body in the Upper Atmosphere." Goddard Space Flight Center and George Washington University, 6 June 1965.
14. D. A. Whittaker, "Electrostatic Characteristics of a Thor Nose Cone." Technical Report TR-999. Diamond Ordnance Fuze Laboratories, Ordnance Corps, Department of the Army, 1 February 1962.

# REFERENCES ON SYSTEM EFFECTS & SPECIFIC PHENOMENA LEADING TO EFFECTS

1. J. C. Abbey and T. E. Upham, "An Investigation of Electrostatically Induced Failures in Teflon Hose." Aeroquip Corp., Jackson, Michigan, April 1961.
2. Leonard Aronowitz, "Rocket Engine-Generated Voltage as a Source of Electromagnetic Interference and Electronic Component Damage on Interplanetary Vehicles." Grumman Aircraft Engineering Corporation, Bethpage, New York.
3. J. C. Axtell, "Preliminary Minute-man Electrostatic Charge Studies, Model WS-133a." The Boeing Company, Seattle, Washington, 1963 [Contract AF04(647)-580].
4. Rodney A. Boudreaux and Frederick G. Etheridge, "Altitude Control Rocket Exhaust Plume Experiments." Technical Report AFRL-TR-67-3. North American Aviation, Inc., El Segundo, California, February 1967.
5. C. L. Brundin, "Effects of Charged Particles on the Motion of an Earth Satellite." *AIAA Journal*, Vol 1, No. 11, November 1963.
6. A. J. Butts and R. W. Ellison, "Control of Electrostatic Hazards in Spacecraft." Presented at the Workshop on Electromagnetic Interference in Spacecraft, Jet Propulsion Laboratory, Pasadena, California, February 1968 (See NASA TM 33-402, JPL/CIT, Pasadena, California, December 15, 1968).
7. W. Coleman and J. Hoffman, "Consequences of Electrostatic Phenomena on the Lunar Mission (Saturn)." Technical Report PPS 64/386. North American Aviation, Inc., El Segundo, California.
8. J. E. Drummond and D. J. Nelson, "Electrical Hazards of Docking in Space." Technical Report DL-82-0525. Boeing Scientific Research Laboratories, Seattle, Washington, April 1966.
9. R. W. Ellison, "Control of Electrostatic Hazards in Spacecraft." *IEEE Transactions in Electromagnetic Compatibility*, August 1969.
10. R. W. Ellison, "Investigation of Ionization Phenomena of Titan IIIC." Technical Report TM-G453/20-66-17. Martin Marietta Corporation, Denver, Colorado, 14 March 1966.
11. R. W. Ellison, "Rocket Exhaust-Initiated Breakdown in Electrical Connectors at Altitude." Presented at the Second Workshop on Voltage Breakdown at Low Air Pressures, Jet Propulsion Laboratory, Pasadena, California, February 1969.
12. R. W. Ellison and V. J. Siminski, "Research on the Influence of Ions on Rocket Combustion." Technical Report RMD-204-Q5, Thiokol Chemical Corporation, 30 May 1959.
13. R. W. Ellison, "Summary Report on Electrostatic Phenomena on Titan III." Martin Marietta Corporation, Denver, Colorado.

14. R. M. Fristrom, F. A. Oyhus, and G. H. Albrecht, "Charge Buildup on Solid Rockets as a Flame Burst Mechanism," *Journal of the American Rocket Society*, November 1962.
15. P. E. Grear, "Electrostatic Measurement Experiment, Scout Vehicle 131-R," Technical Report NASA CR-477. Ling-Temco-Vought, Inc.
16. T. L. Harlor, A. R. Jordan, and D. G. Murcay, "Development of Aircraft Discharge Methods, Final Report." Denver Research Institute, University of Denver, Denver, Colorado, April 1956 [Contract AF33(616)-157].
17. M. N. Huberman, "Measurement of the Energy Dissipated in the Electrostatic Spraying Process," *Journal of Applied Physics*, Vol 41, No. 2, p. 578, 1970.
18. Philip Krupen, "Measuring the Electric Charge on a Missile in Flight," Technical Report TR-856. Diamond Ordnance Fuze Laboratory, Ordnance Corps, Department of the Army.
19. N. Leuder, "Investigation of Electrostatic Charging and Radio Interference on DS-1400 X Glide Bomb," Translation Report F-TS-1824-RE. Headquarters, Air Materiel Command, Wright Field, Dayton, Ohio, June 1947.
20. G. F. McGowan, T. J. Goyette, and K. V. Gentry, "Investigation of Guidance System Anomalies on Titan III Vehicles C-10 and C-14," Technical Report MCR-67-347. Martin Marietta Corporation, Denver, Colorado, October 1967 [Contract AF04(695)-150].
21. N. Richard Mesnard, "Integrated System Testing for Assurance of Electromagnetic Compatibility of Unmanned Spacecraft," Presented at the AAS/ORSA Meeting, Denver, Colorado, 18 June 1969.
22. G. Miller, "Electrostatic Tests on Titan IIIC Payload Fairing Panels, Test 2794," Martin Marietta Corporation, Denver, Colorado, 25 January 1968.
23. P. Molmud, "Frictional Electricity in Missile Systems," *Journal of the American Rocket Society*, pp. 73 and 74, January 1959.
24. L. K. Monteith and J. R. Hauser, "Space-Charge Effects in Insulators Resulting from Electron Irradiation," *Journal of Applied Physics*, Vol 38, No. 13, December 1967.
25. J. E. Nanevich, et al., "Development and Testing of Techniques for Precipitation Static Interference Reduction, Final Report," SRI Project 2848. Stanford Research Institute, Menlo Park, California, January 1962 [Contract AF33(616)-6561].
26. J. E. Nanevich, E. F. Vance, and W. C. Wadsworth, "Low-Altitude, Long-Range, All-Weather Vehicle Interference Investigation," Technical Report AFAL-TR-65-239, Parts I and II. Air Force Avionics Laboratory, Wright-Patterson Air Force Base, Ohio, December 1965.
27. B. J. O'Brien, S. C. Freden, and J. R. Bates, "Degradation of Apollo 11 Deployed Instruments Because of Lunar Module Ascent Effects," *Journal of Applied Physics*, Vol 41, No. 11, p. 4538, 1970.
28. K. G. Payne and F. J. Weinberg, "A Preliminary Investigation of Field-Induced Ion Movement in Flame Gases and Its Applications," *Proceedings of the Royal Society, A*, Vol 250, No. 195, pp. 316 thru 336.
29. R. J. Pilie and J. W. Ford, "A Study of Instrument Errors in the Measurement of Electrostatic Fields and the Design of a New Electric Field Meter," Technical Report RM-824-P-4. Cornell Aeronautical Laboratory, Inc., Buffalo, New York, 21 February 1955.
30. Herbert Ackland Fohl, "Some Effects of Nonuniform Fields on Dielectrics," *Journal of Applied Physics*, Vol 29, No. 8, p. 1182, 1958.
31. Samuel Sabaroff, "Sources and Effects of Electrical Charge Accumulation and Dissipation on Spacecraft," Presented at the G-EMC Meeting of IEEE, Los Angeles, California, 21 January 1965.
32. E. B. Smith, "Electrostatic Voltage Generated by Launch Vehicles," Aerospace Corporation, El Segundo, California.
33. A. L. Stanley, "Electrostatic Charge Experiment," Gemini Electronics Design Note 411-133P-175. McDonnell Aircraft Corporation, St. Louis, Missouri, 14 December 1964.
34. E. L. Strauss, T. H. Hay, D. L. Carlson, and J. V. Mumford, "Investigation and Application of Ablative Coating for the Titan IIIC Universal Payload Fairing," Technical Report MCR-69-41. Martin Marietta Corporation, Denver, Colorado, 10 January 1969. (Also, MCR-69-41, Supplement 1, 3 February 1969.)
35. R. L. Tanner and J. E. Nanevich, "Precipitation Charging and Corona-Generated Interference in Aircraft," Technical Report 73, SRI Project 2494. Stanford Research Institute, Menlo Park, California, April 1961 [Contract AF19(604)-345J].
36. J. Rimas Vaisnys, "Development of Electrical Potentials in Supersonic Nozzles," *Journal of Applied Physics*, Vol 38, No. 11, October 1967.
37. E. F. Vance and J. E. Nanevich, "Rocket Motor Charging Experiments," Technical Report AFCRL-66-497. Stanford Research Institute, Menlo Park, California, June 1966.
38. E. F. Vance, L. B. Seely, and J. E. Nanevich, "Effects of Vehicle Electrification on Apollo Electroexplosive Devices, Final Report," SRI Project 5101. Stanford Research Institute, Menlo Park, California, December 1964 (Contract NAS9-3154).

# Techniques for the Study of Noise Generation and Coupling

E. F. Vance  
Stanford Research Institute

## ABSTRACT

Some limitations on transient and single-frequency analysis of system transfer functions are discussed. These include zeros caused by rectangular excitation pulses and by truncation of the transient responses. In addition, the limitations on obtaining transfer functions from transient data due to the dynamic range of the transient oscillograms is discussed. The use of scale models to obtain transient responses of complicated systems is described by citing several examples in which scale modeling has been used.

STUDIES OF TRANSIENT RESPONSES of systems under the influence of the nuclear electromagnetic pulse (EMP) have resulted in the development of techniques for generating fast-rising electromagnetic waves and guiding or radiating these transient waves to produce a simulated EMP environment. Studies of system responses in these simulated environments have been accompanied by analytical efforts to determine the coupling of the transient waves to typical structures, such as antennas and transmission lines, that are commonly found in many systems. For very large and complicated systems, however, it may be extremely expensive or impossible to produce an accurately simulated environment enveloping the entire system to determine experimentally the system response, but, on the other hand, the system may be so complex that one would have a rather low confidence in a purely analytical approach to determining its transient response. To help define the simulation and coupling problem in such cases, scale modeling techniques have been developed that are very useful in determining which coupling characteristics are dominant and what properties of the incident wave must be accurately simulated.

This paper will briefly discuss some of the techniques that have been used to evaluate the transient response of systems to fast rising electromagnetic pulses. In addition some practical limitations of the often-used equivalence of frequency domain and time domain analysis will be discussed.

Many of the transients encountered in the analysis of system responses can be approximated by two-exponential pulses. As is illustrated in Figure 1, the two-exponential pulse can assume

many forms, depending on the viewing time and the exponents. Figures 1a through 1e are all two exponential pulses with real exponents. Note however, that Figures 1b, 1c, and 1d, which at first appear to be quite different waveforms, can be visualized as the same pulse plotted on different time scales. Thus if the waveform of Figure 1d is plotted on a compressed time scale, we obtain Figure 1b, and if the leading edge of Figure 1d is plotted on an expanded time scale, we obtain the waveform of Figure 1c. When we scale the viewing time, we inversely scale the frequency spectrum, so that when Figure 1a is viewed in the compressed time of Figure 1b, we are "seeing" only the flat part of the frequency spectrum of Figure 1d. Similarly, when Figure 1d is "seen" as Figure 1c, we are seeing only the portion of the spectrum with slope  $f^{-2}$ . From similar considerations the waveform of Figure 1e, viewed in a compressed time scale becomes the impulse of Figure 1b, and viewed on an expanded time scale becomes the step function of Figure 1a.

Such exercises in scaling time and frequency are useful in diagnosing system responses to pulses such as the one shown in Figure 1d. A system stimulated by this pulse "thinks" it sees a ramp ( $f^{-2}$  spectrum) early in time, but later it "thinks" it sees a step function ( $f^{-1}$  spectrum), and very late in time, it "thinks" it has seen an impulse. Since the step and ramp responses are readily derivable from the impulse response (by one or two integrations, respectively), the approximate response to a pulse such as that of Figure 1d can be synthesized from an impulse response. Conversely, the impulse response, in the frequency domain, can be synthesized from the frequency domain response of the system to the pulse of Figure 1d, providing there is sufficient dynamic range in the frequency domain data.

## REQUIREMENTS OF THE MEASUREMENT

Since there is an apparent equivalence of frequency and time through the Fourier transform, it may be inferred that all transient testing could be done in the frequency domain using single-frequency, continuous-wave (CW)

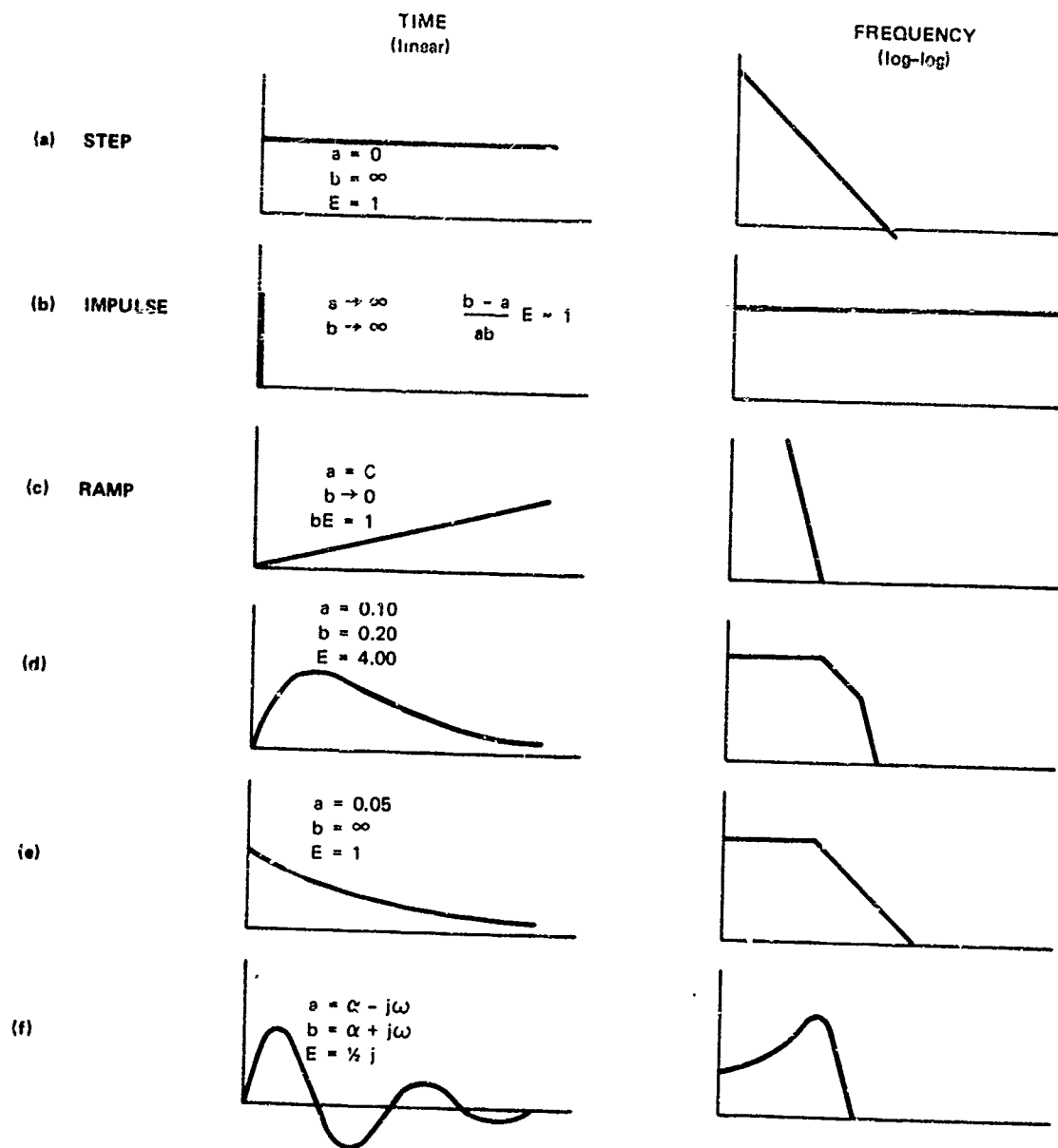


FIGURE 1 WAVE SHAPES THAT CAN BE APPROXIMATED BY  $e = E(e^{-at} - e^{-bt})$

measurements to determine the spectrum of the impulse response. This approach has the advantage that the transfer function so obtained can be used to determine the system response to any transient. The use of CW measurements and the Fourier transform implicitly implies that the system is linear under the transient conditions of interest. If this presumption is valid, one must further consider the quantity of frequency-domain data required to perform the inverse Fourier transform and obtain the transient response.

Let us assume that the transient stimulus is of the form shown in Figure 1d in which the exponential coefficients  $a$  and  $b$  are finite and greater than zero, and that  $b \gg a$ . Then

$$e(t) = E(e^{-at} - e^{-bt})$$

and the Fourier transform of  $e(t)$  is

$$E(\omega) = \frac{(b-a) E}{(a + j\omega)(b + j\omega)}$$

To adequately define the spectrum of this pulse (and the spectrum of the system response to the pulse) we must measure the system transfer function over a range of frequencies that extends from well below the first break in the pulse spectrum to well above the second break. The first break occurs at

$$f_1 \approx \frac{a}{2\pi}$$

and the second break occurs at

$$f_2 \approx \frac{b}{2\pi}$$

or in terms of the pulse rise time constant  $\tau_r = 1/b$  and the decay time constant  $\tau_d = 1/a$ ,

$$f_1 \approx \frac{1}{2\pi\tau_d} \quad \text{and} \quad f_2 \approx \frac{1}{2\pi\tau_r}$$

If we plan on using the fast Fourier transform to obtain the inverse transform, we are further constrained to equal increments of frequency so that

$$\Delta f = \text{Constant} \ll f_1$$

To perform the numerical integration

$$f(t) = \frac{1}{\pi} \int_{<2\pi f_1}^{>2\pi f_2} F(\omega) e^{j\omega t} d\omega$$

$$\approx \frac{1}{\pi} \sum_{n=1}^N F(n\Delta\omega) e^{jn\Delta\omega t} \Delta\omega,$$

therefore, we require

$$N \gg \frac{f_2}{f_1} \approx \frac{\tau_d}{\tau_r}$$

measurements of the magnitude and phase of the transfer function. For a pulse whose rise is 10 nanoseconds and whose duration is 1 microsecond,

$$N \gg \frac{10^{-6}}{10^{-8}} = 100.$$

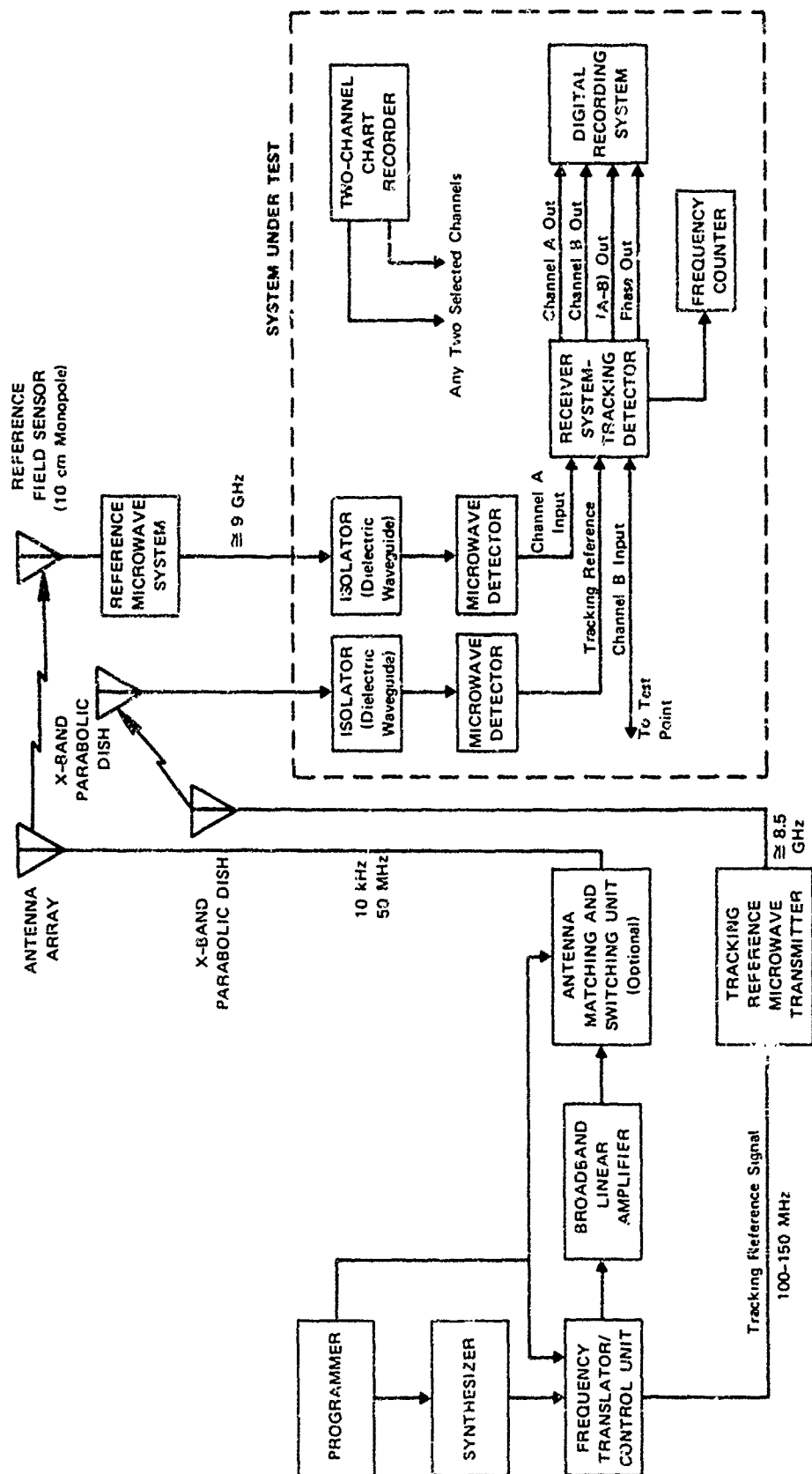
It is not an uncommon requirement that 500 to 1000 frequencies are needed to obtain a reliable inverse transform for a pulse spectrum having a duration-to-rise-time ratio of 100. Even with fairly sophisticated equipment, of the order of one second may be required to make a measurement at each frequency. With 1000 measurements to be made, the complete transfer function will require of the order of 15 minutes to measure. With less sophisticated instrumentation these measurements might take several hours to make.

Somewhat fewer frequencies may be used if the slower transform techniques which do not require equal increments of frequency is used. Some measurement time may then be saved at the expense of somewhat more computer time for the transformation process.

The block diagram of an automatic CW measurement system that was designed and built at SRI for system transfer function measurement is shown in Figure 2. This equipment was designed to obtain, conveniently and rapidly, transfer functions that describe the response of a system to an electromagnetic environment. The principal elements of the system are:

- . A transmitter, which provides signals to drive an antenna array or the system under test
- . A microwave system which furnishes a tracking reference signal to the tracking detector receiver
- . A tracking detector receiver, which provides the transfer function between the reference and test point signals
- . A microwave system which furnishes a reference drive function for the tracking detector receiver





TA-7995-258

FIGURE 2 BLOCK DIAGRAM, DIGITAL RECORDING CW MEASUREMENT SYSTEM

An analog paper chart recorder and digital magnetic tape recording system.

Transmitter frequencies from 10 kHz to 50 MHz and receiver tracking reference frequencies from 100.01 MHz to 150 MHz are derived from a Hewlett-Packard 5105A frequency synthesizer, externally controlled by an SRI-constructed digital programmer and a punched paper tape program reader. The frequency stepping rate and off-time period are variable parameters of the programmer; for most data runs, a rate of about one step per second is used with an off time of approximately 300 ms.

The receiving system consists of two units; an SRI-constructed RF and IF unit, and an extensively modified Hewlett-Packard 676A tracking detector. The system is the equivalent of a dual-channel receiver that can be tuned to any desired frequency between 10 kHz and 50 MHz by injecting a tracking reference signal at a frequency 100 MHz higher than the desired receive frequency. The receiver processes the input signal and provides a dc voltage output for each channel proportional to the log of the input signal over an 80-dB dynamic range. Additional circuitry measures the phase difference between Channels A and B and the amplitude difference (A-B). Since the (A-B) channel output is actually proportional to

$$\log(A) - \log(B) = \log \frac{A}{B},$$

it can be used to measure a transfer function directly, if one channel is considered to be a driving function. Dielectric waveguide isolation links in the x-band system for supplying the tracking reference signal and excitation field sensor signal to the receiving system are used to avoid compromising the integrity of the system shield.

To avoid the lengthy measurement process that seems necessary to adequately define the CW transfer function with manual measurement one may conclude that this transfer function could be obtained more simply from the transient data. Thus, for example, one would record the exciting waveform and the response waveform, Fourier transform each, and divide the transformed response by the transformed excitation to obtain the transfer function. Because the transients require only a few microseconds to record, it appears that the transfer function which took minutes or hours to measure with CW instrumentation requires only microseconds to measure with transients recorded on an oscilloscope. To be sure, the transient data must be processed to obtain the transfer function, but these, it may be

contended, are largely machine operations that can be performed quickly and economically.

Let us examine this proposition more carefully. Just as it takes 500 to 1000 frequency samples to adequately define the transfer function, it will take approximately the same number of time samples to adequately define the input and response waveforms for Fourier transformation. Thus two or more oscillograms, with accurate time-ties between successive oscillograms, may be required to define each waveform. A more severe limitation on the process of obtaining transfer functions from transient data, however, is the dynamic range that can be achieved from oscillograms. Since there is an upper limit of a few centimeters in the usable deflection of an oscilloscope trace, and a lower limit of a few hundredths of a centimeter in trace width, there is an inherent limit in the accuracy of the oscillogram, even if no error exists in the sensor and signal processing components. This accuracy limit leads to a limit in dynamic range or bandwidth (or both) in the Fourier transformed data. The dynamic range of the transformed data is usually limited to about 40 dB. Because the transfer function is the ratio of two such transforms (the excitation and the response), the dynamic range of the transform function may be considerably less than 40 dB (often less than 20 dB).

An example of a transfer function computed from transient data is illustrated in Figure 3. This transfer function was obtained from very well-behaved oscillograms, so that the more general problems of trace dim-out, time-tying, etc., that may be encountered in transient data were not present. In addition, the transfer function was for a simple tubular shield that could be accurately analyzed to give

$$Z_T = R_0 \frac{\gamma T}{\sinh \gamma T}$$

where

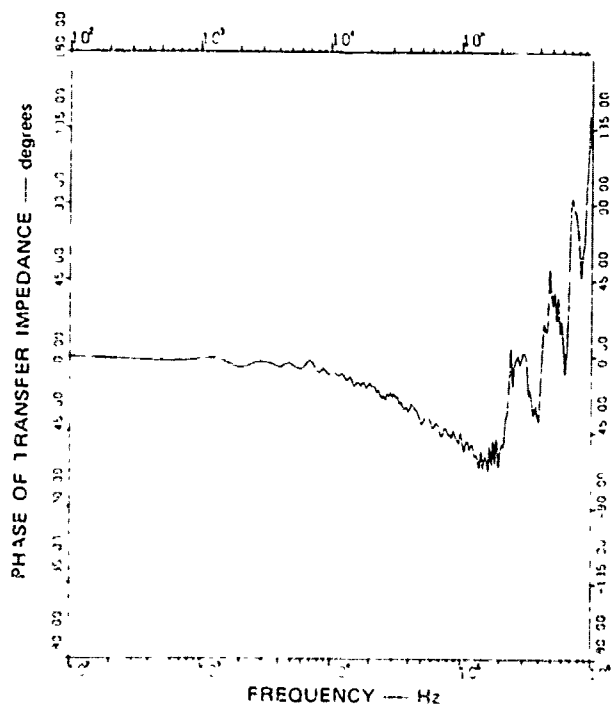
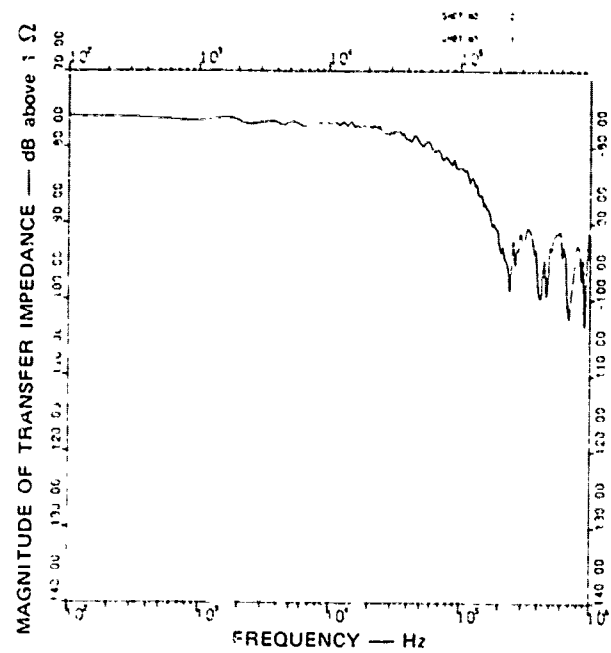
$$\gamma = (1 + j) \sqrt{\pi f \mu \sigma}$$

and  $\mu$ ,  $\sigma$ ,  $T$ , and  $R_0$  are independent of frequency. Thus at high frequencies the transfer function should behave as

$$|Z_T| \approx \frac{2}{\sqrt{2}} R_0 T \sqrt{\pi f \mu \sigma} e^{-\sqrt{\pi f \mu \sigma} T}$$

$$Z_T \approx \frac{\pi}{4} - \sqrt{\pi f \mu \sigma} T.$$

It is apparent that both the magnitude and phase of the transfer function of Figure 3 became



TA-1404 9

FIGURE 3 MAGNITUDE AND PHASE OF A TRANSFER FUNCTION OBTAINED FROM TRANSIENT DATA

erratic when the magnitude has decreased 20 dB from its maximum value.

An additional problem that may be encountered in acquiring and processing transient data to obtain transfer functions is related to the spectrum of rectangular pulses. Let us define the rectangular pulse as

$$R(t, \tau) = R, \quad 0 \leq t \leq \tau \\ = 0, \quad t > \tau$$

The Fourier transform of this pulse is

$$R(\omega, \tau) = R\tau \frac{\sin \omega\tau/2}{\omega\tau/2} e^{-j\omega\tau/2}$$

Because of the  $(\sin \omega\tau/2)/(\omega\tau/2)$  term in this transform, the magnitude of the pulse spectrum goes to zero at

$$\frac{\omega\tau}{2} = n\pi \quad (n = 0, 1, 2, \dots)$$

The spectrum of a rectangular pulse of area 1 is shown in Figure 4 to illustrate these zeros. This characteristic of the rectangular pulse is important for two reasons. First, if a rectangular pulse is used as the excitation pulse, the transfer function obtained from processing the transient data will be cluttered with spikes which occur at each point where the excitation pulse spectrum goes to zero (since the response spectrum is divided by the excitation spectrum). These spikes often make the transfer function unintelligible. Second, if the wave forms (from any source) are truncated before the transient reaches zero, this is equivalent to changing the pulse from  $e(t)$  to  $e(t)R(t, \tau)$ ; the spectrum of function  $e(t)R(t, \tau)$  contains all the zeros that the spectrum of  $R(t, \tau)$  contains, so that the clutter problem described above is encountered even if the source spectrum was "void-free". If both the excitation  $e(t)$  and the response  $r(t)$  are truncated, the transfer function will contain zeros from the truncated response and poles (spikes) from dividing by the zeros in the truncated excitation spectrum. The transfer function so obtained may therefore be utterly useless. (An analogous aliasing of the time domain responses occurs when the frequency spectra are improperly truncated or the sampling rate is inadequate.)

To summarize the discussion of transfer function measurements, it is noted that the CW method can provide an accurate measurement of transfer function over a large dynamic range, but a very large number of measurements is required and fairly sophisticated equipment is

necessary to efficiently measure the magnitude and phase of the transfer function over a useable range of frequencies. With the transient method of determining transfer functions, fairly simple equipment can be used to obtain the data rapidly, but dynamic range and useable spectrum may be quite limited, and the data acquisition, processing, and interpretation are subject to many subtle pitfalls.

#### SCALE MODEL TECHNIQUES

In discussing the waveforms of Figure 1 it was noted that the impulse and step functions might be represented by an exponential pulse viewed on compressed or expanded time scales. Because the velocity of propagation of an electromagnetic wave is finite (in free space the wave travels one foot in one nanosecond), the appearance of the pulse may also be related to the scale of the system. Thus, for example, a rectangular pulse 10 ns wide will induce a step function response in a system of conductors whose maximum dimension is less than one inch, whereas it will induce the impulse response in a system of conductors whose minimum dimension is more than 100 ft. Such concepts lead to the idea of using scale models to study transient responses of systems. Thus, for example, if a 1/10 scale model of a system is excited with a transient whose temporal characteristics are 10 times as fast as the full scale transient, the system response will be a transient whose temporal characteristics are also 10 times as fast as a full scale pulse. Because the linear dimensions are a factor of 10 smaller, however, the working space and transient power required are greatly reduced. Transient measurements on scale models are particularly useful for

- (1) defining excitation requirements such as wave front planarity, uniformity of field strength, area of coverage, rise time, and duration, all of which affect the cost of simulators for illuminating large systems.
- (2) Studying the coupling of the electromagnetic wave to elements of the system to verify and guide analytical efforts, to assess directional effects, and to investigate the degree of coupling to major system components.
- (3) determine the current and field distribution on major elements of

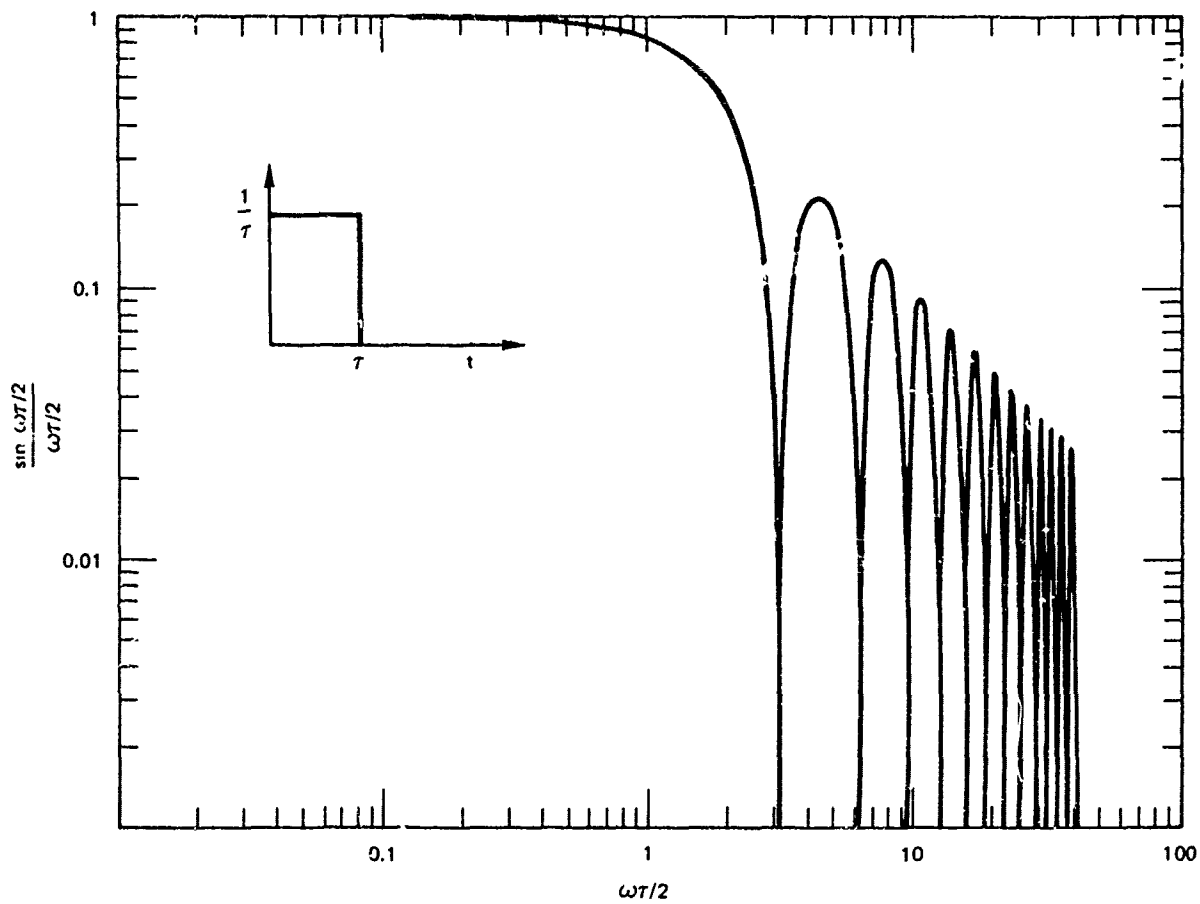


FIGURE 4 MAGNITUDE OF THE SPECTRUM OF A RECTANGULAR PULSE

the system so that full scale excitation requirements can be established (e.g., currents that must be injected on long appendages such as power lines, communication cables, etc., to simulate the transients propagating into the system on those conductors).

- (4) evaluating simulator concepts prior to design and construction of the full scale simulator.

Some examples of scale model experiments that have been performed at SRI will be described briefly to illustrate the type of applications for which modeling is particularly well suited.

The first example, illustrated in Figure 5, is only partially scaled in dimensions. The purpose of this model was to evaluate methods of terminating a charged transmission line pulse source in order to add an exponential decay to the rectangular pulse produced by the discharge of the transmission lines (to avoid zeros in the pulse spectrum discussed earlier). The full-scale pulse source was to be operated at several hundred kilovolts, so that trial-and-error techniques would be very expensive on the full scale system, as would rigorous analysis of the system response taking into account all of the transmission line effects with complex RLC terminations. Using the low-voltage model illustrated in Figure 5a, however, it was possible, in the course of a few hours, to assess the effect of a wide variety of RLC terminations and select a realizable combination of R, L, C, and line length that would achieve the desired goals. In addition to determining what the best combinations of these parameters were, however, it was also learned how bad some of the poorer combinations were, so that as the full scale design progressed and tradeoffs became necessary, the probable effect of compromises in the design was better understood. This by-product of the use of scale models as an aid in the design of complex and expensive systems is one of the major advantages of modeling that is often overlooked. The model in this case was constructed of low-voltage components of the type that would be found in most electronics stockrooms, and assembly in a breadboard fashion was adequate for these experiments. Construction of the model was, therefore, neither expensive nor technically difficult.

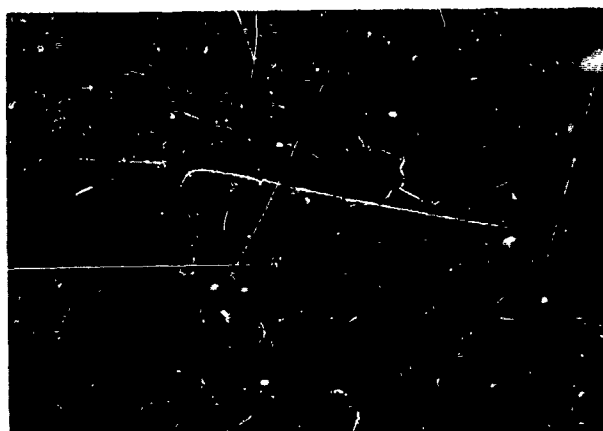
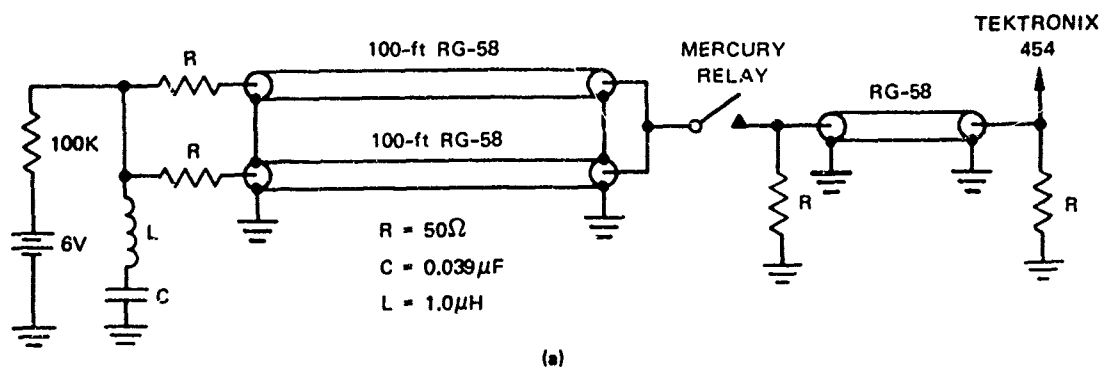
A second example is illustrated in Figure 6. In this case, the objective was to obtain information to aid in the design of a horizontal dipole antenna for radiating a fast rise-time transient with an exponentially decaying tail. The full scale dipole was to be operated near the ground and fed with a transient source of several

megavolts. The radiating dipole was expected to be several hundred feet long, and composed of a biconic section for launching the leading edge followed by a cylindrical section for the late-time part of the pulse.

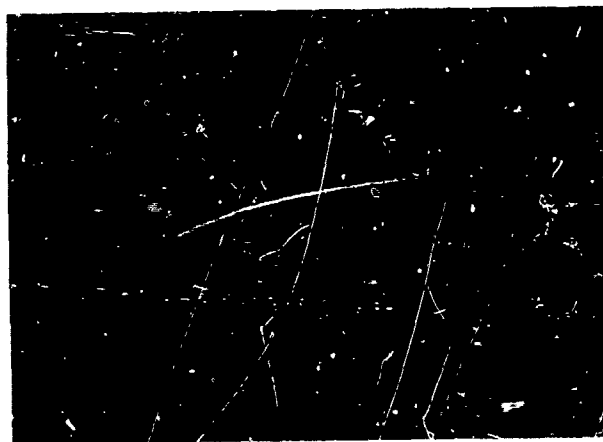
Numerous dipole configurations, including tapered resistance loading of the elements and various termination configurations and impedances, were studied on 1/150th scale models in the laboratory. For some of these studies, the complete antenna was modeled, while for others, it was convenient to model only half the antenna and use a ground plane image to produce the effects of the other half. The latter technique is illustrated in Figure 6 along with the transient magnetic field pulses measured in the vicinity of the model. A repetitive pulser that uses a charged capacitor or charged transmission line switched onto the load by a chatter-free mercury-wetted relay was used as the pulse source for these experiments. Pulse rise times of 0.3 ns were obtained with this pulser. The fields of the pulse antenna were measured with small slot and parallel plate antennas mounted along the ground plane. A sampling oscilloscope with an X-Y recorder was used to record the transients.

Many inexpensive sheet-metal models were used in this experiment to study particular features of the dipole. To study the effect of the biconic feed structure on the leading edge, for example, models larger than 1/150th scale of the feed structure were used. Smaller models were used to study the late-time behavior, since the late time behavior was found to be independent of the pulse rise-time. Other models were used to determine the effects of making the cylindrical dipole elements from a grid of wires rather than sheet-metal. Many other design questions, such as the behavior of the radiated waveform when the ground-reflected wave returns to the antenna element and the antenna behavior change from that of a biconic radiator to that of a cylindrical transmission line, were studied in detail. As a result of the model studies, the final design of the full-scale system was significantly improved, and the confidence in the predicted operating characteristics was greatly enhanced.

A system-oriented example illustrating a model of a large, ground-based system with many interconnecting conductors and several very long utility conductors is shown in Figure 7. The model study of this system had two goals. First, it was desired to determine the requirements for an electromagnetic simulator to be used to illuminate the facility with a transient wave. Second, it was desired to determine the current magnitudes and waveforms



(b) SWEEP: 200 ns/div  
VERTICAL: 1.0 V/div



(c) SWEEP: 10 ns/div  
VERTICAL: 1.0 V/div

TA-7390-15

FIGURE 5 MODEL OF CHARGED TRANSMISSION LINE PULSE SOURCE

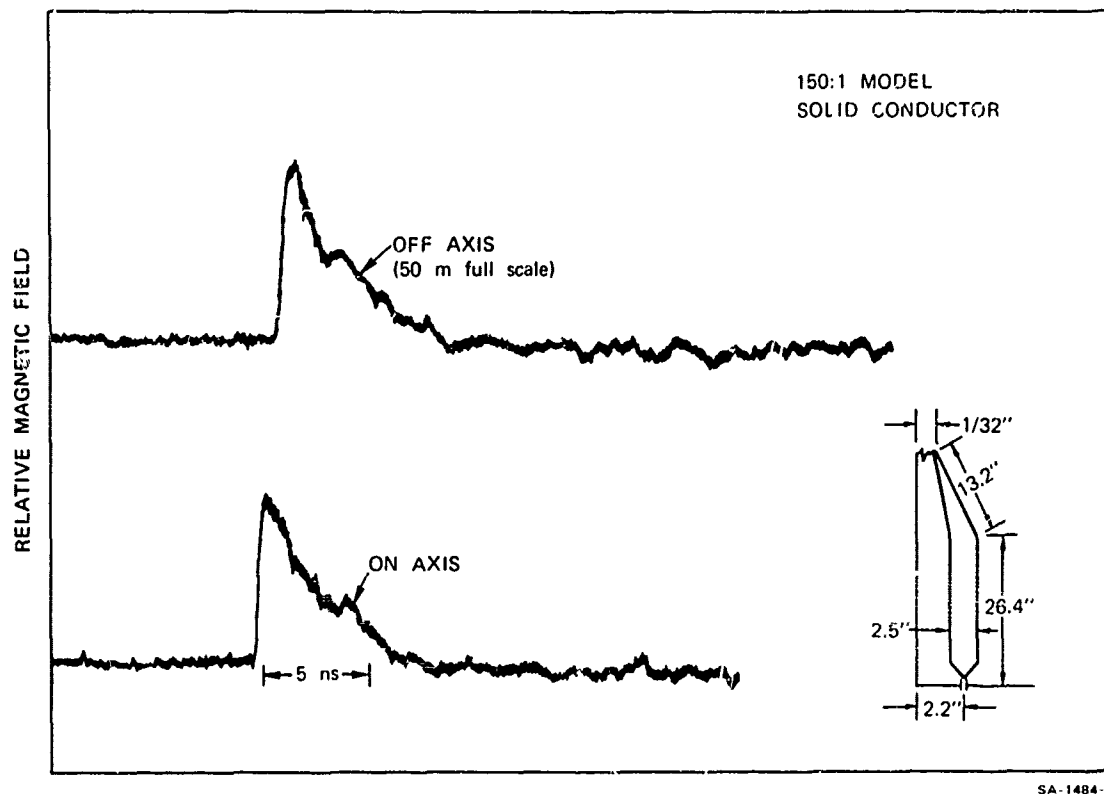


FIGURE 6 RADIAL MAGNETIC FIELD FROM A CAPACITIVELY FED DIPOLE  
AT 8.5-m FULL-SCALE HEIGHT



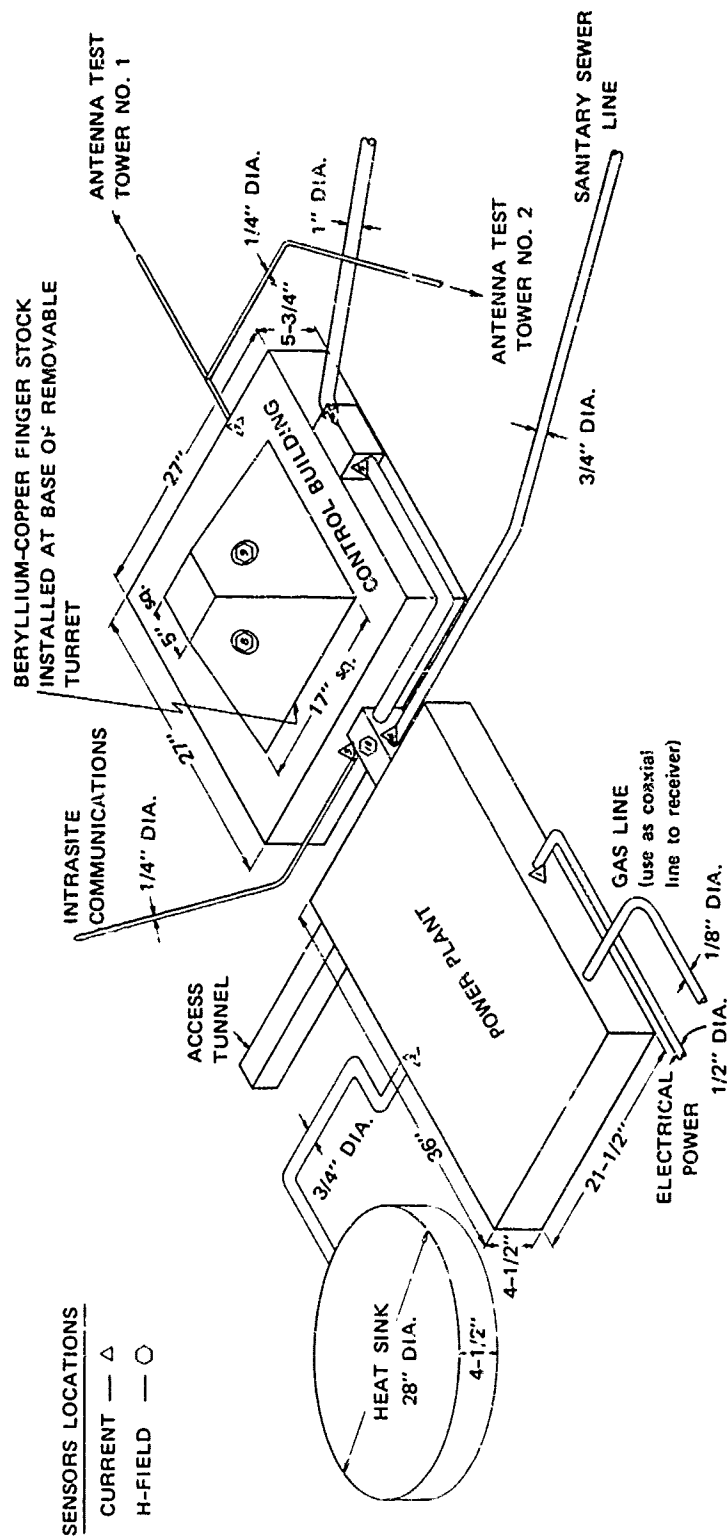


FIGURE 7 SCALE MODEL OF A COMPLEX FACILITY USED TO STUDY EFFECTS OF WAVEFRONT PLANARITY AND UNIFORMITY, AND DIRECTIONAL EFFECTS

at key points in the facility to assist in determining the effects of coupling through the power system, cable shields, etc., to the internal components of the system.

Using a 1/100th scale model of the facility illuminated with a pulsed dipole radiator, currents and fields at selected points in the facility were measured for various degrees of planarity and uniformity of the incident transient fields obtained by varying the range between the radiating dipole and the modeled facility. The directivity of the facility as a transient receiver was also studied. The information gained from this study permitted simulator requirements, such as planarity and uniformity of the wavefront, area of illumination, and portability of the simulator, which significantly affect the cost, to be evaluated quantitatively. The magnitude and waveforms of the currents induced in the long conductors providing electric power, gas, and sewage service to the facility provide a basis for evaluating the effect of these appendages on the system shielding effectiveness. In addition, the magnitude and waveform of current that must be injected on these conductors to test the full scale system has been established.

Because of the complex shape of the system illustrated in Figure 7, one would have limited confidence in a purely analytical attempt to estimate the transient response of even the major features of the system. On the other hand, a measurement program to determine the system response on the full-scale operational system would be very expensive (because it is a field operation), limited in scope (because many desirable test points are inaccessible), and would probably require removing the facility from operational status (or at least compromising its operational status). Using a scale model, made of sheet-metal, wire, tubing, and other conventional materials, accurate measurements of the magnitude and waveform of the transient response at any point on the facility for any angle of incidence or polarization of the transient wave can be made very economically.

A final example illustrates the use of scale models as an analytic tool. In the case illustrated in Figure 8, the coupling of transients to transmission lines was studied by illuminating a section of scaled transmission line with the transient field radiated by a pulsed dipole antenna. The current and voltage induced in a transmission line were analyzed many years ago. The solution for the current and wave for a wire over finitely conducting ground are very complicated, even in the frequency domain, and it is difficult to visualize the interaction phenomena from these solutions. From a combin-

ation of analysis and experiments on scale models, however, it has been possible to cast the solutions in a form that permits obtaining an approximate response in time domain by inspection, because many uncertainties about the relative importance of radiation and ground effects were quickly eliminated by the experiments. With the model, it was also possible to quickly study the effects of angle of incidence of the transient wave, effects of varying configuration parameters such as line height or length, and the effect of adding elements such as various loads at the terminals, extraneous ground wires, etc.

An example of the estimated and measured responses of the wire-over-ground with a vertical ground lead at one end (as shown in Figure 8) is shown in Figure 9. The incident waveform is a step function arriving from the direction of the open end of the wire at an elevation angle  $\psi$  of 30 degrees. The response consists of the superposition of the current induced in the horizontal conductor by the horizontal component of electric field and the current induced in the riser by the vertical component of electric field. The field itself consists of two components--the direct ray and the ground-reflected ray. Each of these induces two components of current--a forward traveling component and a backward traveling component. In Figure 9, only the forward components traveling toward the base of the riser are observed, since the backward traveling components must propagate to the open end of the line and back before they are observed at the base of the riser. At the base of the riser, one first sees the current in the riser building up as it propagates in from further up the riser. After  $h \sin \psi / c = h/2c$ , all this current has arrived at the base, and current induced in the horizontal wire begins to arrive. This current opposes the riser current, and the total current begins to decrease. After  $2h \sin \psi / c = 2h/c$ , the ground reflected wave forces the field along the horizontal conductor to zero, so that the current can no longer build up. The current then remains constant until reflections (which occur much later) from the open end arrive. The experimental data illustrates these characteristics of the response, as well as some effects of the finitely conducting ground, on the response of the horizontal conductor. Because of the imperfect ground, the ground reflected wave does not completely "turn-off" the horizontal field driving the wire, so the current continues to rise slowly after the reflected wave arrives.

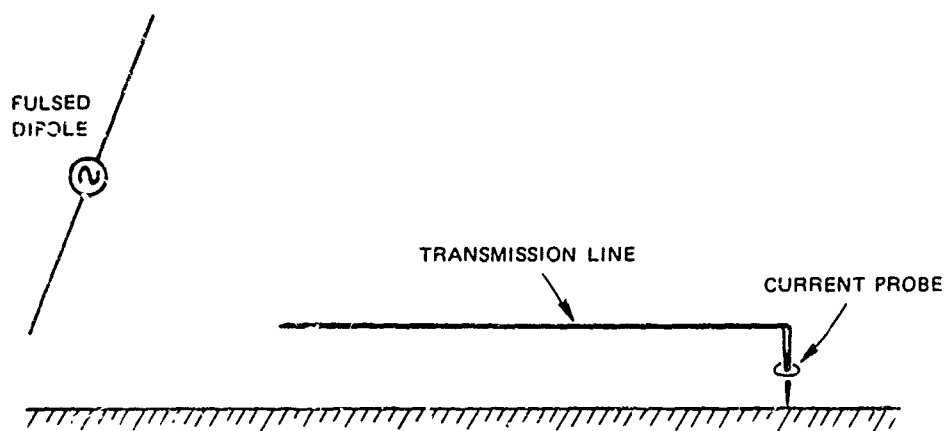
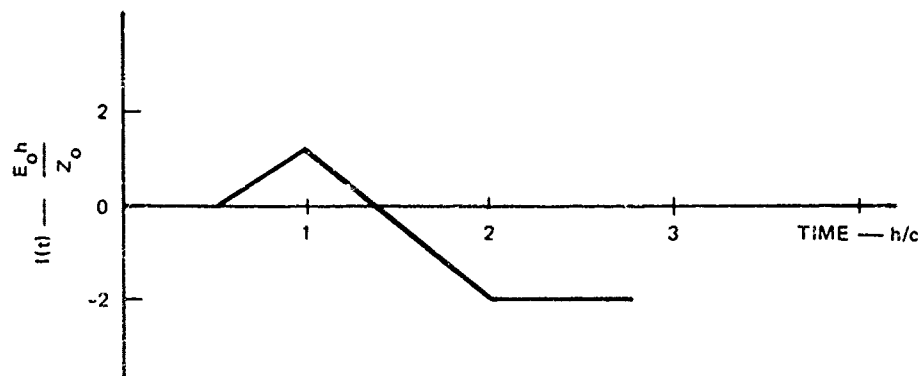
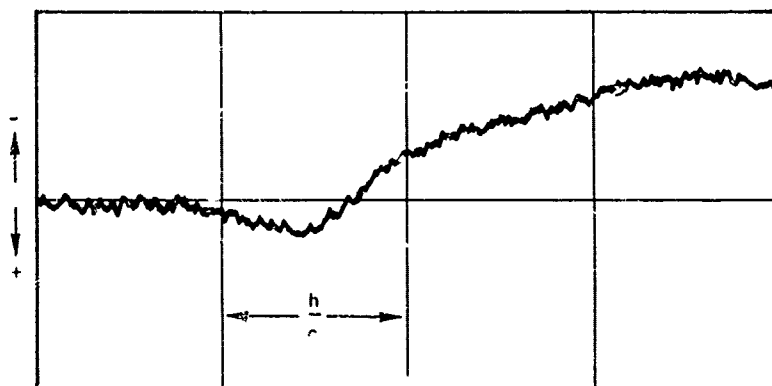


FIGURE 8 SCALE MODEL EXPERIMENT TO STUDY COUPLING TO TRANSMISSION LINE



(a) ESTIMATED RESPONSE TO STEP FUNCTION



(b) RESPONSE MEASURED WITH SCALE MODEL

FIGURE 9 RESPONSE OF HORIZONTAL CONDUCTOR WITH VERTICAL RISER TO VERTICALLY POLARIZED WAVE INCIDENT AT  $30^\circ$  ELEVATION ANGLE

## CONCLUSION

Experience with the use of scale models to study fast transient phenomena has demonstrated that this technique is a very economical and accurate method of studying parametric variations on simple, as well as complicated, systems. Viewed as an analog computer, it delivers the results quickly and in the desired (transient) form, whereas other processes must break the problem into small increments to perform the processing and then add them together again to obtain the desired solution. Although digital computers are efficient at performing these operations, the opportunities for error are plentiful and sometimes hidden. Furthermore, analytical/digital computer techniques for solving complicated problems in electromagnetic transients are very expensive, both in professional effort to develop and program suitable formulations of the solution and in machine time necessary to calculate the results. The interpretation of the computed result, however, is usually no more difficult than the interpretation of analog data from a model.

## Structure of Lightning Noise--Especially Above HF

N. Cianos, G. M. Oetzel, and E. T. Pierce  
Stanford Research Institute

### ABSTRACT

The following paper summarizes the characteristics of the radiation fields due to lightning. The fields are shown to vary with time, frequency, and distance from the discharge, and the variations in time and frequency are correlated with the different stages (leader-streamers, return strokes, and recoil streamers) of the lightning flash. It is very important to recognize that the radiation from lightning does not consist of one impulse but generally includes many. At VHF, for example, a single flash usually generates about  $10^4$  identifiable pulses.

At VLF the radiated fields are largely created by the return strokes and recoil streamers, while at HF and VHF they are associated with the various leader-streamer processes. As the frequency increases into the microwaves spectrum (centimeter wavelengths) the fields once again appear to be associated with the return stroke. It is important to understand the basic characteristics of the lightning radio emissions since they can couple into electrical and electronic equipment causing noise and errors as well as producing damage to some types of solid-state circuit components. Yet lightning noise is not entirely disadvantageous. As an example applying to the aviation industry, it is shown how the VHF lightning emissions can be used to locate thunderstorms and potentially to provide methods for vectoring aircraft around thunderstorms.

IT IS WELL KNOWN that lightning discharges produce electric and magnetic fields that vary with time, frequency, and distances. The characteristics of these fields are of practical importance since they can affect the performance of electrical equipment. For example, the radiated fields can produce interruptions or errors in computers, cause failures in electronic circuitry (particularly with solid-state devices) and create noise in communications equipment. On the other hand, these fields can sometimes be used to practical advantage--for example, to locate thunderstorms.

As previously described by the introductory papers on the fundamental aspects of lightning (1-3)\* a lightning flash consists of

various stages with each stage having characteristic currents. Briefly, for most of the flash duration leader-streamer processes are occurring. These involve the advance of a charge-carrying channel by a series of comparatively minor sparks that occur in rapid succession. The most intense of these minor sparks are the well-known "steps;" these are often present during the advance, from the base of the cloud to the earth, of the leader-streamer which initiates the flash to ground. Usually--and particularly for streamer processes within a cloud--it is difficult to distinguish the electrical signal associated with each small spark involved in advancing the streamer; it is only the aggregate electrostatic effect or the radiated electromagnetic "noise" that can easily be recognized.

If an advancing charge-carrying leader encounters a concentration of charge of opposite sign, there is a rapid recoil surge of current backward along the advancing channel. The electrical and luminous effects produced by such surges are readily identified. In the case of intracloud discharges, the phenomena accompanying the sudden surges are described as K changes. Although these are pronounced, far more intense effects accompany the return strokes of the flash to ground. In an earth discharge, the initial leader-channel typically carries negative charge downward from the cloud. When contact with the ground is made, a very intense upward surge of luminosity toward the cloud occurs; this is a return stroke. There may be several return strokes contained within a flash to earth. During the intervals between return strokes it is believed that leader streamers carrying positive charge probe into the cloud from the upper part of the channel energized by the return stroke. If such a positive leader encounters a medium-sized concentration of negative charge within the cloud, there is a recoil streamer giving a K change. Occasionally the recoil may be sufficiently intense to extend as far as the ground; in these instances the recoil streamer is known as a dart leader. In its passage, the dart leader recharges the original channel negatively, so that when the dart reaches the earth the conditions are suitable for another return stroke to surge upward. It is noteworthy that K changes are present both for intracloud discharges and for flashes to earth (between return strokes or after the final

\*Numbers in parentheses designate References at end of paper.

return stroke). On the other hand, true return strokes occur only for the discharge to earth, since it is solely in this case that one extremity of the spark is a large, homogeneous, good electrical conductor.

The fields produced by lightning are different for each stage, and very complex in many respects. A considerable amount of effort has gone into their understanding and interpretation, since a large portion of our knowledge of lightning processes is based on a variety of electric and magnetic-field measurements. In general, the fields produced by lightning consist of the far fields or radiated components and the near fields or static and induction components. Analytically, these far- and near-field components can be approximately represented by

$$E_T = \frac{1}{4\pi\epsilon_0} \left[ \int \frac{M_t dt}{D^3} + \frac{M_t}{cD^2} + \frac{1}{c^2 D} \frac{dM_t}{dt} \right] \quad (1)$$

where  $M_t$  is the current moment,  $2i_t l_t \sim i_t$  being the current and  $l_t$  being the length of the current channel energized by  $i_t$ . Of course, retarded values of time ( $t - D/c$ ) are implied and  $\epsilon_0$  is the permittivity of free space. The first term of  $E_t$  is the static field, the second term is the induction term, and the third term is the radiation field. It can be seen from Eq. (1) that the relative contribution of these components to the total field is dependent on the frequency and distance from the source. If  $E_t$  were expressed in the frequency domain, then the three components would be equal when  $D = c/(2\pi f)$ . Generally speaking, for distances greater than 15 km and frequencies exceeding 3 kHz, the radiated fields are dominant. Reviews of the radiated fields have been presented by Horner (4) and by Oetzel and Pierce (5). Extensive references to electrostatic-field measurements can be found in the standard texts (6-9). The following, however, summarizes the characteristics of the radiated field components only.

#### RADIATION FIELDS

The structure of the electromagnetic radiation from lightning varies with frequency and time as schematically illustrated in Figure 1. For this analysis, the fields only for close (within ~ 100 km) lightning are presented; propagational degradation is therefore not considered. The electric fields for a typical ground and cloud flash are shown, illustrating the relative magnitudes of the fields at various frequencies. At very low frequencies, VLF (3 to 30 kHz), the pulses are discrete and are generated principally by the return stroke and/

or recoil streamers (K-changes). As the frequency increases, the number of pulses per flash also increases, with a maximum of about  $10^4$  per discharge for frequencies between 30 to 300 MHz (VHF); the disturbance accompanying the flash is then quasi-continuous. These pulses appear to be associated with the initial leader, including its stops, and also with the electrical-breakdown processes accompanying probing leaders moving within the cloud. These probing leaders can occur, for a flash to earth, between return strokes or after the final stroke; for an intra-cloud discharge their presence is possible at almost any stage of the discharge. We note the interesting feature that the signals at HF and VHF associated with return strokes and K changes are not strong, and are indeed partly "quenched" following the occurrence of return strokes and K changes. It is believed that this quenching is due to a temporary absence of probing leaders. As frequency is further increased beyond the V.F. range, there is a sharp decrease in the number of pulses until at centimetric wavelengths (~ GHz) the pulses are again well separated and associated with the macroscopic features of the return strokes.

Peak pulse amplitudes are reached, for a flash to earth, at frequencies of about 5 kHz. With increasing frequency up to about  $10^4$  MHz there is a general decrease in amplitude, which approximately follows an inverse frequency dependency. However, over substantial sections of the spectrum between 10 kHz and  $10^4$  MHz there are probably appreciable deviations from this simple law. Figures 2 and 3\* illustrate the spectral characteristics of the radio emissions from close lightning. The results--which present information from several sources--have been normalized to a distance of 10 km. Figure 2 represents the amplitude spectrum,  $S(f)$ , of the return-stroke signals, while Figure 3 is the peak amplitude,  $e_p$ , for a receiver of bandwidth 1 kHz and for all lightning-generated emissions. The relation between  $S(f)$  and  $e_p$  is complicated, as described by Horner (4), who has derived a relation between  $S(f)$  and  $e_p$  for a narrow-bandwidth receiver. For illustrative purposes, though, Figures 2 and 3 can be approximately interconnected (18) if the ordinate scale of Figure 2 is multiplied by  $10^3$ , as shown by the solid curve in Figure 3. It should be noted that for frequencies below 100 kHz where the signals are discrete pulses, the field is scaled linearly with bandwidth. At 5 kHz the spectrum of the return-stroke pulse (Figure 2)

\*The references for Figure 3 are: Takagi (10), Horner (11), Iwata (12), Hallgren (13), Oetzel (5), Atlas (14), Schafer (15), Cianos-Oetzel (16), Kosarev (17), and Horner (4).

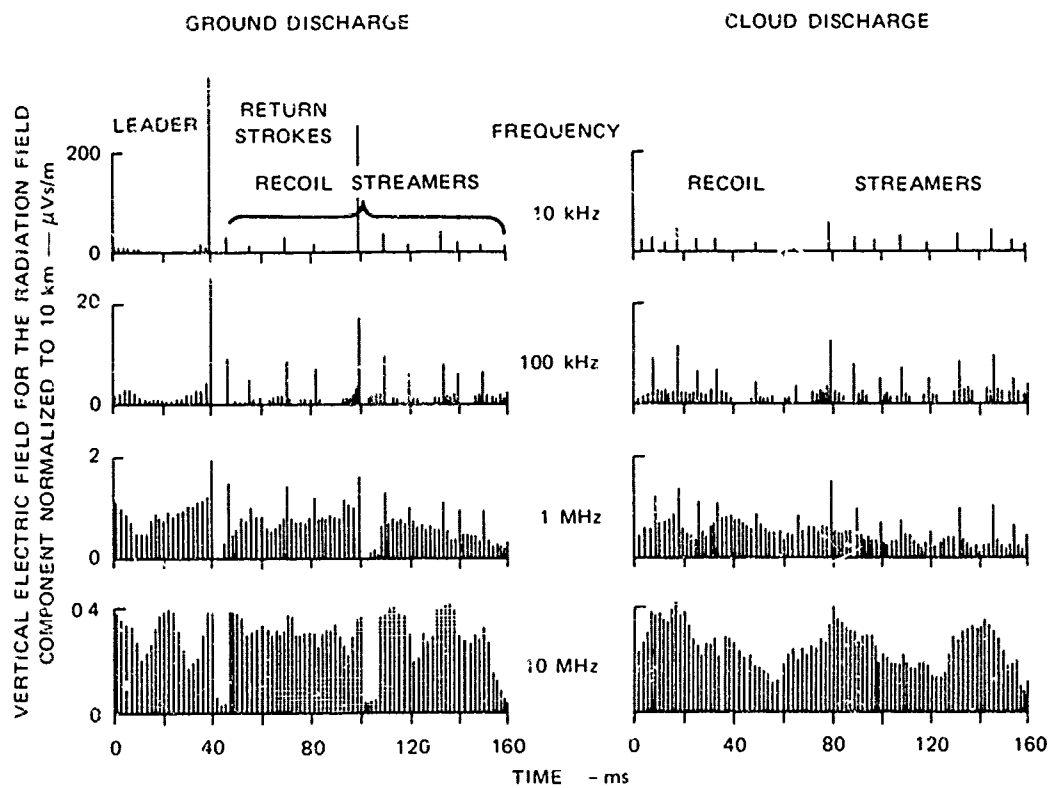


FIGURE 1 STRUCTURE OF THE FIELDS RADIATED BY LIGHTNING AS A FUNCTION OF TIME AND FREQUENCY



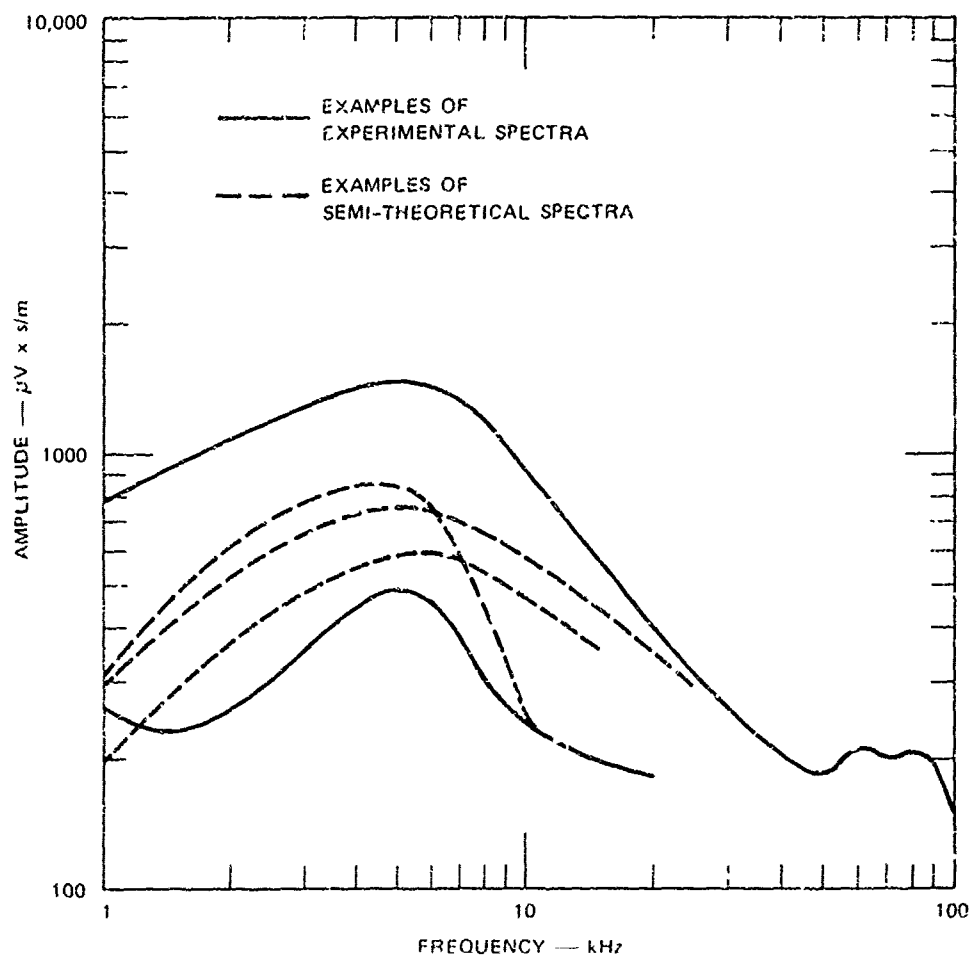


FIGURE 2 AMPLITUDE SPECTRUM OF RETURN-STROKE SIGNALS RADIATED BY LIGHTNING

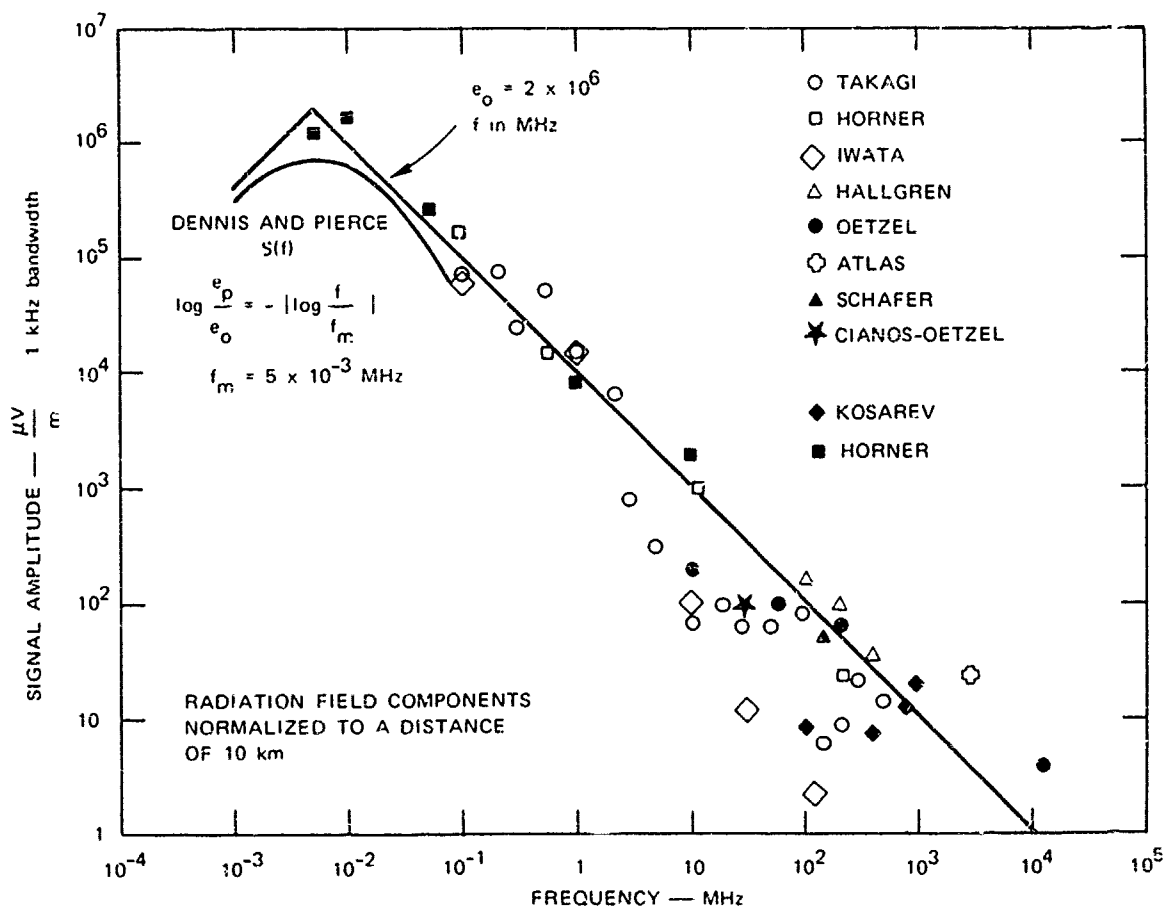


FIGURE 3 PEAK RECEIVED AMPLITUDE FOR SIGNALS RADIATED BY LIGHTNING

exceeds the spectrum of a K-change pulse by more than an order of magnitude. But at 100 kHz the two spectra are more comparable.

Analytic models describing the frequency dependence of the radiated fields on the physical processes are not well developed for the entire spectrum. However, at frequencies less than 100 kHz, several models describing the radiation from the return stroke are available (18). Despite these shortcomings, a model relating the field strength over a wide range of frequencies is often required. An empirical relation between the peak field strength,  $e_p$ , and the frequency, based on a form previously derived (19), is

$$\log \frac{e_p}{e_0} = - \left| \log \frac{f}{f_m} \right| \quad \text{for } f \geq 1 \text{ kHz} \quad (2)$$

where  $e_0 = 2 \times 10^6 \mu\text{V/m}$  in a 1-kHz bandwidth and the frequency mode,  $f_m$ , is  $5 \times 10^{-3}$  MHz, the frequency,  $f$ , being expressed in megahertz. Then  $e_p$  is the field strength in  $\mu\text{V/m}$  in a 1-kHz bandwidth and normalized to a distance of 10 km. Equation (2) is shown in Figure 3. It is a reasonable fit to the entire experimental data from  $10^{-3}$  to  $10^4$  MHz. It should be noted that the model for  $e_p$  represents the average or typical field strength, but that  $e_p$  also has a statistical behavior generally obeying a log-normal distribution with a standard deviation of about 6 dB relative to the mean (4,5). Equation 2 is only an analytical tool and does not imply any physical justification. The radiation fields are scaled linearly with distance for distances exceeding 10 km, as square-root of the bandwidth for frequencies greater than 100 kHz, and linearly with bandwidth for frequencies less than 100 kHz (4, 18).

A word of caution regarding the use of Figures 2 and 3 is in order. These figures have been normalized to a distance of 10 km, and it has been indicated that a scaling inversely with distance is appropriate for greater distances. It is, however, a very dangerous procedure to apply an inverse scaling to distances appreciably less than 10 km. For example, at VLF the lengths of the radiating channels are an appreciable fraction of 10 km and there is consequently no orderly change in magnitude with distance at the closer ranges (4). Also it appears that the subsidiary sparks providing most of the radiation at HF and VHF are usually located within the thundercloud; consequently, they are seldom very close to ground equipment but may be close to an airplane.

#### SUMMARY

The behavior of the radio emissions from

close lightning may be summarized by stating that a multitude of subsidiary sparks of many different types are involved--e.g., step leaders and return strokes. In addition, the larger the current peak in a given type of spark, the longer the energized channel, the lower the frequency at which peak signal is radiated, and the less frequent the occurrence of the particular kind of spark. High-current channels tend to be orientated vertically (especially the return stroke); however, minor subsidiary discharges are much more randomly disposed.

It cannot be over emphasized that a lightning flash involves this multiplicity of sparks and consequently a protracted and complicated generation of radio signals. It is still a common misconception that the lightning discharge occurs as one single large spark, and that therefore all radio emissions are produced almost simultaneously as in the case of the nuclear electromagnetic pulse (EMP) (20). In reality the time histories of the lightning emissions and of the EMP are quite different, and comparisons of equipment response to the two types of signal should entail intelligent recognition of this fact. For example, at HF the EMP would generate one very large pulse while a typical lightning flash might create ten thousand small pulses. Designs of equipment can be conceived that could survive the single large pulse but would fail under the repetition of the small pulses.

Although the radiated noise from lightning often has its detrimental effects such as interfering with radio communications, the lightning radio emissions can be used as mentioned in the introduction, to indicate thunderstorm positions. An example of this type of use is now discussed; the technique described is especially applicable to close (< 100 km) lightning and to aircraft operations.

VLF radio-location techniques are well established for locating distant thunderstorms (> 100 km), but for various reasons these methods are not very well suited for accurately locating close lightning (4). Recently, a new technique has been demonstrated for accurately locating close lightning using its VHF noise emissions (16). The essential feature of this technique, which is based on a time-of-arrival approach, is that modern equipment enables a short baseline to be used. Consequently, confusion caused by the multiplicity of VHF pulses is avoided, and it is possible to establish the azimuth of a flash from two sensors located quite close together--for example, at the extremities of an aircraft. Thus the technique could be profitably applied operationally when it is of practical interest for aircraft to avoid flying into thunderstorms in order to

minimize the chances of being struck by lightning and to avoid the strong turbulence associated with thunderstorms. It would be most interesting to add a Cianos-Oetzel-Pierce lightning locator (16) to an airplane so as to complement its weather radar. In this way the troublesome question, which thunderstorm cells indicated on the radar are active and producing lightning, could be answered. Such a combination of techniques would aid pilots in determining the optimum flight pattern during thundery conditions.

#### ACKNOWLEDGMENT

Preparation of this paper was supported by the United States Office of Naval Research under Contract N00014-71-C-0106. Accordingly, reproduction of this paper in whole or in part is permitted for any purpose of the United States Government.

#### REFERENCES

1. B. Vonnegut, "Basic Thunderstorm and Lightning Phenomena," presented in these proceedings.
2. M. Brook and C. Moore, "Instrumentation and Measurements Associated with Lightning Strikes," presented in these proceedings.
3. M. A. Uman, "Natural Lightning and Simulated Lightning," presented in these proceedings.
4. F. Horner, "Radio Noise from Thunderstorms." In "Advances in Radio Research," Vol 2, J. A. Saxton, ed., Academic Press, New York, 1964, pp 122-215.
5. G. N. Oetzel and E. T. Pierce, "The Radio Emissions from Close Lightning." In "Planetary Electrodynamics," Vol 1, S. C. Coroniti and J. Hughes, eds., Gordon and Breach, New York, New York, 1969, pp 543-571.
6. M. A. Uman, "Lightning." McGraw-Hill Book Co., Inc., New York, New York, 1969.
7. B. F. Schonland, "The Lightning Discharge." In "Handbuch Der Physik," Vol 22, Springer-Verlag, OHF, Berlin, 1956, pp 567-628.
8. D. J. Malan, "Physics of Lightning." The English Universities Press, London, 1963.
9. J. A. Chalmers, "Atmospheric Electricity." Pergamon Press, New York, New York, 1967.
10. M. Takagi and T. Takeuti, "Atmospheric Radiation from Lightning Discharges." Proc. Res. Inst. Atmos. (Nagoya University), Vol 10, 1963, pp 1-11.
11. F. Horner and P. A. Bradley, "The Spectra of Atmospherics from Near Lightning Discharges." J. Atmos. Terrest. Phys., Vol 26, 1964, pp 1155-1166.
12. A. Iwata and Masahiro Kanada, "On the Nature of the Frequency Spectrum of Atmospherics Source Signals." Proc. Res. Inst. Atmos. (Nagoya University), Vol 14, 1967, pp 1-6.
13. R. E. Hallgren and R. B. MacDonald, "Atmospherics from Lightning 100 to 600 MHz." Report No. 63-538-89, IBM Federal Systems Division, 1963.
14. D. Atlas, "Radar Lightning Echoes and Atmospherics in Vertical Cross-Sections." In "Recent Advances in Atmospheric Electricity," L. G. Smith, ed., Pergamon Press, London, 1959, pp 441-458.
15. J. P. Schafer and W. M. Goodall, "Peak Field Strengths of Atmospherics Due to Local Thunderstorms at 150 Megacycles." Proc. IRE, Vol 27, 1939, pp 202-207.
16. N. Cianos, G. N. Oetzel, and E. T. Pierce, "A Technique for Accurately Locating Lightning at Close Ranges." (To be published in J. Appl. Meteorol., October 1972.)
17. E. L. Kosarev, V. G. Zatsepin, and A. V. Metrofanov, "Ultrahigh Frequency Radiation from Lightnings." J. Geophys. Res., Vol 75, December 20, 1970, pp 7524-7530.
18. E. T. Pierce, "The Thunderstorm as a Source of Atmospheric Noise at Frequencies between 1 and 100 kHz." Special Technical Report 2, Contract DASA01-68-C-0073, SRI Project 7045, prepared for the Defense Atomic Support Agency, Washington, D.C. 20305, June 1969.
19. A. S. Dennis and E. T. Pierce, "The Return Stroke of the Lightning Flash to Earth as a Source of VLF Atmospherics." Radio Sci., Vol 68D, 1964, pp 777-794.
20. W. Sollfrey, "Effects on High-Frequency Electromagnetic Radiation from Low Altitude Nuclear Explosions." Proc. IEEE, Vol 53, No 12, December 1965, pp 2035-2042.

SESSION III

ELECTRIFICATION-OPERATIONAL PROBLEMS

DR. J.G. BRELAND, CHAIRMAN & ORGANIZER

U.S. AIR FORCE, F.J. SEILER RESEARCH LABORATORY, AFSC

## Electrification-Operational Problems

### Introduction to Session

Captain John G. Breland, Jr.  
Frank J. Seiler Research Laboratory

This session is designed to emphasize operational electrification problems, both actual and potential. With the ever increasing complexity of aircraft over the past twenty years, more and more emphasis has been placed on total system performance over a widely varied flight profile. This has required the art to be advanced significantly with each new commercial and military aircraft system produced.

As the basic costs of systems increase, larger percentages of available monies are required for design and development. This leaves smaller and smaller amounts for testing and evaluation. This is especially unfortunate since communication between structural and electronic engineers is often very poor although material-atmospheric interaction accounts for a majority of electrification problems. The current interest in returning to lower frequency communication necessitates that electronic and design/material engineers re-establish clear and effective interchange of knowledge.

The papers to be presented in this session cover two topics. The first two will discuss the results of p-static on certain communication and navigation systems. The second group will discuss the interaction of non-metallic materials with the airstream.

Significant improvements in radome coatings have been made in the past few years and these new systems are now ready for use on aircraft. Electrical properties of windshields have received only superficial attention during the previous conferences. The inclusion of several papers on this topic is an attempt to partially rectify this omission. These discussions along with an Air Force Windshield Symposium in 1973 should prove highly beneficial to designer and electrical engineer alike.

Operational problems resulting from tribo-electric charging will continue to occur if for no other reason than 95 percent of Air Force personnel don't realize that static electrification exists. Today, however, no aircraft system designer can afford not to realize it. It is hoped that the current discussions will prevent someone from having an "operational problem" in the future.

## Static Electricity Problems--VLF/LORAN Systems

John B. Chown, Joseph E. Nanevitz  
Stanford Research Institute

### ABSTRACT

Currently under development are new aircraft navigational systems operating at LF and VLF. This portion of the radio frequency spectrum is particularly susceptible to precipitation static interference. Results of analysis and ground tests on a LORAN-D system are presented. This work demonstrates that proper attention to p-static elimination is essential to all-weather system operation.

WHEN AIRCRAFT FIRST began to be equipped with radio communication and navigation systems, the first navigation aids included the ADF system and the LF range. Both of these systems operated at frequencies of hundreds of kHz, and both were affected by precipitation static interference unless careful precautions were taken. More recently, navigation aids, particularly on small military aircraft, operated at VHF and above where the precipitation static problem is less severe.

Now, once again, navigation systems operating in the hundred kHz range are being developed and used in operational situations. Thus although this portion of the spectrum is inherently more prone to vehicle-generated interference, the features of systems operating at these frequencies are so attractive that they outweigh the noise problems. For example, a modern LORAN-D with associated logic system can solve extremely complex navigation problems relieving the pilot of a large fraction of his normal work load. Unfortunately unless proper precautions are taken, all of this capability can be nullified by precipitation static as soon as the aircraft enters a cloud.

The noise sources that must be considered are: (1), (2)\*

- (1) Sparks between unbonded metal sections,
- (2) Corona discharges from points of high electric field, and
- (3) Streamer discharges over the surface of a charged dielectric.

Sparks between unbonded conductors, which generate severe noise with frequency components extending to the VHF regions can disable most receiving systems on the aircraft--including the LORAN-D canopy installation. This source

of noise can be eliminated by ensuring that all metal parts of the aircraft are properly electrically bonded.

Corona discharges occur wherever on the aircraft the electric field intensity is sufficiently high to cause breakdown of the air. Since, for a given airplane voltage, the highest fields occur at the extremities of the aircraft, discharges occur first from the extremities. At aircraft operating altitudes, the discharge occurs in the form of a series of short current pulses containing noise components in the HF region. This noise couples into all antennas on the aircraft, including the LORAN-D canopy installation. The corona noise level can be reduced to negligible magnitudes--50 to 60 dB by installing passive dischargers at those high-field locations on the aircraft where corona discharges would normally occur. (3)

Streamer discharges occur whenever frictional charging resulting from dust or precipitation impact causes a plastic region on the frontal surface of the aircraft to become charged with respect to the rest of the airframe. The bound charge on the plastic is relieved by a series of surface discharges "streamers" to the airframe. These streamers are an energetic source of noise, particularly when the coupling is high--as in the case of an antenna located immediately below the charged plastic surface. Furthermore, the power spectrum of streamer noise is flat up to 500 kHz frequency, at which point it begins to fall off with increasing frequency at 6 dB per octave. Thus, low-frequency systems--such as LORAN-D--are most affected by streamer discharge noise. Streamer noise is most easily eliminated by coating the outside surface of the plastic with conductive material to permit the charge to flow away as rapidly as it arrives, thereby eliminating the discharges that are the source of noise. Unfortunately, there are no satisfactory optically transparent conductive materials, so that the conductive coating scheme cannot be used in the case of antennas mounted inside plastic surfaces--such as canopies and windshields, which must remain transparent to light. Thus, when a canopy antenna installation is being considered, great care must be exercised to make certain that

\* Numbers in parentheses designate References at end of paper

streamers on the windshield and frontal surfaces of the canopy do not couple sufficient noise into the antenna to cause the system to malfunction.

The frictional charging, which results in precipitation static interference, occurs whenever an aircraft is operated in precipitation containing ice crystals. It has been the authors' experience that virtually all clouds above 20,000 ft are composed of ice crystals and produce vehicle electrification. Below 20,000 ft, some clouds are composed of liquid water and produce very little charging. Other clouds below 20,000 ft contain ice crystals and statistically produced the highest charging currents observed. Therefore, to be certain that the system is truly capable of all-weather operation, it must be immune to precipitation static interference.

#### CORONA INTERFERENCE

An idea of the magnitude of the corona noise problem likely to be encountered in the case of a LORAN-D system installed on an F-111 aircraft can be obtained through the proper application of laboratory and flight test data generated on KC-135 aircraft.

The noise field induced in the belly antenna on the KC-135 prototype aircraft (4) is shown in Figure 1. The noise field above 1 MHz is influenced by the airframe resonances; however, so that for a smaller aircraft, these resonance effects will occur at higher frequencies. According to Figure 2 (reproduced from Reference 4), the noise current should fall off as  $1/\omega$  above 1 MHz at 20,000 ft altitude. For small electric dipole type antennas, the equivalent noise field  $E_n$  is related to the noise current  $I_n$  by (4)

$$|E_n| = \frac{|I_n|}{\omega \epsilon_0 a} \quad (1)$$

where  $a$  is the induction area of the antenna, (4) and  $\epsilon_0 = (1/36 \pi) \times 10^{-9}$  farad/meter. Thus the noise field should fall off as  $1/\omega^2$  above 1 MHz until the resonance effects are encountered on the smaller aircraft. Assuming that the resonance effects will be the same on the small aircraft as on the larger aircraft, the noise field on a one-half-scale aircraft has been plotted on Figure 1. This should represent approximately the form of the noise field on the F-111A.

To obtain the magnitude of the noise field, account must be taken of the effect of aircraft size on charging rate, coupling, and antenna

effective induction area. The antenna noise field may be expressed in terms of the source spectrum  $D(\omega)$ , the coupling factor  $\psi(\omega)$ , and the effective induction area  $a$  by (4)

$$E_n = k [D(\omega) \psi(\omega)/a] \quad (2)$$

Since the source spectrum  $D(\omega)$  is proportional to the square root of the discharge current  $I$ , Eq. (2) can be rewritten

$$E_n = k' [\sqrt{I} \psi(\omega)/a] \quad (3)$$

From Ref. 3, the coupling factor  $\psi(\omega)$  varies as the square root of the scale  $s$  of the aircraft ( $s > 1$ ). Thus,

$$\psi_{1/s} = \psi/s$$

Since everything about the general form of the aircraft (including antenna size) is scaled, the induction area  $a$  varies as the inverse square of the scale  $s$ , so that

$$a_{1/s} = a/s^2$$

The noise field on the  $1/s$  scale aircraft can thus be written

$$E_{n(1/s)} = k' [\sqrt{I_{1/s}} \psi(\omega)/a] s^{5/2}, \quad (4)$$

or, in terms of the noise field on the KC-135,

$$E_{n(1/s)} = \sqrt{\frac{I_{1/s}}{I}} s^{5/2} E_n, \quad (5)$$

where  $E_n$  is the value given by the adjusted curve of Figure 1 for a discharge current  $I$  of 250  $\mu$ A. The values of  $I_{1/s}$  will be taken from Figure 3, which is reproduced from Ref. 5. (These values will be slightly high because the scale size is  $2/3$  in Figure 3 instead of  $1/2$ ). The results of this calculation are presented in Figure 4. The atmospheric noise field strength was obtained from Ref. 6. These values were adjusted for a 1-kHz bandwidth and plotted in Figure 4 along with the corona noise field strength computed from Eq. (5). The corona noise field strength is seen to be 40 to 60 dB greater than the daytime atmospheric noise throughout the 0.1 to 10 MHz frequency range. The corona noise field strength is also 20 to 40 dB greater than the night-time atmospheric noise throughout the same frequency range.

The implications of noise on the operation of a LORAN-D system are as follows: The LORAN-D



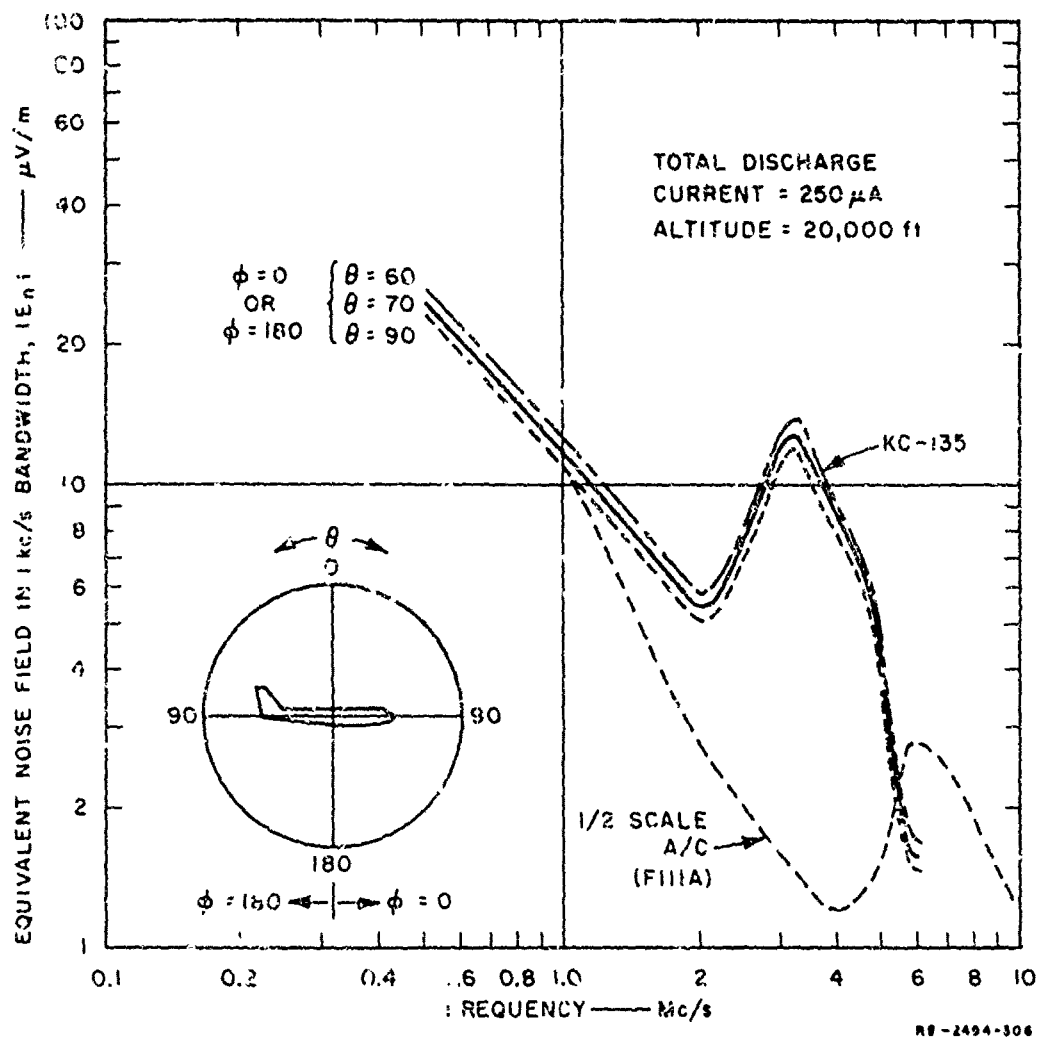


FIGURE 1 EQUIVALENT NOISE FIELDS AT CANOPY OR BELLY-ANTENNA LOCATION

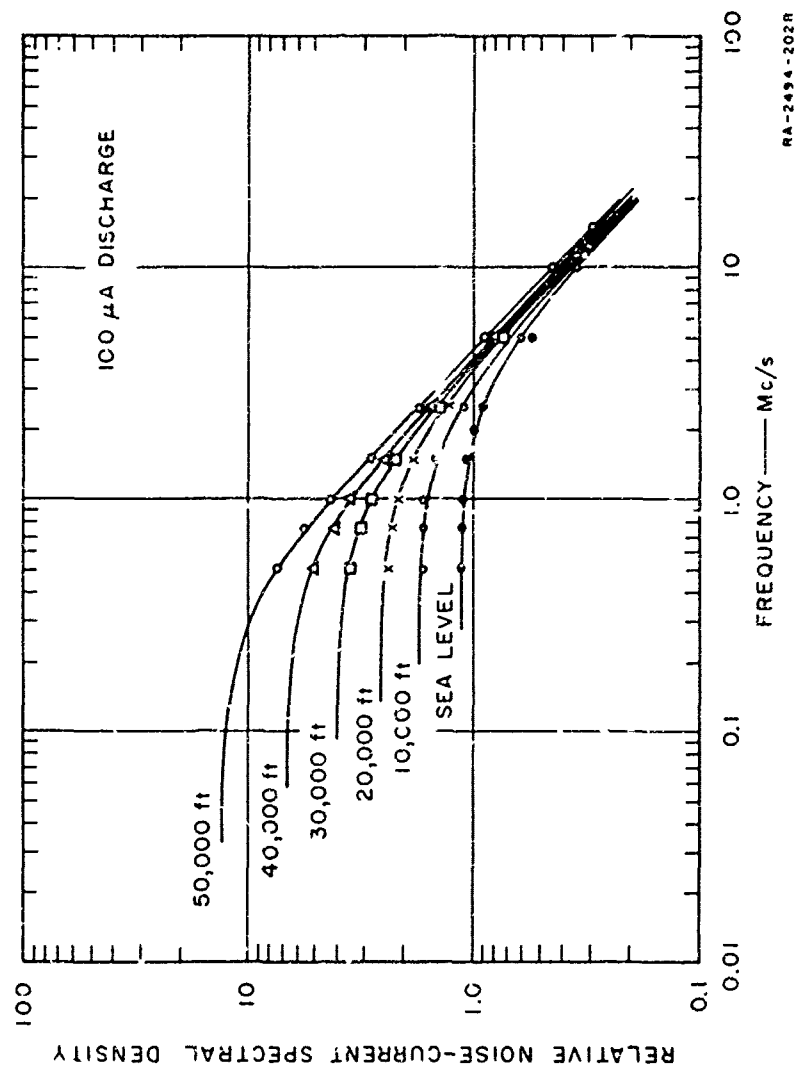


FIGURE 2 NORMALIZED CORONA NOISE SPECTRUM FROM TRAILING EDGE

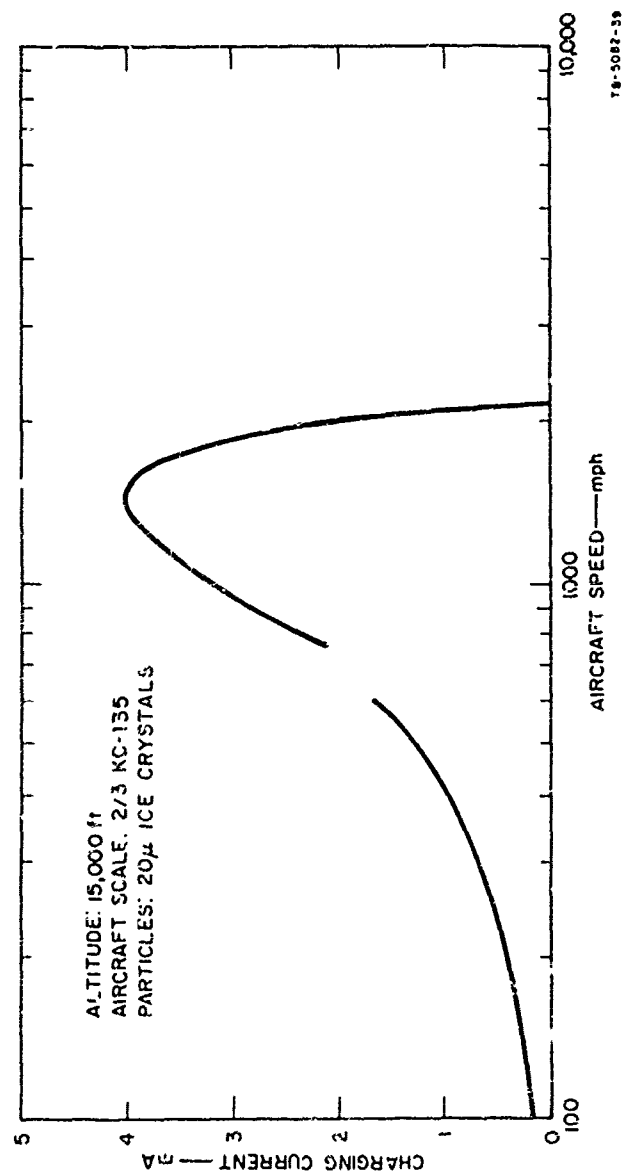


FIGURE 3 PREDICTED CHARGING CURRENT FOR ADVANCED AIRCRAFT

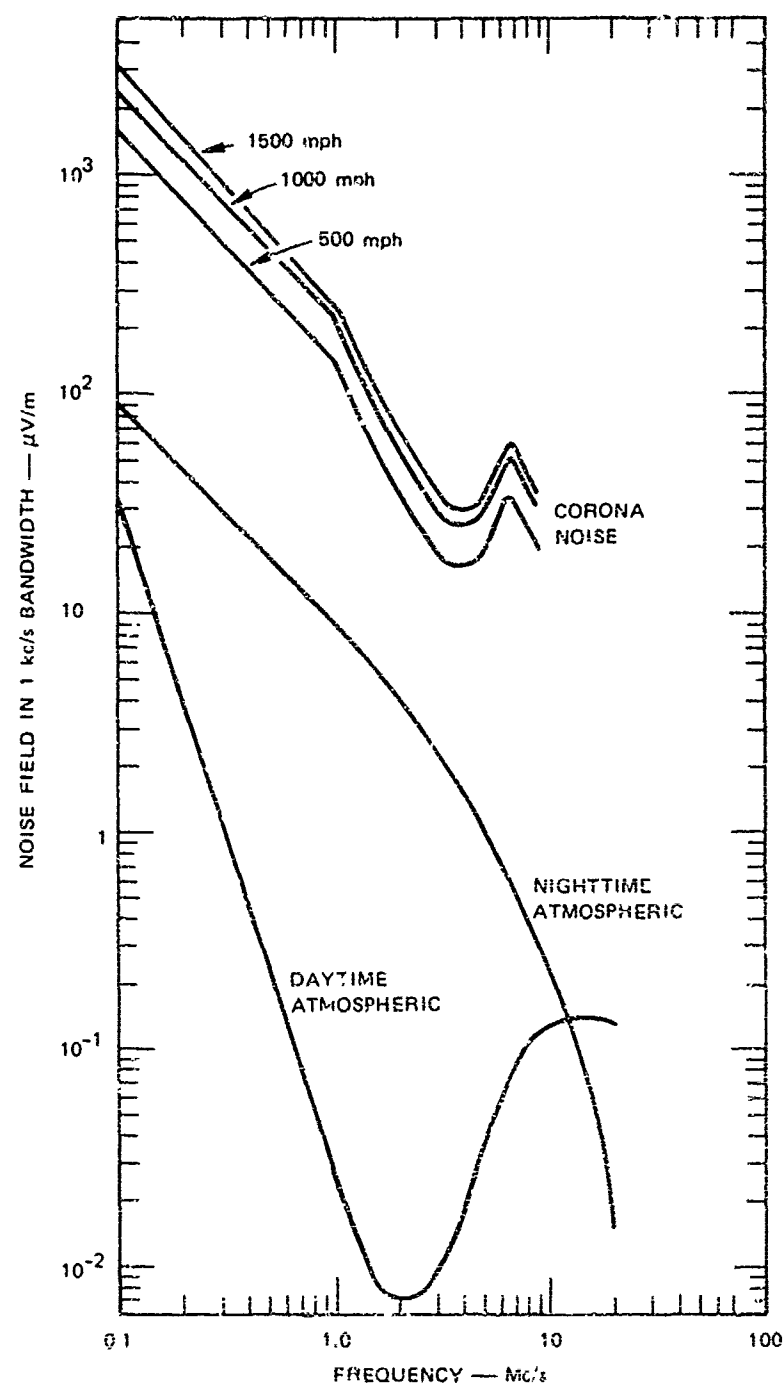


FIGURE 4 ANTICIPATED NOISE FIELDS FOR BELLY ANTENNA

system designer can buy improved performance until he has reduced his system input noise figure to the atmospheric noise level. From this observation we can infer that such systems are now, or ultimately will be, operating at the atmospheric noise level limit. From Figure 4, we see that corona noise will severely degrade the performance of such a system. In particular, the analysis indicates that 40 dB of corona noise reduction is required to reduce the corona noise levels to the daytime atmospheric level.

#### NOISE EXPERIMENTS ON LORAN-D EQUIPPED AIRCRAFT

GENERAL - Ground tests were conducted on an F-105 aircraft equipped with a LORAN-D system and with a canopy LORAN-D antenna installed. (7) The antenna is made using 1/2-inch wide adhesive-backed copper tape attached to the inside of the canopy as shown in Figure 5. The tape was soldered at each junction. The measured antenna capacity was 70 pF and the estimated effective height, based on similarly located antennas, was  $\approx 0.35$  m.

The LORAN-D\* antenna coupler was mounted in the aircraft. The cables connecting the coupler to the receiver were brought out aft of the canopy to the ground. Provisions were also made to bring out a lead directly from the antenna; this antenna lead was connected to an EMI receiver (Empire Model 105). This configuration was used during the survey of the aircraft for possible noise sources that would be coupled into the LORAN antenna system. The receiver was operated from the ground 60-Hz power system.

AIRCRAFT BONDING AND RESISTIVITY - The initial work consisted of an inspection of the LORAN-D antenna installation as well as the aircraft itself. At this time resistance measurements were made to check the bonding between airframe sections; particular attention was given to the canopy frame sections and adjacent structures. The tests indicated that proper bonding was provided and that no noise should be expected from discharges between sections of the airframe.

To locate regions where possible surface streamers can be anticipated, surface resistivity measurements were made on the plastic structures and antenna covers. It was found that, without exception, the resistivity was very high:  $> 2 \times 10^8$  ohms per square. This level is too high to be effective in prohibiting surface charge buildup. The paint used on the surfaces--apparently a rain erosion coating--

was either of the MIL-C-7439A (USAF) Class I type (no resistive material added) or Class II (with additive) that had been applied some time ago and deteriorated.

Similar measurements made on an operational F-4 aircraft indicated that here too, the surface resistivity of the dielectric frontal surfaces was so high that it probably would be ineffective in draining away charge as it arrived on the surfaces. (Unreported measurements made by authors.)

NOISE STUDIES - A portable spark noise source was used to investigate the coupling between the antenna and possible streamer corona noise sources on the aircraft. (5) The value of a measurement of this sort is that it provides an indication of the probable severity of the noise from various potential sources. Often, such a measurement saves much time by eliminating from consideration noise sources whose coupling to the antenna is too low to result in serious interference.

The portable noise source was used in conjunction with the EMI receiver to survey the aircraft (150 kHz). The results of the measurements are presented in Figure 6. The numbers at various locations on the airframe indicate the dB reading observed on the receiver's signal strength meter when the noise source was held at that location. Without the noise source on, the "no signal" meter reading was -6 dB.

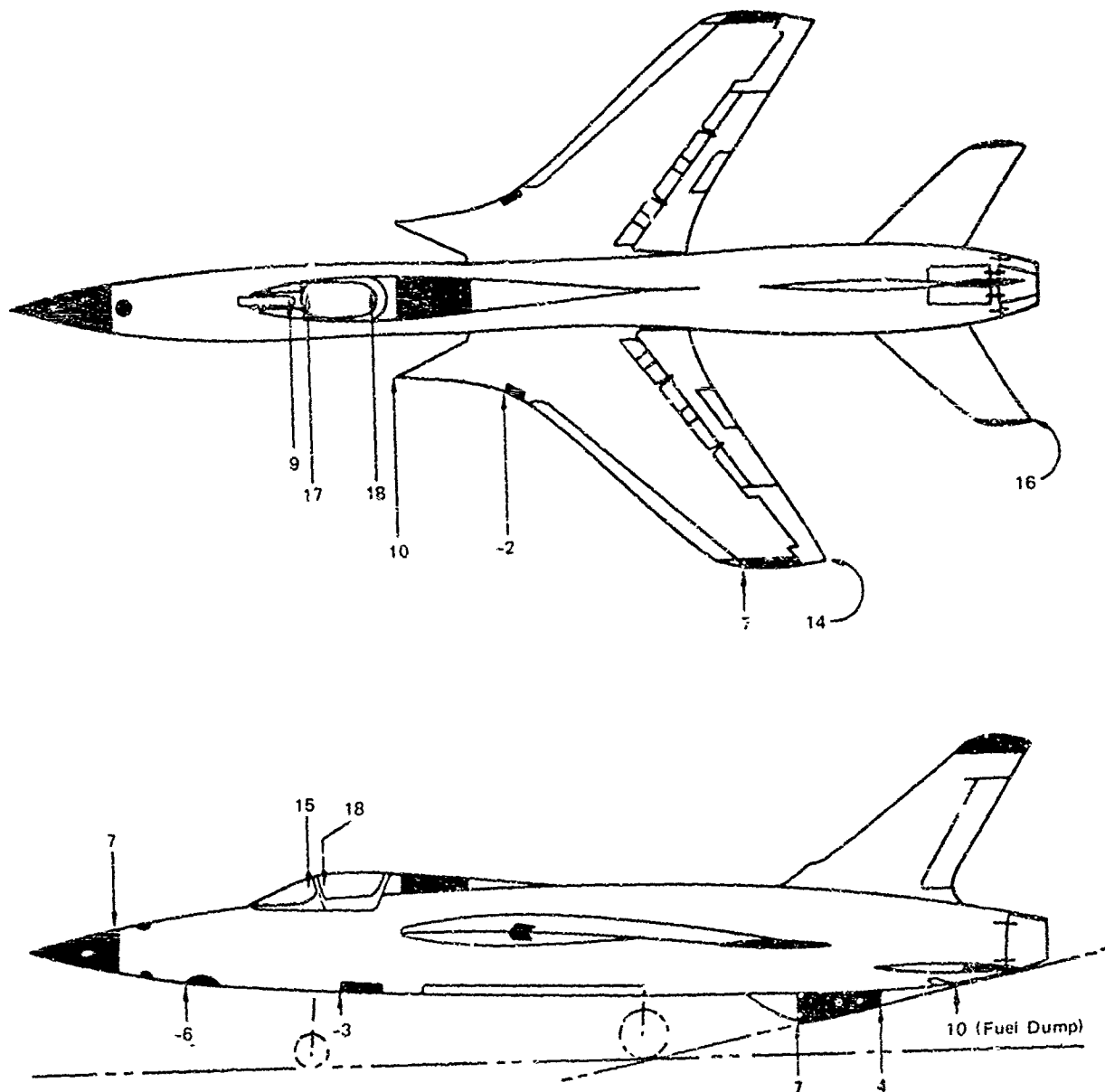
It is interesting at this time to compare the ground test data of Figure 6 with the predicted noise data of Figure 4. For the wing tip and elevator tip, the ground measurements indicate that the noise, coupled from the noise source was 20 and 22 dB respectively above the ambient noise level. From Ref. 5 we find that the spark noise source is roughly equivalent to a corona discharge equal to the spark source current (15  $\mu$ A). Adjusting this to a discharge current of 1.5 mA (corresponding to the discharge current from the aircraft at 500 mph in Figure 4) the noise power goes up by 20 dB and we obtain a noise level of 40 to 42 dB above ambient. This is in good agreement with Figure 4 which indicates that 100 kHz corona noise for charging conditions corresponding to a speed of 500 mph is approximately 40 dB above daytime atmospheric. (The measurements were made during daylight hours on a ramp removed from factory buildings.) Thus, the ground test data confirm the prediction that corona discharges from the extremities can generate noise fields in the vicinity of the canopy several orders of magnitude above the ambient noise level.

\* AN/AR-92 receiver



TA-7796-2

FIGURE 5 LORAN-D CANOPY ANTENNA



NOTE Reference Level = -6 dB  
Surfaces shown in black are made of dielectric material

FIGURE 6 RESULTS OF NOISE-COUPPLING SURVEY

The data of Figure 6 indicate that other regions of high coupling (where noise can be generated) exist on the aircraft.

It should be noted that, with the exception of the canopy region, the noise can in most cases be eliminated by the use of static dischargers that keep the aircraft potential below the corona threshold of the structure itself and by covering plastic surfaces with lossy paint to prohibit charge buildup and subsequent streamer ing. With the exception of the canopy itself which must remain optically transparent so that the normal opaque resistive coatings cannot be applied. Accordingly, the canopy must receive special attention.

To directly study the noise generated by charging of frontal plastic surfaces in the vicinity of the receiving antenna, a portable sand blaster was used to blow lycopodium powder onto the plastic frontal surfaces to simulate the frictional charging caused by impinging precipitation particles in flight. The noise generated in the LORAN receiver was monitored. During the dust-charging experiment, measurements were made of the current flowing from the plastic surface to the airframe. The current density levels can then be compared to the levels experienced on frontal surfaces of aircraft in actual flight. Thus, some estimate of the severity of the test can be made. The charging current is measured by placing a conductor around the area to be exposed to the blowing powder. The average current flowing from the section of dielectric surface under-going charging to the fuselage is then monitored. Two such current patches are visible in the side and front windshield in Figure 7.

Lycopodium powder charging was carried out on all the dielectric surfaces indicated in Figure 6 with the exception of the tail cap and the painted fiberglass cover aft of the cockpit.

The plastic surfaces that produced significant

noise in the canopy antenna system are listed in the order of the severity of the coupled noise:

- (1) Canopy
- (2) Side windshield
- (3) Front windshield
- (4) Nose radome
- (5) Ventral fin
- (6) UHF-ADF antenna cover.

The noise level produced by powder blown on the windshields and canopy was, as one would expect, much more severe than at the other locations. The current measurements indicated that charging rates on the order of  $2 \mu\text{A}/\text{ft}^2$  were obtained during the tests. Previous flight test data indicate that this current level could easily be experienced on the F-105 aircraft operating in ice-crystal clouds (1-4).

The AN/ARN-92 LORAN-D receiver saturated when lycopodium powder was blown on the frontal surface of the windshield just below the canopy so that there was a tangential flow of particles over the canopy producing 1- to  $2 \mu\text{A}/\text{ft}^2$  charging current.

Appropriate circuitry changes to the LORAN receiver were made to enable relative amplitudes of the generated noise and received LORAN signals to be monitored on an oscilloscope. The strongest LORAN signal received was from the slave station located 170 miles from the test site. Its signal was used as a reference for the noise tests. Auxiliary attenuators were used to prevent receiver overloading. Results of the powder charging tests are shown in Table I.

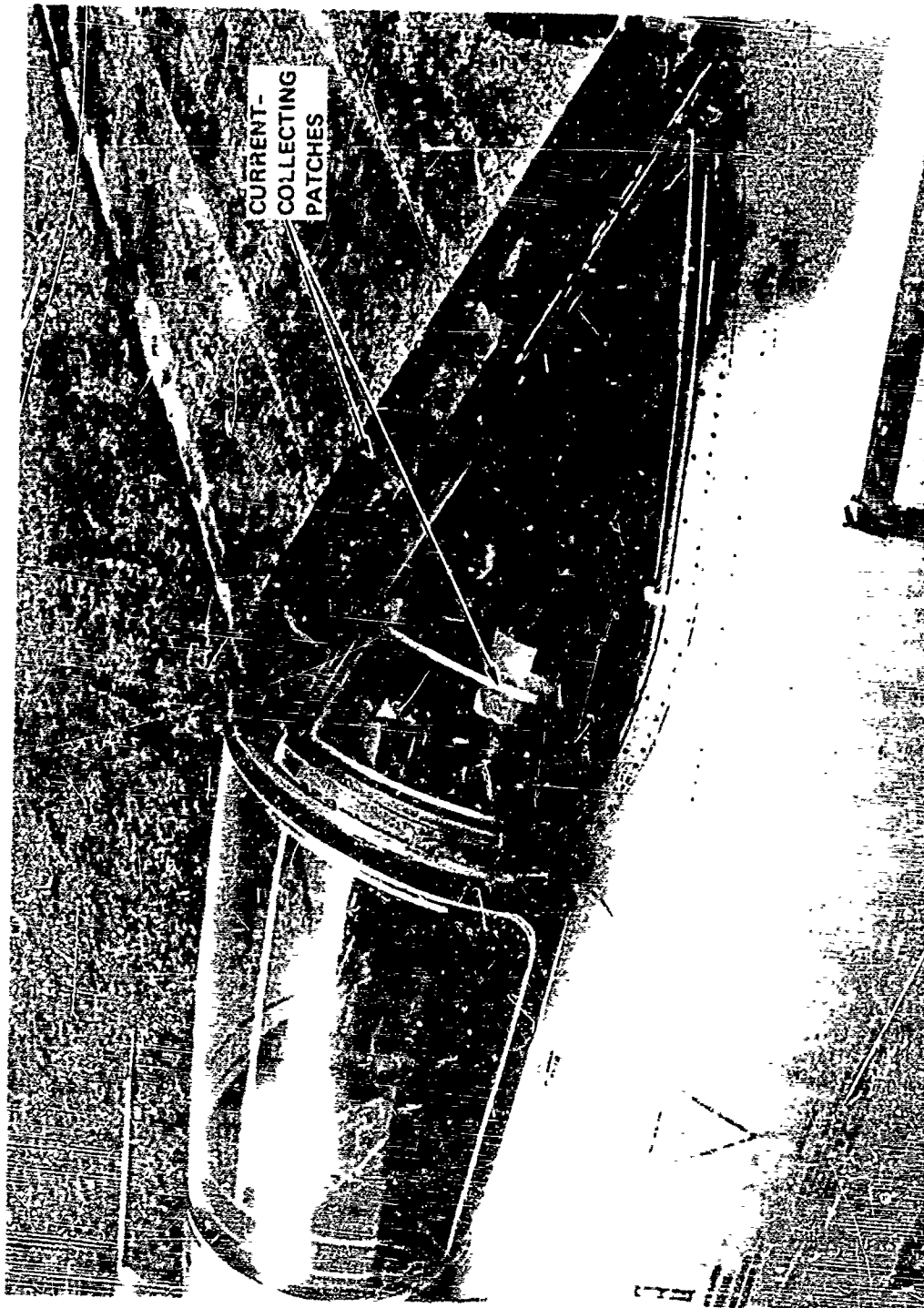
In summary, the ground tests showed that a charging current of 1 to  $2 \mu\text{A}/\text{ft}^2$  of canopy surface would cause the LORAN-D receiver to lose track. Previous flight test measurements have shown typical charging levels of 10 to  $30 \mu\text{A}/\text{ft}^2$  of effective frontal area. The in-flight particle impingement and the resulting

Table I

NOISE LEVEL GENERATED BY BLOWING LYCOPODIUM POWDER ON CANOPY

Location and Angle	Reference Signal (V peak to peak)	Noise Signal (V peak to peak)	Receiver Gain (dB)	Noise-to-Signal Ratio
Forward canopy centerline at $0^\circ$	0.6	13	28	21.7
Forward side windshield at $0^\circ$	0.6	11	28	18.4
Forward side canopy at $20^\circ$	0.6	12	28	20.0
Aft side canopy at $20^\circ$	0.6	12	28	20.0





TA-7796-4

FIGURE 7 WINDSHIELD AND CANOPY AREA, SHOWING LOCATION OF CURRENT-COLLECTING PATCHES

charging current to the canopy cannot be determined by ground test: While the blowing powder simulates the charging mechanism and charging levels encountered by frontal areas in flight through particulate matter, it does not simulate the fluid mechanics of flight.

#### CONCLUSIONS

Ground tests of the F-105 are in good general agreement with the outcomes anticipated on the basis of earlier aircraft flight and ground tests and laboratory studies (1-3).

Measurements on the F-105 verified that electrostatic charging of the canopy results in one of the most serious sources of LORAN-D noise. Although other potential precipitation static noise sources capable of producing comparable antenna noise levels were located on the aircraft, the others generally can be eliminated through the judicious application of such well-tested precipitation-static noise-reduction techniques as passive dischargers and conductive paints. The canopy, since it must remain optically transparent, is very difficult to treat. It must be recalled, however, that the ground tests demonstrated only that severe noise would be generated in the LORAN-D antenna provided precipitation charging as low as  $2 \mu\text{A}$  occurred on the canopy. The question of whether or not canopy charging currents of this magnitude can be expected in flight remains to be answered. (The aerodynamic problem of calculating precipitation particle trajectories around the complex structure consisting of a canopy mounted on an aircraft fuselage is so complicated that flight testing will be necessary.) Some insight into the problem can be gained from the results of previous flight tests, which indicate that canopy currents of  $2 \mu\text{A}$  or so are not unreasonably high. From Figure 7 it appears that the F-105 canopy is sufficiently similar to the B-47 canopy that the canopy intercepting area calculations of Table VI, (2) can be applied to the F-105, which indicates that the projected frontal area of the side windshields and of the main canopy each approach  $1 \text{ ft}^2$ . Flight test data indicate that charging rates of 10 to  $30 \mu\text{A}/\text{ft}^2$  are normal in ice-crystal clouds (3). Thus, if even only 10 percent of the projected frontal area of the canopy is effective in intercepting precipitation particles, currents of  $2 \mu\text{A}$  can be generated.

Many other potential sources of precipitation static interference were located. For example, corona discharges from the wing and tail airfoil extremities will cause serious interference. Corona noise from these sources can, of course, be reduced to acceptable levels through the

installation of passive dischargers on the airfoil extremities.

It is understood that the operational F-105 and other aircraft incorporating LORAN-D installations will be equipped with a pitot-static tube protruding forward from the radome. Experience on the SAAB Draken aircraft indicates that a pitot-static tube in this location reaches corona discharge threshold at very low airplane potential. Noise coupling to this point is high (probably higher than the coupling to the radome rim in Figure 6 would indicate--the ground test aircraft used a wing-tip-mounted pitot tube instead of a radome-mounted unit, so that direct measurements could not be made) so that corona discharges from the pitot-static tube will generate severe interference. A further difficulty with pitot tube corona is that if the corona threshold is indeed low, devising an acceptable fix is difficult since generally no modification of the pitot tube is permitted.

The ground tests demonstrate that streamer discharges occurring on the radome and on the plastic portion of the ventral fin can cause interference in the LORAN-D system. Surface resistance measurements on these surfaces on the ground test aircraft indicated that either a nonconducting rain erosion coating had been applied to them or that the conducting coating had deteriorated sufficiently that it was no longer serviceable (i.e., the surface resistance was so high that streamers could occur under typical precipitation charging conditions). (On the LORAN-D equipped aircraft therefore, it will be necessary to make certain that the coating on the ventral fin is actually conducting (resistivity of the order of 1 to 10 megohms per square).

In conclusion, it may be stated that, concurrent with LORAN-D system installation, anti-precipitation static techniques must be applied to the aircraft in question. In view of the subtlety of some noise generation and coupling mechanisms, the system flight test after installation should include flight through ice crystal clouds to ascertain that all of the noise sources have indeed been identified and adequately treated.

#### REFERENCES

1. R. L. Farnett and J. E. Nanevich, "Radio Noise Generated on Aircraft Surfaces," Final Report, Contract AF33(616)-2761, SRI Project 1267, Stanford Research Institute, Menlo Park, California (September 1956), AD 108 651

2. J. E. Nanevich, "A Study of Precipitation-Static Noise Generation in Aircraft Canopy Antennas," AFRCR-TN-57-583, Tech. Report 62, Contract AF 19(604)-1296, SRI Project 1197, Stanford Research Institute, Menlo Park, California (December 1957), AD 133 623.

3. J. E. Nanevich, E. F. Vance, R. L. Tanner, and G. R. Hilbers, "Development and Testing of Techniques for Precipitation Static Interference Reduction." ASD-TDR-62-38, Final Report, Contract AF 33(616)-6561, SRI Project 2848, Stanford Research Institute, Menlo Park, California (January 1962), AD 272 807.

4. R. L. Tanner and J. E. Nanevich, "Precipitation Charging and Corona-Generated Interference in Aircraft," Technical Report 73, SRI Project 2494, AFRL 336, Contract AF 19(604)-3458, Stanford Research Institute, Menlo Park, California (April 1961).

5. J. E. Nanevich, E. F. Vance, W. C. Wadsworth, and J. A. Martin, "Low-Altitude Long-Range All-Weather Vehicle Interference Investigation," Part I: Laboratory Investigation, Technical Report AFAL-TR-65-239, Part 1, Contract AF 33(615)-1934, SRI Project 5082, Stanford Research Institute, Menlo Park, California (August 1965).

6. Reference Data for Engineers, Fourth Edition, p. 762 (International Telephone & Telegraph Corporation, New York, New York 1956).

7. J. E. Nanevich, J. B. Chown, and W. C. Wadsworth, "F-105 LORAN-D Precipitation Static Problem" Final Report, Purchase Order m-33378 from Granger Associates, Palo Alto, Ca., SRI Project 7796, Stanford Research Institute, Menlo Park, California (March 1969).

# ILS/VOR Navigation and Approach Errors From Precipitation Static Interference

## Part I - Basic Concepts

J. D. Robb  
Lightning & Transients Research Institute

### ABSTRACT

Reports of precipitation static effects on VHF navigation receivers have resulted in some laboratory and in-flight investigations of the phenomena. The following mechanism is suggested for explaining the effect: the differences in the audio transient responses of the FM and AM channels in the VHF omni range audio navigation signal circuitry result in random but coherent output pulse pairs which are detected by the phase comparator circuitry as a true VOR station. The existence of the phenomena has been demonstrated and what is now required is data on the frequency of occurrence and types of equipment affected.

PRECIPITATION STATIC EFFECTS on VHF receivers were found to be very infrequent in the joint Army-Navy precipitation static research program, with which LTRI was associated in supplying special instrumentation and high voltage equipment (1)\*, as the effects lasted for only a matter of minutes and generally only under very severe snow charging or more often under thunderstorm electrical crossfield conditions (the presence of the aircraft in thunderstorm electrification regions). Because of the infrequent occurrence and short duration it was not considered to be a serious problem, particularly because of the relatively sparse air traffic in 1946 when the researches were carried out. Although much excellent work has since been done on precipitation static effects, particularly in the series of reports from Stanford Research Institute, such as (2), apparently little consideration has been given to precipitation static effects on VHF navigation receivers based apparently on the lack of reports of problems from the airline industry.

A number of reports received by LTRI several years ago again raised the question as to possible effects of precipitation static radio interference on VHF navigation systems. Upon inquiry, reports of temporary navigation receiver errors apparently attributable to precipitation static effects were received as illustrated in attached Appendix A. Laboratory tests made on general aviation VHF navigation receivers indicated that under some atmospheric electrical conditions, an erroneous semi-stable bearing indication could be observed on the Course Deviation Indicator (CDI) which gave no evidence that it was erroneous. It could be tracked and no error flag was evident. Some variation in the VOR error was noted but the

variations were sufficiently slow that they could not necessarily be observed by a pilot under instrument conditions.

It was suggested that some new investigations of VHF precipitation static should probably be carried out in view of continuing approach accidents which, although attributable to many other causes, should be considered in view of the demonstrated laboratory effects. The FAA reported that no evidence other than reports from LTRI could be found regarding such effects. Continued reports to LTRI still indicated a problem and discussions with Dayton Aircraft Products (DAP) of Fort Lauderdale, Florida resulted in DAP company funding a program. Their company aircraft was instrumented with electric field meters, and recording microammeters connected to several of the wick dischargers. It also included a DC power supply of 50,000 volts maximum, capable of charging the aircraft through a discharge probe consisting of a wick discharger in an insulated bushing. This is a standard research technique for simulating precipitation static self charge effects. With this installation it was found that the VOR localizer signals could be affected with definite course offsets which could be flown as if they were a true course but showing no error flag. The errors were not repeatable on different flights indicating that the mechanisms were not entirely understood.

It had been originally assumed that the effects would be present only under severe conditions of intense corona. But in-flight measurements on the DAP aircraft indicated that effects could be present with lower currents directly off the antenna, all of which will be discussed in Part II by Mr. Robert Truax. The system was shown to military R&D personnel and discussed with FAA personnel and was followed by the issuance of an FAA engineering report. (3)

Our present interest is to establish the extent of the problem and the type of equipment affected. The purpose of this report is to alert the aircraft industry as to a potential problem for consideration in the design of their own aircraft and radio navigation equipment.

### VOR SYSTEM OPERATION

In the VOR (VHF omni range) navigation system, two types of audio modulation signals are superimposed on the VHF carrier; an FM signal which is constant in all directions from the station and an AM signal whose phase with respect to the FM signal is varied with direction. Phase resolvers in the VOR receiver audio converter circuitry determine the phase difference between the two signals and thus

\*Numbers in parentheses designate References at end of paper.

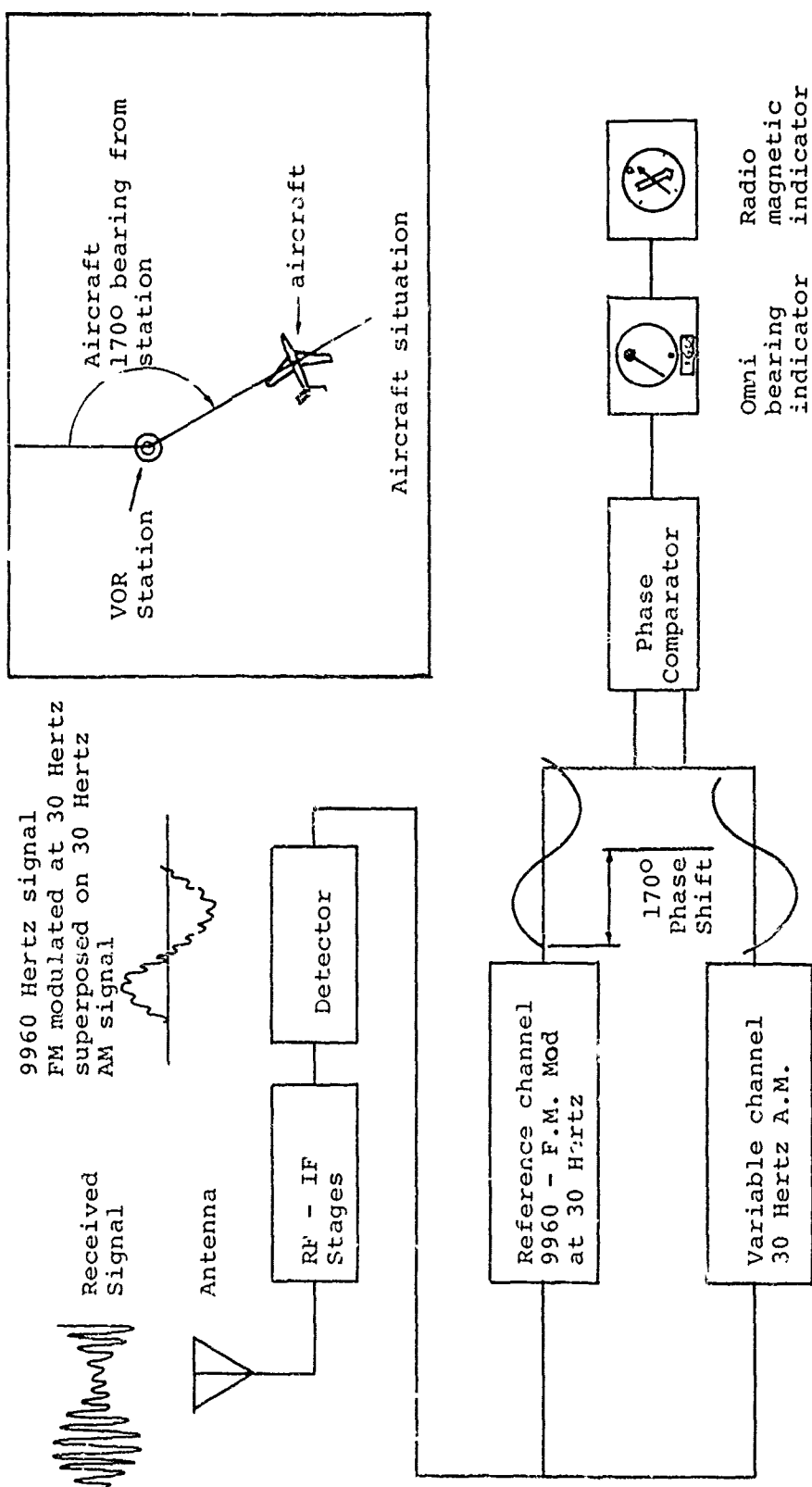


Figure 1. Block diagram VOR system operation.

determine the bearing of the aircraft from the ground base transmitter as illustrated in Figure 1.

#### PRECIPITATION STATIC WAVEFORMS

Nearly all papers published on the subject of precipitation static interference are presented in terms of a regular pulse train of Trichel negative corona pulses. The audio character of the signals, however, varies widely under actual precipitation static conditions. The descriptions from the original "Army-Navy Precipitation Static Project" publication for pilots described sounds of (1) frying eggs, (2) violins, (3) seltzer bottles, (4) the dumping of ashes, etc. This variability in natural precipitation static interference is also found in the variations observed in the laboratory generated precipitation static and points up the problem of attempting to reproduce it in the laboratory. Physical parameters which may effect the characteristics of the interference and the effects on VOR/ILS receivers probably include as a minimum electrode shape, air density, humidity and air velocity.

LTRI is attempting to relate the corona discharge phenomena of the various types to the pulse response waveforms in the aircraft receiver and to the audio pulses in VOR converter circuitry. The negative corona burst consists of electron avalanches induced under high electric field conditions from electrodes such as an aircraft antenna or a sharp metal wingtip. The individual pulse waveshapes may be described mathematically as a double exponential with an exponential front rising in less than 10 nanoseconds and an exponential tail decaying in approximately 100 nanoseconds as shown in Figure 2. The positive corona pulse, which is equally probable under thunderstorm conditions, has much slower rise and decay times but also must be considered in any study of VOR effects. The repetition rates will vary through a complete range from single discrete audio pulses in the receiver up to several megahertz. The Fourier output spectrum of the negative pulses shows spectrum content up into the UHF region of one-half gigahertz as shown in Figure 3. Corona waveshape variation with electrode shape and with altitude is shown in the oscillograms of Figure 4. (4) Effects on Automatic Direction Finders (ADF's) are shown in Figure 5. (5)

This interference is capable of reproducing nearly any known type of phase, amplitude or pulse modulation response in aircraft navigation, communication and digital data systems and is indistinguishable except for lack of intelligence from true modulated signals. The individual pulse discharges may not appear to be similar to the various navigation signals transmitted such as VOR transmissions but the receiver response can be.

Relative  
Amplitude

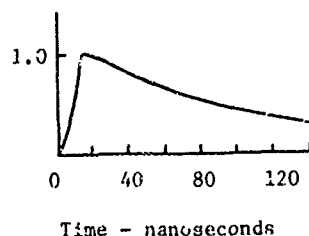


Figure 2. Waveshape of individual corona pulse - negative polarity.

Relative  
Amplitude

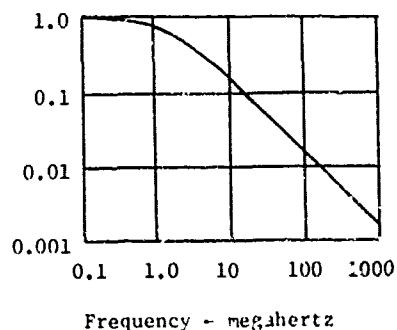


Figure 3. Fourier spectrum of corona pulse.

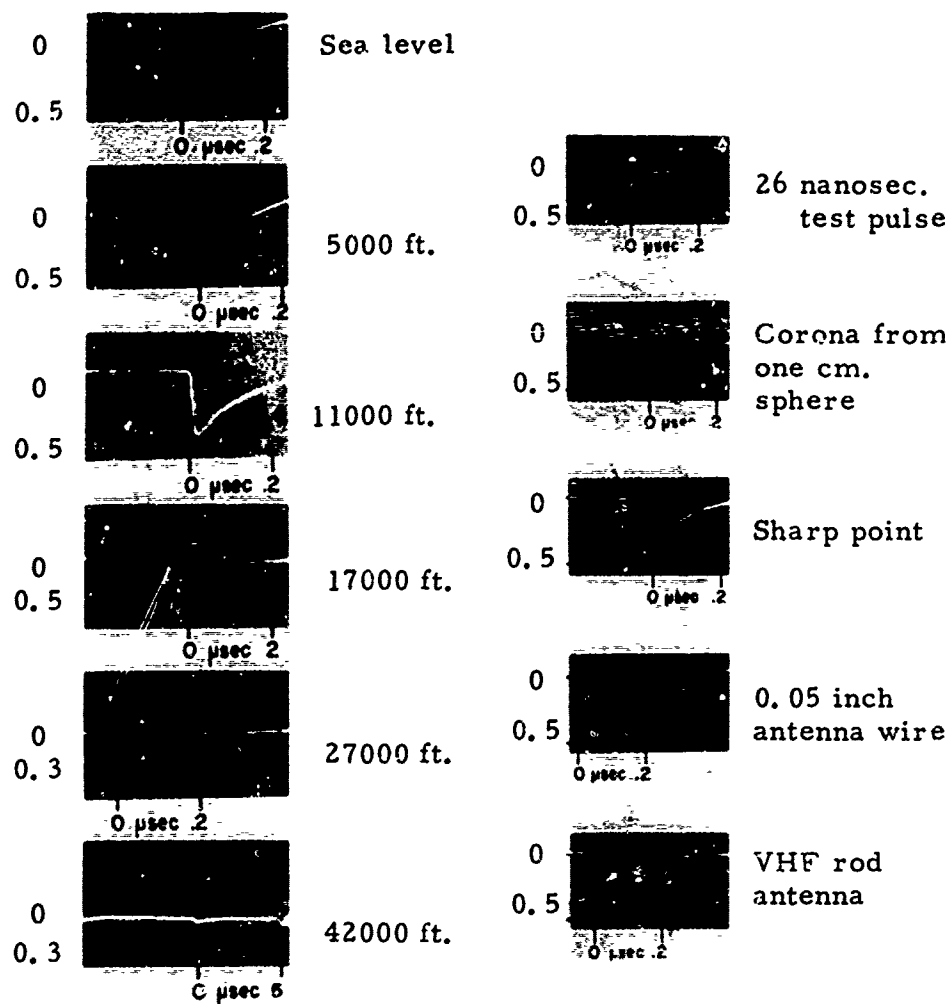


Figure 4. Corona waveform variation with altitude (left) and electrode type (right)

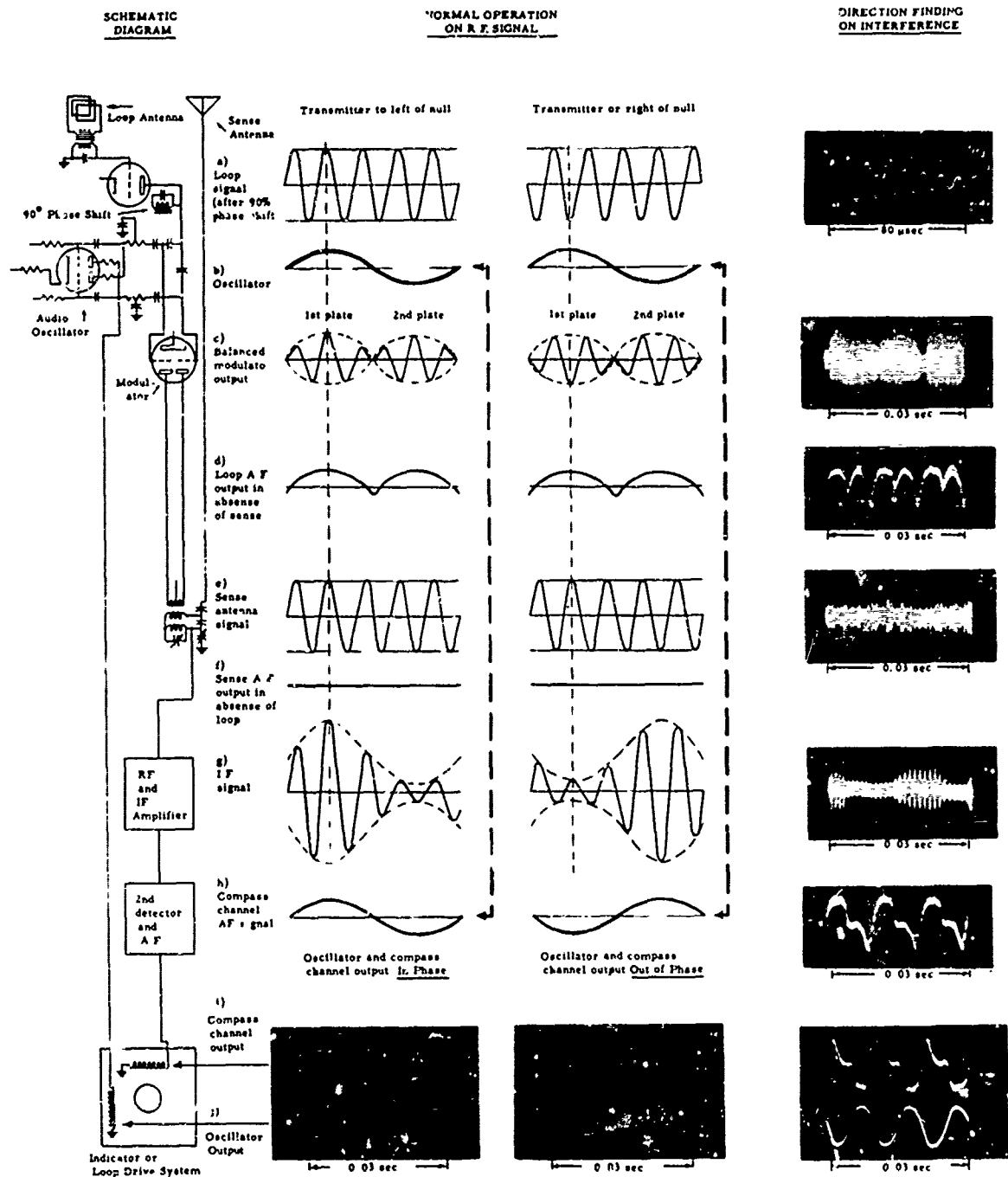


Figure 5. Schematic diagram of automatic radio compass direction finding on an interference source and on an RF signal.



## ERROR MECHANISMS

The brief studies to date indicate an error mechanism which is as follows: Under either strong external thunderstorm cross fields (exogenous conditions) or intense snow charging, with aircraft self potentials, (autogenous charging), the resultant electric field produces corona discharge avalanches off the antennas. These result in audio pulses out of the receiver which, after passing through the VOR converter, are shaped differently according to the audio transient response of the FM and AM channel circuitry. Thus, repetitive audio pulses into the VOR converter from a receiver will result in a fixed phase difference indication on the Course Deviation Indicator (CDI) on the instrument panel determined purely by the relative difference in transient response of the FM and AM channels. As the error flag circuitry is essentially also a phase comparator circuit (and in some cases detects only one channel), it will also indicate an apparently valid signal from the pulse waveform signals received and therefore show no error flag.

In flight, the resultant signal is a mixture of the interference signal and the station being received. The sum of the two input signals will vary with the aircraft bearing as a result of the part of the signal from the ground station which does vary with bearing, thus producing a trackable indication. False station passages are also indicated by erroneous "To-From" reversals. The receiver response is illustrated in Figure 6 and shows how the corona pulses are stretched out in the high Q IF stages to near millisecond duration from their original sub-microsecond lengths. The millisecond audio input pulses to the VOR converter result in pulse pairs from the converter which though random in spacing are coherent in time and phase and thus produce an omni bearing indication.

## EFFECTS OF MODERN NARROW BAND CIRCUITRY

It has been suggested that because of the almost continuously varying repetition rate from corona interference under either thunderstorm or friction charging conditions that narrow band audio filters used in the more modern VOR converter circuitry would not be susceptible to this type of interference. Preliminary tests in the laboratory have indicated the opposite and this may be understood in terms of corona pulse interference on basic receiver circuitry of any type. For example, major systems have been designed with extremely narrow IF band widths in order to reduce precipitation static interference but tests have indicated that they are much worse than standard receivers. This may be understood in terms of the non-linear circuit effects. If the receivers were truly linear, then the reduction of band width would improve receiver response in the presence of corona interference.

What actually occurs, however, is that the corona pulses produce crest pulse voltages of the order of one volt in receiver circuitry tuned to microvolts and shock excite the various tuned stages of the receiver into saturation. As a result the receiver responds with impulse responses corresponding to the corona pulses.

## CONCLUSIONS

Laboratory and in-flight investigations of precipitation static effects on VOR receivers have indicated that stable error signals can be introduced which can result in serious course errors during instrument approaches. The intensity of the effect does not depend upon the quality of the receiver but rather upon the chance selection of the VOR converter circuitry components which determine their relative transient response. Further studies are definitely needed for determining what types of equipment are affected and with what frequency of occurrence. Suggested preliminary approaches preventing this phenomenon or alerting the pilot are presented in the companion paper Part II.

## REFERENCES

1. R. Gunn et al., "Army-Navy Precipitation Static Project," Proc. IRE Vol. 34, Nos. 4 and 5 (1946).
2. J. E. Nanevich, E. F. Vance, R. L. Tanner, G. R. Hilbers, "Development and Testing of Techniques for Precipitation Static Interference Reduction," Final Report, USAF Contract AF33(616)-6561, January 1962.
3. D. S. Salmond, "Report of Effects of Precipitation Static on Airborne Navigation Systems," FAA Report No. FS-130-3, 15 October 1971.
4. M. M. Newman and J. D. Robb, "Aircraft Corona Variation With Altitude," Proceedings of the National Electronic Conference, Vol. 8, January 1953.
5. M. M. Newman and J. D. Robb, "Automatic Radio Compass Operation in the Presence of Interference," Appendix I, L&T Report #317, 3rd Interim Report, USAF Contract AF 33(616)-2459, December 1954.

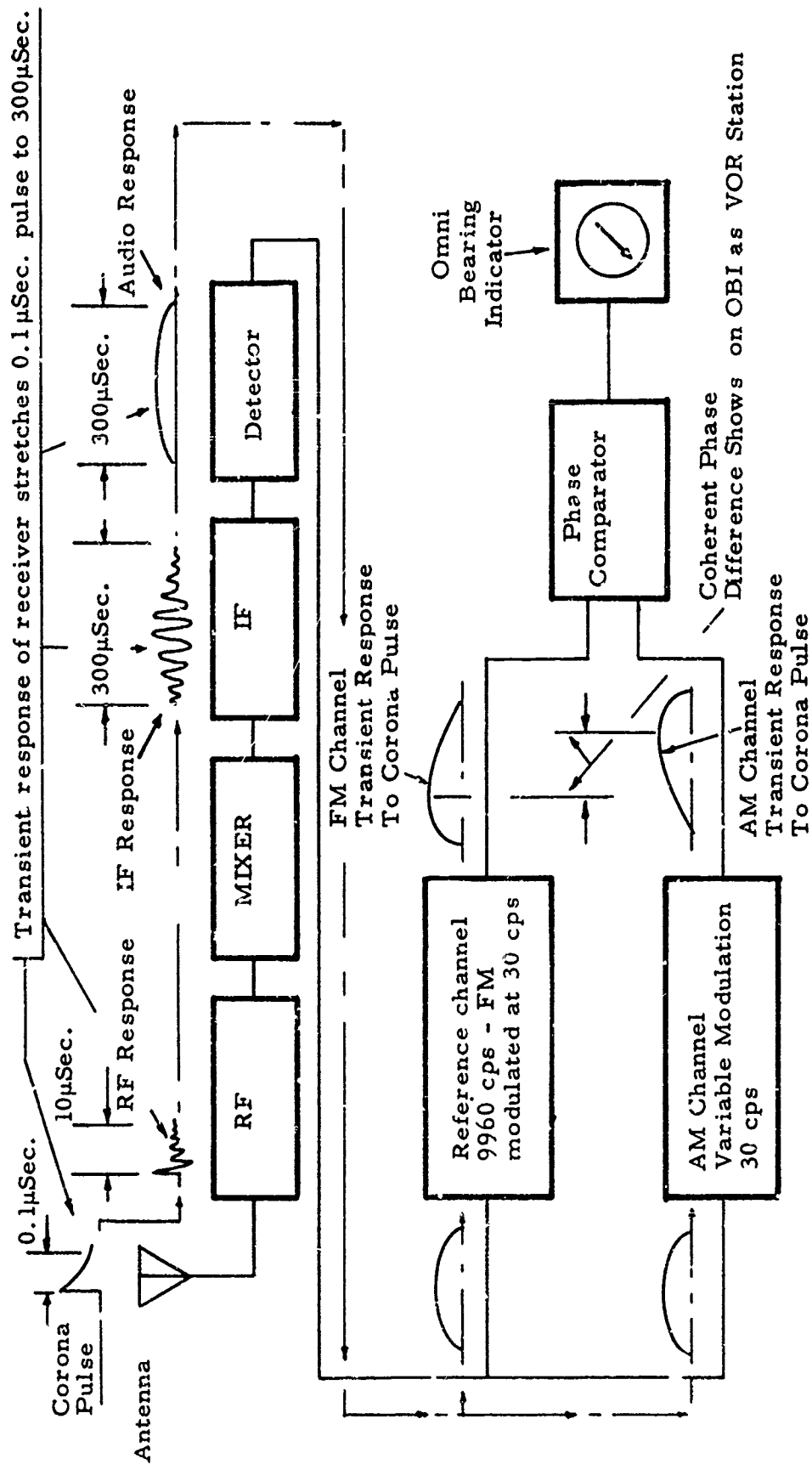


Figure 6. A suggested mechanism for VOR erroneous omni bearing indications from corona interference.

## IIS/VOR Navigation and Approach Errors- Part 2 Experimental Investigations

Robert L. Truax  
The Truax Company

### ABSTRACT

Localizer and VOR course errors, without appearance of a warning flag, due to corona discharge interference have been demonstrated in both the laboratory and in flight. Glide slope errors due to corona interference have not been investigated. However, the similarity between glide slope and Localizer signal processing gives cause to suspect that glide slope errors due to corona interference are possible. The Localizer and VOR course errors were most stable and repeatable under conditions of strong desired signal reception and relatively weak corona current conditions. Stable in-flight VOR course errors ranging from a few degrees to errors of up to 30 degrees have been observed and demonstrated. False To-From indications have been demonstrated in the laboratory. One Localizer Approach, with the aircraft artificially charged, was made by an Air Force pilot, and witnessed by an Air Force Aeronautical Systems Division engineer, which paralleled the actual approach course at a distance estimated to be eight to twelve miles--with the course needle centered and no evidence of a warning flag nor interference. In-flight data was obtained by using conventional, accepted artificial charging techniques. The errors were demonstrated using several general aviation navigation system types and the military AN/ARN-58.

VHF NAVIGATION COURSE ERRORS have been reported from time-to-time by various pilots. Some of these reports have come to the attention of LTRI and myself. Official recognition has been given to at least three causes of such errors. These recognized causes are: 1. aircraft flying over the ground Localizer antenna (1)\*; 2. temporary structural, or similar, interference in the near-field of VHF ground station antennas (2), and; 3. VHF multipath propagation (3).

These explanations, however, did not seem to fit all reported instances. Including observations of my own during actual instrument flight conditions since the early 1950's.

Unfortunately course errors under actual instrument flight conditions are difficult to identify and exact condi-

tions extremely difficult, if not impossible, to duplicate. But the emergence of a wide area radar coverage in the Air Traffic Control (ATC) system does reveal that course "deviations" in flight are not uncommon.

Professional pilots can recount times they've been told, "Radar shows you to be 'x' miles off the airway centerline." Yet, both VOR's agree that the aircraft is on the airway. And, the professionals comply with FAR 91.25, which requires a VOR accuracy check and record every 10 flight hours and 10 days. But, when the pilot checks his equipment again at flight termination, "It's still within limits."

"What do you report? Who do you report it to?"

Some reports and observations indicated that concurrent "P-Static" was evident.

VHF is not immune to P-Static interference!

Early reports, and subsequent work, states that VHF interference due to P-Static is less frequent than at lower frequencies (4). An analysis of the corona pulse waveforms indicates that the interference energy is down about 40 db at VHF navigation frequencies. But to receivers sensitive to signals of as little as 0.1 microvolts, at higher electrostatic charging rates the interference can disrupt reception. Arcing, or bonding, noise pulses have spectrums essentially flat in energy to 100 MHz.

DC-8 aircraft did indeed experience VHF P-Static interference in their early utilization (5).

LITERATURE RESEARCH showed that past investigations, and instrumentation, has been largely limited to reduction of electrostatic noise and the shock excitation of affected receiver front ends. With the exception of an ADF investigation by LTRI (6), past investigations have seemed to be concerned principally with voice or other aural communications. No information seems to be available on the effect of electrostatic interference on

\* Numbers in parentheses designate References at the end of Paper.

modern data signaling techniques. Yet the trend in aircraft communication and navigation has already largely removed the operator and pilot from the aural monitoring loop. This is evidenced by such common systems as Omega, LORAN, ADP, HF teletype, VOR, ILS, TACAN, DME and Transponders. And, recently there is much talk of future systems where ATC communication will be via data link, instead of voice.

Further, flight test in instrumented aircraft in two independent programs showed that electrostatic events were much more common during actual instrument flight conditions than previously indicated (7) (8). This is probably due to the facts that: 1. most recent research has been accomplished on jet aircraft which routinely operate above the weather, and; 2. civil and military operational aircraft are not instrumented to identify or record electrostatic events.

These factors led to laboratory, then flight, investigations of the possibility of electrostatic interference to VOR and Localizer signals. The flight investigation was possible only because at that time Dayton Aircraft Products, Inc. had an aircraft equipped with an artificial charging system and field mills that was being used to evaluate a new type of discharger.

THE RESULTS OF THE LABORATORY RESEARCH were briefly reported at the 1970 "Lightning and Static Electricity Conference." But the work was accomplished too late to be incorporated in the written paper.

The laboratory test configuration is shown in block diagram in Figure 1 of this paper.

Table 1 summarizes the data taken during the laboratory tests.

These tests were necessarily limited, since the VOR/LOC Navigation System and the Boonton H-14 Signal Generator were on loan. This also prohibited instrumenting the VOR/LOC system

to observe the mechanisms of the error generation.

However, the limited investigation proved that repeatable, stable course errors could be created by corona discharge interference. The VOR course needle could be centered during such interference by rotating the Omni Bearing Selector (OBS). It was also found that a To-From indicator reversal, or false station passage, could be caused. The magnitude of the course errors could be varied by changing the corona current.

In the Localizer mode, varying the corona current made it possible to move the indicator needle to the right or left. Or, to center the needle with an off-course signal from the Signal Generator.

In general it was noted that the errors were most stable, and a warning flag least likely, when a comparatively strong desired signal was present and a relatively weak corona current was used. Lower level desired signals and higher level corona currents resulted in erratic course indications and erratic or positive warning flag operation.

These laboratory tests were later duplicated in the Localizer mode, with the AN/ARN-58 at Wright-Patterson AFB. These latter tests were witnessed and conducted by several Air Force personnel at that time.

THE AIRBORNE COURSE ERROR INVESTIGATION was principally conducted in a Cessna 320 aircraft. This aircraft was equipped with a 0 to 50 KV artificial charging system and field mills. The aircraft also had dischargers and insulated antennas installed. Electrostatic voltages as high as 500 KV in cross field conditions and about 100 KV in snow had previously been measured on the aircraft.

The first attempts to introduce VOR/LOC errors were made with the dischargers and insulated antennas in-

Table 1-Laboratory data summary

Corona Current $\mu$ a	Signal Generator $\mu$ v	Course Error		Flag
		VOR	LOC	
0	10	no	no	yes
0	100	no	no	no
0	2,000	no	no	no
10	100	yes	yes	int*
10	2,000	yes	yes	no
20	100	yes	yes	yes
20	2,000	yes	yes	no
40	100	no	no	yes
40	2,000	no	no	yes

int\*=intermittant

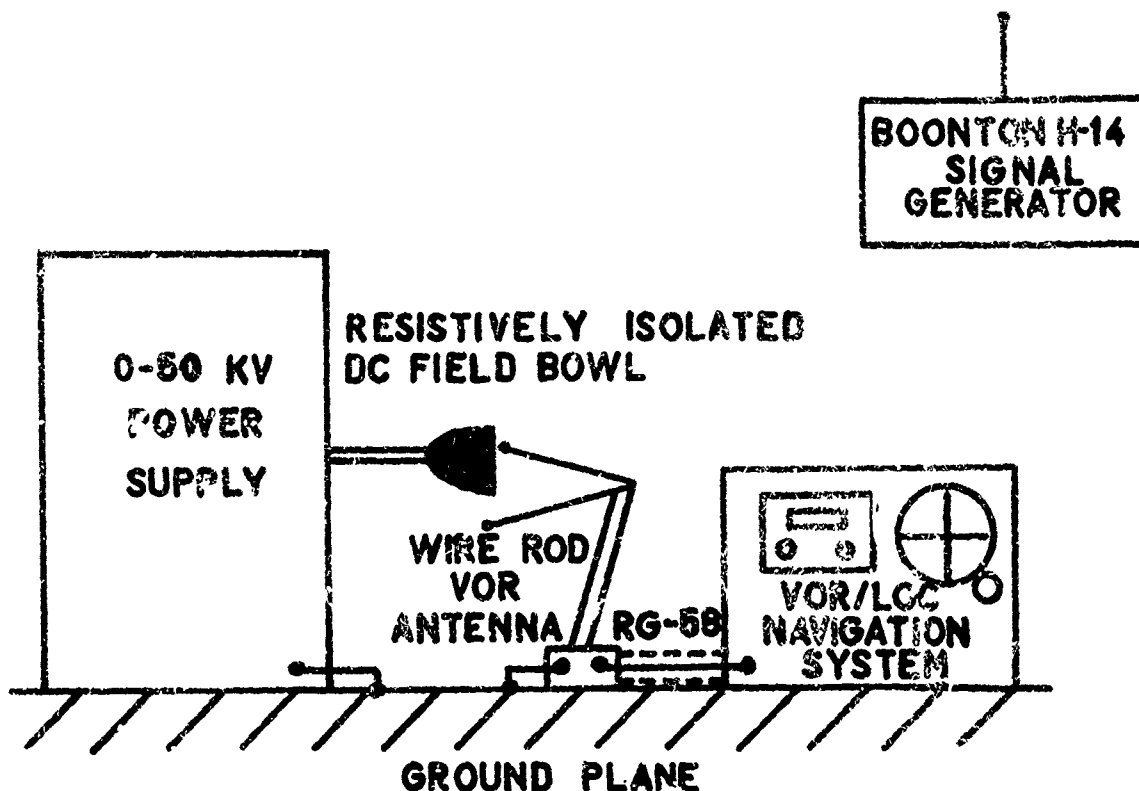


Fig. 1 LABORATORY TEST CONFIGURATION

stalled. They were unsuccessful, at least with the 50 KV artificial charging limitation.

The dischargers were then removed. Occasional course needle movements could be collated with switching the artificial charging system on and off at 50 KV. But the errors were very small, if any, and the data not repeatable.

A commercially available wire rod antenna was obtained. In still air at sea level and standard atmospheric conditions the corona threshold of this antenna was measured at 18 KV. The antenna was installed in a conventional location, for small aircraft, under the tail, just forward of the plastic tail cone.

With the dischargers removed, corona currents up to 20 microamperes at 50 KV were measured in flight. With dischargers installed no current from the antenna was obtained within the 50 KV power supply limitations. Later tests showed no evidence of VOR/LCC errors with dischargers installed and this potential limitation. Unfortunately antenna corona currents could not be measured with the antenna connected to the receiver.

Using the wire rod antenna and removing the dischargers, flight tests showed that repeatable VOR course errors, without warning flags, of up to 30 degrees could be achieved. Evidence of these course errors were demonstrated in flight to Air Force engineers.

On one occasion 12 VOR approaches were flown to the Palm Beach International airport. The first 3 were for calibration with the artificial charging system off. All three were to Minimum Descent Altitude (MDA) and brought the aircraft over the runway, within the runway width. The final approach was made under the same conditions, with identical results.

The other 8 approaches were flown with the artificial charging system set at 35 to 40 KV and indicating about 20 microamperes of current. These approaches all took the aircraft directly over the VOR ground station, but were terminated at the MDA outside the airport boundaries. The final approach path appeared to be identical in each instance.

Figure 2 indicates the aircraft's flight path during the approaches when course errors were experienced. Note on the approach plate comprising Fig-

**PALM BEACH INTERNATIONAL**  
WEST PALM BEACH, FLORIDA



ure 2 that the VOR is situated only 2.8 nautical miles from the runway threshold.

A very brief flight test was conducted under similar circumstances with the VOR 30 Hz variable phase channel monitored on an oscilloscope. A definite phase shift could be observed. At other times the signal appeared to have a second harmonic type distortion. Unfortunately the oscilloscope was not equipped to obtain photographic records.

The aircraft's approximate flight path during the most dramatic Localizer course error is portrayed in Figure 3.

This flight was especially intriguing because of the circumstances under which it occurred. Major Johnson, Wright-Patterson AFB Flight Safety Officer was flying the aircraft and I occupied the copilot seat. John Robb, LTRI and Charley Seth, ERVCC, Air Force occupied the cabin with the artificial charging system.

We had departed the Dayton VOR, cleared for an ILS approach to the Dayton Municipal Airport. The approach was intended to be a calibration approach to demonstrate that the airborne and ground equipment were operating properly.

Unbeknownst to the flight crew the artificial charging system was turned on by Robb to demonstrate its operation.

The course needle centered and Major Johnson turned to his final approach heading and descended to the initial approach altitude. Further descent was not made since the outer marker was never received. After the time to reach the field had elapsed, Approach Control called and asked our intentions, advising us, "Radar shows you to be 12 miles northeast of Dayton Airport."

Visibility was about 5 miles in haze. We'd flown past the airport on the apparent ILS centerline, without even seeing the runway! We later estimate that we'd paralleled the actual ILS course at a distance laterally of about 8 miles.

THE FAA WAS ADVISED immediately when the course errors were demonstrated in the laboratory. They were further advised of the results of the flight tests.

But before further demonstrations could be made the local FAA General Aviation District Office (GADO) advised that the aircraft would have to be

licensed in the Experimental Category or the equipment removed. The alternative was a very expensive time-consuming Supplemental Type Certificate (STC). Investigation revealed that any later modification or change would require additional STC action. The GADO would not even permit the dischargers to be installed without Experimental or STC action. This effectively ended the research.

Proposals were made to the FAA by LTRI and The Truax Company to extend the knowledge obtained in these tests. The FAA declined the proposals giving as their reasons the lack of reported errors due to this cause (not surprising, since aircraft are not equipped to identify electrostatic occurrences) and the Literature Search attributed to the FAA in the bibliography at the end of this paper.

RELATED TO THE FREQUENCY OF CHARGING OCCURRENCES, The Truax Company Beechcraft Bonanza was instrumented to measure corona discharge from a wire rod VHF communications antenna. The sensitivity of the antenna insulation failure detector was set at 150 microampere-seconds. On one 55 minute flight in typical Florida cumulus and scattered thunderstorm conditions the corona current from the VHF antenna exceeded that level 9 times. Of especial interest, 4 of the occurrences were inside the outer marker on an ILS approach to Fort Lauderdale International Airport. Figure 4 pictures a similar antenna insulation failure detector.

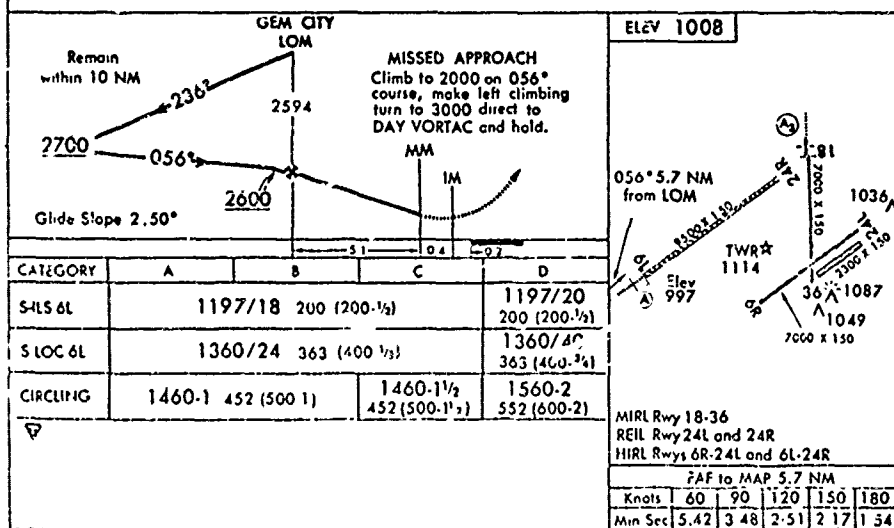
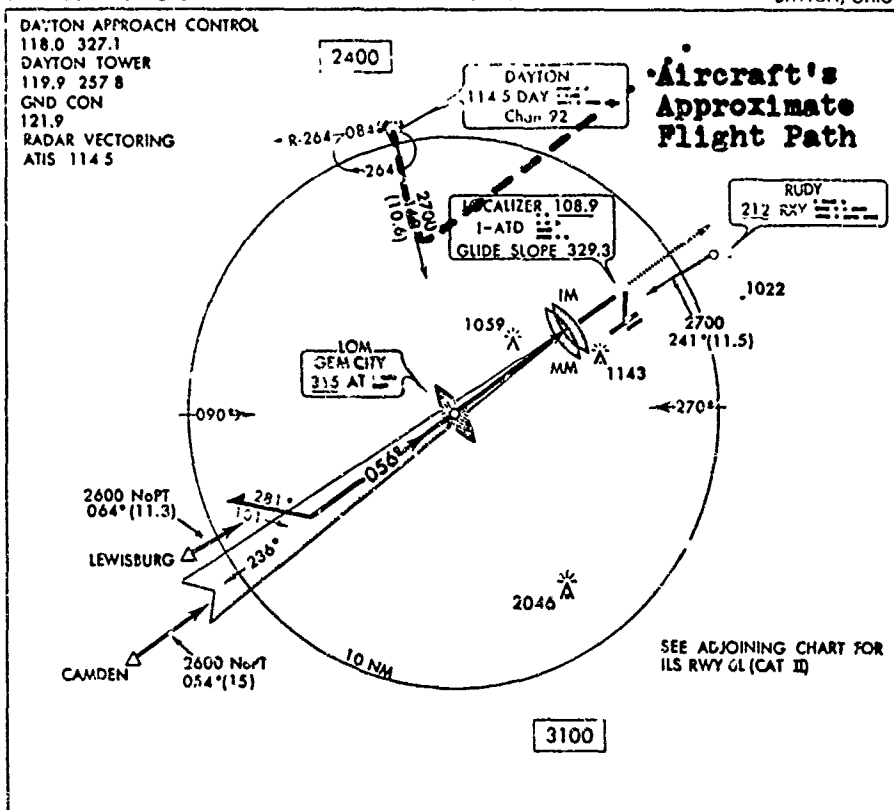
IN CONCLUSION, errors to VOR and Localizer equipments can result from electrostatic interference. This has been demonstrated in the laboratory and in flight.

The work thus begun should be extended in both laboratory and flight conditions--including known conditions

# ILS RWY 6L

AL-107 (FAA)

JAMES M. COX-DA...ON MUNI  
DAYTON, OHIO



ILS RWY 6L

2 MAR 1972

39°54'N - 84°13'W

PUBLISHED BY NOS NOAA TO THE PUBLIC

JAMES M. COX DAYTON MUNI

Fig. 3 AIRCRAFT'S APPROXIMATE GROUND TRACK WITH LOCALIZER COURSE ERROR





Fig. 4 ANTENNA INSULATION FAILURE DETECTOR

of natural charging events. Once sufficient knowledge is obtained, navigation systems should be designed that are immune to such interference or at least warn aircrews of its presence.

Probably, in light of the research reported in these present papers, all airborne data type communications and navigation systems should be investigated for susceptibility to errors under electrostatic interference conditions. At least from VLF through L-band frequencies, where such interference has already been observed.

Flight test work in an appropriately instrumented aircraft should be continued. This will require a military aircraft which is exempt from the Federal Air Regulations. Or, a waiver from the FAA of FAR 91.42 (a), (2) and (d), (2) for a civil aircraft, so it can be flown in actual instrument conditions and for compensation, as an Experimental aircraft.

Lastly, standards are long overdue for qualification of dischargers for use on IFR aircraft. Also, for implementation of other proven, accepted electrostatic noise reduction techniques, such as, use of insulated antennas and resistive coatings on plastic frontal surfaces (9) (10).

#### REFERENCES

1. DOT, FAA, "Instrument Flying Handbook," AC 61-27B.
2. Superintendent of Documents, "Airman's Information Manual, Part 3, Notices to Airman."
3. DOT, FAA, "Course Needle Oscillations on VHF Omnidirectional (VOR) Receivers," AC No. 91-18.
4. R. Gunn et al, "Army-Navy Precipitation Static Project," Proc. IRE 34, 4 and 5 (1946).
5. R. L. Tanner and J. E. Nanevich, "Precipitation Charging and Corona-Generated Interference in Aircraft," AFRCL 336, Contract AF 19 (604)-3458.
6. M. M. Newman and J. D. Robb, "Automatic Radio Compass Operation in the Presence of Interference," L & T #317, Contract AF 33(616)-249.
7. R. L. Truax, "Electrostatic Charging and Noise Quieting," Paper No. 700926, 1970 Lightning and Static Electricity Conference.
8. N. Ray and D. Decker, "P-3 Aircraft Preliminary Electrostatic White Noise Investigation," Report No. WST-185R-71, Contract N00421-71-C-6250.
9. DOT, FAA, "Reduction of Precipitation Static Interference in Aircraft," DO-5, 68-47, May 19, 1947.
10. D. S. Salmond, DOT, FAA, "Report of Effects of Precipitation Static

on Airborne Navigation Systems," Report No. FS-130-3.

#### FAA CITED LITERATURE SEARCH RE: "ELECTROSTATIC VOR/ILS COURSE ERRORS"

1. D. C. Hogg, "Satellite Communications and Atmospheric Water-Prent and Future," Aug. 29-Sep. 6, 1969, Proceedings P.1-5.
2. G. Flachenecker, "A Lightning Protected Transistorized Receiving Antenna," Nachrichten Technische Zeitschrift, Vol. 22, P. 557-564.
3. S. V. C. Aiyar and S. J. Bhat, "VHF Atmospheric Radio Noise," Institution of Telecommunication Engineers, Journal, Vol. 15, P. 293, 294.
4. K. S. McCormick and J. I. Strickland, "Slant Path Microwave Attenuation Due to Precipitation," IEEE, Proc. Sep. 30-Oct. 2, 1968.
5. J. E. Nanevich and E. F. Vance, "Precipitation Static Interference on Aircraft in the Mach 1 to Mach 4 Speed Range," IEEE, Supplement, Vol. AES-3, P. 628-638.
6. J. V. N. Granger, "Precipitation Static Protection for Jet Aircraft, Summary Report."
7. R. K. Crane, "Simultaneous Radar and Radiometer Measurements of Rain Shower structure," Lincoln Lab, MIT.
8. R. K. Crane, "A Comparison Between Monostatic and Bistatic Scattering from Rain and Thin Turbulent Layers," Lincoln Lab., MIT.
9. K. A. Moore, "Precipitation Static Noise Problems on Operational Aircraft," 1968 Lightning and Static Electricity Conference.
10. E. B. Minihan and M. E. Rogers, "Correlation of DECCA VHF Equipment Malfunctions with Degree of Static Activity Recorded During Flights with an S61N Helicopter in Thunderstorm Conditions," RAE, Farnborough, England.
11. L. T. Tushkov, "Thermal Radio Emission from an Ice Cover in the UHF-Band," Aztec School of Languages, Inc. Maynard, Mass.
12. B. G. Kutuza, "Experimental Investigation of Attenuation and Radio Emission from Rain in the UHF-Band," Aztec School of Languages, Inc., Maynard, Mass.
13. A. S. Dennis, "The Scattering of the Radio Waves by Hail and Wet Snow, Final Report," SRI, Menlo Park, Ca.
14. N. W. Ray and W. T. Walker, "Lightning Protection Improvements and Precipitation Static Noise Quieting Investigation of the P-3 Aircraft, Interim Report," NATC, Patuxent River, Md.

15. R. V. Grossang, "F-4D Precipitation Static Flight Test, Final Report," 10 Aug. 1970-2 Jan. 1971.

16. J. W. Curtis and T. A. Ryan, Elimination and Generation of Air Vehicle Precipitation Static Noise for the XB-70," North American Aviation, Inc., Los Angeles, Ca.

17. P. F. Weilminster, "Feasibility of using Radioisotopes for Elimination or Reduction of Precipitation Static Problems as Related to Aircraft" AFSC, Wright Patterson, AFB.

## Conductive Polymeric Coatings for Combined Anti Static Properties and Erosion Resistance

George F. Schmitt, Jr.  
Air Force Materials Laboratory

### ABSTRACT

The complexities involved in development of conductive coatings having subsonic rain erosion resistance, good dielectric transmission properties, and ease of applicability are described. Carbon black-pigmented elastomeric polymeric coatings having surface resistivity of 0.5 to 15 megohms per square, dielectric constant of 3.5, loss tangent of 0.060, and one-way power transmission of 92.8% at 9.375 GHz at room temperature for precipitation static discharge and static electricity protection have been developed.

The critical effects of pigment loading and coating formulation on the conductive surface characteristics of the applied coating are discussed.

DAMAGE TO reinforced composite materials because of precipitation static discharge during flight has long been a problem for aircraft operations. This damage is in the form of burn-through spots or holes on honeycomb laminate skins which may be serious enough to structurally weaken the structure or provide a path for moisture to get into the core of the honeycomb. The presence of moisture in the core disrupts the electrical transmission properties and the radar does not perform as designed.

Another problem associated with nonmetallic structures is that of static charge build-up during flight with subsequent discharge when contacted by personnel on the ground. A serious hazard exists in this area as is well known. In addition the generation of broadband radio frequency noise by triboelectric contact with precipitation, cross fields, and engine produced ionization is a major problem. Streamer currents, corona discharge and arcing between structural members are phenomena resulting from charging during flight (1).

Conductive coatings applied to the surface of non-metallic structures provide a means of reducing or eliminating the precipitation static and static electricity problems. However, any exposed reinforced composite structure absolutely requires rain erosion protection. Elastomeric coatings which provide this erosion resistance must be formulated with conductive pigments for antistatic

protection while maintaining dielectric transmission and substantial erosion resistance. Other necessary properties are good weatherability including retention of rain erosion resistance, transmission properties, and surface resistivity after prolonged outdoor exposure and appropriate application techniques and cure properties. Repair of the coatings themselves as well as strippability, if the coating must be removed, are also required (2).

The incorporation of these requirements and coatings developments to fulfill them are discussed below.

### MATERIALS DEVELOPMENTS

DIELECTRIC TRANSMISSION AND CONDUCTIVITY - Approximately fifteen years ago when the first antistatic coatings for non-metallic structures were developed, coatings of varying levels of conductivity, typically expressed as surface resistivity and measured by a megohmmeter, were formulated with different amounts of carbon black pigments and these were flight tested in service (3). Those with a surface resistivity of 0.5 to 15 megohms provided the appropriate degree of antistatic protection for the radomes and this was adopted in Specification MIL-C-7439B.

When the current MIL-Spec polyurethane erosion resistant coatings were being developed in 1967-1968 it was determined that the same values of surface resistivity would still be appropriate to provide sufficient protection against static charge buildup. To obtain a proper level of surface resistivity, 0.5-15 megohms, the MIL-C-83231 Type II polyurethane coating, were pigmented with sufficient conductive carbon black to attain this resistivity. Greater or lesser amounts resulted in too much or too little conductivity.

The effect of pigmentation level on the conductivity (surface resistivity) and dielectric transmission properties of the coating is shown in Table I and Figure 1. The conductivity (inverse of the resistivity) was achieved with a pigment loading of 5-7% (based on vehicle solids) which provided acceptable transmission properties of

TABLE I  
SURFACE RESISTIVITY AND TRANSMISSION AS A  
FUNCTION OF PIGMENT LOADING

Panel No.	Percentage of Carbon Black Pigment <sup>*</sup>	Surface Conductivity <sup>**</sup> (Megohms <sup>-1</sup> )	Dielectric Transmission (%) <sup>***</sup>
A	5	0.04	92.3
B	6	0.167 - 0.25	93.0
C	7	1.0	-
D	10	33.3	91.9
E	7 (10 mils thick)	1.0	88.0

\* Carbon black is Vulcan XC-72R

Panels A through D and 10 mils of clear polyurethane plus 2 mils of pigmented carbon black topcoat

Panel E is 10 mils of 7% carbon black coating only

\*\* Reciprocal of surface resistivity measured with 500 volt DC megohm bridge.

\*\*\* At 9,375 GHz and room temperature as a percentage of transmission through a bare control panel.

TABLE II  
\* ELECTRICAL CONDUCTIVITY OF FLUOROCARBON FORMULATIONS

Fluorocarbon A				100
Carbon Black A				25
Magnesium Oxide A				15
				Conductive
Fluorocarbon A	100	100	AF-C-935	100
Carbon Black B	10	15	100	100
Magnesium Oxide A	5	5	20	20
	Non-Cond.	Non-Cond.	5	15
			Conductive	Conductive
Fluorocarbon A			100	100
Carbon Black B			20	25
Magnesium Oxide B			10	15
			Non-Cond.	Non-Cond.
Fluorocarbon A	100		100	
Carbon Black B	10		20	
Zinc Oxide	10		10	
	Non-Cond.		Non-Cond.	
Fluorocarbon A	100		100	
Carbon Black B	10		20	
			Blisters	
			Conductive	
Fluorocarbon	100		100	
Carbon Black B	10		20	
	Non-Cond.		Erodes	
			Conductive	

\* Measured with Megohmmeter - Model No. 5C-1000 - The Winslow Company, and spring-loaded probes spaced 6 inches apart.

Conductive - measurement of 0.1-15 megohms/square

Non-Conductive - measurement of infinite resistivity.

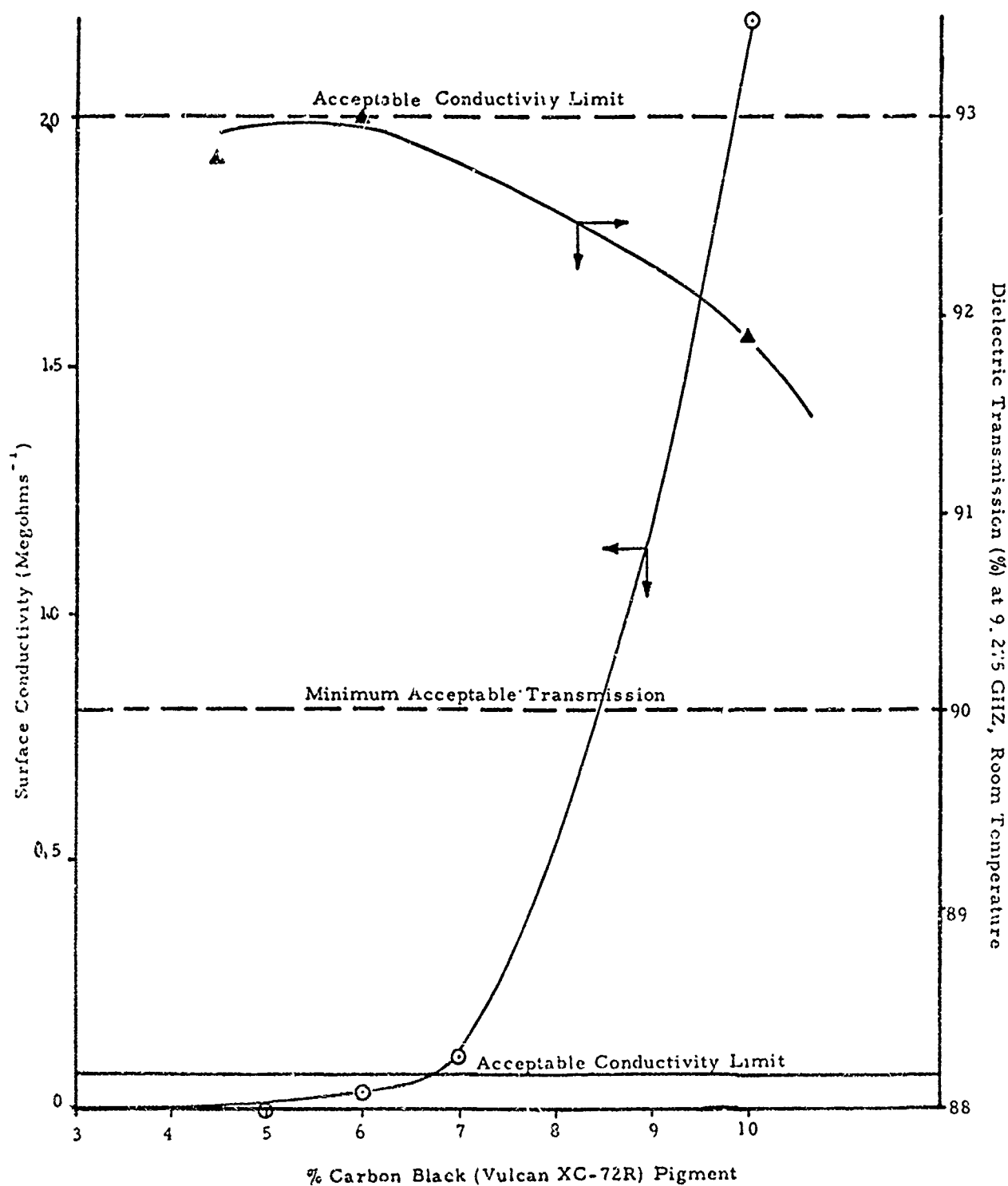


Figure 1. Surface Conductivity and Transmission vs. % Carbon Black Pigment in Polyurethane Coating

92.3 - 92%. With proper dispersion techniques, 5% by weight loading of carbon black gave acceptable resistivity; this was incorporated into a topcoat of the polyurethane base resin. This topcoat is applied in a 2 mil thickness over 10 mils base coating which contains 1/8% carbon black for coloration only. This approach maximized the erosion resistance of the antistatic coating system since the use of 5% black polyurethane for the full 12 mil thickness would result in less erosion resistance (because the presence of a high loading of pigment or filler invariably reduces the erosion resistance) and would reduce the transmission properties (because of the amount of conductive carbon in a 12 mil thick coating) to an unacceptable level (6). For example formulation C in Table I when applied at 10 mils total thickness gave only 88.0% transmission at 9.375 GHz, room temperature. This is an unacceptable degradation in the radar transmission properties.

Only Vulcan XC-72R conductive carbon black from Cabot Corporation provided a conductive coating at 5% weight loading.

As can be seen in Figure 1 only a narrow range of pigmentation levels existed which would provide anti-static conductivity levels and still maintain acceptable dielectric transmission properties.

A similar approach was employed in developing the high temperature fluorocarbon erosion resistant coating (AF-C-934) and antistatic topcoat (AF-C-935) (2), which has a resistivity of 0.5-15 megohms. The fluorocarbon coatings contain minimum levels of carbon black and magnesium oxide (which serves as a stabilizer for the curing reactions) fillers to maximize erosion performance. With the fluorocarbon system a loading of 20% weight carbon black based on vehicle solids was necessary. The influence and interaction of conductive pigment and fillers on the coatings surface electrical properties is illustrated in Table II. Note in the first column that the formulation is not conductive with 10% carbon black regardless of other type of filler (magnesium oxide or zinc oxide). In the second row across, the carbon black loading must be increased to 20% to provide a conductive coating but that once this level of pigmentation is utilized, the stabilizing filler can be increased to 15% and the coating remains conductive. However, if a magnesium oxide which mask the effect of the carbon black is used (See third row of Table II), even increasing the carbon black to 25% does not result in a conductive coating. The substitution of zinc oxide for magnesium oxide as a

stabilizer for the curing reactions reduces the conductivity to an unacceptable level as shown in row 5 of Table II.

Attempts were made to formulate conductive coatings without the stabilizing filler using two different fluorocarbon polymers but the coatings were unacceptable from inadequate cure, blistering and erosion standpoints.

The optimum formulation for the antistatic erosion coating is shown in the table as AF-C-935. This fluorocarbon is applied in a 2 mil thickness over the base fluorocarbon coating which is 10 mils thick.

**EROSION RESISTANCE** - One of the keys to developing elastomeric coatings which exhibit the greatest erosion resistance is the extensive use of rotating arm apparatus to characterize the dynamic response of these coatings to the rain environment. One rotating arm is located at the Air Force Materials Laboratory (4). In these experiments the coated materials specimens are fastened on the tips of a propeller-like blade, spun at velocities of 500 MPH typically, through artificial rain (at AFML, 1.0 inch/hour simulated intensity of 1.8 mm diameter drops) which impinges on the surface. The specimens are exposed in this environment until failure of the coating by penetration to the substrate, which is determined by observation of the specimens while running through use of a stroboscopic light and closed circuit TV camera (See Figure 1). The performance of coatings in the rotating arm apparatus has been correlated to actual flight test results both as to rankings of various materials and the actual modes of failure of the materials themselves.

The coating penetration phenomenon caused by continued droplet impingement on the surface varies for different types of coatings (5). For example, neoprene coatings gradually wear away with a true erosion phenomenon on the surface. Epoxy or polyester coatings possess no erosion resistance at all and fail by brittle rupture of the coating. Polyurethanes do not erode on the surface but suffer localized failures at a weak spot in the substrate under the coating or at a defect in the coating surface after prolonged exposure. This has been noted for polyurethane-coated glass-epoxy laminates where under long exposure times (up to 180 minutes), the failure is the result of eventual crushing and breakdown of the laminate by repeated water droplet impacts. The neoprene coating does not have even sufficient

strength to withstand the water impact like the urethane and hence tears with subsequent droplets causing massive damage to the laminate when the neoprene is removed. The fluorocarbon erodes in much the same manner as the neoprene but withstands rain impingement longer.

The erosion performance of these coatings is compared as a function of thickness in Figure 2. As may be seen, the polyurethanes offer at least five times the erosion resistance of the neoprene and reports from actual service tests indicate up to a tenfold improvement in life of the coating during repeated flight exposure. The failure times for a 0.012" polyurethane on glass-epoxy laminates are 120-160 minutes at 500 MPH in 1 inch/hour simulated rainfall (AFML rig) compared to 40 minutes for the neoprene and 55 minutes for the fluorocarbon in the same conditions. The 12 mils thickness is a minimum for attainment of any substantial erosion resistance; at thinner sections, elastomeric coatings fail rapidly in the rain environment.

A summary of properties of the rain erosion resistant elastomeric radome coatings is given in Table III. See Figure 3 for a photograph of a C-141 radome coated with antistatic MIL-C-83231 Type II polyurethane showing the aluminum lightning arrestor strips (6).

**WEATHERING AND APPLICATION** - The ability of the elastomeric erosion coatings to maintain their conductivity and erosion resistance after prolonged outdoor weathering is a key requirement. The most serious deficiency in the old MIL-C-7349B neoprene coatings was their embrittlement within a short time, 2-3 months with loss of erosion resistance and loss of conductive properties. Although the mechanism whereby this conductivity change occurs, whether polymer degradation, pigment migration, or other chemical change, is unknown, the weathered neoprene coatings would no longer provide precipitation static or static discharge protection.

The newly developed coatings, MIL-C-83231 polyurethane and high temperature fluorocarbon, are more stable to the ultraviolet light, ozone, and adverse weather effects and exhibit little change in erosion resistance, transmission properties or surface resistivity even after a year of Florida weathering (7). This is important because the maintenance of their resiliency is the key to providing erosion protection.

For application of the coating, sprayability is essential. Furthermore, rapid build-up of coating, minimum time between

coats, and cure at room temperature are desirable. If recoating becomes necessary (in many cases because of ground-caused damage, not erosion or static burn-through) a system for stripping the coating must exist. Such procedures have been developed for all erosion coatings.

## CONCLUSIONS

Coatings for precipitation static and static electricity discharge protection of nonmetallic reinforced composites must combine conductivity, rain erosion resistance, radar transmission properties, weatherability and ease of application and repair.

Two layer coatings based upon neoprene, polyurethane, and fluorocarbon elastomers pigmented with carbon black have been developed to provide an optimum combination of these properties.

Polyurethane (MIL-C-83231) and fluorocarbon (AF-C-934 and AF-C-935) erosion coatings provide long term resistance to degradation by outdoor weathering while the neoprene (MIL-C-7439B) degrades rapidly.

By properly selecting conductive carbon blacks and stabilizing oxide fillers, conductive fluorocarbon coatings can be formulated which maintain their erosion resistance and other properties.

The amount of carbon black in conductive erosion resistant topcoats governs the electrical transmission of the erosion protective coating system (basecoat plus topcoat).

## REFERENCES

1. R. L. Truax, "Electrostatic Charging and Noise Quieting," 1970 Lightning and Static Electricity Conference, 9-11 December 1970, pp 157-174.
2. G. F. Schmitt, Jr. "Synthesis of Elevated Temperature Resistant, Erosion Resistant Polymeric Coatings," Proceedings of the Eleventh Symposium on Electromagnetic Windows, Air Force Avionics Laboratory Georgia Institute of Technology, August 1972.
3. R. T. Schwartz, Private Communication, August 1969.
4. C. J. Hurley and G. F. Schmitt, Jr., "Development and Calibration of a Mach 1.2 Rain Erosion Test Apparatus", Air Force Materials Laboratory, Technical Report AFML-TR-70-240, October 1970.
5. G. F. Schmitt, Jr. "Erosion Behavior of Polymeric Coatings and Composites at Subsonic Velocities," Proceedings of the Third International Conference on Rain Erosion and



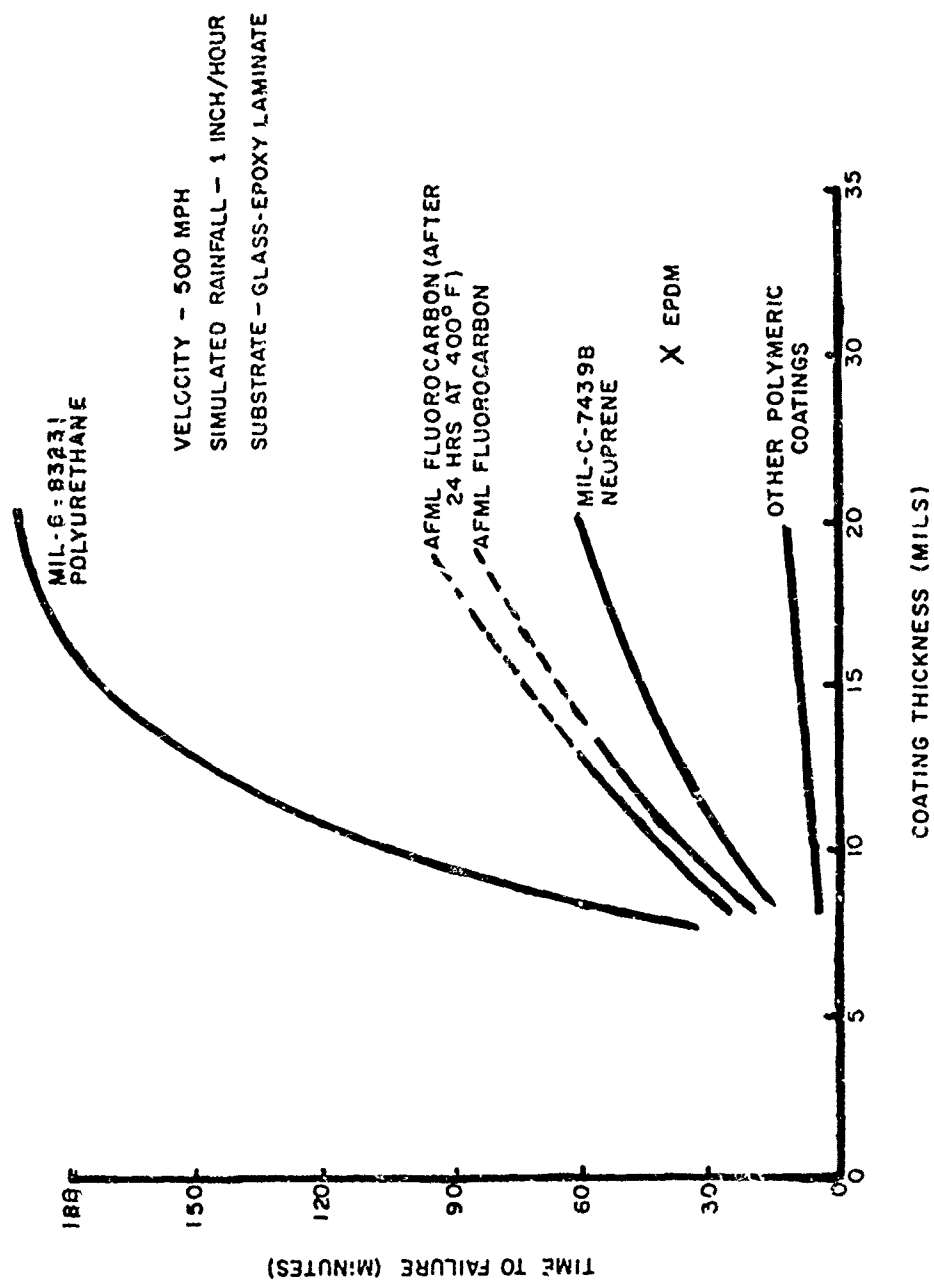


Figure 2 Comparison of Polymeric Coatings Performance in Rotating Arm Apparatus

TABLE III

Coating	Dielectric Constant	Loss (1) Tangent	One way power		Surface (3)		Erosion (4)	
			Transmission (%)		Resistivity (megohms/sq)		Resistance	
			Initial	Aft 6 mos Fla weather	Initial	Aft 6 mos Fla weather	Initial	Aft 6 mos Fla weather
MIL-C-7439B Neopren Type II	3.11	0.047	98.8	97.6	30	0	40.0	25.0
MIL-C-83231 Polyurethane Type I	3.16	0.059	93.4	93.4	-	-	165	180.0
MIL-C-83231 Polyurethane Type II Antistatic	-	-	92.8	91.6	5	0.8	165	180.0
AF-C-934 Fluorocarbon Type I	3.77	0.055	94.0	92.0	0.5-15	0.5-15	55	70
AF-C-935 Fluorocarbon Type II Antistatic	-	-	90.5	90.0	0.5-15	0.5-15	60	70

(1) Room temperature at 9.375 GHZ

(2) % Transmission relative to blank panel at 9.375 GHZ (20° Parallel) at room temp.

(3) Measured with Megohmmeter Model No. 56-1000 - The Winslow Company and spring loaded probes spaced 6 inches apart.

(4) In minutes to failure at 500 MPH, 1 inch/hour simulated rainfall (1.8 mm dia drops)

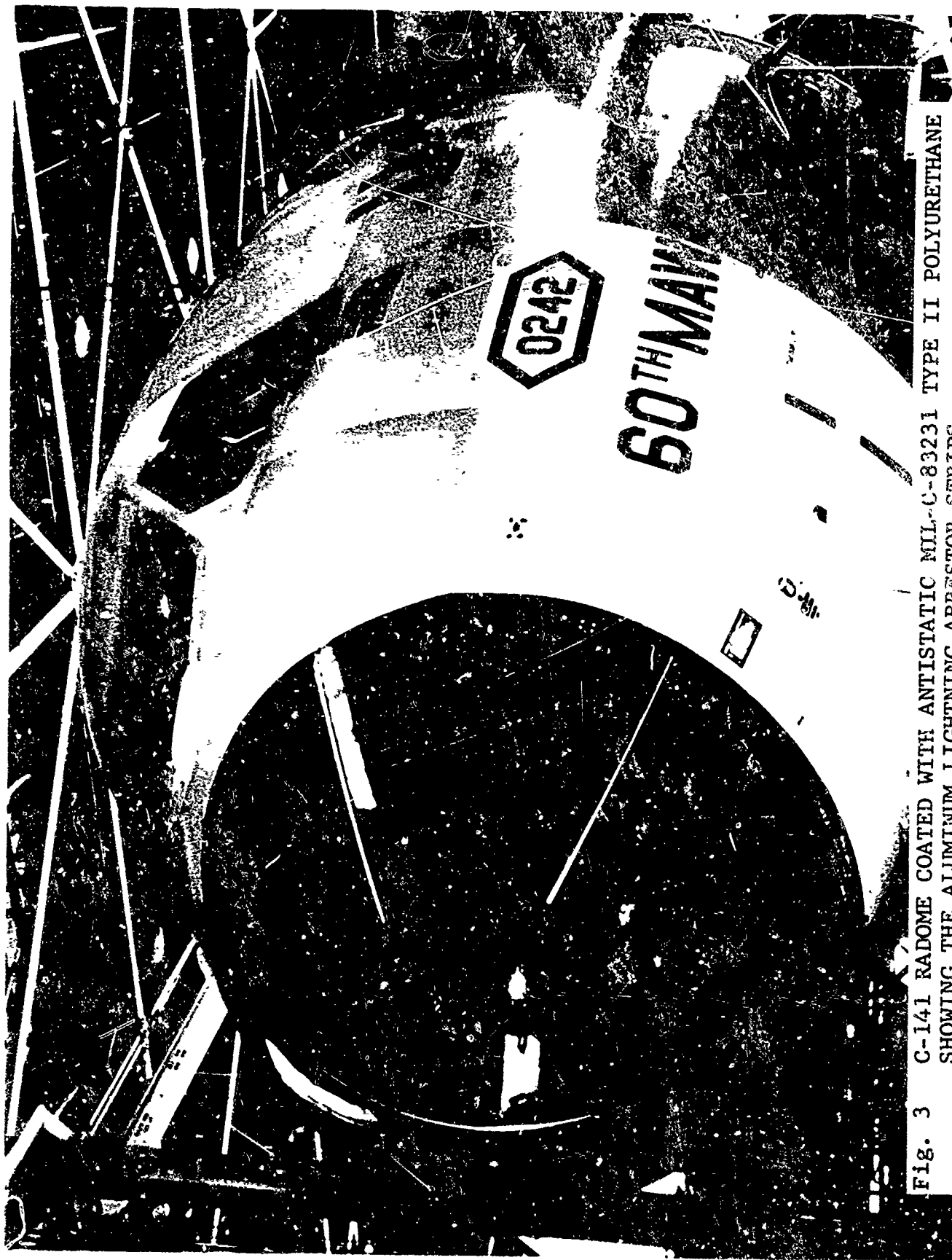


Fig. 3 C-141 RADOME COATED WITH ANTISTATIC MIL-C-83231 TYPE II POLYURETHANE  
SHOWING THE ALUMINUM LIGHTNING ARRESTOR STRIPS

Associated Phenomena, Royal Aircraft Establishment, England, August 1970. Volume I, pp 107-146.

6. G. F. Schmitt, Jr. "Polyurethane Coatings for Subsonic Radome Rain Erosion Protection" Proceedings of the Tenth Symposium on Electromagnetic Windows, Georgia Institute of Technology, pp 74-79, July 1970.

7. J. F. Moraveck, "Polyurethane Coatings for Subsonic Rain Erosion Protection," Aerospace Adhesives and Elastomers - 1970, National SAMPE Technical Conference Series Volume 2, pp 425-440, October 1970.

## A Review of Air Force Experience With Static Electricity Problems on Aircraft Windshields

Robert E. Wittman  
Air Force Materials Laboratory

### ABSTRACT

The Air Force is confronted continuously with problems related to lightning. One area that is conspicuous by its relative insensitivity to direct strikes is that of windshields and canopies basically because the transparent materials used in these components are in themselves very poor conductors as compared to metals. Conversely they are good insulators or dielectrics.

The bulk of aircraft windshields utilize two materials in construction, namely, acrylic plastics and glass. Of the two, glass has the lowest surface resistance ( $\sim 10^{12}$  ohm). The somewhat open silica network in the structure allows hydration which is not as evident in the acrylics ( $\sim 10^{16}$  ohm). Glass is about 10,000 times as good a conductor as acrylic under comparable conditions.

All aircraft are subjected to frictional interactions with air and any particles suspended in air, with the resultant acquisition of an electrostatic charge to the aircraft. Highly conductive materials allow these charges to move freely and be removed by one of several techniques or natural reactions. Non-conductors must rely predominantly on interactions with charged ions to lose their charge.

Acrylics and glass, by their non-conductive nature, restrict the lateral movement of a surface charge and, consequently

will isolate and hold a charge much longer than a conducting material. Providing a single discharge path through such arrangements as a grounding strap relieves only the area in the proximity of the strap. Design requirements for specific windshields (shape, materials, thickness, anti-icing needs, etc.) combined with the operating environment can produce a set of conditions that will allow a build up and retention of a static charge that can produce a personnel safety hazard ranging from minor electrical shocks to severe burns as well as damaging the windshield itself.

Precipitation static build up and retention on aircraft windshields and windows does not constitute a wide-spread Air Force problem. Quite a bit of information on this subject was generated just after World War II and was almost all completely related to communications and the interference created by the charging phenomena.

A brief analysis of factors such as transparent metallic coatings, materials thickness, etc., which contribute toward producing a precipitation static-problem on aircraft windshields will be given. Specific windshield designs which enhance static build-up will be discussed. Observations and conclusions on attempted solutions to the problem will be reviewed.

## Windshield Static Electrification Problems

### Commercial Aircraft Experience and Protection Parameters

M.M. Newman, J.D. Kobb and J.R. Stahmann  
Lightning & Transients Research Institute

#### ABSTRACT

Static electrification effects on aircraft electrical heated windshields have been known for many years, being reported in the first Symposium on Lightning Protection for Aircraft in 1948 (1)\*. The associated effects include: (a) induced static electrification pulses on windshield heater circuitry, (b) puncture of windshield outer panels, (c) interference with pilot's vision during instrument approaches, (d) thunderstorm crossfield transients intensification in heater circuitry and (e) shock hazards to ground personnel. The principal solution to all of the above problems include the use of external conductive coatings and surge protection devices on the heater circuitry. Erosion resistant conducting coatings, one of the major problem areas, have been developed for glass but remain to be developed for plastic windshields.

STATIC ELECTRIFICATION puncture of aircraft windshields has been reported as early as 1948 in the first Symposium on Lightning Protection for Aircraft. (1) Reports were received of a Pan American Airways aircraft having its windshield shattered during a lightning strike incident shortly after leaving Shannon, Ireland for the U.S. The windshield was electrically heated but used fine wires in the heating element rather than a metallized continuous coating presently in use. Experiments were carried out on windshield samples in a study with Pittsburgh Plate Glass Company, who manufactured the windshields and the investigations indicated that the punctures were more likely due to the effects of friction charging on the windshield or combinations of friction charging effects and rapid thunderstorm crossfield transients rather than due simply to electric field changes from a lightning strike to the aircraft. Conductive coatings were recommended as a preventive measure and were developed by Pittsburgh Plate Glass in the form of an external Nesa coating for alleviating the problem. Since that time, occasional reports have been received of problems with windshields utilizing electrically heated coatings below the outer lamination and investigations of the problem showed that one of the principal difficulties was the failure of ground crews to properly analyze the source of the problem. Although windshield problems can arise from a variety of causes other than static electrification of the outer surface, for example by faulty temperature controllers and mechanical stresses, it is very seldom that maintenance personnel con-

sider the possibility of static electrification puncture until it is specifically pointed out.

As aircraft have become larger and as more emphasis is placed on good visibility, the windshields are becoming larger with increasing static electrification problems because of the increased potentials which can result. At any specific altitude there is a limited horizontal electrical gradient which can be sustained across the windshield surface and consequently the larger the windshield size the greater the gradient which can be sustained and the greater the total potential which can be accumulated.

#### PROBLEMS

There are four principal problems associated with atmospheric electrical effects on aircraft windshields. These are:

- (a) direct precipitation charge accumulation and puncture of the windshield outer glass with possible electrical damage to the windshield's control circuitry,
- (b) electrification of the outer glass with surface flashover resulting in high voltage induced transients and resultant damage to the windshield electrical heating control circuitry,
- (c) induced voltages from the presence of the aircraft in thunderstorm crossfield regions resulting in electromagnetic pulse coupling into the controller circuitry,
- (d) visible windshield electrification interfering with pilot's visibility during instrument approaches,
- (e) shock hazards to ground maintenance personnel.

#### SOLUTIONS

The solutions to the problem include the use of volume or surface resistivity to limit the potentials which can be accumulated on the windshield surface under the most severe charging conditions. Also a variety of electrical circuit protection devices are now available for protection of the electrical heating circuitry.

The principal coating presently in use for glass outer panels is stannous-oxide which can be fused into the glass exterior surface to sufficient depth that erosion should not seriously reduce the resistivity of the external surface coating during the life of the windshield. Plastic external windshield surfaces required in some applications present a more difficult problem for which there has been to date no truly successful solution developed. However, multiple layered coatings are presently under development which offer some promise.

Calculations have been carried out on the volume and surface resistivities required for an incident friction charging rate of 40 microamperes per square foot, a maximum rate, and for combinations of volume and surface resistivity as presented in Table I. These are applicable to both glass and plastics.

\*Numbers in parentheses designate Reference at end of paper.

**TABLE 1**

Voltage on Windshield for Severe Snow Friction Charge Rate  
of 40 Microamperes Per Square Foot  
for Various Volume ( $\rho_v$ ) and Surface ( $\rho_s$ ) Resistivities\*  
( $\rho_v$  in ohm meters,  $\rho_s$  in ohms per square)

		Ohms per square					
$\rho_v$	$\infty$	$10^{12}$	$10^{11}$	$10^{10}$	$10^9$	$10^8$	
( $\Omega$ -m) ( $\Omega$ -cm)		25075300	2507530	250753	25075	2508	
$10^{12}$ $10^{14}$	1246500	981000	779592	207995	24580	--	
$10^{11}$ $10^{13}$	124650	114826	98100	77959	20800	2458	
$10^{10}$ $10^{12}$	12465	12331	11482	9810	7796	2080	
$10^9$ $10^{11}$	1247	1245	1233	1148	981.0	779.6	
$10^8$ $10^{10}$	124.7	--	124.5	123.3	114.8	98.1	

Surface flashover to windshield mounting frame will limit voltage to about 300,000 volts maximum for the dimensions of the windshield, about 30 inches edge to edge.

One other associated problem is that of thunderstorm crossfield coupling into the electric heating circuitry in spite of the use of external resistive coatings. As shown in Appendix I an incident electric field of 5,000 volts per centimeter which has been actually measured in flight just previous to lightning strikes, will produce on a large windshield without a conductive coating a potential on the metallized heater element of about 4000 volts.

shown in the table, the addition of resistive coatings with the magnitudes used on commercial aircraft windshields can reduce the problem but not eliminate it, thus some type of windshield protection circuitry should be utilized in view of the excellent coupling through the heating element which can act as an antenna into the aircraft interior electrical system.

#### SUMMARY

External conducting coatings have provided a satisfactory solution to the problem of friction electrification puncture and surge damage to heater circuitry when used in conjunction with circuit protection devices. The principal remaining problem is the development of erosion resistant conducting coatings for plastic windshields. There is also a need for the education of design and maintenance personnel that they may be aware of the effect in order to prevent it in new designs or recognize it when it occurs in the field in order that preventive measures can be taken.

#### REFERENCE

1. "Proceedings of the 1948 Symposium on Lightning Protection for Aircraft," Lightning & Transients Research Institute, Minneapolis, Minnesota, Nov. 8-9, 1948, ATI 76514.

#### APPENDIX I

##### Attenuation of Thunderstorm Induced Surges on Windshield Subsurface Heating Elements by Resistive Surface Coatings

Thunderstorm crossfields can induce charge separation in vehicles in flight. This charge will also be induced in subsurface or surface coatings of windshields as illustrated in Figure 1. A release of the thunderstorm charge by a remote lightning discharge will immediately release the charge separation on the aircraft, however, the charge on the windshield will be released more slowly as it must leak off through the resistive surface coating. Thus a remote lightning stroke will cause a charge separation to occur on the aircraft between the skin and the surface or subsurface coating resulting in an induced voltage on the heater circuit wiring. As the inter-resistive layer capacity  $C_1$  is very large (about 10,000

2 pfs) the addition of a surface coating will divide the voltage in proportion to the windshield outer coating capacity to the thunderstorm charge region  $C_2$  and the inner heating

layer capacity to the aircraft  $C_1$ .  $C_2$  and  $C_1$  will be of the same order of magnitude, or a few hundred picofarads for a large windshield. Measurement of these two capacities will permit calculation of the reduction ratio.

$$\frac{\text{Voltage (coating)}}{\text{Voltage (no coating)}} = \frac{C_2}{C_1 + C_2}$$

The calculations for maximum incident thunderstorm fields of 500,000 volts per meter show voltages on the heater circuitry of about 2000 volts with surface coatings and about double that for uncoated windshields.



# Windshield cross section

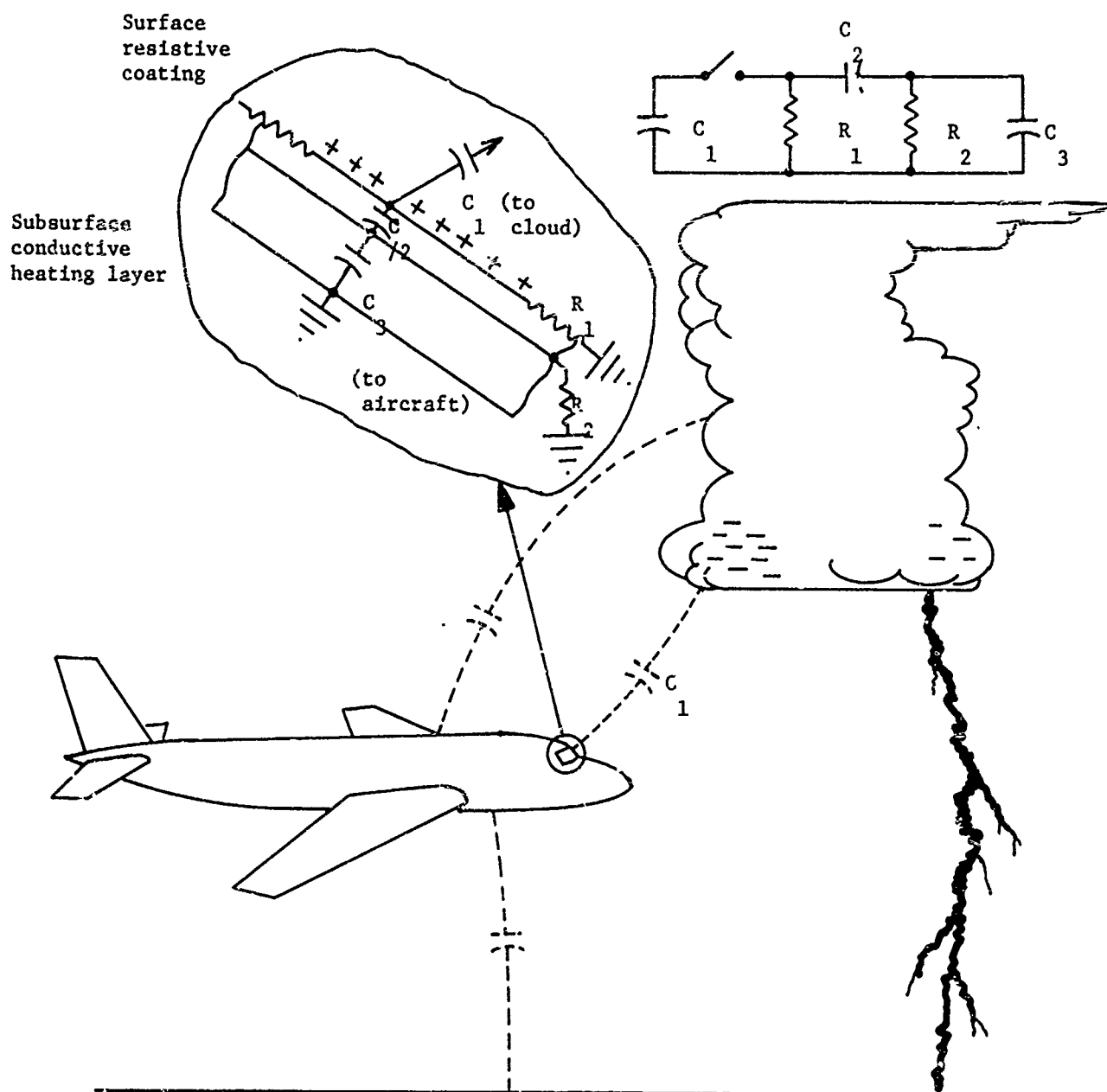


**Figure 1.** Attenuation of thunderstorm induced surges in aircraft windshield heating layer by surface coatings.

WINDSHIELD RELATED PROBLEMS - A  
MANUFACTURER'S VIEW

F. H. GILLERY, SENIOR SCIENTIST  
PPG INDUSTRIES, INC.

ABSTRACT

A discussion of the well-documented cases of windshield failure thought to have been caused by electrostatic build-up will be presented, and an interpretation of the effects in light of the windshield design will be made.

Finally, several methods of preventing or minimizing failure will be analyzed and recommendations made for future designs.

## Windshield Related Electrostatic Problems

### Electrification Studies on the 747

Rowan O. Brick  
The Boeing Company  
Commercial Airplane Group

Several study programs have been conducted by The Boeing Company to determine the relationship between electrostatics and some unexplained windshield failures that have occurred in flight.

The purpose of the presentation will be to discuss study programs that were conducted to determine how electrostatic particle charging and lightning strikes would affect the windshield. The following study programs will be reviewed.

1. Investigation of windshield charging in flight.
2. The effects of electrostatic pulses on the windshield heater controls.
3. The simulation of lightning puncture of the outer glass ply by dielectric strength tests.
4. The simulation of particle charging to investigate the windshield surface flash-over characteristics.

As a result of the study programs changes were made on the production windshields. Windshield failures after the production changes will be compared to earlier windshield failures to determine if the changes were helpful in eliminating some of the suspected electrostatic problems.

SESSION IV

MISSILES AND SPACECRAFT

R.W. ELLISON, CHAIRMAN & ORGANIZER

MARTIN MARIETTA CORPORATION - DENVER DIVISION

## Introduction of the Session

R. W. Ellison  
Martin Marietta Aerospace

THE MISSILE AND ROCKET session for this conference addresses the in-flight aspects of static electricity. The papers discuss flight data on the magnitudes of the electrification, the effects that have been encountered in flight, ground tests that lead to corrective measures prior to flight, and are concluded by a paper summarizing the important practical aspects of the flight electrification phenomena. One of the papers includes data implicating electrification as a factor in contamination control.

The subject and the papers for this session were chosen to increase awareness among aerospace engineers that static electricity must be considered during the design, testing, and system analysis phases of space projects. Most aerospace engineers, as well as a majority of designers of satellite instruments, have been barely aware that static electricity occurs and has significance in their work; only a few have been adequately knowledgeable of this matter. The authors of the papers in this session are, in substantial measure, both pioneers and experts in the subject.

The USSR has also been active over the last decade in studying the electrification of spacecraft. Perhaps the earliest measurements of electric fields on orbital spacecraft were those of Imyanitov and Gurevich. The USSR literature available suggests the Russians have encountered substantial problems with static electricity; however, the known reports do not identify the in-flight effects that were troublesome nor the subsystems that were affected. Certainly their early instruments to measure particles and fields in the upper atmosphere were involved--as were our own--but no specific details are available. Recent reports suggest that a high level of activity in the USSR continues to be concerned with the effects of static electrification.

Future progress in understanding the magnitudes of electric fields arising on spacecraft is being hindered by the lack of direct measurement of E-fields. Since the last conference, measurements have been made on a Thor-Delta flight, and direct measurements on a Titan III booster will be reported in the next paper. But no direct measurements have been made on lunar orbital, lunar surface, earth orbital, or interplanetary missions. Measurements on such missions will be mandatory to provide the firm foundation required to make progress in this discipline. Until now, we have been almost

entirely dependent on inferences deduced from space science data. I strongly urge this audience to initiate and support proposals for adding field mills or their equivalent to programs with which they are involved. The instruments are available, some are qualified for the environment of space, and their use on future missions is strongly recommended.

For interplanetary missions, it has been suggested that contaminants, as they sublime, may continue to lose mass in environments which prohibit a loss of electrical charge. This concept would lead to very high charge-to-mass ratios for the particles in the vicinity of spacecraft that are known to have substantial voltages. It is anticipated that such questions may be investigated in the near future and that some answers may be available in time for the next conference.

In conclusion, two areas of experimental work--field measurements and particulate electrification in space--may merit our attention in the near future as we begin to apply our existing knowledge to the systems, subsystems, and sensors that will be used in space missions for defense, civil, and scientific programs.

## Results of Titan III Flight Electrostatic Experiments

J. E. Nanovicz  
Stanford Research Institute

### ABSTRACT

Flight test and ground test experiments were conducted during the launch of two Titan III C rockets to study Titan rocket vehicle electrification. The results of the experiments indicate that many of the electrification processes observed on aircraft also occur on large rockets. Rocket motor charging currents of the order of 50 to 100  $\mu$ A raise the potential of the rocket to hundreds of kilovolts even during a clear weather launch. Frontal precipitation charging rates measured on the Titan are in good agreement with aircraft data. Streamer discharges were shown to occur on plastic frontal surfaces of the rocket exposed to precipitation particle impact. The charge transferred per streamer is in good agreement with data obtained during aircraft flight tests.

The high rocket exhaust temperature result in interesting differences between aircraft and rocket potential. Of particular interest is the indication that the highly-conducting portion of the rocket exhaust extends to 650 ft aft of the rocket.

ROCKETS AND SPACE vehicles can acquire electrical charge of various amounts from such processes as triboelectric charging from particulate matter; plasma processes in the ionosphere, radiation belts, and solar wind; photoelectric charging from high-energy radiation; and engine charging from various processes occurring in the combustion chambers of rocket engines. Of these charging processes, triboelectric charging and engine charging appear to be the predominant sources of detrimental vehicle charging from the standpoint of producing high vehicle potentials that lead to sparks, corona, and streamers. (1-7)

On the Titan III-C vehicle, anomalous Missile Guidance Computer (MGC) responses have been observed during the flights of Vehicles C-10 and C-14. Ground tests of the MGC indicate that similar responses can be produced by sparks to the computer case or by electrical discharges near the computer system. In addition, the Titan III-C payload fairing is coated with an ableting material on which charge may accumulate, and the fairing was not positively bonded to the missile frame. Thus, it was strongly suspected

that the anomalies observed on Vehicles C-10 and C-14 were of electrostatic origin.

The objectives of this program were to study the vehicle electrification mechanisms and charging-current magnitudes on the Titan III-C rocket vehicle in an effort to better understand the processes by which electromagnetic impulses capable of affecting system operation might be generated. The objectives were achieved by developing and calibrating special flight-test instrumentation and installing and operating it on two Titan III-C rockets during scheduled firings. The instrumentation is designed to measure vehicle potential, charging current arriving on a metal frontal surface, and streamers generated on a small dielectric frontal surface (8).

Actual installation of the instrumentation on the Titan III-C test vehicle was accomplished at the Eastern Test Range by the Martin-Marietta Corporation on a separate contract.

During the Titan III instrument development and fabrication period, Apollo 12 was struck by lightning during launch, and SRI scientists participated in two series of ground experiments (one on Apollo 13 and the second on Apollo 14) to investigate the electrical characteristics of the Apollo rocket and its plume (9). These Apollo experiments were conducted with no electrostatic instrumentation on the rocket, while the Titan III-C experiments were to be conducted with no ground-based electrostatic instrumentation. It was observed that both programs would be considerably strengthened at a relatively little expense if provisions were made to include ground-based measurements on the Titan program. Accordingly, a set of ground-based field meters was fabricated and emplaced around the Titan III-C launch complex for each launch.

### INSTRUMENTATION

FLIGHT - The instrumentation system was developed (8) to measure the following parameters during the flight of the test vehicle:

- (1) Instantaneous vehicle potential
- (2) Charging rate
- (3) Impinging particle count
- (4) Streamer discharge PRF
- (5) Streamer discharge current

<sup>\*</sup> Numbers in parentheses designate References at end of paper

(6) Ambient electron density.

An electric-field-meter system is used to measure vehicle potential. The field strength measured at a point on the surface of the vehicle by the field meter is directly proportional to the vehicle potential; thus a measure of the field strength is tantamount to a measure of vehicle potential. The vehicle can be charged by frictional electrification by rocket-engine operation.

A charging patch located on the nose of the rocket is used to measure the charging produced by impinging dust or precipitation particles only (10). The charging-rate patch consists of an electrically isolated conductor on the outside of the vehicle subject to the impingement of dust or precipitation. The electronic circuitry associated with this patch is designed to measure the current flowing to the patch and to count the number of particles impinging.

In an effort to further study the breakdown processes occurring on a rocket vehicle, provisions were made to count the streamer pulses generated by charging of a small, insulating region of the vehicle nose. The electronic circuitry used for the streamer studies includes provisions for measuring the streamer current and for counting the number of streamers generated.

The Langmuir probes for studies during orbit injection are similar to those designed and fabricated by SRI for use by AFRL in their Trailblazer experiments (11). The probe consists of an isolated conductor biased negatively with respect to the skin so that it collects saturation ion current. The magnitude of the current is related to the electron density in the immediate vicinity of the probe (12).

**Field Meter** - The field meter developed for this program is of the rotating vane design. The detector head is mounted in a hole in the skin in such a manner that the meter vanes are exposed to the exterior of the vehicle as shown in Figure 1. Movement of the grounded rotor shown in the figure causes the stator to be alternately exposed to and shielded from the exterior environment. In this way an alternating signal is generated in the stator as the rotor chops the ambient electric field at the skin or as it chops a convection current to the skin. The flight test system included provisions for separating the "electric field" signal from the "convection current" signal (8).

To ensure its proper operation, the field meter must not be located near plastic surfaces which may accumulate charge and distort the electric field at the meter location. In determining a location for the field-meter sensor, the transtage (13) (Stage III) of the vehicle was attractive because this section remains

intact and operational until payload orbital injection seven hours after launch. This part of the fairing is covered with a 5-mil-thick layer of special, thermal-control silicon paint of sufficient electrical quality to maintain an electric charge on its surface for extended periods of time. This problem was overcome by installing a 21-by-30-inch sheet of Alzak (an electropolished, anodized soft aluminum) on the skin of the vehicle surrounding the field meter. This material has suitable optical characteristics for use as a thermal-control material on the surface of the Titan III-C, and laboratory tests demonstrated that it retains a sufficiently small charge on its surface to permit it to be used around the field meter.

**Charging Rate and Particle Counter** - The charging rate and particle count are determined with one sensor and appropriate signal processing. The particle counting is done by processing pulses produced by individual particle charge deposited on the sensor plate. The charging rate is obtained from the average current flowing to the plate as a result of these charge deposits.

A photograph of the particle sensor is shown in Figure 2. The entire assembly is made of 0.090-inch-thick stainless steel pieces cemented to a fiberglass substrate. The particle electrode is simply the 3-by-30 cm rectangle of stainless steel shown in the lower part of the photograph. Ideally, for best particle-pulse definition, the sensor should be a conducting strip with its longest axis oriented at right angles to the flight path. With this arrangement, particles remain close to the skin as they cross the sensor electrode and gap and generate short, high-amplitude pulses.

The instrumentation for studying frontal charging is shown in block form in Figure 3. Particles impinging on the sensor induce current pulses, the ac components of which are fed through the coupling capacitor, C, to the input of the pulse amplifier located immediately behind the sensor. The input resistor, R, is chosen so that  $1/RC$  (where  $C_s$  is the stray capacitance to ground of the input circuit) is small compared to the time between successive pulses. The pulses out of the amplifier are fed to an absolute-value amplifier. The unipolar pulses from the output are used to trigger a pair of one-shot multivibrators. The output from each multivibrator is integrated and used to drive a channel of the telemetry system. Since all of the output pulses produced by a particular multivibrator are of identical shape, the output from the integrator is linearly proportional to the PRF of the pulses at the input. Thus the output is linearly

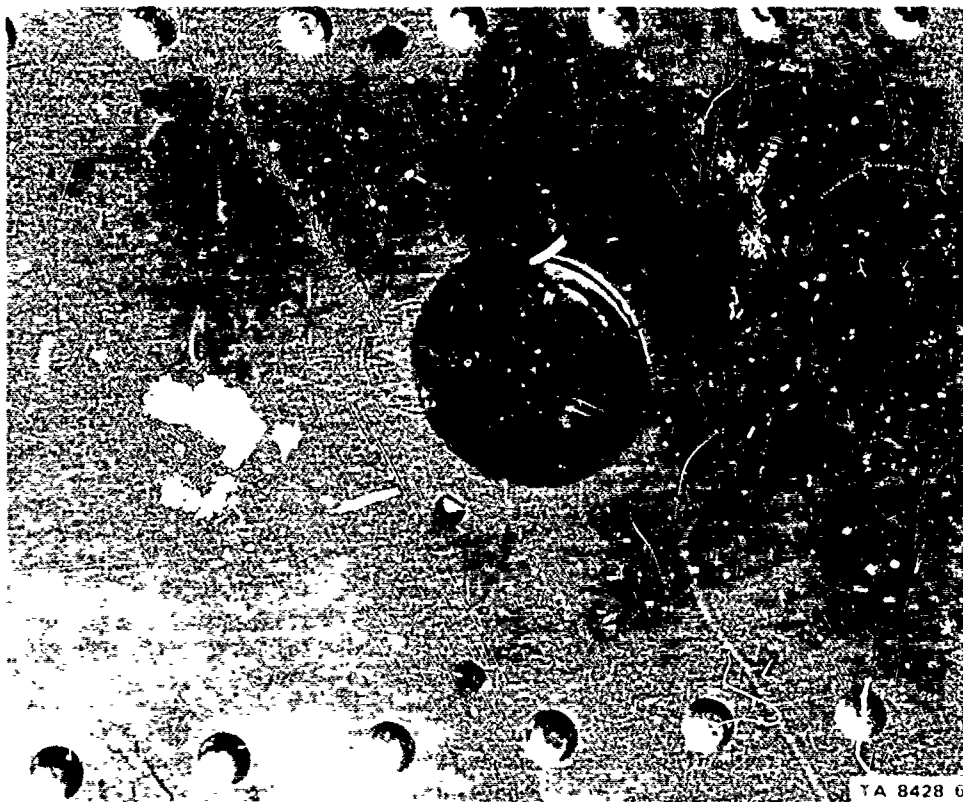


FIGURE 1 FIELD-METER INSTALLATION ON TITAN-III ROCKET



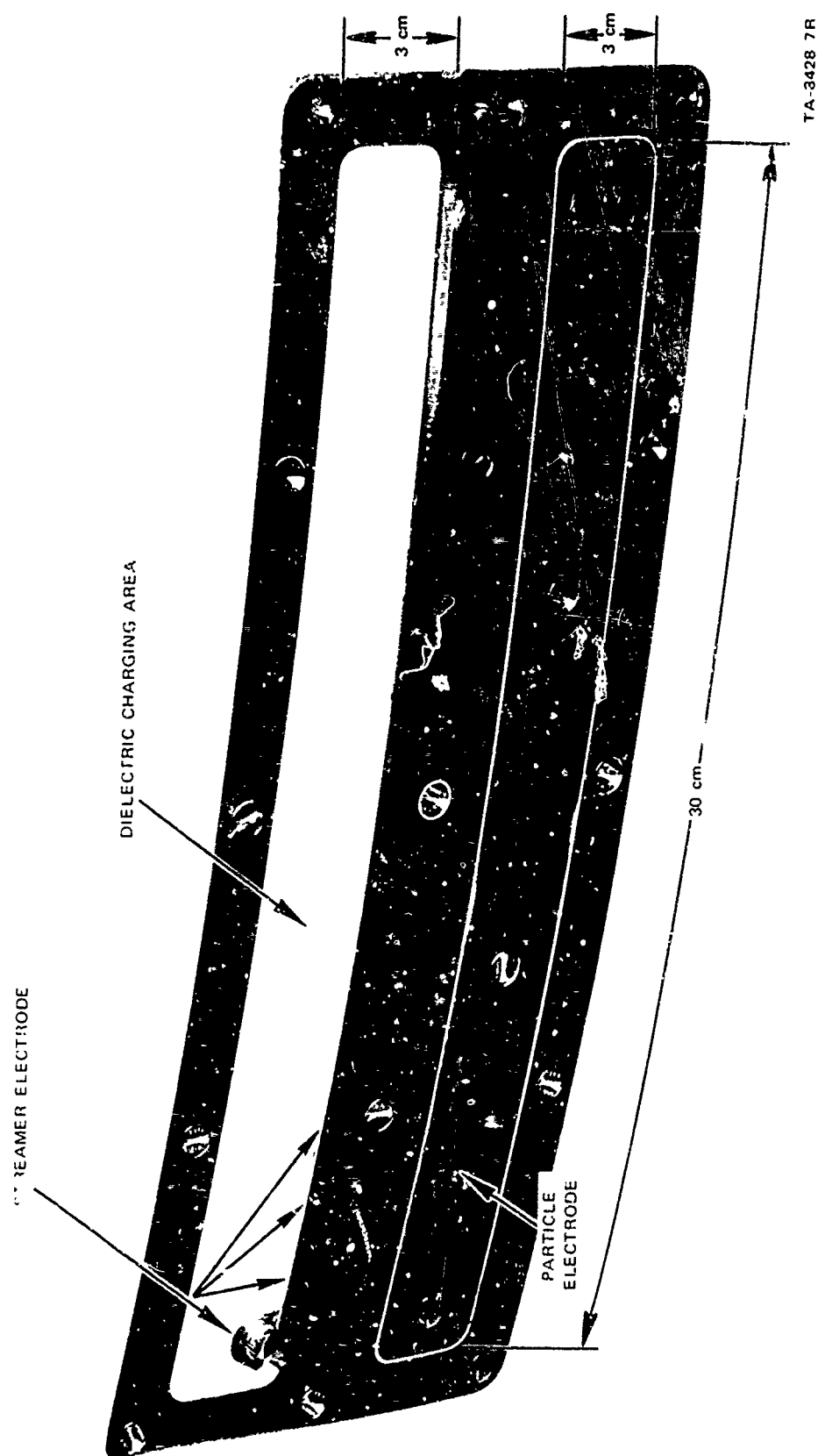
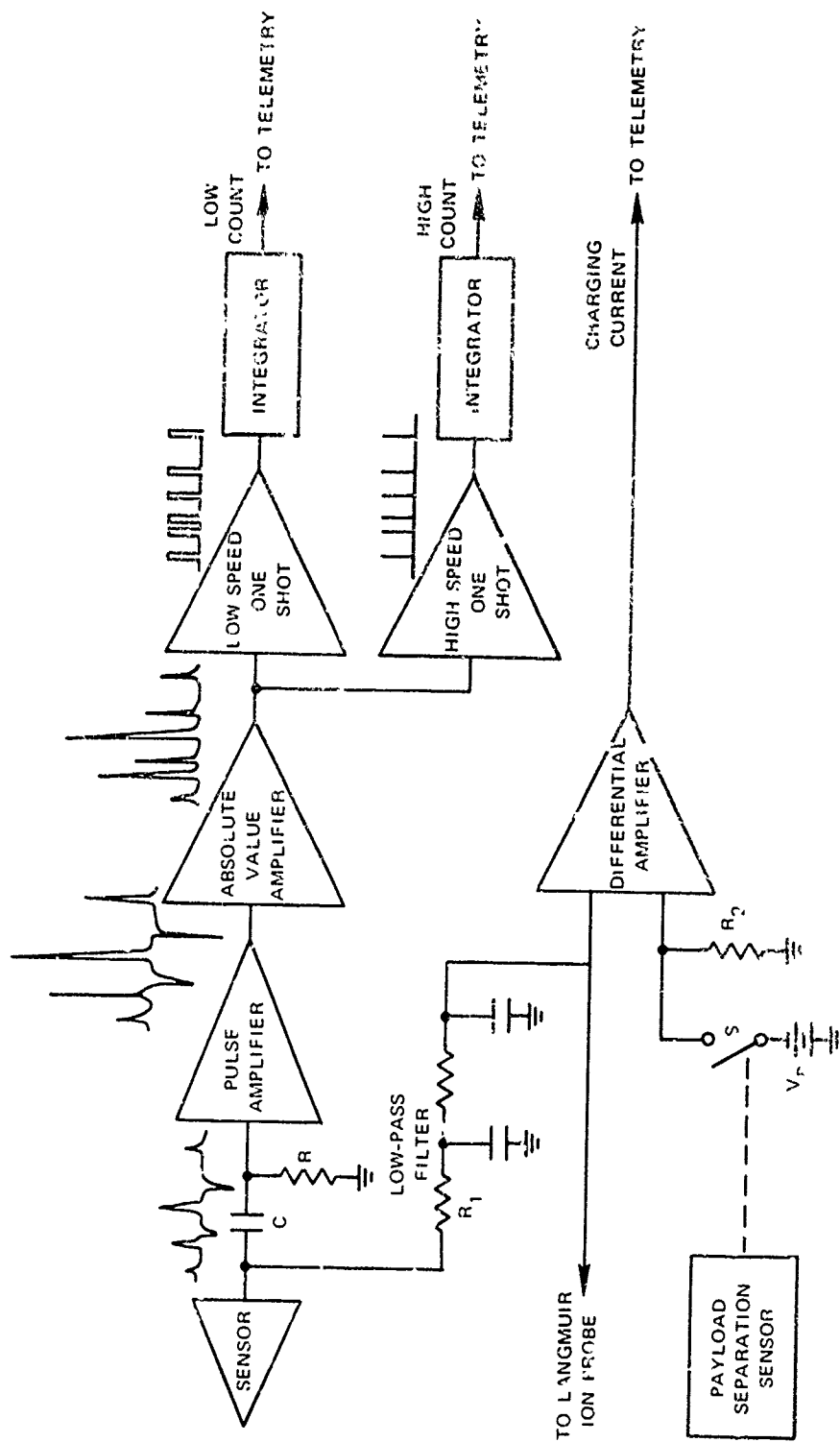


FIGURE 2 PARTICLE/STREAMER SENSOR



TA-8428-4

FIGURE 3 BLOCK DIAGRAM OF CHARGING RATE AND PARTICLE COUNT SYSTEM

proportional to the particle impingement rate. Wider dynamic range for the system is achieved by setting the multivibrator constants such that the top one produces wider pulses than the lower one. Thus, for a given pulse rate, the top multivibrator produces a higher dc output from its integrator than the lower one.

The dc component of the current deposited on the probe flows to ground through the low-pass RC filter, the input resistance of the differential amplifier, and  $R_2$ . The voltage developed by this current flowing through the differential amplifier input is amplified and used to drive a telemetry channel. Switch S is open the entire time that frontal charging measurements are being made, so that the power supply  $V_p$  is not connected to the differential amplifier during this time. The purpose of the power supply, the switch, and the ion-probe lead is to permit the particle current circuitry to be used as a Langmuir ion probe in the ionosphere. In this paper, consideration will be limited to the atmospheric portion of the flights.

#### Streamer Counter and Dielectric Charging -

The streamer patch is designed to provide a direct measure of frontal-dielectric-surface charging and streamer-discharge occurrence. The streamer pulse rate and streamer current to an isolated dielectric patch were measured using signal-processing electronics similar to that used with the particle-charging system discussed in the previous section.

The form of the sensor evolved for streamer studies is shown in the upper part of the photograph of Figure 2. A region of dielectric 3 by 30 cm is exposed to impinging particles. The streamer electrode is a 0.005-inch-thick plate of stainless steel insulated from the rest of the structure and protruding 0.005 inch over the dielectric from the lower edge of the rim and the dielectric region. Charge deposited on the dielectric surface is relieved by streamers to the streamer electrode or to the surrounding metal structure. These streamer discharges generate pulses in the streamer-sensor electrode. The dc current flowing to the streamer electrode is very nearly equal to one-half the charging current arriving on the isolated dielectric region (the other half of the current flows to the grounded surrounding structure).

The electronic system used for the streamer studies is of the same form as that indicated in Figure 3. Since streamer pulses are much more energetic than the pulses generated by individual precipitation or dust particles, the gain of the pulse amplifier in the system is reduced. The dc-current-measuring system is identical to that used in the particle-charging

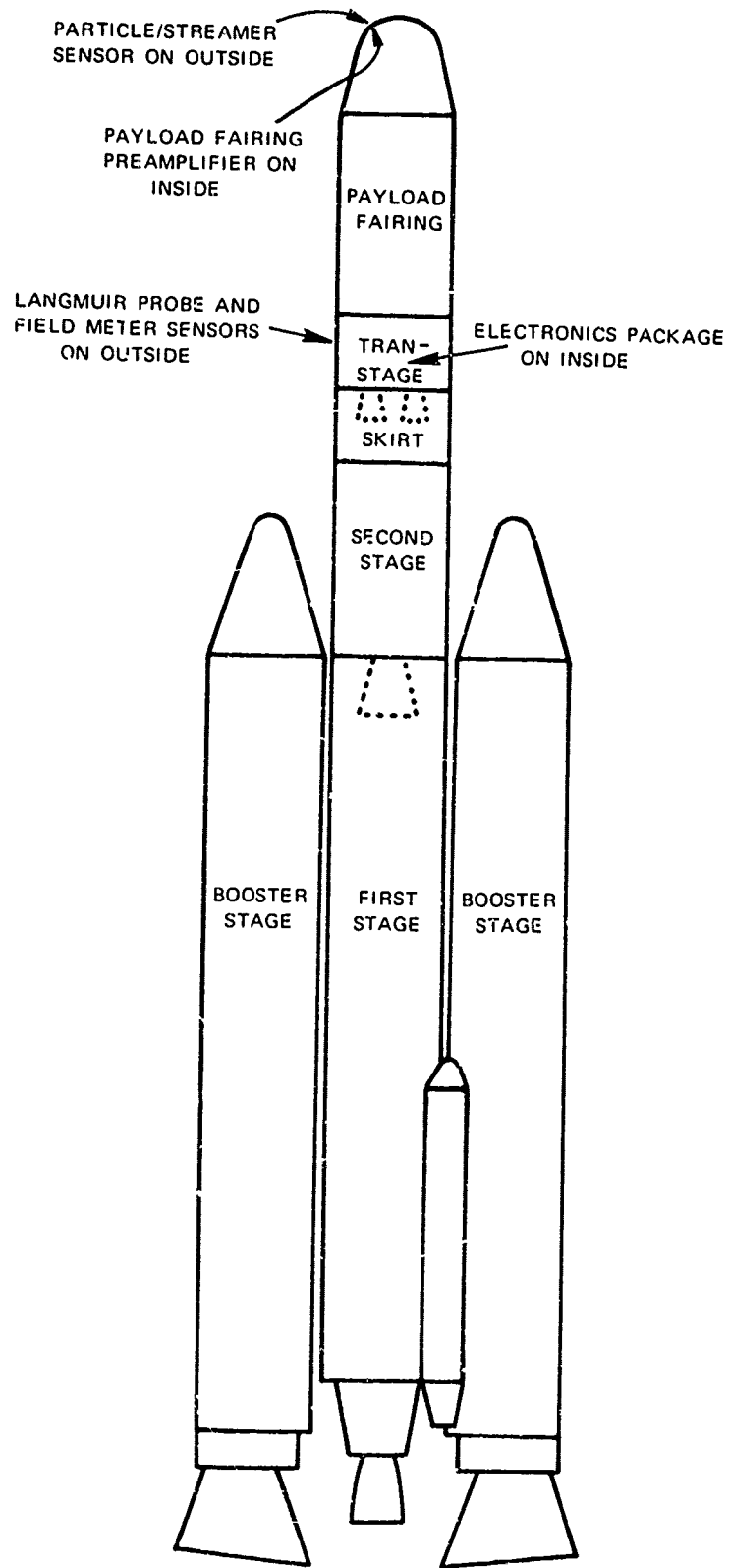
studies, since the charging areas are very nearly the same in the two cases, and the currents should be the same.

Installation on Test Vehicle - The general form of the Titan III-C test vehicle and the physical placement of the electrostatic study instrumentation on it is shown in Figure 4. All of the electronics and sensors are located either in the transtage or the payload fairing. Both of these structures stay with the vehicle throughout the early staging. The payload fairing is jettisoned 280 seconds into the flight at an altitude of 400,000 feet. The transtage remains intact and operating until the time of payload orbit injection.

A more detailed illustration of the instrument locations is shown in Figure 5. The particle/streamer sensor is installed on the outside surface of a door in the nose of the payload fairing. This location was chosen because it places the surface of the sensor at roughly  $45^\circ$  to the axis of the rocket. This location is away from the stagnation region at the nose, but still not so far back on the rocket that the sensor is shielded from the particles. A location on the vehicle at  $90^\circ$  from the target direction was chosen to minimize changes in particle impingement resulting from changing airflow patterns about the probe during vehicle maneuvering. The in-flight maneuvering of the Titan III-C is such that the pitch of the rocket (in the plane of the target direction) is non-zero, and changes from time to time during the flight. No deliberate changes are made, however, in the yaw direction, and the yaw angle is maintained near zero throughout the flight. Thus the airflow patterns about the sensor should be constant during flight.

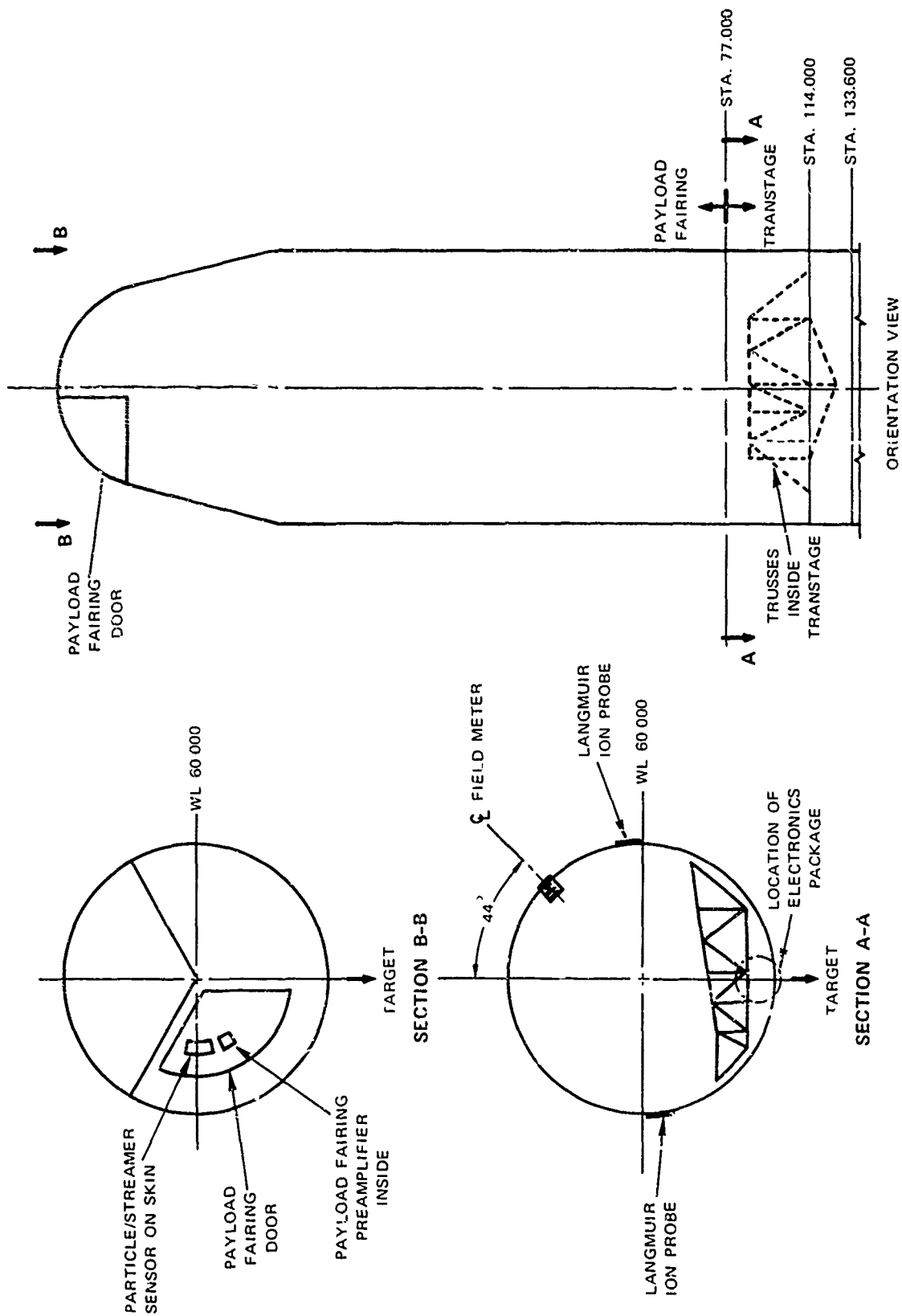
To avoid particle impingement, the field-meter sensor was located on the side of the rocket away from the target direction. Since the vehicle operates in a pitch-up attitude during much of the launch trajectory, the back side of the vehicle is shielded from particles.

GROUND - As was indicated earlier, the purpose of the Titan ground experiments was to generate data to supplement that from the flight vehicle, and to provide a common set of measurements to unify the Apollo and Titan electrostatic experiments. As is indicated in Ref. 9, the Apollo experiments were designed to use launch perturbations in ground electrostatic field structure to infer as much as possible about the electrical appearance of the launch vehicle (i.e., is the vehicle highly charged, or is the conducting portion of the plume thousands of feet long?). The SRI



TA-8428-10

FIGURE 4 SKETCH OF TITAN III-C TEST VEHICLE



TA-8428-11

FIGURE 5 LOCATION OF INSTRUMENTATION AND SENSORS ON T TAN III-C TEST VEHICLE

instrumentation for the Apollo experiments consisted largely of field meters arrayed on the ground around the launch pad and on the launch tower. A similar ground installation was used for the Titan launches.

A drawing of the Titan launch pad showing field meter locations is shown in Figure 6. During the early part of the launch, the rocket exhaust is directed eastward via the exhaust duct. To minimize coupling to the exhaust products (which generally are charged), a set of field meters A, B, and C was set out in a line to the south of the pad at right angles to the exhaust duct. Field meter D was positioned slightly north of the exhaust duct axis to couple strongly to the exhaust products. Field meter E was located on the top of the tower to couple strongly to the rocket as it moves by the tower in an effort to measure the potential of the vehicle as it moves by.

A photograph of a typical ground field-meter installation is shown in Figure 7. All of the electronics and the strip-chart recorder were housed in a plywood box that protected the system from the weather and provided a convenient base for sandbagging to protect the instrumentation from the launch blast. The field-meter detector head is positioned upside down 13½ inches above ground and a few feet toward the pad from the instrumentation box. (Inverted field meter operation avoids problems with motor bearing and insulator design when the sensor must be operated in rain.) Electrostatic cage calibrations provided the true ambient electrostatic field from the field that was read at the detector face.

A photograph of the field meter installation on top of the umbilical tower is shown in Figure 8. The field meter detector head is positioned upside down 20 inches above top of the tower. The field meter installed on the umbilical tower is one of the heavy-duty units developed for the Titan III onboard field measurements, and was qualified to a 160 dB acoustic environment, and to 1360 g peak shock (8). Electrostatic cage calibrations indicate that the ambient electrostatic field at the field meter location on top of the tower is 27 percent of the field reading at the meter face. Also the ambient field that would exist at ground level is 12 percent of the ambient field at the top of the tower at the field meter location. Thus, to obtain true tower top fields, field meter E readings must be multiplied by 0.27 while, to obtain the true ground field, field meter E readings must be multiplied by  $.12 \times .27 = .032$

## FLIGHT TESTS

GENERAL - Instrumentation was carried on two rockets. The first experiment was conducted on Titan III C-20 launched in early Spring of 1971. (For interpreting the records, the time of solid rocket motor, SRM, ignition was 0743:01.24 GMT.) The second experiment was conducted on Titan III C-21 launched in Fall 1971. For C-21, SRM ignition occurred at 0309:05.44 GMT. A general Titan III mission is described in Ref. 14. Both vehicles were launched at the Air Force Easter Test Range (AFETR) on a 93-degree flight azimuth.

AIRBORNE DATA - Titan III C-20 - A clear, stable atmosphere with no cloud formations existed in the AFETR area at the time of C-20 launch. All test instruments worked both on the ground and in flight to synchronous orbit injection.

Onboard instrument data for the first minute after launch are shown in Figure 9. In general, particle and streamer sensor activity was very minimal. This is to be expected in view of the clear weather conditions at the time of launch. In fact, the only indications from these two sensors in this flight regime consist of a few particle counts (25 - 50 pulses/sec measured starting at roughly 20 kft altitude.) There was no accompanying indication of particle or streamer current and no change in vehicle potential indicating charge accumulation on the rocket. It is not clear, therefore, what interpretation should be placed on the burst of particle counter activity.

The field meter record at the time of launch is far more interesting. In view of the existing stable and clear meteorological conditions at launch, rocket charging is evidently caused by processes in the ionized rocket exhaust. It is seen that the C-20 vehicle begins charging negatively about 2 seconds after SRM ignition. The rocket potential remains at approximately -20 Kv until about 8 seconds after lift off (at 0743:09.5) when the rocket altitude is 650 ft. The subsequent abrupt increase in negative potential can be interpreted to indicate that the highly conductive portion of the rocket exhaust breaks contact with the ground at 650 ft. This behavior is consistent with the Apollo work of Uman (15); he has indicated that the visible rocket plume (length approximately 625 ft at ground level) is a uniformly good conductor, but that the conductivity drops quite rapidly with further increasing distance along the exhaust trail.

The C-20 vehicle reaches 200 kv negative potential about 12 seconds after SRM ignition

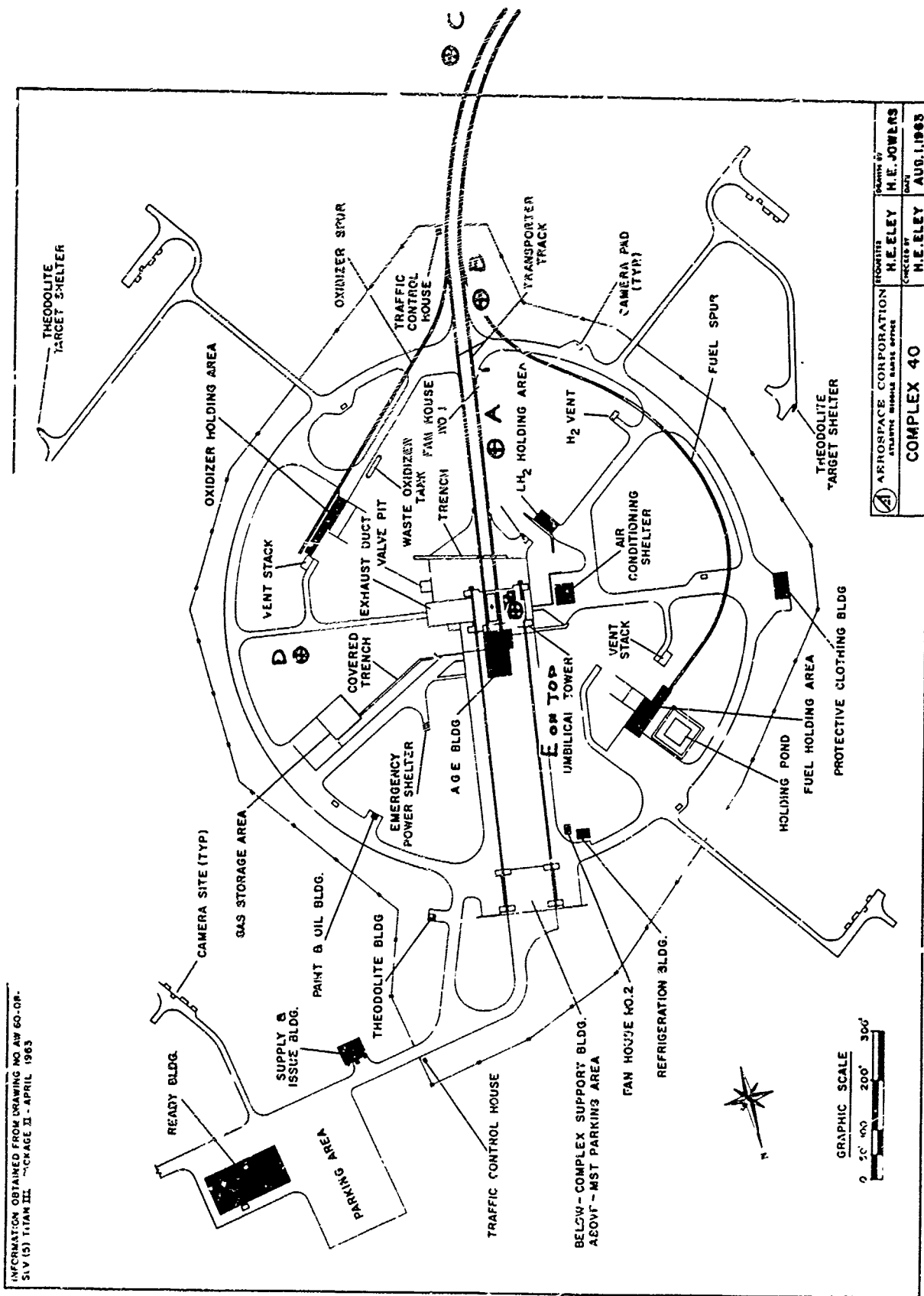
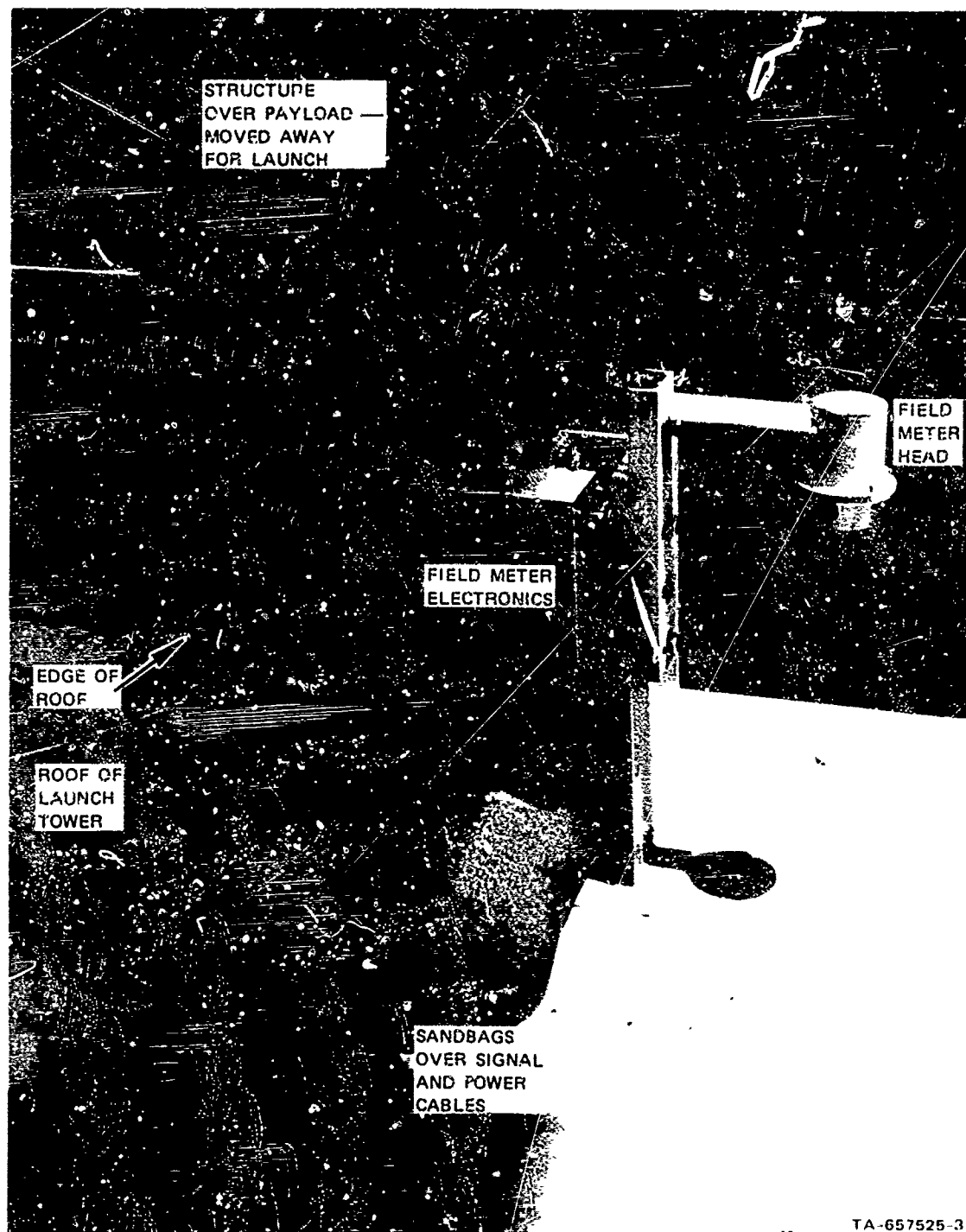


FIGURE 6 GROUND FIELD METER INSTALLATION ON TITAN III FIRING



FIGURE 7 TYPICAL TITAN III GROUND FIELD METER INSTALLATION





TA-657525-3

FIGURE 8 FIELD METER INSTALLATION ON TITAN III UMBILICAL TOWER

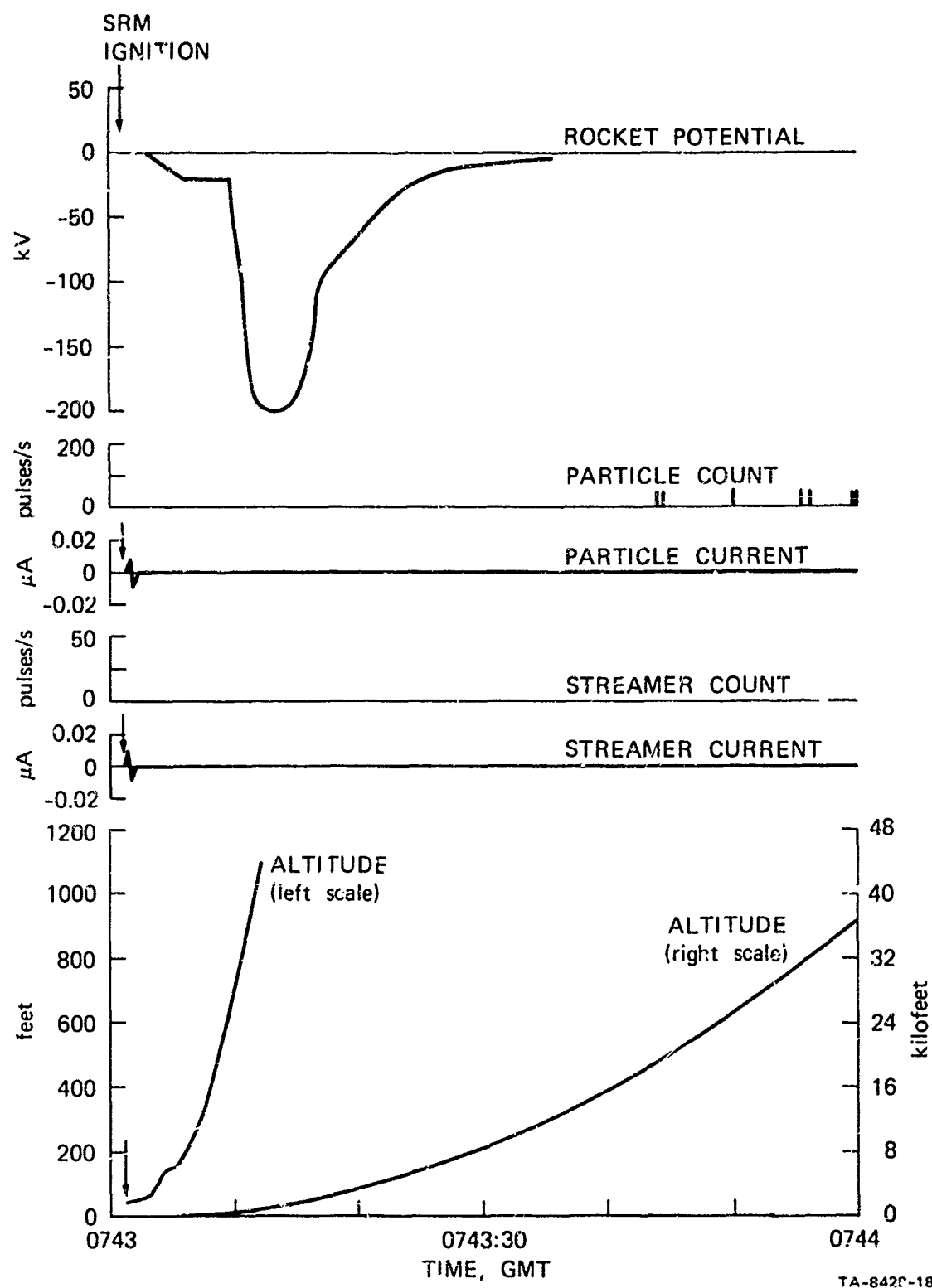


FIGURE 9 LAUNCH DATA FROM TITAN III C-20

at an altitude of 1.4 kft. The potential is held nearly constant at 200 kV for nearly 5 seconds. (Limiting probably occurs as the result of corona discharges from vehicle extremities.) Altogether, the rocket potential remains above 50 kV between 800 and 4000 ft. (9 to 20 seconds after ignition). At these altitudes, the vehicle as viewed by camera is trailed by an exhaust plume removed from local exhaust clouds generated in the launch area. The vehicle returns to approximately zero potential 34 seconds after launch at an altitude of 12 kft. At this altitude the rocket plume is not visible in the launch movies. This behavior agrees with aircraft experience where engine charging current monotonically decreases as the aircraft climbs.

It is interesting at this time to use the rate of change of rocket potential to estimate rocket engine charging current. From Figure 9 we observe that, during the period of rapid potential increase,  $\Delta V/\Delta t = -10^5$  volts/sec. From measurements made on a scale model of the Titan III C vehicle the self capacitance  $C$  of the vehicle is (1000 pf). The charging current  $i_{ch}$  is given by

$$\begin{aligned} i_{ch} &= C \Delta V/\Delta t \\ &= 10^{-9} \times 10^5 \\ &= -100 \mu A \end{aligned}$$

Both the polarity and magnitude of the charging current are in good agreement with engine charging currents observed on large American jet aircraft (16). These currents were in the range 100 - 200  $\mu A$  for "dry" take offs, and increased by a factor of 3 to 5 during water injection. In a series of tests on 17 small solid-fuel motors, Boeing measured charging currents in connection with its Minuteman program (17). The motors were in the 200-to-500 pound thrust range. The charging currents varied from less than 0.1 microamperes for the 200-pound-thrust-motors, to slightly over 2 microamperes for the 500-pound motors. The motors apparently charged to a negative polarity. Although it is not clear how one should scale data from 200-500 pound rocket to apply to a Titan III C with a thrust of  $1.2 \times 10^6$  pounds, at least the polarities are in agreement, and the small rocket motor current is substantially smaller.

The principal period of particle counter activity during the launch of Titan III C-20 is shown in Figure 10. Here occasional bursts of counting  $\approx 50$  pps occurred at random times. There was no corresponding indication of either

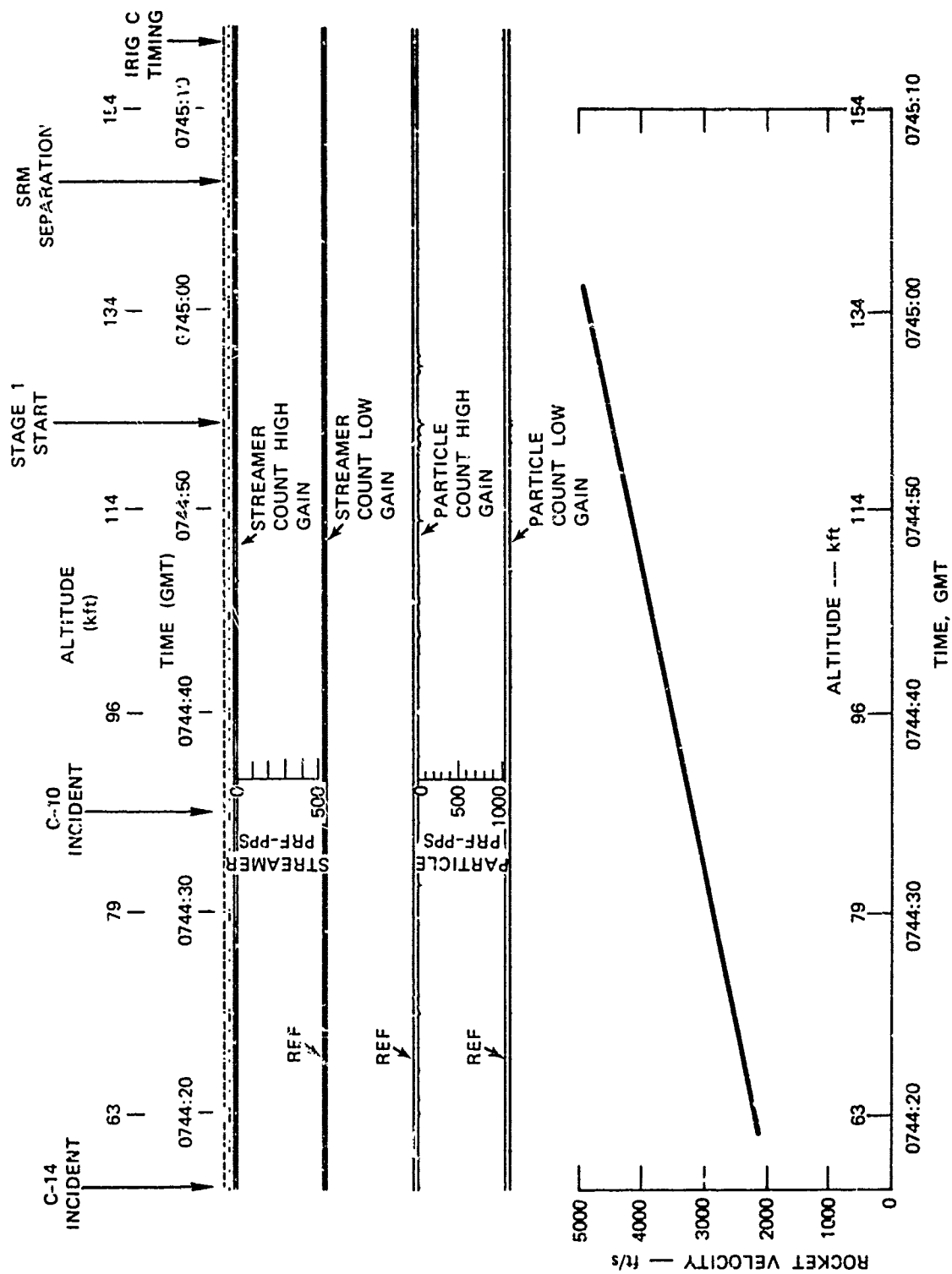
particle current or streamer current. A single streamer pulse is indicated at 0744:46.4. Interestingly, this is the altitude regime at which the computer anomalies on Titans C-10 and C-14 occurred. (The altitudes of occurrence are shown in Figure 10.) Evidences of particle impact at this altitude were not expected when the experiment was being planned since appreciable particulate matter does not usually occur at this altitude. Nacreous clouds do occur in the range 60-120 kft, however, and it is possible that they were present the night of the launch. An effort is underway to obtain independent evidence for the existence of nacreous clouds over AFETR the night of C-20 launch.

Evidence that the current and field meter systems were functioning at the 100 kft altitude regime and that the absence of current indications is not due to instrumental malfunction is given in Figure 11 which shows the records of these systems at the time of solid rocket motor (SRM) jettison. At this time, two rockets (exhausts directed toward the Titan I stage) are activated to move the solid, strap on rockets away from the main vehicle. The operation of the jettison rockets bathes the vehicle (including the transtage) in exhaust products. This exhaust striking the Langmuir ion probe sensors undoubtedly generates the charging currents which saturate both channels of both the particle current and streamer current systems. The same exhaust products impinging on the field meter sensor produce the noisy records shown. It must be concluded, therefore, that the particle counts of Figure 10 were indeed not accompanied by appreciable charging current.

In this regard, it is interesting to calculate the magnitude of particle probe charging current that might be expected under these circumstances. Flight test measurements of particle impact charging made on high speed jet aircraft indicate that, following impact, atmospheric ice crystals acquire charges of up to 50  $\mu C$ . Let us assume that the particles of Figure 10 acquired the same charge upon impact. Since we have 50 particles per second striking the probe per second depositing a charge of  $5 \times 10^{-11}$  coulombs per impact, the current arriving on the probe will be

$$\begin{aligned} i_{probe} &= 50 \times 5 \times 10^{-11} \text{ coul/sec.} \\ &= .0025 \mu A \end{aligned}$$

Unfortunately, the full scale deflection of the sensitive particle and streamer current



TA-687325-7R

FIGURE 10 ILLUSTRATING PRINCIPAL PERIOD OF PARTICLE COUNTER ACTIVITY DURING LAUNCH OF TITAN III C-20

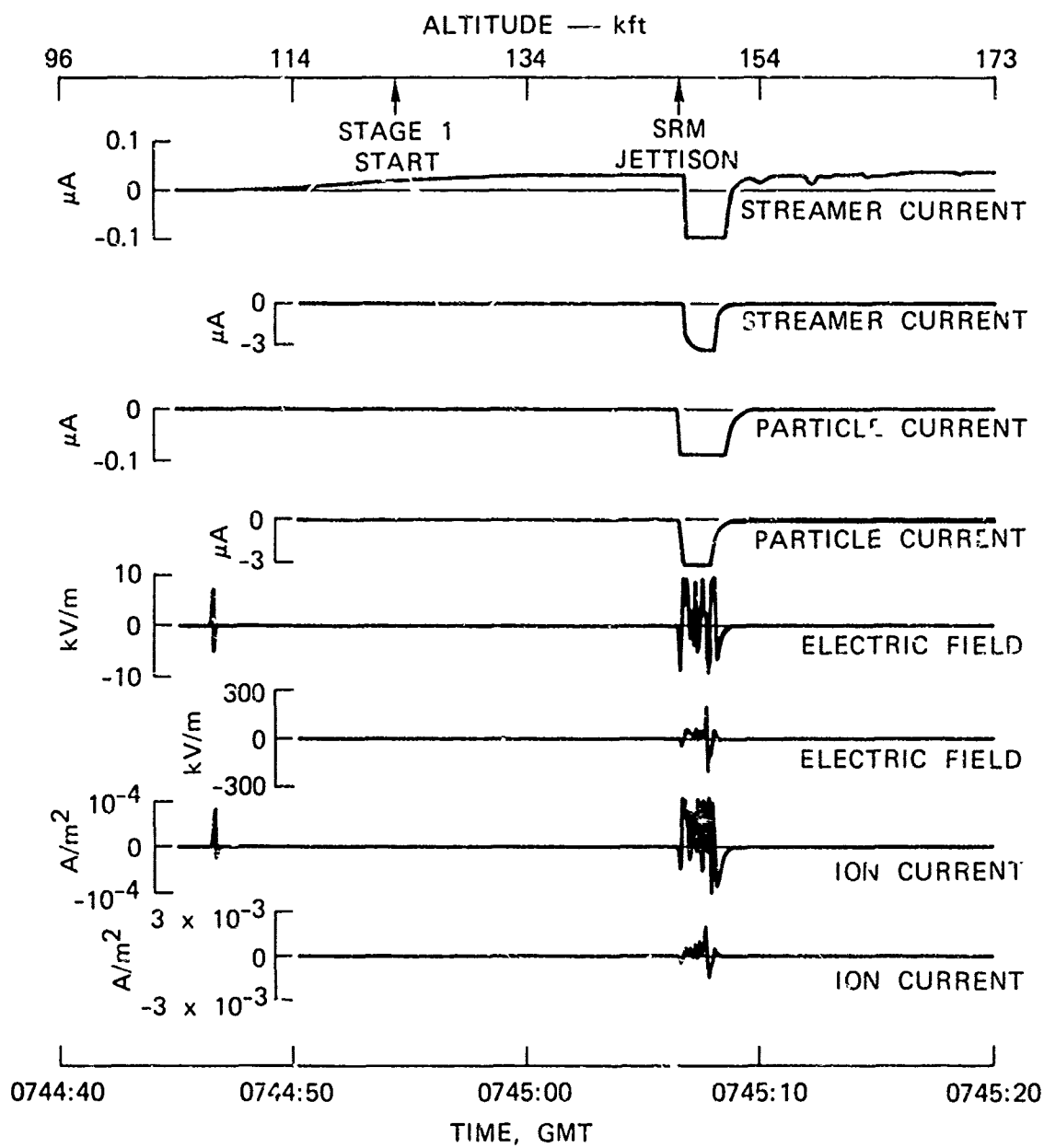


FIGURE 11 MEASUREMENTS DURING FIRST STAGING OF TITAN III C-20

channels is  $0.1 \mu\text{A}$  so that a current of  $0.0025 \mu\text{A}$  is right at the limit of detectability of the current measuring system. Accordingly, it is not surprising that there is no indication of charging current accompanying the evidences of particle impact.

Before leaving the question of the encounter with particles at 100 kft altitude, it is interesting to invoke a further test. Experiments involving the firing of 5/32-in-diam. steel balls through clouds of ice crystals and dust indicate that charging by impact with the ice crystals was zero at velocities 3500 ft/sec and above, while impact with dust particles produces charging to velocities of 4000 - 5000 ft/sec depending upon the type of dust (19). The velocity profile shown in the lower portion of Figure 10 indicates that, at this time, the rocket velocity is in the regime where particle impact charging is marginally possible. (It is not clear that the data obtained with 5/32-in-diam. balls at sea level should be applied on a one-to-one basis to a 10-ft-diam. rocket at high altitude. Thus it is conceivable that charging could persist to the velocities shown in Figure 10.) It appears, therefore, that the evidence of particle impact of Figure 10 must be accepted as real.

Titan III C-21 - At the time of C-21 launch, rain of varying intensity was falling on the launch pad, and heavy cloud formations existed at high altitudes (e.g., 10 to 40 kft). Again all instrumentation worked both on the ground and in flight to synchronous orbit injection.

Data generated by onboard instruments during the first minute after C-21 launch are shown in Figure 12. This record obviously shows far more activity than the C-20 data in Figure 9. Inspecting the rocket potential record in Figure 12 we see that in the first two seconds after ignition, the field meter indicated a field change corresponding to a positive potential of 50 kV on the rocket. It is not clear what physical explanation should be offered for this initial positive potential excursion. The rocket has barely moved from the pad so that the plume is certainly in good contact with the ground so that, based on the C-20 experience, one would expect the rocket potential to be low. Seeking some transitory charging process involving the rain does not seem promising because the field meter was exposed to the rain and its reading was steady until SRM ignition.

Following the initial positive excursion, the potential assumed a low negative value and remained there until 0309:14 when the rocket reached 650 ft altitude. At this time the potential rapidly increased to a maximum value

of -100 kV. This rapid potential change again suggests that the conductive plume broke contact with the ground when the rocket reaches 650 ft. The rate of potential increase is  $\Delta V/\Delta t = -5.5 \times 10^4$  volt/sec. This corresponds to a charging current of  $i_{\text{chg}} = 5.5 \times 10^4 (10^{-9}) = 55 \mu\text{A}$  which is roughly half the rocket motor charging current observed during the launch of C-20. After reaching -100 kV, the rocket potential gradually decreased and remained within the range  $\pm 15$  kV for the rest of the flight through the atmosphere.

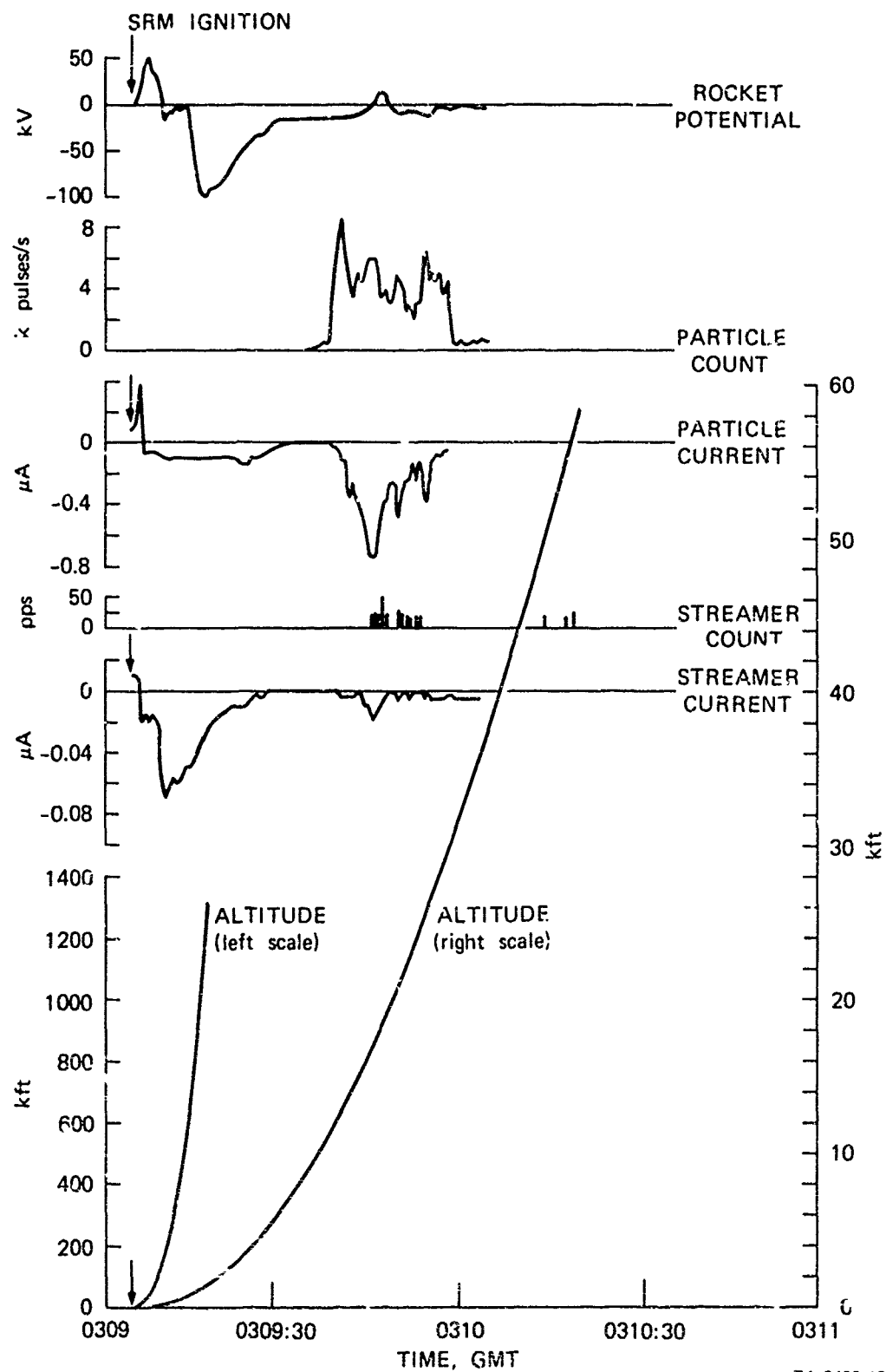
Both the particle and streamer current channels indicate that negative charge is arriving on the sensor immediately after SRM ignition. It is very likely that these sensor currents do not represent actual charge arriving on the vehicle, but rather are electrochemical currents flowing in each probe system because the probes are wet from the rain. (The probes were uncovered prior to launch.) Although the sensors were made entirely of stainless steel, there is often sufficient difference in the metals that battery action can occur. This effect was often observed on aircraft flights through rain where it was found that the current would gradually go to zero after the aircraft left the rain cloud and the probe dried.

True charging by precipitation begins unequivocally at 0309:36 at an altitude of 10 kft when the particle counter first indicates particle impacts. Particle counting and particle current persist until 0310:00 when the rocket reaches 32 kft altitude. The data indicate that negative charge is arriving on the rocket. This is in agreement with the charging polarity observed during aircraft flight in precipitation.

Further comparisons with aircraft flight test results will be interesting. For example, at 0309:45 when the particle current is maximum  $i_p = 0.8 \mu\text{A}$ , the particle count  $N$  is  $6 \times 10^3$  particles/sec and the rocket velocity  $v$  is roughly 1000 ft/sec = 305 m/sec. Since the particle probe area is  $A = 100 \text{ cm}^2 \approx 0.1 \text{ ft}^2$ , this means that the frontal charging rate  $i/A = 0.8/0.1 = 8 \mu\text{A}/\text{ft}^2$ . This value is in excellent agreement with aircraft flight test experience (18) which indicates peak frontal charging of 5 to  $10 \mu\text{A}/\text{ft}^2$  in cirrus and  $30 \mu\text{A}/\text{ft}^2$  in frontal snow.

The particle density  $\rho$  in the cloud can be found from

$$\rho = \frac{N}{Av} \\ = \frac{6 \times 10^3}{.01(305)}$$



TA-8428-17

FIGURE 12 LAUNCH DATA FROM TITAN III C-21

$$= 2 \times 10^3 \text{ particles/m}^3$$

Aircraft flight test experience (18) indicates that typical maximum particle concentrations are, for cirrus type clouds,  $2 \times 10^4$  particles/ $\text{m}^3$  and for a thunderhead  $6 \times 10^4$  particles/ $\text{m}^3$ . Thus, the Titan particle density data are an order of magnitude below the maximum values measured in the aircraft flight test programs.

The charge  $q_p$  acquired by each impinging particle can be found simply by dividing the particle current by the particle count

$$\begin{aligned} q_p &= i_p / N \\ &= \frac{.8 \times 10^{-6}}{6 \times 10^3} = 1.3 \times 10^{-10} \\ &= 130 \mu\mu \text{ coul.} \end{aligned}$$

Normally charges of the order of  $10 \mu\mu$  coul are measured during aircraft flight tests. This probably means that not all of the particles striking the probe were counted, so that the actual particle concentration in the clouds was most likely of the order of  $10^4$  particles/ $\text{m}^3$ .

The streamer study instrumentation also generated interesting data during the period of maximum precipitation charging. It should be noted that streamer counting does not start until 0309:45 almost 10 sec after the onset of particle counting. This is reasonable because the plastic surface takes time to become charged before streamer discharges can occur. It is also interesting that the streamer current is not steady, but there are bursts of current corresponding to bursts of streamer occurrence. The charge  $q_s$  transferred per streamer discharge can be estimated from the streamer current  $i_s$  and the streamer count  $N_s$  from the relation

$$q_s = \frac{i_s}{N_s}$$

For the period of maximum streamer current at 0309:45, we find  $i_s = 2 \times 10^{-8}$  amp and  $N = 20$  so that

$$\begin{aligned} q_s &= \frac{2 \times 10^{-8}}{20} \\ &= 10^{-9} \text{ coul.} \end{aligned}$$

This result is in perfect agreement with the results of ground and flight test studies of streamer processes, where it was found that the charge transferred per streamer was  $1-1.5 \times 10^{-9}$

coul.

Although many aspects of the Titan II C-21 electrostatic behavior have been similar to that observed on large jet aircraft there are important differences. Figure 13 shows plots of the potential of the Titan III C-20 and C-21 together with a typical record of the potential of a 707 aircraft during take off. In the case of the 707, engine charging causes the potential to rise to 100 to 150 kV (depending on whether water injection or dry engine operation is being used) immediately when the wheels leave the ground. In the case of the Titan III-C, the conductivity of the exhaust plume in contact with the ground holds the potential down until at an altitude of 650 ft contact is broken. Then the potential rises to hundreds of kV.

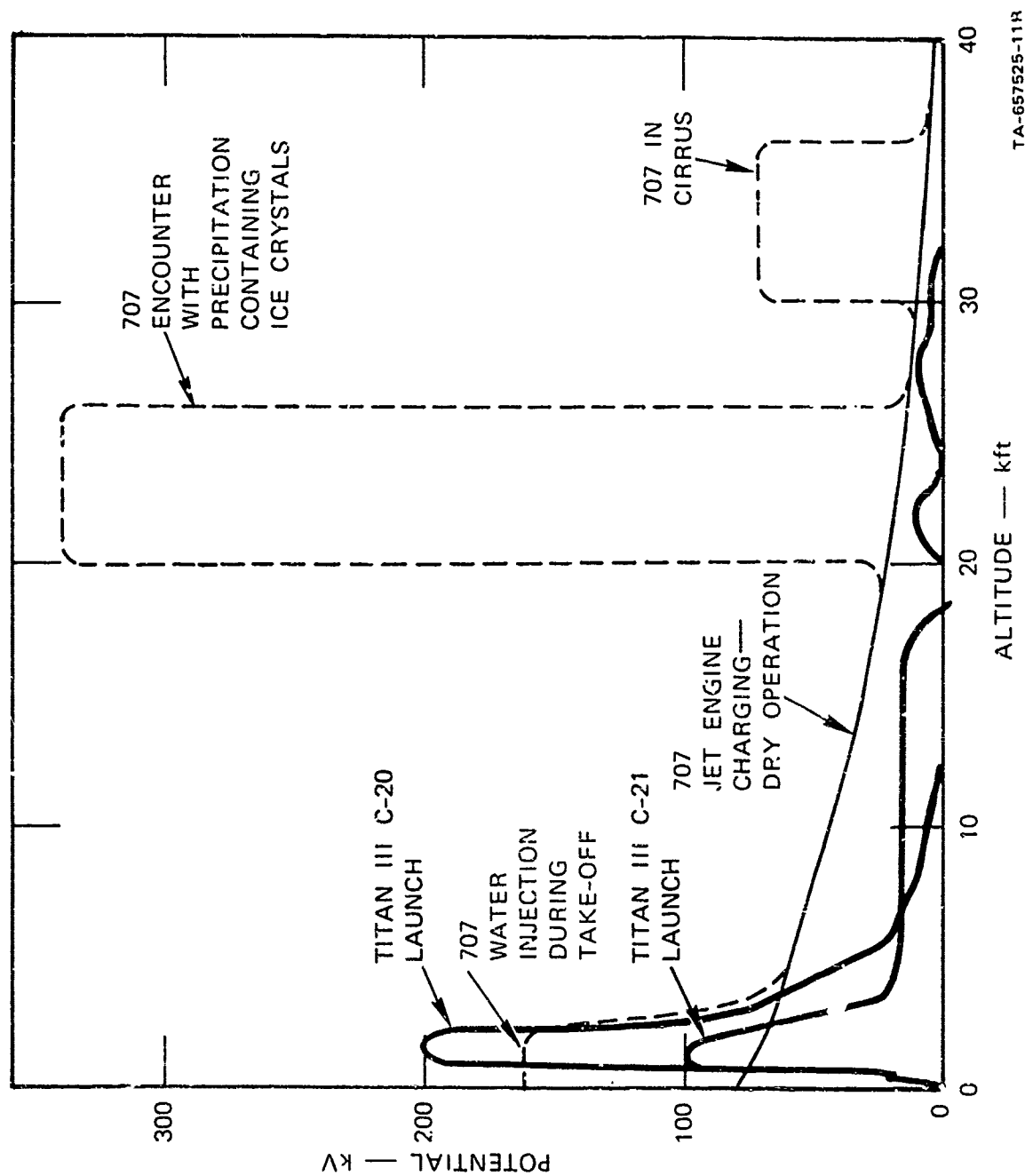
As the 707 climbs, in clear weather, its potential gradually decreases monotonically to zero. If the 707 encounters precipitation, its potential rises to hundreds of kV (the precise value depends on the density and type of cloud). The potential of Titan III-C, also decreases to zero as the rocket climbs. However, the Titan potential is only slightly affected by an encounter with precipitation. For example, in Figure 12 at time 0309:45 we showed that the frontal charging current is  $8 \mu\text{A}/\text{ft}^2$ . (At this charging rate, the 707 potential would reach 150 kV). This insensitivity of rocket potential to charging undoubtedly stems from the high conductivity of the high temperature rocket plume. Similar behavior is observed on fighter aircraft equipped with afterburners. For example, in flight tests on an F-4 at Eglin AFB, it was observed that operating the afterburner on take off increased the engine charging thereby increasing the aircraft potential. On the other hand, if the aircraft was at operational altitude, the activation of the afterburners served to help discharge the aircraft and reduce its potential.

Although there was additional activity observed on certain of the electrostatic study instruments up to altitudes of several hundred kft, its significance is not clear yet, and will not be discussed here.

GROUND DATA - Titan III C-20 - Data generated by the ground instrumentation array during the launch of Titan III C-20 are shown in Figure 14. The launch tower field meter records (shown to the time the motors reached the top of the tower) can be interpreted to indicate that a negatively charged body passed the top of the tower. This is in agreement

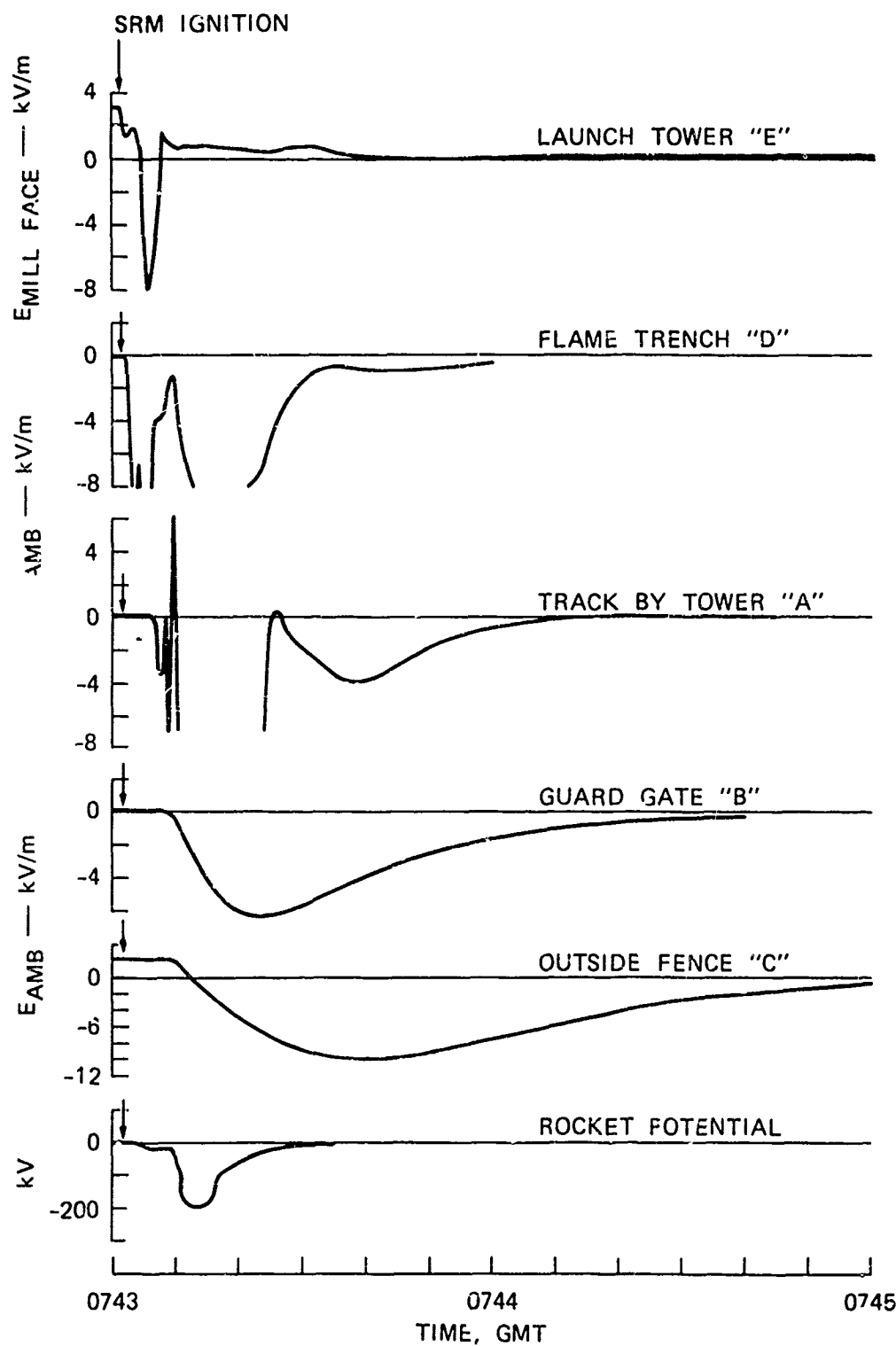
\* Report on these flight tests currently under preparation at SRI.





TA-657525-11R

FIGURE 13 COMPARING POTENTIAL OF 707 AIRCRAFT IN FLIGHT AND TITAN III IN LAUNCH



TA-657525-9H

FIGURE 14 GROUND INSTRUMENTATION DATA FROM TITAN III C-20 LAUNCH

with the onboard instrumentation which indicated that the rocket acquired negative charge at liftoff.

The flame trench field meter indicated that negatively charged exhaust products reached the vicinity of the field meter immediately after SRM ignition. Some consideration is in order of the fact that although the rocket charged negatively indicating that the exhaust gases leaving the rocket were positively charged, yet the flame trench effluent is negatively charged. The most plausible explanation is that although the exhaust as it leaves the rocket may be slightly positively charged, it subsequently strikes the exhaust trench where it erodes the concrete surface causing electrification to occur. The exhaust also can pick up charge by interacting with water from the deluge in the exhaust trench. This interaction with material in the trench evidently produces negative charging which completely overwhelms the initial positive charge in the rocket exhaust.

The time history of the records at the remaining ground field meter locations indicates that the fields in the vicinity of the launch pad are generated by the exhaust clouds rather than by charge on the rocket. For example, the field at site C does not reach its maximum until the rocket potential shown at the bottom of Figure 14 for reference has reached zero. Also, calculations not presented here indicate that the magnitude of the measured charge on the rocket is inconsistent with the observed ground fields.

Titan III C-21 - The ground data from Titan III C-21 are shown in Figure 15. Their behavior is similar to that observed for C-20. Again the launch tower field meter record is consistent with a negatively-charged body moving by. The behavior of the rest of the field meters indicates that again the exhaust clouds were negatively charged. The fields associated with the launch of C-21 are roughly half those observed on C-20. Again the time history of the ground records agrees that they were not generated by charge on the rocket vehicle since the field at site B, for example, reaches its peak considerably after the rocket potential has peaked.

Apollo 14 (for comparison) - For comparison, the results of SRI ground field measurements reproduced from Ref. 9 are shown in Figure 16. The field meter arrangement was similar to that employed for the Titan experiments and is presented in Ref. 9, but will not be discussed here. The launch tower field meter indicates a positive field change accompanying lift off indicating that the engines charged the Apollo 14 vehicle positively. (It will be recalled that both

Titans charged negatively.) At the time the engines reach the field meter, the measured field magnitude indicates that the rocket potential is less than 6000 V. This result is in good agreement with the Titan experiments in which it was argued that the rocket potential remained relatively low until the rocket plume broke contact with the ground.

On the remaining ground field meters the field changes were in the positive direction indicating that predominantly positive exhaust clouds were generated by the launch, whereas, negatively charged clouds were observed in the Titan experiments. There is evidence in the Apollo ground data for the existence of different charge polarities in different parts of the cloud. Thus it is not surprising that different gross effects were observed on the two vehicles since both polarities of charging undoubtedly occur on both launches, and the gross fields are determined by which process dominates.

#### CONCLUSIONS

The Titan III experiments generated a variety of significant results. Of great interest is the fact that the rocket appears to be connected to earth until it reaches an altitude of 650 feet. This means that the rocket is trailed by a highly conducting plume 650 ft long. The presence of this plume is significant in many situations (for example, in making determinations of the likelihood of lightning strikes to the rocket).

The experiments indicate that, in the early stages of the launch, the rocket motors charge the vehicle to potentials of hundreds of kilovolts. Accordingly, corona discharges can be expected from prominent protrusions from the vehicle.

At higher altitudes, the rocket motors serve to discharge the vehicle so that high vehicle potentials and corona discharges do not occur during flight through precipitation.

Precipitation charging of the frontal surfaces does occur as in the case of aircraft. The charging rates measured on the Titan are in good agreement with aircraft data. Evidences of frictional charging by particles were present to altitudes of 100 kft (where nacreous clouds occur).

Streamer discharges on dielectric frontal surfaces of the Titan were shown to occur. The characteristics of these discharges appear to be in good agreement with aircraft experience. (It should be noted that the frontal charging and the resulting streamers occur in spite of the fact that the vehicle as a whole is at low

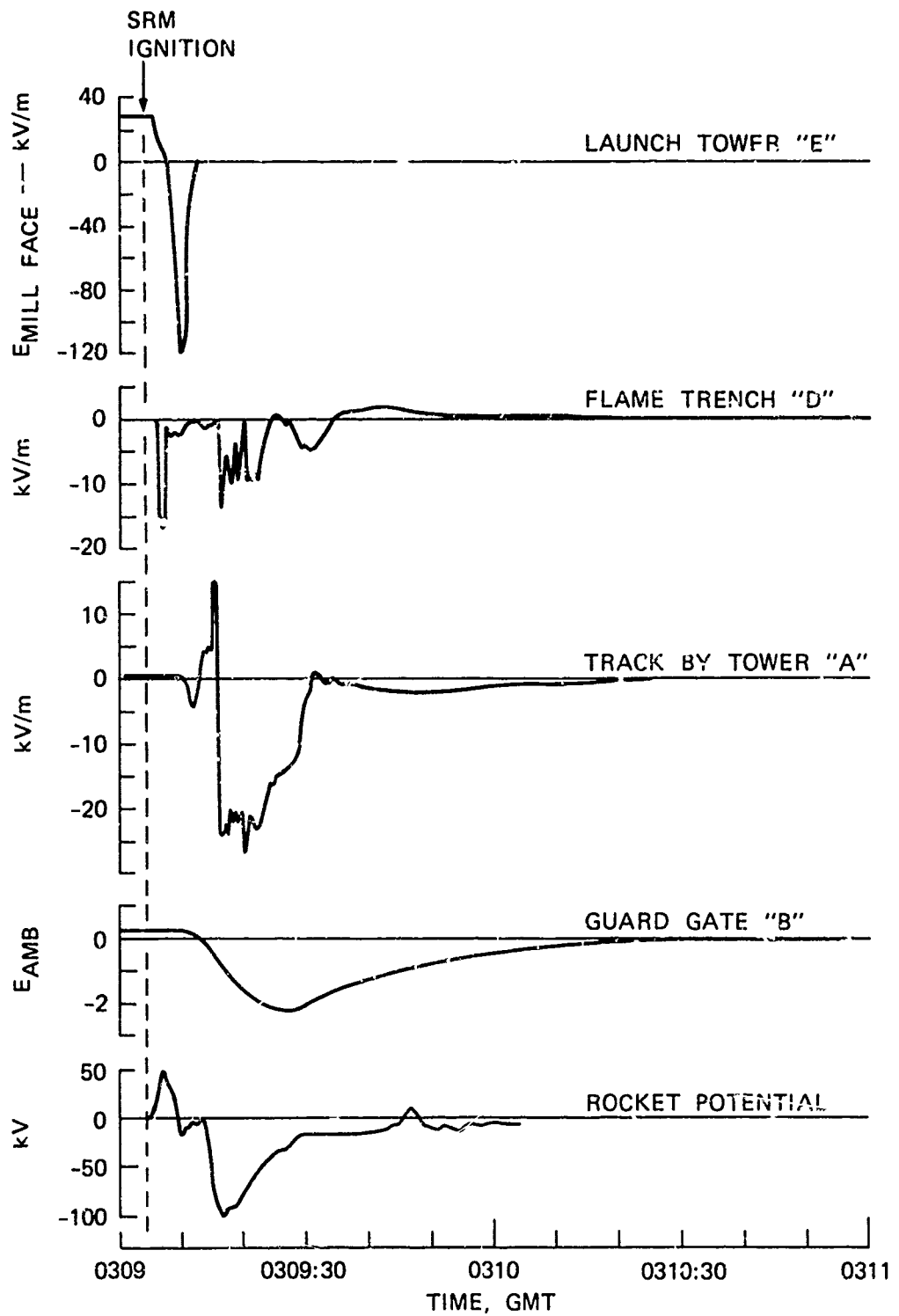
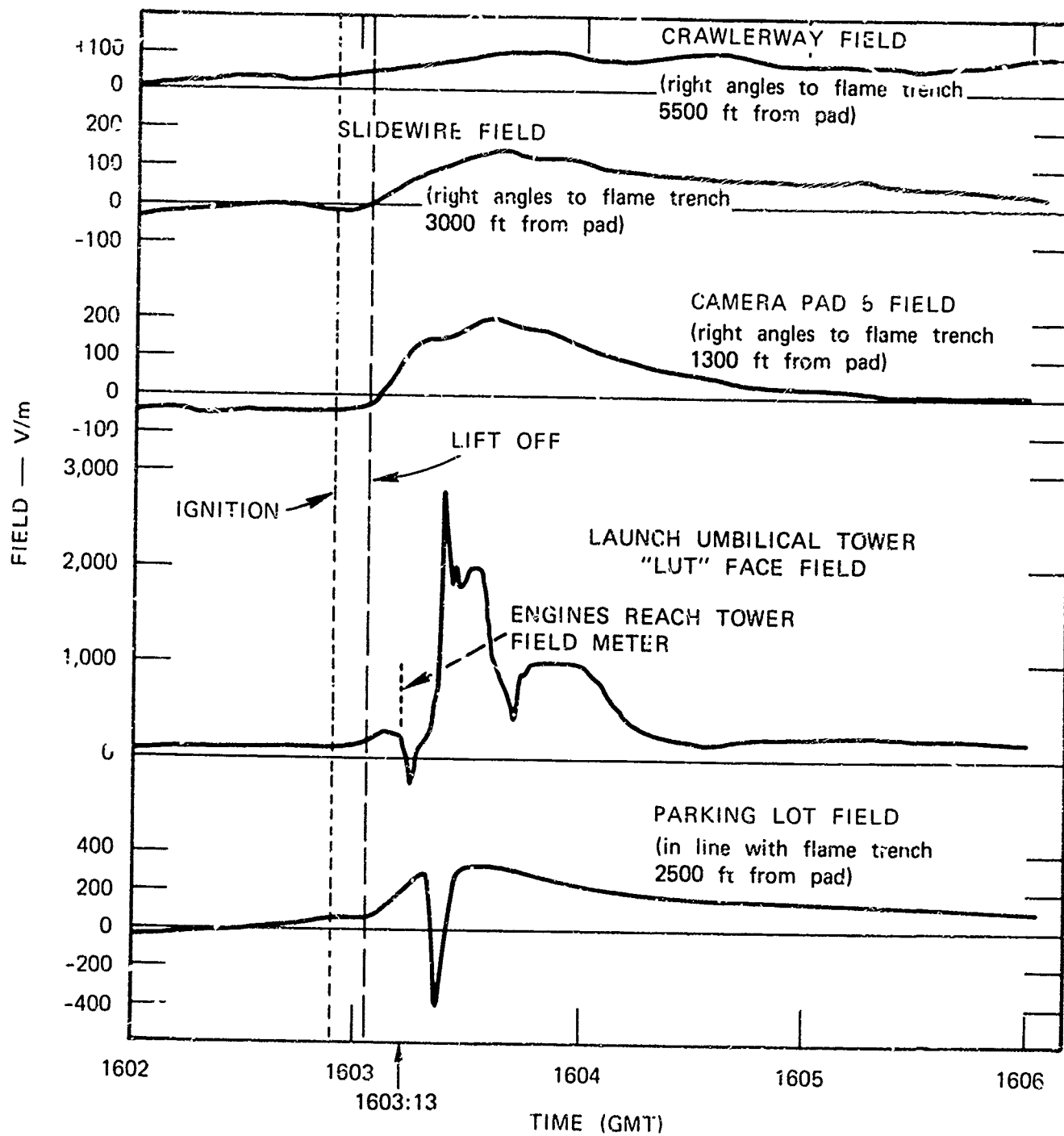


FIGURE 15 GROUND INSTRUMENTATION DATA FROM TITAN III C-21 LAUNCH



TA-657525-8R

FIGURE 16 SRI DATA FROM APOLLO 14

potential as the result of the rocket motor discharging).

Finally, the experiments indicate that the electric fields in the vicinity of the launch pad are so dominated by the charged clouds associated with the launch that relying solely on ground field measurements to infer the rocket's behavior is not likely to be fruitful.

The general conclusion from these experiments is that static electrification by large rockets does indeed occur, but that it differs in detail from that observed on aircraft. The same precautions regarding precipitation static observed in aircraft design should be applied to rockets. In particular, care should be exercised to avoid unbonded metal frontal surfaces since these will lead to highly noisy spark discharges from the unbonded member to the adjacent airframe. If sensitive systems are carried on the vehicle, provisions, such as the use of conductive surface coatings, should be made to eliminate streaming on dielectric frontal surfaces.

#### ACKNOWLEDGEMENTS

The work reported in this paper was conducted on Air Force Contract F33615-70-C-1406. The work was administered under the direction of the Systems Engineering Group (RTD) of the Air Force Avionics Laboratory, Wright-Patterson Air Force Base, Ohio. Mr. C. R. Austin, AFWL/WRE was the task engineer.

Many people and organizations contributed to the success of the flight test program. G. R. Hilbers of SRI was responsible for the design and fabrication of the flight test instrumentation. H. Heritage of Aerospace Corp. and Capt. T. Lang of SAMSO saw to it that all personnel and organizations involved in the program worked effectively and expeditiously toward to goal of instrumenting the test vehicle. N. Fox of Martin Marietta was responsible for integrating the instrumentation into the test rocket. Finally, the author is grateful to many people at AFETR who participated in the installation, checkout, and launch of the test vehicles.

#### REFERENCES

1. E. F. Vance, L. B. Seely, and J. E. Nanevicz, "Effects of Vehicle Electrification on Apollo Electro-Explosive Devices," Final Report, Contract NAS-9-3154, SRI Project 3101, Stanford Research Institute, Menlo Park, California (December 1964).
2. L. Aronowitz, "Rocket-Engine-Generated Voltage as a Source of Electromagnetic Interference and Electronic Component Damage on Interplanetary Vehicles," paper presented at IEEE Space Electronics Symposium, Miami Beach, Florida, 2-4 November 1965.
3. "Electrical Boundary Currents Generated by Plasma Flow," *Applied Physics Letters* 6, pp. 215-216 (1965).
4. P. Molmud, "Frictional Electricity in Missile Systems," *J. Am. Roc. Soc.*, pp. 73-74 (January 1969).
5. W. K. Luckow, "Spacecraft Electrostatic Phenomena," SID 64-422-1, Space and Information Systems Division, North American Aviation, Inc., Downey California (February 1964).
6. E. F. Vance and J. E. Nanevicz, "Rocket Motor Charging Experiments," Scientific Report No. 2, Contract AF 19(628)-4800, SRI Project 5359, Stanford Research Institute, Menlo Park, California (December 1967).
7. J. E. Nanevicz, E. F. Vance, W. C. Wadsworth, and J. A. Martin, "Low-Altitude, Long-Range All-Weather Vehicle Interference Investigation," Tech. Report AFAL-TR-65-236 Contract AF 33(615)-1934, SRI Project 5082, Stanford Research Institute, Menlo Park, California (December 1965).
8. J. E. Nanevicz, "Progress in the Study of Titan Vehicle Electrostatic Environment," Engineering Data Design Evaluation Report, Contract F33615-70-C-1406, SRI Project 8428, Stanford Research Institute, Menlo Park, California (May 1971).
9. J. E. Nanevicz, E. T. Pierce, and A. L. Whitham, "Measurements in Atmospheric Electricity Designed to Improve Launch Safety During the Apollo Series," Final Report, Contract NAS 9-11357, SRI Project 8940, Stanford Research Institute, Menlo Park, California (June 1972).
10. J. E. Nanevicz, E. F. Vance, and W. C. Wadsworth, "Low-Altitude, Long Range All-Weather Vehicle Interference Investigation: Development of Flight Test Instrumentation, Part II," Tech. Report AFAL-TR-65-239, Contract AF 33(615)-1934 SRI Project 5082, Stanford Research Institute, Menlo Park, California (December 1966).
11. J. E. Nanevicz, and J. B. Chown, "SRI Experiments on AFCRL Nike-Cajun Rocket AD 6.842 and on Trailblazer II," Scientific Report 8, Contract AF 19(628)-4800, SRI Project 5359, Stanford Research Institute, Menlo Park, California (December 1967).
12. W. E. Scharfman and H. R. Bredfeldt, "Use of the Langmuir Probe to Determine the Electron Density and Temperature Surrounding Reentry Vehicles," Final Report, Contract NAS1-4872, SRI Project 5771, Stanford Research Institute, Menlo Park, California (December 1966).

13. L. J. Paustian, Titan III-C Payload Users' Guide, Martin-Marietta Corp., Denver Division, Denver, Colorado (January 1968).

14. K. E. Bessett, "T III-C Vehicle 20 Final 3D Guidance Reference Trajectory Reissue A," MCR-70-414, Martin-Marietta Corp., Denver, Colorado (April 1971).

15. M. A. Uman, "Electrical Breakdown in the Apollo 12/Saturn V First Stage Exhaust," Report 70-SCS-HIVOL-R1, Westinghouse Research Laboratories, Pittsburgh, Pennsylvania (1970).

16. J. E. Nanevich, E. F. Vance, R. L. Tanner, and G. R. Hilbers, "Development and Testing of Techniques for Precipitation Static Interference Reduction," Final Report, Contract AF 33(616)-6561, SRI Project 2848, Stanford Research Institute, Menlo Park, California (January 1962).

17. J. E. Axtell, "Preliminary Minuteman Electrostatic Charge Studies," Model No. WS-133A, Contract AF 04(647)-580, The Boeing Company, Seattle, Washington (1963).

18. R. L. Tanner and J. E. Nanevich, "Precipitation Charging and Corona-Generated Interference in Aircraft," ACRL 336, Tech. Report 73, Contract AF 19(604)-3458, SRI Project 2494, Stanford Research Institute, Menlo Park, California (April 1961).

19. J. E. Nanevich, E. F. Vance, W. C. Wadsworth, and J. A. Martin, "Low-Altitude, Long-Range All-Weather Vehicle Interferences Investigation," Tech. Report AFAL-TR-65-239, Contract AF 33(615)-1934, SRI Project 5082, Stanford Research Institute, Menlo Park, California (December 1965).

20. J. E. Nanevich, "A Study of Precipitation-Static Noise Generation in Aircraft Canopy Antennas," Tech. Report 62, SRI Project 1197, Contract AF 19(604)-1296, Stanford Research Institute, Menlo Park, California (December 1957).

## Static Electricity in the Apollo and Skylab Spacecraft

Andrew E. Potter, Jr., and B. R. Baker  
NASA Manned Spacecraft Center  
Houston, Texas

### ABSTRACT

Reports of electric sparks produced by static charges on the Apollo space suit prompted an investigation of static electricity ignition hazards and communications interferences in the Apollo spacecraft. The production of static electricity by contact of a space-suited man with the spacecraft was studied by rubbing the space-suited man with various materials and by measuring the voltage produced. Approximately 2 milli-joules of electric energy were accumulated by the space-suited man; this amount is sufficient to ignite combustible gas vapors and mists. Static electricity ignition tests conducted on solid combustibles (logbook paper and cotton fabric) in the spacecraft showed that ignition of these solid materials by 2 millijoules of electric energy was not possible.

Biomedical sensors attached to the man's body and plugged into the spacecraft electronics provide an effective grounding path so that no danger of electrostatic charge buildup exists. However, static electricity drainage through the biomedical sensors temporarily interferes with cardiac measurements. This interference is minimized by adding a resistor in parallel to the ground circuit. Since no effective means of charge buildup existed, and no ignitable materials existed, it was concluded that ignition hazards from static electricity were effectively zero in the Apollo spacecraft.

In addition to the space suit, other sources of static electricity were studied. The static electricity accumulated by the Teflon Velcro and the food bags did not present a problem. However, the Teflon-coated glass fiber cloth items (the constant-wear garment, tool bags, sleeping bags, and suit-storage bags) became electrically charged while in use. Storage lockers on the command module floor are subject to frequent contact with insulating materials (such as sleeping bags), and the lockers were found to accumulate static electricity before they were grounded to the spacecraft structure. The lithium hydroxide canisters in the command module accumulated large static charges when removed from the storage lockers. Grounding of the canisters eliminated this effect.

A survey of the Skylab spacecraft to locate sources of static electricity was performed. No hazardous conditions were located. Some minor interference problems with electronic gear were found and corrected.

**INTRODUCTION** During the effort to remove all flammable materials from the Apollo spacecraft, combustible fabrics were replaced, whenever possible, with noncombustible glass fiber cloth. Following the replacement, previously unnoted static electricity effects occurred. For example, sparks were discharged during removal of equipment from the spacecraft wall, donning of suits, and installation of a glass-fiber-cloth-covered umbilical cable, which had previously been dragged across the command module (CM) floor.

These incidents of static electricity in the Apollo spacecraft prompted an investigation, since for several reasons, static electricity sparks are considered hazardous. (References 1, 2, 3, and 4)

The most obvious reason is the danger of a spark igniting combustible material in the spacecraft. Other hazardous effects of static electricity sparks are interference with communications or telemetered data and the involuntary reflex movements associated with discharge of a spark from a body. The objective of this investigation was to evaluate the static electricity ignition hazards resulting from electrostatic charges. This evaluation was accomplished by comparing the amount of electrical energy that was accumulated with the amount of energy required to ignite flammable materials in the spacecraft.

Static electricity accumulation by the space-suited man was the major concern in the investigation of static electricity in the Apollo spacecraft. However, the entire spacecraft was surveyed to locate and evaluate other sources of electric charges. Static electricity interferences with communications and instrument readings were also studied. Sufficient spark ignition data for evaluation of the static electricity ignition hazard were not available; therefore, measurements were made of minimum spark ignition energy for typical flammable materials in the spacecraft.

### MINIMUM IGNITION ENERGY

The minimum ignition energy (MIE) has been extensively investigated for many combustible mixtures. For gaseous mixtures, the MIE is a definite quantity which depends on the type of fuel, on fuel concentration, and to a lesser extent, on the electrode configuration.

Representative values for gaseous mixtures are as follows (refs. 1 and 2): For hydrocarbon-air mixtures at 1 atmosphere, MIE



values are in the range of 0.2 to 0.4 millijoule of spark energy. In a hydrocarbon-pure oxygen mixture at 1 atmosphere, MIE values range from 0.002 to 0.004 millijoule of spark energy. Lowering the pressure from 1 atmosphere to one-third atmosphere increases the MIE so that hydrocarbon-oxygen mixtures at one-third atmosphere have MIE values ranging from 0.02 to 0.04 millijoule of spark energy. (The Apollo spacecraft cabin atmosphere is pure oxygen at one-third atmosphere.) Hydrogen is the most easily ignited fuel, with MIE values 10 times less than the MIE values for hydrocarbons.

The energy required to ignite gas vapors or mists is not well defined because the spark energy must be divided in two parts; one part is used to evaporate the liquid fuel, and the other part is used to ignite the gaseous combustible mixture resulting from the evaporation. Generally, approximately 1 millijoule of spark energy is required for the ignition of fuel droplets in air (ref. 1). Fuel droplets in oxygen are expected to require less energy for ignition. The decrease is not expected to be a large one because much of the spark energy is used for fuel evaporation. Approximately the same amount of fuel must be evaporated in both air and oxygen because substitution of oxygen for air does not have a large effect on the lean flammability limit.

The energy required to ignite dusts or fibrous materials is poorly defined. A considerable amount of energy is required in order to vaporize a solid before ignition; therefore, 10 millijoules has been given (ref. 1) as an approximate energy requirement for ignition. Substitution of oxygen for air is expected to have little effect on this value. Because the MIE for solid materials is variable, measurement of the MIE for typical solid flammable materials present in the Apollo spacecraft was desirable.

#### MINIMUM IGNITION ENERGY FOR SOLID COMBUSTIBLES IN THE APOLLO SPACECRAFT

The Apollo spacecraft was surveyed for the presence of flammable materials on March 1, 1968. Logbook paper and cotton underwear were identified as the only easily flammable materials that would exist in the flight-qualified spacecraft. By passing capacitor sparks of known energy through the logbook paper and cotton underwear, their ignition characteristics were measured.

The spark ignition apparatus used for measuring the ignition characteristics of the logbook paper and cotton underwear is shown schematically in figure 1. The cloth or paper sample being tested was clamped loosely to a 1-inch-diameter copper disk electrode, which was electrically grounded to the metal chamber wall. A sharply pointed steel electrode was placed approximately 0.5 centimeter from the disk electrode. The pointed steel electrode passed from the chamber through a window, from which ignition was observed. The

spark generator was calibrated by discharging sparks through a 100-megohm high-voltage resistor. Voltage across the resistor was measured as a function of time with an oscilloscope. The effective capacitance  $C$  of the circuit was calculated from the rate of decay of voltage across the 100-megohm resistor, and the actual voltage  $V$  available was considered to be the initial peak voltage. The spark energy  $E$  was calculated from the relation  $E = 0.5CV^2$ .

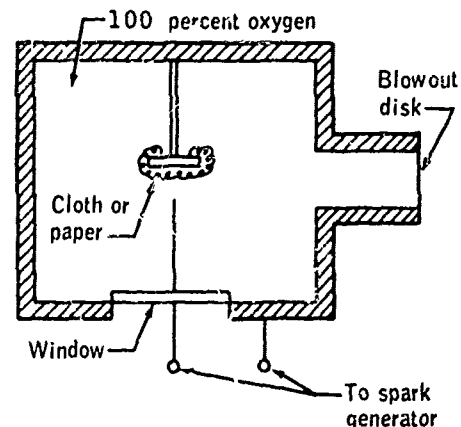


Figure 1. - Schematic diagram of spark ignition test chamber.

Measurement of the ignition characteristics of logbook paper and cotton underwear showed no defined ignition limit and the ignition appeared to be statistical. The following procedure was used to measure the ignition characteristics of the two materials. The spark generator was adjusted to give a spark of moderate energy. The spark was repeated until an ignition occurred or until 20 sparks had passed. If ignition occurred, the spark energy was decreased, and the procedure was repeated. If 20 sparks were passed without an ignition, the spark energy was increased, and the procedure was repeated. Prior to installation in the test chamber, the samples of cloth and paper were rubbed with sandpaper to generate as much lint as possible. Prior to starting the spark tests, the test chamber was evacuated to a pressure of less than 10 microns with the cloth or paper sample in place to remove all traces of moisture from the material. During the spark tests, a moderate flow of the test atmosphere was maintained throughout the chamber. For most of the tests, the disk electrode and pointed steel spark electrode were maintained approximately 5 millimeters apart. The distance between the two electrodes was varied in one series of tests with no apparent effect on the results.

The results of the spark tests on the logbook paper are shown in table I, and the results of the test on the cotton fabric are shown in table II.

TABLE II. - SPARK IGNITION OF COTTON CLOTH

Spark energy, mJ	Number of sparks	Results
16.5 psia oxygen, Feb. 29, 1968		
12	26	No ignition
20	21	1 ignition
26	28	No ignition
32	14	No ignition
41	21	No ignition
52	21	No ignition
74	5	1 ignition
16.5 psia oxygen, Mar. 6, 1968		
9	8	1 ignition
12	6	1 ignition
20	16	2 ignitions

The ignition of the logbook paper in a 16.5-psia, 100-percent-oxygen atmosphere was difficult. No ignitions occurred until 120-millijoule sparks were used. The sparks were observed to puncture the paper at all energies. To prevent a spark from passing through the hole made by the previous spark, the pointed electrode was moved after each spark.

The cotton fabric sample was ignited by sparks with energies as low as 9 millijoules in one test series, while 20 millijoules of spark energy were required in order to ignite the fabric in another test series. Change of the atmosphere from 16.5-psia pure oxygen to a 16.5-psia, 60-percent-oxygen, 40-percent-nitrogen mixture had little effect. Use of only 9 millijoules of spark energy yielded ignition in both atmospheres. However, a change of pressure from 16.5 to 6.2 psia in the pure-oxygen atmosphere had a pronounced effect. At the lower pressure, no ignition occurred up to energies of 170 millijoules. Higher energies were not available from the spark generator.

#### CAPACITANCE MEASUREMENTS

The objective of capacitance measurements is to determine where significant amounts of static electricity might accumulate on a space-suited man. To accomplish this objective, capacitance relative to the electrical ground was measured at different points. The results show (table III) that the most important point for charge accumulation is the body of the man inside the space suit. The observed body capacitance values of approximately 200 micromicrofarads are similar to values reported in reference 1.

#### STATIC ELECTRIFICATION OF SPACE SUITS

The inner lining of the space suit contains several alternating layers of metallized plastic. The capacitance of these layers relative to one another is large, but the capacitance of the layers relative to the electrical ground appears to be negligible. Contact with the metallized plastic layers was made by inserting a pin through the material on the back flap of the space suit. The result was surprising, because the capacitance of the metallized plastic layers relative to the electrical ground was expected to be at least as large as the body capacitance. A possible explanation is that the various pieces of metallized plastic sewn together to make the inner lining are not in electrical contact with one another.

#### VOLTAGE MEASUREMENTS

The electrostatic voltages, generated by contact of the space suit with various materials, were measured with an electrostatic voltmeter. To achieve electrical isolation for these tests, the space-suited man stood on an insulated plastic platform. Air hoses, communications links, and biomedical sensors were disconnected. The degree of electrical isolation for this configuration was tested by charging the space-suited man and measuring the electrostatic voltage generated by his suit as a function of time. The electrostatic voltage remained constant over periods of approximately 5 minutes, which indicated that the electrical leakage resistance was more than  $10^{12}$  ohms. Charging of the space-suited man was performed by a second man who rubbed the space suit with sheets of various materials.

TABLE II. - SPARK IGNITION OF COTTON CLOTH

Spark energy, mJ	Number of sparks	Results
16.5 psia oxygen, Feb. 29, 1968		
12	26	No ignition
20	21	1 ignition
26	28	No ignition
32	14	No ignition
41	21	No ignition
52	21	No ignition
74	5	1 ignition
16.5 psia oxygen, Mar. 6, 1968		
9	8	1 ignition
12	6	1 ignition
20	16	2 ignitions
6.2 psia oxygen, Mar. 6, 1968		
20	20	No ignition
32	20	No ignition
47	20	No ignition
100	20	No ignition
130	20	No ignition
150	21	No ignition
170	22	No ignition
16.5 psia total pressure: 10.0 psia oxygen, 6.5 psia nitrogen, Mar. 6, 1968		
9	10	1 ignition
12	10	1 ignition
20	10	2 ignitions
32	40	1 ignition
42	20	1 ignition
52	12	1 ignition
75	30	1 ignition
100	3	1 ignition

In the first test series, the electrostatic voltage was measured at different points on the space-suited man after rubbing his suit with Beta 4190B glass fiber cloth. The electrostatic voltages measured at 30 percent relative humidity were as follows: space-suit arm, 4.3 kilovolts; arm ring, 3.4 kilovolts; neck ring, 2.2 kilovolts; and bare hand, 2.2 kilovolts. Repeated measurements of the same locations showed that the voltage differences that appeared to exist between various points on the space suit are the result of the method of measurement. After the space-suited man was charged by rubbing his suit with the glass fiber cloth, voltage was measured by touching a lead from the electrostatic voltmeter to the point of measurement. The voltmeter lead was then removed and the voltmeter was discharged. Voltage was then measured at a different point. Invariably,

the voltage was less in each succeeding measurement. The decrease in voltage was partially caused by leakage of the charge and partially by the 10-micromicrofarad capacitance of the voltmeter, which was discharged following each measurement.

To investigate the charge buildup on the space-suited man, the voltmeter was attached to his hand before the charge was generated on the space suit. Voltage was observed as a function of time after the space suit was charged. A qualitative representation of the charge buildup is shown in figure 2. An initial rapid decrease in voltage is followed by a small increase, which, in turn, is followed by a slower decrease to a steady value. In the steady condition, the suit surface and the man's body are observed to be at the same voltage. Possibly, the redistribution of

TABLE III. - CAPACITANCE AT VARIOUS POINTS ON  
STANDING MEN WEARING SPACE SUITS

Measuring point	Capacitance, $\mu\text{F}$	
	Suit 1	Suit 2
Hand (glove removed)	200	185
Neck ring (blue part)	1	1
Neck ring (silver part)	36	26
Air exhaust fitting	2	1
Air inlet fitting	1	1
Zipper	54	66
Wrist ring	1	1
Wrist ring gage clamp	33	34
Pin through back flap of suit material	--	2

charges throughout the man/space-suit combination is observed in this experiment.

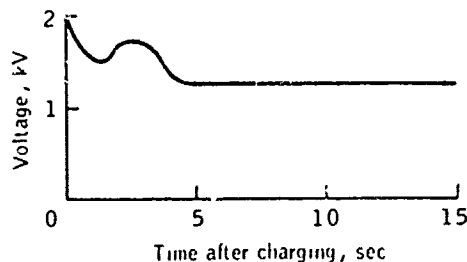


Figure 2. - Voltage on the body of space-suited man as a function of time after suit charging.

A second test series was run to determine the effect of contact material on the electrostatic voltage produced by rubbing the space-suit. During these tests, voltages were lower (in the 1-kilovolt range) than voltages observed in the first test series (in the 2- to 4-kilovolt range). Either the high relative humidity (in the 50- to 60-percent range) during the second test series or the ionized air from the electronic equipment in the test room (or both) could have lowered the kilovolt range during this second test series. The re-

sults of this test shown in table IV, demonstrate that the Beta 4190B glass fiber cloth is the most favorable static electricity generator tested, while other materials yielded only approximately two-thirds as much voltage as the Beta 4190B glass fiber cloth.

TABLE IV. - STATIC VOLTAGE  
PRODUCED ON SPACE-SUITED MAN  
BY DIFFERENT MATERIALS

Material	Static voltage, kV
Glass fiber cloth:	
Beta 4190B	1.6
Beta 4484	.8
Tellon-coated glass fiber cloth:	
Armalon	1.0
Beta cloth	.3
T-162-42 TEF	1.0
Other:	
Blue nylon	1.0
Metallized mylar	0

TABLE V. - EFFECT OF RELATIVE HUMIDITY ON ELECTROSTATIC VOLTAGE

Relative humidity, percent	Maximum voltage, kV
69	2.4
50	3.0
24	3.9

The relative humidity has a significant effect on static electricity generation because of the effect of relative humidity on surface resistance as discussed in the appendix. During a third test series, the effect of relative humidity on static electricity generation was studied. The space-suited man was placed inside a wood chamber in which the humidity was controlled. Electrostatic charge was generated on the space-suited man by rubbing the suit with a Beta 4190B glass fiber cloth. The electrostatic voltage produced by the Beta 4190B glass fiber cloth was measured at the man's hand. The results in table V show that the electrostatic voltage increased as the humidity decreased. However, at the lowest relative humidity available (24 percent), the voltage was only 3.9 kilovolts. A value of 4.3 kilovolts was observed in an earlier test made at 30 percent relative humidity. At the 24-percent relative humidity level, the test subject developed 0.5 kilovolt of static electricity standing still and 3.0 kilovolts of static electricity by shuffling his feet.

#### EVALUATION OF IGNITION HAZARD FROM ELECTROSTATIC CHARGES ON A SPACE SUIT

The maximum capacitance in the man/space-suit system was found to be equal to the capacitance of the man's body, which is approximately 200 micromicrofarads. The maximum voltage observed under a wide range of conditions was 4.3 kilovolts. Therefore, the maximum electrical energy stored in the man's body was  $0.5 (200 \times 10^{-12}) (4.3 \times 10^3)^2$ , or approximately 2 millijoules. Ignition of combustibles in the spacecraft require the following minimum amounts of energy: Ignition of gas vapors requires approximately 0.02 millijoule (at 0.33 atmosphere of pure oxygen); ignition of gas mists requires approximately 1 millijoule; and ignition of combustible solids re-

quires 10 to 100 millijoules. A comparison of the spark energy available with the spark energy required for ignition indicates that electrostatic energy sufficient to ignite gas vapors and mists, but not sufficient to ignite solids, can accumulate on the space suit.

#### ELIMINATION OF ELECTROSTATIC CHARGES FROM THE SPACE SUIT

Although the accumulation of electrostatic charge does not present a hazard in the absence of combustible gas vapors and mists, accumulation of charges is undesirable. To make charge accumulation negligible, the body of the space-suited man must be electrically grounded to the spacecraft structure. As explained in the appendix and verified by a grounding test, even large resistances to the electrical ground (as high as  $10^8$  ohms) are acceptable.

The grounding test was performed in the following manner. One terminal of a 100-megohm resistor was electrically attached to the body of a space-suited man, while the other terminal was kept free. The space-suited man was then charged by rubbing his suit. After the electrostatic voltage became constant, the free terminal of the 100-megohm resistor was connected to the electrical ground. The voltage dropped to zero in less than 1 second. In a second grounding test, both terminals of the 100-megohm resistor were connected simultaneously (one to the space-suited man, the other to the electrical ground), and the suit was rubbed to generate static electricity. No electrostatic voltage was measured on the space-suited man.

Because the biomedical sensors are attached to the space-suited man's body, the sensors could possibly provide a grounding path. Earlier in the Apollo Program, a direct electrical connection from the astronaut's body to the spacecraft electrical ground had been provided, but the connection was removed to prevent possible electrical shocks. The circuits of the remaining biomedical sensors were examined to see if a grounding path existed. A section of the drawing of the electrocardiogram (ECG) assembly is illustrated in figure 3. Two ECG sensors are attached to the electrical ground circuit by two 22-megohm resistors wired in parallel. Thus, the ECG leads provide an 11-megohm grounding path for static electricity from the space-suited man's body. Grounding tests showed that a 100-megohm grounding path was sufficient; therefore, no significant buildup of static electricity in the space-suited man should exist as long as the ECG leads are connected as illustrated in figure 3.

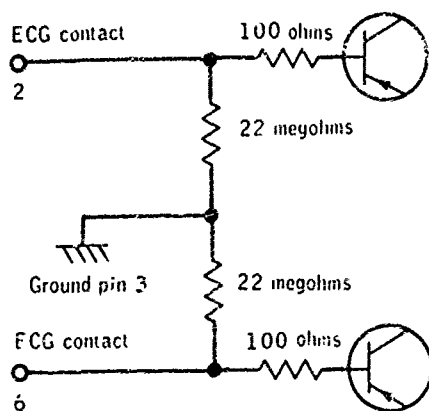


Figure 3. - Schematic section of ECG assembly electrical circuit in bioharness.

Since the current flow from the electrostatic charge drainage usually ranges from  $10^{-8}$  to  $10^{-9}$  amperes and since grounding resistance is approximately 10 megohms, voltages of 10 to 100 millivolts will appear on the ECG sensors. This voltage is similar in magnitude to the voltages normally measured by the ECG sensors. Consequently, interference with ECG readings of cardiac voltages was expected. This voltage interference was verified during crew compartment fit and function tests for SC 103 on July 17, 1968. Two space-suited men were fitted with ECG sensors in the flight configuration. When one man rubbed his arm across the space suit of the other man, large temporary disturbances in the ECG readings were observed.

#### DISCOVERY AND REMOVAL OF STATIC ELECTRICITY HAZARDS FROM SOURCES OTHER THAN THE SPACE-SUIT

Many sources of static electricity other than the space suit exist in the spacecraft. The relative importance of these sources can be determined only in operational tests, in which men occupy the spacecraft and simulate the tasks to be performed in flight. During the simulations, four effects of static electricity were observed by the crewmen; three of which were considered potentially hazardous. The spacecraft was modified to eliminate each hazard.

The first effect of static electricity occurred when the surface of the space-suit glove was charged by handling various objects. When the charged glove touched the face of a C<sub>1</sub> gage, the gage reading was altered by the electrostatic charge. However, this electrostatic charge effect presented no hazard and was disregarded.

The first electrostatic effect considered to be hazardous was produced by the plastic couch cover. Voltages up to 10,000 volts were observed on the couch cover after use of the couch by the crewmen. Furthermore, the voltage appeared to leak off the couch cover very slowly. While there was no danger of sparks directly from the couch cover (because of its insulating nature), a real danger of induced voltages in conducting objects such as space-suited men and tools that moved into the vicinity of the charged couch cover existed. Such induced voltages in conducting objects could produce dangerous sparks. The effects of these induced voltages were noted by crewmen who observed their body hair standing up when they lay on the couch.

Two methods were studied to eliminate the electrostatic charge generated by the couch cover. First, commercial antistatic coatings were applied to the couch cover material. This method proved ineffective because the coatings would not stick to the Teflon-coated material. A second method was to shorten the electrical path to the spacecraft electrical ground to increase the rate of electrical discharge of the couch cover material. Elimination of the electrostatic charge generated by the couch cover was accomplished by installing a grounded metal screen underneath the couch cover. This method proved effective in reducing voltages to less than 100 volts.

A second potentially hazardous situation became evident during SC 103 simulated altitude test runs. When lithium hydroxide canisters were withdrawn from the storage lockers, electric sparks were seen and heard by the crewmen. The sparks were observed to jump from the canister to the storage locker at the instant of withdrawal. Laboratory tests were performed to determine the amount of energy in the sparks. Storage lockers from SC 103 and lithium hydroxide canisters from both SC 101 (Apollo 6) and SC 103 were used for these tests. The lithium hydroxide canisters from the two spacecraft had similar outer dimensions and internal construction, but the outer canister wall of the SC 101 canisters was made of stainless steel and the outer wall of the SC 103 canisters was made of Teflon-coated aluminum. To hold the lithium hydroxide canisters snugly in place, the storage lockers were lined internally with pads of Teflon and silicone rubber. When the canisters were pushed into the storage locker, the pads compressed to make the canisters fit securely. These pads provided nearly complete electrical insulation between the canister and the locker. Measurements showed the resistance between the lithium hydroxide canister and the storage locker to be greater than 10,000 megohms.

Voltages and capacitances for the lithium canister relative to the storage locker were measured for a standard test configuration. The canister was installed in the

locker, momentarily grounded, and then rapidly withdrawn to a position where the canister bottom was about one-half inch from the locker top. This configuration corresponded approximately to the configuration in which sparking occurred. The spark jumped from the bottom of the canister to the top of the locker as the canister came completely out of the locker.

The capacitance of the lithium hydroxide canister relative to the storage locker was approximately 30 picofarads in the test configuration, and the voltage was approximately 10,000 volts. These values were approximately the same for all storage lockers tested; the values corresponded to a theoretical spark energy of approximately 1.5 millijoules. The theoretical spark energy is sufficient to ignite gas vapors or mists, but it is not sufficient to ignite solid combustibles. Elimination of the canister/storage lockers spark source was considered necessary, and elimination was accomplished by grounding the lithium hydroxide canisters during insertion and withdrawal. The canisters in the LM and in the PLSS were also tested. No static electricity charges were found in these two articles because of the absence of an insulating liner inside the storage lockers.

During simulation of lunar surface activities, a third potentially hazardous static electricity effect was found. The lunar sample receiving containers are hoisted into the LM by means of a Teflon fabric belt and metallic pulley combination. It was found that the hoisting operation electrically charged the belt to approximately 5000 volts. The charged belt produced strong attractive forces in powdered minerals (hematite and basalt). When the charged belt was placed 1 inch above a tray of powdered mineral, a substantial quantity of powder flew vertically upward and stuck to the belt. This alerted investigators that the belt might carry the lunar dust (which could be either toxic or flammable) into the LM along with the lunar sample container. To prevent this, the belt was sewn in a zigzag pattern with metal thread. The conducting metal thread effectively reduced the electrical charge to only a few hundred volts and completely eliminated dust pickup due to electrostatic charge.

#### STATIC ELECTRICITY IN THE SKYLAB PROGRAM

The experience gained in the Apollo program leads one to expect that static electric effects will be observed in the Skylab program. Consequently, the Skylab spacecraft was systematically surveyed to locate sources of static electricity. Careful inspections were made of the Orbital Workshop, Airlock Module, and the Multiple Docking Adapter to identify any devices, systems, or activities which could produce static electricity during operation of the spacecraft. A large number of

minor sources similar to those of Apollo were located, such as sleeping bags, stowage of metallic objects (i.e. LiOH canisters) in insulated lockers, etc. No major sources were found except possibly the astronaut himself.

The maximum static electrification level for a space-suited astronaut was established as 5000 volts in the Apollo program. In the Skylab program, similar voltages are expected for fully suited astronauts. The highly insulating nature of the surface of the suit makes possible the accumulation of a charge of this magnitude.

However, the Skylab astronauts do not wear a suit for most of their operations, and the voltage level established for the suited man is not appropriate for estimating static electric effects on these operations. Consequently, tests were performed to determine the maximum voltage to which a Skylab astronaut could become charged while wearing everyday garments. A detailed description of the test follows:

Two subjects were suited in the apparel to be worn during Skylab missions and placed in an enclosure in which the relative humidity was held below 40%. The subjects were in the enclosure for 20 minutes before tests were performed to allow the subjects and clothing to stabilize at the lower humidity. The resistance between the subjects' skin and building ground was measured to be greater than  $10^{12}$  ohms. Tests and their results were as follows: Subject 1, the fully suited subject, removed his jacket. Subject 1, was rubbed by subject 2 across the back on his undergarment with a cotton towel, Nomex, Beta cloth and flight jacket: When rubbed with cotton towel - 3000 volts built up on the body and clothing. When rubbed with Nomex - Zero volts on the body and - 1000 volts on the undergarment (the spot which was rubbed). When rubbed with Beta cloth - 1500 volts on the body and clothing. When rubbed with a second jacket - 0 volts on body, 200 volts on jacket.

It was concluded that the Skylab astronauts wearing their everyday garments will not become charged to static voltages greater than 3000 volts during normal activities in the spacecraft. This represents an approximate upper limit reached under extreme conditions, and will rarely if ever be experienced by the astronauts. The amount of electrical energy available is less than half that from the fully-suited astronaut, and is insufficient to ignite solid or fibrous combustibles, and most mists. Gases could be ignited. The hazard is considered to be negligibly small, because of the extreme difficulty of generating this amount of static electricity on the subject while wearing Skylab everyday garments. While a negligible ignition hazard is anticipated, static electricity could produce undesirable effects on sensitive circuits.

Biomedical instrumentation for measurement of brain waves and cardiac activity is sensitive to small electric charges. The

energy from common static electric discharges is sufficient to produce noise in the circuits, and in extreme cases may seriously damage the circuits.

Two sets of instrumentation were identified as possible problem areas, the electroencephalographic experiment (M133) and the electrocardiogram experiment (M093). Discussions of static electric effects on these experiments and proposed solutions to these effects are as follows:

Skylab Experiment (M133). Static electric discharge to the electroencephalographic sensors of experiment M133 when the subject dons the cap containing these sensors is a real possibility. These sensors are extremely sensitive, and damage to the circuits could easily be produced by such a discharge. A solution to the problem was implemented, in which conductive thread was sewn into the cap in a position where the astronaut must touch the thread when he grasps the cap to put it on. The metallic thread is grounded by a high resistance, sufficient to both discharge static electricity and protect against electro shock.

Skylab Experiment (M133). Static electroencephalographic sensors of experiment (M133) when the subject dons the cap containing these sensors is a real possibility. These sensors are extremely sensitive, and damage to the circuits could easily be produced by such a discharge. A solution to the problem was implemented, in which conductive thread was sewn into the cap in a position where the astronaut must touch the thread when he grasps the cap to put it on. The metallic thread is grounded by a high resistance, sufficient to both discharge static electricity and protect against electro shock.

Skylab Experiment (M093). A series of experiments on static electric effects on the electrocardiogram system of Experiment M093 were performed. Results indicated no problems existed other than generation of occasional noise spikes.

#### CONCLUSIONS

The amount of static electricity that can be accumulated by a space-suited man, who is electrically isolated, is sufficient to ignite combustible gas vapors and mists but is not sufficient to ignite combustible solids found in the Apollo spacecraft. Connection of the biomedical sensors to the space-suited man provides a grounding path sufficient to prevent appreciable charge buildup. Consequently, no hazard exists when the biomedical sensors are connected to the space-suited man. Temporary interference with biomedical sensor readings occurs during static-charge drainage. This interference can be minimized by providing a 0.1- to 1.0- megohm path parallel to the ground circuit. (A complete short circuit to the ground would be more

suitable, but it cannot be used because of an electric shock hazard.)

Other static electricity ignition hazards were discovered during operational tests of the spacecraft. These hazards included a highly charged plastic couch cover, spark discharge from lithium hydroxide canisters, and poorly grounded storage lockers. The couch cover hazard was eliminated by installing a grounded metal screen underneath the couch cover. The lithium hydroxide canister hazard and the storage locker hazard were eliminated by proper grounding. A survey of Skylab for static electricity revealed no new or outstanding problems.

#### REFERENCES

1. F. G. Eichel, *Electrostatics*. Chem. Eng., vol. 74, no. 6, Mar. 1967, pp. 153-167.
2. M. V. Blanc, P. G. Guest, G. Von Elbe, and B. Lewis, "Ignition of Explosive Gas Mixtures by Electric Sparks." Third Symposium on Combustion and Flame and Explosion Phenomena, William and Wilkins Co., 1949, pp. 363-367.
3. Leonard B. Loeb, "Static Electrification." Springer-Verlag, 1958
4. W. F. Cooper, "The Practical Estimation of Electrostatic Hazards." J. Appl Phys., vol. 4, supplement 2, 1953, pp. S71-S77.



## The Role of Electrostatics in Skylab Contaminant Behavior\*

H. E. Beaver and R. W. Ellison  
Martin Marietta Aerospace

### ABSTRACT

Skylab is an experimental space station that will be launched early in 1973 by the National Aeronautics and Space Administration. The station is a 100-ton complex of highly versatile laboratories whose capabilities for multipurpose scientific investigation are unmatched by any institution on Earth. Its three-man crews will carry out over 50 major research programs in earth resources, solar astronomy, zero-g manufacturing, medicine, and a variety of other areas. This work requires instruments of the highest sensitivity, and this inherently implies that they will be susceptible to extremely minute amounts of contaminants. A comprehensive program of contamination control has been effected both analytically, experimentally, and through major hardware controls.

The role of electrostatics in contaminant behavior is not established. This paper discusses the possibility that contaminant deposits and particulate clouds may be substantially influenced by static charges on the spacecraft and the contaminants themselves, and reviews the evidence of such charges.

SKYLAB WILL BE THE first manned space effort after the Apollo lunar exploration program.

During its 8 months in orbit the Skylab Cluster (fig. 1) will pass above all parts of the Earth within 3450 miles of the equator, its delicate sensors finding and recording new information about the sun and the Milky Way, the earth's atmospheric sheath, remote and sparsely inhabited areas, the earth's composition, and even about man himself. The data from these experiments will be of direct benefit to man in agriculture, forestry, oceanography, geography, geology, water and land management, communications, and ecology and pollution control.

The Skylab mission begins with liftoff of the unmanned Orbital Workshop from Kennedy Space Center. The Skylab workshop is launched by a two-stage Saturn V vehicle from Pad A of Launch Complex 39--where lunar flights begin--and is inserted into a near-circular orbit at an altitude of 435 km and at an inclination of 50 degrees from the equator. During the first 7½ hours of flight, commands are issued to jettison the payload shroud, maneuver the workshop into a sun-pointing mode, rotate the ATM solar observatory 90 degrees to its operating position, and deploy all solar-cell panels. The ATM pointing con-

\*Work supported by the National Aeronautics and Space Administration.



Fig. 1 - Skylab Cluster

trol system is activated to maintain the sun-pointing attitude, and the CWS is pressurized in preparation for docking of the CSM and entry of the astronauts.

One day after the first launch, a Saturn IB vehicle launches the CSM and its three-man crew from Pad B at KSC Launch Complex 39. The CSM is first inserted into an interim elliptical orbit 93 to 138 miles above the earth. Using its service propulsion system, the CSM then climbs to rendezvous with Skylab and docks to the axial port of the MDA, thus completing the cluster. Crewmen enter and activate Skylab for habitation. The CSM is powered down so that only the essential elements of the communication, instrumentation, and thermal control systems remain in operation. In the OWS, the astronauts conduct assigned experiments which, on Flight 2, stress medical and solar research and evaluation of long-term habitability of the Skylab. In addition, the crewmen activate and check out the earth resources experiments and the ATM solar observatory. On the 27th day the crewmen prepare Skylab for storage in orbit; on the 28th day they board the CSM, deorbit, and splash down in the West Atlantic recovery area.

Sixty days later, a second CSM and another three-man crew are launched from KSC. Orbital insertion, rendezvous, and docking are the same as on Flight 2. This mission can last up to 56 days and is similar to that of Flight 2, but places more emphasis on solar astronomy and earth resources experiments.

The third CSM and its crew are launched approximately 1 month after the Flight 3 crew returns to earth. This mission completes the objectives of the planned experiments and provides additional data on the crew's adaptability and performance during the planned 56-day flight.

The data accumulated from the many Skylab experiments will literally take years to assess. For example, one experiment in the earth resources experiment package will provide over 21,600 separate photographs in several different spectral bands, covering various areas of the earth.

It was recognized early in the program that accomplishing the planned scientific objectives would depend to a large extent on the amount of surface contamination on the exterior of the vehicle. For example, many of the science experiments rely on clean optics; thermal control coatings must stay clean to control the temperature of the vehicle; and electrical power systems could be degraded by contamination on the solar cells.

A major interdisciplinary program was undertaken to identify possible sources of contamination and all susceptible hardware and to develop a mathematical model to predict the effects of contamination. As a result of this analysis the following actions have been implemented:

- (1) The contaminant system has been tested and shown to create no detrimental effects.
- (2) The overboard vent has been eliminated.
- (3) The disposal system has been rerouted to the waste tank, where effluent must pass through multiple filters before being vented overboard.
- (4) The questionable outgassing materials have been replaced or baked out.
- (5) All measures known to control corona have been imposed on all hardware, and tests to demonstrate corona-free operation have been required.

Because of the criticality of the Skylab experiments and the relatively long life of the spacecraft, all mechanisms through which the contaminants can be attracted onto and become bound to vehicle surfaces have been rigorously scrutinized. These analyses show that the electrostatic charge of the vehicle, though small, could attract particles, and that these particles could then be bound to the surfaces through contact potentials or triboelectric charges.

Particles charged by venting and dumping, for example, will be retained indefinitely or collected by the spacecraft if their velocity of emission does not exceed

$$v_e = \sqrt{\frac{2qV_s}{m}} \quad (1)$$

where  $q/m$  is the charge-to-mass ratio of a charged particle emitted by a spacecraft having a potential of  $V_s$ . If the spacecraft has a potential of 20 v and can be represented as a sphere with a radius of 5 m, then the escape velocities for several typical values of  $q/m$  will be as shown in Table 1.

Equation (1) indicates that highly charged particles will be retained and even collected unless they are vented and dumped at high velocities. Typically, water droplets in turbulent flow can reach values of  $q/m$  as high as 0.1 coulomb per kg. Coal dust has been measured at several thousandths of a coulomb per kg. In general, high-velocity flow, spraying, or atomization leads to high charge-

Table 1 - Electrostatic Behavior of Charged Particles

Parameter	Charge-to-Mass Ratio, coulomb/kg			
	$10^{-6}$	$10^{-4}$	$10^{-2}$	$10^0$
$V_e$ , m/sec	$6.3 \times 10^{-3}$	$6.3 \times 10^{-2}$	$6.3 \times 10^{-1}$	6.3
$r_{50}$ , m	6.67	6.67	6.67	6.67
$t_{50}$ , sec	$1.6 \times 10^5$	$1.6 \times 10^4$	$1.6 \times 10^3$	$1.6 \times 10^2$
$V_e$ = velocity for charged particles to escape spacecraft at 20 v. $r_{50}$ = radius for particles emitted at $\frac{V_e}{2}$ to turn around $t_{50}$ = time for particles emitted $\frac{V_e}{2}$ to turn around				

to-mass ratios on a significant fraction of the particulates dispensed, and a substantial increase must also occur in the spacecraft potential since the charge imparted to the spacecraft must be equal and opposite to the charge imparted to the particles.

It is well recognized that launch ignition will cause the Saturn booster to acquire a charge of several hundred kilovolts. This charge develops as burning ionized gases are expelled from the engines, causing an accumulation of electrons on the engine bells and structure. However, during this phase of flight, Skylab is enclosed within the payload shroud, and since electrostatic charges primarily appear on external surfaces, it is protected. Furthermore, during the coast phases that follow engine cutoff, the large charge is rapidly dissipated by the free electrons and/or ions at orbital altitudes. Thus, from an analytical standpoint, we can assume that the Skylab Orbiting Assembly arrives in orbit with a zero net charge.

#### SKYLAB ENVIRONMENT

Beginning with the early Sputnik and Vanguard satellites, considerable empirical data have been accumulated on the conditions of space at different altitudes. Skylab will orbit with a velocity of  $7.5 \times 10^5$  cm/sec at an altitude of 435 km. At this altitude the number of electrons and ions are nearly equal, and range between  $5 \times 10^4$  and  $3 \times 10^5$  per  $\text{cm}^3$  (see Table 2). However, due to differences in mass and temperature, and because they move randomly between collisions at a velocity of only 1 to  $2 \times 10^5$  cm/sec, traveling at a small fraction of the spacecraft's speed, the ions are swept out by the spacecraft, leaving a wake. The electrons, on the other hand, are constrained by the magnetic field and are moving helically along the geomagnetic field lines at a velocity notably greater than that of the spacecraft, interacting on all exposed surfaces of the vehicle. The net result is that the electrons about the spacecraft tend to be uniformly distributed, but that the density of ions in the wake is reduced below ambient values, while the ion density ahead of the vehicle is increased.

Table 2 - The Skylab Environment at 435 km

Parameter	U. S. Standard Atmosphere, 1962	T. M. Donahue, "Science," Vol 159, No. 3814, 1968
number density	$1.234 \times 10^8 \text{ cm}^{-3}$	
Particle speed	1.283 km/sec	
Collision frequency	0.094 sec <sup>-1</sup>	
Mean free path	13.69 km	
Molecular weight	19.16 amu	
Kinetic temperature	1487.37 °K	
Molecular-scale temperature	2249.05 °K	
Density	$3.925 \times 10^{-12} \text{ kg/m}^3$	
Pressure	$1.9 \times 10^{-8} \text{ torr}$	
Atomic oxygen number density		$1.1 \times 10^8 \text{ cm}^{-3}$
Helium number density		$3 \times 10^6 \text{ cm}^{-3}$
Atomic hydrogen number density		$5 \times 10^5 \text{ cm}^{-3}$
Electron number density		(a) $5 \times 10^4 \text{ cm}^{-3}$
Oxygen ion (O <sup>+</sup> ) number density		$3.8 \times 10^4 \text{ cm}^{-3}$
Hydrogen ion (H <sup>+</sup> ) number density		$1 \times 10^4 \text{ cm}^{-3}$
Helium ion (He <sup>+</sup> ) number density		$1.6 \times 10^3 \text{ cm}^{-3}$

(a) W. Calvert, "Science," Vol 154, No. 3746, 1966, reports  $3 \times 10^5 \text{ cm}^{-3}$ .

## CHARGE RESULTING FROM SPACE PLASMA

To prevent the following analysis from becoming unduly complicated, we can reduce the Skylab vehicle to its equivalent geometrical shape. Neglecting the solar-panel wings and the Apollo Telescope Mount, the basic configuration is that of a cylinder 40 m long and 6.6 m in diameter. This cylinder has an area of 898 m<sup>2</sup>, which is equivalent to the area of a sphere 8.4 m in diameter.

Skylab will have an orbital velocity of  $7.7 \times 10^5 \text{ cm/sec}$ . Thus, it will be traveling approximately five times faster than the free ions and more than ten times slower than the free electrons. As a result, there will be a concentration of ions impacting the forward portion of the vehicle, but electrons will impact the vehicle from all directions. This will cause the electron current to the vehicle to be larger than the ion current. In effect, the vehicle will take on a negative potential such that all but that number of higher-energy electrons sufficient to balance the ion current are repelled.

Brundin<sup>(2)</sup> has shown that on a spherical metal body, such as that shown in Figure 2, the respective electron and ion currents can be described by:

$$I_e = -eN_e v_s \pi R^2 C_e \quad (2)$$

and

$$I_i = eN_i 4\pi R^2 \left( \frac{KT}{2\pi M_e} \right)^{1/2} e^{-\left( e\phi_s / KT \right)} C_i \quad (3)$$

where

$e$  = electron charge =  $1.6 \times 10^{-19}$  coulomb

$N_i, N_e$  = density of electrons or ions per cc

$R$  = radius of spacecraft

$C_i, C_e$  = shielding constants ( $\approx 1$ )

$v_s$  = velocity of spacecraft

$M_e$  = mass of electron

$K$  = Boltzmann's constant

$T$  = temperature of plasma

$\phi_s$  = charge on spacecraft

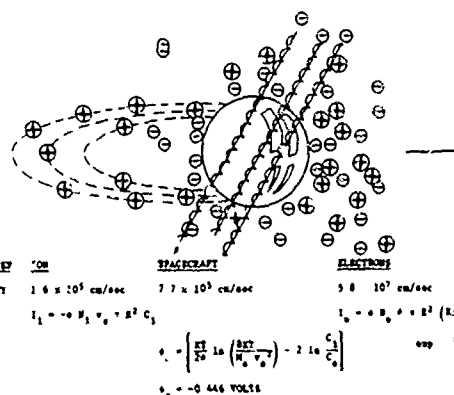


Fig. 2 - Plasma Charge Effects on a Spherical Spacecraft

By summing the ion and electron currents and solving for the spacecraft charge  $\phi_s$ , we obtain

$$\phi_s = \frac{KT}{2e} \left[ \ln \left( \frac{8KT}{\pi M_e v_s^2} \right) - 2 \ln \frac{C_i}{C_e} \right] \quad (4)$$

When the appropriate numerical values are substituted in the equation, the charge on the spacecraft resulting from motion through the plasma at an altitude of 400 km is found to be about  $-1/2 \text{ v}$ .

## CHARGE DUE TO PHOTOELECTRIC EFFECTS

Solar radiant energy falling on the spacecraft will cause electrons to be emitted from the vehicle. This electron current flowing away from the spacecraft will tend to counteract the charge accumulated from plasma effects.

The resultant vehicle charge ( $\phi_s$ ) when photoelectric effects are included is

$$\phi_s = \frac{KT}{2e} \left\{ \ln \left( \frac{8KT}{\pi M_e v_s^2} \right) - 2 \ln \left[ C_i - \frac{I_{PH}}{v_s \pi R^2 N_e e} \right] + 2 \ln C_e \right\} \quad (5)$$

where

$I_{PH}$  = photoelectric current, coulombs.

that this equation is similar to Eq ( ) except that the second term has been modified to include the photoelectric current.

Measured values of  $I_{PH}/\pi R^2$  from Explorer and other spacecraft show that currents of less than  $10^{-4}$  amp per sq m are to be expected.

Inserting the appropriate numerical values alters the spacecraft charge by less than 0.1%; i.e., the photoelectric contribution is negligible.

#### CHARGE FROM MOTION THROUGH THE MAGNETOSPHERE

For the usual unmanned spacecraft, which is of small dimensions (1 or 2 m in diameter) and symmetrical, the voltage created by motion through the magnetosphere is insignificant. However, when we consider a vehicle the size and shape of Skylab, then the electromagnetic force becomes appreciable.

Consider a cylindrical metal tube 40 m long, 6.6 m in diameter, and moving through earth's magnetic field at a velocity of 7.7 km/sec (see Fig. 3). It is immediately apparent that a sizeable voltage is generated.

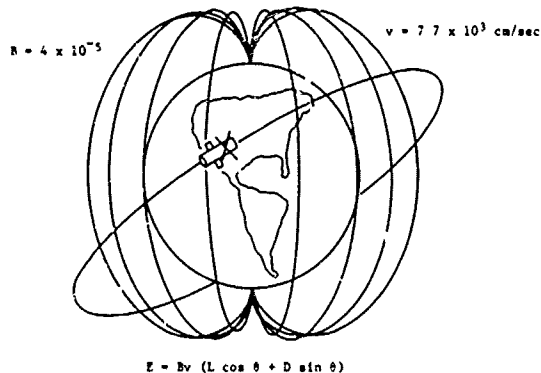


Fig. 3 - Charge on a Spacecraft Traveling in the Geomagnetic Field

We must also consider that Skylab flies in two different attitudes. Its primary attitude is solar inertial, in which the solar arrays or major axis of the vehicle are pointed sunward. The alternate attitude is with the Z-local vertical axis toward the nadir; this is the attitude in which an airplane normally operates. These different attitudes act to cause differing vehicle axes to be normal to the geomagnetic field. Thus, differing induced voltages are present as the attitude changes.

Since Skylab's orbit is oriented  $50^\circ$  to the equator, the vehicle moves alternately northward and southward, and normal to the magnetic field at the extremes. This motion through the geomagnetic field generates an alternating voltage component of 1 Hz per

orbit across the cylinder and another component longitudinal to the cylinder. Considering the cylindrical form of Skylab, the voltage generated on the vehicle will be

$$E = Bv(L \cos \theta + D \sin \theta)$$

where

$B$  = magnetic field intensity =  $4 \times 10^{-5}$  weber at 400 km  
 $v$  =  $7.7 \times 10^3$  m/sec  
 $L$  = length of vehicle = 40 m  
 $D$  = diameter of vehicle = 6.6 m  
 $\theta$  = angle between spacecraft and direction of magnetic field

When  $\theta = 0^\circ$ , a longitudinal voltage of 12.6 v is generated along the length of the vehicle. When the spacecraft is oriented so that  $\theta = 90^\circ$ , a voltage of 2.06 v is generated across the vehicle.

Skylab is launched at an inclination of  $50^\circ$  from the equator. Neglecting geomagnetic anomalies, the angle  $\theta$  will be closer to  $50^\circ$ . At this angle, the voltage generated on the vehicle will then be

$$E = (4 \times 10^5) (7.7 \times 10^3) (40 \cos \theta + 6.6 \sin \theta)$$

This voltage will appear as a d-c gradient along the length of the vehicle on which an a-c component of frequency equal to the orbit period is superimposed. In any case, the charge from this source will be much larger than the electrostatic charge from motion through the plasma.

As the spacecraft changes orientation with respect to the magnetosphere, the magnitude of the charge changes and may, in some orientations, reverse polarity. As this occurs, various areas of the spacecraft's surface become more or less attractive to ionized-particle contaminants and electrons.

#### CHARGE EFFECTS FROM RCS ENGINE FIRINGS

In considering electrostatic charges on the Skylab Cluster, the firing of the reaction control engines on the Command and Service Module has little effect. These engines will be used to dock the Apollo CSM with the MDA, and to make orbital adjustments during the mission.

The voltage developed on the spacecraft by RCS engine firings can be estimated from the integral of current with time measured in a typical test firing. Since the spacecraft capacitance can be calculated very roughly as about 930 pf, the magnitude of the charge is given by

$$\frac{\int i_{RCS} dt}{C} = v_s$$

References 3 and 4 analyze the effects of charges from small rocket engines operating in a space environment. These studies are unanimous in their conclusion that small rock-

ecs with non-ablative engine bells produce very low-potential energized particles. A potential of  $\pm 5$  v appears to be the maximum charge to be expected, and then only with engine firings of considerable duration.

Since the Skylab RCS engines will only be operated at infrequent intervals, and then for relatively short periods, the small charge they produce can be disregarded.

#### CHARGES FROM LIQUID DUMPING

In the late nineteenth century, it was discovered that a waterfall has an electric field of several hundred volts per meter. This field is apparently caused by the mechanical disruption of the stream from impingement on the rocks below. This same effect has been observed under many other circumstances and is a source of concern in cleaning supertankers and in transferring fuel between aircraft in flight.

Skylab, in its earlier configuration, vented certain liquids overboard. The cloud of ice particles created by this venting raised concern about surface deposits and the lifetime of the cloud. It was believed that venting might charge the vehicle while charging the droplets, and that electrostatic effects would aggravate the potential problem by making the cloud take longer to clear, increasing the amount of surface contamination, and introducing highly charged particles into high-voltage regions of sensors. From the start, Skylab was configured so that no straight line of sight existed between sources of contaminants and critical surfaces. Two series of tests were performed to determine whether this line-of-sight protection could be negated by electrostatic forces pulling particles to critical surfaces, but the results were generally inconclusive. Even though the data did not show that electrostatic forces dominated the transportation of contaminants, the vent lines were rerouted through the waste tank, and the effluent was filtered to ensure that no escaping particle would be larger than a few microns.

As a part of the contamination test program for Skylab, Martin Marietta conducted several series of tests to simulate the dumping of water from the environmental condensate system to space.

In the first group of tests, a stream of distilled water was pumped through three different types of nozzles in a thermal vacuum chamber. The nozzle panel was insulated from the chamber walls using material with a resistance of  $2 \times 10^{12}$  ohms.

At the start of each test, the vacuum chamber was pumped down to a pressure altitude of 175,000 ft. During the tests, the equivalent altitude decreased to 150,000 ft due to the volume of water introduced in the chamber.

The triboelectric charge was measured with a sensitive research electrostatic voltmeter, which had a range of 200 v full-scale.

All measurements were made between the nozzle panel and the wall of the chamber.

At a pressure of 10 psia, the triboelectric charge ranged from 45 to 60 v, depending on the particular nozzle, and the charge built up from 2 to 50 sec. At 100 psia the voltages were between 70 and 180 v. In an earlier setup in this chamber, the highest reading observed was 1800 v.

In the last test, a large, 45-ft-high by 25-ft-diameter thermal-vacuum chamber cooled with  $\text{LN}_2$  was used. Condensate was vented at a rate of 1 gallon in 11 minutes, and the nozzle charging current was measured using a Keithley 410 electrometer. The current was erratic, swinging alternately positive and negative for the first 7 minutes, and finally settling out at a constant polarity between  $10^{-6}$  and  $10^{-7}$  amp for the remaining period. A rough average of the readings is  $3 \times 10^{-7}$  amp.

Under these conditions, a spacecraft with a capacitance of 930 pf would be charged at a rate of 320 volts per second, and would reach an ultimate potential of 210 kv after 11 minutes if the current were continuous, of one polarity, and if there were no mechanism for discharge. However, such voltages cannot be achieved, even in the ionosphere, because the rapidly increasing potential would attract and return the appropriately charged effluents before such high potentials were generated. In the ionosphere, the tendency to charge will be negated by the drawing in of ions or electrons, and an upper limit of 200 v seems likely.

Photographs of liquids vented into a very high vacuum show that a small fraction of the particles cross the tracks of the remaining particles. In our own tests and in tests at JPL, these anomalous tracks remain unexplained. Electrostatics has been involved and may, perhaps, be ultimately established as the causative agent. Astronaut reports and Apollo photographs also confirm the existence of anomalous trajectories (see Fig. 4 and 5).



Fig. 4 - Water Jet into Air Streaming into Vacuum (Courtesy of C. Miller, Jet Propulsion Laboratory)



Fig. 5 - Water Injected Directly into Low-Temperature, High-Vacuum Chamber

#### MECHANISMS OF VEHICLE DISCHARGE

It was shown earlier that collisions with charged particles in the space environment cause the charge on Skylab to build up to an equilibrium potential of small magnitude. At this point a sheath is established about the vehicle that effectively shields it from further contact with the plasma particles.

The thickness of the plasma sheath is about 0.44 cm, equal to the Debye length. The concentration of charged particles, ions, or electrons in the sheath depends on the magnitude and polarity of the charge, which for an idealized Skylab has been shown to be about  $-4$  v.

The sheath of electrons is also the mechanism whereby the vehicle is discharged when charge mechanisms other than plasma-charged particles drive the vehicle from its equilibrium potential. The conductivity of the sheath and the capacitance of the vehicle (930 pf) combine to determine the time constant that is effective in discharging the spacecraft. The complex geometry and surface properties of Skylab combine with these sheath properties to render computations of discharge currents and rates intractable.

#### PERTUBATIONS TO ANALYSIS

Skylab is covered to a large extent with dielectric thermal control paints. The white paint has a resistivity of  $1.3 \times 10^{15}$  ohm-cm; the black paint,  $10^{11}$  ohm-cm. These values can be higher after exposure to vacuum. Thus, the discharge can be extended by many orders of magnitude, and may require seconds.

The charge pattern of the vehicle will also be distorted by the solar panels of the OWS and ATM. These solar panels are constructed of numerous strings of solar batteries, in series. For instance, one ATM subpanel is constructed of 360 solar batteries, with the positive and negative interconnections interspersed over the surface of the panel. One end of each series string is grounded; the

other end is at 90 to 125 v dc. Since the average voltage of the panels is 50 v, the solar-cell arrays are considered as being at a mean voltage of +50 v from the body of the vehicle. Of course, they are insulated from the body of the vehicle and are also environmentally protected with covers of fused quartz, which has a resistivity of  $10^{18}$  ohm-cm.

Assuming the solar panels are at this +50 v average level, it is apparent that an ion sheath will be formed over the panels, whereas the body of the vehicle will be at a small negative potential and the plasma sheath about the vehicle will be highly non-uniform. As a result, there can be substantial voltage across the paints, the solar cells, the quartz covers, and the insulation blankets. The problem is not tractable.

#### OTHER TRIBOELECTRIC EFFECTS

In addition to the triboelectric effects that result from dumping liquids, the triboelectric effect of contact potentials is also important in analyzing possible contamination mechanisms for Skylab. Table 3 lists the relevant physical properties for Skylab materials.

In the latter part of the nineteenth century, Alfred Coehn, of Germany determined that the amount of electrostatic charge generated between two materials in contact is determined by the difference in their dielectric constants. The material with the largest dielectric constant will have the positive polarity.<sup>(5,6)</sup> This relationship is expressed in Coehn's equation as

$$Q_{1-2} = k (K_1 - K_2)^2$$

where

$Q_{1-2}$  = resultant charge differential, esu

$K_1, K_2$  = respective dielectric constants of the two materials in contact

$k$  = Coehn's constant

H. R. Richards, working on a fellowship at Princeton University, spent considerable time empirically verifying Coehn's constant. He tested many materials and determined the average value of Coehn's constant as  $k = 4.4$ .

Using Coehn's Law, we can analyze several probable situations that may arise during Skylab operations. For example, the condensate dumped from the Airlock Module is water mixed with human sweat and breath. As such, it closely approximates a salt solution and would have a similar dielectric constant of 6.1. If a droplet of this condensate should contact the magnesium fluoride (MgF<sub>2</sub>) coating of the S190 experiment window, a contact potential will be generated. MgF<sub>2</sub> has a dielectric constant of 1.9, so the charge will be

Table 3 - Skylab - Triboelectric Series

Material	Leakage Source or Vehicle Location <sup>a</sup>	Dielectric Constant	dc Resistivity, ohm-cm	Time Constant, RC, sec	Reference
Nitrogen	1,2,3,4	1.000547			2,8
Oxygen	1,2, 4	1.000494			2,8
Clean Water	3	-78 at 25°C	$2 \times 10^{11}$	$6.24 \times 10^{14}$	1
Neoprene	5	-6.4 at 25°C	$6 \times 10^{12}$	$3.9 \times 10^{13}$	1
Polyurethane	5	-6.7 at 25°C	$1 \times 10^{13}$	$6.7 \times 10^{13}$	1
Zinc Sulphide	8	-5.3			
Clean Ice	3	4.8	$8 \times 10^{11}$	$3.89 \times 10^{12}$	1
Glass-Boro Silicate-Crown	6	4.05	$8 \times 10^{11}$	$3 \times 10^{13}$	1
Glass Fused Silica	7a	3.85	$1 \times 10^{13}$	$3.85 \times 10^{13}$	3,10
Fused Quartz-Mirror	7b	2.25	$1 \times 10^{16}$		
Infrasil-Fused Quartz	8	3.77	$1 \times 10^{16}$	$3.77 \times 10^{16}$	4,10
Aqueous NaCl	3	6.1			2
Nylon	5	3.5	$6 \times 10^{13}$	$2.1 \times 10^{15}$	1
Mylar	5	3.0	$4 \times 10^{15}$	$1.4 \times 10^{15}$	1
Paper	5	3.29	$8 \times 10^{13}$	$2.6 \times 10^{14}$	1
Teflon	5	2.04	$5 \times 10^{15}$	$1.02 \times 10^{16}$	1
Magnesium Fluoride	9	1.95	$1.39 \times 10^8$	$2.7 \times 10^8$	6,7
Liquid Urine	9	1.8	$5.7 \times 10^1$	$1.02 \times 10^2$	5,6
Liquid Oxygen	1,2,3,4	1.5 at 80°K	$6 \times 10^{12}$	$7.5 \times 10^{14}$	8
Liquid Nitrogen	1,2,3,4	1.454 at -203°C	$8 \times 10^{10}$	$11.3 \times 10^{12}$	8
Liquid Hydrogen	1,2,3,4	1.228 at 20°K	$1 \times 10^{13}$	$9.16 \times 10^{14}$	8
Germanium		16.6	$9 \times 10^0$	$14.9 \times 10^1$	9
Silicon	5	13	$8.5 \times 10^{-3}$	$1.1 \times 10^2$	2,9
Carbon	5		$1.4 \times 10^{-3}$		2
Stainless Steel	11		$90 \times 10^{-6}$		2
Titanium	5		$47.8 \times 10^{-5}$		2
Iron	5		$9.7 \times 10^{-6}$		2
Cobalt	5		$9.7 \times 10^{-6}$		2
Nickel	5		$6.9 \times 10^{-6}$		2
Zinc	5		$6 \times 10^{-6}$		2
Manganese	5		$5 \times 10^{-6}$		2
Aluminum	5		$2.62 \times 10^{-6}$		2
Chromium	5		$2.6 \times 10^{-6}$		2
Gold	5		$2.44 \times 10^{-6}$		2
Copper	5		$1.69 \times 10^{-6}$		2
UREA (PlasSkin Natural)	Listed only for Ref	7.1	$2 \times 10^{12}$		
Vehicle Paints					
White-RV 602 & ZnO <sub>2</sub>	1,2,3,4	2.3	$1.32 \times 10^{13}$		11
Black-Catalac-463-3-8	1,2,3,4	6.27	$9.5 \times 10^{10}$		11
Fecal Moisture	10	65-85% (Moisture of bulk material)			5
Waste Food	10				5

<sup>a</sup>Leakage Sources or Vehicle Locations:

- |  |   |
|--|---|
| 1 - CSN                                | 7a - S191 Fused Silica Window                           |
| 2 - CM                                 | 7b - Quartz Overcoat on S191 Mirrors                    |
| 3 - AM                                 | 8 - S192 Infrasil Window or Germanium Window            |
| 4 - MDA                                | 9 - Magnesium Fluoride Coating on 6 and 7a              |
| 5 - Ventline Experiment M479, M512     | 10 - Leakage from OWS, Waste Tank                       |
| 6 - S190 Boron Silicate - Crown Window | 11 - Steel Pipes from Waste Tank and Vehicle Structures |
|  | 12 - Exterior Thermal Control Coatings                  |

## References:

- 1 - A. F. Von Hippel, "Dielectric Materials and Applications," MIT Technology Press and Wiley & Sons, 1958
- 2 - "International Critical Tables," McGraw-Hill, 1932
- 3 - Corning Glass - "Fused Silica 7940 Data Sheet #FS-6," March 1966
- 4 - Amerel Optics, Inc. - "TI7 Infrasil 1 - Data Sheet"
- 5 - D. B. Putnam, "Composition and Concentrative Properties of Human Urine," McDonnell-Douglas Astronautics Co-DAC-61125-F-1
- 6 - Condon and Odishaw, "Handbook of Physics," McGraw-Hill, 1958
- 7 - "Optical Design Handbook," MIL-HDM-141
- 8 - "Handbook of Chemistry and Physics," 41st Edition, Chemical Rubber Publishing Company
- 9 - W. L. Volz, "Handbook of Military Infrared Technology," Office of Naval Research, Washington, D.C., 1951
- 10 - Vendor Information
- 11 - Laboratory Test at Martin Marietta

$$Q = 4.4 (6.1 - 1.9)^2 \\ = 75.6 \text{ esu.}$$

Since the dielectric constant of the droplet is larger, its charge will have a positive polarity.

From electrostatics, we know that the force resulting from an electrostatic charge is equal to

$$F = \frac{Q^2}{r}$$

where

F = the attractive force, dynes

Q = the charge, esu

r = the separation distance between materials, cm

For simplicity, we will assume that  $r = 1 \times 10^{-6}$  cm = 100 Å. Using this separation distance, the attractive force between the droplet and the window surface is

$$F = \frac{(75.6)^2}{(1 \times 10^{-6})^2}$$

$$= 5.7 \times 10^{15} \text{ dynes, or } 5.7 \times 10^{10} \text{ newtons.}$$

A similar situation may result from operation of Experiment M479 (Manufacturing Technology). One of the residues vented to space from this experiment will be Teflon particles. The dielectric constant of Teflon is 2.04. It is possible, due to their relative proximity, that a Teflon particle might contact the quartz (SiO<sub>2</sub>) coating of the primary mirror of Experiment S191 (infrared spectrometer). If this occurs, the resultant charge will be

$$Q = 4.4 (3.77 - 2.04)^2 = 13.4 \text{ esu,}$$

and the attractive force between the particle and the window will then be

$$F = \frac{(13.4)^2}{(1 \times 10^{-6})^2} = 1.75 \times 10^{14} \text{ dynes.}$$

These examples show that contact potentials can result in a very large attractive force to bind the contaminant particles on the windows.

Although these forces appear to be extremely large, they have been corroborated from other fields of endeavor. D. K. Donald investigated particle adhesion on various substrates used in the graphics industry. By using beads of substrate, covering them with other powdered materials, and spinning the combinations in a centrifuge, he determined the adhesive forces of contact potential for numerous compounds. In his experiments he found that some combinations of materials can withstand accelerations up to 30,000 g before they separate.

These results seem to indicate why dirt and mud spots adhere so strongly to our auto-

mobile windshields. It also explains how an airplane flying through an atmosphere containing dust can get dirty even while flying 600 mph. The electronic theory of adhesion was also studied to a great extent by B. V. Derjaguin and V. P. Smilger.<sup>(9)</sup>

Using the dielectric constants and the bulk or surface resistivities from Table 3, it is feasible to develop an approximate time constant that is indicative of the time required for a contact charge to bleed off.

The resistivity of MgF<sub>2</sub> is  $1.39 \times 10^8$  ohm-cm, and its dielectric constant is 1.9. The product of these two factors is  $2.7 \times 10^8$ , which is an approximate time constant in seconds. Thus, it is seen that after a particle is attracted to a surface, it may be expected to remain there for a considerable time, even through the duration of the Skylab mission.

Although the precise dielectric constant is not generally known for metallic materials, the constant is very large. From considerations in physical optics, it can be shown that the "dielectric constant" closely approximates the square of the index of refraction. For reflective metals,  $n$  becomes very large and the dielectric constant approaches infinity. However, the magnitude of the dielectric constant is largely offset by the very low resistivity of metals. Steel exhibits an average resistivity of  $90 \times 10^{-6}$  ohm-cm; and the resistivity of gold is only  $2.44 \times 10^{-6}$  ohm-cm. Consequently, even though a large instantaneous charge may occur when a particulate material is in contact with metal surfaces, the charge dissipates in microseconds due to the low resistivity of the metal.

Table 3 is a triboelectric table of Skylab materials. This table can be used to estimate the contact potential between vehicle surfaces and contaminants.

#### ADDITIONAL DATA FROM SPACE

Some recent results from the Apollo lunar program show clear evidence of electrostatic forces controlling contamination. In some cases lunar dust has been seen to "jump" to dielectric surfaces and remain there against lunar gravity in a geometrical pattern associated with an electrostatic field (see Fig. 5 and 7). Other indications pertain to density measurements of neutral and charged molecules. Surprisingly, the sunlit surface of the moon appears to have densities of neutral molecules and ions that are not so far different from the values in the upper F<sup>2</sup> ionosphere where Skylab orbits.

The striking evidence that electrostatics controls the transportation and deposition of lunar dust combines with the other evidence (of near-ionospheric properties at the lunar surface) to necessitate continued attention to the question: How large is the role of electrostatics in spacecraft contamination?





Fig. 6 - Lunar Dust Experiment  
[Courtesy of T. Gold, Cornell Univ.  
(NASA Photo)]



Fig. 7 - Dust on ALSEP  
[Courtesy of H. Collicott, Bendix Corp.  
(NASA Photo)]

#### REFERENCES

1. Gerard Fournier, "Interactions Between a Satellite and the Ionosphere and Applications to Drag and Probe-Measurement Problems." *Journal of the Astronautical Sciences*, Vol XVIII, No. 5.
2. Clark J. Brundin, "Effects of Charged Particles on the Motion of an Earth Satellite." *AIAA Journal*, Vol 1, No. 11, p 2529, November 1963.
3. Leonard Aronowite, "Rocket Engine-Generated Voltage as a Source of Electromagnetic Interference and Electronic Component Damage on Interplanetary Vehicles." Grumman Aircraft Engineering Corporation, Bethpage, New York.
4. W. S. West, J. V. Gore, M. A. Kashi, and H. W. Bilsky, "Spacecraft Charge Buildup Analysis." Technical Report NASA SP 276, 1971.
5. Robin Beach, "Preventing Static Electricity Fires." Three-Part Series in *Chemical Engineering*; 21 December 1964, 4 January 1965, and 1 February 1965.
6. W. R. Harper, "Contact and Frictional Electrification." Oxford University Press, London, 1967.
7. D. K. Donald, "Electrostatic Contribution to Powder-Particle Adhesion." *Journal of Applied Physics*, Vol 40, No. 7, June 1969.
8. E. T. Pierce, "Pertanker Explosions." *Proceedings of the 1970 Lightning and Static Electricity Conference*.
9. B. V. Derjaguin and V. P. Smilga, "Adhesion Fundamentals and Practice - The Electronic Theory of Adhesion." Part III, Chapter 6. Gordon and Breach Science Publishers, New York, 1969.

## Electrostatic Potentials Developed by ATS-5

Sherman E. DeForest  
University of California, San Diego

### ABSTRACT

Investigation of the properties of low-energy particles measured on board ATS-5 show that the synchronous spacecraft can charge to -12,000 volts in eclipse, and several hundred volts in sunlight. Differential charging can produce local fields of several thousands of volts per meter in the near vicinity of the spacecraft surface. Time constants for charging can be less than a second to tens of minutes.

ATS-5 WAS LAUNCHED INTO SYNCHRONOUS ORBIT on August 12, 1969. Shortly thereafter, it was stationed at  $105^{\circ}$  W longitude (local midnight at 0700 UT) with orbital inclination of  $2.30^{\circ}$ . Before launch, research groups at both the University of California, San Diego and Lockheed, Palo Alto had insisted that conducting collars be placed around the apertures of low-energy particle detectors. This was meant to be a partial shield against local electric fields which could affect particle counting rates. In addition, some concern was expressed about the fact that the viewing cones of two instruments looked out through a cylinder of solar cells. The general geometry is shown in Figure 1. In flight, ATS spins at about 100 rpm about the longitudinal axis. The spin axis is oriented parallel to the earth's axis.

Within weeks it was obvious that these precautions had not been sufficient to prevent differential charging from taking place in the vicinity of the end detector. The big surprise, however, was that certain puzzling particle events could be shown to be due to the whole spacecraft charging to thousands of volts. No one else had reported seeing these kinds of potentials developed on spacecraft, although several predictions of a few volts potential had been made. Therefore, a paper (1) was written which discussed this charging with emphasis on a model that had been developed to predict it. This paper will review that work, then discuss some more recent work on the differential charging, and finally present some evidence of effects which have not been satisfactorily explained yet.

### INSTRUMENTATION

The UCSD plasma detector is shown schematically in Figure 2. Four such detectors are provided on ATS-5. They are arranged in electron-proton pairs looking parallel and perpendicular to the spin axis. The energy range from 50 eV to 50 keV is covered in 62 logarithmically placed steps. A complete scan takes about 20 seconds.

## TOTAL SPACECRAFT CHARGING

**ECLIPSES** - The plasma environment seen at synchronous altitude is quite different from that seen at lower altitudes (2,3,4). Particularly in the midnight region, great variability of plasma density and temperature is found. In addition, a synchronous spacecraft goes into eclipse for periods of about 1/2 hour every night for a period of 3 to 4 weeks on either side of an equinox. Therefore, the satellite's response to any given plasma in both darkness and sunlight must be known.

This is demonstrated by the data shown in Figure 3. It contains 24 hours of data taken on October 16, 1969. The format is a plot of energy versus time for both electrons and protons. Note that the energy scale for protons is reversed so that zero energy electrons and protons have the same origin. The gray scale is modulated by the counting rate with low rates being dark. The scale is allowed to overflow and recycle. The highest proton counting rates in the figure are black. For more details on this method of presentation, see reference (3).

These data (which are taken only from detectors looking perpendicular to the spin axis) show a sudden change in character at about 0620 UT and return to what would appear to be a normal development at 0720 UT. It is not surprising that this type of event was first thought to be a crossing of a particle trapping boundary from closed to open and back. One of the first papers presented on these data even suggested this explanation (5). However, the orbit calculation showed that on this night, and every other night when such events occur, the spacecraft enters and leaves eclipse at exactly the times of the event. For this reason, we had to assume that the apparent changes in spectra are due to some effect local to the spacecraft.

The most obvious explanation is that ATS is charging to a negative potential of about 4200 volts in eclipse. This is shown to be the case by considering the detailed spectra. Figure 4 shows a cut taken through the previous figure just prior to the event. Data from both sets of detectors are shown in the figure with the perpendicular at the top. Data from the two directions have been separated by a factor of 100 for convenience. From the integrals calculated at the top of this figure, it is seen that the plasma has a density of about  $1/\text{cm}^3$ . The electrons have a temperature of about 3000 electron volts, and the protons have a temperature of about 10,000 electron volts. Both species are roughly Maxwellian in shape.

Figure 5 is in the same format, but is taken from the middle of the event. Note the sharp cut-off in proton below a certain energy. In both of these figures, energy flux, which is nearly proportional to counting rate, has been plotted.

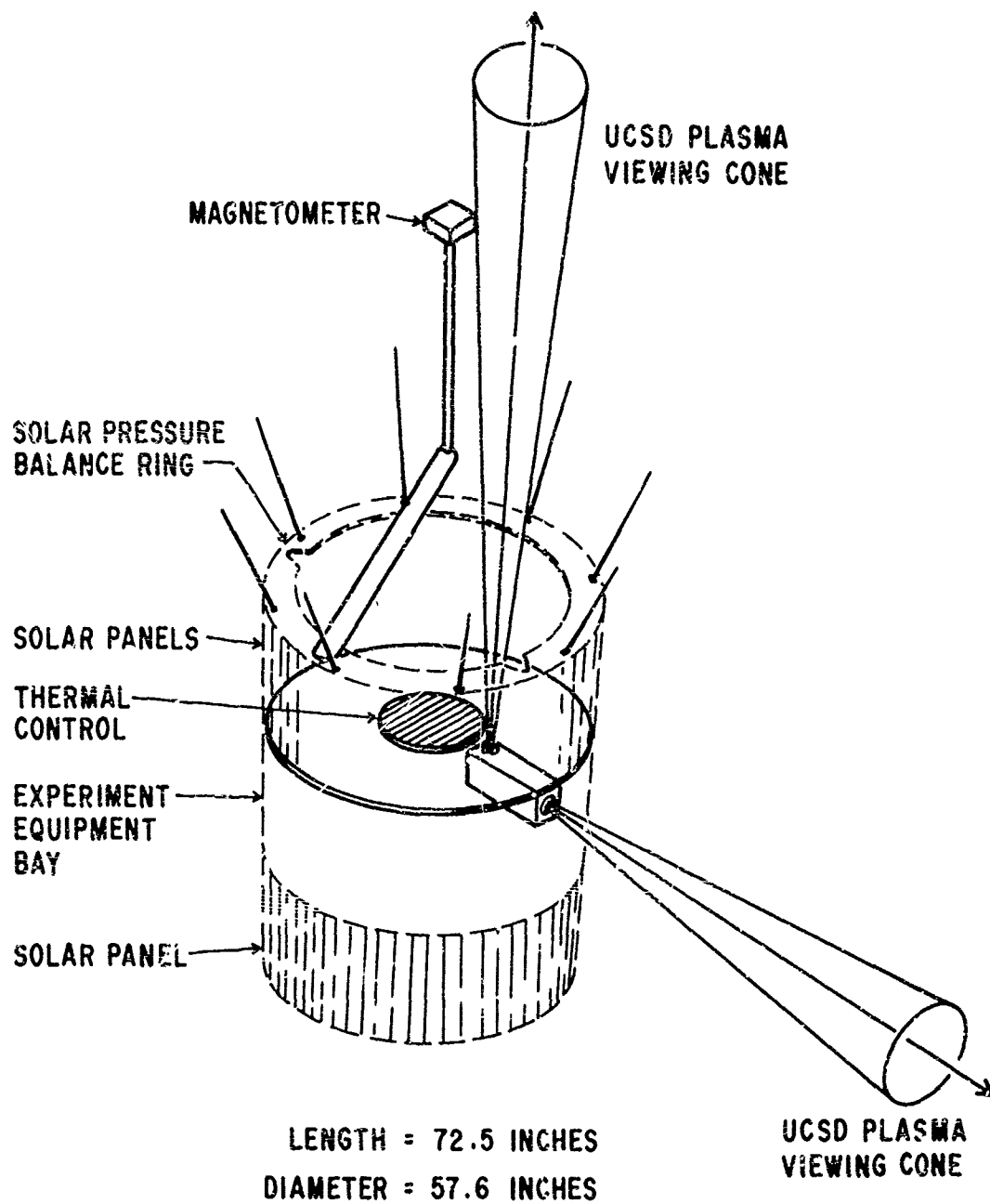


Fig. 1 - Schematic representation of ATS-5.

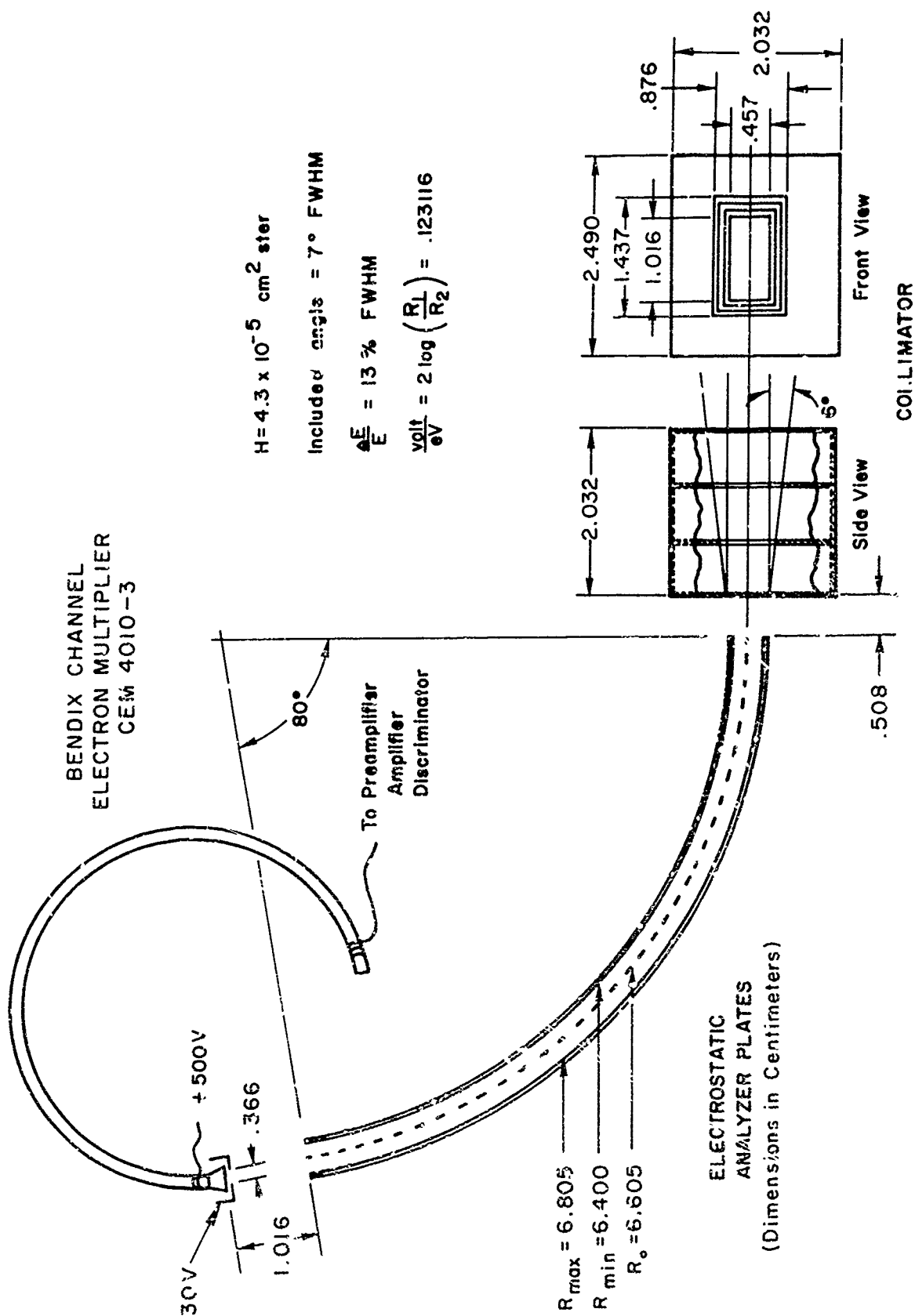


Fig. 2 - Schematic representation of the UCSD plasma detector on ATS-5.

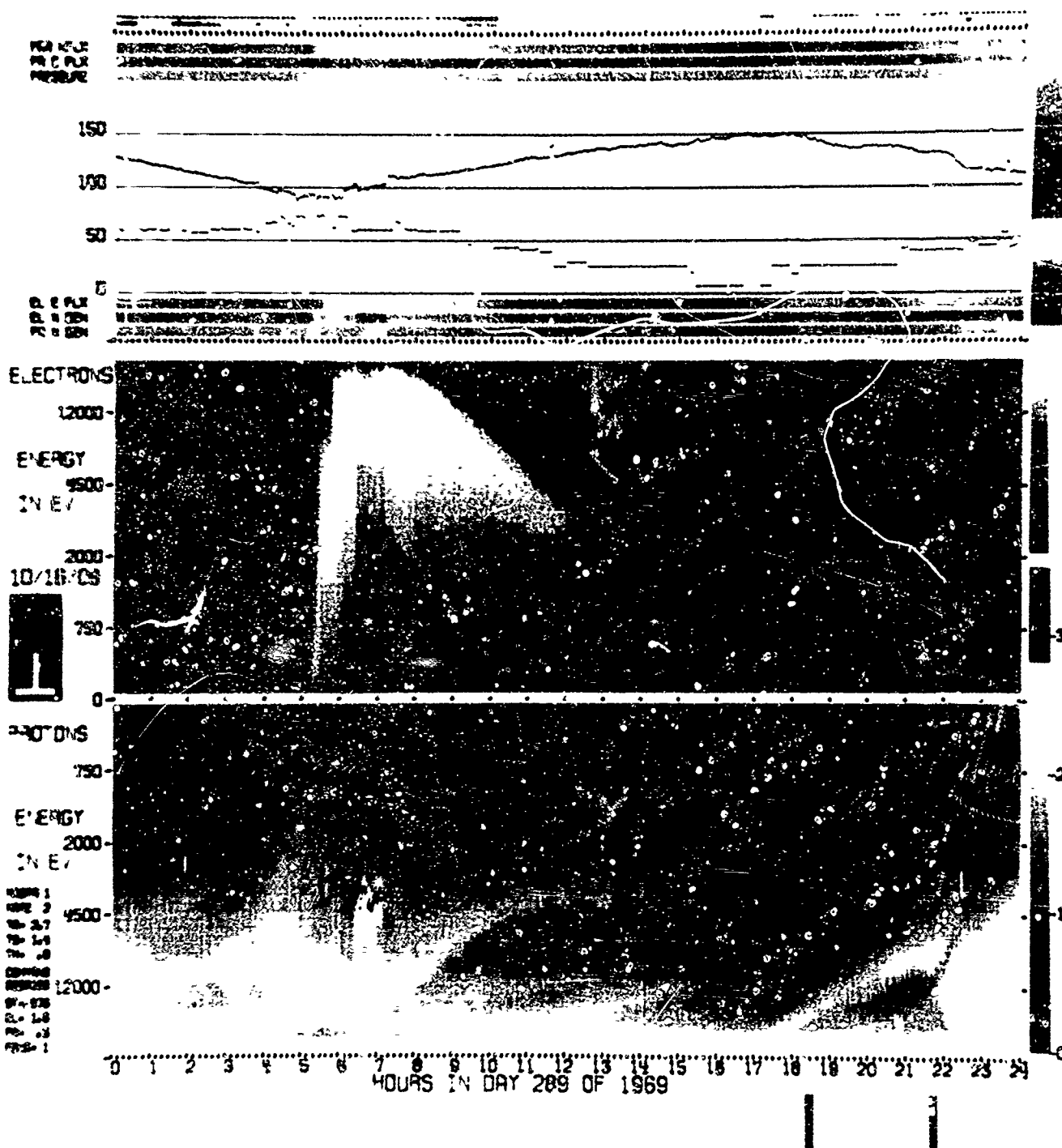
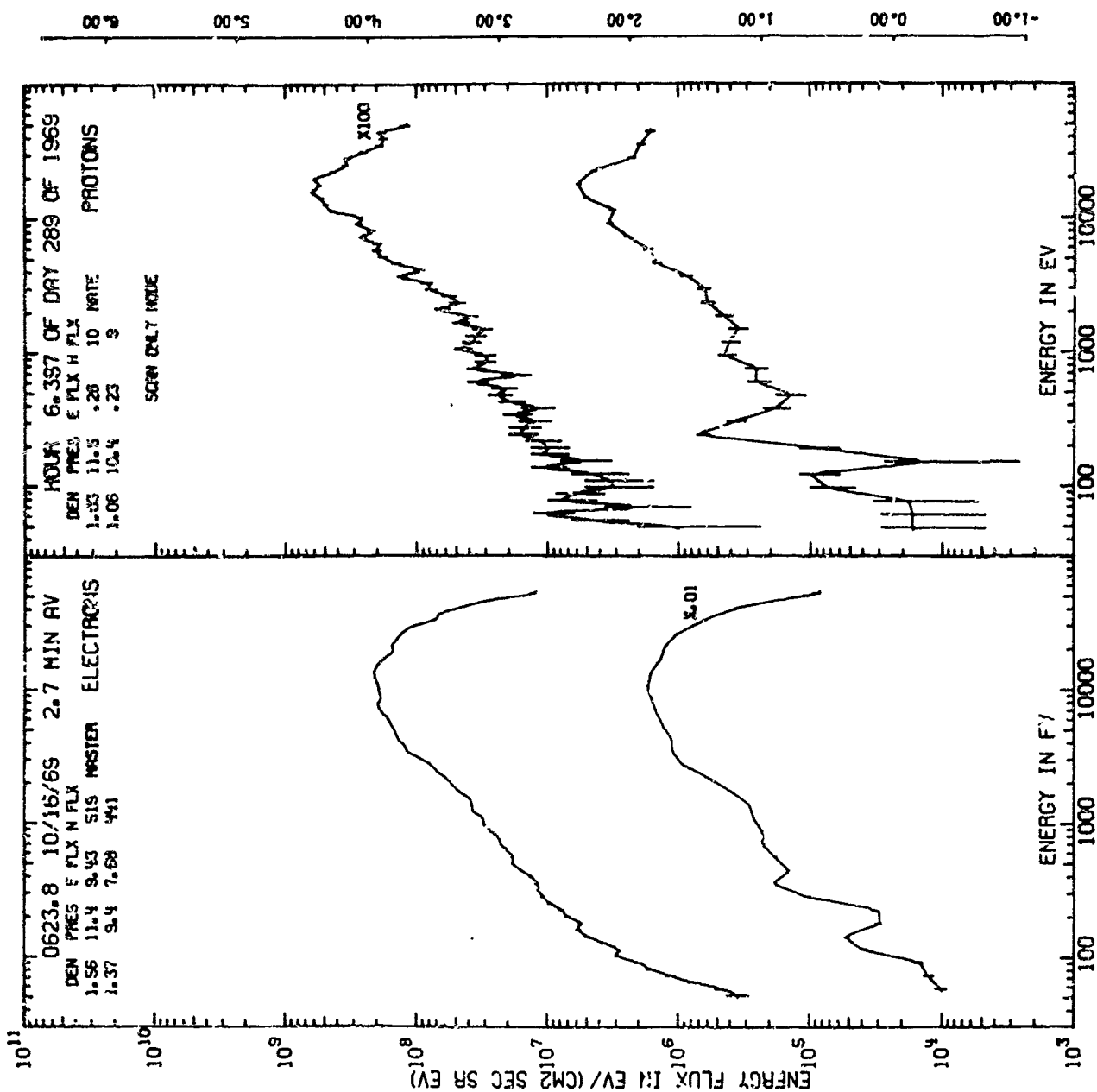


Fig. 3 - Spectrogram of data taken perpendicular to spin axis on October 16, 1969.



4956 12/17/70 1

Fig. 4 - Pre-eclipse particle data on October 16, 1969 (top curves are data perpendicular to the spin axis; bottom curves are parallel).



When the same data are replotted as phase space density against energy as in Figure 6, the charging hypothesis is confirmed. In this representation, the data are seen to be almost identical except for an offset of 4.2 keV, and not only are the electron and proton spectra offset in opposite directions, as they should be, but also the shift in both cases is the same amount that would have been predicted from the location of the proton cutoff. This is emphasized by the parallel solid lines drawn through the electron data at a constant separation of 4.2 keV. The largest deviation from this simple explanation is in the 30- to 50 keV electrons, but from Figure 3, we know that the electron spectrum is changing fast enough in this time period to account for this discrepancy.

Other examples would show much the same story. This particular case was chosen for publication only because it has a relatively simple injection with fairly stable spectra.

ATS-5 does not charge to high potentials during every eclipse. An injection of hot plasma must precede the eclipse by not more than approximately 3 hours for significant charging to take place. On the average, slightly more than half of the eclipses result in charging. On several days, injections has taken place while the spacecraft was in the shadow. The spacecraft went from almost zero potential to a very large potential within a single scan.

**SUNLIGHT** - ATS-5 can also charge to several hundred volts in the sunlight. All such events are confined to the midnight to dawn time sector. This might have been expected by the nature of injections at midnight, but another feature of sunlight charging is that it only happens during the winter months. This has been true from launch until the most recently analyzed data of spring 1972.

A typical charging event would be to about -150 volts for a period of 5 minutes to an hour.

The seasonal effect must be due to the seasonal variation in the magnetosphere which causes ATS to cut through higher lines of force during the summer. Therefore, occurrence of this effect is probably a function of the location at which the spacecraft is parked. Detailed magnetospheric mappings would have to be made before a prediction of sunlight charging could be made for other longitudes.

**THEORY OF CHARGING** - A theory to explain these total charging events has been developed and presented in detail elsewhere (1). The technique will be only summarized here.

As a first step, it was assumed that the spacecraft was made of aluminum, and then standard laboratory values were used to predict backscattered electrons (6), secondary electrons due to both incoming protons and electrons (7), and photo-electrons (8). No

corrections were made for magnetic or wake effects.

The spectra of outgoing electrons as produced by incoming particles was then calculated for several representative charging events. Keeping the outgoing spectral shapes constant, the normalization was varied to obtain an indicated zero net flux to the spacecraft. An excellent fit was found when the surface was emitting only about 1/4 as many electrons of pure aluminum would.

The best value for the photo-electron flux produced by ATS-5 was obtained by considering the sunlight charging events. We calculated  $8.2 \times 10^{-10}$  amp/cm<sup>2</sup> as compared with  $3 \times 10^{-9}$  amp/cm<sup>2</sup> for pure aluminum measured on a rocket flight (7).

A side effect of this calculation was to predict that the spacecraft normally is about one volt positive potential in the night region. This prediction has also been made in a recent paper by Grard (9).

Figure 7 shows the predicted net flux to ATS-5 as a function of potential using this model and the pre-eclipse data from Figure 4 with the assumption that the photoelectron flux has been turned off. The proper potential is predicted to within the resolution of the instrument.

#### DIFFERENTIAL CHARGING

**IN SUNLIGHT** - The total charging events are spectacular oddities which have been useful in developing the theory of charging, but several types of differential charging are more important to particle experimenters in that they can happen all the time.

It will be remembered that the one set of detectors look parallel to the spin axis of the spacecraft, yet in Figure 8 a large modulation is seen in the protons looking along the spin axis. This modulation is at the spin frequency. Simultaneously, there is a cut-off in the electron spectrum. The modulation of the protons increases to higher energies as the cut-off in the electron spectrum increases. Perpendicular detectors see neither effect, but the parallel detectors see similar events on every active day from the autumnal equinox to the vernal equinox.

As was seen in Figure 1, the parallel detectors are at least partially shielded from the external plasma by a ring of solar cells with several antennae and a boom on it. Initially, we thought that sunlight was being reflected down into the cavity by one of these booms. Something (most likely the thermal control unit) would then change up in the way that would be expected in the dark. Then the periodic illumination of the cavity temporarily decreases the potential. The net effect would be to produce an electric field that is dependent on the spin angle.

A better explanation can be deduced from the special event shown in Figure 9, which



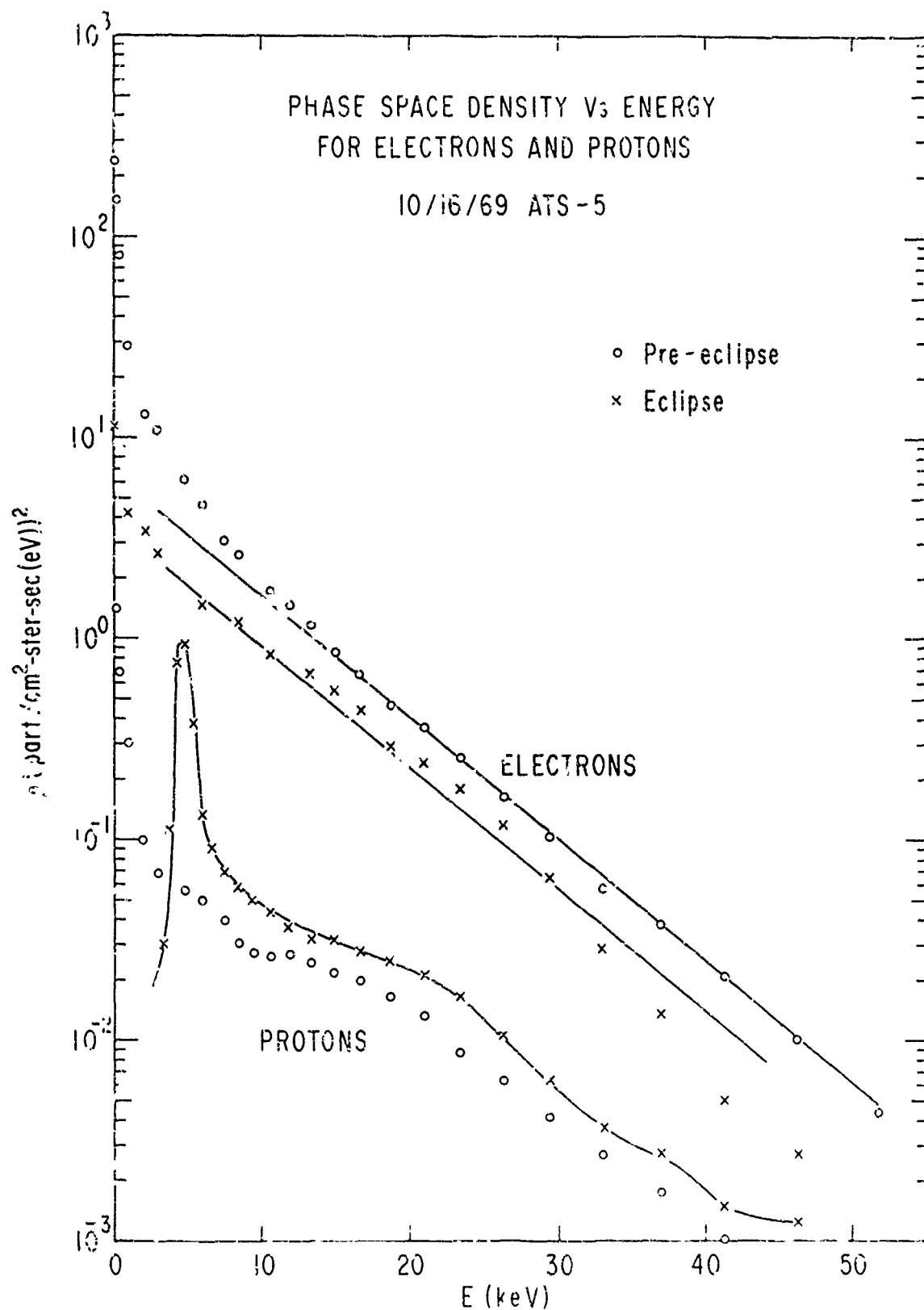


Fig. 6 - Phase space density of particles before and during eclipse.

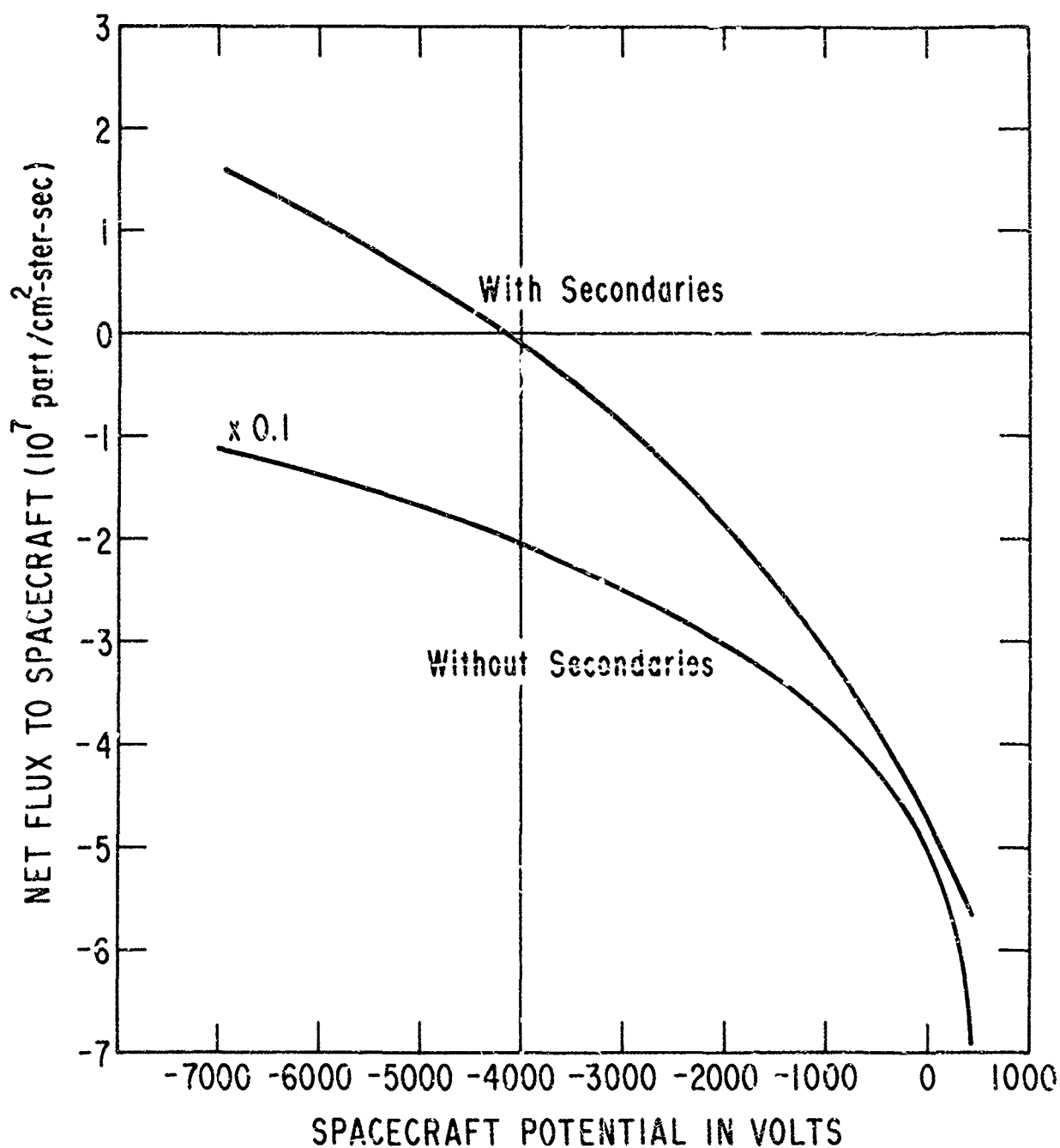


Fig. 7 - Theoretical net flux to ATS-5 versus spacecraft potential during eclipse.

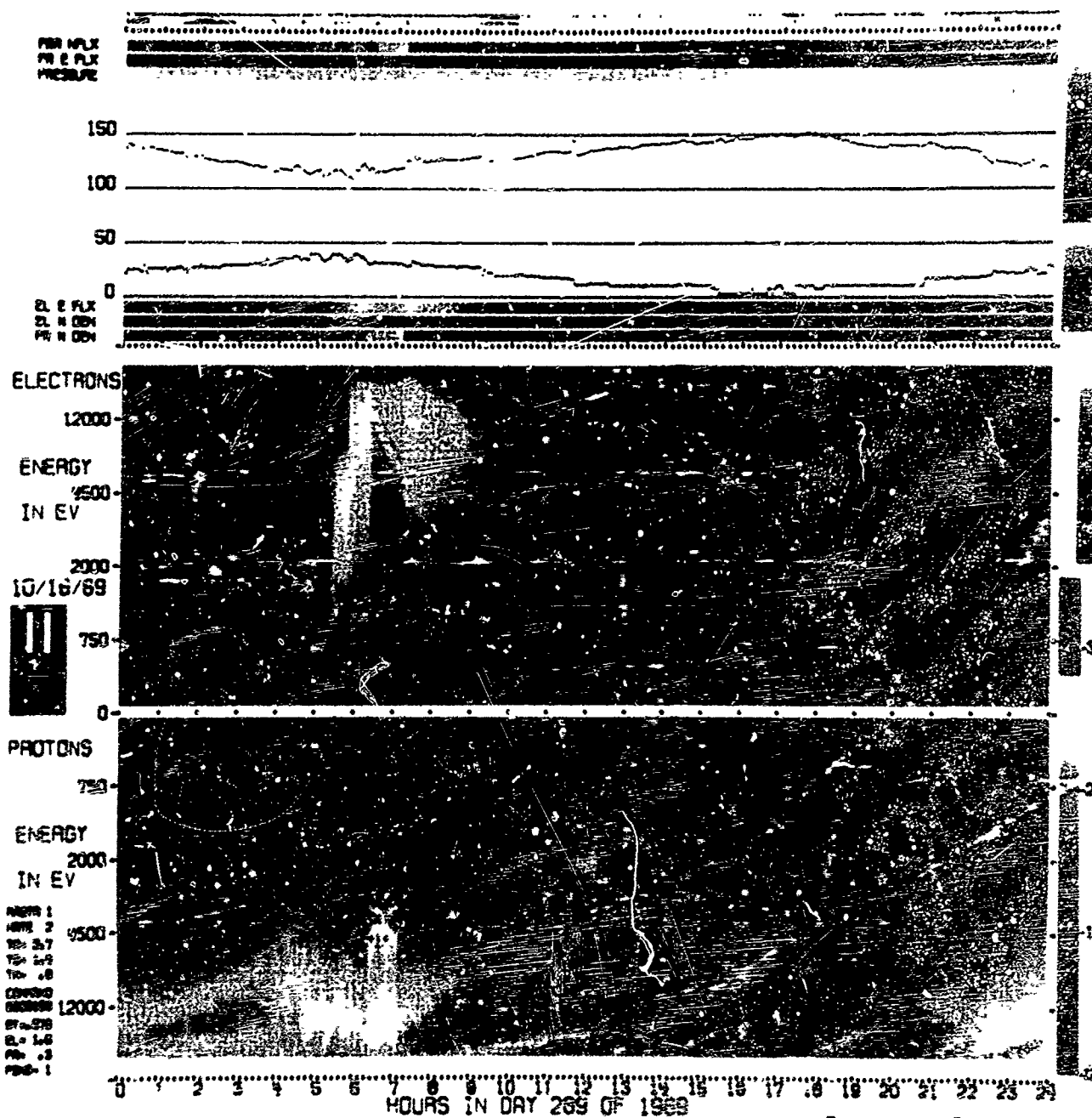


Fig. 8 - Spectrogram of data taken parallel to spin axis on November 10, 1969.

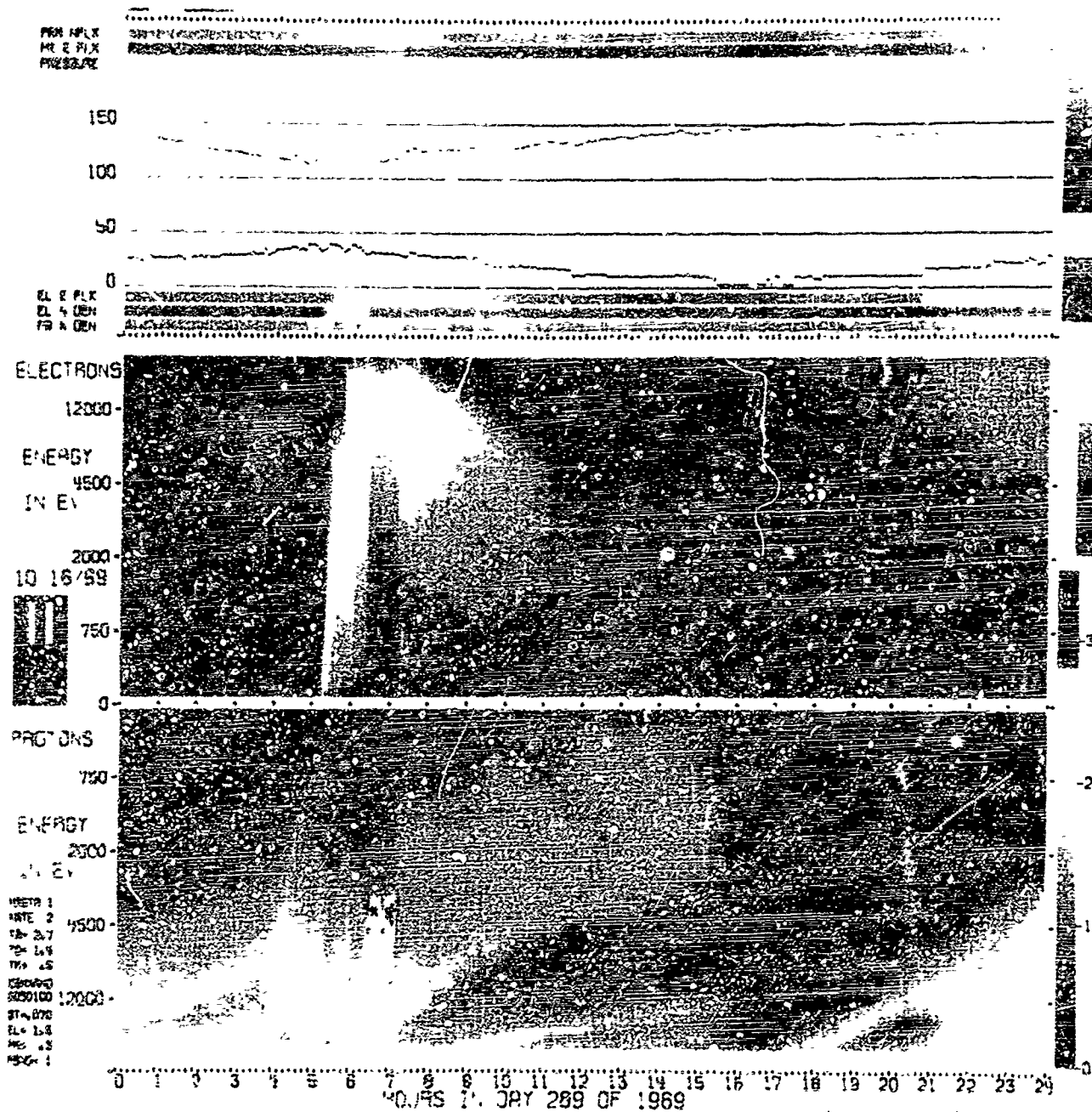


Fig. 9 - Spectrogram of data taken parallel to spin axis on October 16, 1969.

contain data from the parallel detector for the same eclipsing event as previously shown. A slight differential charging had taken place starting at about 0600 UT, coincident with the main injection. During the eclipse, this feature slowly disappears over about 20 minutes. After leaving the eclipse, the differential feature does not return immediately, but rather builds up with a similar time constant. The same general type of behavior is seen on all eclipsing events when there has been differential charging before entering the shadow.

The capacitance of the spacecraft to the outside plasma is of the order of picofarads, but the capacitance formed by an oxidized layer of aluminum on top of metal can be several thousands of picofarads per square centimeter. The events shown in Figure 9 can then be explained by saying that in the dark part of the solar cell cavity something charges up in the same manner as eclipse charging. When the spacecraft enters the earth's shadow, it charges up through an effective capacitor of about 1 picofarad. The previously charged surface then finds itself several thousands of volts above its equilibrium potential, and proceeds to discharge, but it is working through a much larger capacitance back to the main spacecraft body. Similarly, this large capacitor takes several minutes to charge up after leaving the shadow.

The proton modulation as seen in Figure 8 is then thought to be the result of a changing  $E \times B$  force acting on incoming particles. During typical differential charging events, the angle between the spin axis and the local magnetic field is about  $30^\circ$ .

This phenomenon occurs until the annual precession of the plane of the orbit tips the spacecraft far enough to illuminate the cavity continuously.

While the perpendicular detector never sees such striking events, a non-spin modulated notch is frequently seen in the lowest energy electron channels. A possible explanation of this could be a slight charging of the solar cell covers in sunlight with a discharge time long compared to a spin period (about .5 sec). ATS-5 is a particularly simple spacecraft in exterior configuration, and that probably simplifies differential charging problems for the perpendicular detector, but differential charging might be expected on any spacecraft operating in the outer magnetosphere, depending on its configuration and orientation to the sun. This is particularly important when measuring plasma flows by looking at modulations in a spinning detector.

The magnitudes of electric fields produced in the vicinity of the parallel detectors can be estimated to be of the order of thousands of volts per meter.

**IN SHADOW** - Figure 10 shows the parallel detector's response during an eclipse. No

particles are seen below the cutoff energy. However, in Figure 11 we see the perpendicular data taken at the same time, and there is a definite peak in counting rate below the cutoff. Figure 12 shows four scans taken during the event. The presence of these particles is particularly difficult to explain since they do not occur on every charging (cf. Figure 5). They have too high a flux to have been created by ionizing neutrals in the vicinity of the spacecraft. Elastic scattering of ions near the spacecraft is also much too weak a source. The most likely candidate at this time seems to be particles sputtered from surfaces of the spacecraft which are not at the same potential as the main body. Data on sputtering (10) would indicate that the incoming fluxes are strong enough to produce these particles. However, the exact nature of these particles cannot yet be determined, and we still have no adequate explanation of why they occur sometimes and not others.

#### SUMMARY

Many types of surface charging phenomena have been seen on ATS-5. Some have not yet been adequately explained. At this time, it is known that the spacecraft can charge to well over 10,000 volts in eclipse, and to several hundreds of volts in sunlight. Differential charging which produces fields of at several thousands of volts per meter have also been seen. Time constants for charging can range from a fraction of seconds to tens of minutes depending on the surface being charged.

All of these effects are serious hazards to the study of low-energy natural plasmas. Particle optics and accessibility can become hopelessly snarled in these fields.

The possibility of subsystem failure due to discharge of these potentials exists, and may already have been observed (11).

#### ACKNOWLEDGEMENT

Many fruitful conversations with Prof. C. E. McIlwain have helped to understand these data. The work was supported by NASA Contract NAS 5-10364 and Grant NGL 05-005-007.

#### REFERENCES

1. S. E. DeForest, "Spacecraft Charging at Synchronous Orbit," J. Geophys. Res. 77, 651, 1972.
2. C. R. Chappel, K. K. Harris, and G. W. Sharp, "A Study of the Influence of Magnetic Activity on the Location of the Plasma-pause as Measured byOGO 5," J. Geophys. Res. 75, 50, 1970.
3. S. E. DeForest, and C. E. McIlwain, "Plasma Clouds in the Magnetosphere," J. Geophys. Res. 76, 3587, 1971.
4. L. A. Frank, and K. L. Ackerson, "Local Time Survey of Plasma at Low Altitudes

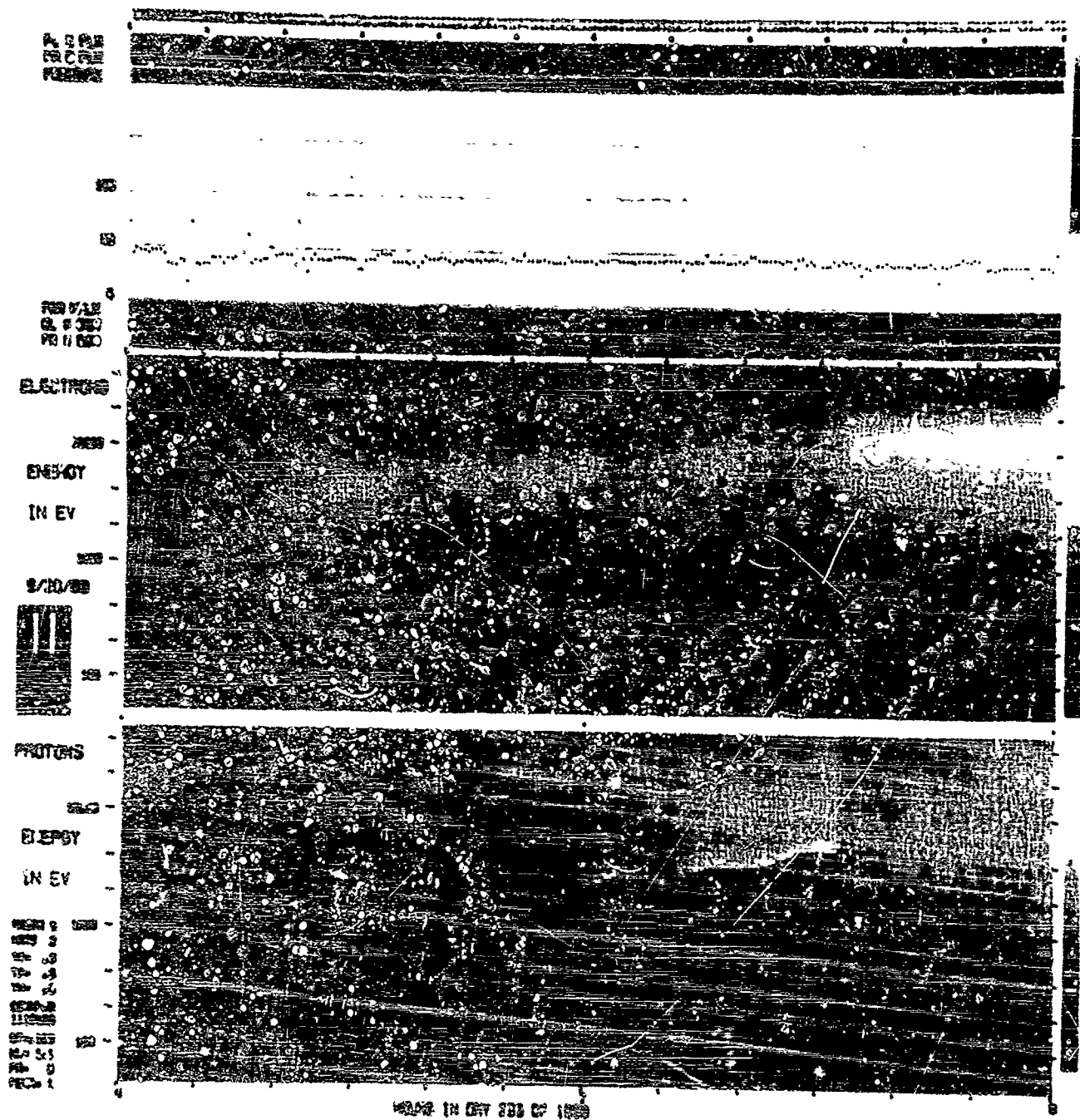


Fig. 10 - Spectrogram of data taken parallel to spin axis on September 20, 1960.

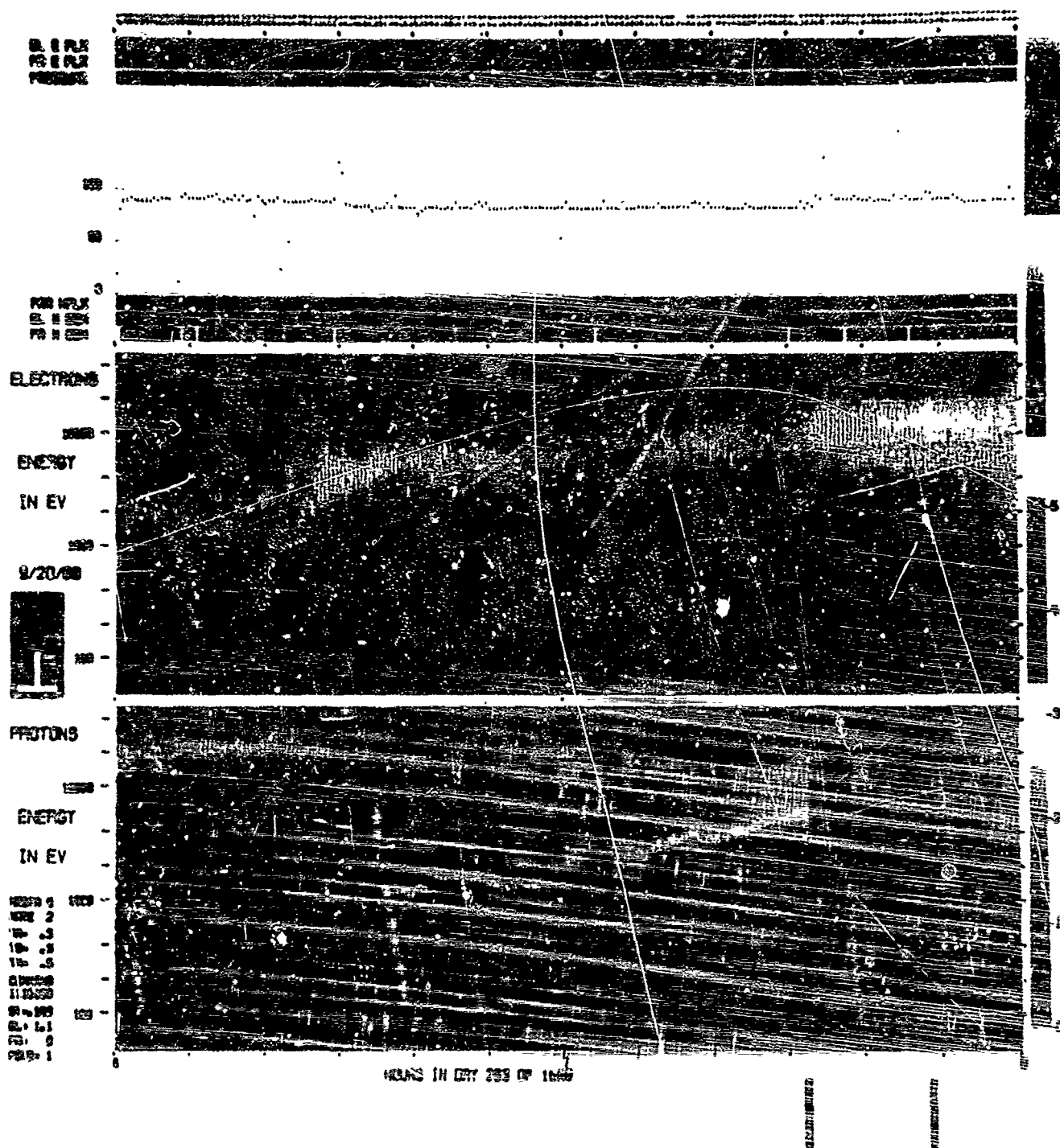
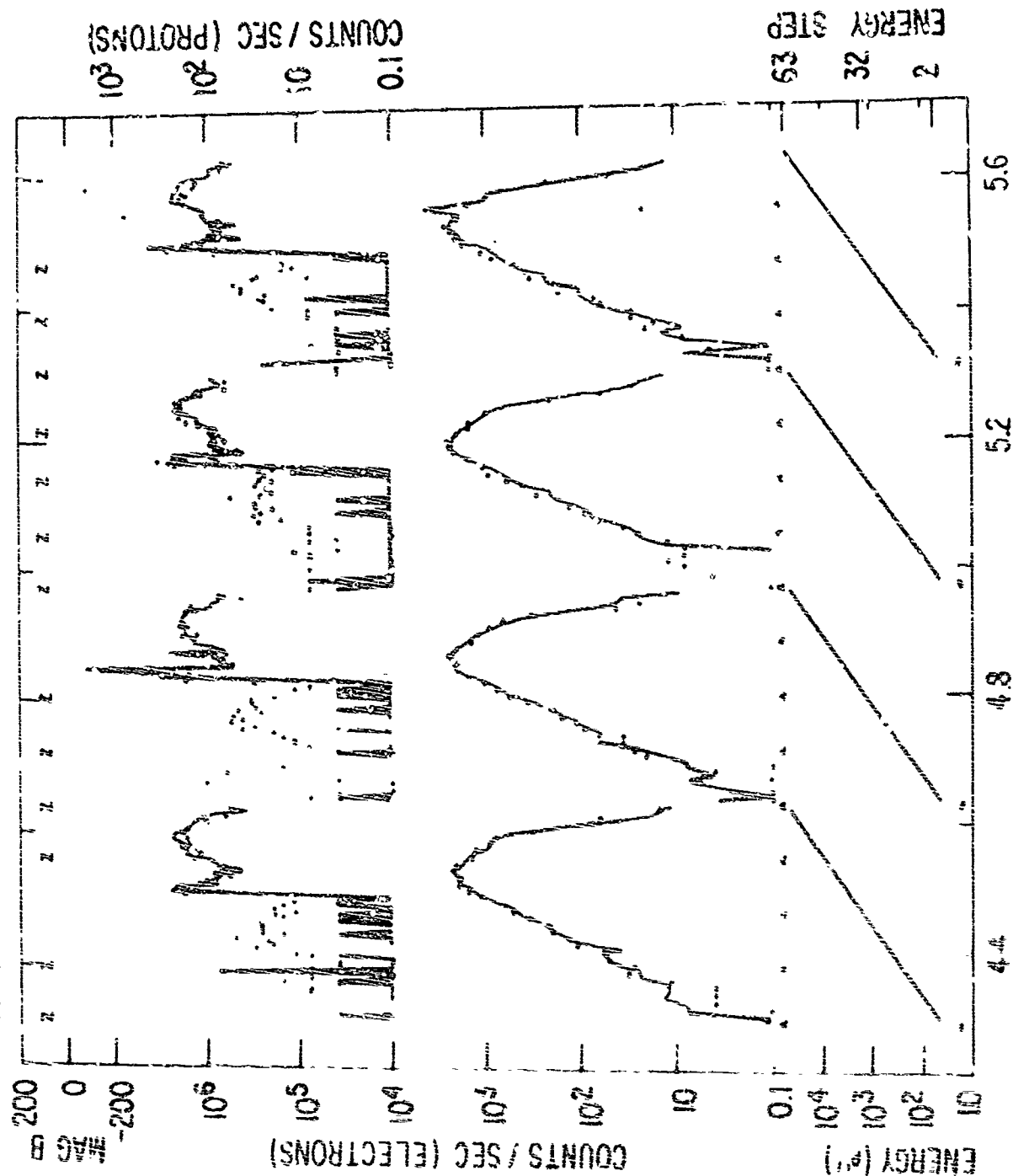


Fig. 11 - Spectrogram of data taken perpendicular to spin axis on September 20, 1969.



9/20/69 DAY OF YEAR 263 SEQ 312528 MASTER 4 MATE 2



HOUR 7 TIME (MINUTES)

FIGURE 1 - Partial solar eclipse on September 20, 1969.



Over the Auroral Zones," J. Geophys. Res. 77, 4116, 1972.

5. S. E. DeForest, "Initial Results of the ATS-5 Plasma Experiment," ECS 150, 660, 1969.

6. E. J. Sternglass, "Backscattering of Kilovolt Electrons from Solids," Phys. Rev. 95, 345, 1954.

7. E. C. Whipple, "The Equilibrium Electric Potential of a Body in the Upper Atmosphere and Interplanetary Space," Ph.D. thesis, George Washington University, Washington, D.C. 1965; also published as NASA Tech. Note X-615-65-296, 1965.

8. H. E. Hinteregger, K. R. Damon, and L. H. Hall, "Analysis of Photoelectrons from Solar Extreme Ultraviolet," J. Geophys. Res. 64, 961, 1959.

9. R. J. L. Grard, "Properties of the Satellite Photoelectron Sheath Derived from Photoemission Laboratory Measurements" submitted to J. Geophys. Res., 1972.

10. J. Strong, "Procedures in Experimental Physics, Prentice-Hall, Englewoodcliffs, N.J., 1938.

11. R. Fredrichs, and F. Scarf, "Observations of Spacecraft Charging Effects in Energetic Plasma Regions," presented at ESLAB Symposium on Photon and Particle Interaction with Surfaces in Space, Noordwijk, Holland, 1972.

## Electrostatic Charges Acquired by Spacecraft and Their Possible Effects on Instruments

Elden C. Whipple, Jr.

National Oceanic and Atmospheric Administration

### ABSTRACT

The important charging mechanisms for a spacecraft in the ionosphere are the collection of ions and electrons from the ionospheric plasma. Expected and measured spacecraft potentials (measured with respect to the ambient plasma) are on the order of the equivalent electron temperature, namely, a few tenths of a volt negative. At higher altitudes where the plasma density is lower, photoemission of electrons caused by sunlight drives spacecraft potentials positive. Other mechanisms that can at times affect spacecraft charges are secondary emission of electrons, the induced electric field caused by spacecraft motion in the earth's magnetic field, and electric fields on exposed spacecraft surfaces. Large negative potentials have been observed during magnetic storms in the earth's shadow and have been attributed to the effect of large fluxes of energetic electrons. Spacecraft potentials must be taken into account in the design and interpretation of charged particle experiments in the upper atmosphere.

### THE SPACECRAFT ENVIRONMENT

THE ELECTROSTATIC CHARGE acquired by a spacecraft is determined primarily by the spacecraft environment. The lowest altitude at which a satellite can be maintained is about 250 km (about 150 miles), and at this altitude the environment is characterized by an extremely low atmospheric pressure, about  $10^{-10}$  atmospheres. Yet in spite of the rarefied nature of the environment compared to the atmosphere at the surface of the earth, it is primarily the interaction of the spacecraft with that fraction of the environmental particles that are charged that determines the electrostatic charge acquired by the spacecraft.

In addition to the low atmospheric density, the spacecraft environment is characterized by sunlight, except of course for that part of the satellite orbit which is in the earth's shadow. The flux of solar photons includes ultraviolet and x-ray wavelengths which are absent at the earth's surface because of the absorbing effect of the denser portions of the earth's atmosphere. These shorter wavelengths of the solar spectrum are responsible for producing the charged particles, ions and electrons, which constitute the ionosphere at satellite altitudes. The number density of ions or electrons ranges from about  $10^3/\text{cm}^3$  at the peak of the ionosphere (300 km) to about  $1/\text{cm}^3$  in the earth's magnetosphere. In addition to their ionizing action, these energetic photons can affect the spacecraft

charge directly, by knocking electrons out of the surface material when they impact. At higher altitudes where atmospheric particle densities are extremely low, this phenomenon of photoemission can be the dominant mechanism in determining the spacecraft charge.

The temperature of the atmosphere at these altitudes is on the order of 1000°K. It is convenient to use the electron-volt (eV) as an energy unit. On this scale, the atmospheric particles have energies of about 0.1 eV and are frequently called thermal particles. In contrast, there are energetic particles present in the Van Allen belts and in the magnetosphere with energies of thousands (keV) and millions (MeV) of electron-volts. Although the fluxes of particles with these large energies are usually small compared to the fluxes of thermal particles, there are times, especially at higher altitudes in the magnetosphere, when these energetic particle fluxes can affect spacecraft charges.

Finally, the motion of the charged particles in the spacecraft environment is dominated by the earth's magnetic field, which must therefore be taken into account in calculating the charge acquired by a spacecraft. The term ionosphere is used for that part of the atmosphere where the charged particle density is controlled by collisions between the particles as well as by the magnetic field. Above a few thousand kilometers altitude, collisions are so infrequent (the mean-free-path is on the order of or larger than the dimensions of the earth) that the charged particle densities and fluxes are determined by the earth's magnetic field and its interaction with the solar plasma streaming from the sun (the solar wind). Hence the term magnetosphere is used for this outer portion of the earth's atmosphere.

### CHARGING MECHANISMS

When an ion or an electron strikes a spacecraft surface, the particle charge is in general acquired by the spacecraft. In the case of an electron incident upon a metal surface, the electron is absorbed into the conduction layer of the metal. There is a small probability at thermal energies, about 5%, that the electron will be reflected before absorption. At higher energies the electron may be absorbed and then re-emitted with other electrons that have been excited being emitted also. The ratio of the number of emitted electrons to the number incident is called the "secondary electron yield". A typical yield curve versus energy of the incident electrons is shown in Figure 1.

When an ion approaches a metal surface it is neutralized at low incident energies by pulling an electron out of the metal before the surface is reached. The neutral atom then strikes the surface and rebounds, so that the net effect on the metal is the acquisition of one positive charge. Occasion-

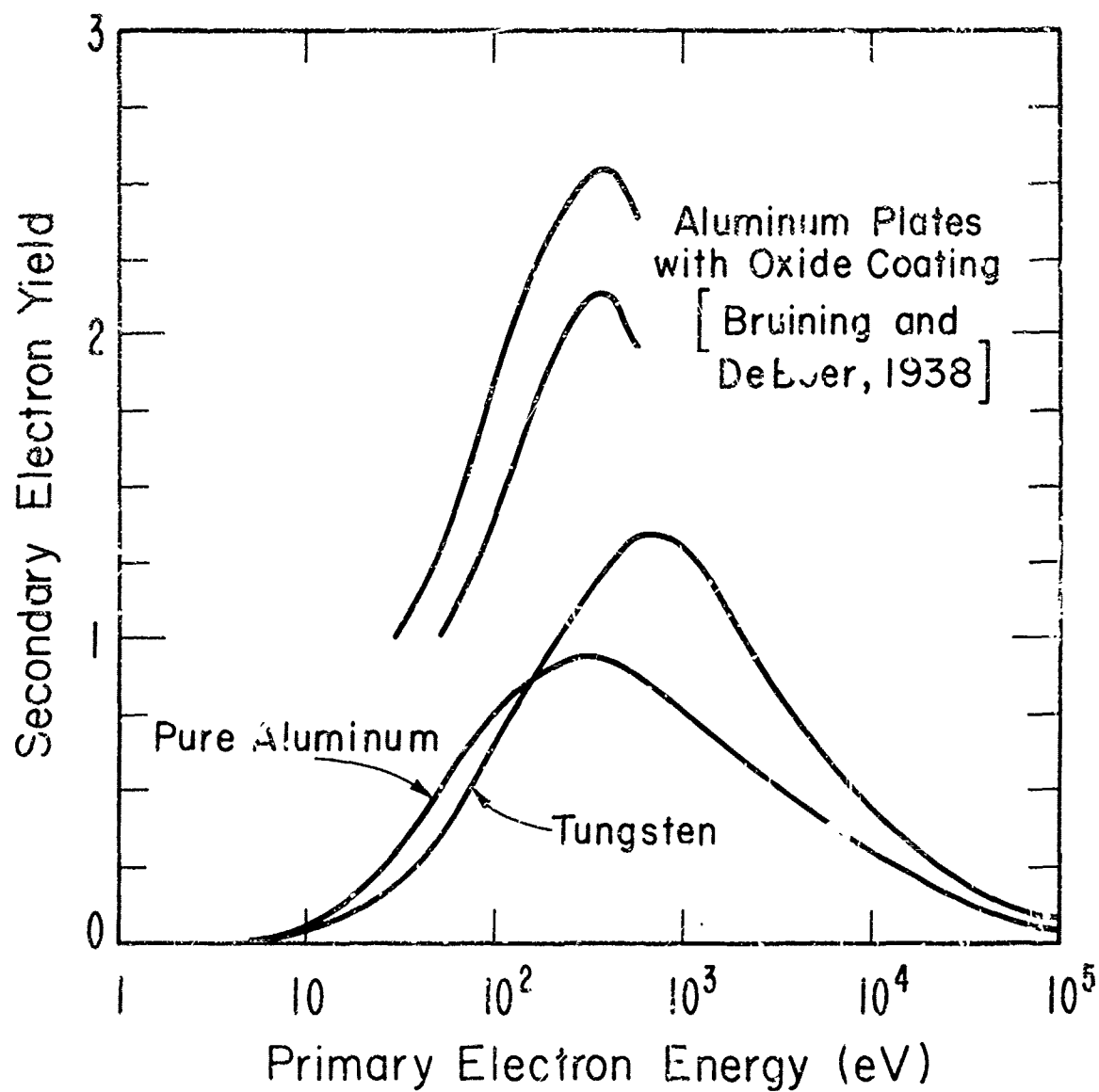


Fig. 1 - Secondary electron yields for aluminum and tungsten on electron impact.

ally, more than one electron is pulled out of the metal. The ratio of the average number of additional emitted electrons to the number of incident ions is called the "secondary yield for ion impact." It is only weakly dependent on the ion energy below a few keV. At higher energies the ion actually impacts the metal and a larger number of electrons can be emitted as a result. Some typical yields for protons incident on aluminum and tungsten are shown in Figure 2.

The behavior of charged particles incident upon insulating surfaces is less well understood. Electrons may be caught and bound in the surface layer of the material at the point of impact until they are released by some mechanism such as an incident ion. The binding forces and mobility of the charged particles on the surface are strongly dependent on the nature of the material.

The rate at which charged particles are incident upon a spacecraft depends both upon the number of charged particles in the vicinity of the spacecraft and upon the particle trajectories. The particle trajectories are determined by the thermal velocities of the particles and by the forces exerted on them by magnetic and electric fields. Since the electric field around the spacecraft depends not only on the charge on the spacecraft but also on the space charge distribution in the vicinity of the spacecraft, it is apparent that the calculation of the total ion or electron current is an extremely complicated problem.

The fate of electrons that are emitted from spacecraft due to ion or electron impact or to photoemission is also dependent upon the local electric and magnetic fields as well as upon their initial velocity. If the spacecraft is charged positively, the emitted electrons may return to the spacecraft without escaping and hence not contribute to the current balance. Photoemission current densities due to sunlight are on the order of  $3 \times 10^{-9}$  amp/cm<sup>2</sup> (1)\*. The photoelectrons are probably emitted isotropically with a distribution of velocities corresponding to an energy of 2 to 3 eV.

The equilibrium charge residing on a spacecraft is determined by the condition that there be no net current to the spacecraft--if it can be assumed that the spacecraft is a conducting body at a uniform potential. If the spacecraft is not a conducting body, then each point of the surface will reach its own local equilibrium potential determined by the condition of zero current density at each point. The problem, then, of determining spacecraft charge involves calculating all the possible currents to the spacecraft as a function of total charge on the spacecraft, and determining what charge is required to produce zero net current. It is obvious that a realistic calculation will be extremely complicated; however,

fairly realistic equilibrium potentials can be obtained with some simplifying assumptions for factors such as the spacecraft geometry and material and for the collected currents.

#### OTHER FACTORS AFFECTING SPACECRAFT CHARGE

There are a number of other factors that must be taken into account in considering the charging mechanisms. One of the most important of these is the spacecraft motion. A typical satellite velocity in near-earth orbit is about 8 km/sec. Typical thermal velocities in the ionosphere are from 1 to 6 km/sec for ions, the lower velocity corresponding to oxygen ions ( $O^+$ ) which dominate at the lower altitudes and the higher velocity corresponding to protons ( $H^+$ ) which dominate at higher altitudes. In contrast, the thermal velocity for electrons is much higher, about 200 km/sec. Consequently, a satellite is supersonic with respect to the ions but subsonic with respect to the electrons. One result of the satellite motion, therefore, is an ion wake. The region immediately behind the satellite is depleted of ions, but not depleted of electrons. The wake region is a tail-like conical region of negative space charge and consequently negative potential. The extent and other characteristics of the wake depend primarily upon the ion composition, but also upon the magnetic field. Wakes have been detected behind spacecraft (2), and some theoretical work has been attempted with the aim of calculating wake characteristics (3). It is apparent that the wake can affect the collection of ions and electrons to the rear of a spacecraft.

Another effect of spacecraft motion is an induced electric field caused by the motion of a conducting body across the earth's magnetic field lines. The induced field will cause polarization such that the field due to the polarization charge exactly cancels the induction field in the interior of the body. The polarization charge, in turn, is the source of a real field external to and carried along with the body which depends on the geometry and the environmental plasma. Its effect on particle collection may be described by saying that the potential of the surface of the spacecraft varies linearly with distance in the  $\vec{V} \times \vec{B}$  direction. This effect can be particularly important if the spacecraft carries long antennas. One end of the antenna will tend to be "pinned" to a potential near the plasma potential, while the other end may reach a high negative value given by  $(\vec{V} \times \vec{B}) \cdot \vec{L}$ , where  $L$  is the length of the antenna. The quantity  $(\vec{V} \times \vec{B})$  can be as high as 0.2 volts/meter, so that long antennas of several hundred meters such as have been used on the topside sounding satellites and on the radio astronomy satellite can cause large potential excursions.

As mentioned above, the magnetic field of the earth also affects particle collection because of the spiral nature of the charged

\* Numbers in parenthesis designate References at end of paper.

# SECONDARY YIELD OF ELECTRONS FOR PROTON IMPACT AT ENERGIES ABOVE 1 KEV

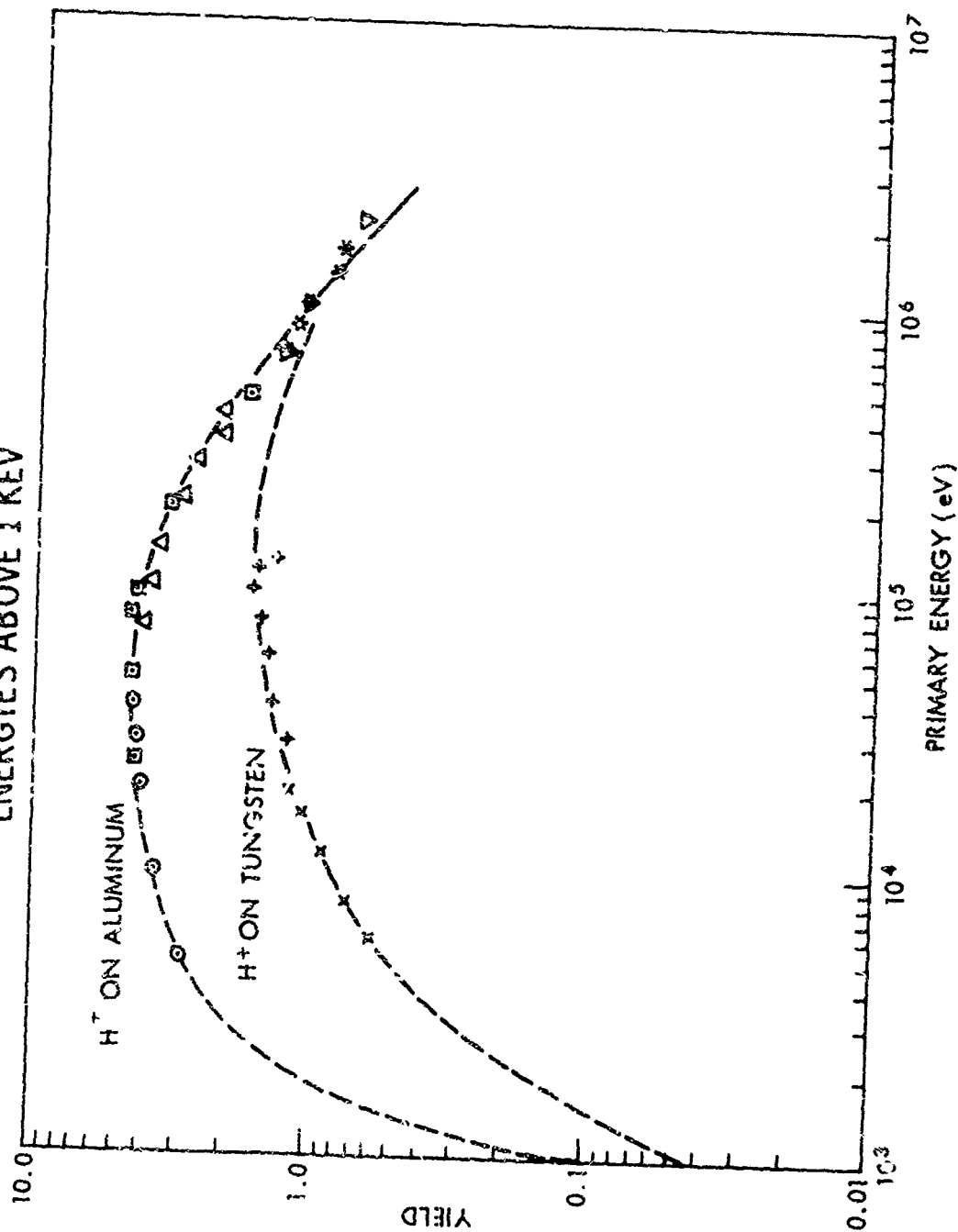


Fig. 2 - Secondary yield of electrons for proton impact at energies above 1 kev.

particle trajectories about the field lines. The gyroradius for electrons is a few centimeters; for ions, a few meters.

The influence of surface material properties on secondary emission and photoemission has already been discussed. If a spacecraft has a significant magnetic moment or dc or rf electric fields on exposed surfaces, these can also affect particle collection and hence the spacecraft charge.

#### TYPICAL SPACECRAFT POTENTIALS

Because of the fact that electrons have higher thermal velocities than ions, there is a larger flux of electrons than ions from the ionospheric plasma to a body such as a spacecraft. Hence a negative charge is accumulated until enough electrons are repelled that the electron and ion currents are equal. To a good approximation, except in the wake region, the electron current density to a negatively charged body at a potential  $V$  is given by

$$J_e = ne(kT/2\pi m_e)^{1/2} \exp(Ve/kT) \quad (1)$$

where  $n$  is the local electron density and  $T$  the temperature ( $e$  is the unit charge,  $k$  is Boltzmann's constant and  $m_e$  the electron mass). The coefficient of the exponential function is called the random current density and would be the current density of electrons to an uncharged surface. At the peak of the ionosphere it is on the order of  $10^{-6}$  to  $10^{-7}$  amp/cm<sup>2</sup>. Because of the heavier ion mass and consequent lower thermal velocity, the ion random current density is about an order of magnitude smaller, but is still quite a bit larger than the photoemission current density of about  $3 \times 10^{-9}$  amp/cm<sup>2</sup>. Hence photoemission effects can be disregarded throughout a large part of the ionosphere.

The simple exponential dependence of the electron current density on potential is due to two things: first, the large thermal velocity of the electrons compared to the satellite velocity means that the satellite can essentially be regarded as being at rest; the electron velocities are isotropic in the satellite reference frame. Second, the calculation of currents in a repulsive force field is much more straightforward than for attractive force fields because space charge effects can in general be disregarded. Neither of these factors is true for the ions which means that the ion current calculation is much more complicated and in general must be done numerically. An approximate expression that is valid for small potentials and large Mach numbers is the so-called ram current expression that describes the current that would be collected by a body sweeping up all the ions in its path if the ions were stationary:

$$I_+ = n e v_s A \quad (2)$$

In this expression,  $v_s$  is the satellite velocity

and  $A$  is the cross-sectional area of the satellite in the direction of motion.

The effect of an attractive potential is to increase the effective cross-section of the spacecraft. The effectiveness of the potential in "reaching out" and pulling in additional ions is best described through the concept of the "Debye Length" which is a measure of the distance over which a charge is shielded in a plasma. The larger the Debye length, the more effective is the potential, with an infinite Debye length corresponding to an unshielded Coulomb field. As the electron density decreases, the Debye length increases according to the relation

$$L = (\epsilon_0 kT/ne^2)^{1/2} \quad (3)$$

where  $\epsilon_0$  is the free space permittivity. In the upper atmosphere the Debye length ranges from a few mm in the ionosphere to several meters in the magnetosphere. An accurate calculation for the ion current to an attractive body in a plasma has only been done for spheres and cylinders at rest by Laframboise (4). A convenient approximation that has been used assumes a spherically symmetric Debye potential distribution,

$$V(r) = V_s (R/r) \exp\{-(R-r)/L\} \quad (4)$$

and then employs the results of ion trajectory calculations to obtain ion current densities. Some typical ion current-voltage curves for various ratios of the Debye length to the body radius are shown in Figure 3.

If the total electron and ion currents from expressions such as (1) and (2) are equated, it can be seen that the equilibrium potential is negative and is given very nearly by the equivalent electron temperature multiplied by a logarithmic function that is near unity and only weakly dependent on other factors. Since the electron temperature is about 0.1 eV, spacecraft potentials should also be typically a few tenths of a volt negative. This is indeed the magnitude of potentials that have generally been measured on spacecraft near the earth. Table 1 lists some measurements of spacecraft potential. Most of the satellites in this table which show larger or positive potentials were either in orbits that took them well into the magnetosphere or solar wind, or else had long antennas or surfaces where electric fields were exposed to the plasma. In the outer ionosphere or in the magnetosphere where the thermal plasma density is low, photoemission becomes the predominant positive current and spacecraft potentials tend to become positive. All of the positive potentials in Table 1 were obtained on satellites with orbits that took them well into the magnetosphere or into interplanetary space.

Charging currents due to fluxes of energetic particles are generally smaller than photoemission currents and would not affect

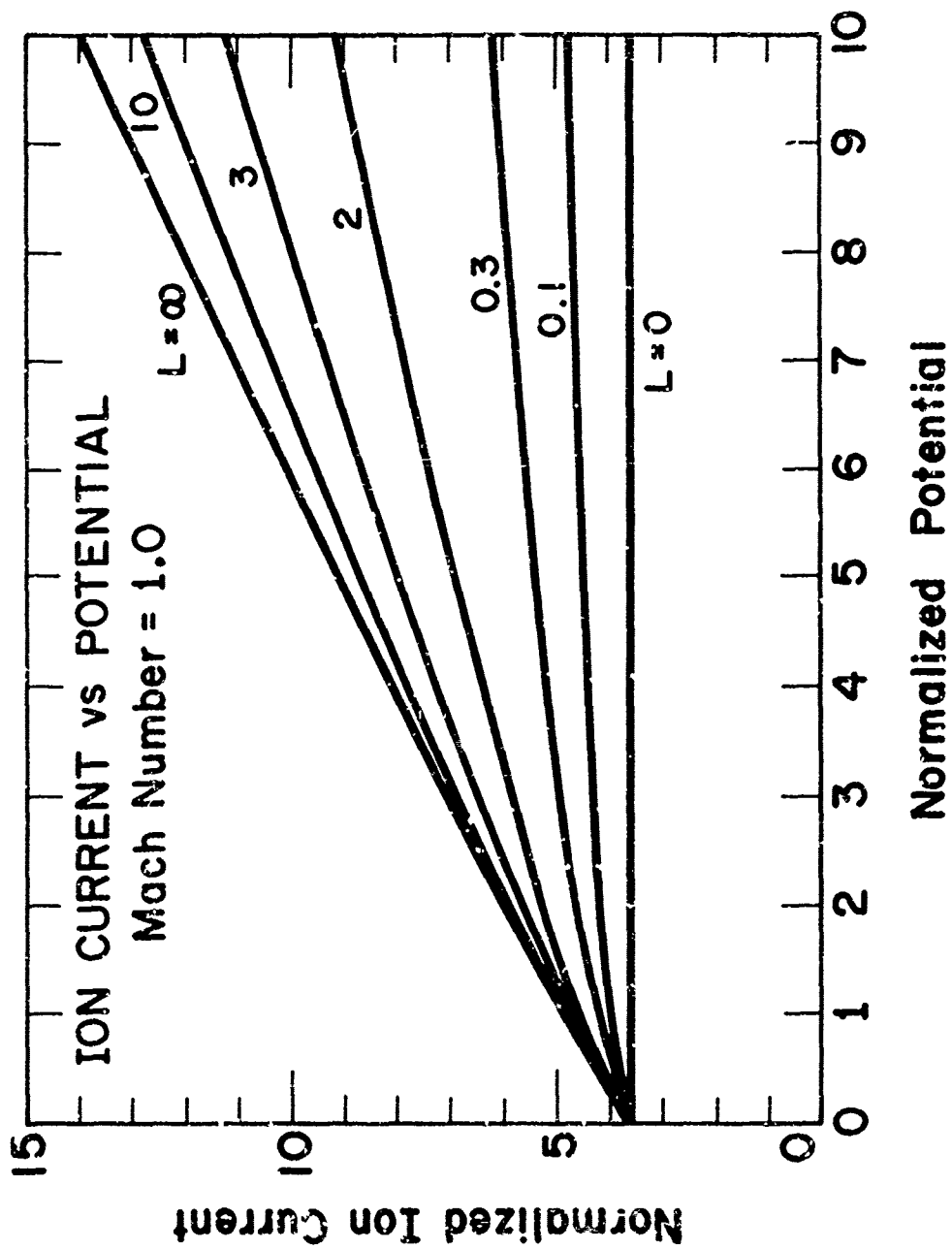


Fig. 3 - Ion current density to a sphere with a Debye potential.

## SOME MEASUREMENTS OF SATELLITE POTENTIAL

Satellite	Launch Date	Experiment	Satellite Potential & Comments
Sputnik 3	5/15/58	Ion Traps	Negative to -6 volts
Explorer 8	11/3/60	Ion & Electron Traps	Normal No solar cells, some effect from r.f. probe
Discoverer 32	10/13/61	Ion Trap	Normal
Cosmos 2	4/6/62	Langmuir Probe & Ion Traps	Negative potential increased by positive potentials on outer grids of traps.
Air Force Satellite	4/17/62	Ion Trap	Negative to -20 volts
Ariel 1	4/26/62	Langmuir Probes	Normal* up to -1.0 volt
Explorer 17	4/3/63	Langmuir Probe	Normal* up to -1.0 volt at night
Tiros 7	6/19/63	Langmuir Probe	Normal*. Negative solar cells.
IMP A (Expl. 18)	11/27/63	Electron Trap	1-2 volts positive, Positive solar cells
Explorer 20	8/25/64	Langmuir Probe	Negative to -8 volts, Positive solar cells
OGO 1	9/5/64	I&E Traps Mass Spectr.	Negative to -15 volts, Positive solar cells
IMP B (Expl. 21)	10/4/64	Electron Trap	1-2 volts positive, Positive solar cells
Explorer 22	10/10/64	Langmuir Probe	Negative, exceeding -4 volts at times. Some positive solar cells
Explorer 27	4/29/65	Langmuir Probe	Negative to -8 volts. Some solar cell terminals coated
IMP C (Expl. 28)	5/29/65	Electron Trap	1-2 volts positive, Positive solar cells.
OGO 2	10/14/65	Ion, Electron Trap Mass Spectr.	Negative to -3 volts, solar cell terminals coated.

\* "Normal" means a few tenths of a volt negative near the earth.

spacecraft potentials appreciably if the spacecraft were in sunlight. However, magnetic storms can increase the flux of energetic particles and affect satellite potentials. There have been cases of satellites in the magnetosphere that experienced very large negative potentials when they entered the earth's shadow. DeForest (5) measured a potential as large as  $10^4$  volts negative on ATS-5 during simultaneous magnetic storm and eclipse conditions. Frank (6) has reported fluctuations of several hundred volts in particle energies measured with an instrument on IMP-5 which he attributes to spacecraft potential fluctuations. Scarf (7) has suggested that there is evidence from some satellites in the magnetosphere that differential charging has occurred on different insulated portions of the spacecraft such that electric fields as large as kilovolts/meter occur between different portions of the spacecraft.

### EFFECTS OF SPACECRAFT CHARGE ON MEASUREMENTS

One of the most obvious effects of spacecraft charge on measurements is shown in Figures 4 and 5 where the ion current collected by an ion trap on the OGO-1 satellite is plotted against the retarding potential applied to one of the grids of the trap. The ion trap is essentially similar to a conventional vacuum tube with the ionospheric plasma acting as a cathode in providing ions and electrons. One or more grids are applied with a potential which selects the ions or electrons that can reach the collector according to their energy, so that the current-voltage curve yields information about the energy and number density of the particles in the plasma. In Figure 4 the spacecraft is in the earth's shadow, and the ion current falls rapidly to a background value when the retarding potential reaches about 2 volts. Five minutes later, as shown in Figure 5, the spacecraft is in sunlight, and now the ion current does not cut off until the retarding potential



# Ion Mode in Eclipse, 1910 UT 26 Mar 1965

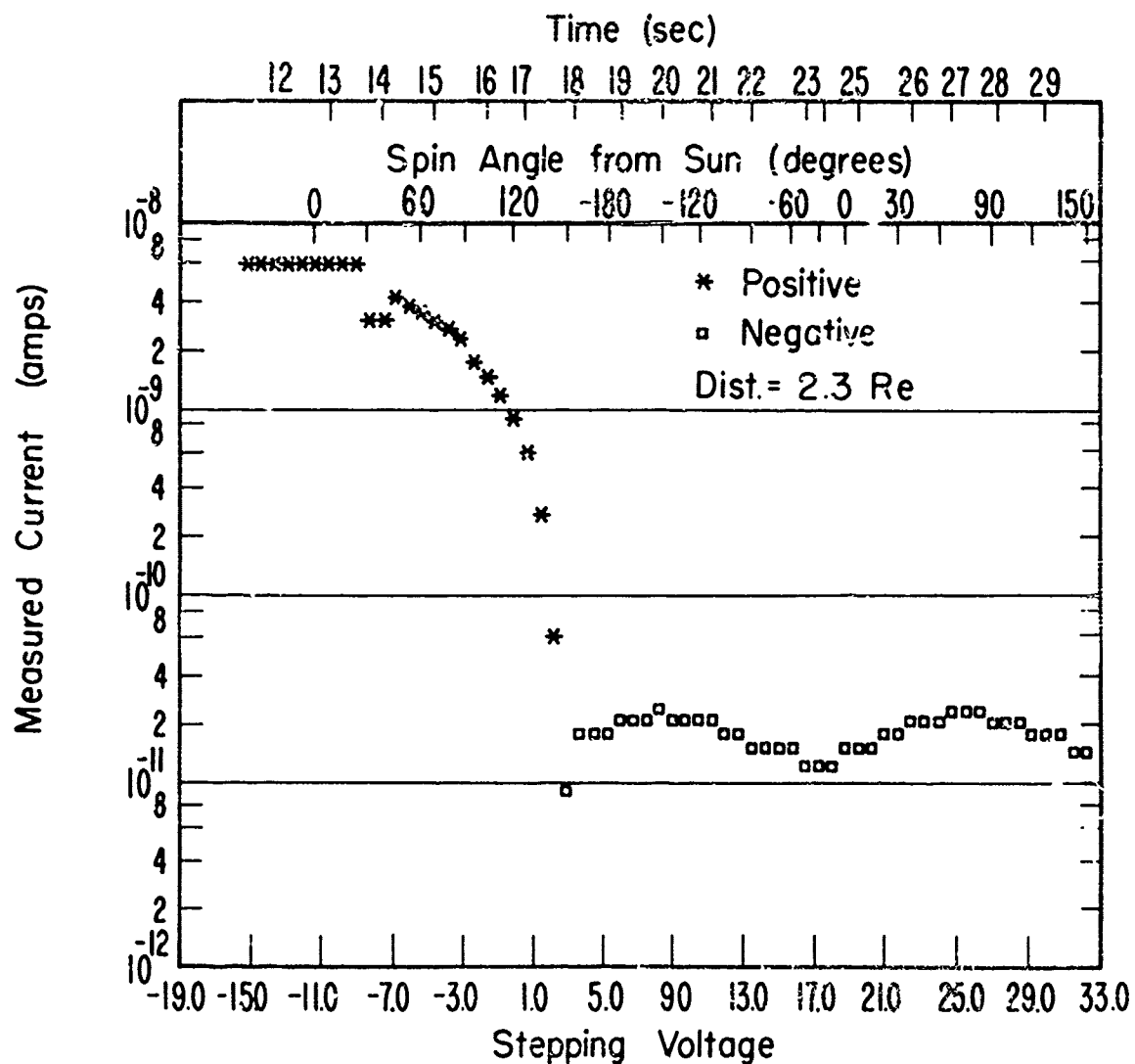


Fig. 4 - Ion current to the ion trap on OGO 1 in the earth's shadow.

# Ion Mode in Sunlight, 1915 UT 26 Mar. 1965

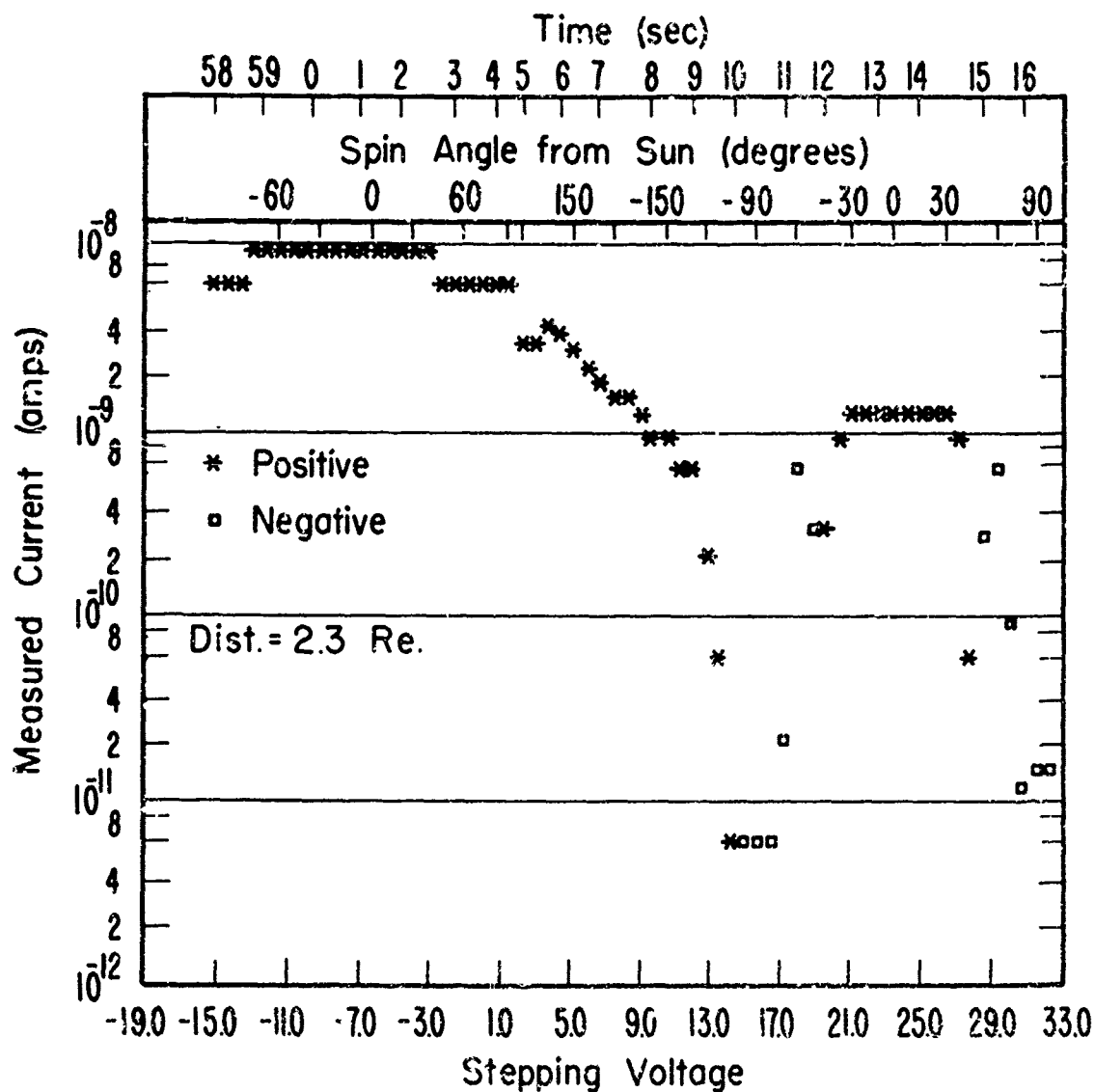


Fig. 5 - Ion current to the ion trap on OGO 1 in sunlight.

reaches about 14 volts. The peak in current at 25 volts is due to photoemission from the grids and collector. The spacecraft potential has changed by about 12 volts in a negative direction as the satellite moved from darkness into sunlight, and the current-voltage curve has been shifted along the voltage axis by a corresponding amount. Any kind of ion or electron collector will see an apparent shift of the energy of the particles by an amount corresponding to the spacecraft potential shift, and this effect is what has been used to infer the spacecraft potentials in Table 1. In this particular example, the potential shift is not due to photoemission, but to the effect of the solar cell paddles in acting as electron collectors when they reached their full potential in sunlight. Figure 6 illustrates how the cut-off potential for the ions changes as the satellite moves further out in the magnetosphere. The spacecraft potential becomes less negative as photoemission becomes more important at higher altitudes and the cut-off potential moves to lower values. It is possible that some of the steep gradients in ion density that have been reported in the outer ionosphere (8) are partially a result of decreasing ion currents caused by an increasing positive spacecraft potential.

If the plasma particles have low kinetic energies it is possible that none will be collected at all by an instrument. Hoffman (9) found that at times near apogee the Explorer 31 spacecraft potential becomes positive, so that no positive ions reached his ion mass spectrometer in spite of a -6 volt drawing-in potential on his aperture grid. Narcisi et al. (10) experienced a similar result for negative ions on a rocket flight when the rocket potential was about -0.5 volts. Conversely, an attractive spacecraft potential may enhance the collected current significantly so that it becomes difficult to relate the measured current to the ion density in the plasma. Figure 7 illustrates the helium ion current enhancement by a -6 volt spacecraft potential (11). The ion current can be increased by almost two orders of magnitude when the experiment is facing the direction of motion, and by much more than this at other angles. These results were obtained by numerical calculation of ion trajectories for an infinite Debye length. However, even at Debye lengths as small as 10 cm there can still be an enhancement of the ion current of a factor of 3 at small angles of attack to more than an order of magnitude at large angles.

At the large spacecraft potentials reported by DeForest of hundreds and even thousands of volts it is easy to imagine instrumental effects such as breakdown of insulators or corona discharges through escaping gases near outgassing materials. Such phenomena could occur even more easily if different portions of the spacecraft which are electrically isolated charge to different potentials.

Finally, it is possible to speculate about what might happen to a spacecraft sent

to the vicinity of the planet Jupiter where there are probably large electron fluxes with energies of several MeV. On the dark side of the planet in its outer atmosphere where the density of the thermal plasma is low, it is possible that spacecraft potentials would be of the order of millions of volts.

#### REFERENCES

1. E. C. Whipple, Jr., "The Equilibrium Electric Potential of a Body in the Upper Atmosphere and in Interplanetary Space," Ph.D. Thesis, The George Washington University, 1965; also published as NASA Tech. Note X-61565-296, 1965.
2. U. Samir and A. P. Willmore, "The Distribution of Charged Particles Near a Moving Spacecraft," *Planet. Space Sci.*, **13**, 285, 1965.
3. A. V. Gurevich, *Planet. Space Sci.*, **9**, 321, 1962.
4. J. G. Laframboise, "Theory of Spherical Langmuir Probes in a Collisionless, Maxwellian Plasma at Rest," Report No. 100, Institute for Aerospace Studies, University of Toronto, 1966.
5. S. E. DeForest, "Spacecraft Charging at Synchronous Orbit," *J. Geophys. Res.*, **77**, 651, 1972.
6. L. Frank, personal communication.
7. F. Scarf, personal communication.
8. H. C. Brinton, R. A. Fickett, and H. A. Taylor, Jr., "Thermal Ion Structure of the Plasmasphere," *Planet. Space Sci.*, **16**, 899, 1968.
9. J. H. Hoffman, "Ion Mass Spectrometer on Explorer 31 Satellite," *Proc. IEEE*, **57**, No. 6, 1063, 1969.
10. R. S. Narcisi, A. D. Bailey, and L. D. Lucca, "Composition Measurements of Negative Ions in the D and Lower E Regions," *Trans. Amer. Geophys. Union*, **49**, 149, 1968.
11. L. W. Parker and E. C. Whipple, Jr., "Theory of Spacecraft Sheath Structure, Potential, and Velocity Effects on Ion Measurements by Traps and Mass Spectrometers," *J. Geophys. Res.*, **75**, 4720, 1970.

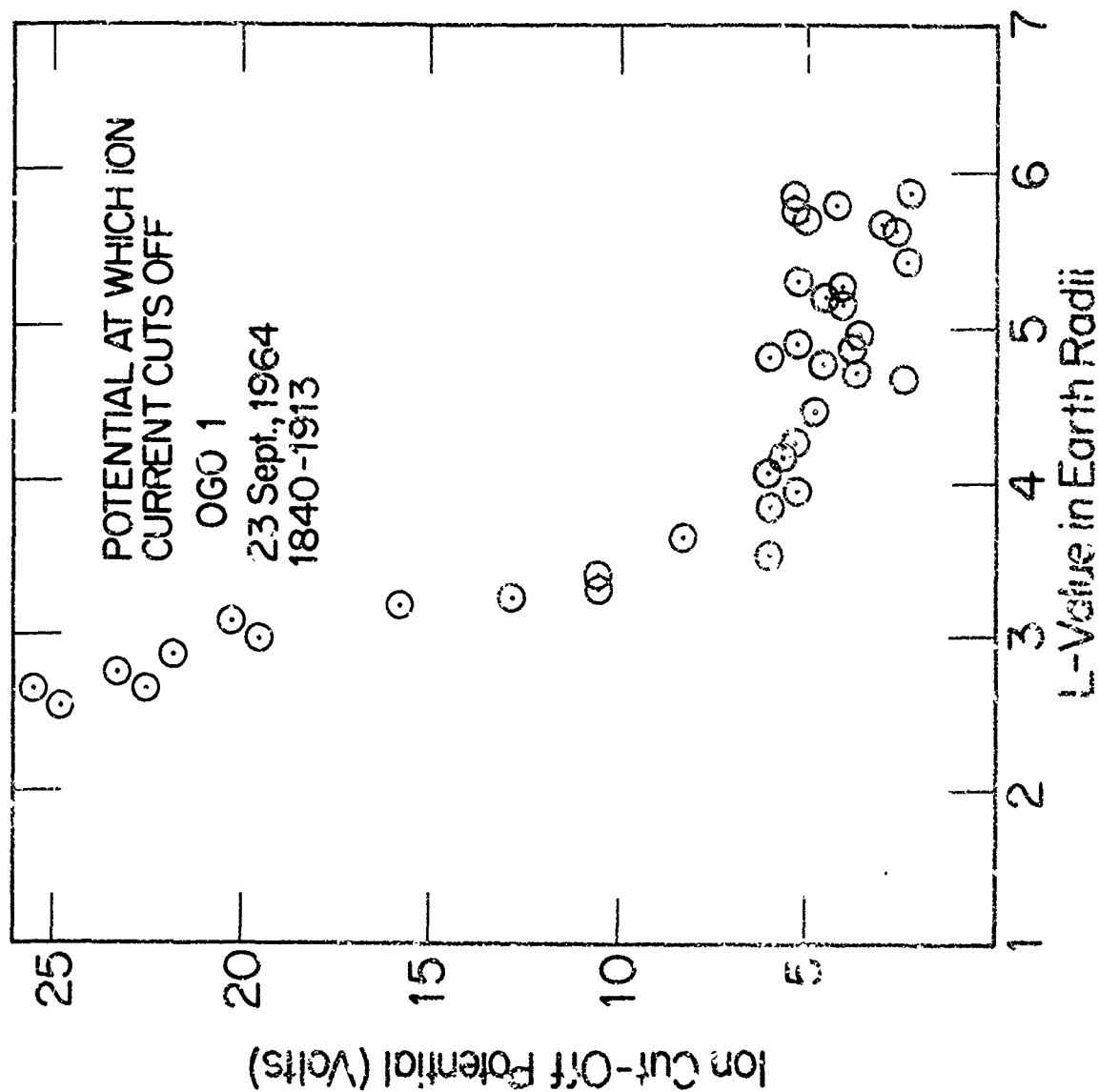


Fig. 6 - Potential at which the ion current measured by the ion trap on OGO 1 cuts off.

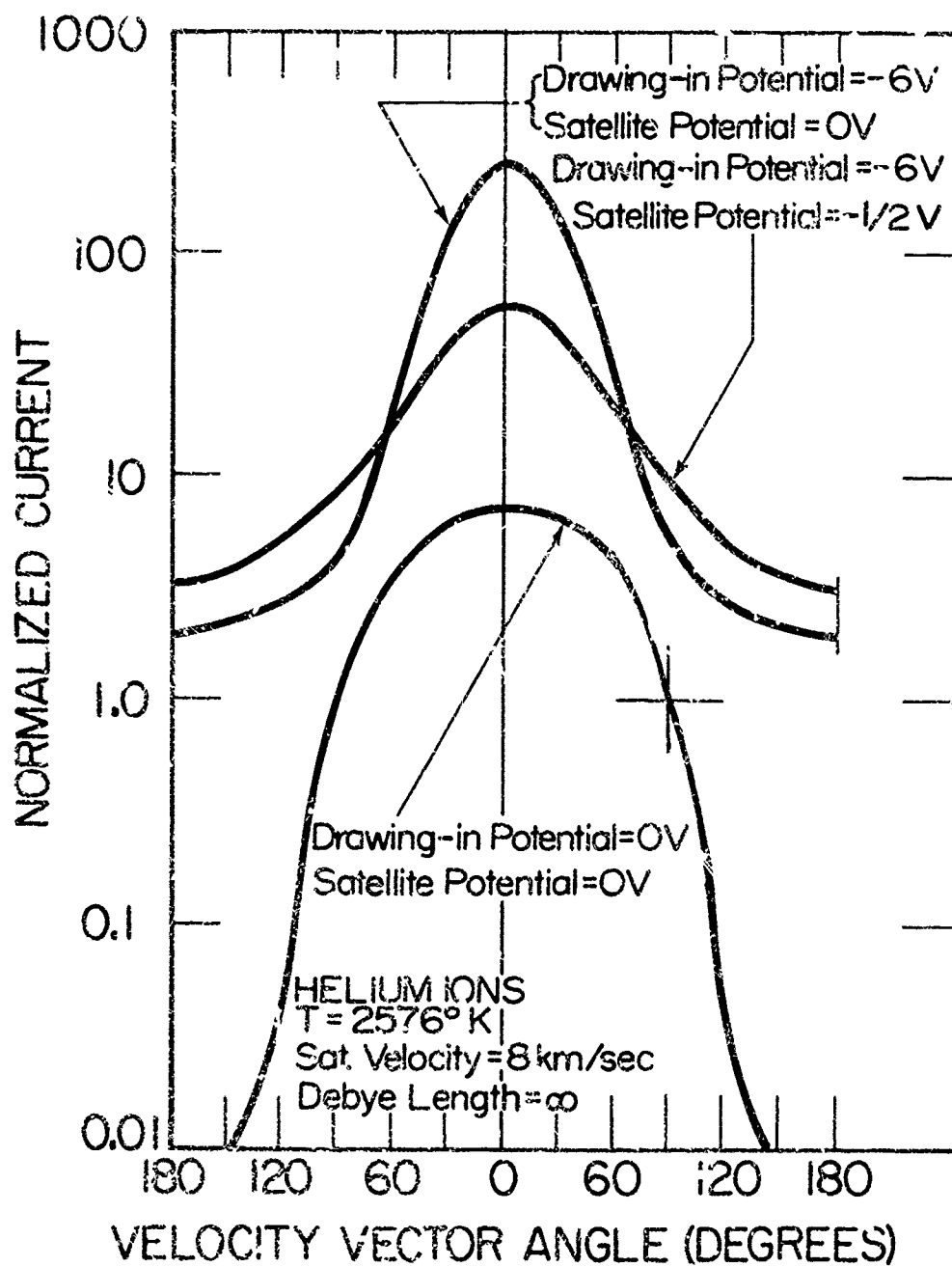


Fig. 7 - Theoretical effects of drawing-in potential and satellite potential on the helium ion current measured by a mass spectrometer on a satellite.

SESSION V

AIRCRAFT I

G.L. WEINSTOCK, CHAIRMAN & ORGANIZER

MCDONNELL DOUGLAS CORPORATION

## Session Introduction - Aircraft I

G.L. Weinstock, McDonnell Aircraft Company

This session comprises the significant phases of lightning interaction with the total aircraft vehicle. Various types of air vehicles, such as commercial, general aviation, military aircraft and helicopters are addressed. The session includes the fundamental aspects of the lightning/aircraft relationship in the papers on lightning mechanisms and lightning triggering. The session also covers attach point studies, design and application of lightning protective systems, testing programs and statistical surveys of lightning strike incidents.

A few years ago there was an aura of mystery surrounding aircraft lightning protection. Now analytic methods are being developed leading to a better understanding of the various lightning and static electricity parameters. As a result of this, certain testing methods can be shown to be more accurate than others. As an example, the use of ungrounded models for attach point testing may be more valid than the use of grounded models. Thus analytic methods provide an important complementary tool to lightning simulation testing. Using an analytic approach will not eliminate full-scale testing or even model tests. However it will provide a systematic means to reduce the amount of experimentation required in a parametric study, and to restrict and concentrate the testing to those areas expected to be most beneficial. It will also provide for better interpretation of the test data. A compilation of data describing natural lightning is now available and should be valuable in improving laboratory lightning simulation, and complete strike histories are being tabulated which can be related back to analysis, design and test methods. Thus significant progress in the solution of aircraft/lightning situations has been made since the last conference, and some of these accomplishments are presented in this session.

## Triggered Lightning and Its Application to Rockets and Aircraft

Edward T. Pierce  
Stanford Research Institute

### ABSTRACT

Man can modify the natural environment in many ways that can initiate lightning; among these are discharges triggered by high-rise buildings, by rockets, by aircraft, and so on. It is shown that almost all incidents of triggered lightning occur when the ambient field is some 10 kV/m or more, and the potential discontinuity between the conductor initiating the lightning and the adjacent atmosphere approaches a million volts. Some instances with aircraft, however, diverge from the second criterion; the importance of self-charge is considered in this respect. An assessment is made of the chances of triggered lightning occurring during operations involving aircraft and rockets.

NATURAL LIGHTNING is believed to demand two conditions for its occurrence. Firstly, there must be a generally strong electrification within a cloud, with electric fields exceeding 10 kV/m being typical. Secondly, this electrification must be substantially intensified locally by various physical processes, thus producing electric fields sufficiently large for streamer--and therefore lightning--initiation (1)\*. Both conditions appear to be necessary for lightning occurrence; the local "hot-spot" is essential for initial breakdown, while the resulting streamer can propagate and develop into a full-scale discharge only if the general ambient electric field is high.

Triggered lightning seems to obey the same criteria as ordinary lightning (2). In almost all instances of triggered lightning, natural electrification processes provide the high ambient fields, but the necessary field concentration for initiation or triggering is caused by man. Typically, the extremity of some man-made conducting object is the point at which the field concentration occurs.

It is convenient to differentiate between triggered lightning, occurring when the object is electrically connected to the ground (e.g., a high-rise building), and that taking place when the object is in free flight, isolated from the earth (e.g., aircraft and rockets).

\* Numbers in parentheses designate References at end of paper.

### TRIGGERED LIGHTNING--OBJECTS IN CONTACT WITH GROUND

Figure 1 illustrates some realized (and one possible) occurrences. Flashes initiated by high-rise buildings (Figure 1a) take place frequently, while instances of wire-carrying rocket (Figure 1c) and depth-charge (Figure 1d) triggering have occurred; examples of all three types of initiation are shown in Figure 2a, b, and c. The cargo-helicopter example (Figure 1b) has never actually been reported as occurring. However, as Solak (3) has indicated, it could quite possibly take place when a helicopter operating in a thundery environment is approaching the ground. Equipotentials are shown on Figure 1; the region of field intensification, where initial breakdown is most likely to occur, is of course at the extremity of the object where the equipotentials approach each other most closely.

It has already been suggested that two conditions--a high general ambient field and a local intensification of that field--are necessary for lightning occurrence. Estimates of the ambient field,  $E_a$ , are readily made for many instances of triggered lightning; these are based on measurements made either at the time of the incidents or under comparable conditions. A quantitative measure of the effective degree of field intensification is more difficult to define, since the morphology of the field distribution around a pointed conductor depends on the geometry of the conducting surface. However, a convenient indicator of the intensification is the voltage difference,  $V_D$ , between the ground and the unperturbed atmosphere at the height,  $H$ , of the object triggering the lightning;  $V_D$  effectively represents the voltage discontinuity between the tip of the object and the adjacent atmosphere. If the electric field is vertically directed and given by  $E_h$  at height,  $h$ , above the ground, then

$$V_D(H) = \int_0^H E_h \cdot dh$$

It is generally believed that under thundery conditions  $E_h$  will increase with height, although evidence on the amount of the increase



----- EQUIPOTENTIALS

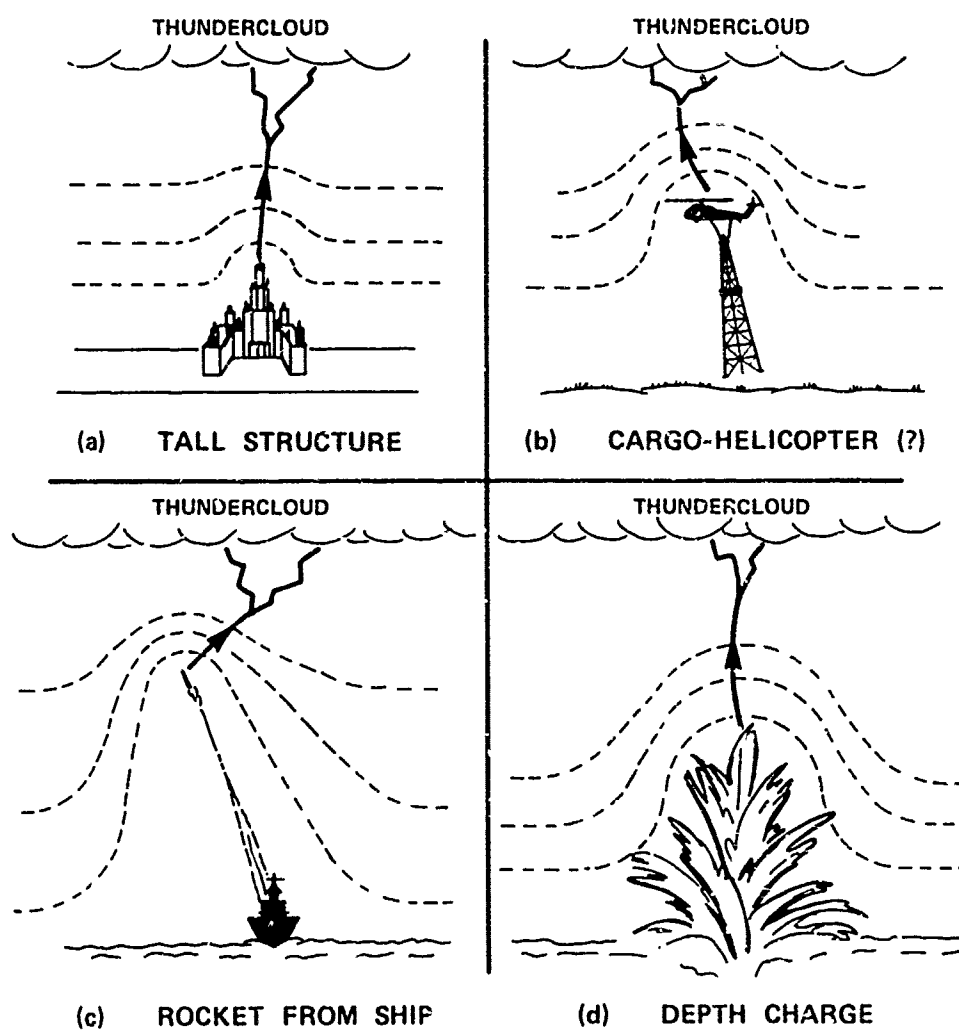
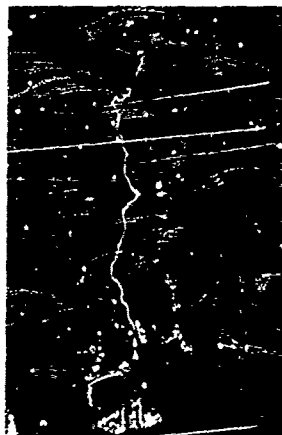
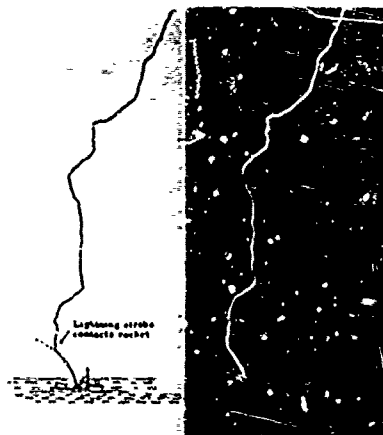


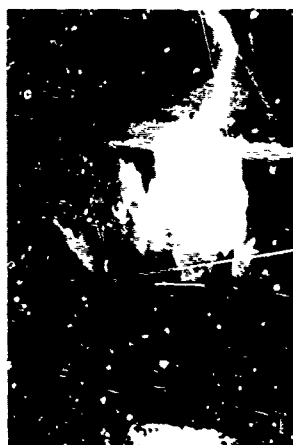
FIGURE 1 EXAMPLES (diagrammatic) OF TRIGGERED LIGHTNING



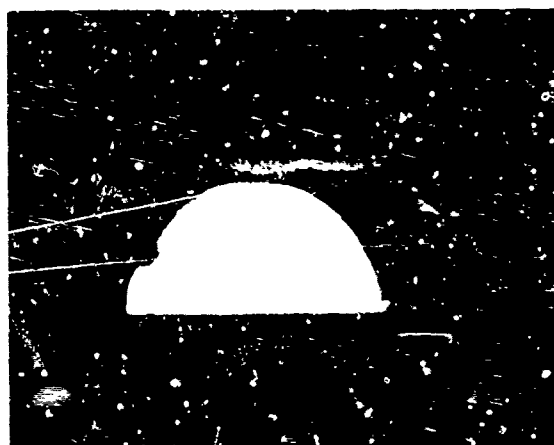
(a) TALL BUILDING



(b) ROCKET



(c) DEPTH CHARGE



(d) NUCLEAR

LA-4454-24

FIGURE 2 INSTANCES OF TRIGGERED LIGHTNING

is uncertain.

The well-instrumented experiments of Newman and his collaborators (4,5) on lightning triggering by rocket-borne wires, yield accurate estimates for  $E_a$  and  $V_D$ . For the depth-charge event (6) the height of the water-column at the time of triggering (in other words,  $H$ ) is known, and, by analogy with the rocket-borne wire incidents,  $E_a$  and  $V_D$  can be deduced. In the case of discharges initiated from tall objects, values of  $E_a$  and  $V_D$  can be derived for specific structures such as the Empire State Building (7) and the towers on Monte San Salvatore (8); in the latter case the effective height of the towers is much increased by the configuration of the mountain (2).

The statistics of discharges involving tall towers and high-rise buildings can be manipulated to give values of  $E_a$  and  $V_D$ . Figure 3 based on the available data (3), shows that triggered flashes initiated by upward leaders from tall structures do not occur for structures with heights less than about 150 m. Since the ground-level field below a thundercloud rarely exceeds 10 kV/m, it follows that the critical values of 10 kV/m and 150 m can be associated, giving  $V_D = 150 \times 10 \text{ kV} = 1.5 \text{ MV}$  (assuming no increase of field with height). It is possible to analyze the statistical data on field-magnitude distributions, and on lightning strikes to high structures, in much greater depth; such analysis enables, for example, the strike probability--whether by triggered or natural lightning--to be assessed at any time for a structure of given height located anywhere in the world (9, and unpublished work).

Figure 2d shows a very unusual incident; it is of lightning initiated from instrumentation towers following the first thermonuclear explosion in 1952. This type of triggered lightning differs from all others in that not only the local field intensification but also the general electrification is man-made, being caused by gamma rays generated in the explosion (10).

#### TRIGGERED LIGHTNING--OBJECTS IN FLIGHT

Figure 4 illustrates, in a manner similar to that of Figure 1, how lightning can be initiated by aircraft and rockets. However, the representations are probably far less realistic than those of Figure 1. Specifically the diagrams of Figure 4 assume that the objects are in electrical equilibrium with their surroundings so that there is no potential difference between the mid-planes of the aircraft (and of the rocket-exhaust combination) and the adjacent atmosphere; in other words, the object lies

on the appropriate median equipotential. It is unlikely that this equilibrium situation will ever be attained or even approached. The natural conductivity of the atmosphere is not great, so that if a conducting body is suddenly introduced it takes a substantial time before electrical equilibrium is achieved. Furthermore, the equilibrium situation varies with position and especially altitude; thus an ascending rocket or aircraft will be perpetually attempting an adjustment that is never realized. Most important of all, aircraft and rockets experience substantial and variable charging currents due to engine action and encounters with atmospheric particles; the resulting changing self-charge almost guarantees that there can never be exact electrical harmony with the surrounding atmosphere.

Estimates of the general ambient field,  $E_a$ , are available for most of the triggered lightning incidents involving aircraft and rockets. The models of Figure 4 are--admittedly--probably incorrect, but there is no obvious simple way in which these models can be made truly more realistic as regards typical conditions. If we adopt the diagrams of Figure 4, then the voltage discontinuity  $V_D$  is approximately  $1/2(E_a l)$  where  $l$  is the length of the conductor involved. If the ambient field is horizontally directed (Figure 4c) we have  $V_D \approx 1/2(E_a l_h)$  where  $l_h$  is the horizontal dimension; in the case of a vertical ambient field (Figure 4a and 4b) we have, correspondingly,  $V_D \approx 1/2(E_a l_v)$ . Note that in the case of a rocket the length is effectively extended by the conducting plume.

The best known triggered lightning incidents involving rockets are the strikes shortly after the launch of the Apollo 12 space vehicle. This launch was made into clouds that, although not active thunderclouds, were undoubtedly strongly electrified. Surface fields of a few kV/m were being experienced (5), and allowing for some field increase with height it is probable that  $E_a$  within the clouds was at least 10 kV/m. The actual length--110 m--of the vehicle is augmented electrically by perhaps some 200 m of conducting exhaust plume (2, 11), thus giving an effective electrical length of about 400 m; hence,  $V_D$  can be estimated.

Although reports of aircraft being struck by lightning are common, it cannot usually be determined whether or not the flash was triggered by the aircraft. However, there are at least two occasions of lightning (12, 13) when well-instrumented aircraft on research flight were penetrating dissipating thunderclouds that were no longer producing lightning. The only flashes that occurred during these penetrations were to the aircraft, and there seems no doubt

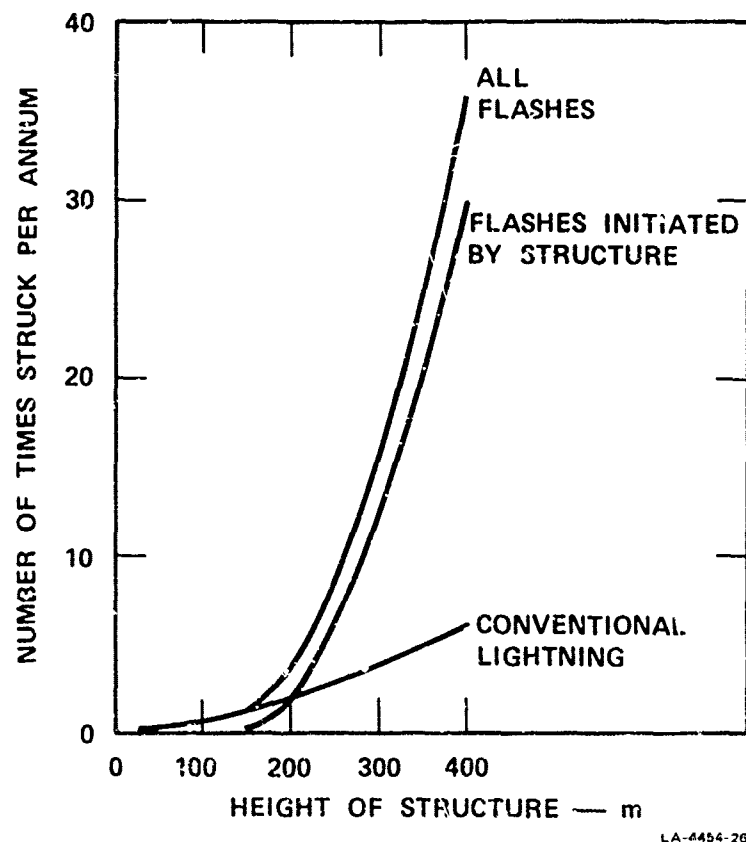


FIGURE 3 DATA ON FLASHES TO TALL STRUCTURES  
(Isoceraunic Level — 32)

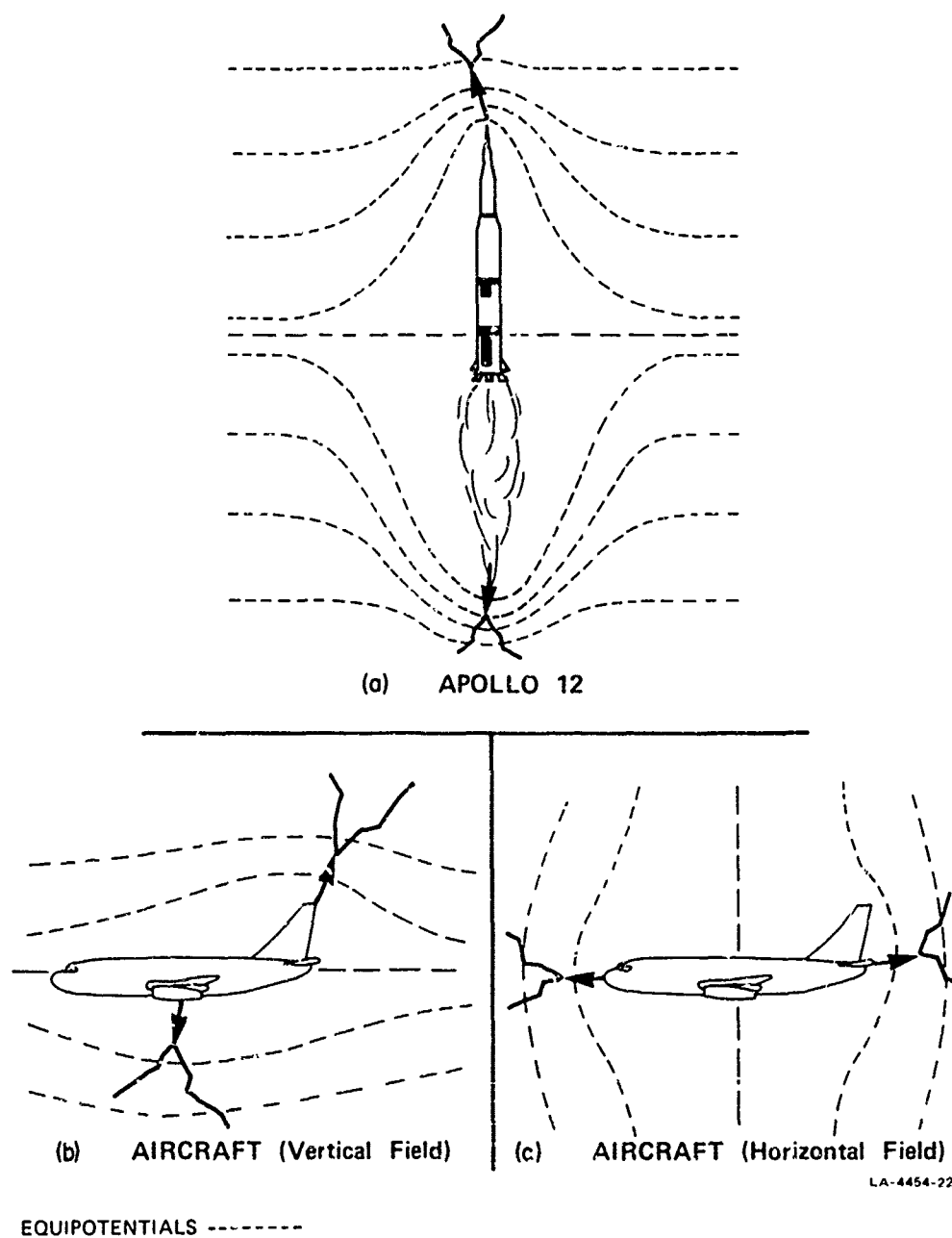


FIGURE 4 FURTHER EXAMPLES (diagrammatic) OF TRIGGERED LIGHTNING

Table 1 - Triggered Lightning Incidents

Type of Incident	Ambient Field, $E_a$ (kV/m)	Conductor Dimension --Height or Length (m)	Voltage Discontinuity, $V_D$ (MV = $10^6$ V)
Objects Connected to Ground			
• Rocket trailing wire	18	100 to 300	1.8 to 5.4
• Depth-charge incident	10 to 20 (?)	70	0.7 to 1.4
• Empire State Building	5	380	1.9
• Monte San Salvatore Tower	$\geq 3$	$\sim 270^*$	$\geq 0.8$
• Statistics of flashes to tall structures	$\geq 10$	$\sim 150$	$\geq 1.5$
• Thermonuclear explosions	$\sim 30$	$\sim 10$	$\sim 0.3$
Objects in Flight			
• Apollo 12 Rocket	$\geq 10$	$\sim 400^{**}$	$\geq 2.0$
• F-100	30 (vertical) 6 (horizontal)	6 (vertical) 15 (horizontal)	0.09 0.045 (Plus contribution due to self-charge on aircraft-- indicated as $\sim 1.9$ MV)
• DC-6	16 (vertical) 2 (horizontal)	9 (vertical) 36 (horizontal)	0.072 0.036 (Plus contribution due to self-charge on aircraft)

\* Effectively extended by shape of mountain.

\*\* With allowance for conducting exhaust.

therefore that the aircraft triggered the flashes. Both horizontal and vertical components of the ambient electric field were being measured at the time of the strikes, so that, since the dimensions of the aircraft are known,  $V_D$  can be estimated.

#### DISCUSSION

Table 1 summarizes the information on the various instances of triggered lightning discussed above. We note that for all the incidents the values of ambient field are well within an order of magnitude of 10 kV/m. The estimates of voltage discontinuity are approximately 1 MV with the exception of the aircraft incidents for which  $V_D$  is apparently only about 50 kV (0.05 MV). However, it should be recalled that the representations of Figure 4 and the analysis yielding  $V_D$  [ $V_D = 1/2(E_a l)$ ] ignore any effects due to charge on the aircraft. It is well known that when aircraft are flying under full engine power or colliding with precipitation particles in the atmosphere, the resulting charging currents soon raise the aircraft potential to a value of several hundred kilovolts with respect to the neighboring atmosphere (14). This potential difference is presumably available to supplement the voltage discontinuity  $V_D$  calculated from the ambient field alone, and thus it will facilitate the initiation of leader breakdown. It is note-

worthy that the strikes triggered by the DC-6 occurred when the aircraft was encountering a mixture of rain and graupel (13); precipitation-impact currents are notoriously large under such circumstances. For the F-100 incidents, sufficient experimental data are available for the charge on the aircraft--and therefore the supplemental potential difference--to be calculated (5, 12). Rough estimates indicate supplemental potentials approaching a million volts, and also the very significant feature of a rapid increase in aircraft charge immediately prior to the triggered strike.

If we adopt the two criteria--a general ambient field of some 10 kV/m, and a local potential discontinuity of about a megavolt ( $10^6$  V)--as being necessary and sufficient conditions for triggered lightning, we can estimate the chances of its occurrence under various circumstances. Table 2 indicates the fields existing for certain meteorological conditions. We note that general fields exceeding 10 kV/m are usually experienced only in thunderstorms and heavy showers. However, high fields can be encountered within stratiform clouds, such as nimbostratus, on rare occasions, and there are Russian reports of lightning triggered by aircraft sometimes occurring within these clouds (15).

As regards the second condition--a voltage discontinuity of about a megavolt--the discontinuity due to the ambient field,  $E_a$ , is approximately  $1/2(E_a l)$ . This increases with  $E_a$  and the

Table 2 - Electric Fields Associated with Various Meteorological Situations

Meteorological Situation	Typical Field within Cloud (kV/m)	Extreme Field within Cloud (kV/m)	Chance of Aircraft Triggering Lightning
Fair Weather	0.2		
Non-Precipitating Clouds			
• Fog	0.6		
• Stratus/Stratocumulus	0.6	2	Negligible
• Small Convective Cumuli	1.0	10	Extremely Slight
Precipitating Clouds			
• Steady Rain--Quiet Atmosphere--Nimbostratus	0.5	20	Very Slight
• Steady Rain--Unstable Atmosphere	2.0	40	Slight
• Heavy Showery Rain	10 to 20	100	Appreciable
• Steady Light Snow	0.5	?	Very Slight ?
• Heavy Snow and Snow Showers	5.0	?	Appreciable ?
• Thunderstorms	10 to 100	> 300	Substantial

dimension  $l$ . Thus the larger the aircraft or rocket the more likely it is to trigger lightning. Note also that for rockets the length is effectively extended by the conducting exhaust trail. The conductivity of the trail depends, among other factors, on the rocket fuel and the length of time the trail has been in existence; the latter factor suggests that the faster the rocket, the more probable is the occurrence of triggered lightning. However, we have noted that in the case of strikes to aircraft the necessary voltage discontinuity is probably due more to charge on the aircraft than to the ambient field and the aircraft dimension. Since aircraft--and presumably rockets--charge strongly when under full engine power or encountering precipitation particles, it follows that the critical voltage discontinuity is often approached in flights through all types of clouds, and that the more important criterion is therefore the magnitude of the general ambient field. A corollary to this argument is that techniques such as active dischargers (16) that minimize the charge carried by aircraft also reduce the likelihood of triggered lightning.

Qualitative assessments, based on the above discussion, of the chances for triggered lightning are included in the last column of Table 2.

#### ACKNOWLEDGMENT

Preparation of this paper was supported by the United States Office of Naval Research under Contract N00014-71-C-0106. Accordingly, reproduction of this paper in whole or in part is permitted for any purpose of the United States Government.

#### REFERENCES

1. G. A. Dawson and D. G. Duff, "Initiation of Cloud-Ground Lightning Strokes." *J. Geophys. Res.*, Vol 75, 1967, pp 5858-5867.
2. E. T. Pierce, "Triggered Lightning and Some Unsuspected Lightning Hazards." *Naval Research Reviews*, Vol XXV, No 3, March 1972, pp 14-28.
3. B. J. Solak, "Influence of Lightning and Static Electricity as Applied to Helicopter Design." *Proc. 1970 Lightning and Static Electricity Conf.*, Air Force Avionics Laboratory, 1970, pp 179-187.
4. M. M. Newman, J. R. Stahman, J. D. Robb, E. A. Lewis, S. G. Martin, and L. V. Zinn, "Triggered Lightning Strokes at Very Close Range." *J. Geophys. Res.*, Vol 72, 1967, pp 4761-4764.
5. D. R. Fitzgerald, "Aircraft and Rocket Triggered Natural Lightning Discharges." *Proc. 1970 Lightning and Static Electricity Conf.*, Air Force Avionics Laboratory, 1970, pp 3-9.
6. M. Brook, G. Armstrong, R. P. H. Winder, B. Vonnegut, and C. B. Moore, "Artificial Initiation of Lightning Discharges." *J. Geophys. Res.*, Vol 66, 1961, pp 3967-3969.
7. C. E. R. Bruce, "The Initiation of Long Electrical Discharges." *Proc. Roy. Soc.*, Vol 183A, 1944, pp 228-242.
8. D. Müller-Hillebrand, "The Physics of the Lightning Discharge." *Elektrotech. Z(A)*, Vol 82, 1961, pp 232-249.
9. E. T. Pierce, "Lightning Discharges to Tail Structures." *EOS*, Vol 51, No 4, April 1970, p 301.

10. M. A. Uman, D. F. Seacord, G. H. Price and E. T. Pierce, "Lightning Induced by Thermo-nuclear Detonations." J. Geophys. Res., Vol 77, 1972, pp 1591-1596.

11. M. A. Uman, "Electrical Breakdown in the Apollo 12/Saturn V First Stage Exhaust." Research Report 70-9C8-HIVCL-R1, Westinghouse Research Laboratories, Pittsburgh, 1970.

12. D. R. Fitzgerald, "Probable Aircraft 'Triggering' of Lightning in Certain Thunderstorms." Monthly Weather Review, Vol 95, 1967, pp 835-842.

13. W. E. Cobb and F. J. Holitza, "A Note on Lightning Strikes to Aircraft." Monthly Weather Review, Vol 96, 1968, pp 807-808.

14. J. E. Nanevich and R. L. Tanner, "Some Techniques for the Elimination of Corona Discharge Noise in Aircraft Antennas." Proc. IEEE, Vol 52, 1964, pp 53-59.

15. I. M. Imianitov, Y. V. Chubarina, and V. M. Shvarts, "Elektrichestvo Oblakov." Gidrometeorologicheskoye Press, Leningrad, 1971.

16. J. E. Nanevich and G. R. Hilbers, "Flight Test Evaluation of an Active Discharger System," Interim Technical Report 1 (Phase II) to Air Force Avionics Laboratory under Contract F33615-68-C-1359, SRI Project 7104, Stanford Research Institute, Menlo Park, California, February 1970.



N. Cianos and E. T. Pierce  
Stanford Research Institute

ABSTRACT

The following discussion summarizes a recent report on lightning environments as applied to engineering problems.

IN THE FIRST SESSION of this conference, the fundamental nature of lightning and instrumentation methods for measuring its characteristics have been presented (1,2)\*, and the nature of natural lightning and simulated lightning has been compared (3). Of course, lightning simulation has become an important part of testing and evaluating equipment exposed to lightning strikes. But in addition to the simulated testing, statistical and analytical methods for evaluating the hazards to equipment due to lightning are also needed. However, a consistent set of analytical and statistical models of lightning environments for engineering usage is greatly lacking even though a great amount of basic information is available in the literature and in the usual references (4,5). A recent report (6) reviews and colligates information on the physical characteristics of lightning and shows how this information can be used for engineering applications in estimating the lightning sensitivity of equipment. The purpose of this discussion is to summarize the contents of that report.

The major emphasis of the report (6) is on the ground lightning environment and includes the climatological as well as the physical parameters of lightning.

The climatological data, available in the form of thunderstorm-day statistics is important, since this information can be used to determine the lightning-flash incidence in a given area at any time of day and month of the year at any location. Expressions are derived relating the thunderstorm day statistics to the flash incidence. Also, the degree to which lightning incidence is modified by the presence of high structures is indicated. Of course, lightning incidence is a vital factor in determining the economics of avoiding lightning hazards. Elaborate protective measures are obviously far more justifiable for high-lightning-exposure areas such as Florida than they are for flat deserts where thunderstorms rarely occur. Even in low-exposure regions, however,

especially sensitive sites such as explosives factories and missile installations may require particular consideration.

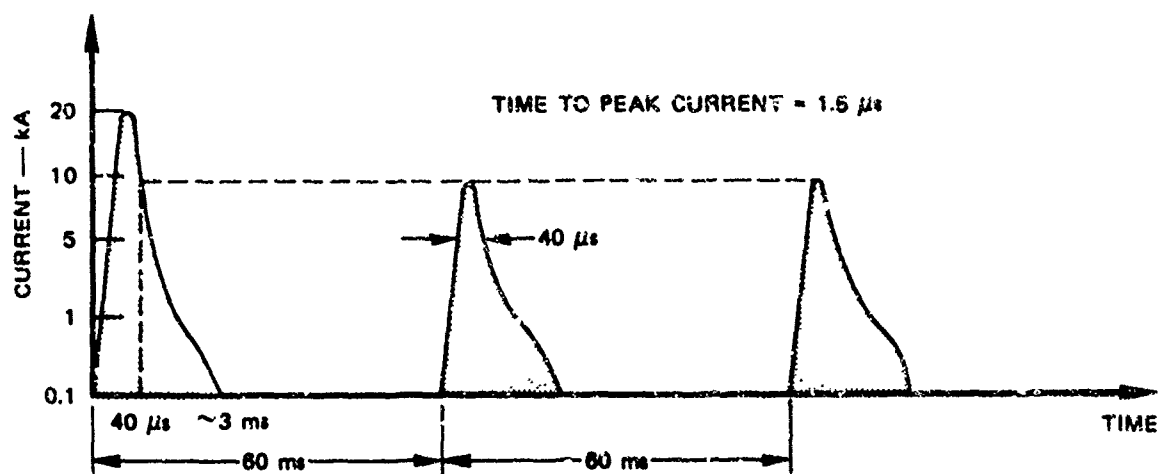
A substantial part of the report deals with the characteristics of lightning flashes to ground. Statistical distributions are given for many of the parameters likely to create problems for the engineer; median and extreme values are specified as illustrated in Table 1. With the exception of the statistics on the number of return strokes per flash, the statistics for all the parameters listed in Table 1 are modeled as log-normal distributions. The information presented is based on a critical survey of data available in the literature, and in some instances this critical process has led to a partial rejection of some previously accepted values. The degree of interconnection of the parameters is discussed; this can be a very important point in the assessment of lightning hazards.

Several models for lightning are derived and expressed in convenient analytical forms. It is emphasized that caution in the derivation process is necessary so as to obtain models that are both physically plausible and internally self-consistent. Two types of models are identified--basic models developed solely from the physical properties of lightning, and applied models modified appropriately for use with equipment, the lightning sensitivity of which is partially defined. Basic models are presented for typical and severe flashes; in the latter case the criterion of the severity for a lightning parameter is taken as approximately the two-percent point on the statistical distribution. An example of an applied model is also given. Basic models for the typical types of lightning flashes are schematically shown in Figure 1 of the report, where Figure 1(a) illustrates the case in which the flash does not contain a continuing current, and Figure 1(b) illustrates the case in which a continuing current is included.

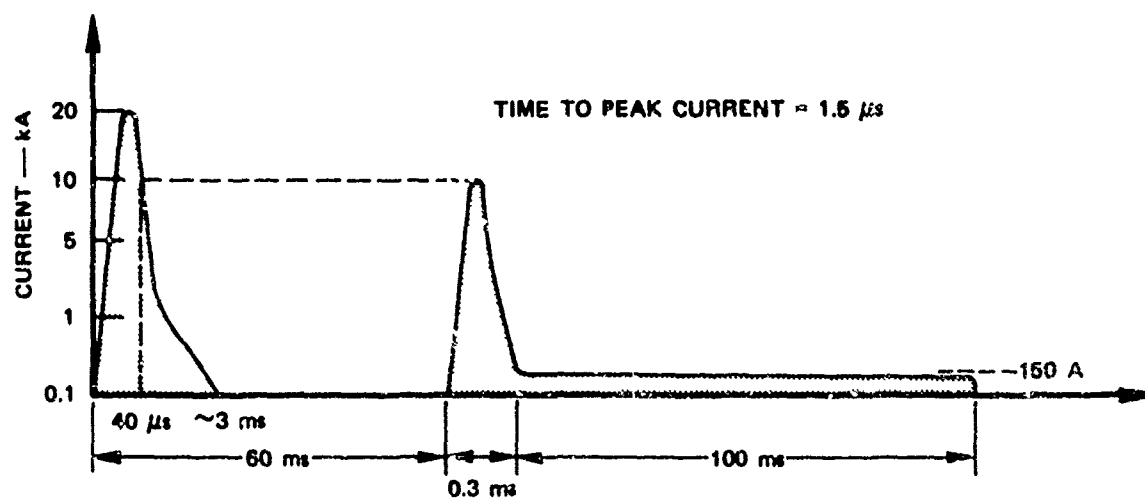
As mentioned, the main emphasis of the report (6) is on the direct effects of flashes to ground. However, discussions are also given of the physical characteristics of intracloud discharges, and of the static and electromagnetic fields generated by lightning.

In summary, this report (8) provides an extensive survey of lightning environments as

\*Numbers in parentheses designate References at end of paper.



(a) FLASH WITHOUT ANY CONTINUING CURRENT STAGES



(b) FLASH WITH FINAL STAGE CONTINUING CURRENT

FIGURE 1 TIME HISTORY OF TYPICAL (basic) LIGHTNING MODELS

applied to evaluating the lightning hazards in engineering analysis.

#### REFERENCES

1. P. Vonnegut, "Static Thunderstorms and Lightning Phenomena," presented in these proceedings.
2. M. Brook and C. Moore, "Instrumentation and Measurements Associated with Lightning Strikes," presented in these proceedings.
3. M. A. Uman, "Natural Lightning and

Simulated Lightning," presented in these proceedings.

4. M. A. Uman, Lightning. McGraw-Hill Book Co., Inc., New York, New York, 1969.
5. B. F. Schonland "The Lightning Discharge." In Handbuch der Physik, Vol 22, Springer-Verlag, OHF, Berlin, 1956, pp 567-628.
6. N. Cianos and E. T. Pierce, "A Ground-Lightning Environment for Engineering Usage," Technical Report 1, SRI Project 1834, Contract D S-2817-A3, Stanford Research Institute, Menlo Park, California, 1972.

This work supported by the McDonnell Douglas Astronautics Company under contract from the Bell Telephone Laboratories and the U.S. Army Safeguard System Command.

Table 1 - Properties of Statistical Distributions for Lightning Parameters

Parameter* \ Percentage of Occurrence	2 %	10 %	50 %	90 %	98 %
Number of return strokes	10 to 11	5 to 6	2 to 3	---	---
Duration of flash (ms)	850	480	180	68	36
Time between strokes (ms)	320	170	60	26	11
Return stroke <sup>†</sup> (kA)	140	65	20	3.2	3.1
Charge transfer per flash (C)	200	75	15	2.7	1
Time to peak current (μs)	12	5.8	1.8	0.66	0.25
Rates of current rise (kA/μs)	100	58	22	9.5	3.5
Current half value time (μs)	170	100	45	17	10.5
Duration of continuing current (ms)	400	260	160	84	58
Continuing current (A)	520	310	140	60	33
Charge in continuing current (C)	110	64	26	12	7

\* Note that not all of the parameters are independent. Some judgement must be made in using the values for consistency.

<sup>†</sup> Values for first stroke.

## Aircraft Initiation of Lightning

J.F. Shaffer

McDonnell Aircraft Company  
McDonnell Douglas Corporation  
St. Louis, Missouri

### ABSTRACT

Analytical results and lightning simulation testing show that an aircraft can trigger lightning when flying in a highly charged atmospheric environment. For such an environment, the electric field intensification of the aircraft is high enough to initiate lightning which otherwise may not have occurred naturally. It is shown that an external source of charge is required to support an aircraft initiated discharge.

The electric fields surrounding an F-4 and B-52 aircraft were determined from the electrostatic integral field equations using an algorithm which included: actual aircraft geometry; an external cloud electric field, and a net charge on the aircraft. Capacitance of the aircraft has been determined and consequently the charged vehicle potential and electrostatic field energy obtained. The algorithm has also been used to obtain the maximum net charge an F-4 and B-52 aircraft can hold before self discharge corona begins. The effect on these parameters caused by varying aircraft size is discussed.

The jet engine exhaust has been analyzed to determine if it is sufficiently conductive to extend the electrical length of the aircraft. A statistical study of lightning strikes to F-4 aircraft is presented showing the effects of geographical distribution and a nose mounted pitot mast.

### INTRODUCTION

The question "Can aircraft trigger lightning?" has long been asked. There has been much debate on whether or not an aircraft by its presence can cause a lightning strike which otherwise would not have occurred. The implication of this question is: If indeed an aircraft can trigger lightning, then what are the mechanisms involved and what can be done to reduce the effect.

There are several positive indications that a conducting body in an electrified environment can initiate lightning. Fitzgerald<sup>(1)</sup> in the Rough Rider Program has presented evidence that the presence of an aircraft can trigger a lightning strike which otherwise would not have occurred. Kasmir<sup>(2)</sup> and Newman<sup>(3)</sup> have tried with various degrees of success to initiate lightning by firing rockets into charged clouds. However, some of these rocket experiments<sup>(3)</sup> had a grounded trailing wire behind the rocket. Since charge could then flow from ground to the vehicle, the basic electrostatic field phenomenon is different from that of an aircraft which is isolated from ground. Thus, some careful distinctions need to be made in applying the results of a particular experiment to that of an aircraft. In addition, there have been laboratory experiments<sup>(4)</sup> where high

voltage breakdown has been initiated by a water drop falling into a high electric field region near the high voltage electrode.

In each of these experiments, it is the electric field disturbance surrounding the vehicle which is thought to initiate or trigger the breakdown. The electric fields surrounding a metallic object are altered since the electrode must be a constant potential surface with no tangential component of field at the electrode surface. The fields adjacent to the electrode are changed from the magnitude of the field far from the electrode. Intensification of the electric field is of interest since the higher field can initiate a discharge which might not otherwise have occurred naturally.

Pierce<sup>(5)</sup> has surveyed instances of lightning initiated by man's activities and has concluded that for lightning incidents, the usual values of ambient electric fields are on the order of 10 kV/m and the voltage discontinuity between the object initiating lightning and adjacent atmosphere is about  $10^6$  V. Basic electrostatic theory indicates that the amount of energy that an electric charge (and hence a streamer) can acquire in moving from one location to another is proportional to the potential difference between two points. If these points are some distance away from a field disturbing object where the potential remains unchanged, then a streamer or lightning stroke which passes through the electrode does not gain additional energy because of the presence of the object. Thus, the presence of an aircraft can at most only divert the lightning path and does not add significantly to the path length.

On a physical basis, the following questions concerning possible aircraft initiation of lightning need to be answered: 1) Are the electric fields surrounding the vehicle high enough to initiate breakdown?, 2) Can the vehicle sustain a streamer once initiated?, 3) What is the effect of a net charge on the electric fields in the neighborhood of the vehicle?, and 4) What is the effect of possible ionization in the jet engine exhaust?

An answer to these questions is presented in this paper. The following topics will be discussed: 1) a statistical survey of lightning strikes to F-4 aircraft; 2) breakdown criteria for streamer formation, 3) electrostatic field analysis including effects of net charge on vehicle; 4) jet engine exhaust study, and 5) laboratory high voltage experiments.

### STATISTICAL SUMMARY

To provide a background from which to study aircraft initiation of lightning, a statistical analysis of lightning strikes to F-4 Phantom aircraft is presented. Since the

Supported by Air Force Avionics Laboratories Contract F33615-71-C-1581.

F-4's have a large number of flight hours, and some F-4 models have a nose pitot mast while others do not, a statistical summary provides relevant comparisons.

The study involved RF-4C and F-4E (both with nose pitot mast) and F-4C and F-4D (without pitot mast) models of the Phantom aircraft. A five year time period from April 1967 to April 1972 was investigated for which there were 56 strikes from which to form a data base. The strike data were taken from official Air Force Lightning Reports.

The percent of lightning strikes as a function of the time of year is presented in Fig. 1. Since most of the strike data were for the Northern Hemisphere, the data indicate that the frequency of strikes correlates with spring and summer thunder storm activity.

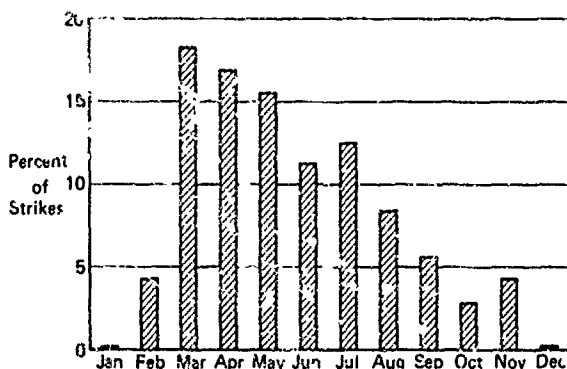


Figure 1 - Lightning strikes to F-4 aircraft as a function of time of year

The percentage of strikes as a function of altitude is presented in Fig. 2. The data show that aircraft flying at lower altitudes are more susceptible to lightning strikes.

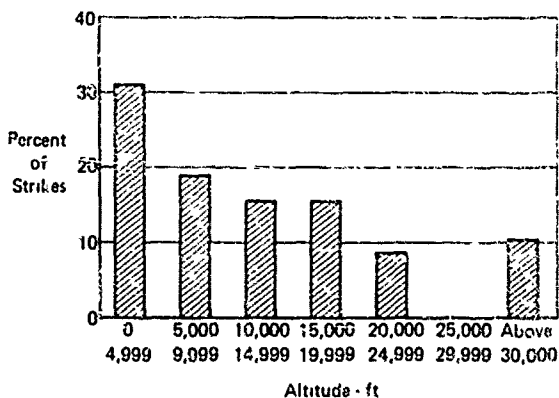


Figure 2 - Lightning strikes to F-4 aircraft as a function of altitude

The rate of lightning strikes (number of strikes per one hundred thousand flight hours) for the various models of F-4's as a function of geography is presented in Fig. 3. The data indicate that Europe has a much higher rate of strikes, which may be attributable to a greater number of days of inclement weather and/or to geographical restrictions in flight corridors. The aircraft with nose mounted pitot masts, the RF-4C and F-4E, show much

higher rates of strikes. This phenomenon may be caused by the fact (shown later) that the electric field intensification factors are greater for the nose pitot mast than for any other extremities of the aircraft.

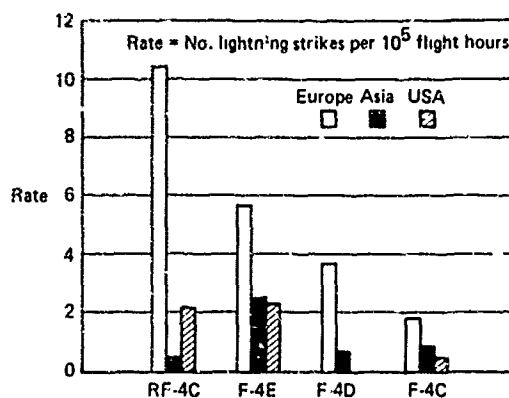


Figure 3 - Rates of lightning strikes to F-4's

#### BREAKDOWN CRITERIA

The physical mechanism for the initiation and propagation of lightning should be discussed so that possible aircraft initiation of lightning can be explored. Breakdown at atmospheric pressures over distances greater than 1 cm takes place by way of streamer development. The streamers form weakly ionized channels which traverse a path between two sources of charge forming a path for a bright discharge or return stroke. Streamers which do not cross the discharge gap do not cause breakdown and are generally then called corona.

Streamers develop or are "initiated" from a Townsend avalanche process which relates to the build-up of a space charge in an applied external electric field. When the space charge density passes a critical level, so that the space charge field approaches that of the external field, a new mechanism for charge propagation occurs - the streamer<sup>(6)</sup>. The streamer forms when the local photoionization-formed charge adjacent to an avalanche enhances its development. The conditions under which this process begins define streamer initiation. Meeke and Craggs<sup>(7)</sup> give the requirement as approximately  $10^8$  charged particles in an avalanche head for transition to a streamer. This is translated to a requirement on the ratio of field strength to pressure,  $E/P$ , and the distance,  $X_c$ , over which an avalanche is converted to a streamer. The ratio  $E/P$  is related to the first Townsend ionization coefficient,  $\alpha$ , by means of Fig. 4. The conditions for transition to a streamer are <sup>(7)</sup>:

$$\int_0^{X_c} \alpha \left( \frac{E}{P} \right) dx \sim 20. \quad (i)$$

Since  $X_c$  is generally limited to several centimeters, the initiation condition requires the ionization coefficient,  $\alpha$ , to have an appreciable value (approximately 5 to 10) over the distance  $X_c$ . It is noted from Fig. 4 that

a small relative change in the electric field  $E$  results in a large variation on  $\alpha$ . For  $\alpha$  to have a value in the range of 5 to 10, field strengths of 27 to 30 kV/cm are required. Once a streamer has formed, the electric field required for continued propagation is much smaller.

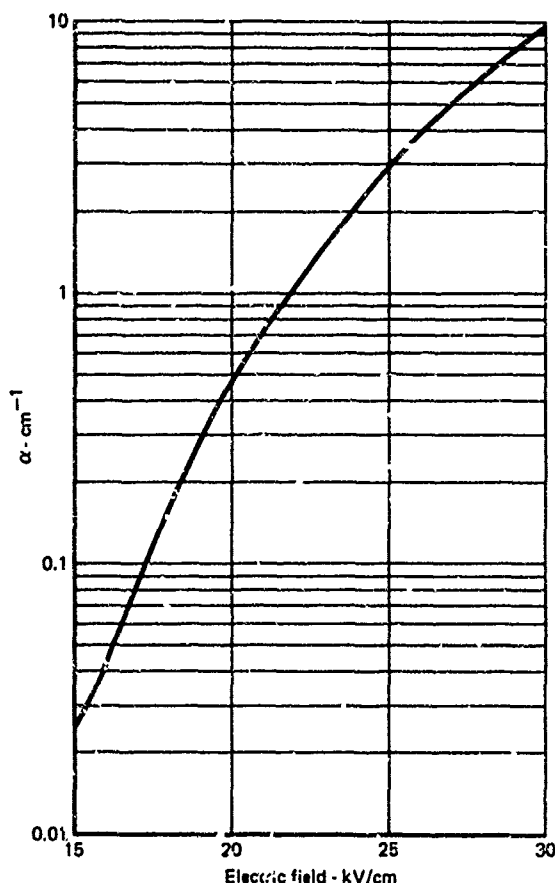


Figure 4 - First Townsend coefficient for electron multiplication vs electric field strength ( $P = 760$  Torr)

Phelps<sup>(4)</sup> has shown in laboratory experiments that an ambient field of 7 kV/cm is enough for continued streamer propagation. Streamers require energy to propagate<sup>(8)</sup> which may be gained from the ambient field. However, streamers can propagate in zero field regions if they gained sufficient initial energy<sup>(8)</sup>.

#### ELECTRIC FIELD ANALYSIS

The introduction of a metallic object into an external electric field, such as is found in an electrified cloud environment, disturbs and intensifies the field.<sup>(9)</sup> Also, net charge on an aircraft results in an electric field surrounding the vehicle. It is the purpose of the electrostatic field analysis to determine these fields so that they can be related to streamer initiation. The analysis will also determine the aircraft capacitance so that for a given vehicle charge, the resulting potential and electrostatic field energy can be found.

The electrostatic integral field equations for potential

and electric field are solved for actual aircraft geometry using the "method of moments"<sup>(10)</sup> with point matching. The surface charge distribution of the aircraft, approximated by a set of point charges, is obtained.

The potential and electric field at any point in space caused by a charge distribution  $\rho(\vec{r})$  is given by:

$$V(\vec{r}) = \frac{1}{4\pi\epsilon_0} \int \frac{\rho(\vec{r}')}{|\vec{r} - \vec{r}'|} d^3\vec{r}' + V_{\text{ext}}; \quad (2)$$

$$\vec{E}(\vec{r}) = \frac{1}{4\pi\epsilon_0} \int \rho(\vec{r}') \frac{(\vec{r} - \vec{r}')}{|\vec{r} - \vec{r}'|^3} d^3\vec{r}' + \vec{E}_{\text{ext}}; \quad (3)$$

where the principle of superposition has been used to incorporate the external applied electric field,  $E_{\text{ext}}$ , and its associated electric potential,  $V_{\text{ext}}$ .

The unknown is the charge distribution,  $\rho(\vec{r})$ , on the electrodes. The method of moments approximates  $\rho(\vec{r})$  by a set of  $N$  discrete point charges resulting in the following expressions:

$$V(\vec{r}) = \frac{1}{4\pi\epsilon_0} \sum_{i=1}^N \frac{q_i}{|\vec{r} - \vec{r}_i|} + V_{\text{ext}}; \quad (4)$$

$$\vec{E}(\vec{r}) = \frac{1}{4\pi\epsilon_0} \sum_{i=1}^N q_i \frac{(\vec{r} - \vec{r}_i)}{|\vec{r} - \vec{r}_i|^3} + \vec{E}_{\text{ext}}; \quad (5)$$

This set of equations forms the basis from which the potential and electric field are determined once the discrete charges,  $q_i$ , are known. The determination of  $q_i$  and the potential on the electrodes which are described by a net charge results in a set of simultaneous equations which are solved on a computer. Up to 200 charges have been used to represent the aircraft (resulting in 200 simultaneous equations).

The McDonnell electrostatic analysis algorithm has the following general features: electric field and potential determined anywhere in space caused by any number of arbitrarily shaped electrodes; each electrode (object) can be described by either its potential or net charge, the solution then obtaining the other unknown parameter; external electric field of any orientation may be inputted; charge distribution on electrode obtained; and capacitance relationships obtained.

An electrostatic analysis has been performed for F-4 and B-52 aircraft. A comparison of the results from these two aircraft will also allow a determination of the effect of vehicle size. The electric field  $E_T$  (scalar magnitude) is presented in units of the external applied field  $E_{\infty}$ . This parameter,  $E_T/E_{\infty}$ , is defined as the field intensification factor.

The intensification factors are a maximum at the aircraft surface and then fall-off with distance from the vehicle. Several representative values at the surface of an F-4 (for the appropriate orientation of the external field) are illustrated in Fig. 5. The nose pitot mast has the highest intensification, and the fuselage back has a low value. The magnitudes of these field intensification factors correlate very well with the usual lightning attachment points.

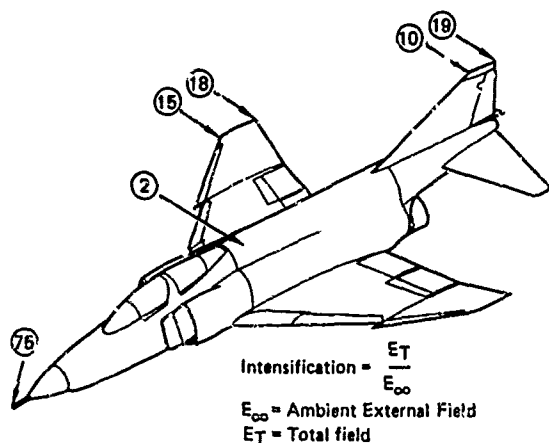


Figure 5 - Electric field intensification at the surface for selected locations

The intensification factors as a function of distance from the aircraft are shown in Fig. 6 for F-4 pitot mast, and Figs. 7 and 8 for the wing tips of the F-4 and B-52. The maximum values of intensification are relatively the same; however, the rate of fall of the fields is vastly different. The larger B-52 has a greater range of electrical influence than does the smaller F-4. A net charge on the vehicle has the effect of increasing the electric fields and extending the electrical region of influence of the aircraft.

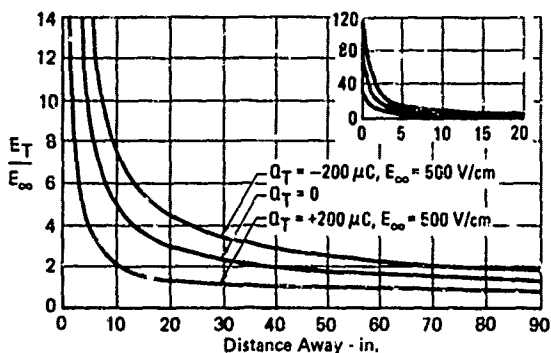


Figure 6 - F-4 pitot boom electric field intensification (Horizontal nose-tail field)

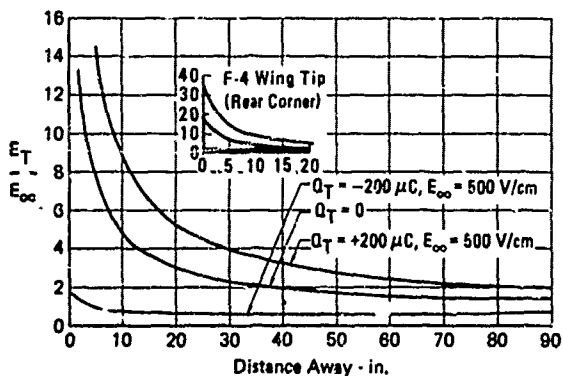


Figure 7 - F-4 wing tip electric field intensification (Horizontal wing tip-wing tip field)

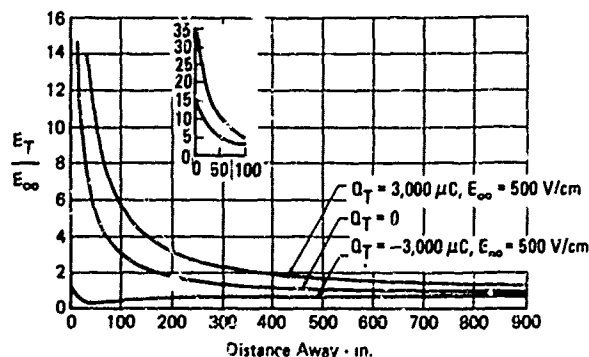


Figure 8 - B-52 wing tip electric field intensification (wing tip - wing tip field)

The values chosen for the vertical and horizontal electric fields, 4000 V/cm and 500 V/cm, respectively, represent the maximum measured in an electrified cloud environment<sup>(11)</sup>.

The net charges of 200  $\mu\text{C}$  for the F-4 and 3000  $\mu\text{C}$  for the B-52 represent the estimated maximum charge these vehicles can hold before the electric fields at the aircraft extremities and sharp points become high enough for charge loss mechanisms (corona) to occur. For example, a net charge of 200  $\mu\text{C}$  on the F-4 results in a field of 20 kV/cm at the pitot mast. Refer to the insert on Fig. 9.

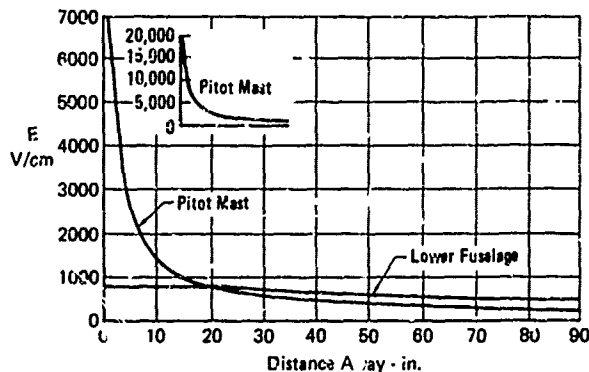


Figure 9 - Electric field from charged F-4 (No external field, net charge  $Q_T = +200 \mu\text{C}$ )

The electrical size or region of electrical influence is shown in Figs. 10 and 11 for the F-4 and B-52 in an external vertical field. The contour shown is for an intensification factor of 1.1, that is, where the external field has been intensified by 10%. In each case the contour extends approximately one body diameter from the aircraft. The electrical size is thus seen to be proportional to the physical size of the aircraft.

Aircraft capacitance, and potential and electrostatic field energy, for the estimated maximum vehicle net charge are shown in Table 1. Since the aircraft capacitance is very small, it does not take much charge to raise the vehicle potential to a very significant level. Three thousand micro-coulombs, which is the charge transferred by a current of 3 mA in 1 sec, raises the B-52

potential to several million volts. The net electrostatic energy for a B-52 with a net charge of 3000  $\mu\text{C}$ , is 3400 J which is the energy consumed by a 100 W light bulb in 34 sec.

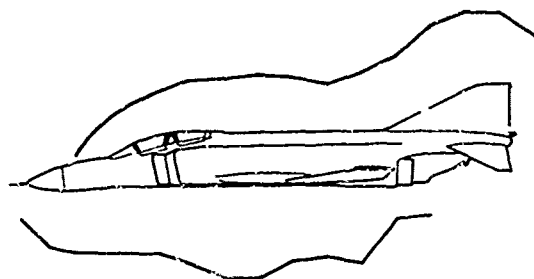


Figure 10 - F-4 electrical size  
(F-4 electric field intensification contour for  $E_T/E_\infty = 1.1$ , vertical field,  $Q_T = 0$ )

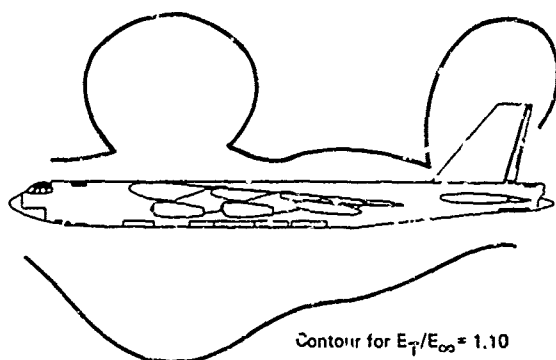


Figure 11 - B-52 electrical size  
(Vertical field,  $Q_T = 0$ )

Table 1  
Aircraft electrical parameters

	B-52	F-4
Capacitance	1310 pF	420 pF
Estimated Maximum Net Charge	3000 $\mu\text{C}$	200 $\mu\text{C}$
Vehicle Potential	$2.3 \times 10^6 \text{ V}$	$4.7 \times 10^5 \text{ V}$
Electrostatic Energy	3400 J	47 J

The net energy in the electrostatic field attributable to a charge on the vehicle is proportional to  $Q_T^2$ . This follows from the basic energy relationship  $E = 1/2 QV$ , along with the capacitance relationship  $Q = CV$ , so that

$$E = \frac{1}{2} \frac{Q^2}{C}$$

If an aircraft size can be characterized by a linear dimension  $L$ , then the following approximate relationships hold:

Aircraft Capacitance  $\sim L$   
Maximum Net Charge  $\sim L^2$  (surface area)  
Potential (at Max Charge)  $\sim L$   
Energy (at Max Charge)  $\sim L^3$  (Volume)

Capacitance proportional to vehicle length can be seen from Table 1 where the ratio of B-52 to F-4 capacitance is approximately the same ratio as their respective lengths, 3:1. This compares analytically to the capacitance of a spherical object which is proportional to its characteristic length, the radius. The maximum net charge is proportional to vehicle surface area since the factor controlling the charge loss mechanism is the vehicle surface electric fields, and these are proportional to surface charge density (assuming comparable local geometry).

The maximum vehicle potential and electrostatic energy, proportional, respectively, to characteristic length  $L$  and  $L^3$ , follows from basic electrostatics.

$$V = Q/C \sim L^2/L = L; E = \frac{1}{2} QV \sim L^2 \cdot L = L^3$$

It should be emphasized that these relationships are for gross comparisons only. More accurate results should be obtained from an exact analysis.

#### AIRCRAFT ELECTROSTATIC FIELD ANALYSIS SUMMARY

The field intensification factors, while high at the surface of the aircraft extremities (75 at the pitot mast, refer to the insert on Fig. 5) fall off rapidly as a function of distance from the vehicle. Large and small aircraft have relatively the same maximum values of field intensification since this is determined mostly by local geometry. The rate of fall-off, however, is inversely proportional to vehicle size, so that the region of electrical influence is proportional to vehicle size.

The effect of a net charge on a vehicle is to increase the electric fields surrounding the vehicle. The region of electrical influence is also extended. The electrostatic field energy is proportional to the net charge squared,  $Q_T^2$ . The electric fields around an aircraft at maximum charge are high enough to initiate streamers - which in turn, provide the charge loss mechanism to prevent infinite buildup of charge.

The electric field intensification factors are high enough and extend far enough to initiate streamers when the aircraft is flying in an external electric field of the magnitudes that have been measured. For example, the field at the pitot mast when the aircraft is in an external field of 500 V/cm is  $15 \times 37.5 \text{ kV/cm}$  - more than enough field strength to initiate breakdown at atmospheric pressure.

The amount of charge the aircraft can supply an initiated streamer, however, is extremely limited, 200  $\mu\text{C}$  for the F-4 and 3000  $\mu\text{C}$  for the B-52. This is the maximum amount that a charged aircraft or even an uncharged aircraft can contribute to a developing streamer. For an uncharged aircraft causing a streamer, the vehicle will become charged, the polarity such as to reduce the electric field at the extremity initiating the streamer. The charge which can be transferred is then just the maximum charge the vehicle can hold. Thus



larger aircraft can support more "streaming", however slight, than a smaller aircraft since the maximum charge is proportional to surface area.

Therefore, the fields at the aircraft extremities are high enough to initiate streamers and an aircraft can initiate lightning when flying in highly charged atmospheric conditions where there is an external source of charge.

## JET ENGINE EXHAUST

The ions and electrons found in a jet engine exhaust have a possibility of providing a conductive path extending behind the aircraft. Ions and electrons in the exhaust are formed in the combustion chamber as a result of chemical reactions taking place between the compressed intake air and jet fuel - see Fig. 12. The regions for various thermodynamic assumptions - equilibrium and partial nonequilibrium thermochemistry in the combustion chamber, and equilibrium and frozen expansion flow - are also illustrated in Fig. 12.

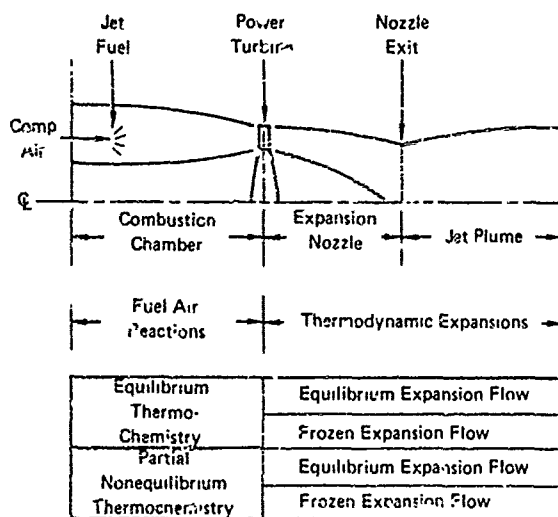


Figure 12 - Aerothermochemical analysis of jet engine exhaust

Typical engine operating conditions (non-afterburning) for modern high performance aircraft were chosen for the analysis<sup>(12)</sup>. The combustion temperature was determined by using the minimum heating value of JP-4 fuel, neglecting the heat loss to the wall, and taking into account a boundary layer temperature profile. The resulting thermodynamic conditions in the combustion chamber were: pressure ~ 4.5 atm, temperature ~ 850 to 2000K, air fuel ratio 31.25 to 125, and JP-4 fuel with a net minimum heating value of 42,900 J/g.

The important chemical elements of JP-4 fuel are the hydrocarbons (paraffins, aromatics, and olefins) and the impurities of sulfur and alkaline metals. A model of 38 selected species was used to calculate the chemical composition in the combustion chamber at elevated temperatures. These species represented the principal

chemical contributions from the jet fuel, air, and the combustion products.

The equilibrium composition was calculated according to the minimum free energy method<sup>(13)</sup>. This method seeks the solution to a set of simultaneous equations in which temperature and pressure are the independent variables and the concentration of each specie is the dependent variable.

A typical result for major ion and electron concentrations is shown in Fig. 13. Table 2 summarizes the electron concentration in the combustion chamber calculated for various thermodynamic situations.

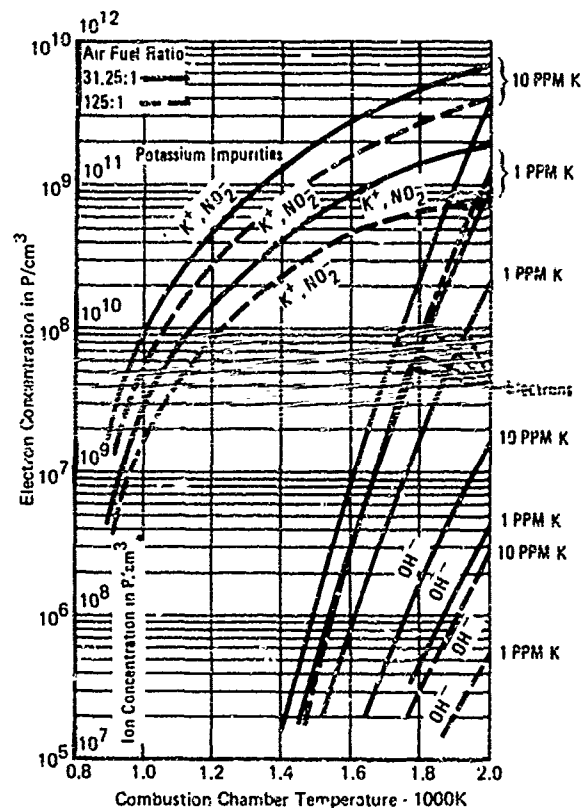


Figure 13 - Equilibrium composition for combustion chamber at 4.55 atm

Table 2 - Electron analysis from combustion chamber to jet exhaust  
(Electron concentration ( $N_e$ ) in combustion chamber)

Air Fuel Ratio	Combustion Temperature	Alkaline Impurities	$N_e$ (P/cm <sup>3</sup> )	Thermodynamic Condition
125	1054K	10 PPM K	$4.5 \times 10^{-1}$	Equilibrium Condition Exists
		1 PPM K	$1.4 \times 10^{-1}$	
31.25	2000K	10 PPM K	$4.2 \times 10^{-9}$	Equilibrium Condition Exists
		1 PPM K	$1.05 \times 10^{-9}$	
125	1054K	10 and 1 PPM K	$3 \times 10^{-9}$	Partial Equilibrium Condition Exists
31.25	2000K	10 and 1 PPM K	$1.65 \times 10^{-15}$	Equilibrium Condition Exists

The region of interest, however, is the exhaust plume downstream from the combustion chamber. The hot gases undergo expansion in the expansion nozzle and plume. The thermodynamics of the expansion flow vary between complete equilibrium and frozen flow. For equilibrium, the chemical composition readjusts itself completely to flow temperature and pressure, while for frozen flow composition, no chemical reactions take place. These two expansions represent the two extreme cases for the resulting values of concentrations.

The electron concentration in the exhaust plume for various alkaline metal impurity levels and flow assumptions is shown in Table 3. The results bracket well the measured values of ion density and inferred electron densities<sup>(14)</sup>.

Table 3 - Electron concentration in jet exhaust

Electron Concentrations (P/cm <sup>3</sup> )		Remarks	Alkaline Impurities
Combustion Chamber	Exhaust Plume		
$4.2 \times 10^6$	$1.9 \times 10^5$	Equilibrium Flow	10 PPM K
	$8.2 \times 10^5$	Frozen Flow	
$1.05 \times 10^9$	$6 \times 10^{-1}$	Equilibrium Flow	1 PPM K
	$2 \times 10^8$	Frozen Flow	
$3 \times 10^9$	$5 \times 10^{-3}$	Equilibrium Flow	10 and 1 PPM K
	$5.9 \times 10^8$	Frozen Flow	
$1.65 \times 10^{15}$	$3.3 \times 10^8$	Equilibrium Flow	10 and 1 PPM K
	$3.2 \times 10^{14}$	Frozen Flow	

The following summarizes the results of the jet engine exhaust aerothermochemical study. The electron number density is much smaller than the ion density (Fig. 13). The electron density is critically dependent upon alkaline impurity levels in the fuel, combustion temperature, and the assumed thermodynamic conditions.

A comparison of electron concentrations for various situations is presented in Table 4. The electron concentration in the jet exhaust is small compared with that in a lightning streamer head, a rocket exhaust and a metal.

Table 4 - A comparison of electron concentration values

Electron Concentration in	Quantity	Notes
Free Atmosphere	$10^{-10} \text{ P/cm}^3$	
Jet Exhaust at 1 Nozzle Diameter Down the Nozzle Exit Plane	$10^{-3} - 10^9 \text{ P/cm}^3$	Calculated Values in This Investigation
	$10^3 - 10^6 \text{ P/cm}^3$	Inferred from Ion Density Measurement
Lightning Streamer Head	$10^{12} \text{ P/cm}^3$	Ref. 6
Rocket Exhaust	$10^{12} \text{ P/cm}^3$	
Typical Metal	$10^{22} \text{ P/cm}^3$	

Thus, the jet exhaust plume is not very conductive and does not represent a significant electrical extension of the aircraft.

Even though there is a small amount of free charge (ions and electrons) in the jet exhaust, there are no high fields associated with this region of the aircraft. The charge in the exhaust plume, since it is diffuse in distribution and has no sharp geometrical shapes, does not intensify external electric fields. The high fields required for streamer initiation are not present.

Since the exhaust plume is not very conductive, and is not a region of high fields, it is not a significant factor for lightning initiation.

## LABORATORY LIGHTNING MECHANISMS TEST

Laboratory high voltage tests were performed in the McDonnell Lightning Simulation Laboratory to investigate various breakdown mechanisms. An object was placed in the high voltage discharge gap and the change in the "just fire" breakdown voltage noted. The results were normalized to the unperturbed breakdown potential and given as a percent reduction:

$$\% = \frac{V_0 - V}{V_0} \times 100 \quad (6)$$

where  $V$  and  $V_0$  are the "just fire" breakdown voltages with and without an object present in the gap respectively.

With a sphere as the test object, several possible factors that might influence breakdown could be isolated and examined on an individual basis.

The following parameters which could influence or initiate breakdown were tested: type of breakdown streamer (polarity of high voltage electrode); position of object in gap; relative size of object; net charge on object; increased local field intensification (sharp point); local adjacent ionization (polonium radioactive strip); and uniform/nonuniform electric field distribution (disk-to-disk and point-to-disk electrodes).

Figure 14 is a picture of the disk-to-disk electrode test set up. The disks were 24 in. diam with a 13 in. vertical spacing, the lower grounded disk being 31 in. above the floor (ground image plane).

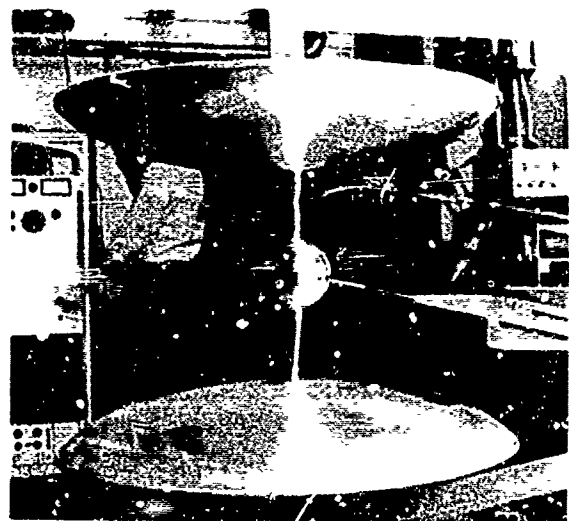


Figure 14 - Experimental test setup

The electric field distribution on the axis between the disk electrodes was calculated with the McDonnell electrostatic analysis algorithm described previously and the results are shown in Fig. 15. With no sphere in the gap, the field at the high voltage electrode is higher than that at the grounded electrode because of ground plane image effects. With a sphere the electric field adjacent to it is much higher than at the electrodes. Thus the sphere has produced a very significant disturbance in the field distribution.

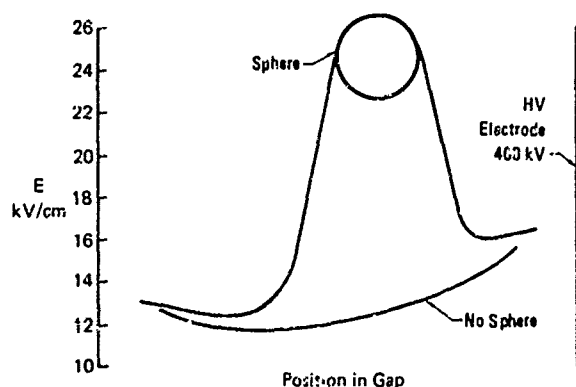


Figure 15 - Disk electrodes centerline electric field

The percent reduction in the "just fire" voltage attributable to a 4 in. diam sphere at various locations between the disk electrodes was measured. The results are shown in Fig. 16 for positive and negative high voltage output polarities. Two very significant effects are seen.

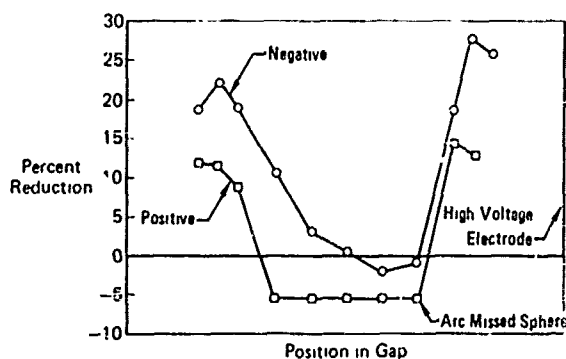


Figure 16 - Percent reduction of "just fire" voltage due to 4 in. sphere in 13 in. gap

When the sphere is in the vicinity of either the high voltage or ground electrode, an appreciable reduction in the voltage required for breakdown occurs. This reduction takes place only when the intensified fields about the sphere augment the electric fields at the electrodes. Since breakdown occurs for a given field strength independent of the presence of the sphere, the disk electrode field augmented by the sphere results in breakdown at a lower voltage. The reduction in

the "just fire" breakdown voltage occurs only when the intensified fields about the sphere interact with an external source of charge on the electrode.

When the sphere is in the center of the gap there is no reduction in the "just fire" breakdown voltage. The voltage required for breakdown is the same with or without the presence of the sphere. From Fig. 15, the electric fields at the sphere are at least twice what they are at the electrodes, yet no breakdown enhancement occurred. This indicates that high fields alone will not lower the breakdown voltage and that the amount of charge the isolated sphere can contribute to the breakdown process is extremely limited, in conformance with the previous analysis. With the sphere in the center of the gap where it does not influence the fields at the electrodes, the voltage required for breakdown is unaltered in accordance with basic electrostatic theory. For a streamer initiated at the disk electrode, the energy gained in moving a charge from one point to another is proportional only to the voltage difference of these two points and not to the electric field distribution.

This test shows that breakdown is enhanced only when a high field occurs in the presence of a charge source. The high field initiates a streamer and the charge source "feeds" the streamer development process so that it will propagate across the gap and cause breakdown.

The effects on breakdown attributable to the various parameters listed previously were slight when compared with the location of the sphere in the gap. A summary for disk-to-disk electrodes is presented in Table 5.

Table 5  
Laboratory test results (effect in reducing breakdown potential for disk-to-disk electrodes)

Varied Parameter	Streamer (High Voltage Polarity)	
	Positive	Negative
Positive Net Charge	No Effect	Aids
Negative Net Charge	No Effect	Aids
Point Up (Toward H.V.)	Aids	No Effect
Point Down (Ground)	Aids	Aids
Ionization Up (Toward H.V.)	No Effect	Aids
Ionization Down (Ground)	Aids	Slight Aid
Position in Gap	Great Effect	Great Effect

Several comments are in order. The effect of a different diameter sphere was in direct proportion to its physical size indicating that the electrical size is proportional to physical size. The difference between a uniform field (disk-to-disk) and a highly nonuniform field (point-to-disk) were slight, indicating almost no dependence upon field distribution. Local ionization adjacent to the sphere

in the direction of the field caused some aid in break-down; however, when the ionization was oriented at right angles to the field, there was no effect. This indicates that the local ionization will give a slight aid when in a high field region. Further discussion of these results can be found in Ref. 15.

#### LIGHTNING MECHANISM SUMMARY

As a result of this program, the following conclusions can be reached.

- 1) Aircraft can trigger lightning when flying in a source charge such as a charged cloud.
- 2) Lightning not triggered by an aircraft will at most only be diverted; the total path of the lightning travel is not influenced by an aircraft.
- 3) Nose mounted pitot masts increase lightning hazard.
- 4) Jet exhaust is not a significant factor in lightning initiation.
- 5) Static charges on aircraft increase the lightning hazard, thus static discharges reduce the lightning hazard.

#### ACKNOWLEDGEMENT

Appreciation is expressed to Dr. T.C. Peng of McDonnell Douglas Research Laboratories for the Aerothermochemical Jet Engine Exhaust Analysis and K.E. Maxwell of McDonnell Aircraft Company who performed the laboratory tests.

#### REFERENCES

- 1 D.R. Fitzgerald, "Probable Aircraft Triggering of Lightning in Certain Thunderstorms", *Monthly Weather Review* 95, 835 (1967)
- 2 H.W. Kasemir, Memo Dated August 19, 1970, Subject Report on Lightning Discharges Triggered by Rockets at Langmuir Observatory, Socorro, New Mexico, NASA Contract CC-88025
- 3 M.M. Newman, J.R. Stahman, J.D. Robb, E.A. Lewis, S.G. Martin, and L.V. Zinn, "Triggered Lightning Strokes at Very Close Range", *J. Geophys. Res.* 72, 4761 (1967)
- 4 C.T. Phelps, "Field-Enhanced Propagation of Corona Streamers", *J. Geophys. Res.* 76, 5799 (1971)
- 5 E.T. Fierce, "Triggered Lightning and some Unsuspected Lightning Hazards", 138th Annual Meeting of the American Association for the Advancement of Science, Philadelphia, December 1971.
- 6 E. Nasser, *Fundamentals of Gaseous Ionization and Plasma Electronics*, Wiley-Interscience, 1971
- 7 J.M. Mink and J.D. Criggs, *Electrical Breakdown of Gases*, Oxford Press, 1953.
- 8 G.A. Dawson, "The Life Time of Positive Streamers in a Point-to-Plane Gap in Atmospheric Air", *Z. Physik* 183, 172 (1965)
- 9 B. Vonnegut, "Electrical Behavior of an Airplane in a Thunderstorm", FAA Tech. Report No. FAA-ADS-36, February 1965.
- 10 R.F. Harrington, *Field Computation by Moment Methods*, The Macmillan Co., 1968.
- 11 D.R. Fitzgerald, "USAF Flight Lightning Research", Lightning and Static Electricity Conference, 3-5 December 1968 AFAL Tech Rpt TR-68-290, Part II
- 12 Data from General Electric, J79-GE-10/17, Estimated Performance Model SP. E2039 and E2029, (January 1965).
- 13 T.C. Peng, P.M. Doane, and H.J. Fivel, "Modern Optimization of Equilibrium Air Plasmas from  $10^{-4}$  to  $10^3$  atm and 1000 to 10,000K," McDonnell Douglas Report G996 (March 1969)
- 14 R.T. Fowler, "Ion Collection by Electrostatic Probe in a Jet Exhaust", Graduate Thesis of Air Force Institute of Technology, WPAFB, Ohio (June 1970).
- 15 J.F. Shaeffer and G.L. Weinstock, "Lightning Mechanism Related to High Performance Aircraft", AFAL report to be published

## General Aviation Lightning Effects and Protection

J.A. Plumer  
General Electric Company  
Corporate Research and Development

### ABSTRACT

Increasing operation of general aviation aircraft under IFR conditions may increase their susceptibility to lightning strikes. Most aircraft are afforded good protection against adverse lightning effects by virtue of their all-metallic construction. The increasing use of fiberglass and other nonmetals in new aircraft construction raises the question of their possible vulnerability to lightning. A program was sponsored at General Electric by FAA to evaluate lightning effects on some of these materials and components, and develop protection design guidelines if warranted. This paper describes the work performed on a typical fiberglass wing tip fuel tank. Simulated lightning tests showed that lightning strikes can ignite fuel-air mixtures inside the tank. A protective diverter system was applied and found to be effective under both stationary and swept-stroke simulated lightning test conditions.

INCREASING NUMBERS of single and multi-engine general aviation aircraft, coupled with the greater availability and use of sophisticated avionics, makes operation of these aircraft under IFR conditions more common. As a result, their susceptibility to lightning strikes may increase. Coupled with this is another trend toward greater application of nonmetallic materials in aircraft structural and fuel systems, and greater use of solid state components in avionics. This combination results in greater potential vulnerability to lightning strikes, and may require that specific lightning protective measures be developed and applied if operational reliability and flight safety are to be maintained. Protective measures suitable for all-metallic aircraft, for example, may not be adequate for aircraft with some fiberglass or plastic sections. The all-metallic airframe is in many ways quite compatible with basic lightning protection requirements, and often only minor design modifications have been needed to provide adequate lightning protection.

Lightning effects on aircraft can be categorized basically as follows:

- (1) Effects on aircraft structural materials and systems.
- (2) Effects on aircraft fuel systems.
- (3) Effects on aircraft electrical and avionics systems.
- (4) Effects on personnel.

Before lightning protection can be designed and applied to aircraft with these

newer materials and components, their degree of vulnerability, if any, to lightning strikes must be established. For this reason, the Federal Aviation Administration instituted a program with General Electric Company (1)\* to evaluate typical design features of light aircraft to determine their possible vulnerability to lightning and develop design guides for protective measures.

As an example of the processes involved, this paper describes the vulnerability assessment, development and verification of a protective diverter system for a typical light aircraft fuel tank of nonmetallic construction. Similar tests and studies were also made on examples of electrical and structural systems under the FAA program, and the results of these will be given in the program final report.

For the fuel tank evaluation, a typical light aircraft wing tip fuel tank made of fiberglass was furnished by FAA. A drawing of the tank is shown in Figure 1. It is constructed of resin-impregnated fiberglass cloth covered on the outside with a nonconductive white paint, with a wall thickness 0.065 inches. A 7-inch diameter cutout was made in the tank to allow for internal inspection and to serve as a "blow-out" panel during fuel ignition tests.

### PRELIMINARY TANK VULNERABILITY STUDY

At the beginning of the program, a study of the tank structure was made to identify characteristics which could contribute to ignition hazards when subjected to a direct lightning stroke or static electric fields such as exist when the aircraft is within an atmospheric electric field or being electrically charged by precipitation.

A number of metallic components inside the tank were identified which could create high electrical stress and resultant corona under such conditions. These are listed below by numbers which identify their location on Figure 2.

- (1) The plain end on the vent pipe outlet has sharp edges which could produce corona.
- (2) Several sharp edges exist on the fuel level sensing device which could produce corona.
- (3) The fuel line strainer has a pointed configuration which could produce corona.

\*Numbers in parentheses designate References at end of paper.

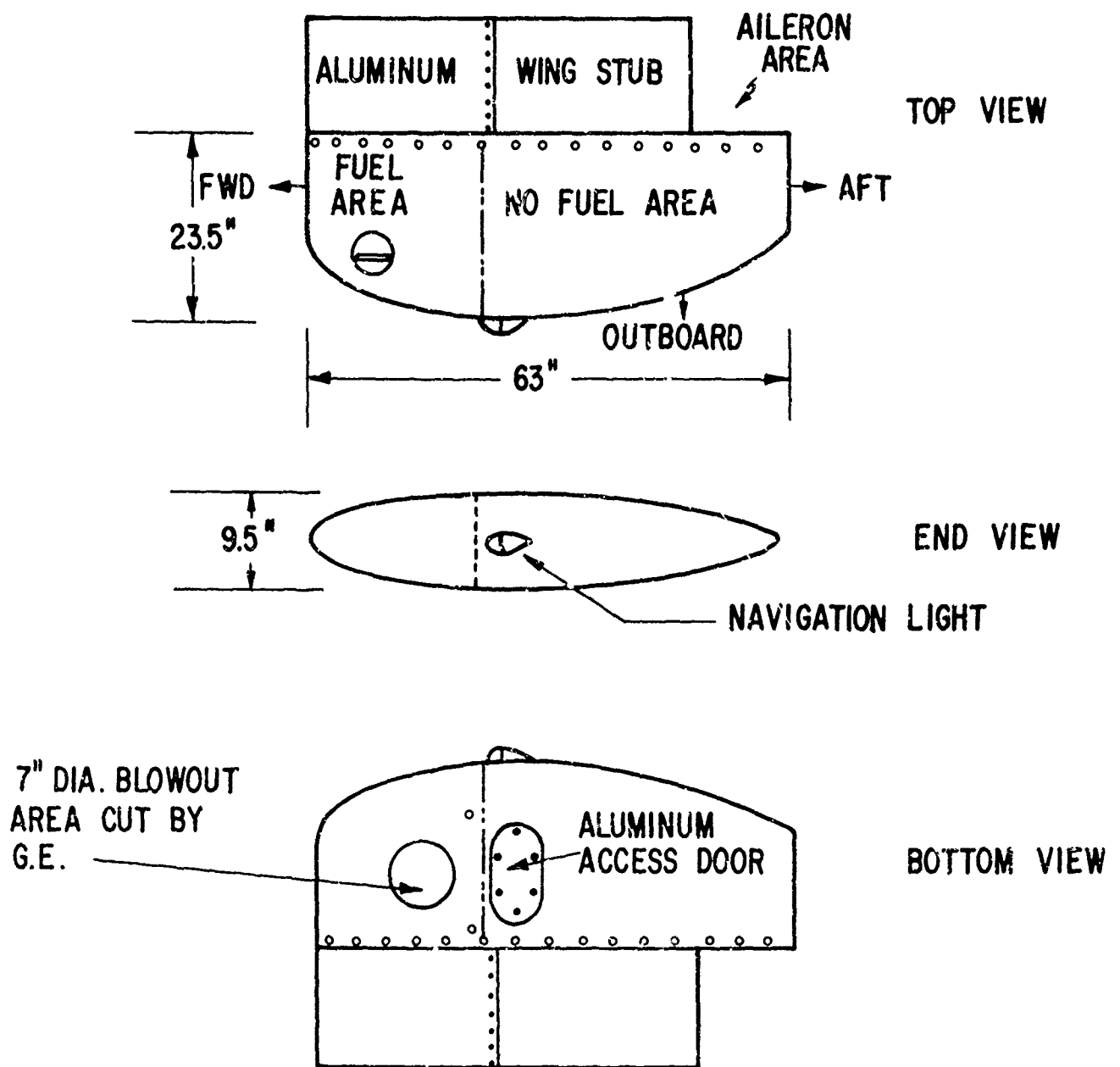


FIGURE 1. - FIBERGLASS WING TIP FUEL TANK UTILIZED IN LIGHTNING TEST PROGRAM.

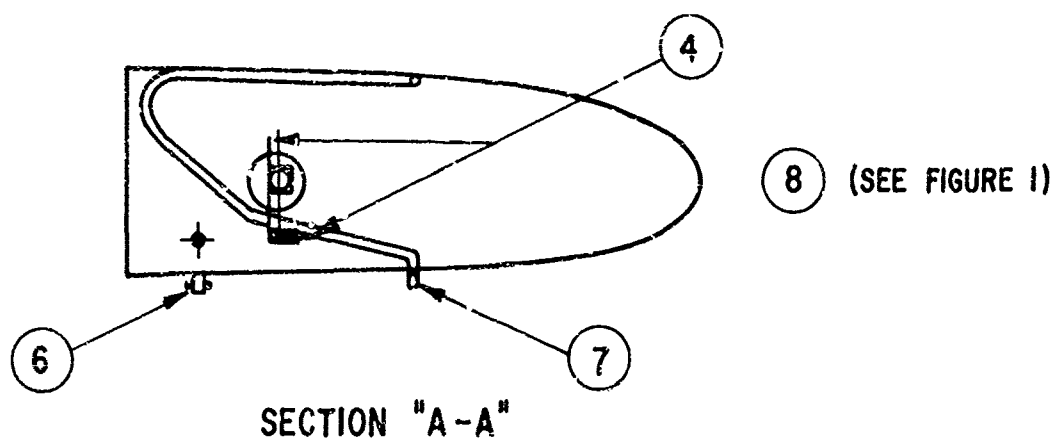
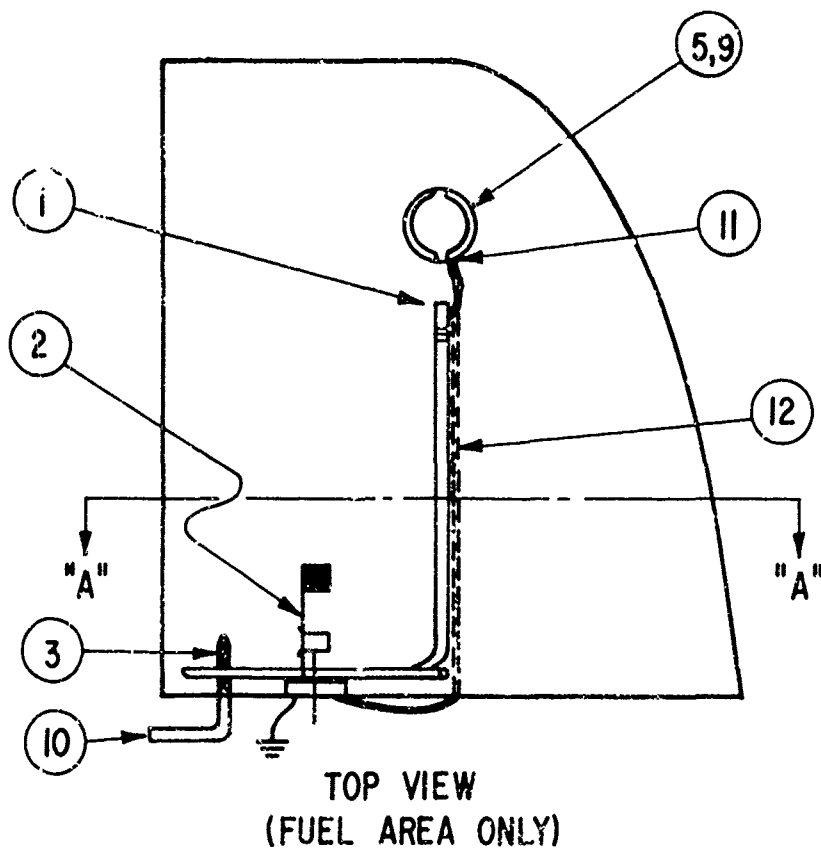


FIGURE 2. - POINTS OF POSSIBLE VULNERABILITY TO LIGHTNING OR STATIC ELECTRICITY.

(4) The sharp end of the wire supporting the fuel float could produce corona.

(5) The filler cap receptacle has a 1" deep tube wall projecting into the tank which could produce corona.

There are also several external tank components which may be susceptible to direct lightning strike attachment. These are:

(6) The tank drain plug protrudes outside and is not bonded to the airframe. This could produce an attachment point for lightning, but no subsequent conductive path for the current.

(7) The vent outlet protrudes about 1" and may be susceptible to direct lightning strokes.

(8) Although not an integral part of the fuel tank proper, the position lamp is susceptible to a direct stroke (see Figure 1).

(9) The filler cap is not of the "lightning protected" type and may produce sparking if struck.

Some of the bonding and grounding provisions found in the tank were not adequate to safely carry lightning currents. These are:

(10) The fuel line is not firmly grounded to the aluminum wing stub, creating possible electrostatic sparks between the line and other hardware.

(11) The filler cap receptacle is grounded to the vent pipe and sender unit by a ground braid whose arrangement may be conducive to inductive sparks and of insufficient size to carry full scale lightning currents.

(12) The embedded ground braid could cause severe blast damage to the fiberglass tank skin if it were to carry high amplitude lightning currents and explode.

In addition to the above characteristics, there is the overriding possibility that oncoming lightning flashes may puncture the fiberglass skin and attach directly to any of the internal metallic components pictured in Figure 2.

In order to determine the extent to which each of the above factors actually contributes to tank vulnerability, laboratory tests were performed wherein the tank was subjected to simulated static electric fields and lightning strokes.

#### STATIC ELECTRICITY VULNERABILITY TESTS

Static electricity tests were performed to determine if ignition of a flammable fuel-air mixture within the tank could occur from corona generated on any external or internal tank components by virtue of the tank's presence in ambient static electric fields of external origin or self-generated fields created by precipitation-static charging of the airframe. For each test, a flammable mixture of 5.97 cc of commercially available 100 octane gasoline per cubic foot of air was placed in the tank. This mixture was determined to be the optimum explosive mixture of aviation gasoline in air by an

experimental program of measurements of explosion pressures for a variety of fuel-air mixtures performed by Fenwal, Inc., under contract to General Electric. For each ignition test, the gasoline was injected into the tip tank, evaporated at room temperature and mixed with air for 5 minutes by a 5" diameter nylon fan within the tank. After the fan was turned off, the mixture was allowed to become stagnant for several minutes and the test performed. A mylar covering taped over the blow-out hole was burned away and replaced after each ignition.

To simulate an ambient electrostatic field the tank was placed in a quasi-uniform DC field created as shown in Figure 3. The anode was a 50" O.D. rubber inner tube with an aluminum foil insert. The cathode was a single sheet of aluminum approximately five feet square. The spacing between electrodes was 32 1/2 inches and the test piece was placed midway between the electrodes. The electrodes were energized by the 1,000,000 volt, 1 ampere DC generator loaded by a 0.5  $\mu$ f capacitor bank at the GE High Voltage Laboratory.

Voltage was increased rapidly to the inception level of audible corona (approximately 300 kV). At this point voltage was increased in 50 kV steps to 400 kV, then in 20 kV steps to 460 kV. Beyond 460 kV all increases in voltage were made in 10 kV steps until anode-to-cathode flashover occurred. Throughout the application of voltage, each level was held for one minute before progressing to the next level.

At no time during these tests did ignition of the fuel/air mixture occur as a result of corona off of metal components within the fuel tank. During these tests a maximum average field gradient of 590 kV/meter was applied, exceeding that in a thunderstorm region (2).

To determine whether or not an induced corona discharge emanating from an object within the tank would ignite the fuel/air mixture, a nail was inserted within the fuel tank through the mylar blowout cover and voltage applied to it. Ignition did occur just above the inception level of visual corona, at 70 kV.

With each "run" a voltage level was obtained where breakdown of the air gap occurred (ranging from 435 kV to 490 kV). In each case the discharge path passed through the wing tank structure. In several cases ignition of the fuel/air mixture resulted from the discharge.

This test series showed that even when the wing tip tank assembly is within an ambient electric field sufficient to produce visible and audible corona at external appendages on the tank, corona generated inside the tank, if any, is insufficient to cause ignition, even at voltages approaching the flashover potential of the quasi-uniform ambient field in air. Thus, the tank failed to permit ignition under conditions of ambient electric field stress approximating those



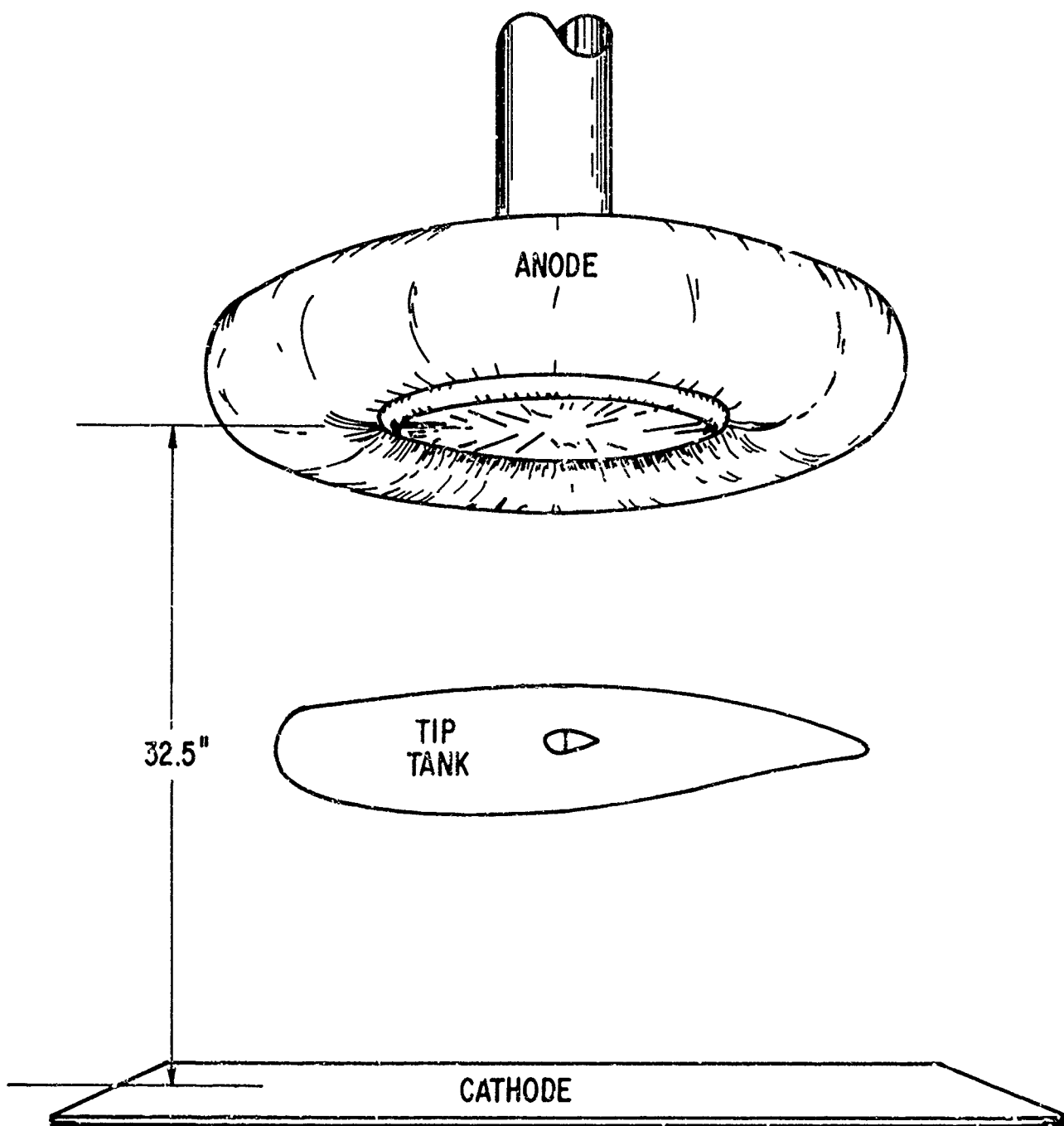


FIGURE 3 - ELECTRODE CONFIGURATION FOR AMBIENT ELECTROSTATIC FIELD TESTS.

existing in thunderstorm regions at stresses up to that at which a lightning flash would form.

A flashover through the tip tank, however, often caused an ignition. In some cases the specific cause, such as arc attachment to the unprotected filler cap, was evident; however, at other times the cause was obscure.

Next it was necessary to investigate the effects of corona which is self-generated, by virtue of the airframe being at a high voltage, as from F-static. In this case voltage was applied directly to the tip tank above a ground plane as shown in Figure 4. The tank was charged with fuel/air in the same manner as before.

At an electrode spacing,  $h$ , of 24 inches, audible and faintly visible corona was evident at applied voltages exceeding 100 KV, but no ignitions occurred. The air gap between tip tank and ground plane flashed over at 240 KV, again resulting in no ignition.

The gap was increased to 76 inches and voltage increased in 50 KV steps to 750 KV, holding each level for a minimum of one minute. At 750 KV the external tank glowed with excessive corona, but no ignition occurred.

To show that the fuel/air mixture was ignitable, a nail was again extended into the tank and again ignition occurred. These tests were repeated several times with the same results.

The ambient and self-generated electrostatic field tests just described showed that flammable fuel-air mixtures within this tip tank will not ignite when fields surrounding the tank, of either external or self-generated origin, are increased in intensity up to the flashover stress level of the ambient air.

#### LIGHTNING STRIKE SUSCEPTIBILITY TESTS

The tip tank was next subjected to simulated lightning strike tests to determine points of possible stroke attachment and to answer the question of whether a lightning flash will creep over the outside of the fiberglass or puncture the fiberglass to terminate on a metallic component within. For these tests the tank was supported horizontally by an insulating cylinder and subjected to simulated lightning strikes from an electrode suspended above a variety of locations on the tank surface. Both top and bottom of the tank were tested in this manner. The same fuel-air mixtures as used for the static electricity tests were inserted in the tank for each test.

Lightning strike reports (References 3 and 4) show that stroke attachments are pretty well scattered over wing tip surfaces, to a point several feet inboard of the edges and tips. Thus, the gap between the electrode and the tank surface was kept small enough so that the stroke was purposely directed to different spots on the tank surface. Since temporal and geometric descriptions of the electric field just prior to flashover of the gap between the aircraft and the oncoming lightning leader are

not available, the tests were made at close-in electrode positions averaging 7.5 cm normal to the tank surface with an applied voltage waveshape of  $150 \times 3000 \mu s$ , and repeated at a shorter, faster rising waveshape of  $1.7 \times 37 \mu s$ . Another series was made at a much greater gap spacing averaging 50 cm with front-of-wave flashovers applied at an even faster rate-of-rise of 1380 KV/ $\mu s$ . These waveforms are shown on Figure 5. Tests were made under this wide envelope of test conditions in the hope of encompassing those most representative of natural lightning.

When the electrode was placed above the aluminum wing stub or near any other external metallic object, most arcs flashed directly to the metal. When the electrode was above a fiberglass area, most arcs flashed to the fiberglass skin and either flashed along the outside surface to exposed metal, or punctured to a metal object beneath. The metallic objects contacted when arcs punctured the tank are listed in Table 1:

Table 1 - Metallic Objects Contacted Inside Tank

Object	Location on Figure 2
vent pipe beneath skin (all along its length)	1
embedded ground braid (all along its length)	12
sender float wire (with float in full or empty positions)	2

The external metallic objects contacted by the surface flashovers are listed in Table 2:

Table 2 - External Metallic Objects Contacted

Object	Location on Figure 2
filler cap	5
vent outlet	7
drain valve	6

The wing stub, navigation light housing and tank fastening screws (to wing stub) were also contacted. Whenever the fiberglass was punctured, ignition of the fuel-air mixture occurred. The only time surface flashovers resulted in ignition was when the filler cap was contacted, resulting in sparking between the filler cap and its receptacle. The faster rising voltage waveshapes produced flashovers at shorter times and higher voltages, enabling more direct flashovers to occur via puncture in the fiberglass. Thus, the slowly rising  $150 \times 3000 \mu s$  waveform resulted in the least percentage of punctures; whereas the faster rising voltages of the  $1.7 \times 37 \mu s$  and

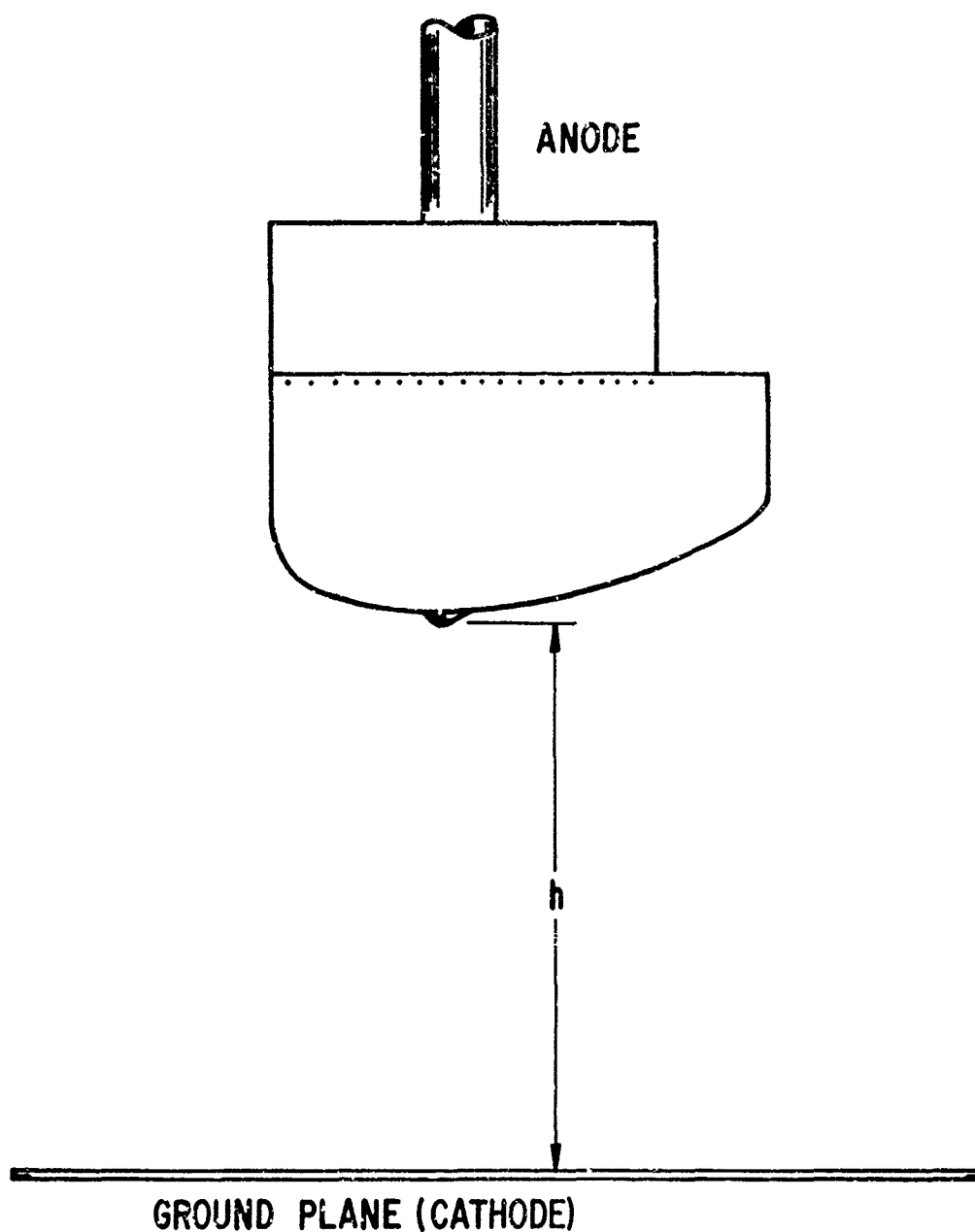
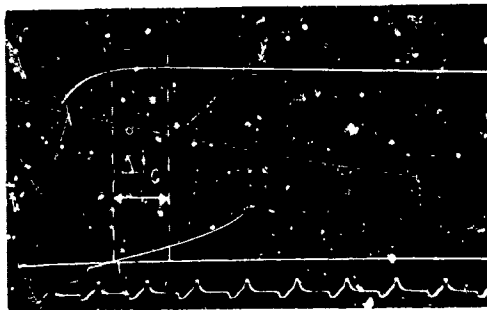


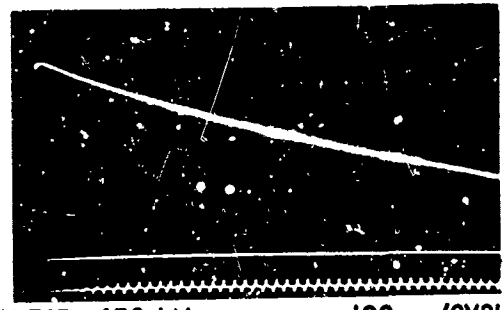
FIGURE 4 - ELECTRODE CONFIGURATION FOR SELF-GENERATED  
STATIC ELECTRICITY TESTS.

LONG WAVE  
(150 x 3000  $\mu$ s)



CREST = 430 kV

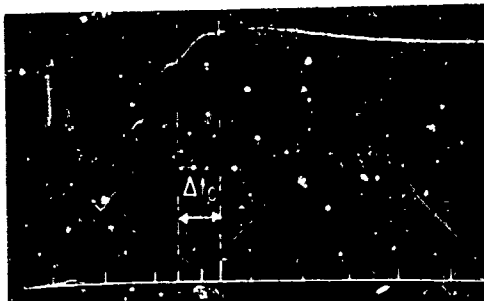
50  $\mu$ s/CYCLE



CREST = 430 kV

100  $\mu$ s/CYCLE

SHORT WAVE  
(17 x 37  $\mu$ s)



CREST = 185 kV

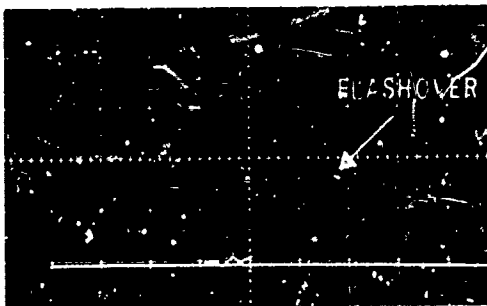
0.5  $\mu$ s/cm.



CREST = 185 kV

5  $\mu$ s/CYCLE

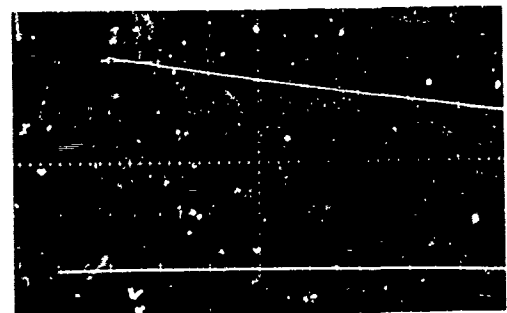
FRONT OF WAVE  
(1380 kV/ $\mu$ s)



CREST = 690 kV

0.5  $\mu$ s/cm.

(17.5" AIR GAP)



CREST = 956 kV

5  $\mu$ s/cm.

FIGURE 5. SIMULATED LIGHTNING VOLTAGE WAVESHAPES APPLIED FOR LIGHTNING STRIKE ATTACHMENT AND BREAKDOWN TESTS. (NOTE: VOLTAGE AMPLITUDES SHOWN ARE NOT NECESSARILY THE ONLY AMPLITUDES APPLIED.)

front-of-wave tests resulted in most punctures, as shown in Table 3. Aside from demonstrating that the tank is vulnerable to lightning, the test results show that the degree of this vulnerability is dependent not only on the tank design but on test voltage waveshape and electrode position.

It should be noted that these high voltage tests are performed at very low arc current levels as compared with natural lightning. The maximum currents of 1000 amperes or less, therefore, did not damage the fiberglass or other tank components as natural lightning would. This enabled a large number of tests to be performed on the single tank available. An epoxy sealer was successful in filling some of the punctures to prevent subsequent flashovers from passing through.

#### PROTECTIVE DIVERTER

Based on the high voltage test results, a protective diverter system made of aluminum straps  $0.5" \times 0.064"$  was designed, mocked-up and applied to the tank as shown in Figure 6. The diverter was clamped beneath the navigation light housing, fastened to the aluminum stub wing by sheet metal screws and wired and soldered to the vent outlet and drain valve on the bottom of the tank. The basic arrangement is designed to receive all lightning strikes and preclude punctures. Therefore, it was positioned to shield internal metallic components, including the braze and vent lines running beneath the skin between filler cap receptacle and tank separation wall. The filler cap is among the objects most frequently struck, so its receptacle was attached to the diverter system via a piece of strap as shown in Figure 6. This strap was also positioned to shield the metal vent line and internal grounding braid running beneath the skin (see Fig. 2, loc. 12), at this location.

Because the high voltage tests at the 1380 kV/ $\mu$ s rate-of-rise and 50 cm gap resulted in the highest degree of vulnerability, this test was repeated with the diverter applied to the tank. There were no punctures this time and no ignitions, except when the filler cap was struck, which again resulted in sparking to its receptacle. When the cap-to-receptacle bond was improved with aluminum foil jammed in between, sparking and resultant ignitions were prevented.

The only time the diverter proved ineffective was when the float wire was near the top or bottom tank walls as when the tank is either full of fuel or empty. In these cases the wire was too close to the tank wall to allow the diverter to be effective, and flashes striking the tank skin in this region punctured it and terminated on the float wire. Use of a non-metallic float support or positioning of the float and sender unit within a region effectively shielded by the diverter would eliminate this problem.

Since there are no metallic components inside the tank forward of the filler cap, the

need for the diverter around the outboard and leading edges is questioned. Because the tank skin is thin with respect to the surface flash-over distance required for strikes hitting the leading edge, its contribution to overall breakdown strength between the skin attachment point and the nearest metal diminishes for points increasingly forward on the skin. While most arcs will remain outside of the tank, the protection afforded by the skin itself is not deemed sufficient enough and the diverter was applied. The trailing edge diverter was also applied, to prevent physical damage to the skin in the event of lightning strikes in this region.

#### LIGHTNING CURRENT TESTS

Once an effective arrangement for the diverter system was determined, its ability to safely conduct lightning currents was evaluated by test. With the diverter applied and a fuel-air mixture in the tank as before, simulated lightning currents were delivered to all sections of the diverter, with the aluminum wing stub connected to the return side of the current generators so that test currents flowed from the diverter straps to the wing stub as they normally would in flight, where the other lightning attachment point is elsewhere on the aircraft. Composite current waveforms, including a high amplitude simulated stroke followed by a low amplitude, long duration continuing current were applied. Other tests were made in which only the stroke currents were applied. Unidirectional  $8 \times 17 \mu$ s simulated strokes with peak amplitudes from 50 kA to 120 kA, combined with continuing currents of between 0 and 336 coulombs were applied. Examples of these waveshapes are shown on Figure 7. A total of 37 test currents were delivered to all parts of the diverter and also the exposed vent outlet, drain valve and fuel filler cap. The diverter afforded adequate protection in all cases. Only strokes to the unprotected filler cap caused ignitions.

Stroke currents alone do not damage the  $0.5" \times 0.060"$  aluminum strap, as the  $i^2t$  value of the 100 kA stroke alone ( $\approx 1 \times 10^5$  amp<sup>2</sup>-sec.) are insufficient to raise the temperature of the diverter straps, with a cross-sectional area of 20 mm<sup>2</sup>, more than a few degrees centigrade. The more damaging component of lightning was found to be the continuing currents, as shown in Table 4.

A repeat of the last condition given in Table 4, showed that the diverter was still effective in preventing fuel ignition, although considerable paint was scorched from the fiberglass surface near the broken diverter.

Diverter strap of smaller cross-sectional areas also provide satisfactory protection, if the lightning flash remains attached to it after a strap is burned in two and several inches or more burned away. Protective effectiveness may diminish if significant

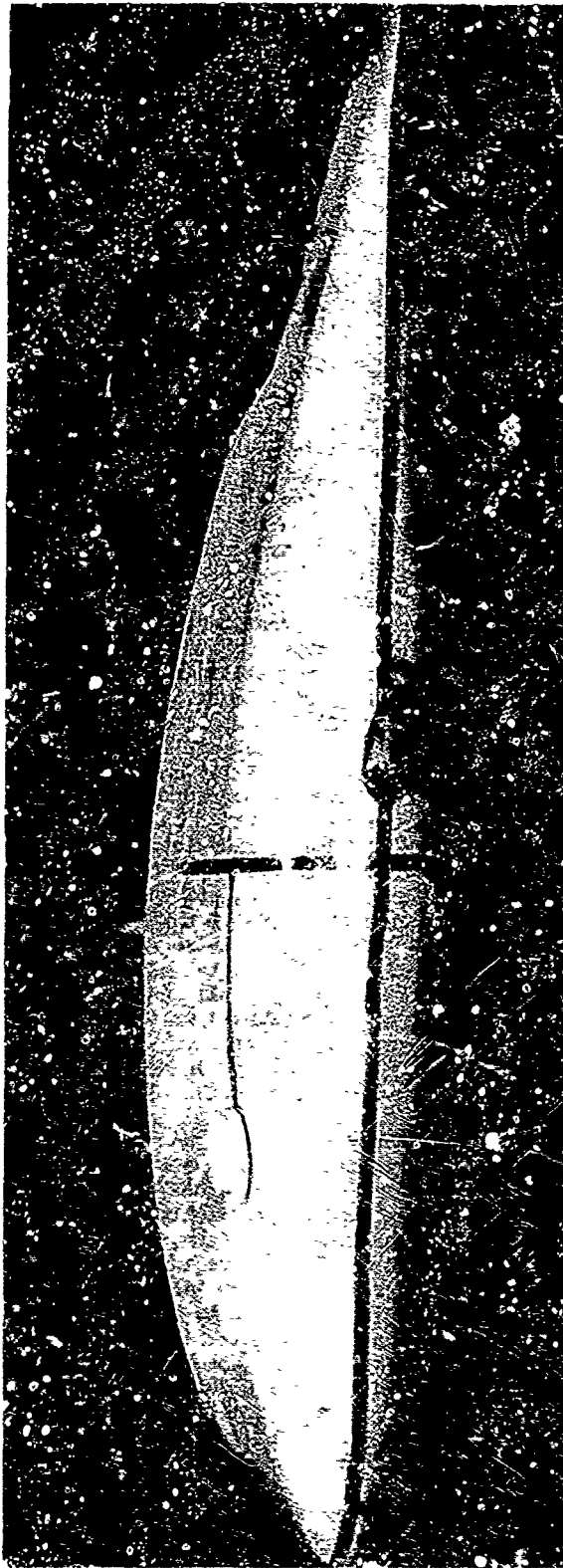
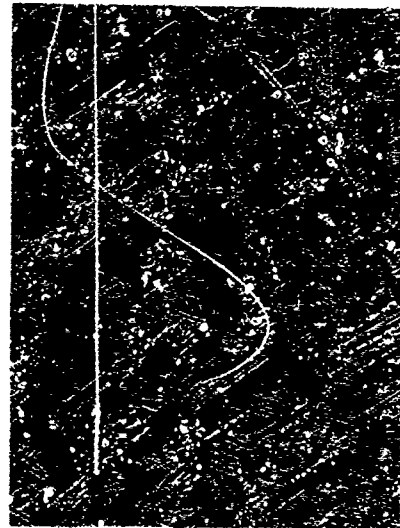


FIGURE 6 - 0.5" x 0.064" ALUMINUM DIVERTER SYSTEM APPLIED TO FIBERGLASS TIP TANK.

100 kA

160 COULOMBS



30 kA/cm.

5  $\mu$ s/cm.

STROKE CURRENT



84 A/cm.

0.2 ms/cm.

CONTINUING CURRENT

FIGURE 7 - SIMULATED LIGHTNING CURRENTS APPLIED FOR DIVERTER VERIFICATION TESTS.

Table 3 - Applied Voltage vs. Tank Puncture

Waveform ( $\mu$ s)	dv/dt (kV/ $\mu$ s)	Average Test Voltage (kV)	Average Air Gaps (Normal to Tank Skin - cm)	Percent of Flashovers Resulting in Punctures
150 x 3000	3	120	7.5	20
1.7 x 37	300	350	7.5	30
Front-of-wav	1380	700	50	63

Table 4 - Continuing Current Effects on 0.5" x .060" Aluminum Diverter Straps (Main)

Continuing Current			Effects on Diverter Strap
Average Amplitude (amps)	Time Duration (sec)	Charge Transfer (coulombs)	
--	(100 kA Stroke Current Only)	--	Surface pitting only
176	0.44	77	Eroded 15% through
167	0.96	160	Eroded 50% through
168	1.1	185	Eroded in two
168	2.0	336	Eroded in two and 2" eroded from one end

amounts of the strap are eroded away by a previous strike. Since aircraft are sometimes subjected to more than one strike, a strap of sufficient cross-section to maintain its effectiveness after receiving at least one flash is advisable for protection of a flight-critical component, such as a fuel tank. Cianos and Pierce (5) have constructed a 2% extreme lightning model based on the 2% extreme of many statistical summaries of the critical parameters of lightning flashes to earth. This model is a 10 stroke multiple-stroke flash with stroke currents of up to 140 kA and a total charge transferred to earth of 200 coulombs, of which 77% is carried by the continuing currents. (The "average" flash probably carries only 10% of this). Cloud-to-cloud flashes occurring at altitudes above 5,000 feet perhaps, are thought to be less severe, but since general aviation aircraft are commonly operated at altitudes of less than 5,000 feet, the ground-flash statistics are probably applicable. While not exactly the same as this model, the currents applied in this test series are of the same order of magnitude and therefore represent a relatively severe flash.

#### SWEPT STROKE TESTS

The foregoing discussion assumes that all of the current delivered by a lightning flash enters the diverter at one spot. In terms of diverter damage, this condition is likely to be the most severe. As an aircraft flies through the relatively stationary lightning arc, however, the arc apparently stretches somewhat along the line of flight as the original attachment spot moves forward with the aircraft. Sometime later the arc reattaches itself to the airframe at a point further aft. If the flash persists longer, the process may be repeated a number of times. The factors governing the tenacity, or dwell time, of the arc at its initial attachment points and the formation of new attachment points are not yet well understood. Brick, et al, (6), have suggested that new attachment points form on metallic surfaces when the stretched arc voltage drop exceeds the breakdown potential of the air (and any dielectric coatings) between the stretched arc and the surface. Plumer (7) has suggested that subsequent attachment points are also dependent on discontinuities in the lightning waveform and the presence of multiple strokes-especially in relation to nonmetallic surfaces. In any event, strike evidence (3) and (4), shows that such attachment points usually follow each other in a line parallel to the direction of flight. Since the protective diverter straps applied to this tank are not all parallel to the flight direction, it was decided to test the protected tank in a "swept stroke" environment to determine if successive strokes or dwell points will become reattached to other locations on the diverter system or if they may puncture or damage the fiberglass in between. Simulation of the dynamic relationship between a lightning stroke channel and a moving air-

craft surface, while maintaining all important electrical parameters involved, is a formidable task which has yet to be accomplished. The method utilized in this case is described in Reference 7 and is an attempt to simulate multiple stroke and high voltage characteristics thought important with respect to nonmetallic aircraft surfaces. In this case, the tank and aluminum wing stub were supported by a wooden cradle atop a truck and driven at 35 miles per hour through a one million volt, 60 hertz field. The tank was filled with an ignitable fuel-air mixture as before, and high-speed motion pictures were taken of the resulting flashovers and arc attachments to the tank. With 60 hertz high voltage, nonsustained flashovers were made to occur one or more times on each positive half cycle, providing flashover separations of from 1 to 16 milliseconds, which are similar to those of natural lightning. Sustained, continuous arcs were also generated, to more closely represent a continuing current. A total of 30 runs were made, each providing between 1 and 100 flashovers to the tank. Most of these tests were made with the diverter on, and it was 100% successful in preventing ignition or damage to the tank. Punctures and subsequent ignitions occurred on other runs with the diverter removed. The high-speed motion pictures showed that the nonsustained multiple stroke flashovers followed the same path to the vicinity of the tank but flashed directly or crept over the surface to the nearest diverter strap in each case. The continuous arcs were capable of stretching across the widest distance between any two straps in the line of flight before reattachment occurred.

The swept-stroke tests thus provided an additional degree of confidence in the diverter's ability to intercept oncoming lightning flashes and protect the tank. When properly installed and bonded to the metallic components discussed heretofore, this diverter and a lightning protected filler cap assembly should greatly minimize the risks of damage to the tank as a result of lightning. Care must be taken to design any permanent diverter installation so that the high temperature gaseous products at the point of arc attachment will be readily vented outward and not be contained and damage the fiberglass skin enclosing the fuel. In general, the full skin thickness of fiberglass should be between the diverter and the fuel. If much different from the completely external installation used in this evaluation, a prototype should be made first and tested with simulated lightning.

#### CONCLUSIONS

Static electricity and lightning simulation tests were performed on a typical light aircraft wing tip fuel tank made of fiberglass. The following conclusions can be drawn from the data.



(1) This tank was not vulnerable to fuel-air ignition as a result of DC fields of ambient or airframe origin, at field stress levels up to those sufficient to cause visible corona on external tank fittings or flashover of the surrounding air. These levels equal or exceed those expected in a thunderstorm region.

(2) The tank is susceptible and vulnerable to lightning strikes. At least 20% of oncoming high voltage test waveforms punctured the fiberglass and ignited the fuel-air mixture within.

(3) The applied voltage waveform utilized for the tests is significant in determining the results obtained. Front-of-wave flashovers at 1380 kV/ $\mu$ s resulted in 3 times as many tank punctures as slower rising 150 x 3000 usec waveforms. Electrode positioning is also significant.

(4) A protective diverter system made of 0.5" x 0.064" aluminum straps and applied as shown in Figure 6 was 100% successful in preventing tank punctures and ignition therefrom under the most severe of the high voltage test conditions applied.

(5) The diverter system remains effective after a simulated lightning flash of at least 120 kA (8 x 17  $\mu$ s) and 336 coulombs of charge have been delivered to it, although strap burn-through occurs at 185 coulombs.

(6) The diverter system on the tank was 100% effective in "catching" swept continuous and multiple stroke flashes formed by 1,000,000 volt 60 hertz sustained and non-sustained breakdowns when driven through them at a rate of 35 mph.

(7) With the protective diverter system applied, the only remaining tank vulnerability to lightning was via the fuel filler cap, which was of the nonprotected type and caused internal sparking.

#### ACKNOWLEDGEMENT

The author wishes to acknowledge the support of the Federal Aviation Administration, National Aviation Facilities Experimental Center, for this work, and the assistance of Mr. D.M. Millar of that agency as program manager. The contribution to this work by Mr. K.J. Lloyd of General Electric is also appreciated.

#### REFERENCES

1. Contract DOT-FA72NA-656, "Evaluation of Light Aircraft Fuel Tanks for Hazards Associated with Atmospheric Electrical Phenomena", Federal Aviation Administration, NAFEC.

2. F.A. Fisher, et al, "Lighting Effects Relating to Aircraft Part II - Characteristics of Simulated Lightning Flashes and Their Effects on Lightning Arresters and Avionic Equipment" AFAL-TR-72-5, January, 1972.

3. B.L. Perry, "Lightning Strike Hazards and Requirements", AFAL-TR-68-290, Part II, pp. 81-103, May, 1969.

4. J.A. Plumer, "Data From the Airlines Lightning Strike Reporting Project", Summary Report No. 71-1, 31 Dec. 1971. General Electric Corporate R&D report No. GPR-72-008.

5. Cianos and Pierce, "An Extreme Lightning Model for Flashes to Earth", Stanford Research Institute memo/note June 1, 1972.

6. R.O. Brick, L.L. Oh, and S.D. Schneider, "The Effects of Lightning Attachment Phenomena on Aircraft Design", Paper No. 700925, 1970 Lightning and Static Electricity Conference Proceedings, December, 1970.

7. J.A. Plumer and A.F. Rohlf's, "A Laboratory Test Technique for Evaluating Swept Stroke Effects on Aircraft", Paper No. 20, Proceedings of the 10th National Conference on Environmental Effects on Aircraft and Propulsion Systems, Naval Air Propulsion Test Center, Trenton, N.J. May, 1971.

## AIRCRAFT LIGHTNING PROTECTION DESIGN CONSIDERATIONS

by

M. P. Amason  
G. J. Casell  
J. T. Kung  
J. A. LaManna  
W. W. McCloud

Douglas Aircraft Company  
McDonnell Douglas Corporation  
Long Beach, California

### ABSTRACT

Lightning protection design considerations for present and next generation aircraft are presented. The zonal lightning protection design concept is described and basic design criteria for Zone 1, Zone 2, and Zone 3 lightning protection regions are established. Special design considerations for the following critical aircraft components are discussed: nose radome, fuel system, antenna system, p-static discharger installation, light housing, nose pitot boom, canopy, structure, and electrical circuit. Also, general design considerations for aircraft constructed of boron and graphite epoxy composite and glass fiber reinforced plastic materials are presented.

THE PURPOSE of this paper is to discuss the various phases of the aircraft lightning strike phenomena and the practices that should be employed to ensure a trouble-free design. It is the intent to assess the lightning parameters that are of concern and relate them to the design of aircraft components.

Lightning strikes involving aircraft are a common occurrence. The majority of these lightning strikes occur at low altitudes, in and below the cloud level, and during the takeoff and landing phases of aircraft operation. The greater number of short hop commercial flights has increased the exposure rate of aircraft to the lightning environment. Military aircraft sometimes fly missions which require them to remain at low altitudes in a lightning environment for long periods of time. The improvement of modern flight instrumentation has made it possible for aircraft to fly between thunder clouds rather than avoiding the entire storm area. Also, the large number of aircraft flying today has resulted in numerous aircraft lightning strike events.

General design considerations for aircraft lightning protection are the prevention of structural failure, flight control system damage, fuel explosion, and electrical or avionics systems malfunction, caused by lightning encounter. Special considerations must be provided for the protection of advanced composite structures and modern solid state computers. Lightning protection may also be required to reduce the maintenance effort on a cost effective basis.

The zonal lightning protection concept is described and used to establish lightning protection design requirements for aircraft components located in the various regions of the aircraft. Examples of lightning protection system design,

fabrication, and testing techniques for specific aircraft components are given.

This paper describes the factors considered in the design of aircraft lightning protection systems. Many of the specific design details are contained in the reference material. Much of the information presented may be familiar to those working intimately in this field. However, it is particularly for those designers who are less familiar with the subject that this paper is directed.

### AIRCRAFT LIGHTNING STRIKE PHENOMENA

**LIGHTNING STRIKE PHENOMENA** - Measured data indicate that the cloud-to-ground lightning strike phenomena generally contain three phases: the prestrike phase, the high peak current phase, and the heavy coulomb phase. The cloud-to-cloud and other types of lightning strike phenomena are not well understood due to the difficulty in collecting and measuring data. However, it is generally believed that they are similar to the cloud-to-ground strike phenomena but contain less energy (1).<sup>\*</sup> Therefore, the cloud-to-ground lightning strike characteristics are considered conservative when used as the design criteria for aircraft lightning protection.

**Prestrike Phase** - As a lightning stepped leader approaches an extremity of the aircraft, high stress streamers are initiated. The aircraft becomes a part of the stepped leader channel when one of these streamers is selected and contacted by the stepped leader, Figure 1. Propagation of the stepped leader will continue from other aircraft extremities until one of the branches of the stepped leader reaches the ground. The average velocity of propagation of stepped leader is 0.5 foot per microsecond and the average charge in the whole stepped leader channel is 5 coulombs (2).

**High Peak Current Phase** - The return stroke starts immediately following the completion of the stepped leader channel between cloud and ground. It contains a high peak current with an average value of 10 to 20 kiloamperes and a maximum value of up to 200 kiloamperes. This high peak current has a fast rate of rise, an average rate of 10

<sup>\*</sup>Numbers in parentheses designate References at end of paper.

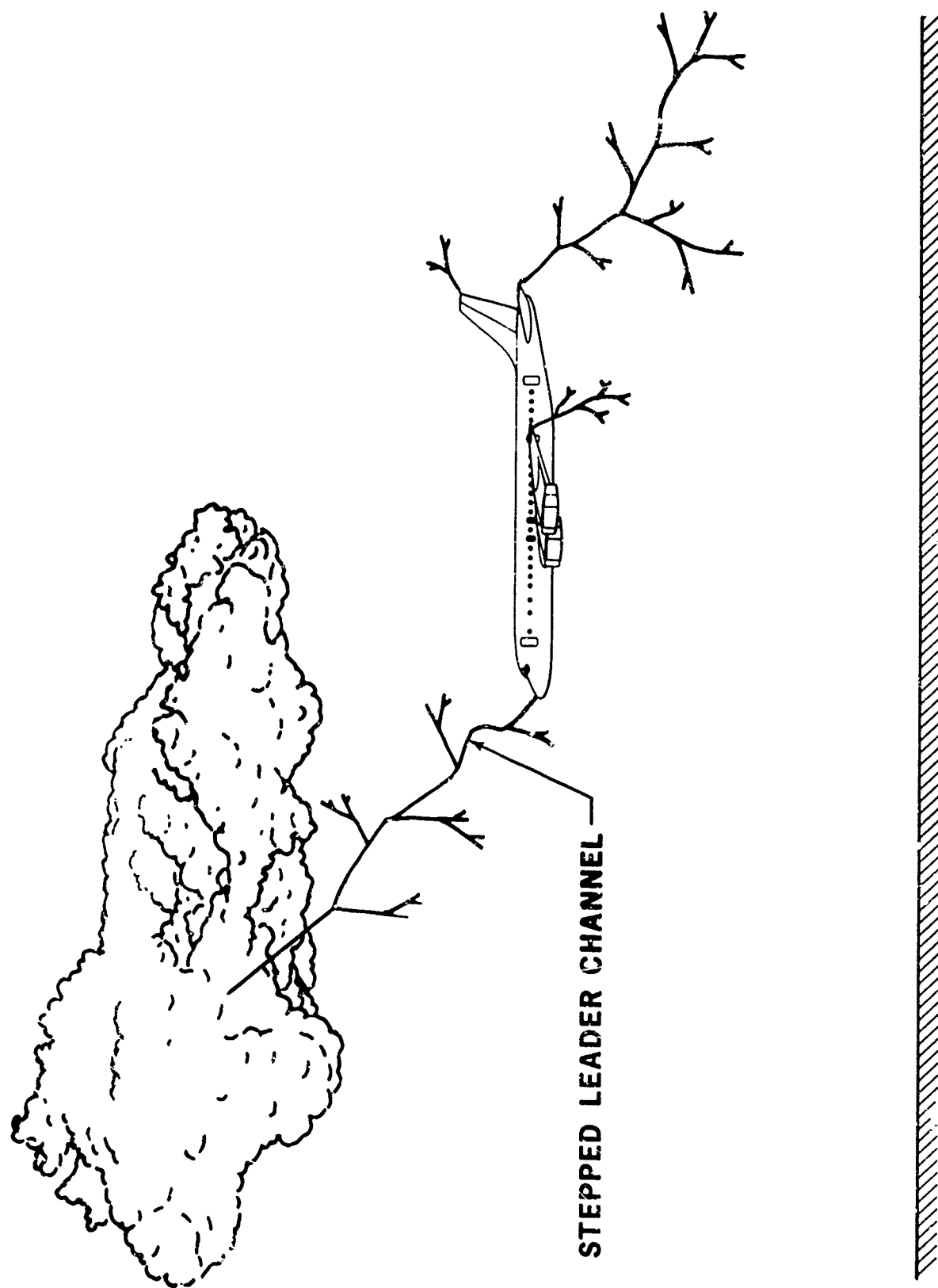


Fig. 1 - Aircraft during lightning prestrike phase

kiloamperes per microsecond and a maximum rate of 100 kiloamperes per microsecond. The average time to half of the peak current value is 40 microseconds. The initial return stroke is usually followed by 3 to 4 high peak current restrikes at somewhat lower amplitude and at millisecond intervals (2, 3, 4, and 5).

**Heavy Coulomb Phase** - A low continuing current flow normally follows the initial return stroke, having a magnitude of 100 to 200 amperes. The average duration of the continuing current flow is 174 milliseconds with a maximum duration of up to 1 second. The average total charge transfer is 31 coulombs, but a maximum charge transfer can be up to 200 coulombs (6).

Figure 2 shows the composite current waveform of the high peak current phase and the heavy coulomb phase of natural lightning stroke which is used as the design criteria for aircraft lightning protection.

**SWEPT-STROKE PHENOMENA** - The lightning channel is somewhat stationary in space while it is transferring charges. When an aircraft is involved, it becomes part of the channel. However, due to the speed of the aircraft and the length of time that lightning channel exists, the aircraft can move relative to the lightning channel. When a forward extremity such as the aircraft nose and wing mounted engines or fuel pods are involved, the aircraft surface moves through the lightning channel. Thus, the lightning channel appears to sweep back over the aircraft surface as illustrated in Figure 3. This is the swept-stroke phenomena. As the sweeping action occurs, local surface features of the aircraft can cause the lightning channel to contact and remain at various locations for different periods of time. Therefore, a portion or the entire heavy coulomb phase and the restrikes of lightning current may be involved in the swept-stroke action.

**DAMAGE PHENOMENA** - The types of damage caused to aircraft components by lightning are related to the three phases of lightning current transfer discussed above.

**Thermal Vaporization** - The high peak current phase of the lightning stroke consists of the transfer of a large amount of charge in a short period of time, a few microseconds. This charge transfer can result in fast thermal vaporization of material. If this occurs in a confined area, a high vaporization pressure can be created. This pressure can be of sufficient magnitude to cause extensive structural damage. Figure 4 shows extensive structural damage caused by a lightning stroke to an unprotected radome. The vaporization of metallic and other type materials and the heating of the air inside the radome housing created the high internal pressure that caused this structural failure. In some instances, large parts have been blown from the aircraft.

**Burning and Eroding** - The heavy coulomb phase of a lightning stroke can cause severe burning and eroding damage to aircraft structures. The most severe damage occurs when the lightning channel dwells or hangs on one point of the aircraft for the entire period of lightning current transfer. This can result in holes up to a few inches in diameter on the aircraft skin.

**Magnetic Force** - The current flow during the high peak current phase of lightning through sharp bends or corners of aircraft structure, can cause intensive magnetic flux interaction. In certain cases, the resulting magnetic forces can

twist, rip, distort, and tear structures away from rivets, screws, and other fasteners.

**Fuel Explosion** - High stress streamers are initiated from the aircraft extremities during the prestrike phase. Certain types of fuel vents located at these extremities are susceptible to streamer conditions. If streamers are initiated from the fuel vent opening while the fuel vapor condition is critical, local explosion may occur. If this explosion is not properly controlled, flames can propagate into the fuel tank area and cause a major fuel explosion.

The flow of lightning current through aircraft structures during the high peak current phase can cause sparking at poorly designed structural joints. If the sparking occurs inside the fuel tank or critical fuel vapor area, and the fuel vapor/air condition is critical, an explosion may occur.

The burning and eroding damage caused by the heavy coulomb phase of lightning current is critical when it occurs to the skin of fuel tanks or fuel vapor areas. The resulting burn-through penetration and in certain cases, hot spots on the internal surface of the skin can ignite fuel vapor and cause fuel explosions.

**Electrical Current Conduction** - The flow of lightning current, even a small portion of it through electrical components, can cause damage. In most cases, a varying degree of damage will result to both the component and the associated small gauge wiring.

**Electromagnetic Coupling** - The fast rate of rise of current during the high peak current phase can cause the electromagnetic coupling effect to the nearby electrical wiring systems and electronic components. This coupling effect can be severe enough to result in the following hazards:

- Electrical shock to the pilot by the conduction through wiring circuits
- Failure of the electrical systems by the false trigger of relays
- Malfunction of the avionic and control systems by affecting solid-state devices.

## ZONAL LIGHTNING PROTECTION DESIGN CONCEPT

**DEFINITION** - The aircraft surfaces can be divided into three zones (7), with each zone having different lightning attachment and/or transfer characteristics. They are defined as follows:

- Zone 1: Surfaces of the aircraft for which there is a high probability of direct lightning stroke attachment.
- Zone 2: Surfaces of the aircraft for which there is a high probability of a lightning stroke being swept rearward from a Zone 1 point of direct stroke attachment.
- Zone 3: The aircraft areas other than those covered by Zone 1 and Zone 2 regions.

Figure 5 shows lightning strike zones of a typical aircraft.

**ATTACH POINT STUDY** - Lightning attach points include the extremities of the aircraft surface. In addition to these obvious attach points, lightning can attach to the leading edge with a high degree of sweep back wings, certain high-lift leading edge devices, control surfaces during certain operational phases, canopies, and minor protrusions located near high field gradient points on the aircraft. All attach points including the nonobvious ones should be identified in

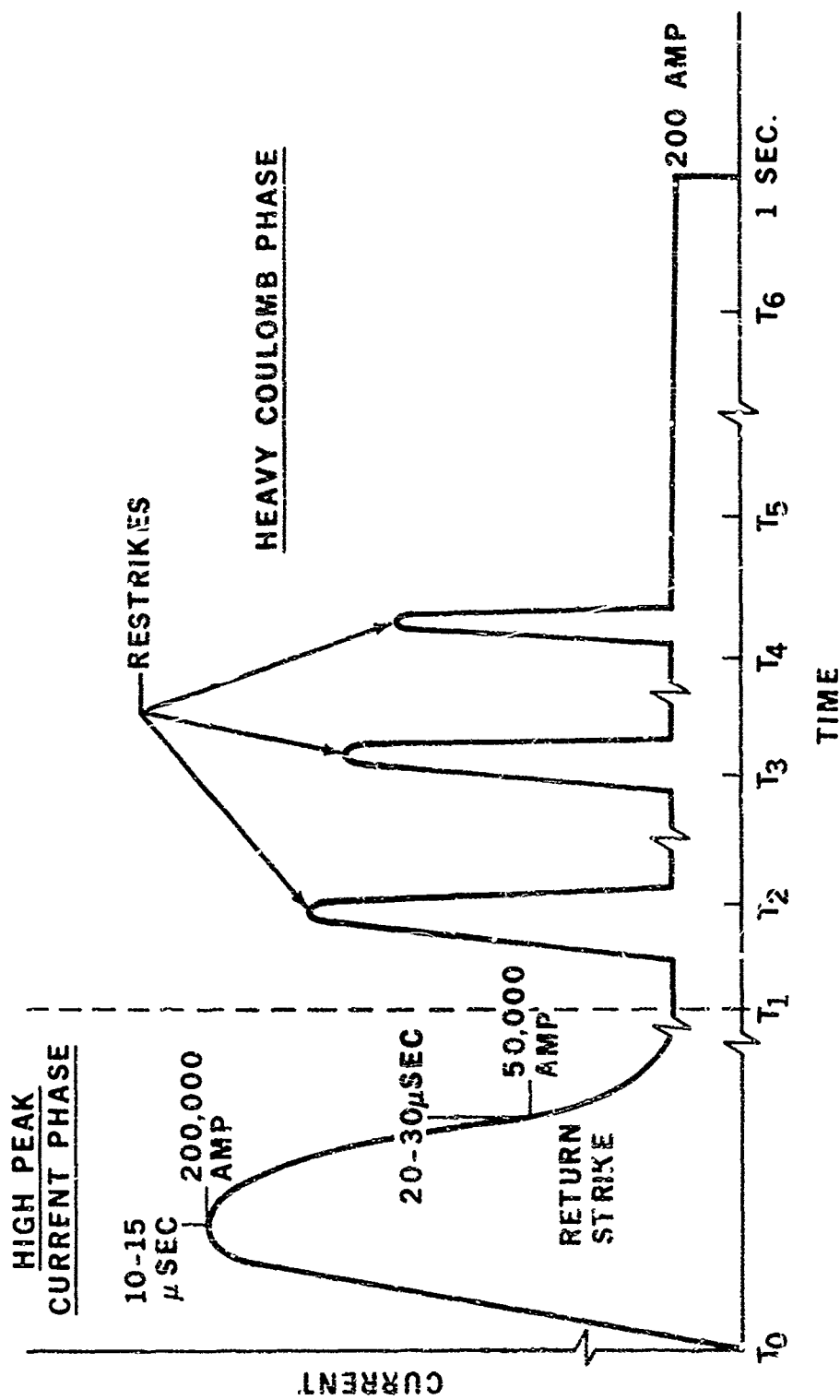


Fig. 2 - Composite natural lightning strike current waveform

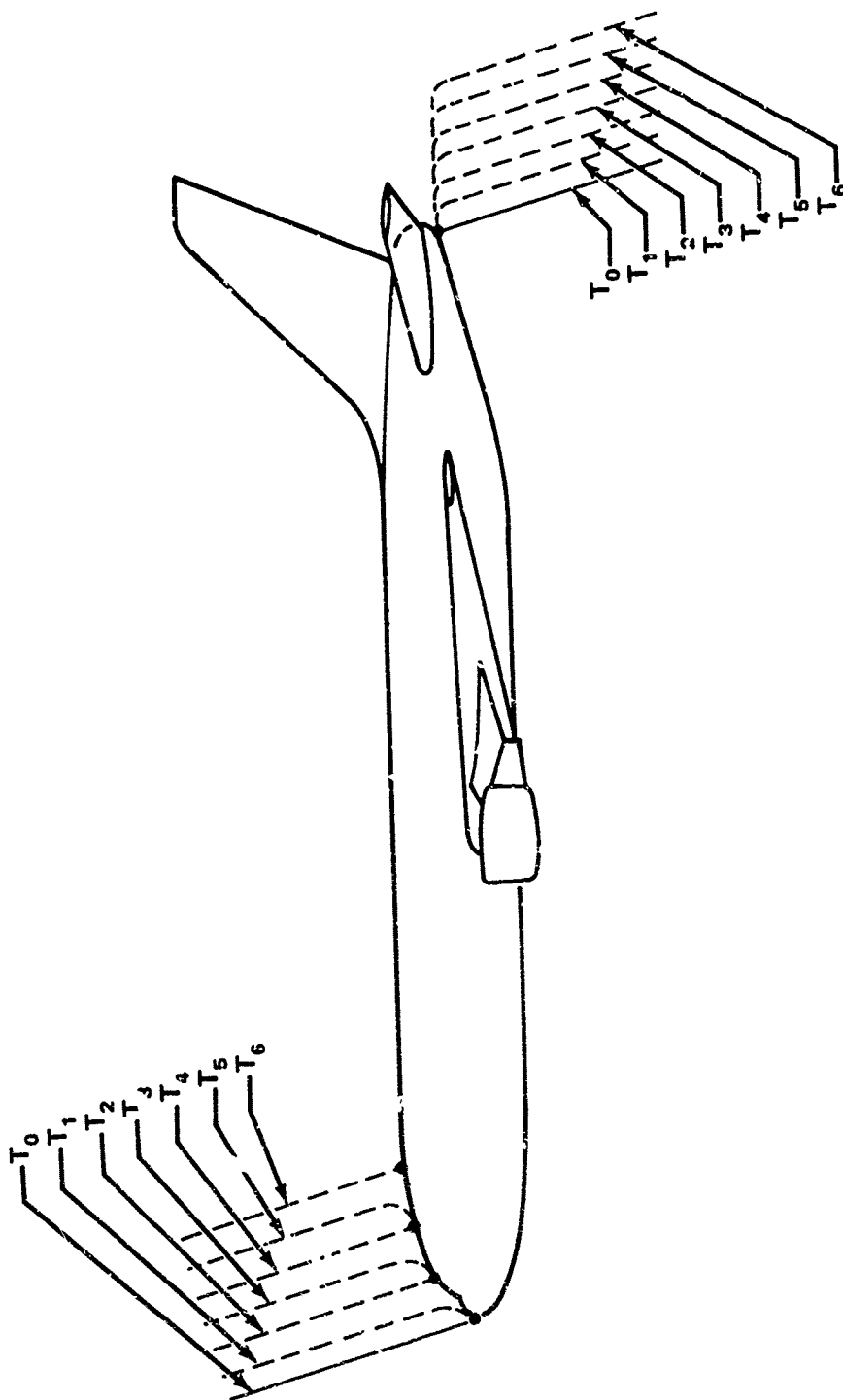


Fig. 3 - Swept-stroke phenomena



Fig. 4 - Lightning damage to unprotected nose radome

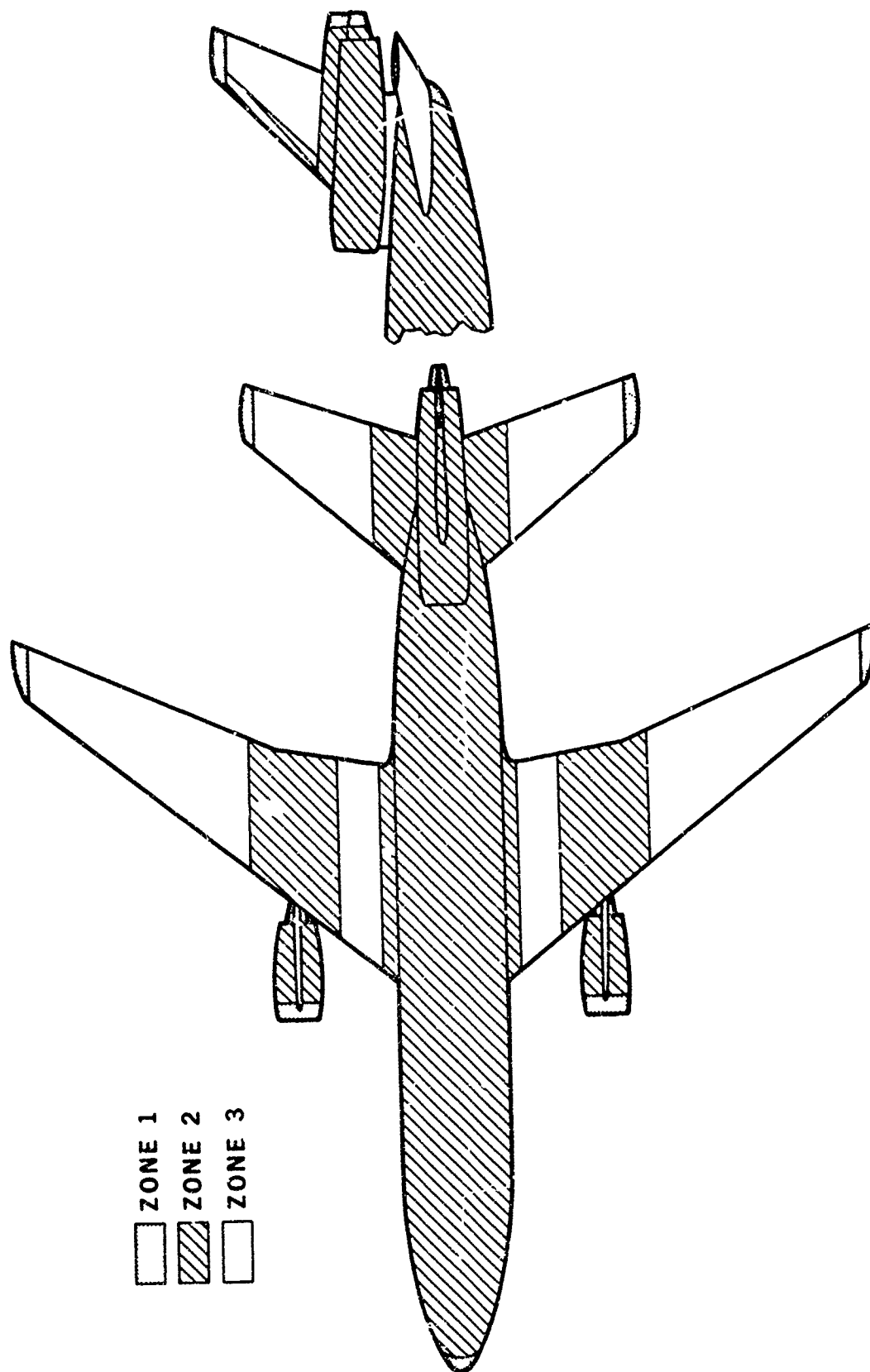


Fig. 5 - Typical aircraft lightning strike zones



the early stages of aircraft design so that lightning protection zones and thus protection design requirements can be established.

The lightning strike zones of an aircraft can be determined through the laboratory attach point study (8). The aircraft model should be of adequate size to allow for the proper modeling of candidate nonobvious attach points. One such model is shown in Figure 6, during an attach point test shot. The longest dimension of this model is approximately 5 feet. It should be noted that the control surfaces of the wing are at the most critical positions for lightning strike attachment. A high voltage generator capable of producing an arc of two to three times the longest dimension of the aircraft model should be used.

The model aircraft may be mounted on a three-axis rotatable fixture so that it can be located at any position relative to the arc channel. Lightning tests should be conducted from various striking positions and enough data collected to determine all direct lightning stroke attach points and thus Zone 1 regions of the aircraft.

Zone 2 regions of the aircraft can then be determined by identifying all surfaces which extend 18 inches laterally to each side of airflow lines passing through the Zone 1 forward protrusion attach points. Other areas of the aircraft are defined as the Zone 3 region (Figure 5).

**DESIGN CRITERIA** - Lightning protection design criteria should be established on the basis of the Zone 1, 2, and 3 regions.

**Zone 1 Region** - The high peak current phase of lightning stroke is involved at all points of direct attachment. Thus, the design of aircraft components located in the Zone 1 regions must consider the transfer of lightning current described above for this phase. In addition, if the lightning channel dwells or hangs on, such as in the trailing edge attach point case, the design must consider the heavy coulomb phase of the lightning current transfer. In the case of certain leading edge attach points, the lightning channel may not dwell or hang on long enough for the transfer of the heavy coulomb phase of lightning current; therefore, only the peak current phase may apply. In the fuel vent area, the protection against the prestrike streamering and stepped leader condition should also be considered.

**Zone 2 Region** - In Zone 2 regions the swept-stroke and restrike criteria are considered. The design of aircraft components located where lightning attachment can dwell or hang on, such as trailing edge areas, must consider the protection against both the restrike and the heavy coulomb phase of lightning current transfer. Components located at the other areas should consider the protection against the swept-stroke and restrike only.

**Zone 3 Region** - In Zone 3 regions the lightning current transfer criteria of both the high peak current phase and the heavy coulomb phase are considered. Efficient transfer of lightning current from one region to another on the surface of the aircraft is the principal requirement.

## DESIGN CONSIDERATIONS

The first step after the establishment of the lightning strike zones should be to evaluate the various aircraft components and identify the critical components requiring lightning protection. Design considerations for these critical components should be determined according to their

vulnerability, function, and location. Lightning protection design should also consider all inflight environmental effects as well as the serviceability and maintainability of proposed protection systems. Special design considerations for certain selected components are discussed relative to their locations in the Zone 1, 2, and 3 regions.

### ZONE 1 REGION -

**Nose Radome** - The nose of an aircraft, even though highly vulnerable to lightning strikes, is an ideal location for radar, ECM, and glideslope antennas. These antennas when housed within the reinforced plastic nose radome can be the main source of ionized streamers created at the nose of the aircraft during the prestrike phase. These streamers sometimes pass through an unprotected radome creating a potential path for the main lightning stroke.

The systems used for protecting radomes from lightning damage have been described previously by Douglas (9). These systems all provide an electrostatic shield over the radome. This shield usually consists of conductive strips installed on the outer surface of the radome as shown in Figure 7. If properly designed the strip installation can reduce the streamers from the antenna inside the radome while providing a new source of streamers outside the radome. Lightning can then attach to these streamers and travel down the strips to the fuselage without damaging the radome or antennas.

Devices available for protecting radomes from lightning damage include metal foil strips, permanent metal bars, and segmented metal/resistance strips illustrated in Figure 8.

Special design considerations are as follows:

- Selection of the type of lightning protection strip for a particular radome design takes into consideration the radome outer skin thickness, aerodynamic drag requirements, and the operational frequencies of nearby antennas.
- The thin metal foil strips\* have been used when the aerodynamic drag requirements prevent the thicker bars from being installed on the external surface of the radome. The thin foil strips provide only one stroke protection since they vaporize when struck by lightning. The outer skin of the radome must be thick enough to prevent damage to the radome when the foil strip explodes during vaporization. Thick foil strips may also be used, but they release more energy during vaporization than the thinner foil strips and, therefore, require a thicker radome outer skin. The magnitude of the vaporization explosion is also affected by the type of metal used in the foil strips.

A radio frequency noise source may be created if the metal foil strips are improperly grounded, or if fatigue cracks occur in the strips. Fatigue cracks are caused, generally, by improperly adhesive bonding the strips to the radome surface. Satisfactory installations of 0.004-inch-thick foil strips can be achieved, when proper grounding and bonding methods are used. Extreme care should be taken when designing grounding and bonding mechanisms for the strips.

- Permanent metal bars can be used in place of the metal foil strips to provide lightning protection. The metal bars should be of sufficient cross section to prevent vaporization or distortion of the strip near the point of stroke contact. Metal bars can withstand repeated lightning strokes from

\*Douglas U.S. Patent No. RE 25,417, 1963.

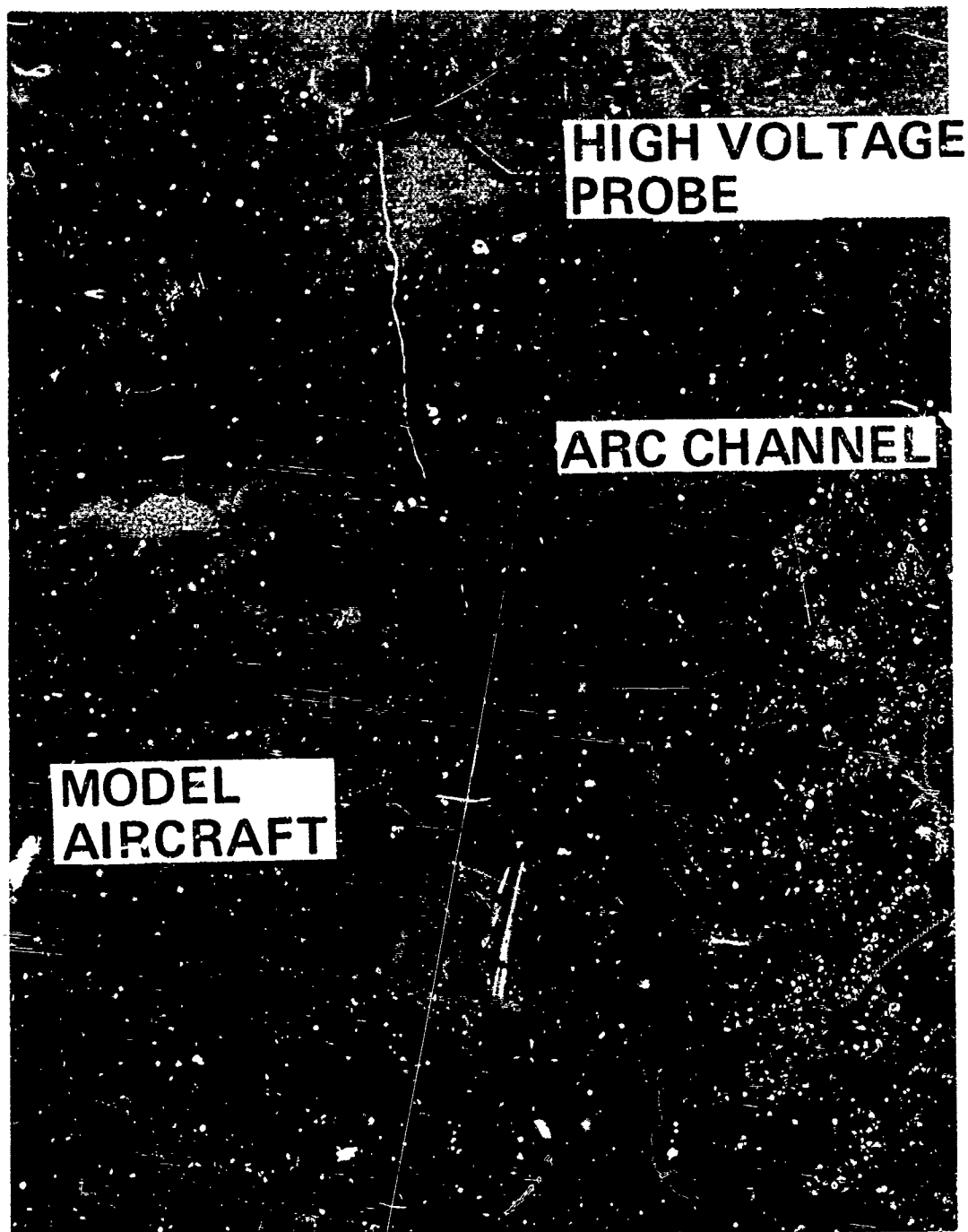


Fig. 6 - Attach point lightning test

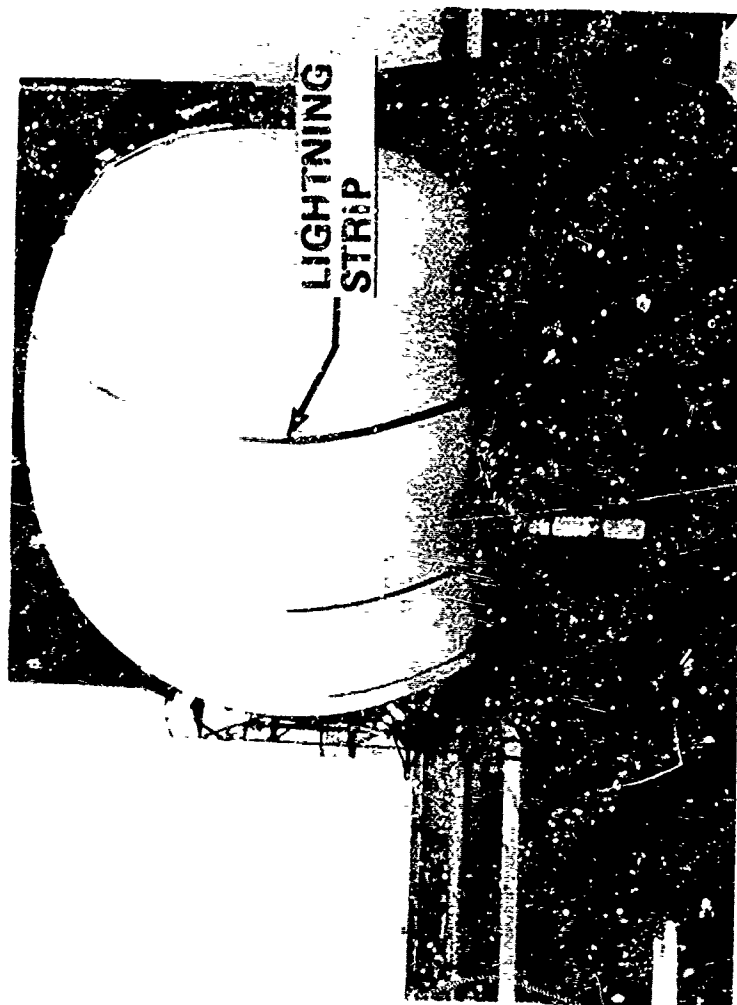


Fig. 7 - Typical nose radome lightning strip installations

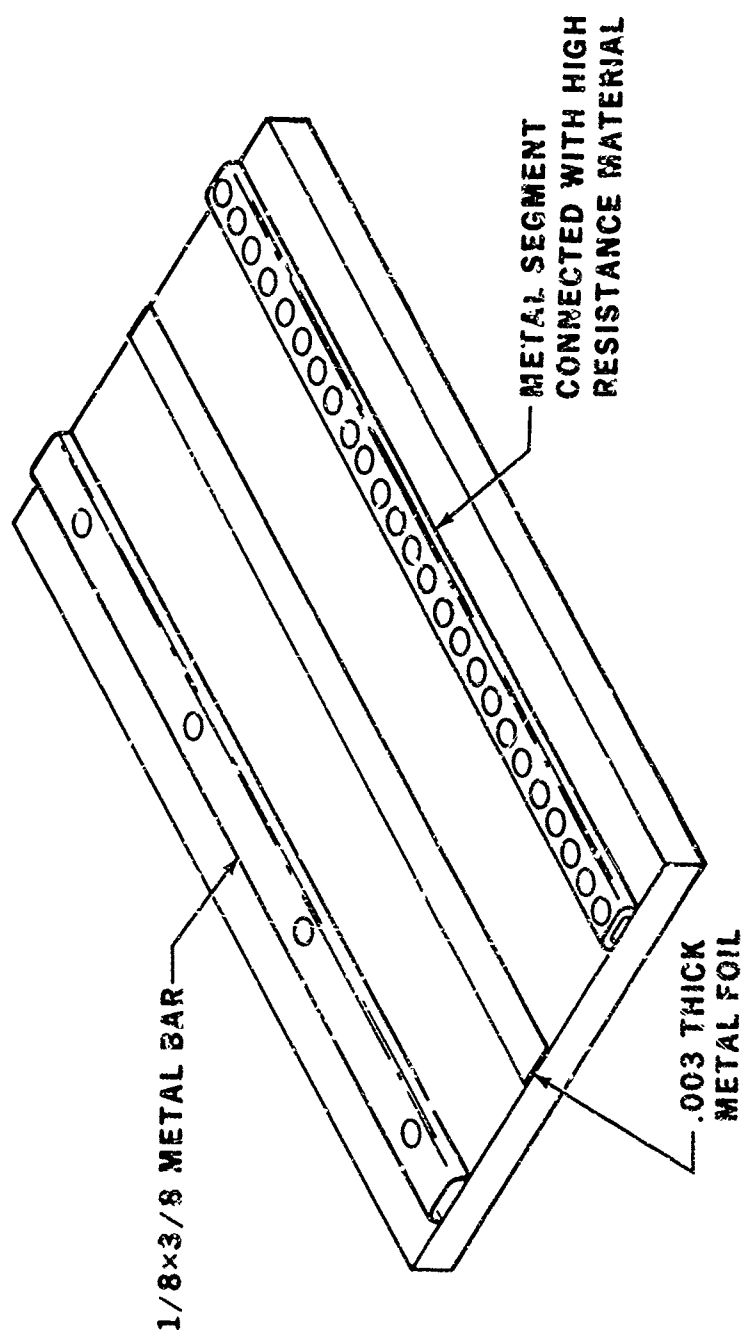


Fig. 8 - Radome lightning protection strips

the same direction. Generally, they eliminate the problems associated with thin foil strips. The attachment and grounding mechanisms for the strips should be carefully designed to withstand the most severe lightning strokes. Special considerations should be made in the design of the connection joint between the bars and radome metal frames so that the magnetic forces generated by the lightning current transfer through the joint will not damage it.

The expansion of gases around a lightning channel can damage the radome outer skin at the point of lightning impact. The radome can also be damaged if the expansion of gases is restricted by thick coatings over the metal bars. This is particularly true for thin metal foil strips. The outer skin of the radome should be designed to prevent this type damage.

- The Douglas segmented lightning protection strips\*\* may be used for those cases where the degree of distortion caused by the continuous metallic strips is not acceptable, antenna field and cause varying degrees of antenna pattern distortion. This pattern degradation is unacceptable for many types of antenna installations. These segmented lightning strips not only have insignificant effects on antenna radiation patterns, but also can withstand repeated lightning strikes and have good aerodynamic characteristics. This system consists of metal segments connected by appropriate resistance material. The size of the metal segments should normally be less than  $1/8$  wavelength at the highest operating frequency of the antennas housed within or adjacent to the radome. Larger segments are acceptable for many applications, however. An example of a simulated high-voltage lightning strike to a nose radome protected by the segmented strips is shown in Figure 9.

**Fuel System** — Fuel system components located in Zone I regions include wing tip tanks, pod tanks, and fuel vents. These components should be designed to withstand direct lightning current discharges without the initiation of fuel explosion (10 and 11).

Special design considerations are as follows:

- The fuel tank wall should have adequate skin thickness to prevent burn-through penetration or hot spots which can cause fuel ignition (12). Penetration can also be prevented at a forward point of attachment by the reduction of the lightning channel dwell time. This can be accomplished by providing a conductive surface aft of the attach point, over which the lightning channel can easily sweep back.
- Fuel tank elements, such as tubing, fuel connections, access doors, filler caps, probes, valves, and structural joints, should be designed to avoid the initiation of sparks inside the fuel tanks or critical fuel vapor area during the transfer of lightning current. This can be accomplished by good electrical bonding practices and the appropriate design of structural joints to ensure that sparking, if any, occurs externally and not within critical areas (13).
- Fuel vents should be kept away from Zone I regions. However, if this is not possible, protective means should be provided to prevent fuel explosion during the prestrike phase of lightning stroke (14). Flush or submerged vents can be used to prevent the initiation of streamers during the prestrike phase. For certain installations, diverter rods can

be used to advantage by directing lightning attachment away from the fuel vent. Also, when required, flame arresters can be installed in the vent system to prevent flame propagation into the fuel vent area.

Lightning tests are generally required to demonstrate the satisfactory suppression of internal sparking in the fuel tank area. Fuel tank elements used should be the actual production parts and the mockup of the adjacent areas should be made with the actual fabrication and installation methods.

**Antenna System** — Antenna systems commonly located in Zone I regions include HF, Loran, VHF flush tail tip, glideslope, and radar antennas. Lightning strikes to poorly designed systems may damage the antenna, associated wiring, and communication or navigation systems connected to it. Even though the physical damage to the antenna may be acceptable, lightning protection should be provided to prevent lightning current from transferring through the wiring circuit and damaging other associated systems (15). In certain cases, dual antenna system installations may be required.

Special design considerations are as follows:

- Lightning arrester installations may be used to protect certain ungrounded antenna systems, such as the isolated section type HF antenna. Figure 10 shows a typical installation. It includes a special spark gap between the antenna and aircraft metal structure, a dc blocking capacitor, and a static electricity leak resistor, all encased in a metal/glass enclosure. This installation can be located within the antenna assembly and carefully grounded to the aircraft metal structure.
- Lightning diverter rods can be used to control the lightning strike attach point on antenna systems. Figure 11 shows a simulated lightning test on a diverter rod installation of an antenna system. Lightning arresters may also be installed in the antenna wiring circuit for the secondary protection where personal or aircraft safety is involved.
- The glideslope and radar antenna systems are normally located inside the nose radome housing. Lightning protection for these antenna systems is not required if the nose radome is well protected. However, if this is not the case, lightning arresters should be installed in the wiring circuit of these antenna systems to prevent the associated systems being damaged by lightning.

**P-Static Discharger Installation** — P-static discharger installations, Figure 12, are normally located at the extremities of the aircraft wing and tail assemblies, and are frequently struck by lightning. The lightning current transfer characteristics of the aircraft p-static discharger installation have been previously investigated by Douglas (16). It was concluded that, if properly designed, the trailing-edge type p-static discharger installation can provide local lightning protection for the associated aircraft trailing-edge structure.

Special design considerations are as follows:

- The discharger installation should have a metal shank section with approximately 2 inches extending beyond the aircraft trailing edge to absorb lightning current burning and eroding damage. Figure 13, View A shows an example of severe burning and eroding damage caused by a natural lightning stroke to a well-designed discharger metal shank section. No damage occurred to the aircraft structure during this lightning stroke incident. Figure 13, View B shows the

\*\*Douglas U.S. Patent No. 3,416,027, 1968.

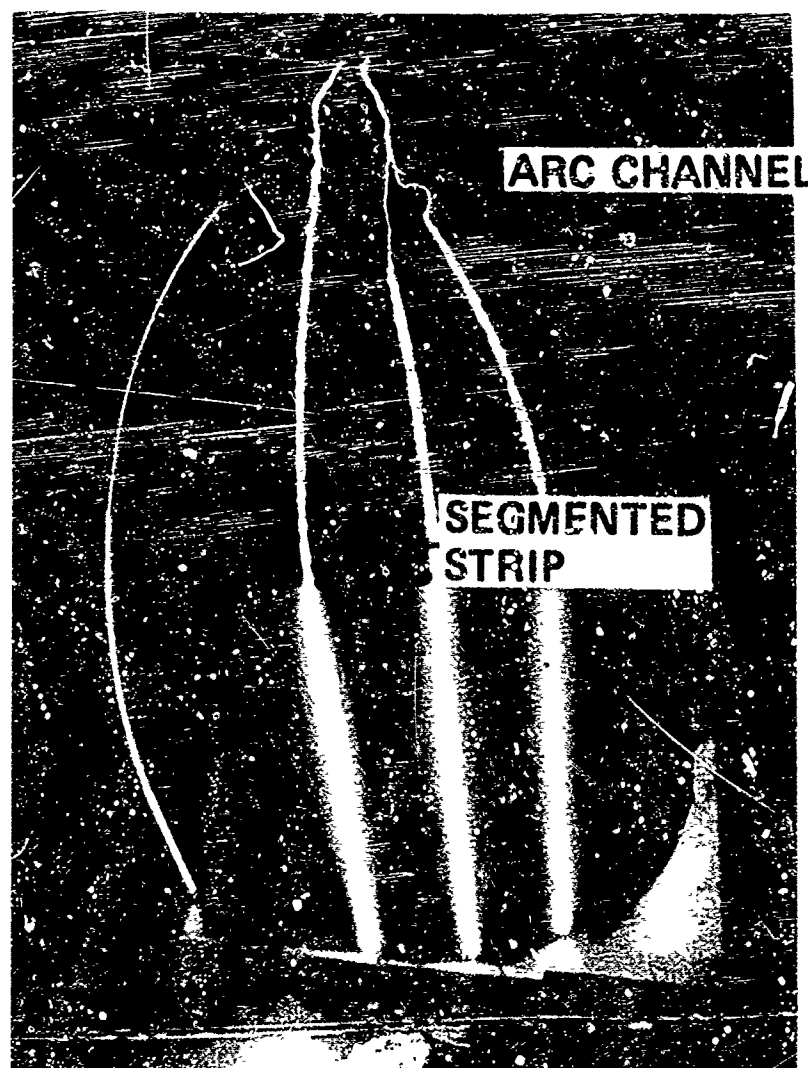


Fig. 9 - Nose radome lightning test

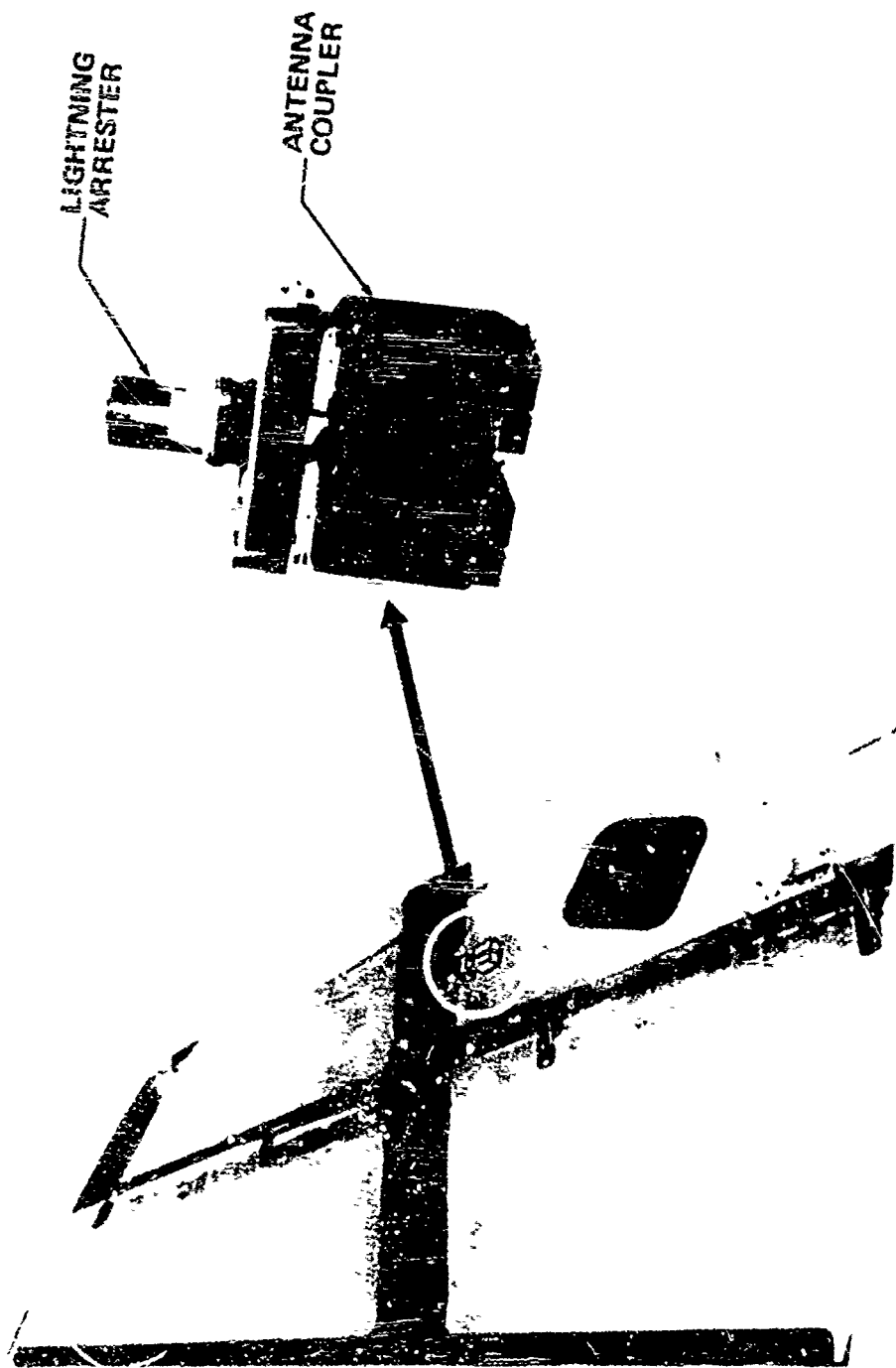


Fig. 10 - HF tip cap antenna and lightning arrester installation

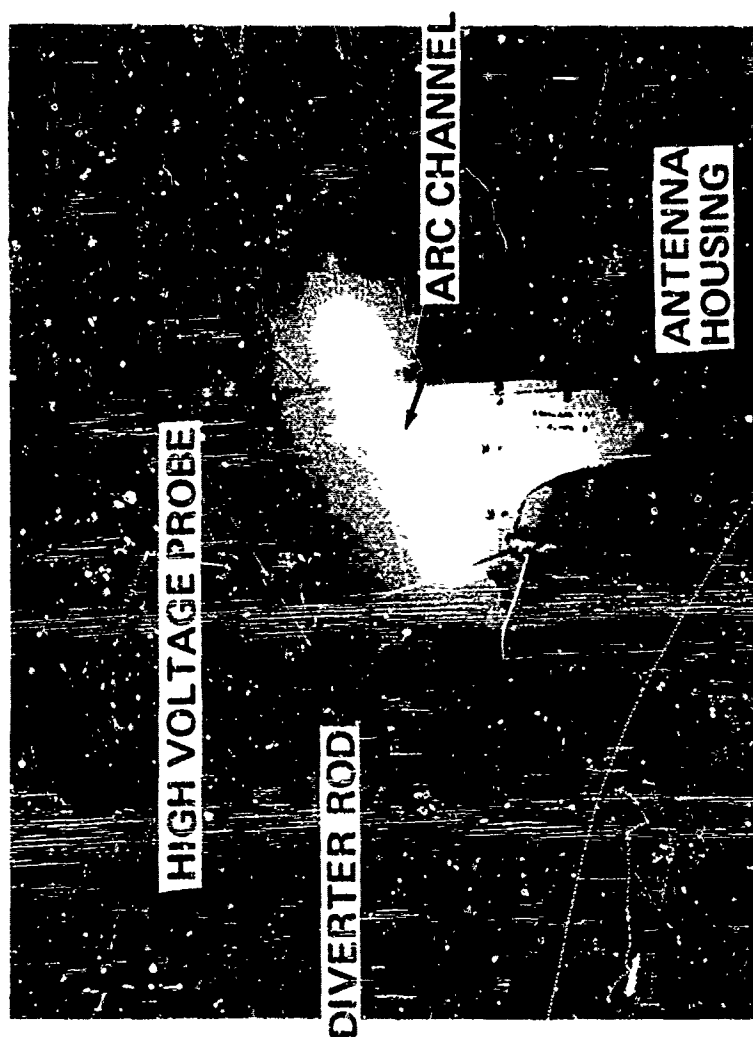
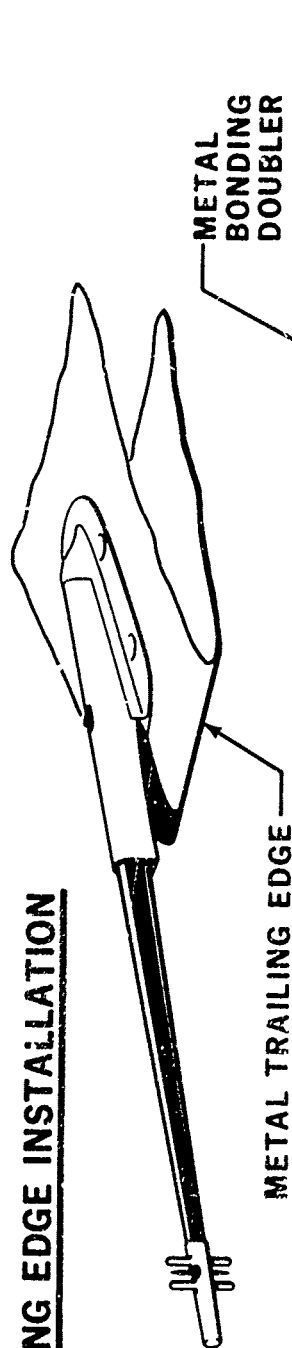


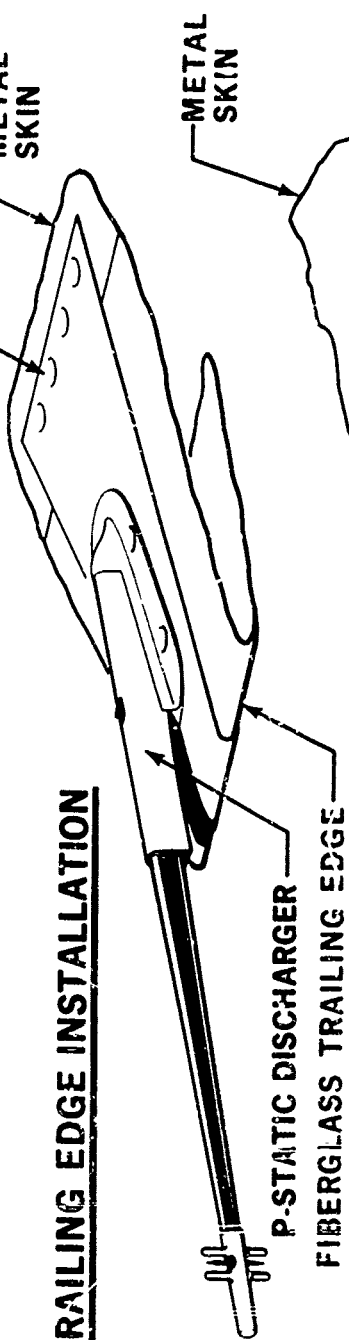
Fig. 1.1 - Diverter rod installation lightning test



### METAL TRAILING EDGE INSTALLATION



### FIBERGLASS TRAILING EDGE INSTALLATION



### TIP INSTALLATION

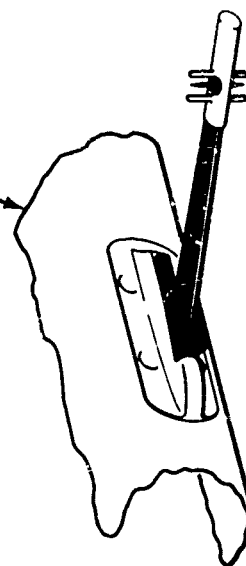


Fig. 12 -- Typical aircraft p-static discharger installations



View A - Damage to discharger from natural lightning stroke



View B - Damage to structure from simulated lightning test

Fig. 13 - Burning and eroding damage

type of damage that would have occurred to the aircraft structure, had a discharger with a poorly designed (short) metal shank section been installed at the same location.

- Riveted discharger retainer installations using non-corrosive PR 1422 adhesive, as a faying surface seal, can transfer lightning current satisfactorily. The previous requirement for the use of silver adhesive in the discharger retainer installation for lightning protection is not justified.

**Light Housing** - Certain aircraft have navigation lights installed at the extremities of the aircraft wing and tail assemblies. These housings are frequently struck by lightning with resulting damage to the housing structure and light bulbs. Figure 14 shows typical lightning damage of a light housing. View A shows the crazed glass housing and the eroded metal base caused by direct lightning stroke attachment. View B shows the eroded edge of the metal base caused by the transfer of lightning current through a poorly bonded joint between the light housing and the airframe.

Special design considerations are as follows:

- The surface conductivity and dielectric strength of the glass housing should be evaluated to assure that lightning current will flash over the glass surface to the metal base rather than fracturing or penetrating the glass housing and attaching to the light bulb and associated wiring circuit. If this is not possible, lightning conductive surge protectors should be used for the wiring circuit near lightning attachment points.
- The metal base of the light housing should be properly designed and electrically bonded to the airframe to prevent damage caused by the transfer of lightning current.
- When necessary, a lightning diverter or diverter-discharger (a regular trailing-edge type discharger mounted on an extended metal base) can be used to prevent lightning from striking the light housing (16). Figure 15 shows the development lightning protection tests of the diverter-discharger installation for an aft wing tip navigation light housing. View A shows a long diverter-discharger installation on top of the light assembly that failed to protect the outboard corner of the light housing. View B shows an installation at the outboard wing tip, which was too short to protect the inboard corner. View C shows an installation which successfully intercepted a lightning stroke. View D is the final design.

**Nose Pitot Boom** - Certain aircraft have a pitot boom installation on the nose radome as shown in Figure 16. This installation normally consists of a long metallic pitot tube with an anti-icing electric heater system inside the tube, air tubes connecting the instrumentation in the cockpit, and heater wires connected to the electrical system. The air tubes are normally made of plastic materials to avoid the distortion of the radar antenna radiation pattern. Lightning protection techniques for this installation have been investigated and reported by McDonnell Aircraft Company (17).

Special design considerations are as follows:

- Sufficient metal cross section areas should be provided at the forward tip of the pitot tube so that the tube will not be deformed and the airflow into the tube will not be affected by the direct attachment of lightning strokes.
- The flow of lightning current through electric heater wires which can vaporize the wires and damage the radome housing should be avoided. This can be accomplished by providing a metallic tube or by using one of the lightning

strip protection systems to transfer lightning current from the pitot tube to aircraft metallic structure.

- The electric voltage induced in the heater wires during the transfer of lightning current should be reduced to a safe level. This may be accomplished by twisting the wires and/or enclosing the wires in a metallic tube. Where necessary, a voltage surge protector can be incorporated in the heater wire circuit near the aft edge of the radome.

**Canopy** Aircraft canopies may be vulnerable to direct lightning stroke attachment (18). McDonnell Douglas Aircraft Company has investigated and published data (19) relative to the theoretical and experimental evaluation of the canopy lightning strike phenomena, and lightning protection methods.

Special design considerations are as follows:

- The primary hazard of lightning strike to an aircraft canopy is the lightning current penetration of the canopy and contact to the pilot. The construction and material of the canopy should be analyzed and tested for the lightning current surface flashover versus penetration characteristics.
- The lightning streamer condition inside the canopy during the prestrike phase should be evaluated. Medical study may be required to study the shock or streamer effect, if any, associated with the personal safety of the pilot.
- Lightning tests should be conducted to demonstrate that the canopy structure can withstand the transfer of lightning current without damage sufficient to create unsafe inflight conditions.
- If study indicates that special lightning protection systems are required, lightning strip protection methods discussed previously for nose radomes may be used.

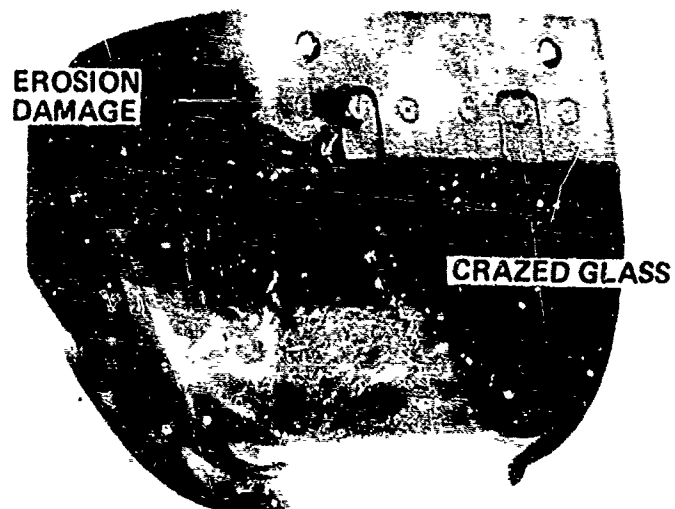
## ZONE 2 REGION -

**Fuel System** - Integral fuel tanks and pod tanks in the wing area fall in this region. Swept-stroke and restrike lightning current may attach to the fuel tank skin surface aft of forward attach points such as engines, pylons, and pod tanks. Fuel tank elements requiring lightning protection considerations include access doors, probes, filler caps and fuel vents. The special design considerations are similar to those discussed previously for the fuel system in Zone 1 regions, except that the swept-stroke and restrike lightning criteria are applied. Boeing Company and Lightning and Transients Research Institute have investigated and published data (20, 21) relative to the skin thickness requirement using aluminum and titanium materials and surface coating effects for fuel tanks in this region. Where the lightning channel can dwell or hang on, such as the trailing edge of pod tanks, the skin thickness should be designed to withstand the transfer of heavy coulomb phase of lightning current, without causing penetration or hot spots which may result in fuel explosion.

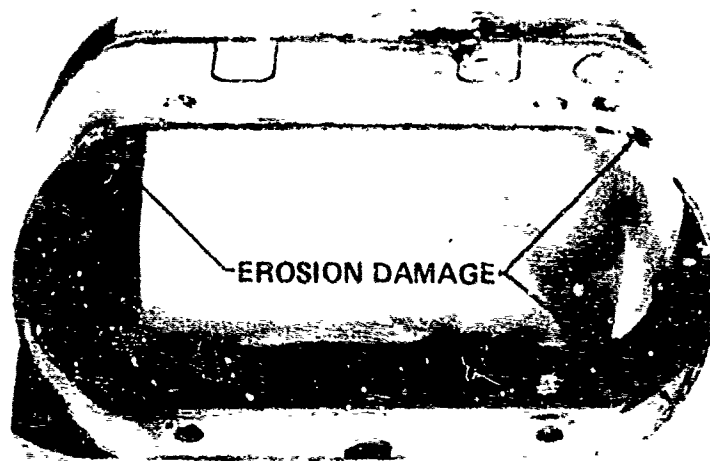
**Antenna System** - Antenna systems located in this region include VHF blade, ADF, and Loran antennas. Lightning protection design, if required, should be provided to prevent lightning current from transferring through the wiring circuit and damaging associated systems.

Special design considerations are as follows:

- Lightning arresters should be used in antenna wiring circuit to protect ungrounded antenna systems, as required.
- Proper electrical bonding should be provided for grounded antenna systems so that lightning current can

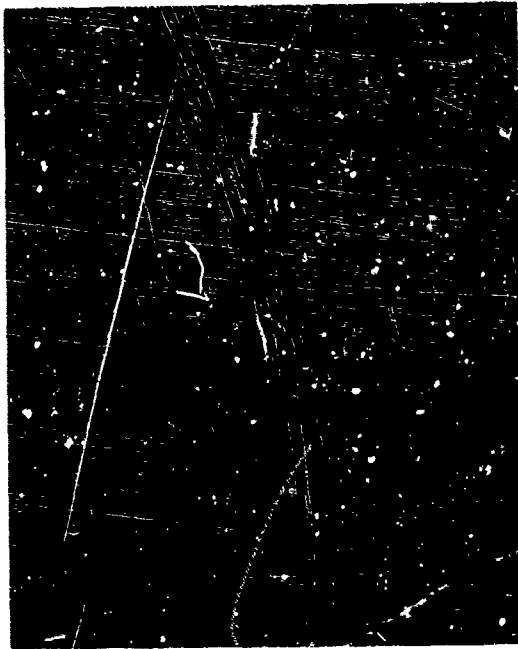


View A - Damage from direct lightning strike attachment



View B - Damage from lightning current transfer

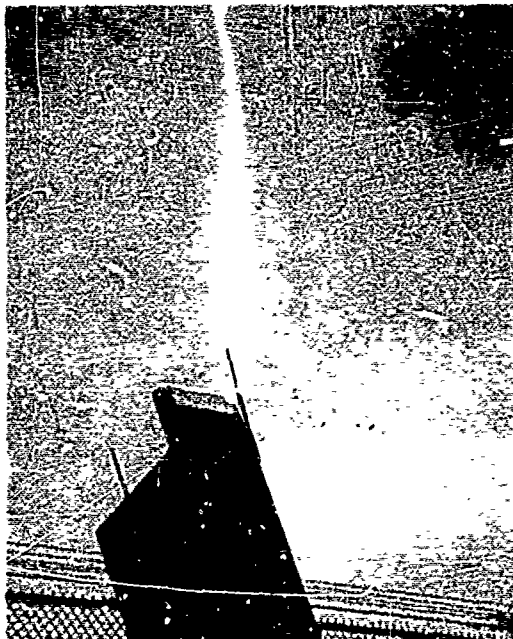
Fig. 14 - Light housing lightning damage



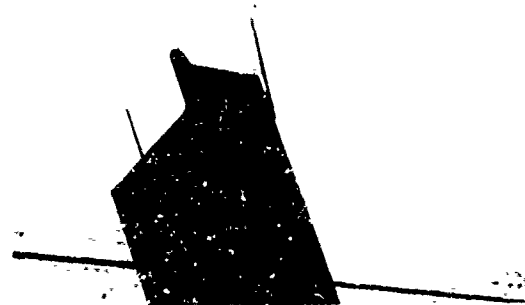
View A - Intense streamer current from the outboard corner



View B - Lightning current attached to the inboard corner



View C - Lightning current attached to the diverter-discharger



View D - Successfully tested installation

Fig. 15 - Aft wing tip light housing diverter-discharger installation lightning test

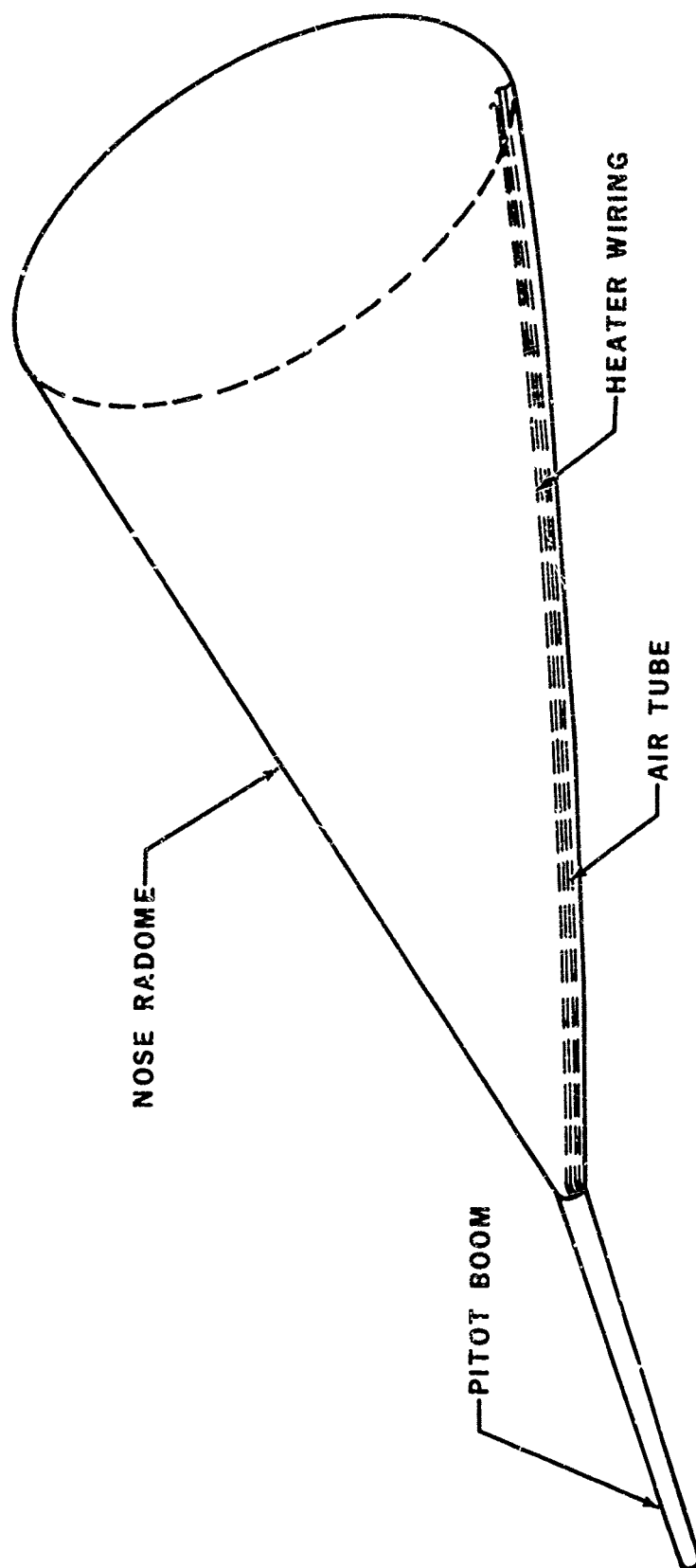


Fig. 16 - Nose pitot boom installation

transfer from the antenna to aircraft metal structure without causing burning damage in the joint interface.

### ZONE 3 REGION -

**Structure** - Conventional metal structures are usually riveted or bolted together. These types of structural joints can transfer lightning current satisfactorily. The advanced structural fabrication techniques quite often use adhesive bond methods to assemble structures. The adhesive materials used are normally nonconductive. Thus, ideal conductive paths for the transfer of lightning current do not exist. Therefore, special means must be incorporated to structures to provide adequate lightning current paths to avoid extensive damage (13).

Special design considerations are as follows:

- The use of other metal structures and conductive structural joints for lightning current transfer.
- The use of a few metal fasteners through the adhesive bonded interfaces to provide a conductive lightning current path.
- The use of the peripheral transfer design concept (16): the transfer of lightning current peripheral across the unsealed edges of the structural joint with minimum burning damage at the edges.
- The use of conductive adhesives for the structural joints should be prevented due to the undesirable corrosion characteristics of these adhesives.

**Fuel System** - The main consideration here is the transfer of lightning current across this region without the initiation of sparks inside the fuel tank and critical fuel vapor area. Normally, good structural bonding techniques such as rivets and bolts, will provide adequate conductive path for the transfer of lightning current.

**Antenna System** - Antenna systems located in this region do not require special lightning protection design considerations. Normal installation and bonding techniques are sufficient to shield lightning current from transferring through the wiring circuit of these systems.

**Electrical Circuit** - Lightning current transfers from one extremity of the aircraft to another across numerous conductive structural elements. Electrical circuits located close to these structural elements or using the structure as a ground return path, are susceptible to lightning impulse coupling. The vulnerability of the electrical, navigational, communication, instrumentation, or control systems involved, depends primarily on the specific characteristics of the system. Thus, careful analysis and measurements must be made before each system malfunction mode can be identified. It should be noted, however, that the increasing use of solid state circuits, with low threshold-of-failure voltages, requires that a judicious search be made to identify possible problem areas. Measurements and analysis of lightning induced voltages in aircraft electrical circuits have been made by various organizations. One such program sponsored by the NASA and conducted by General Electric High Voltage Laboratory has been reported (22). Douglas has also made investigations in this area.

Special design considerations are as follows:

- The measured and analytical data for certain simulated conditions should be carefully used in a system analysis to define each system malfunction mode and thus establish appropriate protection requirements.

- Voltage surge protectors and band-pass filters may be installed to reduce transient voltage effects.
- Rerouting, shielding, and twisting of wiring may be considered for the reduction of transient voltage effects to an acceptable level.
- The use of aircraft structures for ground return paths should be avoided for critical systems.

### ADVANCED COMPOSITE AIRCRAFT

**GRAPHITE/BORON EPOXY COMPOSITE AIRCRAFT** - Graphite and boron epoxy composite structures are much less conductive both electrically and thermally than conventional metal structures; therefore, new lightning protection design concepts are required. The general design concept here is to prevent any lightning current from attaching to or transferring through these composite structures. If this is not possible, appropriate lightning current transfer paths should be established and properly designed to prevent damage to composite structures and associated structural joints resulting from the transfer of lightning current. Also, the aircraft as a whole should have external conductive paths to transfer lightning current from one extremity of the aircraft to the others across Zones 1, 2, and 3.

**Zone 1 Region** - Laboratory simulated lightning test results have indicated that boron and graphite epoxy composite structures can be severely damaged when struck by lightning (23, 24). Certain protection systems, such as flame sprayed aluminum or silver coatings, aluminum wire mesh, and thin foil aluminum strips, have been developed by the industry (25, 26). However, while most of these systems may sustain considerable damage during lightning current transfer, they require expensive repair. Thus, from a maintenance point of view, these systems are not desirable. Also, these protection systems can only reduce damage to composite structures, they cannot completely eliminate it. The resulting hidden damage in the structures and the progressive damage by repeated contacts may become a problem.

Douglas lightning protection design experience indicates that it is highly desirable to retain the conventional metal structural components in the Zone 1 regions for direct lightning strike attachment protection. However, for certain designs, the weight reduction requirement may indicate the necessity of using composite structural components in these areas. In this case it may be possible to protect the composite structure using one of the metallic lightning strip protection systems described for the nose radome in the extremity area of the structure as a compromised design. To prevent damage to the conductive composite structures, a nonconductive type adhesive should be used to isolate the lightning strips from the structure. Lightning tests should be conducted to demonstrate that lightning current will indeed attach to the metal strips and transfer through the designed lightning current path avoiding the composite structure path.

**Zone 2 Region** - The dielectric shielding technique provides a promising approach for lightning protection of boron and graphite epoxy composite aircraft structures located in the Zone 2 region of an aircraft. The principle is to apply dielectric materials over the composite skin panel

and use their dielectric shielding strengths to prevent the reattachment of swept-stroke and restrike lightning current to the composite skin panel. The metal bar protection system shown in Figure 17 can be used in conjunction with the dielectric shielding system for the protection of a longer span of composite skin surface. This approach is based on the assumption that sufficient metal structure would be used in the associated Zone 1 region for direct lightning stroke attachment (27).

In the past 2 years, Douglas has conducted swept-stroke and restrike lightning tests over large size (4 by 8 feet) boron and graphite epoxy composite skin panels. Test results indicated that this dielectric shielding approach is feasible. Additional development work is currently being carried out by Douglas to facilitate the use of this technique on actual aircraft flight installations.

The aluminum mesh surface protection technique (28) is another approach. This technique utilizes thin aluminum wire fabric to cover the composite skin panel so that most of the swept-stroke and restrike lightning current will attach to and travel through the aluminum wire fabric. When using this protection system design precautions should be undertaken to avoid the following hazards:

- Sparking at bolts and joints in the fuel tank or critical fuel vapor area during the transfer of lightning current.
- Structural strength degradation of the composite skin panel at the point of lightning attachment and associated joints that provide the current path to aircraft.
- Progressive undetected structural degradation caused by repeated strikes during the life of the aircraft.

**Zone 3 Region** – The basic design concept here is to prevent lightning current from transferring through composite structures located in these regions by providing adequate conductive paths across these regions. Metal strips or bars may be used to transfer lightning current across this region. However, they should be properly designed to avoid sharp bends or corners, which may be damaged by the magnetic forces during the transfer of lightning current.

If this is not possible, composite laminates and associated structural joints should be designed in such a manner so as to prevent damage resulting from the transfer of lightning current. Techniques of increasing the lightning current carrying capabilities for boron and graphite epoxy composite laminates are being investigated by General Electric High Voltage Laboratory and the Philco-Ford Corporation (29, 30). Douglas is currently studying the lightning current transfer characteristics through composite-to-composite and metal-to-composite structural joints with the objective of establishing design requirements for the safe transfer of various types of lightning current.

The electromagnetic shielding properties of composite skin panels are much poorer than conventional metal skin panels (31). Thus, electrical wiring systems located within structures containing composite skin panels are more vulnerable to lightning current impulse coupling. The following design guides can be undertaken to reduce the coupling voltage to a safe level.

- The use of appropriate ground return paths for electrical wiring systems.
- The shielding of exposed critical wiring by enclosing in a grounded metal conduit.
- The twisting of wire pairs of critical circuits.

- The proper orientation and location of wires within the structure.

**GLASS FIBER REINFORCED COMPOSITE AIRCRAFT** – The glass or nonconductive fiber reinforced plastic aircraft is not immune to lightning strikes. In fact, a composite aircraft whether fabricated using conductive or nonconductive reinforcement fibers is more difficult to protect from lightning than an aircraft with a metal skin. This is because the conventional metal skin can satisfactorily shield metal control cables, fuel tanks, engines, and other critical components and the pilot and passengers from lightning. Special features must be added to a plastic aircraft to provide the necessary lightning protection.

An aircraft extremity, even though fabricated of a material normally considered to be nonconductive, can provide a high gradient point to which lightning may attach. A lightning stroke can enter the reinforced plastic structure causing severe damage if the structure is moisture contaminated or houses conductive components. The zones for a plastic aircraft may be somewhat different than for the conventional metal aircraft. Metal cables, wires, tubes, etc., may terminate halfway to the tip of the wing presenting a potential direct attach point at the center of the wing rather than at the wing tip. This would create different Zone 1, 2, and 3 regions than normally considered for metal aircraft.

Local attach point studies for plastic aircraft should be made on full-scale aircraft or full-scale sections, such as the nose radome, rather than scale models. This is because the thickness of the dielectric walls affects the streamer characteristics of the metal components within the structure. These tests would aid in establishing accurate Zone 1, 2, and 3 areas for a specific aircraft design.

**Zone 1 Region** – Zone 1 regions on a plastic aircraft can be protected by using metal skins, lightning diverter rods, or electrostatic shielding of the type discussed for the nose radome. Where possible, the use of metal components within plastic aircraft, which may become a direct attach point, should be avoided. Metal control cables should also be shielded as required.

Electrical wiring circuits located within plastic fuel tanks on wing tips may present a particular hazard for plastic aircraft. The wires can provide an attach point and conductive paths for lightning current in a highly vulnerable area. The wires would vaporize when struck by lightning creating an explosive force which can cause severe structural damage and possible fuel ignition. Thus, the installation of wiring or other metal components in the tip tanks should be avoided. If necessary, the plastic tip tanks can be protected in a manner similar to other plastic sections of the aircraft. Care should be taken to assure that both Zone 1 and Zone 2 protection of the tip tanks is considered.

**Zone 2 Region** – Metal components such as wiring and cables in Zone 2 regions can be protected from swept strokes using metal bars or frames which provide external conductive paths normal to the airstream as shown in Figure 17. The lightning channel may then "hang on" and transfer from one bar to the next shielding metal component on the aircraft. Spacing between the metal bars is a function of the dielectric strength of the wall and the shape and distance from the wall of conductive objects housed within the structure. Metal bars installed parallel to the airstream will not provide swept-stroke protection unless



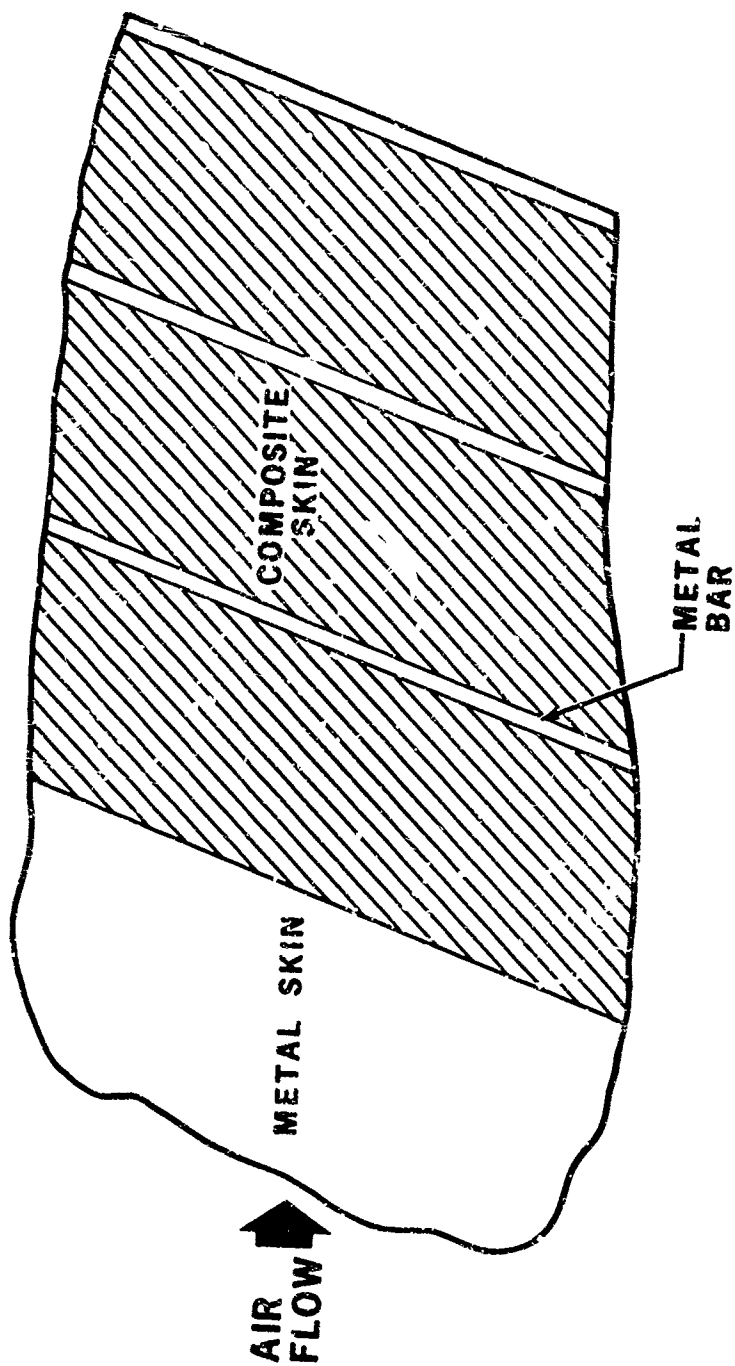


Fig. 17 - Metal bar protection system on composite skin panel

they extend to the leading edge of the vulnerable area as shown in Figure 18. Where the parallel metal bars are installed aft of a metal section, the lightning channel may sweep between two bars puncturing the wall as it sweeps back attaching to metal components beneath the plastic structure as shown in Figure 19.

**Zone 3 Region** - Hazards of electrical wires used in conjunction with fuel tanks have been discussed. Except for fuel ignition, the same hazards exist for any unprotected wiring in the aircraft including the wiring to lights which are normally located at the aircraft extremities. Further, the transfer of lightning current through an electrical wire in a plastic aircraft can cause failure of the power generating system and a direct hazard to the pilot. Lightning arresters or surge protectors may be used in these wiring circuits as required.

A pilot is usually well shielded from lightning in a metal aircraft even though special protection features may be required for canopies. In a plastic aircraft the pilot can be protected using the same systems discussed above. The canopy can be protected using one of the systems discussed under canopies in this paper. The canopy protection system would probably include an external metal ring around the base of the canopy.

External metal strips or bars should be installed in this region, as required, to transfer lightning current from one extremity of the aircraft to another. These installations should be designed to avoid sharp bends or corners which may be damaged by the magnetic forces during the transfer of lightning current.

## CONCLUSIONS

Many different types of lightning protection techniques are required to be incorporated in a single aircraft to provide for safe operation in the lightning environment. They are developed for each individual aircraft component according to its specific application and location on an aircraft. The various phases of the lightning strike phenomena, such as the prestrike phase, the high peak current phase, and the heavy coulomb phase, have different damaging effects on aircraft components. The zonal design concept can be used to divide the aircraft into regions, such as the direct attachment region, the swept-stroke and restrike region, and the lightning current transfer region, which can be specifically related to the various phases of the lightning strike.

Through the above methods appropriate lightning protection designs can be developed. These protection designs require the consideration of all inflight environmental effects as well as the serviceability and maintainability of proposed protection systems. In certain cases, the protection system side effects, such as the p-static effect, the antenna radiation effect, and the electromagnetic shielding effect, become important aircraft system performance considerations. These side effects should be identified early in the design of the aircraft so that appropriate lightning protection systems that are compatible with all aircraft system performance requirements, can be developed and incorporated.

The aircraft lightning protection design considerations discussed in this paper are based upon available information. Many factors are still unknown, especially those associated

with the prestrike and the cloud-to-cloud lightning stroke phenomena, which may have an effect on certain lightning protection design features. Research efforts should be continued until all phases of the natural lightning strike to aircraft phenomena can be understood, and improved design criteria of aircraft lightning protection can be established.

## REFERENCES

1. N. Cianos and E. T. Pierce. "A Ground Lightning Environment for Engineering Usage." SRI Project 1834, Contract Number L.S. 2817-A3. Prepared for McDonnell Douglas Astronautics Company, August 1972.
2. M. A. Uman. "Lightning." McGraw Hill, New York, 1969.
3. R. J. Fisher and M. A. Uman. "Measured Electric Field Rise Times for First and Subsequent Lightning Return Strokes." *Journal of Geophysical Research*, Volume 77, pp. 399-406, January 20, 1972.
4. M. A. Uman. "Comparison of Lightning and a Long Laboratory Spark." *Proceedings of the IEEE*, Vol. 59, No. 4, pp. 457-466, April 1971.
5. M. M. Newman, J. R. Stahmann, and J. D. Robb. "Experimental Study of Triggered Natural Lightning Discharges." FAA Report No. DS-67-3, Lightning and Transients Research Institute, March 1967.
6. D. F. Williams and M. Brook. "Magnetic Measurements of Thunderstorm Currents." *Journal of Geophysical Research*, Volume 68, No. 10, pp. 3243-3247, May 15, 1963.
7. "Protection of Aircraft Fuel Systems Against Lightning." FAA Advisory Circular AC 20-53, October 1967.
8. J. R. Stahmann. "Model Studies of Stroke Probability to Selected Points on Aerospace Vehicles." SAE Paper 700915, 1970 Lightning and Static Electricity Conference, December 1970.
9. M. P. Amason and G. J. Cassell. "Radome Lightning Protection Techniques." Douglas Aircraft Company, Technical Paper No. 5839. 20th Annual Symposium on United States Air Force Antenna Research and Development, 13-15 October 1970.
10. M. M. Newman, J. D. Robb, and J. R. Stahmann. "Lightning Protection Measures for Aircraft Fuel Systems, Phase I." FAA Technical Report ADS-17, May 1964.
11. C. C. Bolta, R. Friedman, G. M. Griner, M. Markels, Jr., M. W. Tobriner, and C. Von Elbe. "Lightning Protection Measures for Aircraft Fuel Systems, Phase II." FAA Technical Report ADS-18, May 1964.
12. R. O. Brick. "A Method for Establishing Lightning-Resistance/Skin-Thickness Requirements for Aircraft." Lightning and Static Electricity Conference, 3-5 December 1968; AFAL-TR-68-290, Part II, May 1969.
13. R. O. Brick, et al. "The Significance of Advanced Structural Fabrication Techniques on Aircraft Lightning Protection." SAE Paper 680290. The Boeing Company, April 1967.
14. M. Markels and J. M. Spurlock. "Aircraft Fuel Vent Line Sensitivity to Lightning Effects." Lightning and Static Electricity Conference, 3-5 December 1968; AFAL-TR-68-290 Part II, May 1969.
15. M. P. Amason. "Douglas Aircraft Company Lightning Protection Research and Development Capabilities."

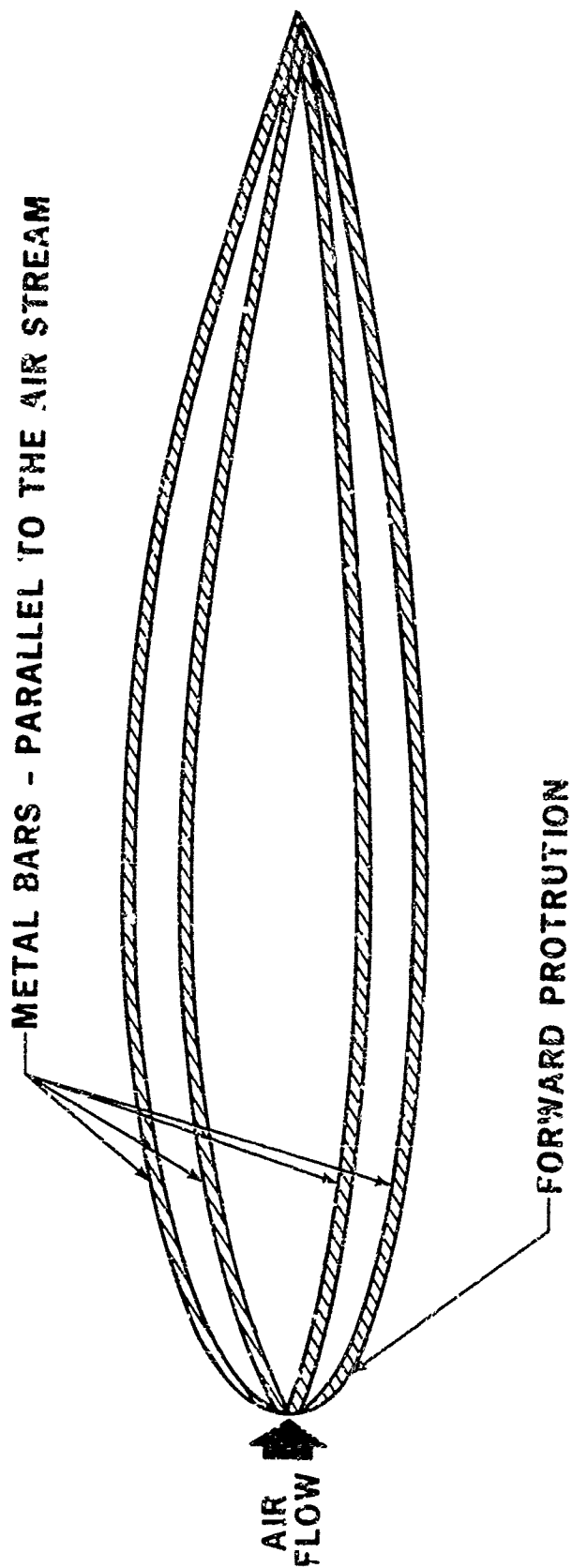


Fig. 18 - Metal bar protection system

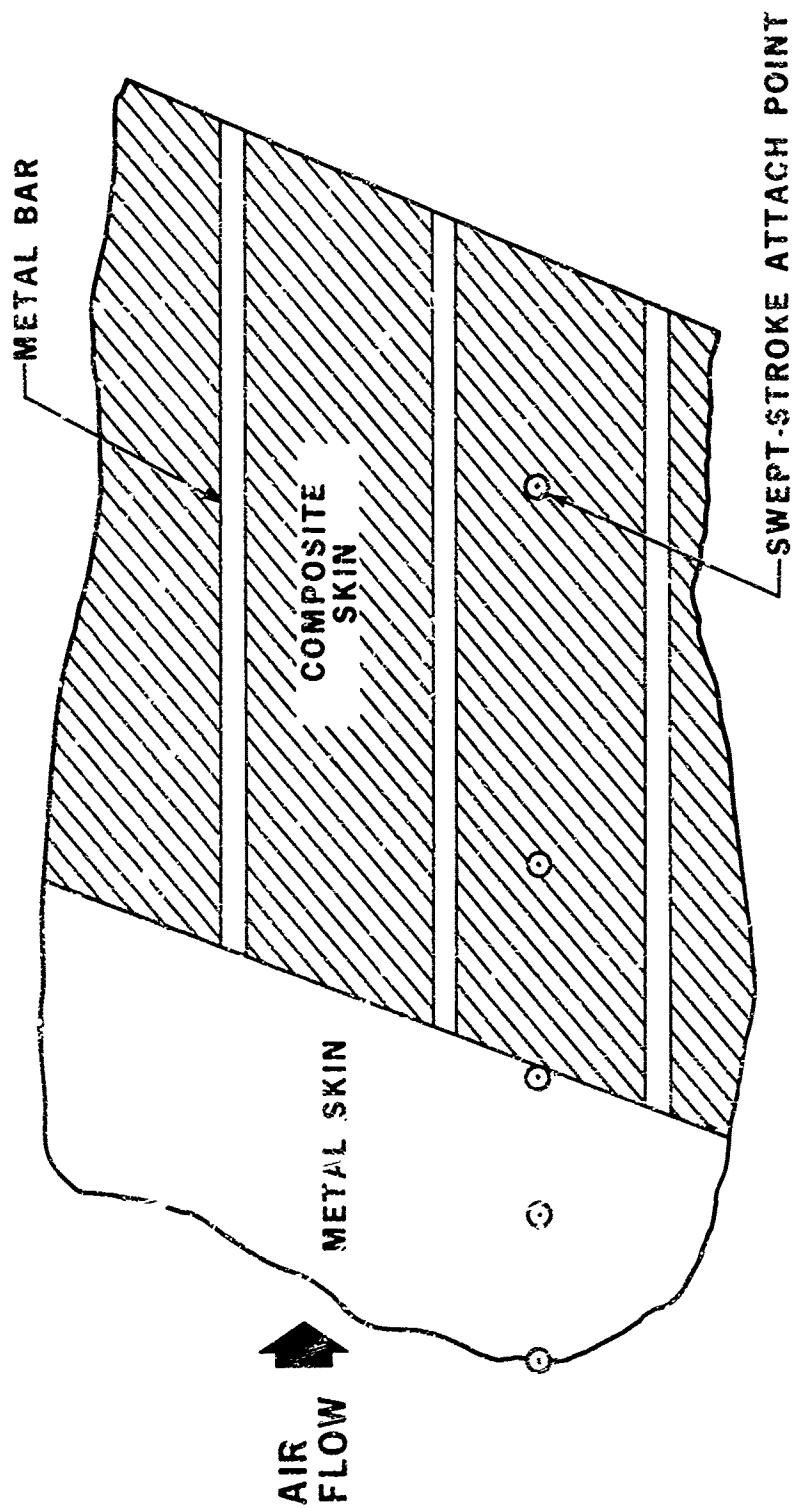


Fig. 19 - Unsatisfactory metal bar protection system

Douglas Aircraft Company, Technical Paper No. 5692, November 1969.

16. M. P. Amason and J. T. Kung, "Lightning Current Transfer Characteristics of the P-Static Discharger Installations." Douglas Aircraft Company, SAE Paper No. 700923. Lightning and Static Electricity Conference, 9-11 December 1970.

17. G. L. Weinstock and B. F. Arnold, "Improvement of Lightning Protection on USAF and FMS Aircraft." McDonnell Aircraft Company, Final Report for ECP 8137, Report No. MDC A1288, 20 August 1971.

18. R. Aston, "F-15 Scale Model Lightning Attach Point Study." McDonnell Aircraft Company, Report No. A0719, November 1970.

19. R. Aston, R. Gorton, and G. L. Weinstock, "Lightning Protection Techniques for Large Canopies on High Speed Aircraft." McDonnell Aircraft Company, Technical Report AFAL-TR-72-49, January 1972.

20. R. O. Brick, L. L. Oh, and S. D. Schneider, "The Effects of Lightning Attachment Phenomena on Aircraft Design." The Boeing Company, SAE Paper 700925. 1970 Lightning and Static Electricity Conference, 9-11 December 1970.

21. "Lightning Discharge Sweeping Effects on Current Pitting of Painted Aircraft Skins." Lightning and Transients Research Institute, Report No. 530, April 1971.

22. K. J. Lloyd, J. A. Plumer, and L. C. Walko, "Measurements and Analysis of Lightning-Induced Voltages in Aircraft Electrical Circuits." General Electric High Voltage Laboratory. NASA CR-1744, February 1971.

23. J. C. Kelly and H. S. Schwarta, "Investigation of Lightning Strike Damage to Epoxy Laminates Reinforced with Boron and High Modulus Graphite Fibers." Lightning and Static Electricity Conference, 3-5 December 1968, AFAL-TR-68-290, Part II, May 1969.

24. M. P. Amason and J. T. Kung, "Lightning Protection of Advanced Composite Aircraft Structure." Douglas Aircraft Company, Report No. MDC J5002, December 1970.

25. R. O. Brick, C. H. King, and J. T. Quinlivan, "Coatings for Lightning Protection of Structural Reinforced Plastics." The Boeing Company, Technical Report AFML-TR-70-303, Part I, March 1971; and Part II, February 1972.

26. G. T. Woodrum, "Lightning Protection for Advanced Composite Aircraft Structures." SAE Paper No. 700935. Lightning and Static Electricity Conference, 9-11 December 1970.

27. M. P. Amason and J. T. Kung, "Dielectric Shielding Lightning Protection for Composite Aircraft Structures." Douglas Aircraft Company, Technical Paper No. 6037, published in 1972 Lightning and Static Electricity Conference, December 1972.

28. H. T. Clark, "Advanced Development on Vulnerability/Survivability of Advanced Composite Structures." McDonnell Aircraft Company, AFML Contract No. F33615-71-C-1414, Report No. MDC A1530, January 1972.

29. A. P. Penton, J. L. Perry, and K. J. Lloyd, "The Effects of High Intensity Electrical Currents on Advanced Composite Materials." NASC Contract No. N00019-71-C-0063, Philco-Ford Corporation, Report No. U-5018, March 1972.

30. J. L. Perry and K. E. Crouch, "The Effects of High Intensity Electrical Currents on Advanced Composite Materials." NASC Contract N00019-72-C-0205, Quarterly Progress Report No. 1, Philco-Ford Corporation, June 1972.

31. F. A. Fisher and W. M. Fassell, "Lightning Effects Relating to Aircraft Part I - Lightning Effects on and Electromagnetic Shielding Properties of Boron and Graphite Reinforced Composite Materials." Technical Report AFAL-TR-72-5; General Electric High Voltage Laboratory, January 1972.

## B-1 Lightning and Electrification Program

Harry Z. Wilson  
North American Rockwell (NR)

John D. Robb  
Lightning and Transients Research Institute  
(LTRI)

### ABSTRACT

Lightning and electrification protection programs are now recognized by the military, NASA, and the FAA as being essential for most aerospace vehicles. Safety of flight, the cost per vehicle, and the importance of completing the assigned mission are some of the factors that weigh in favor of such programs. In particular, the hazard to aircraft increases with size, speed, and low-level flying, and with greater use of nonmetallic materials, sensitive solid-state devices, and computerized flight control. Therefore, it was determined early in the design stages that lightning and electrification protection would be incorporated into the B-1 aircraft.

FAMILIARIZATION with the B-1 aircraft will be gained by observing Figures 1, 2, and 3.

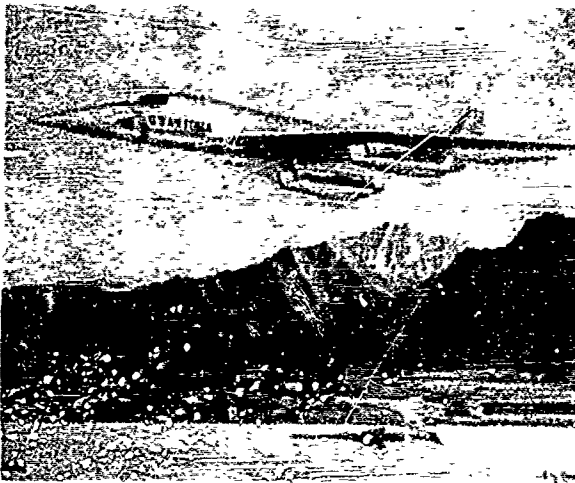


Fig. 1.

Three such aircraft are presently under construction to provide the Air Force with the necessary information, through research, development, test, and engineering (RDTE), with which to base a production decision. The first two will be equipped with basic flight equipment to provide proof that the aircraft will fulfill the aerodynamic and structural requirements.

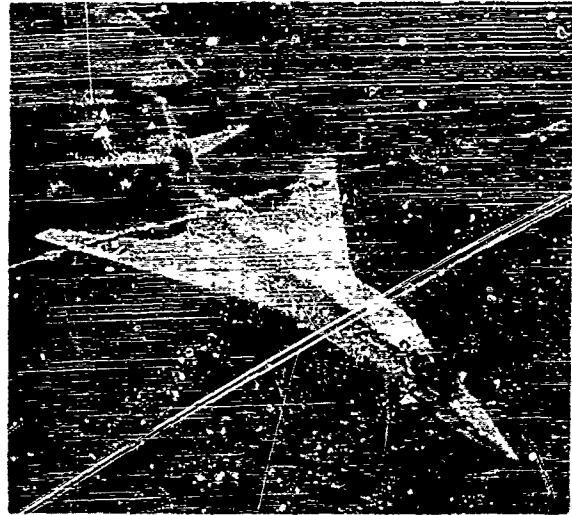


Fig. 2.

The third air vehicle will be equipped with offensive avionics to verify its strike capabilities, i.e., radar penetration and weapons delivery.

The B-1 has a wing span of 136 feet when the wings are forward and 78 feet when the wings are swept aft. Its length is 148 feet, its height 34 feet, and its gross weight from

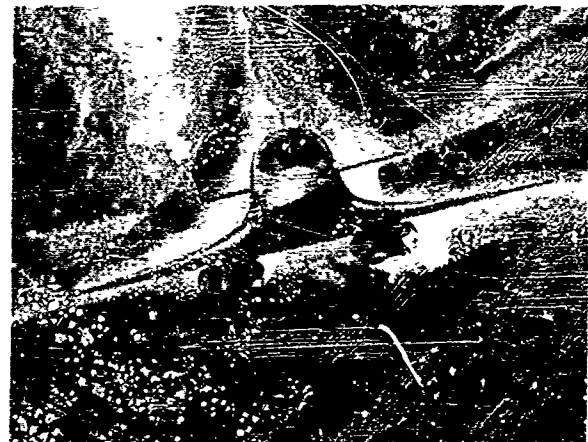


Fig. 3.

350,000 to 400,000 pounds. It has four General Electric jet engines, each of the 30,000-pounds thrust class. Its speed is almost mach 1 for low-level penetration and above mach 2 at high altitude. Air vehicle No. 1 is scheduled for rollout in February 1974 and its first flight is scheduled in May of that year.

The B-1 is an all-weather aircraft, capable of completing the most severe of military missions despite the ever-present atmospheric hazards due to the effects of lightning strikes and precipitation static (P-static).

#### LIGHTNING AND P-STATIC CONTRACT REQUIREMENTS

The requirements for the system, which consists of the B-1 Air Vehicle, the Ground Support Equipment, and the Training Equipment, are outlined in the B-1 system specification. It requires compliance with MIL-E-6751D, which covers bonding, lightning, and static electricity.

The Prime Item Development Specification covers the B-1 vehicle only. In addition, it requires compliance with MIL-F-38363 for fuel system bonding and lightning hazards, with FAA AC20-53 for lightning protection of the fuel system, and with MIL-C-38373 for lightning protection of the fuel tank filter cap. It is intended that the B-1 will be "designed to" and "tested for" compliance with these specifications. For the three RDT&E air vehicles, the lightning test requirements were amended to add, "Lightning strike tests will be conducted only where it cannot be shown by analysis or similarity of previous design that a lightning strike does not constitute a safety-of-flight hazard." In other words, it must be determined if the RDT&E B-1 can fly safely without the section or component under consideration. If it can, LTRI, which is providing engineering assistance, will determine the required protection without tests. If it cannot, LTRI must determine the required protection design and verify by tests.

#### PROGRAM TASKS

A program plan was developed to insure that the B-1 is designed and developed to comply with the lightning and electrification (P-static) requirements. It outlined the tasks of the various in-house design groups and LTRI, and specified those required to budget the funds necessary to carry out the program. A work schedule was also included.

A test plan was developed for describing the tests necessary to determine the areas on the aircraft most likely to be struck by lightning, and the number of static dischargers required and their locations.

#### DESIGN REVIEWS

Preliminary design reviews were conducted with the various in-house engineering design groups and with a representative of LTRI early in the program. Protection recommendations, within the scope of the contractual specifications, were made on the spot as each engineer presented the structural design for which he was responsible. This provided timely direction which, for the most part, could be implemented into the program with little or no difficulty. Equally important, basic protection was designed into the aircraft through continuous bonding as contrasted to the less desirable add-on protection.

Test results and design recommendations received from LTRI are directed to the corresponding engineering design groups via the protection engineering supervisor for incorporation into the RDT&E aircraft.

#### MODEL TESTS

Model studies were conducted to determine the probability of strikes to the various parts of the aircraft (Figure 4). The strike point data also points up unusual strike patterns which might not be anticipated from analysis of similar aircraft, such as strikes to both communications antennas observed by LTRI in earlier aircraft test programs.

It is worth noting in this partial sequence of tests (Figure 5) that lightning strikes are attracted to the horizontal and vertical tail tips, thus providing protection to the tail cone. Also, the top forward blade antenna and the nose pitot boom provide protection against direct strikes to the windshields and nose radome.

Ninety percent of the strike points involved the nose pitot boom, the wingtips, and the vertical and horizontal stabilizer tips (Table I). Other strike points are presented in the table, as well as the percentage of strike points for another swing-wing aircraft which may be used for comparison.

Electrolytic tank plots of the model (Figure 6) were conducted to provide the basis for the determination of antenna and airframe threshold potentials, and the static discharger configuration.

These tank plots were drawn in the vertical and horizontal planes with the wings swept in various positions. From this data, the discharger locations were determined. The major factors utilized in optimizing discharger locations are the trailing edge electric field and the discharger spacing. As a rule, the



Fig. 4 - B-1 model lightning strike test.

discharger threshold and its discharge capability is improved with the increasing electric field produced as a result of the aircraft geometry. This increasing electric field is shown by the narrower spacing of the equipotential lines in the two-dimensional plot shown in Figure 7. These equipotentials were measured in a three-dimensional electrolytic tank. The plot thus indicates that a concentration of dischargers should be placed near the trailing edge tips. Conversely, wind tunnel studies by LTRI have shown that locating dischargers too closely together reduces their discharge capacity due to their inherent shielding quality; for example, two dischargers with no spacing between them would have little better performance than a single discharger. Combining the trailing edge electric field effects with the discharger shielding function will yield an optimized configuration. This must be modified by the space charge effects formed by the particle charging of forward areas and the interference produced

by other trailing edge components such as fuel jetison tubes and aileron edges. Also, the plots permitted the quantitative P-static performance in terms of corona threshold potentials.

In Figure 8, the threshold potentials are shown on the aircraft without dischargers. The difference between the aircraft potentials shown and the discharger threshold potential illustrates that the discharger increases the corona threshold potential of the basic airframe. The major functions of the discharger are to reduce the aircraft potential and to quietly dissipate the accumulated charge due to atmospheric precipitation and engine exhaust, thereby permitting operation of the HF communications in low-signal strength areas. It was initially determined that 44 dischargers were needed for each B-1 aircraft. This number was reduced to 41 due to the location of the fuel dump at each wingtip, and provisions for the future installation of an antenna within the vertical tail tip. The primary emphasis in the precipitation static program for the B-1 has been a balanced approach to include, in addition to an adequate discharger installation, the use of resistance paints on forward dielectric skin areas and careful attention to bonding of electrically floating external skin sections.

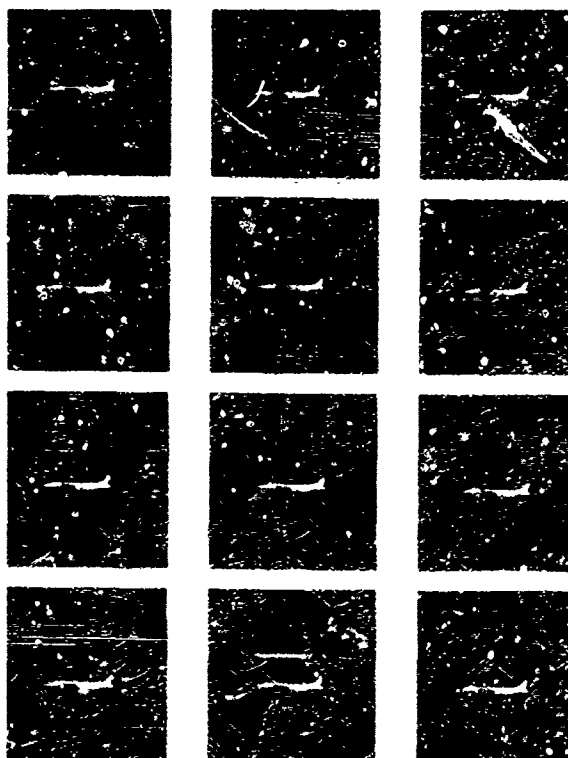


Fig. 5 - Partial sequence of 1.5-million-volt strikes to model about pitch axis.



Table I  
PERCENT DISTRIBUTION OF STRIKE POINTS  
B-1 MODEL STUDIES

	Configuration				Other (1) Swing- Wing Aircraft
	(1) I	(2) II	(3) III	(4) IV	
Pitot boom	25.0	25.0	26.0	28.0	24.0
Wingtips	41.0	40.0	39.0	40.0	38.0
Vertical Stabilizer	9.7	10.0	10.0	10.0	13.0
Horizontal stabilizer	14.0	14.0	15.0	14.0	15.0
Engine	4.2	2.3	2.3	1.4	7.0
Mode control fin	0.5	0.5	0.9	0	-
Top antennas	0.9	1.4	1.4	1.4	-
Forward radome base	0	0	0	0	0
Aft radome base (or tail cone)	2.8	3.7	3.2	2.3	1.0
Windshield eyebrow	0.5	0.5	0.5	0.5	2.0
Fuselage, bottom forward	0	0.9	0	0	0
External stores	0	0	2.0	2.8	0

- (1) No external stores
- (2) With external bombs
- (3) With external missiles
- (4) With external fuel tanks

#### SECTIONS AND COMPONENTS TESTS

As the model test progressed, a design review was implemented with the many engineering design groups, and specific aircraft sections and components were recommended to be evaluated and/or tested.

The B-1 sections and components which are to undergo lightning and P-static evaluation

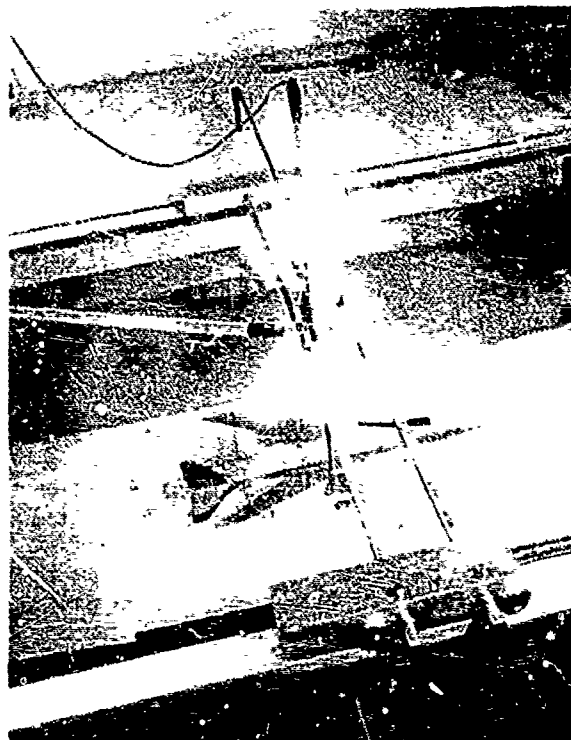


Fig. 6 - B-1 model in electrolytic tank over ground plane.

and/or tests are:

#### Safety of Flight Items

- Forward upper and lower wing glove panels
- Energy transfer system
- Horizontal tail spindle bearings
- Radomes
- Windshield/window
- Fuel system components
- External lights
- Pitot boom assembly

#### Engineering Test and Evaluation Items

- Wingtip
- Fin tip
- Blade antenna
- Special test panels
- Fuselage splices
- Wing splices
- Nonmetallic surfaces
- Door seals

#### After Production Decision Items

- Wing slat, wing flap, and mode control bearings
- Aft upper wing glove panel
- Wing pivot structure

The tests began in June of this year and are being conducted at LTRI. Except for five items which will be tested after production decision, the tests are scheduled to be completed in August 1974.

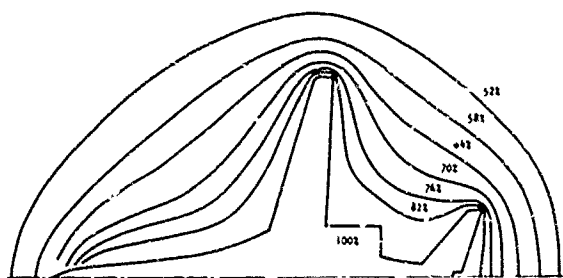


Fig. 7 - Equipotential lines in horizontal plane with wings forward.

#### GENERAL DESIGN CONSIDERATIONS

(1) One of the first considerations confronting NR involved the bonding requirements of MIL-B-5087B versus the corrosion prevention requirements of MIL-F-7179D and the Prime Item Development Specification. The requirements outlined in these specifications are almost in direct conflict with each other; one requires the metallic bonds to have high electrical conductivity, while the others allow no electrical conductivity where the mating surfaces are exposed to the atmosphere. One might think that internal base metal bonds with sealants around the outside periphery would suffice. However, this design is very difficult to maintain because of the continual flexing of each joint while the aircraft is flying. Thus, the sealant may crack and let moisture penetrate the joint.

Therefore, a test plan outlining a series of tests was prepared. It specifies testing a number of samples configured from the ideal electrical bond (bare metal to bare metal), to the ideal bond for preventing corrosion (two coats of primer dried over anodized surfaces),

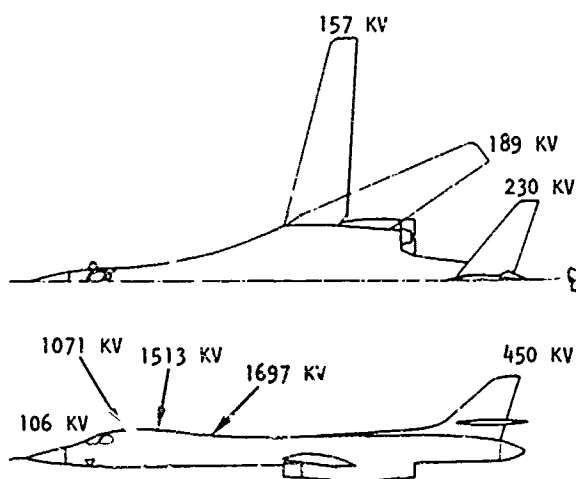


Fig. 8 - Potentials required to bring the aircraft extremities to corona threshold.

with various combinations in between. The results are expected to guide us in the preparation and mating of metal surfaces throughout the construction of the aircraft. (See Figure 9.)

Lightning currents are of sufficient magnitude to penetrate, to some degree, through the joint bonding no matter what configuration is used. However, it will be of interest to determine their destructive effects with respect to the corrosion prevention materials.

(2) There is need for a white, anti-static paint which will withstand high temperatures, have antierosion qualities, and measure 10 to 50 megohms per square. If a paint with these characteristics were applied to all nonmetallic surfaces, it would fulfill a particular set of requirements imposed on the B-1. After an extensive search, a material claimed to be capable of fulfilling

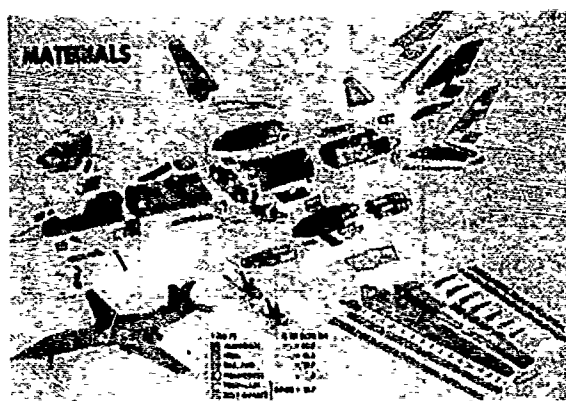


Fig. 9 - Exploded view of B-1 showing materials used.

these requirements was found. This material will be tested to determine its acceptance for use in the B-1 program.

(3) The lightning protection designs for nonmetallic skin surfaces currently being tested include the application of flame-sprayed aluminum, the application of aluminum foil, and the application of a fine mesh aluminum screen. Methods of establishing adequate electrical bonds to the metallic frames are also being investigated. Economics, and the ease of installation and replacement, will play a major role in the selection of the design to be used.

(4) Static dischargers will be installed on the B-1. The plan is to provide two parallel approaches regarding the design of the dischargers themselves. The first is to use and flight test off-the-shelf F-111 hardware, which has flown in an environment similar to the B-1 (high-mach, swing-wing), with minor

modifications to provide assurance that RDT&E schedule dates will be met. The second approach is to develop B-1 tailored designs and have these designs ready in the event that the available dischargers do not prove completely satisfactory. In addition to providing noise quieting, we are looking for a discharger that can withstand high temperatures for long periods of time, is lightweight and causes little or no drag, has antierosion qualities, provides local lightning protection for the aircraft (does not easily cause skin burning), and has good reliability and long service life.

(5) A controlled circuit grounding scheme has been implemented throughout the B-1 system. The aircraft electrical power system is basically a single-point grounded neutral wire return with few exceptions. The electronic circuits are, for the most part, isolated from power by transformers, and grounded to structure only where it is deemed necessary. Each circuit ground is being analyzed in detail by the electromagnetic compatibility engineers. Since lightning may enter the aircraft and damage electrical/electronic circuits and the equipment they are connected to, it was found desirable to prevent those circuits classified as "mission essential," "safety-of-flight," and those appearing at the external surface of the aircraft from being multipoint grounded. This is thought to deter lightning currents from entering at one ground point, traveling along the wire through wire bundles and equipment, and leaving by way of the other ground point(s). This scheme is desirable from an electromagnetic compatibility viewpoint, also. In addition, the circuits exposed to the external surface through electromagnetic windows, such as the nose pitot boom heater wires, the window and windshield-heater circuits, antenna circuits, and all external lights, have secondary protective spark-gap devices as well.

The electrical/electronic wiring is enclosed in conduit runs between shielded equipment bays for protection from the nuclear electromagnetic pulse. In a few isolated cases, where the circuits are terminated outside an equipment bay, the wire that extends beyond the conduit is covered with a braided shield. The shields and conduit are grounded to structure so that any stray electrical energy that is impressed or induced on the shields or conduit may be dissipated directly to structure. These drainage paths, together with spark-gap drainage devices and sufficient conductivity through skin joints, are expected to provide the protection necessary to keep most of the lightning and P-static energies on the external surface of the aircraft.

## SPECIFIC DESIGN CONSIDERATIONS

(1) Normally, the heater wire dielectric strength in the nose pitot boom is approximately 700 volts. The pitot heater wiring will be carried back to the forward bulkhead through copper tubing to reduce the coupled potentials from the lightning currents' high inductive voltages. This voltage across the heater wiring inside the tubing is approximately equal to the product of the tubing resistance and the lightning current or about 500 volts plus the end joint bonding resistance. There will be several parallel paths between the boom and the forward bulkhead through which the energy, from a lightning strike to the boom, must travel. If our "best effort" bonds measure 2.5 milliohms dc resistance per bond, it is estimated that a current flow of 200,000 amperes through these bonds would create between 970 and 1,350 volts potential at the nose boom depending on the number of joints in the final design. This exceeds the dielectric strength (700 volts) of the usual heater wire construction and is considered a potential hazard.

The present protection design includes a dielectric strength of 1,000 volts which has been assured by several vendors without increasing the diameter of the boom, an isolation transformer which has been inserted into the circuit to increase the heater wire dielectric strength to structure, and spark-gap protectors which have been placed across each line to structure between the transformer and the boom, to drain abnormal currents.

(2) The nose radome is about 12-feet long, pointed, and made of polyimide quartz. For obvious reasons, the radar equipment engineers prefer not to have any metal on the radome. However, from a lightning and P-static protection viewpoint, metal strips or buttons should be placed on its surface in addition to an antistatic coating. This type of protection, together with the nose pitot boom acting as a lightning rod, should provide ample protection for the radome. Since it is not known at this time what degradation effects this protection design produces with respect to the operation of the internal radar equipment, the radome will be tested with and without this protection and a trade-off study will be made.

(3) It was recognized at the beginning of the B-1 program that a permanent antistatic coating was needed for the windshields and windows. Glass was thought to be an ideal material, for an applied tin-oxide antistatic coating could be tested at supersonic speeds. However, glass did not fulfill all the requirements imposed, as a 4-pound bird having a

velocity of 650 m.p.h, directed at a 25-degree angle to the windshield, resulted in extensive fracturing and reduced visibility. Also, the glass would have to be approximately 1.4 inches thick to prevent bird penetration.

Comparing an all-glass with an all-plastic 17-square-foot windshield, the glass was found to be the same thickness, 2.2 times heavier, three times more expensive, and to have more optical distortion due to its curvature. Also, glass fractures extensively due to bird impact. Therefore, it was determined that the windshields and windows would be made of plastic. This design is shown in Figure 10.

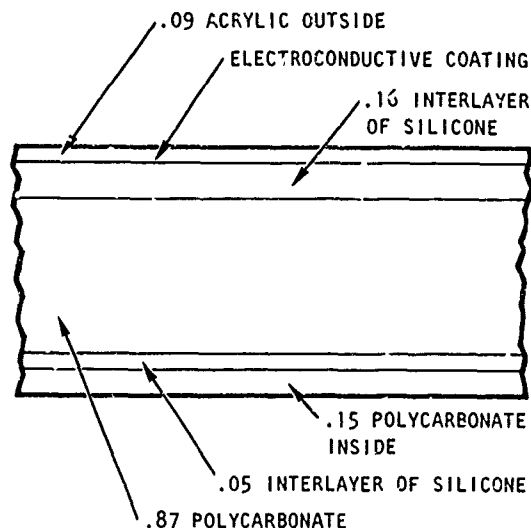


Fig. 10 - B-1 windshield design.

The basic problem with large aircraft windshields is that particle friction charging of the external dielectric surface can store large energies in the parallel plate capacitor formed by the external charge and interior electrical heating coatings. This charge, when accumulated to a sufficient potential, can spark-over to the exterior mounting frame of the windshield, thus inducing large potentials into the heater circuitry potentials corresponding to the discharge of a 60,000-picofarad capacitor charged to 60,000 to 100,000 volts. Because of the obscure nature of this effect, of which most ground maintenance personnel are not aware, such failures are generally attributed to other causes such as electrical component failure in the heater control circuitry, bad relays, etc. Also, if the windshields are sufficiently large and the outer dielectric layer between the external charge and the heating layer is sufficiently thin, puncture may occur to the interior heating layer resulting in shattering of the

windshield outer ply. Also, radio interference is generated by the almost continuous streamer across the windshield exterior during penetration through dry particle clouds. Thus, conductive coatings of some type are necessary on the windshield exterior to limit the external potentials which can be accumulated and thus eliminate the damages which can be produced.

An approach is being tried which has been successfully used on nontransparent radome coatings in which a conducting rubber is covered by a thin layer of 5 to 10 mils of an insulating rubber surface. Because of the large surface area and thin dielectric coating, the external charge can drift through the low resistance of the thin layers to the sub-surface conductive coating to limit the precipitation static potentials. This approach is being proposed by Goodyear Aerospace Corporation for the B-1 windshield in which the plastic outer windshield ply is being covered with two transparent coatings - one conducting to bleed the charge off and an external hard coating to withstand the severe in-flight erosion environment.

(4) All fuel system components will be evaluated. Many will be tested for lightning and/or P-static protection in accordance with the innovations program. These are included in the foregoing list of sections and components to be tested.

The fuel tank skin thicknesses have been designed to fulfill the lightning protection requirements of the FAA Advisory Circular 20-53. This circular specifies 0.030-inch aluminum or the equivalent to prevent penetration of a dwell stroke in the zone 1 area. Zone 1 is defined as the area within 18 inches of the leading edge of the wings (they sweep back more than 45 degrees) and wingtips, the trailing edge of the horizontal tail and horizontal tail tips, and the vertical tail tip. Also included are the nose pitot boom, nose and aft radomes, antennas, external stores, air inlet ducts, and engine nacelles. The present B-1 design provides an aluminum thickness slightly less than 0.080 inch over a portion of the zone 2 fuselage fuel tanks. The design also provides a nitrogen inerting system in the fuel tanks for protection against fire and explosions resulting from incendiary projectiles. The inerting system is designed to supply nitrogen for the entire mission. However, this may be cycled for the purpose of supplying the nitrogen only when it is needed. When the fuel tanks are inerted, protection against lightning is provided.

(5) Bonding across the movable wing

poses a problem as the wing is designed to slide over plastic runners for a considerable distance. The only practical location for bonding the wing to the wing carry-through structure is at the wing pivot. The bonding conductor should be of highly conducting metal, such as copper, and shaped in the form of a flexiole tube. This configuration presents a minimum impedance through which the current is expected to flow. However, there will be many metallic "tubes" across the wing pivot which are needed to transport hydraulic fluids and fuel and to house electrical circuit wires. The conductivity is considered ample, and an additional bond is probably not required. However, an adequate bond path is being provided in addition to these tubes and conduit, and the entire configuration is to be tested for lightning protection, after production decision.

(6) The surface of the wingtip is fiberglass honeycomb construction. The tip has a large aluminum cast bow around its periphery, except for an 8-inch wingtip light, which provides a direct electrical path to the wing structure. This tip has the capability of adapting to a wire mesh placed over its surface at a later date without great difficulty should the results from lightning tests dictate its inclusion.

(7) The wingtip light sits in a pie-shaped, quarter-segment, metal frame. Its 1/4-inch-thick glass has no metal around its outside edge which is approximately 8 inches in length. The lamp sits in the apex of the metal frame in excess of 2 inches from the outside edge of the glass. It is believed that a lightning strike will attach itself to the metal frame rather than shatter the glass to reach the lamp inside. However, backup spark-gap protectors will be placed between the auto transformer and the lamp to limit the energy coupled from a lightning strike to the lamp's circuit. The wingtip with its light will undergo lightning and P-static tests in order to determine further design refinements.

(8) The mode control bearing (the bearing for the forward small canard-type wing surface), the wing slat bearing, and the wing flap bearing will be tested after production go-ahead, as none have been determined to involve safety-of-flight. However, the horizontal tail spindle bearings will be tested during the RDT&E program and adequate protection will be applied.

(9) The third RDT&E aircraft may have a radome at the aft end of the vertical stabilizer tip to accommodate several internal

antennas. At this aft end, it is desirable to place a static discharger for the reduction of RF noise. However, any metal appearing in the view of the antennas, other than a discharger needle, would be detrimental to the operation of the internal equipment. Therefore, our lightning and P-static protection design for the vertical stabilizer tip includes a discharger rod that extends beyond the aft tip, a metal shank approximately 2 inches long for lightning protection, a metal base metallicly fastened to a wire mesh imbedded in the top of the radome forward of the antenna view, and adequate bonding of the mesh to the aircraft structure. The entire vertical tail tip will be tested at LTRI for verification of this design.

#### INSTALLATION REQUIREMENTS AND VERIFICATION

Installation requirements and specific instructions will appear on installation drawings. Verification by inspections and tests will be formally presented in an in-house process specification.

Bonding requirements for structure and skin joints will be determined from laboratory tests. Direct current and low-frequency measurements will be made with the hardware installed on a random sampling basis, as well as selected items that will be specified for each aircraft. Direct correlation between the test samples and the assembly line hardware is expected with these two types of measurements.

#### FLIGHT TEST VERIFICATION

A flight test will be conducted with all the electronics operating to verify the effectiveness of the static dischargers. The minimum testing requirements for the effects of airframe electrification, propulsion system charging, corona discharge, etc., will be accomplished by flying under conditions maximizing these effects while operating equipments and testing for degradation of operation.

#### SUMMARY

There are many design areas which require RDT&E effort in order to fulfill the B-1 requirements. These include (1) radomes, (2) windshields and windows, (3) other plastic material surfaces, (4) metallic bonding versus corrosion prevention, (5) a white antistatic paint, (6) static dischargers for the swing wing, and (7) protection for the vertical tail

tip. NR has developed and is implementing a program which will fulfill the B-1 lightning and electrification protection requirements.

#### ACKNOWLEDGEMENTS

The invaluable assistance and technical support rendered by Messrs. Dennis F. Baseley, B-1 SPO Technical Advisor, and Robert B. Shanks, Accident Prevention Aerospace Engineer, Directorate of Aerospace Safety, which have been instrumental in making the B-1 lightning and P-static protection program a success, are hereby acknowledged.

Experimental Investigation of Problems  
Associated with Discharging Hovering  
Helicopters

J. E. Nanevich and D. G. Douglas  
Stanford Research Institute

S. Blair Potente  
U.S. Army Material Research and  
Development Laboratory

B. J. Solak  
Boeing Company, Vertol Division

ABSTRACT

Laboratory and flight tests were performed to investigate various active discharger systems, and sensing problems as they relate to the Boeing 301 HUH Helicopter. Excellent agreement between laboratory studies and flight tests were obtained.

The experiments show that while high net current ( $> 600 \mu A$ ) discharger designs were probably feasible for the HUH helicopter, the accurate sensing of the helicopter potential (with respect to ground) would be very difficult when the helicopter was operated in an external space charge environment.

WHEN CONSIDERING the problem of maintaining the potential to ground of a hovering helicopter near zero, it becomes apparent that the most crucial problems are: a) Devising a scheme for accurately measuring the helicopter-to-ground potential in the presence of charged particles, discharged ions, and external electric fields; and, b) Designing and positioning a discharging element on the helicopter capable of removing from the aircraft the requisite discharge current. There are many other problems associated with the development of a functioning active discharging system such as designing a high voltage supply capable of operating in the helicopter environment, designing a stable servo system, etc., but unless the problems of sensing and discharging have been solved, all other problems are academic.

A review of the general problem quickly indicated that any approach to this investigation must lean heavily on experiment. The geometry of the helicopter is sufficiently complicated that a purely analytical approach to a study of the electrostatic fields in its vicinity is difficult. The problem is further complicated by the fact that a hovering helicopter may not be located in a field-free, charge-free region, but can be surrounded by charged precipitation particles, discharged ions, etc., severely

complicating the sensing problem. The primary limit on current discharged from an element is established by the ion cloud formed about the element by the discharge products, and the complicated airflows which cannot be simulated adequately. Proper description of all of these parameters in sufficient detail to permit an accurate analytic solution appeared impossibly difficult, and an experimental approach was followed instead.

Since flight tests can be very expensive and marginally productive unless they are carefully planned to eliminate as much random testing as possible, it dictated that the flight tests be preceded by thorough laboratory and ground tests to serve as a guide to determining the ultimate course of the flight tests.

With the above arguments in mind, it was decided that the program would be conducted in three phases. In the first, laboratory simulations of various designs of dischargers were carried out at SRI to investigate likely approaches, and to weed out those which proved to be undesirable. In the second phase, ground tests were carried out on a CH-47 helicopter at Boeing Vertol to verify the laboratory results, and to investigate the workability of proposed flight test systems in an actual helicopter environment. In the third phase, flight tests were conducted at the Yuma Proving Grounds, Yuma, Arizona, using an instrumented CH-47 helicopter.

LABORATORY INVESTIGATION OF DISCHARGER DESIGNS

Experience in designing fixed-wing aircraft discharging systems indicates that it is essential that the discharge products be injected into a high velocity airstream to carry them away and minimize the limitation of the discharge by the presence of the discharge ion cloud. In addition, it is important that the discharge products be directed away from any

field sensing devices being used to measure aircraft potential. In casting about for likely locations for discharging elements on a helicopter, one is immediately led to the tips of the rotor blades since these are regions of clearly-defined, high-velocity airflow. Unfortunately, active discharging elements located on the blades greatly complicates rotor design. A second (smaller and slower) region of directed airflow away from the helicopter exists in the engine exhausts. The feasibility of locating discharging elements here was investigated on the present program. A third region of directed airflow away from the helicopter is located amidships in the region where the two rotors intersect. The functioning of a discharging element in this location was also investigated.

In designing a discharging system, one must select a discharger configuration, a discharger location, and an operating potential. Many combinations of these parameters are possible, and to test all of the combinations in flight would be prohibitively expensive. It was decided, therefore, that a helicopter mock up would be used in a laboratory program to investigate a wide variety of discharger arrangements, and to select the most promising for further investigation during the ground and flight tests.

To expedite the investigation of the various design parameters, an operating full-scale model of the discharging system, aft fuselage, and left engine was assembled in the laboratory. This was accomplished by modifying an existing water-wave wind-tunnel facility in the Electromagnetic Sciences Laboratory at SRI. By modifying it slightly it was possible to use this air source to feed a 22-inch-diameter cylindrical tube simulating the helicopter engine exhaust, and achieve a range of exhaust velocities from zero up to 125 fps. The "engine" and full-scale mock up of the aft part of the Chinook helicopter is shown in Figure 1.

Velocity profile measurements indicated that at a position one tail-pipe diameter downstream of the exit plane the flow was still very clearly defined and had not grown appreciably in diameter. Farther downstream, the boundary of the flow slowly became less clearly defined, and the flow became turbulent. These results were interesting, in that they indicate there was little flow actually impinging on the body of the helicopter to cause recirculation. Although the maximum flow velocity in the simulator "engine" was lower than the 300 fps engine exhaust velocity on the CH-47 it was felt that it was sufficiently high to permit realistic investigation of the effects of changes in discharging-element design parameters.

Before testing started in the facility, a variety of possible discharging-element designs were conceived and assembled. Some of these designs were mechanically awkward, while others appeared to be electrically less desirable than others. These "ugly duckling" were deliberately included in the laboratory testing to make certain that no satisfactory design was accidentally discarded as the result of unjustified, preconceived bias.

Several recirculation patches were installed on the mock up so that recirculation currents to the airframe could be measured as well as the recirculation current to the "engine", and the power supply voltage and current fed to the discharger. These measurements, together with a measurement of the current blown downstream in the exhaust allowed an accurate estimate of the effectiveness of the candidate discharger to be made.

Although detailed data were taken for each discharger configuration, it is instructive to look first only at the data for top windspeed and highest supply voltage to see how discharge current varies with discharger configuration. Data for the single discharge point are presented in this abbreviated form in Figure 2. In Column 1 it is observed that as the discharge point is moved farther downwind from the "engine" exhaust plane, the power supply current decreases and the net discharge current increases. These results indicate that the net discharge current achievable is limited by recirculation to the airframe in the immediate vicinity of the discharging element. For this reason, discharging elements positioned far back from the fuselage result in a higher net discharge current even though they are located in a region of somewhat reduced flow velocity.

In Column 2, the effect of moving the discharge point away from the center line of the engine is illustrated. The vertical position V along the centerline resulted in maximum net discharge current. Although moving the point away from the skin to Positions A or B reduced the power supply current, it also reduced the net discharge current. As might be expected, moving the point toward the skin to C increases the power supply current (as the result of increased recirculation) but also reduces the net discharge current. Apparently discharge current is maximized when the ion density is uniformly distributed throughout the exhaust.

Column 3 illustrates the effect of using an auxiliary electrode in an effort to achieve the desired discharge current at lower power supply voltage. Although the power supply current is drastically increased, most of this current flows to the auxiliary ring, and the





FIGURE 1 LABORATORY MOCK UP OF CH-47 HELICOPTER FUSELAGE AND ENGINE

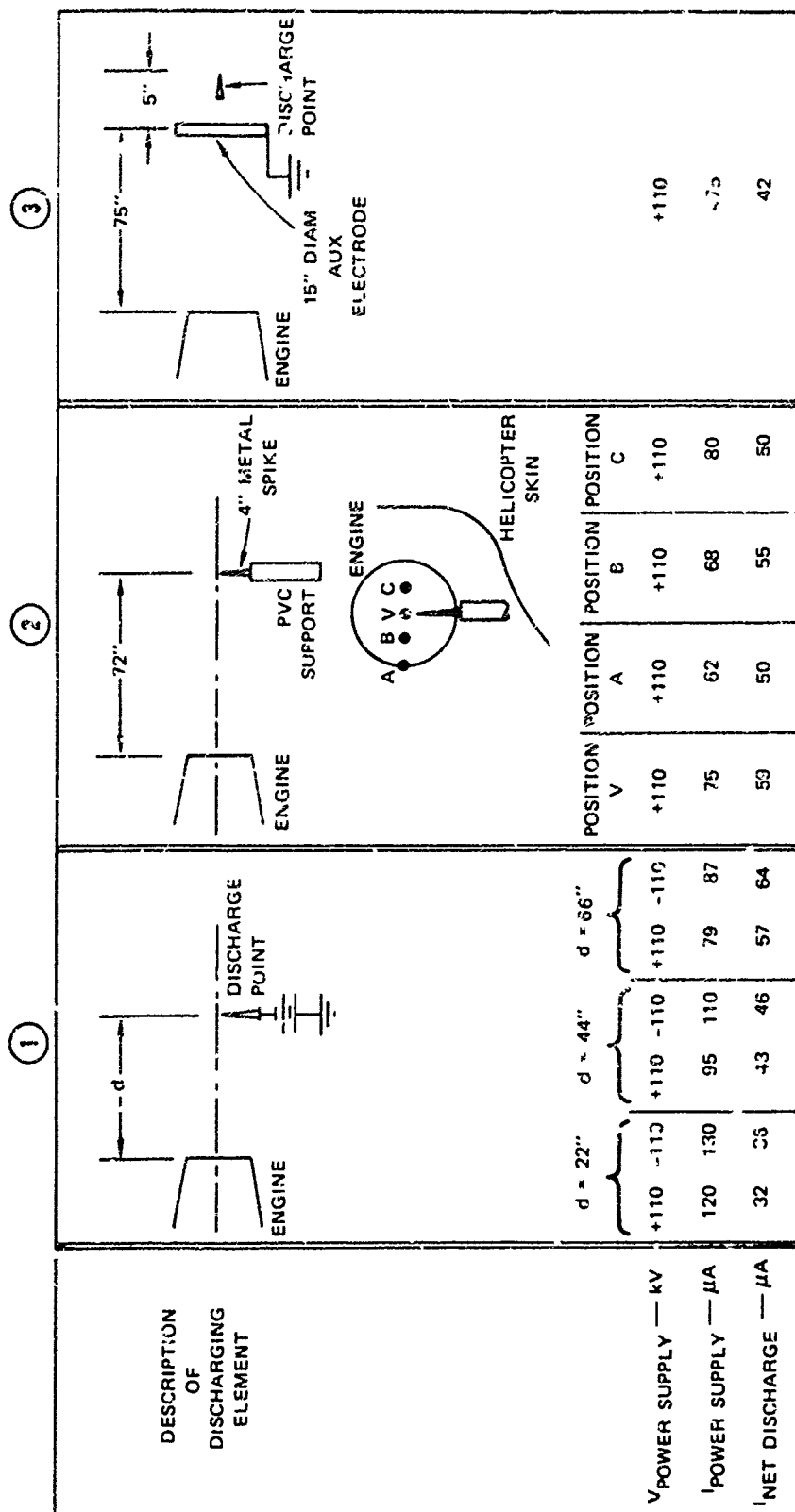


FIGURE 2 GENERAL RESULTS OF EXPERIMENTS WITH DISCHARGER CONFIGURATIONS INVOLVING A SINGLE POINT FOR WINDSPEED = 125 fps

net current is lower than it would have been without the ring.

Results of experiments with various combinations of ring-shaped discharging elements are presented in Figure 3. Column 1 indicates that the net discharging current is relatively independent of the diameter of a single ring used as the discharge element. It should also be noted that this current is almost identical with that obtained with a single point in Column 1 of Figure 2 (positive polarity).

Column 2 of Figure 3 illustrates the results of experiments with discharging elements composed of a discharging ring and an auxiliary ring of the same diameter. Again the performance of the system is evidently not very sensitive to ring diameter. The spacing between the rings does affect system performance, since the spacing determines the maximum power supply voltage that can be used without flashover. In the case of a 2-inch spacing, this is 40 kV. With a 6-inch spacing it was possible to use 90 to 97 kV without flashover. These results indicate that spacings as small as 2 inches are impractical in that they do not permit significant power supply current before flashover. Even a spacing of 6 inches is inadequate to avoid flashover at 110 kV. Finally, it is apparent that at the 125 fps exhaust velocity, substantial recirculation to the ground ring occurs, so that the net discharge current achieved is lower than with a single ring in Column 1.

The results of a series of experiments with rings of unequal size are summarized in Column 3. Although there is some variation in details between these data and those in Column 2, there appears to be no reason to choose one over the other.

Column 4 illustrates the reduction in net discharge current that occurs as the discharging assembly is moved closer to the engine. This is in agreement with the results obtained with a single discharge point in Column 1 of Figure 2.

The last experiment with ring discharger configurations is illustrated in Column 5. It consisted of a pin-filled, 8-inch-diameter ring concentrically mounted inside a 15-inch diameter auxiliary electrode. For the windspeeds available, the recirculation with this arrangement is very high and the net discharge current is low.

In addition to the single point and ring discharger configurations discussed above, several other designs were built and evaluated on the mock up. These designs included small diameter wires placed in various orientations with respect to the exhaust velocity vector, long metal bars similarly placed, etc., but the structural form of these designs was poor and will not be discussed here.

In Figure 4, results were presented of a typical set of measurements exploring in detail the way in which discharger currents are related to power supply voltage. At low power supply voltages, the electric field generated by the supply voltage on the discharging element and the coulomb force generated by the self charge on the ion beam itself are both low, resulting in low recirculating current so that  $I_{net}$  almost equals  $I_{ps}$ . As power supply voltage is increased, it increases the magnitude of both the field generated by the discharging element, and the coulomb forces generated by the increased charge density in the ion beam. The net result is that the recirculation current increases with increased power supply voltage. The increasing recirculation current manifests itself as a divergence between the net discharge current and the power supply current. For the discharger geometry of Figure 4, the system is quite efficient even with a power supply voltage of 110 kV (86% of the power supply current is discharged), and the power supply voltage could probably be doubled without requiring unacceptably high power supply currents.

Figure 5 illustrates the way in which various currents are affected by changes in exhaust velocity. Obviously, as velocity is increased, the net discharge current increases; first, as a lower than first power of velocity, then approaching a linear dependence. The recirculation of current  $I_{body}$  is maximum at zero velocity when the applied field and coulomb field have unlimited time to act on the discharged ions to cause them to be recirculated. As the exhaust velocity is increased, the ions are carried away faster and the recirculation current is diminished. The reduced recirculation current at high windspeeds causes the power supply current to approach the net discharge current.

Andrews and Forrest (1)<sup>N</sup>, in a report received subsequent to these tests, report data which confirm the results described above.

#### HELICOPTER GROUND TESTS OF DISCHARGER DESIGNS

In planning the CH-47 ground tests at Vertol, it was argued that they should be designed to verify laboratory results, to expose interesting discharging element designs to a more nearly true in-flight environment (involving acoustic noise, high temperature, soot, etc.), and to look for unexpected developments. It was felt, furthermore, that the ground tests should be of clearly circumscribed

\* Numbers in parentheses designate References at end of paper.

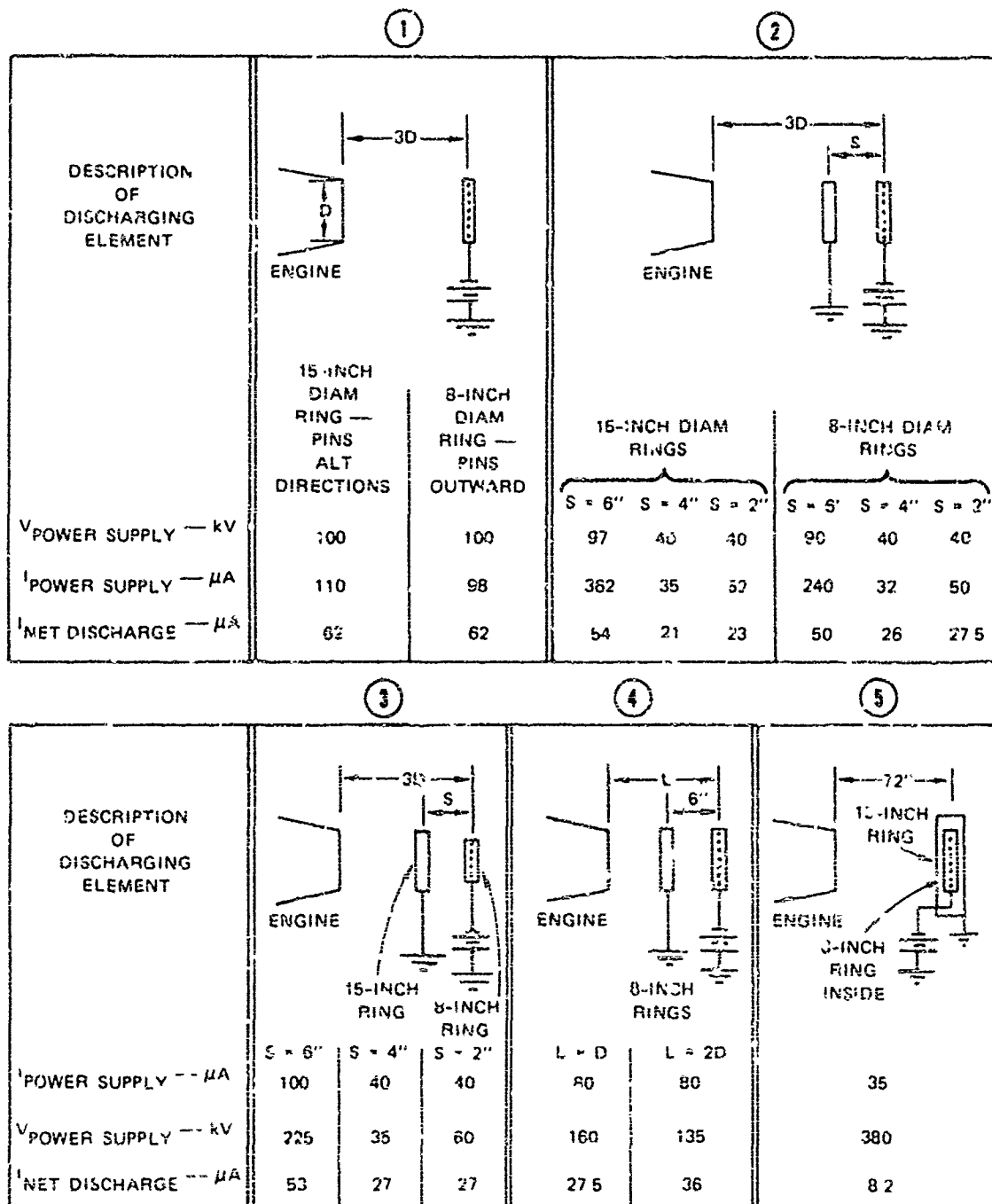


FIGURE 3 GENERAL RESULTS OF EXPERIMENTS INVOLVING RINGS AS DISCHARGING ELEMENTS FOR WINDSPEED = 125 fps

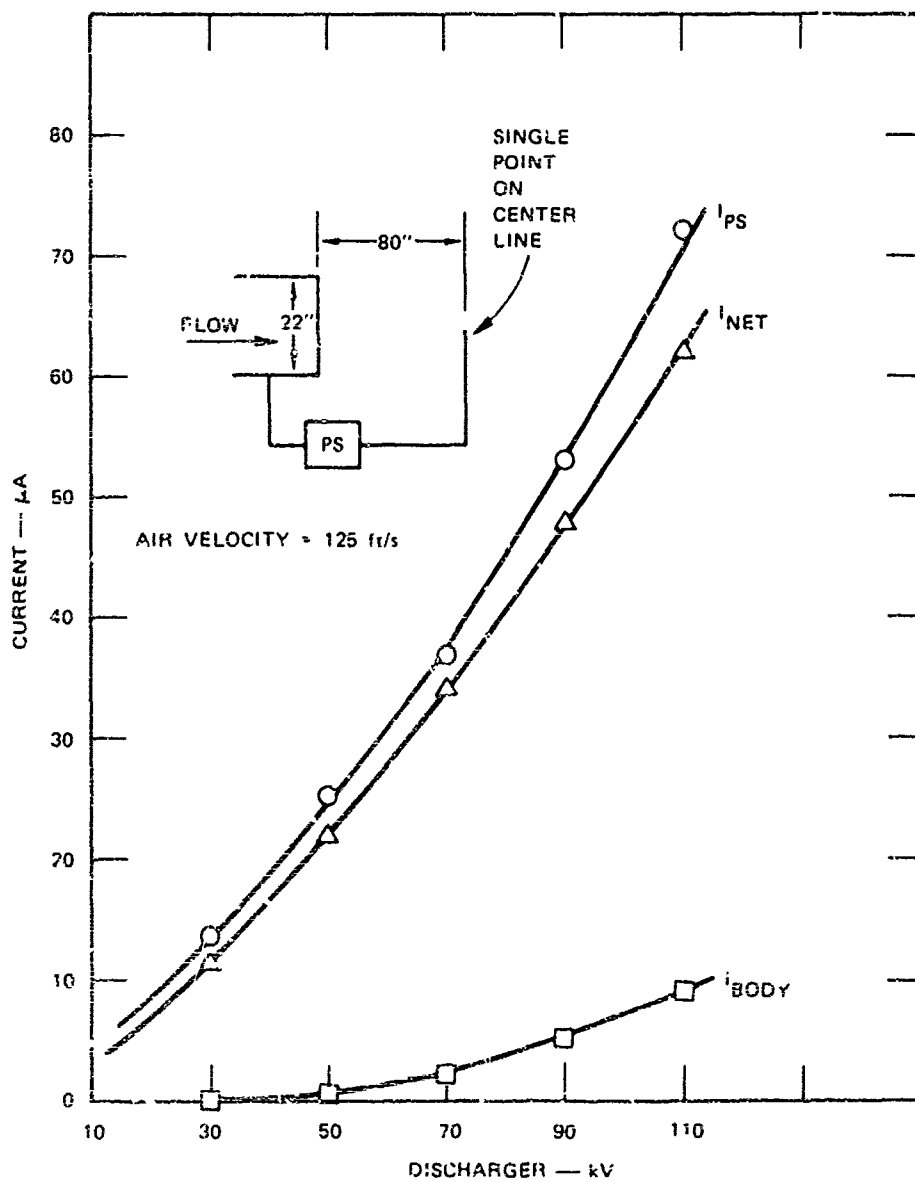


FIGURE 4 RELATIONSHIPS BETWEEN CURRENTS AS POWER SUPPLY VOLTAGE IS VARIED

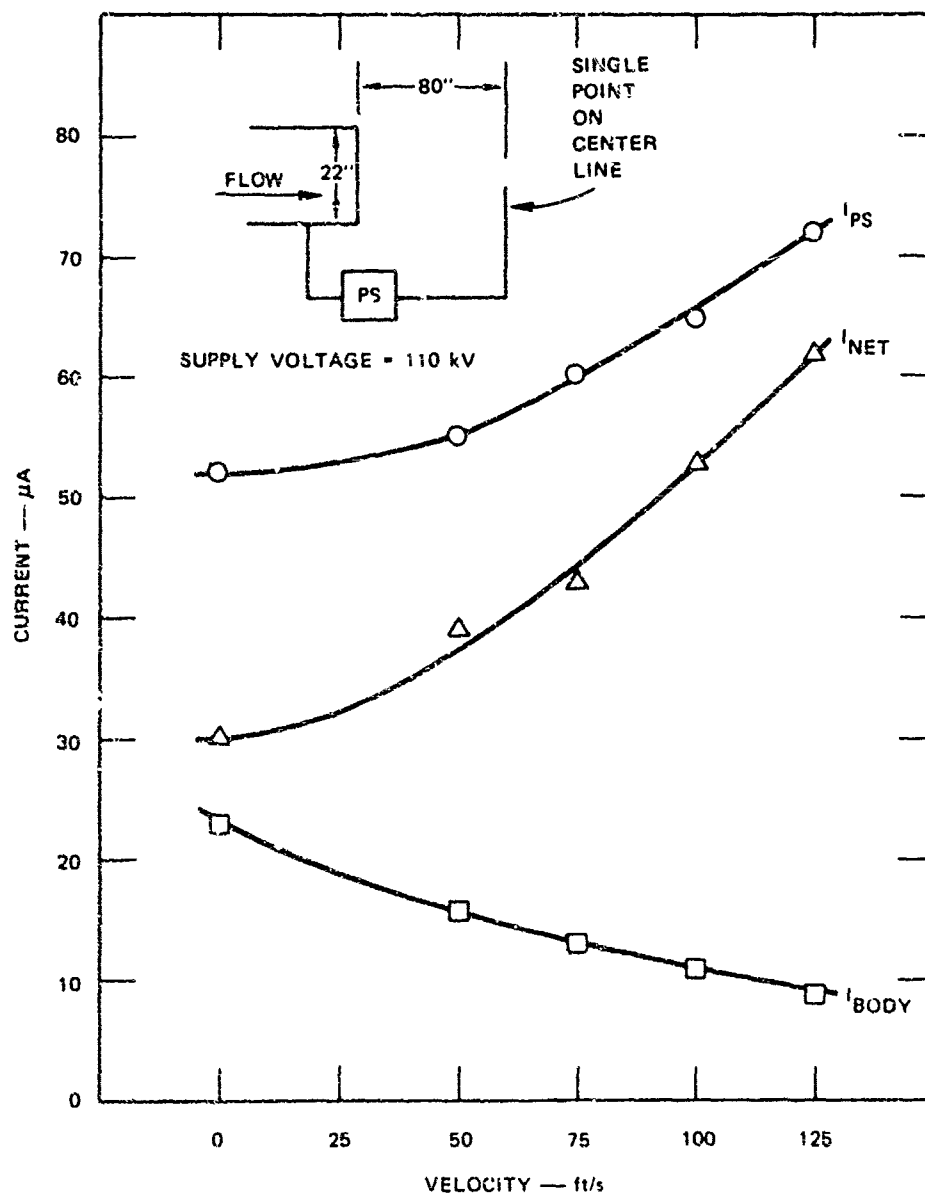


FIGURE 5 RELATIONSHIP BETWEEN CURRENTS AS AIRSPEED IS VARIED

scope, since they are considerably more expensive than the laboratory tests, but are not representative in all respects of the in-flight situation. Accordingly, it was decided that the discharging elements to be investigated would be confined to a single-point discharger and a 12-inch diameter ring discharger, each of which would be used alone or in conjunction with a 12-inch diameter auxiliary discharge electrode for a total of four different configurations.

At the conclusion of the ground tests, a review of the data available indicated that both the laboratory and the ground test data were in good agreement, and that substantial increases in net discharge current accrued from increasing discharger spacing behind the engine exit plane, at least up to the maximum distance  $d = 3D$  investigated (The results of these ground tests will not be discussed in detail here). It was decided that the laboratory investigation should be extended to greater spacings to determine when the current ceases to increase. The results of the work are shown in Figure 6. It is evident that considerable improvement accrued for each configuration tested by increasing the spacing up to  $d = 5D$ . The discharger efficiency curves also plotted in Figure 6 indicate that the increased discharger current is achieved largely by virtue of increased efficiency (i.e. reduced recirculation to the skin). Efficiency  $\eta$  is defined by

$$\eta = 100 \frac{\text{Net Discharge Current}}{\text{Power Supply Current}}$$

Beyond a spacing of  $5D$ , the improvement achieved by decreased recirculation obtained by increasing distance to the skin is counterbalanced by degraded performance stemming from increased difficulty in getting discharge products removed as the result of immersing the discharging element in a region of low-speed, diffuse, and considerably turbulent flow.

#### FLIGHT TESTS OF DISCHARGING ELEMENTS

For the Yuma, Arizona flight test investigation of discharging elements, the instrumentation was arranged as shown in Figure 7. Tests were made of three basic discharging elements: A single point or a ring located in one (and in some cases both) of the engine exhausts; and an "outrigger" discharger shown in Figure 8. The outrigger discharger system consisted of a four-foot-long, 1-inch diameter aluminum tube mounted amidships on each side of the helicopter six feet outboard from the skin. A sharpened wire was installed at each end of each bar to provide four widely-spaced, low-threshold corona

points. In view of the results of the laboratory tests shown in Figure 6, provisions were made on the flight test aircraft to position the discharging element up to 5 engine exhaust diameters aft of the engine exit plane. The structure for accomplishing this is visible in Figure 8.

In discussing the various charging and discharging phenomena it is of considerable importance to agree upon a convention when discussing the signs of various charged particles. The sign convention used in this paper is shown in Figure 9.

In reviewing the results of the flight tests, it is interesting to determine the degree to which they agree with the laboratory and ground tests. In Figure 10 the net discharge current for a single point discharger is plotted for comparison with the current discharged from a single ring at the same location ( $d = 5D$ ) in the helicopter engine exhaust. The two sets of data obviously lie along the lines of best fit. This result substantiates the laboratory and ground test data which indicated that a single point and a single ring constitute equally satisfactory discharging elements. Shown for comparison in Figure 10 is a laboratory experimental curve of discharge current measured at the same spacing behind the engine exit plane, and with a wind velocity of 100 fps. The laboratory data predict a somewhat higher discharge current than was measured in flight. This disparity probably stems from the difference in temperature between the laboratory "engine" exhaust and that of the actual aircraft engine. The higher temperature of the real engine exhaust implies higher ion mobility permitting higher recirculation current which results in a lower net discharge current.

With the effectively low directed wind velocities associated with the CH-47 turbine exhaust, it is necessary to move the discharging element far from the fuselage to reduce current recirculation to a tolerable level. This means that high power supply voltages must be used to generate the corona discharge current required. Thus the engine exhaust discharger may be considered to be a high-impedance system. (From Figure 10 for  $V = 200\text{kV}$ ,  $i = 100 \mu\text{A}$  therefore  $R = 2000 \text{ M}\Omega$ ). In the case of the active discharger developed for jet aircraft (2), the high windspeed and low air temperature permitted the discharging element to be placed in close proximity to the airframe without any recirculation. There it was possible to achieve discharge currents of 1 mA for power supply potentials of 60 kV so that  $R = 60 \text{ M}\Omega$ .

In a further effort to verify and extend the laboratory work during the flight tests,

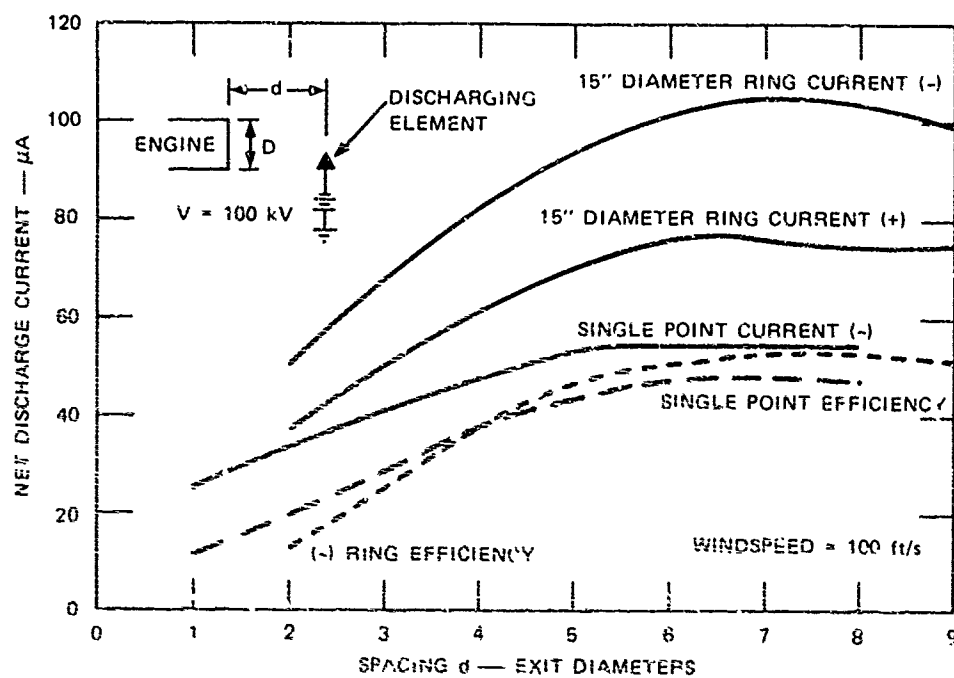


FIGURE 6 LABORATORY INVESTIGATION OF EXTENDED DISCHARGER SPACING



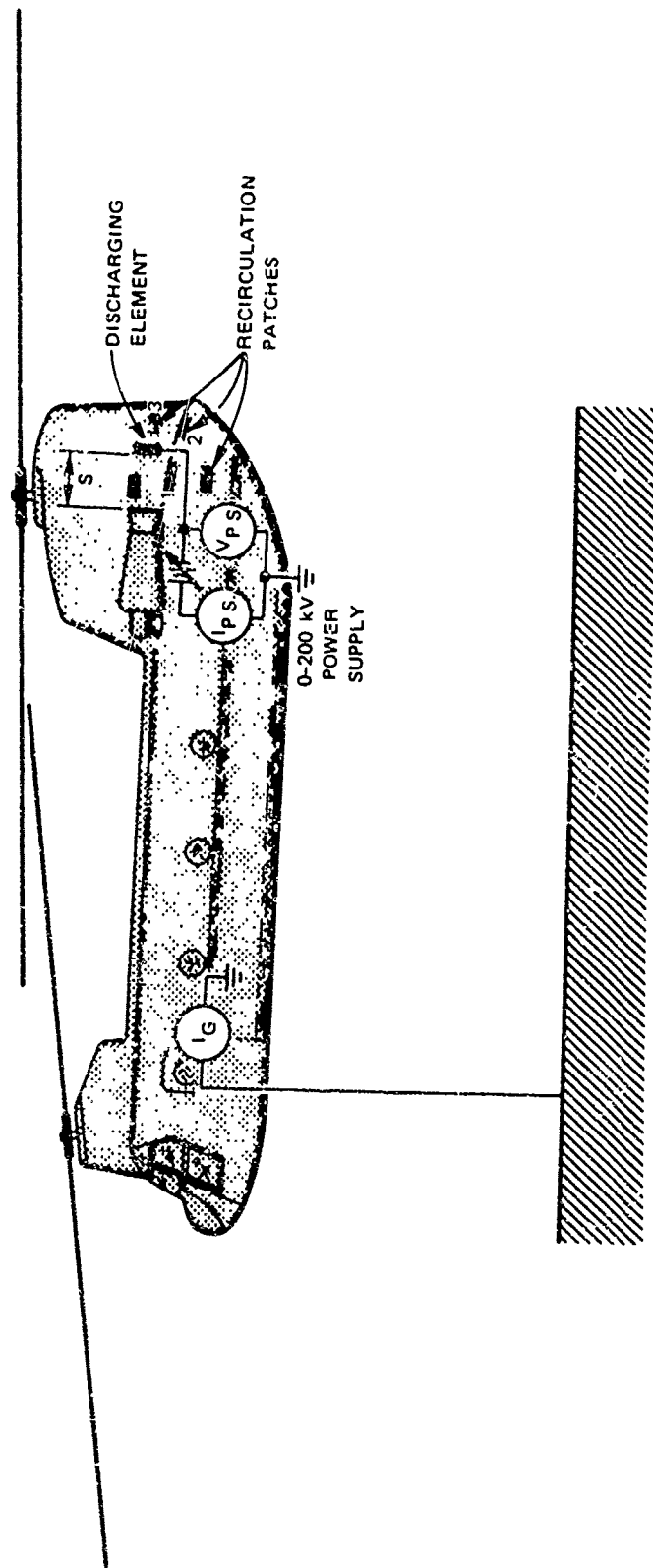


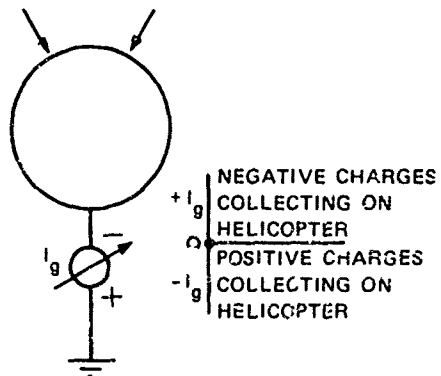
FIGURE 7 LAYOUT OF INSTRUMENTATION FOR DISSIPATOR TESTS



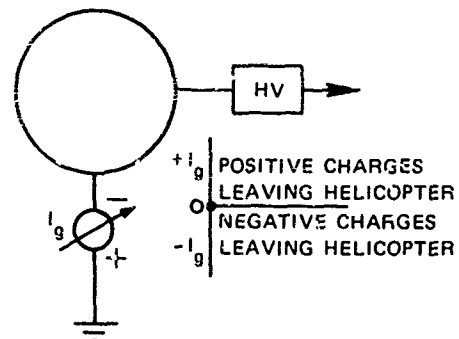
FIGURE 8 PHOTOGRAPH OF CH-47 FLIGHT TEST AIRCRAFT

## CURRENT

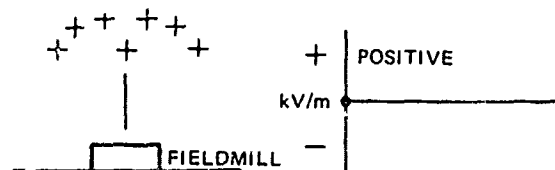
### TRIBOELECTRIC CHARGING



### DISSIPATION



## FIELDS



### FIELDMILLS ON HELICOPTER

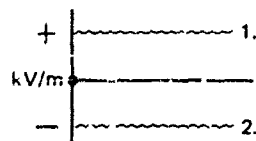
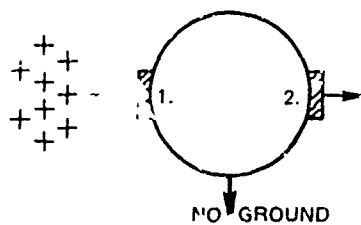
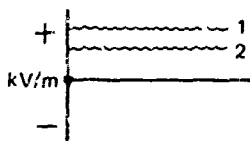
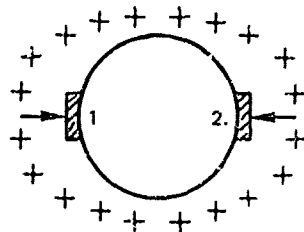


FIGURE 9 SIGN CONVENTIONS FOR CURRENTS AND FIELDS

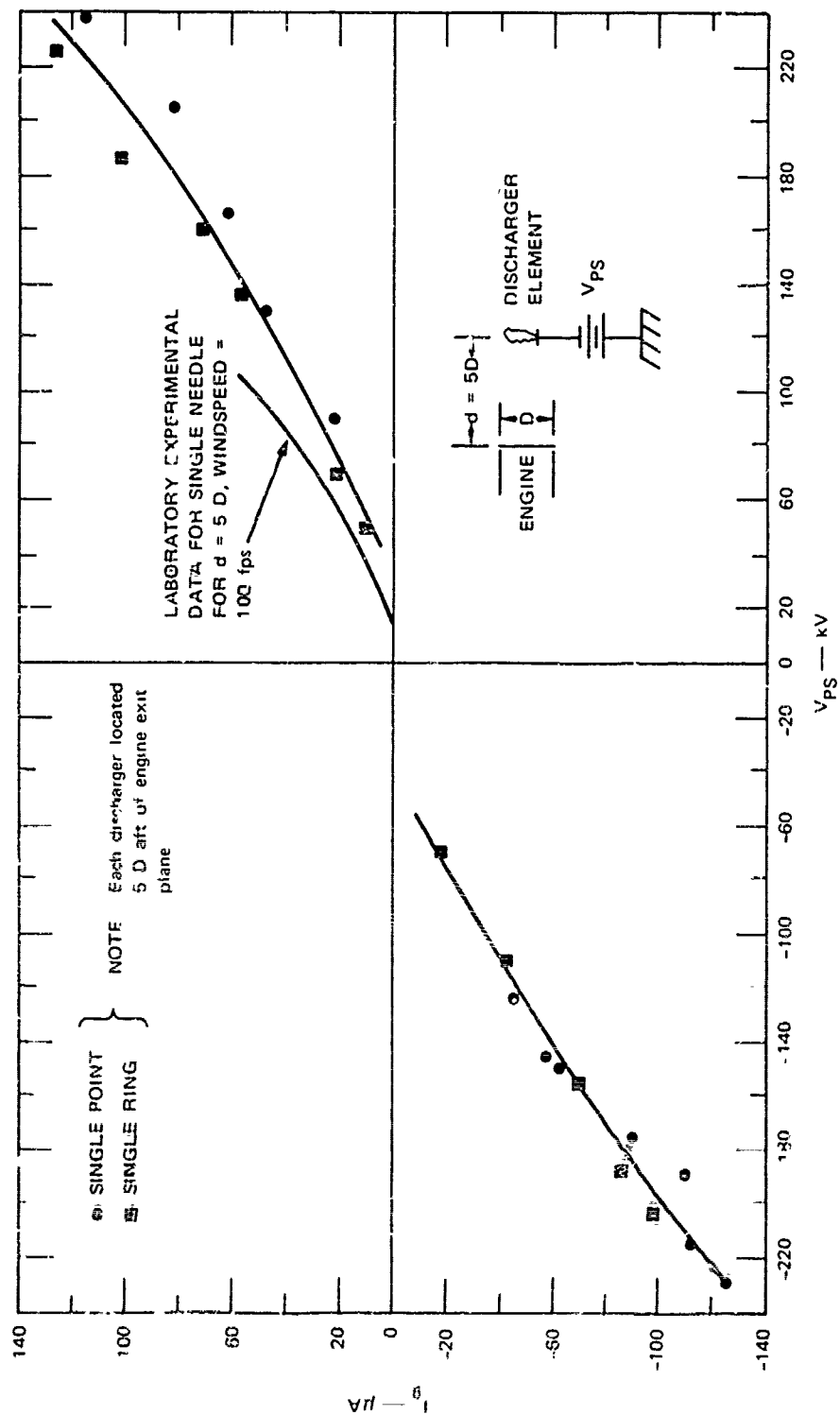


FIGURE 9 FLIGHT TEST COMPARISON OF SINGLE RING AND SINGLE POINT DISCHARGERS IN ENGINE EXHAUST (clean environment)

an investigation was made of the effect on discharge currents of varying the position of the discharging element in the exhaust plume. The results of such a flight test experiment are shown in Figure 11. Here, in agreement with the laboratory results, we see that increased net discharge current can be achieved by increasing the spacing from  $2\frac{3}{4} D$  to  $5D$ . In addition, it was found that, with the ring at  $d = 2\frac{3}{4} D$ , it is sufficiently close to the fuselage that flashover occurred from the ring to the fuselage at voltages in excess of 120 to 160 kV depending on the power supply polarity. Increasing the spacing to  $d = 5D$  increased the net discharge current at the lower voltages and, at the same time, permitted the full power supply voltage of 220 kV to be applied to the discharger.

Figure 12 illustrates the results of an investigation of the degree to which dischargers located in one engine interact with and limit the current that can be discharged from an identical system in the other engine. The results of these experiments indicate that, on the CH-47, the engines are sufficiently far apart that, at the lower power supply voltages, discharging in both exhausts doubles the discharge current. At the higher discharge current levels, there is some interaction, and the current discharged from two engines is not quite twice the current discharged from a single engine.

The results of tests with the outrigger discharger system in a clean environment are shown in Figure 13. Comparing Figure 13 with Figure 11, we find that at a given power supply voltage the outrigger system discharged roughly twice the current discharged by the single ring at  $d = 5D$ .

For some of the tests, the discharging system was arranged in the "maximum dissipation" configuration in which the outrigger system and the ring located at  $d = 5D$  in the engine exhaust were both connected to the power supply. The results of such a series of tests are shown in Figure 14. Comparing these data with those of Figures 13 and 11 we find that the "maximum dissipation" current is very nearly equal to the sum of the current discharged by the outriggers alone and the ring alone. Referring again to Figure 14, we observe that there is considerable difference between the data for each of the hover altitudes. Why this should be is not clear since the effect is not so pronounced for either of the dischargers used singly. Perhaps it has to do with the fact that when larger absolute values of current are discharged, the problem of space charge current limitation by the ion cloud assumes increased importance. In this case any process which gets rid of the space charge or minimizes its effects assumes added importance.

Dissipation testing was also carried out in a dusty environment generated by hovering freshly-disked sand. Results of such tests using the outrigger system are shown in Figure 15.

The ground current flowing when the power supply voltage is set to zero represents the frictional charging current to the helicopter. (This is the current we would like to be able to null with the active discharge system.) It can be seen from this figure that by adjusting the power supply voltage, it is possible to increase the ground current, set it to zero, or even to reverse its polarity, and that the curves are almost identical to the clean environment data of Figure 14, displaced to account for the triboelectric charging current.

#### SENSOR FIDELITY FLIGHT TESTS

One of the most difficult problems associated with the development of a satisfactory active discharging system is that of devising a sensing scheme capable of providing an indication of the helicopter-to-ground potential under all operational conditions. Typical environments might include dust, dry snow, electrified rain, and the ion cloud generated by discharge from the dissipator element. Ideally, the sensing element should function without any connection to the ground. A field meter or "field mill" immediately suggests itself as the sensing device.

In considering the workability of a simple field meter sensing scheme, we argue that; if a charged body is suspended in charge-free, field free space, there is a unique relationship between the electric field intensity at a particular point on the body, and the potential of that body. In particular, the fields are zero when the potential is zero. In this case, a field meter is an ideal device for measuring the potential of the body. At the other extreme, if we allow any arbitrary distribution of charges and applied fields around the body in question, there is no unique relationship between electric field structure about the body, and its potential to ground. So that no measurement we can make on the body can tell us its potential.

In planning this program, it was felt that the actual operational situation would lie somewhere between the two extremes discussed above. It was observed further that it would be fruitless to try to settle the question of sensing either by purely analytic methods or by laboratory experiments since the problem involves the interaction between poorly understood frictional charging processes,

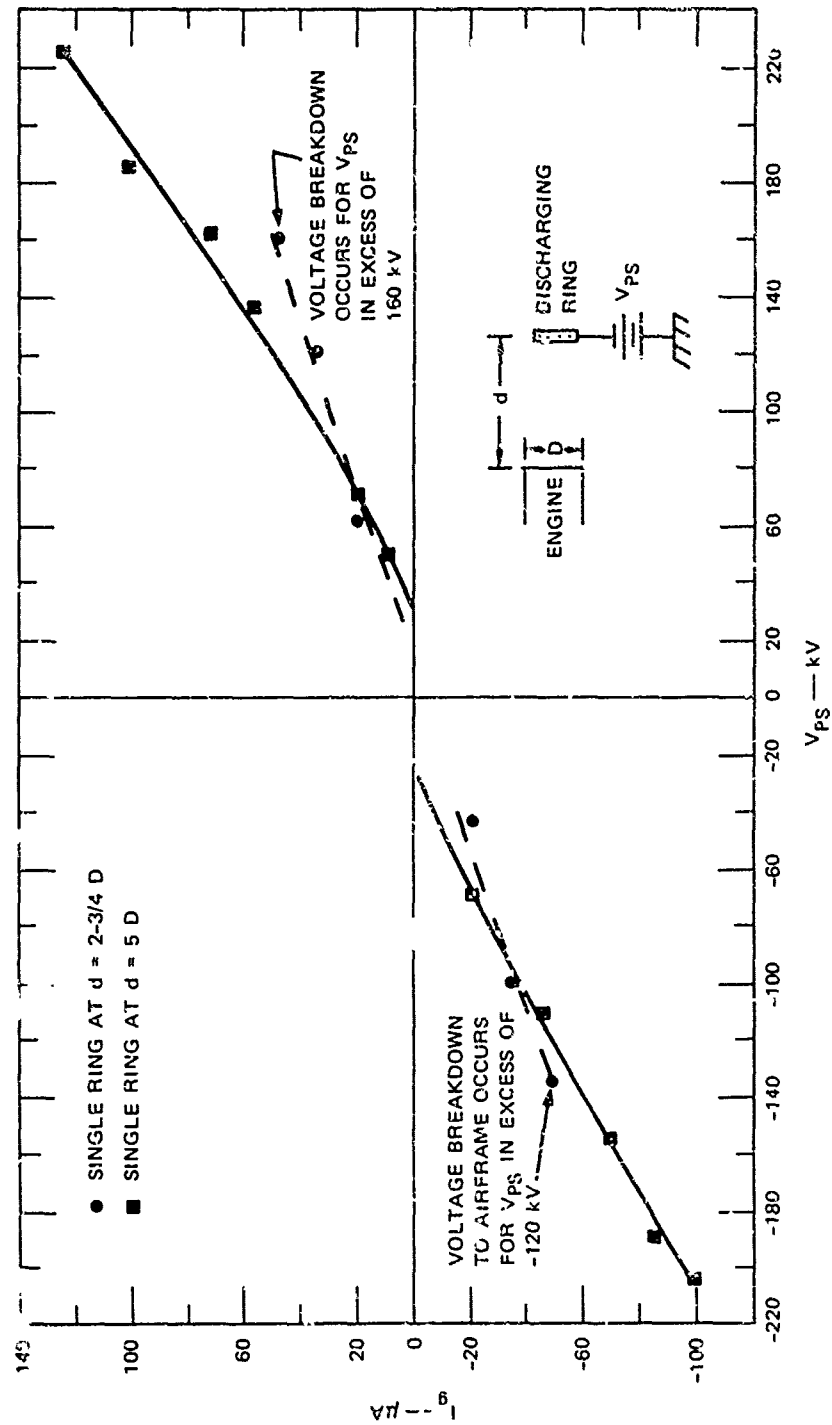


FIGURE 11 FLIGHT TEST INVESTIGATION OF EFFECT OF DISCHARGING ELEMENT AS A FUNCTION OF DISTANCE AFT OF ENGINE EXIT PLANE (clean environment)

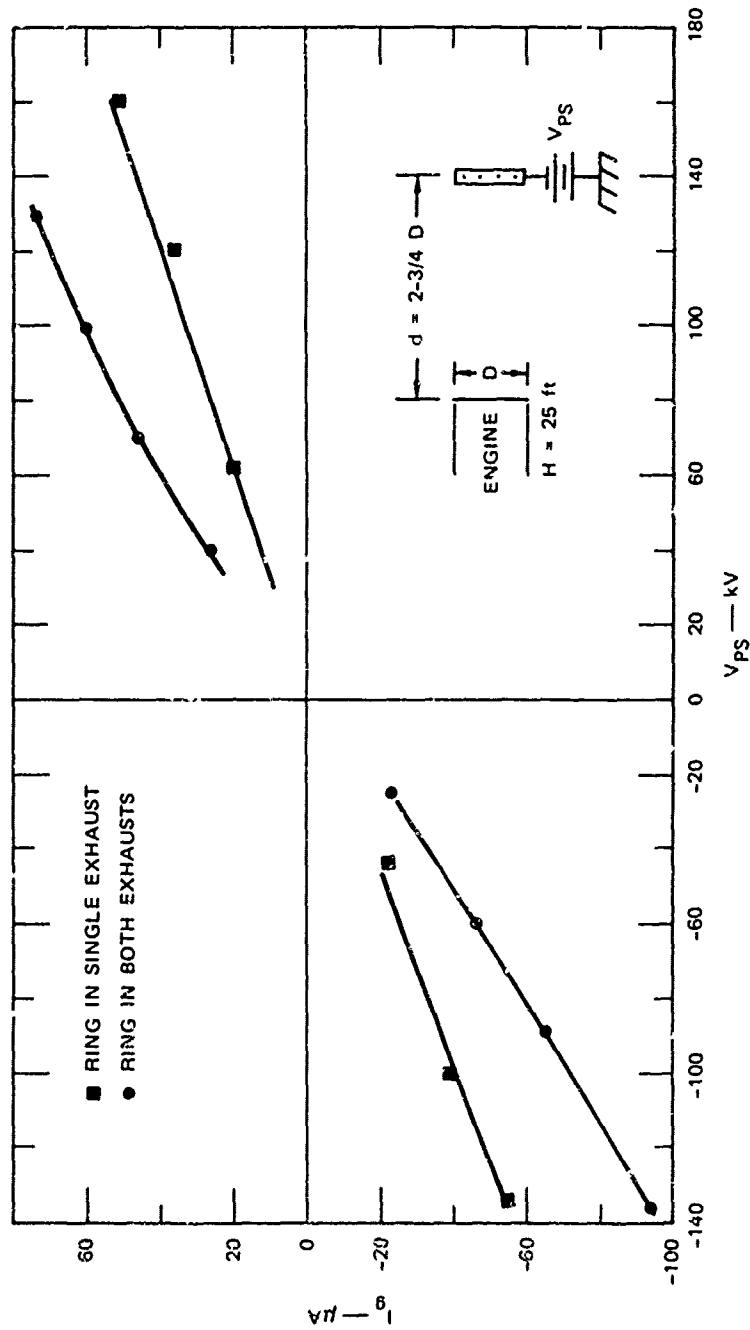


FIGURE 12 FLIGHT TEST COMPARISON OF DISCHARGE CURRENT FROM DISCHARGING ELEMENTS IN ONE vs. TWO ENGINE EXHAUSTS (clean environment)

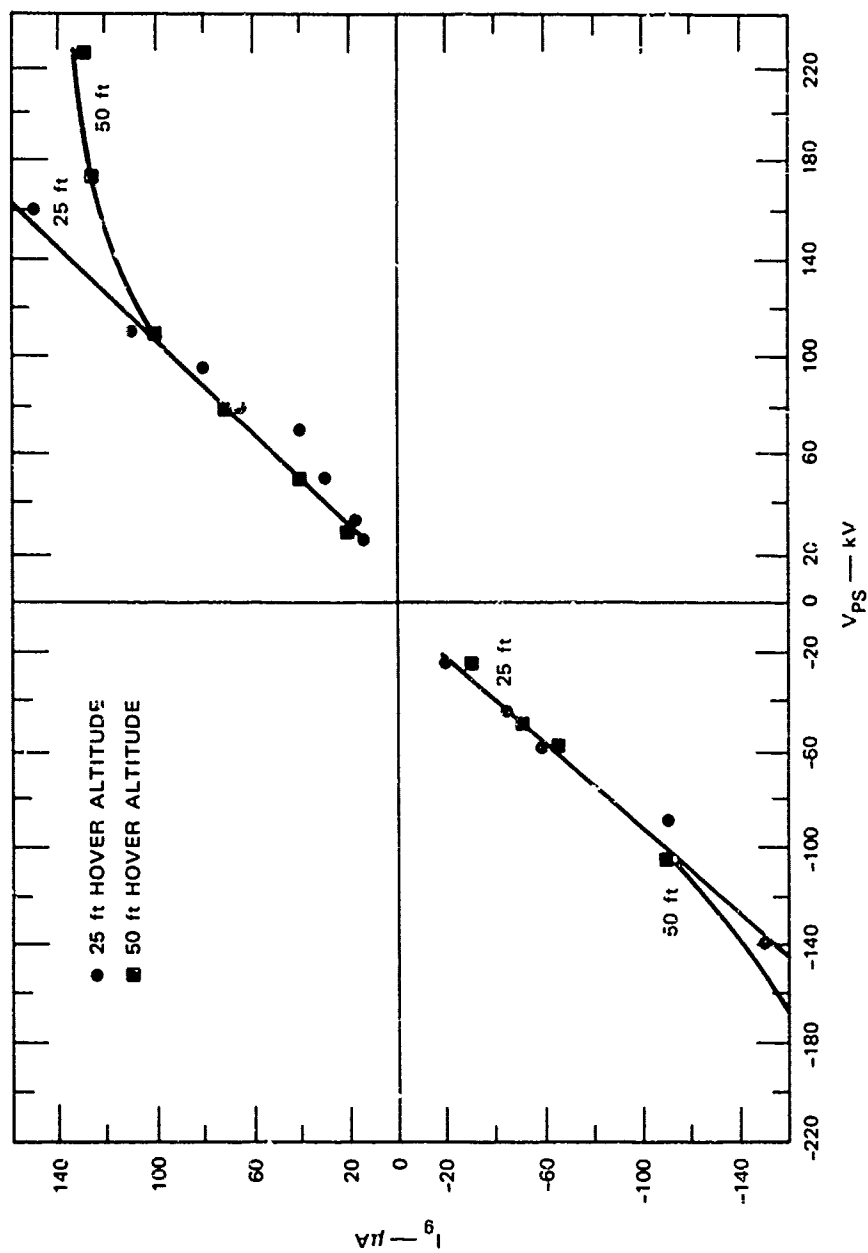


FIGURE 13 FLIGHT TEST INVESTIGATION OF OUTRIGGER DISCHARGER CURRENTS AS AFFECTED BY HELICOPTER HOVER ALTITUDE (clean environment)



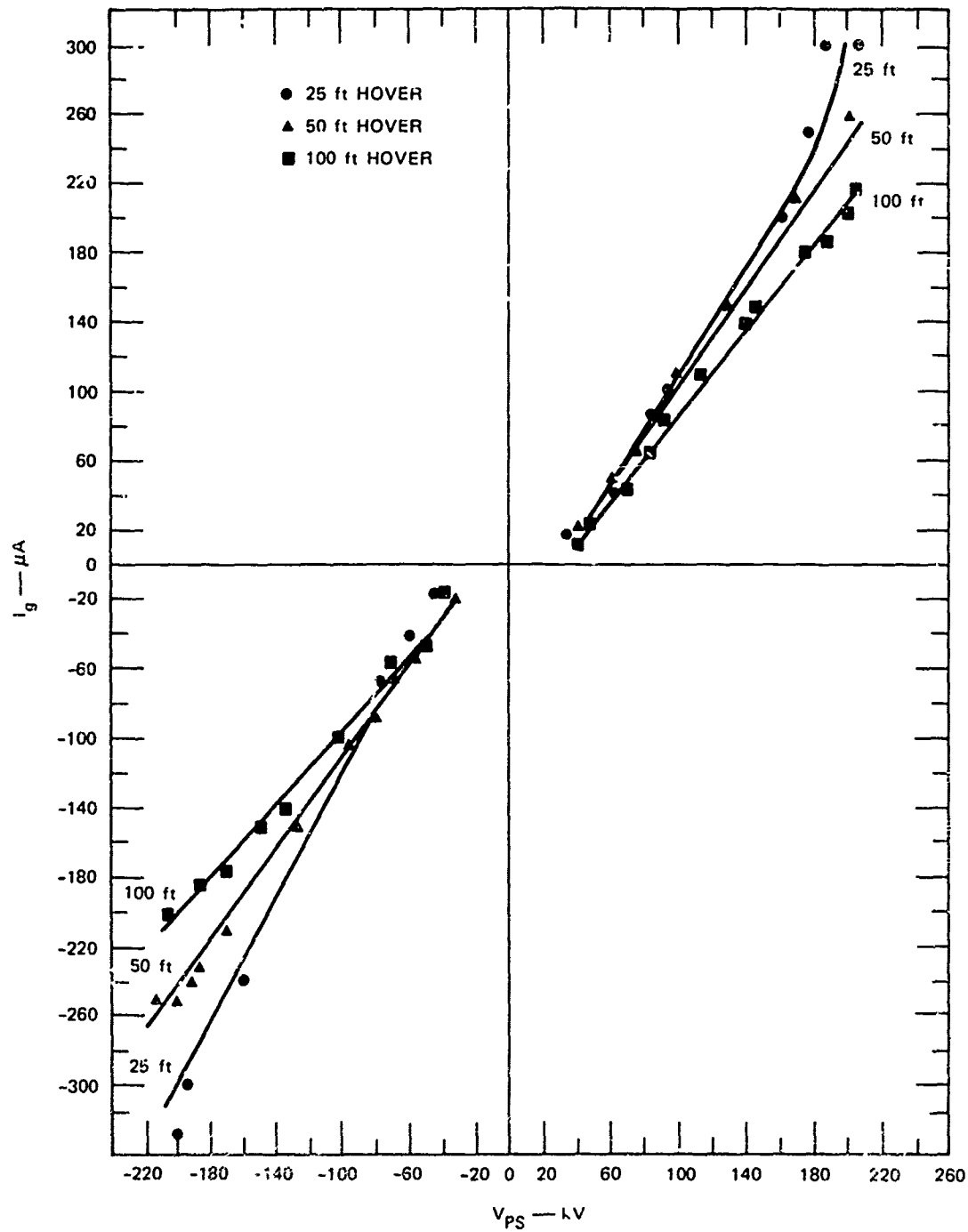


FIGURE 14 "MAXIMUM DISSIPATION" FLIGHT TESTS USING OUTRIGGER SYSTEM AND SINGLE RING AT  $d = 5 D$  (clean environment)

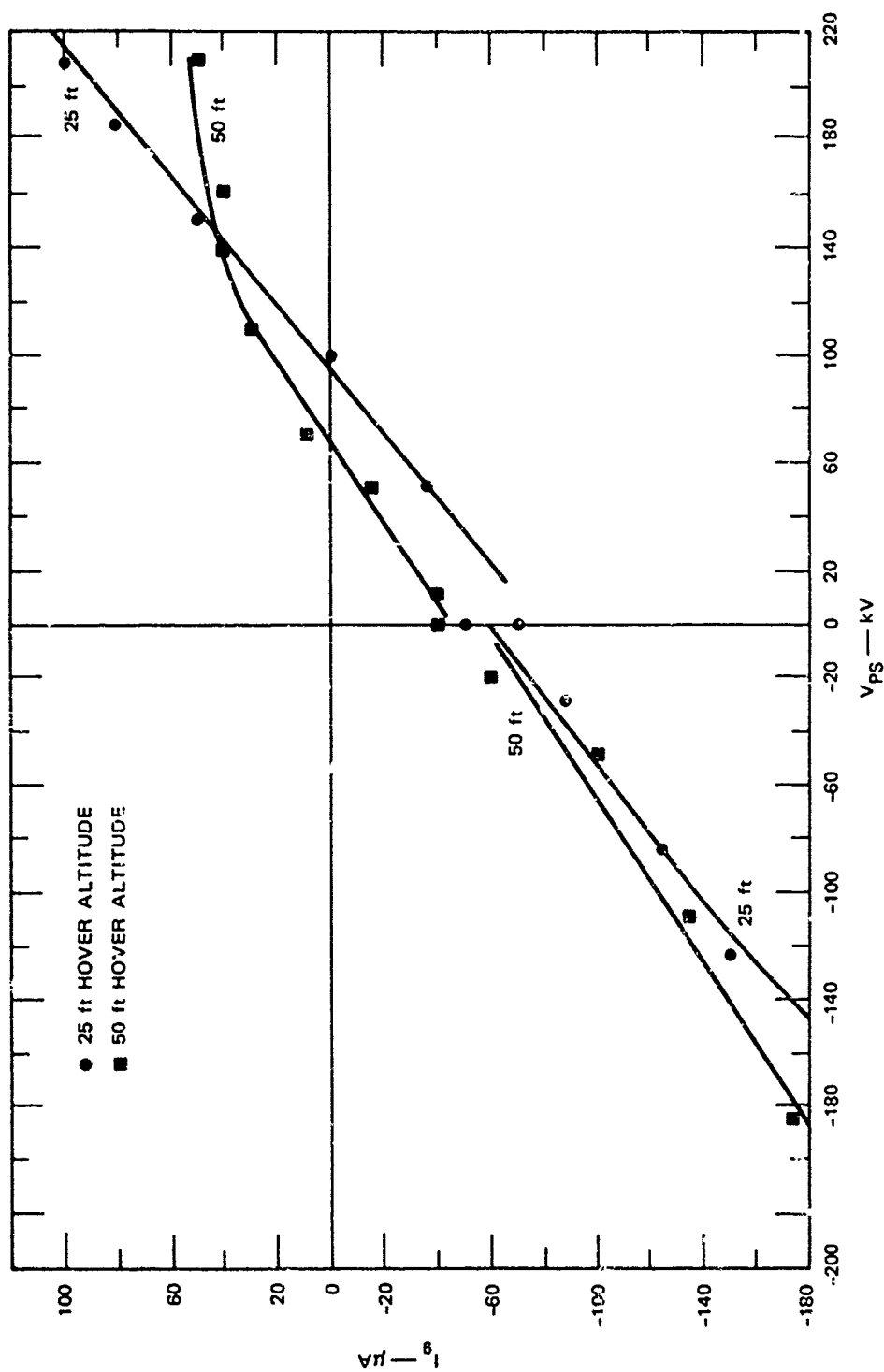


FIGURE 15 FLIGHT TEST; INVESTIGATION OF CURRENT DISSIPATION, USING OUTRIGGER DISCHARGERS, AS AFFECTED BY HELICOPTER HOVER ALTITUDE (dust environment)

complex airflows, and tortuous recombination processes. Accordingly no effort was made to investigate the sensing problem in the laboratory or during the Vertol CH-47 ground tests.

For the flight test investigation of sensor fidelity, the helicopter was equipped with a total of four electric field meters (field mills). Two of the field mills are visible in the photograph of Figure 8. The overall arrangement of the field meters is shown in the sketch of Figure 16.

Provisions were made to suspend field meter #1 from the helicopter by means of a nylon rope passed through the cargo hatch. This arrangement simulates the mounting of a field meter on the helicopter cargo hook. It was argued that this arrangement minimized the amount of charged material between the sensor and earth, and would therefore have considerable promise of sensing the true helicopter-to-ground potential.

Field meter #2 was located on the underside of the helicopter near the nose in the region often used in the past for field meter installations. This field meter serves to tie together data from this experiment with earlier work. Field meter #4 was installed on the side of the fuselage roughly centered in both the vertical and fore-and-aft directions. Field meter #3 was mounted on the top of the fuselage roughly centered fore-and-aft, and slightly to the left of the fuselage centerline. The purpose for field meters 3 and 4 was to investigate the possibility of using multiple field meter installations to sort out the effects of charged dust and ion clouds in the vicinity of the hovering helicopter and to infer from these readings the true helicopter-to-ground potential.

The sensor fidelity instrumentation system included a set of 5 ground-based field meters which, for all but one of the tests, were arrayed under the hovering helicopter. This field meter system permitted study of the way in which discharge ion and charged dust clouds are distributed and how they affect the electrostatic field structure in the vicinity of the helicopter. Two basic ground field meter arrangements were used during the sensor fidelity tests. The configuration employed during any particular test is shown with the data from that test.

The most fundamental sensor fidelity flight test experiment (illustrated in Figures 16 and 17) consisted of determining the relationships between the various field meter readings and the aircraft potential. For this experiment, the ground wire was connected to the power supply high voltage terminal. In this way, the helicopter potential with respect to ground is simply the power supply voltage.

Figure 16 presents the results of measurements on the cargo hook field meter. First we observe that a positive field meter indication is obtained upon the application of a positive power supply voltage. This is in keeping with the sign convention for field meters illustrated in Figure 9 where a positive charge above the field meter is interpreted as a positive field indication (this is the convention employed by atmospheric electricians). Next, we observe that, for a given voltage and hover altitude, the field meter reading depends critically upon the field meter sensor altitude. As  $h$  is decreased, the protrusion of field meter #1 increases so that it produces a greater concentration of field about itself. For very small  $h$ , the proximity of the ground further enhances the field.

Returning to an inspection of Figure 16, we find that  $E_1$  varies linearly with  $V_{ps}$  until corona threshold evidenced by non zero power supply current is reached, and some corona current is discharged. At this time the slope of the curve decreases. Physically this behavior can be explained as follows: The aircraft is charged negatively with respect to the earth so that, to the field meters, the outside world looks positive and they give a positive indication. When corona threshold is reached, negative charge begins to leave the tips of the rotor blades and is driven toward the ground by the rotor downwash. This negative charge in the vicinity of the helicopter makes the outside world look less positive so that the field meter reading is reduced. (This same effect of corona space charge was reported in Reference (3) in connection with hovering tests conducted on CH-34C and UH-1A helicopters.) The effect is apparent only on the data for  $h = H$  because at  $h = 5$  and  $H = 15$ , the field meter output saturates before corona threshold is reached.

Calibration data for the three fuselage mounted field meters are shown in Figure 17. Their behavior and sensitivities are similar to that of field meter #1 when it is at fuselage level (i.e., for  $h = H$ ).

In another set of experiments, the helicopter was grounded and hovered over an array of ground field meters as shown in Figure 18. These tests were carried out in a "clean" area, that is, an area in which there was no dust stirred up by the hovering helicopter. Current was discharged from the cuttrigger discharger and readings were made of electric field intensities both on the aircraft and on the ground array. With this arrangement the helicopter is held at ground potential at all times so that there is no contribution to the electric field

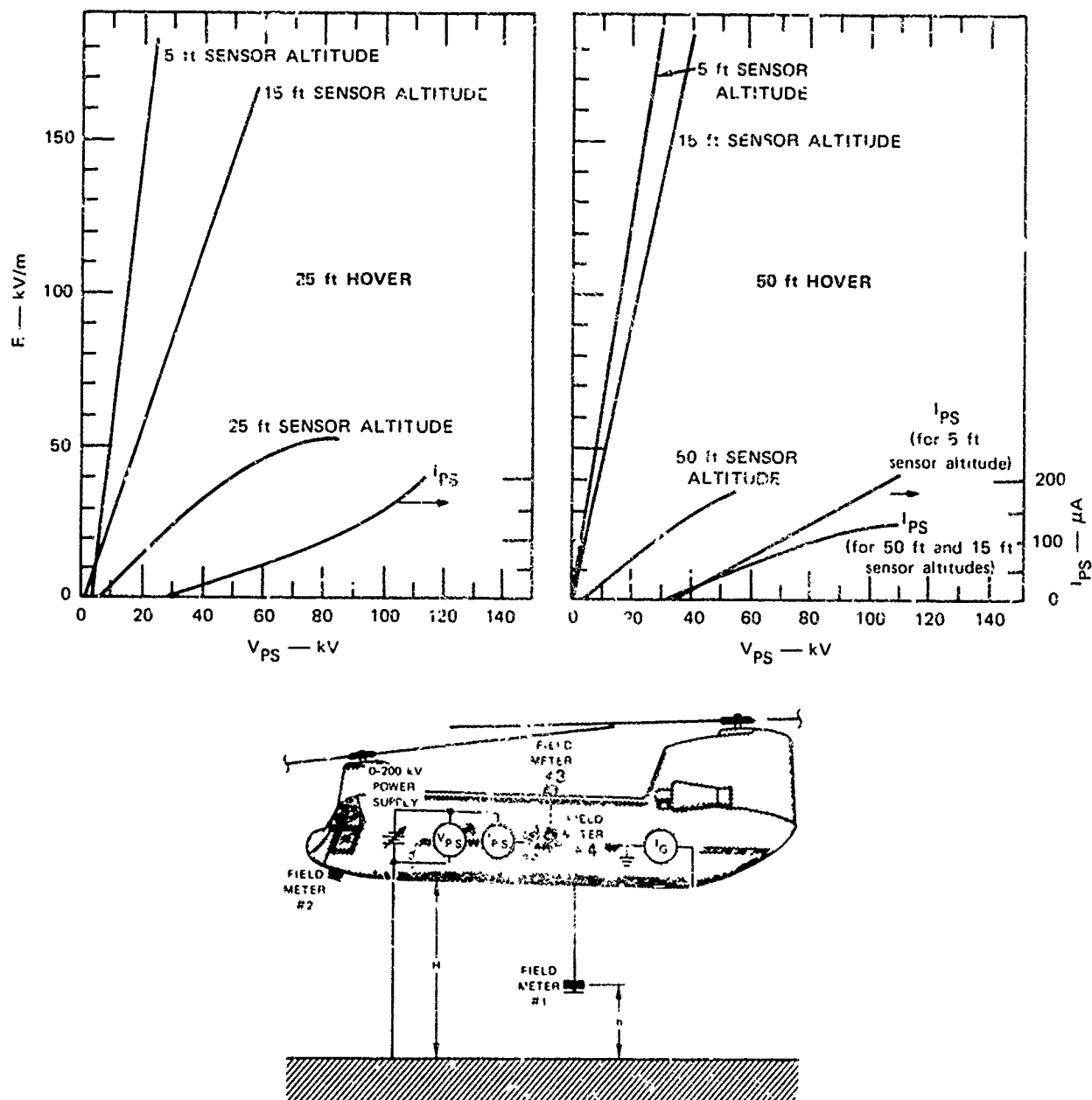


FIGURE 16 FLIGHT TEST CALIBRATION OF CARGO HOOK FIELD METER

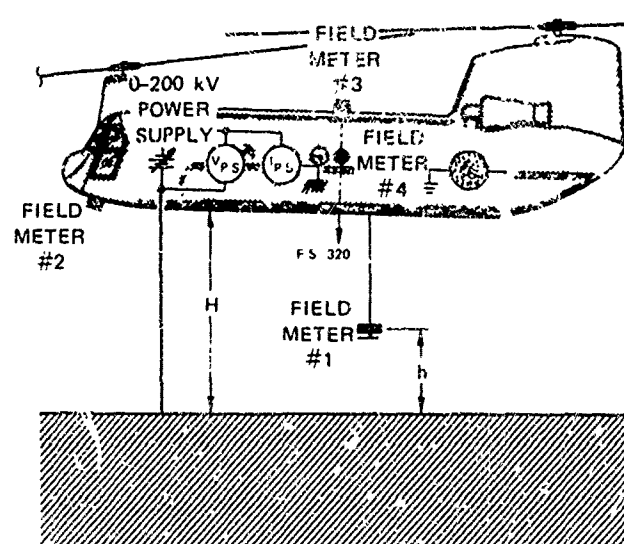
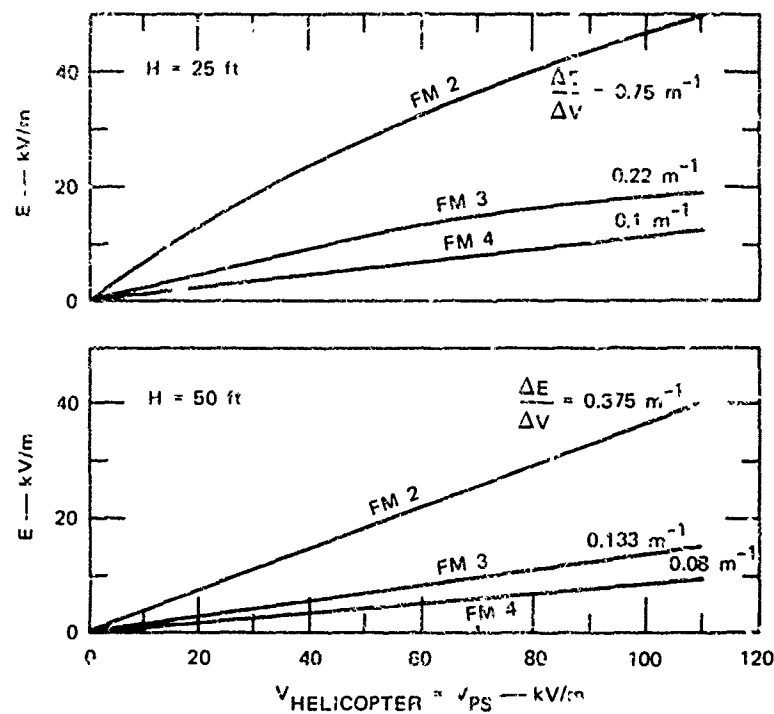


FIGURE 17 FLIGHT TEST CALIBRATION OF HELICOPTER FIELD METERS

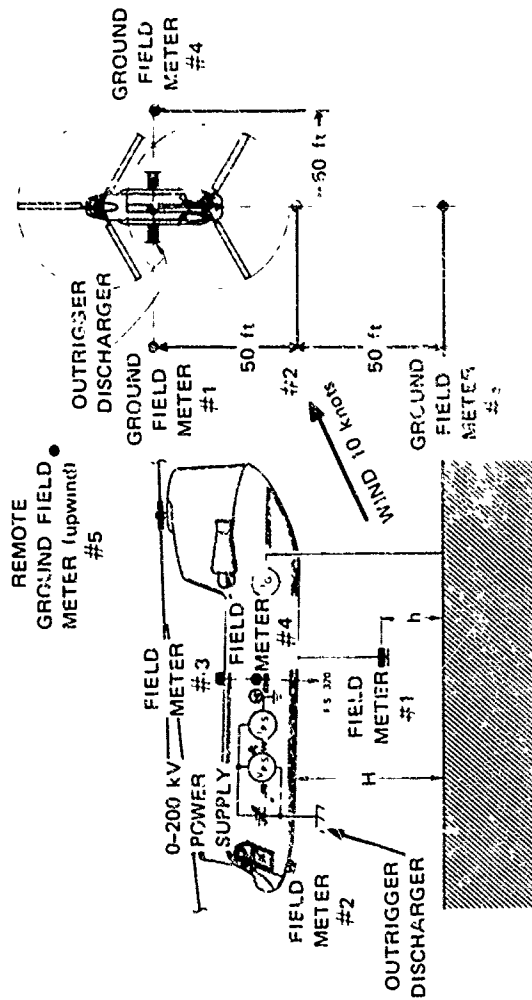
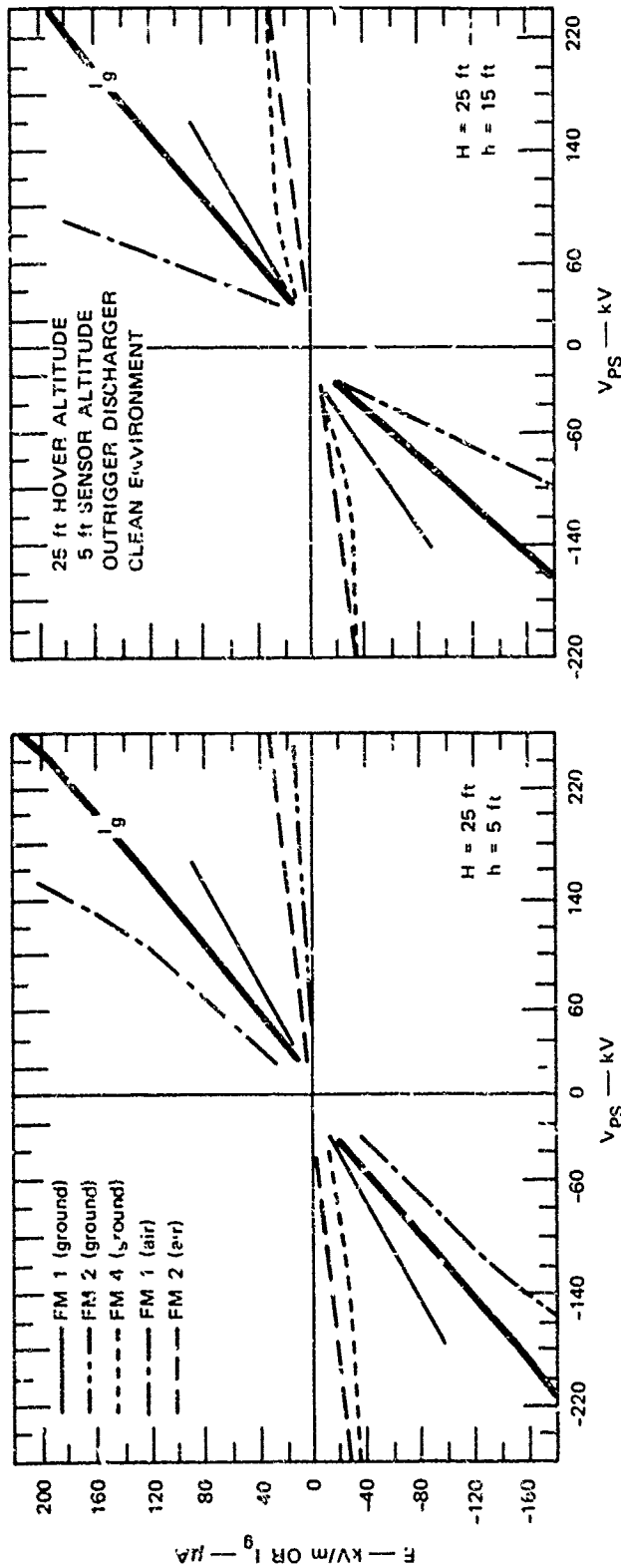


FIGURE 18 SENSOR FIDELITY FLIGHT TESTS WITH OUTRIGGER DISCHARGER (clean area)

structure from net charge on the helicopter. Thus, in the absence of perturbing influences, the airborne field meters should read zero. The only sources of electric field around the helicopter are the potential applied to the discharging element, and the space charge generated by the discharge ion cloud. A laboratory model experiment demonstrated that the power supply potential produced negligible fields at all of the field meter locations. Thus the large electric fields measured on the airborne field meters in Figure 18 are predominantly due to the ion cloud generated by the discharger which is blown around the various field mills by the rotor-wash. Further examination of Figure 18 shows that the ion cloud produced by the outrigger discharger is blown down into the ground array giving large values of the electric field.

In an effort to better understand the effect of the discharger-produced ion cloud, additional experiments were carried out using various discharger locations. Figure 19 shows the results of one such experiment when the discharger in the left engine exhaust was used to supply the ions. It can be seen from this figure that the ion cloud's perturbation of airborne field meter #1's reading has a somewhat smaller effect than the outrigger discharger-produced cloud shown in Figure 18. The ring discharger ion cloud has a markedly smaller effect on airborne field meter #2 than does the outrigger-produced cloud. This difference is attributable to the fact that the ion cloud produced at the outrigger location is blown about in relatively close proximity to the #1 and #2 airborne field meter whereas the discharger located far back produces an ion cloud which, due to the engine exhaust and rotor-down wash flow pattern, is unable to strongly influence the #2 airborne field meter and to a lesser extent, the #1 airborne field meter.

The extent of the ion clouds migration can be observed in the ground field meters. Referring again to Figure 19, it is seen that the #2 ground field meter gives a higher field reading than does the #1 ground field meter (the #2 ground field meter was beneath and somewhat behind the ring discharger; the #1 ground field meter was directly beneath the CH-47 cargo hatch). The results of these tests indicate that in order to correctly infer the helicopter potential, it is essential that the field meter location be chosen such that there is minimal effect from the discharger ion cloud since the field meter cannot differentiate between the "desired" component of electric field due to aircraft-to-ground potential and an electric field produced by an ion produced space charge.

The sensor fidelity tests were extended to determine the effects of an actual operating environment upon the performance of the field meters. The helicopter was operated in an area of plowed desert sand at the Yuma Proving Ground to reflect a severe natural charging environment.

Before an understanding of the various observed phenomena was possible, it was necessary to determine the effects of blowing dust in the absence of the helicopter. This was accomplished during a series of "fly-by" measurements: The ground array of field mills was laid out in a cross array configuration and the helicopter was used as a wind source to blow the dust over the sensors. The helicopter was flown past the ground array, at an altitude of 50 ft on the upwind side, at a speed of 5 knots which was slow enough to allow a good sized dust cloud to develop, and yet fast enough so that the dust cloud did not rise to contact any part of the helicopter.

The results of these fly-bys were consistent and the ground field mills indicated that as the dust cloud blew across the surface of the earth, it became positively charged. The airborne instrumentation was not used during these tests.

The initial natural charging sensor fidelity tests were made at various hover altitudes and sensor #1 altitudes with the helicopter grounded. During these tests, the electric fields on the airborne and ground systems were recorded as a function of time. Results typical of the observed electric fields are shown in Figure 20 for a hover altitude of 50 ft and the #1 sensor altitude of 25 ft. It should be repeated here that the hovering helicopter was kept at ground potential through the ground line, and as such any measured electric field other than zero represents an error in the measurement of the helicopter-earth electric field. Figure 20 shows the charging current,  $I_g$ , the airborne field meter data and the ground field meter data recorded over a 35 second period.  $T = 0$  denotes roughly where take-off occurred and the hover altitude of 50 ft over the ground array was established at approximately 15 seconds. It is observed from this figure that  $I_g$ , the charging current, rapidly increases to about 300  $\mu A$  and then at about  $t = 15$  seconds slowly begins to decay. This decay is due to the rotor wash blowing the dust away from the measurement site. It is also observed from this figure that except for sporadic instances all of the ground field meters and airborne field meters #1, #3, and #4 measured positive electric fields. This is in agreement with the fly-by tests discussed

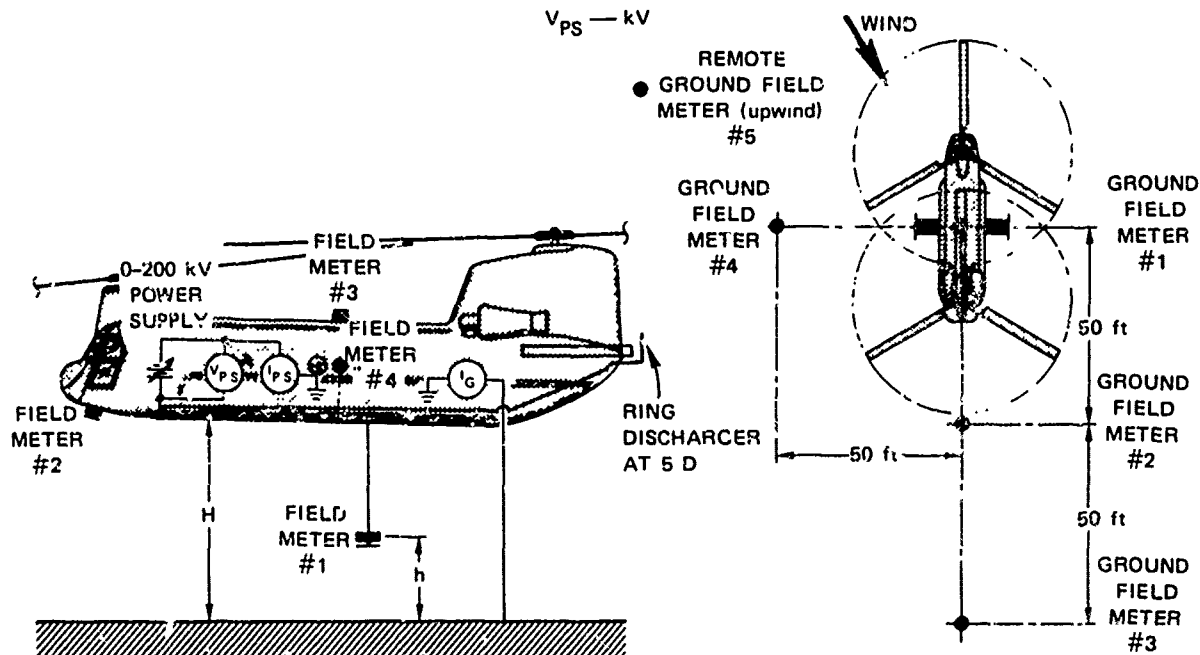
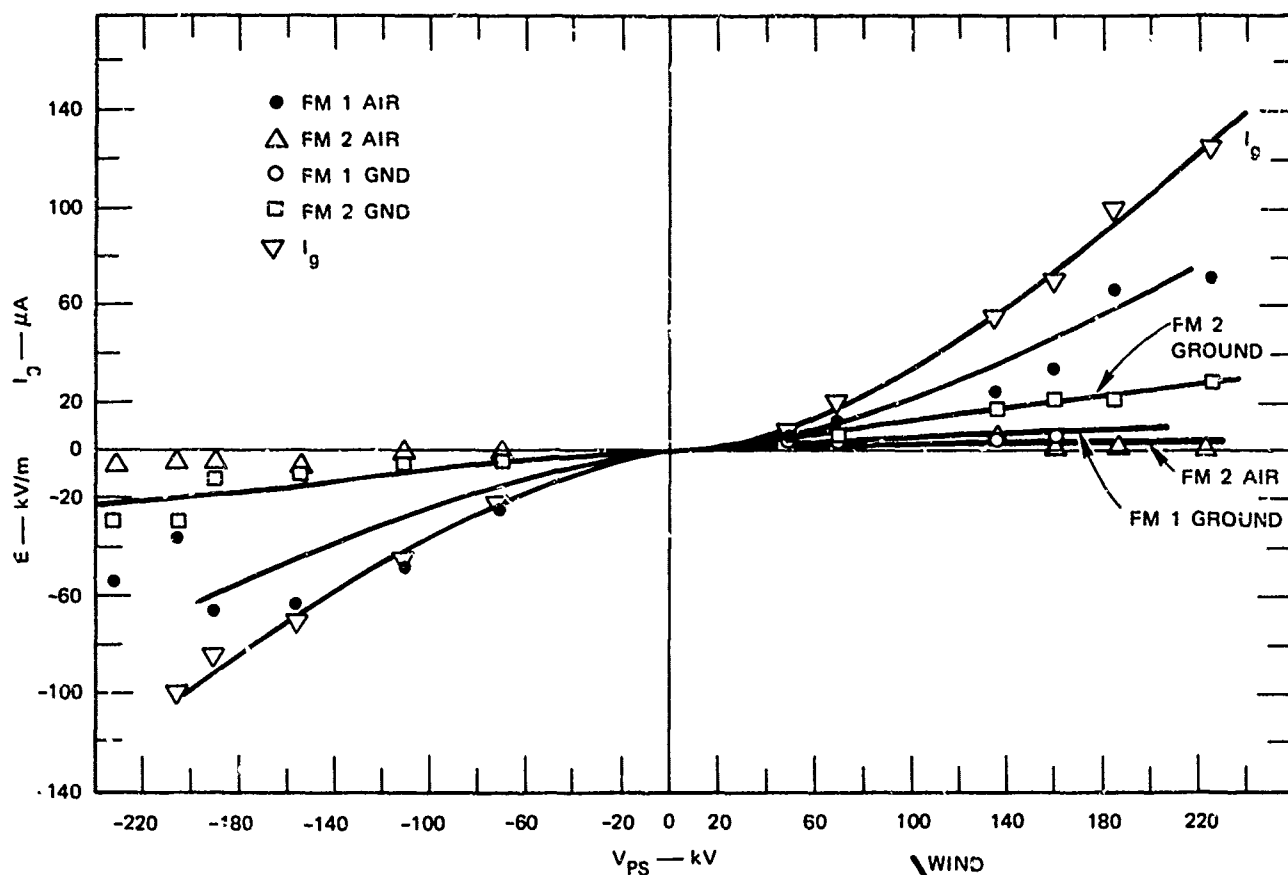


FIGURE 19 SENSOR FIDELITY FLIGHT TESTS USING RING AT 5 D FOR ARTIFICIAL CHARGING



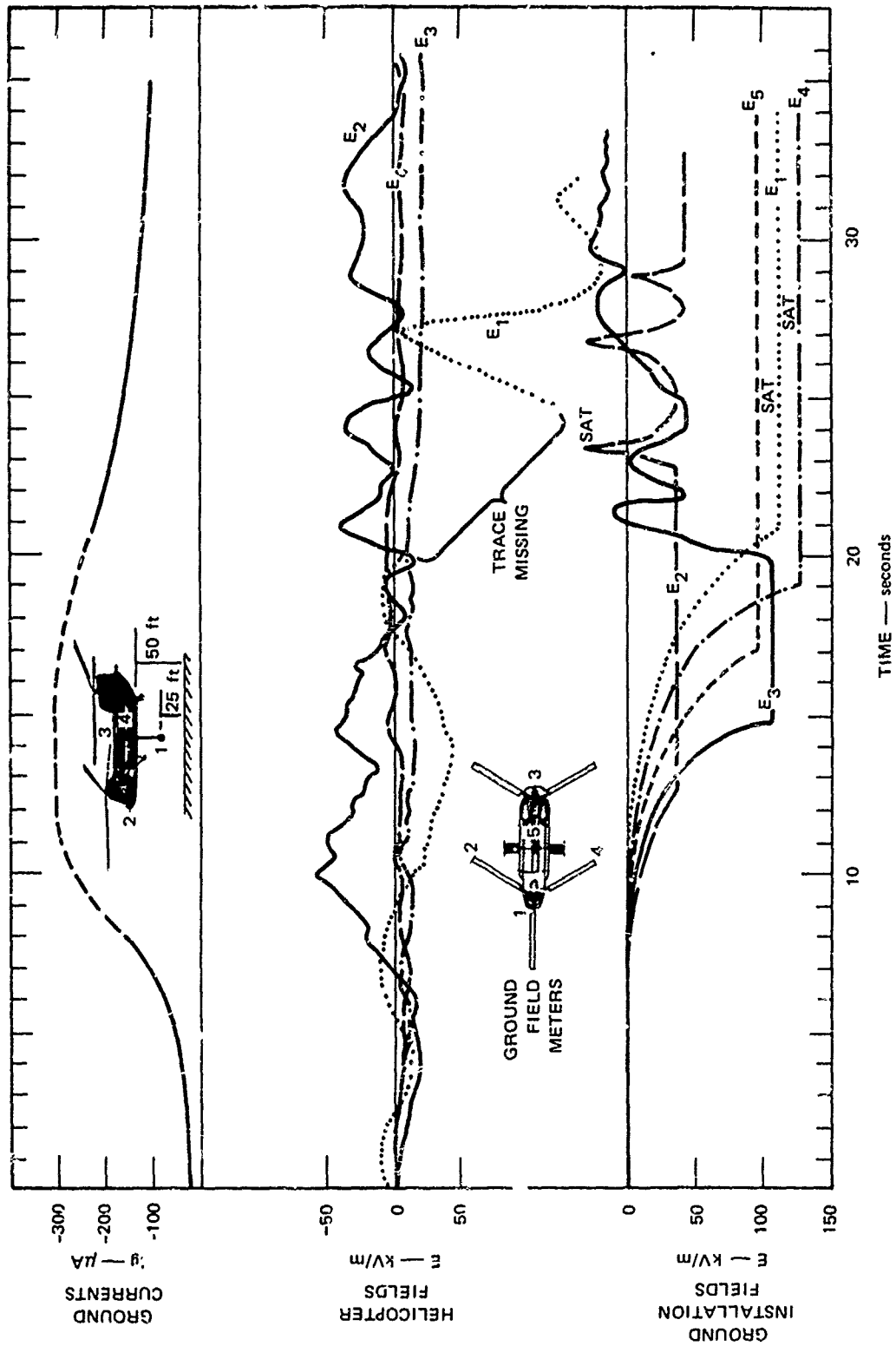


FIGURE 20 OBSERVATION OF ELECTRIC FIELDS ON VARIOUS SENSORS MEASURED AS A FUNCTION OF TIME

earlier, and it indicates that the field meters were looking into a region of positive (relative to the helicopter, charge, according to our sign convention - see Figure 9). The negative electric field measured by airborne #2 is somewhat open to conjecture due to the lack of supportive data, but it is felt that this behavior could be due to the frictional charging of the plastic cockpit canopy and the proximity of field mill #2 to that canopy. The variation of the measured field as a function of time (from the #1 airborne mill) was subjected to statistical analysis and it was found that during hover operations in dust, with the helicopter grounded, the dischargers inactive, the #1 mill measured electric fields in excess of 20 kv/m about 75% of the time, and fields in excess of 50 kv/m about 65% of the time. The helicopter potentials inferred from these readings would then be >30 kv 75% of the time, and >80 kv 65% of the time (refer to Figure 16). A similar although less detailed, analysis was performed on airborne field meters #2, #3, and #4. The preliminary results of this analysis indicate that although the measured electric fields were less than those obtained on the cargo hook sensor, the inferred potentials from meters 2, 3, and 4 (see Figure 17) had approximately the same magnitudes and distribution as described above. These large errors are due to the cloud of charged dust particles swirling about the aircraft, and influencing the field meter readings in the same way as was done by the ion cloud created by the outrigger discharger discussed earlier.

In an additional attempt to understand the relation between helicopter potential and the measured electric fields, natural charging with the helicopter grounded was observed as discussed above and then the ground line was disconnected, allowing the helicopter to acquire a charge. Figure 21 shows data typical of these tests. In the previous figure,  $t = 0$  denotes roughly the time of take-off to hover and hover was established over the ground arrays at approximately  $t = 15$  seconds. It is observed from Figure 21 that the behavior of the airborne and ground field mills is similar in behavior to those of Figure 20 before the ground line was disconnected. When the grounded line was disconnected at  $t = 68$  seconds it is observed that the airborne field meters indicate a negative charge. This is consistent with the idea that, after the ground line is snapped, the helicopter begins to acquire a positive charge from the previously charged dust and from its own triboelectric process during the rotor blades collisions with the dust particles. After contacting the helicopter the dust particles blow down and away with a reduced positive (or zero, or negative) charge. This

cloud then appears negative to the airborne field meters, because the meters measure field with respect to the helicopter. The ground array of field meters, however, are still looking into a positive electric field due to the positively charged dust, and the (now) acquired positive charge on the helicopter.

Additional ground disconnect experiments were carried out in the "clean" area to verify the dust measurements made in Phillips Drop Zone. The results of these clean tests are shown in Figure 22 for a 25 ft hover with a 5 ft #1 sensor altitude. A low, negative polarity, power supply voltage was used during these tests to try to obtain about the same average "artificial" charging as was obtained while hovering in the dust. It can be seen from this figure that, prior to the ground disconnect, the airborne field meters are, as expected, looking into a small negative ion region due to the down-washed negative ion cloud produced by the ring discharger mounted five exhaust nozzle diameters behind the left engine. The ground array, it is observed, is also measuring a very small negative field. At  $t = 22$  seconds the grounding wire was snapped and it is seen that the airborne field meters indicate an immediate increase in the observed field. This is consistent with previous experiments and it shows that the helicopter is becoming more positively charged than the environment around it. It is also seen that the ground field meter indicates an increasing positive charge which indicates that the electric field from the helicopter becomes much stronger and over powers the field due to the ion space charge. At about  $t = 40$  seconds it is observed from the figure that the measured fields begin to decrease in magnitude even though the voltage supply ions to the discharger remains constant. It is felt that this is attributable to the fact that the helicopter acquires enough charge to put it into corona, and the corona tends to lower the observed fields.

## CONCLUSIONS

The experiment discussed above has shown excellent agreement between laboratory tests, ground tests, and flight tests. It has demonstrated that laboratory work is a useful and economical tool for investigating concepts related to discharger operation and design.

Laboratory tests and flight tests have confirmed that discharger designs capable of discharging the design goals of at least 600  $\mu$ A net current are probably achievable for application to the Boeing 301 HLH helicopter.

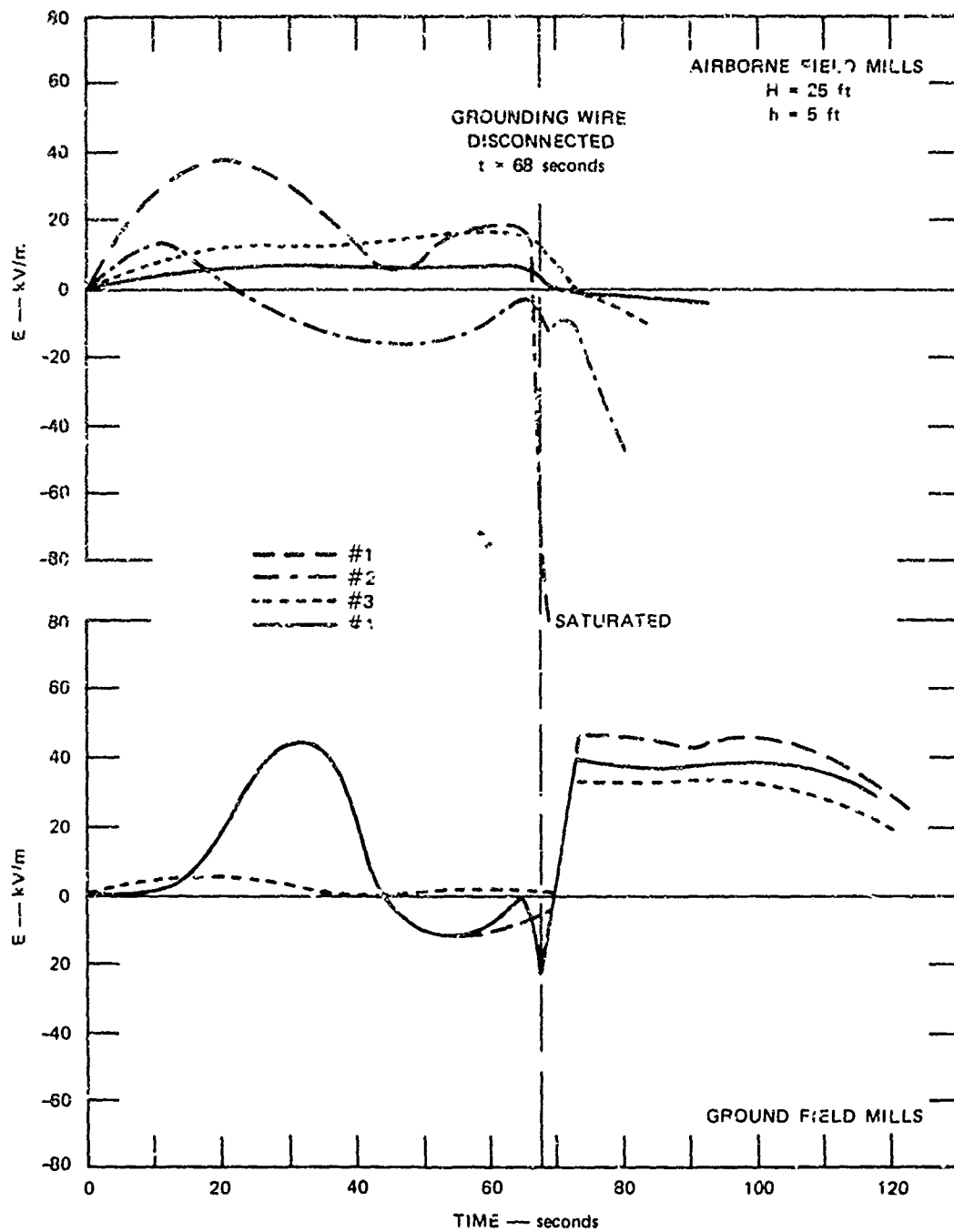


FIGURE 21 MEASURED ELECTRIC FIELD AS A FUNCTION OF TIME DURING GROUND DISCONNECT EXPERIMENT WHILE HOVERING IN DUST

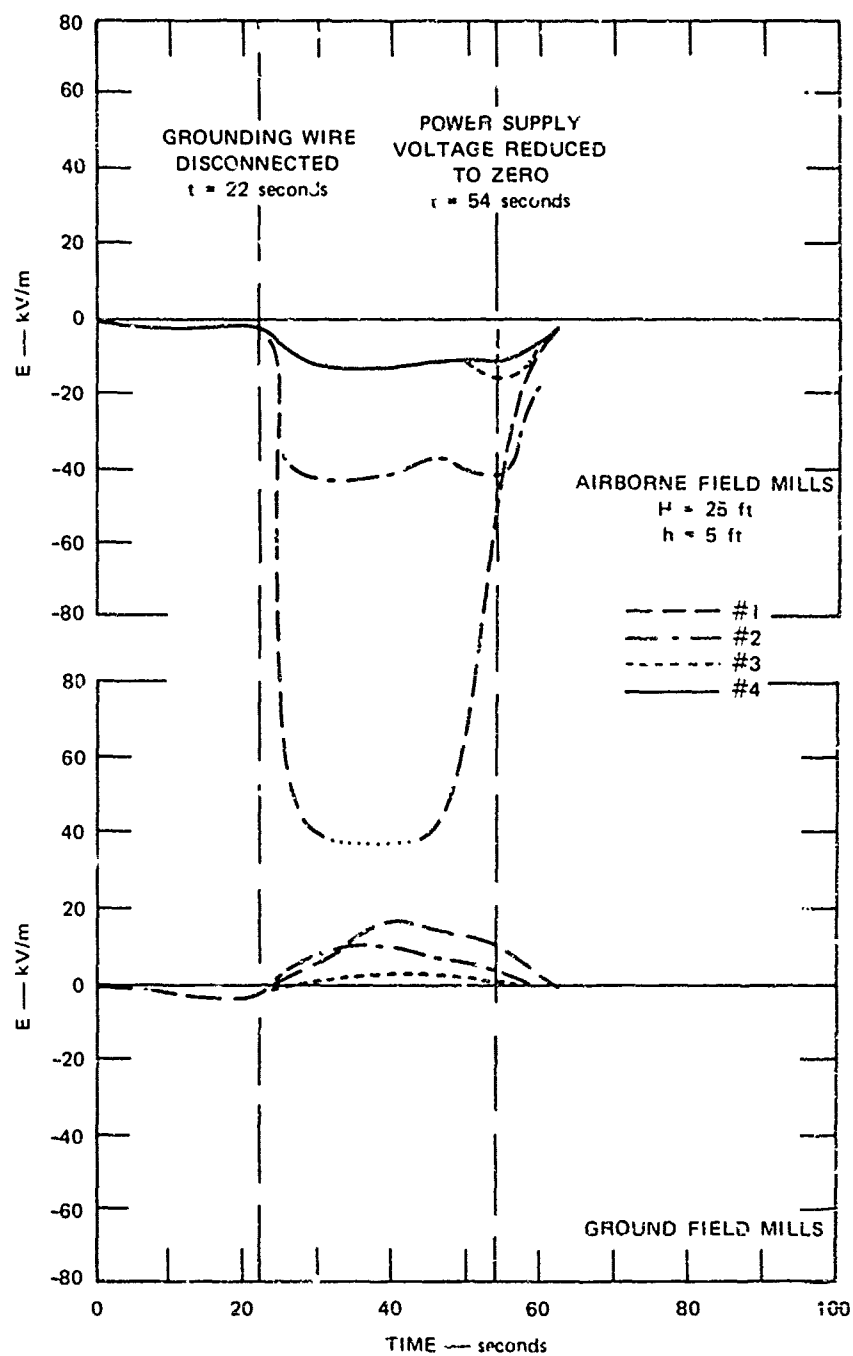


FIGURE 22 MEASURED ELECTRIC FIELD AS A FUNCTION OF TIME DURING GROUND DISCONNECT EXPERIMENT WHILE HOVERING IN A CLEAN AREA

These tests also indicated that existing discharger technology is sufficient to achieve that goal.

The flight test data taken during the Yuma tests and the laboratory measurements program indicate that optimum discharger designs are those which place the discharging electrode standing isolated in the exhaust flow. These designs allow one or more corona points to be inserted into the turbine exhaust at a location as far removed from the fuselage as possible, to minimize recirculation, yet close enough to the turbine exhaust nozzle to provide strong convective flows to remove the discharged ions. Moving the discharger far out into the exhaust plume allows large displacements from the fuselage and, in addition, it allows the discharger to be in a region of low temperature, and hence, lower ion mobility which aids the discharging process.

The flight tests conducted at the Yuma Proving Grounds indicate that accurate sensing of the helicopter-earth electric field by a simple field meter, or an array of meters is very difficult to achieve when the helicopter is operating in an environment containing charged ions, and other solutions to the problem might be easier to achieve. Electric field measurements made with sensors located on the nose, side, top and hanging from the cargo hook have shown that the field meters can provide inaccurate measurements of field when the charged ions are charged dust particles, or even the ion cloud generated by the discharger which is attempting to reduce the helicopter potential. An array of field meters located beneath the hovering helicopter indicates that although the electric field emanating from it can be accurately determined when there is no naturally occurring charging taking place, the ground sensing problem becomes just as much a problem as the airborne sensing when the helicopter is in the presence of dust.

#### ACKNOWLEDGEMENT

The authors wish to acknowledge the help of Mr. Charles King of Boeing, Seattle who was responsible for integrating the test instrumentation into the flight test aircraft. The authors also wish to acknowledge the personnel of the Yuma Proving Grounds for their support during the flight test operations, the U.S. Army CH-47 Flight Crew for their outstanding effort and enthusiasm during the flight operations, and Mr. David Granger and Timothy McCullough of SRI for the technical assistance they provided during program.

#### REFERENCES

1. T. R. Andrews and R. H. Forrest, "Evaluation of an Active Electrostatic Discharger Mounted on the Engine Exhaust of a Helicopter", Technical Report 71219, Royal Aircraft Establishment, Farnborough, England, November, 1971.
2. J. E. Nanevich and G. R. Hilbers, "Flight Test Evaluation of an Active Discharger System," Interim Technical Report 1 (Phase II), Contract F33615-68-C-1359, SRI Project 7104, Stanford Research Institute, Menlo Park, California (February 1970).
3. W. G. Hocver, "Loran D Electrostatic RFI and Nail Field Discharger Flight Tests," Granger Associates, Palo Alto, California (January 1967).

Data from the Airlines Lightning Strike  
Reporting Project

J.A. Plumer  
General Electric Company  
Corporate Research and Development

ABSTRACT

A cooperative lightning strike reporting project has begun in which five U.S. commercial airlines report lightning strike incidents to General Electric for analysis and correlation. The objective of this program is to obtain more data on the effects of lightning on advanced aircraft and flight systems, and relate these effects to the known characteristics of the lightning strike event, such as flash attachment points and intensity. Periodic summaries of data and analyses are made and disseminated to interested aircraft companies, airlines and government agencies. Forty-six strike incidents were included in the first summary covering 1971 data which is the basis of this paper. The summary includes data on Boeing 707, 727, 737, 747 and McDonnell-Douglas DC-8 and DC-9 aircraft. The 46 incidents included 16 with no reported damage to the aircraft. Among the effects reported were 12 incidents with radome damage, 15 involving interference or damage to avionics and 3 involving lightning arrester failure on HF antenna systems. Of great concern were two instances of AC generator trip-off, and the most elusive of an explanation were two incidents of reported "balls of fire" within the cabin. The data also shows that most aircraft were struck at altitudes of between 10 and 22 thousand feet but as high as 37,000 feet. Cooperation by most airline pilots has been excellent, and continued interest and support is needed if the data base is to grow and provide this needed input to most effectively guide the course of future research on aircraft lightning effects and protection development.

THE AIRLINES LIGHTNING STRIKE REPORTING PROJECT has the objective of obtaining a greater understanding of the conditions under which aircraft are struck by lightning and the resultant effects therefrom on aircraft structural, electrical and avionics systems and personnel. Of particular interest are the effects of lightning on new and advanced avionics systems and airframe structural materials, for which operational experience and lightning strike data are relatively limited. Toward this end, five U.S. commercial airlines began forwarding data on lightning strike incidents, in June of 1971, to the G.E. High Voltage Laboratory, in a cooperative program wherein the airlines were provided with questionnaire-type report forms for flight and ground crews to record pertinent aspects of each incident. This form, a copy of which is shown on Figure 1, was designed with the aid of participating airlines

and is an outgrowth of one designed earlier for possible Air Force use, under a program sponsored by the Air Force Avionics Laboratory.

The participating airlines are:

AMERICAN AIRLINES  
BRANIFF INTERNATIONAL  
CONTINENTAL AIRLINES  
EASTERN AIR LINES  
UNITED AIR LINES

This data is to be periodically compiled and reported, with appropriate correlations, to interested organizations and research laboratories concerned with various aspects of the phenomenology of lightning effects on aircraft. It is hoped to continue the project for several more years and expand the data base by the addition of more airline participants and other operators of airfleets, including general aviation aircraft for which little lightning strike data has been recorded and summarized.

Over 100 completed report forms have been received from participating airlines, however, only the data from the 46 strikes of 1971 has been reduced and summarized as of this writing (August 1972). Therefore it is this data which is reported herein. Each incident report remains on file and, in general, statistical summaries presented in each data summary report will be based on the cumulative total of all incidents reported in the project to date.

Recognizing that 46 strikes is a very small data base on which to show meaningful correlations, few have been presented in this first summary report. As the project proceeds, additional correlations will be developed. The following paragraphs summarize the lightning strike conditions and resulting effects reported for 1971.

CONDITIONS WHEN STRUCK

Figure 2 is a bar graph showing frequency of lightning strikes versus altitude. In interpreting this graph, it should be remembered that the altitude at which a strike occurs depends not only on the electrical situation of the atmosphere at a certain altitude, but also upon the frequency of operational use of a certain altitude by the aircraft. The graph shows that most strikes have been received at altitudes of between 10,000 and 22,000 feet, but it is interesting to note that about 5% were received at altitudes above 30,000 feet. One strike, not shown on

# LIGHTNING STRIKE INCIDENT REPORT

## INSTRUCTIONS

The purpose of this report is to gather data relating lightning strike incidents to aircraft type and flying conditions. This data will be used in support of research efforts leading to the development of lightning protection systems.

Please complete and file this report immediately following your flight, providing as much as the requested data as you can.

PART I - TO BE COMPLETED BY THE FLIGHT CREW.

PART II - TO BE COMPLETED BY THE GROUND CREW.

<u>PART I (TO BE COMPLETED BY FLIGHT CREW):</u>				
<u>Operational Conditions at Time of Strike</u>				
• Flight No.	Date	Time of Strike	Aircraft type	
• Route	To	DMF Reading	Miles from	
• Altitude	Ft.;	Air Speed	Kts.;	
• Condition:	Approach	Climb	Level Flight	Other
• Area Weather:	Cloud Type	% Cover	Ceiling (ft.)	Tops at (ft.)
				Temp. (°C)
• At time of strike aircraft was:	Above Clouds	Within Clouds	Below Ceiling	
• Experiencing:	None	Light	Mod.	Heavy
	Turbulence			
• Experiencing Precipitation in form of:	Rain	Sleet	Hail	Snow
• Were There Lightning Flashes in Vicinity	Before	After	Strike?	
• Were You Aware of Electrical Activity (Static)	Before	After	Strike?	
• Was St. cloud Fire Visible Before Strike?	Yes	No		
	<u>Experienced: (Check Which)</u>		<u>Any Effects on: (Check Which)</u>	
	<u>Interference</u>	<u>Outage</u>		
Compass	1 2	1 2	AC Power System	
Weather Radar	1 2	1 2	DC Power System	
VOR Receiver	1 2	1 2	Stiffening of Controls	
ILS G/A	1 2	1 2	Engine Flameout	
LF ADS	1 2	1 2		
INS	1 2 3	1 2 3	<u>Any Effects on Personnel, such as:</u>	
Radio Alt.	1 2	1 2	Flash Blindness	
CAS	1	1	Electric Shock	
VHF	1 2 3	1 2 3		
HF	1 2	1		
Cabin P.A.	1	1		
Voice Amp. System	1	1		
Additional Comments (Further Description of Effects Check Above)				
PART I Completed By				

PLEASE TURN TO REVERSE SIDE FOR PART II, TO BE COMPLETED BY GROUND CREW

NVL FORM LSRP-5

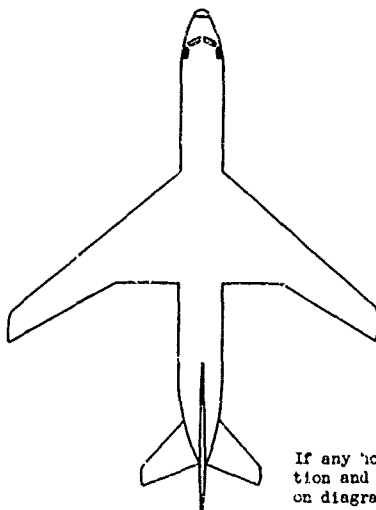
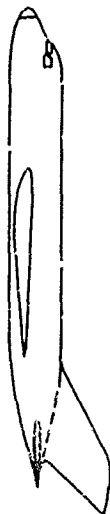
FIGURE 1- LIGHTNING STRIKE INCIDENT REPORT FORM

**PART II (TO BE COMPLETED BY GROUND CREW):**

Please mark stroke attachment points (burn marks) on generalized aircraft sketch below. Add engines or other components, if necessary, to show attachment points.

Indicate whether top or bottom, starboard or port, etc.

Sketch here an enlargement of the area struck (i.e., wing tip, flap, etc.). Show details, such as successive pitting (swept stroke) markings, etc. Please attach photographs if possible.



If any holes were burned through the skin, indicate location and diameter (key to locations indicated by numbers on diagram above).

<u>Location</u>	<u>Hole Diam. (in.)</u>
1	_____
2	_____
3	_____

- Describe any damage to aircraft structure or external components believed to be the result of the lightning strike \_\_\_\_\_

- Describe any damage to avionics or electrical components believed to have occurred as a result of the lightning strike \_\_\_\_\_

PART II Completed by \_\_\_\_\_

Fold in Thirds with this Address Side Visible, Staple and Mail

Place  
First Class  
Postage Here

TO: GENERAL ELECTRIC COMPANY  
HIGH VOLTAGE LABORATORY  
BLDG. C, ROOM 202  
100 WOODLAWN AVENUE  
PITTSFIELD, MASS. 01201

ATTN. LIGHTNING STRIKE REPORTING PROJECT

FIGURE 1- (CONTINUED)



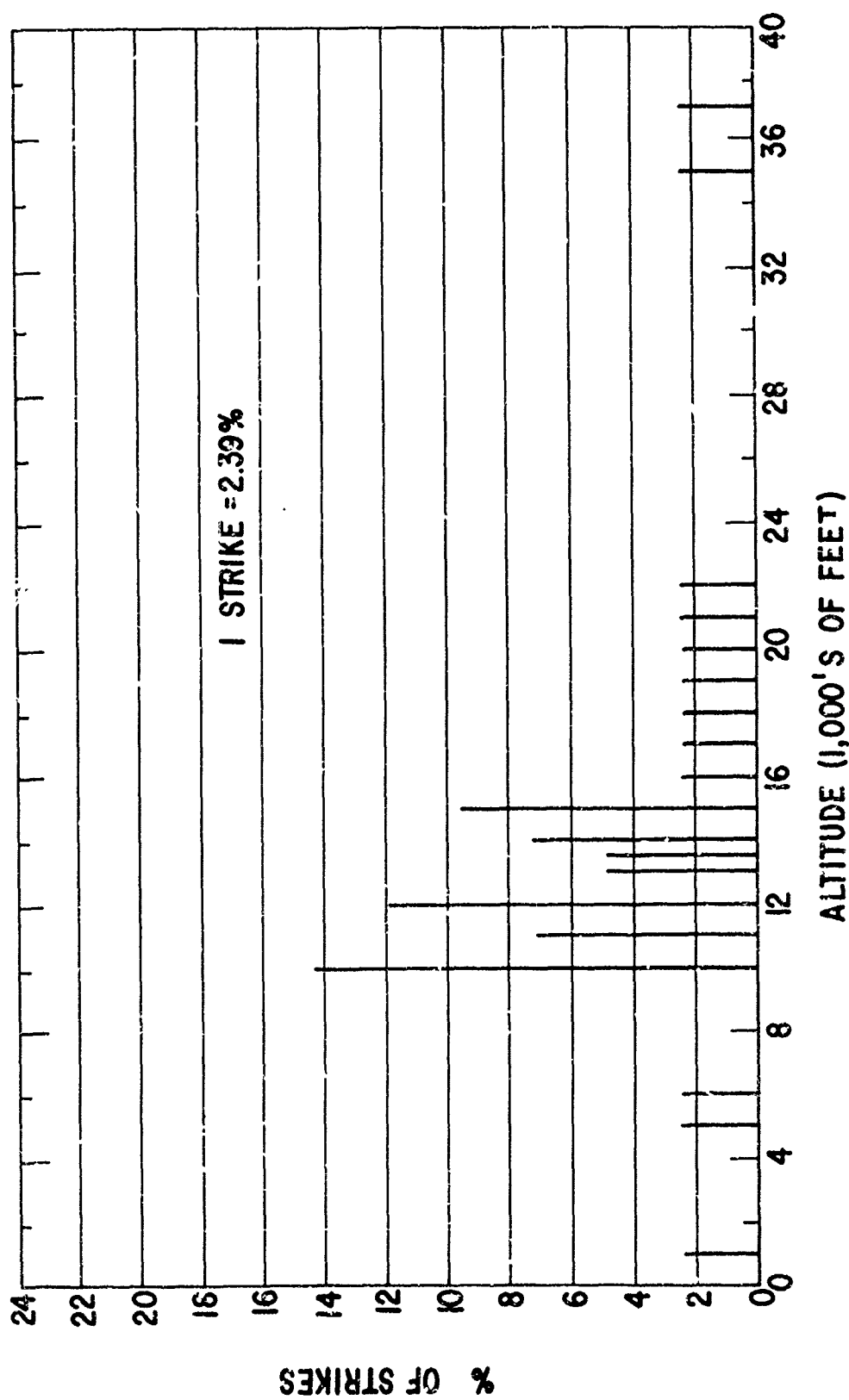


FIGURE 2 - STRIKE OCCURRENCE VS. ALTITUDE

the graph, was also received by an aircraft on the ground.

Weather conditions in the vicinity of the aircraft when struck include the following, based on a total of 46 incidents reported:

- In 30 of the incidents the aircraft was known to be within a cloud.
- In 27 cases the aircraft was experiencing turbulence.
- In 27 incidents precipitation in the form of rain, freezing rain, sleet or snow was reported.
- In 23 cases electrical activity (earphone static and/or St. Elmo's fire) was evident before the strike.

#### EFFECTS ON THE AIRCRAFT

When an aircraft is struck by lightning it nearly always becomes part of the path the flash is taking to another ultimate destination. This is because the aircraft itself has little capacity to store electrical charge, as compared with the amount of charge (coulombs) which we know actually flows in a lightning flash. Thus, in each incident there will normally be two points where the lightning actually attaches itself to the aircraft: an "entry" and an "exit" point. Sometimes, due to branching of the flash, there may be more than one entry or exit point.

The most obvious effects of lightning on the aircraft are therefore those such as pitting or puncture, which occur at the attachment points.

Of the 46 incidents reported:

16 reported no effects of any kind except minor pitting or burned marks on the aircraft.

12 reported radome damage of some degree, including puncture.

10 reported static discharger wicks burned off.

The passage of lightning current through the airframe between these points may be the cause of other effects. These may result from magnetic field interaction with aircraft electrical circuits, or ohmic heating of resistive materials, for example. Relatively little data presently exists concerning the extent of such effects or their relationship to the lightning strike characteristics. To the extent possible, one of the objectives of this project is to learn more about the relationship of these effects to lightning.

Where sufficient information has been reported to enable it, the data is being organized to show the two (or more) attachment points, thereby indicating the main portions of the aircraft through which lightning currents traveled, for comparison with corresponding effects. The data are subdivided according to aircraft type and presented on Table I.

Among the incidents particularly noteworthy are the following:

- In 2 cases the strike apparently caused an AC generator to trip-off the line.

- In 2 incidents "balls of fire" were seen by flight attendants to enter the cabin through a window or pass down the aisle.

- Lightning arresters in HF antenna systems were blown out in 3 or 4 incidents and apparently failed to protect HF system components in several other incidents.

- No holes were burned through metallic aircraft skin in any incident reported, although several stabilizer skin panels were torn off of a 747 in one incident.

- In no case of an incident of a strike in the air were any personnel injured.

#### CONCLUDING DISCUSSION

The preceding data provide some interesting opportunities to compare basic lightning current flow paths with resulting effects on various components or systems. In most cases, additional information about the affected systems will be required before the specific cause of each effect can be defined. Since publication of the first data summary report (1) several airframe companies and other organizations have volunteered additional supporting information or made suggestions for improvements in presentation of data. This assistance is gratefully appreciated and will be taken advantage of as the program proceeds, so that the data can be made as useful as possible. A larger data base would be possible if additional airlines would cooperate in the project, and it is hoped that other airlines will join the project in the near future.

#### ACKNOWLEDGMENTS

The author wishes to thank American Airlines, Braniff International, Continental Airlines, Eastern Air Lines and United Air Lines for their support in organizing the project and providing the data reported herein. Assistance and advice from many other individuals and organizations is also gratefully appreciated.

#### REFERENCES

1. J.A. Plumer, "Data from the Airlines Lightning Strike Reporting Project," Summary Report 71-1, December 1971.

\*Numbers in parentheses designate References at end of paper.

Table 1 - Attachment Points and Effects

B-707

Attachment Points		Effects
Nose (pitot tube)	and HF antenna	• No. 1-HF tuner would not tune
Static air temp probe	and ?	• Static air temp probe burned out
Radome (1/2" hole and burn marks)	and ?	• No. 1 radar outage

B-727

Swept stroke along lower right side of fuselage from nose gear door to leading edge of wing root	and Vertical stabilizer (?)	• No. 1 and No. 2 compass systems out • ADF coupler in tail inoperative
Co-pilot's forward windshield	and ?	• Approx. 15 cracks from upper center corner to right side of co-pilot's forward windshield (no pressure fluctuations)
Swept stroke leaving 6 shiny spots 1/8" to 1/4" in size, in line 5" apart beginning just aft of radome on right, lower side of fuselage in front of nose gear door	and Oscillating tail light	• Flew off oscillating tail light lens and burned out light • Blew out two tail lightning arresters • Stewardess said "ball of fire" moved down aisle of cabin
Right wing tip	and Left wing tip (?)	• 90° error in both compass systems
Nose (?)	and Right wing tip trailing edge lamp	• Compass system "acted up" after strike "had to keep resetting" • "Felt one jolt on controls" • Crew flash blindness--was outside with heads close to windshields. • Lens and bulb broken on trailing edge light, all collar rivets burned and top side of collar pulled away from wing 1/4"
Radome	and Right wing tip outboard static discharger	• Chip of paint removed from radome • Outboard static wick knocked off at skin attachment point
Radome (1/8" hole)	and Swept stroke along fuselage leaving 12 to 15 burned marks running from main entrance door aft to No. 1 engine	• 1/8" hole in radome • 12 to 15 burned marks in skin
?	and ?	• Interference on No. 1 & 2 ILS-G/S • Differential fault on No. 3 generator
Nose (?)	and Left wing tip static discharger	• One trailing edge static discharger blown off

Table 1 - (Continued)

B-727

Attachment Points			Effects
Radome (2 pin-holes)	<u>and</u>	Swept stroke along fuselage from lower nose aft to left nose gear door	<ul style="list-style-type: none"> <li>• 2 pin-holes in radome</li> <li>• Interference-weather radar and No. 2 VHF</li> </ul>
Left outboard wingtip static discharger	<u>and</u>	?	<ul style="list-style-type: none"> <li>• "Flash and thump"</li> <li>• Interference in radio altimeter</li> </ul>
Left outboard elevator	<u>and</u>	?	<ul style="list-style-type: none"> <li>• No. 3 generator tripped</li> <li>• Discharge wick burned</li> </ul>
HF Antenna	<u>and</u>	Swear strike leaving 5 marks along belly of fuselage	<ul style="list-style-type: none"> <li>• Both HF's inoperative</li> <li>• Damaged lightning arrester and No. 1 HF coupler</li> </ul>

B-747

Radome (small burned spot)	<u>and</u>	Right horizontal and vertical stabilizers	<ul style="list-style-type: none"> <li>• 20x37" portion of upper skin panel missing on right stabilizer outboard of elevators</li> <li>• 19x29" portion of right stabilizer lower skin panel missing</li> <li>• Right tail light missing and electrical wiring damaged</li> <li>• Slight damage to right outboard elevator</li> <li>• Damage to right stabilizer trailing edge rib</li> <li>• Streaks on outer surface of first nine passenger windows on right side of fuselage</li> </ul>
Radome (?) (Destroyed by hail)	<u>and</u>	All static dischargers on wing and empenage tips	<ul style="list-style-type: none"> <li>• All static discharge wicks missing or burned down to short stubs</li> </ul>

DC-8

Radome (3 pin-holes)	<u>and</u>	Ground power umbilical cables	<ul style="list-style-type: none"> <li>• All ADF's inoperative</li> <li>• All altimeters off 400'</li> <li>• Flt-recorder light stays on</li> <li>• Aircraft would not accept AC power after strike</li> <li>• Worker loading aircraft knocked unconscious</li> </ul>
(Plane struck while on ground at airport)			
Radome (2 1/4" holes)	<u>and</u>	Both wing tip static wicks (burned) <u>and</u> Right stabilizer leading edge 12" out from fuselage <u>and</u> Several rivets burned on right stabilizer leading edge from top of front spar to bottom approx. 4' from tip	

Table 1 - (Continued)

DC-9

Attachment Points		Effects
Swept stroke creating 5 burned marks along 4" path on fuselage below left wing	<u>and</u>	VHF and UHF antennas <ul style="list-style-type: none"> <li>• VHF and UHF antennas required replacement</li> <li>• 10° spread in compass system</li> </ul>
Swept stroke creating 6 pit marks between nose and forward loading door	<u>and</u>	Flash entered passenger door and went out window in galley door <ul style="list-style-type: none"> <li>• One flight attendant was struck in the hands but not injured</li> </ul>
Radome (destroyed by hail) <u>and</u> Auxiliary pitot head	<u>and</u>	No. 2 VHF antenna <ul style="list-style-type: none"> <li>• Outage both compasses</li> <li>• Momentary crew disorientation</li> </ul>

SESSION VI

ADVANCED COMPOSITES, MATERIALS, AND STRUCTURES

H.S. SCHWARTZ, CHAIRMAN & ORGANIZER

U.S. AIR FORCE MATERIALS LABORATORY

Introduction to the Session on Advanced  
Composites, Materials, and Structures

H. S. Schwartz  
Air Force Materials Laboratory

ABSTRACT

The use of external aircraft components made of nonelectrically conducting materials (e.g. glass fiber reinforced plastics for radomes and transparent plastics for canopies) and poorly electrically conducting materials (e.g. boron and graphite fiber reinforced plastics for structures) require special design attention to assure resistance to structural damage when struck by lightning. Lightning protection techniques for radomes and canopies have been known and used for a number of years. More recently, lightning protection techniques and coatings have been developed for boron and graphite fiber reinforced plastics. An additional design consideration is the protection of electrical circuits housed within these materials from electromagnetic fields which may induce extraneous voltage, thereby causing malfunctions. Some research has been done in this area but additional research and information is needed for electrical design purposes.

FOR AN AIRCRAFT or other aerospace vehicle to have maximum resistance to the damaging effect of lightning, at a high confidence level, it is recommended by most authorities that the lightning current be confined to the outer surface or skin of the vehicle. An ideal situation would be for the aircraft surface to be a continuous aluminum skin, without any area of electrical discontinuity. Obviously, this situation does not exist for real aircraft, since certain functions and mission performance aspects necessitate the use of nonelectrically conductive materials on the outer surface. For example, windshields and canopies are either transparent plastic or glass, and radome materials are glass fiber reinforced plastic. These materials are good dielectrics and generally have a high dielectric strength (good resistance to puncture when a high voltage is imposed across the thickness of the material). When lightning strikes or sweeps across the surface of these materials, their high dielectric strength resists puncture over a certain distance called the "surface flashover distance". This surface flashover capability of good dielectric materials permits the use of the "spaced conductive element" approach for lightning protection. In this approach, aluminum or other conductive metal strips connected at one end to the metal airframe are placed on the surface, at a distance from each other slightly less than the surface flashover distance. When lightning strikes such a protected surface, it (should) flash over to the conductive metal strip and thence be conducted

to the airframe without significant damage occurring.

For radomes, windshields, and canopies, nonelectrically conductive materials are used of necessity. There are no suitable high electrical conductivity materials for these uses. However, in the structural materials area, there are options available to the designer. During the last few years structural fiber reinforced plastics have been developed which give lighter weight, more fatigue resistant aircraft structures than metals. Specifically these are boron fiber reinforced plastics and graphite fiber reinforced plastics. These materials are so attractive from a structural performance standpoint that they will very likely be used in a broad range of structural applications in aircraft in the coming years, even though neither material is a good electrical conductor.

Boron fiber reinforced plastics are macroscopically a dielectric material analogous to glass fiber reinforced plastics. Microscopically, however, they consist of an array of conductive elements in an electrically insulating two phase matrix. Boron fibers are made by chemical vapor deposition of boron on a heated tungsten wire. During the fiber formation process, most of the tungsten "core" is converted to tungsten borides. The conducting elements in the composite are the tungsten or tungsten boride "cores" of the boron filaments. One phase of the insulating matrix is the boron "sheath" which surrounds the core; the other phase of insulating matrix is the plastic (e.g. epoxy) which surrounds the boron fibers. When an unprotected boron fiber plastic composite is exposed to sufficiently high voltages and current, (representing moderately severe lightning strikes) dielectric breakdown of the insulating phases occurs. Current flows in the core raising its temperature, and causing it to expand against the restraint by the boron sheath. When the strain caused by the core expansion exceeds the maximum strain capability of the boron sheath, the boron cracks, both longitudinally and radially causing the loss of structural integrity of the composite.

Graphite fiber reinforced plastics are quite different, electrically, from boron fiber reinforced plastics. Graphite fibers are homogeneous from an engineering standpoint, and have moderate electrical conductivity. When graphite fibers are combined with a plastic laminating resin to form a composite, the composite has measurable electrical conductivity under low voltage

(no dielectric breakdown) conditions. When an unprotected graphite fiber plastic composite is exposed to sufficiently high voltage and current, current enters the graphite fibers by both direct conduction and dielectric breakdown of the plastic laminating resin. The graphite fibers are heated to a temperature sufficiently high to cause pyrolysis (decomposition, vaporization) of the plastic laminating resin in contact with the graphite fibers, causing loss of structural integrity of composite.

In order to assure that boron and graphite fiber reinforced plastic composites would maintain structural integrity after being struck by lightning, various protective materials and techniques have been evaluated and developed during the past few years. The approach which has been demonstrated to be most effective is the use of an electrically conductive coating or overlay over the surface. Aluminum foil, flame sprayed aluminum and aluminum wire fabrics have been shown to be effective in protecting boron and graphite fiber reinforced plastics from structural damage at peak currents as high as 200KA. In the interest of objectivity no assessment will be made here of which coating system is best using various criteria such as performance, weight, cost, fabricability, durability, etc. The information presented at the 1968, 1970 and 1972 Lightning and Static Electricity Conferences should be adequate for the reader to draw his own conclusions as to which coating has the best balance of properties. (1), (2)\*. The important point is that from a structural standpoint, boron and graphite fiber reinforced plastics can be protected from lightning damage with coatings weighing no more than that of about two coats of paint. Information to substantiate this statement has been presented at the 1970 Lightning and Static Electricity Conference and additional corroborating information will be presented at this conference in this session. In addition, one of the papers to be presented at this session will present information on development and evaluation of a lightning protection system for a flight scale boron fiber reinforced plastic aircraft structure.

Although the principles of protecting boron and graphite fiber reinforced plastics from structural damage by lightning have been established, there are still certain engineering details that will probably have to be worked out or evaluated for specific applications. For example, suppose a boron or graphite composite skin covered with a lightning protective coating is fastened with metal rivets or bolts to a metal spar or rib. Will the lightning current be confined to the coating, go through the fastener to the substructure, spread out in the composite, or do a combination of these things? This sort of

evaluation of detail design is analogous to what has been required in other areas of lightning protection, such as protection for fuel systems, helicopter rotor blades, etc, so we are really following a philosophy that has already been established.

The prototype development work and production applications of boron and graphite fiber reinforced plastics in aircraft structures have also focused attention on the "electromagnetic compatibility" aspects of these composite materials. The term "electromagnetic compatibility" as used here refers to the influence of the composite materials on the functioning of on-board electrical and electronic circuitry in the presence of both external electromagnetic fields and fields generated by on-board circuitry. The electromagnetic shielding properties of bare boron and graphite fiber reinforced plastics are several orders of magnitude less than that of aluminum of equivalent thickness. Some shielding will be provided by a conductive lightning protective coating on the external surface of the composite. However, it is likely that special design attention will have to be given to this area to assure the desired electrical performance.

Designing for electromagnetic compatibility will require the availability of analytical design procedures, information on electrical properties of materials, and data on the performance of electrical and electronic circuitry housed within representative composite material components to validate the analysis and design procedure. Some work to provide some of the required information has already been done and is being reported at this conference. However, a great deal of additional work is needed to provide the remaining required information and to provide a high confidence level in the ability to design for and provide assurance for adequate electrical performance. We also need to maintain the dialogue among the engineers and scientists representing the various disciplines that are relevant to this area. Conferences such as this are one way in which this can be accomplished or at least catalyzed. After the conference is over we will hopefully maintain communication among organizations and individuals which is so vital to advancing the technology.

\*Numbers in parentheses designate References at end of paper.



#### REFERENCES

1. L. G. Kelly and H. S. Schwartz, "Investigation of Lightning Strike Damage to Epoxy Laminates Reinforced with Boron and High Modulus Graphite Fibers". Lightning and Static Electricity Conference, 3-5 December 1968. Technical Report AFAL-TR-68-290, Part II., pp. 485-519. May 1969.
2. J. G. Breland, Jr., J. T. Quinlivan and C. J. Kuo, "Lightning Protective Coatings for Boron and Graphite Fiber Reinforced Plastics". Lightning and Static Electricity Conference, 9-11 December 1970, pp 233-251.

Current Flow Phenomena in Boron and  
Graphite Fiber Reinforced Composites  
Exposed to Simulated Lightning

John L. Perry  
Philco-Ford Corporation

Kenneth J. Lloyd  
General Electric Company

ABSTRACT

Damage due to the flow of high energy electrical current in boron and graphite reinforced plastic matrix composites was studied on both a filament and composite level. Degradation levels were established for these composites at various simulated lightning waveform shapes and current amplitudes. Electric current flow and its effect was measured in current restricted paths of unidirectional oriented composites and also in current dispersion paths of multioriented composites. It was found that the total electric energy input and the heat dissipation were the most important factors in the degradation mechanism. Composite specimens of boron reinforced filaments fail at a filament level, whereas those of graphite reinforced filaments fail at the matrix level.

A JOINT exploratory research program between the Aeronutronic Division of Philco-Ford and General Electric Company's High Voltage Laboratory has been concerned with electric current induced damage in boron and graphite reinforced plastic matrix composites (1)\*. This program was initiated and sponsored by the Naval Air Systems Command in response to data presentation which demonstrated that boron filament epoxy composites were extensively degraded as the result of high intensity electric current flow (2). The significance of the data depends upon the probability that extensive usage of these lightweight, strong and stiff composites will be made in future generation aircraft; coupled with the distinct possibility that such electrical current damage could occur to these composites as the result of a lightning strike to the aircraft.

The overall objective of this program was to perform research into the effects of high intensity electric currents on advanced filament reinforced plastic composites. Specifically, the work was to be directed toward those current high strength and modulus filament types that have been developed for use in structural composites for advanced aircraft. Also, the electric currents to be used in the study were to be representative of those that

might occur as the result of a lightning strike to the surface of an aircraft. Following this overall approach, the program was oriented to study the processes involved in electric flow through filaments and composites and in the determination of the mechanisms of any damage resulting from the current flow. Introductory to this, however, was the materials selections and characterizations that were made preparatory to the current flow and damage mechanisms research.

The approach which was used in this program was to expose the filaments and composites to the passage of electrical current by injecting the current into the specimen and causing the current to flow through the filament or the composite. The program did not include studies of the highly severe type damages that might result at the point of lightning stroke attachment. Instead, the program studied the effects of and current flow processes involved when the electric current from such a strike disperses throughout surrounding structures of advanced boron or graphite filament reinforced plastic composites such as are planned for use in advanced military aircraft

MATERIALS AND TEST SPECIMENS

In the program both filaments and epoxy resin composites of boron and graphite filaments were evaluated. The boron filaments included both the standard filament manufactured with a tungsten substrate core and also included those in which the boron is chemically vapor deposited onto a substrate carbon core filament. Two varieties of graphite filament were investigated, a graphite tow produced from a polyacrylonitrile precursor and a graphite yarn manufactured from a rayon precursor. The specific filamentary reinforcements were:

1. Hitco's - HMG 50 graphite yarn.
2. Courtauld's - HMS graphite tow.
3. United Aircraft Corp. - Boron filaments with tungsten core.
4. Supplied by the Air Force Material Laboratory - Boron filaments with carbon core.
5. Union Carbide - Thornei 75S graphite yarn.
6. Whittaker - Modmer II graphite tow.

\* Numbers in parentheses designate References at end of paper.

7. Minnesota Mining's SP-272 boron epoxy prepreg. The epoxy resin matrices in the composites were Dow Chemical's DEN 438/MNA, Whittaker's 1004, and 3M's PR 279 resin which is the resin system in their SP-272 prepreg. Test specimens included: (1) 15-inch pieces of filament, (2) unidirectional 7" x 0.5" x 0.025" tensile specimens, (3) unidirectional 6" x 0.5" x 0.1" flexural specimens, and (4) multioriented ply composite panels possessing four electrical injection attachment sites. The electrical current exposure levels were obtained by the use of a single current pulse with a wave shape front time generally in the range of 3-4 microsecond and a tail time of 22-24 microseconds.

#### EVALUATION OF BORON/TUNGSTEN CORE FILAMENT AND BORON/CARBON CORE FILAMENT

It has been previously reported that boron/tungsten core filaments begin to degrade when exposed to electrical current injection levels at  $3.7 \times 10^4$  amps/cm<sup>2</sup> of filament cross-sectional area. Above this amperage level tensile strength reduction is rapid with total filament disintegration occurring at levels of  $8.0 \times 10^4$  amps/cm<sup>2</sup> (1). Figure 1 is a typical photograph of a boron/tungsten filament which has been exposed to a high degradation level of current. At damage thresholds the energy that is dispersed within the core is dissipated as heat and results in a thermal expansion to a degree that cracks the outer boron sheath. As illustrated by the specimen in Figure 1, this temperature can be of such magnitude as to melt the tungsten core, and as confirmed by scanning electron microprobe determination the molten tungsten core will actually flow into the cracks in the boron sheath. Figure 2 shows the same type of failure (axial cracking) of the boron/carbon core as was found with the boron/tungsten core. It appears that regardless of whether manufactured using a tungsten wire or a carbon monofilament substrate, the electrical conduction of the boron filament is still via the substrate core, due to the extremely low conductivity of the boron so deposited. It was determined that the degradation level of the boron-carbon core filaments compares to that of the boron-tungsten core filaments ( $3.7 \times 10^4$  amps/cm<sup>2</sup>) and that the majority of the current is carried by the core because of the very low conductivity of the boron sheath.

#### DAMAGE INSPECTION OF ELECTRICALLY EXPOSED BORON FILAMENTS

It has been observed that boron filament epoxy composites that have been degraded by electrical current contain some filaments that are cracked and some that are not. Photomicrographic studies showed that the proportion of the number of filaments with radial

cracks was higher in more severely degraded composites. These observations contributed to the suspicion that there is considerable variation in the conductivity of boron filaments within the composites, with the higher conductivity filaments carrying current and being damaged. This would be true only if the cracks in filaments are not local. In other words, is a filament that is observed to be cracked at one point in the composite also cracked at other points along its length, or are all filaments cracked locally at different points along their length? Attempts to trace single filaments micrographically along their lengths in a composite were not successful. Also, such observations were not possible in single boron filament electrical exposures. At a point where any cracking occurred in the absence of a confining plastic matrix the filaments would fall apart into a multitude of fine pieces. Therefore, in order to prevent this filament disarray, it was decided to encapsulate individual boron filaments within a resinous sheath. The embedment of the filament in a resin casting was to prevent any displacement of individual pieces caused by electrical degradation and to allow photomicrographs to be made along the length in order to determine if the damage is of a continuous or a local nature. Boron filaments were encased within a plastic casting by centering each filament within a thermoplastic soda straw. After closing one end, the straw was filled with a mixture of epoxy and polyamide resins (50-50 mixture of Epon 828 and Versamid 140), cured at room temperature and removed from the straw. The embedded filament specimen configuration was 7 inches in length, 0.20 inch diameter with a free end of the filament 3/4 inch in length protruding from each end of the casting. The specimens were exposed to 5.8, and  $10 \times 10^4$  amps/cm<sup>2</sup> (3 x 24 microsecond waveform) based on the cross-sectional area. Specimens from each series were mounted, polished, and photomicrographed at three positions along the length of the fiber 1/4 inch, 2 inches, and 4 inches from one end in order to ascertain the severity and location of the degraded area in the filament. Representative photomicrographs from each group are shown in Figures 3, 4, and 5. The specimen in Figure 3 which was exposed to  $5.0 \times 10^4$  amps/cm<sup>2</sup> of filament cross-sectional area had axial cracking present at the 2 inch and 4 inch position but not at the 1/4 inch position. The specimen in Figure 4 which was exposed to  $8.0 \times 10^4$  amps/cm<sup>2</sup> of filament cross-sectional area was cracked at all three locations (1/4 inch, 2 inch, and 4 inch) and the degradation (axial cracks) were more severe than was seen in the specimen in Figure 3 which was exposed to a lower current test. The specimen in Figure 5 which was exposed to  $10.0 \times 10^4$  amps/cm<sup>2</sup> of filament cross-sectional area was cracked at all three locations and was the most severely

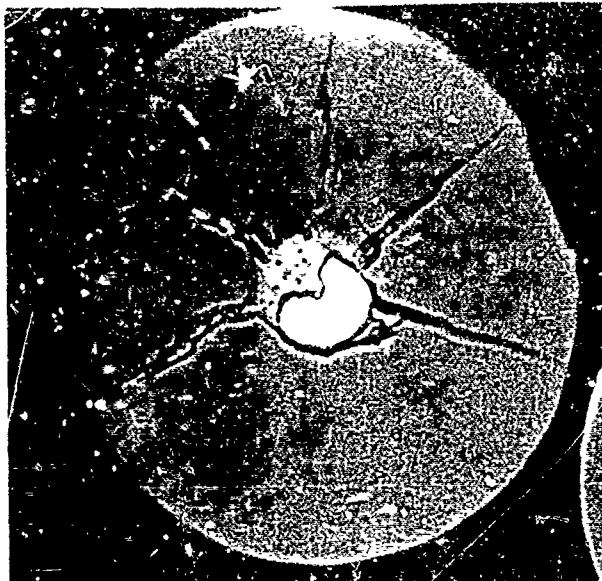


Fig. 1 - VIEW OF DAMAGED BORON TUNGSTEN  
CORE FILAMENT IN COMPOSITE  
SPECIMEN (800X)

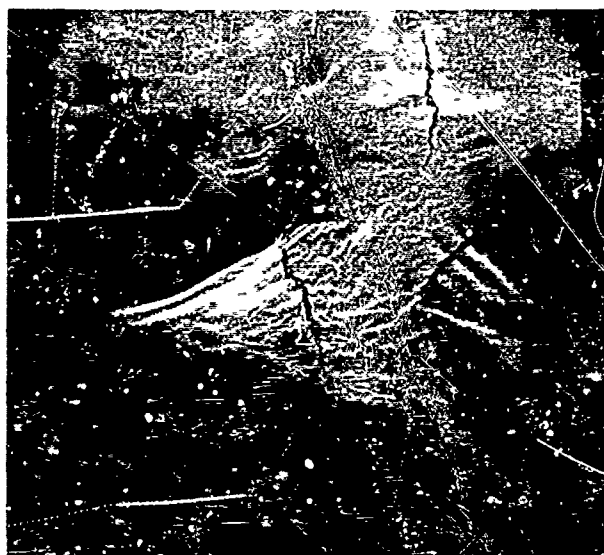
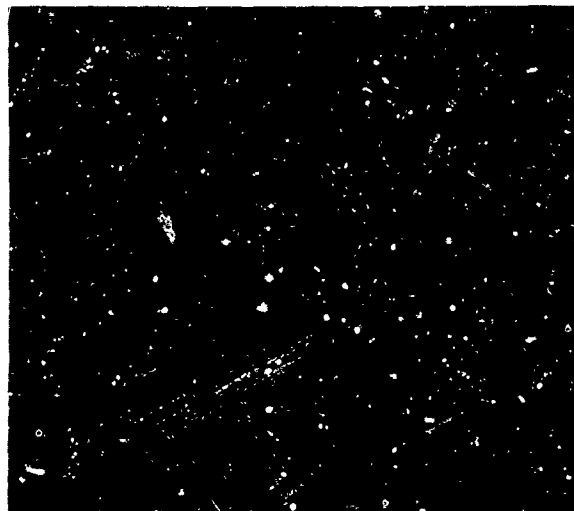


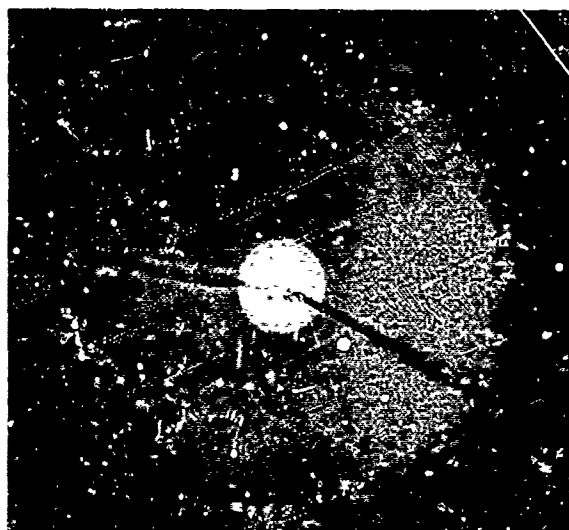
Fig. 2 - BORON CARBON CORE FILAMENT  
EXPOSED TO  $3.7 \times 10^4$  amps/  
 $\text{cm}^2$  CURRENT INJECTION,  
(200X) LONGITUDINAL VIEW



A. (800X)

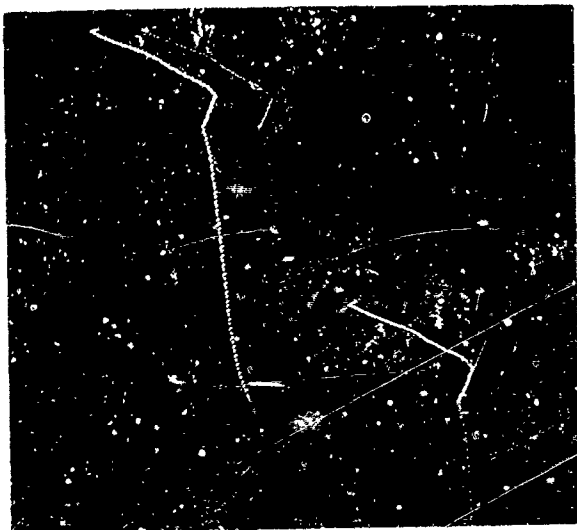


B. (800X)

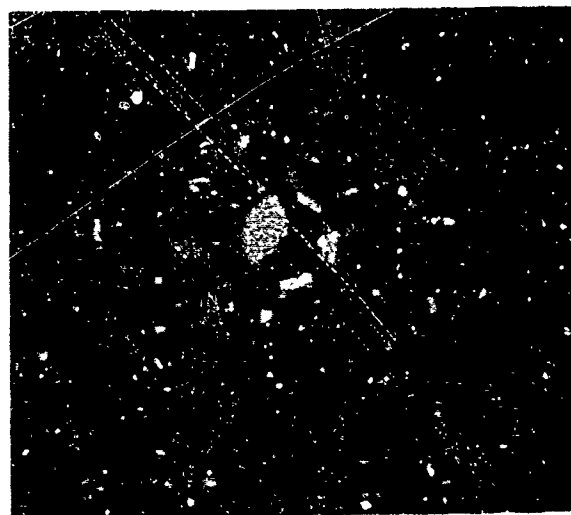


C. (800X)

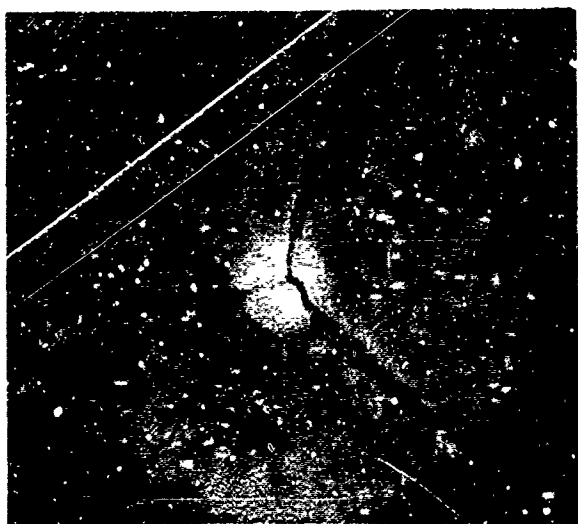
Fig. 3 - SPECIMEN NO. 22, BORON FILAMENT AFTER EXPOSURE TO  $5.0 \times 10^4$  amps/cm<sup>2</sup> ELECTRIC CURRENT INTENSITY. (A = CROSS-SECTIONAL VIEW 1/4 INCH FROM FILAMENT END; B = CROSS-SECTIONAL VIEW OF 2 INCHES FROM FILAMENT END; C = CROSS SECTIONAL VIEW 4 INCHES FROM FILAMENT END.)



A. (800X)

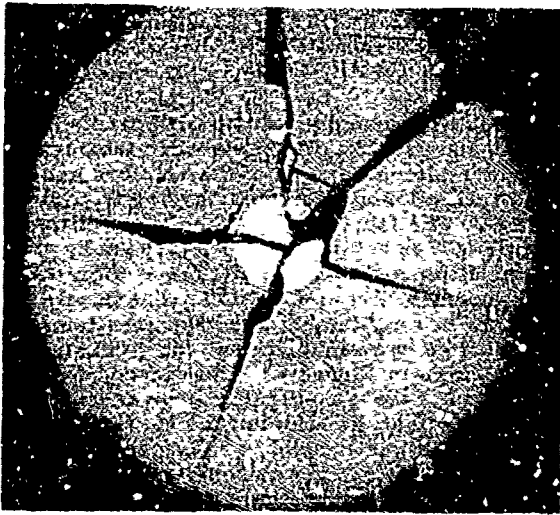


B. (800X)

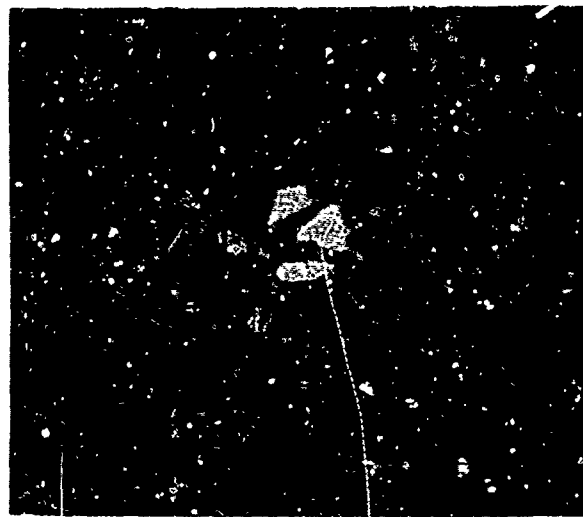


C. (800X)

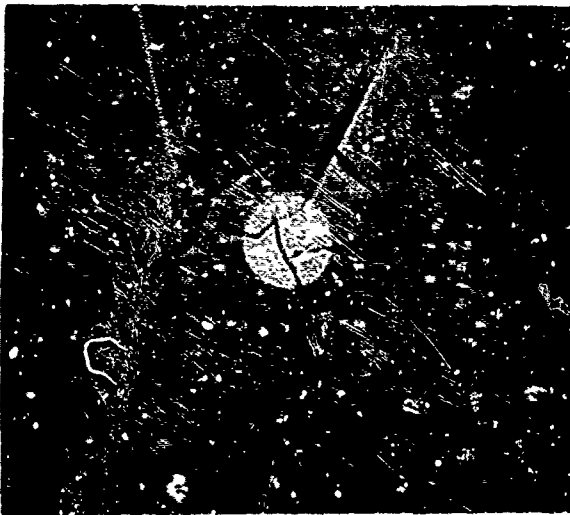
Fig. 4 - SPECIMEN NO. 23, BORON FILAMENT AFTER EXPOSURE TO  $8.0 \times 10^4$  amps/cm<sup>2</sup> ELECTRIC CURRENT INTENSITY (A = CROSS-SECTIONAL VIEW 1/4 INCH FROM FILAMENT END; B = CROSS-SECTIONAL VIEW 2 INCHES FROM FILAMENT END; C = CROSS-SECTIONAL VIEW 4 INCHES FROM FILAMENT END)



A. (800X)



B. (800X)



C. (800X)

Fig. 5 - BORON FILAMENT AFTER EXPOSURE TO  $10.0 \times 10^4$  amps/cm<sup>2</sup> ELECTRIC CURRENT INTENSITIES. (A = CROSS-SECTIONAL VIEW 1/4 INCH FROM FILAMENT END; B = CROSS-SECTIONAL VIEW 2 INCHES FROM FILAMENT END; C = CROSS-SECTIONAL VIEW 4 INCHES FROM FILAMENT END)

degraded of all three specimens. The photomicrographs clearly indicate the following:

1. The degradation is directly related to the injection current level.
2. The boron filament (degraded by the passage of electrical current) is characterized by circumferential and axial cracking of the tungsten core and the boron shell.
3. The degradation appears to be of a local nature (Figure 3) at lower levels of damaging current flow and may appear at weak locations of the specimens.
4. The degradation appears to be continuous along the filament length (Figures 4 and 5) for those specimens which have been exposed to higher current injection levels.

#### INFLUENCE OF WAVEFORM SHAPE UPON THE DEGREE OF DEGRADATION

Available data indicate that current flow resulting from lightning strikes rises to a maximum amplitude in a short period of time and decays over a much longer period of time. The rise is referred to as front time ( $t_f$ ) and the decay as tail time ( $t_t$ ). Typical peaks have front times of 1-10 microseconds and tail times of 10-50 microseconds. Prior work has shown that degradation levels in boron epoxy composites could be correlated to the resistive energy dissipation of electric current flow in such composites (1). However, in the previous work a single current waveform was utilized and the exposure levels were changed by varying the crest amplitude of the current. As it was suspected that the degree of degradation was not solely dependent upon the crest amplitude, further testing was accomplished with boron and graphite epoxy composites in which front times and tail times of the wave shapes were varied.

Unidirectional tensile specimens (0.025 inch thickness x 0.10 inch width x 7 inch length) were fabricated of HMG-50 graphite with DEN 438-MNA epoxy and of 3 M's SP-272 boron epoxy tape. Each end of the individual specimens was scarfed, vapor honed and nickel plated for electrical contact. Specimens were exposed to various current crest level variables and waveform variables. Four variations in waveform were investigated:  $t_f$  and  $t_t$  of 1 x 10, 3 x 10, 3 x 24, and 3 x 50 microseconds. Variations in the current intensity injected, based on the total cross-sectional area of the filaments in each specimen, in amps/cm<sup>2</sup> were in the range of 5 to 60 x 10<sup>4</sup> for boron composites and 10 to 33 x 10<sup>4</sup> for the graphite composites.

The relation of the percent tensile strength degradation for three waveforms at various current crest levels is graphically presented in Figure 6 for both the boron-epoxy and graphite-epoxy composites. It appears that one relationship holds true for both the boron and graphite composites, i.e., damage in both composites is directly related to the total energy deposition.

#### ELECTRICAL CURRENT FLOW PATHS IN MULTIORIENTED BORON AND GRAPHITE FILAMENT COMPOSITES

Multi-oriented ply composite panels of boron and graphite filaments were fabricated in which alternate plies of the reinforcement were directionally oriented varying from 0° to 90°. The fabrication of the panels utilized 3M SP-272 boron filament/PR-279 epoxy composition and Modmor II filament/Whittaker 1004 epoxy resin composition. The panels of both the boron filament and graphite filament composites were machined to the configurations shown in Figure 7. The reasons for selection of these configurations was to place cutouts so that the effect of the current flow to different points could be measured as a function of the number of non-interrupted filament conduction paths. Each point of electrical contact was nickel plated for that purpose. After electrical exposure the panels were dissected and flexural specimens were taken from various locations in order to determine areas of electric current damage. To determine percent loss in strength due to the electrical exposures an identical panel of each material and configuration was dissected and flexural specimens from identical locations tested. The degradation at each location then was expressed as a percentage reduction in flexural strength from the three point bending flexural test. Figures 8 and 9 present the data obtained during the electrical injection testing of boron and graphite composite panels which were fabricated using ply orientations of 0°, +45°, -45° and 90°. In each figure, point No. 1 is the point of current injection. Points No. 2, 3, and 4 were connected to ground and the amplitude of current injected to point No. 1 and exiting points 2, 3, and 4 was measured.

The location of the flexural specimens tested after electrical injection are drawn on the panel configurations and the percent degradation as measured for each specimen is noted within the rectangle that denotes each specimen. Two current injection levels were selected for each panel. The first level was of a low non-degrading magnitude to evaluate current flow paths, in the absence of degradation, due to current flow. The second was of a higher current level to insure composite damage in order to study relative locations of such damage.

The studies performed with the several combinations of filament orientations and composite panel geometries show that: In boron filament epoxy composites the electric current will flow predominantly in the boron filaments that intersect the point where the current is introduced into the panel.

Electric current flow in graphite filament epoxy composites appears to be isotropic in that equal flow is independent of filament orientation. The current flow proceeds to several ground contact points independent of



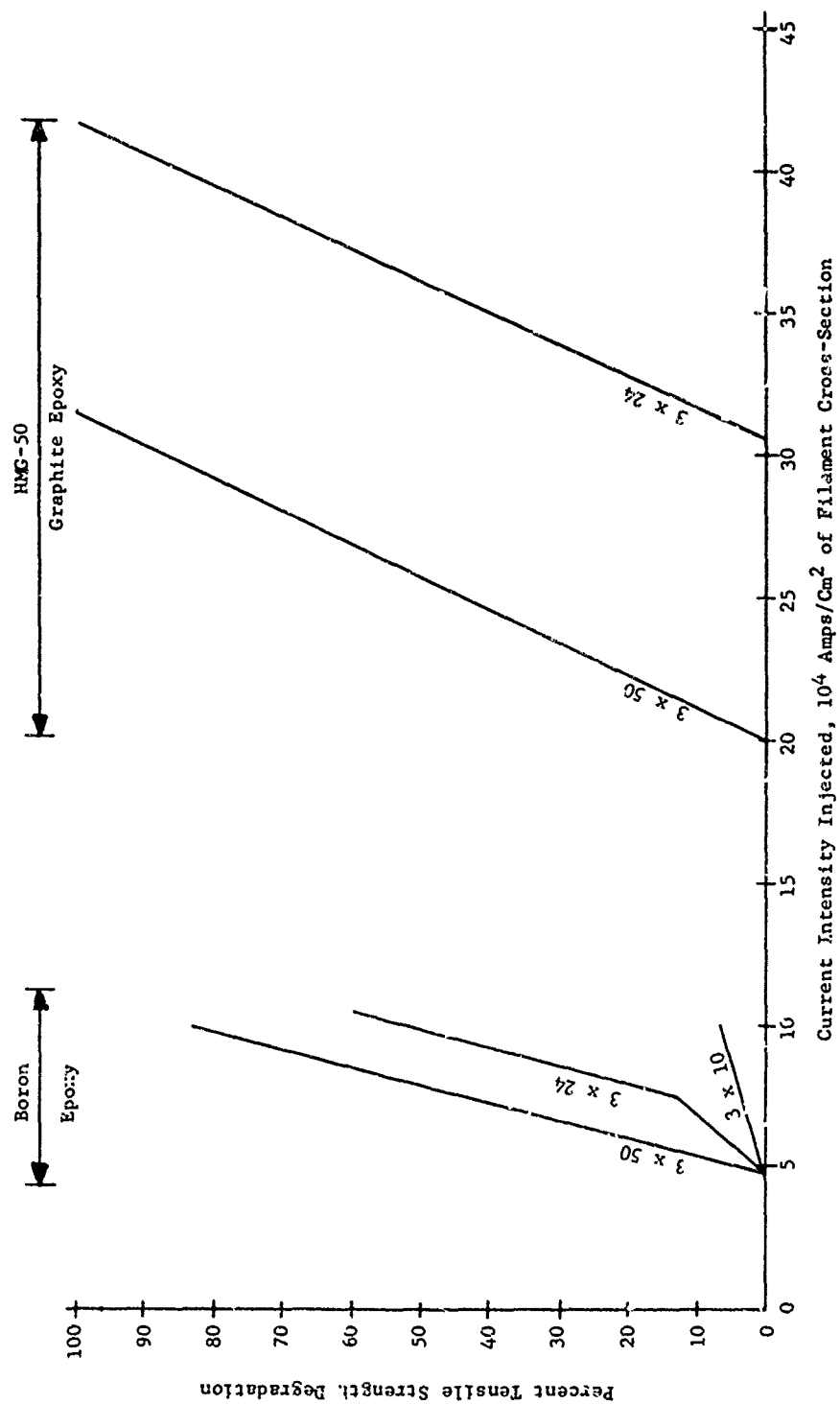
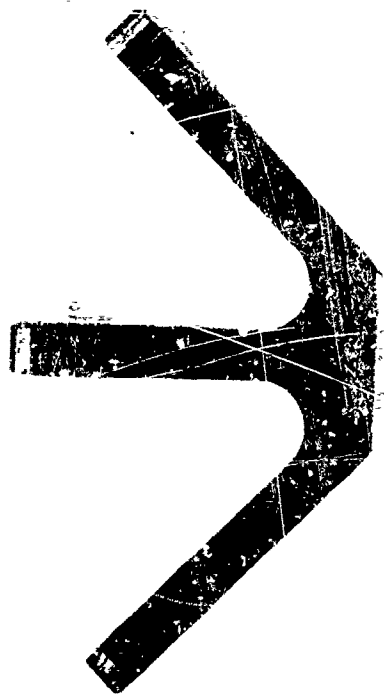


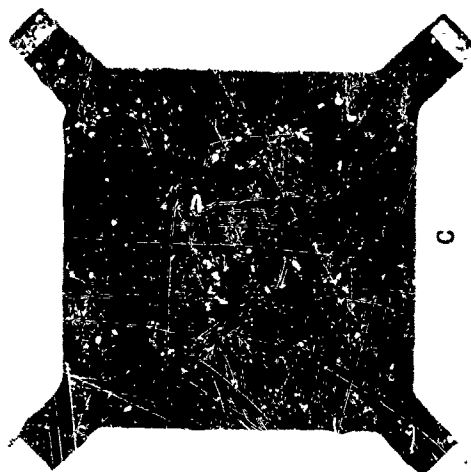
Fig. 6 - Tensile strength degradation at various waveform and current amplitudes for boron and graphite epoxy composites



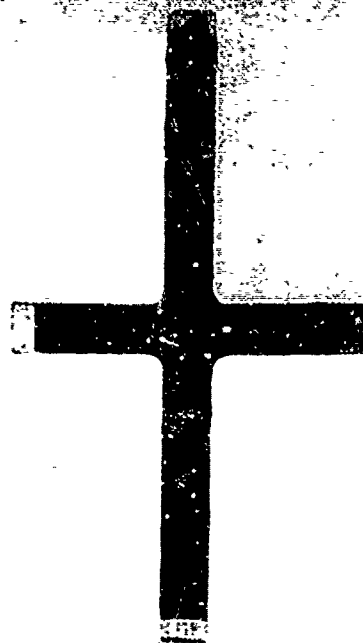
A



B



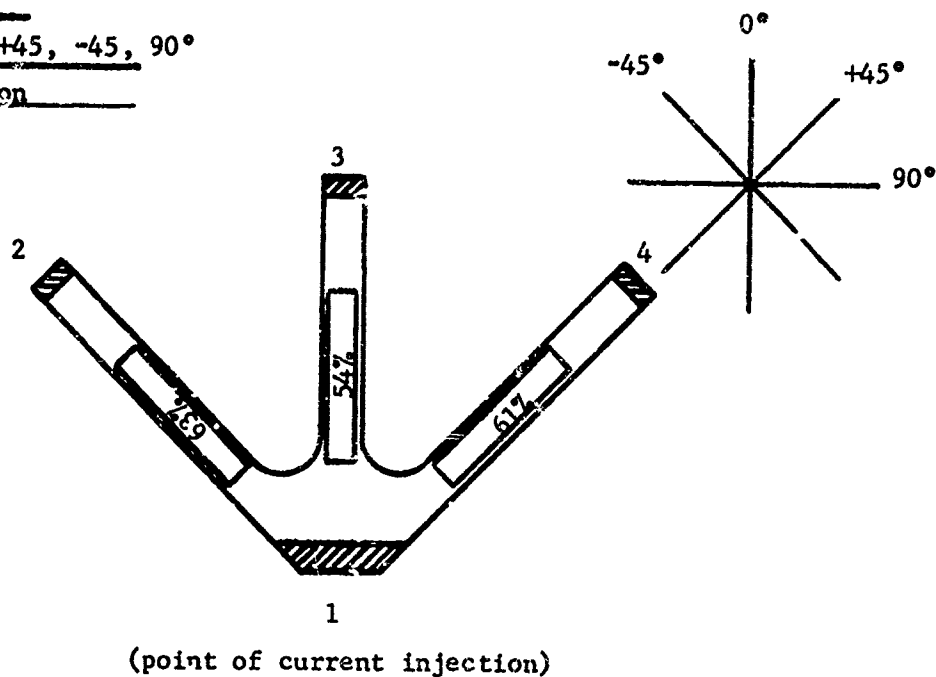
C



D

Fig. 7 - Four types of configurations of multioriented ply composite test specimens for electrical current flow path evaluations.

Panel BA-1a  
 Plies 12  
 Orientation 0, +45, -45, 90°  
 Filaments Boron



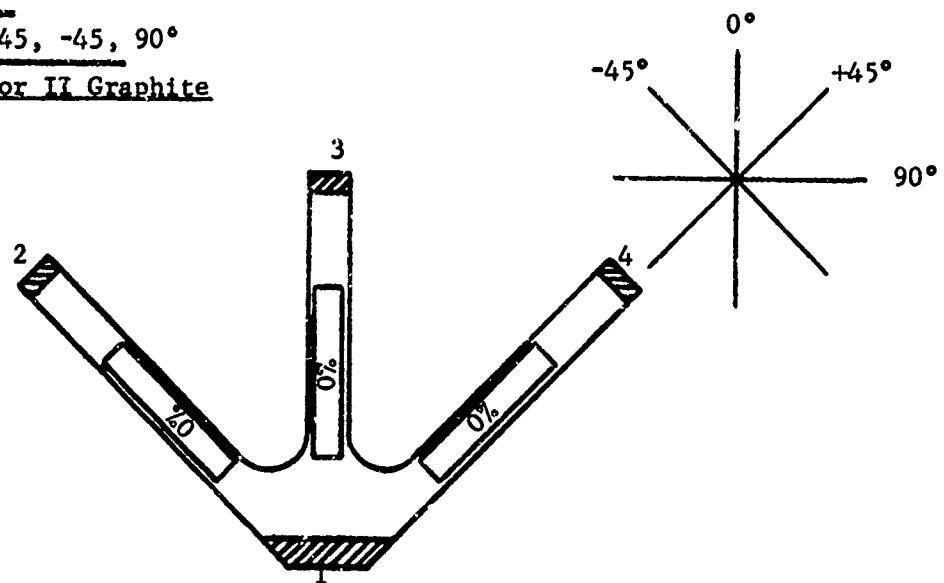
Low level current level (100%) 3,570 amps  
 High level current level (100%) 13,000 amps

	Current Flow in Percent			
	Term 1	Term 2	Term 3	Term 4
Low Level	100	34.7	32.8	32.5
High Level	100	38.4	No oscillogram	

	Resistance in Ohms Between		
	1-2	1-3	1-4
Before low level current injection	1.57	1.41	1.49
Between low and high levels	1.15	1.07	1.18
After high level current injection	53,800	46,800	49,900

Fig. 8 - Panel BA-1a

Panel GA-1a  
 Plies 8  
 Orientation 0, +45, -45, 90°  
 Filaments Modmor II Graphite



(point of current injection)

Low level current level (100%) 23,700 amps

High level current level (100%) 35,200 amps

	Current Flow in Percent			
	Term 1	Term 2	Term 3	Term 4
Low Level	100	32	36.5	31.5
High Level	100	31.6	37.6	30.8

	Resistance in Ohms Between		
	1-2	1-3	1-4
Before Low Level Current Injection	0.320	0.230	0.284
Between Low and High Levels	0.350	0.257	0.356
After High Level Current Injection	0.338	0.234	0.650

Fig. 9 - Panel GA-1a

whether or not there are filaments in the direction of the current flow.

## CONCLUSIONS

1. Investigations have verified that the substitution of a carbon monofilament for the tungsten wire commonly used as a substrate for the manufacture of boron filaments does not significantly affect the damage mechanisms or threshold of damage resulting from high intensity electric current flow.

2. Electric current injection tests were performed on single boron filaments that were encapsulated in plastic to study crack frequency as a function of the severity of the current injection. At damage threshold levels of current injections the radial cracks in boron filaments are localized, probably in weaker areas of the filaments. At higher levels the radial cracks become more severe in number at any one location on the length of filament and cracks are perpetuated throughout the length of filament so exposed.

3. The controlling factor in the degree of degradation for the boron and graphite composites is the total energy that is resistively dissipated within the composites. In other words, the same degree of degradation can be produced by low current amplitude, long duration current waveforms as was produced by very high current amplitude, short duration current waveforms.

4. Studies were performed with boron and graphite composites fabricated using different ply filament orientation ( $0^\circ$  to  $90^\circ$ ) which varied the amount of fibers in the direct current flow path. For boron composites it was determined that the electric current will flow predominantly in those fibers that directly connect to the area in which the current is introduced into the panel. For graphite composites the flow was independent of filament orientation and the current flowed not only to those areas which were directly linked by conductive fibers but also to those areas in which there was no direct fiber connection with the electrical injection sites.

## REFERENCES

1. A. P. Penton, J. L. Perry, and K. J. Lloyd, "The Effects of High Intensity Electrical Currents on Advanced Composite Materials," Final Report, Contract N00019-70-C-0073, dated 15 September 1970, Final Report, Contract N00019-71-C-0063 dated 21 March 1972.

2. Lightning and Static Electricity Conference, 3-5 December 1968, AFAL-TR-68-290, Part II, May 1969.

## Electromagnetic Shielding Properties of Composite Materials

F.A. Fisher  
General Electric Company  
Corporate Research and Development

### ABSTRACT

Boron-epoxy and graphite-epoxy composite materials have electromagnetic shielding capabilities that are poorer than aluminum by several orders of magnitude. Measured magnetic-field attenuations provided by 0.120 inch thick graphite-epoxy ranged from 6 dB at 1 MHz to 20 dB at 6 MHz. Boron, having higher resistivity than graphite, has correspondingly lower shielding effectiveness. Conductive coatings used for lightning protection may add substantially to the shielding provided by a composite material. A coating of silver paint 0.003" thick raised the shielding effectiveness of 0.040" thick graphite-epoxy from 17 dB to 25 dB at 20 MHz while a coating of flame-sprayed aluminum raised the effectiveness of 0.083" boron-epoxy from about 6 dB at 5 MHz to 33 dB. None of the painted or flame-sprayed coatings however approach the shielding effectiveness of a metal sheet or foil. Aluminum foil only 0.0016" thick provides nearly 50 dB of shielding at 10 MHz. An implication of the poor shielding effectiveness of the composite materials is that as composite materials replace aluminum, the electromagnetic shielding provided inadvertently, and at no cost or weight penalty, by structural designers will diminish. The designers and users of electrical and avionic equipment in aircraft of the future must assume the responsibility of shielding against the electromagnetic effects of lightning and assume the burden of justifying the resulting costs and weights.

LIGHTNING PROTECTION of aircraft involves not only protection against the direct burning and blasting effects of lightning, but against the electromagnetic interference associated with lightning as well.

Electromagnetic interference is perhaps too mild a term to use in connection with lightning. Electromagnetic damage potential is perhaps a more valid term. Control of the electromagnetic damage potential associated with lightning is a many-sided problem. Some key questions are:

- (1) What electromagnetic threat level is presented to an airplane by a lightning stroke?
- (2) What shielding is provided against the electromagnetic fields?
- (3) What kind of surge voltages and currents are produced on aircraft electrical systems?
- (4) What is the vulnerability of avionic equipment to the fields, voltages and currents associated with a lightning strike?

This paper deals with the second question above. It is prompted by the observation that

the newer composite materials have much less electromagnetic shielding capability than the historically used aluminum. Increasing use of composite materials, coupled with increasing susceptibility and vulnerability of avionic equipment implies the potential for severe hazards in the future.

During a series of tests, investigating further the mechanism of damage to composite materials in the event of a lightning flash, a number of boron-epoxy and graphite-epoxy test panels of various thicknesses and coatings were available. A number of these were tested for their electromagnetic shielding capability, both under high level pulse conditions and under low level CW conditions.

### PULSE MEASUREMENTS OF SHIELDING FACTORS

The original goal during this program was to measure electromagnetic fields at points on the back side of the composite sheets during the high current tests on the panels and to relate these measurements to the intrinsic shielding effectiveness of the panels.

The idea proved not to be as attractive as it originally seemed. Measurements of shielding factors obtained with continuous wave (CW) test techniques yielded more useful data. Nevertheless, some interesting data was obtained under high current pulse conditions.

The principle of measurement involved measuring the magnetic field produced inside a steel tank (29 inches diameter, 38 inches high) by the flow of current across an opening in the top of the tank.

The composite panel under test was placed over the opening in the top of the tank and a magnetic field produced by a high current discharge circulated through a one-turn loop two feet in diameter and one foot above the panel.

The magnetic field produced by the flow of current through the loop was measured by a field sensor consisting of three orthogonally-mounted loop antennas, each of two-inch diameter and wound with 10 turns. A changing magnetic field inside the tank would induce in these loops signals proportional to the time rate-of-change of the field, the output from each coil being proportional to the vector component of the field. The outputs of the coils were coupled to three identical integrating amplifiers, the outputs of which were thus proportional to the H-field inside the test enclosure. The coils were placed 1 foot below the panel.

The surge current was produced by the discharge of a 54  $\mu$ f, 50 KV capacitor bank. The current was oscillatory with a period of 2.75  $\mu$ s, corresponding to a frequency of 36.4 kHz. Currents ranged from 43 kA, (kilo-amperes) to 130 kA, producing ambient fields inside the test enclosure (no test panel in place) of 130 A-T/M (ampere turns per meter) to 440 A-T/M.

The panels tested were graphite-epoxy,

circular in shape (13 inches diameter) and either 0.040" (4 ply) or 0.120" (16 ply) thick. The materials were Union Carbide Thorne1-50 graphite yarn and Union Carbide Bakelite ERIA 2256 resin. Panels were either uncoated or coated with silver paint of about 0.003" thickness. Test results are given in Table I.

The panels provided very little shielding, 0.5-1.5 dB. As a comparison a thin sheet of aluminum foil of 0.0016" thickness provided over 20 dB shielding.

#### CONTINUOUS WAVE MEASUREMENTS OF SHIELDING FACTORS

The best data shielding effectiveness of the composite materials was obtained with CW measurement. The measurement technique employed was one described by Eckersley (1).

The principle of measurement is shown on Figure 1. A constant current was maintained in a transmitting loop while a receiving loop was connected to a detector. The relative readings of the detector with and without a test specimen between the loops was related to the shielding effectiveness of the specimen. For most metallic materials a ground on each coil is sufficient to prevent electrostatic pickup and erroneous measurements. With these nonmetallic materials it was found that a single ground on each coil was not sufficient, and that each coil had to be completely screened to prevent errors due to electric-field coupling through the material. This alone was a measure of the poor shielding effectiveness of these materials, since even the thinnest sheet of metal provides almost complete shielding against a high impedance electric field if it is well grounded. The transmitting and receiving coils were identical, each consisting of 25 turns wound on an 0.75 inch diameter coil form.

The transmitting coil was excited with an oscillator and wideband amplifier, creating a magnetic field (H-Field) between the transmitting and receiving coils, thereby producing a voltage across the receiving coil. The receiving coil was connected by coaxial cable to a Tektronix 1A1 plug-in mounted in a Tektronix Type 547 oscilloscope, which served as a detector.

The procedure was to establish at a specific frequency an ambient voltage level, as read on the oscilloscope, with the coils coaxial and the test panel absent. It was important that the distance between the coils, with and without the composite sample in place be the same, since the energy coupled between two coils at close spacings varies inversely as the cube of the distance between them.

The current in the transmitting coil was kept constant during the tests, and was monitored using a Tektronix Type 131 current probe. A change in current in the transmitting coil could be caused by reflection of part of the created H-field back to the transmitting coil

when the test panel is placed between the two coils. This change in Current, I, would change the ambient voltage level and an error would result in measurement and subsequent attenuation calculation.

The amount of H-field attenuation afforded by the shielding properties of the composite material was calculated by:

$$\text{Attenuation} = 20 \log \frac{V_1}{V_2} \quad (1)$$

where  $V_1$  is the ambient voltage reading and  $V_2$  is the voltage reading on the oscilloscope with the composite material placed between the coils. The energy transfer between two closely spaced loops was primarily a condition of magnetic coupling, and thus the attenuation values measured in this fashion are applicable chiefly when the shield material is to be used against low impedance or predominately magnetic fields.

To avoid fringing effects the receiving coil was placed in a metal enclosure and during tests the composite test panel was placed over an opening in the top of the metal enclosure.

An initial series of measurements was made on four materials:

- (1) 0.125" thick aluminum plate
- (2) 0.0016" thick aluminum foil
- (3) .0625" mesh bronze screen
- (4) a boron-epoxy laminate

As might be expected, the laminated material produced little electromagnetic shielding. The measurements on the other materials show some anomalies, the shielding effectiveness not increasing uniformly with frequency. It was these anomalies that led to the conclusion that the transmitting and receiving coils had to be well-shielded. While the absolute accuracy of the data of Figure 2 is questionable, it does indicate the relative shielding effectiveness that may be expected from some representative materials.

Once the measurement technique was debugged, measurements were made on the following types of composite materials:

- (1) 13" diameter graphite panels with no protective coating - 0.040" and 0.120" thickness.
- (2) 13" diameter graphite panels with silver-paint coating - 0.040" and 0.120" thickness.
- (3) 6" x 12" rectangular graphite panels with black carbon coating - one thickness - 0.083".
- (4) 6" x 12" rectangular graphite panels with black carbon coating.
- (5) 6" x 12" rectangular boron panels with black carbon coating.
- (6) 6" x 12" rectangular graphite panels with silver-paint coating.

\*Numbers in parentheses designate references at end of paper.

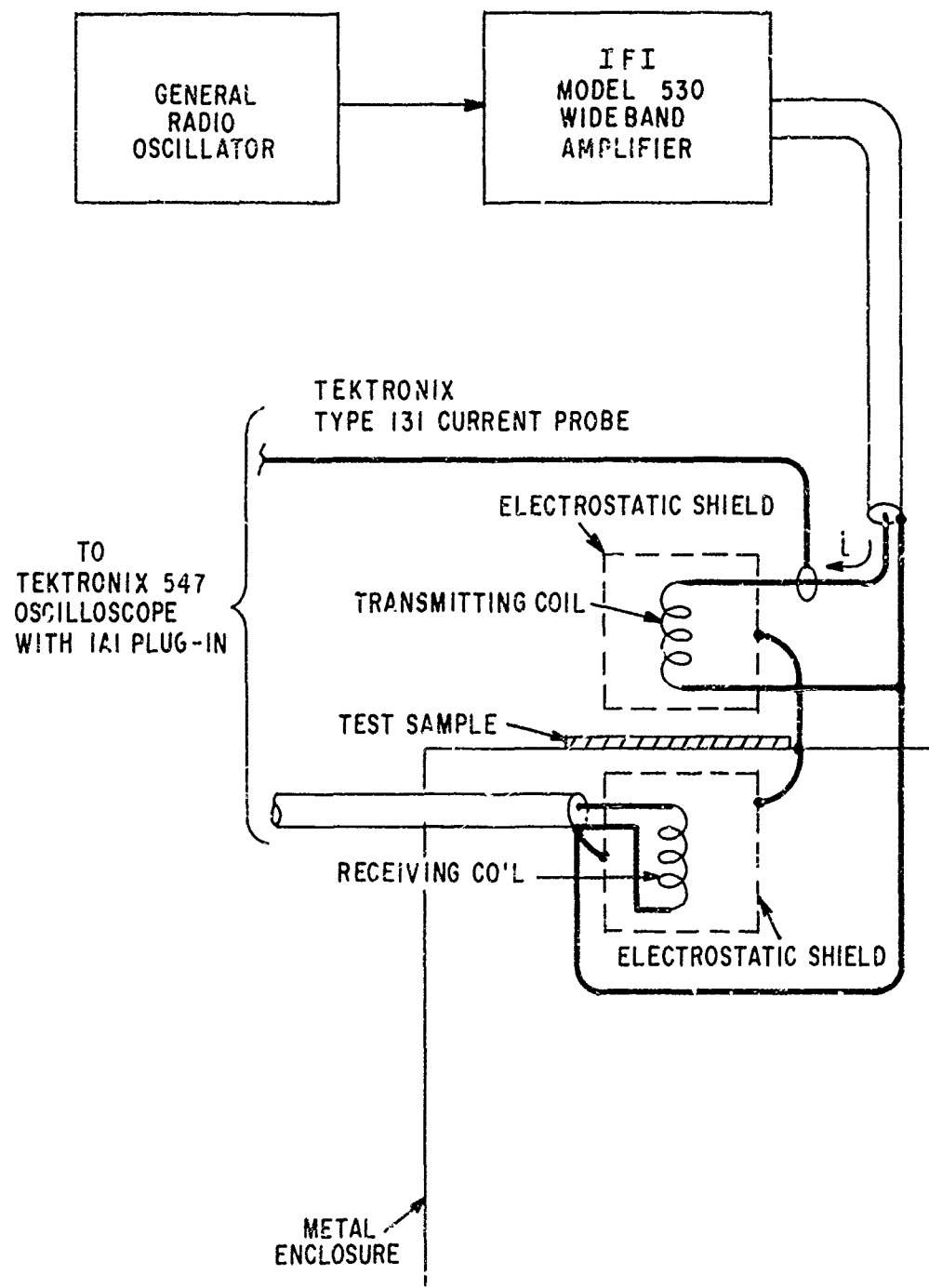


FIGURE 1 - TEST SETUP FOR SHIELDING EFFECTIVENESS TESTS.



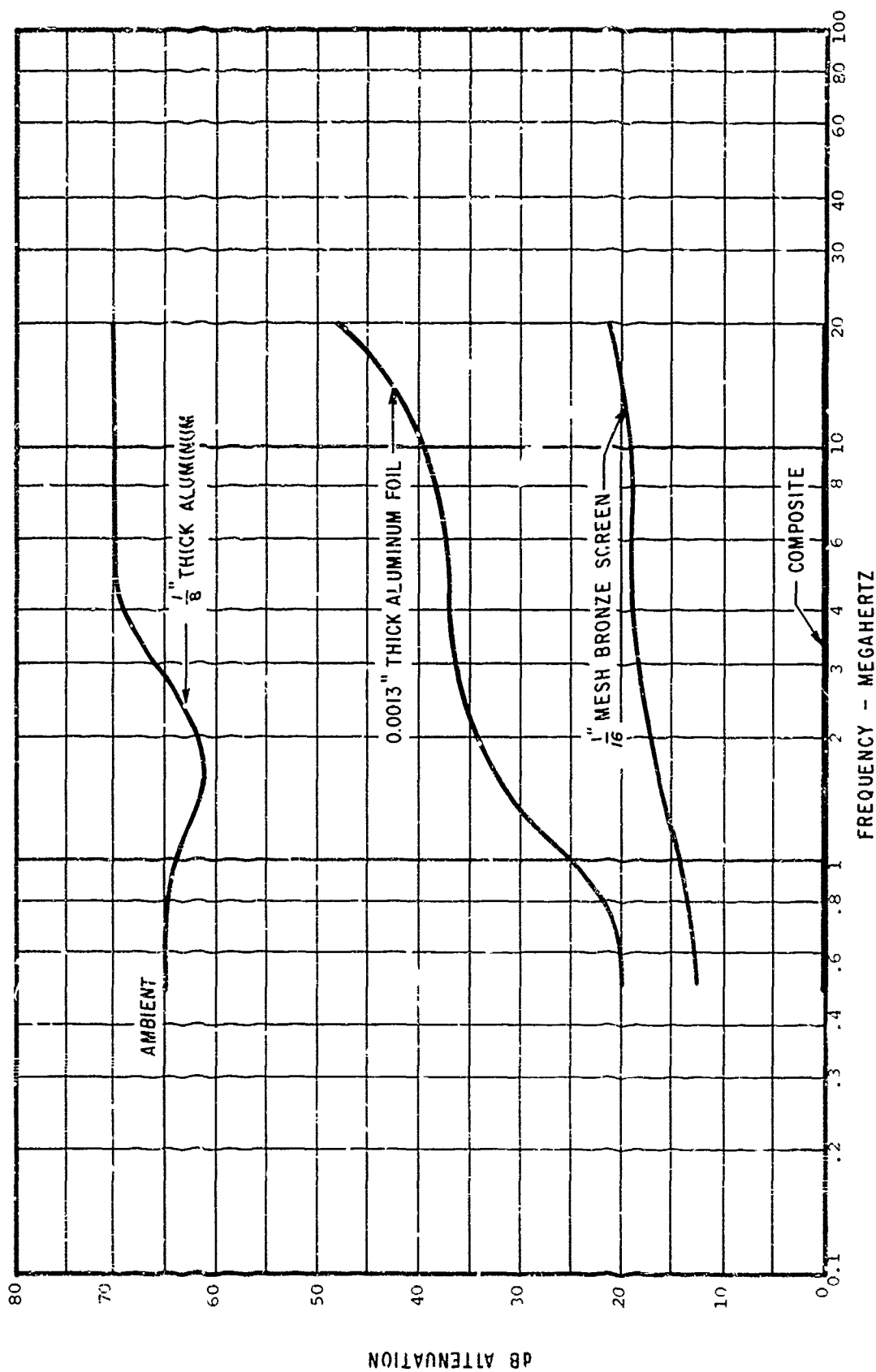


FIGURE 2 - H - FIELD SHIELDING EFFECTIVENESS OF REPRESENTATIVE MATERIALS.

Table 1 - H-Field Shielding Factor Measurements Using a Damped-Oscillatory of 36.4 kHz

Thickness	Coating	Current Level kA	Ambient Field* A.T/M	Absolute Field A.T/M	Shielding dB
.040	none	43.4	130	120	0.7
.040	none	84.4	241	227	0.5
.040	none	130	360	348	0.3
.040	silver paint	84.4	241	227	0.5
.040	silver paint	84.4	241	226	0.5
.040	silver paint	84.4	241	221	0.5
.040	silver paint	84.4	241	227	0.5
.040	silver paint	130	360	336	0.6
.120	silver paint	101	440	384	1.2
.120	none	102	440	373	1.4
.120 *	none	102	440	388	1.1
.120 *	none	107	418	385	0.7
.120	silver paint	107	418	378	0.9
.120	silver paint	107	418	378	1.1
1.6 mil aluminum foil		130	360	16.5	26.8
1.6 mil aluminum foil		107	418	32	22.8

\* 0°-45°-90° ply lay-up. All other panels were 0°-90° lay-up.

(7) 6" x 12" rectangular boron panels with silver-paint coating.

(8) 6" x 12" rectangular graphite panels with flame-sprayed aluminum coating.

(9) 6" x 12" rectangular boron panels with flame-sprayed aluminum coating.

The results of the measurements are shown on Figures 3 and 4. Strictly speaking, the data is valid only for the coil spacing used in these tests since the coil spacing effects the impedance of the magnetic field and the shielding is determined in part by the impedance mismatch between the field and the shielding material. However, implications of the data are quite clear.

(1) The shielding effectiveness of both graphite-epoxy and boron-epoxy materials is much less than an equivalent thickness of aluminum.

(2) A thin piece of aluminum foil has much greater shielding effectiveness than even a 0.120" panel of graphite-epoxy.

(3) Graphite-epoxy, by virtue of its higher conductivity, provides more effective shielding than does boron-epoxy.

(4) The conductive coatings likely to be needed for control of the direct burning and blasting effects of lightning will probably have more effectiveness as electromagnetic shields than do the composite materials they protect.

(5) Measurements made at high field conditions at a frequency of 35 MHz are in agreement with the CW measurements made at low levels.

Some other observations on test results that are not readily apparent from the above data are:

(1) In no case did panel orientation or ply lay-up seem to affect the test data.

(2) During the high field tests made with the surge generator, there did not appear to be any non-linearities due to differences in field level. The measured attenuations were quite small however, and any non-linearities would have been hard to detect.

Apparently there is sufficient contact between the fibers in the different plies that effective contact is made between plies, in spite of the fact that the individual fibers are held together by nonconductive epoxy binder.

Our measurements of shielding effectiveness of panels covered with flame-sprayed aluminum indicated that most of the shielding came from the aluminum. Values of 16 dB and 20dB were measured at 0.5 MHz and 1.0 MHz for .083" boron with a coating of flame-sprayed aluminum. The thickness of the aluminum on the particular panel under test was not known, but on two other panels the aluminum was between 0.010 and 0.020" thick. Eckersley (1) measured shielding factors of 30, 37 and 43 dB at 0.5 MHz for a 5, 10 and 20 mil thickness of aluminum. Apparently, the electrical contact between the particles of aluminum was not as good as that used by Eckersley.

#### COMPARISON WITH OTHER INVESTIGATIONS

Similar measurements of shielding effectiveness of boron and graphite composite materials have also been made by Schulz (2). His data is in general agreement with the data obtained during this study. An excerpt of his data is presented in Figure 5. His data covers the range 10-500 MHz and thus complements the previous data, extending it to higher frequencies. The agreement is quite good. He observed shielding factors in the range of 16 dB for .0375" thick graphite and 30 MHz whereas, we observed 17 dB at 20 MHz on 0.040" graphite. He observed about 3 dB on 0.105" thick boron at 30 MHz whereas, we observed about 16 dB on 0.083" boron with a black carbon coating at 20 MHz. He also observed that panels with alternating ply lay-ups gave significantly better shielding performance than a panel with all fibers arranged in parallel; a configuration we did not study. This is an indication that there is generally good contact between the plies in the different layers.

#### ACKNOWLEDGEMENT

Data presented in this paper was developed in connection with contract F33(15-70-C-1144, performed for the USAF Avionics Laboratory (3). Test samples were supplied by Messrs. H.S. Schwartz and I.G. Kelly of the Air Force Materials Laboratory.

#### REFERENCES

1. A. Eckersley, "H-Field Shielding Effectiveness of Flame-Sprayed and Thin Solid Aluminum and Copper Sheets", IEEE Transactions on Electromagnetic Compatibility, March, 1968.
2. R.B. Schulz, "RF Shielding and Electrical Properties of Boron and Carbon Fiber Reinforced Composites", 1972 International Electromagnetic Compatibility Symposium Record, pp. 180-184.
3. F.A. Fisher and W.M. Facsell, "Lightning Effects Relating to Aircraft" - Part I - "Lightning Effects On and Electromagnetic Shielding Properties of Boron and Graphite Reinforced Composite Materials", Technical Report AFAL-TR-72-5, January, 1972.

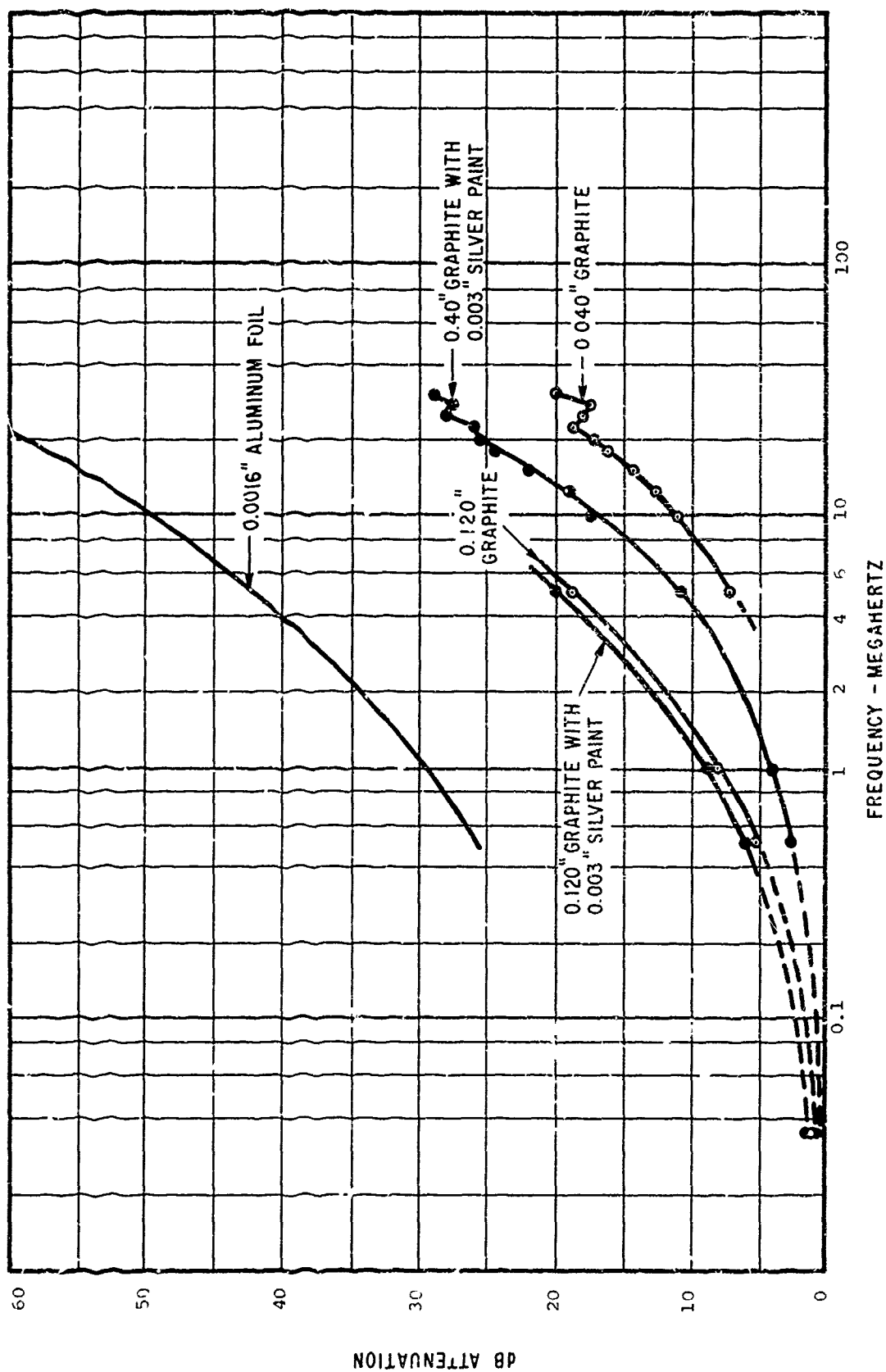


FIGURE 3 - SHIELDING FACTOR MEASUREMENTS ON 13-INCH DIAMETER GRAPHITE PANELS.

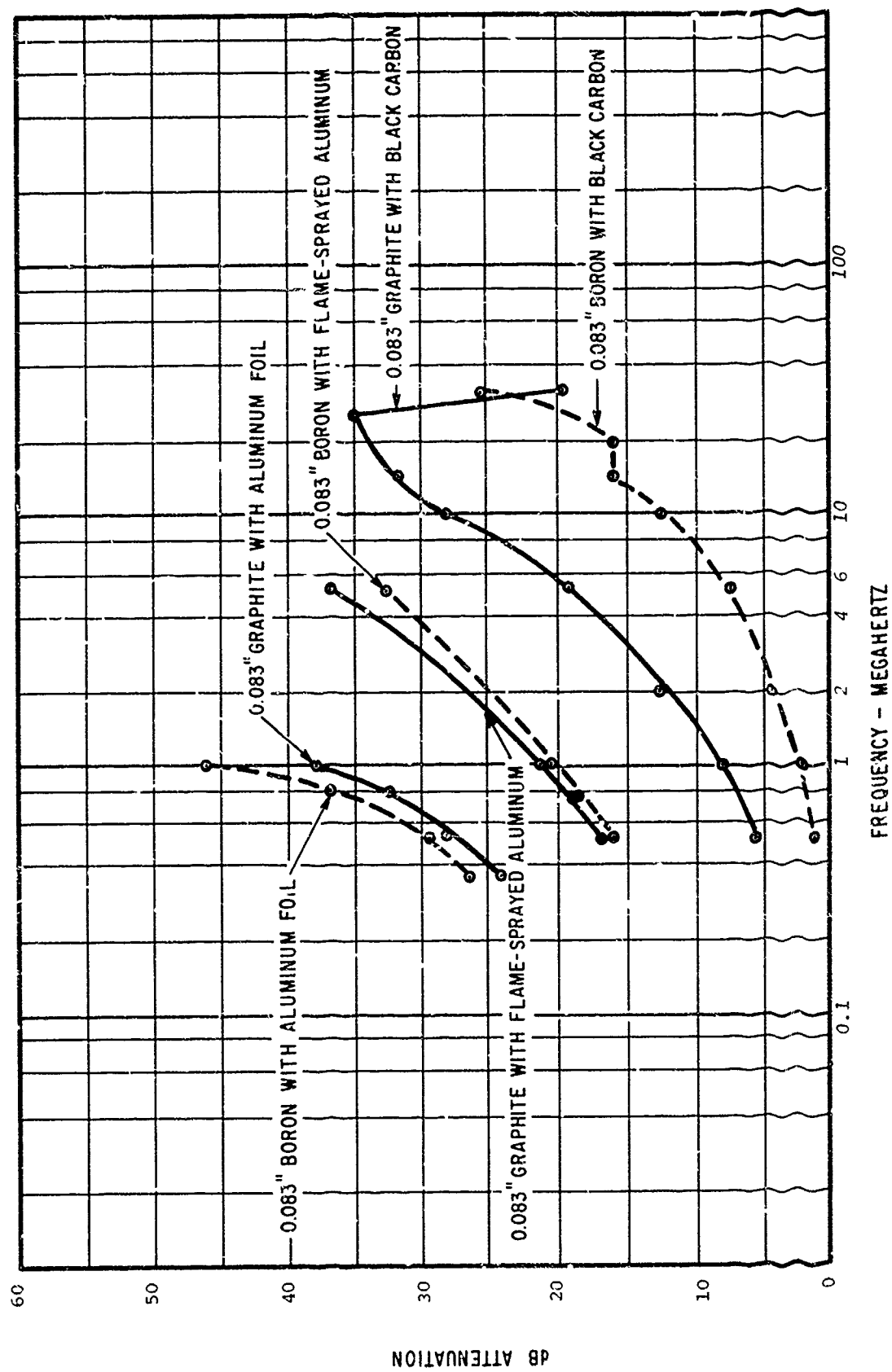


FIGURE 4 - SHIELDING FACTOR MEASUREMENTS ON 6" x 12" GRAPHITE AND BORON PANELS.

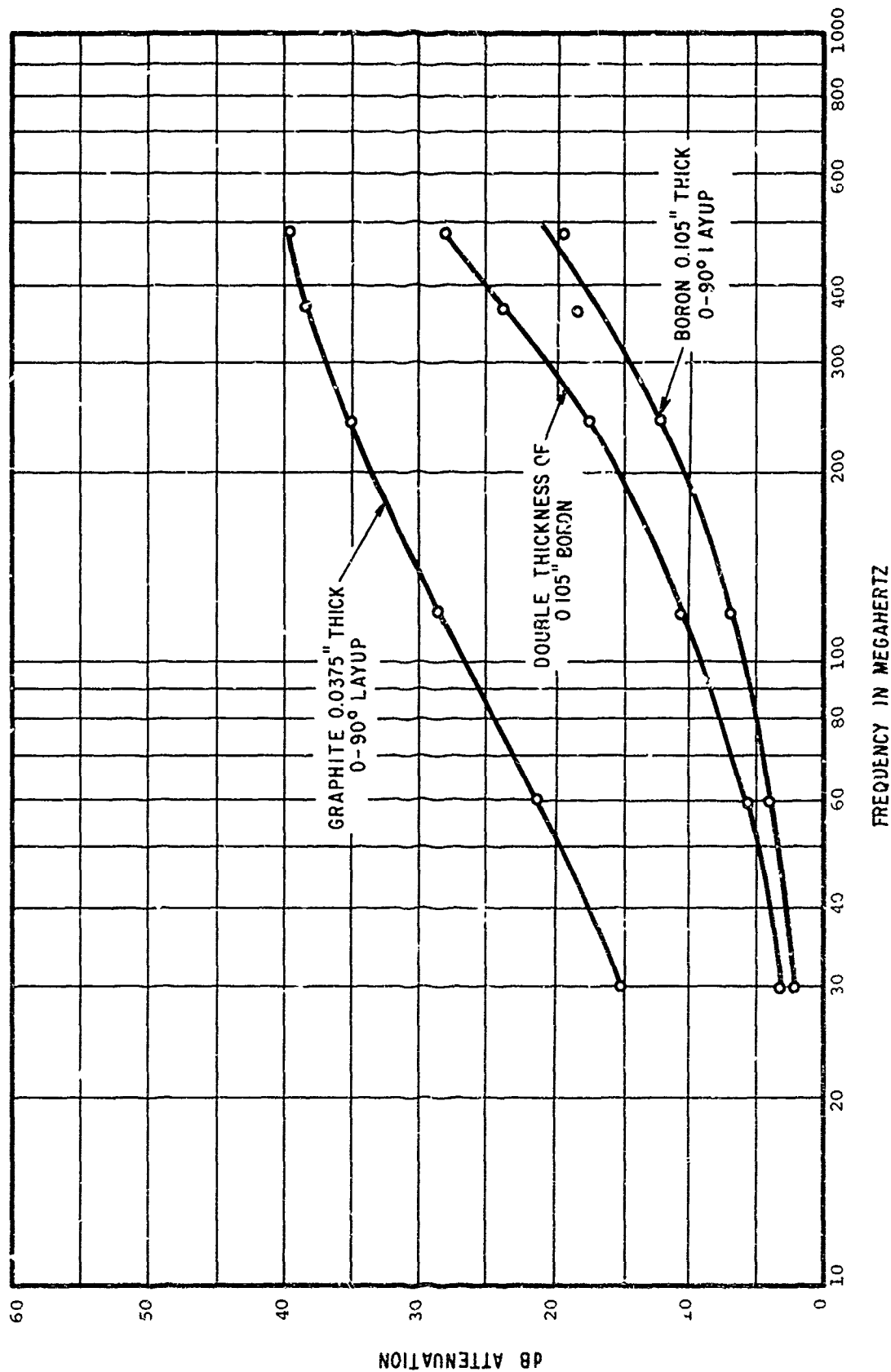


FIGURE 5 - SHIELDING EFFECTIVENESS OF COMPOSITE MATERIALS

## New Developments in Lightning Protective Coatings for Advanced Structural Composites

Dr. John Quinlivan, The Boeing Company  
Mr. J. H. Weaver, Air Force Materials Laboratory

### ABSTRACT

Light weight coatings and coating systems have been developed with improved capabilities compared to the currently available metal foil and conductive paints for protecting boron-filament and graphite-fiber reinforced plastic composites from structural damage by simulated lightning strikes. These coatings were 200 x 200 mesh aluminum wire fabric, 120 x 120 mesh aluminum wire fabric and a coating containing aluminized glass filaments. These coatings all use a continuous metal member as the protective element. Each of these was found capable of preventing any mechanical damage to the composite at the 100-kA test level. Very local and minor damage was frequently, but not always, detected after 200-kA testing. Where there is damage, it is restricted to a small area and can be easily repaired.

**BORON-FILAMENT-** and graphite-fiber-reinforced plastics exhibit entirely different behavior from their aluminum counterparts when struck by lightning. Techniques employed to protect conventional aluminum aircraft and their dielectric components are not directly applicable to advanced composite structures. The conductive, tungsten-rich core of the boron filament and the inherent conductivity of the graphite fiber render their reinforced plastics dielectrically inhomogeneous. As a result, these plastics require some form of lightning protection.

The Air Force Materials Laboratory, under contract to The Boeing Company, initiated a program to develop lightning discharge protective coatings for application to external surfaces of boron and graphite fiber reinforced plastic aircraft structural components that had superior performance and fabricability to the aluminum foil and silver paint which were then considered "state-of-the-art". The goals of the program were to develop light weight, easily applied, environmentally resistant coating systems which would protect boron and graphite fiber reinforced plastics from serious structural damage when struck by simulated lightning having peak currents as high as 200,000 amperes and charge transfers as high as 200 coulombs.

Selected coating systems were applied to boron-filament-and/or graphite-fiber-reinforced epoxy laminates. The coated panels were exposed to the required adverse environments (if any) and subjected to artificial lightning discharges. The performance of the coating system was determined by visual damage analysis, microscopy, and the residual mechanical properties of the composite. Successful coating systems were subjected to lightning restrikes to provide additional data and greater confidence levels for the coating systems.

### COATING DEVELOPMENT

**REINFORCED PLASTIC SUBSTRATES -** The boron filaments were manufactured by the Hamilton Standard Division of United Aircraft Corporation. The filaments were impregnated with a high-temperature epoxy resin by the Minnesota Mining and Manufacturing Co., and marketed under the designation "Scotchply" SP-272. Two forms of impregnated tape were used: one employed a style 104 glass scrim carrier, the other did not.

The graphite fibers were manufactured by the Union Carbide Corporation. The Thornel 40S graphite yarn was impregnated with WRD 1004, an epoxy resin, by the Research and Development Division, Whittaker Corporation. Thornel 50 fibers were impregnated with BP 907 epoxy resin (American Cyanamid Corporation).

**Test Panels -** The boron-filament-and graphite-fiber-reinforced laminates consisted of several plies in an alternating 0° - 90° orientation. The boron-filament-reinforced laminates were constructed symmetrically about the center ply, with the glass carrier fabric (if any) providing the outer surfaces. Generally, the laminates were five plies thick. A few 14-ply laminates were prepared for special testing. The test panels varied in size from 6- by 12-in. to 12- by 12-in.

Unidirectional and bidirectional laminates were specially fabricated for control tensile test data. The unidirectional laminates were seven plies and the bidirectional

laminates were five plies. The doublers were prepared from four plies of Narmco 551-181 and were bonded to laminates using an oven cure (90 min at 260°F) under vacuum bag pressure. Surface preparation of the laminate included scouring with Scotch-brite followed by MEK wipe. The laminate plate with the four bonded doubler strips was cut into 1/2 in.-wide specimens using a diamond cutoff wheel and surface grinding techniques.

The boron-filament-reinforced and ThorneI 50-fiber-reinforced composites were autoclave cured in accordance with standard techniques.

**COATINGS** - This paper describes the development of woven wire fabric and aluminized glass coatings for utilization as protective coatings for lightning strike protection of structural reinforced plastics.

**Wire Fabrics** - Woven wire fabric was purchased from Pacific Wire Products Company. The pertinent fabric parameters are as follows:

Fabric	Mesh Density	Wire Diameter (in)
Aluminum	120 x 120	0.004
Aluminum	200 x 200	0.0021

Figure 1 shows a 200 x 200 woven wire fabric. These fabrics were integrally bonded to the composite substrates during laminate manufacture.

It was necessary to add resin to the laminates to ensure proper resin flow and encapsulation of the fabric. This was accomplished either by impregnating the fabric with BP 907 laminating dispersion or by adding sufficient unsupported BP 907 adhesive film. Additional resin was not necessary for proper part manufacture with ThorneI 50S/1004 when the 200 by 200 mesh fabric was used. Sufficient resin flowed from the composite into the mesh to encapsulate the coating fully and provide a smooth exterior panel surface.

The layup procedure for integral bonding was to apply the resin-impregnated wire fabric coating to the tool side of the part. The required number of prepregs of the high modulus material was laid against the wire fabric coating. Standard layup techniques were used in fabricating the reinforced composite test panels for autoclave curing. The cure cycle (temperature-time) was adjusted according to panel thickness and the heat-up rate characteristics of the tool.

**Aluminized Glass Filaments** - Aluminized glass filaments were obtained from the Lundy Technical Center, Lundy Electronics and Systems, Inc. The filaments were furnished

on commercial textile cones containing 20-filament strands. Two types of material were obtained. In one, all 20 filaments were metallized; in the other, only 7 (of 20) were metallized. The filament consists of a metal thread bonded to a glass thread, as shown in Figure 2. Each thread is approximately 0.5 mil diameter. The filament uses the aluminum thread for electrical conductivity and the glass thread for mechanical strength.

Unidirectional layers of aluminized glass filaments were prepared by two procedures:

a. The filaments were wound into a single layer of BP 907-impregnated, style 104 glass cloth (224 strands per inch)

b. The filaments were wet wound, impregnating them with BP 907 epoxy resin (448 strands per inch).

Using the partially metallized strands, the two layers contained 155 and 3100 conductive filaments per inch, respectively. The scrim-containing layer has a cured thickness of 3.6 mils per ply, of which approximately 1 mil is the scrim cloth. A single ply weighs 4.5 lb/100 sq. ft. No fabrication difficulties were encountered with this material.

The fully metallized strands were prepared by wet-winding techniques only. These layers contained 4480 or 9060 conductive filaments per lineal inch. The cured layers were approximately 2.3 and 3.6 mils thick and weighed 2.2 and 3.6 lb/100 sq ft/ply, respectively. The different cure schedules for boron and graphite did not change these properties.

**ENVIRONMENTAL PAINT COATINGS** - Primer coating for environmental paint coatings was P-148, a product manufactured by Andrew Brown Company, and qualified to MIL-P-7962B. The lacquer topcoat was qualified to MIL-L-19537C and manufactured by the same company. The materials were applied per specification, except that the pretreatment coating MIL-C-8514 was not applied.

**ENVIRONMENTAL TESTS** - Coated and uncoated boron-filament- and graphite-fiber-reinforced laminates were exposed to the following environments:

- 140°F and 100% relative humidity
- Salt spray (3% NaCl)
- Immersion in hydraulic fluid (Skydrol 500A)
- Immersion in jet fuel (JP-4)
- Weather-O-Meter (FED-STD-141, method 6152)

Upon completion of these exposures, the samples were removed and subjected to



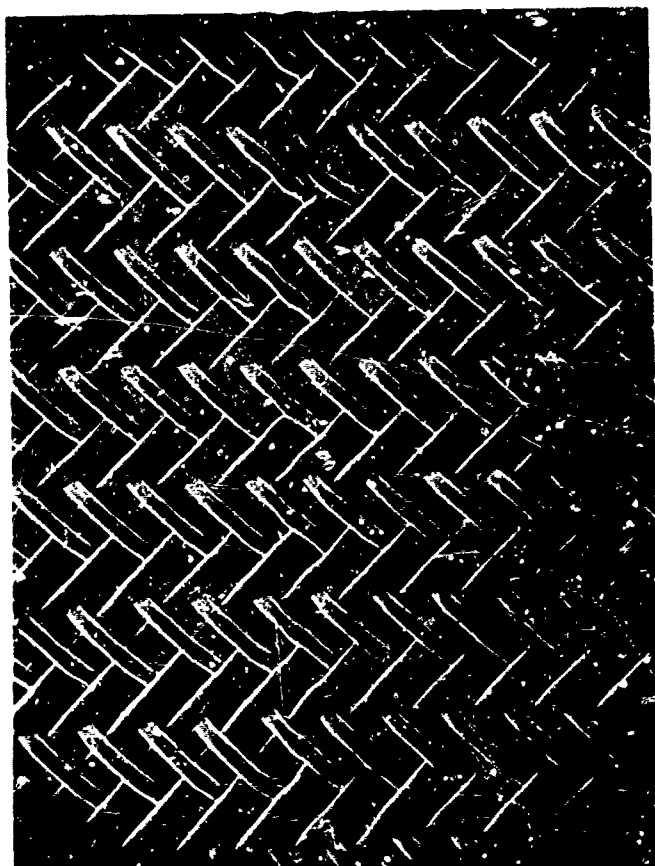


Fig. 1      200 x 200 mesh aluminum wire fabric (X37)

## Aluminized Glass Filament (900 X)

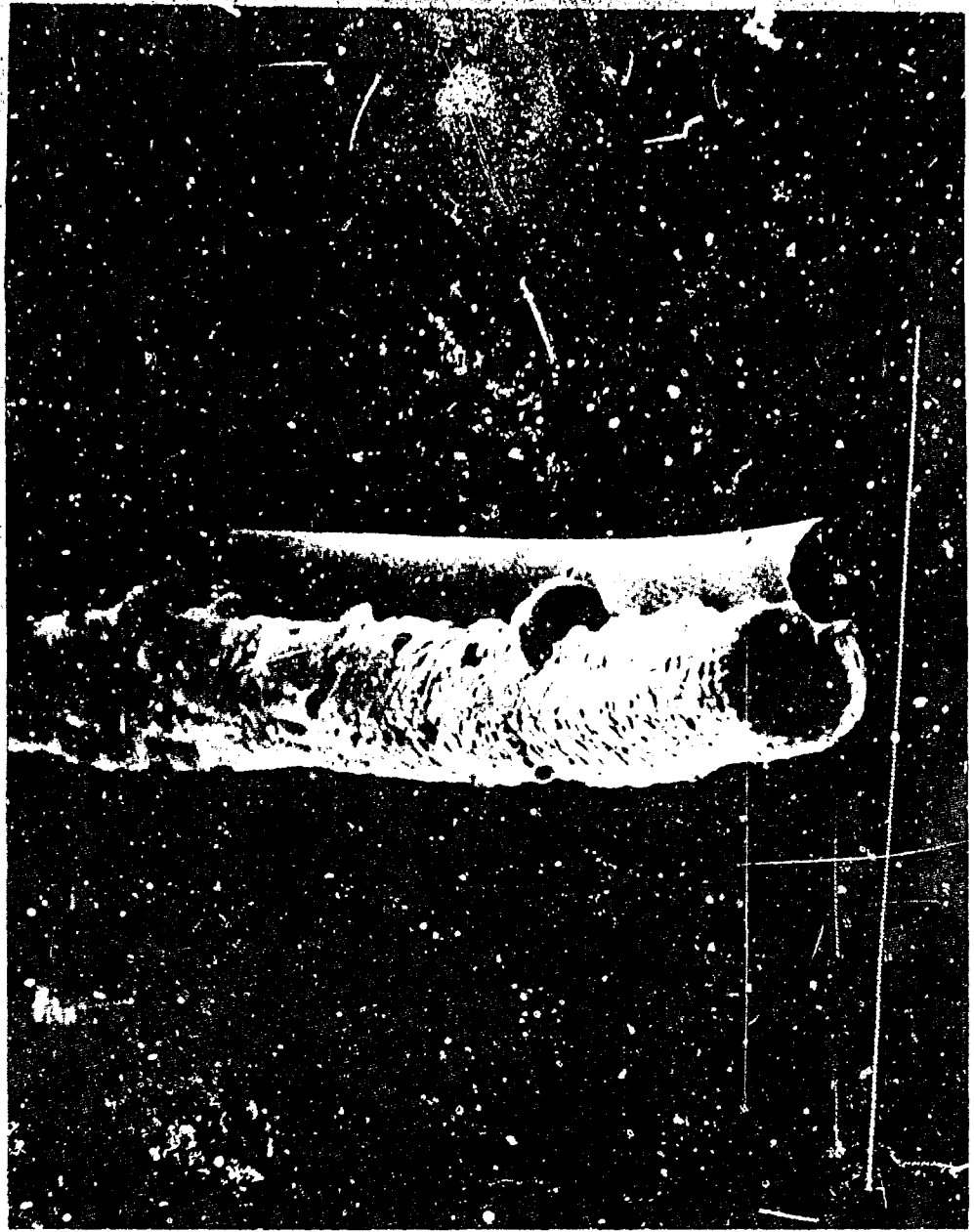


Fig. 2 Aluminized glass filament (X900)

simulated lightning discharges to determine if the environmental exposure altered the lightning protective qualities of the coatings. In general, the coatings were not visibly altered by any of these environments, and all tests except salt spray were discontinued after 30 days' exposure.

## LIGHTNING TESTS

**LIGHTNING TEST APPARATUS** - Past studies have shown that the damage introduced by a natural lightning stroke is composed primarily of two parts: a high-current component, which causes thermal and electrical heating damage. The high-current discharge is usually a crest current with a peak amplitude from 10 to 200 kA and a pulse duration of up to approximately 50  $\mu$ s. A high-coulomb component is usually a long-duration, low-amplitude current component (a few hundred milliseconds to a few seconds' duration and from less than a hundred amperes to a few thousand amperes).

All aspects or properties of natural lightning cannot be simulated in the laboratory due to limited space and energy available as well as the lack of a complete understanding of a lightning stroke; however, for the present study, a test discharge with the following requisite characteristics was used:

a. A high-current component rising from zero to a crest value of 200-kA in 10  $\mu$ s and a pulse duration of 20  $\mu$ s with  $\pm 50\%$  tolerance on time

b. A MIL-A-9094C, type-C, high-coulomb, transfer discharge with total charge transfer equal to or exceeding 200 coulombs in 2 sec or less.

For the initial screening of candidate lightning protective coatings, a high-current component rising from zero to a crest value of 100-kA in 10  $\mu$ s and a pulse duration of 20  $\mu$ s with  $\pm 50\%$  on time was used. Application of this moderately severe stroke not only screened coating candidates for further investigation and test but also identify protective coatings which would be adequate for areas requiring only secondary protection such as the zone II or III areas of an airplane.

The laboratory test setup is shown in Figure 3. The test panel was clamped to an 18- by 18-in. phenolic panel that was bolted to the Faraday cage and was electrically isolated from the cage except for the ground strap clamped to one end of the panel. This configuration ensured that the discharge current passed through the maximum available coating surface of a test panel. A 1/4 inch

diameter tungsten probe was used to direct the discharge to the test panel and a 1/4 in. gap was maintained between the probe and the panel.

**HIGH-CURRENT GENERATOR** - The energy source used to generate a 100-kA crest was provided by a 42  $\mu$ F capacitor bank with a positive-grounded supply, i. e., the discharge probe injected discharging electrons toward the test panel to simulate a more severe damage situation than that of a positive probe, should the system have a negative-grounded power supply. The capacitor bank normally produced an underdamped oscillatory discharge. An improved switching technique was developed that gives reliable 200-kA discharges and can be used as a unipolar trigger for high-coulomb discharges.

Oscillograph displays obtained during the testing of protective coatings for both 100 and 200-kA discharges are shown in Figure 4. Some oscillograph traces obtained using the ignitron switch are also displayed, for comparison. Note that the coatings on the test samples are low impedance and present the most difficult condition for obtaining a unipolar discharge.

**TWO-COMPONENT GENERATOR** - A block diagram of a two-component lightning generator is shown in Figure 5. The high-current component generator first established an arc between the discharge probe and the test item; the high-coulomb component generator then followed on by discharging a dc component through the established ionized channel to the test panel. The charged high-voltage capacitor bank was isolated electrically from the battery bank by switch  $S_1$ . These high-current and high-coulomb components were isolated transiently from each other by the isolation coil. The total discharge was terminated by opening switch  $S_T$ .

Two 430-V battery carts were used for the required high-coulomb component. Each steel cart measured 73 by 49 in. and was 50 in. high, had 36 automotive batteries (12V), and a total weight of about 2200 lb. With a series connection, the system was capable of discharging a dc level up to 700 A and maintaining an arc with a gap of up to a half inch.

The development of a series fuse switch allowed high-coulomb discharges to be triggered with a unipolar high-current discharge. This was possible because the associated circuit of the discharge generator with the series fuse had no shunting components. Figure 6 shows the oscillograph displays of the high-current trigger and the high-coulomb discharge obtained in a test panel.

## Laboratory Test Setup

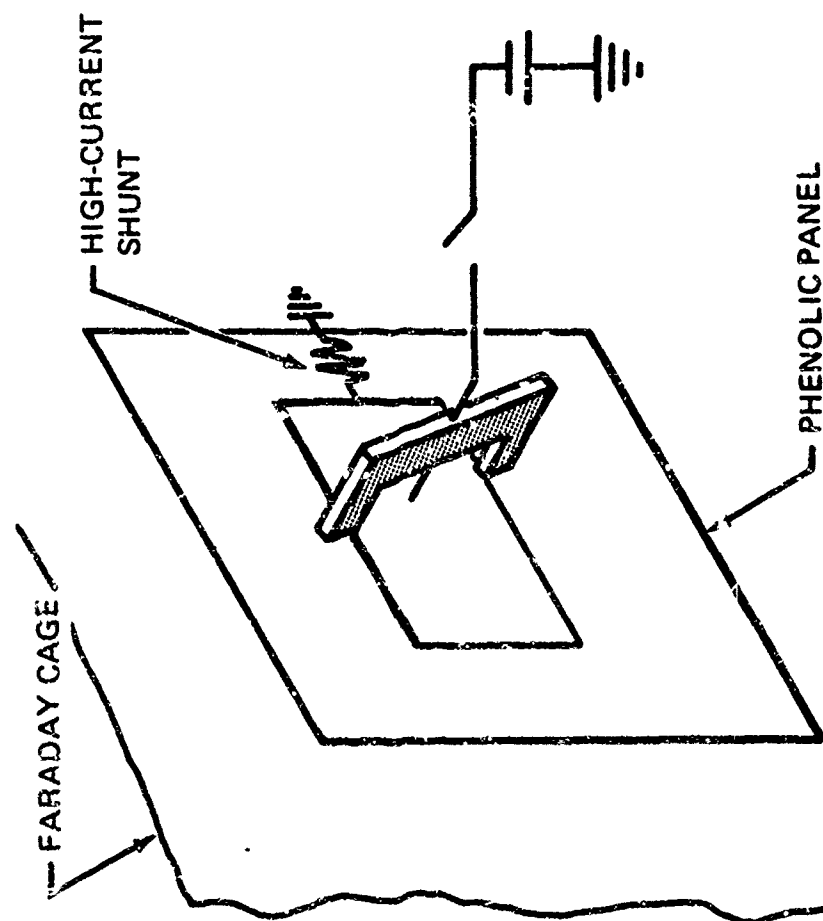
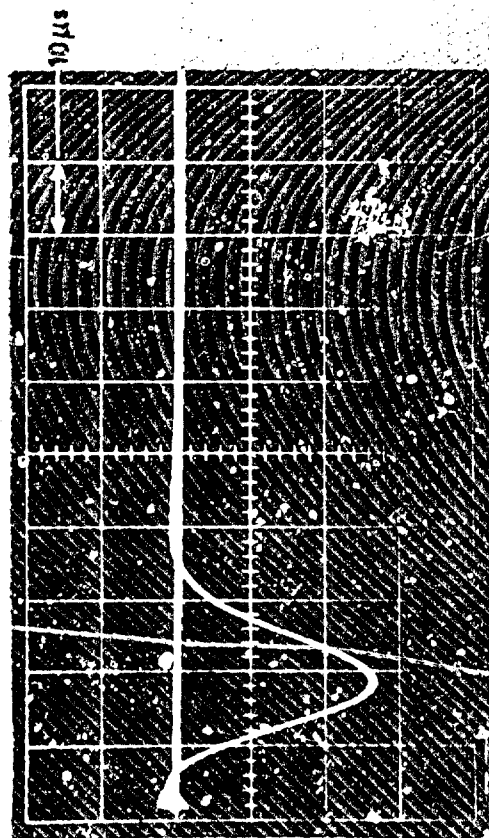


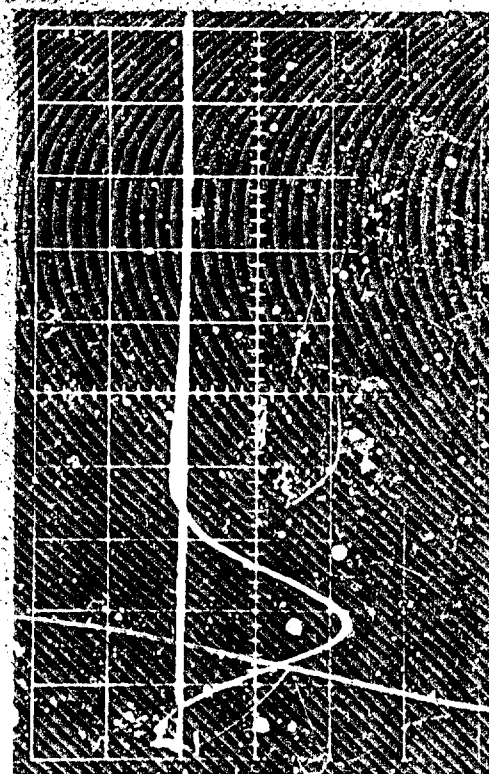
Fig. 3 Laboratory test setup

# Oscilloscope Traces

## A. TRACES USING FUSE SWITCH

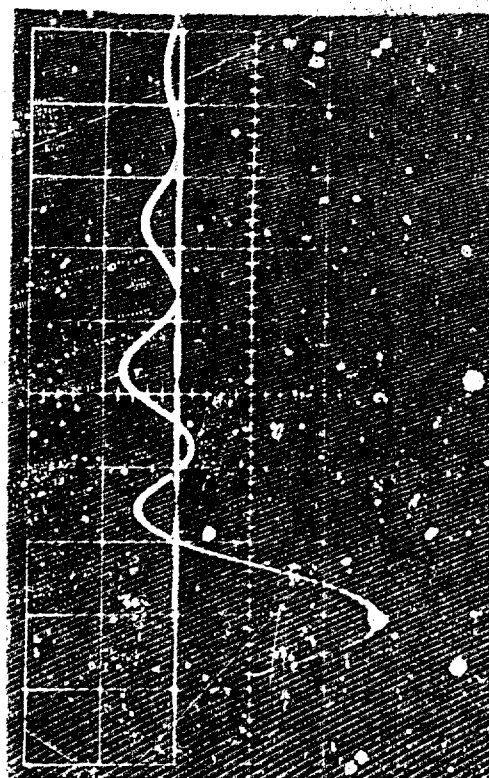


431-BR18-A109N-ALCO PEAK CURRENT - 100 KA

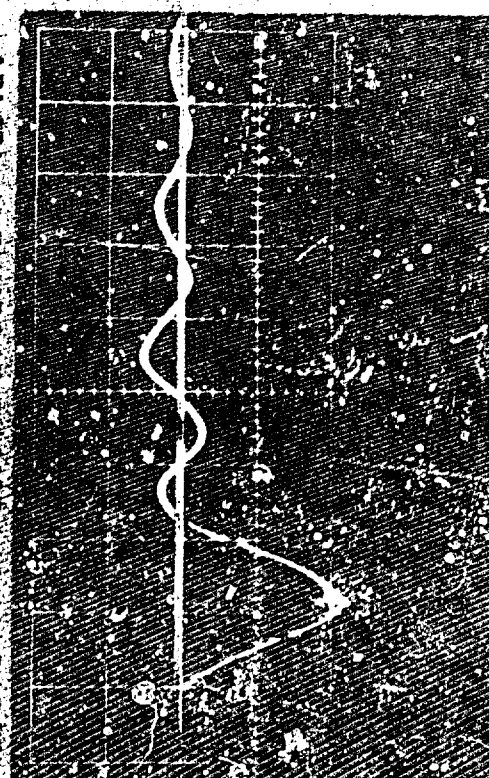


424-GP87-A109N-ALCO PEAK CURRENT - 200 KA

## B. TRACES USING IGNITRON SWITCH



436-BR84-A106N-ALCO PEAK CURRENT - 100 KA



458-GP73-AC09C-A104Z PEAK CURRENT - 108 KA

Fig. 4 Oscilloscope Traces

# Schematic Diagram of Two Component Generator

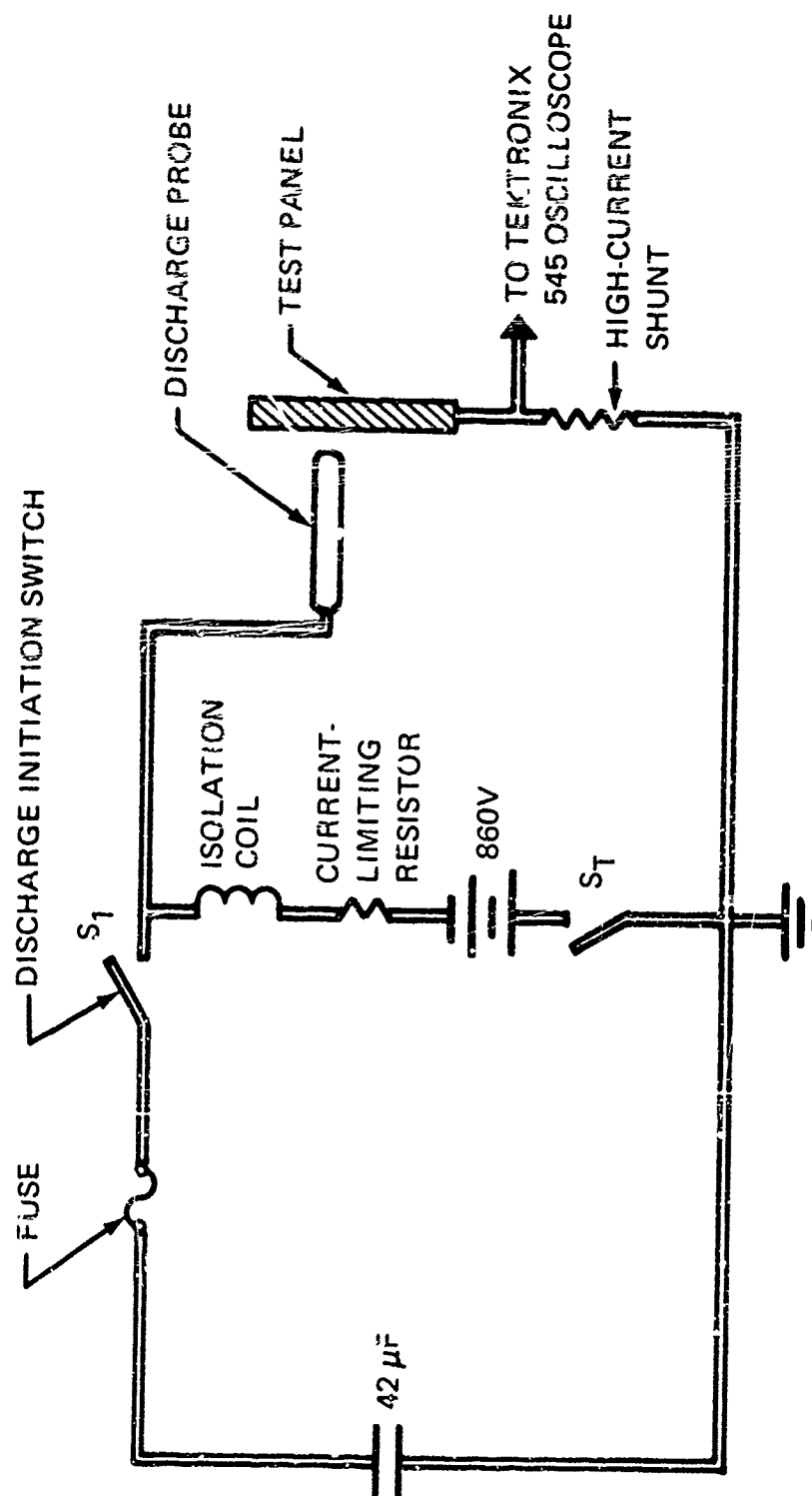


Fig. 5 Schematic diagram of two component generator

## High-Current, High-Coulomb Oscillograph Traces

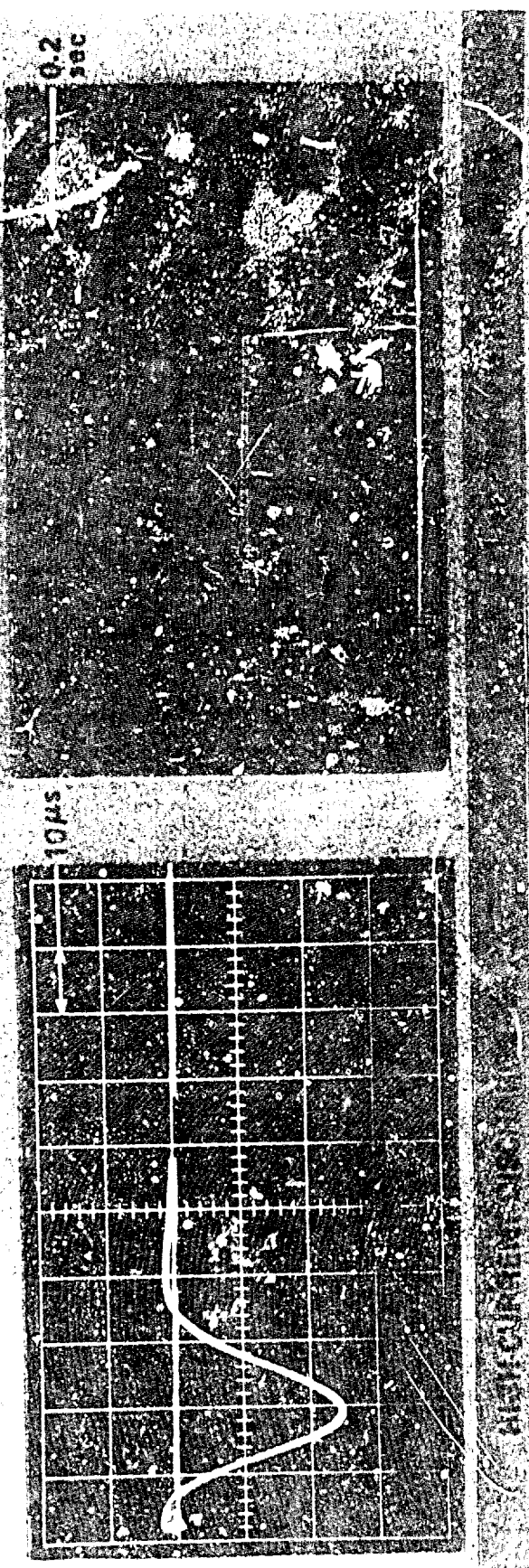


Fig. 6 High-current, high-coulomb oscillograph traces

## LIGHTNING TEST RESULTS

**HIGH-CURRENT TESTS** - Unprotected boron-filament- and graphite-fiber-reinforced plastics are severely damaged by high-current flow through the reinforcement. In boron-filament-reinforced plastics, the current causes the filaments to crack and break. This can result in the total loss of useful mechanical strength. Peak currents as low as 40-kA have totally destroyed the strength and rigidity of 6- by 12-in., five-ply laminates. Larger laminates may not be totally destroyed at this current level but suffer significant reductions in strength. In graphite-fiber-reinforced plastics, Joule heating of the fiber causes resin pyrolysis and, eventually, fiber destruction by a mechanical whipping action. The damage is less widespread than that of comparable boron composites, however. In both composites, the damage is not limited to the arc contact zone but travels toward electrical ground.

**Metal Wire Fabrics** - Metal wire fabrics have been found to provide excellent protection to boron and graphite fiber plastics from simulated high-current lightning tests, based on laboratory tests. The fabrics possess the hand and drape necessary for use as an overlay on complex contoured parts. Additionally, the composite matrix fully encapsulates the fabric and protects it from the environment. A wide range of tests have found aluminum wire fabrics very resistant to environmental exposures including prolonged (90-day) salt spray; 30-day immersion in jet fuel, hydraulic fluid, or boiling water; Weather-O-Meter testing (FED-STD-141, method 6152); or prolonged exposure to hot, humid (140°F, 100% relative humidity) conditions. Environmentally exposed laminates were found to be unchanged when compared with unexposed controls and performed equally well when subject to high-current discharge. In this regard, these coatings outperform others since most other coatings are susceptible to corrosion as determined by salt spray exposure. This is particularly true of unprotected metal foils which suffer extreme corrosion. Resin encapsulated wire fabrics are protected from the corrosive action of this environment by the resin. Since bare metal is not exposed to the environment, corrosion is retarded.

In this program, aluminum wire fabrics were found to provide the best combination of lightning protection, light weight, environmental resistance and ease of application. For 200 by 200 mesh woven aluminum wire

fabric, the area density of 0.019 lb/sq ft. A 120 by 120 mesh fabric has an area density of 0.042 lb/sq ft. These weights are increased to 0.036 and 0.072 lb/sq ft, respectively, if one accounts for the resin required for encapsulation of the fabric. Some weight saving is possible by employing calendered wire cloth. This serves to reduce the thickness of the cloth by flattening the intersections of the wires. Weight savings occur because less resin is required to encapsulate the flattened mesh. As a point of reference, 6-mil-thick aluminum foil has an area weight of 0.084 lb/sq ft. The weights of environmentally protective topcoats or adhesive required for bonding the foil (or fabric) must be added to these figures.

The outstanding performance of wire fabrics as lightning protective coatings is due to their use of the skin effect for electrical conduction. The skin area of a 200 by 200 mesh wire fabric, using a 0.0021-in., diameter wire, is over 200 times that of the area actually coated by the fabrics. Consequently, the fabric is highly efficient in conducting electricity away from the arc contact zone. This fabric has been found capable of withstanding successive 100-kA discharges at the same location with little visible damage to the fabric and no reduction in the mechanical strength of the coated laminate. At the 200-kA level, the only significant damage to the coated boron laminate is directly under the arc contact zone and the residual tensile strength of coupons taken directly under the arc contact zone is typically 80% of the panel average (Figure 7). The residual tensile strengths of graphite-fiber-reinforced coupons at the damage zone were 85%, 84%, 71% and 89% of the undamaged values. Of these, only the lowest was statistically significant.

Paint coatings can be expected to be used on aircraft structures for various reasons, such as camouflage, environmental protection and marking. Paint coatings over the 200 x 200 mesh wire fabric confined the electrical energy (100-kA) to a smaller surface area resulting in an increase in the amount of damage to the coating i. e., a greater amount of wire is vaporized or melted. However, composite residual tensile strengths are unchanged, indicating little or no reduction in the effectiveness of the lightning strike protective coating. At the 200-kA test current level, with the painted lightning strike protective system over graphite-fiber-reinforced composites, damage at the arc contact zone is visible as exposed resin-free graphite fibers. These are visible





Fig. 7 Boron-filament-reinforced epoxy laminate coated with 200 x 200 mesh aluminum wire fabric after exposure to 200-kA

in Figure 8. Three different tests of two different laminates have found the damage limited to the 1/2-to 1-inch, -wide arc contact zone. With boron-filament-reinforced laminates (paint over wire mesh coating), the damage zone is limited to a 1-1/2- to 2-in. -wide area which is readily repairable.

Heavier, 120 by 120 mesh aluminum wire fabric also provides an excellent level of lightning protection. Figure 9 depicts the visual results of a boron fiber reinforced laminate coated with 120 by 120 mesh wire fabric after exposure to 203-kA discharge. Slight discoloration is noted with no visual damage to the substrate. When the 120 by 120 mesh wire fabric is painted and exposed to a 193-kA discharge, there is removal of the paint with some aluminum wire vaporization at the contact point. This is shown in Figure 10. Residual mechanical properties indicated no loss of strength due to the high-current exposure.

**Aluminized Glass Filaments** - The concept of electrically conductive coatings using fine wires as the current-carrying member has been extended through the use of aluminized glass. Unidirectional layers consisting of several thousand conducting members per linear inch can be fabricated using current filament winding technology. Model studies used copper wires as the conductive filament. These studies found it necessary to use at least two orthogonal layers to provide good lightning protection. The fact that the wires were electrically insulated from one another did not prevent the coatings from performing satisfactorily. These findings were confirmed with aluminized glass coatings.

Optimum coatings of aluminized glass used two layers of fibers. The fibers in each layer were aligned in one direction only, and it is necessary that the fibers in one layer be orthogonal to those of the other layer. Excellent results were obtained with coatings containing 4500 aluminized filaments per linear inch per ply. Two-ply coatings satisfactorily protected boron-filament-reinforced composites from current levels as high as 180- to 190-kA. None of the coupons cut near the arc contact zone had lost mechanical strength or stiffness. Four plies of filaments were required to protect graphite-fiber-reinforced composites. However, they did not prevent some loss of tensile strength at the arc contact zone. For example, the contact zone had a tensile strength of 14 ksi in panel, while the remainder of the panel averaged 59 ksi. Some typical results with this type of coating are shown in Figure 11.

Aluminized glass filaments provide excellent high-current protection for boron-filament-reinforced plastics. Coating area weights of 0.040 lb/sq ft (including resin) are easily prepared and handled. This coating is less satisfactory for graphite-fiber-reinforced plastics since a heavier (0.080 lb/sq ft) coating weight appears to be required. Corrosion may be a problem with this aluminum-carbon galvanic couple since panels exposed to a 3% salt spray for 30 days underwent severe corrosion especially about the edges. Coatings applied to boron-fiber-reinforced laminates did not undergo corrosion when exposed to similar conditions. These differences are illustrated in Figure 12.

**HIGH-COULOMB TESTS** - High-coulomb tests involve long-duration, high-temperature areas that can cause severe burning damage to both aluminum and composites, although this type of damage is frequently quite localized. Nevertheless, no coating can withstand an extremely high coulomb test when the arc is confined to a small surface area. The coatings burn away almost immediately, and the arc will attach itself to the conductive panel. Damage then propagates toward electrical ground.

**Metal Wire Fabric** - High-coulomb tests of wire-fabric-coated laminates yielded two types of results: those in which the arc attached at only one point on the surface and those where it did not. In the latter instances, little or no damage to the substrates was observed. The "wandering" of the arc was unpredictable but occurred most frequently with coated boron-filament-reinforced plastics. A coating of 200 by 200 mesh aluminum wire fabric with an underlayer of epoxy-resin-impregnated, style 120, glass fabric produced arc wandering at a test level of 232 C. The result for boron is shown in Figure 13. Residual tensile tests of this laminate found no damage, nor was damage observed when the substrate was graphite (coulomb transfer 165 C). The presence of the glass fabric insulating layer greatly improved the performance of this coating system.

When the arc did not wander on the coating surface, burning damage to the coating and the composite substrate occurred. Furthermore, the damage to five-ply boron laminates appears to be linear with the number of coulombs transferred. Figure 14 shows the relationship between the size of the hole and the test level in coulombs for 200 by 200 mesh, aluminum wire fabric coated, boron-filament-reinforced laminates. The area damaged increases linearly with an

**Painted Graphite-Fiber-Reinforced Epoxy Laminate  
Coated with 200 by 200 Mesh Aluminum Wire Fabric  
After Exposure to 190 kA**



**Fig. 8** Painted graphite-fiber-reinforced epoxy laminate coated with 200 x 200 mesh aluminum wire fabric after exposure to 190-kA



Fig. 9 Boron-filament-reinforced epoxy laminate coated with 120 x 120 mesh aluminum wire fabric after exposure to 203-kA





Fig. 10 Painted boron-filament-reinforced epoxy laminate coated with 120 x  
120 mesh aluminum wire fabric after exposure to 196-kA

Aluminized, Glass-Coated, Graphite-Epoxy Laminates  
After Exposure to High-Currents

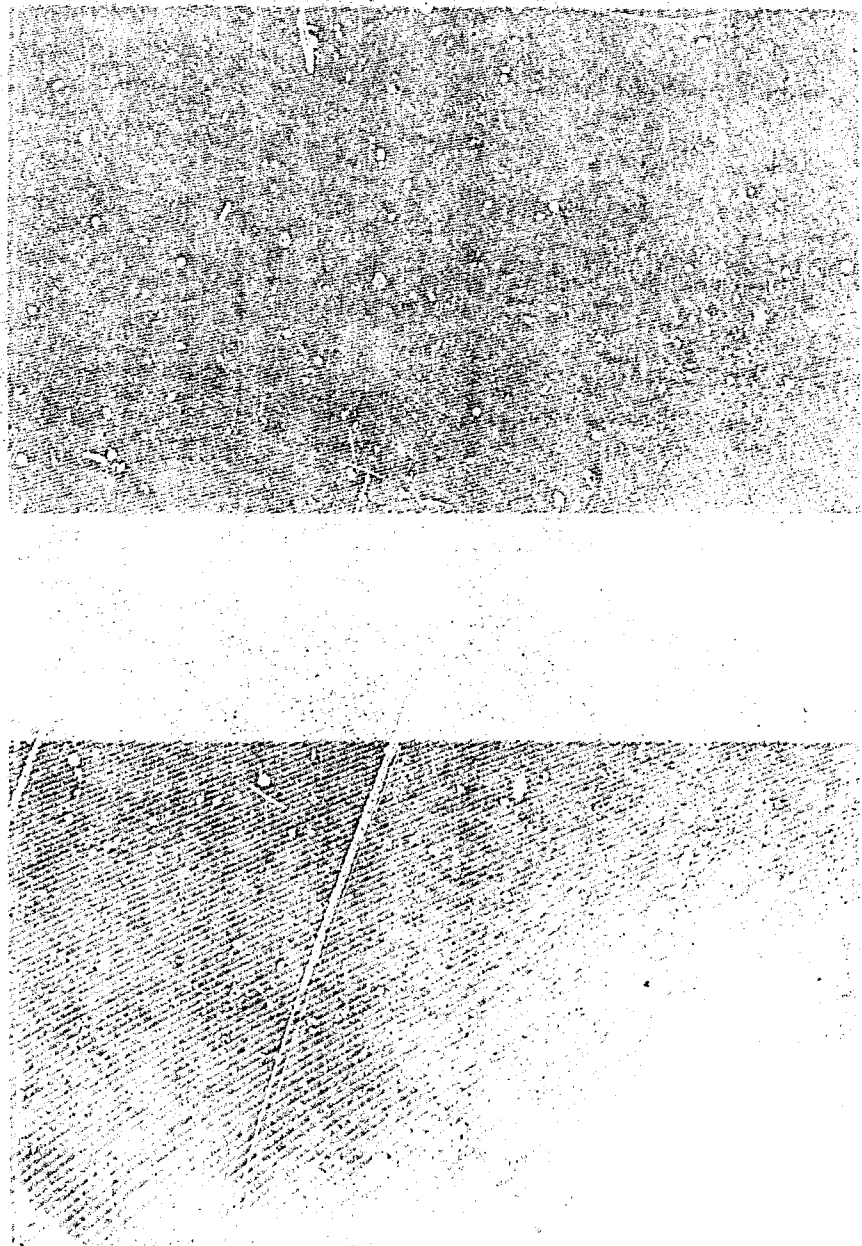


Fig. 11 Aluminized, glass-coated, graphite-epoxy laminates after exposure to high-current tests



Aluminized, Glass-Coated,  
Graphite-Epoxy (left) and Boron-Epoxy (right) Laminates  
After Exposure to 3% Salt Spray for 30 Days:  
Graphite-Epoxy Laminate Displays Coating Corrosion

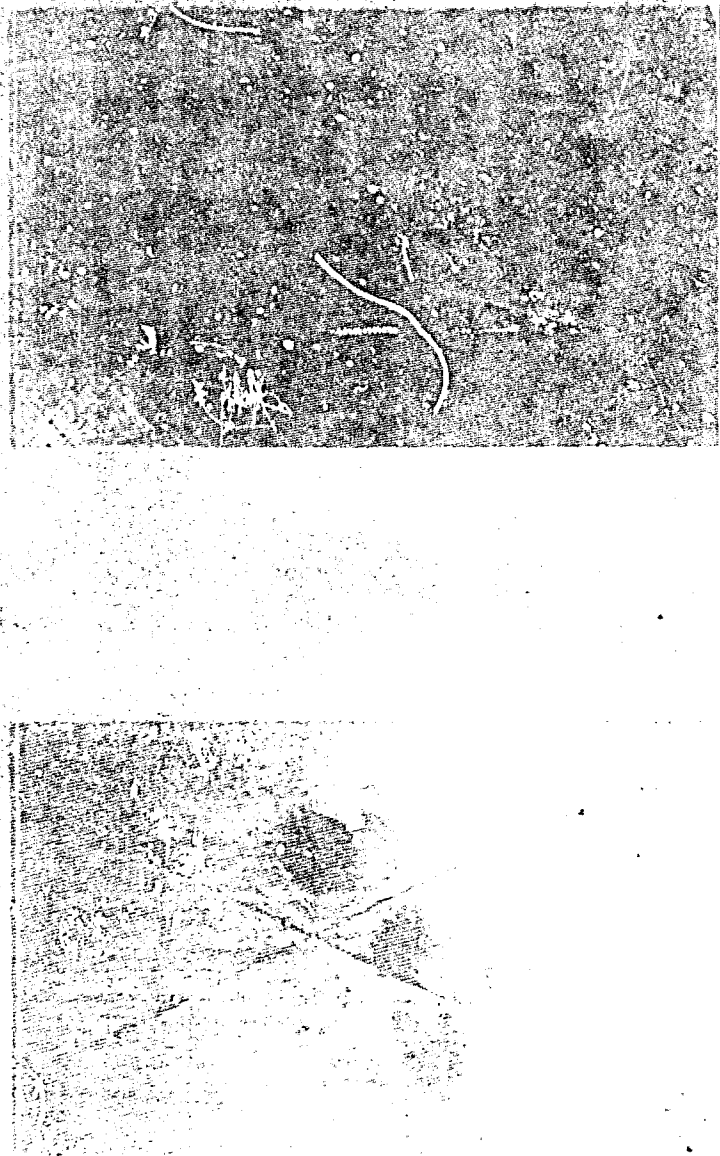


Fig. 12 Aluminized, glass-coated, graphite-epoxy (left) and boron-epoxy (right) laminates after exposure to 3% salt spray for 30 days

**Aluminum-Wire-Fabric-Coated,  
Boron-Filament-Reinforced Epoxy  
After Exposure to 232 C**

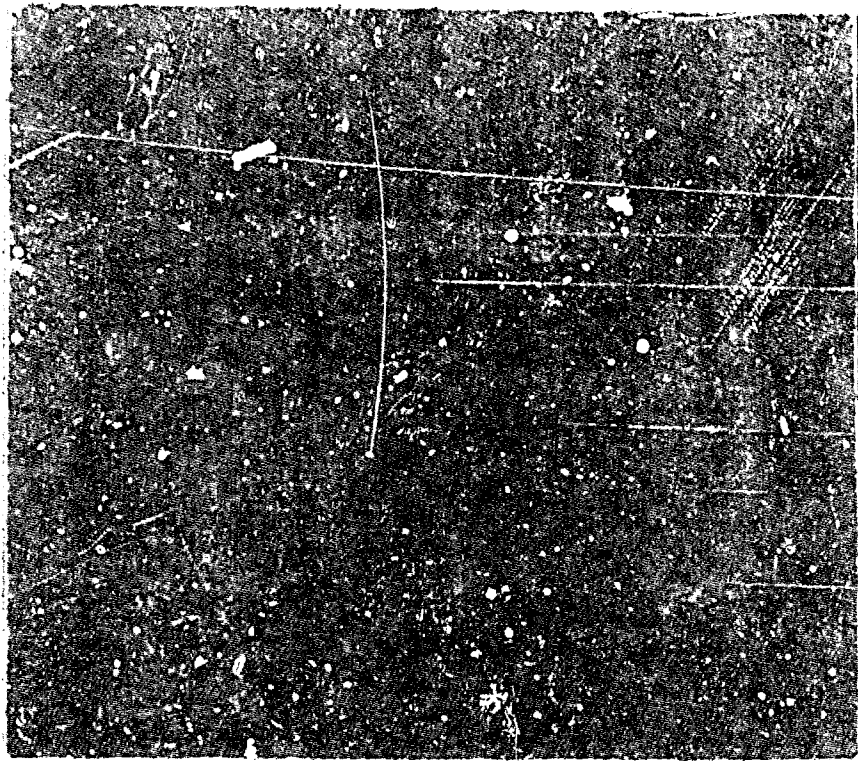


Fig. 13 Aluminum-wire-fabric coated boron-filament-reinforced epoxy  
after exposure to 232 coulombs



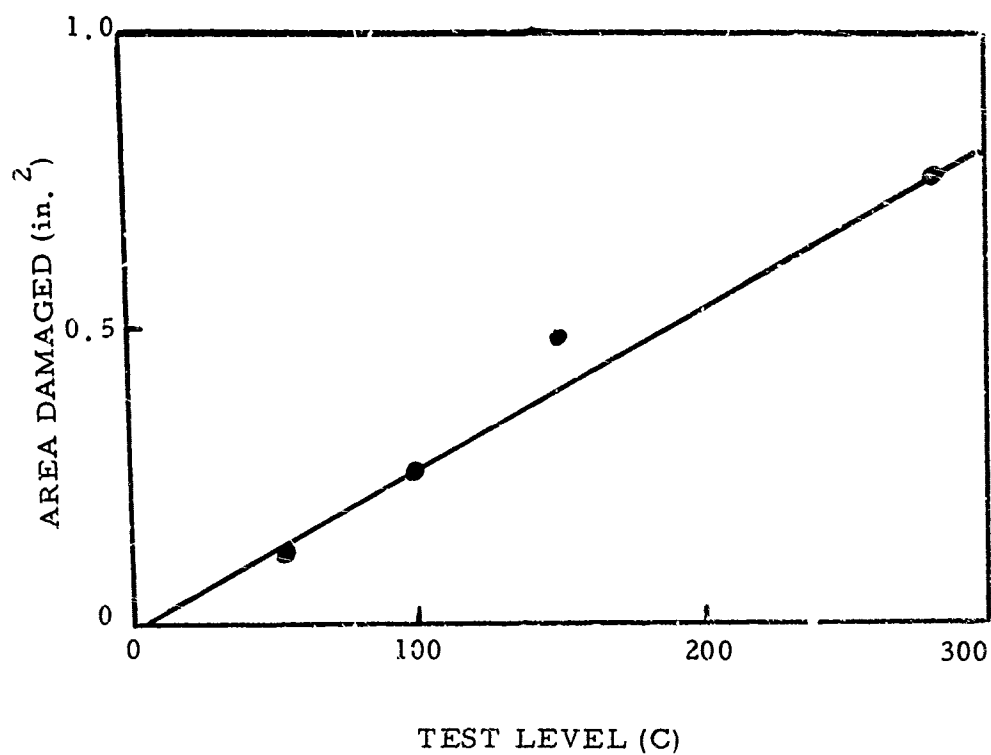


Figure 14. Damage Versus Coulombs Transferred for 200 by 200 Mesh, Aluminum-Wire-Fabric-Coated, Boron-Filament-Reinforced Laminates

increase in the test level. Residual mechanical properties of the laminates indicate the damage was restricted to the visible burn areas. Generally, the boundaries of the burn zone were quite sharp.

That localized damage does occur with high-coulomb tests was proven with flexural strength tests of two 14-ply laminates coated with 200 by 200 mesh and 120 by 120 aluminum wire fabric. The data are given in Table 1. For these tests, the laminates were cut into five 1-in. wide strips, labeled 1- to -5 such that -1 and -5 were the edge strips, -3 was the center, etc. Each strip was then cut into two parts with the parts nearest electrical ground labeled -6 through -10. Thus, -3 and -8 were cut from the center, -5 and -10 from the right edge, etc. The coupons were tested per ASTM D790, with a 32-to-1 span-to depth ratio.

The test data show reduction of strength in the graphite-fiber-reinforced laminate only at the burn center. Even between the burn center and electrical ground no damage was detectable. The boron-filament-reinforced laminate was undamaged as the arc wandered across the surface, burning the coating of all specimens except -6 and -7.

Aluminized Glass Filaments - Very similar behavior was observed with aluminized, glass-fiber-coated laminates. If the arc wandered, little or no damage occurred. If the arc attached to the reinforcing filaments, damage occurred. A 200-C transfer test to a two-ply coating (4960 conductive filaments per inch) burned a 1-in. -diameter hole through the boron-filament-reinforced laminate and caused mechanical damage in a 2-1/2 in. -diameter area. Yet, a 180-C transfer test to a similarly coated graphite-fiber-reinforced laminate caused no damage as the arc wandered on the panel surface. Figure 15 shows the results for high coulomb test utilizing the aluminized glass filaments. This series of tests indicates that localized damage caused by the high-coulomb component of the lightning stroke will occur unless the arc wanders or sweeps across the test surface. Since the arc would be expected to be swept to some extent across the surface of an aircraft in flight, it is anticipated that the in-flight damage would be less than the damage in laboratory tests where the arc remained attached at one point.

## CONCLUSIONS

1. Several improved lightweight coatings were developed to protect boron and graphite-reinforced plastic composites from the high-

current component of an artificial lightning stroke. These coatings are: 200 by 200 mesh aluminum wire fabric, 120 by 120 mesh aluminum wire fabric, and a coating containing aluminized glass filaments.

2. These coating can withstand re-strikes at the 100-kA test level with no coating repair required. At the 200-kA test level, very local and minor damage may occur to the coating and the coating can be easily repaired.

3. The wire fabric coatings were resistant to normal aircraft environments including salt spray, relative humidity and fluid resistance. In general, the coatings were not altered by any of these environments and still provided satisfactory lightning protection to the composites after exposure.

4. The coatings were successful in preventing structural damage to boron and graphite fiber reinforced plastics at currents as high as 200-kA. In some of the tests at 200-kA there was very minor, localized damage at the point of stroke attachment. Where such damage did occur, it was limited to an area of the order of one inch in diameter, which would be about the same size of damaged area, as aluminum sheet of the same thickness exposed to the same current level.




Reproduced from  
best available copy. 

Fig. 15 Aluminized, glass coated, graphite epoxy laminate after exposure to 194-kA and 180 coulombs

TABLE 1

## Residual Flexural Properties of Aluminum-Fabric-Coated Laminates

Boron reinforcement (140-C test level)			Graphite reinforcement (206-C test level)		
Specimen 120 x 120 mesh	Flexural Strength (ksi)	Flexural Modulus (psi x 10 <sup>6</sup> )	Specimen 200 x 200 mesh	Flexural Strength (ksi)	Flexural Modulus (psi x 10 <sup>6</sup> )
323-1*	88.2	11.3	446-1	63.4	13.7
-2*	97.8	12.7	-2*	64.3	13.8
-3*	87.9	11.6	-3	43.3	11.5
-4*	97.1	11.6	-4	69.7	14.1
-5	93.1	11.7	-5	64.8	13.5
-6	87.5	11.8	-6	60.5	13.6
-7*	93.0	12.1	-7	64.7	14.1
-8*	82.6	11.1	-8	59.8	14.0
-9*	91.1	12.1	-9	62.2	14.2
-10*	<u>87.9</u>	<u>11.8</u>	-10	<u>68.8</u>	<u>14.4</u>
Avg	90.6	11.8	Avg	62.2	13.7

\* Visible damage to coating

# DIELECTRIC SHIELDING LIGHTNING PROTECTION FOR COMPOSITE AIRCRAFT STRUCTURES

by

J. T. Kung  
M. P. Amason

Douglas Aircraft Company  
McDonnell Douglas Corporation  
Long Beach, California

## ABSTRACT

Boron and graphite epoxy composite aircraft structures are vulnerable to lightning-strike damage. Douglas has taken a new approach to develop appropriate lightning protection techniques for these structures, based on the zonal lightning protection design concept. An extensive research program has been carried out to investigate lightning protection techniques for composite structures located in the Zone 2, swept-stroke, and restrike areas. A series of lightning tests was conducted on 4- by 8-foot panels and test results indicated that the dielectric shielding technique can be utilized to provide adequate lightning protection.

**SIGNIFICANT WEIGHT SAVING** can be realized by substituting boron and graphite epoxy composite materials for conventional metals in certain structural elements of aircraft. However, these materials are not electrically or thermally as conductive as conventional metals, and laboratory test results have indicated that lightning strikes can seriously degrade the structural integrity of parts made of these composite materials.

In 1970, Douglas made an overview of all lightning and static electricity related problems associated with the use of boron and graphite epoxy composite structures in aircraft (1)\*. This study indicated that various types of lightning protection methods should be developed for this type of structure so that they can be efficiently used in the various regions of aircraft. The lightning protection design requirements for this type of structure should be established based on the region of the aircraft where it is used. Environmental effects, as well as the serviceability and maintainability of proposed protection systems, should also be considered.

A review of industry activities in this area (2 and 3) indicates that most of the effort has been concentrated on the development of conductive surface shielding methods to provide protection against the direct lightning stroke condition. An assessment of the aircraft lightning strike phenomena (4) indicates that most aircraft structural parts are not located in regions requiring protection against such severe conditions. While conductive surface shielding methods can be used to provide more than adequate protection for structures located in the less stringent swept-stroke and restrike regions, their usage may not be cost effective. In addition, the use of these protection methods can reduce, but not completely eliminate, lightning damage to composite structures (2).

In view of the above, Douglas has considered other approaches for the development of lightning protection for composite structures located in the swept-stroke and restrike regions of an aircraft. This has resulted in the development of a new approach utilizing the dielectric-shielding concept. The design objective of this approach is to prevent the swept-stroke and restrike lightning current from attaching to, or transferring through, the composite structures by shielding them with dielectric coatings and films.

## DESIGN CONCEPTS

**ZONAL PROTECTION DESIGN CONCEPT** — When struck by lightning, an aircraft becomes involved in various phases of the lightning current transfer. For the purpose of defining lightning protection requirements, the aircraft surfaces can be divided into three major zones (5):

- Zone 1: Surfaces of the aircraft for which there is a high probability of direct lightning stroke attachment.
- Zone 2: Surfaces of the aircraft for which there is a high probability of a lightning stroke being swept rearward from a Zone 1 point of direct stroke attachment.
- Zone 3: The aircraft areas other than those covered by Zone 1 and Zone 2 regions.

Figure 1 shows the lightning strike zones of a typical aircraft. These zone regions were defined from the analysis of laboratory lightning test results obtained using a scale aircraft model. Since the lightning attachment and/or transfer characteristics in each zone region are not the same, lightning protection design considerations for aircraft structures in each zone region are different. Therefore, appropriate lightning protection designs for advanced composite structures should be developed according to their specific applications on an aircraft.

**SWEPT-STROKE PHENOMENA** — An aircraft becomes a part of the lightning discharge channel when struck by lightning. Figure 2 shows the probable current waveform of the most severe lightning stroke. The aircraft, due to its speed, may move a distance of several hundred feet during the entire lightning event. Since the lightning channel is somewhat stationary in space, the aircraft will fly through the established lightning channel when an attachment occurs to a forward protrusion point on the aircraft. As a result, the lightning channel may make intermittent contacts with the aircraft surface aft of the initial attach point. Thus, the lightning channel appears to sweep back over the aircraft surface as illustrated in Figure 3. This is the swept-stroke phenomena. When a lightning restrike occurs, it usually follows the same lightning channel if it occurs

\*Numbers in parentheses designate References at end of paper.

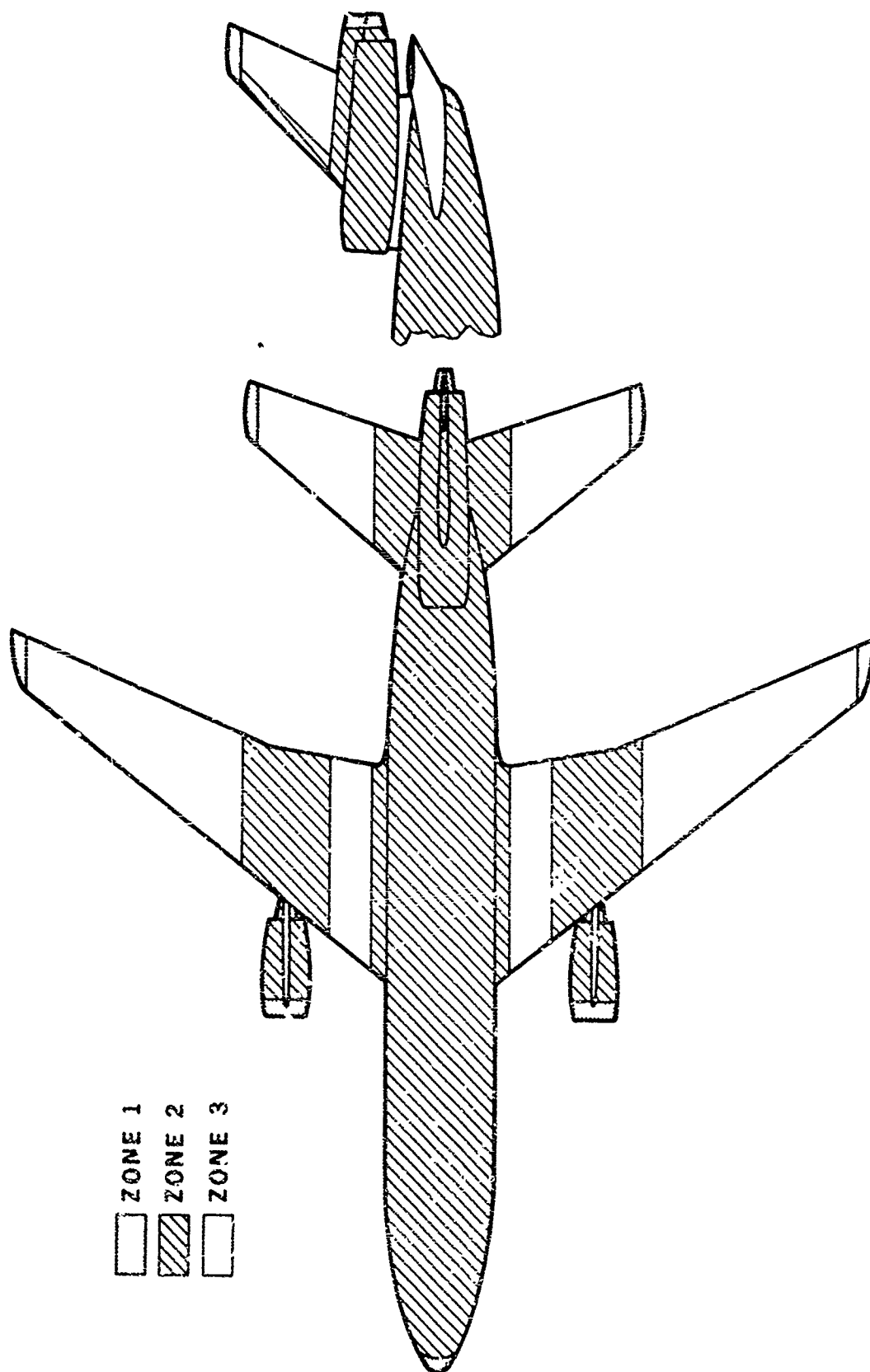


Fig. 1 - Typical aircraft lightning strike zones

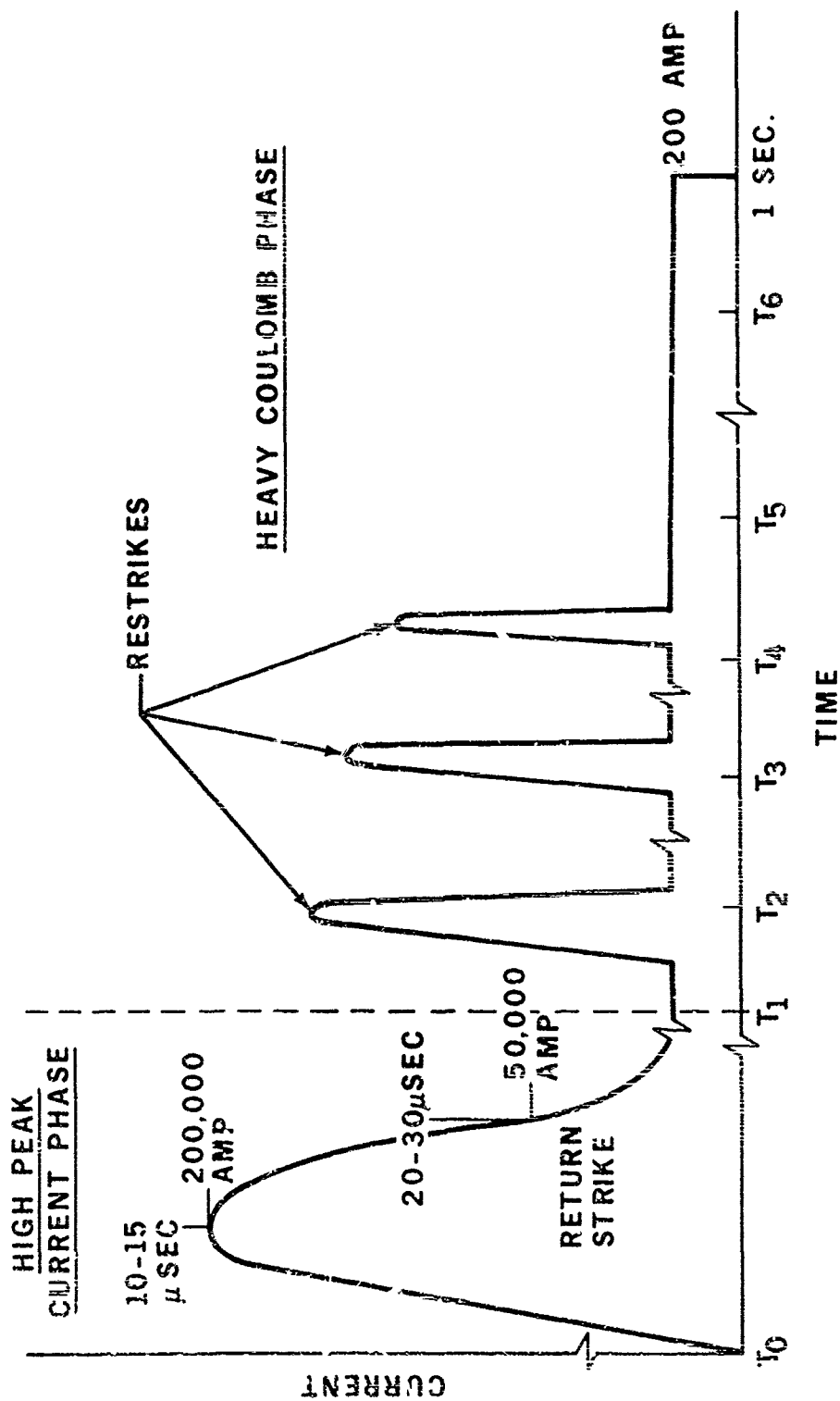


Fig. 2 - Critical lightning current waveform

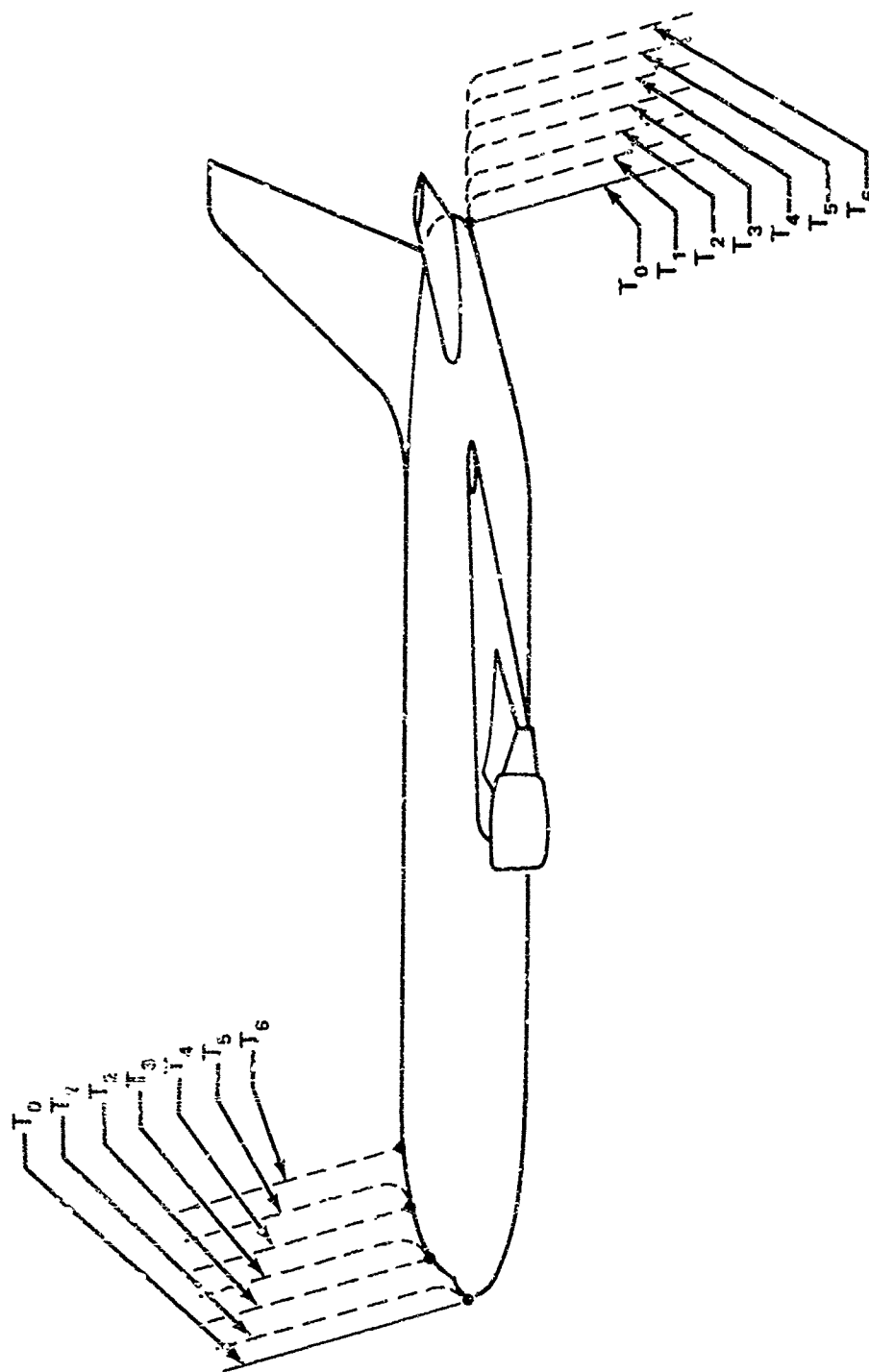


Fig. 3 - Swept-stroke phenomena



within 100 milliseconds of the initial return stroke (6). Hence, restrikes can be part of the swept-stroke phenomena.

**DIELECTRIC SHIELDING DESIGN CONCEPT** - A complete lightning protection system includes two fundamental parts: a conductive part which provides lightning current paths and an isolation part which shields the protection object from the lightning current paths. The isolation part of the protection system is as important as the conductive part. In the past few years, most of the research effort for advanced composite structures in the industry has been concentrated on the development of the conductive part of the system. The isolation part, however, appears to have been neglected.

Boeing and Lightning and Transients Research Institute (LTRI) have investigated the dwell time characteristics of swept-stroke attach points on metal skin surfaces in the fuel tank area (7 and 8). These investigations indicated that when coatings were used on the external metal surface located in swept-stroke regions, the lightning channel would dwell at specific points on the metal surface and not sweep smoothly as it would across the bare metal surface. The surface coatings provided a dielectric shield over the metal skin surface. This created a condition that made it difficult for the lightning channel to contact a new point during the sweeping event, thus prolonging the dwell time at each attach point.

An analysis made by Douglas indicates that certain dielectric materials can be used to provide boron and graphite composite structures with dielectric shielding protection against lightning attachment in Zone 2 regions. Since the longer dwell time of the lightning channel at a point on the skin panel will result in a larger separation distance between attach points during the swept-stroke, this can be used to advantage for composite skin panels. The distance between lightning attach points can be extended by increasing the dielectric strength of the surface coating. Therefore, the attachment of lightning swept-stroke and restrike current to a certain span of composite skin panel can be prevented by the external surface application of materials with sufficient dielectric strength.

This design concept assumes that an attach point occurs forward of the composite skin panel on a metal surface. Metallic leading edge structures may be used for this purpose since they also provide ideal rain erosion protection for composite structures. If required, a metal surface component should also be used aft of the composite skin panel for the dwelling or hanging on of the lightning channel.

#### LABORATORY INVESTIGATIONS

**TEST SETUP** - LTRI swept-stroke and restrike lightning test facilities were utilized for laboratory investigations. Figure 4 shows the schematic diagram of the test setup while Figure 5 shows the typical swept-stroke current waveform. This waveform reflects a peak amplitude of 500 amperes which decays exponentially to zero in about 20 milliseconds. The restrike high voltage generator produces a current discharge of 15 kiloampere peak amplitude at a frequency of 150,000 Hz and a settling time of 30 microseconds, as shown in Figure 6. The wind tunnel can provide a wind velocity of from 130 to 250 mph during the lightning test. After the lightning channel is established

between the lightning rod and test panel, the wind blows the channel across the test panel. The upper end of the lightning channel also moves along the metal lightning rod allowing the arc channel to follow the windstream. The lightning channel may be swept over a range of 30 to 55 inches from the initial attach point depending upon the wind velocity provided during the 20-millisecond discharging period.

A Polaroid camera is used to take the still photograph of each lightning test shot. In addition, a high-speed Fastex movie camera is used to record the movement of lightning channel at a speed of approximately 2,000 frames per second.

**TEST SAMPLES** - Boron and graphite epoxy composite panels with different types of dielectric surface coatings were lightning tested to demonstrate the feasibility of the dielectric-shielding concept. Common surface coating-type materials were tested first since all external composite skins would require them for environmental protection and other purposes. A test panel is described in Figure 7 and Table 1. Two such panels, with four composite skins, were tested. The polyurethane coating was selected for test since it is the type of finish coating that would normally be used over composite skins. On the No. 2 skin surface, an additional coating of 10-mil epoxy was used to provide extra dielectric shielding strength. The Astrocoat coating, which provides good rain erosion protection, was also tested.

The attachment characteristics of swept-stroke and restrike lightning current on a graphite epoxy composite skin bonded to aluminum honeycomb core were also investigated. See Figure 8 and Table 2.

**TEST RESULTS** - Figure 9 shows a typical swept-stroke lightning test. During this test, the lightning channel dwelled on the forward aluminum bar while being swept over the composite skin. In the latter part of the test, the lightning channel was reattached to the aft aluminum bar and detached from the forward dwell point without contacting the intervening composite skin. Test results indicate that the dielectric surface coating applied to this sample was sufficient to prevent lightning attachment to the composite skin for the span involved. Figure 10 shows a failure case and Figure 11 shows the puncture damage that resulted to the composite skin.

Figure 12 shows a restrike test and the discharge current waveform. The restrike was triggered at 16 milliseconds after the initiation of the swept-stroke. The composite skin was not contacted by lightning current during this lightning test. Figure 13 shows the clips of the Fastex movie film in which the entire swept-stroke and restrike event was recorded.

In the first frame of the film clips, a small spark was recorded at the top of the thin wire and a larger one at the bottom. These sparks are expected since the thin wire was loosely attached by tapes to the overhead lightning rod and aluminum test panel. The thin wire was partially vaporized both at the top and bottom in the second frame, by the heat generated during the flow of high current. The third frame shows the thin wire completely vaporized. The movement of the lightning channel was clearly recorded starting from the fourth frame. The 27th frame shows that the restrike current flowed through the existing lightning channel, but it is difficult to see the attach point since the

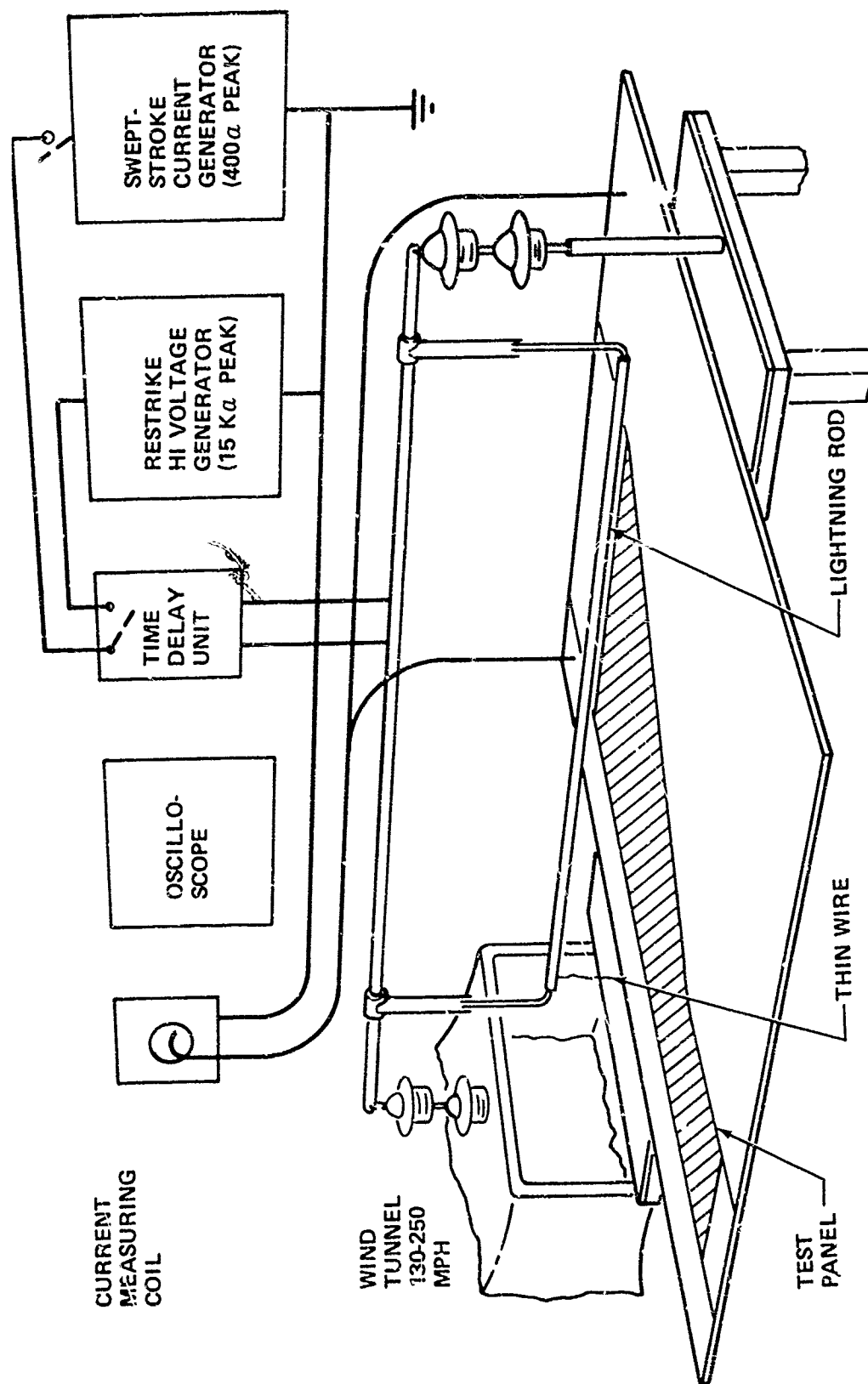


Fig. 4 - LTRI swept-stroke and restrike lightning test schematic diagram

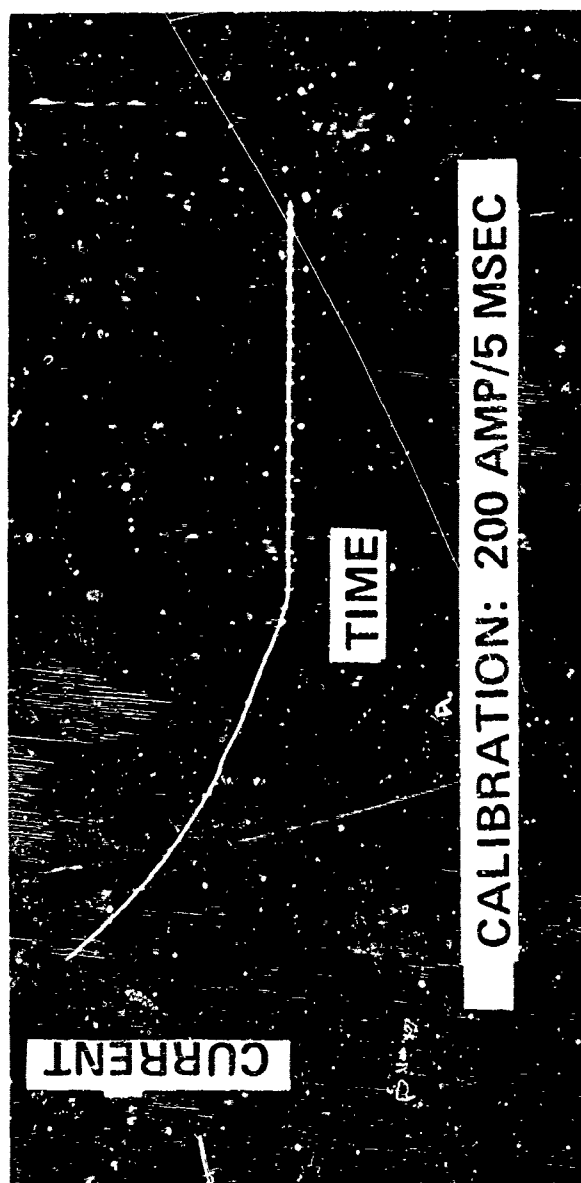
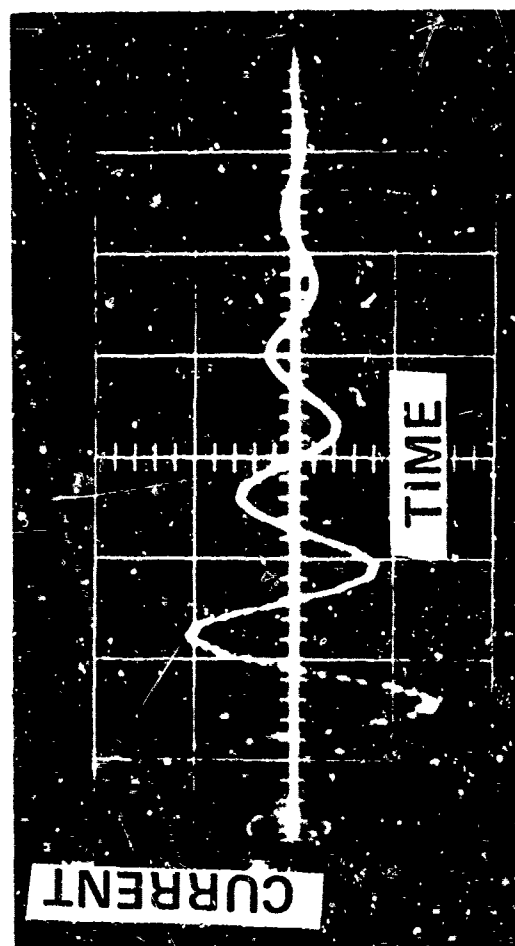


Fig. 5 - Typical swept-stroke test current waveform



CALIBRATION: 6,000 AMP / 5 $\mu$  SEC

Fig. 6 - Typical restriking test current waveform

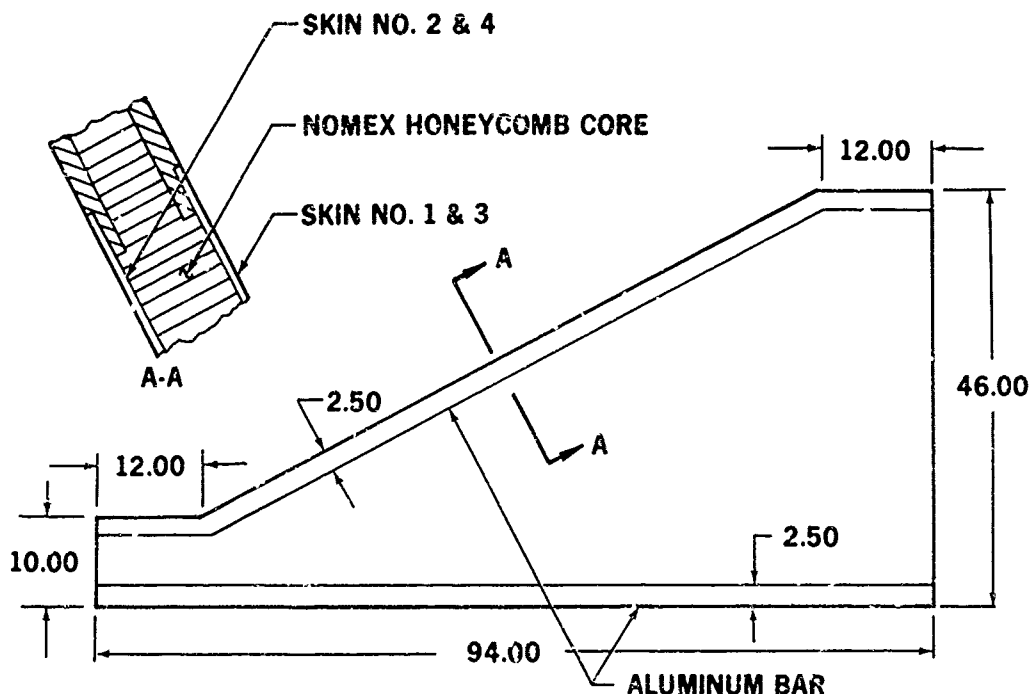


Fig. 7 - Composite test panel

Table 1 - Composite test panel material description

SKIN	COMPOSITE AND SURFACE COATING MATERIAL
1	4 LAYERS GRAPHITE FILAMENT* (FERRO PREG C-1313 GLC 4T/E-350) AND 3 MIL POLYURETHANE COATING (DPS 4.50-62)
2	4 LAYERS GRAPHITE FILAMENT* (FERRO PREG C-1313 GLC 4T/E-350), 10 MIL EPOXY COATING (DPM 110 CLEAR), AND 3 MIL POLYURETHANE COATING (DPS 4.50-62)
3	4 LAYERS GRAPHITE FILAMENT* (FERRO PREG C-1313 GLC 5T/E-350), 2 LAYERS BORON FIBER** (NARMCO 5505), AND 3 MIL POLYURETHANE COATING (DPS 4.50-62)
4	4 LAYERS GRAPHITE FILAMENT* (FERRO PREG C-1313 GLC 5T/E-350) AND 7.3 MIL ASTROCOAT RAIN EROSION COATING

\*FILAMENT LAYER ORIENTATION:  $+45^{\circ}$ ,  $-45^{\circ}$ ,  $-45^{\circ}$ ,  $+45^{\circ}$ .

\*\*FIBER LAYER ORIENTATION:  $0^{\circ}$ ,  $0^{\circ}$  (PARALLEL TO THE STRAIGHT ALUMINUM BAR)

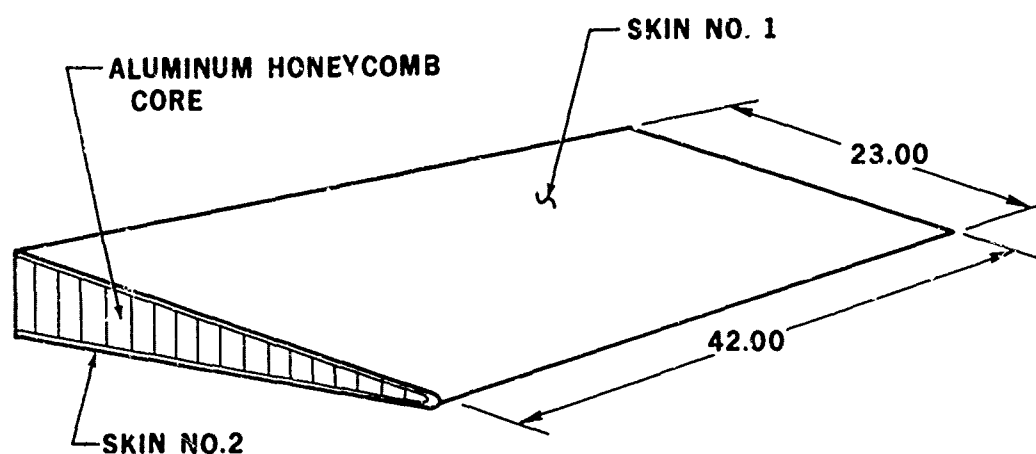


Fig. 8 - Graphite epoxy composite flap

Table 2 - Graphite epoxy composite flap material description

SKIN	COMPOSITE AND SURFACE COATING MATERIAL
1	4 LAYERS GRAPHITE FILAMENT* (NARMCO 50206) AND 3 MIL POLYURETHANE COATING (DPS 4.50-62)
2	4 LAYERS GRAPHITE FILAMENT* (NARMCO 50206), 10 MIL EPOXY COATING (DPM 110 CLEAR), AND 3 MIL POLYURETHANE COATING (DPS 4.50-62)

\*FILAMENT LAYER ORIENTATION:  $+45^{\circ}$ ,  $-45^{\circ}$ ,  $-45^{\circ}$ ,  $+45^{\circ}$ .

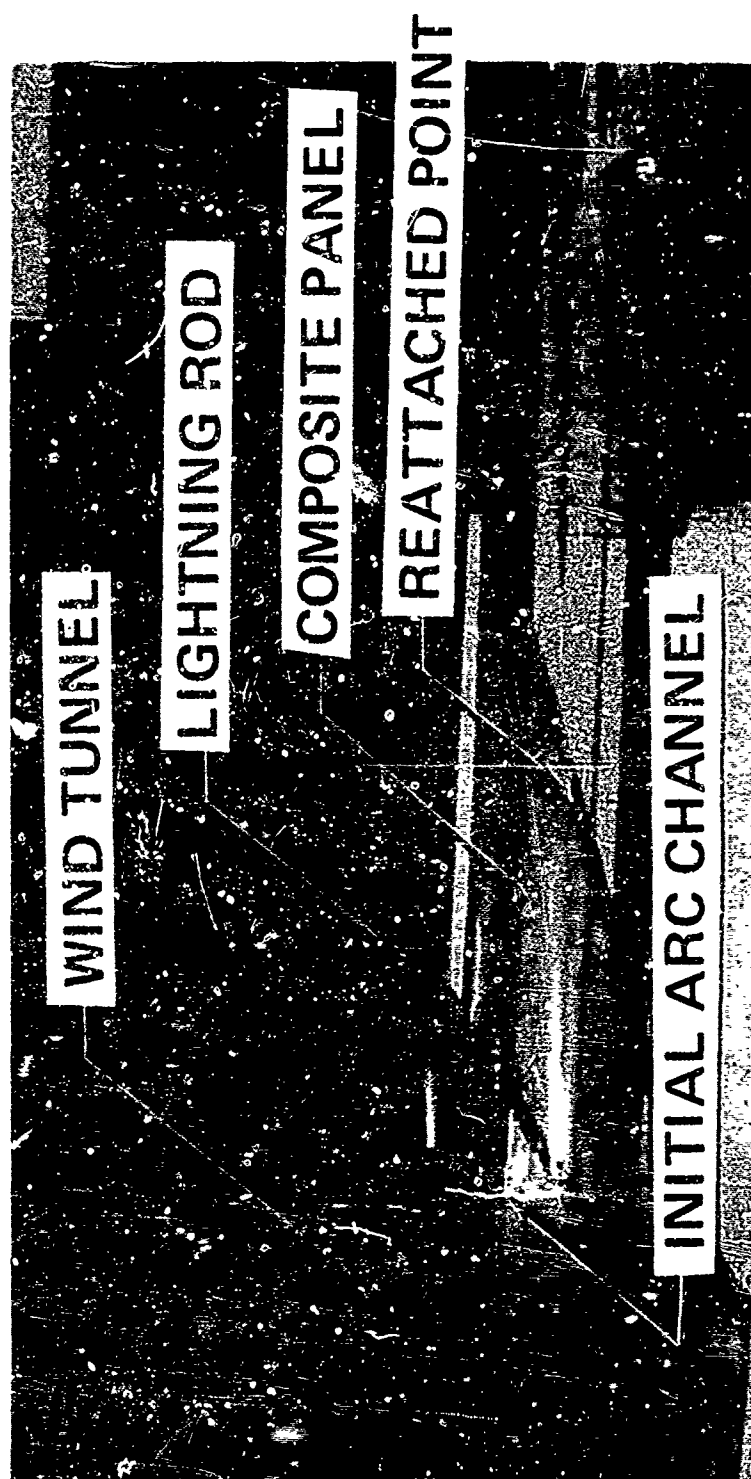


Fig. 9 - Typical swept-stroke lightning test

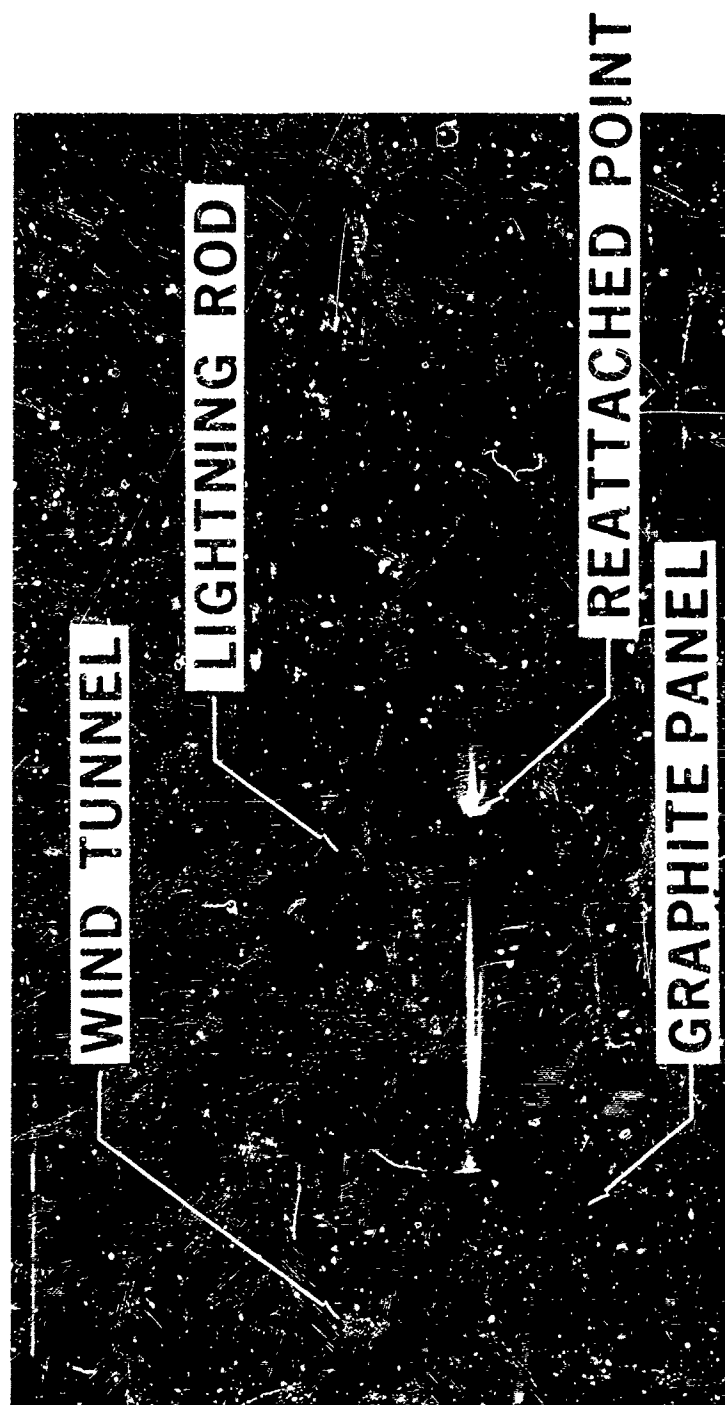
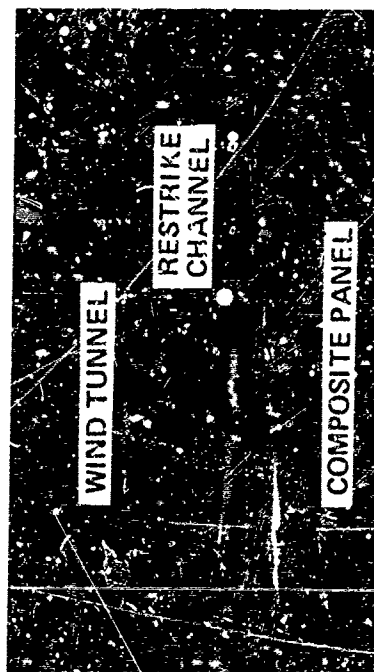


Fig. 10 - A test failure on composite skin panel

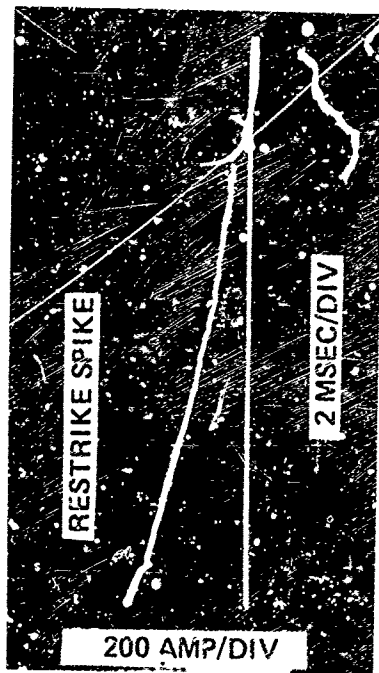




Fig. 11 - Damage resulting from swept-stroke attachment



HANGING OVER 31 IN. SPAN



RESTRIKE AT 16 MSEC

Fig. 12 - Restrike lightning test and current waveform - I

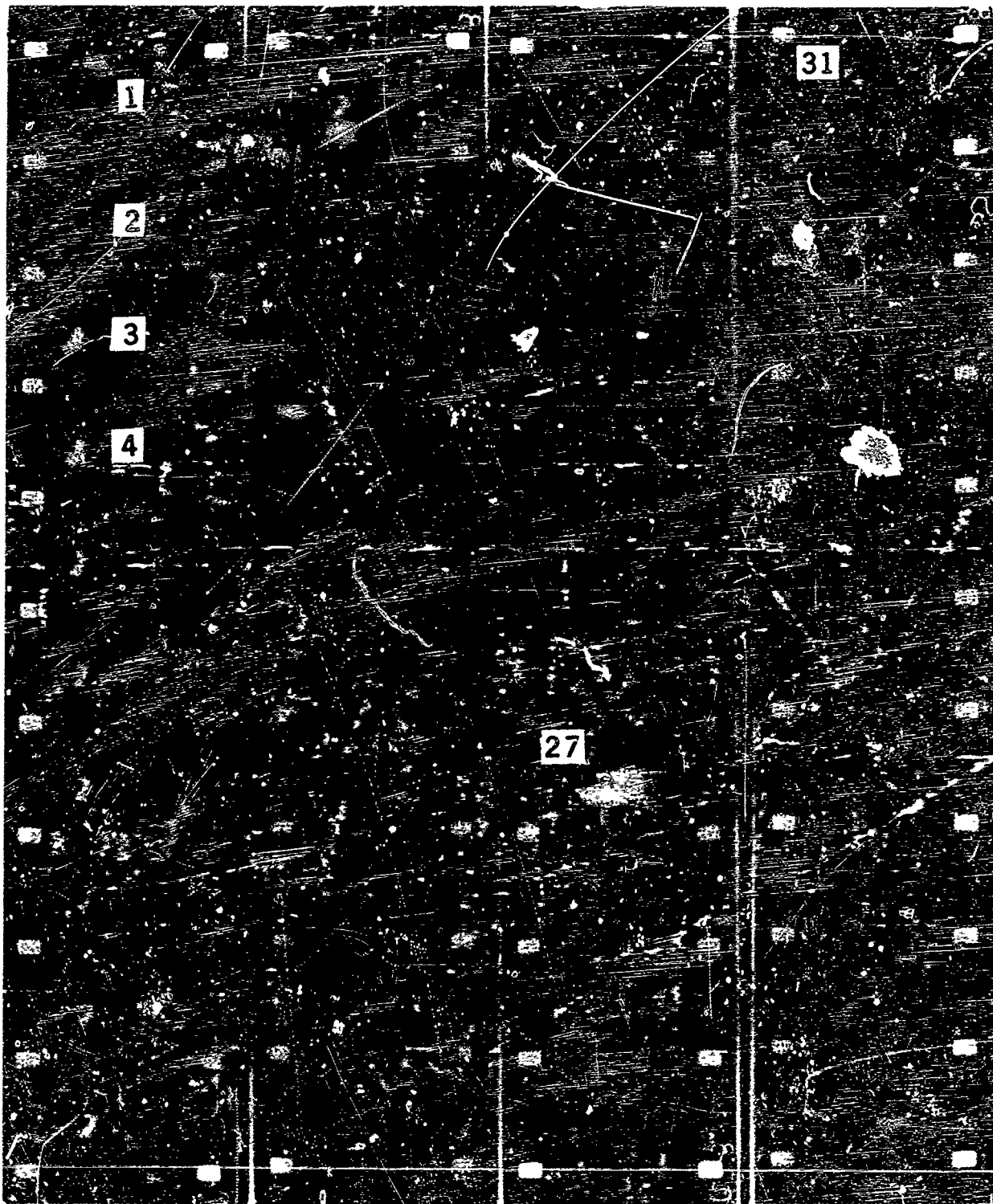


Fig. 13 - Fastex movie film clips of restriking lightning test

picture has been overexposed. However, the still photo of the same event, Figure 12, recorded a clear restrike channel attaching back to the forward aluminum bar. The 31st frame shows the lightning channel disconnected from the top lightning rod indicating the cease of lightning current flow. This is also shown in the current waveform, Figure 12. The lightning current magnitude reduces to zero two milliseconds after the restrike discharge. The remaining part of the film clips show the decreasing illumination of the plasma channel.

The exact film speed of the Fastex movie can be calculated from Figures 12 and 13. The restrike event at 16 milliseconds is shown in the 27th frame of the film clips. This corresponds to a film speed of 0.59 millisecond per frame.

Figure 14 shows another successful restrike test. During this test, the restrike current did not follow the existing swept-stroke channel, but instead attached to the aft aluminum bar, as shown in the still photo. This demonstrates that sufficient shielding strength was provided for the composite skin by the dielectric surface coating.

The effect of using exposed metallic structural ribs for the attachment of the lightning channel between dielectrically shielded composite skin panels has been investigated. Thin metal foil strips were used to simulate these ribs. The strips were applied both perpendicular and parallel to the windstream. Figure 15 shows the test panel and Figure 16 shows one of the swept-stroke tests. Test results indicate that strips positioned perpendicular to the windstream can be effectively used for the reattachment of lightning current. Thus, this method can be used over dielectrically shielded composite skin surface for the protection of longer spans. The strips positioned parallel to the windstream, however, failed to provide any diversion function for the swept-stroke channel.

The effect of electrically grounding the graphite epoxy composite skin on the attachment characteristics of swept-stroke lightning channel also has been investigated. Figure 17 shows the test results. In this case, a 24-inch air gap was intentionally provided at the trailing edge of the composite flap. It should be noted that for the ungrounded skin case, the lightning channel dwelled on the forward aluminum bar for the entire period of lightning test. However, when the skin surface was grounded the lightning channel attached to the forward aluminum bar and then reattached to the trailing edge of the composite flap where it dwelled until the channel decayed.

Fifty swept-stroke test shots and 20 restrike test shots were made on boron and graphite composite skin panels shielded with various types of dielectric coatings. The span protections afforded for each configuration for both swept-stroke and restrike tests are summarized in Table 3. Test results have verified that the restrike condition is more critical than the simple swept-stroke condition. The test results have been analyzed and significant findings are as follows:

- The boron epoxy composite skin has an inherent degree of dielectric shielding strength which makes this type of skin easier to protect than the graphite skin.

- The aluminum honeycomb core underneath a composite skin does not have appreciable effect on the shielding characteristics of dielectric surface coatings when considering swept-stroke and restrike conditions.

- A 10-mil coating of epoxy plus a 3-mil polyurethane coating system can provide over a 48-inch span protection for swept-stroke and 31-inch span protection for restrike when applied to the graphite epoxy composite skin. More investigations, using higher restrike peak current, are necessary for further verification. This protection system applied to the boron skin has not been tested. However, a longer span of protection is expected.

- Metal foil strips or exposed metallic structural ribs, positioned perpendicular to the windstream over the dielectrically shielded composite skin surface can be used for the protection of longer spans. Metal strips or ribs positioned parallel to the windstream may not provide a diversion function to the swept-stroke channel.

- Electrical grounding of the graphite epoxy composite skin surface may affect the swept-stroke lightning channel attachment characteristics by weakening the dielectric shielding protection system. Therefore, it may be desirable to isolate the composite skin surface from the adjacent metal structures.

- An analysis of these results indicates that higher dielectric strength materials may be beneficial for large skin panel protections and also for weight saving considerations. Douglas is investigating certain dielectric films for the next phase of this research program.

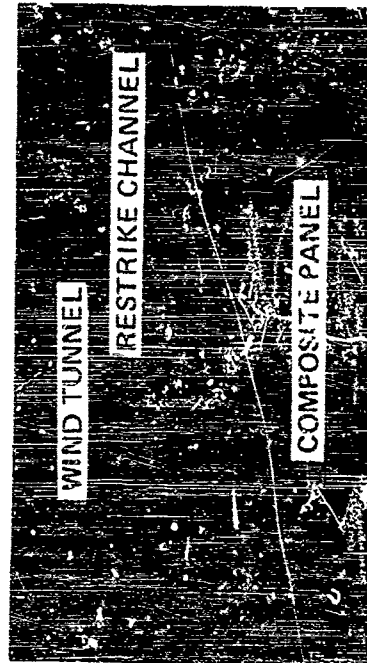
## CONCLUSION

Various lightning protection design techniques are required for advanced composite aircraft structures. These techniques should be developed for each individual structure according to its specific application and location on an aircraft.

The dielectric surface shielding method presented in this paper has shown that adequate protection has been provided for certain spans of composite skin panels located in the swept-stroke and restrike region of the aircraft.

## REFERENCES

1. M. P. Amason and J. I. Kung, "Lightning Protection on Advanced Composite Aircraft Structures," Douglas Report No. MDC 15002, Douglas Aircraft Company, Long Beach, California, December 1970.
2. R. O. Bruck, C. H. King, and J. T. Quinliven, "Coatings for Lightning Protection of Structural Reinforced Plastics," Technical Report AFML-TR-70-303 Part I, The Boeing Company, February 1972.
3. G. T. Woodrum, "Lightning Protection for Advanced Composite Aircraft Structures," SAE Paper No. 700935, Lightning and Static Electricity Conference, 9-11 December 1970.



SWEEPING ACROSS 22 IN. SPAN



RESTRIKE AT 15 MSEC

Fig. 14 - Restrike lightning test and current waveform - II

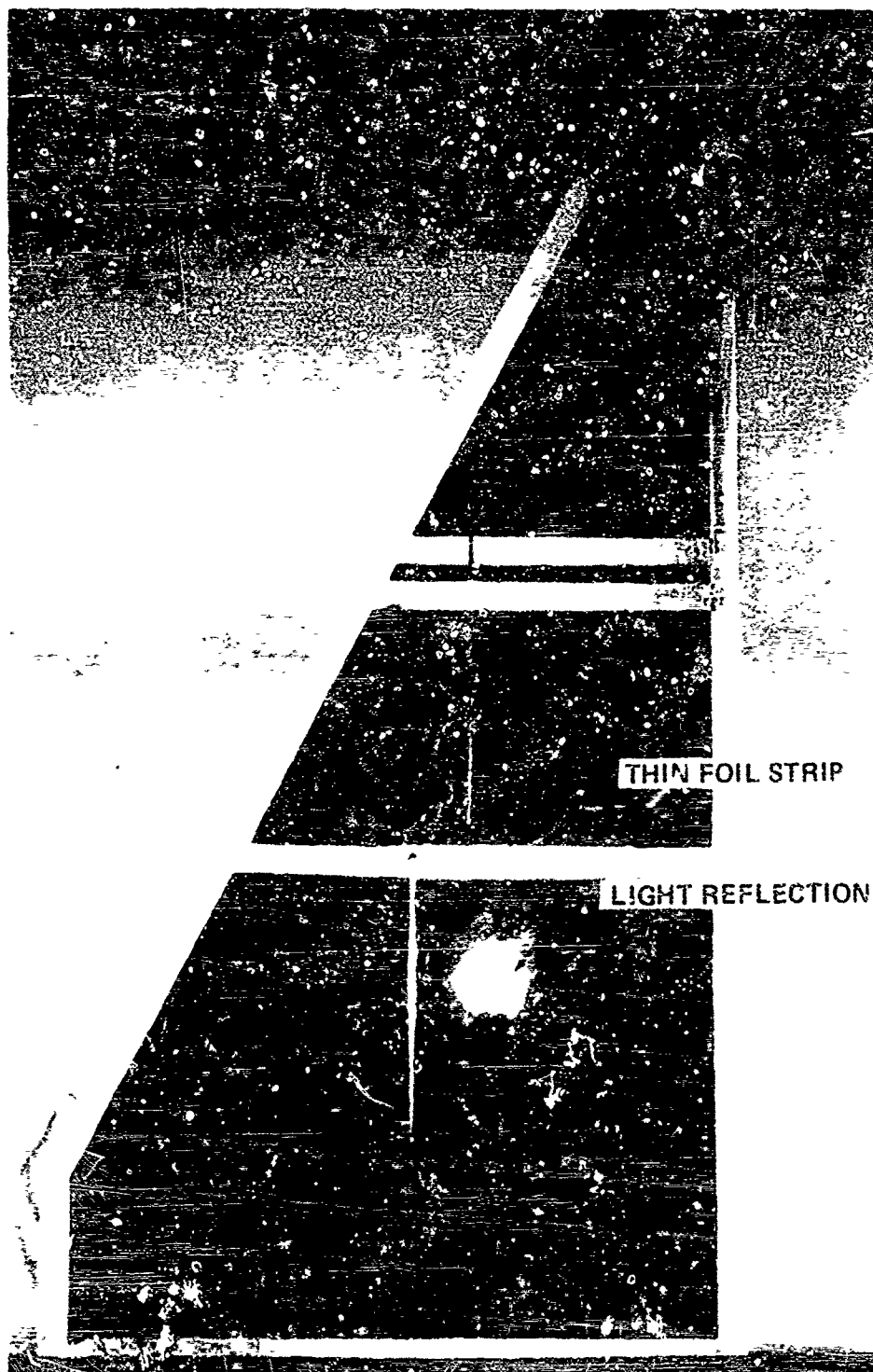


Fig. 15 - Swept-stroke lightning diversion test panel

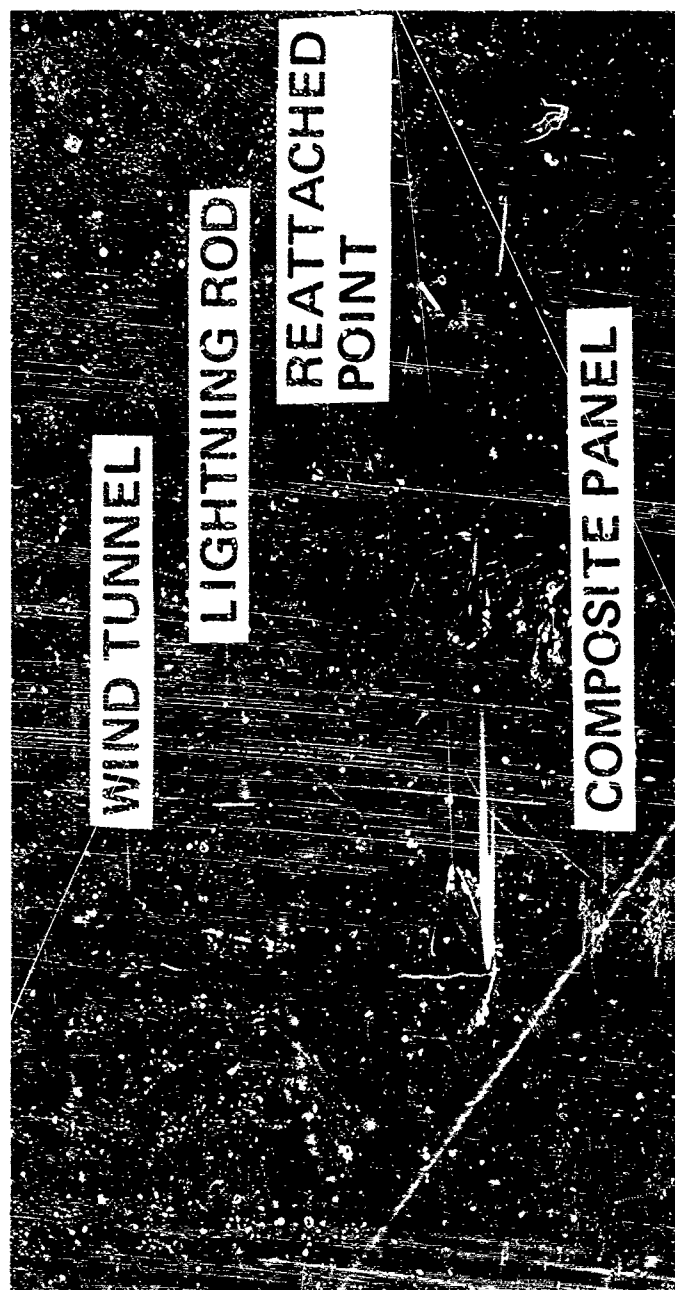
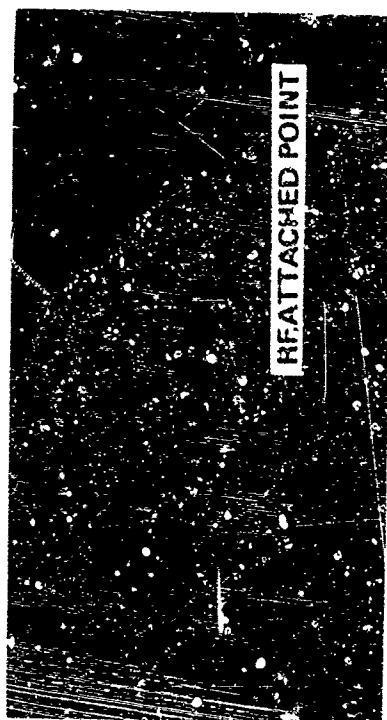


Fig. 16 - Swept-stroke lightning diversion test



**SKIN SURFACE UNGROUNDED**



**SKIN SURFACE GROUNDED**

Fig. 17 - Graphite epoxy composite skin surface grounding effect



Table 3 - Summary of swept-stroke and restrike lightning test on advanced composite panels

TEST SAMPLE	HONEYCOMB CORE	SPAN PROTECTION (INCHES)	
		SWEPT STROKE	RESTRIKE
BORON + 0.003 POLYURETHANE	NOMEX	51.5*	19.0
GRAPHITE + 0.003 POLYURETHANE	NOMEX	35.5	FAILURE
GRAPHITE + 0.010 EPOXY + 0.003 POLYURETHANE	NOMEX	48.0*	31.0
GRAPHITE + 0.007 ASTROCOAT	NOMEX	48.0*	24.5
GRAPHITE + 0.003 POLYURETHANE	ALUMINUM	22.0*	FAILURE
GRAPHITE + 0.010 EPOXY + 0.003 POLYURETHANE	ALUMINUM	-----	22.0*

\* NO FAILURE (SAMPLE SIZE LIMITED)

4. M. P. Amason, G. J. Cassell, J. T. Kung, J. A. La Manna, and W. W. McCloud, "Aircraft Lightning Protection Design Considerations." Douglas Aircraft Company, Technical Paper No. 6043. Published in 1972 Lightning and Static Electricity Conference, December 1972.

5. "Protection of Aircraft Fuel Systems Against Lightning." FAA Advisory Circular AC 20-53, October 1967.

6. M. A. Uman, "Comparison of Lightning and a Long Laboratory Spark." Proceedings of the IEEE, Vol. 59, No. 4, pp. 457-466, April 1971.

7. R. O. Brick, L. L. Oh, and S. D. Schneider, "The Effects of Lightning Attachment Phenomena on Aircraft Design." SAE Paper No. 700925. Lightning and Static Electricity Conference, 9-11 December 1970.

8. "Lightning Discharge Sweeping Effects on Current Pitting of Painted Aircraft Skins." Lightning and Transient Research Institute, Report No. 530, April 1971.

## Lightning Protection for Aircraft Sandwich Structures with Boron/Epoxy Composite Skins

George Lubin and Sam Dastin  
Grumman Aerospace Corporation

### ABSTRACT

Boron/epoxy composites are relatively new materials for aircraft structures and there was very little data on the lightning resistance at the time the first production part, the F-14A horizontal stabilizer was initiated. This part was designed as a full-depth, aluminum honeycomb sandwich with boron/epoxy skins of varying thickness. Specimens reproducing this design were fabricated and tested under laboratory conditions to simulate exposure to lightning. Certain specimens were unprotected control specimens others had various types of protective surfaces. Protection included sprayed aluminum, aluminum and titanium foils of various thickness, conductive coatings, aluminum wire mesh and laminated metal foil, solid, perforated and in strips of various width.

Preliminary tests indicated that unprotected boron/epoxy sandwich panels with aluminum core were severely damaged by lightning strikes in excess of 100,000 amperes. Conductive paint gave a limited improvement but not sufficient protection. Sprayed aluminum coatings and bonded metal foils were very effective. Additional tests and full-scale stabilizer tests proved out the panel test results and a final pattern of aluminum foil strips was developed on the maximum effectiveness - lowest weight basis.

The PRIMARY PURPOSE of the boron/epoxy lightning exposure study was to develop the minimum weight-minimum cost protection system required by the stabilizer for the F-14A aircraft to resist 200,000 ampere discharges. This stabilizer consists of a full-depth, honeycomb base structure with boron/epoxy skins and aluminum core, and aluminum leading edge, aluminum trailing edge and an aluminum cap, (Figure 1). The boron/epoxy skins have titanium edge sections and a titanium plate at the pivot fitting. These titanium parts have tapered steps chem-milled on both sides and are bonded to the boron layer (co-cured) during the autoclave curing cycle.

The initial opinion of the designers was that since all the exposed edges of the part were metallic, little or no protection should be required. However, a study of lightning strikes on various types of aircraft, particularly, the fiberglass radomes indicated that either the lightning may strike a non-metallic surface, or the passage of lightning bolt across a surface, which occurs in flight, may also seriously damage a non-conductive component. Since the behavior of boron/epoxy

structures was not well known, a study to determine its resistance to lightning strikes was initiated.

The vulnerability of boron/epoxy structures to high-amperage discharges had been originally determined by the early Air Force tests which showed that many sample sandwich panels were extremely sensitive to lightning and tended to explode when hit by discharges of 100,000 amperes and higher. To determine the actual resistance of production parts a comprehensive program was initiated at Grumman. The first part of this study involved the exposure of test panels with and without protection to various simulated lightning exposures and the evaluation of the effects of such exposures. The second part consisted of full-scale tests on an actual F-14A boron/epoxy stabilizer. The final pattern of the protective system was developed as the result of these full scale tests.

### TEST PANEL STUDY

The initial panels used were two single-skin boron/epoxy panels, 0.060 inch thick, one with a sprayed aluminum coating and the other with a conductive epoxy coating. The aluminum sprayed panel was fabricated by first spraying 0.008 inch of aluminum on a metal plate and then molding a boron skin integrally on the surface of the aluminum. The results of the tests on the sprayed panel are shown on Figure 2.

The surface was etched by the discharge but the panel was not punctured even by a 200,000 ampere strike but some surface damage was apparent. Flexural tests of specimens from the damaged area showed a 30% drop in mechanical strength. The panel with 0.003 inch conductive epoxy coating was penetrated by both 100,000 ampere and 200,000 ampere lightning strikes and was not tested further.

The panel tests on sandwich panels consisted initially of seven panels listed in Table I. The facing skins for these panels were fabricated from Narmco 5505 boron/epoxy tape. The core was aluminum honeycomb, 3/4 inch thick, 1/8 inch cell size and 5 pounds per cu. feet density. For the back skins, fiberglass panels, 0.060 inch thick were used. The skins were bonded to the honeycomb using Metlbond 239 adhesive. Grounding strips were bonded to panels with Hyso 4239-3487 con-



Figure 1 - F-14 Boron/Epoxy Stabilizer

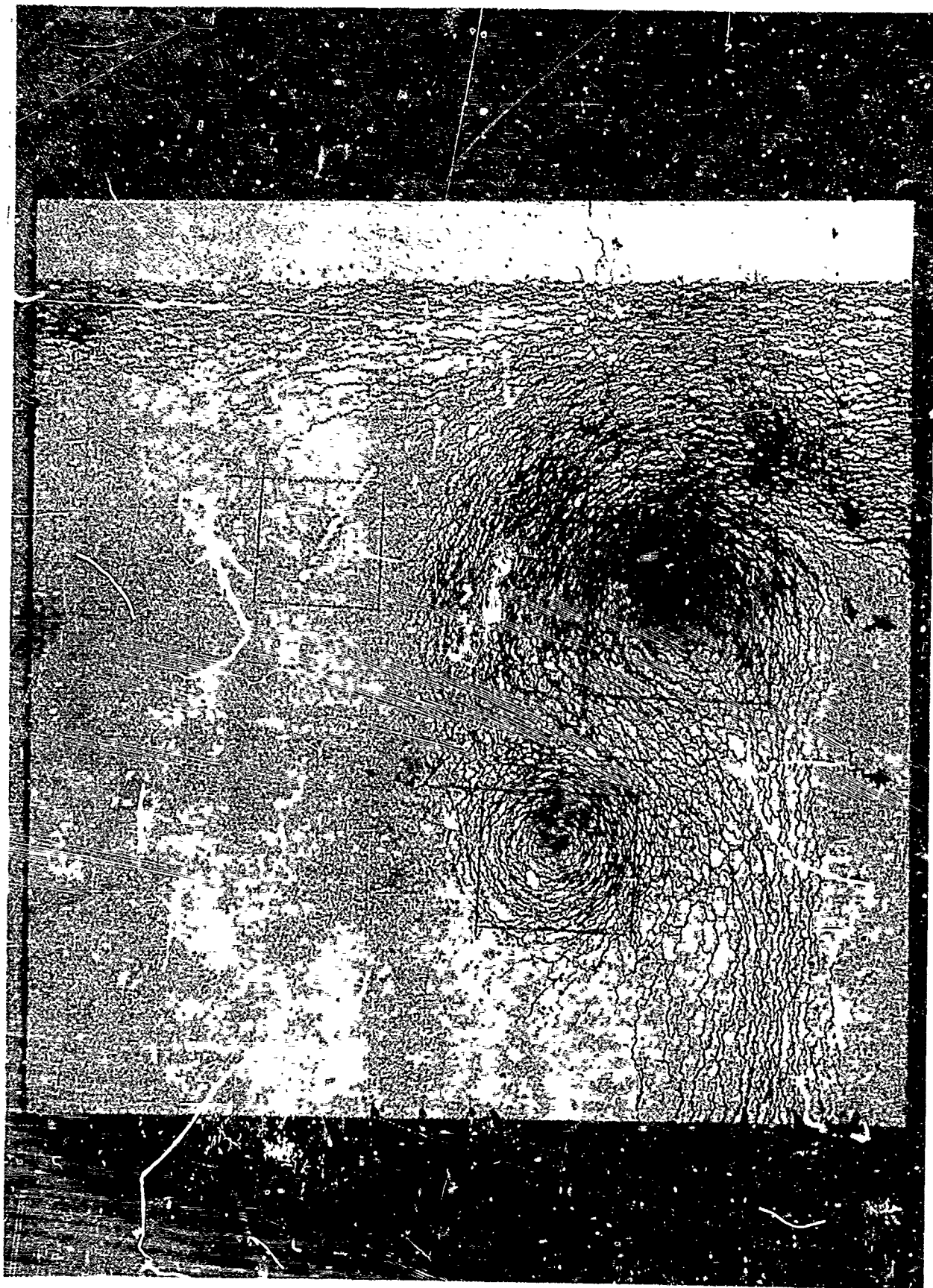


Figure 2 - Aluminum Sprayed Boron/Epoxy Panel

TABLE I  
DESCRIPTION OF BORON-EPOXY SKIN/ALUMINUM HONEYCOMB CORE SANDWICH TEST PANELS

Panel No.	Boron-Epoxy Skin		Panel Size, inches	Type of Protection	Reference No.
	Type	Thickness, inch			
A	12 Crossed Plies	0.062	9x9	0.006-inch-thick aluminum foil	Fig. 3
B	12 Crossed Plies	0.062	9x9	0.006-inch-thick, one-inch-wide aluminum foil strips spaced one inch apart	
C	12 Crossed Plies	0.062	9x9	0.006-inch-thick aluminum foil with 1/2-inch-diameter holes on one-inch centers	Fig. 4
F	12 Crossed Plies	0.062	9x9	None (originally had 0.006-inch-thick, one-inch-wide aluminum foil strip spaced two inches apart)	Fig. 5
G	12 Crossed Plies	0.062	9x9	0.006-inch-thick, one-inch wide aluminum foil strips spaced 2 3/4 inches apart	
H	15 Unidirectional Plies	0.082	12x12	0.012-inch-thick titanium foil	None
I	15 Crossed Plies	0.086	12x12	0.008-inch-thick titanium foil	None

ductive epoxy adhesive. Protective aluminum foil and titanium foil were bonded to the boron/epoxy skins with non-conductive Metlbond 329 adhesive.

The use of bonded metal foil on the surface of boron/epoxy rather than of sprayed aluminum was necessitated by the method of molding actual production skins for F-14A stabilizer. The mold surface was the faying surface of the skin (the surface which was to be bonded to the honeycomb) and the air-passage surface was the bag surface. For the aluminum sprayed layer to be effective, it must be first sprayed on the mold and be bonded to the skin during the actual cure operation. Aluminum sprayed on top of a cured boron/epoxy surface does not adhere sufficiently to withstand the air pressures under flight conditions.

#### TEST PROCEDURE

Since it is prohibitively expensive to simulate actual lightning strikes under laboratory conditions, three types of laboratory tests have been developed as a compromise. These are high-

voltage, high-current, and high-energy (high coulomb) strikes. Past studies of actual lightning strikes and aircraft structures have shown that a high-current strike at 200,000 amperes and 48,000 volts should be the standard test to evaluate the lightning resistance of proposed structures. This test is called out by Paragraph 3.3.4.5 of Military Specification B5087B.

Artificial Lightning Discharge tests on Panels A, B, C, F, G, H, and I were performed by the Lightning and Transients Research Institute of Minneapolis, Minnesota. These tests were sponsored by the Air Force Material Laboratory (Wright-Patterson Air Force Base) and were conducted under the supervision of Mr. L. Kelly of that laboratory and Dr. C. Robb of the Institute.<sup>(1)</sup> Test conditions used are listed in Table II.

(1) Lightning and Transient Research Institute Report on Contract No. F33615-68-C-1534 of September 12, 1969

## TYPES OF TESTS

Three types of test discharges were used to simulate the effects of natural lightning. High-voltage, long-arc discharges of moderate energy were used to determine the strike points and current paths. High-current discharges of high energy and high-charge-transfer discharges of long-time duration were used to evaluate the damage which would be produced. The high-voltage, long-arc discharges and the high-current discharges can be combined in a single discharge but the more extensive damage resulting from the high currents and high-charge transfers generally obscures the contact points and current paths which would be shown by the high-voltage long-arc discharges and thus are performed separately.

Oscillograms showing the high-current damped oscillatory waveform and the high-charge transfer waveform are presented in Figure 6. The long-arc discharges were also of a damped oscillatory nature but with a crest current of approximately 15 kiloamperes and a charge transfer of about 0.01 coulomb versus up to 200 kiloamperes and 3 coulombs for the high current discharges. The oscillatory discharges are slightly more severe than the unipolarity discharges typical of natural lightning.

For the high-voltage tests, a discharge electrode with a one-half-inch-diameter tip was positioned over the test panel and the protection strips and aluminum honeycomb core were grounded.

First, intense electrical impulse fields were applied to the sample to produce the predischARGE streamering which guides natural lightning discharges into an aircraft and thus determines the strike points. The points from which the most intense streamers initiate are the most probable points of lightning strike. The intense electric fields are applied by placing a high-voltage electrode over the test sample and bringing up the voltage until streamering occurs but not high enough to produce a discharge. In the initial tests, the most intense streamering occurred off the edge of the panel. Because of a lack of time the streamer tests were discontinued and tests with long-arc discharges to the test panels were begun.

A 0.6-megavolt discharge to Panel E with resultant edge arcing due to laminate current flow is shown in Figure 7. As listed in Table II, the discharges fired through a 30-inch gap struck the edges of the panel. However, with the gap shortened to 6 inches and with the protection strips spaced 2-1/2 inches apart on panel G, one discharge struck the composite material between the protection strips (Figure 14).

Some laminate damage was observed due to this discharge, although it appeared to be less than had been observed for similar tests of earlier composite panels without the foil strip protection. The protection strips apparently not only reduced the probability of strikes to the exposed boron panel but also reduced the damage to the boron probably because part of the current was conducted over the external surface by an arc to the protection strip rather than through the material itself. The above discharge to the exposed boron section rather than to the adjacent aluminum protection strips indicated that streamers can emanate from the boron material between the strips to guide in a natural lightning discharge even though the few streamering photographs which were taken did not indicate major streamering except from panel and strip edges.

Next, high-current artificial lightning discharges were fired to various panels with and without the protection strips. The panels were mounted on an insulated backing plate and the protection foils and honeycomb core were returned to ground via a high-current measurement circuit used for current recording. A discharge gap of approximately 1/2 inch was used for the tests.

A 200-kiloampere discharge to Panel F with the protection strips removed produced major damage in the boron epoxy skin and honeycomb core as illustrated in the photograph of Figure 8. However, this damage appeared to be substantially less than observed in earlier similar tests of other honeycomb core composite material, one possible explanation being that in the earlier tests either the skin or the aluminum core was of thinner material.

High-current discharges to the panels with continuous aluminum and titanium foils and perforated aluminum foil generally produced local holes in the foil but no visible laminate damage as illustrated in Figures 9, 10, 11 and 12. For Panel A with a 6-mil aluminum foil, a 100-kiloampere discharge burned approximately a one-inch-diameter hole in the foil and a 200-kiloampere discharge burned approximately a 1-1/2-inch-diameter hole in the foil but no boron laminate damage was noted. A 200-kiloampere discharge to the heavier 8-mil, aluminum-coated Panel I produced a similar but smaller hole in the foil and again no laminate damage was observed.

Both the 6-mil perforated aluminum foil of panel C and the 12-mil titanium foil of Panel H showed approximately 2-1/2-inch-diameter holes due to 200-kiloampere discharges but, as for the other continuous foils, no laminate damage was observed for either panel.

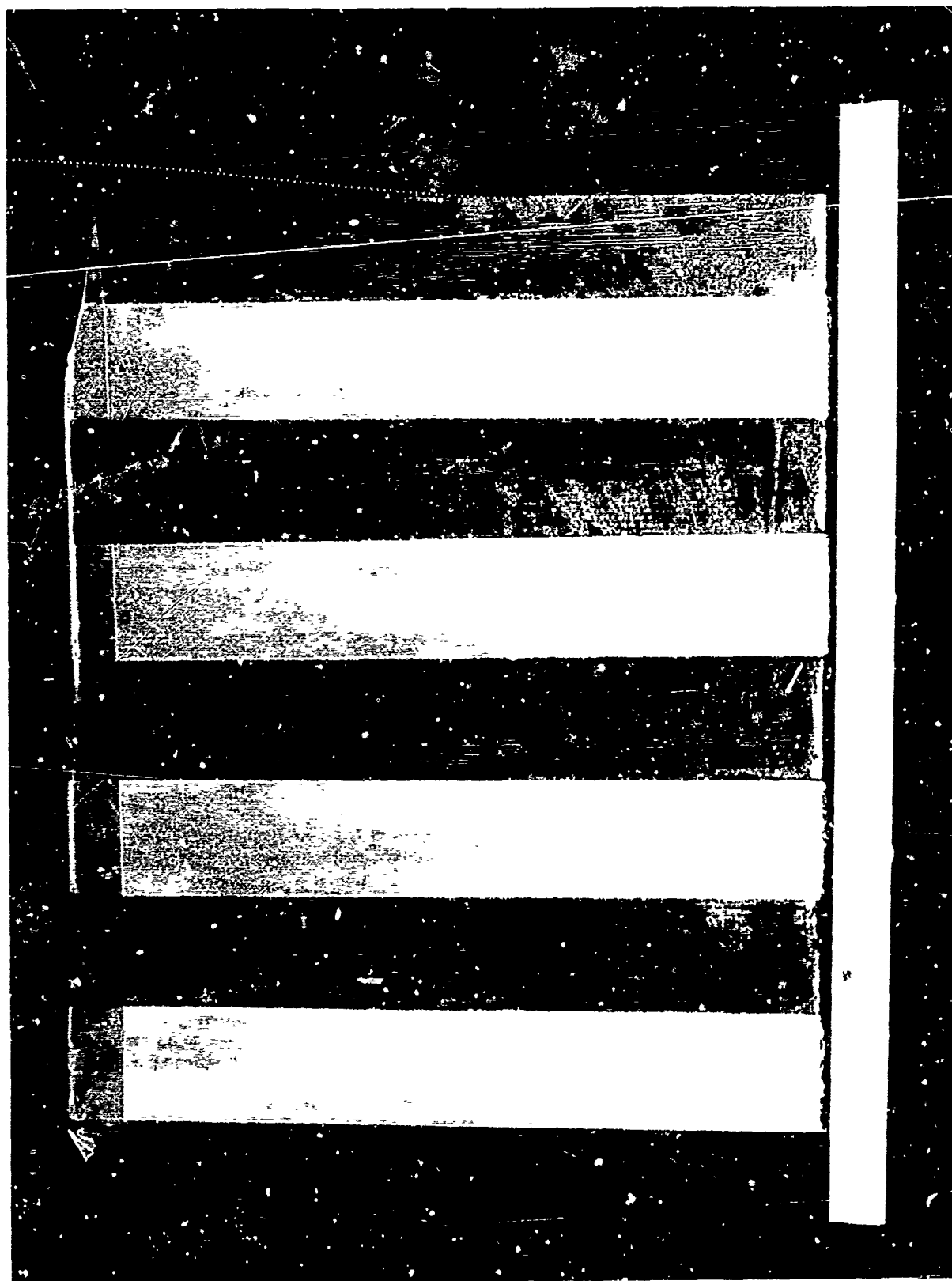


Figure 3 - Boron/Epoxy Sandwich Panel with 1 Inch Aluminum Strips Spaced 1 Inch



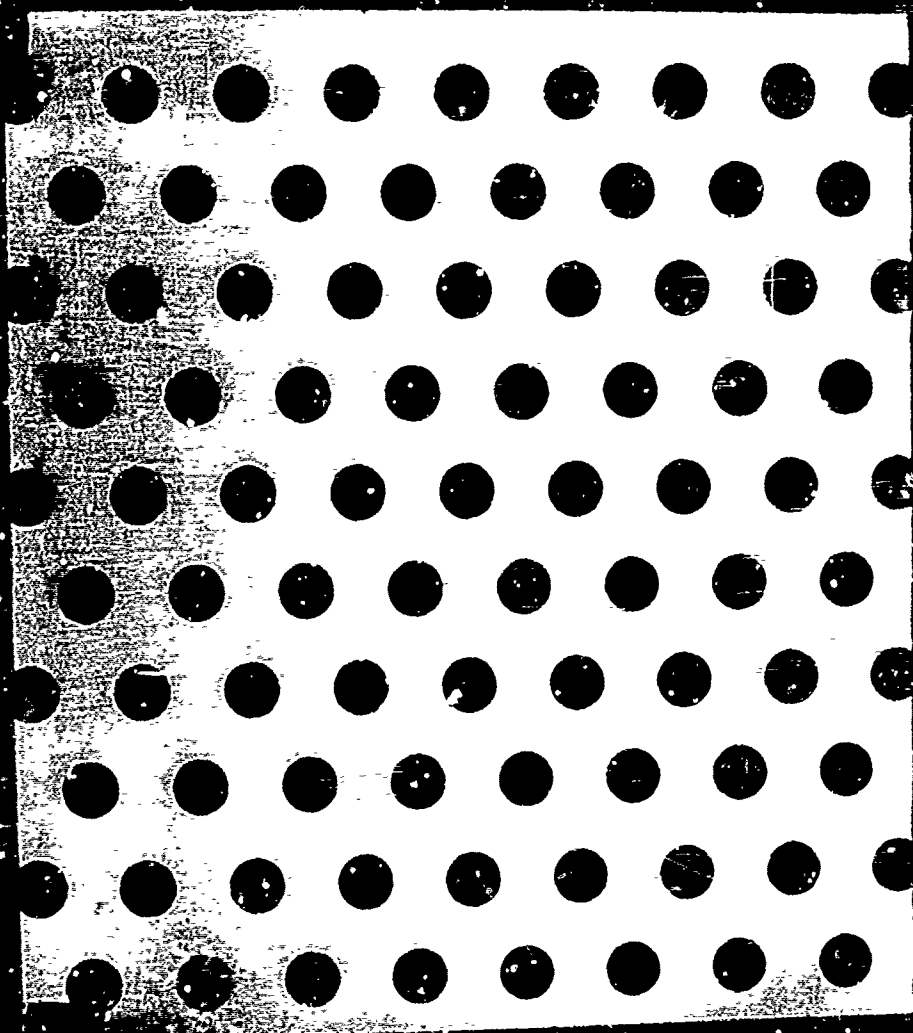


Figure 4 - Boron/Epoxy Sandwich Panel with Perforated Aluminum Foil

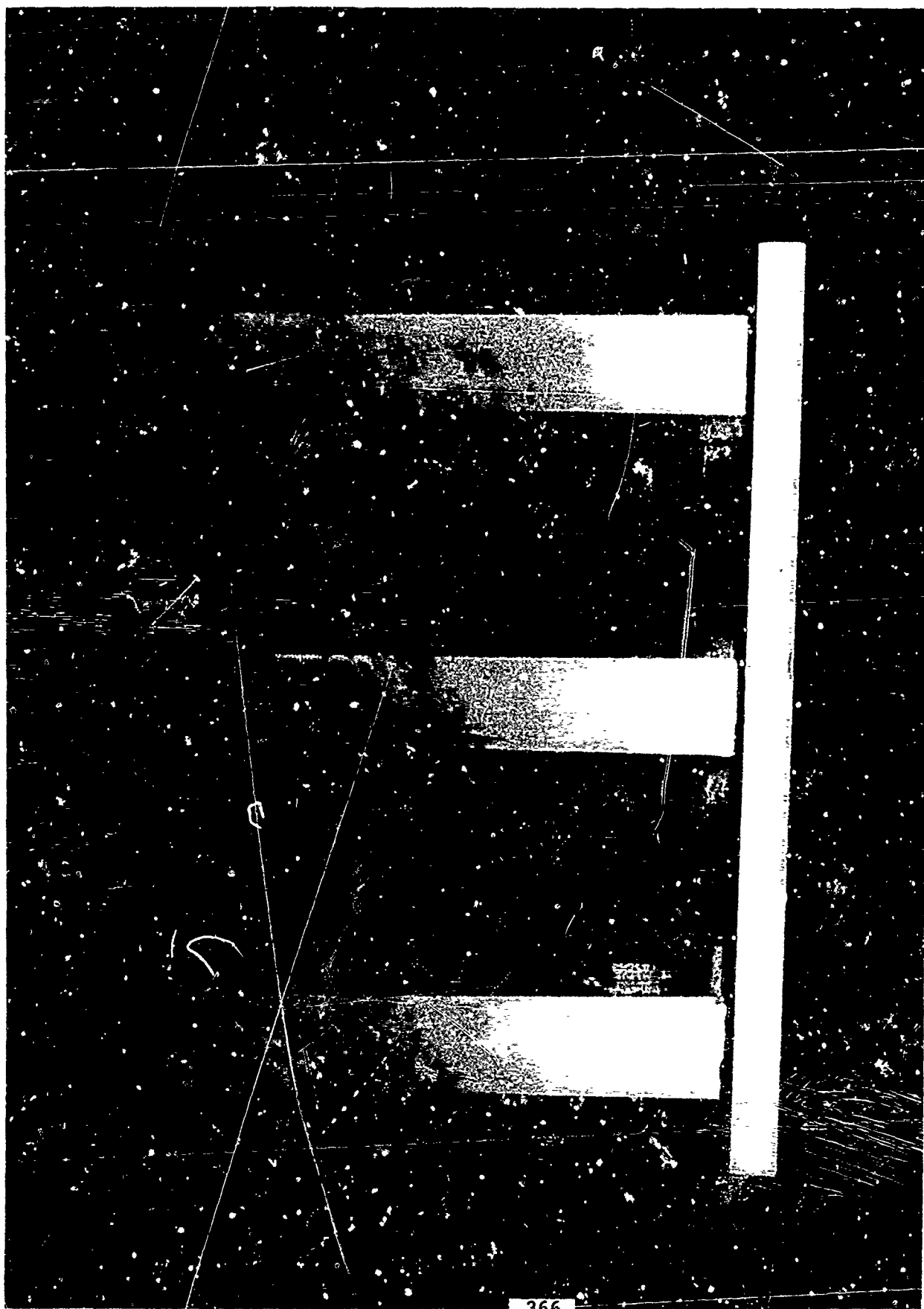


Figure 5 - Boron/Epoxy Sandwich Panel with 1 Inch Aluminum Strips Spaced 2 3/4 Inch

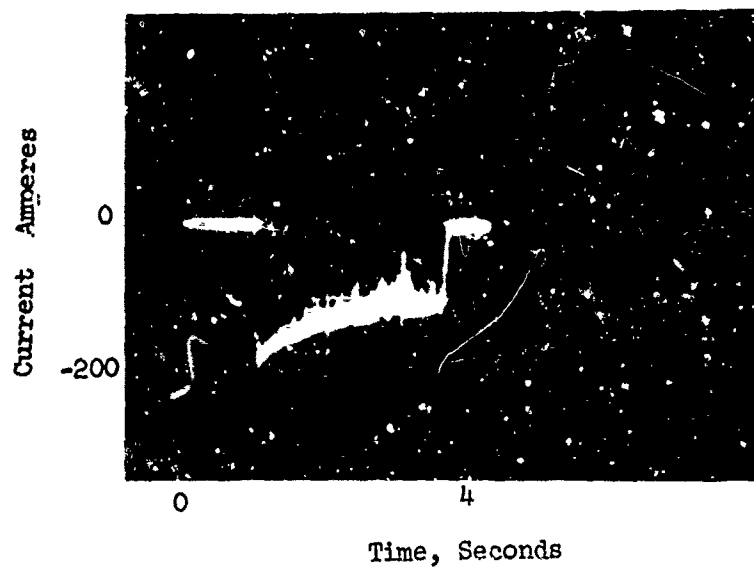
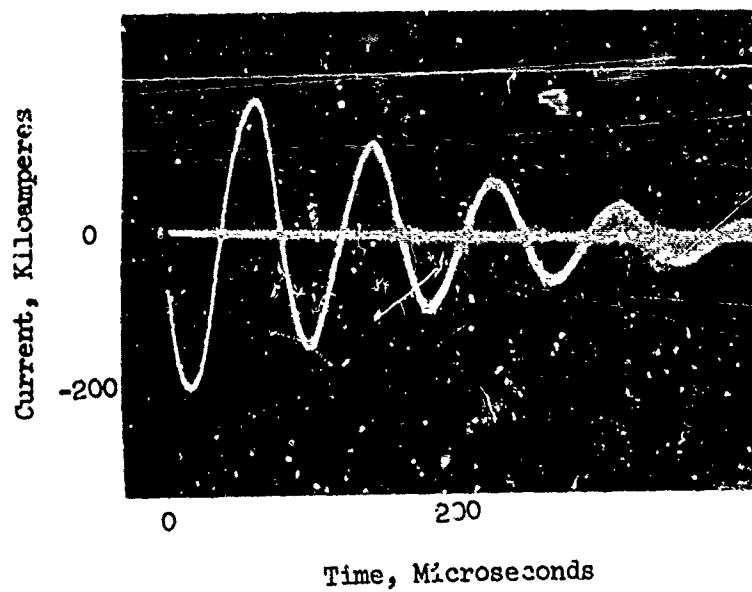


Figure 6 Typical Current Oscillograms



Figure 7 High-Voltage, Long-Arc-Discharge to  
Panel E with Arcing Along Panel Edges

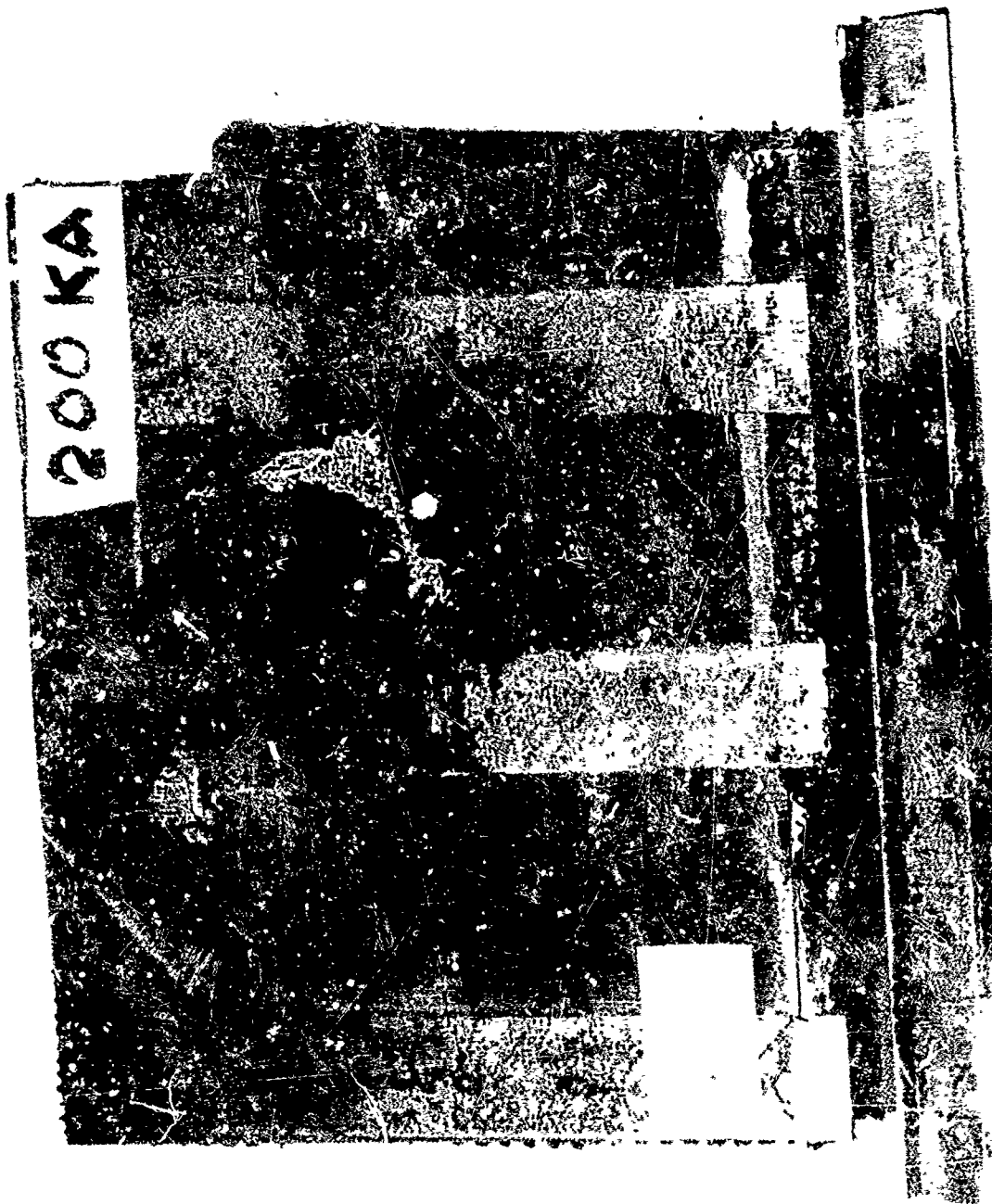


Figure 8 - Panel F with Aluminum Strips Removed After a 200 Kf. Lightning Strike

Figure 9 - Panel A After Exposure to Artificial Lightning Discharge

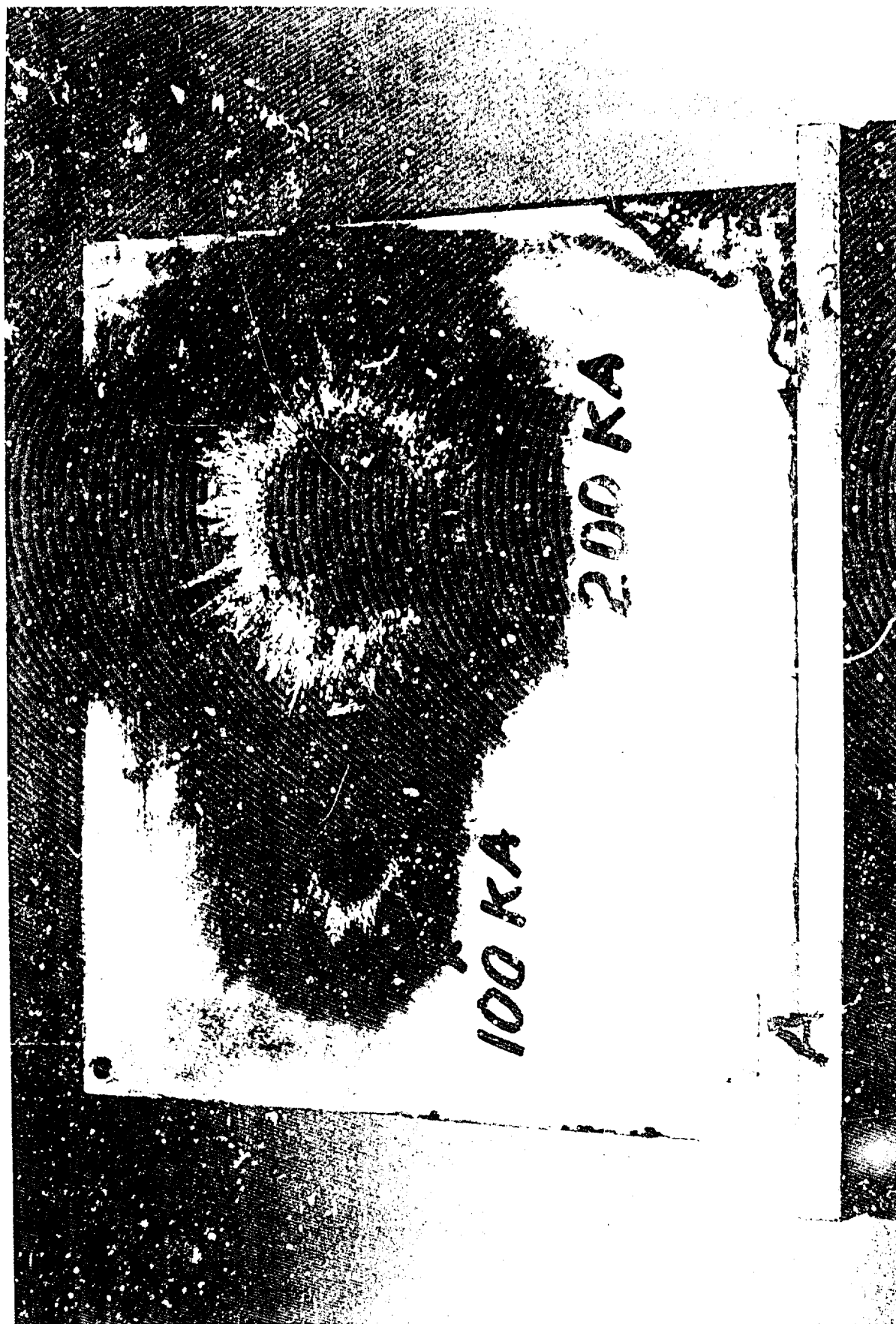


Figure 10 - Panel C After a 200 KA Lightning Strike



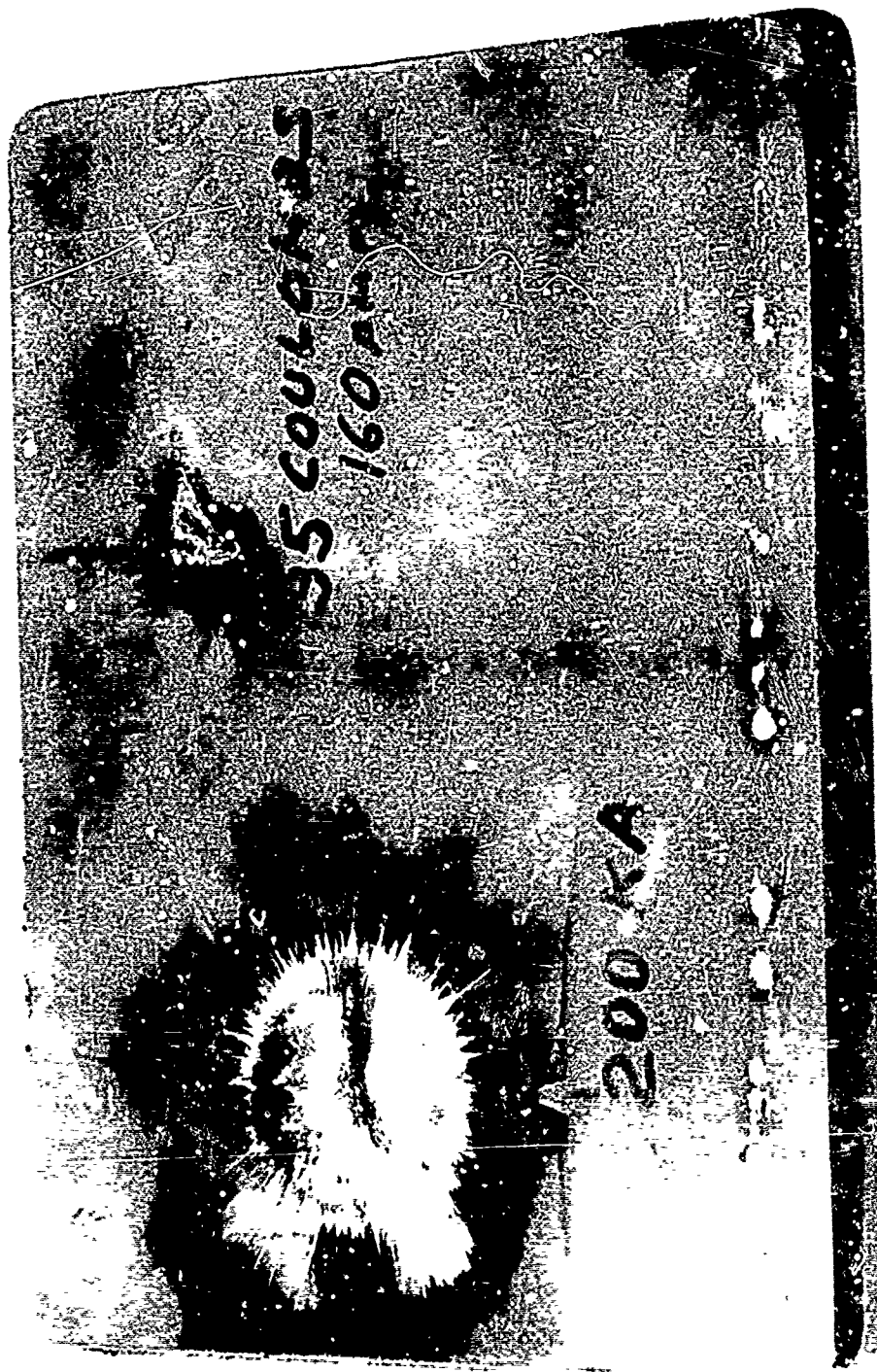


Figure 11 - Panel H After a 200 KA and a High Current (35 Coulombs) Lightning Strike





350 COFF.  
140 AMP.

TABLE II  
ARTIFICIAL LIGHTNING TEST DATA FOR  
BORON COMPOSITE PANELS WITH ALUMINUM GRID PROTECTION

Test No.	Figure No.	Panel No. and Dist	Long Arc (probe to panel in.)	HI Current (kiloamps)	HI Coulomb (coulombs)	Comments
1		E 1-1/2" spacing	30	0	0	Arc to chopping gap electrode
2		E	30	0	0	To panel edge
3		E	6	0	0	Arc split to strips
4		E	2/4	0	0	Arc to strips
5	14	G 2-1/2" spacing	6	0	0	To composite, slight delamination
6	14	G	20	0	0	To panel edge
7	14	G	36	0	0	To chopping electrode, streamer photograph
8	14	G	36	0	0	To chopping electrode, streamer photograph
9	14	G	35	0	0	To chopping electrode, streamer photograph
10	9	A 6 mil alum foil		100	0	Foil locally burned away, no delamination
11	9	A	2	200	0	Foil burned away, no delamination
12	13	B 1-1/4" spacing		200	0	Foil strips burned off. To strip
13	10	C perforated foil		200		Foil locally burned away
14	11	H 12 mil titanium foil		200	0	Foil locally delaminated from panel
15	12	I 8 mil alum foil		200	0	Foil locally burned away
16	14	G 2-3/4" spacing		200	0	Local delamination and strips burned off
17	11	H			35	Several pits in titanium foil

TABLE II (Continued)

Test No.	Figure No.	Panel No. and Dist	Long Arc (probe to panel in.)	HI Current (kiloamps)	HI Coulomb (coulombs)	Comments
18	12	I			35	Approx. 1 in. diameter hole in foil
19	12	I			350	Approx. 3 in. diameter hole in foil
20	8	F foil strips removed		200	0	Approx. 2-3 in. diameter hole and alum honeycomb locally vaporized

High-current tests of the panels with 6-mil aluminum foil strips indicated that the strips greatly minimized panel damage even for the largest strip spacing tested of 2-3/4 inches. The 200-kiloampere discharge fired to a strip on Panel B (Figure 13) vaporized and blew off three strips but no delamination was noted in the panel.

The discharge to Panel G illustrated the effectiveness of the strips at a 2-3/4 inch spacing for a discharge fired directly to the boron material midway between the protection strips. As indicated in Figure 14, the adjacent strips were vaporized and only local pitting of the boron material was observed. This damage can be compared with that observed for the somewhat lower amplitude discharge to the unprotected Panel F where extensive laminate and core damage was noted. Apparently most of the discharge current was carried by the surface flashover to the protection strips in spite of the discharge probe being within 1/2 inch of the boron material.

Finally, several tests were made with high-charge-transfer, long-time-duration discharges typical of the continuing components of a natural lightning strike. The 35 and 250-coulomb discharges to the 12-mil titanium skin of Panel H and the 3-mil aluminum skin of Panel I produced local burning away of the foil and some heat damage due to the arc to the underlying boron composite.

After being subjected to the lightning discharge tests, the panels (with the exception of Panel F which was too severely damaged) were chemically milled with standard caustic solution to remove the aluminum surface foil and honeycomb core. Flexural strength specimens were then cut from both undamaged (control) and damaged areas of the panel as shown in Figures 15 to 20.

Flexural strength data obtained are summarized in Table III. Visual inspection of the test panels and analysis of the flexural strength values indicated that:

- o Unprotected panels can be severely damaged by lightning strikes.
- o The perforated and full-scale aluminum and titanium foil are very effective in preventing lightning damage to boron/epoxy structures.
- o The one-inch-wide, 6-mil aluminum foil strips are effective in diverting direct strikes away from the unprotected boron composite segments as well as in reducing the damage when a strike does contact an unprotected segment.
- o The low-current, high-coulomb discharges typical of continuing components in the natural lightning discharge produce considerable metal erosion and some heat indications in the boron.
- o Discharges to the aluminum surfaced boron composite burned away the aluminum coating exposing the boron composite but not necessarily damaging it to any extent as determined visually.

#### ADDITIONAL LIGHTNING DISCHARGE TESTS

Additional lightning discharge tests were conducted at the General Electric facility in Pittsfield, Massachusetts, on honeycomb sandwich panels more representative of actual aircraft-type structures. The effects of boron-epoxy skin thickness and the density and thickness of aluminum honeycomb core on resistance to lightning strike damage were studied. The sandwich panels used are listed in Table IV. These panels were designed and fabricated as part of an Air Force Contract (2). It was planned to subject these panels to end-compression and beam-bending tests after they had been exposed to lightning strikes. If the damage was excessive, the panels were to be repaired and then tested. All panels except the BR 103-1 were

TABLE III  
ROOM-TEMPERATURE FLEXURAL STRENGTH OF LIGHTNING-DAMAGED  
BORON-EPOXY SKIN/ALUMINUM HONEYCOMB SANDWICH PANELS

Panel	Control Specimens			Specimens from Damaged Areas		
	Spec. No.	Flexural Str., psi	Flexural Modulus, psi x 10 <sup>6</sup>	Spec. No.	Flexural Str., psi	Flexural Modulus, psi x 10 <sup>6</sup>
A*	A-1	154,000	17.90	A-3	150,000	17.30
	A-2	145,000	17.30	A-4	154,000	18.00
	A-10	147,000	17.20	A-5	148,000	17.90
	A-11	145,000	16.80	A-6	149,000	17.80
	Avg	147,800	17.30	A-7	146,000	18.30
				A-12	145,000	17.30
				A-13	142,000	17.50
				A-14	149,000	17.40
				A-15	142,000	17.60
B*	B-1	152,000	17.60	B-3	123,500	16.90
	B-2	159,000	17.30	B-4	116,000	16.80
	Avg	155,500	17.45	B-5	127,000	17.70
				B-6	128,000	17.10
				B-7	136,000	16.90
C*	C-1	155,000	17.10	C-3	145,500	17.30
	C-2	146,000	16.60	C-4	147,200	16.90
	Avg	150,500	16.85	C-5	108,000	16.50
				C-6	150,500	16.60
				C-7	145,000	16.70
G*	G-0	115,000	15.90	G-2	115,000	13.50
	G-1	121,000	16.00	G-3	97,400	11.50
	G-9	157,000	17.70	G-4	77,500	10.60
	G-10	149,000	17.00	G-5	29,900	--
	Avg	134,000	16.70	G-6	90,500	12.40
				G-11	149,900	16.70
				G-12	115,000	13.80
				G-13	79,700	12.70
				G-14	96,200	12.20
H*	H-1	276,000	33.00	H-3	280,000	32.10
	H-2	274,000	31.20	H-4	288,000	33.20
	H-11	276,000	31.20	H-5	268,000	33.60
	H-12	280,000	33.00	H-6	282,000	32.80
	Avg	276,500	32.14	H-7	274,000	33.40
				H-8	274,000	33.80
				H-9	296,000	34.00
				H-10	277,000	33.50

TABLE III (Continued)

Panel	Control Specimens			Specimens from Damaged Areas		
	Spec No.	Flexural Str., psi	Flexural Modulus, psi x 10 <sup>6</sup>	Spec. No.	Flexural Str., psi	Flexural Modulus, psi x 10 <sup>6</sup>
I*	I-1	157,500	19.70	I-3	151,000	19.90
	I-2	152,200	20.00	I-4	147,000	20.70
	I-8	155,000	19.20	I-5	141,000	19.80
	I-9	158,500	19.60	I-6	157,000	19.80
	I-13	149,000	20.20	I-7	156,000	19.40
	I-14	136,000	20.40			
	Avg	154,400	19.74			
				I-10	150,000	20.20
				I-11	155,000	20.00
				I-12	155,000	19.90
				I-15	139,000	19.70
				I-16	116,500	16.00
				I-17	60,100	---
				I-18	88,000	13.00
				I-19	126,500	18.70

\*Test span was 2.00 inches for Panels A, B, C, and G, and 2.50 inches for Panels H and I.  
 Reported values are based on a normalized thickness of 0.005 inch per ply on laminates oriented (44%-0°, 44%~+45°, 12%-90°).

TABLE IV  
RESULTS OF LIGHTNING DISCHARGE TESTS AT THE GENERAL ELECTRIC  
FACILITY IN PITTSFIELD, MASSACHUSETTS

Specimen No. (2)	Skin Thickness, inches	Test Description and Results
BR 109-3	0.250	Lightning Discharge Test Setup Specimen before exposure to lightning discharge
↓	↓	49-KA strike on side 2 (upper left)
BR 109-1	↓	73-KA strike on side 2 (upper right)
↓	↓	111-KA strike on side 2 (lower left)
BR 103-3	0.045	111-KA strike on side 2 (edge view shows charring)
↓	↓	168-KA strike on side 2 (extensive damage on face)
BR 108-1	↓	168-KA strike on side 2 (edge showing core damage)
↓	↓	149-KA strike on side 1 (penetration of skin and extensive damage)
BR 108-3	↓	88-KA and 134-KA strikes on side 1 (extensive face damage and penetration after 134-KA strike)
↓	↓	Same specimen-reverse side (charring at ground areas)
BR 108-3	↓	84-KA and 111-KA strikes on side 2 (light surface pitting)
↓	↓	107-KA strike on side 1 (considerable pitting and charring)
BR 103-1	0.045	Same specimen with charring on far side
		73-KA strike on side 1 (extensive damage and core blow-out at edge)
		Same specimen showing edge detail
		Reverse side with further edge charring
		107-KA strike on side 2 (deep hole in honeycomb core)
		Same specimen (edge view showing charring)
		Setup in which the specimen is not grounded directly but is laid up on insulators
		72-KA strike on side 2 (penetration and edge charring)
		Same specimen-reverse side (shows spark exit)
		72-KA strike on same side using grounded connection
		Aluminum mesh specimen with 154-KA and 203-KA strikes (minor face damage)
		Edge of same specimen showing severe delamination of skin from core

Figure 13 - Panel B After a 200 KA and a High Voltage Lightning Strikes





Figure 14 - Panel G After a 200 KA and a High Voltage Lightning Strike



FIG. 15 - TEST SPECIMEN/ PATTERN OF PANEL A



FIG. 16 - TEST SPECIMEN PATTERN OF PANEL B

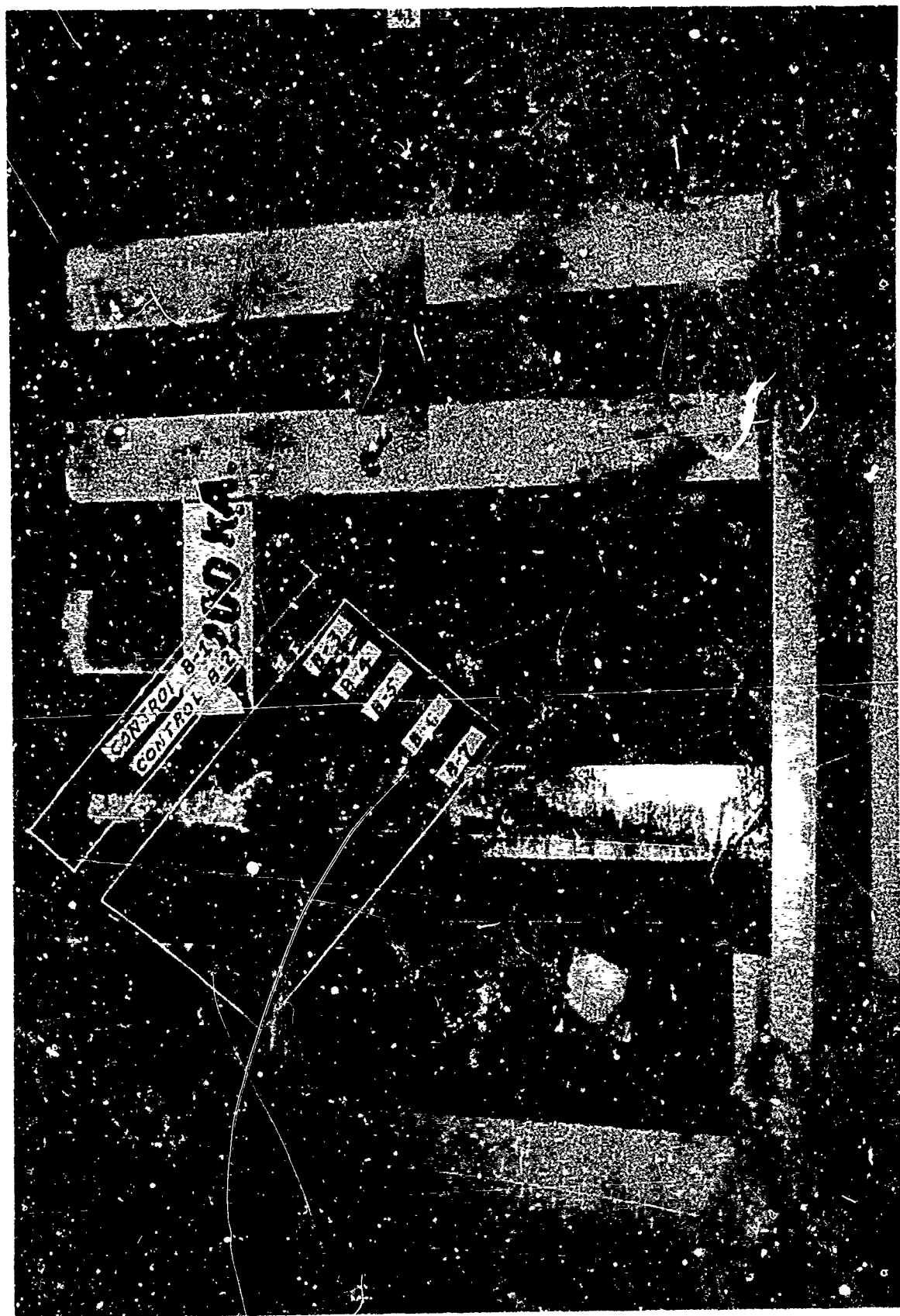


FIG. 17 6-TEST SPECIMEN PATTERN ON PANEL C



FIG. 18 - TEST SPECIMEN PATTERN OF PANEL G

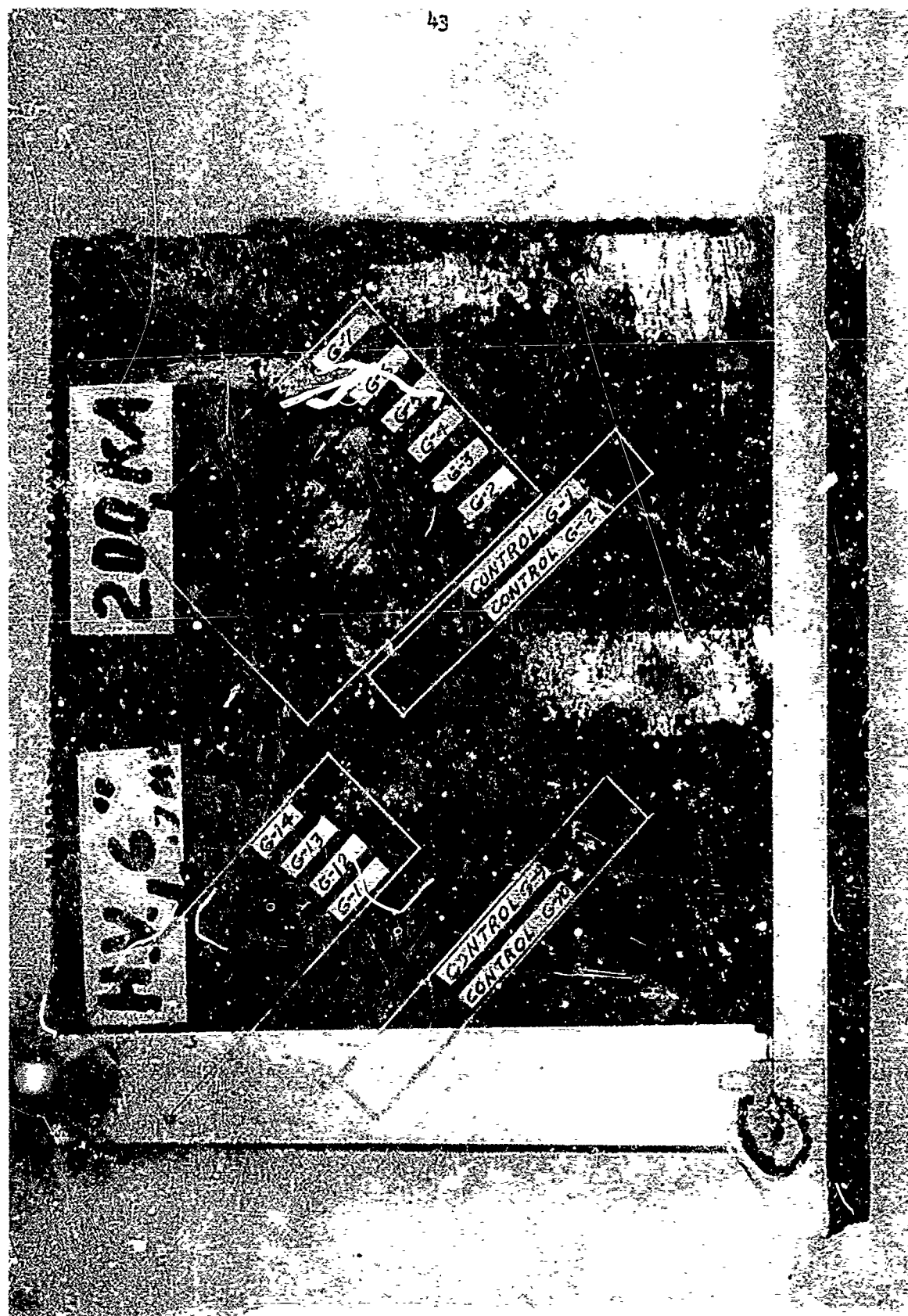


FIG. 191 - TEST SPECIMEN PAKET OF PANEL H

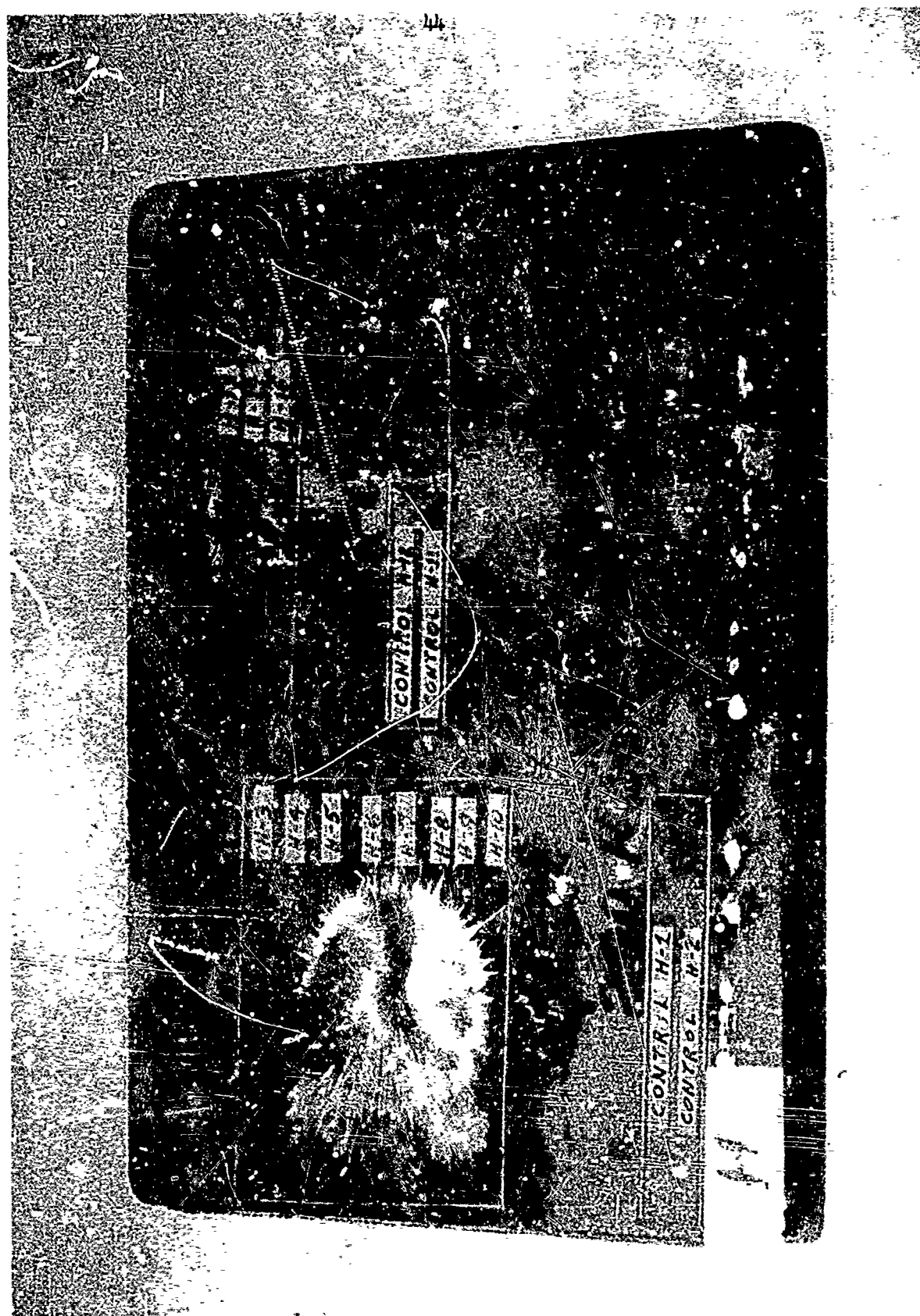
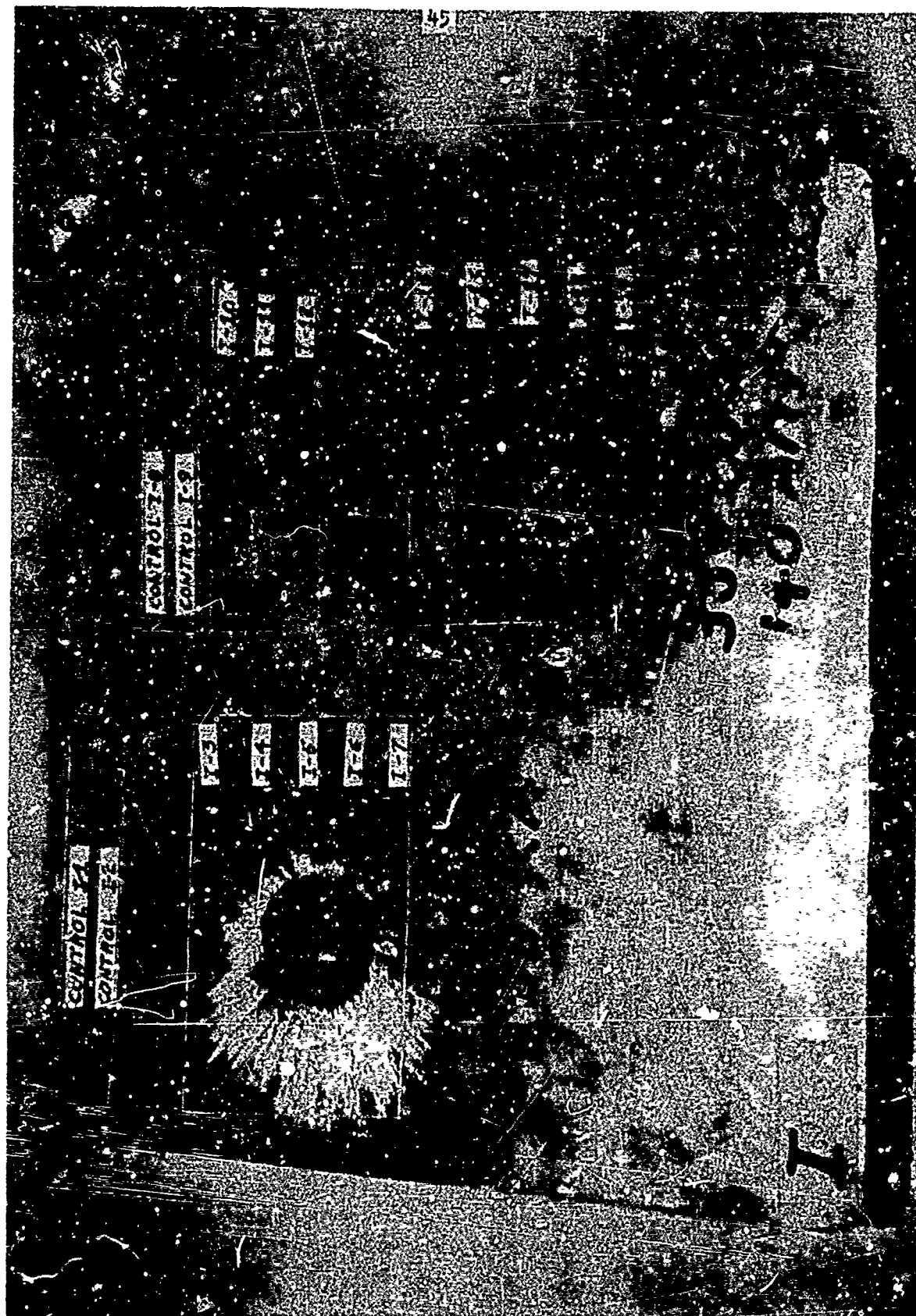




FIG. 20 - TEST SPECIMEN PATTERN OF PANEL I



given an 0.003 to 0.006-inch-thick coating of silver-epoxy conductive paint. The BR 103-1 panels had an aluminum mesh laminated on one surface. The test plan involved a gradual increase in the lightning current with successive shots on one side of the specimen until severe damage had occurred. The lightning current would then be reduced by about 25,000 amperes before exposing the other side of the panels. The test setup is shown on Figure 21 and 22. Some of the exposed panels are shown in Figures 23 through 28. The test results are listed on Table IV.

The test results indicate that thick boron-epoxy skins resist lightning-strike damage better than thin boron-epoxy skins and that the thickness and density of the aluminum honeycomb core have little effect on the degree of damage sustained by sandwich panels. Repeated lightning strikes, even of a lower magnitude than those used in the General Electric Tests, cause cumulative damage which tends to propagate through the aluminum honeycomb core normal to the lightning strike direction. The silver-epoxy conductive paint is not as effective in providing protection against lightning strikes as aluminum foil or spray. Aluminum mesh protects boron-epoxy surfaces but did not prevent delamination of the boron-epoxy skins from the honeycomb core for the one panel used in this study.

#### TEST PROGRAM FOR F-14A HORIZONTAL STABILIZER

The purpose of this program for the actual flight component was to develop the lightest weight design to adequately protect the boron composite skin from lightning strike damage and satisfy the lightning protection requirements of Military Specification MIL-B-5087B.

The lightning test program was conducted on a full-scale horizontal stabilizer and representative stabilizer designs fabricated by Grumman. Each configuration tested depicted the lightning protection system as it would be incorporated onto a production horizontal stabilizer. The tests were conducted at the Lightning and Transient Research Institute (LTRI) Miami, Florida facility and included the following protection schemes:

#### TEST CONFIGURATIONS

- No protection over boron skin (see Figure 29).
- 0.008" thick, aluminum foil over the entire outboard 1/3 of the boron skin. 1" wide, 0.008" thick, aluminum strips spaced 1" apart over the middle 1/3 of the boron skin and 1" wide, 0.008" thick, aluminum strips spaced 2" apart over the inboard 1/3 of the

boron skin. See Figure 30.

- 1" wide, 0.008" thick, conductive paint strips spaced 2" apart over the inboard 1/3 of the boron skin and 1" apart over the remaining 2/3 of the boron skin. See Figure 31.
- 2" wide, 0.004" thick, aluminum strips spaced 2 1/4" apart. See Figure 32.
- 1" wide, 0.008" thick, aluminum strips spaced 2 1/2" apart over the boron skin. See Figure 33.
- 1" wide, 0.008" thick, aluminum strips spaced 3" apart over the boron skin. See Figure 34.
- 1" wide, 0.008" thick, aluminum strips spaced 4" apart over the boron skin. See Figure 35.
- 1" wide, 0.008" thick, aluminum strips spaced 5" apart over the boron skin. See Figure 36.

NOTES: (1) Aluminum used was type 2024-T81.

(2) Conductive paint used was a silver filled epoxy, Hysol 4238/3475.

#### TESTS PERFORMED

The tests consisted of (1) High Voltage Strike - Without Windstream, (2) High Voltage Swept Stroke - With Windstream, (3) High Current Damage and (4) Electrical Bonding Resistance Measurements.

#### HIGH VOLTAGE STRIKE - WITHOUT WINDSTREAM

These tests were performed as illustrated in Figure 37. The tests consisted of firing high voltage discharges, from nine predetermined locations, to determine where approaching (direct) lightning strikes attach to the horizontal stabilizer. The number of discharges fired at the test configuration and locations were determined by analysis, utilizing the spacing between protection strips as a reference.

#### HIGH VOLTAGE SWEPT STROKE - WITH WINDSTREAM

These tests were performed as illustrated in Figures 38 and 39. The tests consisted of firing multiple discharges, initiated at the stabilizer leading edge in a 130-mph airstream, to determine where the initial and restrike components, of a swept stroke, impinge upon the horizontal stabilizer. The number of discharges fired at the test configuration was determined by analysis, utilizing the spacing between protection strips as a reference.

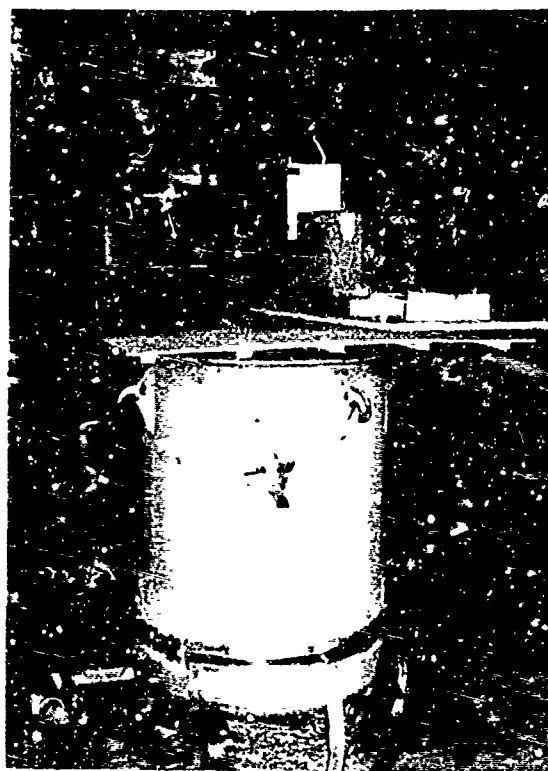


Figure 21

G.E. Lightning Discharge Test Setup

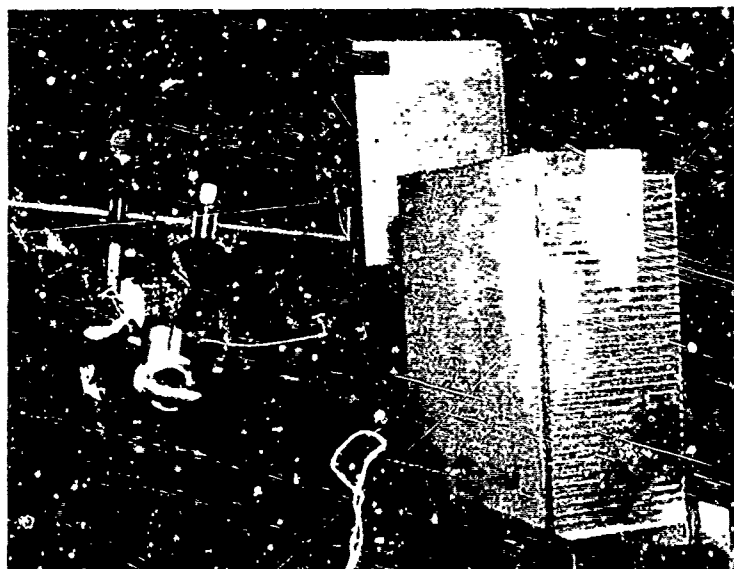


Figure 22

BR-109-3 Specimen Before Exposure to Lightning Discharge.





Figure 23

BR-109-3 Specimen After Exposure to 49KA Discharge.

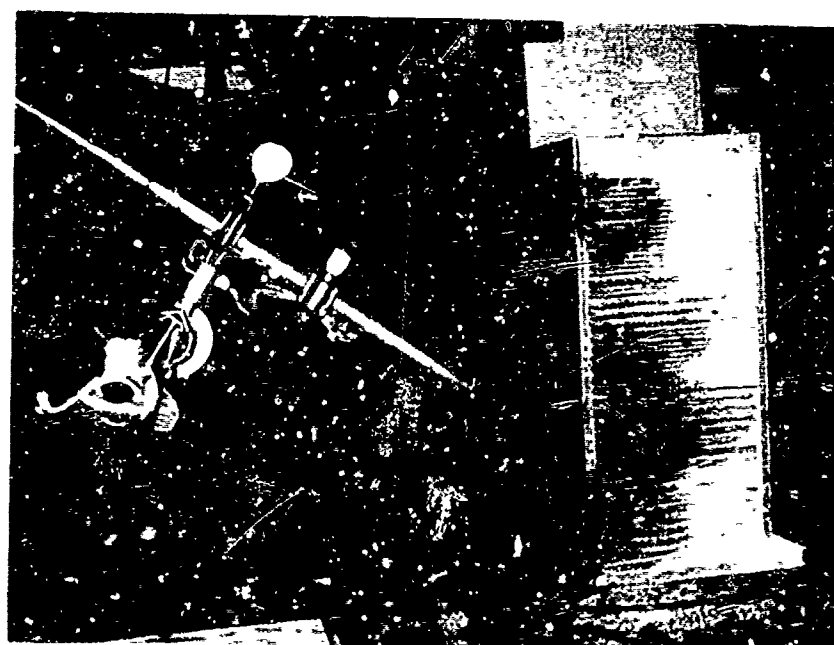


Figure 24

Edge View of BR-109-3 Specimen After Exposure to 111-KA Discharge Showing Charring on Honeycomb Core.

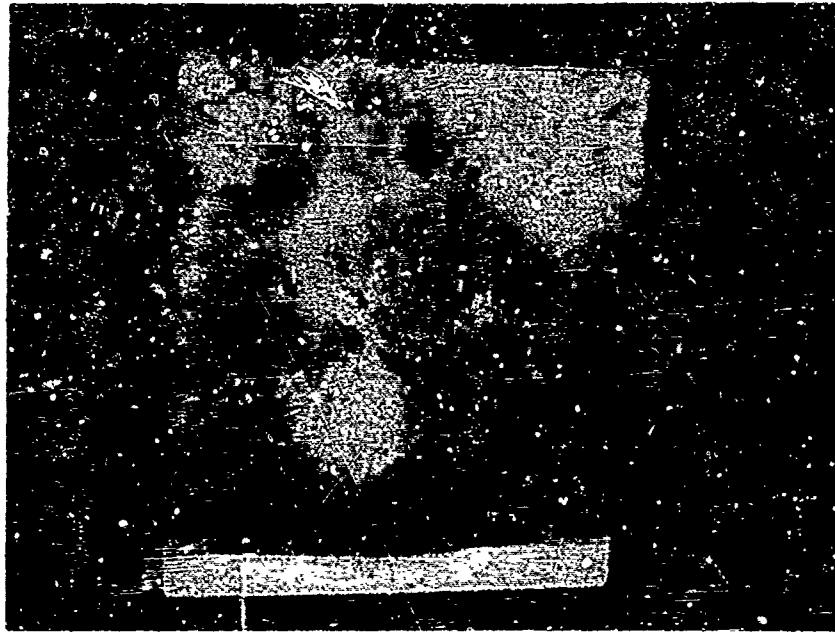


Figure 25

BR-109-3 Specimen After Exposure to 149KA Discharge Showing Skin Penetration.

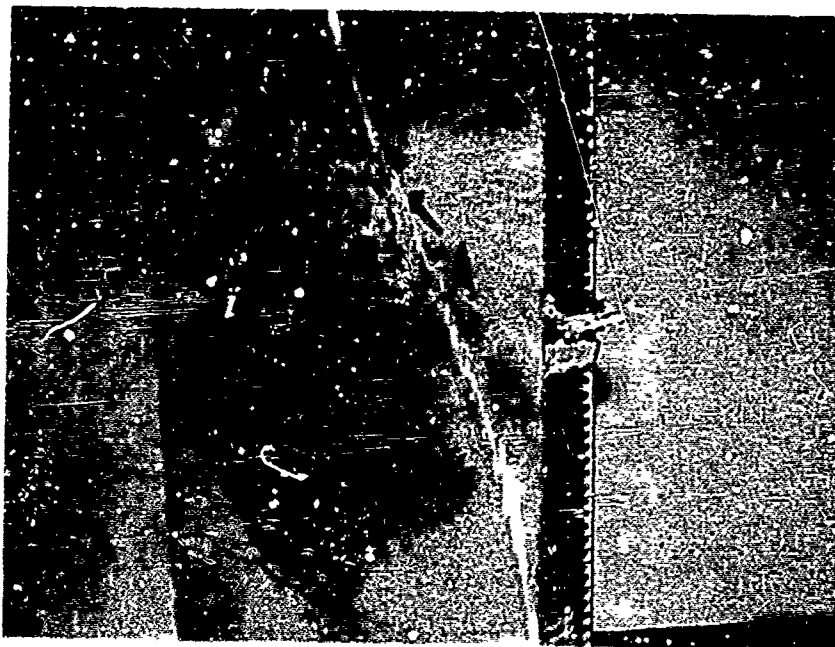


Figure 26

Edge Damage to BR-103-3 Specimen After Exposure to 73KA Discharge.



Figure 27

BR-108-1 Specimen After Exposure  
to 107 KA Discharge.



Figure 28

BR-103-01 Specimen After Exposure to 154 and 203  
KA Discharges - Showing Severe Delamination but no  
Surface Damage (Specimen with wire mesh on surface).

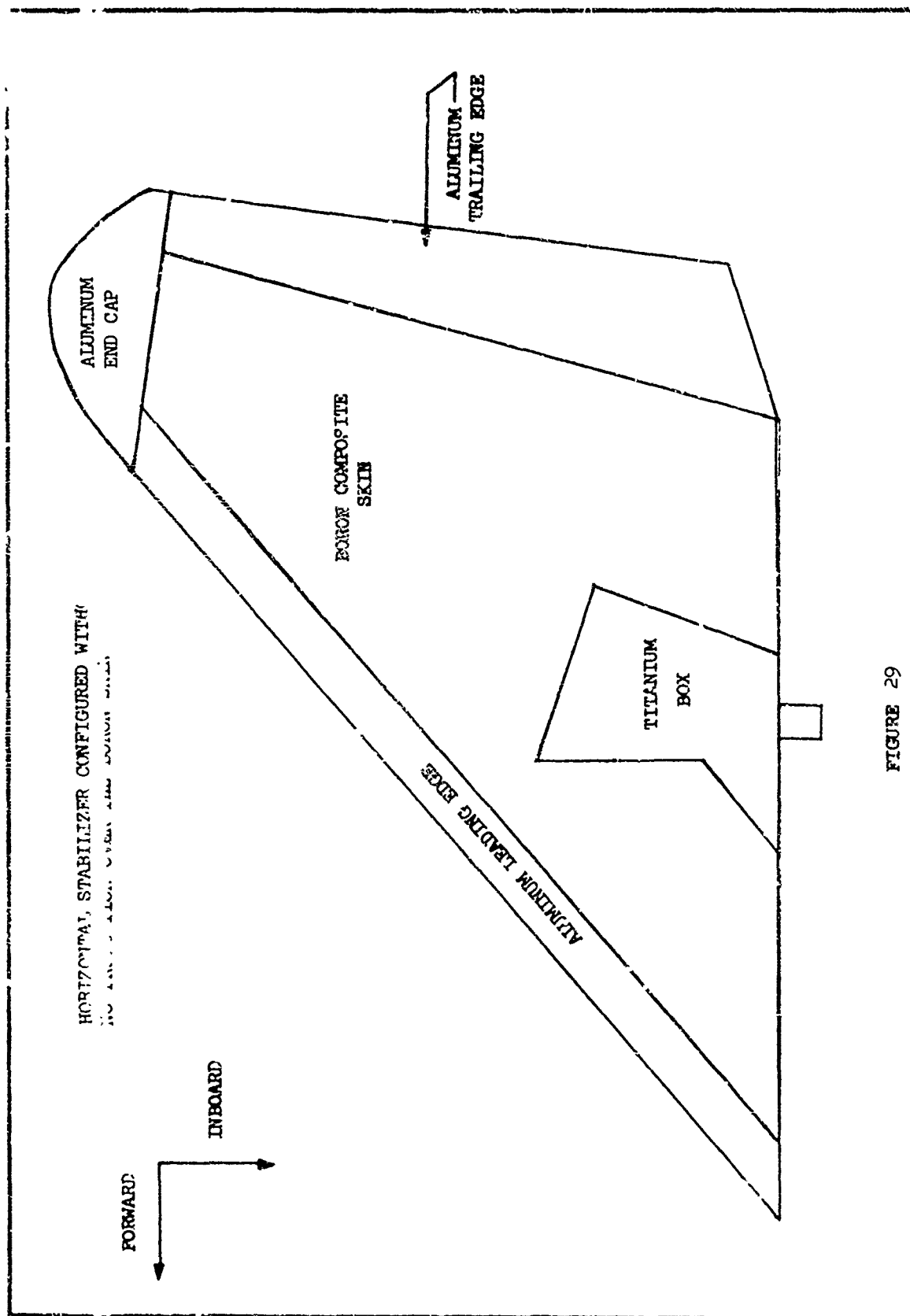


FIGURE 29

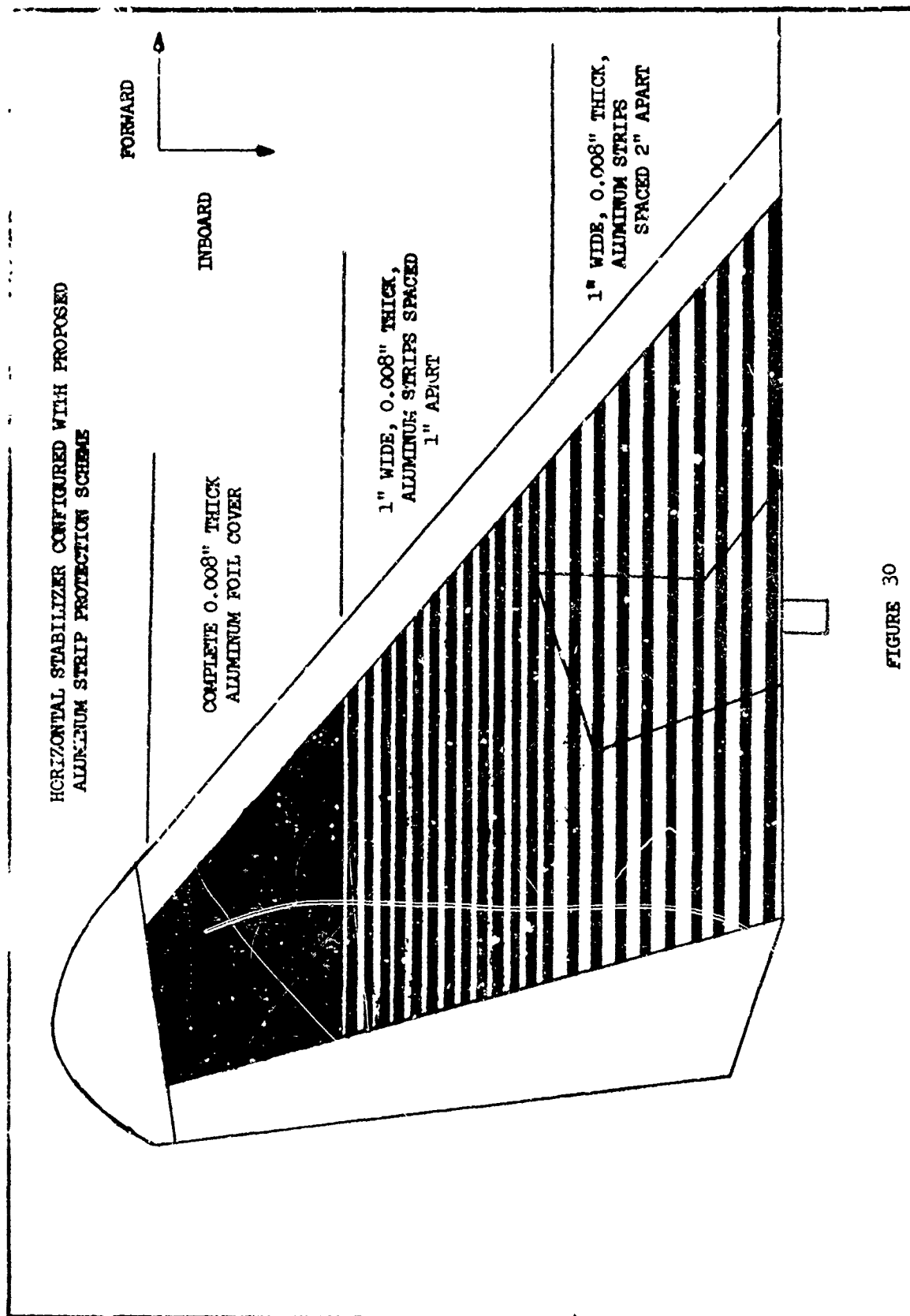


FIGURE 30

HORIZONTAL STABILIZER CONFIGURED WITH 1" WIDE,  
0.005" THICK CONDUCTIVE PAINT STRIPS SPACED  
2" APART ON THE INBOARD 1/3 OF THE STABILIZER  
AND 1" APART ON THE REMAINING 2/3 OF THE  
STABILIZER.

FORWARD

INBOARD

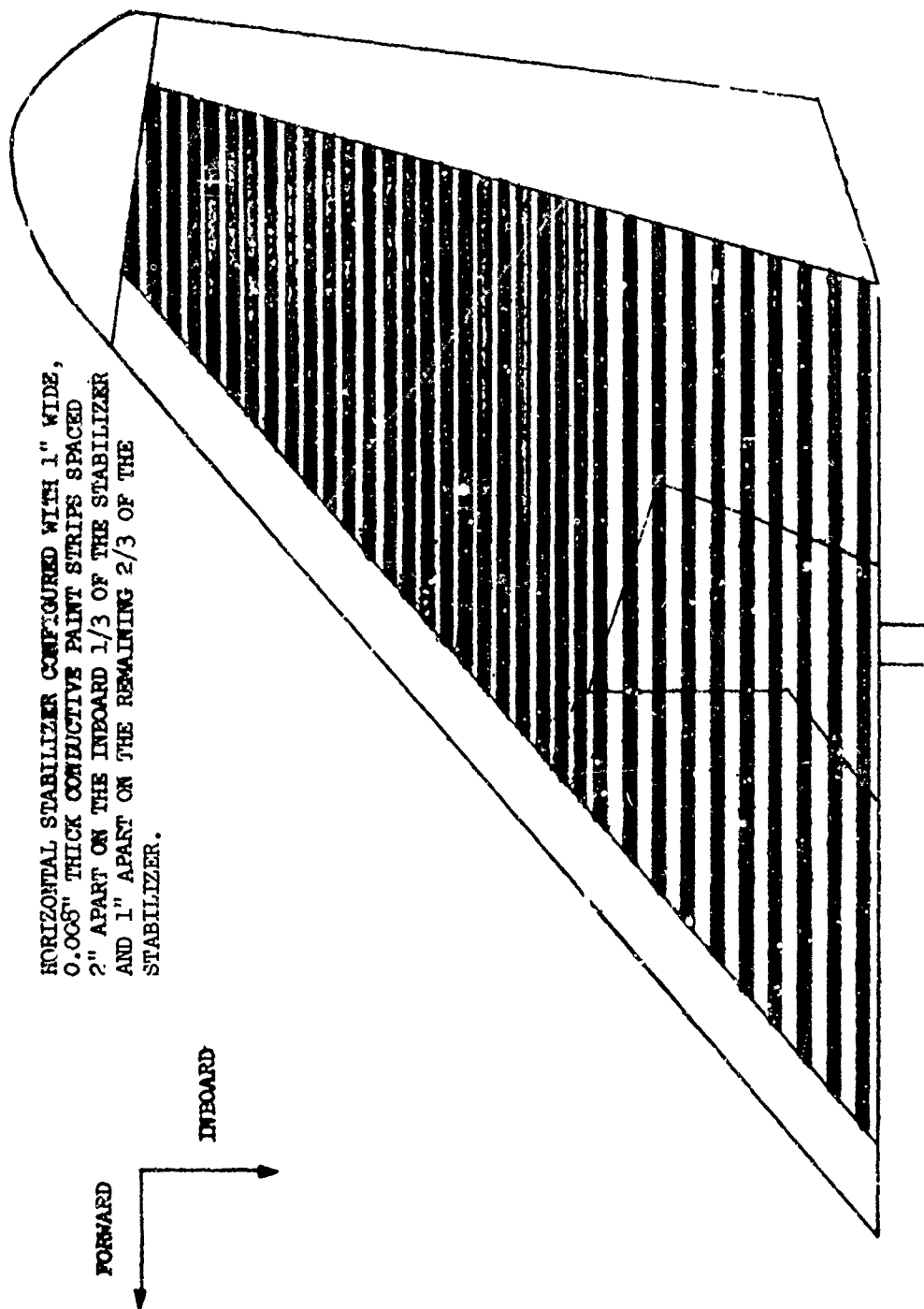
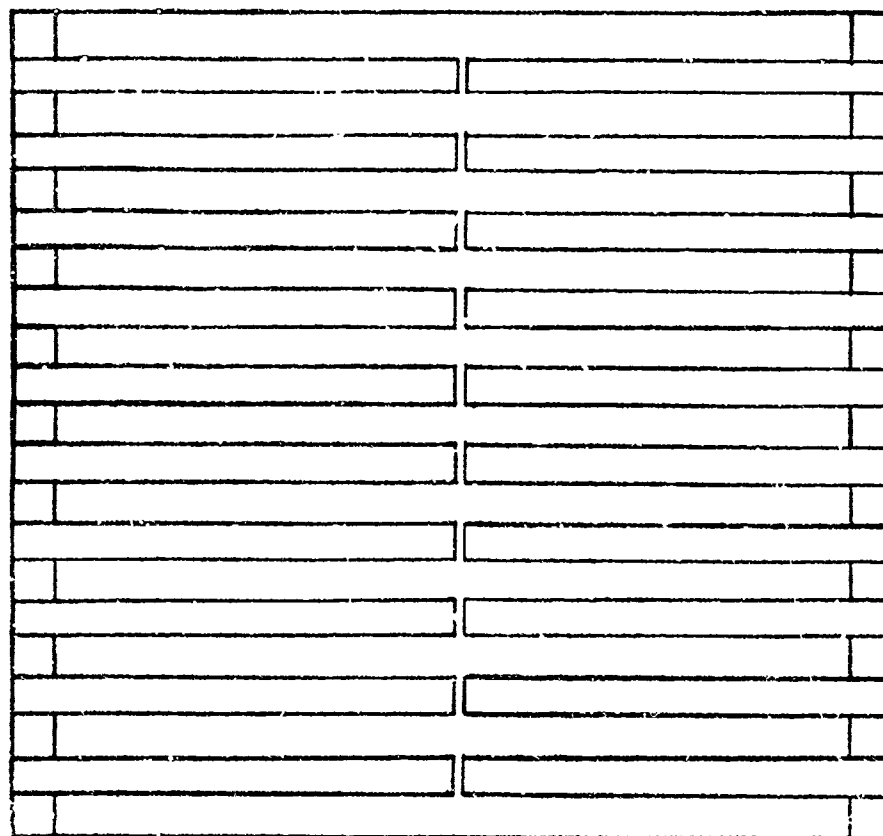


FIGURE 31

48"x48"x0.100" BORON COMPOSITE PANEL WITH 2" WIDE, 0.004" THICK, ALUMINUM STRIPS  
SPACED  $2\frac{1}{8}$ " APART WITH A 0.004" THICK FIBERGLASS FILLER BETWEEN STRIPS  
AND RELIABOND 350 CONDUCTIVE ADHESIVE PER GRUMMAN STANDARD GALOO U



→ ← 1/8" maximum spacing

aluminum strips typical

NOTE: 1/8" maximum spacing to minimize differential thermal expansion between aluminum and boron

FIGURE 32

HORIZONTAL, STABILIZER CONFIGURED WITH 1" WIDE,  
0.008" THICK, ALUMINUM STRIPS SPACED  $2\frac{1}{2}$ " APART

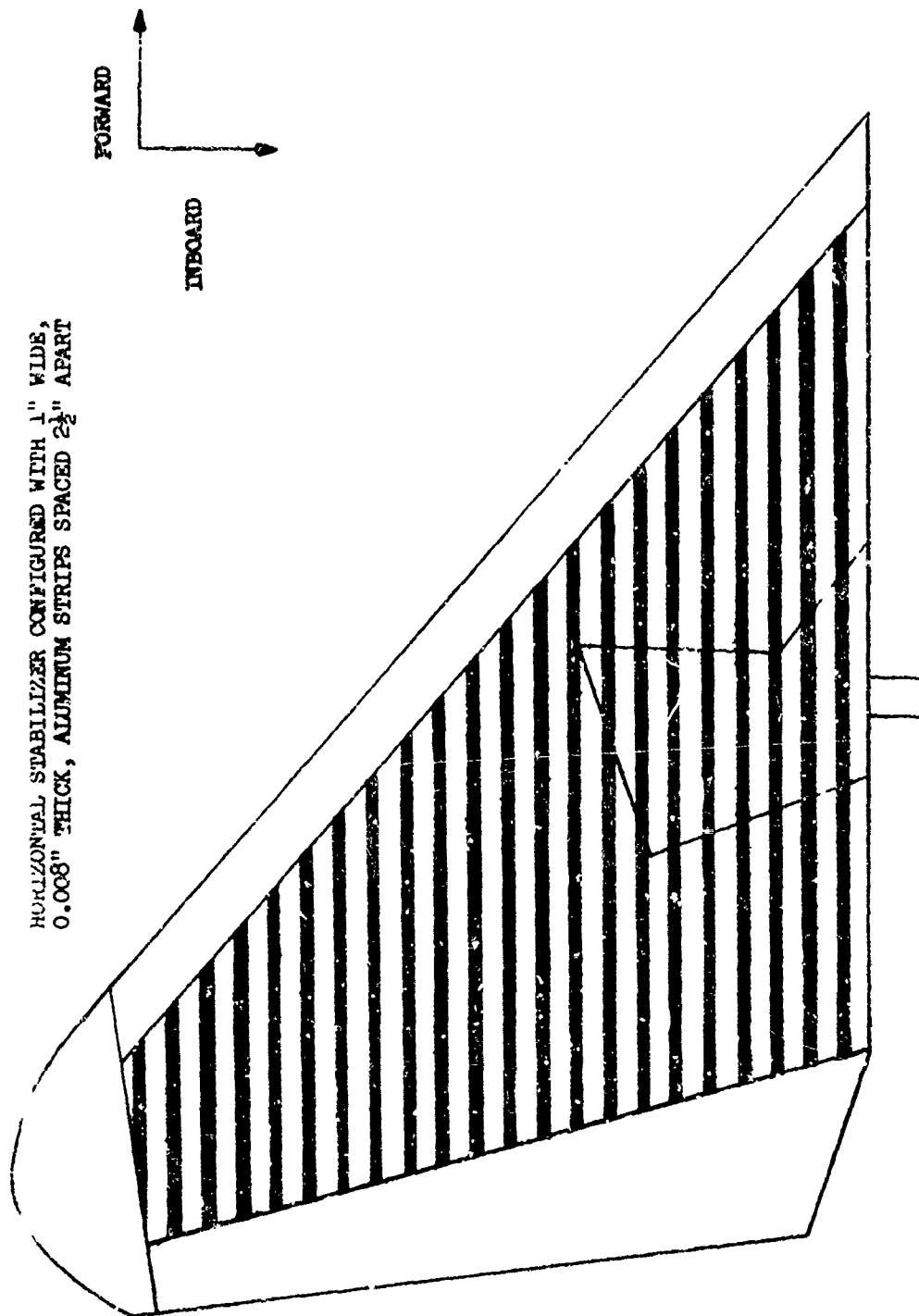


FIGURE 33



HORIZONTAL STABILIZER CONFIGURED WITH 1" WIDE,  
0.008" THICK, ALUMINUM STRIPS SPACED 3" APART

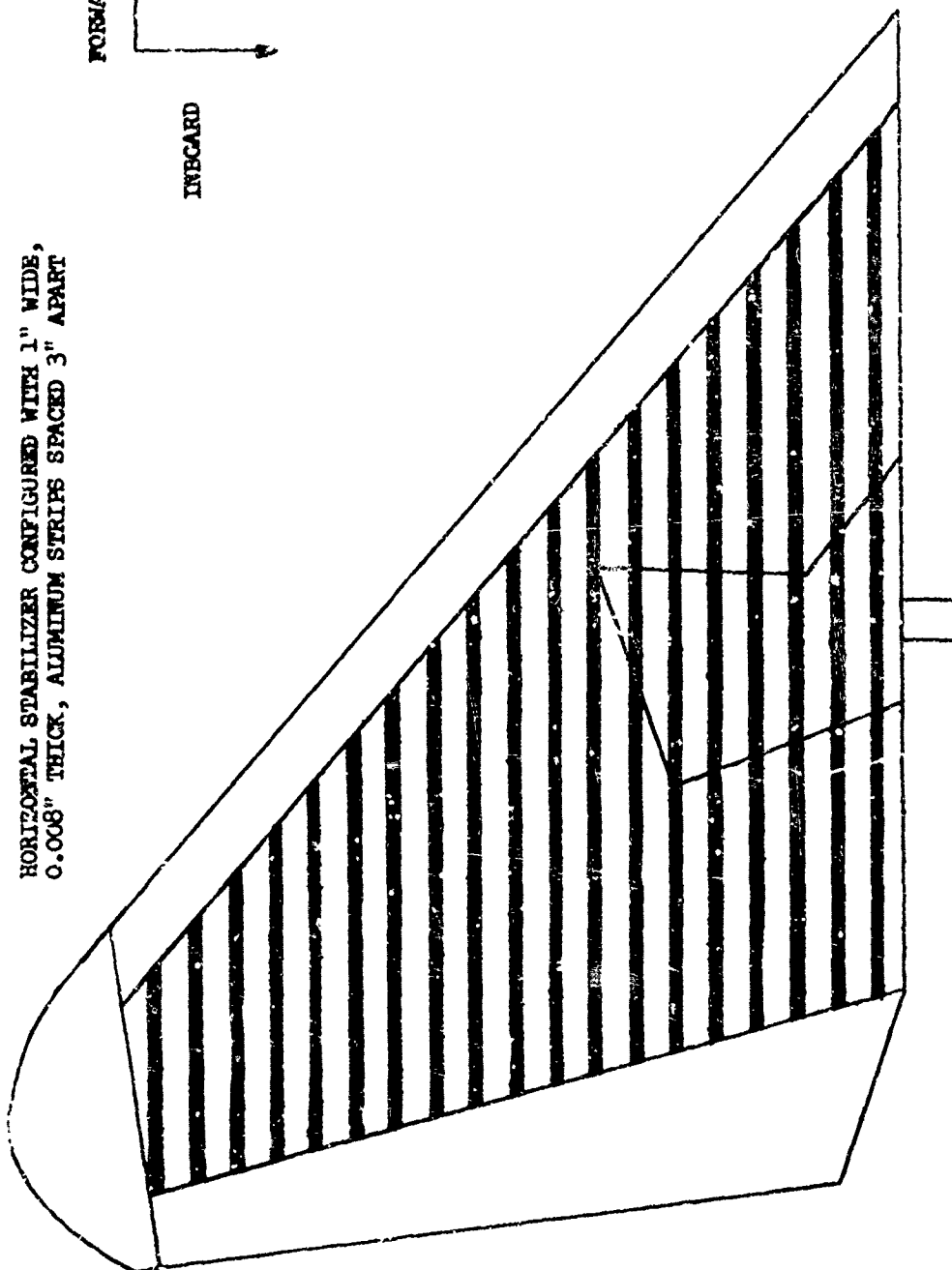
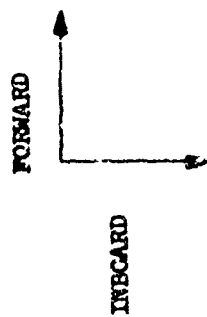


FIGURE 34

HORIZONTAL STABILIZER COMPOSED WITH 1" WIDE,  
0.008" THICK, ALUMINUM STRIPS SPACED  $\frac{1}{4}$ " APART

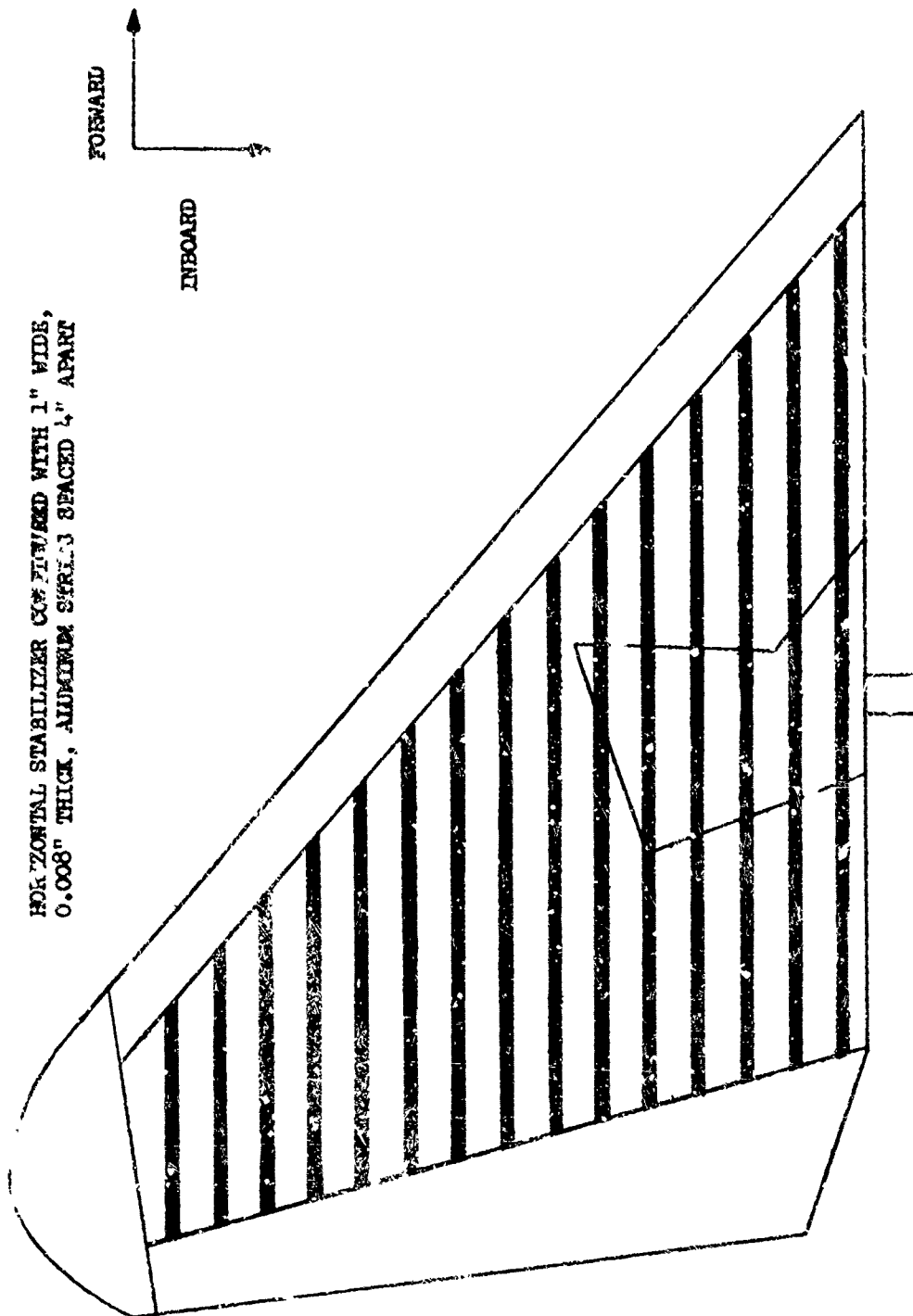


FIGURE 35

HORIZONTAL STABILIZER CONFIGURED WITH 1" WIDE,  
0.008" THICK, ALUMINUM STRIPS SPACED 5" APART

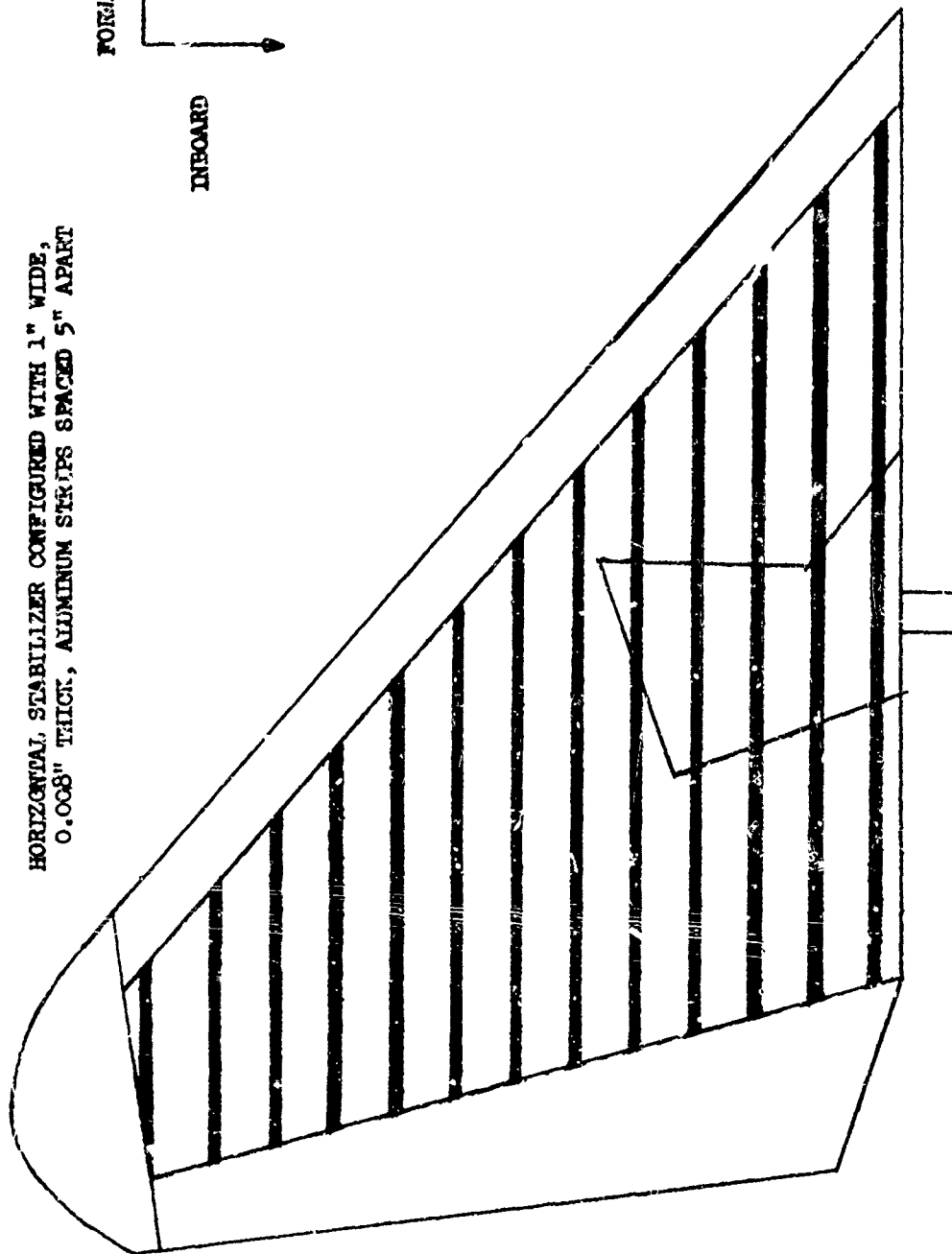
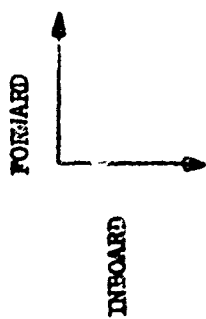
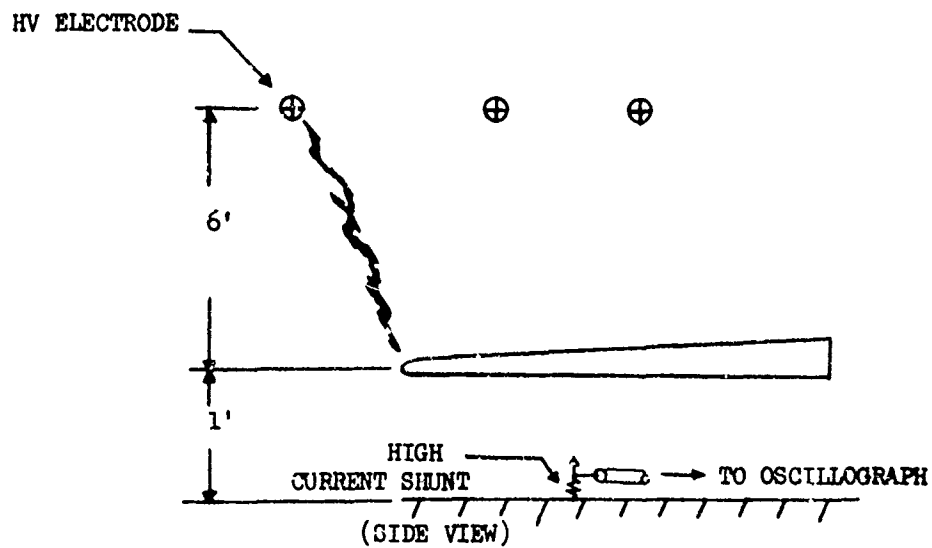
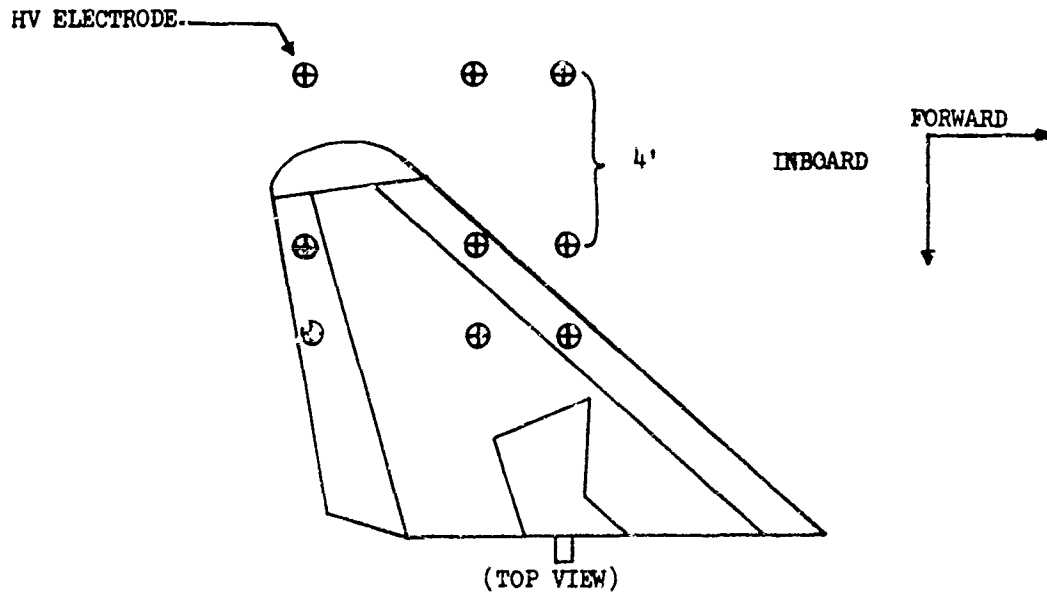


FIGURE 36

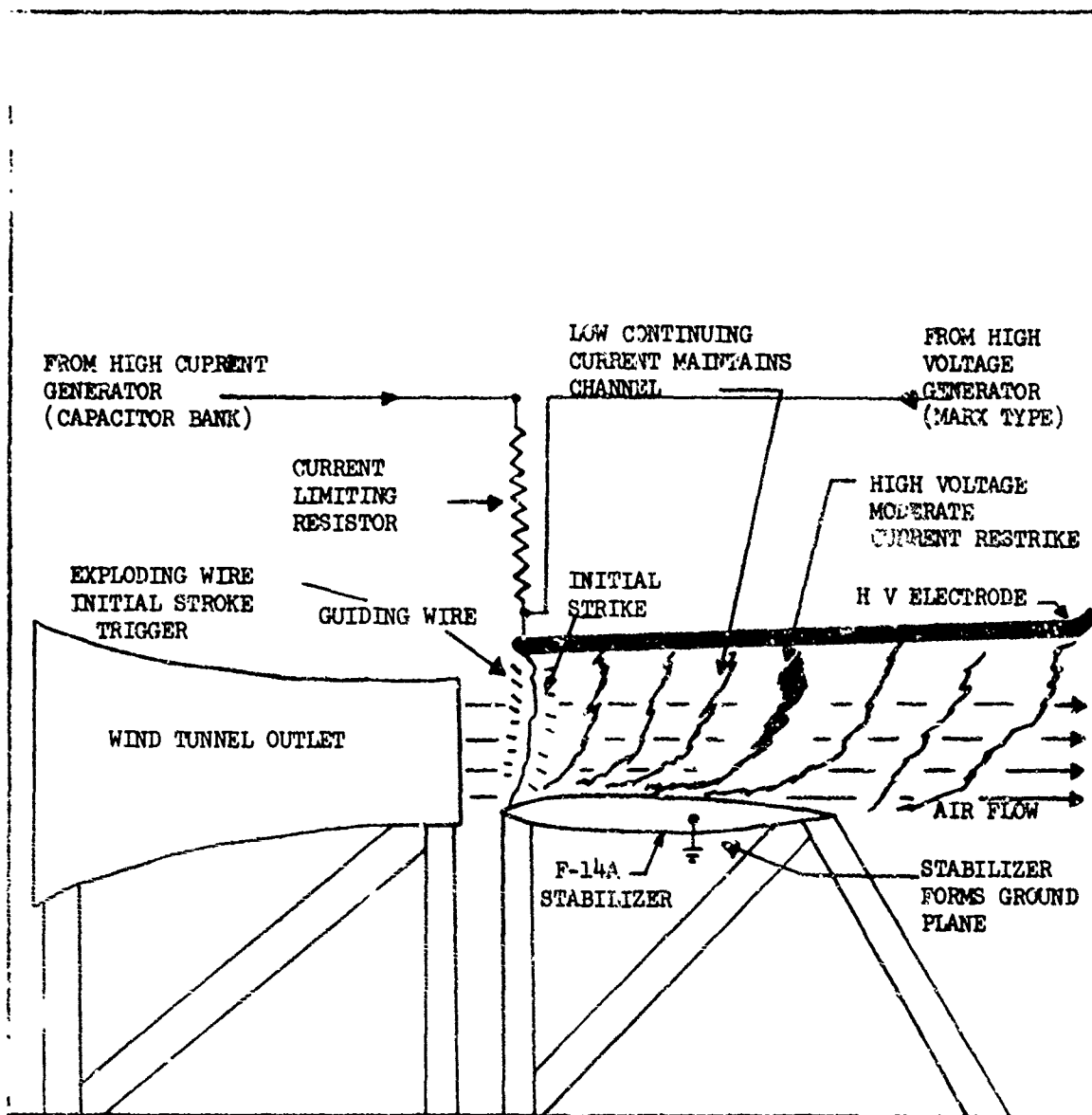


⊕ - HIGH VOLTAGE TEST ELECTRODE POSITIONS



TEST SETUP: HIGH VOLTAGE STRIKE STUDY - WITHOUT WINDSTREAM

FIGURE 37



TEST SETUP; HIGH VOLTAGE SWEEP STROKE STUDY - WITH WINDSTREAM

FIGURE 38

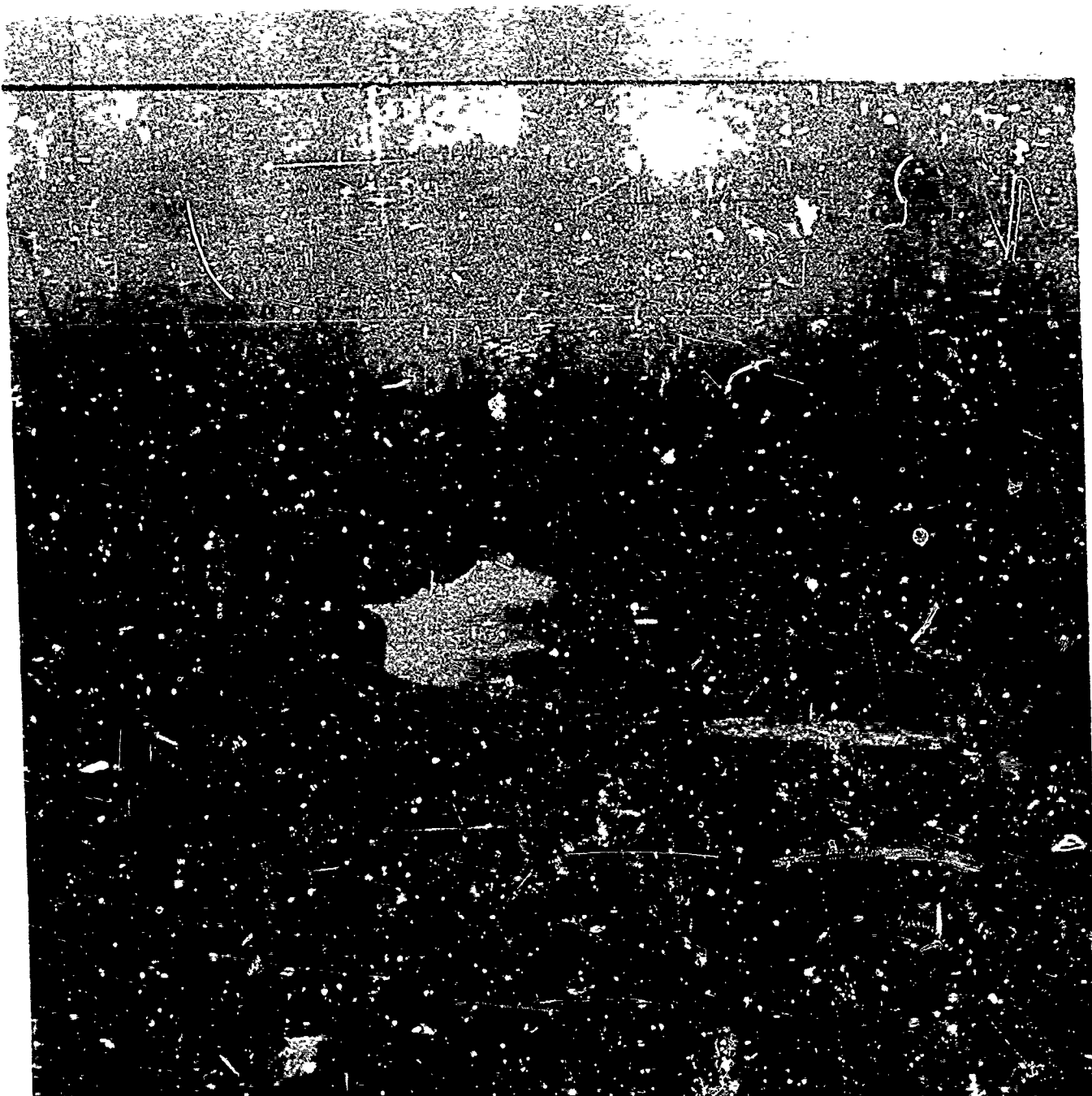


Figure 39 - Swept stroke discharge initiated at left to leading edge, moves at a low current level toward the right where the restrike occurs.

## HIGH CURRENT DAMAGE

These tests were performed as illustrated in Figure 40. The test consisted of firing high current discharges at the attachment points observed during the High Voltage Strike Study (Without Windstream) and High Voltage Swept Stroke Study (With Windstream) to determine if lightning strike damage would result.

## ELECTRICAL BONDING RESISTANCE MEASUREMENTS

These measurements were performed as illustrated in Figure 41. The test determine the resistance across the metal-to-metal joints of the horizontal stabilizer.

## TEST RESULTS

A summary of the test results is presented below:

- The horizontal stabilizer, with no protection over the boron skin, failed to provide adequate lightning protection for the exposed boron area. Thirty strikes were initiated to the stabilizer. Fourteen hit the metal periphery, thirteen hit the exposed boron area and three missed the stabilizer completely. The results of this test are depicted in Figures 42 and 43.
- The horizontal stabilizer, with 0.003 inch thick, aluminum foil cover over the outboard 1/3 of the boron skin one inch wide, 0.008 inch thick, aluminum strips spaced one inch apart over the middle 1/3 of the boron skin and one-inch-wide, 0.008 inch thick, aluminum strips spaced 2 inches apart over the inboard 1/3 of the boron skin, provide adequate lightning protection for the exposed boron area. Thirty strikes were initiated to the stabilizer. Ten hit the metal periphery, fourteen hit the aluminum strips and three missed the stabilizer completely. No strikes hit the exposed boron area. The results of this test are depicted in Figures 45 and 46.
- The horizontal stabilizer, with one inch wide, 0.008 inch thick, conductive paint strips spaced 2 inches apart over the inboard 1/3 of the boron skin and one inch apart over the remaining 2/3 of the boron skin, failed to provide adequate lightning protection for the exposed boron area. The High Voltage Strike Study (Without Windstream) was not completed because the conductive paint strips could not protect the boron skin from the high voltage, low current discharges (17,000 amps peak).
- The horizontal stabilizer design with 2 inch wide, 0.004 inch thick, aluminum strips spaced 2 1/4 inches over the boron skin, provided adequate lightning protection for the exposed boron area. Twenty-eight strikes were initiated and twenty-eight discharges hit the aluminum strips. No strikes hit the boron area. The results of this test are depicted in Figure 46.
- The horizontal stabilizer with, one-inch wide, 0.008 inch thick, aluminum strips spaced 2 1/2 inches apart over the boron skin, provided adequate lightning protection for the exposed boron area. One hundred and twenty six strikes were initiated to the stabilizer. Forty-six hit the metal periphery, sixty-six hit the aluminum strips and fourteen missed the stabilizer completely. No strikes hit the exposed boron area.
- The horizontal stabilizer with one-inch wide, 0.008 inch thick, aluminum strips spaced 3 inches apart over the boron skin, failed to provide adequate lightning protection for the exposed boron area. One hundred and eight strikes were initiated to the stabilizer. Fifty-two hit the metal periphery, thirty-seven hit the aluminum strips, seven hit the exposed boron area and twelve missed the stabilizer completely.
- The horizontal stabilizer, with one-inch-wide, 0.008 inch thick, aluminum strips spaced 4 inches apart over the boron skin, failed to provide adequate lightning protection for the exposed boron area. One hundred and thirty-five strikes were initiated to the stabilizer. Fifty hit the metal periphery, fifty-seven hit the aluminum strips, thirteen hit the exposed boron area and fifteen missed the stabilizer completely.
- The horizontal stabilizer, with one-inch-wide, 0.008 inch thick, aluminum strips spaced 5 inches apart over the boron skin, failed to provide adequate lightning protection for the exposed boron area. One hundred and sixty-two strikes were initiated to the stabilizer. Seventy-four hit the metal periphery, thirty-nine hit the aluminum strips, thirty-one hit the exposed boron area and eighteen missed the stabilizer completely.
- The resistance measurements performed across the metal-to-metal joints of the horizontal stabilizer were satisfactory and less than the maximum allowable value of 0.0025 ohm.

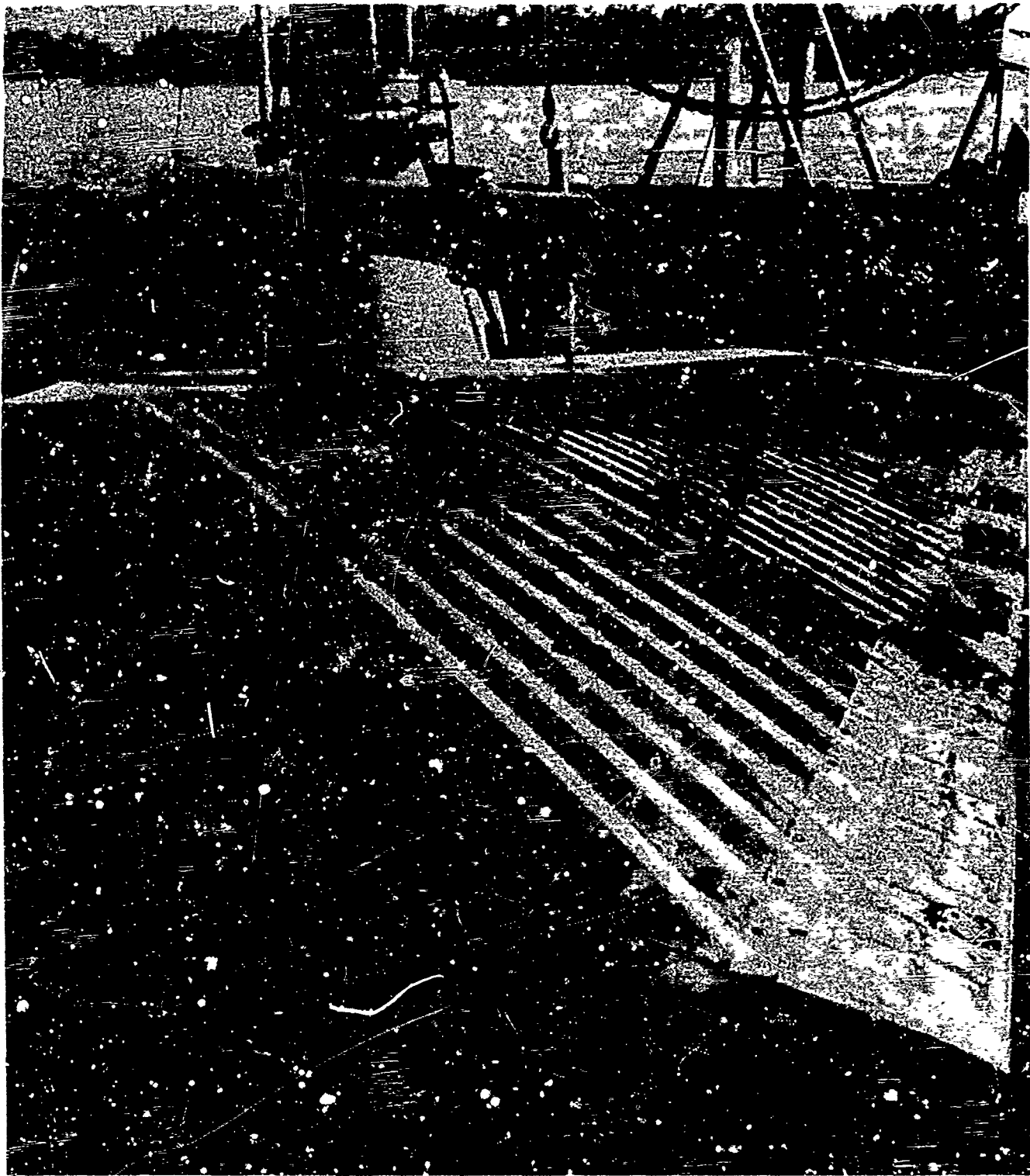


Figure 40 - Test arrangement for high current tests of stabilizer.



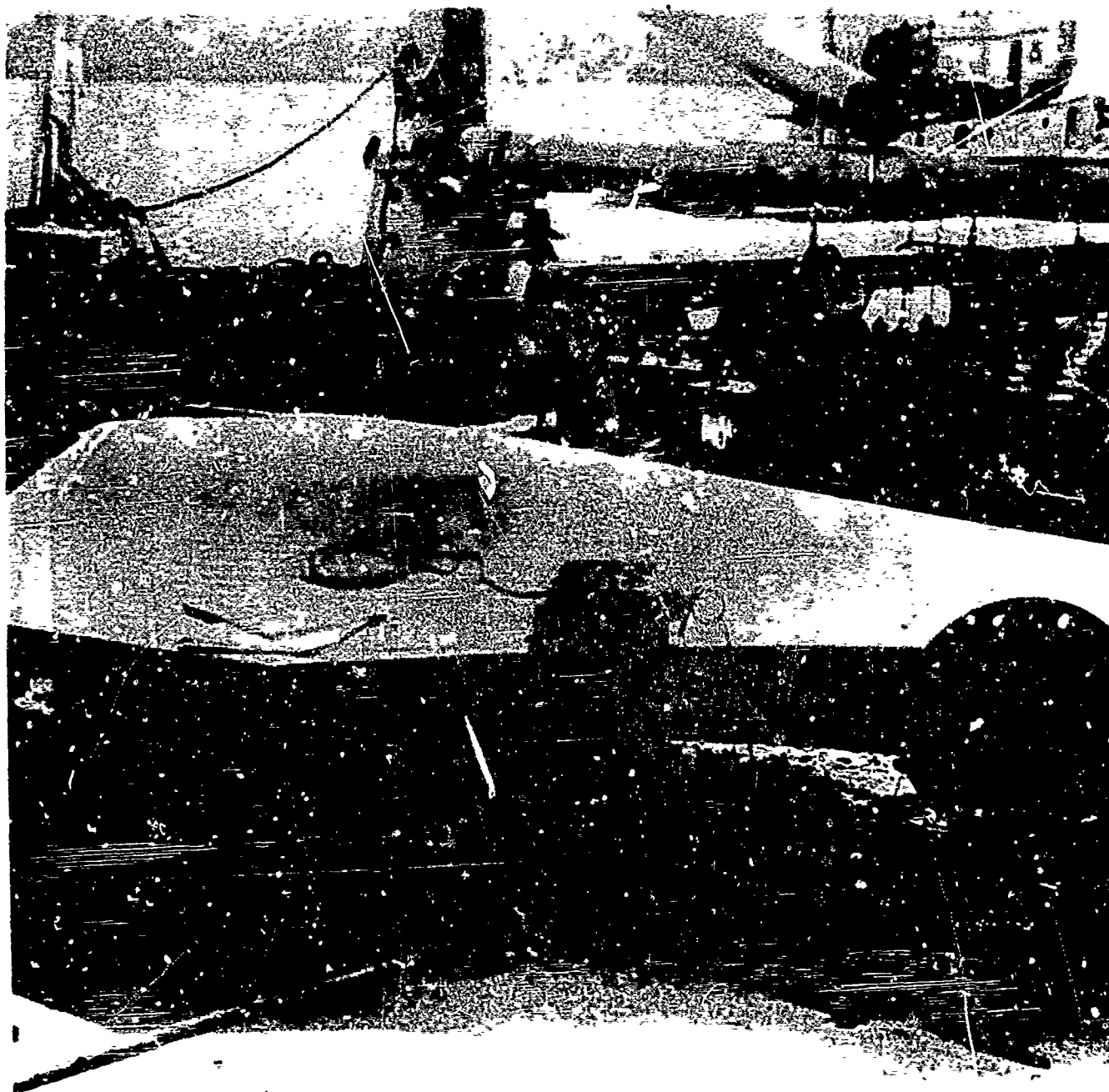


Figure 41 - Photograph of test arrangement for measurement of bonding resistance.



Figure 42 - Photograph of high voltage long arc discharge to unprotected side of Boron stabilizer.



Figure 43 - 200 kilovolt discharge to unprotected side of stabilizer produces half-inch hole and delamination.

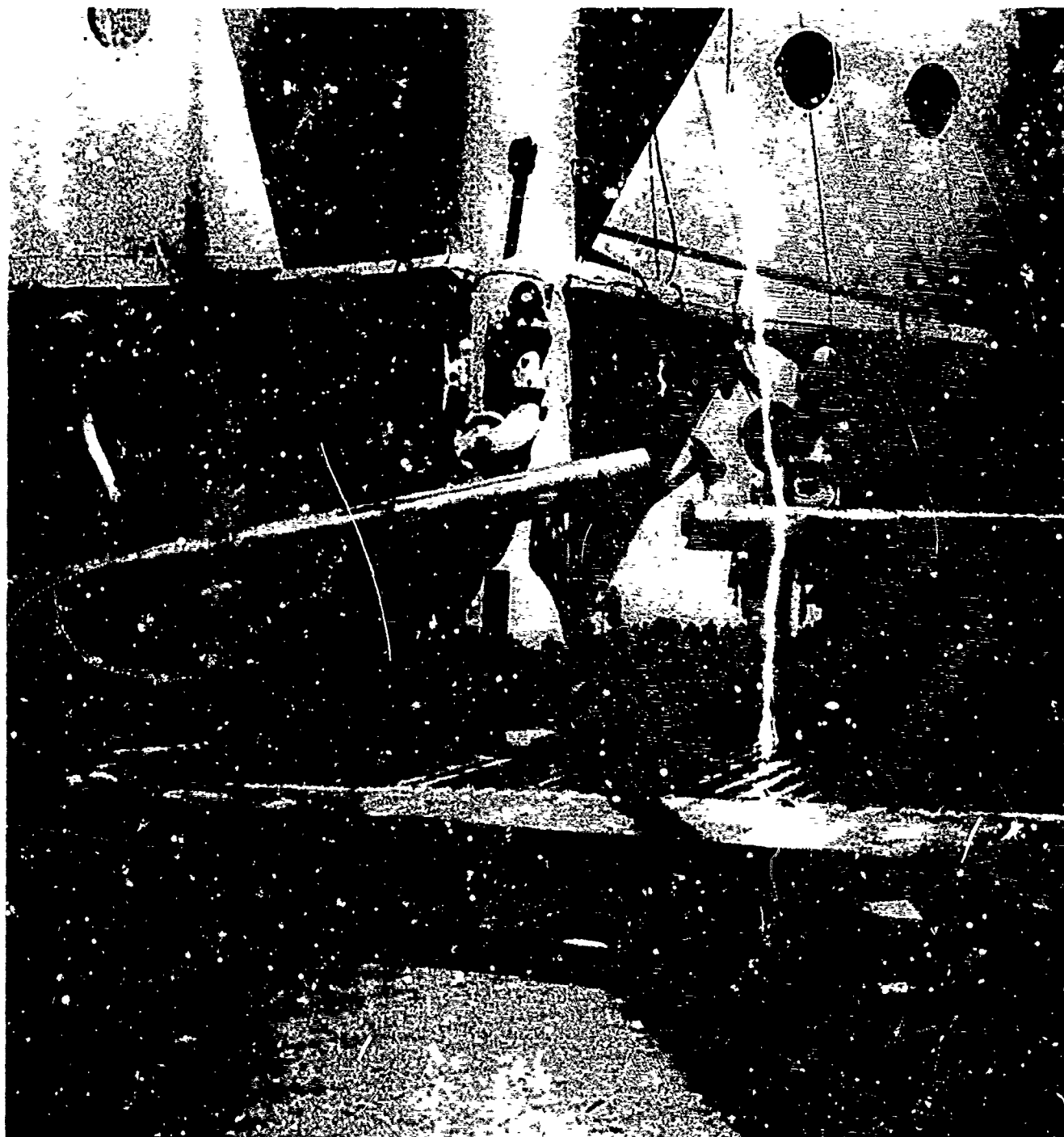


Figure 44 - Photograph of high voltage long arc discharge to protected side of Boron stabilizer.



Figure 45 - Swept stroke discharges produces light pitting of metal protection strips.



Figure 46 - 200 kilovolt discharge to protected side of stabilizer lifts the foil strips but shows no evidence of significant damage to the stabilizer surface.

## CONCLUSIONS

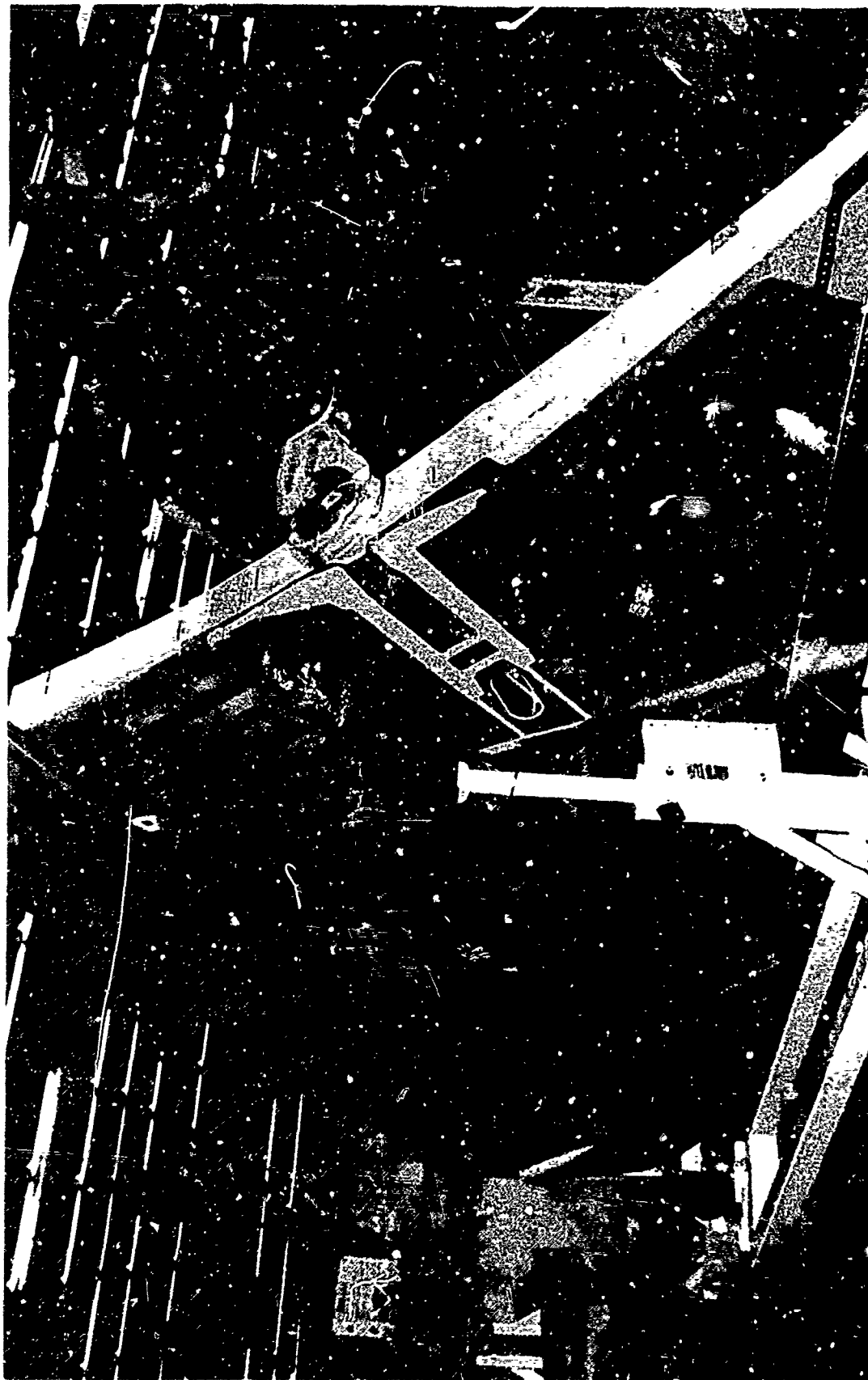
Based on the results of this test, the following is concluded:

- Five protection schemes (one inch wide, 0.008 inch thick, aluminum strips spaced either 1, 1 1/2, 2, or 2 1/2 inches apart and 2 inches wide, 0.004 inch thick, aluminum strips spaced 2 1/4 inches apart) were developed for use on the F-14A horizontal stabilizer which provide adequate protection from lightning strike damage and satisfy the requirements of MIL-B-5087B.
- The lightest weight scheme consists of 2 inch wide, 0.004 inch thick, aluminum strips spaced 2 1/4 inches apart.
- The aluminum strip protection schemes utilizing 3, 4 and 5 inch spacing failed to provide adequate lightning protection and meet the requirements of MIL-B-5087B.
- The conductive paint protection scheme was demonstrated to be totally inadequate.
- The final horizontal stabilizer design complies with the electrical bonding requirements of MIL-B-5087B.

The lightning protection scheme developed for the F-14A horizontal stabilizer as a result of the test program as shown on Figure 47, consists of placing 2 inch-wide, 0.004 inch-thick, aluminum strips spaced 2 1/4 inches apart over the boron skin on both the upper and lower skins. Tests were not made on stabilizers having strips protected with exterior coatings.

## REFERENCES

1. Lightning and Transient Research Institute Report of September 12, 1969 on Contract No. F33615-68-C-1534.
2. Repair Technology for Boron/Epoxy Composites, AFML-TR-71-270 of February, 1972.
3. Grumman Report F-14 Aircraft Lightning Program, No. A51-340-R-72-16 of 31 July 1972.



LIGHTNING PROTECTION FOR THE ZORON COMPOSITE HORIZONTAL STABILIZER

FIGURE 47



SESSION VII

ELECTROSTATICS IN AVIATION FUEL SYSTEMS

J.B. GODWIN, CHAIRMAN & ORGANIZER

U.S. AIR FORCE, DIRECTORATE OF AEROSPACE FUELS

Introduction of Electrostatics in  
Aviation Fuel Systems Sessions

J. B. Godwin, Jr., P.E.  
US Air Force  
Directorate of Aerospace Fuels

ABSTRACT

In previous sessions, you have heard presentations on nature's natural phenomena of static electricity "Lightning" and electrostatic build up on space vehicles and aircraft. This session will be devoted to electrostatic charging of fuel during handling and the hazards associated with a wide variety of varying parameters, which are constantly changing with the advent of new materials and large volume aircraft receipts. These include the 74' and C-5A types of aircraft.

Static electricity is as old as mankind and received little attention, until the first catastrophic incident in the petroleum industry, which appeared to be from an unknown source. It was then the petroleum industry devoted total efforts as a matter of self-survival and today, extensive studies are being made by both industry and government activities. The incendiary ignition mechanism of explosive mixtures chooses no boundaries and is a mutual problem to both industry and government.

For years the results of explosions due to static electricity were based on so called "old wives tales" and in 1958 a concentrated effort was mustered by Dr. Klinckenberg, the author of a bible of standards in the field of static electricity. No records of any consequence were maintained as to where an event occurred and what type equipment that was involved until 1960. At this time, the American Petroleum Institute (API) formed the Static Electricity Committee who compiled incident reports with supporting data.

Following World War II, the development of the turbo jet engine type aircraft resulted in research for a new type and more readily available high energy jet fuel for these aircraft. This set the stage for a new set of standards for the safe handling of these types of fuels. Aircraft were being lost on the ground during fuel servicing, but other problems were manifested which were resulting in the losses of bulk storage tankage, barges, railroad tankers, seagoing tankers,

and refueling vehicles (transport trucks) as a result of explosions due to sparking of the fuel in the vapor space above the liquid.

New techniques were developed for the safe handling of jet fuel because of its different characteristics in electrical conductivities versus aviation gasoline with tetra-ethyl-lead (TEL). Certain types of jet fuel were more prone to electrostatic generation. JP-4 jet fuel in layman's language is a 50-50 blend of kerosene and straight run gasoline. By the very nature of JP-4's electrical properties, it restricts flow velocities to a maximum of 7 Ft/Sec, requires assured electrical interconnection of handling systems and a 30 second minimum relaxation time in ferrous metal systems. New electrostatic charge relaxing methods have been developed and some are currently under extensive testing. These procedures were to reduce generated charges to a safe level in relationship to the discharge from the filter/separator, which in itself is "prolific static generator."

In this session, you will be presented a full spectrum analysis of the electrostatic charging characteristic of flowing hydrocarbon fuels in fixed and servicing systems with measures for retardation of these charges, design criteria utilizing new state-of-the-art materials, research and development, and trends of jet fuels of the future. As your session chairman and organizer, I have assembled the most knowledgeable gentlemen in the world on the subject of electrostatics. They are recognized as professional experts, my only regret is that we will cover many subjects in such a short period.

## Principles of Electrostatics in Aircraft Fuel Systems

Joseph T. Leonard  
Naval Research Laboratory

### ABSTRACT

A survey is presented on the subject of the generation and dissipation of electrostatic charge during aircraft fueling. The types of discharges that can take place inside of aircraft fuel tanks during fueling are described and methods of eliminating discharges are discussed.

GENERATION OF ELECTROSTATIC CHARGE by hydrocarbon liquids has long been recognized as a potential hazard by the petroleum industry. In 1958 Klinkenberg and van der Minne (1)\* published an excellent monograph on the subject including a review of research conducted by Royal Dutch/Shell which led to the development of an antistatic additive suitable for use in turbine and other fuels. Other segments of the petroleum industry have also been active in research on electrostatics, spurred on, no doubt, by a number of fires and explosions involving tank trucks, aircraft and tankers. According to a recent survey (2) covering the period 1960-1969, there were 116 fires resulting from static electricity generated by the fuel during tank truck loadings. Over the same period, there were 33 incidents involving aircraft; 12 of which involved aviation gasoline, 15 with JP-4 and 1 with kerosine (3). Since then, two more explosions have occurred while fueling commercial aircraft with kerosine (4). The latter incidents took place within a period of seven months at the same airport and involved the same type of aircraft. Although a number of fires of suspected electrostatic origin have taken place

while loading tankers with petroleum products (5), recent explosions aboard three very large crude carriers during tank cleaning operations (6) have intensified interest in electrostatic charge generation.

The purpose of this survey is to review the state-of-the-art on the subject of electrostatic charge generation as related to aircraft fueling. Although a number of reviews on the subject have been written (4,7,8,9,10,11,12), this survey will endeavor to present an in-depth study of those aspects of the problem which deal specifically with aircraft fueling.

### THE PROBLEM

Whenever a hydrocarbon liquid, such as a jet fuel, flows with respect to another surface, a charge is generated in the liquid. Although the exact nature of the charging mechanism is not completely understood, it is generally held that the charge is due to ionic impurities present in the hydrocarbon in parts-per-million or parts-per-billion quantities. When the fuel is at rest, the impurities are adsorbed at the interface between the fuel and the walls of the container, with one part of the ionic material showing a rather strong attachment for either the fuel or the solid surface. This type of attachment is illustrated in Figure 1a which shows fuel in contact with the wall of a pipe. In this

---

\* Numbers in parentheses designate References at end of paper.

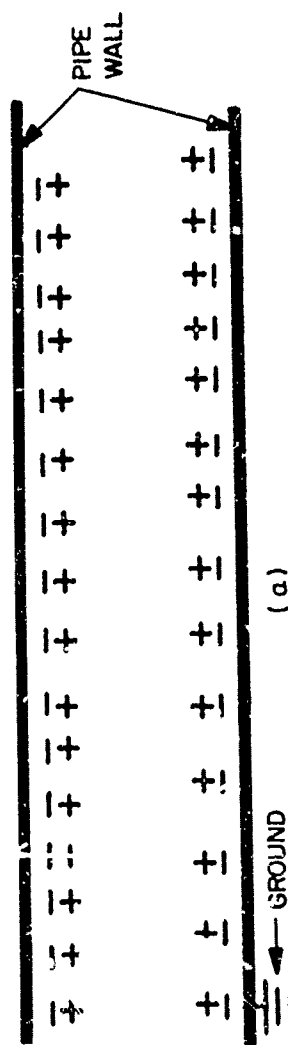


Fig. 1a - Fuel at rest in a pipe showing adsorption of ionic impurities at pipe wall.

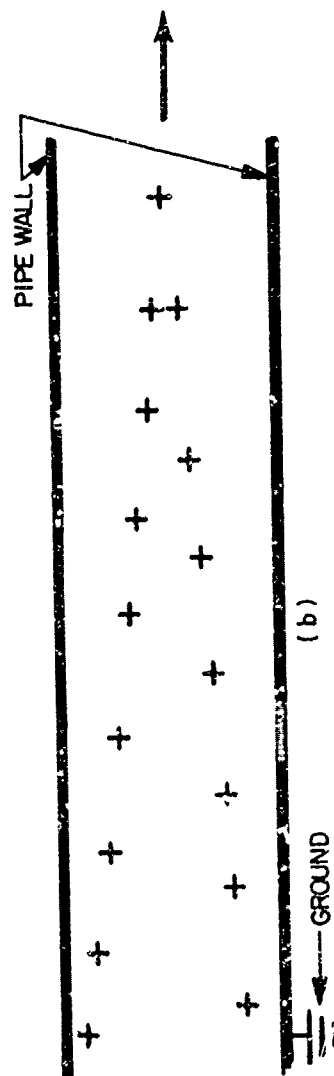


Fig. 1b - Separation of charge as fuel flows through pipe.

example, the negative portion of the ionic material is depicted as being more strongly attracted to the solid surface, but since the numbers of positive and negative charges are equal, there is no net charge on the fuel. However, when the fuel begins to flow (Figure 1b), the positive charges are swept along by the fuel while the negative charges leak to ground. Thus, the fuel acquires a net positive charge as it moves through the system. In a similar manner, the fuel would receive a negative charge if the positive portion of the ionic material were preferentially adsorbed at the solid surface.

When the charged fuel is loaded into a receiving tank, either of two possibilities will occur: (1) the charge will relax harmlessly to the walls of the tank or, (2) if the conductivity of the fuel is sufficiently low, the charge may accumulate giving rise to high potentials on the fuel surface. If somewhere in the tank the local potential exceeds the breakdown value for the vapor space, a discharge will occur. Whether or not the vapor will ignite depends on the composition of the vapor and the nature of the discharge.

#### CHARGE GENERATION DURING AIRCRAFT FUELING

The situation with respect to aircraft fueling presents a somewhat more complicated picture than flow through a pipe due, primarily, to the use of filter/separators and fuel monitors which greatly increase the level of charge on the fuel. A typical aircraft fueling operation is illustrated in Figure 2 together with an indication of the level of charge on the fuel as it passes through each piece of equipment. Since charge separation is a surface effect and since filter/separators provide a tremendous amount of surface area upon

which charge separation can take place in a comparatively short period of time, the level of charge on the fuel emerging from the filter/separator may be increased by a factor of 100 or more as compared with flow through the hydrant line. A more detailed illustration of the charge separation process in a typical two-stage filter/separator is presented in Figure 3. The first stage, the filter-coalescer, removes dirt and coalesces water. The coalescer may charge the fuel positively, as shown in the figure, or negatively. The second stage, the water separator, allows the fuel to pass but causes the coalesced water to settle out. The coalescer may increase the charge on the fuel, as indicated by Type A in the figure, or decrease it, as shown by Type B. The use of two different types of filter media, each of which places the opposite sign of charge on a fuel, has been demonstrated on a laboratory scale as a means of neutralizing charge on a fuel, but full scale tests have not been carried out (13). The unpredictable and sometimes variable nature of the charging process in field tests would militate against the success of this method of charge reduction.

The level of charge on a fuel coming out of a filter separator, or at any point in the system, can be determined by placing a charge measuring device, such as the AO Smith Charge Measuring System (14), in the line. This device measures the charge density in the fuel,  $Q$ , from which the streaming current can be calculated from the following equations (12):

$$i = Qv, \quad (1)$$

where  $i$  = Streaming current  
(microamperes,  $\mu A$ )  
 $Q$  = Charge Density  
(microcoulombs/  
meter<sup>3</sup>,  $\mu C/m^3$ )  
 $v$  = Volumetric Flow Rate  
(meter<sup>3</sup>/second,  
m<sup>3</sup>/sec)

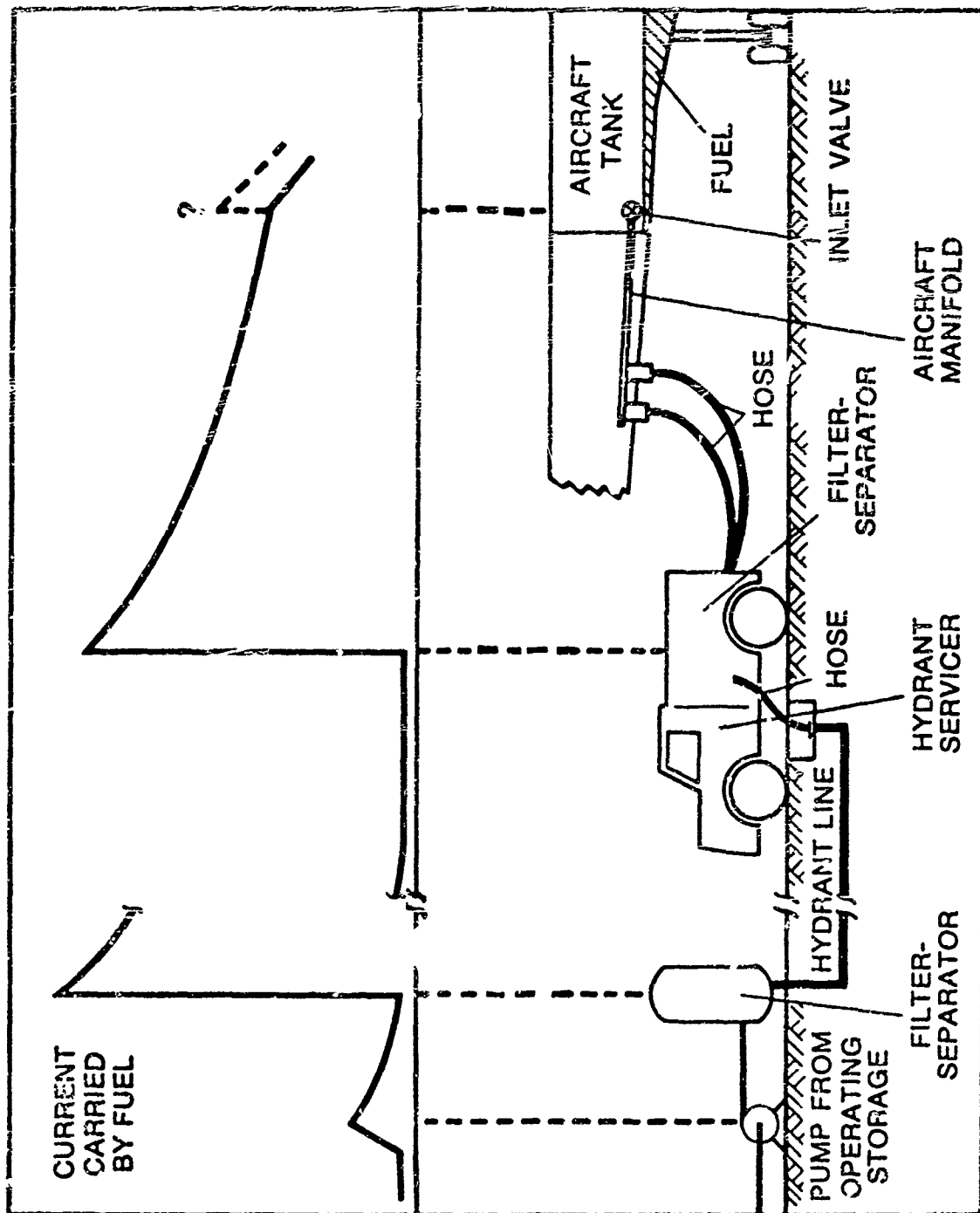


Fig. 2 - Generation of electrostatic charge during aircraft fueling (12).

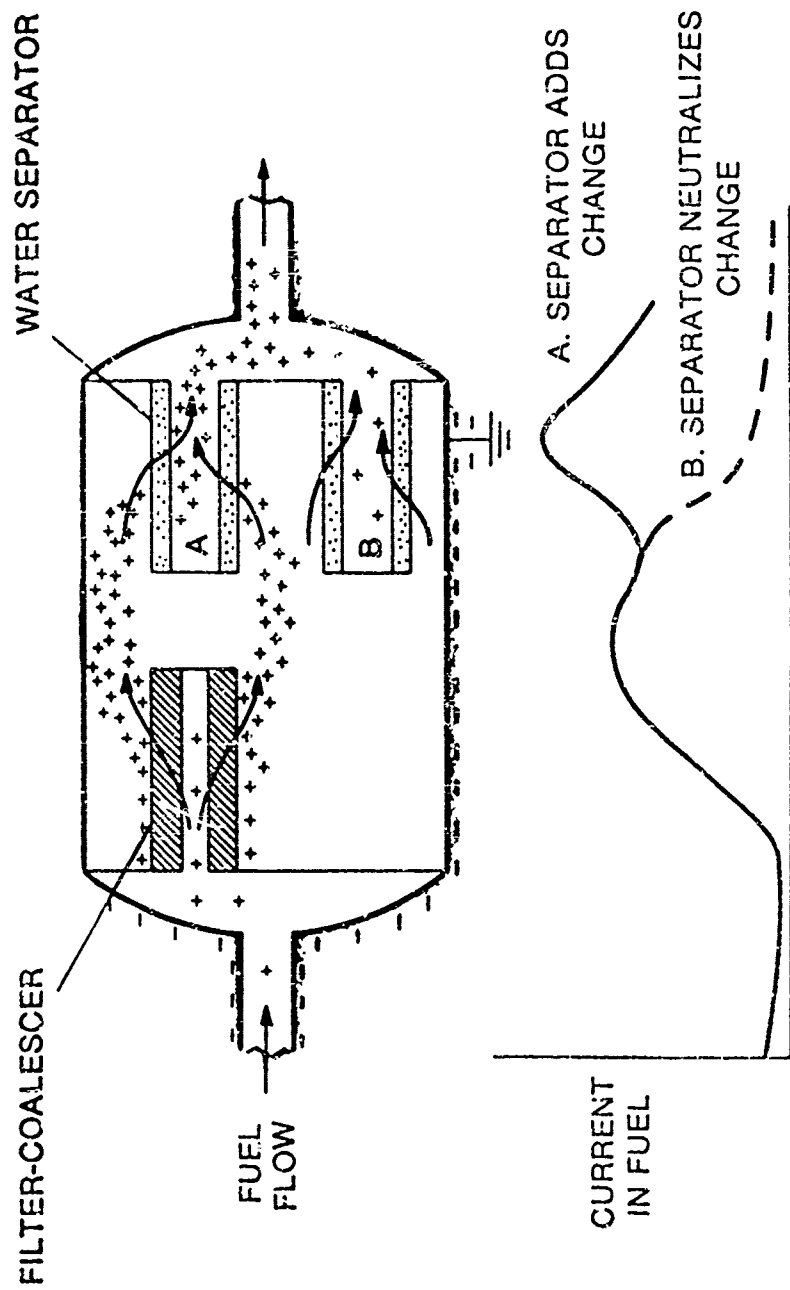


Fig. 3 - Charge separation in a filter/separator (12).

The charge density is a function of flow rate ( $v$ ), the area ( $A$ ), and the characteristics ( $X$ ) of the fuel/surface interface, i.e.,

$$Q=f(v,A,X) \quad (2)$$

The factor,  $X$ , represents the charging tendency. It is an unpredictable factor since it depends on both the type of ionizable materials in the fuel and the properties of the surface presented to the fuel.

The equations predict that for a given fuel with a particular set of coalescer and separator cartridges, the charge density on the fuel should increase with flow rate as shown in Figure 4. While this statement is generally true, conflicting results have been obtained in some field tests (Figure 3), in which the performance of various filters were compared (4). Obviously, the nature of the filter surface is an important factor in charge generation.

As stated above, the charging tendency of a fuel depends on the type of ionizable materials in the fuel. Since the electrical conductivity of the fuel also depends on the presence of ionic material it would seem that the charging tendency of the fuel should also be related to its electrical conductivity. Indeed it has been shown that such a relationship does exist, at least in simple systems involving a single hydrocarbon liquid containing known amounts of specific ionic compounds. For example, it has been shown that for n-heptane containing various amounts of polar additives, the magnitude of the streaming current is dependent upon the conductivity of the hydrocarbon over a wide range of conductivity values (16) - see Figure 6. In these experiments, which were conducted in stainless steel tubes, the sign of the streaming current was

found to vary with the chemical nature of the polar additive, i.e., alcohols, acids, nitrobenzene and an antistatic additive (ASA-1) produced positive currents, whereas ketones, esters and amines gave negative currents. However, at a given conductivity level, the magnitude of the streaming current was the same, regardless of the nature of the polar additive.

Fuels present a much more complicated picture than single compounds since they consist of a wide variety of hydrocarbon types and may contain a number of polar additives and impurities which can alter the charging behavior in an unpredictable fashion. Also, the nature of the surface upon which the charge separation takes place has an effect on both the magnitude of the charge, as shown in Figure 5, and the sign. With JP-5 fuel containing an antistatic additive it was found that the sign of the charge on the fuel passing through a resin-bonded fiber glass filter could be reversed by baking the resin coating off the filter to expose the clean glass surface (13) - see Figure 7.

The above tests were conducted in a laboratory-scale apparatus where it is a relatively simple matter to control fuel conductivity and filter materials. In full-scale tests in which JP-4 and JP-5 fuels of approximately the same electrical conductivity were passed through the same filter/separator, a considerable variation was observed in the charge density of the two fuels as they emerged from the filter (Figure 4). Elsewhere, it has been reported that certain aliphatic amines can increase the filter charging of kerosene by a factor of 100 without increasing the conductivity of the fuel (4). Also, the presence of fuel monitors can have a profound effect on the charging tendency of a fuel (12). Data obtained during simulated aircraft



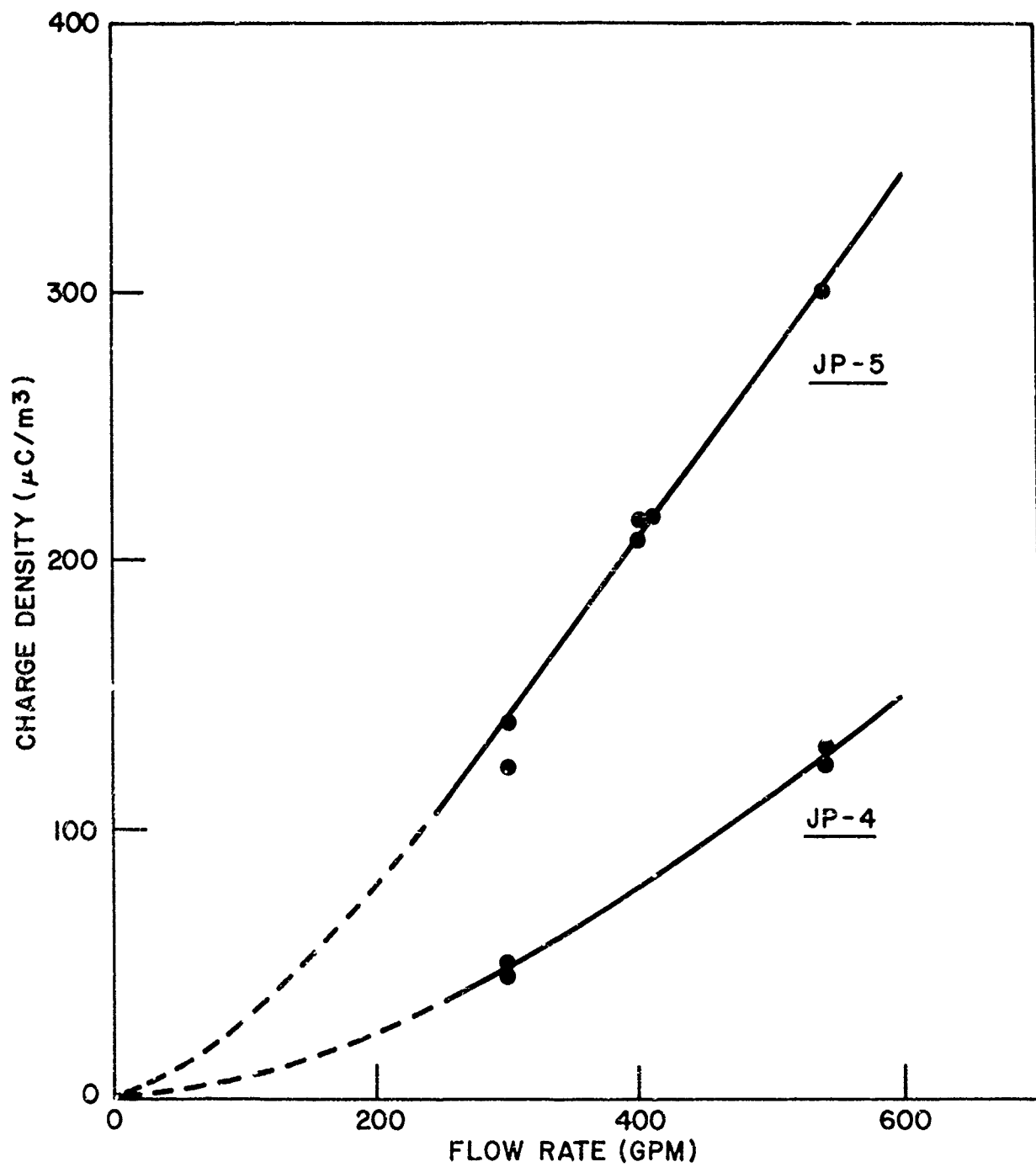


Fig. 4 - Charge density at filter as a function of flow rate for JP-4 and JP-5 fuels (15).

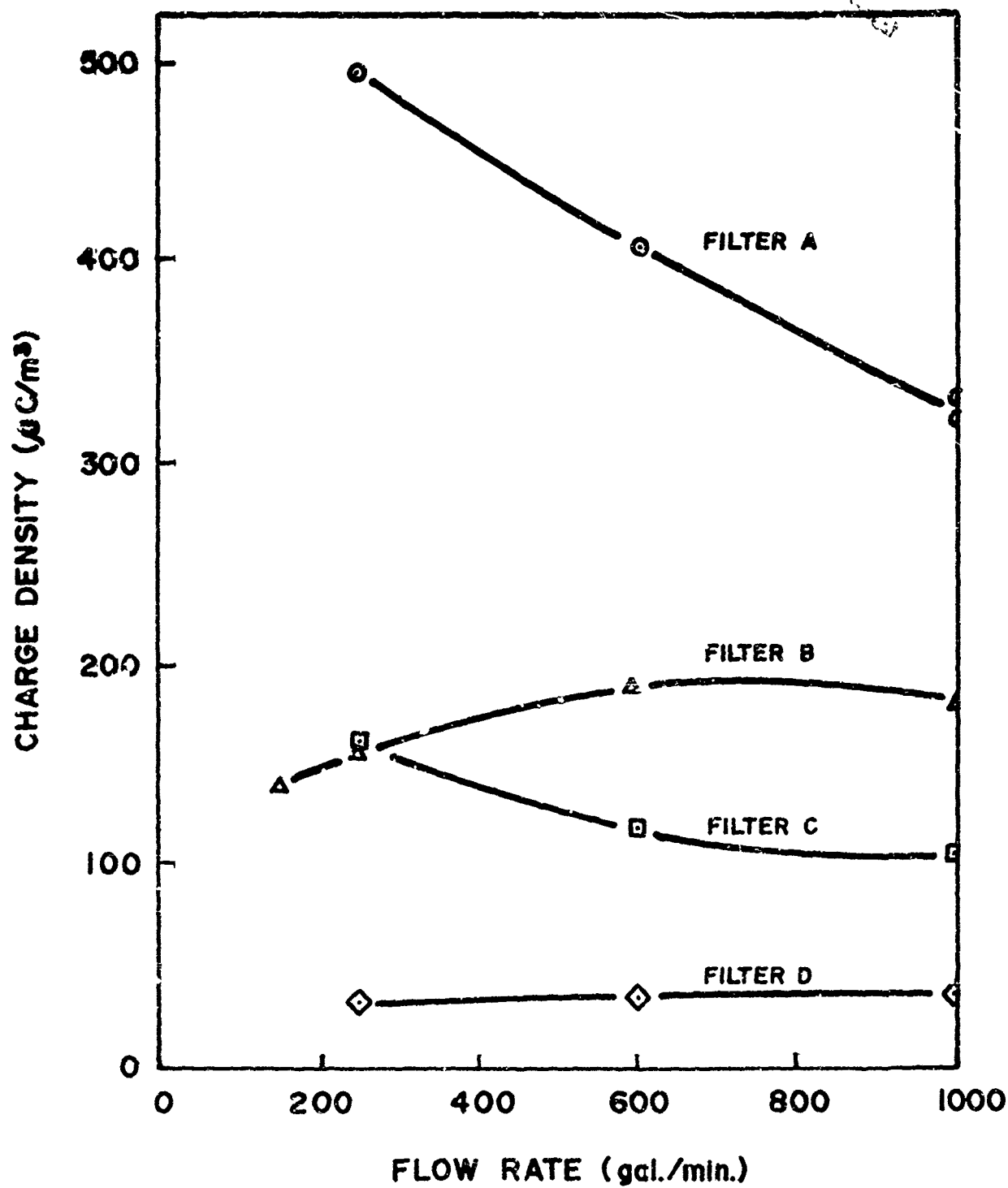
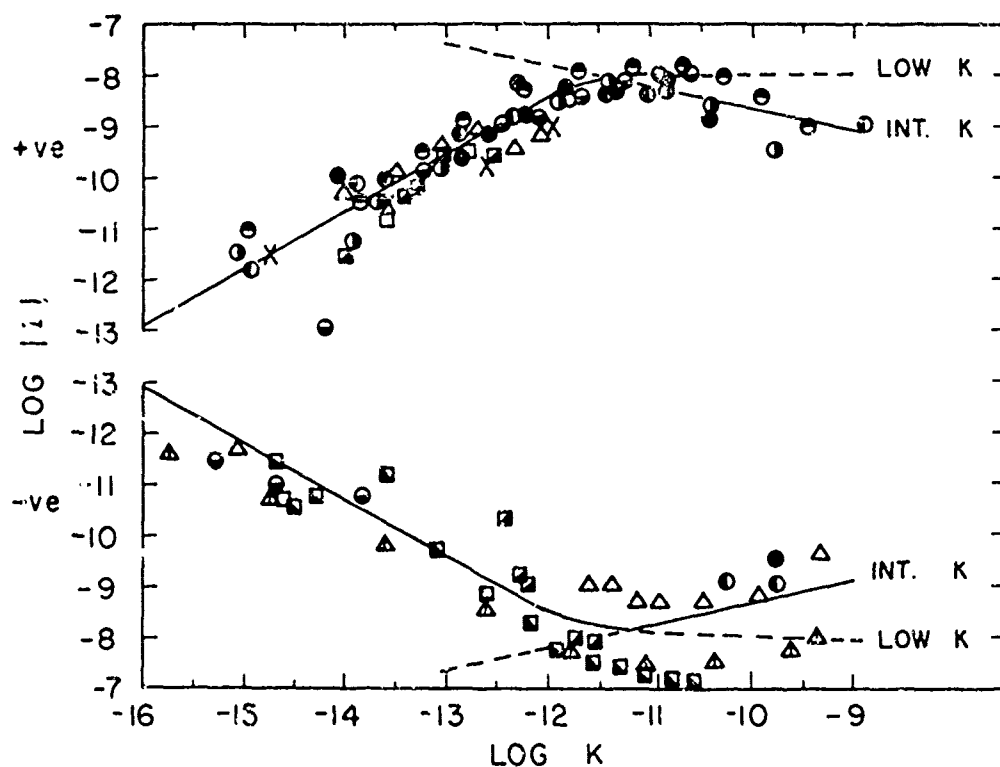


Fig. 5 - Effect of filter type on charge density of aviation kerosene (4).



- |               |                           |
|---------------|---------------------------|
| ● ETHANOL     | ■ ISOPROPYL ACETATE       |
| ○ PROPANOL    | □ ETHYL ACETATE           |
| ● ISOPROPANOL | △ ACETONE                 |
| ○ BUTANOL     | △ CYCLOHEXANONE           |
| ● 2-PENTANOL  | X ASA # 1 (KOSZMAN et al) |

$N_{Re} = 22,000$

Fig. 6 - Effect of different polar additives on sign of streaming current for n-heptane as a function of conductivity (16).

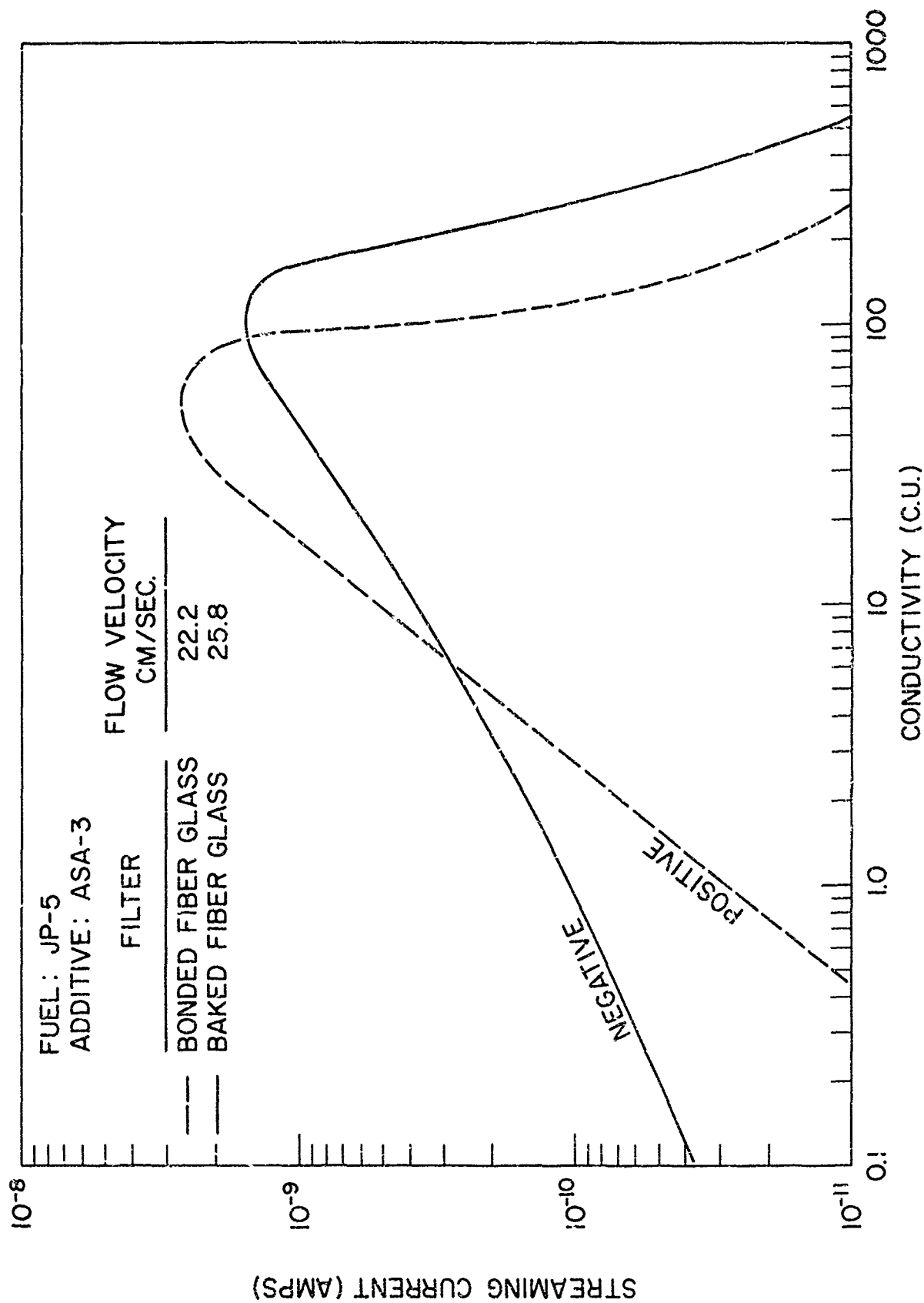


Fig. 7 - Effect of filter material on the sign of the streaming current for JP-5 fuel (13).

fueling (Figure 8) show that the charge density on a fuel can be increased by a factor of 4 to 5 when fuel monitors are used. The obvious conclusion is that the charging of fuels in full scale equipment is the net result of a number of uncontrollable factors, such as the chemical nature of the additives and impurities in the fuel, as well as the properties of the surfaces upon which charge separation takes place. Consequently, it is not possible to predict the charging tendency of a fuel under field conditions from the known properties of the fuel.

#### CHARGE RELAXATION

As shown in Figure 2, when the fuel emerges from the filter/separator, the charge begins to relax or dissipate. Actually, some charge generation takes place in the piping downstream of the filter/separator, but for short runs it is negligible in comparison with the charge generated by the filter. The rate at which the charge dissipates depends on the electrical conductivity of the fuel as shown by the equation (12):

$$Q_t = Q_0 e^{-tk/\epsilon\epsilon_0} \quad (3)$$

where  $Q_t$  = charge after time,  $t$  (e.g.,  $\mu\text{C}/\text{m}^3$ )  
 $Q_0$  = initial charge (e.g.,  $\mu\text{C}/\text{m}^3$ )  
 $t$  = elapsed time (seconds)  
 $k$  = rest fuel conductivity (mhos/m)  
 $\epsilon$  = relative dielectric constant, a dimensionless quantity which varies only slightly for hydrocarbon fuels and has a value of about 2

$\epsilon_0$  = the absolute dielectric constant of a vacuum ( $8.854 \times 10^{-12}$  ampere seconds/volt meter).

Since charge relaxation is an exponential process, it is customary to define relaxation time,  $r$ , as the time required for the original charge to decay to 36.8% of its original value:

$$\frac{Q_t}{Q_0} = 0.368 = e^{-1} \quad (4)$$

and  $r$  is related to  $k$  by the following relationship:

$$r = \frac{\epsilon\epsilon_0}{k} = \frac{17.7 \times 10^{-12}}{k} \quad (5)$$

$$\approx \frac{18 \times 10^{-12}}{k}$$

The conductivity of fuels is usually described in terms of conductivity units, CU, or, in the International System, picosiemens/m, which are related as follows:

$$1 \text{ CU} = 1 \text{ picosiemens/meter}$$

$$(\text{pS/m}) = 10^{-12} \text{ Siemens/meter}$$

$$= 10^{-12} \text{ mhos/m} = 10^{-14} \text{ mhos/cm}$$

According to the above equation, the relaxation time for fuels would be expected to vary with rest conductivity as follows:

Conductivity,	Relaxation Time,
CU	Seconds
0.01	1800
0.1	180
1.0	18
10.0	1.8
100.0	0.18

A world-wide survey of the electrical conductivity of turbine fuels showed that at the time of the survey (1965), 43% of the samples had conductivities of less than 1 CU and

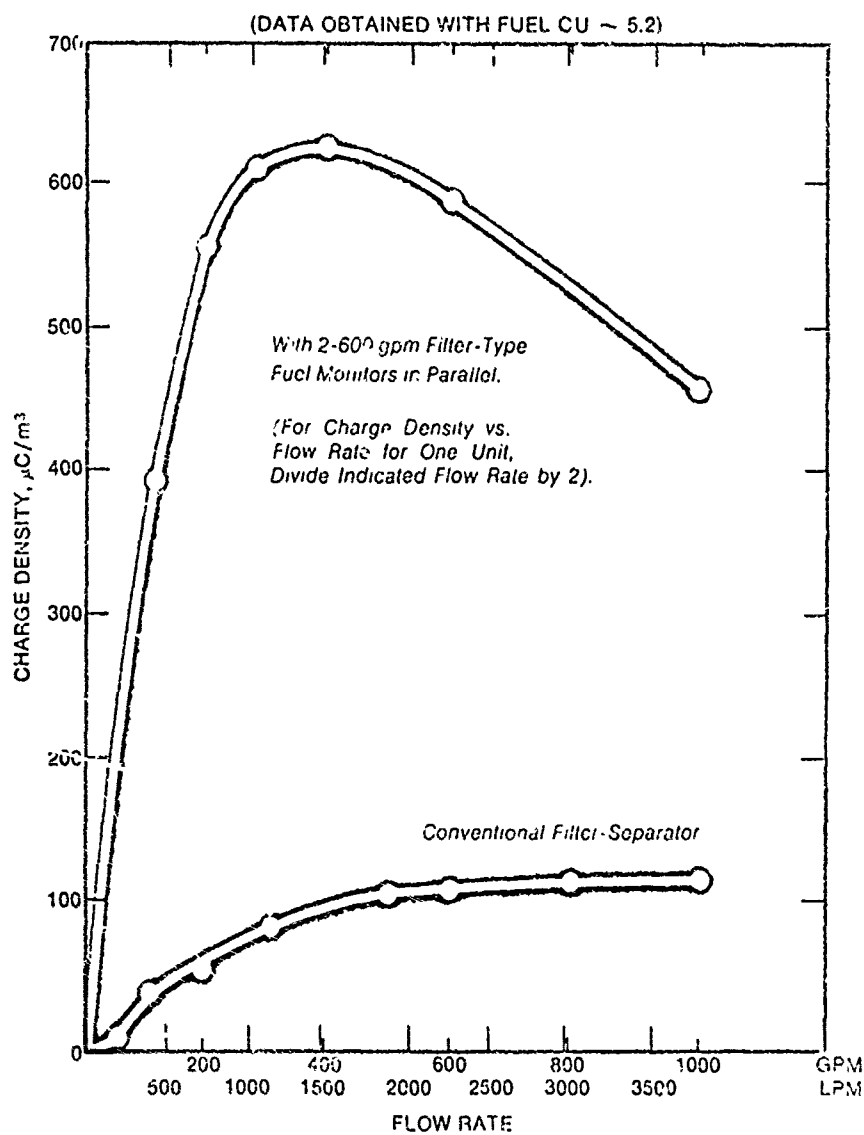


Fig. 8 - Effect of fuel monitor on charge generation (12).

96% were less than 5 CU (18). These results indicate that relaxation times in excess of 18 seconds would be required to reduce the charge on almost half of the turbine fuels to 36.8% of their original value. Since the residence time of the fuel in the hoses downstream of the second filter/separator in a typical aircraft fueling operation (Figure 2) is at most only a few seconds, the above data would suggest that for lower conductivity fuels most of the charge generated at the filter arrives at the aircraft tank undiminished. Fortunately, this is not always the case. Bustin, et al, (19) have shown that if the conductivity of the fuel is less than 1 CU, the charge relaxes faster than predicted by the above (ohmic) equation. A comparison of the relaxation behavior for a 0.01 CU fuel using both the ohmic and Bustin's hyperbolic theories of charge relaxation is shown in Figure 9. The experimental data points for the low conductivity fuel follow the hyperbolic theory and show that in 30 seconds, over 70% of the charge on the fuel has relaxed as compared with less than 5% predicted by the ohmic theory. For the 1.0 CU fuel, the experimental data follow the ohmic theory. Bustin's theory and a wealth of experience have shown that 30 seconds relaxation time is sufficient to remove most of the charge on a fuel regardless of its conductivity.

For practical purposes, neither Bustin's hyperbolic theory nor the ohmic equation are entirely satisfactory for predicting the rate at which the charge on a fuel will decay. Bustin's theory is inadequate because it requires the use of an unavailable quantity, namely, the ionic mobility, for its solution. With the ohmic theory, the rest conductivity, i.e., the conductivity of the fuel obtained in a weak electrical field (20), is used to calculate relaxation times. Experience

has shown that when fuel is in a highly charged condition, e.g., when emerging from a filter separator, the charge may relax at a faster or a slower rate than predicted from its rest conductivity. According to the data in Figure 10, the effective conductivity of the fuel may differ by a factor of 10 or more from the rest conductivity. Thus, in many cases, rest conductivity provides only a rough indication of the actual charge relaxation behavior of a fuel. However, at present, electrical conductivity is the only measurable quantity that provides any sort of correlation with electrostatic behavior, albeit an imperfect correlation.

It should also be pointed out that the conductivity of hydrocarbon fuels is not a constant but rather increases with temperature, as shown in Figure 11. Thus, in predicting relaxation behavior of a fuel, it may be necessary to apply a correction factor if the temperature of the fuel in question is considerably different from the temperature at which the rest conductivity was measured. The data in Figure 11 indicate that the conductivity of turbine fuels doubles with a temperature increase of 40-50°F.

The amount of charge on the fuel when it arrives at the tank of the aircraft depends on the conductivity of the fuel, the rate at which the charge is generated in the filter and on the residence time of the fuel in the hose downstream of the filter and in the piping of the aircraft (Figure 2). Measurements of the field strengths developed inside of a simulated aircraft fuel tank while being filled with kerosine and JP-4 fuel are shown in Figure 12. The data indicate that the field strength passes through a maximum when the fuel conductivity is between 1-2 CU. Other tests involving a mock up of a Vickers Vanguard

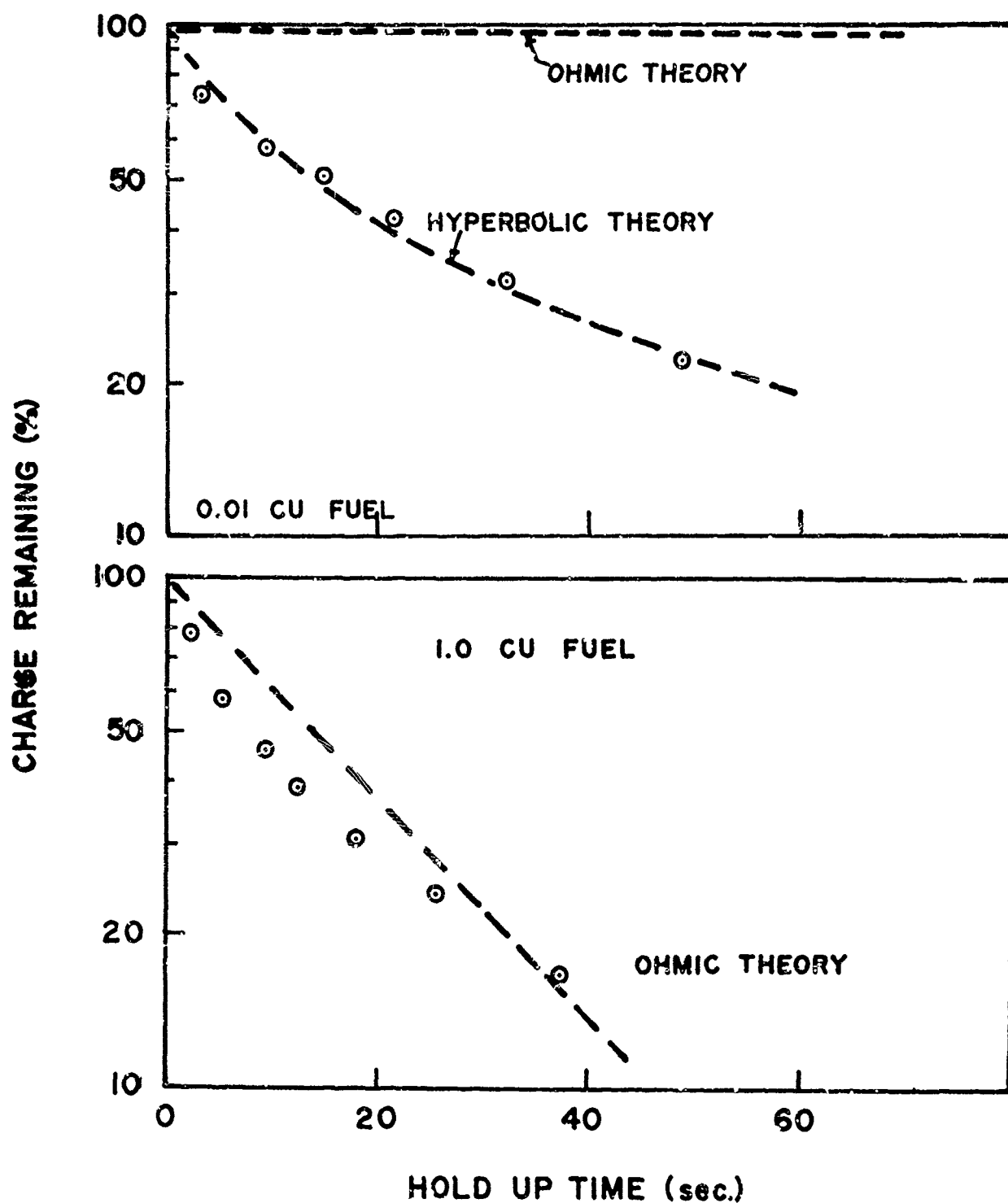


Fig. 9 - Comparison of hyperbolic and ohmic theories in predicting charge relation for fuels with conductivities of 0.01 and 1.0 CU.



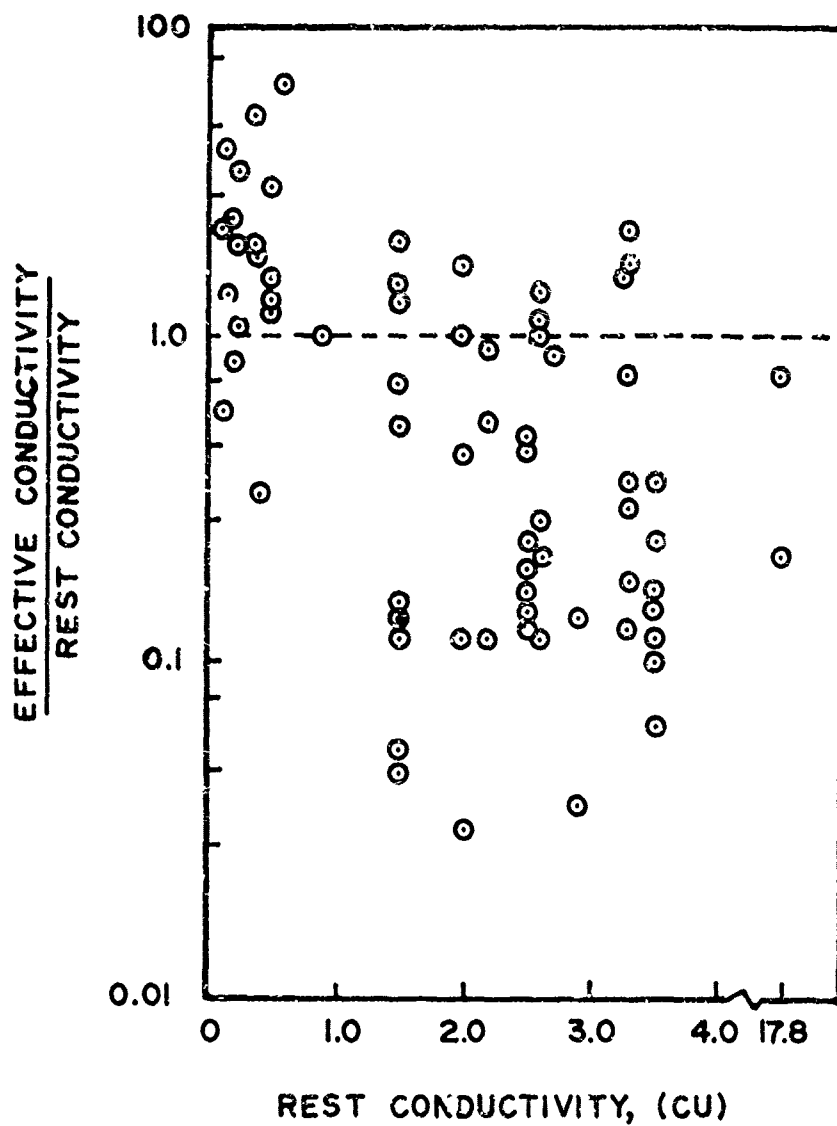


Fig. 10 - Comparison of rest and effective conductivities (4).

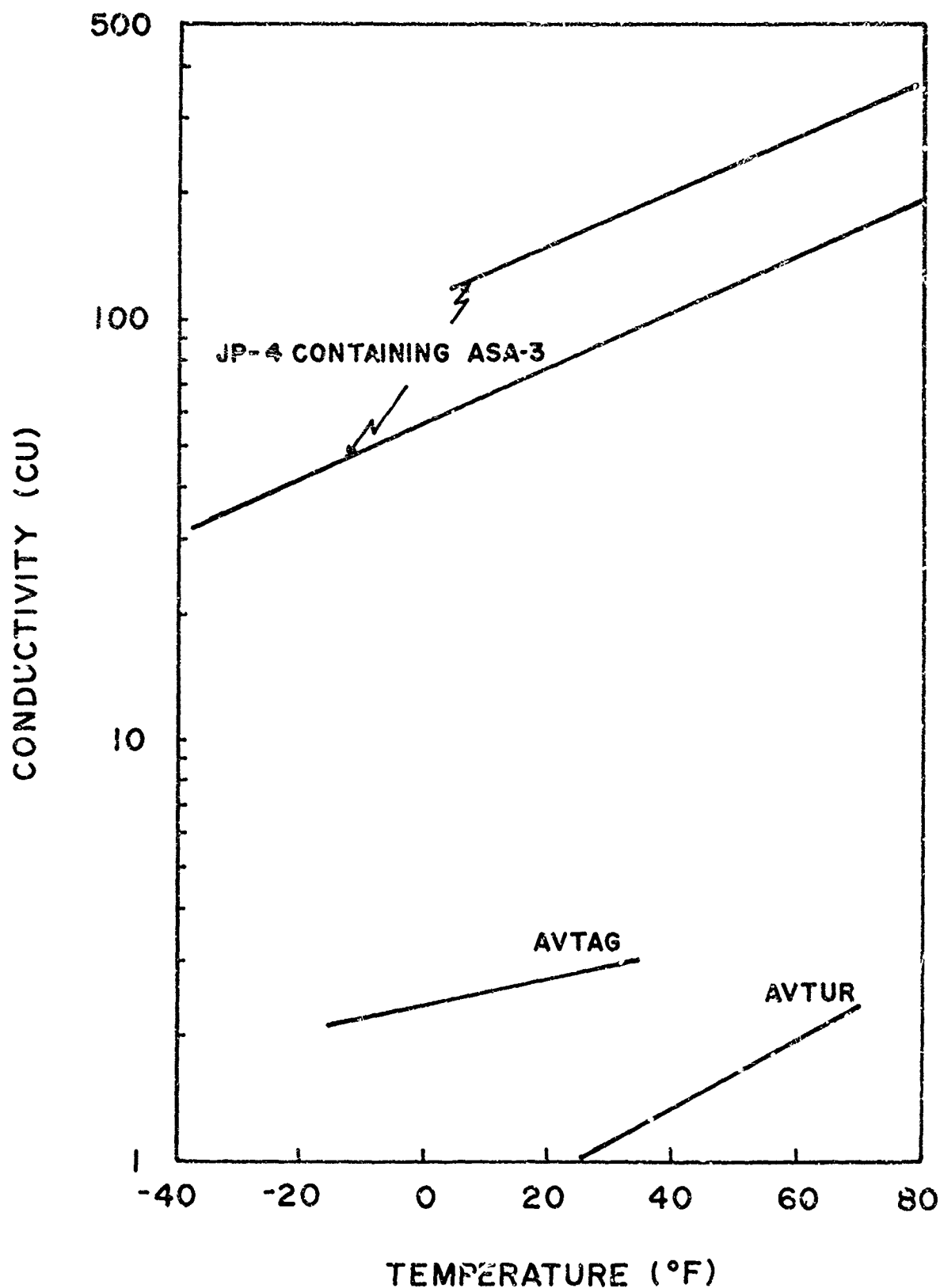


Fig. 11 - Conductivity as a function of temperature for fuels containing ASA-3 (53) and without ASA-3 (7).

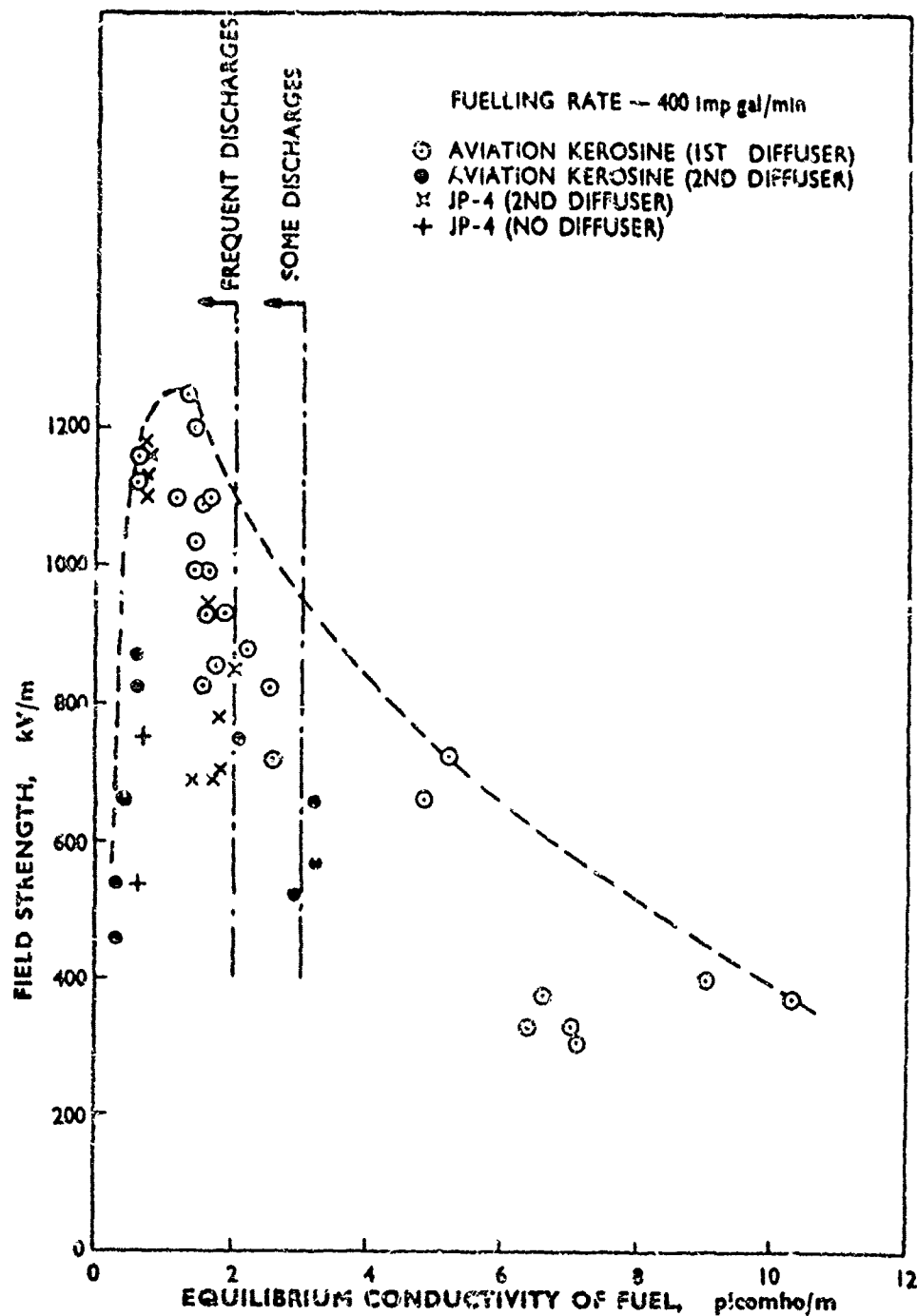


Fig. 12 - Field strength in a simulated fuel tank as a function of fuel conductivity (7).

wing tank show maximum field strengths when the fuel conductivity is in the range of 4-8 CU (Figure 13), with a considerable variation in the field strength levels occurring in adjacent compartments (7). Obviously, field strength measurements are highly dependent on the location and configuration of the tank as well as on the position of the field meter. It will also be noted from a comparison of Figures 12 and 13 with Figure 7 that although the charging tendency of the fuel passes through a maximum when the conductivity is above 10 CU, the maximum field strength in the receiving tank is attained when the fuel conductivity is below 10 CU. The reason, of course, is that although high levels of charge may be generated at the filter when the conductivity of the fuel is above 10 CU, most of this charge relaxes during the few seconds that it takes for the fuel to travel to the tank of the aircraft.

#### DISCHARGES IN AIRCRAFT FUEL TANKS

As stated above, discharges can occur in aircraft fuel tanks if the local potential caused by the charged fuel exceeds the breakdown value for the vapor space. Actually, two modes of discharge are possible as illustrated in Figure 14: one involving a low energy corona or spark discharge from the fuel surface to some grounded projection, and the other, a high energy spark discharge from some unbonded charge collector in the tank. The latter is far more dangerous since the entire amount of charge stored in the unbonded collector is released in a single discharge. By contrast, discharges from a fuel surface involve only a limited area due to low conductivity of the fuel. Tests have shown that when an unbonded charge collector is introduced into a simulated aircraft fuel tank, incendiary spark discharges can take place under

conditions which failed to produce an ignition in the absence of the charge collector (12). Fortunately, unbonded charge collectors are seldom found in aircraft fuel tanks and consequently discharges of this type seldom occur.

If the tank is nearly empty, the inlet device can also serve as the grounded electrode for discharges. Spark discharges to the inlet device during the early stages of filling have been reported as being particularly difficult to suppress (21). However, once the inlet device is covered by the fuel, localized internal discharges in the vicinity of the inlet are of no consequence since they take place under the fuel surface.

The type of discharge that occurs from the fuel surface, i.e., whether spark or corona, depends on the configuration of the electrodes and the field strength (22). Since in the case in question, one of the electrodes is some grounded part of the tank, the configuration of this electrode can vary from a sharp point, as illustrated in Figure 14, to a flat plate as represented by the wall or top of the tank. The other electrode, the fuel surface, may also vary from a flat surface to an unspecified radius of curvature if a foam happens to be present. In the extreme case where both electrodes (the fuel surface and the roof of the tank) resemble parallel plates, the electric field between them is homogeneous and a spark discharge will occur if the field strength is high enough. Most of the time, however, one or both of the electrodes will have a small radius of curvature resulting in an inhomogeneous electric field. If, for example, one of the electrodes is pointed and the other a plate, the field will be intensified around the point and drop off sharply towards the plate. At fairly low field strengths, (ca 200 kV/m) a bluish glow accompanied by an audible hiss,

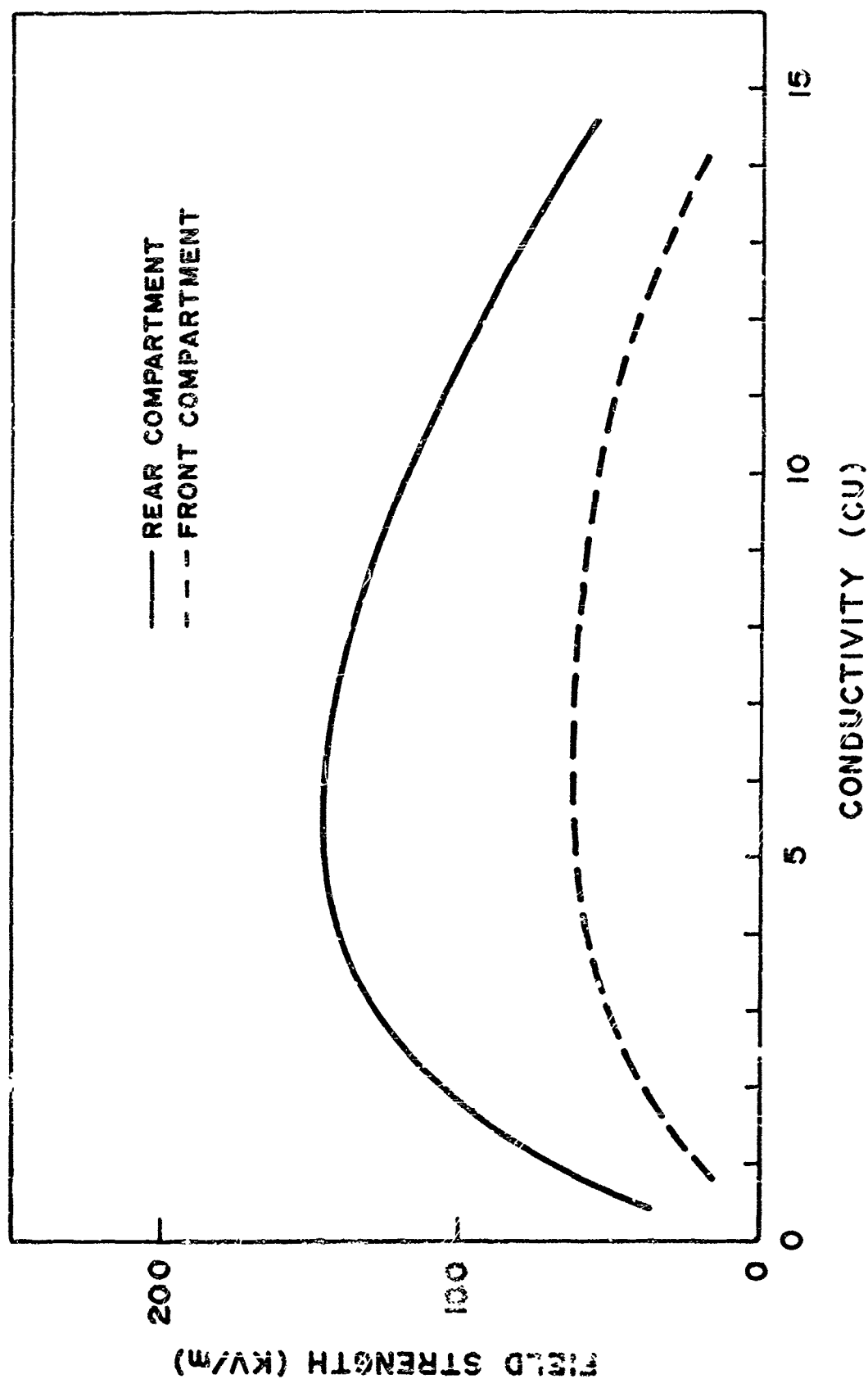


Fig. 13 - Comparison of field strength measurements in adjacent compartments of a Vickers Vanguard wing tank as a function of fuel conductivity.

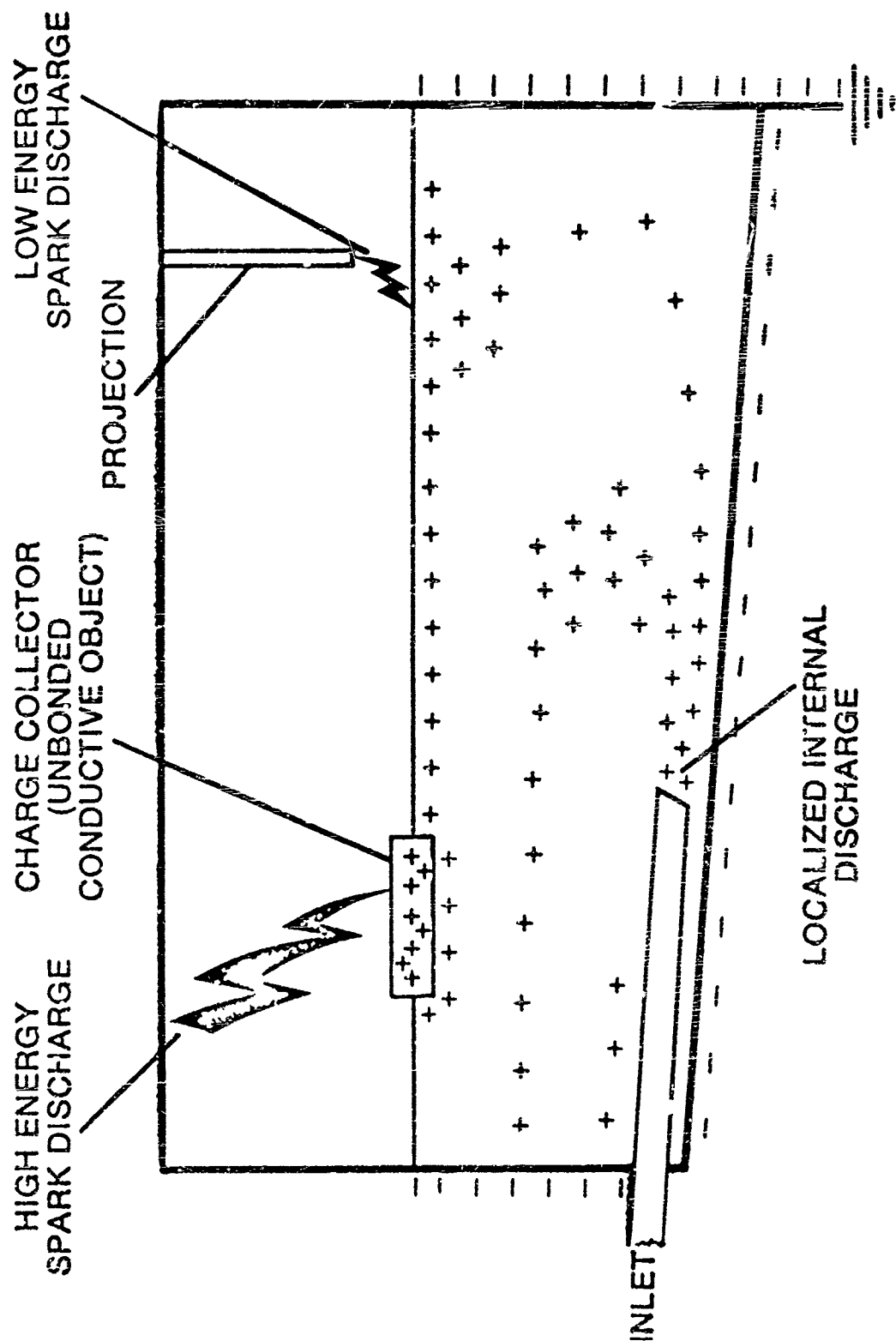


Fig. 14 - Sources of static discharge in a tank (12).

both of which are characteristic of corona discharges, can be seen on the pointed electrode. As the field strength is increased, the intensity of the corona increases up to a point, then becomes silent before passing over to a spark discharge. Thus, depending upon conditions, either corona or spark discharges may be obtained from pointed electrodes.

Due to the limited current supply, corona discharges from a fuel surface usually occur as short bursts, like sparks (9). Each burst is made up of a multiplicity of low energy (ca 20-40  $\mu$ J) discharges which occur at a high frequency (15-80 discharges/sec.) (22). Due to their low energy, corona discharges are generally considered to be non-incendiary. In fact, it has even been suggested that pointed electrodes be placed inside of fuel tanks as a means of harmlessly reducing excess charge on the fuel. However, corona discharges can become incendiary if the current is sufficiently high (23). Also, spark discharges having energies of the order of 0.27 mJ have been reported between a fuel surface and a pointed electrode at small gaps (22). Therefore, in view of their potential incendiary character, corona discharges can not be considered as an entirely safe mechanism for dissipating charge from a fuel surface.

In addition to corona, another type of discharge from a fuel surface, namely a prebreakdown streamer, has been identified (22). The streamers resemble spark discharges in that they are single, discrete discharges and are visible in a darkened room. However, at a given gap width, streamers have only about 1/37 of the energy of a spark discharge and hence are less likely to cause an ignition. More complete descriptions of discharges from a fuel surface may be found in (references 9, 21 and 22).

A typical plot showing the field strength developed inside an aircraft

fuel tank during fueling is presented in Figure 15. The field strength reaches a maximum when the tank is filled and then begins to decrease. The second peak corresponds to a localized condition in which a patch of highly charged fuel reaches the surface. Although the field strength inside of the tank usually reaches a maximum when the tank is filled or shortly thereafter, it doesn't follow that the maximum sparking hazard occurs at this time. Quite the contrary, since in at least two of the incidents involving commercial jet aircraft, explosions occurred during the first half of the filling operation. Also, as mentioned above, in simulated aircraft tank studies, discharges were reported during the early stages of filling (21). The reason for the discrepancy is that the field of vision of the field strength meter includes areas of low and high charge. The meter displays the average field strength within its field of view, not the minimum or maximum. Thus, it is not surprising that although the breakdown value for a spark discharge in air is 3000kV/m, visible sparks having an energy of 0.1 mJ were recorded during a simulated aircraft fueling at a field strength of only 15 kV/m (4). Coincidentally, almost all instances of lightning triggered by man, either accidentally or by design, involve the introduction of a long electrical conductor into a thundery environment where the general electrical field is around 10 kV/m (24). It would appear then that field strength measurements provide a poor indication of hazard during aircraft fueling since the meter obviously does not record what is happening at the time and place where spark breakdown occurs. However, these measurements are of considerable importance in evaluating the relative merits of various methods of reducing electrostatic hazard such as relaxation devices and antistatic additives.

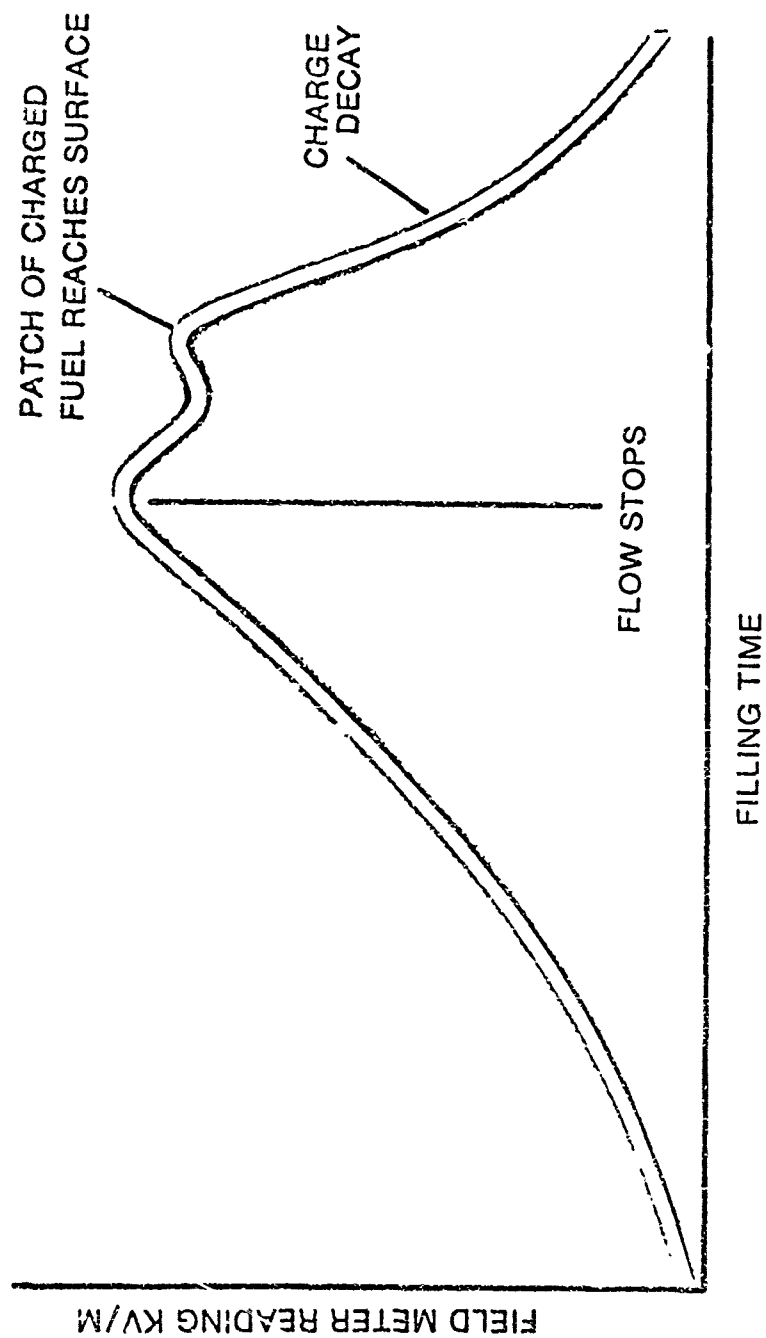


Fig. 15 - Field strength in tank during filling (12).



It has been established in numerous tests carried out in simulated (4,7,9,10,12,21,22,25-35) and in actual aircraft tanks (36-38), that electrical discharges can and do occur during aircraft fueling. In view of the tremendous number of aircraft fueling operations that are carried out daily on a world-wide basis, it seems logical to inquire at this point as to why more explosions have not occurred. Before attempting to answer this question, it is necessary to consider the conditions under which a spark can cause an ignition, which are: (a) the discharge must have sufficient energy, and (b) it must take place in the presence of a combustible fuel/air mixture. The minimum amount of energy required for a spark discharge to ignite an optimum fuel/air mixture under ideal conditions is 0.26 mJ (39). By optimum fuel/air mixture is meant the most easily ignited mixture of fuel in air and ideal conditions refer to glass-flanged metal electrodes at a gap of 0.2 in. As conditions depart from ideality, the energy requirements increase. Thus, changing the fuel/air mixture, the electrode geometry or the gap distance will increase the amount of energy required for ignition. Also, substitution of a high resistivity material, such as a hydrocarbon fuel surface, for one electrode increases the energy requirements for ignition. Thus, the amount of energy required for a discharge from a fuel surface to ignite a propane/air mixture was reported to be 4.7 mJ, twenty times the energy required to ignite the same mixture with a spark discharge between two metal electrodes (40). Although 4.7 mJ may not be the absolute minimum ignition energy for a discharge from a fuel surface, it is apparent that the minimum must be in the range of 0.26 to 4.7 mJ. If so, then the minimum ignition energy for a discharge from

a fuel surface is not quite as high as previously supposed.

In addition to possessing sufficient energy, it is necessary for ignition that the spark discharge take place in the presence of a flammable fuel/air mixture. As suggested in Figure 16, not all fuel/air mixtures can be ignited. Instead, there is a definite concentration range over which mixtures of each hydrocarbon in air will burn. This is called the flammable range. For a material such as n-octane, a hydrocarbon found in jet fuels, the flammable range extends from 0.92 to 6.5 percent of n-octane in air. If the upper limit of this range is exceeded, the mixture becomes too rich in hydrocarbon to be ignited. Likewise, if the fuel vapor concentration falls below the lower limit, insufficient hydrocarbon is present in the vapor space to sustain combustion. Since the amount of hydrocarbon present in the air is proportional to the temperature, the flammable range can also be expressed in terms of temperature limits. Figure 17 presents the temperature-flammability limits for several common fuels. The areas described by the double-headed arrows represent the flammable ranges for the individual fuels. Avgas, for example, is seen to be in the flammable range from -40 to 20°F. Above 20°F, equilibrium mixtures of Avgas in air are too vapor-rich to be ignited. For JP-4, the flammable range extends from -35 to approximately 75°F. Above 75°F, JP-4 passes into the vapor-rich region. For kerosene, the lower flammability limit corresponds to about 110°F, and for JP-5, it is 140°F.

The temperature-flammability limit concept applies only to situations in which the liquid fuel is in equilibrium with its vapor. Consequently these limits should be used only to estimate the composition of a fuel/air mixture in a quiescent tank. At best, they can

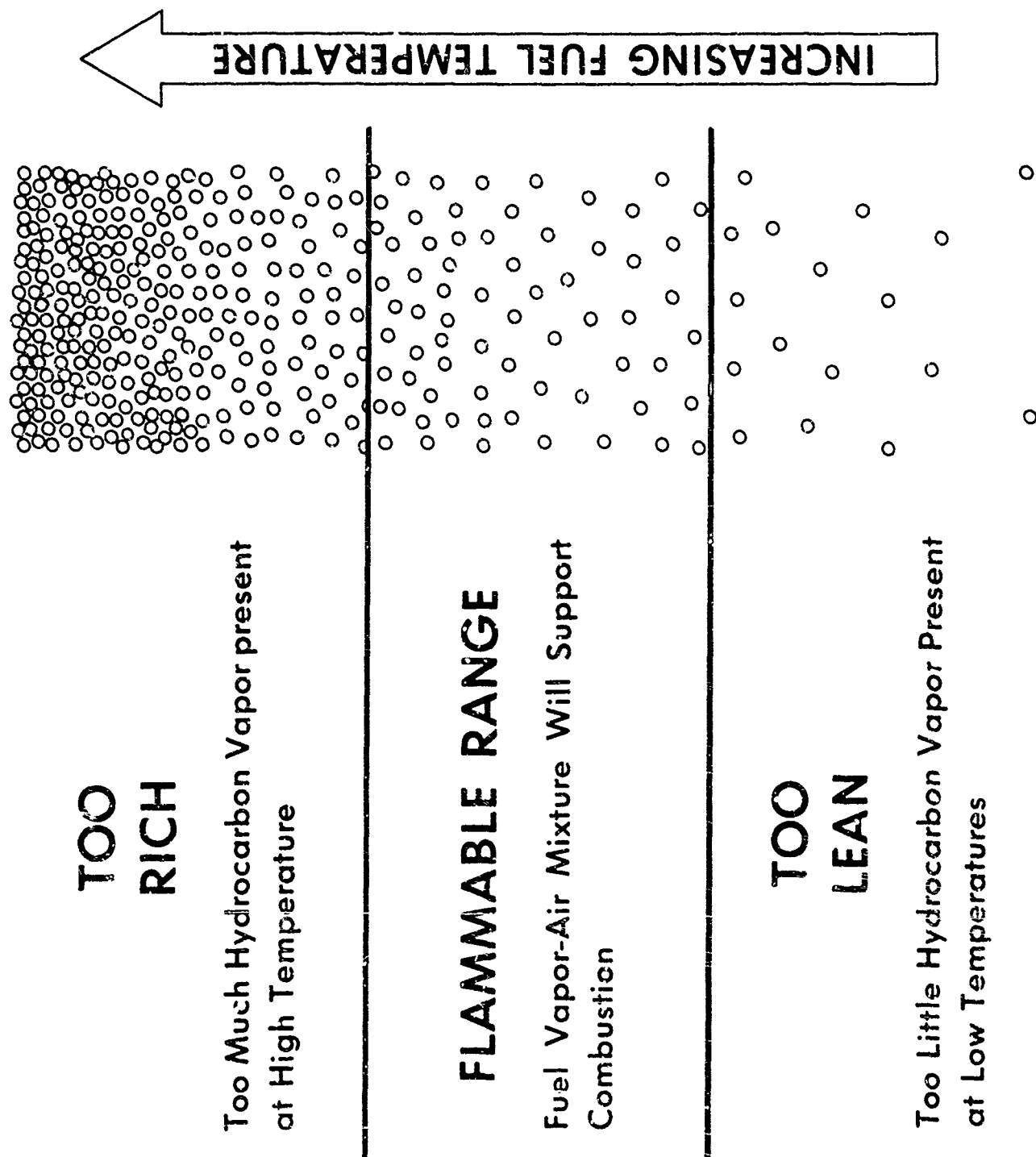
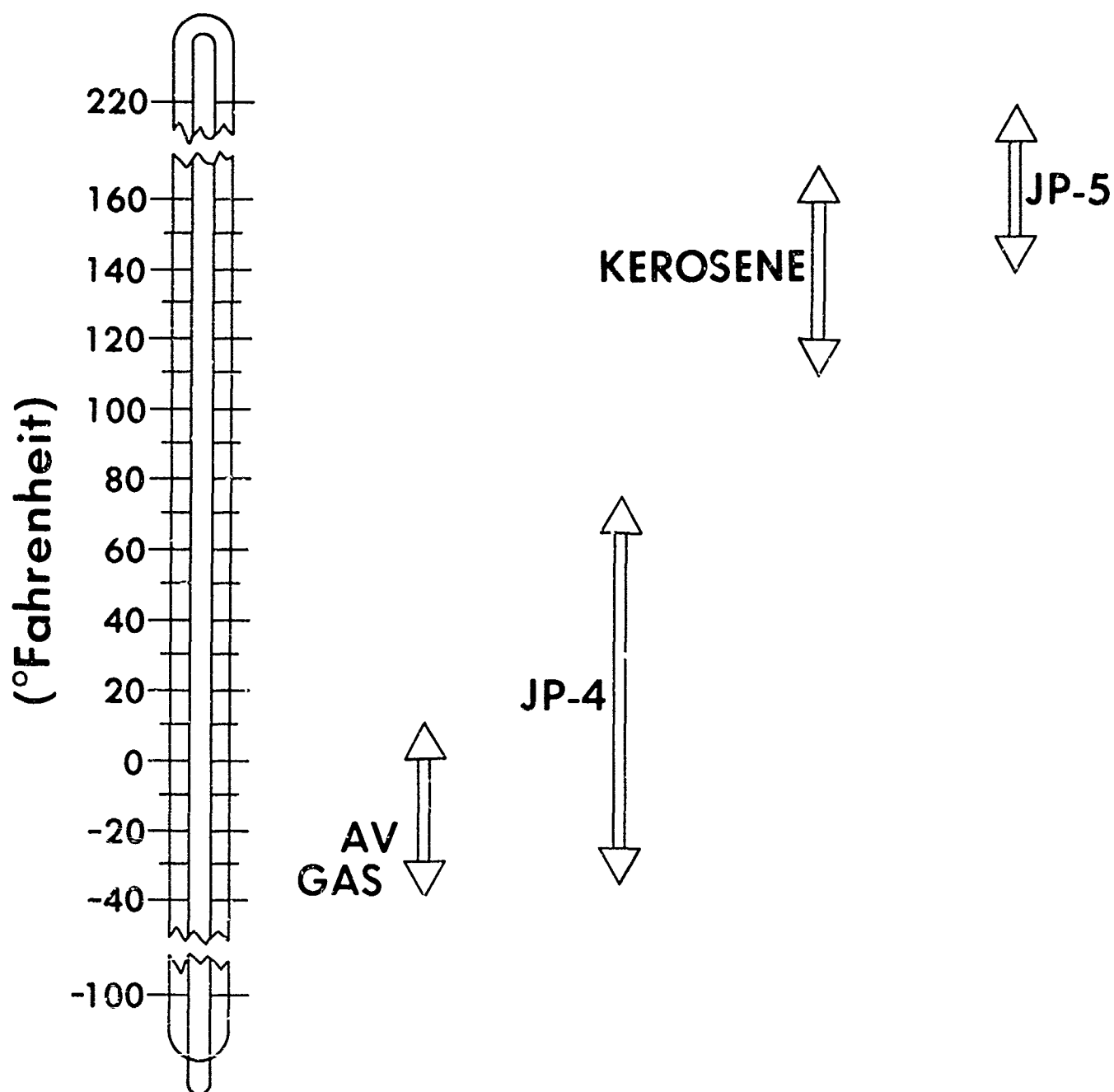


Fig. 16 - Flammability concept.



## TEMPERATURE-FLAMMABILITY LIMITS\* FOR COMMON FUELS

\*Fuel temperature range at sea level within which the vapor in equilibrium with the fuel will form a flammable mixture with air.

Fig. 17 - Temperature flammability limits for common fuels.

serve only as a rough guideline in describing the situation that exists inside an aircraft wing tank during refueling. In practice, these conditions may vary widely from ideality. With kerosene, for example, "flammable" fuel/air mixtures can be produced during fueling at temperatures far below the lower flammability limit for that fuel. In this case, however, the flammable mixtures consist of a foam or mist generated by the splashing action of the fuel or by the fuel inlet valve if it is not submerged.

As shown by the data in Figure 18, the energy requirements for fuel mists or sprays are considerably in excess of the minimum ignition energy of 0.26 mJ. It is interesting to note that in the three explosions that occurred during the fueling of commercial jet aircraft, kerosene was ignited at temperatures far below its flash point.

#### SOLUTIONS

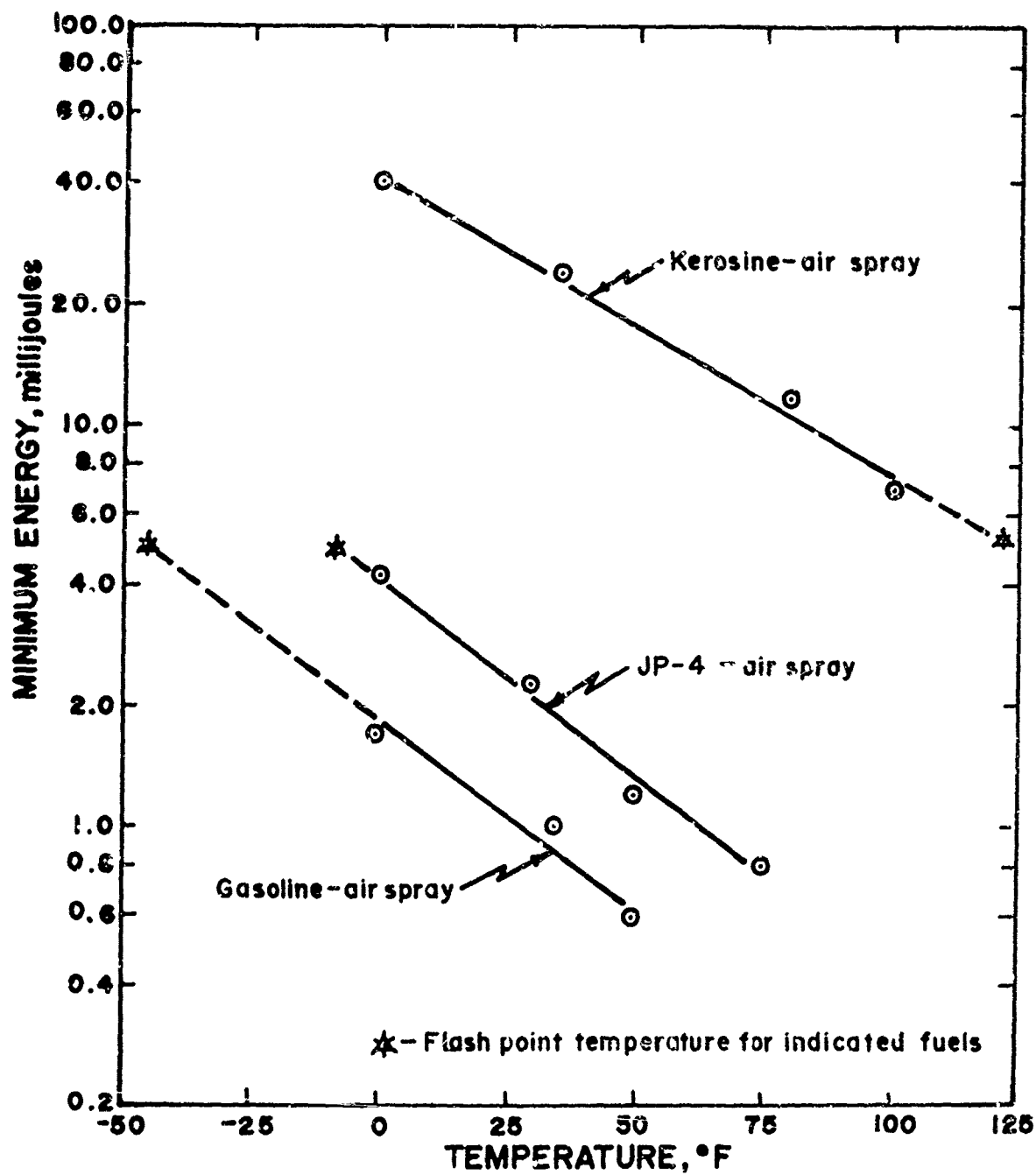
The following solutions have been proposed to reduce or eliminate the electrostatic hazard during aircraft fueling:

1. Inerting the vapor space of the tank with nitrogen or other inert gases.
2. Installation of charge reduction devices.
3. Removal of the final filter/separator.
4. Reduction of flow rates.
5. Use of a static dissipator additive.

Obviously, inerting the vapor space would eliminate the possibility of ignition not only during fueling but also in the event of a lightning strike as well. This solution would require the installation of additional equipment such as cryogenic tanks to

store liquid nitrogen aboard the aircraft plus a dispensing system to ensure that the tanks were continually purged with the inerting gas. The FAA is currently investigating tank inerting with liquid nitrogen (42) and the Air Force is considering the use of catalytic combustor techniques as an alternative method of inerting (43). Other procedures, such as the use of reticulated polyurethane foam to serve as an in situ flame arrestor, and the installation of a rapid release halon fire extinguishment system are being investigated as a means of solving the total fire hazard problem in fuel tanks of which electrostatic ignitions are only a part (44).

At present, there are three devices for reducing electrostatic charge on fuel: the AO Smith Static Charge Reducer [SCR] (14), a 30-second relaxation tank and a new experimental device called the de Gaston Decharger (45). The SCR consists of a 10-inch-diameter pipe, 3 ft. in length containing a 2-inch polyethylene liner through which several rows of sharply pointed electrodes protrude. Passage of the highly charged fuel over the grounded electrodes produces a corona discharge which lowers the charge on the fuel. It has been demonstrated by a number of workers (15, 46-49) that the SCR can reduce the charge generated by a filter/separator during tank truck and fueler loading to less than  $30 \mu\text{C}/\text{m}^3$ , which is reported to be the threshold for incendiary discharges in these tanks (50). Sparking may take place when the charge density is below  $30 \mu\text{C}/\text{m}^3$ , but the energy of these discharges is considered to be insufficient to cause ignition. For safety, a value of  $15 \mu\text{C}/\text{m}^3$  is suggested. The threshold for incendiary discharges in aircraft tanks is not known. Due to variations in size, shape, complexity and inlet configurations found in aircraft fuel tanks, no single value



Minimum spark ignition energies for fuel-air spray mixtures

Fig. 18 - Minimum spark ignition energies for fuel/air spray mixtures (41).

for maximum allowable charge density is likely to be found which will cover all aircraft under all conditions unless it is the minimum value required to initiate sparking in the most spark-prone tank. In simulated tank studies, spark discharges were detected when the charge density on the incoming fuel was as low as  $68 \mu \text{C}/\text{m}^3$  when fueling through a single inlet (12). However, the energy of these discharges was less than 0.06 mJ which is far below the minimum ignition energy for hydrocarbon vapors. Elsewhere, a charge density of approximately  $180 \mu \text{C}/\text{m}^3$  was indicated as the threshold for sparking in a simulated fuel tank (21). The FAA is currently sponsoring a survey of fueling facilities at 10 major airports in the United States to determine typical charge densities on turbine fuel being delivered to aircraft. Still lacking is a reliable correlation between incoming charge density and the onset of incendiary discharges in aircraft fuel tanks.

Another type of charge relaxation device is the 30-second relaxation tank. This device is merely a vessel, usually equipped with baffles, and designed to hold up the fuel for 30 seconds to allow the charge to relax before proceeding through the rest of the system. A recent study showed the SCR and the relaxation tank to be equally effective in reducing charge density on fuels over the conductivity range of 0.1 to 10 CU (15).

The most recently proposed charge relaxation device is the de Gaston Decharger. This device, which is still in the experimental stage of development, consists of a chamber containing a radioactive source to ionize the fuel and render it temporarily more conductive.

For maximum effectiveness, all three relaxation devices have to be located as close as possible to the skin of the aircraft in order to minimize charge generation downstream

of the device. Presumably the SCR could be located on a refueler or hydrant cart but a relaxation chamber capable of providing 30 seconds of relaxation time at flow rates in excess of 600 GPM could hardly be considered portable. It would be premature to comment on the requirements of the de Gaston Decharger at this time. However, due to the weight of the shielding necessary for the radioactive source, it appears that the decharger would also have to be part of a fixed installation.

Reducing the flow rate and/or eliminating the final filter/separator would be unacceptable remedies in view of the requirements for clean dry fuel and minimum turn around times for today's super jets. The benefits to be gained from either of these solutions would be too uncertain to justify the hardships that they would impose.

Finally, the most widely used method of reducing electrostatic charge on hydrocarbon fuels is the addition of the static dissipator additive, ASA-3. The additive is a mixture consisting of equal parts of the chromium salt of an alkylated salicylic acid, calcium disulpho-succinimide and a vinyl/methylacrylate copolymer (51). Since it contains ionic materials, ASA-3 actually increases the charging tendency of fuel in the filter as shown in Figure 7. Other contaminants such as asphaltenes and crude oils (1), Navy Special Fuel Oil (52), oxidized asphalt (12), as well as polar and ionic compounds (16) have a similar effect, again depending on the conductivity of the original fuel. The important point is that as long as the conductivity of the fuel is greater than 50 CU, the charge generated in the filter will dissipate in less than 1/2 second. Thus, in a typical aircraft fueling operation where the residence time of the fuel

in the hoses and piping downstream of the filter is only a few seconds, most of the charge on a fuel containing ASA-3 will dissipate before the fuel reaches the tank provided that the conductivity is greater than 50 CU. Tests in a simulated aircraft fuel tank have confirmed that spark discharges do not occur if the fuel conductivity is above 50 CU (21). Less than 1 ppm of ASA-3 is all that is required to bring the conductivity of a fuel to this level.

After a rather extensive test program by the National Research Council of Canada (53), ASA-3 was introduced into Royal Canadian Air Force fuels on a trial basis in 1962, and became mandatory in Canadian Government Specifications for aviation kerosene and JP-4 in 1964 (4). Also in 1964, the International Air Transport Association revised its Fuel Guidance Material to include the use of ASA-3. The British Ministry of Technology adopted the use of the additive in aviation kerosene in 1968. At present, Canadian and British specifications and IATA guidance material require that sufficient additive be used to ensure that the conductivity of the fuel at the time, place and temperature of delivery to the aircraft is in the range of 50-300 CU (54). A more recent issue of the Canadian Specification will require that the conductivity be in the range of 100-500 CU at 20°C (54).

By 1971, over 10 billion gallons of aviation turbine fuel containing ASA-3 were delivered at over 150 airports throughout the world. In addition, much of the aviation gasoline sold in Canada for some years has contained the additive (4). So far, no significant problems have occurred during the handling or use of fuels containing ASA-3 (4,51). A joint study involving nine oil companies and seven international airfield fueling installations in Europe, the

Middle East and the Far East did not reveal any significant adverse effects on the performance of filter/separator units by fuel containing ASA-3 (4). However, in another test conducted in the United States involving a side by side comparison of filter elements with fuel containing the ASA-3 vs fuel without the additive it was concluded that after a throughput of 200,000 gal./element, element life was reduced somewhat on fuel containing ASA-3 (55).

Depletion of the additive resulting in lowering of fuel conductivity during marine and pipeline shipment has been reported in one study (56) indicating that reinjection of the additive at the airport storage facility may be necessary. Also, since clay filters tend to remove ASA-3, it would be necessary to inject the additive downstream of the clay at airports employing this type of filtration. Concern over depletion, the effect of the additive on the water separation properties of jet fuel and on filter element life, as well as the necessity for making fuel conductivity measurements along the distribution system and at the airport have been the major stumbling blocks to the use of the additive in the United States.

#### CONCLUSIONS

It has been established that, in the absence of protective measures, electrostatic discharges can take place in the vapor space of aircraft fuel tanks during fueling. The fact that these discharges seldom result in fires or explosions can be attributed to the following factors:

- (1) Fuel - With the exclusion of the military, most of the free world's aircraft operate on either kerosene or aviation gasoline, neither of which happens to be in the flammable range at normal fuel handling temperatures (20-100°F). Thus, even if a discharge

should take place while fueling an aircraft with either of these fuels, an ignition would not occur, provided, of course, that the fuel is present as a vapor and not as a mist. When, as a result of improper design or location of inlet devices, either of these fuels enters a tank in the form of a mist or spray, then the resulting fuel/air mixture can be ignited at normal fuel handling temperatures. However, the amount of energy required to ignite fuel mists is considerably greater than the amount required to ignite the same material in the form of a vapor. Tests in simulated and actual aircraft fuel tanks have shown that discharges from a fuel surface seldom have sufficient energy to ignite fuel mists.

Where wide-cut (JP-4) fuel is used, it must be assumed that most of the time the fuel/air mixture in the tank is in the flammable range during fueling. The fact that more ignitions have not occurred when handling this fuel would seem to indicate that other factors, such as the effect of tank configuration on discharge energy, have an overriding influence.

(2) Structure of the fuel tank - Aircraft fuel tanks usually contain structural members, stringers, pumps, probes and other protuberances which encourage low energy corona and pre-breakdown streamer discharges rather than more energetic sparks. In this manner it is believed that much of the charge on the fuel surface is dissipated during fueling without causing an ignition. Even when spark discharges do occur from the fuel surface, they usually do not have sufficient energy to cause an ignition. This is because the amount of energy released in a discharge from a fuel surface per unit length of time is limited by the electrical properties of the fuel. Also due to the high resistivity of the fuel, only a limited area of the

fuel surface can participate in the discharge. These factors tend to reduce the incendiary potential of spark discharges from a fuel surface.

(3) Use of the static dissipator additive - It has been shown that when used at the proper concentration, the static dissipator additive completely eliminates electrostatic discharges during fueling. Since approximately 50% of the aviation fuel sold outside of the United States now contains ASA-3, part of the credit for reducing the incidence of electrostatic ignitions during fueling must be due to the additive.

#### REFERENCES

1. A. Klinkenberg and J. L. van der Minne, "Electrostatics in the Petroleum Industry," Elsevier, Amsterdam, 1958.
2. K. C. Bachman and A. H. Popkin, "Tank Truck Incidents Attributed to Static Electricity, 1960-1969." Report No.: RL-72M-69, Esso Research and Engineering Co., Linden, N. J., Sept. 30, 1969.
3. K. C. Bachman, W. G. Dukek and A. H. Popkin, "Aircraft Incidents Attributed to Static Electricity, 1959-1969." Report No.: RL-45M-69, Esso Research and Engineering Co., Linden, N. J., July 21, 1969.
4. H. Strawson and A. Lewis, "Electrostatic Charging in the Handling of Aviation Fuels," in "AGARD Conference Proceedings No. 84 on Aircraft Fuels, Lubricants and Fire Safety." NATO Advisory Group for Aerospace Research and Development, Nevilly-Sur-Seine, France, 1971, p. 19-1.
5. W. M. Bustin "Static Electricity Studies, Marine Operations," Esso Research and Engineering Co., Linden, N. J., Nov. 9, 1962.



6. D. Van Der Maer, "Electrostatic Charge Generation During Washing of Tanks With Water Sprays - I: General Introduction," in "Static Electrification, 1971." Institute of Physics, London, 1971, p. 153.

7. E. F. Winter, "The Electrostatic Problem in Aircraft Fueling," J. Roy Aeronaut Soc. 66, 429-46, (1962).

8. E. F. Winter, A. Lewis and R. G. Larsen, "Fuel-Handling Problems in the Jet Age," in "Advances in Petroleum Chemistry and Refining." Interscience Publishers, New York, 1963, Vol. VII, p. 137.

9. A. Klinkenberg, "Theoretical Aspects and Practical Implications of Static Electricity in the Petroleum Industry," in "Advances in Petroleum Chemistry and Refining." Interscience Publishers, New York, 1964, Vol. VIII, p. 87.

10. L. Gardner, "The Generation of Static Electricity During Aircraft Refueling," Can. Aero. and Space J. 10, 193, (1964).

11. Maxwell Smith, "Static" in "Aviation Fuels." G. T. Foulis and Co., Ltd., Henley-on-Thames, 1970, p. 181.

12. K. C. Bachman and W. G. Duke, "Static Electricity in Fueling Supercjets," Esso Research and Engineering Co., Linden, N. J., January, 1972.

13. J. T. Leonard and H. W. Carhart, "Effect of Conductivity on Charge Generation in Hydrocarbon Fuels Flowing Through Fibre Glass Filters," J. Colloid and Interface Science 32, 383, 1970.

14. "Generation, Measurement and Reduction of Static Electricity in the Handling of Petroleum Products," AO Smith Meter Systems Division, Erie, Pa. May, 1969.

15. J. T. Leonard and H. W. Carhart, "Reduction of Electrostatic Charge in Jet Fuels During Refueler Loading," NRL Report 7415, Naval Research Laboratory, Washington, D. C., June 20, 1972.

16. H. D. Goodfellow and W. F. Graydon, "Dependence of Electrostatic Charging Currents on Fluid Properties," Can. J. of Chem. Eng. 46, 342 (1963).

17. J. T. Leonard and H. W. Carhart, "Effect of Static Dissipator Additive on the Charging Tendency of Jet Fuels," NRL Report 6952, Naval Research Laboratory, Washington, D. C., November 12, 1969.

18. K. J. Marsh, "Field Measurements of the Generation of Static Electricity During Routine Fueling of Aircraft." Paper presented at the API Mid-Year Meeting, Montreal, 1965.

19. W. M. Hustin, I. Koszman and I. T. Tobye, "New Theory For Static Relaxation in High Resistivity Fuel," Hydrocarbon Process 43, 209 (1964).

20. "Proposed Method of Test for Electrical Conductivity of Aviation Fuels," in "1971 Annual Book of Standards, Part 17." American Society for Testing and Materials, Philadelphia, Pa., p. 1170.

21. C. Bruinzeel, "Electric Discharges During Simulated Aircraft Fueling," J. Inst. Petrol. 49, 473 (1963).

22. J. T. Leonard and H. W. Carhart, "Electrical Discharges From A Fuel Surface," in "Static Electrification. Institute of Physics and the Physical Society, London, May, 1967 p. 100.

23. M. M. Newman and J. D. Robb, "Investigation of Minimum Corona Type Currents for Ignition of Aircraft Fuel Vapors," National Aeronautics and Space Administration, Washington, D. C., 1960.

24. E. T. Pierre, "Triggered Lightning and Some Unsuspected Lightning Hazards," Naval Research Reviews XXV, No. 3, 14 (1972).

25. A. Klinkenberg, "Laboratory and Plant-Scale Experiments on the Generation of Static Electricity," Oil and Gas J. 55, No. 46, 204 (1957).

26. B. V. Poulston, "Static Electricity in Aircraft Fueling," Shell Aviation News, June, 1958.

27. W. M. Bustin, M. P. O'Neill, R. J. Scheverman and C. E. Schlecksler, "Static Electricity Studies on Distillate Fuels." Report No. EE-IT-58; EE-5R-58, Esso Research and Engineering Co., Linden, N. J., Sept. 8, 1958.

28. J. A. Carruthers, "Aviation Fuels Experiments on the Generation of Static Electricity in the Vanguard Fuel Systems Test Rig at Vickers Armstrong, Waybridge, May 9-10, 1959," Report No. 20,161, Project 104, British Petroleum Research Center, May, 1959.

29. "Electrostatic Discharges in Aircraft Fuel System - Phase I," Coordinating Research Council, New York, April, 1960.

30. C. Bruinzeel, C. Luttik, D. Wageraar, E. F. Winter, J. R. Hayden, H. Vernon, S. J. Vallenga, H. L. Dale and A. L. Ludwig, "Static Electricity in Aircraft Fueling; Tests on A Simulated Wing Tank." Thornton Research Centre Report M 206, Shell International Petroleum Co., Ltd., London, April, 1960.

31. J. W. Woodworth and C. Bruinzeel, "Electrostatic Discharge in Aircraft Fueling Operations," Convair Report ZK 026, Dec. 12, 1960.

32. "Electrostatic Discharges in Aircraft Fuel Systems - Phase II," CRC Report 355, Co-ordinating Research Council, Inc., New York, July, 1961.

33. D. N. Harris, A. L. Ludwig and G. Karel, "Electrostatic Discharges in Aircraft Fuel Systems," Paper 583B presented at the S.A.E. National Aerospace Engineering and Manufacturing Meeting, Los Angeles, October, 1962.

34. J. A. Carruthers and K. J. Wigley, "Estimation of Electrostatic Potentials, Fields and Energies in a Rectangular Metal Tank Containing Charged Fuel," J. Inst. Petrol. 48, 180 (1962).

35. J. R. Hayden and E. F. Winter, "Static Electricity in Aircraft Fueling - Tests on the Vickers VC-10 System." Thornton Research Centre Report M218, Shell International Petroleum Co., Ltd, London, May, 1962.

36. D. T. Rogers and J. C. Munday, "Static Electricity Studies in an Aircraft Fuel Tank." Report No. RL-4M-50, Esso Research and Engineering Co., Linden, N. J., November, 1960.

37. C. Bruinzeel, C. Luttik, S. J. Vallenga and L. Gardner, "A Study of Electrostatic Charge Generation During Low Temperature Refueling of Aircraft," Aeronautical Report IR-387, National Research Council of Canada, October, 1963.

38. C. Bruinzeel, C. Luttik and S. J. Vallenga, "Electrostatic Charging Tests on a DC-8 Aircraft," Royal/Dutch Shell, Amsterdam, May, 1963.

39. B. Lewis and G. von Elbe, "Combustion, Flares and Explosions of Gases," 2nd ed., Academic Press, New York, 1961, p. 323.

40. A. R. Lyle and H. Strawson, "Estimation of Electrostatic Hazards in Tank-Filling Operations," in "Static Electrification, 1971," Institute of Physics, London, 1971, p. 234.

41. I. Liebman, I. Spolan, J. M. Kuchta and M. G. Zabetakis, "Ignition of Tank Atmospheres during Fuel Loading Operations," Final Report No. 3914, U. S. Bureau of Mines, Pittsburgh, Pa., 1964.

42. T. G. Horeff, "FAA DC-9 Liquid Nitrogen Fuel Tank Inerting Program," in "Second Conference on Fuel System Fire Safety," Federal Aviation Administration, Washington, D. C., May, 1970, p. 193.

43. R. G. Clodfelter, "Fuel Tank Inerting Using Catalytic Combustion Techniques," in "Second Conference on Fuel System Fire Safety," Federal Aviation Administration, Washington, D. C., May, 1970, p. 141.

44. B. P. Botteri, "Flammability Properties of Jet Fuels and Techniques for Fire and Explosion Suppression," in "AGARD Conference Proceedings No. 84 on Aircraft Fuels, Lubricants and Fire Safety," NATO Advisory Group for Aerospace Research and Development, Nevilly-Sur-Seine, France, 1971, p. 13-1.

45. A. N. de Gaston, "Charge Removal by Irradiation," Paper presented at the SAE National Aerospace and Engineering Manufacturing Meeting, San Diego, Calif., Oct. 2-5, 1972.

46. G. A. Ciotti, "Reduction and Measurement Static Charge in Flowing Fluids," Natl. Safety News, November, 1969.

47. I. Ginsburgh, "Static Charge Reducer," J. Colloid and Interface Sci. 32, 424 (1970).

48. W. L. Bulkley and I. Ginsburgh, "Performance of Static Charge Reducer," SAE Paper 700277 presented at National Air Transportation Meeting, New York, N. Y., April, 1970.

49. C. R. Martel, "An Evaluation of the Static Charge Reducer for Reducing Electrostatic Hazards in the Handling of Hydrocarbon Fuels," Air Force Aero Propulsion Laboratory, WPAFB, Technical Repo. APL-TR-70-22, July, 1970.

50. W. L. Bulkley and I. Ginsburgh, "How to Load Distillates Safely," Hydrocarbon Processing 47, 121 (1968).

51. R. G. Davies and R. W. Knipple, "Experience with Static Dissipator Additive in Aviation Fuels," SAE Paper 700278 presented at National Air Transportation Meeting, New York, N. Y., April, 1970.

52. J. T. Leonard and H. W. Carhart, "Effect of Navy Special Fuel Oil on the Charging Tendency of Jet Fuel," NRL Report 6953, Naval Research Laboratory, Washington, D. C., November 12, 1969.

53. R. G. Davies and M. C. Attou, "RCAF Evaluation of ASA-3 Static Dissipator Additive: Flight Test and Supporting Test Programmes," CAE Report No. 61, Royal Canadian Air Force, April, 1964.

54. L. Gardner and R. B. Whyte, "Jet Fuel Specifications," in "AGARD Conference Proceedings No. 84 on Aircraft Fuels, Lubricants and Fire Safety," NATO Advisory Group for Aerospace Research and Development Nevilly-Sur-Seine, France, 1971, p. 1-1.

55. H. Poitz, "Evaluation of ASA-3 in the United Air Lines Turbine Fuel Handling System at Atlanta Airport," Shell Oil Co., January, 1970.

56. H. F. Jones and E. French, "An Evaluation of the Effectiveness of a Static Dissipator Fuel Additive After Transport in Full Scale Fuel Distribution System." Air Force Propulsion Laboratory, WPAFB, Technical Report AFAPL-TR-69-23, May, 1969.

# Ten Years' Experience of Anti-Static Additives in Aviation Fuels

A. Lewis, Shell Research Limited and  
J. G. Kirtley, Shell International  
Petroleum Company Limited.

## ABSTRACT

Fires and explosions in aircraft or refinery plant have been caused in the past by electrostatic discharges but have been overcome by the use of a conductivity improving additive. The additive works by speeding the relaxation of charges generated in pipelines or filters.

For ten years Shell's ASA-3 additive has provided adequate protection in systems used outside the United States without significant change in fuel quality or any difficulties in fuel handling. This experience involves some 24 million gallons of fuel supplied from over 200 airfields. Limited experience with multi-product pipelines outside the United States and extensive field trials in the USA have indicated that some depletion of the additive occurs, especially where clay filtration is used and that redoping may be necessary.

TEN YEARS AGO the first bulk supplies of aviation fuel were treated with anti-static additive (ASA-3) to increase their conductivity. Since then some 24 billion US gallons have been so treated without trouble. This is the solution adopted by Shell as a preventive measure against electrostatic explosions and fires caused when handling aviation turbine fuels and similar distillate products from refinery to customer and during aircraft fuelling. It is a system widely adopted outside the United States - and additives are used to a limited extent in the United States for non-aviation fuels.

Such an approach has proved over 10 years to be completely effective, very cheap (less than 0.01 c/USG) and the amount of additive used so small that it is of the same order as naturally occurring trace materials in fuels. We strongly recommend this additive approach be accepted universally, because it is obviously in the public interest and it is only when the system is universally adopted that the full advantages can be exploited in relation to the design and operation of fuel handling equipment and aircraft fuel systems.

Since the concentration of additive used is so low the total market for the additive will still be low even if applied universally (ca 75 tons per annum) and it is a doubtful commercial proposition in its own right. In the interests of safety, the additive is made available to any user without restriction.

## THE PROBLEM

It is now widely recognised that when hydrocarbon liquids are moved rapidly through pipes or through filters a separation of charges occurs to an extent depending upon the nature and concentration of ionisable traces in the fuel and upon the flow velocity.

The extent to which these charges accumulate depends upon the conductivity of the fuel and the time available for the charges to relax through the fuel's resistance and to some extent on the nature of the system through which the fuel flows. The potential hazard the accumulated charges represent will depend on the charge remaining in the fuel at the point at which the fuel can form a flammable mixture in contact with air.

### EXISTENCE OF FLAMMABLE ENVIRONMENT -

The curves relating flammability of the equilibrium atmosphere above static fuels to the temperature of the fuels are well known and there is little need to reprint them here. However, the practice of using mixtures of fuels of different volatility in the same aircraft is still current and on the ground the use of the same vehicle for transporting an involatile product immediately after a volatile one (i.e. switch loading) is practised in the USA and in Europe. Thus unless fuelling or loading procedures are varied to allow for the nature of the product being handled it is best to assume that a flammable atmosphere always exists. Even if the atmosphere is not brought into the flammable range by the presence of sufficient fuel vapour it is not possible to preclude always the formation of a flammable fuel mist from incautiously located fuel entry nozzles. The only saving grace in this event is that the energy required for ignition, is greater than for mixtures of air with fuel vapour.

Let us now update our understanding of the influence of handling conditions upon charge generation.

### CHARGE GENERATION - Effect of Flow Rate -

A decrease in flow rate of fuel through pipelines or filters will decrease the charge separation although the effect is by no means linear or consistent in pattern. Figure 1 shows a series of curves of charge density at filter outlet against flow rate. Tests by

Boeing at Minneapolis showed a more consistent pattern with almost proportionality, whilst other work by Esso, indicates a disproportionate effect of flow rate, but it should be remembered that these results also bring some charge relaxation downstream of the filters. However, in general it can be seen that in many cases it may be necessary to reduce the flow rate of the fuel to a very low level in order to reduce significantly the charge generation.

Effect of Filters - The curves in Figure 1 also show that differences between the charging propensities of different filters. The differences in charge generation of fuels depend upon trace compounds present in them and differential adsorption of some of these compounds onto the filter elements results in a variation in the effect of filters with different fuels. Leonard & Carhart (1)\* have tried to develop composite filters which would give a low or zero net charge output, but concluded that because of this interaction between fuel and filter the proposition was not tenable.

As has been said earlier the addition of ASA-3 was made to increase the conductivity of fuels and hence the relaxation of charges. Inevitably since it acts by dissociation into ionised material, it will itself also give rise to charging at the filter or at the pipe interface. However, the net charge carried forward is very much less than it would otherwise be. Figure 2 shows the charge density at a point 2 seconds residence time downstream of a filter element at which charges have been formed. At a conductivity of about 150 pS/m which is the target normally aimed at when using the additive the net residual charge will be negligible. Even at very much lower conductivities as might be met with lower concentrations of additive the residual charge is still low. The charging by the additive has been quoted by some as an adverse property, but it may be seen that taken in its correct context with the increased conductivity conveyed simultaneously the net effect is only beneficial.

ACCUMULATION OF CHARGE - Variation with Net Charge Density - The charge entering the tanks of a tank truck or an aircraft can be potentially hazardous in two respects. If the charge density is sufficiently high the plug of highly charged fuel issuing from the entry nozzle can act as a high potential source giving rise to discharges to nearby earthed surfaces, or secondly the charge can

accumulate within the tank as the liquid rises to give a discharge from the liquid surface to nearby earthed objects.

Let us examine these two possibilities.

Charged Liquid Jets - The charge contained in a jet of fuel entering a tank can be considered in the most pessimistic case to persist in that same form for a finite time before diffusing through the tank, and to act as a high potential jet, to or from which discharges can occur. Whilst the jet will soon be submerged and any discharge will then occur within the liquid there will inevitably be a finite short time when a discharge between the jet and the earthed surroundings could occur in air. By speeding the relaxation of charges before entry and within the jet ASA-3 is effective in removing this hazard; Bruinzeel (2) found that a conductivity of 20 pS/m was sufficient to ensure this safety.

Charge on Liquid Surface - As the liquid rises within the tank concerned, the charges entering the tank will relax through the resistance of the fuel. The lower the resistance of the fuel, i.e. the higher the conductivity, the more rapid the relaxation. Calculations can and have been made of the net charge remaining after a given time of fuelling, and measurements have been made of the resulting fields in the vapour space above fuels. These calculations are based generally on a regular rectangular shaped tank, without any interfering protuberances in the vapour space. The relevance of such calculations has been demonstrated by Carruthers and Wigley (3) and Shell work at Thornton Research Centre showed extremely good agreement except in those cases where discharges affected the field strengths developed.

Figure 3 shows the comparison between measured results and those calculated according to a similar procedure used by Vellenga (4). The values of field strength observed in these and in other reported tests were significantly lower than the 3000 kV/m commonly regarded as the breakdown voltage of dry air. However concentration of fields occurs around projections in the vapour space, and more recent work at Thornton has demonstrated that discharges can occur with projections into the vapour space with the main field strengths as low as 250 kV/m. This is very much in line with observations made much earlier during fuelling tests on a DC-8 aircraft and other mock up tanks when discharges were observed at field strengths around 375 kV/m.

Thus any charge density giving rise to field strengths of this order is suspect, and the pertinent question with regard to aircraft fuelling is whether such charge densities can be avoided. Since in aircraft fuel tanks

\* Numbers in parentheses designate References at end of paper.

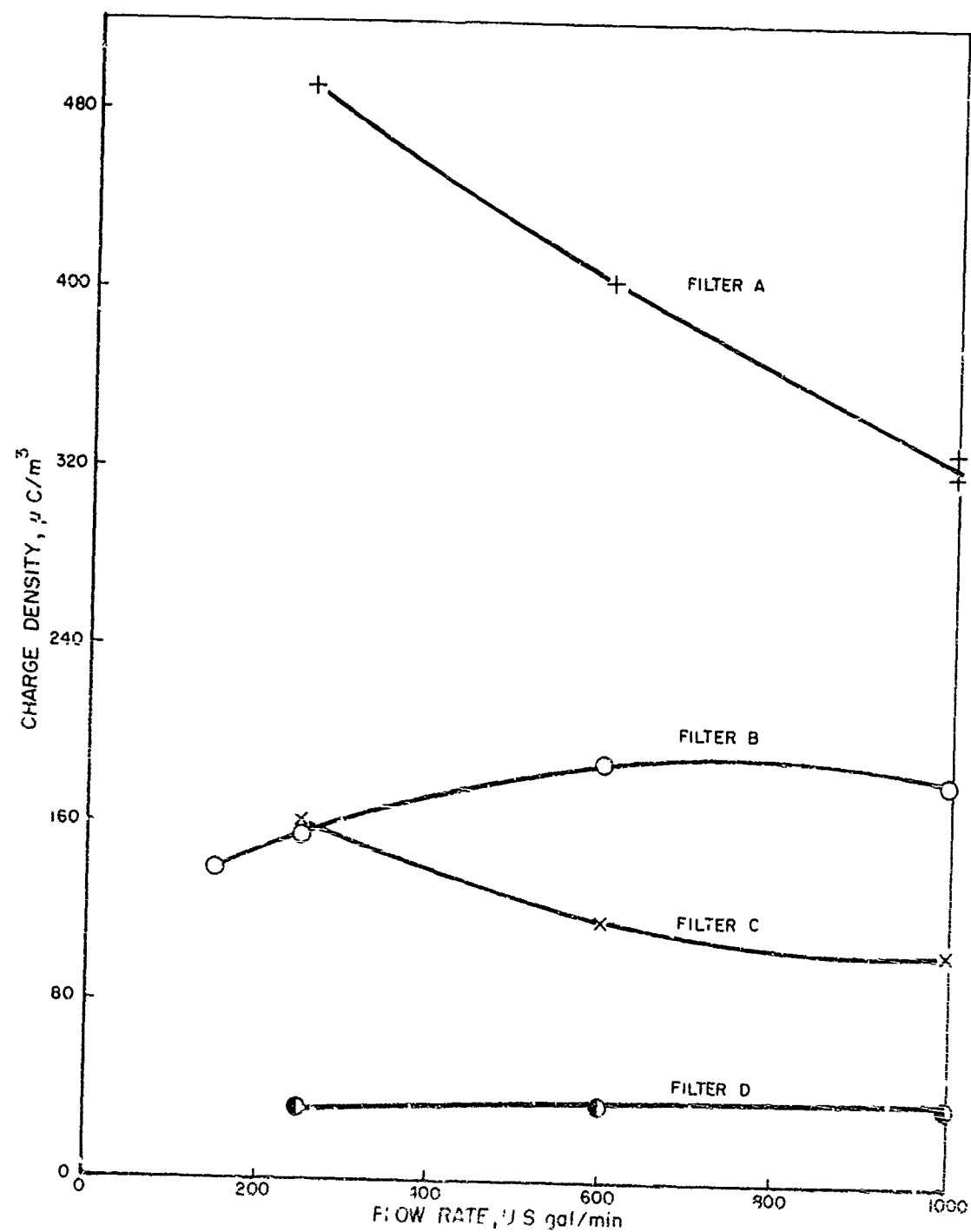


Fig. 1. Filter outlet charge density for four different aircraft fueling filters  
Aviation kerosene, conductivity 2.2 to 3.5 pS/m at 5°C.

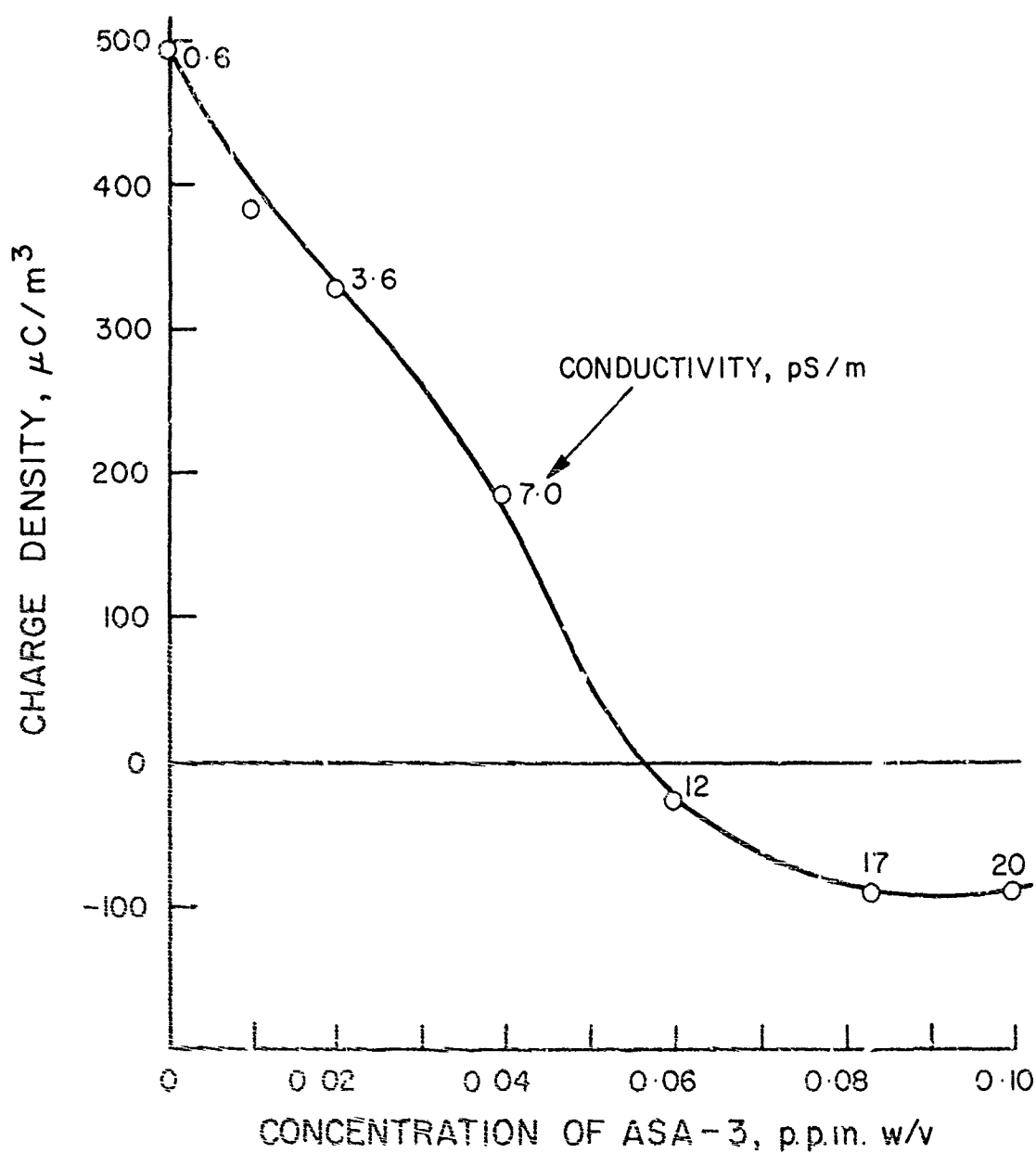


FIG. 2—Effect of ASA-3 concentration on charge density in kerosine measured after 2 seconds residence time downstream of a microfilter



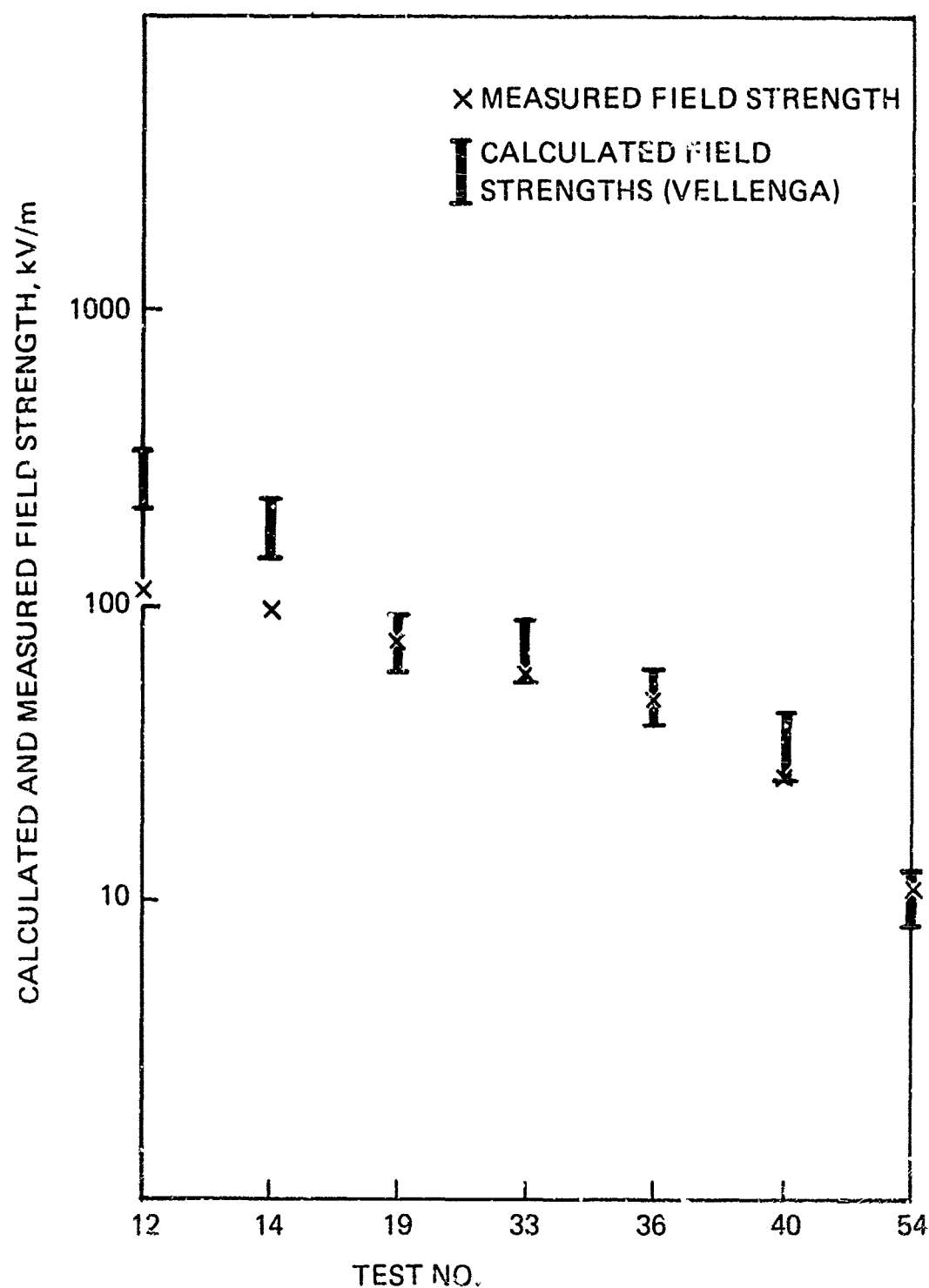


Fig. 3. Comparison of calculated with measured field strengths (using aircraft nozzle)

earthed probes can enter the vapour space over a range of depths within the tank it is essential to take into account the most severe degree of field concentration. To do this we have used a second criterion of equivalent surface potential and calculated for a rectangular tank how the surface potential would vary for different proportions of the tank filled for different inlet charge densities and fuel conductivities. From these results we are able to deduce the maximum charge density which could be tolerated without giving rise to a surface potential greater than the level of 45 kV which from experimental observations would give an incendive discharge to a probe in the vapour space. Such an analysis is by no means precise and at most can only give a general picture. For a particular case studied it has given results as shown in Figure 4 for a hose coupling charge density of  $840 \mu\text{C}/\text{m}^3$ . Thus it may be seen that one might postulate combinations of maximum charge density with conductivity which would give safe conditions. However, for fuels of very low conductivity the relevant level of charge density is likely to be unduly restrictive.

#### THE SOLUTION - ASA-3

The more practical solution then is, we feel, to use an additive to increase the fuel's conductivity, and it was in order to do this that Shell's anti-static additive was developed initially for application to the general handling of petroleum products and later for aviation products.

**COMPOSITION OF ADDITIVE** - It is composed of equal parts of the following three active materials in xylene as a carrier:

- (a) The chromium salt of alkyl salicylic acid.
- (b) The calcium salt of Do-decyl sulfo succinic acid, and
- (c) A methacrylate-vinyl pyridine copolymer.

**EFFECTS OF ADDITIVE** - Typically a concentration of 0.6 p.p.m. w/v (i.e. 0.6 mg/litre) will give a conductivity at 15°C of about 250 pS/m, although the actual value achieved will depend on other trace compounds already present in the fuel. The conductivity will vary with the temperature of the fuel in a log/linear mode. Typical conductivity/temperature curves are shown in Figure 5.

The addition of ionisable material of this kind will affect the charge generation as well as the conductivity. However, the ruling factor is the net balance of charge carried forward into the tanks of aircraft or tank vehicles, and the use of the

effect of high conductivity in speeding relaxation any increase will be eliminated after a short residence time. From early work carried out at Shell's Amsterdam and Thornton laboratories a minimum conductivity level of 50 pS/m has been adopted as having sufficient safety margin above the minimum required to prevent sparking to allow for temperature effects.

It is recognised that other fuel additives, e.g. corrosion inhibitors impart some increase in conductivity. The relevant values for one such additive in common use are included in Figure 6 and are very small. Such additives will also generate charges and the Figure shows that the net balance of charge generated and relaxed over a 2 second period is by no means as attractive as from the ASA-3. The additional inclusion of ASA-3 still neutralises the charge as seen in Figure 7.

**PLASTICS AND GLASS REINFORCED PLASTICS** - The conclusions drawn earlier assume wholly metal tanks. There is however a growing use of plastics materials for the transport of fuels, in particular glass fibre reinforced resins for pipes and storage tanks and epoxy linings for steel tanks. When the materials of construction have specific resistivities of  $10^{12}$  ohm metre or lower they behave in much the same way as metals but for higher resistivities the insulating effects change the picture considerably.

**GRP Pipes** - The charge generated within such pipes is much the same as within pipes of other materials, and in tests at Thornton it has been demonstrated that the generated charges relax to the walls of the pipes during the passage of fuel to the same extent as for steel pipes. However, accumulation of charge on the insulating pipe walls produces a field surrounding the pipes which can give rise to a discharge to a pointed earthed object approaching the pipe and in some instances this discharge can be incendive with energies up to several millijoules. Perforation of PTFE or glass pipes has been reported by some workers but we have not observed this in our experiments with GRP pipes, and our initial fears of discharges from buried GRP pipes to nearby earthed metal pipes in areas of very dry soil, with consequent rupture of the pipes have not been realised.

**GRP Tanks** - In the case of GRP storage tanks the charges entering the tank with the incoming fuel cannot relax to earth unless a bonded object of sufficient surface area exists in contact with the fuel. Thus hazardous fields can exist between the fuel layer and any earthed object within the tank.

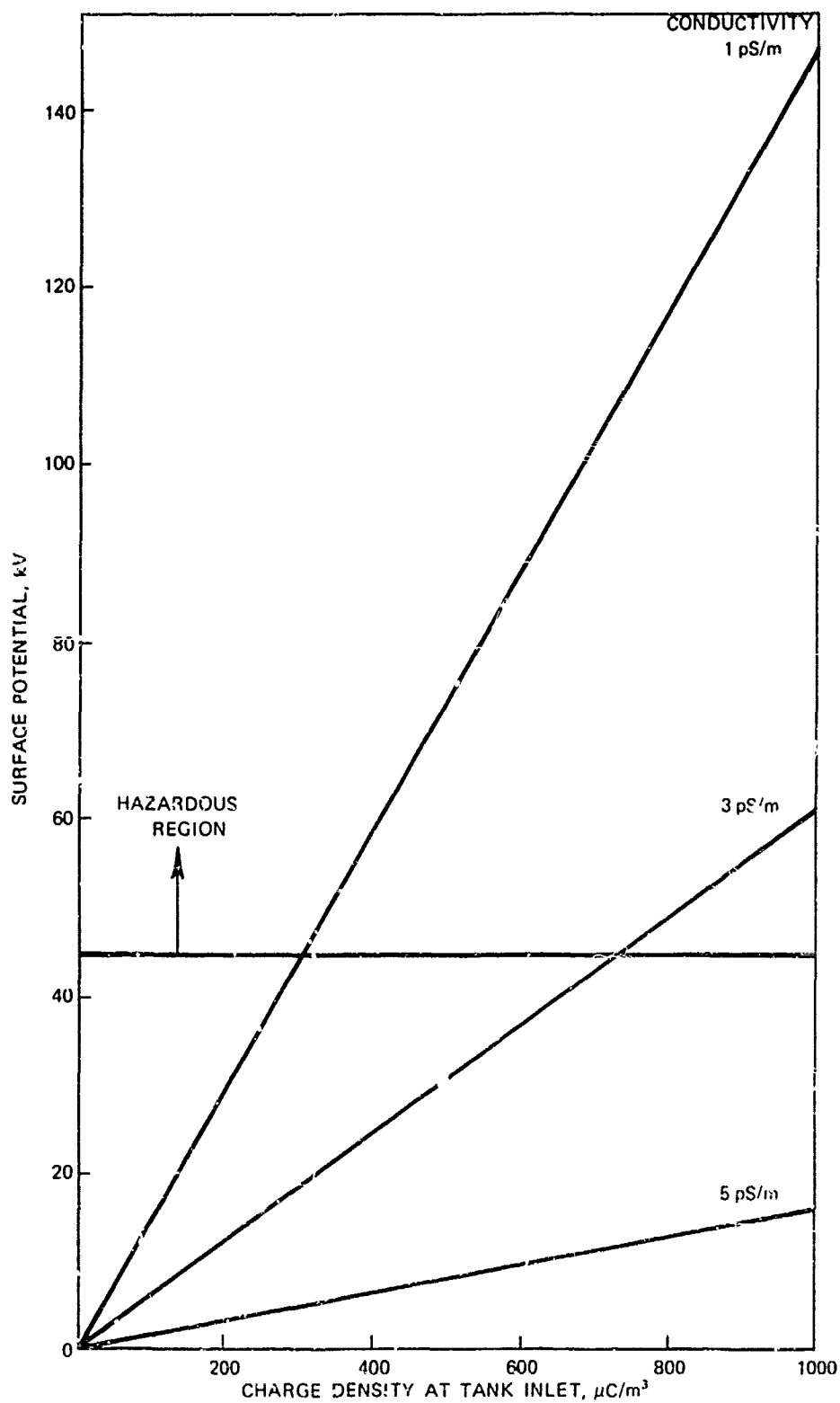


Fig. 4. Surface potentials in one particular aircraft at different charge densities.

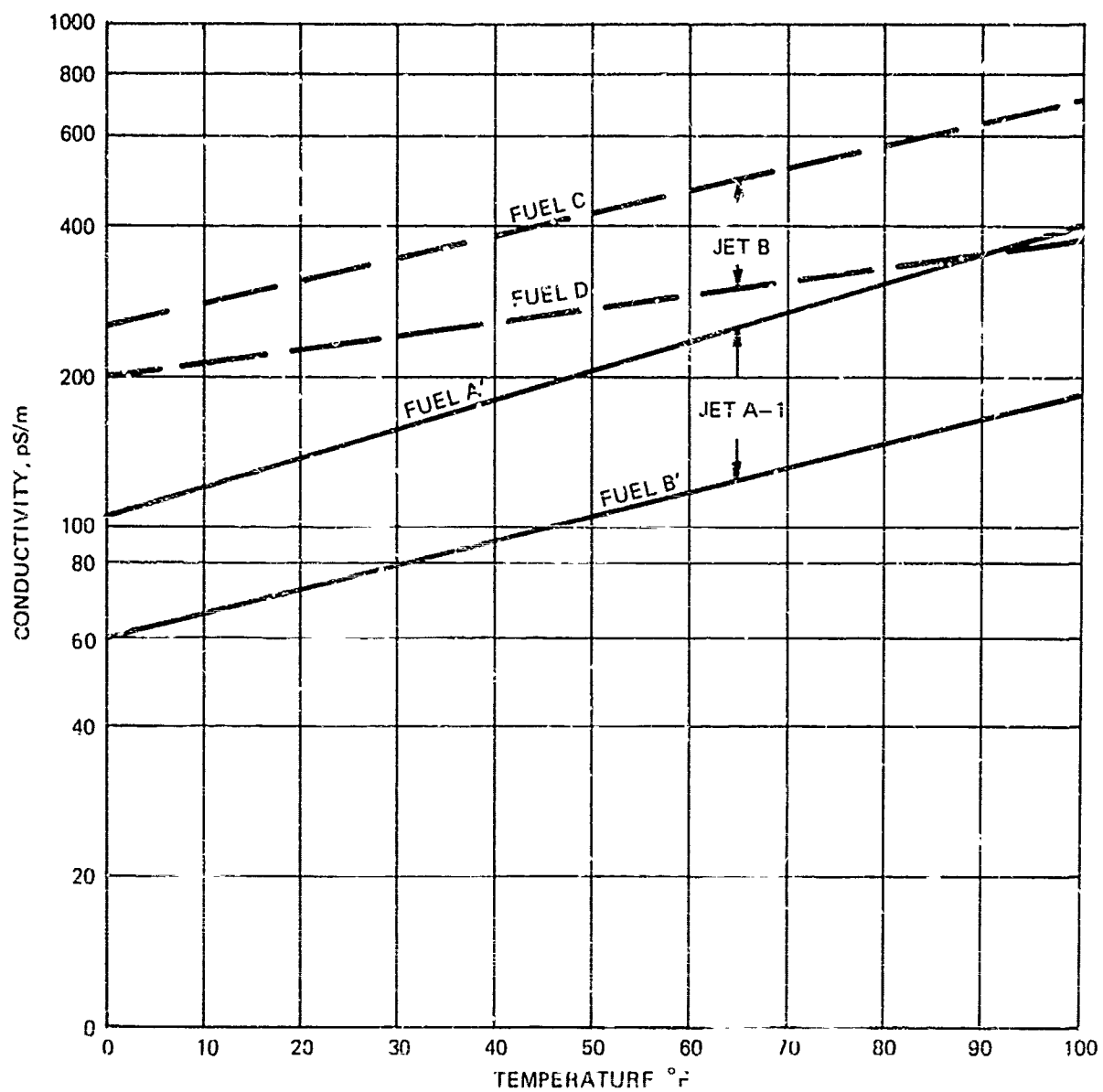


Fig. 5. Variation of conductivity with temperature  
Typical Values

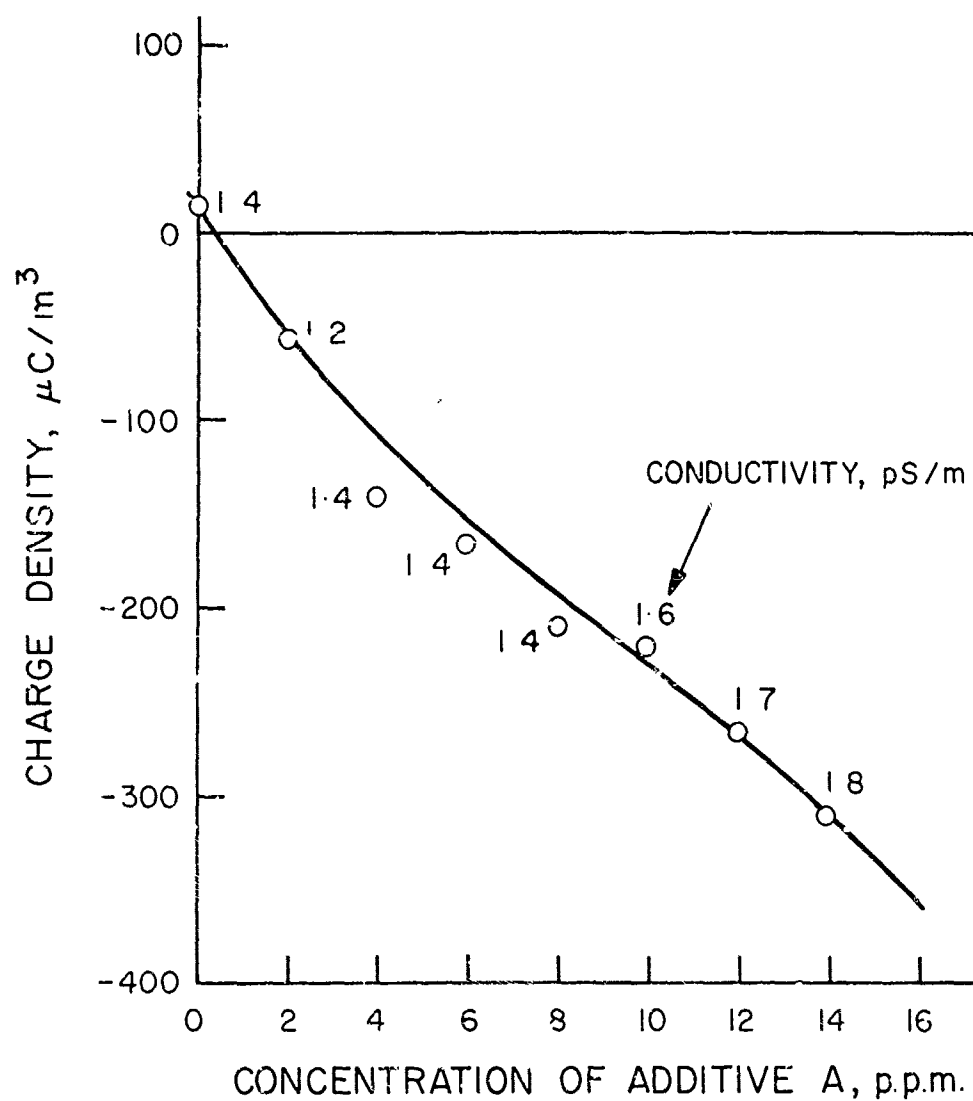


FIG. 6—Effect of concentration of Additive A upon charge density in kerosine measured after 2 seconds residence time downstream of a microfilter

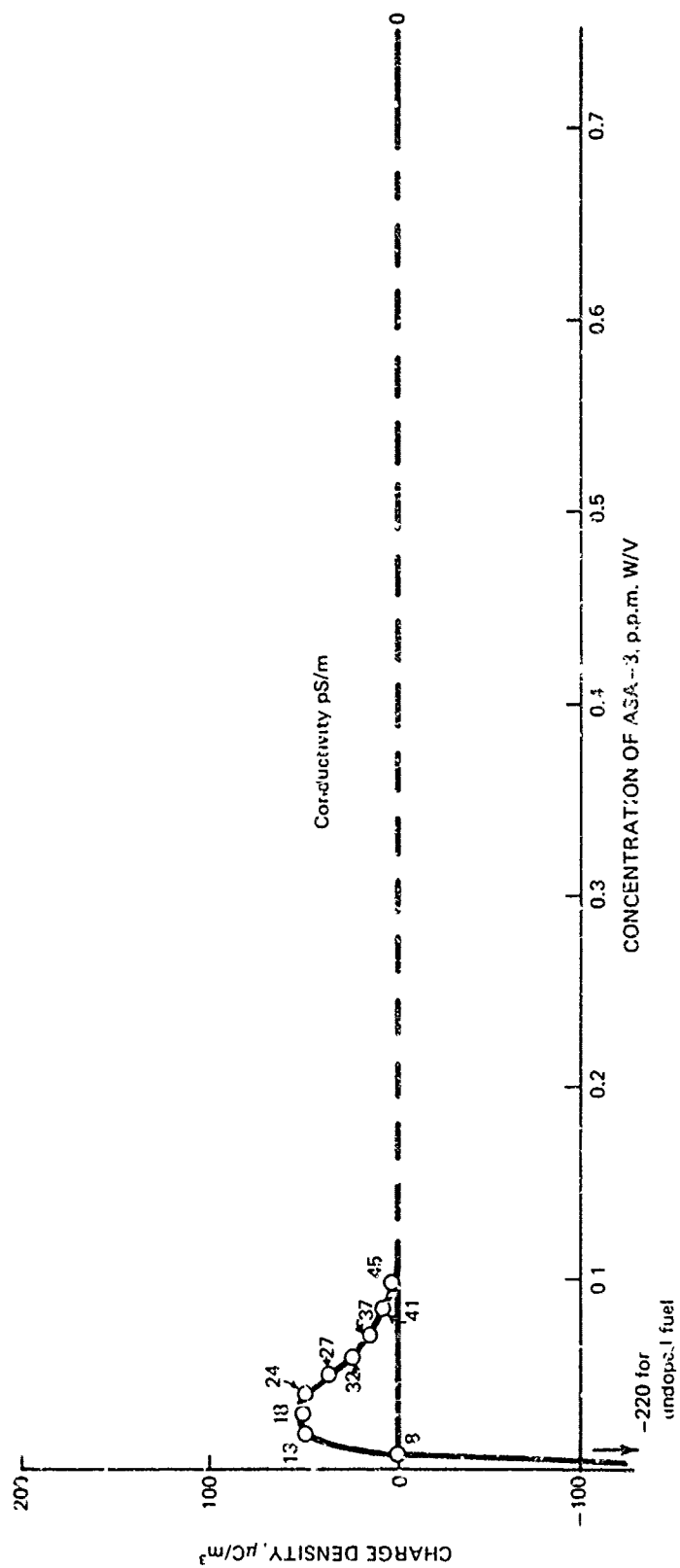


Fig. 7. Effect of ASA-3 concentration on charge density in kerosene + 20 p.p.m. additive A, measured after 2 seconds residence time downstream of a microfilter

A metal plate of about 1 $\frac{1}{2}$  sq. metres area bonded to a bottom loading valve has been found adequate to relax charge to a similar extent to a steel tank, but the rate of relaxation is still of course very dependent upon the conductivity of the fuel.

Tank Linings - A further problem however exists with high resistance linings within tanks, such as epoxy resins. Tests to simulate the behaviour of such a lining have been carried out using a GRP tank surrounded by a wire mesh. Charges in the product move towards the walls of the tank to give a uniform potential and because of the highly resistive layer on the tank walls a finite electric field remains in the vapour space for a long time after filling has stopped and the static charge can remain on the resistive layer even after the product has been drained from the system.

The length of time for which such charges remain a hazard when fuel is present will depend on the integrity of the coating, and the existence within the fuel layer of a grounded metal object. The equilibrium potential within the tank will be a function of the thickness of the coating, being smaller for the conventional thickness of lining than in the case of our tank; we do not consider that this retained charge will be hazardous in the normal case but we intend to confirm our findings in due course with a thinner lining.

In any case the use of the anti-static additive can again only benefit the situation by relaxing the charges to a much greater extent, than in its absence, before the fuel enters the storage tanks.

OTHER FACTORS - Maximum Conductivity - When the additive was first introduced a number of aircraft were fitted with early uncompensated tank contents gauges. Their accuracy was slightly sensitive to fuel conductivity even though the additive had no effect on the dielectric constant of fuels; specification of a maximum conductivity level was therefore considered desirable. A maximum conductivity with the additive of 300 pS/m was adopted initially (and still applies in some specifications) though thorough testing by the R.C.A.F. and gauge manufacturers has shown that this is unduly restrictive with compensated units. The Canadian specifications, based mainly on ensuring adequate conductivity at low temperature, allow higher conductivities than 300 pS/m at high ambient temperatures. The British military specifications now allow up to 600 pS/m where ASA-3 and corrosion inhibitors are used jointly.

Maximum Additive Concentration - The maximum conductivities quoted are compatible with a maximum concentration of 1 p.p.m. w/v.

At this level the additive would contribute an additional 0.04 p.p.m. of inorganic material to fuels. In view of the recognised effects of traces of inorganic compounds, particularly alkaline materials, on high temperature components of engines such as turbine blades, extensive testing was carried out by one engine manufacturer and at Thornton to check the effect on blade materials at 900 and 1000°C. Plate I and II show photomicrographs of sectioned blades used as targets in a laboratory rig for 200 hours. As will be evident no detrimental effect on blade oxidation was noted. Further testing to over 1000 hours confirmed this.

#### FIELD EXPERIENCE

HISTORICAL - Before the additive was used in aviation turbine fuels it was employed in illuminating kerosine and similar non-aviation distillate fuels - and still is - at major Shell refineries in South America and the Eastern hemisphere. A series of trials conducted in non-aviation fuels proved the basic effectiveness of the additive in very low concentrations and the degree of depletion in different distribution systems. The ASA-3 additive formulation incorporates improvements to overcome tendencies to leach out with water which was found in earlier versions. On the basis of these tests therefore, coupled with laboratory tests, concentrations for use in aviation fuels to maximise safety with minimum side effects could be judged.

The first experience was obtained in Canada where the Royal Canadian Air Force started a flight evaluation in May 1962 (5). The experience there also showed there was no difficulty in maintaining conductivity within the desired range.

During 1963 the additive was added to all Shell Jet B supplies to major Canadian airports and in October 1963 to all Jet A-1 supplies by Shell to major Canadian airports. Introduction outside Canada started at the end of 1964 and was limited initially to a few airfields as part of a field evaluation in co-operation with member airlines of the IATA. Further introduction of the additive was relatively slow due in part to the fact that whilst many airlines were quite willing to uplift supplies of doped fuels, they awaited the results of the field evaluation to ensure there were no side effects on power plant operation or life before requesting supplies of doped fuel.

In 1966 the additive became optional in the British Ministry of Aviation Supply (now Ministry of Defence) aviation kerosine type fuel specification D.Eng.R.D.2494 and was used by the Royal Air Force.

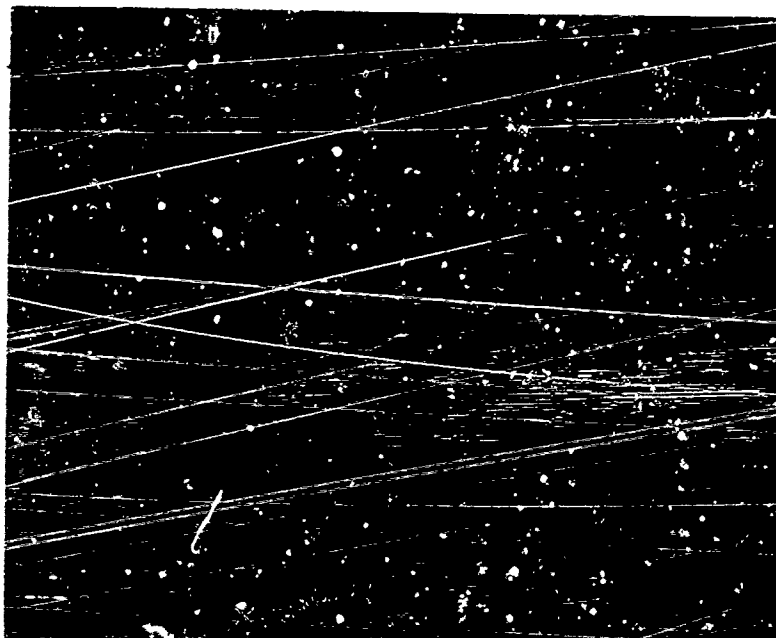


PLATE I — Metallographic section of Nimonic 105 Specimen No 2 after 200 hour test  
(Avtur + A S A 3) x 1000

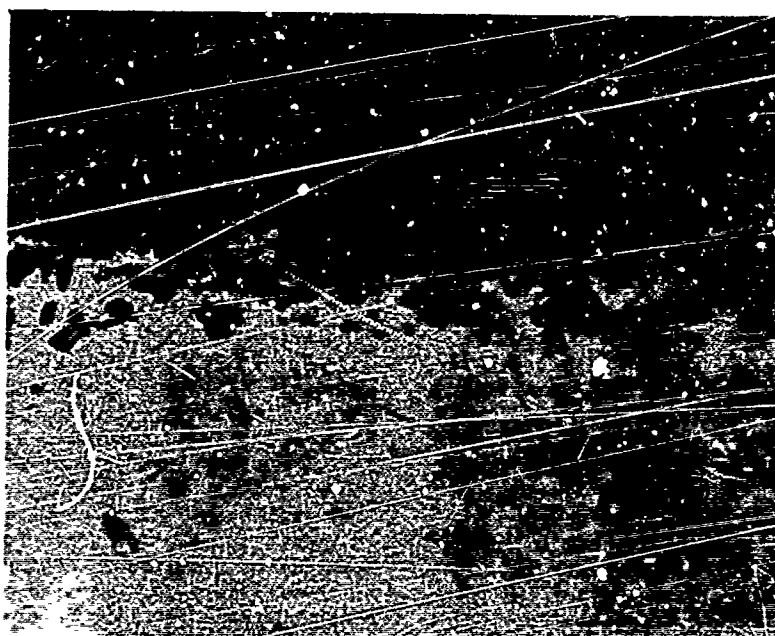


PLATE II — Metallographic section of Nimonic 105 Specimen No 8 after 200 hour test  
(Avtur) x1000



Since 1968 it has been required by many leading international airlines and became generally accepted throughout the free world outside the United States for civil purposes. Today over 90% of aviation kerosine supplies for civil operators outside the United States contain the additive. The history of the introduction of the additive in aviation fuels at major civil airports is given in Table 1. In addition fuel at well over 100 minor airfields also contains ASA-3. The volume of doped fuel supplied annually is expressed in graphical form in Figure 8 and estimates of the total annual civil aviation fuel offtakes outside USA and communist areas are included for comparison.

A brief study of the Table and the Figure shows that experience was gained at an early date at airports widely spaced geographically, with very different climates.

Strict records were kept of conductivity during initial introduction at any airport or at any new phase in the distribution system. It was found there was no difficulty whatsoever in maintaining supplies within the required conductivity range.

During the period up to 1968 it was general practice to dope initially at the airfield to bring the conductivity up to an acceptable level as quickly as possible and thereafter when all airfields supplied from a particular installation or refinery required doped fuel, doping was moved further and further back in the distribution chain to maximise safety.

**FIELD PERFORMANCE** - As described earlier (5) there have been many cases of fires in military aircraft, particularly at low temperatures, before ASA-3 was used - but not since. There have also been three cases of explosions in civil aircraft with undoped fuels, which we are confident could have been avoided with ASA-3 doped fuel.

To the best of our knowledge no problems due to electrostatic discharges have occurred when handling doped products between refinery and airfield, whereas with undoped fuels there have been many incidents, as logged by the API and several have been of a serious nature.

Major airlines, who for years have used a predominance of ASA-3 doped fuel, have reported officially to IATA that there have been no problems in airframes or power plants attributable to the use of the additive.

**INITIAL INTRODUCTION OF THE ADDITIVE** - As mentioned earlier the additive was introduced initially in Shell supplies at certain airfields outside North America for some IATA airlines. This was the only means available to Shell to supply doped fuels because of the use of facilities at other airports which also handled other suppliers'

products. At a later date, following the successful conclusion of the IATA evaluation and a joint petroleum industry evaluation, doped fuel became generally available and the doping-point was moved back to the refinery thus giving complete safety in the distribution chain. It was realised that there was a risk that at the end of the long distribution chain during the initial introduction period there could be fuels with intermediate conductivity - i.e. less than the desired minimum - as doped fuels became mixed with existing undoped fuels in storage. All the evidence at our disposal from full scale fuelling tests and from laboratory studies indicated that this practice did not constitute any additional hazard to that already being run with undoped fuels. To prove the point, additional laboratory work was undertaken which showed that even the minutest amounts of ASA-3 (as little as  $\frac{1}{100}$ th of the maximum allowable concentration) had an overall effect in reducing the charge density in the fuel after due allowance for the relaxation of the charge from filter to aircraft coupling in the practical case (see Figure 2). We have therefore no qualms when introducing ASA-3 doped fuel to an airport to allow doped fuels to gradually replace existing undoped fuel.

**DOPING METHODS** - For maximum safety, the additive should be injected into refinery product streams to protect the whole train of operations through to the airfield (even if it does deplete and redoping is necessary - see next section).

Shell practice at refineries is to make a cocktail of ASA-3 with other additives (for example the anti-oxidant as mandatory in hydrotreated fuels in British specifications). Tests have shown that the performance and stability of the ASA-3 cocktail is satisfactory.

If no other additive is added at the refinery we recommend that a stock solution of ASA-3 up to about 10% should be made up (in aviation kerosine). This is readily handled and is much more convenient than the addition of the additive on its own particularly in view of the very low concentrations employed.

In the simplest case, the additive can be added to storage tanks or bridging vehicles, preferably during replenishment when the movement of fuel in the tanks is quite sufficient to cause rapid homogeneity.

For refinery and pipeline supplies continuous injection is preferable and typical additive injection methods and suggestions are given in the Appendix.

To safeguard their own operations the injection of ASA-3 at Shell refineries has been practised for over 10 years on the full range of distillate products. In the case of

TABLE 1 — Introduction of ASA-3 at major civil airfields

<u>1963</u>	<u>1967</u>	<u>1968</u>	<u>1970</u>	
GANDER MONTREAL OTTAWA QUEBEC TORONTO VANCOUVER WINNIPEG	ATHENS (A-1) BANGKOK (B) BATHURST (GAMBIA) BELEM (BRAZIL) BELFAST BREMEN COPENHAGEN DAR-ES-SALAAM FUKUOKA (JAPAN) GATWICK (UK) GLASGOW (UK) GRONINGEN (HOLLAND) HAMBURG (A-1) HELSINKI HONG KONG ISTANBUL KLAGENFURT (AUSTRIA) KUALA LUMPUR LUTON (UK) MADRID MANCHESTER (UK) MARSEILLE MILAN (LINATE) MILAN (MALPENSA) MONTEVIDEO PANAMA PRESTWICK (UK) RECIFE RIO DE JANEIRO SAO PAULO SINGAPORE STANDSTED (UK) STOCKHOLM TENERIFFE TURIN TUNIS VIENNA (A-1) ZURICH	BARCELONA BEIRUT BIRMINGHAM (UK) CAPE TOWN CHRISTCHURCH (NEW ZEALAND) DURBAN EAST LONDON EDINBURGH FREETOWN (SIERRA LEONE) GUERNSEY JERSEY JOHANNESBURG KUWAIT LIVERPOOL LUNGI (SIERRA LEONE) MALTA NICE PARIS (ORLY) PORT ELIZABETH PORTO ALEGRE ROME ROTTERDAM	ASU DHABI ADDIS ABABA ANKARA ANTWERP ASMARA AUCKLAND BEIRA BERGEN BERLIN BERMUDA BLANTYRE BRUNEI BRUSSELS CAGLIARI (ITALY) CAIRO CORFU DAKAR DANANG ENTEBBE FRANCISTOWN (BOTSWANA) GENOA GOTTENBURG GENEVA GRAZ (AUSTRIA) HANOVER INNSBRUCK JEDDAH KANO KARACHI KEFLAVIK KINGSTON LAE LINZ (AUSTRIA) LISBON LIVINGSTONE	LOURENCO MARQUES LUSAKA MAHE (SEYCHELLES) MALMO MANILA MARACAIBO MOMBASA MONTEGO BAY MUNICH NAIROBI NAPLES NASSAU NDOLA NICOSIA NUREMBERG OPORTO OSTEND PALERMO PORT OF SPAIN PORT MORESBY RABAU (NEW BRITAIN) REYKJAVIK RHODES RIMINI SAIGON SAL (CAPE VERDE IS.) SALONIKA SALZBURG STAVANGER STUTTGART TRONDHEIM VENICE WINDHOEK
<u>1964</u> LONDON (B)				
<u>1965</u> DARWIN DUSSELDORF LAGOS LONDON (A-1) SCHIPHOL (B) SHANNON				
<u>1966</u> ACCRA ADEN AMMAN ATHENS (B) BUENOS AIRES CURACAO GIBRALTAR HAMBURG (B) JERUSALEM OSLO PRESTWICK (B) SCHIPHOL (A-1) TRIPOLI		<u>1969</u> ADELAIDE COLOGNE CORK DOHA DUBLIN FRANKFURT KHARTOUM PALMA DE MAJORCA PORT OF SUDAN		

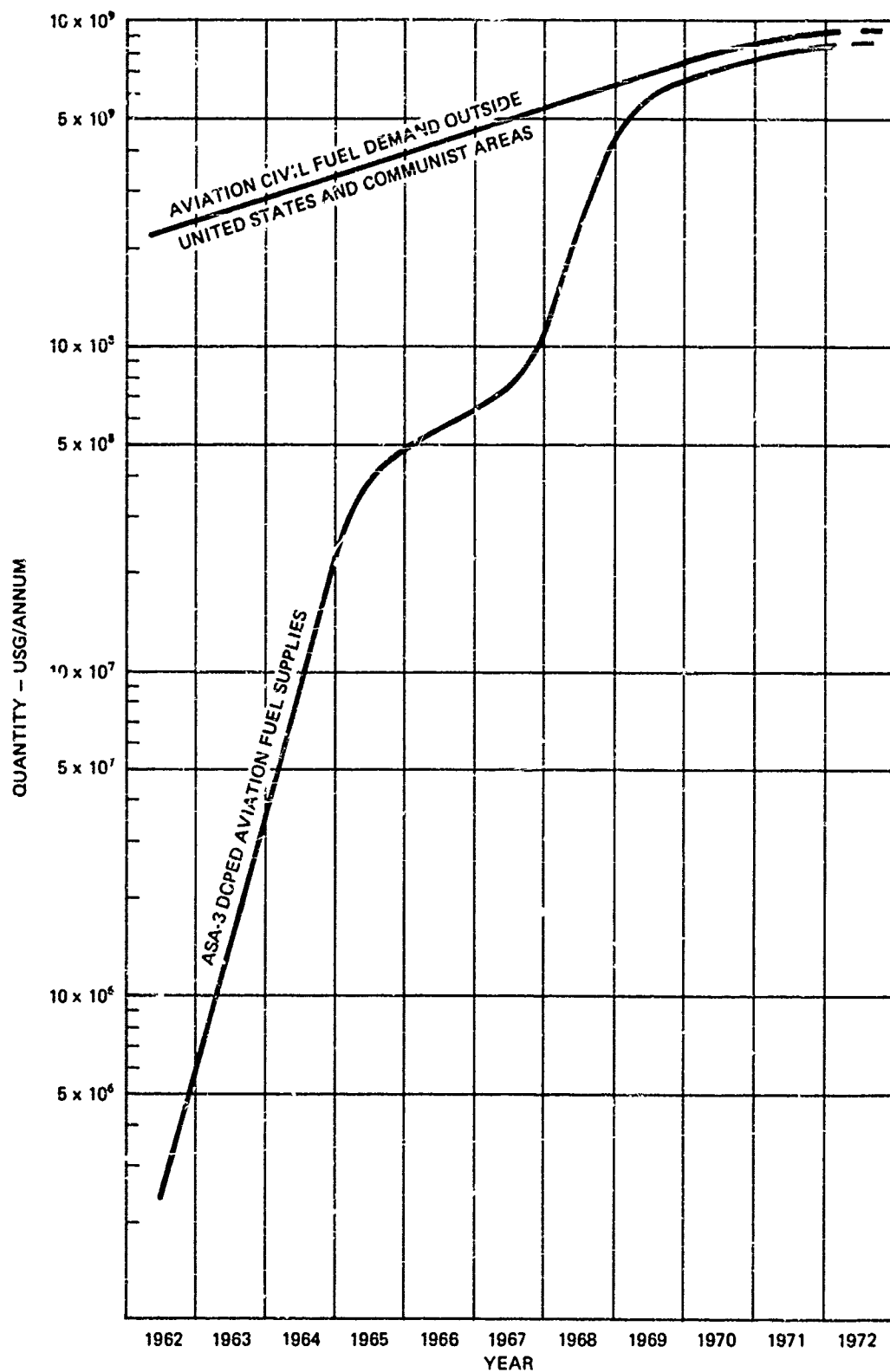


Fig. 8. Growth of supply of ASA-3 doped aviation fuel

aviation fuels however, refinery doping started in Canada at an early date and later spread to Shell refineries in Holland, Switzerland and Argentina by 1967, Italy and the United Kingdom in 1968, but it was only some two years ago that refinery doping became general practice. Shell's policy is to have a target conductivity for turbine fuels of 200 ± 50 conductivity units\* at the refinery. Data obtained during the initial introduction at refineries has shown that this level was adequate to allow for any increase in conductivity when moving fuel from a cold to a warm area and also provides sufficient margin to guarantee a minimum of 50 conductivity units at the aircraft fuelling vehicle in the vast majority of all distribution systems except multi-product pipelines. We have found no difficulty in meeting the target figure with concentrations within the maximum allowable and in the vast majority of cases the concentration is 0.5 to 0.7 mg/L.

The amount of additive used depends

largely on the fuel itself, that is, the treating process and physical cleanliness and to a much smaller extent the normal batch to batch variations in effectiveness of the additive itself. Generally speaking we have found that fuels with high physical cleanliness and low surfactant contents have better additive susceptibilities than those with relatively large amounts of particulate matter which tend to adsorb some of the additive.

We have noted that other additives in combination with ASA-3 do affect the conductivity but where an additive cocktail is used at the refinery, this effect is automatically compensated for by aiming at a particular target conductivity value. The phenolic type anti-oxidants in general have a slight conductivity enhancing effect, whereas fuel soluble corrosion additives have a variable effect according to the particular additive used. The summary of laboratory data on combinations of ASA-3 and fuel soluble corrosion inhibitors is given in Table 2.

**TABLE 2: Influence of Fuel Soluble Corrosion Inhibitors on Electrical Conductivity - Base Fuel Containing 0.7 ppm ASA-3**

Corrosion Inhibitor		Hydrotreated Fuel			Caustic Treated Fuel			Acid Treated Fuel		
		Conductivity Value pS/m	Conductivity Change Due Addition FSCI		Conductivity Value pS/m	Conductivity Change Due Addition FSCI		Conductivity Value pS/m	Conductivity Change Due Addition FSCI	
Type	Addition Level		Value pS/m	%		Value pS/m	%		Value pS/m	%
Hitec B515	MEC	410	+64	+18	105	+25	+18			
	MAC	290	-56	-16						
Hitec B524	MEC	400	+64	+18	170	+30	+21			
	MAC	250	-96	-28						
Tolau 245	MEC	230	-116	-33	34	-56	-40	65	-15	-19
	MAC	250	-96	-28						
Tolad 244	MEC	205	-111	-31	68	-72	-52	45	-35	-44
	MAC	180	-116	-33						
AFA-1	MEC	346	N31	N11				55	-25	-30
	MAC	290	-56	-16						
Apollo PRI-19	MEC	110	-236	-68						
	MAC	95	-251	-72						
Lubrizol 541	MEC	350	+4	+1						
	MAC	350	+4	+1						
Nalco 5400	MEC	345	-1	-						
	MAC	350	+4	+1						

**Note** MEC - Minimum Effective Concentration  
MAC - Maximum Allowable Concentration

\* 1 conductivity unit = 1 pS/m

We would stress that this is laboratory data and in the case of Hitec E515 (Santolene C) we found in the field that there was no difficulty in maintaining the conductivity of Jet B fuel within a desired range by adjusting the ASA-3 additive concentration accordingly. More recently in the case of military fuels for the British Ministry of Defence, the fuel soluble corrosion inhibitor Hitec E515 is added in combination with icing inhibitor at the airfield or some intermediate point in order to maximise its concentration on delivery to the aircraft for fuel pump protective purposes. A study of a large number of readings of conductivity after the addition of the fuel soluble corrosion inhibitor in the field to fuel doped at refineries to a target figure of 200 cu\* indicated average final conductivity of 280 cu and a spread of results of 150-590 cu.

#### CONDUCTIVITY LOSS DURING DISTRIBUTION -

As might be expected from a surface active material, exposure of non-equilibrated surfaces to fuel containing the additive will lead to partial depletion. This is true of storage tanks, pipelines and even filters but experience over the past 10 years with refinery injection of the additive enables us to say that equilibrium conditions are rapidly achieved. Davies and Knipple (5) reported depletion tests in Canada with up to 30% loss of conductivity observed. Experience outside Canada indicates that the major losses occur during ocean transport and shore pumping and that losses during transport by road or rail tanker or in a dedicated pipeline are small. Values recorded for 17 ocean cargoes of aviation turbine fuel are shown in Table 3. In general a loss of conductivity of up to 60% is found, average about 30%, but only very rarely in the case of distribution systems, other than multi-product pipelines, have we found it necessary to redope to ensure that the conductivity at the aircraft is greater than the recommended safe value of 50 cu.

In the case of very long distance transfers especially involving multi-product pipelines greater depletion has been found and we are aware of the work done by the USAF in moving doped fuels from the Gulf of Mexico to Maine. We would comment however that although the conclusion of the programme showed that there was a great loss of additive as judged by conductivity loss, it is our understanding from the data presented (6) that even such a complicated system, with the inclusion of additives, that at no time did the conductivity of the fuel at the time of aircraft fuelling fall below the recommended safe value of 50 cu.

Our experience with multi-product pipelines indicates a wide variation in conductivity loss - presumably due to wall condition - and up to 75% drop in conductivity has been

recorded even in a short (50 mile) line. We have therefore accepted the fact that conductivity monitoring and redoping facilities are essential after multi-product pipeline movements. Nevertheless, the use of multi-product pipelines outside North America is limited and Shell's policy is to continue to use the additive at the refinery to protect operations there and to top-up as necessary at pipeline breakout points.

The use of terminal doping or redoping is made more necessary where clay filters are used near or at airfields for surfactant removal. Tests reported by the Shell Oil Company of the introduction of ASA-3 in the Des Plaines - O'Hare distribution system indicated that clay filtration was found to lower conductivity significantly. The rapid build up in conductivity as fuel throughput increased was most apparent and conductivities downstream of clay soon reached a value greater than the minimum recommended value of 50 cu. It was necessary in these trials to add additional ASA-3 at times to keep the conductivity at the desired level. This trial, involving some 60 million USG of fuel, showed that with a typical North American system of multi-product pipeline, clay treaters and filter separators, that there was no difficulty in maintaining conductivity within the desired range. With the extensive use of clay in the United States for economic reasons, Shell Oil Company recommend that the additive be injected downstream of the clay.

**EFFECT ON FUEL PROPERTIES** - The effect of ASA-3 on general fuel properties is very small indeed and those which are affected are properties which might be expected to be affected by a material which is ionic in nature. These are:

**Thermal Stability** - The additive causes no adverse effect in the CRC-ASTM coker under standard test conditions. Under more severe conditions the additive can cause some improvement. Further, tests on a large scale rig using advanced aircraft filters, heat exchangers and burners have shown that ASA-3 has no effect on deposits in practical systems. Incidentally in this connection the greatest additive effect noted and the cleanest components seen at the end of test in the large scale rig was with a combination of ASA-3, phenolic anti-oxidant and approved metal deactivator: the improvement was equivalent to some 65-75°F in thermal stability threshold temperature.

**WSIM Value** - Incorporation of ASA-3 generally results in a drop in the WSIM value. The amount is variable, in today's high quality fuels with initial WSIM values between 95 and 100, only a drop of a few numbers is obtained. With borderline quality fuels with WSIM values of a range of 85 to 90 the effect can be greater but it is

\* 1 conductivity unit = 1 pS/m

TABLE 3 - CONDUCTIVITY LOSSES DURING OCEAN TRANSPORT OF AVIATION TURBINE FUEL

PORT OF LOADING		PORT OF DISCHARGE			CONDUCTIVITY LOSS BASED ON VALUES CORRECTED FOR TEMPERATURE	
NAME	CONDUCTIVITY PS/M	NAME	BEFORE DISCHARGE - CONDUCTIVITY PS/M	AFTER DISCHARGE - CONDUCTIVITY PS/M	BEFORE DISCHARGE	AFTER DISCHARGE
Pernis (Holland)	150 @ 65°F	Benghazi (Libya)	120-140 @ 23°C ) 230-240 @ 23°C )	110-120 @ 25.5°C	37% Gain 78%	22.6% ) )
Curacao	330 @ 86°F	Portugal	120-210 @ 60-68°F ) (Average 160 @ 61°F)	120-155 @ 66.5°F	32%	42.5%
Curacao/ Cardon	145 @ 77°F	Montreal/Oakville (Canada)		65 @ 77°F		55%
Cardon	110-235 @ 77°F Av. 160 @ 77°F	Montreal/Oakville (Canada)		64 @ 77°F		60%
Cardon	180 @ 77°F	Montreal/Oakville (Canada)		105 @ 77°F		42%
Cardon	140 @ 77°F	Montreal/Oakville (Canada)		86 @ 77°F		39%
Cardon	140 @ 77°F	Montreal/Oakville (Canada)		80 @ 77°F		43%
Curacao	230 @ 86°F	Nassau	185-220 @ 85°F ) (Average 198 @ 85°F)	215 @ 88°F	13%	11%
Curacao	210 @ 86°F	Nassau	150-220 @ 82-87°F ) (Average 200 @ 85°F)	140 @ 79°F	3%	2%
EMS (Iran)	210 @ 95°F	Guam	180 @ 90°F		7.2%	

TABLE 3 - CONDUCTIVITY LOSSES DURING OCEAN TRANSPORT OF AVIATION TURBINE FUEL (CONT'D)

PORT OF LOADING		PORT OF DISCHARGE			CONDUCTIVITY LOSS BASED ON VALUES CORRECTED FOR TEMPERATURE	
NAME	CONDUCTIVITY pS/m	NAME	BEFORE DISCHARGE - CONDUCTIVITY pS/m	AFTER DISCHARGE - CONDUCTIVITY pS/m	BEFORE DISCHARGE	AFTER DISCHARGE
BMS (Iran)	210 @ 84°F	Lourenco Marques (Mozambique)	80-220 @ 74°F (Average 127 @ 74°F)	140 @ 74°F	28.6%	19%
BMS (Iran)	160 @ 70°F	Lourenco Marques (Mozambique)	110-250 @ 86°F (Average 177 @ 86°F)		12.5%	
BMS (Iran)	210 @ 92°F	Colombo (Ceylon)	200 @ 90°F	170-182 @ 82°F (Average 176)	2.5%	2.5%
BMS (Iran)	200 @ 87°F	Colombo (Ceylon)	200 @ 90°F	180 @ 83°F	4%	Nil
BMS (Iran)	210 @ 87°F	Colombo (Ceylon)	190 @ 82°F	180-190 @ 85.5°F (Average 185)	Gain 5%	2.5%
Carden/ Curacao	220 @ 86°F	Nassau	215-240 @ 74.76°F (Average 226 @ 75°F)	155 @ 76°F	Gain 18%	18.2%
Stanlow (England)	165-245 @ 50-57°F Average 212	Ardrossan (Scotland)	140-205 @ 50°F (Average 183)	160-165 @ 49- 50°F (Average 162)	13%	23.5%
AVERAGE	198					

our experience that in all the tests reported, involving well over 1,000 samples, the resultant drop still rarely produces a final value below 70, despite the poor reproducibility of the test.

**EFFECT ON FUEL CLEANLINESS AND FILTRATION** - All fuels to some degree carry particulate material which may be adventitious contamination from the construction of equipment, be generated in storage tanks, in pipelines or may be taken in suspended in the air breathed into tanks. Predominantly the solid burden carried by fuels is iron oxide arising from mill scale dislodged from steel equipment or rust formed on the surfaces of storage tanks or pipe walls. Little other than good house-keeping is required to deal with most of the mill scale and rusting of pipelines is controlled by the use of corrosion inhibitors. Nevertheless some contamination persists and is kept to low levels by careful filtration at the airfields. Regular millipore checks at airfields are used to monitor the performance of these filters and careful examination of the records of such checks following the introduction of ASA-3 has revealed no change in the position. Indeed when ASA-3 was being introduced at Glasgow (Abbotsinch Airport) in 1967 continuous monitoring of the effluent of fixed filtration units was used to verify that the introduction of the additive did not give rise to a release of solids from the walls of the system pipework or partially loaded filter element. Samples taken at the end of the aircraft fuelling hose showed solids levels of below 0.01 mg/litre which were lower than the average for the previous 12 months, and there was no evidence of surges of particles as the ASA-3 was introduced.

As regards the longer term, data has been recorded of particulate matter in aviation fuels at airports before and after the addition of ASA-3. Typical figures from Shell records are given in Figure 9. It will be noted that neither in the short or longer term was any significant increase or decrease in particulate matter.

Similar data was obtained during 1967 and 1968 when an industry evaluation of ASA-3 was conducted at 8 international airfields in Europe and Asia where the fuel was applied by a number of companies. During the evaluation, involving more than 120 million USG of doped fuel, over 1,000 fuel samples were tested for solids, water content and WSIM value before and after the addition of ASA-3 to the system. The supplying fuel companies conducting the evaluation concluded that all the millipores were at a satisfactory low level both during the undoped and doped phases of the evaluation.

In addition they concluded that the water

levels were unaffected by the addition of ASA-3 and under the conditions of the evaluation the ASA-3 increased the conductivity of the fuel to a desirable range of 50 to 300 cu.

It is conceded that in view of the surface active nature of ASA-3 there will be a tendency to maintain solid particles in suspension rather more than in the absence of the additive. Laboratory checks demonstrate, however, that its effect in this respect is significantly less than other surfactants which often are found indigenously in aviation kerosine. Criticisms have been levelled at the additive in respect of this particular feature and suggestions made that one case of accumulations of red iron oxide + 15% sodium chloride in aircraft fuel systems was occasioned by the use of the additive. However, millipore results demonstrate that equilibrium rust levels in the fuel are similar with and without ASA-3 indicating no justification for concern in this respect.

**EFFECT ON FILTER SEPARATORS** - For several years criticism has been levelled at ASA-3 in that being surface active it is adsorbed onto the elements of filter separators. There have been fears that this action would reduce their ability to coalesce water droplets to a sufficient size to be able to settle under gravity. These fears appeared to be supported by laboratory tests for example carried out by some filter/separator manufacturers using MIL-8901A techniques where it was claimed that detrimental effects of the additive were demonstrated.

It is true that the additive is surface active and does adsorb to an equilibrium level onto the separator elements in contact with that fuel. In early Shell laboratory tests some effect was shown under severe conditions of water addition, but the results were never consistent and were in keeping with the considerable variation in performance of individual coalescer elements. This factor therefore has received considerable attention not only by Shell but others to study the effect in the field under evaluation and normal service conditions.

The majority of the experience to date has been most favourable. Full scale tests by Fram of Giamorgan, United Kingdom, in 1964 indicated no effect whatsoever on water contents of fuel downstream of the filter separator element with and without 0.75 mg/l ASA-3. Tests on parallel systems with the same fuel with and without ASA-3 at London Airport in 1966 again showed no significant difference in coalescer element performance after 5 million gallons throughput each of doped and undoped fuel. Subsequently a watch has been kept on filter separator



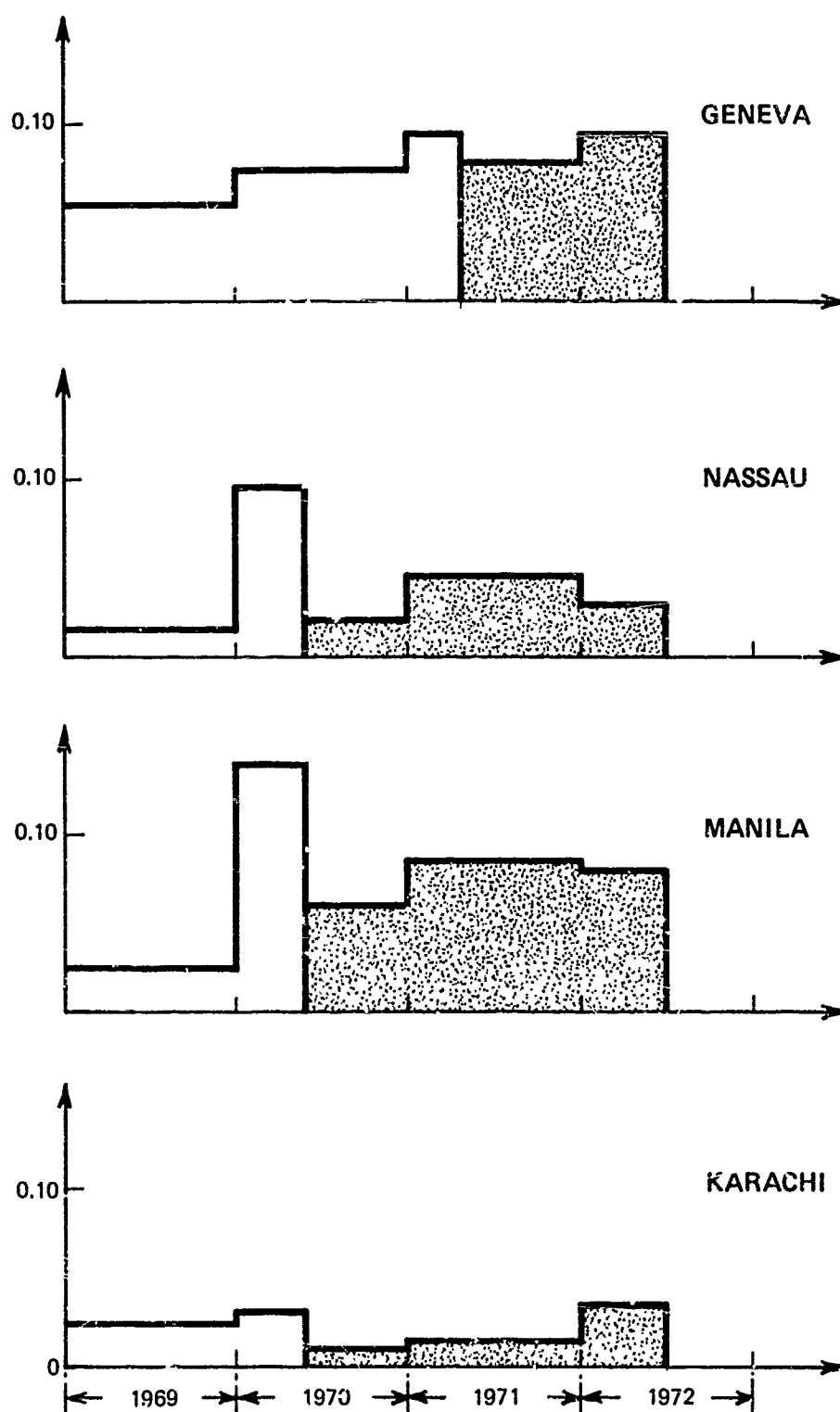


Fig. 9. Typical millipore values before and after use of ASA-3 (MG./L)

performance at airfields where ASA-3 has been introduced by Shell outside the United States and we can say categorically that there has been no significant deterioration in filter separator performance nor any water problems due to filter separator coalescers being disarmed by the ASA-3.

Experience in Canada, reported by Davies and Knipple, indicated that under the severe Canadian conditions both the field experience and the reports from the major filter separator manufacturers indicated no adverse effect on operation efficiency or life due to the incorporation of the anti-static additive.

A study of many fuel evaluations conducted by others or in co-operation with Shell and involving hundreds of millions of gallons have given the following general picture:-

(1) That the performance of filter separators is most variable with undoped fuel, with elements which have never seen fuel with ASA-3.

(2) That in several of the evaluations - for example the co-operative study at 8 major international airports and the USAF evaluation, both mentioned earlier, there was no apparent effect on filter separator performance using ASA-3 doped fuel.

(3) In one field evaluation at Atlanta Georgia by Shell Oil Company in co-operation with United Airlines it was reported that ASA-3 had only a slight effect on filter separator performance with one manufacturer's elements; in the case of a second manufacturer's elements it might be expected that element life would be reduced somewhat with ASA-3 doped fuel.

(4) In a more recent investigation conducted by Shell Oil in co-operation with others at O'Hare as mentioned earlier, some elements performed adequately with ASA-3 doped fuels but others were adversely affected and were not considered suitable for use with ASA-3.

All the above experience indicates that fully satisfactory experience can be achieved in the majority of cases quite naturally, but that for distribution systems which rely completely upon filter separator elements a prudent selection of coalescer model is recommended.

In view of the varying performance of different units and the growing use of ASA-3 the API have developed recently a specification for filter separator elements which incorporates a type test on fuels doped with ASA-3 and other additives. Manufacturers are now offering units which pass these specification requirements and these are giving satisfactory service in the field.

## FURTHER STUDIES

Shell are convinced that a conductivity improving additive can offer a viable system to contain problems due to an electrostatic discharge without significant side effects. Nevertheless the fact that ASA-3 does reduce the WSIM value and also depletes in pipeline and during passage through clay filters has given rise to severe criticisms. A research effort to examine alternative materials continues. To date over 70 have been studied but none have combined a better improvement of conductivity and a lower numerical reduction in WSIM and depletion characteristics. The work continues but it is only fair to point out that we are not optimistic of its success certainly within the short term.

In view of the tremendous cost of clearing additives such as ASA-3 for possible adverse effects on fuel quality or aircraft systems we question whether there is any point in clearing novel additives. From a purely commercial point of view the total sales any additive used at the low concentrations of ASA-3 will be low - even if all the aviation turbine fuel in the world outside communist areas - both military and civil - were doped with ASA-3, the total additive sales would only amount to about 75 tons per annum. To date all the alternative proprietary additives we have seen, whilst being suitable for non-aviation fuels do not appear to be particularly attractive in aviation turbine fuels due to cost, poor additive response or possible side effects. We reiterate that ASA-3 is made available to any user without restriction and has been so since the additive was introduced; thus the present position does not constitute, in our opinion, any impediment to the universal adoption of the system.

## REFERENCES

1. J. T. Leonard and H.W. Carnart, "Effect of Conductivity on Charge Generation in Hydrocarbon Fuels Flowing Through Fibre Glass Filters". *Journal of Colloid and Interface Science*, Vol.32, March 1970, p 383.
2. C. Bruinzeel, "Electric Discharges during Simulated Aircraft Fuelling". *Journal of the Institute of Petroleum*, Vol.49, No.124 (1963) p 473.
3. J. A. Carruthers and K. J. Wigley, "The Estimation of Electrostatic Potentials, Fields and Energies in a Rectangular Metal Tank Containing Charged Fuel". *Journal of the Institute of Petroleum*, Vol.48, June 1962, pp 180-195.

4. S. J. Vallenga, "Estimating the Electric Field Inside a Rectangular Tank with Boundaries at Zero Potential". Applied Scientific Research, Vol.B9, 1961, pp 35-44.

5. R. G. Davies and R. Knipple, "Experience with Static Dissipator Additive in Aviation Fuel". National Air Transportation Meeting, New York, April 20-23 1970. SAE Paper No. 700278.

6. H. F. Jones and E. French, "An Evaluation of the Effectiveness of a Static Dissipator Fuel Additive After Transport in a Full Scale Fuel Distribution System". USAF Report AFAPL-TR-69-23.

## HOW TO ADD ASA-3 TO AVIATION TURBINE FUEL

**STOCK SOLUTION** - Due to the very small quantity of ASA-3 required in the finished product, (about 0.6 p.p.m. mg/litre), it is normally more convenient to make up a stock solution, i.e. a pre-diluted ASA-3 solution and add this to the product.

For example, a stock solution containing 34.1 gm ASA-3, made up to 1 litre with Jet A-1 Fuel (i.e. a 3.4% wt/vol solution approximately), which became known as 'ASA-3 Mix', has been used extensively and successfully. 100 ml of such a stock solution when added to 1,000 Imperial gallons of a product gives a concentration of 0.75 p.p.m. ASA-3 in the finished product. Stock solutions in other proportions can of course be prepared.

**ADDITION METHODS** - Some possible ways for injecting the stock solution are illustrated in Figures 1 to 5 attached. Depending on the rate of injection, the type of equipment used, etc., it is possible that a stock solution of different concentration to that prepared as detailed in the second paragraph above may be necessary or desirable at some locations.

Figure 1 is a diagrammatic arrangement for a simple ratio control system. It operates on the principle, that if two liquids which are to be blended in a specific proportion are passed through an orifice before the point of junction, then the volumetric blend ratio will be in proportion to the ratio of the orifice areas, provided the pressure loss across each orifice is maintained at the same value. Pressures  $P_1$  and  $P_2$  can be equalised by a control valve in the additive line, actuated by a diaphragm, with pressure sensing lines on either side, connected to tappings upstream of the two orifices. Provided the additive stock solution can be pumped in at an adequate pressure a constant blend ratio will be achieved. Such a system can be designed and constructed using conventional control equipment. It is also possible to use a system whereby the blend ratio (additive/product) can be adjusted by using a manually operated accurate type regulating valve with position indicator device in place of the orifice in the additive line. A small meter and strainer in this line will be most helpful to calibrate the equipment and check the performance. Equipment of this nature is made by Elliott-Automation Control Valves Ltd. (Fisher Governor Division) as a packaged unit to include main and additive line control pieces, meter, control valve, regulating valve etc.

Figure 2 is a system using a small proportioning pump, powered by a fractional horse power electric motor. The injection rate of these pumps can be varied by stroke adjustment using a micrometer or similar attachment. The pumps are manufactured in a number of sizes to cover all injection rates, likely to be encountered in practice.

In using such pumps, it is recommended that a calibrated gauge glass or similar attachment is provided on the suction side to verify the injection rate periodically. If the flow rate in the main line varies significantly, it will be necessary to install a flow measuring device (e.g. orifice) in the main line and use this to adjust the stroke or speed of the injection pump to be in proportion to the main flow.

Figure 3 is an example of a self-powered system using a metering pump, such as manufactured by McFarland Engineering and Pump Co. Inc., Houston, Texas or which can be used with some meters such as those manufactured by Avery-Hardoll and Bopp and Reuther, by connecting a small injection pump to the rotor shaft. It is also possible to use small injection pumps on other meters such as those manufactured by Wayne-Smith and Brodie, which are controlled and actuated pneumatically by instrument air, which is normally available at refineries and some installations.

Figures 4 and 5 show two simple and inexpensive non-flow proportional systems, which have to be operated and controlled manually. These have been used successfully for batch wise operation at marketing installations or with aviation fuelling facilities.

Other manual methods, which have also been used satisfactorily for adding ASA-3 at airfields, inland depots and main installations are the following:-

**Product Received by Road or Rail** - Pour the appropriate quantity of stock solution either (a) into each receiving tank or (b) into one compartment of each vehicle and discharge. (The amount used should take into account the total tank contents including dead stock, when a partly filled tank of undoped fuel is to be treated).

**Product Received by Coastal, Inland Waterway Vessels or Tanker** - To provide the greatest measure of protection ASA-3 stock solution should be added in the appropriate quantity to each tank of the ship from which product is to be received.

If for any reason doping on the vessel is impracticable then the appropriate quantity of ASA-3 stock solution should be added to the receiving tank before discharge.

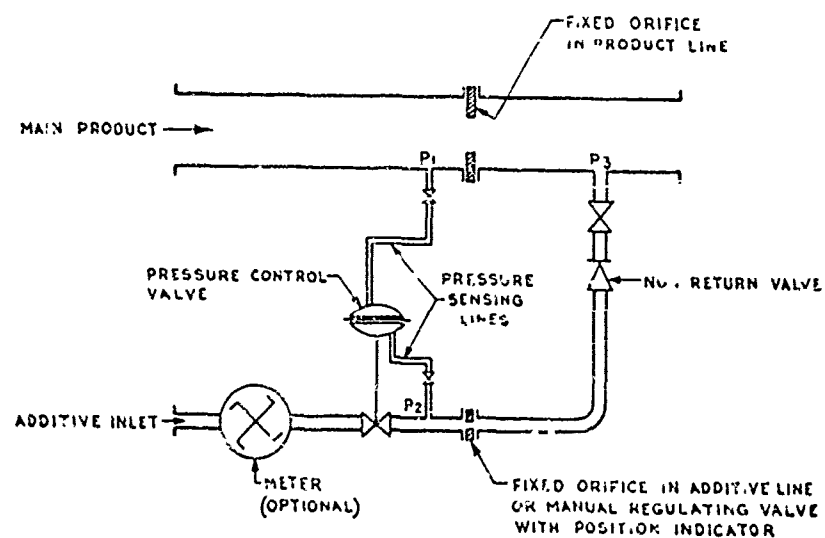


FIGURE 1 SIMPLE RATIO CONTROL SYSTEM

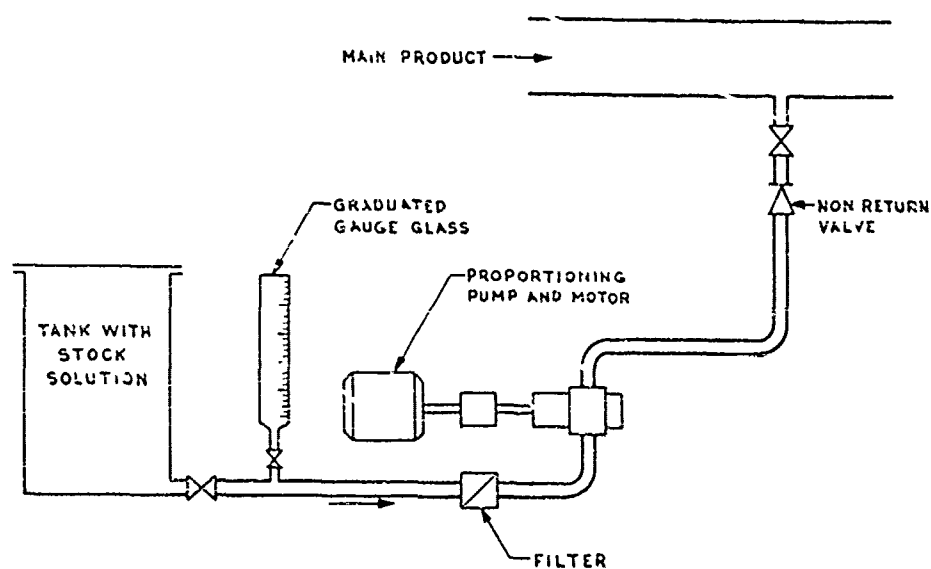


FIGURE 2 INJECTION WITH PROPORTIONING PUMP

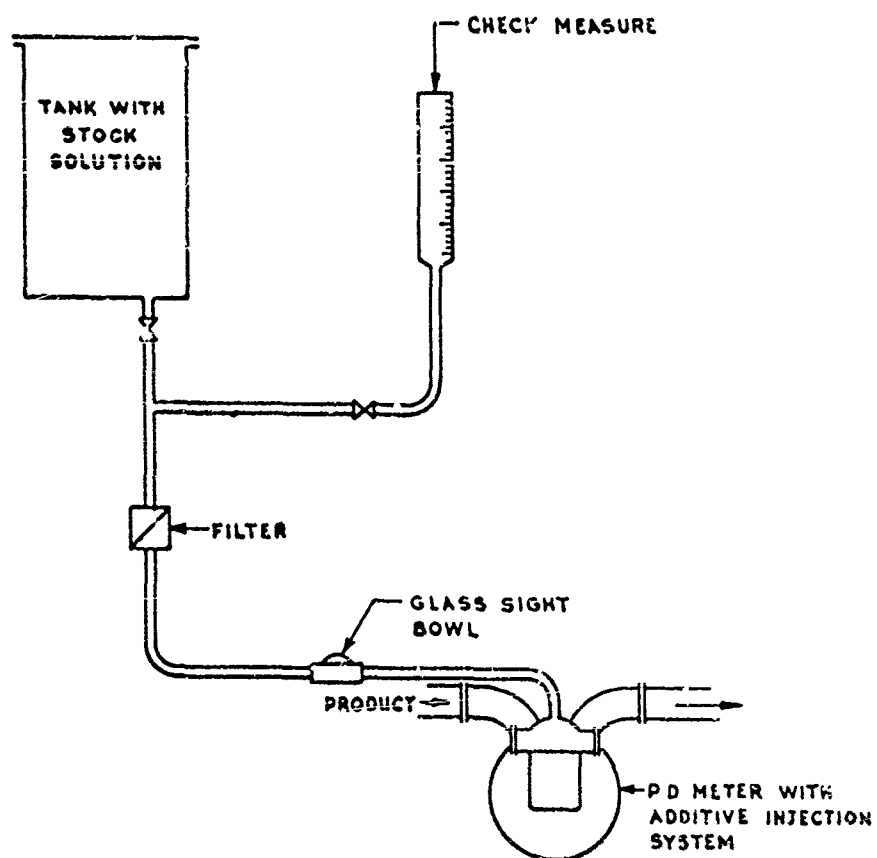


FIGURE 3 INJECTION SYSTEM COUPLED TO PD METER

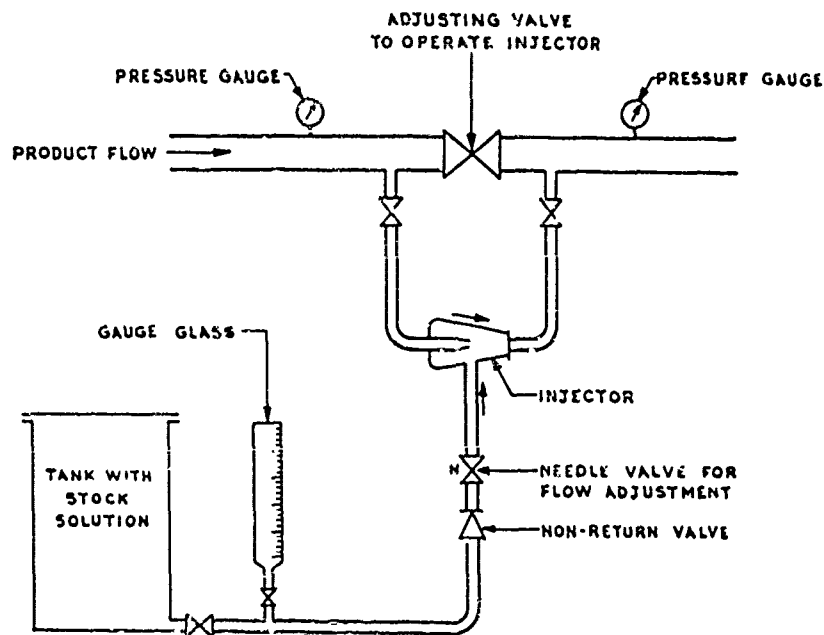


FIGURE 4 SELF ACTUATED SYSTEM WITH HYDRAULIC INJECTOR

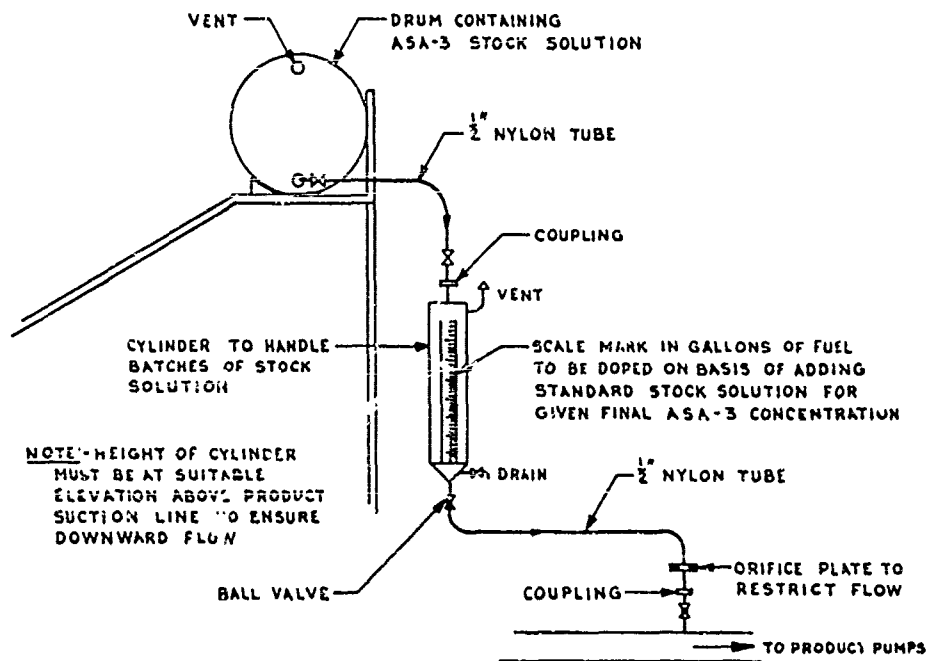


FIGURE 5 INJECTION INTO AVIATION FUELLING FACILITIES

## Protective System Measures For Aviation Fuel Handling

W. G. Dukek & K. C. Bachman  
Esso Research and Engineering Company

### ABSTRACT

There is increasing interest in fiberglass reinforced plastic (FRP) pipe for minimizing contamination in ground handling of aviation fuels. This report presents the results of a study conducted to determine if static electricity hazards would be increased by substituting FRP for metal pipe in such systems. Experiments were conducted in 6 inch diameter, matched volume, carbon steel and Bondstrand 2000 pipes at four fuel conductivities between 0.2 and 5.0 CU and at flow rates between 200 and 1500 GPM at controlled temperatures.

Charge generation in the pipes was low (2.5  $\mu\text{C}/\text{m}^3$  maximum with 0.9 CU fuel at 1200 GPM in steel); generation in FRP was generally less than in steel.

Relaxation in FRP pipe depended on fuel polarity; on the average, relaxation was 8 percent faster, with negatively charged fuel and 30 percent slower with positively charged fuel than in steel. The slower relaxation should not prevent the use of FRP in Type III Air Force hydrant systems handling JP-4 where a minimum of 2 minutes residence time would be available downstream of filter-separator at the maximum flow rates anticipated.

Voltages up to 55 KV were measured on the FRP pipe and sparks up to 1/2 inch long could be discharged from ungrounded metal components on the FRP pipe. These effects should be of no concern in underground installations.

An evaluation of the A. O. Smith Static Charge Reducer (SCR) showed that it was more efficient with positively, than negatively charged fuel and that deposit buildup could reduce its efficiency. The data suggest that static electricity hazards might exist downstream of an SCR although the average charge level is below 30  $\mu\text{C}/\text{m}^3$ .

TWO GENERAL APPROACHES are taken for dealing with the tendency of highly resistive hydrocarbon fluids to generate and accumulate static charges in high-speed flow through a handling system. The first approach attempts to deal with the charged fluid by providing a positive means for charge relaxation processes to occur before the fluid is delivered to the receiving vessel, such as an aircraft tank. The second approach is to minimize charge generation in the first place.

Techniques for dealing with charged fluids either by changing the electrical resistivity of the fluid to speed up charge relaxation--the anti-static additive approach--or by providing a vessel or pipe with sufficient residence time for normal charge relaxation processes--the relaxation tank approach--are well known in the art. A new type of relaxation device which has

been marketed for the past few years is the Static Charge Reducer(1)\*; it is claimed to provide in a fraction of a second the charge reduction equivalent to a relaxation tank.

The second approach, that of minimizing charge generation, has been difficult to achieve in aviation fuel handling systems because the filter-separators which are recognized to be prolific generators of static charge are essential to remove particulates and free water from fuel before it is delivered into aircraft. One course presently being investigated is actively to seek and install the types of filter-coalescers and separators which are inherently low charge generators by virtue of their design or material of construction. Such a program is being carried out by the Coordinating Research Council in full-scale tests of commercial equipment at airports(2).

### PLASTIC PIPE TO ELIMINATE FINAL FILTERS

Another course is represented by the "sanitary system" concept which eliminates the need for the final filter by substituting non-corrosive pipe for the steel normally used for hydrant systems. While ordinary steel, internally coated with plastic, aluminum or stainless steel can eliminate or minimize corrosion, a new material, fiberglass reinforced plastic (FRP), offers some additional advantages which make it attractive. It is less expensive than aluminum or stainless steel, and promises easier and faster installation, has lower friction losses and shows some superior mechanical properties over metal piping.

The use of FRP pipe for aircraft fueling systems has been extremely limited. The Air Force has a few specialized installations including a prototype C-5A facility at Edwards Air Force Base, an underwater POL line at Eniwetok, and a test section at Patrick Air Force Base. One reason for the go-slow approach in the use of FRP in hydrant systems for aircraft fueling has been concern about the possible electrostatic hazards posed by using this non-conductive material in a system that normally uses highly conductive metal. This report summarizes a study carried out for the Air Force in a full-scale Fueling Facility at Esso Research and Engineering Company at Linden, New Jersey to investigate this concern(3).

### WHY PLASTIC PIPE MAY PRESENT A PROBLEM

When charged fluid is introduced into conductive metal pipe, charge carriers migrate to the walls to recombine with charge of opposite polarity through ground. With an excellent electrical insulator like FRP pipe, there is the theoretical possibility that charge recombination processes might be reduced or limited

\* Numbers in parentheses designate References at end of paper.



even if the exterior of the pipe is grounded as in underground installations. The resistivity of FRP pipe could also result in accumulation of charge on its surface leading to voltages high enough to produce discharges to ground; such discharges might puncture the pipe wall or act as an ignition source for flammable vapors.

The primary objective of the Esso Research investigation was to determine if there was any significant difference between FRP and steel pipe in either charge generation or relaxation which might restrict the use of FRP in aviation fuel hydrant systems.

A review of the literature indicated that charge generating characteristics of FRP pipe would be small and little different from metal pipe. With respect to charge relaxation, limited data suggested that charge decay rate would be slower in plastic. Pipe resistivity seemed to be a major factor in determining whether a hazardous situation could develop. For example, visible discharges and voltages high enough to puncture the pipe wall have been observed with Teflon pipe.(4) Only one previous study had been carried out to investigate charge relaxation in a full-scale system using commercially available FRP pipe. The study, carried out at CLA-VAL Corp., Newport Beach, California in early 1969 was of limited value because the fuel electrical properties were not clearly defined.(5)

It was concluded that a side-by-side comparison of both pipe types under closely controlled conditions using fuels covering a range of properties was required before any recommendations could be made regarding the use of FRP in place of metal pipe in aviation fuel handling systems.

#### TEST PROGRAM

In order to study the pertinent variables affecting charge generation and relaxation, experiments were conducted in nominal 6-inch diameter FRP (Bondstrand 2000) and carbon steel pipes which were carefully matched in volume. The pipe sections were installed above ground to facilitate detection of electrical phenomena and to evaluate grounding of FRP pipe. The test pipes were integrated into an existing facility which could provide charged fuel for evaluating charge relaxation or essentially uncharged fuel for evaluation of charge generation in the test pipes.

Charge generation and relaxation were based on continuous measurement of charge densities at the inlet and outlet of each test pipe section. Data were obtained with fuels that ranged in resistivity from a high 5.5 Conductivity Units (CU), representative of JP-4, down to 0.2 CU representative of refined JP-5. Data were obtained over a range of flow rates between 200 and 1500 GPM (equivalent to 3.1 to 15.6 FPS linear velocity). Two lengths of each type of pipe were tested in order to provide a wide range of residence

times to evaluate the charge generation and relaxation processes.

Jet A with a flash point of 120°F was used instead of more volatile JP-4 to minimize the possibility of ignition in case of a fuel spill and also to permit precise control of conductivity by addition of pro-static agent. This control is difficult with JP-4 because of its normal additive package of corrosion inhibitor and anti-icing agent.

A Static Charge Reducer was incorporated into the test facility so that this new technique for relaxation of charged fluid could be compared with conventional relaxation in pipe lengths.

#### TEST FACILITY

The base facility, containing storage tanks, cleanup filters, refrigeration equipment, flow meter and pumps, has been described previously in an Esso Research static report.(6) It contains a 20,000 gallon supply of test fuel, which can be carefully controlled in contaminant level and temperature and supplied to the test pipe sections at flow rates up to 1500 GPM. Epoxy-coated tanks and stainless steel piping insures minimum uncontrolled contamination.

The test section, shown schematically in Figure 1, contains a commercial 1100 GPM filter-separator (F-S) and a pair of 600 GPM filter-monitors (F-M) which deliver charged fuel to the test pipe sections. These units are in parallel with a bypass line through which essentially uncharged fuel can be provided. The filters are electrically isolated by Teflon pads and gaskets so that charge generated in either device can be determined by direct measurement of current flow to ground.

An A. O. Smith Static Charge Reducer (SCR) with a bypass line was installed between the outlet of the filter/filter bypass array and the inlet to the test pipe. A. O. Smith Charge Density Meters (CDM) were installed at the outlet of the filter/filter bypass array and at the inlet and outlet of the test pipe section. Each pipe type was installed in two lengths, as shown in Figure 2; a U approximately 90 ft. long and a W approximately 160 ft. long. Jumpers were provided so that the two pipe lengths could be joined for a total run length of 240 ft. for each pipe type. Fuel was supplied to and removed from the pipe section under test by pairs of 3 inch diameter hoses connected to the pipe section under test through the CDM housings at the pipe inlet and outlet. The CDM housings were connected to the test pipe sections by Victaulic fittings for easy coupling with a given pipe section as illustrated in Figure 3.

To allow for direct and unambiguous comparison of charge generation and relaxation in the two pipe types, their hold-up volumes were carefully matched. Although both were nominal 6" pipes, the I.D. of FRP was 6.265" compared with an I.D. of 6.063" for steel. As a result,

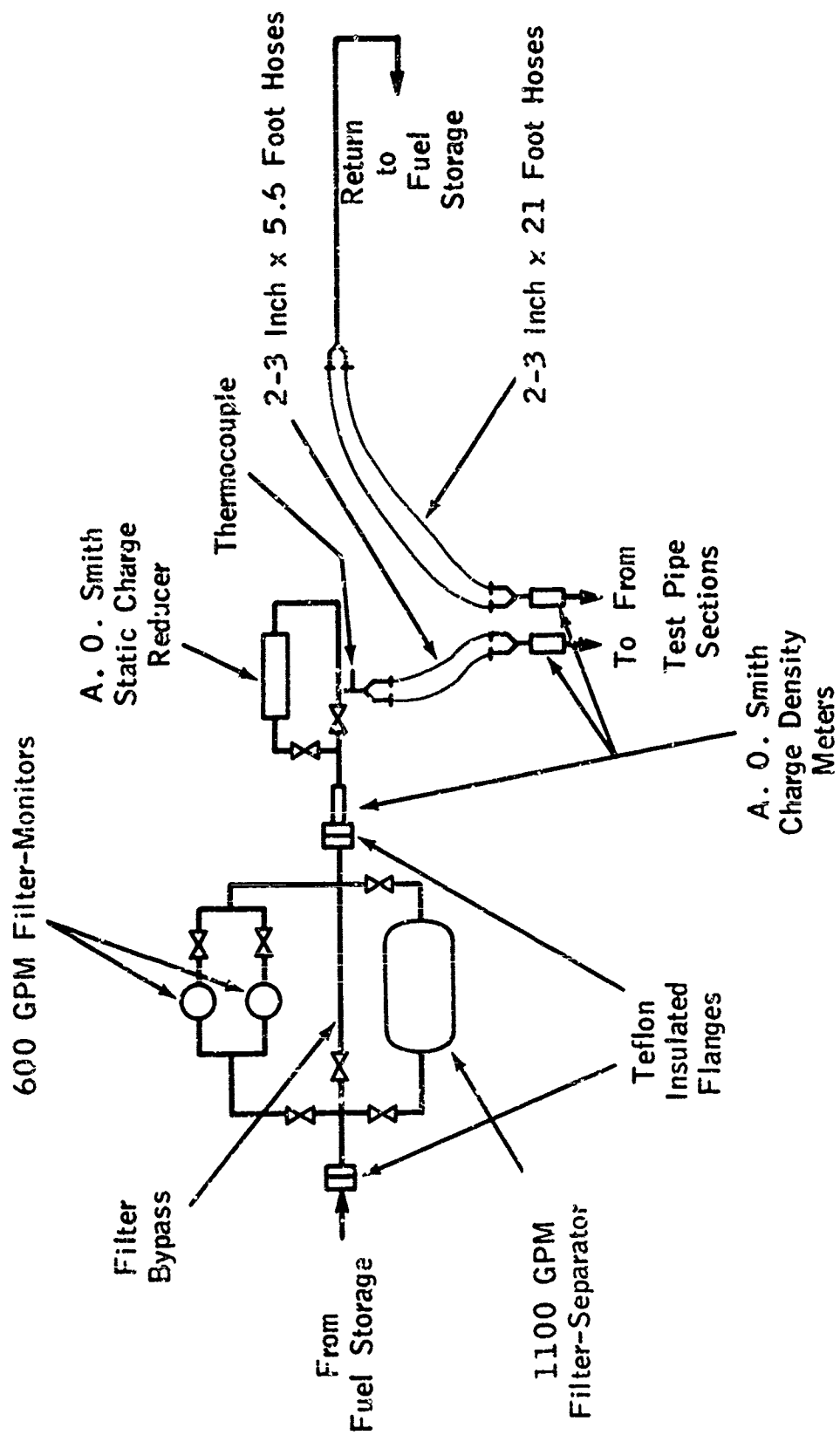


Fig. 1 - Schematic of the test section.

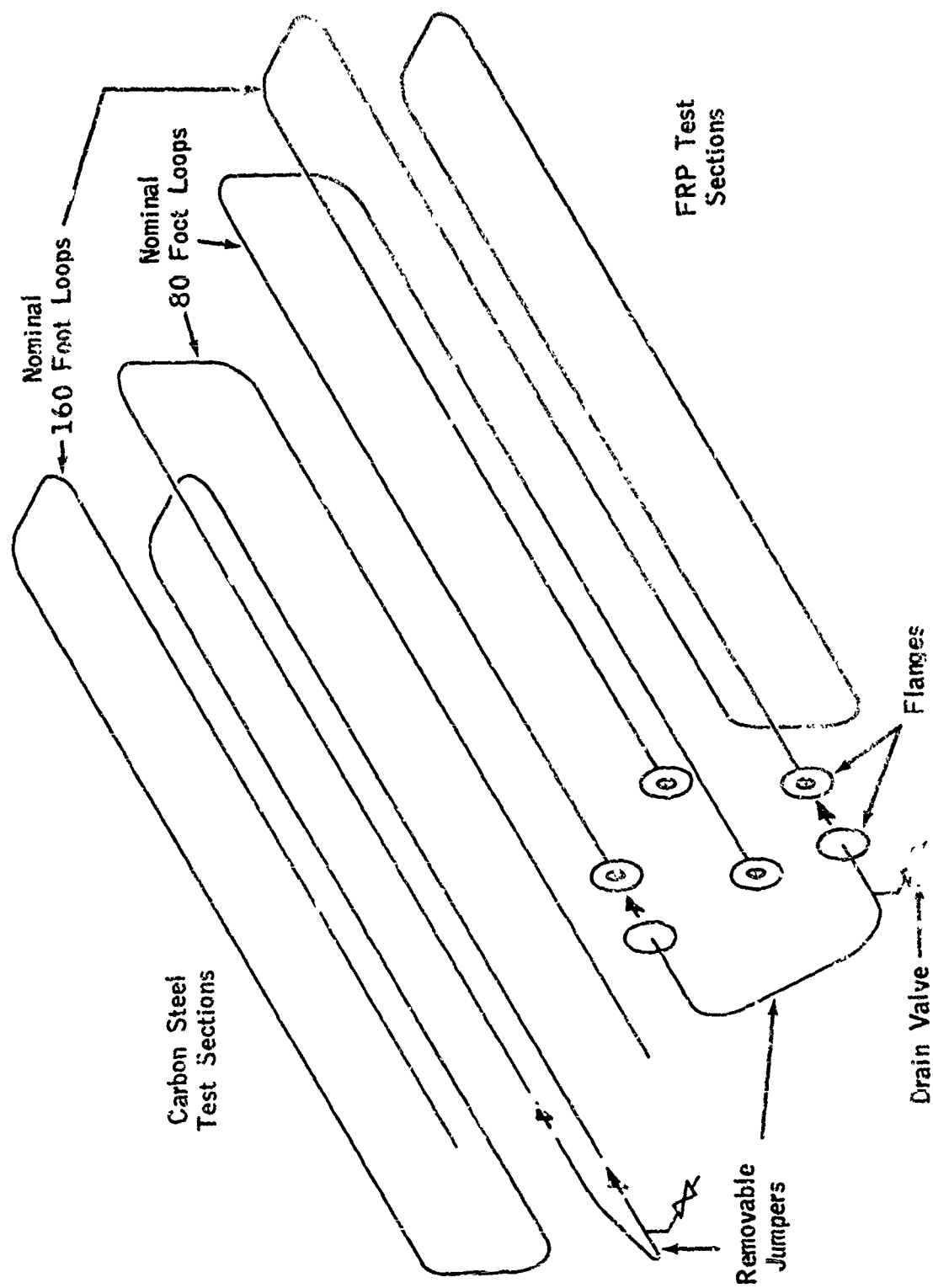


FIG. 2 - Schematic of carbon steel and FRP test pipe installation.

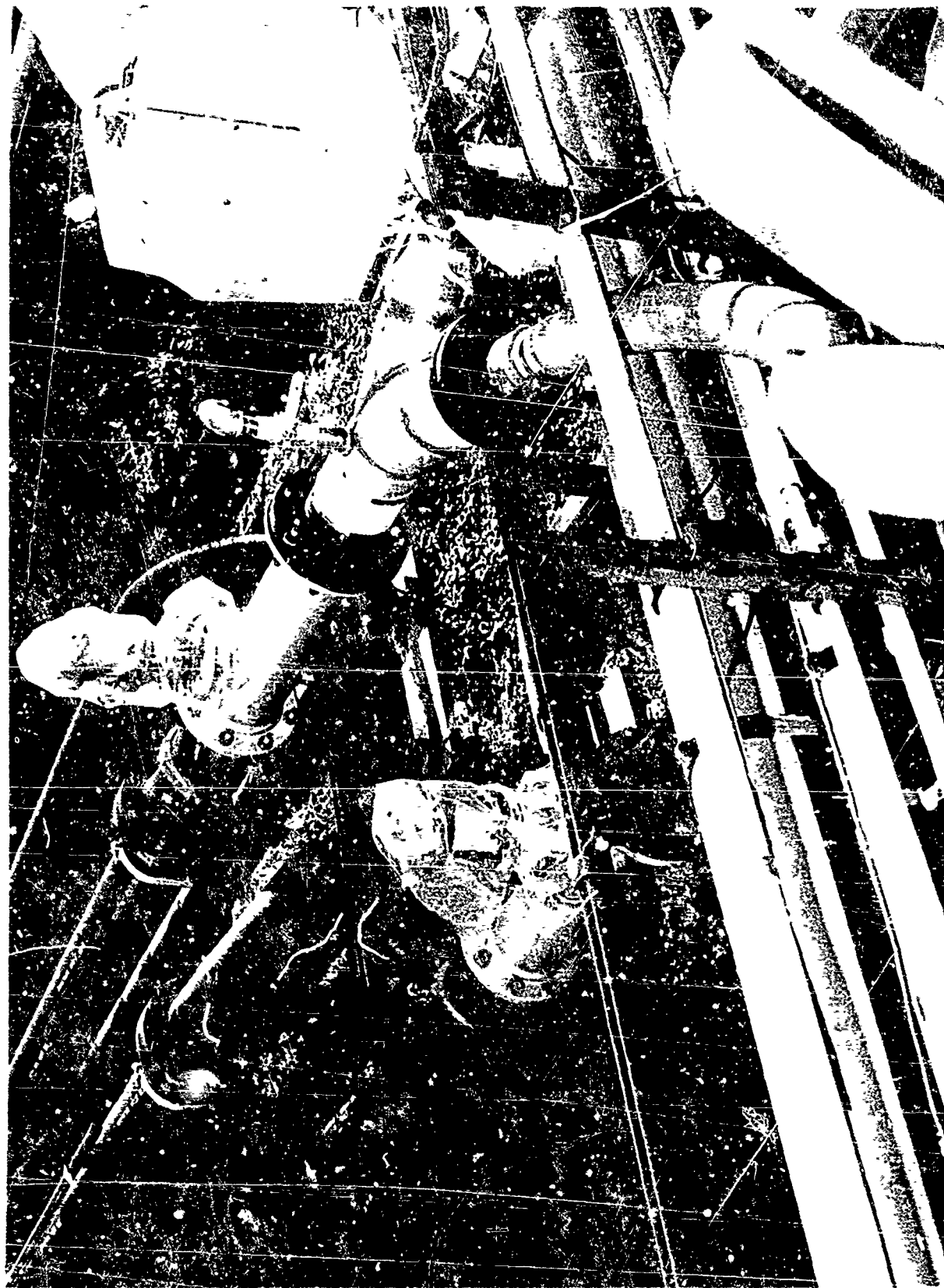


Fig. 3 - View of Charge Density Meters installed on long FRP pipe section  
(Fuel inlet at lower left, outlet at upper center, jumper connecting two  
pipe sections at upper left).

steel runs were somewhat longer than the FRP; the calculated volumes were 136 gal. for the short lengths and about 400 gal. for the long (240 ft.) lengths. An overall view of the Test Facility is shown in Figure 4.

#### TEST INSTRUMENTATION

Charge densities were measured continuously at three locations (outlet of the filter, inlet and outlet of test pipes) during each test using A. C. Smith Charge Density Meters (CDM) (rotating vane field strength meters). The usual Keithley Electrometer was replaced by an amplifier so that the CDM output could be monitored and recorded remotely in an instrument van.

Flow rate was measured with a turbine type Pottermeter, Model 6x5-555X, with an accuracy of 1% at full scale.

Fuel temperature was measured to 0.5°F with a calibrated bimetallic thermometer located ahead of the valve controlling flow to the test section.

Rest conductivity was measured on grab samples collected at random times using the new precision method D 3114 developed by ASTM. Samples were allowed to relax at least 5 minutes before measurement.

Surface voltage was measured with a rotating vane Electrostatic Field Meter, Model 12009-1, made by Comstock & Wescott, Inc., Cambridge, Mass. A special fitting utilized nylon bolts to hold the meter a fixed distance from the pipe.

Spark discharges were detected visually, aurally or by using a walkie-talkie radio. No spark energy measurements were made.

#### TEST PROCEDURE

Prior to use, the FRP pipe was swabbed with hexane-soaked cloths while the carbon steel was sandblasted to bare metal and blown clean with dry air. Prior to testing, the system was flushed with 5000 gals. of Jet A fuel. Each test pipe section was flushed for two hours at 1000 GPM while the fuel was continuously filtered in the 1800 GPM cleanup filter-separator. The cleanup fuel was slopped, new elements were installed in both the F-S and the F-M's of the test section and 20,000 gallons of fresh Jet A were charged to the system for the test program.

The first series of tests were carried out with the fresh Jet A which had a rest conductivity of 0.9 CU. For the next two series, incremental additions of oxidized asphalt were made to increase the fuel conductivity to 3 and then 5.5 CU. For the final series, clay treatment was used to lower the fuel conductivity to about 0.2 CU.

Prior to each test series, the pipe sections were equilibrated with the fuel supply by recirculating at 1000 GPM through the long steel and then the long FRP sections until the conductivity stabilized. During this recirculation, both the F-S and the F-M's were in the

system for equal times to assure their equilibration with the fuel supply.

Temperature was a critical variable in comparing charge relaxation in the two types of pipe. Because the facility was outdoors, the fuel temperature was influenced both by ambient temperature and cloud cover. While it was not possible to run all tests at the same temperature, it was found that judicious use of refrigeration made it possible to match the temperatures within 0.5°F for a given flow rate and inlet charge level in each of the four pipe type/pipe length combinations.

#### TESTS RESULTS

FUEL CONDUCTIVITY VS. TEMPERATURE - Rest conductivities,  $k_0$ , were measured on grab samples collected during each series of tests. An initial measurement was made after the sample was allowed to relax for at least five minutes. A second measurement was generally made after the sample had warmed up in the instrument van. The data from each test fuel were used to find the best fit to the equation

$$\log k_0 = mT + c, \quad (1)$$

where  $k_0$  is expressed in Conductivity Units (CU). The equations were used to define the rest conductivity at the test temperature in each run.

In discussing the data, the nominal rest conductivity of the fuel is used to describe the fuel. It should be noted that a calculated conductivity value can also be derived from charge data during flow. This value is called "effective" conductivity,  $k_e$ , and describes the conductivity of the fuel in the dynamic charged condition.

CHARGE GENERATION IN FRP AND METAL PIPE - To compare charge generating characteristics of FRP vs. metal pipe, fuel was pumped through the filter bypass to keep inlet charge as low as possible. This approach was successful; the inlet charge ranged from 0.5  $\mu\text{C}/\text{m}^3$  at 300 GPM (for 0.2 CU fuel) up to -4.4  $\mu\text{C}/\text{m}^3$  at 1500 GPM (for 5.5 CU fuel). Charge level stabilized at all three measuring points within two minutes after a flow change. Values are considered accurate to  $\pm 0.1 \mu\text{C}/\text{m}^3$ .

The differences in charge densities between pipe inlet and outlet are summarized in Table 1. A positive value indicates that net charge was being generated within the pipe, a negative value generally indicates that charge was being relaxed within the pipe (or that charge of opposite polarity was being generated).

The results show relatively little charge generation in either FRP or steel pipe although steel generated slightly more charge in all cases. With the 3 and 5.5 CU fuels charge relaxation predominated but there was generally a greater decrease in FRP than in steel pipe, indicating that the latter was tending to generate more charge. With 0.2 and 0.9 CU fuels, charge generation generally

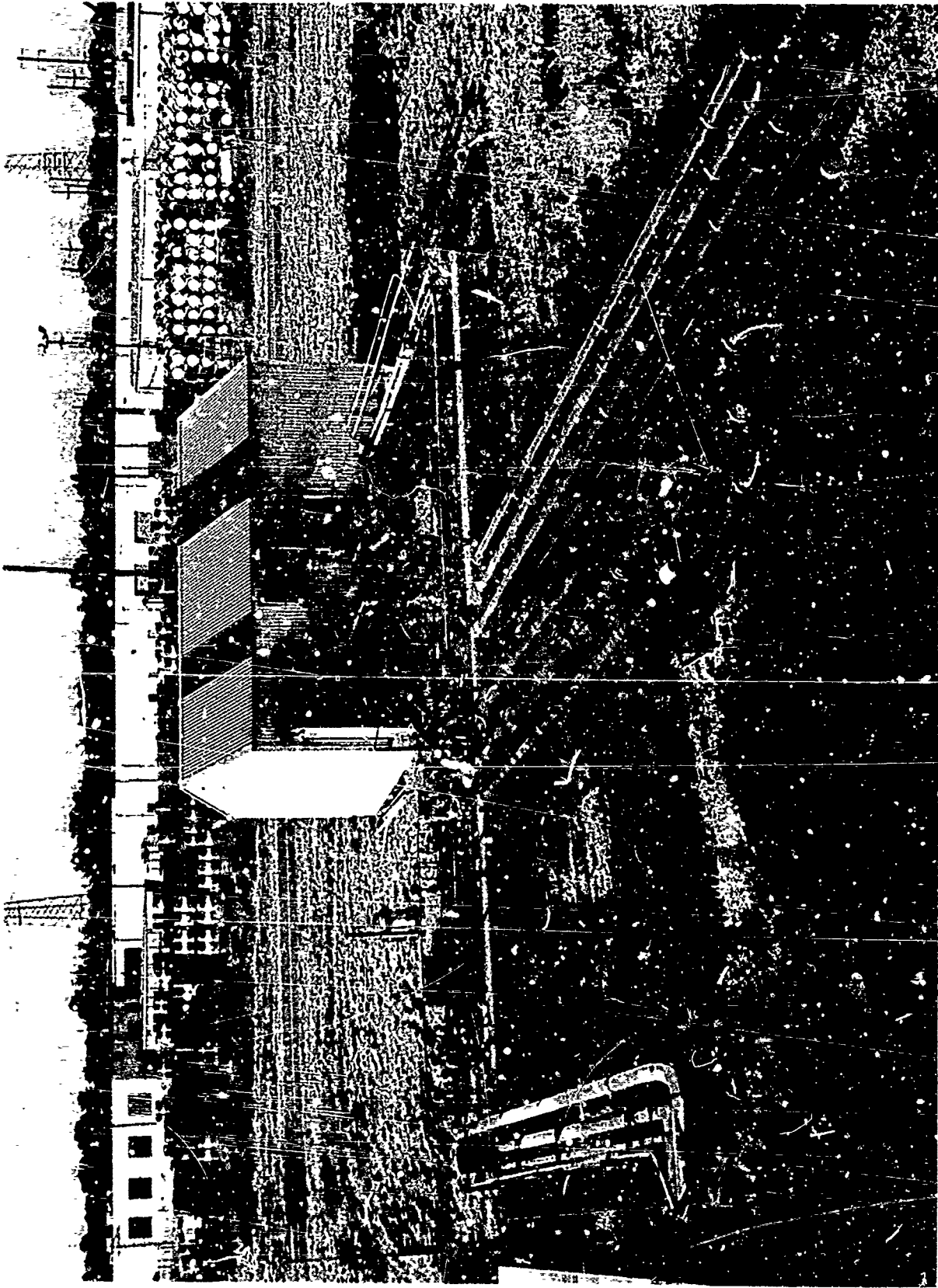


Fig. 4 - Overall view of test section  
(Steel pipe sections at right, FRP sections in center, filter/filter bypass  
array at upper left).

Table 1

Charge Generation in FRP and Carbon Steel Pipe

(A positive value indicates charge was being generated,  
a negative value indicates charge was relaxing.)

Nominal Fuel CU	Pipe Length Pipe Type Flow Rate, GPM	Change in Charge Density Between Pipe Inlet and Pipe Outlet, $\mu\text{C}/\text{m}^3$			
		Short		Long	
		Steel	FRP	Steel	FRP
0.2	300	0.1	0.0	0.2	0.2
	600	0.2	0.1	0.9	0.5
	1200	0.2	0.2	1.3	0.5
	1500	0.4	0.2	1.3	0.4
0.9	300	0.0	-0.5	-0.3	-0.6
	600	0.4	-0.3	0.4	-0.5
	1200	0.8	-0.3	2.5	-0.3
	1500	0.9	0.0	2.5	-0.7
3.	300	-0.8	-0.7(a)	-0.5	-0.6(a)
	600	-0.6	-1.5	-0.5	-1.1(a)
	1200	-0.1	-1.2	-0.6	-2.2(a)
	1500	-0.2	-1.1	-0.2	-2.7
5.5	300	-0.5	-1.3	-0.8	-1.0
	600	-1.2	-1.9	-1.7	-2.5
	1200	-0.3	-1.7	-1.1	-3.7(a)
	1500	0.0	-1.9	-0.4	-4.2

(a) Polarity reversed.

increased with pipe length, but since no increase was noted when the flow rate was increased from 1200 to 1500 GPM, the charge levels reached probably represent equilibrium levels and no further increase would be expected if the pipe lengths were increased. This effect is not apparent with the 3 and 5.5 CU fuels where there is generally a net charge relaxation due to the more rapid relaxation provided by the higher conductivities.

It can be concluded from these data that charge generation in FRP pipe is somewhat less than in steel probably because the internal surface of carbon steel pipe is rough compared with smooth FRP pipe. However, the differences are too small to be of practical significance in the field.

**CHARGE RELAXATION** - The comparison of charge relaxation in FRP vs. steel pipe was made by charging the test fuels in either the 1100 GPM F-S or the pair of 600 GPM F-M's and comparing the rates of charge relaxation under essentially identical conditions. Tests were conducted at flow rates between 300 and 1200 GPM under closely controlled temperatures. Average charge densities generated as a function of flow rate and CU, based on four comparable runs, together with average temperatures, appear in Table 2. As shown in Figure 5, the F-S charged the fuels negatively; the F-M's charged them positively. There was a striking difference between these two filters in response to CU (or impurity level) and to flow rate, the F-S generally showed an increase in charge with flow rate increase and a lower level with increasing CU while the F-M performed almost diametrically opposite.

These differences can be explained in part by geometry of the vessels containing the filters. The F-S case holds 275 gallons of fuel, the F-M case, only 18 gallons, which means that charged fuel has much more opportunity to relax in the F-S than in the monitor at comparable flow rates. The filter media are different and may explain the opposite polarities -- the F-S contains fiberglass depth filter-coalescer elements at the inlet end and treated paper surface filter (separator) elements at the outlet end while the monitor is composed of hundreds of paper wafers in each element providing edge filtration. Each filter element provides very large surface area for charge separation.

Temperature can also affect charge level as noted in Table 2. With the 0.9 CU fuel, tests were repeated when the temperature dropped from 59°F to 36°F. At 1200 GPM, charge levels from the F-S dropped 52  $\mu\text{C}/\text{m}^3$  or about 3  $\mu\text{C}/\text{m}^3$  per degree; little effect could be observed with the F-M's.

Measurement of charge densities in the fuel at the inlet and outlet of each pipe section permitted a calculation of relaxation time,  $\tau$ , which was used to compare relative characteristics of FRP vs. steel pipe. Relaxation time is defined as the time for charge to decay to 36.8% of its original value using the relationship:

$$\tau = t / \ln (Q_0 / Q_t) \quad (2)$$

where  $Q_t$  = charge density at test pipe outlet, in  $\mu\text{C}/\text{m}^3$

$Q_0$  = charge density at test pipe inlet, in  $\mu\text{C}/\text{m}^3$

$t$  = residence time, in seconds, between pipe inlet and outlet at the flow rate tested.

The  $\tau$  values obtained with negatively charged fuel generated by the F-S are summarized in Table 3; the  $\tau$  values for positively charged fuel are in Table 4. No  $\tau$  values are shown for runs in which outlet charge is less than 1  $\mu\text{C}/\text{m}^3$  since small changes in outlet charge at this level, which could be influenced by pipe charge generating characteristics, would have a large effect on  $\tau$ .

When the  $\tau$  values for negatively charged fuel are examined graphically as a function of flow rate and CU level, as in Figure 6, it is observed that  $\tau$  tends to decrease with increasing flow rate as well as increasing CU. With negatively charged fuel, relaxation time in FRP pipe is always less than in steel pipe under the same test conditions. Relaxation time is longer in the long than in the short pipe lengths as shown in Table 3.

Positively charged fuel reveals a different story as shown in Figure 7. Thus  $\tau$  tends to increase with flow rate and to be longer with FRP pipe than steel under identical conditions. Again  $\tau$  is longer in long vs. short pipe lengths. Thus, the data obtained in these runs reveal that there is a difference in charge relaxation between FRP and steel pipe which depends on the polarity of the fuel. When fuel is charged negatively, charge relaxation on FRP pipe proceeds faster; when fuel is charged positively, it proceeds slower.

The difference in relaxation characteristics between FRP and steel pipe, expressed as a percentage change in  $\tau$  ranges from 0 to 18% faster for FRP pipe with negatively charged fuel, averaging 8% faster overall. For positively charged fuel, the range is wider, relaxation takes 8 to 154% longer in FRP pipe. The range is reduced to 8 to 75%, averaging 30% slower overall, if data suspect because of low charge levels or temperature effects is excluded.

To answer the key question as to whether this slower relaxation rate should rule out or limit the use of FRP pipe, it is useful to restate the calculated relaxation times in terms of effective conductivity,  $k_e$ :

$$k_e = 18 / \tau \quad (3)$$

When the ratio of  $k_e$  to rest conductivity,  $k_0$ , is plotted against  $k_0$ , as in Figure 8, the results obtained follow the pattern of previous work shown by the dashed curves. These data indicate that fuel below 1 CU relaxes faster than one would predict from rest conductivity while fuels above 1 CU relax somewhat slower than predicted. The plot also makes clear that



Table 2

Average Charge Densities Generated By  
The Filter-Separator and Filter-Monitors  
as a Function of CU and Flow Rate

Charge Generator	Fuel CU	Charge Density, $\mu\text{C}/\text{m}^3$ , @ GPM(a)			
		300	600	900	1200
(Average Temperatures Shown in Parentheses)					
Filter Separator	0.2	-74(39)	-126(38)	150(37)	-166(38)
	0.9	-51(60)	-102(59)	-	-148(58)
	3.	-4(41)	-16(40)	-	-62(40)
	5.5	5(41)	-2(39)	-22(39)	-44(40)
Filter- Monitors	0.2	12(40)	9(39)	-	6(38)
	0.9	24(57)	20(56)	-	16(55)
	3.	132(44)	118(43)	-	97(42)
	5.5	178(40)	174(39)	159(38)	150(38)
Filter Separator	0.9	-36(38)	-56(36)	-	-96(40)
	0.9	20(37)	16(36)	-	-
Filter- Monitors					

(a) Based on the average of four comparable runs, no repeat runs were included; values in parentheses show average temperature for the four runs.

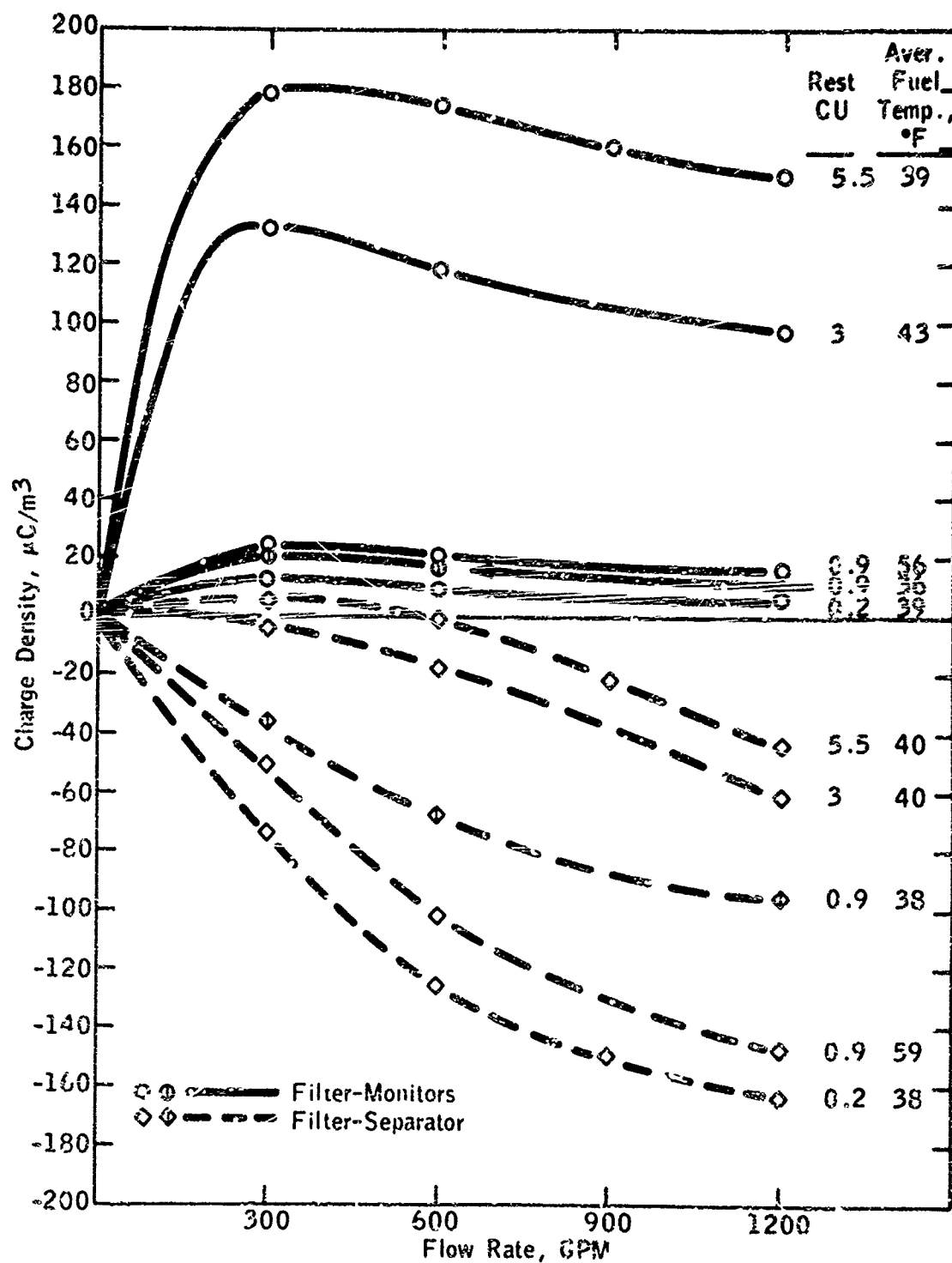


Fig. 5 - Charge generated by F-S and F-M's as a function of fuel conductivity, flow rate and temperature.

Table 3

Relaxation Times for FRP and Steel  
Pipe Obtained with Negatively Charged Fuel  
(Generated by Filter-Separator)

Nominal CU of Fuel	Flow Rate, GPM	Range of Charge Densities at Pipe Inlet, $\mu\text{C}/\text{m}^3$	Relaxation Time, $\tau$ , Seconds			
			FRP Pipe		Steel Pipe	
			Short	Long	Short	Long
0.2	300	-66/-70	56	74	61	77
	600	-115/-120	39	53	41	54
	900	-138/-147	34	44; 45	37	44
	1200	-151/-167	31	40	32; 33	41
0.9	300	-42/-49	32	36	36	40; 40
	600	-86/-97	26	30	29	34
	910	-126/-137	--	24	--	27; 28
	1200	-135/-142	20	23	21	26
3.0	300	0/4	(a)	(a)	(a)	(a)
	600	-6/-20	10.1	(a)	10.4	(a)
	900	-46	--	--	10.0	--
	910	-24/-37	--	10.3	--	12
	1200	-36/-68	8.9	9.9	9.4	11
5.5	300	0.2/0.6	(a)	(a)	(a)	(a)
	600	-1/-7	(a)	(a)	(a)	(a)
	900	-12/-30	5.9	(a)	7.2	9.1; 9.2
	1200	-27/-56	5.8	5.4(b)	6.5	7.5

(a) Charge density at pipe outlet was  $< 1.0 \mu\text{C}/\text{m}^3$ .

(b) Charge density at pipe outlet was  $0.8 \mu\text{C}/\text{m}^3$ .

Table 4

Relaxation Times for FRP and Steel  
Pipe Obtained with Positively Charged Fuel  
(Generated by Filter-Monitor)

Nominal CU of Fuel	Flow Rate, GPM	Range of Charge Densities at Pipe Inlet, $\mu\text{C}/\text{m}^3$	Relaxation Time, $\tau$ , Seconds			
			FRP Pipe		Steel Pipe	
			Short	Long	Short	Long
0.2	200	10/17	55	--	45	--
	300	8/19	56; 57	68	44	52
	600	6/16	60; 58	73	50	48
	1200	4/14	67; 56	60	26	28
0.9	300	14/23	28	31	26	(a)
	600	13/23	26	40	24	24
	910	12/20	--	48	--	24
	1200	11/20	39	51	24	23
3.0	300	68/91	6.7	(a)	5.3(b)	(a)
	600	82/106	12	14	9.1	11
	900	80	--	--	11	--
	910	94/104	--	18	--	14
	1200	76/101	16	21	13	16
5.5	300	63/100	(a)	(a)	(a)	(a)
	600	104/136	7.8	9.4	4.4	(a)
	900	114/137	8.5	9.8	6.2	7.7
	1200	119/134	9.4	10.7	7.5	9.6

(a) Charge density at pipe outlet was  $< 1.0 \mu\text{C}/\text{m}^3$ .

(b) Charge density at pipe outlet was  $0.4 \mu\text{C}/\text{m}^3$ .

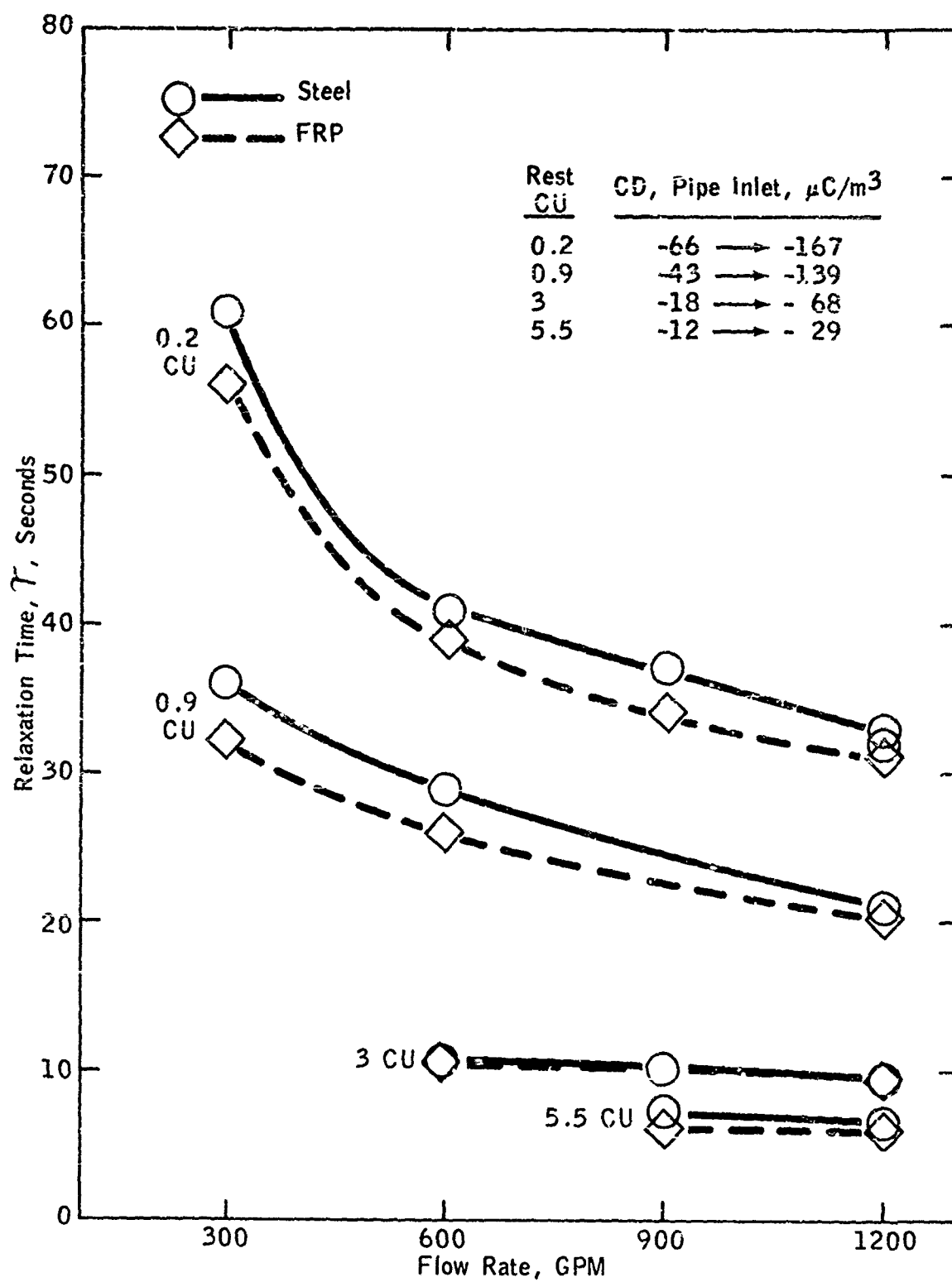


Fig. 6 - Relaxation times in short pipe sections with negatively charged fuel as a function of CU and flow rate.

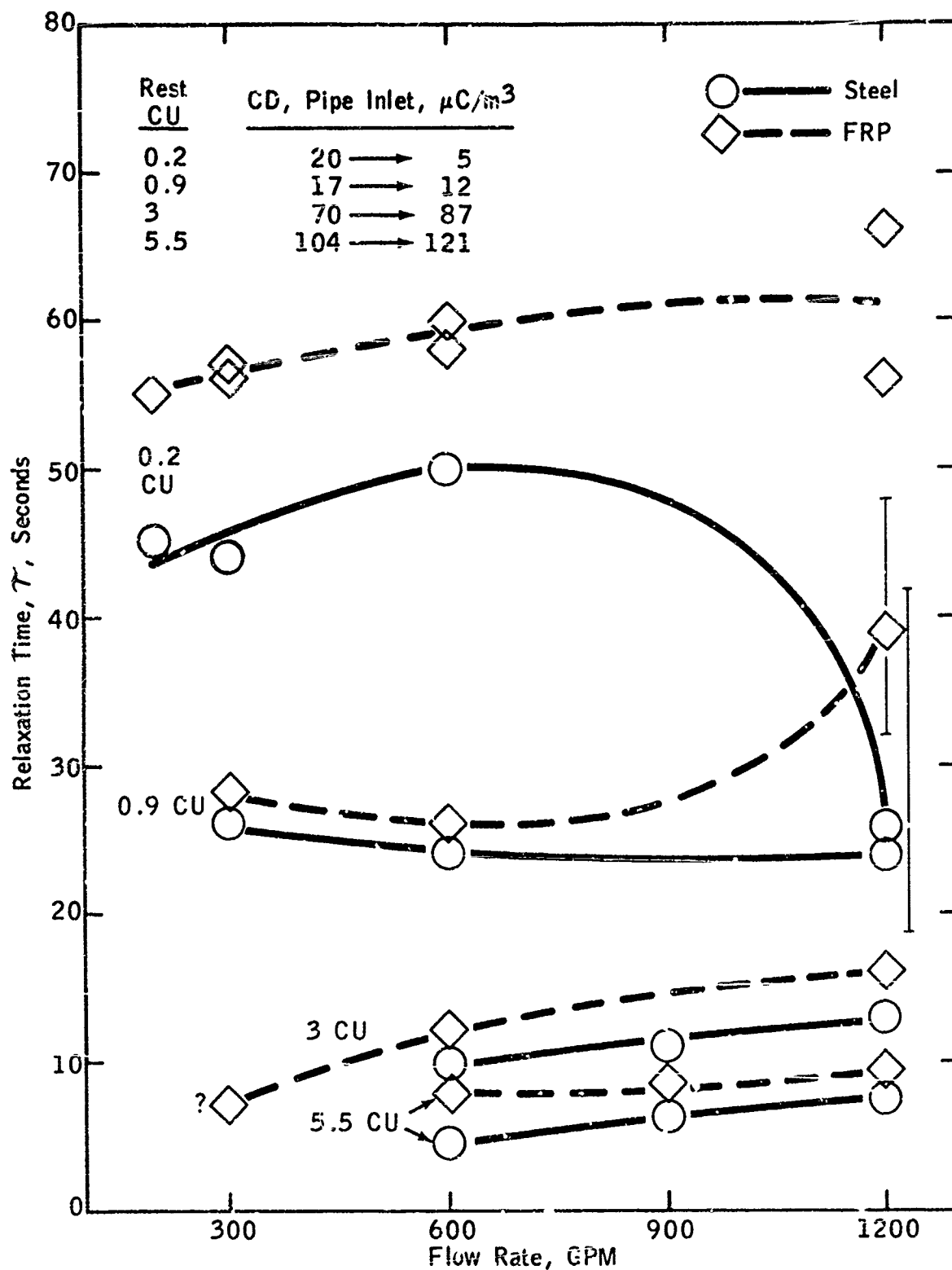


Fig. 7 - Relaxation times in short pipe sections with positively charged fuel as a function of CU and flow rate.

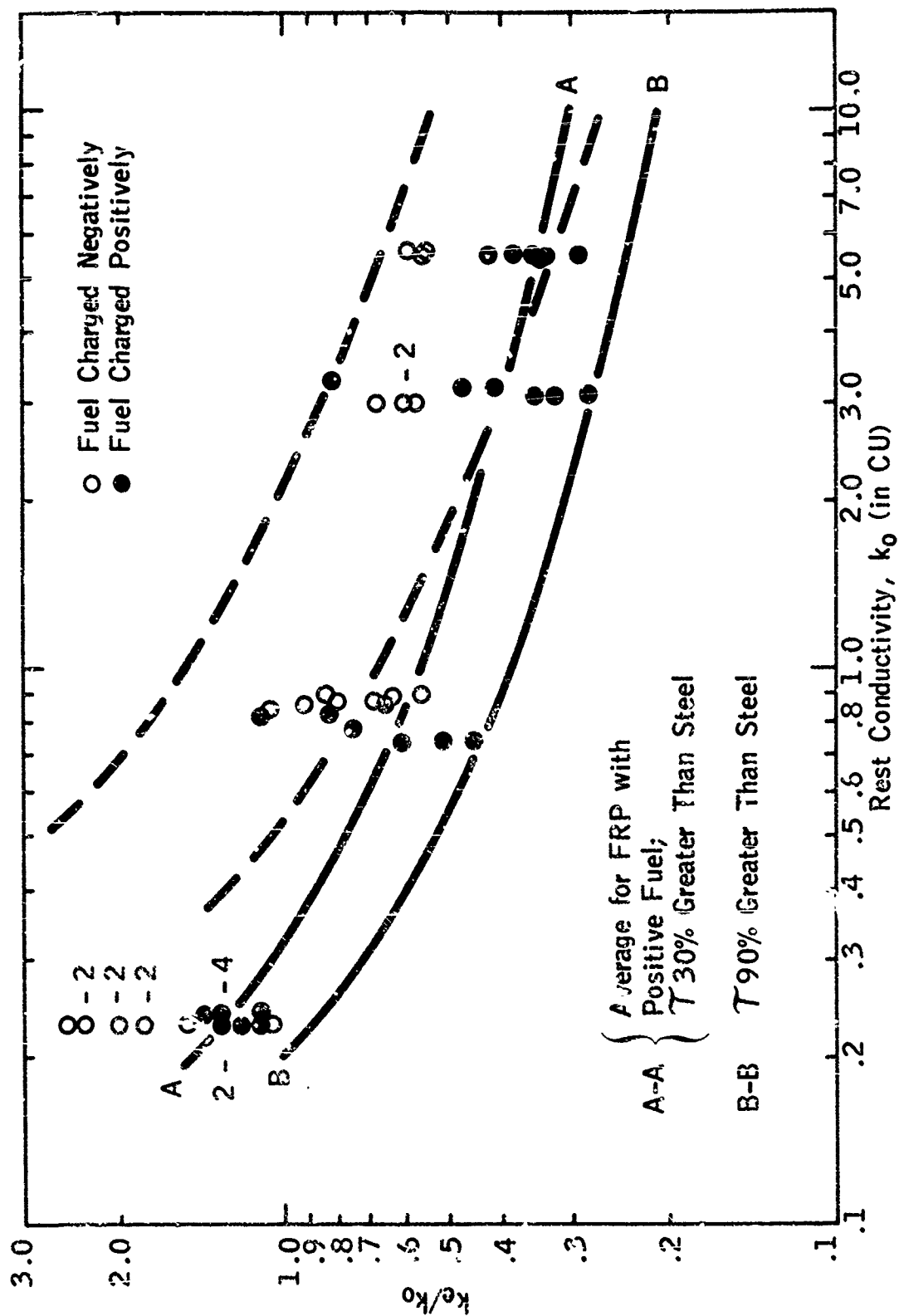


Fig. 8 - Ratio of  $k_e/k_o$  versus  $k_o$  obtained with FRP pipe.

positively charged fuel represents a different family than negatively charged fuel in FRP pipe.

The reason for this faster relaxation of fuel below 1 CU was developed by Bustin (7) who established that the charge decay rate of such fuels was dependent not on conductivity, but on charge level and ion mobility,  $\mu$ , as described by the equation:

$$Q_t = \frac{Q_0}{1 + \frac{\mu Q_0 t}{\epsilon \epsilon_0 \times 10^6}} \quad (4)$$

which is hyperbolic rather than exponential. This decay rate is illustrated by the curves in Figure 9 developed from the test results on the negatively charged 0.2 CU fuel. The solid curves were derived from the above equation for assumed inlet charge levels of 1000 and 100  $\mu\text{C}/\text{m}^3$  and an outlet charge level of 30  $\mu\text{C}/\text{m}^3$  and a calculated ion mobility of  $0.38 \times 10^{-8} \text{ m}^2/\text{volt sec}$ . as derived from the data obtained in this program. For comparison, the straight lines represent ohmic decay based on a rest conductivity,  $k_0$ , of 0.2 CU. While the latter relationship can describe charge relaxation well for fuels above 1 CU, it is obviously deficient for highly refined fuels.

If one examines Figure 9 it is apparent that the initial charge relaxation based on hyperbolic decay is faster than ohmic decay would predict; nevertheless considerable residence time is required for the charge to reach a low level. After 30 seconds of relaxation, the 1000  $\mu\text{C}/\text{m}^3$  fuel would have dropped to 140  $\mu\text{C}/\text{m}^3$ , an 86% decrease in charge; the 100  $\mu\text{C}/\text{m}^3$  fuel would have dropped to 60  $\mu\text{C}/\text{m}^3$ , a decrease of only 40%.

Predicted residence times required to reduce charge to 30  $\mu\text{C}/\text{m}^3$  from inlet levels between 100 and 500  $\mu\text{C}/\text{m}^3$  appear in Table 5. The upper section of the table represents results on standard steel pipe while the middle section represents the effect of increasing relaxation time by 30%, the average observed for FRP pipe with positively charged fuel. The lower section spells out the case for increasing relaxation time by 90%, a value three times higher than the average but representative of the maximum measured with positively charged fuel in the FRP pipe.

For fuels of 1 CU and higher, the steel pipe data were generated using average  $k_e$  values based on the experimental data and assuming ohmic charge decay; data for FRP pipe were generated by increasing the  $\tau$  for steel pipe by 30 or 90%. Steel pipe data for 0.2 CU fuel were generated assuming hyperbolic charge decay and an ion mobility of  $0.38 \times 10^{-8} \text{ m}^2/\text{volt sec}$ ; data for FRP pipe at 0.2 CU were obtained by increasing the residence time values for steel pipe by 30 or 90%.

For Type III Air Force hydrant systems, where FRP pipe has been approved for handling

JP-4, the Air Force has indicated that the minimum length of pipe between a fuel filter and the first fueling station in a typical installation would be 900 to 1000 ft. At the design flow rate of 4 ft./second, the residence time would be 225 to 250 seconds. At 7 ft./second, the maximum flow velocity which such systems might be called on to handle in the future, the residence time would be 130 to 140 seconds.

In Table 5, the asterisks pinpoint the combinations of fuel conductivity and charge level which require residence times above 225 seconds to reach the target value of 30  $\mu\text{C}/\text{m}^3$ . The underlined values note the combinations above 130 seconds, which represents the absolute minimum residence time that would be expected in Type III Air Force hydrant fueling systems. This analysis indicates that 130 seconds of residence time would be adequate to provide relaxation to 30  $\mu\text{C}/\text{m}^3$  for fuel of 1 CU at charge levels up to 500  $\mu\text{C}/\text{m}^3$  at the pipe inlet. A residence time of at least 283 seconds should be provided to protect against the possibility of inadequate charge relaxation in an FRP system with fuel as low as 0.2 CU in conductivity at an inlet charge level of 500  $\mu\text{C}/\text{m}^3$ .

For this study, a charge level of 30  $\mu\text{C}/\text{m}^3$  has been used as the criterion for "safe" fueling. The value was originally proposed by American Oil (1) and has been generally accepted by others in the industry as a reasonable guide. Our own studies on supersonic fueling (6) showed that a minimum charge density of 70  $\mu\text{C}/\text{m}^3$  was required to generate incendiary sparks during fueling if a "charge collector" was present in the receiving tank. Since it is desirable to provide for safe fueling in the most hazardous situations, the use of a maximum of 30  $\mu\text{C}/\text{m}^3$  as a "safe" charge level is considered reasonable.

Although the data in Table 5 were generated with Jet A fuel, there is no reason to expect JP-4 to behave differently. What is not known at present is the range of conductivities of JP-4's and the charging tendency of military filter-separators. Since it is known that corrosion inhibitor tends to act like a weak conductivity additive, it is probable that JP-4's have conductivities of 1 CU or above. A field survey for conductivity and charging tendency of typical JP-4's should make this table useful in deciding whether the charge relaxation characteristics of a particular hydrant system are adequate.

**SURFACE VOLTAGE ON FRP PIPE** - Voltages on the surface of the FRP pipe (the conductivity of steel pipe prevents any buildup of voltage on its surface) were measured at 10 to 20 ft. intervals along the FRP pipe during most runs. The maximum surface voltages observed are summarized in Table 6.

It can be seen that surface voltages generally increase with charge level and are higher on the longer pipe section for a given inlet charge level. The highest voltage



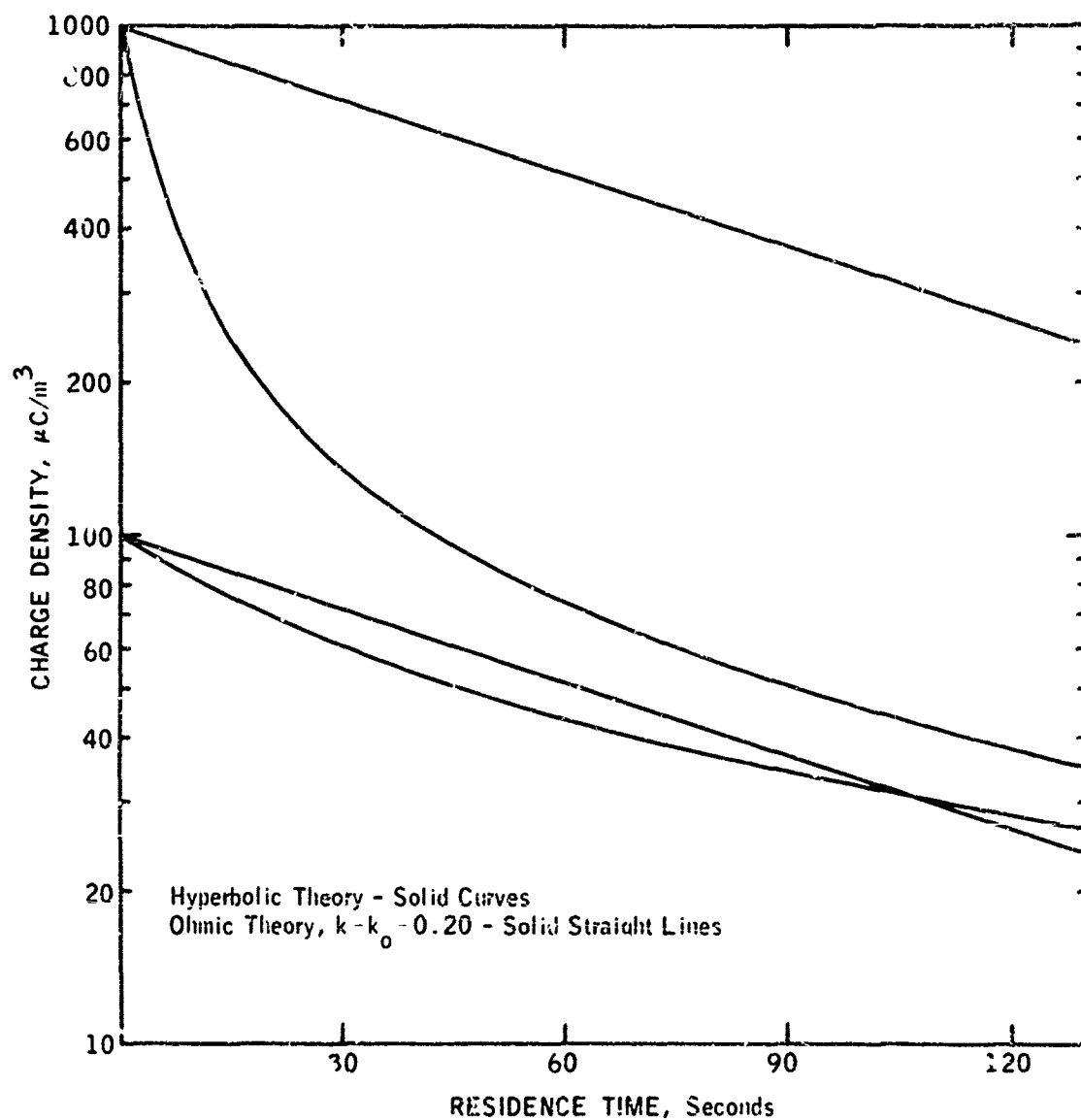


Fig. 9 - Predicted charge density vs. residence time by hyperbolic and ohmic relaxation theories.

Table 5

Predicted Residence Times Required to Reduce  
Charge Density to 30  $\mu\text{C}/\text{m}^3$  in Steel and FRP Pipe

Steel Pipe

$k_0$ , CU	$k_0 k_0$	$k_e$ , CU	$\tau$ , Secs	Residence Time, Seconds, to Reach 30 $\mu\text{C}/\text{m}^3$ from $\mu\text{C}/\text{m}^3$ of:		
				100	300	500
0.2	-	-	-	111	143	149
1.	.74	.74	2.4	28	55	68
3.	.52	1.56	11.5	14	26	32
5.	.46	2.30	7.8	9.4	18	22
10.	.39	3.9	4.6	5.5	10.6	13

FRP Pipe (Assuming Relaxation Time 30% Greater Than Steel)

0.2	-	-	-	144	186	194
1.	.58	.58	31	37	71	87
3.	.40	1.20	15	18	35	42
5.	.36	1.78	10.1	12	23	28
10.	.30	3.0	6.0	7.2	14	17

FRP Pipe (Assuming Relaxation Time 90% Greater Than Steel)

0.2	-	-	-	211	272*	283*
1.	.39	.39	46	55	106	129
3.	.27	.82	22	26	51	62
5.	.24	1.20	15	18	34	42
10.	.21	2.1	8.7	10.4	20	24

**Maximum Surface Voltages Measured on FRP Pipe Using  
Bypass, Filter-Separator and Filter-Monitor**

Using Filter Bypass

Rest CU	Pipe Inlet $\mu\text{C}/\text{m}^3$	Maximum Surface Voltage, KV, at Flow Rate, GPM, and Feet From Inlet Indicated(a)					
		300		600		1200	
		Short	Long	Short	Long	Short	Long
0.2	-0.7 → -1.3	3.0(50)	-4.8(170)	-	-	-	2.2(20)
0.9	1.5 → 3.4	4.3(20)	-	4.6(20)	-	4.6(20)	4.1(30)
	-1.2 → -2.8	-	-	-	-	-	-
3.	-0.9 → -3.8	7.1(30)	.23(50)	-	-.026(150)	-.039(170)	-.108(170)
5.5	-1.3 → -4.2	-1.29(30)	-1.53(160)	6.9(30)	-.018(c)	6.6(30)	6.0(d)
				-1.75(30)	-	-2.4(30)	-2.4(30)

Using Filter-Separator

Rest CU	Pipe Inlet $\mu\text{C}/\text{m}^3$	Maximum Surface Voltage, KV, at Flow Rate, GPM, and Feet From Inlet Indicated(a)					
		300		600		1200	
		Short	Long	Short	Long	Short	Long
0.2	-66 → -161	-11.7(30)	-30(f)	-23(30)	-48(50)	-28(30)	-23(60)
0.9	-44 → -139	-1.26(37)	.21(78)	-5.8(30)	-34(78)	-	-7.1(20)
3.	0 → -68	2.9(20)	-	0.2(10)	.054(50)	-	0.2(10)
5.5	0.3 → -32	-1.29(30)	-	-1.53(30)	4.3(20)	-5.5(30)	-17.7(10)
						-12.4(30)	-34(20)

Using Filter-Monitors

Rest CU	Pipe Inlet $\mu\text{C}/\text{m}^3$	Maximum Surface Voltage, KV, at Flow Rate, GPM, and Feet From Inlet Indicated(a)					
		300		600		1200	
		Short	Long	Short	Long	Short	Long
0.2	7.8 → 4.2	-	14.5(20)	-	-	-	20.5(20)
0.9	17 → 22	.51(30)	4.3(60)	.25(30)	3.8(60)	-	.122(78)
3.	70 → 91	6.0(50)	2.9(60)	5.1(50)	5.5(60)	-	6.9(20)
5.5	(g)	-13.1(30)	16.5(60)	38(20)	55(20)	42(20)	42(20)
						36(10)	30(10)

(a) Values in parentheses indicate distance from pipe inlet in feet at which maximum voltage was measured.  
 (b) 50, 60 and 150 feet (c) 1, 79, 239 (d) 20, 30 feet (e) 79, 170, 190, 230, 239 feet (f) 60, 70 feet  
 (g) Inlet charge densities on long pipe were 73, 131, 129, 125 for each respective flow rate.

observed was 55 KV when pumping 5 CU fuel through the F-M's at 600 GPM. It should be noted that substantial voltages (7.7 KV maximum) were detected even when filters were bypassed.

The low voltage readings with 0.9 CU fuel in the long pipe with the bypass in use were due to early morning fog and high humidity which wet the pipe surface. Similarly the low readings with 3 CU fuel in long pipe when using the bypass and F-S are attributable to a light drizzle which wet the pipe. However, wetting the pipe has no effect on charge relaxation; this was confirmed by a test on 0.2 CU fuel at 900 GPM with the following results:

	Charge Density $\mu\text{C}/\text{m}^3$	
	Pipe Inlet	Pipe Outlet
Before wetting	146.5	112.5
After wetting	146.0	112.0

A plot of surface voltages with distance along the pipe for some typical runs is provided in Figure 10. It shows that voltage increases rapidly at the inlet, falls more gradually toward the outlet and is not particularly affected by location of the stanchions. Actually, the highest voltages were often measured at the first bend, e.g., at 40 ft., sometimes with a polarity reversal.

Pendant water droplets, several aluminum foil wrappings and a metal drain valve were used as "charge collectors" on the FRP pipe. Sparks were generated by bringing a grounded wire or finger into close proximity to the "charge collectors"; sparks were detected by radio, aurally or visually. Spark discharges could barely be detected from water droplets at a surface voltage of 1.5 KV.

Sparks were obtained under all conditions where the fuel was charged either with the F-S or F-M's; Table 6 summarizes the frequency and size of sparks when the fuel was charged positively. Spark discharges increased in frequency as the inlet charge increased. A visible spark was observed with inlet charge as low as  $4.2 \mu\text{C}/\text{m}^3$ . Sparks up to 1/4 inch long were obtained from the drain valve with an inlet charge as low as  $7.2 \mu\text{C}/\text{m}^3$ . No measurements of spark energies were obtained but there is strong indication that the 1/4" spark discharge from a metal valve would have been incendiary.

It was not possible to detect sparks between the FRP pipe surface and a grounded wire under any conditions, even using the radio. However, it was possible to feel and hear discharges if a hand were run over the pipe surface. A surface voltage of 7-10 KV appeared to be required to sense such discharges.

The data on charge relaxation and surface voltage suggest that charge recombination in FRP pipe occurs by electron flow along the inner wall of the pipe to or from metal connections. No change in charge densities was detected when the outer surface of the pipe was made conductive to eliminate surface voltages.

The fact that surface voltages build up with pipe length and decrease rapidly near the pipe ends supports this theory. The results suggest that rate of charge relaxation in FRP pipe could be brought closer to steel by reducing the volume resistivity of the plastic or by grounding the inner wall of the pipe at short intervals.

**EVALUATION OF THE STATIC CHARGE REDUCER -** The Static Charge Reducer (SCR) is claimed by its manufacturer, A. O. Smith Co., Erie, Pa., to reduce charge densities of  $300 \mu\text{C}/\text{m}^3$  or less to  $30 \mu\text{C}/\text{m}^3$  or less at flow rates up to 1200 GPM.(8) It is the only commercially available device for reducing static charge in a flowing fuel and has been extensively used and tested. It was installed as noted in Figure 1 between the filter outlets and the test pipe sections and could be cut in or out by manipulating valves.

The SCR consists of a 3 foot long section of 10 inch diameter pipe lined with a 2" thickness of polyethylene. Sixteen pointed pins, grounded to the pipe, pass through the liner and protrude into the fuel stream as shown in Figure 11. As Figure 11 suggests, it is hypothesized that the charged fluid creates an intense localized field between the point of the grounded pin and the insulating surface in the immediate vicinity causing electrons to be injected into the flowing stream (if the fluid is positively charged), or conversely, to be extracted from the flowing stream (if the fluid is negatively charged).

Initial tests were carried out with 0.9 CU fuel charged negatively by the F-S and positively by the F-M's. The efficiency, determined in terms of absolute charge density values in and out of the SCR, is plotted in Figure 12 against inlet charge level. The dashed lines reveal that SCR efficiency rose only to 50% with negative fuel equivalent to an outlet charge level of  $90 \mu\text{C}/\text{m}^3$ . This was considerably higher than the  $30 \mu\text{C}/\text{m}^3$  claimed by the manufacturer. With positive fuel, the efficiency reached about 60%. These results were surprising because preliminary tests a month earlier had shown higher efficiencies and outlet charges below  $30 \mu\text{C}/\text{m}^3$ .

When the SCR unit was opened for inspection, a very faint gray-brownish discoloration was detected on the polyethylene liner. Numerous small spots were observed and, when cultured, found to contain fungi and bacteria. Although the liner appeared clean after wiping, it required several additional wipings first with hexane-wetted cloths and then chloroform-wetted cloths before the cloth remained unstained, indicating complete removal of deposits.

Data obtained after cleaning show a marked improvement in efficiency as shown by the solid curves in Figure 12. The SCR was not as efficient with negatively charged fuel as with positively charged fuel until an inlet level of  $130 \mu\text{C}/\text{m}^3$  was attained. This difference in response, as a function of fuel polarity, is

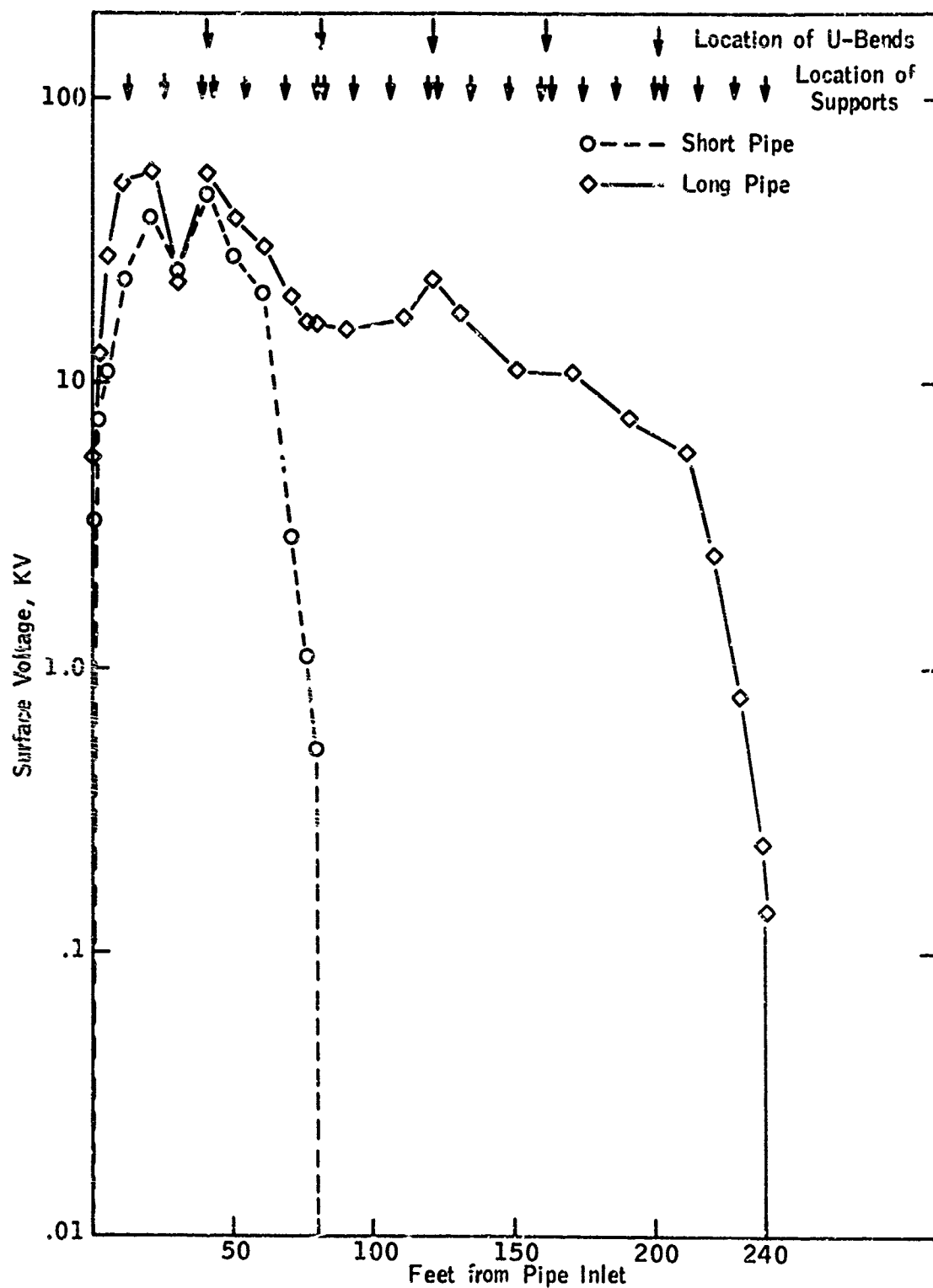


Fig. 10 - Surface voltage versus distance from pipe inlet with positively charged fuel at 5.5 CU and 600 GPM.

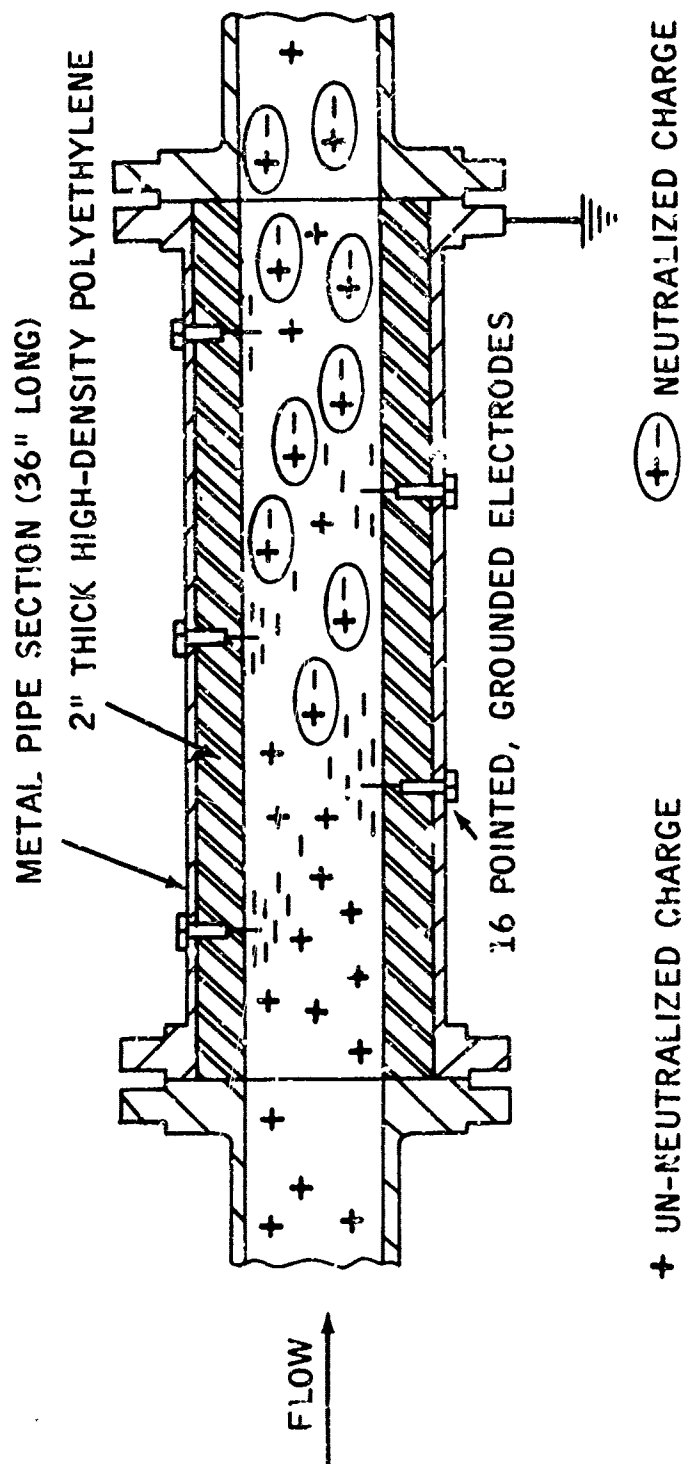


Fig. 11 - The Static Charge Reducer.

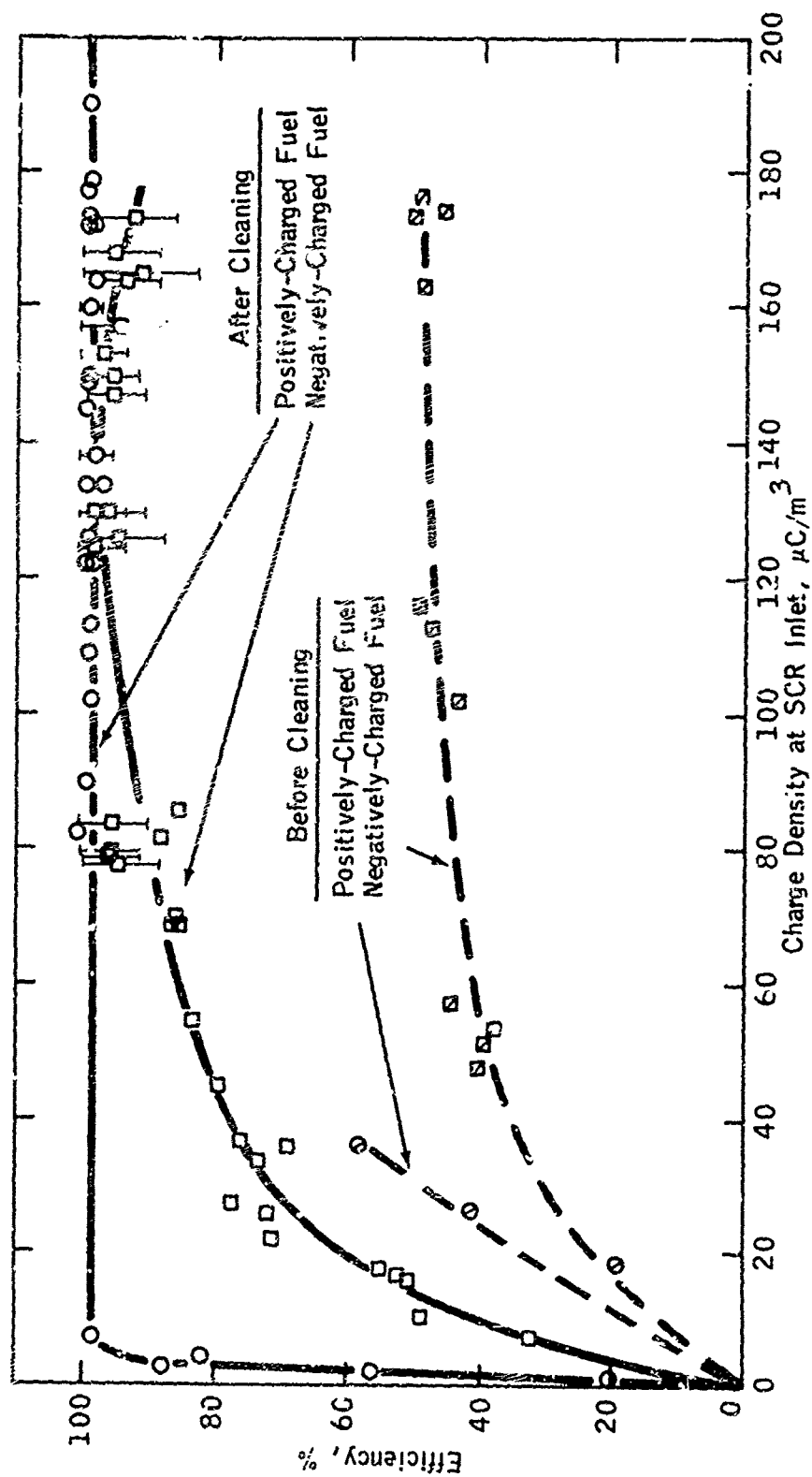


Fig. 12 - SCR efficiency with positive and negative fuel, before and after cleaning.

understandable if one realizes that when fuel with positive charge enters the SCR, electrons flow into the fuel from the pins while with negative fuel, electrons must be extracted from the fuel to flow to ground through the pins, a somewhat more difficult route.

A. O. Smith has recognized the possibility of a loss of efficiency and issued a bulletin (9) recommending checking "not less often than every six months." This program revealed that efficiency could degrade in a month and that continuous monitoring of the SCR would be required.

Irregular oscillations at about 30 cycles/minute were observed in the charge level leaving the SCR over short time periods. Over a period of minutes or more, the average charge level moves up and down irregularly; the largest swings were observed with highly charged 0.2 CU fuel. The range in efficiency which resulted from the latter are shown by the bars in Figure 12.

It was also observed that the charge level at the SCR outlet took considerably longer to reach a low level with the 0.2 CU fuel than with the other fuels. The time for the SCR output to reach  $30 \mu\text{C}/\text{m}^3$  when pumping negatively charged 0.2 CU fuel is shown in Figure 13 as a function of flow rate. The shortest time was about 2 minutes at 900 GPM. Charge levels as high as  $140 \mu\text{C}/\text{m}^3$  were obtained at the SCR outlet upon startup. It is evident that even an efficiently operating SCR will deliver fuel above the  $30 \mu\text{C}/\text{m}^3$  charge level for a considerable time after startup with low conductivity fuel.

During the tests on the SCR, surface voltage measurements were made on the FRP pipe surface into which "relaxed" fuel was being delivered. The maximum voltages for each fuel/flow rate combination are summarized in Table 10. Under conditions where the SCR was operating at 82 to 91% efficiency and delivering a charge of 2 to  $-30 \mu\text{C}/\text{m}^3$ , maximum surface voltages of -22 to -26 KV were observed. Of particular interest was the run with positively charged 5.5 CU fuel at 300 GPM which showed an SCR output of  $-2 \mu\text{C}/\text{m}^3$  and a surface voltage of -23 KV! For comparison, a test run on this fuel using the filter bypass, which delivered fuel of  $-1.3 \mu\text{C}/\text{m}^3$  to the pipe, only produced a surface voltage of 2.4 KV. Thus, the SCR seems to be capable of reducing the charge on the fuel but not the surface voltage on the FRP pipe into which the "relaxed" fuel is delivered.

Observations of spark production from foil wappings and drain valve on the FRP pipe during tests when "relaxed" fuel from the SCR was being pumped support the high voltages measured. Visible sparks 1/4 to 1/2 inch long could be drawn from the drain valve. It appears that the high surface voltages and energetic sparks obtained when the SCR is operating properly is due in some way to the oscillations observed in the charge delivered by the SCR since these oscillations are the only obvious difference between operation of the SCR and the filter bypass.

In summary, the disadvantages of the SCR appear to be loss in efficiency due to deposit buildup, the problem of startup time and the possibility that a low output charge may not truly reflect a safe situation. Of these, the latter is the most serious and requires further investigation.

#### CONCLUSIONS

The following conclusions have been reached as a result of this study:

1. Charge generation in both steel and FRP pipe is very low at flow rates up to 1500 GPM; charge generation in FRP is no greater and is generally less than in steel pipe, probably because the interior of the FRP is smoother.

2. There is a difference in charge relaxation between FRP and steel pipe which depends on the polarity of the charge on the fuel. On the average, relaxation in FRP pipe was 8% faster than in steel with negatively charged fuel and 30% slower than in steel with positively charged fuel. In some runs with positively charged fuel, relaxation in FRP pipe was slower by as much as 75%, e.g., 75% more residence time would be required to obtain the same amount of charge relaxation in FRP as in steel. The slower rate of relaxation should not prevent the use of FRP in Type III Air Force hydrant systems handling JP-4.

3. High voltages can be obtained on the outer surface of FRP pipe. These would not present a problem in buried installations. For above ground installation, all metal fittings should be grounded and, for absolute safety, the pipe should be coated with a non-peeling, non-flaking conductive material or the pipe should be formulated with a higher conductivity so that it can be effectively grounded.

4. The only commercially available device for decreasing the charge level on flowing fuel is the A. O. Smith Static Charge Reducer. It has the disadvantage of losing efficiency if deposits form, or requiring long startup times with low conductivity fuels and, most important, of producing a possibly hazardous situation downstream even when the effluent is below  $30 \mu\text{C}/\text{m}^3$ .

#### RECOMMENDATIONS

This study indicates that an FRP hydrant system with a minimum of 100 seconds of residence time would provide for relaxation to a "safe" charge level for fuel with a minimum CU of 1 at charge levels up to  $500 \mu\text{C}/\text{m}^3$ . Since both CU and charge level are critical to this analysis, it is recommended that a survey be conducted to establish the spectrum of typical JP-4 electrical properties and military filter-separator charging tendency in the field. This survey might involve monitoring fuel and filters at two or more Air Force bases over a period of several months. A similar program, which is currently being conducted by the



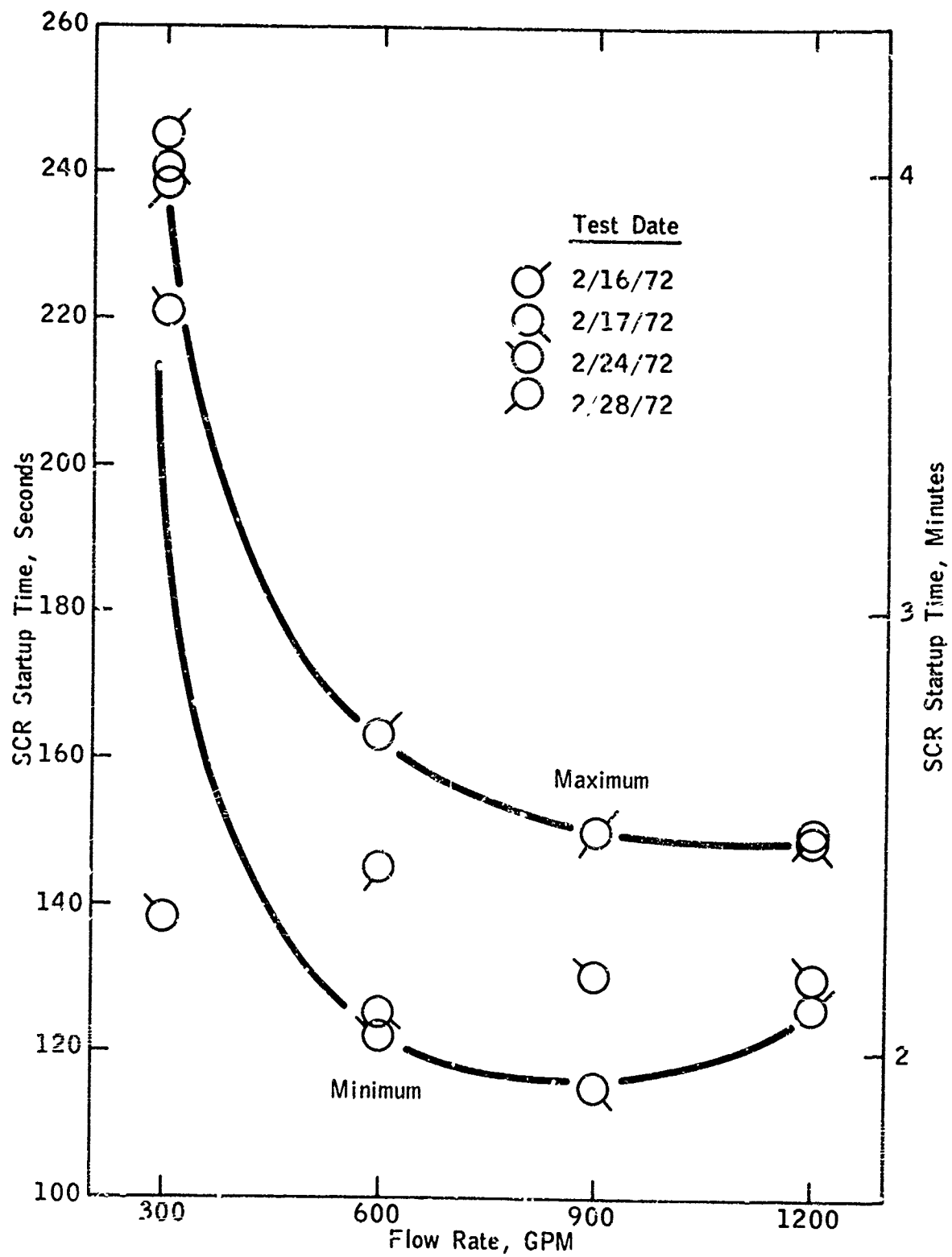


Fig. 13 - SCR startup time versus flow rate with 0.2 CU fuel.

Table 7

Observations on Spark Production Using Filter-Monitors

Nom. Fuel CU	Pipe Lgth.	Flow Rate, GPM	CD, $\mu\text{C}/\text{m}^3$ At Pipe In	Rel. Hum., %	Spark Characteristics Generated By									
					Foil Wrapping @ Feet From Inlet					Valve, @				
					27		48		189	81 Feet		Lgth., Ins.	No./ Sec.	No./ Sec.
					Lgth., Ins.	No./ Sec.	Lgth., Ins.	No./ Sec.		Lgth., Ins.	No./ Sec.			
0.2	Short	300	15.9	-	(a)	2-3	<1/16	1	-	-	-	-	-	-
		600	14.4	-	(a)	2-3	1/16	1	-	-	-	-	-	-
		1200	10.3	-	1/16	2-3	1/16	2-3	-	-	-	-	-	-
	Long	300	7.8	39			3/16	2-3				1/4	1-2	
		600	5.9	40(c)			3/16	2-3				3/16(b)	2-3	
		1200	4.2	41			3/16	2-3				1/16	1-2	
5.5	Short	300	68.9	63	-	-	1/16	2-3	-	-	-	-	-	-
		600	114	60	-	-	1/16	2-3	-	-	-	-	-	-
		900	119	58	-	-	1/8	2	-	-	-	-	-	-
	Long	1200	121	59	-	-	1/4	2-3	-	-	-	-	-	-
		300	73	47	-	-	1/8	3				1/4	2-3	
		600	131	40	-	-	<1/16	3-4	1/16(a)	2	1/4	1/4	3-4	
		900	129	44(c)	-	-	<1/16	3-4	3/16	2	1/4	1/4	3-4	
		1200	145	47	-	-	<1/16	3-4	3/16	2	1/4	1/4	3-4	

(a) Audible on radio only.

(b) 1/4" to finger @ 1 sec.

(c) Estimated.

Table 8

Maximum Surface Voltages Measured on FRP Pipe in SCR Evaluation

## Using Filter-Separator As Charge Generator

Nom. Rest CU	Maximum Surface Voltage, KV, at Flow Rate and Inlet Charge Level, $\mu\text{C}/\text{m}^3$ , Indicated					
	300 GPM		600 GPM		900 GPM	
	Short	Long	Short	Long	Short	Long
0.2	8.1(-8)	-21.5(-9)	7.1(-13)	-21.5(-17)	5.3(-20)	--
0.9	-1.45(-32)	-20(-29)	-6.6(-59)	34(-58)	--	--
3.	4.3(-2.5)	--	2.6(-3)	--	--	--
5.5	--	--	--	--	-3.6(-8)	--

## Using Filter-Monitors As Charge Generator

0.2	--	--	--	--	--	--
0.9	--	--	--	5.0(16)	--	5.5(15)
3.	-6.0(-2)	--	-8.(-3)	--	-5.0(-2)	-11.3(-4)
5.5	-23(-2)	-24.5(-6)	-21.5(-6)	--	-18.1(-3)	--

(a) Values in parentheses indicate maximum inlet charge level,  $\mu\text{C}/\text{m}^3$ .

Coordinating Research Council for the Federal Aviation Administration with commercial fuels and filters, could serve as a model.

It is recommended that when the first FRP installation is made, instrumentation be provided to monitor charge level downstream of a filter and at the pipe exit for a period of time.

The new problem brought to light when using the Static Charge Reducer--i.e., the indication that a low exit level of charge may not reduce surface voltages as expected--requires further investigation. Until the weakness in the SCR is corrected, it is recommended that highly charged fuel be relaxed in the customary way, using a relaxation tank or a length of pipe, either steel or FRP, or provide adequate residence time.

Since the definition of "adequate residence time" is closely related to both charge levels produced by filters and charge levels considered "safe" for tank filling, it is recommended that emphasis be given to low charging filters and to research that may more clearly define acceptable charge levels when fuel is actually introduced into a tank.

#### ACKNOWLEDGEMENT

These results were obtained in a study carried out for the Department of the Air Force, Headquarters Air Force Special Weapons Center (AFSC), Kirtland Air Force Base, New Mexico under Contract No. F29601-71-C-0071.

#### REFERENCES

1. I. Ginsburgh, "The Static Charge Reducer," J. Colloid Interface Science 32 (3), 434-32, 1970..
2. K. H. Strauss, W. G. Dukek, and R. E. Langsten, "The Electrostatic Charging Tendencies of Jet Fuel Filtration Equipment," SAE Preprint 720866, San Diego, October 1972.
3. K. C. Bachman and J. C. Munday, "Evaluation of the Hazard of Static Electricity in Nonmetallic POL Systems-Static Effects in Handling Jet Fuel in Fiberglass Reinforced Plastic Pipe," Technical Report No. AFWL-TR-72-90.
4. M. R. Shafer, D. W. Baker, and K. R. Benson, "Electric Current and Potentials Resulting from the Flow of Charged Liquid Hydrocarbons Thru Short Pipes," J. Res. Nat'l. Bur. Stds. C69 (4), 307-17, 1965.
5. C. W. Young, (HQ AFSC(SCOCM)), "Accumulation and Elimination of Static Electricity in Plastic and Metal Piping," Test Report.
6. K. C. Bachman and W. G. Dukek, "Static Electricity in Fueling of Superjets," Brochure, Esso Research and Engineering Co., Jan. 1972; Esso Air World, 24 No. 6, 147-151 (1972).
7. W. M. Bustin, I. Kozman, and I. T. Tobye, "A New Theory for Static Relaxation From High Resistivity Fuel," API Proc., (III), 44, 548-61, 1964.

8. "Static Charge Reducers" A. O. Smith Bulletin 1.10.1 5M 9-68.

9. "Special Service Bulletin on Possible Damage or Contamination of A.O. Smith - Static Charge Reducer" A. O. Smith, April 1, 1971.

#### SYMBOLS AND TERMINOLOGY

- c = Rest conductivity,  $k_0$ , at 0°F.
- CU = Conductivity Unit, a means of expressing fuel conductivity; 1 CU =  $10^{-12}$  Siemens/meter = 1 Picosiemen/meter.
- $k_e$  = Effective conductivity, i.e. conductivity of charged fuel, expressed in CU.
- $k_0$  = Rest conductivity, i.e., conductivity of uncharged fuel, expressed in CU.
- m = Temperature coefficient for rest conductivity,  $dk_0/dT$ .
- $Q_0$  = Charge density at pipe inlet, expressed as microcoulombs/cubic meter ( $\mu C/m^3$ ).
- $Q_t$  = Charge density at pipe outlet, see  $Q_0$ .
- t = Residence time, i.e. time for charge to decay.
- T = Temperature, °F.
- $\epsilon$  = Dielectric constant of fuel relative to a vacuum, a dimensionless quantity equal to about 2 for hydrocarbons.
- $\epsilon_0$  = Absolute dielectric constant of a vacuum,  $8.854 \times 10^{-12}$  ampere seconds/volt meter.
- $\mu$  = Ion mobility, square meters/volt second.
- $\tau$  = Relaxation Time, i.e. time for charge to decay to 36.8% of original value, seconds.

SESSION VIII

AIRCRAFT II

R.A. PETERSON, CHAIRMAN & ORGANIZER

THE BOEING COMPANY

Aircraft II  
Introduction to Section  
R.A. Peterson, The Boeing Company  
Chairman and Organizer

The papers presented in this, the second session on Aircraft, addresses only the air vehicle and its immediate environment and the effect of this environment on the vehicle's ability to perform in a normal manner.

The authors who have prepared the papers are recognized experts in the field of Lightning and Static electricity as it relates to air vehicles as a total system. Not only have they gained experience over the years by observing and examining damage caused by natural lightning and recognizing the undesirable effects of static electricity, but they have also been able to create artificial models that closely represent the natural phenomena.

One method of approach which has been used very successfully is experimentation using vehicle models, artificial lightning, simulated electric fields and charging mechanisms. A second approach, which has only recently been possible, utilizes a computer to solve the complex equations associated with a mathematical model of lightning and its effect on various vehicle subsystems.

Both of the approaches described above can be effective and the choice usually is determined by complexity of the problem being analyzed. Highly sophisticated weapon systems such as the B-1 lend themselves to the computer analyses approach during the design stage of the vehicle; however, problems that arise as a result of vehicle operational experience usually can be solved more directly by experimentation. With the facilities we have at our disposal today it is relatively straight forward to simulate the operational situation, develop protection systems and then test the system under simulated conditions.

Whatever the approach to the problem may be, this last step is the only way one can be sure that the problem has been corrected. The final tests must be

performed with the actual hardware if at all possible.

The authors of the paper entitled "A Passive Discharge System for the Electrically Charged Hovering Helicopter," were not aware of the planned 1972 Conference on Lightning and Static Electricity until after the agenda had been published; however, we were fortunate enough to receive their excellent paper in time for the printing of these proceedings.

## Lightning Protection Techniques for Large Canopies on High Speed Aircraft\*

Robert Aston, R. Gorton, and G.L. Weinstock  
McDonnell Aircraft Company

### ABSTRACT

The primary hazard from a lightning strike to an aircraft canopy occurs if the canopy punctures and the lightning strikes the pilot. This hazard was analyzed mathematically and was extensively tested on flat polycarbonate sheets, a simulated canopy, and an actual fighter aircraft canopy. The analysis showed that canopy puncture would not occur because of the lower breakdown dielectric strength and the dielectric constant of the surrounding air.

Lightning simulation tests were performed in three steps. First, tests were performed on flat polycarbonate sheets to determine the relationship between surface flashover in air and when breakdown through the material would occur. Puncture of the polycarbonate in air could not be achieved. The second series of tests was performed on an actual canopy to investigate the possibility of puncture by a long spark (between 36 and 80 in.). Tests showed that attachment with long sparks would occur to the metallic framework of the canopy, but not to the polycarbonate material. Using shorter sparks (less than 24 in.), attachment to the polycarbonate canopy was achieved. Surface flashover always occurred, as indicated by the analysis. The third series of tests was to investigate the safety margin of the high speed fighter aircraft canopy. For this purpose, a large sheet of 1/8 in. thick polycarbonate was formed into a flat-bottomed, cylindrical, simulated canopy which was less than half the thickness and considerably larger than an average canopy. The results were similar to the tests on the actual canopy.

Side effects of a lightning strike to the canopy area considered were corona, triggering of the canopy ejection system, and the possibility of the current welding the canopy frame to the aircraft frame. None of these were found to be a hazard.

Three methods of lightning protection were investigated; a solid metal bar outside the canopy, a thin metal strip inside the canopy and an ionizing button strip outside the canopy. All give canopy protection against lightning strikes. The solid metal bar outside the canopy is considered unacceptable because of thermal expansion problems resulting from the different coefficient of thermal expansion between the polycarbonate and the copper or aluminum bar.

LIGHTNING attachment studies and strike histories show that fighter aircraft canopies can be struck by lightning. The purpose of the work described in this paper was to determine by analysis and experimental evaluation the susceptibility of fighter aircraft canopies to lightning strikes and to develop lightning protection methods if required. The initial phase of this program was an analysis of the lightning susceptibility characteristics of a fighter aircraft canopy. High voltage tests were then performed on flat sheets of Lexan (a typical canopy material), a simulated canopy, and a full size canopy. Investigations of the criteria that determine either surface flashover or canopy material puncture were performed on flat Lexan sheets.

An actual aircraft canopy was used to experimentally evaluate and verify the analysis of the primary hazard, canopy puncture, and the secondary hazard, corona inside the canopy.

Tests were also performed on three candidate diverter systems to determine the effectiveness of various protective systems. These included both high current and high voltage tests.

The investigation of corona inside the canopy concluded that corona does not present a serious hazard to the crew. The significant result of this program is that by both analysis and tests, it has been shown that a fighter aircraft canopy of this particular design will not puncture and therefore additional lightning protection is not required.

### CANOPY ELECTRIC FIELD ANALYSIS

An analysis of the electric field distribution about a canopy was made to determine if the maximum sustainable electric fields in air (without air breakdown at atmospheric pressure) would cause dielectric breakdown of the canopy. The objective of the analysis was to determine which would breakdown first as a result of the fields from an approaching lightning stroke. 1) the air above the canopy and hence flashover, or 2) the canopy which would therefore require a canopy lightning protection system.

The physical model chosen for this analysis was that of a hollow dielectric cylinder surrounding a metal cylinder. A uniform electric field,  $E$ , is applied to the system (see Fig. 1). This model was selected because. 1) it represents a worst case in the sense that the inside of the canopy is held at a constant potential by the metal cylinder so that the maximum possible electric fields in the dielectric will be obtained, and 2) the model has a mathematically tractable solution.

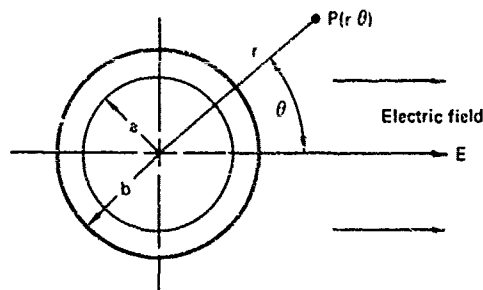


Fig. 1 - Dielectric cylinder in a uniform electric field

\*This work was conducted under U.S. Air Force Contract F33615-71-C-1581

The potential at point  $P(r, \theta)$  is found by standard analytical methods. The potential in air is given by

$$V_{\text{air}} = \left(r - \frac{A}{r}\right) E \cos \theta \quad r > b.$$

In the dielectric:

$$V_{\text{canopy}} = \left(Br - \frac{C}{r}\right) E \cos \theta \quad a < r < b.$$

The coefficients A, B, C are dependent upon the dielectric constant of the canopy, K, and upon the inner and outer radius (a and b) of the dielectric cylinder. These coefficients are given by:

$$\begin{aligned} A &= a^2 & \text{cm}^2 \\ B &= \frac{2b^2}{(K+1)b^2 + (K-1)a^2} \\ C &= B a^2 & \text{cm}^2. \end{aligned}$$

The values for the relative dielectric constant, K, and inner and outer radii (a and b) are 3, 93.98 cm and 94.72 cm respectively. The canopy thickness is 0.29 in. and is made of Lexan (Fig. 2).

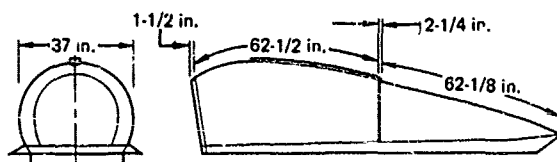


Fig. 2 - Canopy surface dimensions

The maximum potential across the dielectric occurs in the direction of the external electric field ( $\theta = 0$ ,  $\cos \theta = 1$ ). Using the appropriate values for the constants, the maximum voltage across the dielectric is given as

$$\Delta V_{\text{canopy}} = 0.49 E.$$

Thus since atmospheric air breaks down when the electric field is 30 kV/cm, this will correspond to a maximum potential across the dielectric of:

$$\Delta V_{\text{canopy}} = 14.7 \text{ kV.}$$

The long-term thermal breakdown for 0.29 in. thick Lexan is 83 kV. The impulse breakdown potential is 272 kV.

A comparison of these values shows that the maximum electric field which is sustainable in air will not cause a sufficient potential across the dielectric canopy to cause it to puncture. The air adjacent to the canopy will break down, and thus flashover to a metal frame will occur when the canopy is subjected to the high electric fields associated with the lightning strike.

Since the value used for air breakdown was chosen at atmospheric pressure, and since it decreases with a decrease in pressure, the results obtained reflect a worst case for altitude variations.

## HIGH VOLTAGE TESTS ON AN ACTUAL HIGH SPEED FIGHTER AIRCRAFT CANOPY

High voltage tests at 1.4 MV were performed on the canopy (Fig. 3) in a close simulation to the actual conditions to determine if the canopy would puncture. Lightning always attached to the metallic canopy arch when an approaching strike was simulated by a long spark from the electrode located 80 in. above the canopy (Fig. 4). The high voltage electrode was then brought progressively closer to the surface of the canopy while maintaining 1.4 MV. When the electrode was at about 36 in. above the transparency (Fig. 5), attachment to the forward part of the transparency occurred. The attachment point gradually moved aft as the electrode was brought nearer to the transparency surface until it was only 1 in. from the surface.

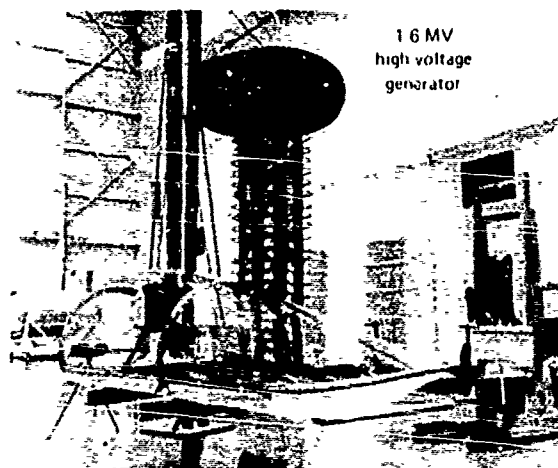


Fig. 3 - High voltage generator and canopy - sideview



Fig. 4 - 1.4 MV strike to unprotected canopy from 80 in.



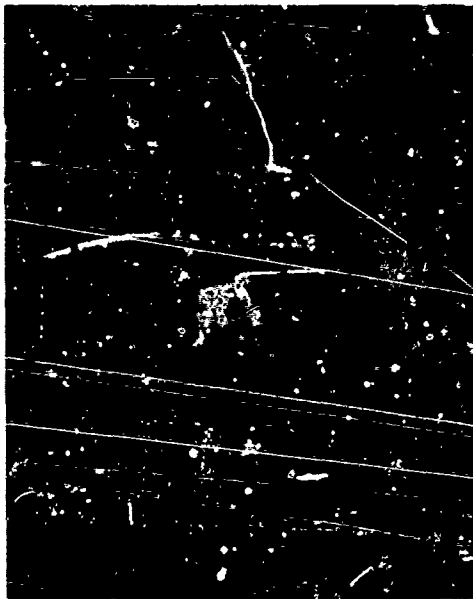


Fig. 5 - 1.4 MV strike to unprotected canopy from 36 in.

Figure 6 shows how air breakdown will occur in all directions at electric field values too low to puncture the Lexan. These conditions might occur in the case of a swept stroke starting from a strike to the forward canopy arch. In none of these configurations did puncture of the canopy occur. This included deliberate "overstressing" by forcing the simulated strike to go to the canopy transparency.

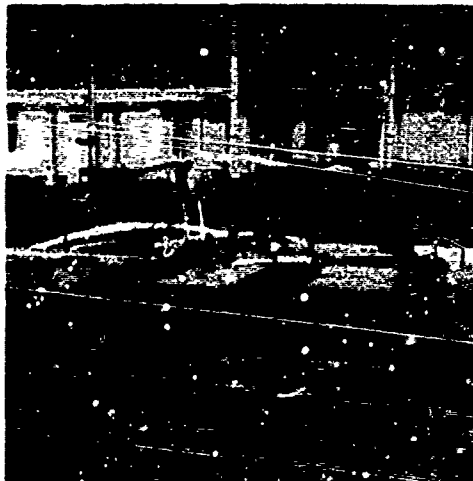


Fig. 6 - 1.4 MV strike to unprotected canopy from 1 in.

#### HIGH VOLTAGE TESTS ON 1/8 IN. THICK SIMULATED CANOPY

In order to establish the existence of a safety margin against puncture, a simulated canopy (Fig. 7) was constructed with a transparency thickness of 0.125 in. as compared with the 0.29 in. thickness of the actual high speed fighter aircraft canopy, and a diameter of about 40 in. as compared with 37 in. for the actual canopy.

A series of high voltage strikes to the simulated "thin"

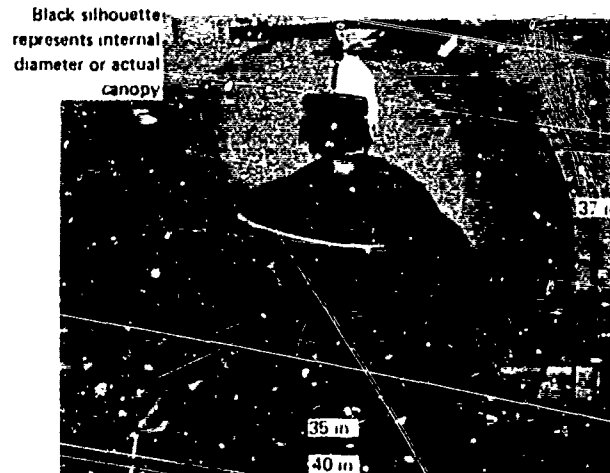


Fig. 7 - End view of 1/8 in. thick Lexan simulated canopy

canopy was performed using approximately 1.3 MV and with a rod electrode at gap distances of 88 in. to 1 in. above the canopy. In none of these configurations did canopy puncture occur.

#### CORONA

Investigations were conducted to assess the magnitude of the corona that would be induced under the canopy by a lightning strike. Photographs of corona streamers from the top of the simulated pilot's seat were obtained.

An actual high speed fighter aircraft canopy was used to determine the magnitude of corona streamering current inside the canopy just before a lightning strike hits the canopy. The upper part of a simulated pilot's seat was fixed inside the canopy and a pilot's helmet was attached to it. The earphones and microphone were grounded. Three cameras were used, one with high speed roll film to photograph low intensity corona inside the canopy and two Polaroid type cameras from different angles to photograph the high intensity spark breakdown and corona outside the canopy.

Corona was studied under two circumstances: 1) with the high voltage generator set at slightly lower than the breakdown value so that a discharge would not occur; and 2) with the high voltage generator set above breakdown so that a spark to some part of the canopy occurred.

The high voltage generator was set for 1.2 MV to 1.3 MV amplitude, and the high voltage electrode was placed approximately 86 in. above the top of the canopy. Photographs of corona streamering were taken during the strike. Photographs of internal corona during a simulated lightning strike show that most corona originates from the top of the pilot seat. No intense sparking was noticeable. Comparison with a reproducible source (a model Van de Graf generator) indicated that the corona is too small to represent a serious pilot hazard even without protection.

#### CONDUCTION OF HIGH CURRENTS

High current tests of 200 kA from the arches to the canopy metal frame were performed. The conduction path from the canopy frame to the airframe is through a number

of parallel paths. Four separate canopy, stainless-steel retaining hooks were clamped to the canopy frame by the canopy counter-balance actuator pressure. Each provided a conductive path between the canopy frame and the air-frame. In addition, two canopy hinges behind the pilot seat also provided a high current conductive path. The tests showed that the canopy metal arches and the attachment hooks and hinges are capable of withstanding 200 kA strikes. Subsequent examination of the screws at the attach point showed evidence of slight damage to the threads of those carrying the current (Fig. 8).

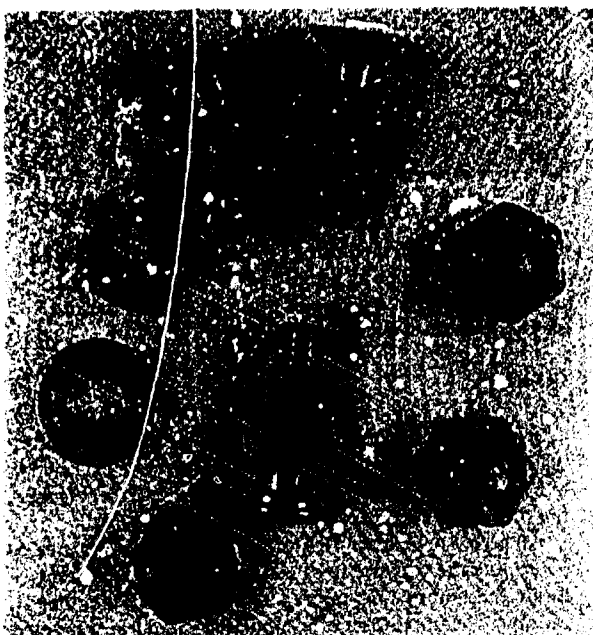


Fig. 8 - Joint screw damaged by 200,000 KA joint test

#### LIGHTNING PROTECTIVE DIVERTER SYSTEMS

Even though the analysis and test showed that the specific fighter aircraft canopy used in this program would not puncture, tests of three candidate diverters were performed. The diverters would be applicable for larger canopies where corona could be a problem or for composites with low dielectric strength that could be punctured by lightning. The following three diverter systems were investigated.

- 1) A solid bar on the outside of the canopy extending from above the back of the pilot's head to the canopy frame.
- 2) A metal strip inside the canopy extending from above the back of the pilot's head to the canopy frame.
- 3) A system of metal buttons on the outside of the canopy extending from above the back of the pilot's head to the canopy frame.

**EXTERNAL SOLID BAR DIVERTER** - This system was a solid aluminum bar 3/8 in. x 0.124 in. x 40 in. long, extending from above the back of the pilot's head to the canopy arch. The temperature rise caused by a high current strike or aerodynamic heating causes considerable differential thermal expansion between the metal bar and the Lexan canopy.

The difference in the thermal expansion rates of Lexan ( $3.75 \times 10^{-5}/^{\circ}\text{F}$ ) and copper ( $0.89 \times 10^{-5}/^{\circ}\text{F}$ ) or aluminum ( $1.59 \times 10^{-5}/^{\circ}\text{F}$ ) is a serious problem. In this case, the expansion problem cannot be minimized by increasing the cross-sectional area of the diverter. Such a large difference in expansion places a considerable strain upon the bond between the diverter and the canopy. In laboratory bond tests, none of the adhesives were found capable of bonding metal to Lexan at the high temperatures anticipated by worst case aerodynamic heating.

Since adhesive attachment of a bar diverter is not feasible, other methods of attachment were examined. Attaching the external metal bar diverter by a sliding mechanism which allows the rod to move longitudinally, could solve the differential expansion problem. However, the sliding mechanism would have to be capable of withstanding the high magnetic forces caused by the high lightning currents and would be undesirable because the total system cross-sectional area would be large and would increase aerodynamic drag and reduce visibility.

Any screw fastening method is also undesirable because a metal screw would introduce the electric field directly into the canopy and a dielectric screw of adequate strength would be too large.

For the reasons discussed in this section, it is therefore considered impractical to use an external solid bar on a high performance aircraft canopy for lightning protection.

**IONIZING BUTTON STRIP DIVERTER OUTSIDE THE CANOPY** - This type of diverter was originally designed and developed by Douglas Aircraft Company for use on commercial aircraft. The button strip diverter, shown in Fig. 9, is constructed of a thin insulating strip with a resistive film coating on the underside and metal buttons (about 10/in.) along the entire length on the top side, with small gaps between each button. The buttons are connected through the strip to the resistive film on the other side. Because of the high resistance between individual buttons, a high current does not flow in the strip itself.

The metal buttons act as a "catalyst" in ionizing the air adjacent to the row of buttons. The low pre-strike current causes a high voltage between adjacent buttons leading to ionization and corona current over the surface of the strip. This leads to breakdown in the air at a reduced voltage, providing a low impedance air path to the end of the strip, which is attached to the metal canopy frame.

Differential expansion problems can be circumvented by using Lexan as the base material in which the buttons are mounted. Since the high current does not flow in the diverter, the magnetic forces do not act on the diverter and available adhesives can be used to attach it to the canopy.

**METAL STRIP DIVERTER UNDER THE CANOPY** - A thin metal strip inside the canopy, extending from a point above the back of the pilot's head to the canopy arch, is also a practical alternative. Since it is inside the canopy, it does not have the aerodynamic problems associated with an external diverter. The low current conducted by the internal diverter means that a small cross-section can be used, so that the mechanical forces (caused by differential expansion) are small, thus, the strip can be held by available adhesives. Since the strip is narrow, visibility restrictions are also less than those of the other two candidate diverters. The internal metal strip, however, is not as

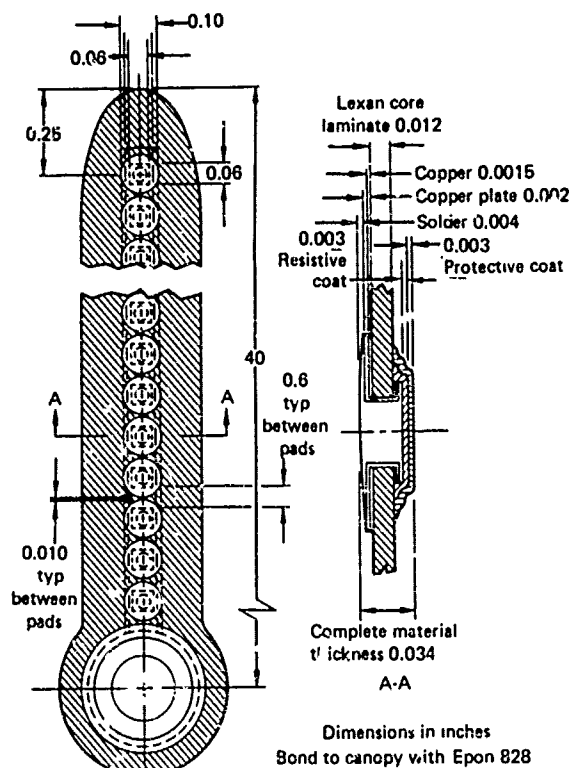


Fig. 9 - Ionizing button strip diverter

effective as the button strip in reducing the surface flash-over voltage. Test results have shown that the electric field required for flashover is 5 kV/in. with the internal diverter compared with 1.2 kV/in. for the button strip and 19 kV/in. without any form of protection.

In order to check the effect of internal diverters on the probability of canopy puncture, two series of high voltage tests were performed. For the first series, a thin, narrow aluminum tape was bonded to the internal surface of the canopy on the longitudinal centerline. Care was taken to ensure that the adhesive did not cover the exposed surface. For the second series, the exposed surface of the diverter tape was completely covered by spraying a thick layer of acrylic adhesive over it. The same high voltage tests were repeated. Neither series of tests resulted in canopy puncture.

## CONCLUSIONS

Analysis and laboratory tests show that canopy puncture will not occur. Although the possibility of a lightning strike to the canopy exists, the tests described herein show that it attaches to the metallic canopy supports. Attachment to the canopy transparency will not normally occur. When a strike attaches to the front canopy arch, a swept stroke may occur. Under these conditions, the strike may sweep aft over the transparency surface and re-attach to the center canopy arch support.

The limiting effect of air upon the maximum electric field will protect the transparency against puncture, and high current tests show that the canopy arch and attachment method is capable of conducting over 200,000 A.

A final judgment of the physiological effects of corona current on the pilot requires a detailed medical study. The engineering conclusions reached are that such corona streamer as exists appears too small to represent a serious hazard to the pilot.

Laboratory tests on the three diverter systems show that all three offer adequate protection against corona. The tests also show that canopy puncture will not occur when equipped with any of these diverter systems.

The results of analysis and tests show that high current heating in the external metal bar can be limited sufficiently with a cross-sectional area greater than 0.023 in.<sup>2</sup>. The thermal expansion caused by aerodynamic heating does not seem to have a satisfactory solution.

Laboratory tests performed on the other two diverter systems show an adequate level of protection against corona and indicate that the internal diverter does not cause canopy puncture.

## ACKNOWLEDGEMENT

Appreciation is expressed to K.J. Maxwell and J.F. Shaeffer of McDonnell Aircraft Company for their contributions to this effort.

## Lightning and Electromagnetic Compatibility Analyses

A Joint Study on Lightning Effects  
for the B-1 Program, Coordinated by  
E.S. Hughes  
North American Rockwell B-1 Division  
Los Angeles, California

J.D. Robb  
Lightning & Transients  
Research Institute  
St. Paul, Minn.

W.R. Johnson  
TRW Systems  
Los Angeles, Calif.

J.A. Plumer  
General Electric Company  
Corporate Research & Development  
Pittsfield, Mass.

### LIGHTNING AND ELECTROMAGNETIC COMPATIBILITY ANALYSES

E. S. Hughes

THE IMPORTANCE OF ANALYZING the effects of lightning on the B-1 bomber has been evident to those responsible for electromagnetic interference and compatibility (EMIC) on the B-1 program for some time. Considerable work has been done in the area of analyzing the physical damage to aircraft due to lightning, however, the effects on internal electronics have not been quantitatively analyzed to date to any acceptable degree.

It appeared that the most effective approach to such an analysis on the B-1 program was to combine and coordinate the knowledge and efforts of experts in different, but related, technical disciplines. The recognized experts in lightning phenomena would develop models of lightning itself, and this data then used by system electromagnetic compatibility (EMC) analysts to determine the effects of electronic subsystems. This is to be accomplished by means of a system level EMC analysis program, such as the Specification Electromagnetic Compatibility Analysis Program (SEMCAP), which is presently being used on the B-1 program for system EMC analysis. This paper comprises three parts by authors with expertise in each of these related disciplines.

Mr. J. D. Robb of the Lightning and Transients Research Institute is recognized as having made significant contributions in the area of lightning research and has developed lightning models for use on the B-1 EMIC analysis program.

Mr. W. R. Johnson of TRW Systems has extensive experience in system EMC analysis and has had major responsibility in the development of the SEMCAP computer program.

Mr. J. A. Plumer of General Electric has done extensive analysis bridging the gap between lightning phenomena and effects on vehicles and their internal systems and cables.

The results presented in this paper represent a major first step in the quantitative prediction and analysis of lightning effects on a complex weapon system and subsystems in terms of total electromagnetic compatibility.

It is hoped that this effort will be continued to develop more refined and explicit models. North American Rockwell would like to take this opportunity to express appreciation to these gentlemen and their companies for this step forward.

### LIGHTNING AND ELECTROMAGNETIC COMPATIBILITY

J.A. Plummer

THE ABILITY OF AN AIRCRAFT to function properly in an all-weather environment is dependent upon interference-free functioning of its electrical and avionics systems in the external electromagnetic environment. One of the most severe environments, and the one the aircraft will be subjected to most often, is that produced by lightning strikes to the aircraft. There are some fundamental differences between the electromagnetic environment created by lightning and that generated from onboard electromagnetic interference (EMI) sources necessitating that this external interference source be given specific consideration in a complete EMC analysis program for a modern aircraft. Briefly, these differences are:

1. The electromagnetic fields generated by lightning currents are of high amplitude, as compared with those generated by onboard avionics and electrical systems.
2. Lightning currents flowing along major sections of the aircraft cause electromagnetic fields to interact with all wiring and components inside as well as outside the airframe, as different from the more localized sources of EMI such as single wires, antennas and "black boxes."

3. Lightning creates one or more discrete EM field pulses as contrasted with an oscillating repetitive field radiated from a corresponding signal in a particular circuit or antenna.

4. The lightning magnetic field is accompanied by an electrostatic field caused by the differences of potential along the structure as well as external to it.

5. Lightning is a flow of high amplitude current through major sections of the aircraft from a low impedance source (visualized as an ideal current generator), as contrasted to the relatively high impedance sources of "conventional" EMI.

Thus, the susceptibility of critical circuits and components to lightning electromagnetic interference must be analyzed to complete the EMC analysis program.

#### MATHEMATICAL MODELS FOR LIGHTNING

J.D. Robb

A MATHEMATICAL MODEL of the thunderstorm electromagnetic fields and currents to which an aircraft is subjected in flight has been developed for use in computer programs previously used for predicting EMC of aerospace vehicles. The computer EMC programs were developed for determining the interaction effects between various circuits in an aircraft including the effects of electric and magnetic field coupling to cables and they are being adapted for determining the effect of lightning strokes and their associated electrical and magnetic fields on the aircraft electrical system. The models are intended to present the near maximum magnitudes and waveforms of the thunderstorm electromagnetic field and lightning currents to which an aircraft would be subjected in flight.

A number of simplifying assumptions are required to bring the problem within a size than can be handled, in view of the extensive computer capacity required for the complex electrical electronic systems on an aircraft such as the B-1. From the almost infinite variety of natural lightning waveforms and magnitudes, a few representative waveforms were selected for input into the SEMCAP program. These, of course, can be easily scaled to higher or lower levels once the program and input waveforms have been established.

The analysis is most easily carried out on the computer in the frequency domain and therefore Fourier components of the input waveforms are used in the program input. It is convenient to use analytical function inputs

to represent the lightning and electromagnetic fields and lightning currents, specifically, double exponentials of the form  $A(e^{-at}-e^{-bt})$ , and a  $\sin^2$  function to handle mathematical discontinuities.

Although the electric fields go down to dc in frequency, these are of less interest for the SEMCAP program as the E field components at the dc level have little effect on any internal aircraft wiring in terms of direct interference. They can produce corona discharges from exposed wiring, but this problem can be more easily handled with techniques utilized in precipitation static control and, therefore, are not included among the models for the SEMCAP program. The fields thus go from large magnitude components with microsecond rise times down to intermediate components with millisecond rise times.

#### MECHANISM OF LIGHTNING STROKE APPROACH AND CONTACT TO AN AIRCRAFT

In considering the mechanisms of lightning stroke current and electromagnetic field coupling to aircraft, it is useful to review the basic mechanisms of stroke contact. A natural lightning discharge initiates from a charge region in a cloud in the form of a step leader which advances in approximately 50-meter steps toward another charged region or toward the earth as illustrated in Figure 1-1.

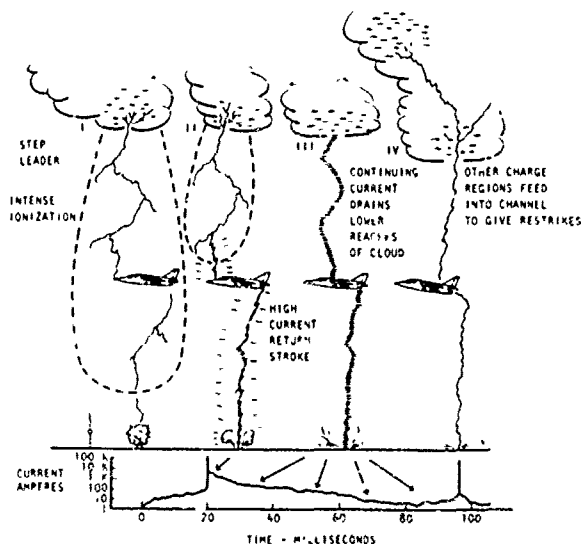


Fig. 1-1 - Illustration of lightning discharge mechanism with corresponding current flow for each phase shown below.

In some cases, the aircraft triggers a lightning discharge which would not have occurred otherwise, and in some cases it merely diverts

the discharge slightly out of its normal path so that the stroke passes through the vehicle.

When the step leader contacts the earth or another charged region, the existence of an ionized conducting path between the earth and the charge region (or two oppositely charged regions in cloud-to-cloud strokes) results in a current pulse in the form of an ionization wave which travels back up the step leader path to the initiating charge region in the cloud. The high current ionizing wave is referred to as the "return stroke" and consists of a fast-rising high-current surge. This is often followed by continuing currents of 100 to 1,000 amperes which may last up to 1 second followed sometimes by high current restrikes, is referred to in the scientific literature as a flash.

As a step leader approaches the vehicle, the intense voltage existing between its tip and the aircraft induces streamers and intense ionization of all the aircraft external surfaces, and particularly from the extremities. Figure 1-2 shows the streamering off a model aircraft subjected to intense electric fields in the laboratory. When the step leader contacts one of the vehicle's extremities through the streamer, the vehicle's potential is immediately raised to the extreme potential of the lightning discharge and additional streamering takes place from the opposite extremities of the vehicle to form the step leader for the continuation of the stroke path to another charge region or to the earth.

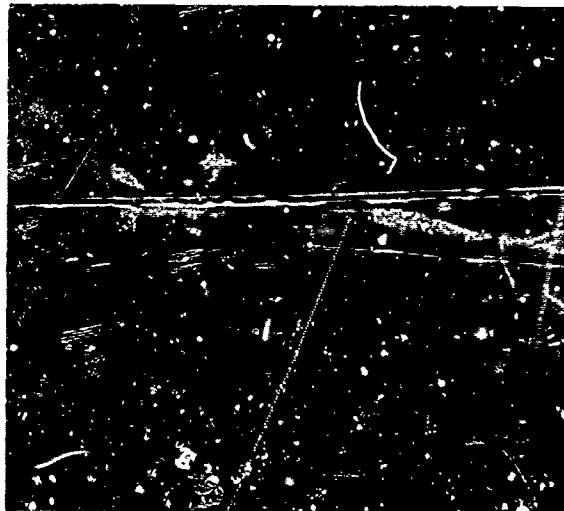


Fig. 1-2 - Streamering effects off a B-1 aircraft model.

Whereas, the stroke generally contacts the aircraft at only a few points, many streamers extend from the aircraft as illustrated in the

figure.

This process thus describes the fields and direct stroke currents to which the aircraft will be subjected. The predominant components for each phase include:

1. Step leader phase - intense electric fields with fast rise times just before contact with the aircraft.
2. Return stroke phase - high current and high current rates of rise with intense magnetic fields.
3. Continuing component phase - reduced electric fields and intermediate magnetic fields.
4. Nearby charge center and nearby strokes - electric and magnetic fields of intermediate magnitude and full range of rise times from DC to micro-seconds.

#### MATHEMATICAL MODELS - E AND H FIELD

SPECIAL MODELS - A simple and fairly rigorous single model for the near zone electric and magnetic fields is a vertical line current representing the natural lightning return stroke (State II of Figure 1-1).

The H field may be simply represented as the field about an infinite vertical line current as illustrated in Figure 1-3 and as derived from the Maxwell integral equation.

$$\oint \vec{H} \cdot d\vec{l} = I$$

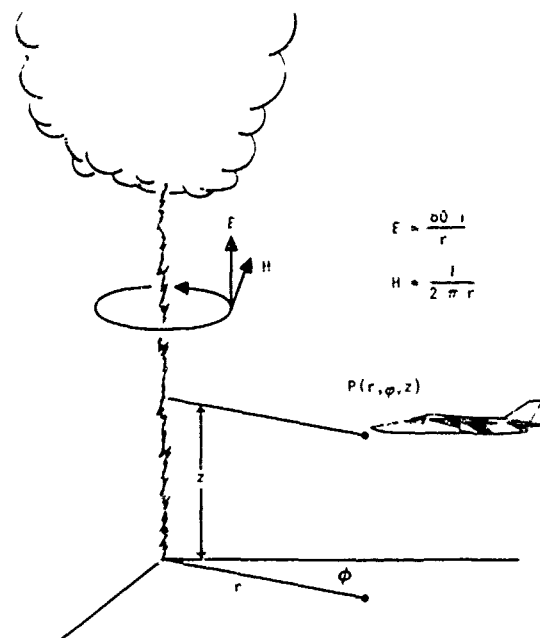


Fig. 1-3 - Mathematical model of E- and H-field lightning geometry.

Integrating about a simple circular path a distance  $r$  from the channel yields:

$$H \cdot 2\pi r = I \quad \text{where } I = \text{channel current}$$

$$H(r, \phi, z) = \frac{I}{2\pi r} \quad r = \text{radius to measurement point} \quad (1)$$

It may be shown that the vertically polarized E field component for a steep current wave front traveling up the channel is

$$E(r, \phi, z) = 60 \frac{I}{r} \quad (2)$$

The two expressions thus give a simple expression for the E and H field variations with distance.

**TIME VARIATION MODELS OF THE ELECTRIC AND MAGNETIC FIELD** - The field variations with time follow the currents directly for both electric and magnetic fields. Measurements indicate field changes of the form

$$F(t) = A(e^{-at} - e^{-bt})$$

A near maximum E field measured in flight is about 500,000 volts/meter. For a crest field of this magnitude in the above equation, A must equal  $6.8 \times 10^5$  because of the decrement

A near maximum H field about the aircraft will be  $2 \times 10^4$  ampere meters for which A must equal about 2.7. Thus the maximum value field models without spacial variation would be

$$E(t) = 6.8 \times 10^5 \times (e^{-at} - e^{-bt}) \quad (3)$$

where  $a = 1.3 \times 10^5$

$$H(t) = 2.7 \times 10^4 \times (e^{-at} - e^{-bt}) \quad (4)$$

where  $b = 1 \times 10^6$

The waveforms are shown in Figure 1-4.

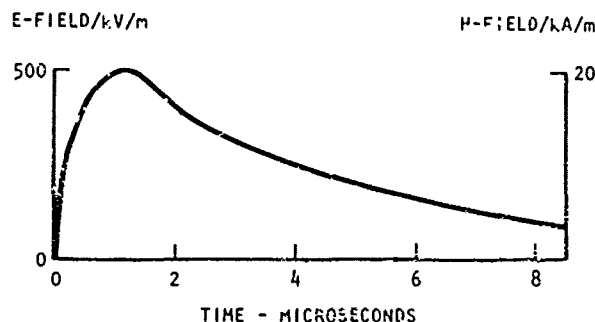


Fig. 1-4 - E- and H-field waveform model.

**COMPLETE MODELS** - The space and time functions can be combined for a more complete descrip-

tion of fields.

$$E(r, \phi, z, t) = E(r, \phi, z) \cdot E(t) \quad (5)$$

$$H(r, \phi, z, t) = H(r, \phi, z) \cdot H(t) \quad (6)$$

A spherical model (a sphere over a ground plane) gives perhaps a more familiar physical picture. The expression for the vertical field component is shown in rectangular coordinates using the sphere over ground plane model, is presented below:

$$E_y = \frac{Q_0 Y}{4} \left\{ \frac{[x^2 + (y_0 - y)^2]^{-3/2}}{[x^2 + (y_0 + y)^2]^{-3/2}} \right\} \quad (7)$$

The complete sphere model would be:

$$E_y(x, y, t) = E_y(x, y) \cdot E(t)$$

In summary, the infinite line current model gives both E and H. The sphere model gives E only but it probably gives a more familiar appearing electric field structure.

Following are some comments on the field orientation. The E field will always be normal to the aircraft regardless of the free space orientation as dictated by Maxwell's equations. The maximum H fields will generally be oriented tangentially to the aircraft skin (from currents flowing in the skin); however, significant H fields could exist from nearby strokes with any orientation. Thus, for the second order H fields, three orthogonal orientations using the three principal axis of the aircraft should perhaps be used to represent the many possible field orientations.

#### DIRECT STRIKE CURRENT MODELS

Two mathematical models may be used for direct stroke currents in the SEMCAP program, one fast rising to represent cloud-to-ground strikes and one with intermediate rise time and current to represent cloud-to-cloud strikes. A third component representing the nearby dc continuing currents is not used as their components are not too significant in producing pulses inside an aircraft. Also, the SEMCAP program does not extend down to dc.

The cloud-to-ground high current model is represented by the double exponential:

$$I = 2.14 \times 10^3 (e^{-at} - e^{-bt}) \quad (3)$$

where  $a = 1.3 \times 10^4$   
 $b = 0.5 \times 10^6$

This is approximately the waveform specified in MIL-B-5087B and also corresponds to the international high voltage test waveform, the 1 x 50 microsecond wave (1  $\mu$ sec to crest, 50  $\mu$ sec to

half value)

The cloud-to-cloud mode is represented by:

$$I = 1.5 \times 10^4 (e^{-at} - e^{-bt})$$

where  $a = 1.3 \times 10^2$   
 $b = 10^3$  (9)

The waveforms are shown in Figures 1-5 and 1-6.

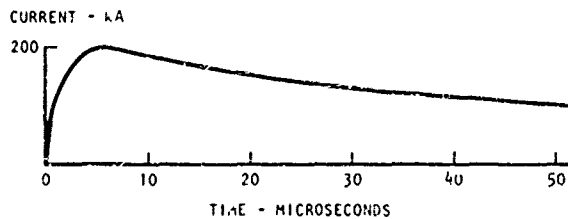


Fig. 1-5 - Direct strike, high current return stroke model waveform (cloud-to-ground).

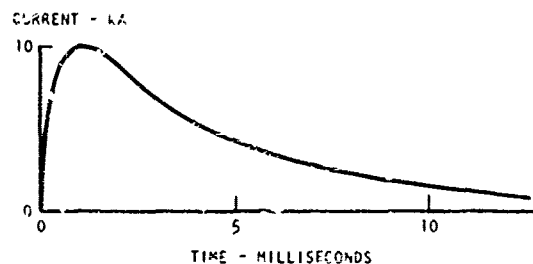


Fig. 1-6 - Direct strike, cloud-to-cloud intermediate current model waveform.

#### MATHEMATICAL MODELS FOR EMC ANALYSIS

W. R. Johnson

SIMPLIFIED MODELS of the spectral density functions for various types of lightning strokes onto or near an aircraft are presented. This data is to be used as input information to a computerized EMC analysis of the B-1 bomber. The models presented are quite simple, and further development to a more sophisticated state is anticipated for future application.

The characteristics of the lightning strokes themselves are provided by John Robb of the Lightning and Transients Research Institute (LTRI), St. Paul, Minnesota, in the preceding section of this paper.

Models are developed to describe the spectral density of various lightning strike conditions. The models developed describe the spectral density of H and E fields, and currents and voltages in the stroke and in the aircraft. The

models cover the following conditions:

- General double exponential current pulse of cloud-to-ground stroke
- The external E and H fields due to a distant stroke
- The internal H field due to high current density in small structural members, such as windshield post
- The internal E field due to a current stroke on the fuselage. (cylindrical model)
- The voltage and current on a wire struck directly by a lightning stroke. Break-down voltage levels due to arresters or arcing is considered."

#### MODELS

##### CONDITION A: GENERAL STROKE, CURRENT MODEL-

The time domain model for general lightning strokes is given by a double exponential function of the form  $I(t) = A(e^{-at} - e^{-bt})$ , (1) where  $a$  is the decay time constant, and  $b$  is the rise time constant.

Information obtained from John Robb of LTRI suggested the use of the following values for equation 1 for cloud-to-ground strikes

$$I(t) = 2.14 \times 10^5 (e^{-1.3 \times 10^4 t} - e^{-.5 \times 10^6 t}) \quad (2)$$

and for cloud to cloud

$$I(t) = 1.5 \times 10^4 (e^{-1.3 \times 10^2 t} - e^{-10^3 t}) \quad (3)$$

From equation 1, the general spectral density function is

$$I(\omega) = A \left[ \frac{\omega_b - \omega_a}{(S + \omega_b)(S + \omega_a)} \right] \quad (4)$$

Where  $\omega_a = a$ ,  $\omega_b = b$ , (as given in equation 1),  $S = j\omega$ .

Equation 4 may be solved for either the cloud-to-ground or cloud-to-cloud stroke by the insertion of the proper  $A$ ,  $a$ ,  $b$  parameters, where  $A$  is current amplitude.

CONDITION B: DISTANT STRIKE, E AND H MODELS - For external E and H fields, the Reference 1, equations 1 and 2, respectively, are evaluated with a driving current source equal to

\*Numbers in parentheses designate References at end of this part of the paper.



equation 4.

$$H = \frac{I(\omega)}{2\pi R} \quad E = \frac{60I(\omega)}{R} \quad (5)$$

Where R is the distance (in meters) from the stroke to the aircraft.

The equation for H( $\omega$ ) is based simply on an infinite length line current whereby Ampere's Law

$$I = \oint H \cdot d\ell$$

The equation for E is based on the time derivative of the magnetic vector potential of that line current.

The E field is based on a moving return stroke current, and is only rigorously correct for  $vt < R$ , where  $v$  = velocity of return stroke =  $3 \times 10^8$  m/sec. For the cloud-to-ground stroke whose current rise time is approximately 4  $\mu$ sec (i.e., approximately 2  $\times$  time constant), the value of  $v \times 4 \times 10^{-6}$  for  $vt=R=0$  is 1.2 km. Therefore, the equation for E field in equation 5 is valid for  $r \gtrsim 5$  km.

CONDITION C: WINDSHIELD POST MODEL - The model for the H field, due to a line current on the surface of the vehicle, is general but was developed specifically for swept stroke current through the windshield post. The model does not have any attenuation for skin, and if there is indeed attenuation, then this factor must be considered. The term "windshield post" will be used for description, with the understanding that the model is valid for any short length line current (i.e., element length  $< \frac{\lambda}{4}$ ).

The windshield post is considered an elemental dipole with the current of equation 4 flowing in it. The H field is then given by the equation

$$R(\omega) = \frac{I(\omega)\ell}{4\pi} \left( \frac{1}{r^2} + \frac{\omega}{rc} \right) \quad (6)$$

Where  $r$  is the mean distance from the post to the point of interest inside the aircraft cockpit,  $\ell$  is the length of the post and  $c = 3 \times 10^8$ .

Where the point of interest is wiring,  $r$  represents the mean distance, and the angle between the post and the wiring is  $0^\circ$  (worst-case).

CONDITION D: FUSELAGE STRIKE MODEL - The model for condition D determines the internal E field due to a surface flow on a cylinder of homogeneous material. Its purpose is to determine the voltage induced on wiring circuits inside the aircraft due to a lightning stroke current

evenly distributed around the fuselage (assumed cylindrical). The model basically uses the driving function of equation 4, and the low- and high-frequency components of the fuselage resistance multiplied by a skin penetration loss function. The model is given for aluminum material as

$$E_{int} = I(\omega) \left( \frac{1}{2\pi r t \sigma} + \frac{3.3 \times 10^{-7} \sqrt{f}}{2\pi r} \right) \cdot B \quad (7)$$

The first term in the brackets is the dc resistance per unit length, and the second term is the skin effect resistance per unit length.

$$B = e^{-t\sqrt{\pi\mu_0 f\sigma}}$$

B is the skin penetration factor.

Where  $\sigma = 3.7 \times 10^7$  rhos/m  
 $\mu_0 = 4 \times 10^{-7}$  H/M  
 $t$  = thickness of fuselage wall (m)  
 $r$  = mean radius of fuselage (m)  
 $f$  = frequency - Hz

CONDITION E: WIRE STRIKE MODEL - This model is to determine the voltage and current spectral density function on a wire struck directly by the lightning stroke. An example might be a lightning strike to a navigation light. The purpose of modeling this circuit is to determine the effect of coupling from the struck circuit to adjacent aircraft wiring. The series of events which occur in such a strike is:

The initial current which flows in the struck circuit is the normal stroke current. After some time, the magnitude of this current times the impedance of the line will reach a voltage breakdown level, either due to the presence of an arrester or the breakdown level between the wire and aircraft structure. The voltage drops to the arc-sustaining level and, due to the low dynamic impedance of the arc, the driving function changes from a current source to a voltage source. The result of these events yield a curve similar to Figure 2-1.

Note that the current in zone 1, i.e., prior to breakdown at  $t_1$ , is not the exponential that was used in equation 1 for the stroke current. If the line length is short (not considered in this paper), the current sees the line inductance and the load resistance. An exponential rise has a finite slope at  $t = 0$  and, therefore, the circuit voltage initially is  $-L \frac{di}{dt}$ , or  $L \cdot A \cdot b$ . For the parameters used in equation 2,  $A = 2.14 \times 10^5$  and  $b = 0.5 \times 10^6$ ,

this yields a voltage for a 1 M line of approximately  $V = 10^{-6} \cdot 2 \times 10^5 \cdot 5 \times 10^6 = 10^6$  at  $t = 0$ . Therefore, the breakdown would occur instantaneously. In reality, the stroke current does not start with a finite slope, and therefore a  $\sin^2$  function is used to simulate the beginning portion of the stroke as given in equation 8.

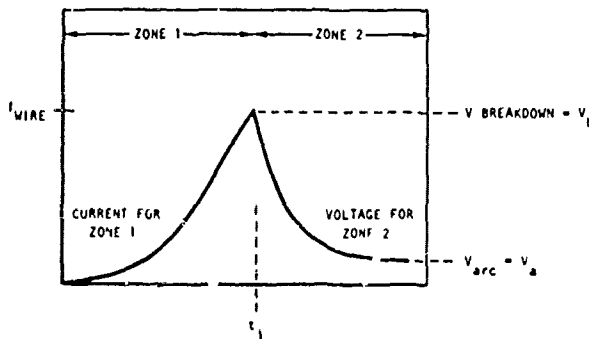


Fig. 2-1 - Wave shape and time due to driving function impedance.

In zone 2 of Figure 2-1 is shown the exponential decay of voltage from breakdown to the arc sustaining voltage. The current of zone 1 is then given by equation 8; the voltage by  $I_1(t) \cdot Z_0$  (i.e., equation 9). The voltage for zone 2 is given by equation 10, and the current for zone 2 is  $\frac{V_2(t)}{Z_0}$  (i.e., equation 11).

$$I(t) = A \sin^2 \frac{\pi t}{T_0} = \left( \frac{A}{2} \right) \left( 1 - \cos \frac{2\pi t}{T_0} \right) \quad (8)$$

Where A is assumed equal to  $2 \times 10^5$  amps and  $T_0$  (the half period of an  $\sin^2$  function) is  $7.4 \times 10^{-6}$  sec. The value of  $T_0$  is determined from the rise time of a  $\sin^2 \frac{\pi t}{T_0}$  function equal

to the rise time of the lightning stroke represented by  $I(t) = A(c^{-at} - e^{-bt})$  where  $\frac{1}{b} = 4.6 \mu\text{sec}$ , as specified in Reference 2-1 by equation 8.

$$V_1(t) = \left( \frac{Z_0 A}{2} \right) \left( 1 - \cos \frac{2\pi t}{T_0} \right) \quad (9)$$

where  $Z_0$  is the characteristic impedance of the wire.

The characteristic impedance is used in lieu of the lumped inductance and resistance due to the line lengths considered for the B-1 (i.e.,  $\approx 30\text{m}$ ). For this line length, the propagation time from wire entry to end and return is  $\frac{60\text{m}}{3 \times 10^8} = 200 \text{ nsec}$ . For the breakdown levels anticipated (i.e., 300 V to 10 KV), the

rise time is very short compared to the propagation time, so the wave front does not see the load boundary condition. Therefore, the wave looks into a quasi-infinite line length and sees only the characteristic impedance of the line. The line length limitation is reached when the line length is less than approximately  $2 \nu t$  where  $\nu$  is the propagation velocity. When the voltage of equation 9 reaches the breakdown voltage  $V_b$ , the voltage drops to the arc sustaining voltage  $V_{\text{arc}}$  according to equation 10. Nominal values of  $V_b$  and  $V_{\text{arc}}$  are  $V_b \approx 300 \text{ V} - 20 \text{ KV}$   $V_{\text{arc}} \approx 30 \text{ V}$  to  $3 \text{ KV}$ , but  $V_b > V_{\text{arc}}$ .

When the voltage of equation 9 reaches  $V_1$ , the voltage falls as

$$V_2(t) = (V_b - V_{\text{arc}}) e^{-\gamma t} \quad (10)$$

and the current decrease is

$$I_2(t) = \frac{V_2(t)}{Z_0} \quad (11)$$

where  $Z_0$  is the characteristic impedance of the wire circuit and  $\gamma$  has been identified between 1 - 10 nsec by Robb (2-1).

The models for voltage and current distribution in the frequency domain are given by the Laplace transform of equations 8 and 10, the voltage spectrum. The transforms were developed by the successive differentiation method outlined in Reference 2-2.

$$V(\omega) = \left[ -Z_0 \frac{S^2 I_1 + S I_2 + I_3 + P I_1}{S^3 + PS} + \frac{V_b - V_{\text{arc}}}{S + \gamma} + \frac{V_{\text{arc}}}{S} \right] e^{-st_1} + K_1 \quad (12)$$

and the current spectrum is

$$I(\omega) = \left[ -\frac{(S^2 I_1 + S I_2 + I_3 + P I_1)}{S^3 + PS} + \frac{1}{Z_0} \left( \frac{V_b - V_{\text{arc}}}{S + \gamma} + \frac{V_{\text{arc}}}{S} \right) \right] e^{-st_1} + K_1 \quad (13)$$

$$\text{Where } I_1 = \frac{A}{2} \left( 1 - \cos \frac{2\pi t_1}{T_0} \right)$$

$$I_2 = \frac{A\pi}{T_0} \sin \frac{2\pi t_1}{T_0}$$

$$I_3 = \frac{2A\pi^2}{T_0^2} \cos \frac{2\pi t_1}{T_0}$$

$$P = \frac{4\pi^2}{T_0^2}$$

$$S = j\omega$$

$$K_1 = \frac{2A\pi^2}{T_0^2}$$

$\gamma$  = Time constant of fall time

$V_{arc}$  = arc sustaining voltage

$V_b$  = breakdown voltage

$t_1$  = time to voltage breakdown

$T_0$  = time to crest of normal stroke

## CONCLUSION

The models presented here merely scratch the surface of the effort required to analyze the results of lightning on the avionics and other electrical and electronics circuitry of aircraft. Much further work is required if the lightning effects are to be quantitatively evaluated.

## REFERENCES

2-1. John D. Robb, "A Lightning Model for the SEMCAP Program - North American B-1," Lightning and Transients Research Institute Report, 23 March 1972.

2-2. Paul Wiley, "Electronic Circuits, Signals and Systems," 1960.

## APPENDIX

This appendix contains example computer printouts for the models described in the body of the report. The output data contained in this appendix used certain parameters for the models which may be changed if different data is supplied. The data output is in a form which may be directly inserted into the SEMCAP program for analysis of the effects of lightning phenomena.

Sample solutions are given for Lightning Models using the parameters indicated. The left column is frequency in Hz, and the right column is in db above 1 ampere, 1 volt, 1 ampere/meter, or 1 volt per meter per Hz of bandwidth. To convert the levels to  $\mu v$ ,  $\mu a$ ,  $\mu v/m$ ,  $\mu a/m$  per MHz, add 240 db.

Standard lightning stroke  
(Cloud-to-Ground) (Equation 4)  
 $I_{peak} = 200,000A$

Time Const (Rise) =  $2 \times 10^{-6}$

Time Const (Fall) =  $77 \times 10^{-6}$  sec

```

RUN
CURRENT SPEC DENSITY FROM STROKE
CURRENT AMP  BETA(LC FREQ)  ALPHA(HI FREQ)
? 214E+3, 1.3E+4, 5E+5
FREQ          DBI/Hz
10            40.059679
15.848932     40.059526
25.118364     40.059141
39.810717     40.053173
63.095734     40.055745
100           40.049651
158.48932     40.03438
251.18364     39.996257
398.10717     39.901945
630.95734     39.673689
1000          39.148135
1584.8932     38.054529
2511.8364     36.124232
3981.0717     33.329299
6309.5734     29.908285
10000         26.129253
15848.932     22.13722
25118.364     17.937965
39810.717     13.39855
63095.734     8.2581627
100000        2.2655466
158489.32     -4.5793713
251183.64     -12.016401
398107.17     -19.770774
630957.34     -27.468992
1000000       -35.5273
1584893.2     -43.611292
2511886.4     -51.604702
3981071.7     -59.502076
6309573.4     -67.60103
10000000      -75.600614
15848932     -83.600448
25118364     -91.600332
39810717     -99.600356
63095734     -107.60035
.1E+09        -115.60034
.15848932E+09 -123.60034
.25118364E+09 -131.60034
.39810717E+09 -139.60034
.63095734E+09 -147.60034
.1E+10        -155.60034
.15848932E+10 -163.60034
.25118364E+10 -171.60034
.39810717E+10 -179.60034
.63095734E+10 -187.60034
.1E+11        -195.60034

```

Reproduced from  
best available copy.

Distant lightning strike  
E and H Fields (Equation 5)  
Distance to Strike 5 km  
I<sub>peak</sub> = 200,000A  
Time Const (Rise) = 2 μsec  
Time Const (Fall) = 77 μsec

RUN  
INPUT AMP, BETA, ALPHA  
? 214E+3, 1.3E+4, 5E+5  
HIS FLD FROD DIST STRIKE

? 5000  
FREQ DBE/HZ DBH/HZ  
10 1.6433039 -49.33318  
15.848932 1.6431506 -49.233472  
25.113864 1.6427655 -49.233157  
39.810717 1.6417983 -49.934324  
63.095734 1.6393697 -49.337253  
100 1.6332755 -49.893347  
158.48932 1.6180049 -49.908617  
251.13864 1.5792318 -49.946741  
398.10717 1.4855695 -50.041053  
630.95734 1.257314 -50.269303  
1000 .73121003E+00 -50.794812  
1584.8932 -3.36184579E+00 -51.839468  
2511.8364 -2.292143 -53.819765  
3981.0717 -5.0370365 -56.613709  
6309.5734 -8.5030903 -60.034713  
10000 -12.287122 -63.813745  
15848.932 -16.279155 -67.305778  
25113.364 -20.47841 -72.005032  
39810.717 -25.017826 -76.544448  
63095.734 -30.158212 -81.634935  
100000 -36.150323 -87.677451  
158459.32 -42.994746 -94.521369  
251183.64 -50.432776 -101.9594  
398107.17 -58.187149 -109.71377  
630957.34 -66.085367 -117.81199  
1000000 -74.044175 -125.5708  
1584893.2 -82.027667 -133.55429  
2511386.4 -90.021077 -141.5477  
3981071.7 -98.018451 -149.54507  
6309573.4 -106.01741 -157.54403  
10000000 -114.01699 -165.54361  
15848932 -122.01432 -173.54345  
25113864 -130.01676 -181.54338  
39810717 -138.01673 -189.54335  
63095734 -146.01672 -197.54334  
.1E+09 -154.01672 -205.54334  
.15848932E+09 -162.01671 -213.54334  
.25113864E+09 -170.01671 -221.54334  
.39810717E+09 -178.01671 -229.54334  
.63095734E+09 -186.01671 -237.54334  
.1E+10 -194.01671 -245.54334  
.15848932E+10 -202.01671 -253.54334  
.25113864E+10 -210.01671 -261.54334  
.39810717E+10 -218.01671 -269.54334  
.63095734E+10 -226.01671 -277.54334  
.1E+11 -234.01671 -285.54334

Strike to Windshield Post  
(Swept Stroke) (Equation 5)  
H fields in cockpit area with no windshield  
attenuation.  
I<sub>peak</sub> = 200,000A  
Time Const (Rise) = 2 μsec  
Time Const (Fall) = 77 μsec  
Distance from Post to wiring = 1m  
Length of Post = 1m

RUN  
CURRENT AMP, BETA(LO FREQ) ALPHA(HI FREQ)  
? 214E+3, 1.3E+4, 5E+5  
H FLD FRM WNDSHLD POST-DRI/M/HZ  
DISTANCE TO WIRES LENGTH OF POST  
? 1, 1

FREQ H FLD DBI/M/HZ  
10 18.075484  
15.848932 18.075331  
25.113864 18.074948  
39.810717 18.073983  
63.095734 18.071559  
100 18.065471  
158.48932 18.050212  
251.13864 18.012105  
398.10717 17.91782  
630.95734 17.639607  
1000 17.16417  
1584.8932 16.07062  
2511.3864 14.140492  
3981.0717 11.345315  
6309.5734 7.9252346  
10000 4.1463734  
15848.932 .13590382E+00  
25118.864 -4.0416659  
39810.717 -8.5784122  
63095.734 -13.71457  
100000 -19.700487  
158489.32 -26.533799  
251183.64 -33.955046  
398107.17 -41.682885  
630957.34 -49.539217  
1000000 -57.432049  
1584893.2 -65.311994  
2511386.4 -73.143779  
3981071.7 -80.291001  
6309573.4 -88.507682  
10000000 -95.93389  
15848932 -103.09605  
25113864 -109.9145  
39810717 -116.31255  
63095734 -122.27177  
.1E+09 -127.776  
.15848932E+09 -132.37947  
.25113864E+09 -137.65553  
.39810717E+09 -142.13345  
.63095734E+09 -146.53385  
.1E+10 -150.76244  
.15848932E+10 -154.90933  
.25113864E+10 -159.00413  
.39810717E+10 -163.04416  
.63095734E+10 -167.10225  
.1E+11 -171.12637

Reproduced from  
best available copy.

# Strike to Fuselage (Equation 7)

$I_{peak} = 200,000A$

Time Const (Rise) = 2  $\mu sec$

Time Const (Fall) = 77  $\mu sec$

Fuselage radius = 3m

Conductivity  $3.7 \times 10$  mho/m

# Strike to Wire (Equations 12 & 13)

$V_{breakdown} = 3000 V$

$V_{arc}$  sustaining = 30 V

Time to breakdown = 20 nsec

Char Z of wire = 200 $\Omega$

Fall time constant = 5 nsec

5 LOAD, FUSLHT, P

END LOAD

5 RUN

CURRENT AMP, BETA (LC FREQ), ALPHA (HI FREQ)

? 214E+3, 1.3E+4, 5E+5

RADIUS, THICKNESS, CONDUCTIVITY

? 3.1E+3, 3.7E+7

FREQ	E INT DBV/HZ	SKIN PEN LOSS
10	-76.772476	-3.3196709E+00
15.848932	-76.775375	-4.1792131E+00
25.118864	-76.780335	-5.2613232E+00
39.810717	-76.783802	-6.6236143E+00
63.095734	-76.803335	-8.3336364E+00
100	-76.82874	-1.0497721
158.48932	-76.874435	-1.3215443
251.18864	-76.960209	-1.6637767
398.10717	-77.123111	-2.0945703
630.95734	-77.468942	-2.6369034
1000	-78.164756	-3.3196709
1584.8932	-79.513043	-4.1792131
2511.8864	-81.819312	-5.2613239
3981.0717	-85.162153	-6.6236143
6309.5734	-89.370829	-8.3336364
10000	-94.266747	-10.497721
15848.932	-99.320962	-13.215443
25118.864	-106.17643	-16.637767
39810.717	-113.6548	-20.945708
63095.734	-122.75466	-26.369034
100000	-134.02565	-33.196709
158489.32	-147.84053	-41.792131
251188.64	-164.4029	-52.613239
398107.17	-184.0413	-66.236143
630957.34	-207.29795	-83.36364
1000000	-235.01621	-104.97721
1584893.2	-268.31726	-132.15443
2511886.4	-303.63967	-166.37767
3981071.7	-357.30468	-209.45703
6309573.4	-418.10312	-263.69034
10000000	-492.44055	-331.96709
15848932	-584.44032	-417.92131
25118864	-695.68692	-526.13239
39810717	-840.94471	-662.36143
63095734	-1018.4698	-833.86364
.1E+09	-1240.3966	-1049.7721
.15848932E+09	-1518.2233	-1321.5443
.25118864E+09	-1865.1724	-1662.37767
.39810717E+09	-2335.6597	-2094.5703
.63095734E+09	-2924.667	-2636.9034
.1E+10	-3600.6723	-3319.6709
.15848932E+10	-4396.6774	-4179.2131
.25118864E+10	-5370.6311	-5261.3239
.39810717E+10	-6584.66	-6623.6143
.63095734E+10	-8080.6632	-8338.6364
.1E+11	-9930.6882	-10497.721

# STRIKE TO WIRE ENTRY

FREQ	DBI/HZ	DBV/HZ
10	-30.538959	15.421641
15.848932	-31.269195	14.751405
25.118864	-31.597908	14.422691
39.810717	-31.736024	14.284576
63.095734	-31.792254	14.228345
100	-31.814842	14.205758
158.48932	-31.823861	14.196739
251.18864	-31.827441	14.193159
398.10717	-31.82883	14.19177
630.95734	-31.829266	14.191313
1000	-31.829228	14.191372
1584.8932	-31.8286	14.192
2511.8864	-31.826831	14.193769
3981.0717	-31.82231	14.19829
6309.5734	-31.810913	14.209687
10000	-31.782206	14.238394
15848.932	-31.709672	14.310928
25118.864	-31.524755	14.495845
39810.717	-31.04212	14.97848
63095.734	-29.696416	16.324184
100000	-24.950987	21.069613
158489.32	-23.290026	22.730574
251188.64	-39.619111	6.4014893
398107.17	-49.526336	3.5057357
630957.34	-58.183256	-12.162656
1000000	-66.433139	-20.412539
1584893.2	-74.534589	-28.513989
2511886.4	-82.581486	-36.563886
3981071.7	-90.628874	-44.608275
6309573.4	-98.707686	-52.687086
10000000	-106.83686	-60.866218
15848932	-115.26347	-69.24284
25118864	-123.53769	-77.517091
39810717	-129.69276	-83.672166
63095734	-135.63426	-89.613684
.1E+09	-143.35027	-97.329685
.15848932E+09	-151.04023	-105.01977
.25118864E+09	-159.0208	-113.00056
.39810717E+09	-166.99032	-120.97063
.63095734E+09	-174.98909	-128.97077
.1E+10	-182.81658	-136.80153
.15848932E+10	-190.56478	-144.55733
.25118864E+10	-197.98004	-151.9883
.39810717E+10	-204.76352	-158.79767
.63095734E+10	-210.68503	-164.74932
.1E+11	-215.77397	-169.86052

Reproduced from  
best available copy.

## LIGHTNING AND ELECTROMAGNETIC COMPATIBILITY ANALYSES CONSIDERATIONS

J. A. Plumer

BECAUSE AVIONICS COMPONENTS are usually localized and enclosed in metal cases which afford substantial electromagnetic shielding, relatively little of the lightning electromagnetic field can link sensitive components within these enclosures, and that which does is probably sufficiently attenuated to be of little consequence. Instead, the most significant interference is first coupled into interconnecting electrical wiring in the form of transient overvoltages. This wiring is unshielded and extends for substantial distances inside the airframe. The first step in the lightning analysis task is therefore to determine the amplitude and pulse waveshape of such voltages, because these define voltages to which the connected avionics components will be subjected. There are two basic mechanisms by which lightning can couple voltages into aircraft electrical wiring. There are commonly referred to as directly coupled voltages and induced voltages. Using a hypothetical electrical wire in an aircraft wing, these two mechanisms are now described.

**DIRECTLY COUPLED VOLTAGES** - Prior to actual attachment to the aircraft, an oncoming lightning flash (stepped leader) will induce corona and streamers from surfaces or appendages on the aircraft where the electric field gradient is great enough. Subsequently, when the electric field strength around protruding objects reaches 5,000 volts per centimeter (3-1)\* a breakdown will commence usually to the point on the aircraft where the field gradient is most severe. If this point happens to be an electrically operated object, such as a wing-tip position lamp, antenna, or stall-warning sensor-switch, for example, connected to power distribution circuits or avionics components by aircraft electrical wiring, the possibility exists for damaging amounts of voltage and/or current to be conducted to such components by the interconnecting circuitry.

Considering a dome lamp, for example, it is possible that an oncoming flash may fracture the globe and bulb glass as shown in Figure 3-1. Such fractures are a common result of lightning strikes and may occur from dielectric puncture or the stroke current blast forces.

\*Numbers in parentheses designate References at end of this part of the paper.

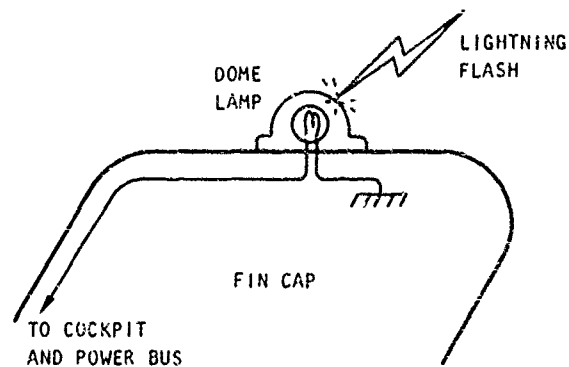


Fig. 3-1 - Lightning flash to dome lamp.

Subsequent attachment of the flash to the bulb filament and lamp socket assembly will provide paths for most of the lightning current to flow to the airframe; however, it is apparent that some portion of this current could flow along the lamp power circuit to the cockpit area. This conducted current will have a waveshape similar to that of the natural lightning current itself, and be limited by the impedance of the lamp circuit as compared with the much lower impedance of the surrounding metal airframe. Even a small percentage of a 100,000-ampere lightning stroke current could far surpass the current handling capability of the lamp circuit, and damage various components associated with the power control and distribution circuitry, however. Exploding wires, insulation fires, and circuit breaker trip-outs have been reported as a result of this.

Coincident with this conducted current will be a conducted voltage pulse, traveling down the wire from the lamp socket. Assuming that the lamp filament is destroyed when the glass is fractured, this voltage will be limited initially by the breakdown voltage level across the terminals of the lamp or socket (whichever is less) and later by the stroke current arc voltage drop as an arc forms across the socket elements. Typically, the impulse voltage breakdown levels of such components, which are determined from a simple test, range between 2 KV and 10 KV. The breakdown voltage limits the amplitude of the voltage pulse which will propagate into the lamp circuit. The waveshape of this voltage pulse approximates the waveshape of the electric field applied by the oncoming lightning flash. After arc-contact with the lamp and flashover across the broken filament terminals, the voltage entering the circuit is further limited to the arc drop, if an arc is maintained across the broken bulb terminal for the duration of the flash. Arc drops are of the order of several hundred volts or less.

Being a very low impedance voltage source, however, a large percentage of this arc voltage will develop across loads at the cockpit end of the circuit with attendant current flow thereto. The results can be damaging.

Protection from such damage can be accomplished by applying lightning diverters at the lamp to prevent stroke attachment and the subsequent events just described. If, due to other requirements, an effective diverter system cannot be used, the lamp assembly itself may be left vulnerable and a suitable surge protector applied to the aircraft circuit at the lamp terminals. Such a protector has the following two functions:

1. Limit the lightning surge voltage entering the circuit to an acceptable amplitude
2. Conduct the ensuing lightning current (or the portion thereof which would enter the lamp circuit) safely to the airframe

The surge protector is shown applied to the lamp terminals on Figure 3-2.

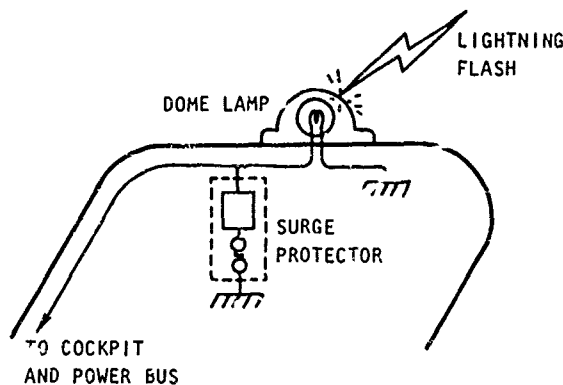


Fig. 3-2 - Surge protector installed on lamp circuit.

A variety of such protectors are available. They must be able to absorb energy as well as limit the surge voltage and safely conduct possible portions of the lightning current. The following information must be obtained before an appropriate protector can be specified:

1. Physical characteristics of the susceptible component (i.e. lamp, antenna, etc)
2. Breakdown voltage of the susceptible component
3. Current-carrying capability of the associated aircraft electrical circuitry
4. Maximum surge voltage and current withstand levels of other equipment to which the circuit is connected

If other components, such as switches, terminal boards, feed-through bushings, or connectors are included in the circuit(s) to the

susceptible components previously mentioned; they may also affect the way surge voltages and current flow in the system. Thus, the aforementioned characteristics of these components must also be known and factored into the foregoing analysis in order to design an effective, properly coordinated protection scheme.

**INDUCED VOLTAGES** - The other mechanism by which lightning can affect aircraft electrical and avionics systems is in the generation of magnetically induced and resistive voltage rises within aircraft electrical circuitry. These voltages may or may not be harmful to the circuits themselves, as well as the avionics equipment to which these circuits are connected. Even if the aircraft has an electrically continuous metallic skin, its noncylindrical geometry will enable some magnetic flux to be present within the wing and fuselage, even if all of the lightning current were to flow through the skin only. This magnetic flux will link electrical circuits within these enclosures, causing induced voltages. Similarly, the finite resistivity of the metallic skin will permit resistive voltage rises within the skin (or structure) along the path of lightning current flow. If an aircraft electrical circuit happens to employ the structure as return path, then this resistive voltage enters this circuit, in-series with the magnetically induced voltage in the same circuit, and any other (normal) steady-state voltages present. Capacitively coupled voltages may also be produced in these circuits; however, the essentially uniform conducting skin of metallic aircraft keeps potential differences among structural elements low, thereby limiting the voltages which can be electrostatically coupled to interior electrical circuits. In practice, experimental measurements have shown magnetic and resistive components to be the most predominant.

The combination of these components is expressible as a function of the lightning current itself, as follows (3-2):

$$e_{oc} = R_s i_L(t) + M \frac{d(1 - e^{-\alpha t}) i_L(t)}{dt} \quad (1)$$

where:

$e_{oc}$  = induced voltage appearing across open circuit terminals

$R_s$  = the effective structural resistance

$M$  = an effective transfer inductance between the lightning current and the particular electrical circuit

$i_L(t)$  = lightning current (a time-varying function)

$\alpha$  = the reciprocal of the time constant of current penetration into the aircraft skin

Because the induced voltages are dependent upon the lightning current, they vary considerably in amplitude and wave shape according to the lightning current parameters of wave shape and amplitude. Induced voltages are also dependent upon the characteristics of the circuit in which they are measured, and the location at which the lightning stroke attaches to the aircraft. From equation 1, it is evident that if the coupling factors,  $R$  and  $M$ , for a particular circuit within an airframe are known, the voltage  $e_{oc}$  in the circuit can be calculated for any assumed lightning current waveform,  $i_L(t)$ .

Due to the fast rise and decay and short time duration of most lightning stroke currents, nearly all of this current will flow in the outer skins of metallic airframes rather than through internal spars and ribs, etc. Assuming that this is so, and also that the current flows uniformly in a linear direction through a structure, its skin can be represented by a very large number,  $n$ , of infinitely small parallel current filaments. Using a wing of an aircraft as an example, this representation would be as shown in Figure 3-3.

Assuming that the wing circuit pictured in Figure 3-3 is "grounded" to the airframe at the outboard end of the wing, the voltage appearing between the inboard end of the conductor and the inboard airframe is equal to the line integral of voltage induced around a plane such as ABCD in Figure 3-3. If it is assumed that all points on the inboard chord of the wing are at the same potential, then any plane passing through conductor AB and intersecting a surface of the wing can be selected to perform this integration, with the same result.

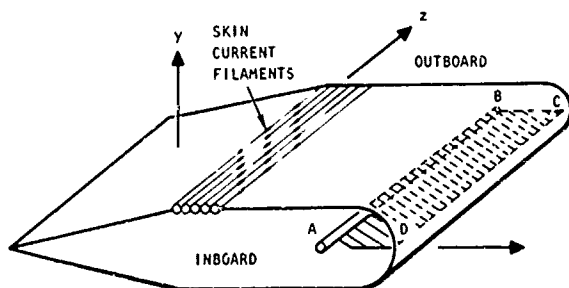


Fig. 3-3 - Electrical representation of wing.

By Faraday's Law (3-3) the voltage magnetically induced along path ABCD is equal to the rate of change of magnetic flux within the loop formed by this path, as follows:

$$e_m = \frac{d\phi}{-dt} \quad (2)$$

If lightning current flows on the wing skin and the skin has a finite resistance, then a resistive voltage drop will appear along CD and contribute to the total voltage along path ABCD. If  $i_L$  represents the entire lightning current, presumed to be equally distributed among all filaments, then the resistive voltage drop included along path CD is given by:

$$e_r = \frac{i_L}{n} \cdot R_n \quad (3)$$

In equation 3,  $R_n$  is the resistance of one current filament, equal to  $n$  times the total wing skin resistance, outboard to inboard.

The magnetically induced voltage is equal to time rate of decrease of the total magnetic flux linking the circuit. This is expressed as:

$$\text{where } e_m = \frac{d\phi}{-dt} \quad (4)$$

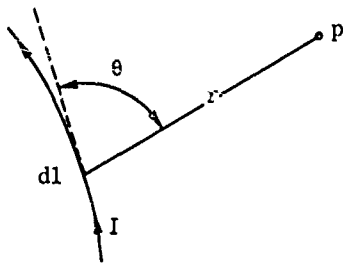
$e$  = total EMF (volts)  
 $\phi$  = total flux (webers)  
 $t$  = time (sec)

If the voltage around the inboard circumference of the wing in Figure 3-3 is assumed to be the same at all points, the voltage between the circuit conductor at A and the inboard circumference will also be the same at any point. Thus, the magnetic flux lines linking all planes defined by the particular wing circuit conductor (AB) and any longitudinal wing intersect will be equal. For purposes of calculation, it is convenient to choose a plan along the axis of symmetry (if available).

The portion of the magnetic flux generated by each of the skin current filaments passing through the plane ABCD must be determined and the total summarized in order to determine the magnetically induced voltage,  $e_m$  as defined in equation 4.

The magnetic flux density produced at some point,  $p$ , with respect to a current filament is defined by the Biot-Savart Law (3-4) as:





$$\text{where: } B = \frac{\mu I}{4\pi} \int \frac{\sin \theta}{r^2} dl \quad (5)$$

$B$  = magnetic flux density (weber per meter<sup>2</sup>)  
 $l, r$  = dimensions in meters  
 $\mu$  = permeability of the medium (for air =  $4 \times 10^{-7}$  henries per meter)

The total flux,  $\phi_n$ , passing through a given area is equal to the product of the area and the component of  $B$  normal to it. Thus,

$$\phi_n = \iint B \cdot ds \quad (6)$$

where:  $\phi_n$  = magnetic flux (webers) contributed by each skin current filament

In the wing circuit problem, the flux density,  $B$ , must be determined as a function of the current  $i_n$  and applicable geometry for each current filament along the wing skin, and integrated over the surface area defined by the plane ABCD, in accordance with equation 6.

Since the assumption has been made, for the present, that the total lightning current,  $i_L$ , is evenly distributed among the  $n$  skin current filaments, the voltage  $e_m$  can be written:

$$e_m = - \sum_{n=1}^{n=n} \frac{d\phi_n}{dt} = - \frac{di_L}{dt} \sum_{n=1}^{n=n} M_n \quad (7)$$

where  $M$  is expressed in henries and  $i_L$  in amperes. Since  $e_n$  is related to  $\frac{di_L}{dt}$  by the function,

$$- \sum_{n=1}^{n=n} M_n = M \quad (8)$$

$M$  operates as a transfer function expressing the magnetic induced voltage in terms of the skin (lightning) current.

To calculate  $M$  for various wing geomet-

ries and circuit conductor positions, a computer program (WING) in BASIC language for use on the General Electric time-sharing computer system has been written. This program also calculates the resistive transfer function,  $R_s$ , based on skin dimensions and resistivity. The values of  $M$  for conductors placed at various locations in the plane of symmetry for one basic wing outline are shown in Figure 3-4.

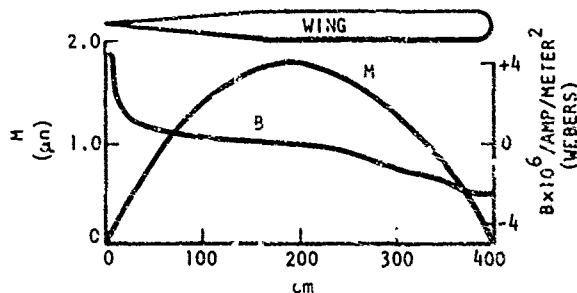


Fig. 3-4 -  $B$  and  $M$  versus conductor location.

The wing in Figure 3-4 is 16 meters long, and the conductor AB traverses its entire length.

Figure 3-4 illustrates that  $M$  and thus, by equation 8, the magnetically induced voltage between conductor AB and the airframe will be a maximum for a conductor 210 centimeters aft of the leading edge. Conductors placed in the leading edge will receive relatively less voltage. It should be remembered that this applies for circuits using the airframe as return only. If it is desired to find the voltage induced in a circuit having a separate return conductor, then the effective coupling factor  $M$  for this case must be determined by integrating equation 6 over the plane defined by the circuit loop itself. For this purpose, the program WING also calculates the flux density per ampere of lightning current,  $B$ , at each conductor location of interest. This information is also plotted in Figure 3-4. From this, it is evident that  $B$  is greatest at the leading and trailing edges of the wing, and minimal at the point where a conductor and the airframe return will link the most flux. Hence, a designer would place parallel-pair or twisted-pair circuits toward the center of the wing to minimize lightning-induced voltages.

The resistive voltage coupled to the circuit, of course, would be the same regardless of location for all circuits using the airframe as return, but would be much less for separate-return circuits.

Once obtained for any circuit of interest, the transfer functions  $R_s$  and  $M$  can be inserted in equation 1 to obtain the amplitude and wave-

shape of the complete lightning-induced voltage in any circuit of interest, as a function of any assumed lightning stroke current characteristics. Another computer program (ETCAL) also in BASIC is available for this purpose (3-2). Using a conductor located 10 centimeters aft of the leading edge skin of the wing of Figure 3-4, as an example, WING calculates transfer functions of

$$R_s = 37 \text{ microhms}$$

$$M = 0.66 \text{ microhenries}$$

and ETCAL calculates an induced voltage peaking at 800 volts. The complete induced-voltage waveshape is shown in Figure 3-5. This information (together with that obtained from the direct coupled analysis) establishes the susceptibility of connected avionics or electric power control circuitry to lightning induced voltages. From here, the lightning EMC study can proceed to analysis of component vulnerability to these voltages and the need for additional protective measures.

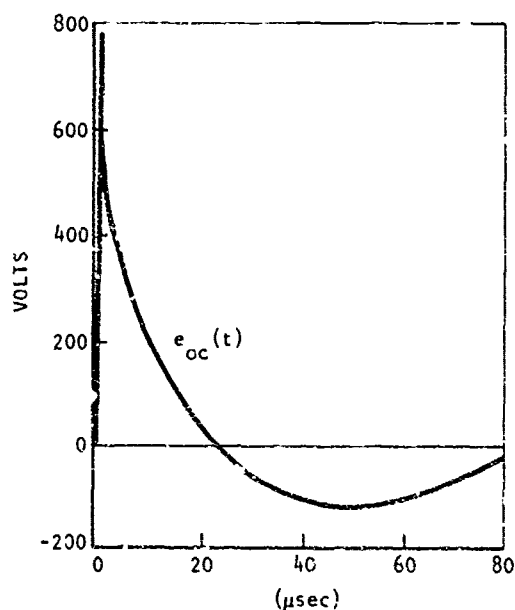


Fig. 3-5 - Voltage induced in conductor AB of Fig. 3-3, located 10 cm aft of leading edge, by 200,000 ampere MIL-B-5087B lightning current flowing uniformly through wing skin.

## CONCLUSION

In the foregoing induced-voltage analysis, the assumption was made that lightning current is evenly distributed across the wing surface. In actuality, this is not so, as the resulting magnetic forces act to concentrate current in the leading and trailing edges. Recent skin current density measurements were made by the General Electric High Voltage Laboratory of currents traveling from the fuselage to an attachment point near the trailing edge position lamp at the tip of a fighter aircraft wing. Preliminary analysis of this data shows the current density to be at least twice as great at the edges as compared with the midchord region. For a conventionally bonded metallic aircraft, skin effect assures that most of the current does indeed flow through the skins. Nevertheless, the effects of direct flux penetration through nonmetallic skin elements and joints, and the presence of ribs, spars, and independent circuit shields will cause the actual voltage to differ somewhat from those calculated by the foregoing analysis. The program WING can be modified to accommodate many of these factors in a straightforward manner. In addition to enabling designers to evaluate the susceptibility of aircraft electrical circuits to lightning while still on the drawing board, the analysis is further evidence that lightning effects are not a mysterious phenomena but conform, as with all other electrical processes, to the established basic laws of electricity and magnetism.

## REFERENCES

- 3-1. F.A. Fisher, B. Macchiaroli, and D.L. Jones, "Lightning Effects Related to Aircraft-Part II-Characteristics of Simulated Lightning Flashes and their Effects on Lightning Arresters and Avionic Equipment." AFAL-TR-72-5, January, 1972.
- 3-2. K.J. Lloyd, J.A. Plumer, and L. J. Walko "Measurements and Analysis of Lightning-Induced Voltages in Aircraft Electrical Systems." NASA CR 1744, February, 1971.
- 3-3. J.D. Kraus, "Electromagnetics." McGraw-Hill Book Co, Inc, 1953, p 287.
- 3-4. *ibid*, p 148.

## Control Surface and Door Hinge Bonding Effectiveness in Modern Aircraft

James R. Stahmann  
Lightning & Transients Research Institute

### ABSTRACT

The practice of indiscriminately placing bond straps across most control surface and door hinge bearings for lightning protection, without first establishing their necessity for safety or noise reduction, is being challenged. Because of the high cost of replacing bonds, broken by flexing in flight, an airline can realize substantial savings by close examination of bonds in questionable locations. Bonding specifications are necessarily generalized to apply to all aerospace systems. By directing attention to specific hinges on doors and control surfaces, advantage can be taken of the inherent bonding as, for example, the self-bonding inherent in a piano type hinge recognized in MIL-B-5087B. Low impedance parallel paths, provided by control actuators and other connections to main structure, are often effective in sharing the lightning current and in preventing noise from static charging. All significant factors should be considered for proper evaluation. Bonding effectiveness can be determined by checks with simulated lightning, using full scale aircraft sections.

BONDING jumpers, used ostensibly to conduct lightning currents across hinges without damaging the bearings or to prevent noise during the discharge of charged surfaces, are being reexamined to determine whether or not they still perform their intended function on modern aircraft. Available specifications, such as the military MIL-B-5087B, necessarily apply to a wide spectrum of aerospace systems. Where bonding maintenance becomes costly and where safety is not jeopardized, an airline can expect significant savings, in one case in excess of \$75,000/year, by carefully reexamining the need for bonds in specific questionable locations. Many bonds have had a high failure rate due to flexing in flight. In certain instances bond removal could improve safety as, for example, where a bond could be blown loose from one or both of its lugs by the lightning discharge. The confusion that exists in the area of bonding requirements is illustrated by the fact that one manufacturer uses almost ten times the number of bonds found necessary by another manufactur-

er of a similar aircraft.

Advantage can be taken of the inherent bonding across the hinge as, for example, the self-bonding property of piano-type hinges. Bearing size and location, parallel paths, bearing inductance and conductivity relative to the bond strap, type of lightning contact to be expected and coupling factor from the bonded surface to a receiver antenna should be considered in a proper evaluation.

In this study the bonding jumpers across selected door and control surface hinges on parts from a Boeing 727 aircraft were checked. The major components selected were:

- (1) Main gear doors, EAL 77DO2051-2053
- (2) Nose gear door, EAL 77DO2154
- (3) Ground spoiler, EAL 77SP3253
- (4) Outboard aileron & tab, EAL 77AI74
- (5) Inboard aileron & tab, EAL 77AI71
- (6) Leading edge flap, EAL 77FL904
- (7) Rudder & tab, EAL 77RU361
- (8) Elevator & tab, EAL 77EL1831-TA121

### SETUPS AND PROCEDURES

Since the parts could not be checked in place on the aircraft, the various setups were designed to insure bond and hinge currents that equaled or exceeded those expected on the aircraft. For example, a door hinge in the aircraft fuselage would carry less current than in our setup since no attempt was made to complete the enclosure. When possible the resistance of the hinge gearings was measured with an ohmmeter. Low resistances, of the order of milliohms, were measured by passing a 10 ampere current through the bearings and measuring the voltage across them. Where a hinge was nonconducting at low voltage, the breakdown voltage was measured. Then the conductivity across the hinge on the actual aircraft, with its actuators and other parallel paths, was also measured from the hinged part to main structure. For the simulated lightning damage checks, standard discharges were applied, first with the bond straps in place and then again with the bond straps removed. The bearings were inspected for pitting or other damage after each test.

## MEASUREMENTS

**HINGE BEARINGS-** The piano-type hinge bearings checked confirmed that these bearings may be considered self-bonded as specified in MIL-B-5087B. The control surface hinge bearings were cylindrical sleeve bearings, usually in a self-aligning ball joint, or the piano-type or both. When a test discharge was passed through a ball joint, the ball was pitted on its external surface, but not on the surfaces in contact during the discharge. The ball could be easily rotated after the test although not as easily as before. There was no evidence of hinge binding. A typical pitted alignment ball and a pitted hinge pin are shown in Fig. 1. The observed pitting was not prevented or significantly reduced by placing a bond strap across the hinge.

**BOND STRAPS-** The bond straps were either stranded aluminum or copper cable measuring between 0.090 and 0.110 inch in diameter. The copper straps were usually covered with insulation. The copper straps had a resistance of about one milliohm and carried a discharge of 75 kiloamperes peak before separating at the lugs to which they were mechanically crimped. Aluminum straps had a higher resistance at the lug fastening points.

Since lightning stroke current components may reach a rate of rise of current of 100 Ka./ $\mu$ sec., the current across a hinge divides according to the inductance of the various parallel paths rather than their resistance due to the high frequency components present. The small diameter bond straps used on the aircraft investigated usually have a higher inductance than the relatively large hinges and thus they carry less current than the hinges, even though their resistance may be lower than that of the hinge. As an illustration, the current in a bond strap across a hinge on the main gear door was measured to be only 20% of the current carried by the hinge.

**MAIN GEAR DOORS-** A main gear door in a setup for checking its hinges is shown in Fig. 2. Two sets of three hinges each are used. Since they are piano-type hinges, they can be considered self-bonded if their resistance is less than 10 milliohms. The resistance measured across the upper hinges was 1.5 milliohms and that across the lower hinges was 0.5 milliohms. Three 200 Ka. peak discharges were applied with bond straps in place and an additional three were applied after the bond straps were removed. No significant hinge pitting or binding was observed after each series of tests.

**NOSE GEAR DOOR-** Two hinges with self-aligning sleeve bearings were checked on the nose gear door. The resistance measured across the hinges was about 0.1 ohm. The first 200 Ka. discharge, applied with the bond straps in place, resulted in pitting at the ball joint, but no joint binding was observed. After three additional 200 Ka. discharges with the bond straps removed, similar pitting was noted, but, again, no restriction of movement of the hinge bearings was evident. One of the ball joints was actually loosened slightly.

**GROUND SPOILER-** The peak current applied to the spoiler hinges was divided with 100 Ka. through the center hinge and 100 Ka. through the two outer hinges. To increase the severity of the test the actuator was not connected. All hinges measured open at low voltage. The breakdown voltage of the center bearing varied from 600 to 1,000 volts. The others required only 50 volts to start conduction. On the aircraft, the spoiler panel was connected to the main structure by parallel paths having a resistance of 3.5 to 5.0 ohms.

One 100 Ka. discharge was applied with the bond straps on and another with the straps removed. The hinge pin of the center bearing was shifted along its axis after the first discharge to separate the pitting obtained with and without the bond straps, Fig. 1. There was no noticeable difference in the pitting obtained with and without the bond straps on. No binding was detected in either case in any of the bearings.

While these hinges were satisfactory in a standard lightning test, some longer duration natural lightning strokes could transfer a larger charge and cause more pitting where the bearing arcs due to a relatively high parallel resistance. Therefore, it would be prudent to retain a bond across these lugs.

For static bonding MIL-B-5087B specifies a connection resistance of less than one ohm. Another source, Vol. 9 of the National Fire Code, suggests a minimum of one megohm. Arcs and sparks are among the most serious noise sources. Assuming a very high charging rate of 100 pamps. for an isolated section, the voltage across one megohm would be 100 volts, not enough to cause sparking in air. Specification of hinge resistance alone does not determine the noise effectiveness of a part since the hinge impedance may be higher. In addition, noise is also produced by any mechanical variation of the impedance,  $dZ/dt$ . Of course, the noise is also only noticeable when a receiving antenna is coupled closely enough to the isolated section.

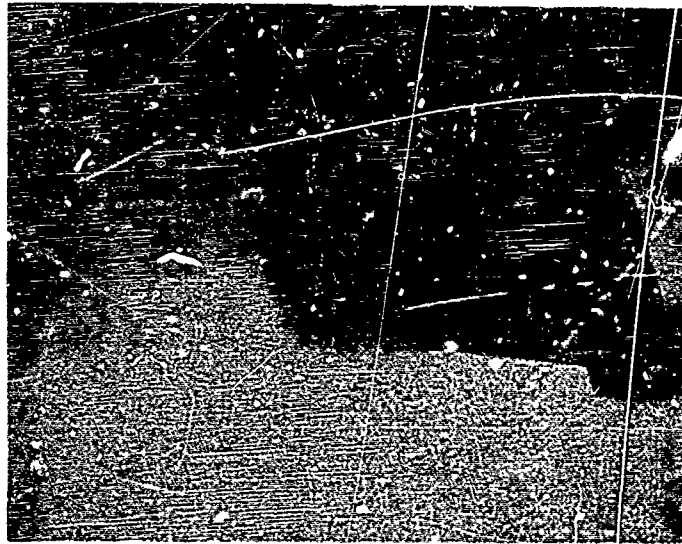


Fig. 1 - Typical pitting on an alignment ball (top photo) of an elevator bearing shows pitting confined to the edges of the ball which has been turned for the photo. Comparative pitting (bottom photo) on a spoiler hinge pin, moved between discharges, shows pitting obtained with and without bonding in place.



Fig. 2 - Setup for checking the hinges of the  
main gear door.

**OUTBOARD AILERON & TAB-** To avoid unnecessary bearing pitting on this part, only two of the four inner hinges of the outboard aileron were connected and the test current was reduced to 120 Ka. peak. The resistance across the inner hinges measured about 0.1 ohm and that across the tab hinges about 17 milliohms. In addition to the hinges described above, the aileron is connected to the main wing structure by piano-type hinges which were disconnected to increase the severity of the test.

One discharge was applied to the inner hinges with the bond straps on and another was applied after removal of the bonds. Slight pitting was noted on the sleeve bearing pin after both discharges. No binding or other malfunction was observed. Similarly, two 200 Ka. peak discharges were passed through the four tab hinges. One bond strap was exploded out of its lug and a nearby metal part was deformed on the first discharge. This raised the possibility of control jamming. No significant pitting or binding was observed after the two discharges.

**INBOARD AILERON & TAB-** The inboard aileron has two inner hinges and three tab hinges. It is also attached with piano-type hinge fittings which were not connected, making the test of the other hinges more severe. The resistance of the inner hinges measured 0.1 to 0.3 ohms and the resistance across the tab hinges was 3 to 5 ohms.

One 200 Ka. peak discharge was applied through the inner and tab bearings in series with the bond straps on and another was applied after their removal. Only slight pitting was observed on the bearings as a result of the discharges. No binding or other deleterious effects were noted.

**LEADING EDGE FLAP-** The leading edge flap has three hinges at the leading edge and three inner hinges. The resistance of the leading edge hinges measured 2.5 to 5.0 ohms and the inner hinges measured 1 to 3 ohms.

One 200 Ka. peak discharge was applied to the leading edge and inner hinges in series with the bond straps on. One of the straps, across a bullnose hinge, exploded out of its lugs. No significant pitting or binding was observed. A second similar discharge was applied after removal of the bond straps. The pitting obtained was essentially the same as that obtained with the bond straps on and no binding of the hinges was observed.

**RUDDER & TAB-** The inner hinge bearings of the rudder, Fig. 3, are normally unbonded. They were typical sleeve bearings in a self-aligning ball joint, Fig. 1. The

resistance measured across the tab hinges was 6 to 8 milliohms.

One 200 Ka. peak discharge was applied through the hinges in series with the tab bond straps on and another was applied after their removal. Only slight pitting was noted on these sleeve type bearings and pins with and without the bond straps on. No binding or other change in the performance of the hinges was noted.

**ELEVATOR & TAB-** The inner and tab hinges of the elevator were also checked. A closeup view of an inner hinge is shown in Fig. 4. The elevator has five inner and five tab hinges. Two bonding jumpers are provided across each group of hinges. The resistance of the tab hinges measured 6 milliohms, but the inner hinges checked open and required 300 to 400 volts for breakdown. The parallel paths on the actual aircraft, however, provided conduction so that, on the aircraft, the resistance across the inner hinges was 0.4 ohms, adequate for static bonding per MIL-B-5087B.

One 200 Ka. discharge was applied to the inner and tab bearings in series with the bonding straps on and another was applied after their removal. The pitting observed after each discharge was essentially the same and no binding or other deleterious effect was noted. Most of the pitting was confined to the normally exposed surfaces of the ball joint rather than on the inner surfaces of the bearing. On the actual aircraft, the elevator is attached with piano-type hinges, Fig. 4, in parallel with the inner hinges checked. Their effect would be to reduce the current in the inner hinges.

## CONCLUDING DISCUSSION

When high current discharges were passed through door and control surface hinges from a 727 aircraft, examination of the bearings showed no fusing or significant binding and no other significant difference in hinge performance, with or without bonding jumpers attached. Therefore, the need for bonding jumpers to conduct lightning currents across the hinges was not demonstrated by these tests. In fact, a question was raised as to whether a bond strap, blown loose from its lugs by the lightning current, might actually become hazardous. Where the parallel path impedance is relatively high, as on the spoiler, a bond might be retained to provide protection against long duration natural discharges which can exceed the standard test levels.



Fig. 3 - Typical rudder self-aligning bearing  
with ball joint.



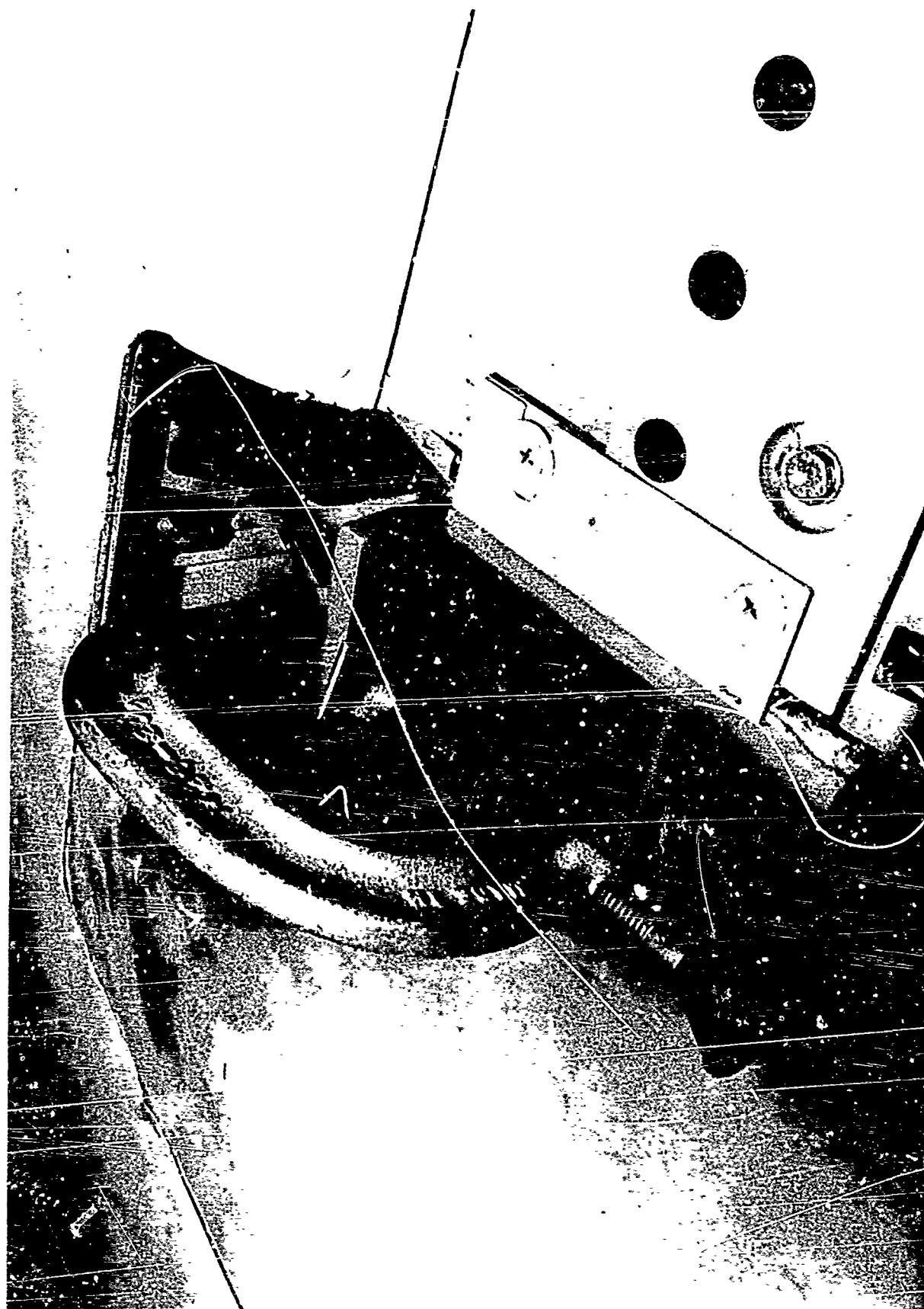


Fig. 4 - Elevator inner hinge bearing and piano-type hinge in foreground.

be higher than that of the standard discharge used for checking bonding.

In the case of noise due to charging of the bonded part, the effectiveness of the part as a noise source depends, among other things, on its coupling factor or location and orientation relative to some receiving antenna. The location of the part also affects its charging rate. The hinge and parallel path impedances are more important than their resistances, since the resistances are usually relatively low at the high receiver frequencies. Any mechanical variation in impedances,  $dZ/dt$ , can be expected to be kept low by the multiple low impedance parallel paths.

This study of the bonding of specific modern aircraft hinges illustrates that the expected effectiveness of hinge bonding for lightning protection or noise reduction should first be established before they are installed, since maintenance costs may be excessive. The piano-type hinges, the large hinges with sleeve type bearings and the parallel paths, found in modern aircraft, make bonding across most hinges ineffective for lightning protection and, in many cases, unnecessary for noise reduction.

#### ACKNOWLEDGEMENTS

This study was conducted jointly by the Lightning & Transients Research Institute and Eastern Airlines Aircraft Engineering, Miami, Florida, with Mr. Chester H. Miller acting as coordinator for Eastern Airlines.

# A Test Technique for Measurement of Lightning-Induced Voltages in Aircraft Electrical Circuitry

Lawrence C. Walko  
General Electric Company  
Corporate Research and Development

Paul T. Hacker  
Aerospace Safety Research and Data Institute  
National Aeronautics and Space Administration  
Lewis Research Center

## ABSTRACT

A test technique has been developed utilizing a portable low-energy impulse generator capable of providing unidirectional current impulses similar to lightning current surges, but at a lower current level, to be used in the investigation of lightning-created induced voltages on aircraft. Such an investigation would aid in determining whether the induced voltages on the circuits are of such a magnitude as to be harmful to equipment connected to the circuit.

The basis for this low-energy test technique is the fact that a linear relationship has been observed to exist between the magnitude of lightning current and the subsequent induced voltages.

Previously, measurements have been made of voltages induced in aircraft circuits by full-scale simulated lightning currents flowing through its skin and structure (1)\*. This is a cumbersome operation at best and may be completely impossible in some cases.

With the portability of this impulse generator, the restrictions as to location of test and test setup time are removed. The portable impulse generator can be taken to a complete aircraft, connected to a certain point on the aircraft, and measurements can be made on the circuitry.

Through use of an F89-J fighter aircraft as a test bed to develop the practicality of this test technique in the field, a usable tool has been made available for lightning-induced voltage studies on all aircraft.

IT IS KNOWN that lightning currents which flow through the skin and structure of a metallic aircraft can induce hazardous voltages into electrical circuits within. There are also incidents of avionics equipment being disabled as a result of lightning stroke to aircraft.

With the knowledge that lightning may cause induced voltages of a magnitude probably sufficient to interfere with or damage sensitive aircraft electrical and avionics equipment (1), a program was initiated by the Aerospace Safety Research and Data Institute, NASA, Lewis Research Center, with the objective to develop a technique to determine the

potential effect upon aircraft electrical systems of lightning currents passing through the skin and structural members of a complete aircraft.

Toward this objective a test technique utilizing a portable low-energy impulse generator, henceforth referred to as a transient analyzer, was developed as a workable tool in the investigation of lightning-induced voltages on aircraft.

Using the complete right wing of a Northrup F89-J aircraft as a test bed and with the use of a complete F89-J aircraft to develop the practicality of field testing, measurements were made of voltages and currents induced in selected wing and fuselage circuits as a result of the lightning currents passing through the wing skin and structural members.

The program was conducted by the High Voltage Laboratory of the General Electric Company in Pittsfield, Massachusetts. This paper outlines the development of the test presented in General Electric report, SRD 72 065.

## OBJECTIVES

In developing a test technique for investigating the effect of lightning currents on aircraft electrical circuits in a complete aircraft a number of design objectives had to be met. These objectives fall into two categories, electrical and physical.

### ELECTRICAL DESIGN OBJECTIVES -

(1) Provide enough charging capability within the transient analyzer to inject a few hundred to a few thousand amperes through a complete aircraft. This would insure that the resultant voltages induced on the aircraft electrical circuitry will range from millivolts to a few volts.

(2) The transient analyzer must produce a current pulse that would induce voltages on aircraft electrical circuitry similar to what the identical circuitry would see if the aircraft were struck by actual lightning. Therefore, the current pulse created by the transient analyzer must be unidirectional, rising \*Numbers in parentheses designate References at end of paper.

to crest and falling to half crest value in times similar to actual lightning. The transient analyzer must also have the capability of producing current pulses similar to accepted lightning test standards, such as MIL-B-5087B.

(3) Since the possibility exists that some induced voltages will be in the millivolt range a measuring system must be provided that would reduce extraneous noise on the system.

(4) The transient analyzer should require no more than standard 110 volts AC power. This is to insure that power requirements can be satisfied in remote test areas either by line power or portable AC generators.

#### PHYSICAL DESIGN OBJECTIVES -

(1) There must be limitations on the size and weight of the transient analyzer. It must be able to be moved, if need be, by the personnel doing the testing, requiring no elaborate devices such as cranes, etc., that would not be available in remote test areas.

(2) Although personnel safety in regard to this test technique has mainly to do with prevention against electrical shock and would seem to be an electrical design objective, it is a physical design objective to provide sufficient grounding devices, warning lights and signs. Since this test technique is to be used in the field without the benefit of AC power interlocked test facilities, such as in a laboratory, adequate precautions must be taken to insure personnel safety.

(3) Due to the many possible locations where tests on an aircraft using this technique could be made the basic test setup must be simple. In fact, if possible, the size of the test site should be governed only by the size of the aircraft to be tested.

(4) Since the test technique utilizes a complete, flyable aircraft as the test piece, the technique must not cause deterioration of the aircraft skin due to the injected current impulses. Such deterioration could occur at higher peak current levels (40 kiloamperes) as used in full scale testing. It is an objective of this test technique not to cause deterioration of the aircraft skin.

Also, the procedure used for connecting on to an electrical circuit for test must be nondestructive to the wiring when connections are made. The connections made to the electrical circuit from the measuring equipment must be simple, but yet must be of a nature as to insure measurement integrity.

(5) Connections must be made on circuits as they are positioned in the aircraft to obtain valid measurements. All access panels and other structural parts providing shielding for the circuits must be kept in place if possible.

#### GEOMETRIC MODELING

The transient analyzer is basically an energy storage device utilizing capacitors as the energy storage units. The capacitors are

charged up to a certain DC voltage using a high voltage DC power supply. When the capacitors are charged to a specific voltage level, the energy is released to the aircraft structure through a sphere gap. By adding resistance and inductance in series with the output of the transient analyzer, the output current wave could be shaped into a unidirectional wave rising from zero to a peak current level in a specific time and falling to half peak value in a specified time.

In designing a transient analyzer to accomplish the objectives listed above the complete test circuit must be taken into consideration. This test circuit includes a complete aircraft structure in series with the transient analyzer impulse circuit. The contribution that an aircraft would make to the test circuit impedance was not completely known.

A complete aircraft was not available during the preliminary design of the aircraft transient analyzer. Therefore, in order to select design parameters for an aircraft transient analyzer capable of injecting the required lightning current wave shapes and current levels through a complete aircraft, the aircraft test circuit, including the aircraft, was geometrically modeled.

A geometric type model is a scale model in which no attempt is made to duplicate the power levels to which the full-size structure is subjected. For this type of model, if scale factors are applied to any three quantities, the scale factors for all other quantities are fixed.

A typical choice of parameter scales is one such that the impedance,  $Z$ , of the model is the same as the impedance of the full-size structure. The impedance scale fixed is thus unity. The length scale was determined by the model aircraft used ( $l = 1/70$ ). A third parameter to conveniently set is the dielectric constant ( $\epsilon = 1$ ). Thus,

$$\text{length} = l = 1/70 \quad (1)$$

$$Z = 1 \quad (2)$$

$$\epsilon = 1 \quad (3)$$

If the impedance,  $Z$ , is 1 then the resistance,  $R$ , of the model is 1. From dimensions of units in the MKS system (2):

$$R = 1 = \frac{Ml^2}{tQ^2} \quad (4)$$

where:

$M$  = mass

$l$  = length

$t$  = time

$Q$  = charge (coulomb)

also from Reference 2:

$$C = \text{capacitance} = \frac{t^2 Q^2}{Ml^2} \quad (5)$$

$$L = \text{inductance} = \frac{MC^2}{Q^2} \quad (6)$$

$$\epsilon = \text{dielectric constant} = \frac{t^2 Q^2}{MC^3} \quad (7)$$

Using equation (4):

$$C = L \cdot t \quad (8)$$

$$\epsilon = \frac{t}{L} \quad (9)$$

then, from equation (3):

$$\epsilon = 1 = \frac{t}{L} \quad (10)$$

$$t = L = 1/70 \quad (11)$$

Thus the length scale ( $L$ ) and the time scale ( $t$ ) are the same. With the length and time scales both equal to  $1/70$ , the scale factors for the component values used in the geometric model are:

$$\text{Resistance} = R = 1$$

$$\text{Inductance} = L/70 = 1/70$$

$$\text{Capacitance} = C/70 = 1/70$$

With this information, aircraft transient analyzer component values were selected to give the desired range of wave shapes, with adequate amplitudes, by simply varying the model component parameters, without having the actual test aircraft. It also allows one to vary other parameters and study the effects.

The entire circuit, representative of a real-life situation was laid out using a  $1/70$  model. The airplane in this case was a plastic model, T33-A jet trainer, similar in size and shape to an F89-J aircraft, which would be used for the actual field tests. The model aircraft was coated with a silver loaded (conductive) paint. (An F89-J model was not available.) The layout of the circuit can be seen in Figure 1.

The current conducting loop was kept a distance of approximately one "wing span" distance from the aircraft in order to minimize return circuit proximity effects. As shown in Figure 2, a 67-volt battery charged up a capacitor,  $C$ , through approximately 400 ohms. The capacitor was then discharged through series resistance,  $R$ , and through the model aircraft. The current,  $i_L$ , returned via the double loop.

The inductance,  $L$ , was the inductance of the complete circuit.

Three current wave shapes were obtained using the model circuit. The circuit components used to create these wave shapes are listed in Table 1 with values for the peak lightning currents obtained.

The initial tests had wiring taped tightly to the ground plane. Model testing continued by raising wiring off the ground

plane to study any associated variations in inductance. The wiring was placed on a sheet of plexiglass. No changes were noted in wave shapes or current amplitudes.

Instead of the double loop return path, a single foil return was used. This would simulate a foil run back under the aircraft. In field testing, comparisons were made between the single return path and the double loop return under the same lightning current test conditions. It was found that for either return path configuration, the lightning wave shapes were similar. In addition during the field tests it was found that resulting induced voltages were the same for either return path configuration. In other words, the proximity effect of current returning to the generator did not noticeably influence the amount of induced voltages in an electrical circuit inside the metal airframe.

From measurements made using this geometric model, the projected maximum amperes obtained with a transient analyzer operating at a charging voltage of 50 KV would be as shown in Table 2.

The projected current output sufficiently met the design objectives. Based on previous induced-voltage measurements, it is clear that lightning current amplitude in excess of 100 amperes would be capable of inducing measurable levels of voltage in the aircraft circuitry. It is also noted from Table 2 that the required values of generator capacitance,  $C$ , did not vary widely. Thus, the generator capacitance could be composed of four 0.5  $\mu\text{f}$  capacitors with 50 kilovolt ratings; one or more of which could be in the circuit as needed for particular wave shapes. It would be possible to obtain a compact 50 kilovolt DC power supply that would suit the needs of the generator. The wave shaping series resistance placed in the generator circuit would be noninductive resistors with values of from 10  $\Omega$  to 50  $\Omega$ . Series inductance,  $L_g$ , needed for the longer wave shapes would be hand-wound coils externally placed in series with the output of the transient analyzer, to make up, together with the inherent test circuit path inductance, the total inductance,  $L$ , required for the desired wave shape.

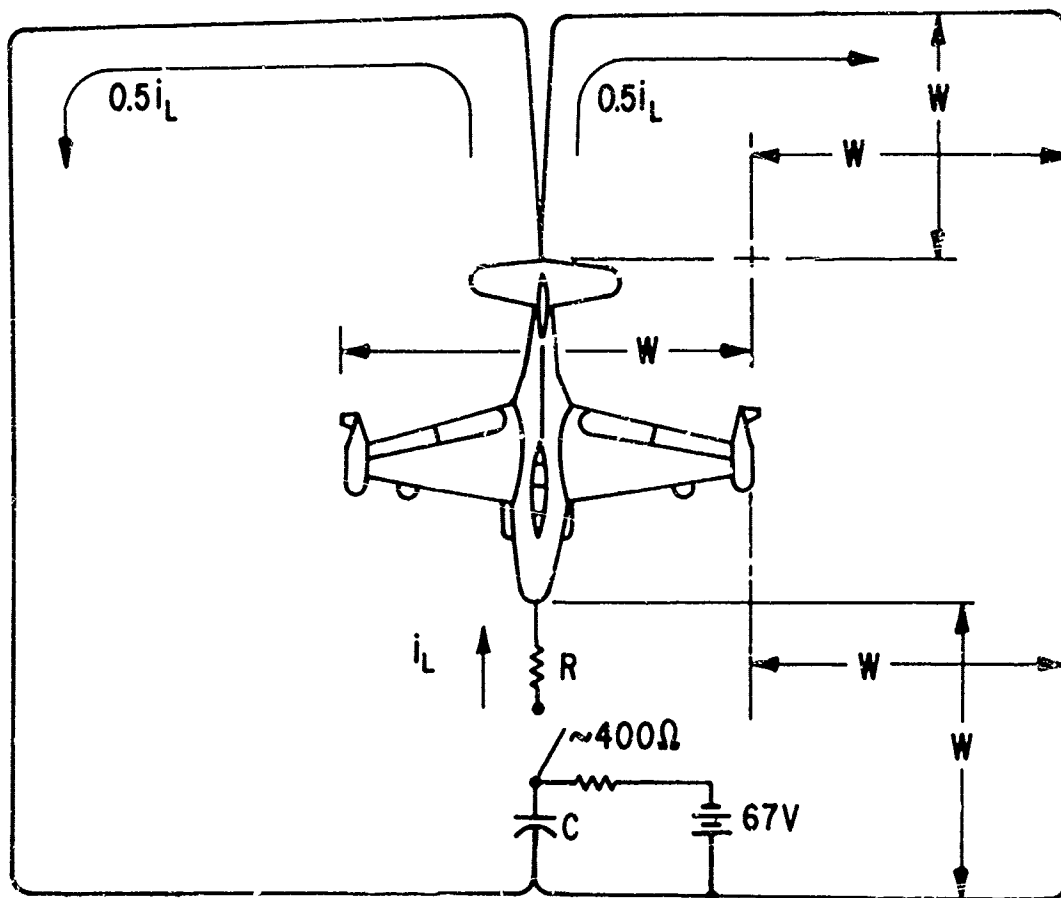
#### DESIGN AND OPERATION OF THE AIRCRAFT TRANSIENT ANALYZER

Keeping in mind the electrical and physical design objectives, the aircraft transient analyzer was built. Figures 3 and 4 show the transient analyzer with its major components.

**HIGH VOLTAGE INSULATION** - Since the design required high charging voltages and relatively high output currents from a device of compact size, the placement of all components important to the operation of the aircraft transient analyzer was very critical. High stresses placed on components by the charging voltage had to be reduced and minimized. Spacings between the high voltage power supply



FIGURE 1 - GEOMETRIC MODEL CIRCUIT LAYOUT OF  
TRANSIENT ANALYZER TEST TECHNIQUE



NOTE 1. "W" EQUALS LENGTH OF WING SPAN

2. NO LUMPED INDUCTANCES WERE INCLUDED. CIRCUIT INDUCTANCE WAS THE DISTRIBUTED SELF AND MUTUAL INDUCTANCES OF EACH BRANCH CIRCUIT.

FIGURE 2- PLAN VIEW OF GEOMETRIC MODEL CIRCUIT LAYOUT OF TRANSIENT ANALYZER TEST TECHNIQUE

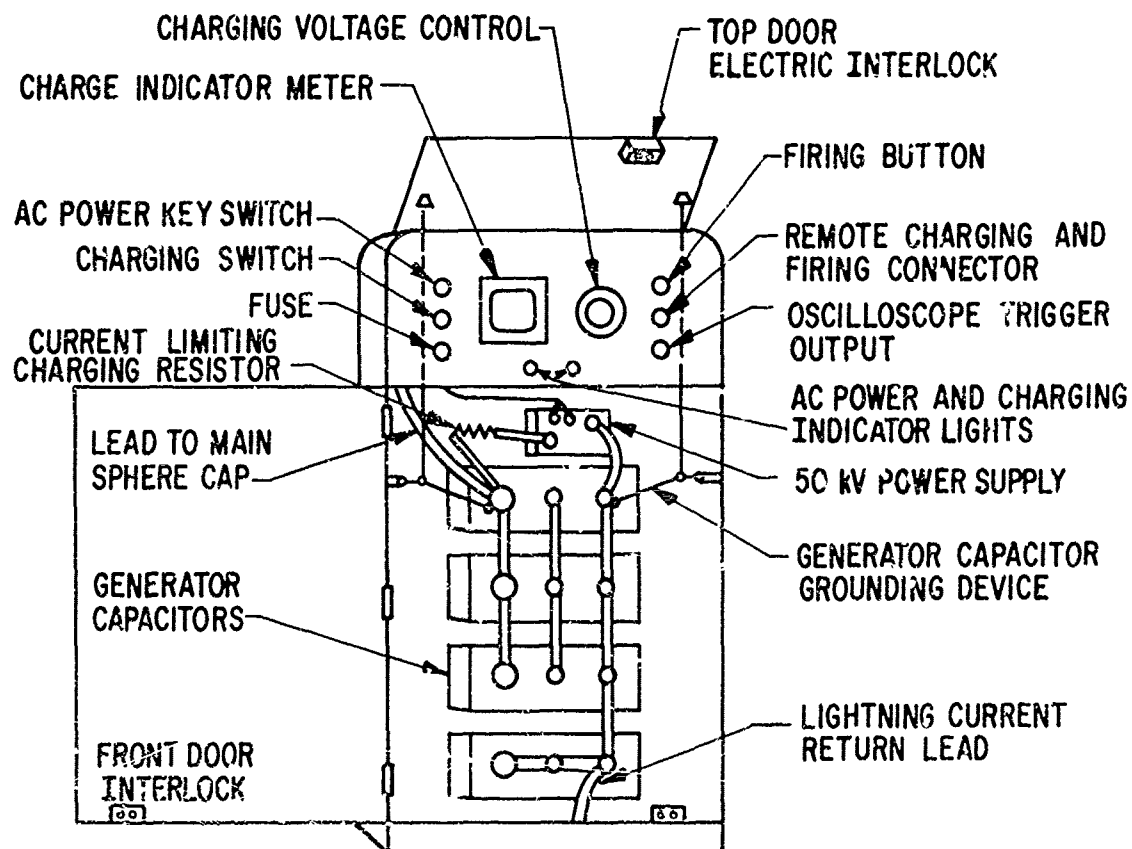
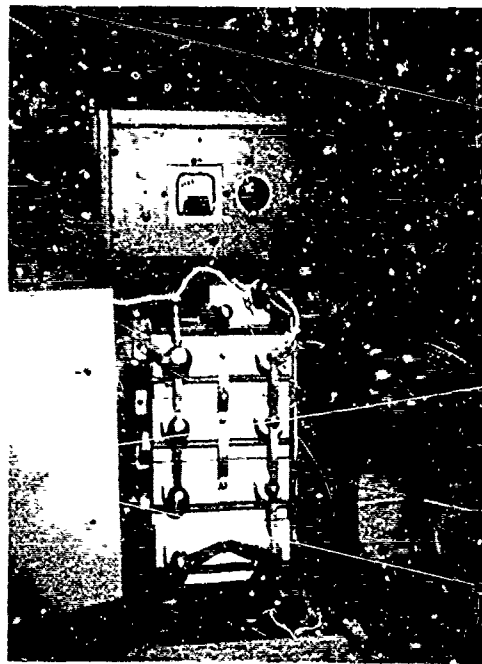


FIGURE 3-AIRCRAFT TRANSIENT ANALYZER SHOWING POWER SUPPLY, GENERATOR CAPACITORS, AND GROUNDING SYSTEM.



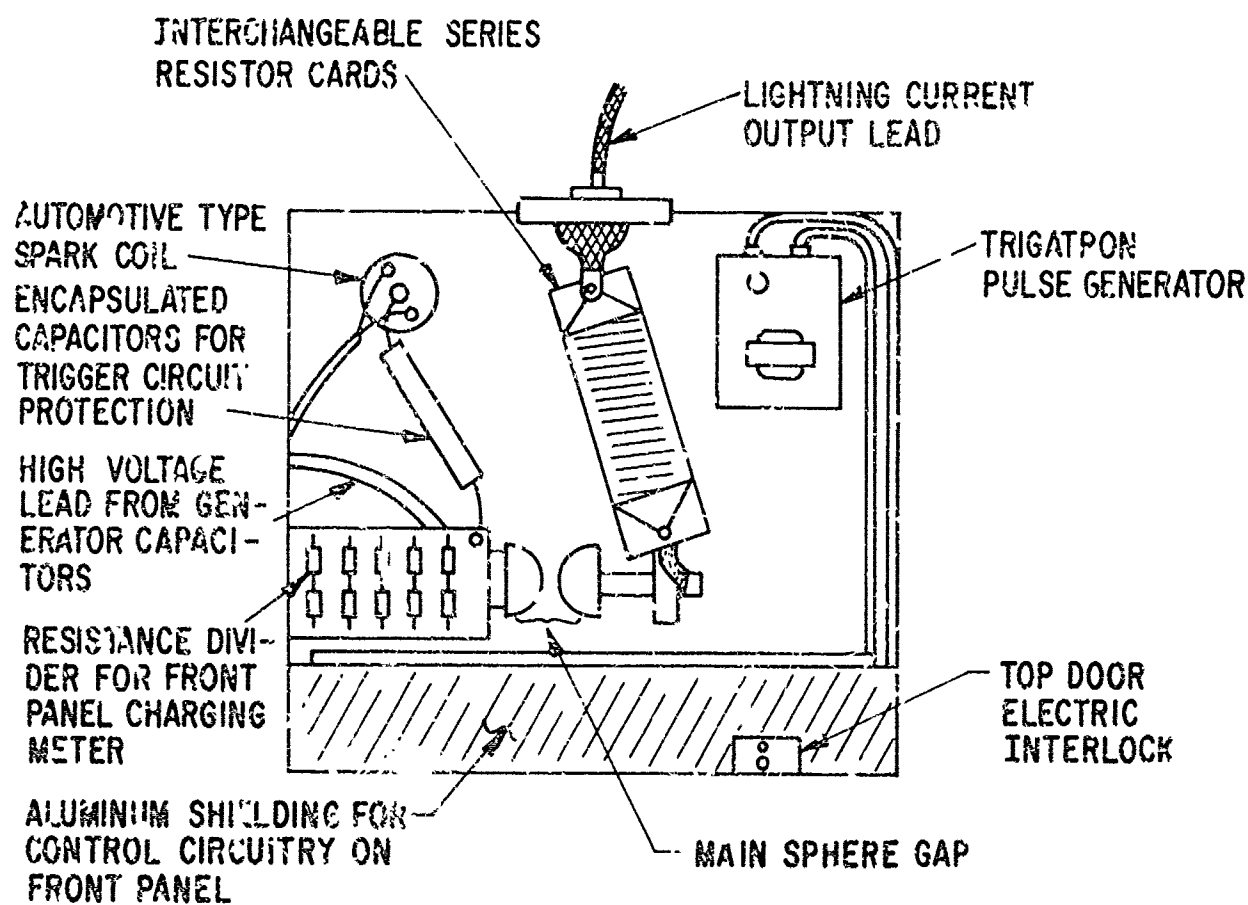


FIGURE 4-EXPOSED TOP VIEW OF AIRCRAFT TRANSIENT ANALYZER SHOWING  
PLACEMENT OF COMPONENTS.

Table 1 - Actual Value of Test Circuit Parameters Used in Geometric Model with Generated Wave Shapes				
Lightning Current Wave Shape Generated (microseconds)	Circuit Inductance, L, 70 (microhenries)	Series Resistance, R, (ohms)	Generator Capacitance, C/70 (microfarads)	Actual Peak Lightning Current, $i_L$ at 40 volts Charging Voltage (amperes)
0.07 x 0.25	model circuit	47	0.007	0.68
0.15 x 0.30	model circuit	12	0.02	1.80
0.40 x 1.0	model circuit + 3.7 microhenries	39	0.03	0.78

Table 2 - Projected Values of Test Circuit Parameters with Projected Peak Lightning Current Obtainable with Aircraft Transient Analyzer with Charging Voltage of 50 Kilovolts				
Lightning Current Waveshape Scaled-Up (microseconds)	Circuit Inductance, L, (microhenries)	Series Resistance, R, (ohms)	Generator Capacitance, C, (microfarads)	Projected Peak Lightning Current, $i_L$ at 50 kilovolts Charging Voltage (amperes)
4.9 x 17.5	circuit	47	0.49	850
10.5 x 21	circuit	12	1.40	2250
23 x 70	circuit + 259 microhenries	39	2.10	975

bushings and the enclosure panels, between the capacitor bushings and the capacitor grounding devices, between capacitor cases and enclosure panels were most critical. DC leakage currents flowing during the capacitor charging period were perhaps the most troublesome. The capacitors used, of the 2-bushing ungrounded case type, were used in this application because of availability. Therefore, the electrical circuit of the transient analyzer called for isolating the cases of the capacitors and several other components from ground. This isolation was needed since with these particular capacitors, the cases are the midpoints of the capacitors, with a maximum of 25 kV possible between each bushing to case and 50 kV between bushings. The isolation in this prototype unit was accomplished by using wood to support the capacitors and Herkolite, a treated laminated insulating material, for supporting and isolating the capacitors. By using grounded-case capacitors much of this insulation could be eliminated.

**AC SAFETY INTERLOCK SYSTEM** - Due to the high voltages used in the production of the simulated lightning current impulses, precautions must be carefully taken to provide personnel safety.

The cabinet used for the transient analyzer is completely enclosed, with energy storage power supply and control components used in the production of the simulated lightning currents included within. External components include any lumped inductance coils and of course the circuit through the aircraft. 115 volts AC power is acquired from an external source, a removable cord from a recessed male outlet mounted in the base of the cabinet.

There are two panel doors that can be opened for access to the charging circuitry, wave shaping elements, sphere gap, and capacitors. The panel doors are interlocked for incoming AC power.

The front panel door not only is interlocked, but has a rod that is inserted through the top access door that locks the front door in a closed position. A capacitor grounding mechanism grounds both terminals of the capacitors when the top access door is opened. To insure complete grounding of the capacitors when changes in the capacitor connections are required, a ground stick is provided for the operator's use to ground the center point of the capacitors, which is the capacitor case itself and all other live elements when the front panel door is opened.

The transient analyzer cabinet is grounded at all times.

#### PRELIMINARY FIELD TESTING

A series of outdoor tests were made to simulate the situation that would be encountered when a complete aircraft was subjected to tests using the aircraft transient analyzer. Grounding configurations and measuring techniques were investigated.

The test piece used for these outdoor tests was a wing from an F29-J aircraft. It was moved to the High Voltage Laboratory outdoor test facility where induced voltage measurements were made on circuits within the wing using the aircraft transient analyzer as the lightning current source. Figure 5 shows the wing in the test area.

**GROUNDING CONFIGURATIONS** - Figure 6 shows the test setup in the outdoor area.

The current from the transient analyzer was injected at points likely to be struck by lightning, the current then flowing down the wing and being removed at the root end, returning to the generator through a foil return path kept isolated from the ground.

The case of the aircraft transient analyzer was grounded and connected to the measurement trailer by an aluminum foil connection. Foil was also placed directly beneath the induced voltage measurement cable. This foil was joined to the foil connecting the transient analyzer and the measurement trailer. All of the simulated lightning current returns to the aircraft transient analyzer after flowing through the wing. Even though there was the foil connection from the root end of the wing to the grounded measurement trailer this foil did not carry any of the lightning current, since all current must return to the negative side of the generator capacitors, which were ungrounded.

There are further comments on grounding in regard to personnel safety, as shown in Figure 7. A complete aircraft is used as the test piece in this example. Since the airframe is grounded, it is safe for a person to touch the airframe during the charging or discharging of the transient analyzer, providing the person is standing on an equally grounded or unbiased surface, such as the earth or a concrete path, etc. Inductive voltage drops around the test circuit loop must add up to the total charge voltage at  $t = 0$  (until current starts to flow in the circuit). However, the relatively low inductance of a large metal airframe results in very low voltage differential along the airframe. Instead, the voltage exists across lumped circuit inductances and the return path or connecting leads. Therefore, both the positive and negative terminals of the transient analyzer are above or below ground by a significant voltage, as shown in Figure 7.

Thus, while the airframe is at ground, the negative side of the transient analyzer can be at a large potential below ground. This is why the negative side of the transient analyzer capacitance must be insulated by at least the full charging voltage from the cabinet, and it is why one cannot arbitrarily ground the negative side of the transient analyzer capacitance to the cabinet. Further study of the above circuit also indicates that a ground stick placed on the positive output lead of the transient analyzer will not necessarily "ground"

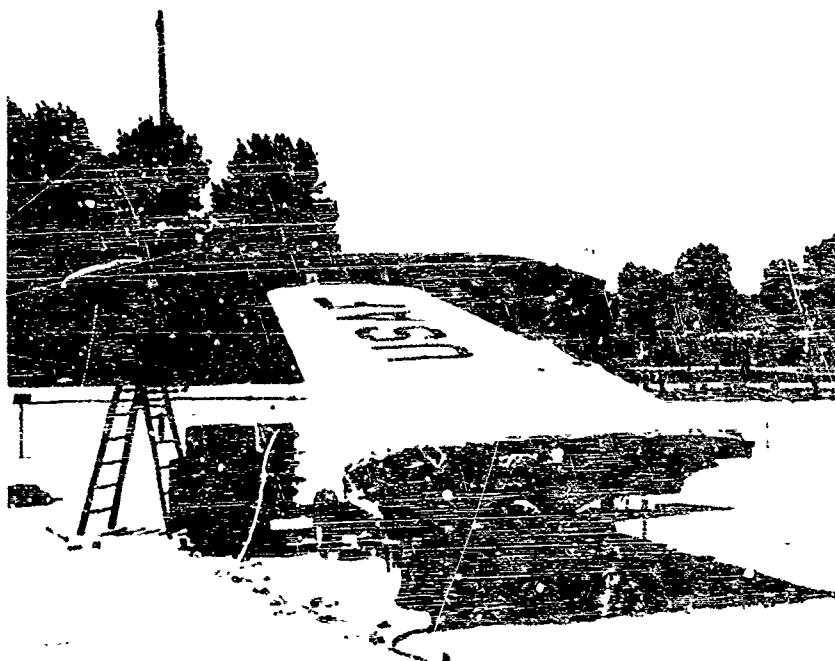


FIGURE 5 - RIGHT WING FROM F89-J AIRCRAFT POSITIONED IN  
G.E. HIGH VOLTAGE LABORATORY OUTDOOR TEST  
AREA FOR PRELIMINARY TESTS USING AIRCRAFT  
TRANSIENT ANALYZER

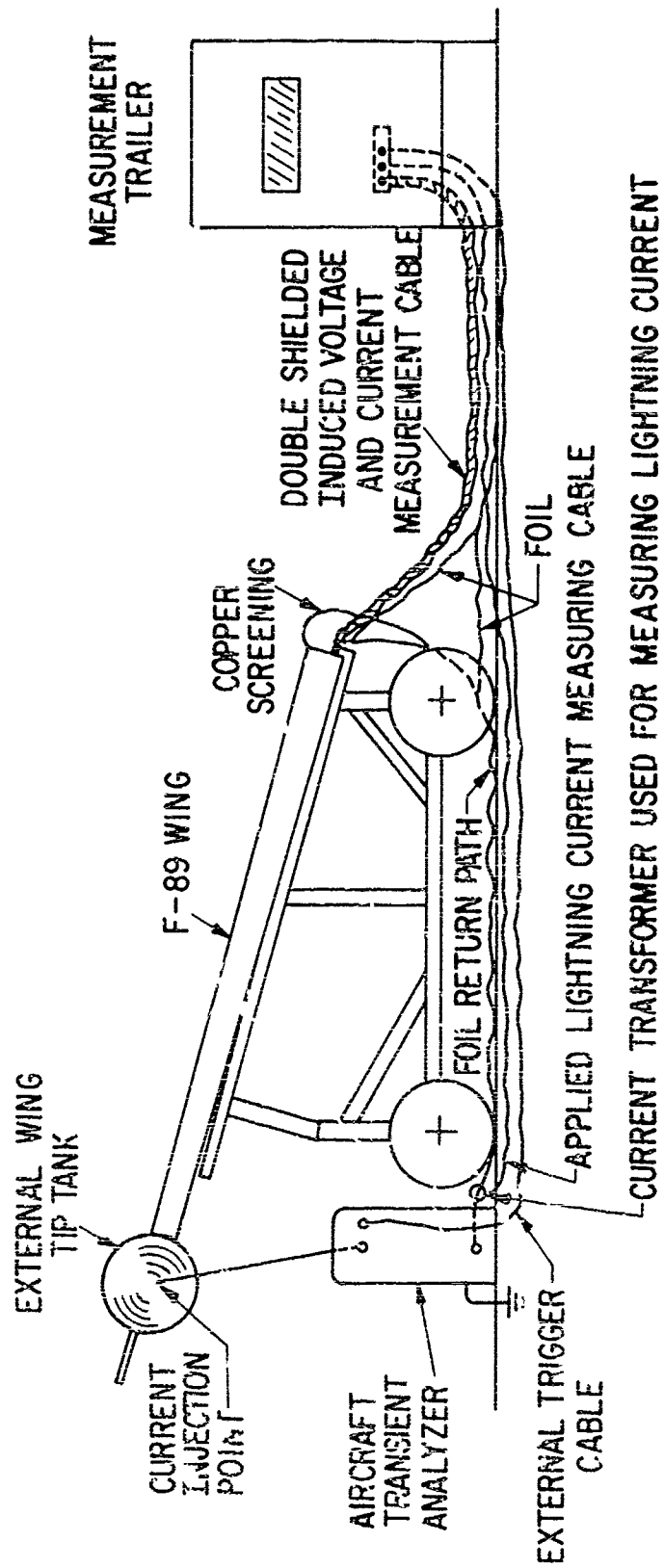


FIGURE 6 - F89 - J WING TEST SET-UP IN HIGH VOLTAGE LABORATORY OUTDOOR TEST FACILITY

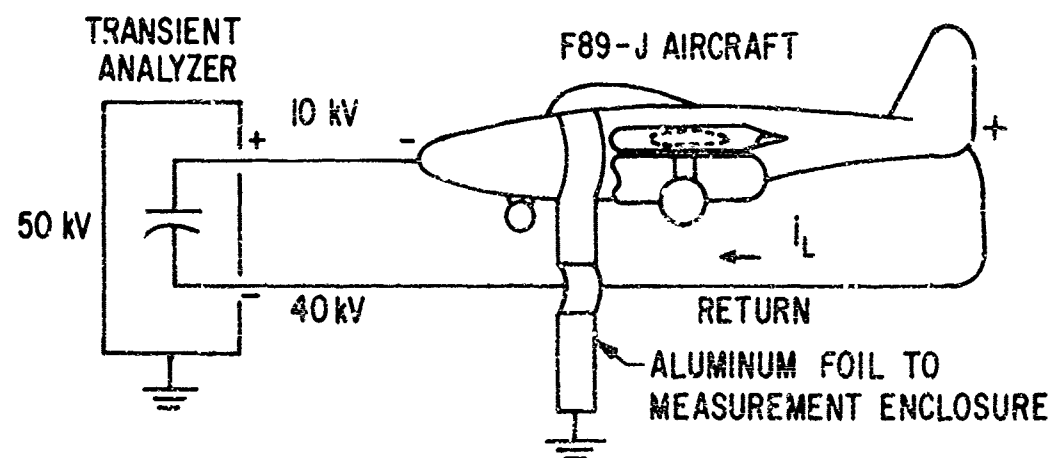


FIGURE 7- DIAGRAM OF TEST CIRCUIT SHOWING ISOLATED LEADS TO AND FROM TRANSIENT ANALYZER

the transient analyzer, as an open circuit return lead could render such a ground completely ineffective.

**DIFFERENTIAL MEASURING SYSTEM** - The simulated lightning current created by the aircraft transient analyzer flows through a wing or other parts of an aircraft creating a magnetic field that induces voltages on electric circuits in the aircraft. A differential measurement system is used to measure voltages induced on the electrical circuitry. The reason for using a differential system is to cancel out error voltages and currents induced in the cable leads by external fields leaking through the measurement cable shields or by cable shield currents induced by such external fields.

Figure 8 shows a comparison of coaxial and differential measurement systems. A coaxial cable system used with this test setup can permit extraneous signals to travel down the cable conductor and shield with the result that the induced voltage seen on the oscilloscope could be the induced voltage plus the extraneous noise.

Figure 8b shows the differential system used. With a differential measurement one conductor is connected to a wing circuit in question. The other conductor is connected to the cable shield and the airframe at the point where the measurement is made. The two conductors are connected to the channel "A" and channel "B" inputs of a Tektronix Type G preamplifier which subtracts one incoming signal from another, with the resultant output being the true induced voltage on the wing circuit.

Further explanation of the differential measurement system is illustrated in Figure 9.

Current is flowing along a wing or any other structural part of the aircraft. The connection to the differential measurement system is shown in the figure as the shielded twin-axial cable connected to a circuit. In a line-to-ground measurement one lead of the twin-axial cable would be connected to the wing and the cable shield.

Figure 9 illustrates two cases where measurement errors could exist. In case (1), if the cable shield is not connected to the airframe at b, the voltage induced along the loop formed by the airframe, aluminum foil, and cable shield appears between the airframe at b (channel "B") and the shield at "a", so that channel "B" alone has a large error voltage in it.

In case (2), if the instrument cable shield at "a" is tied to the airframe at "b", then a circulating current exists in the loop. This circulating current can induce common mode error in both channels "A" and "B" due to current flow in the cable shield. If significant, such an error may saturate the channel "A" and channel "B" amplifiers of the measurement oscilloscopes rendering signal measurements inaccurate.

Thus, to insure valid measurements the aluminum foil ground connection must be

grounded to the airframe as close as possible to the desired zero-voltage reference location on the airframe and solidly connected there. No other ground connections can be made anywhere to the airframe. The measurement cable must be brought to and inside the airframe along the foil and its shield also connected to the airframe at the desired zero-voltage reference location. No loops or "openings" must exist between the foil and the measurement cable shield as shown in Figure 9.

**CURRENT MEASUREMENTS** - The measurement of short circuit currents on the aircraft circuitry was accomplished by using a Pearson current transformer, Model 110A, connected as shown in Figure 10.

The input and output leads to the current transformer are the same leads that would go to channels "A" and "B" of the differential preamplifier in the oscilloscope when induced voltage is being measured.

The simulated lightning current is measured by the use of a Pearson current transformer, model No. 110, with a 0.10 volt per ampere ratio. The current transformer is placed outside the transient analyzer case around the return connection of the transient analyzer as shown in Figure 11.

**OUTCOME OF PRELIMINARY OUTDOOR TESTS** - From the preliminary testing of the aircraft transient analyzer test technique the test procedure to be used in the field on a complete aircraft was perfected. In addition to the grounding configurations and measuring techniques that were investigated a comparison of a single loop and double loop applied current return path was made. Originally, it was thought that the current returning to the aircraft transient analyzer, after flowing through the aircraft, would be in such close proximity to the aircraft as to create an electromagnetic field of an intensity that would influence the induced voltages on the aircraft electrical circuits. This proximity effect was not observed during the geometric model tests and was not observed during the preliminary outdoor tests.

To simplify the test setup it was found that #6 insulated cable could be substituted for the aluminum foil current return path to the transient analyzer with only a slight increase in total circuit inductance. This insulated cable was found to be much easier to work with and insured an isolated current path back to the negative side of the generator capacitors.

#### FIELD TESTS AT CHINA LAKE NAVAL WEAPONS CENTER

After the tryout of the aircraft transient analyzer in the outdoor area of the High Voltage Laboratory, the measurement technique was used on a complete aircraft. This aircraft, an F89-J fighter, was located at the Naval Weapons Center at China Lake, California.

The objective of the tests at China Lake

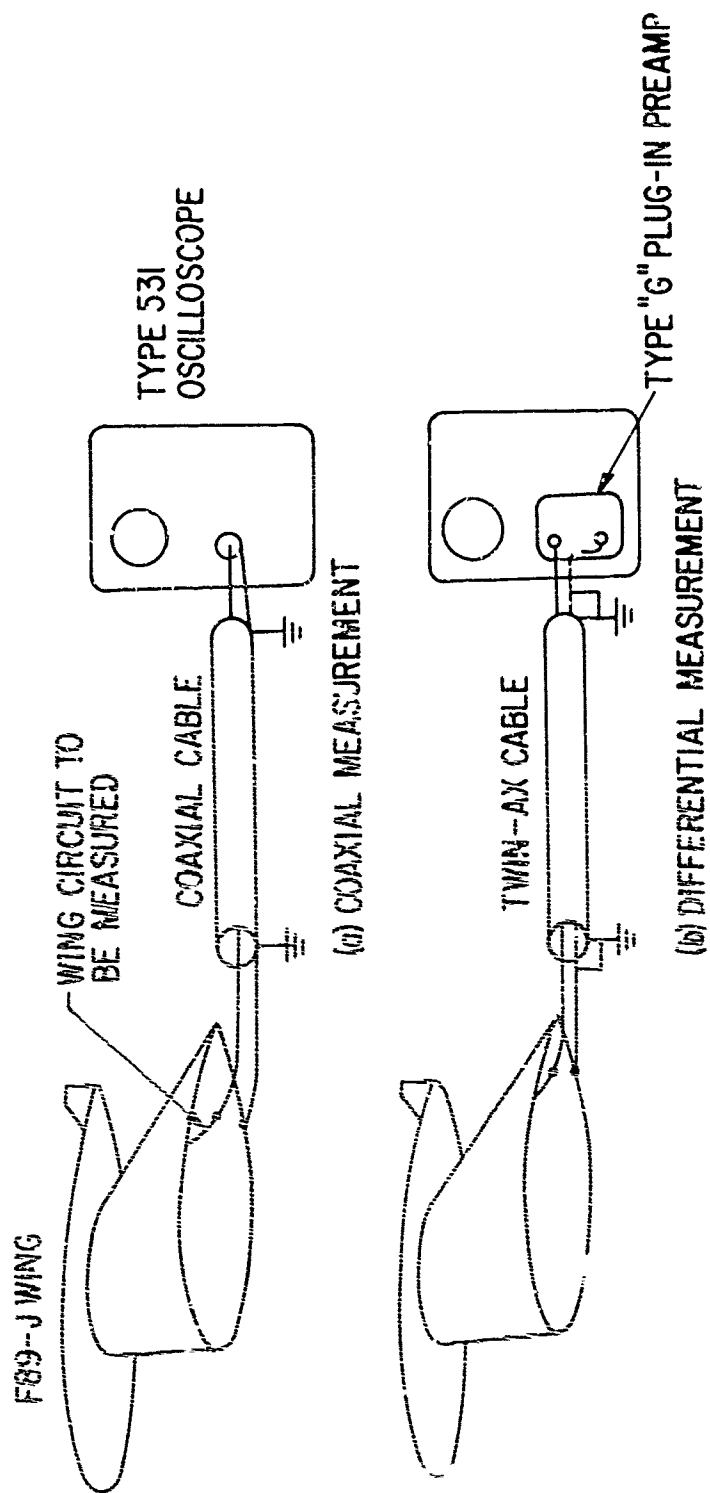


FIGURE 0-- COMPARISON OF COAXIAL AND DIFFERENTIAL MEASUREMENT TECHNIQUES FOR MEASURING LIGHTNING INDUCED VOLTAGE ON AIRCRAFT



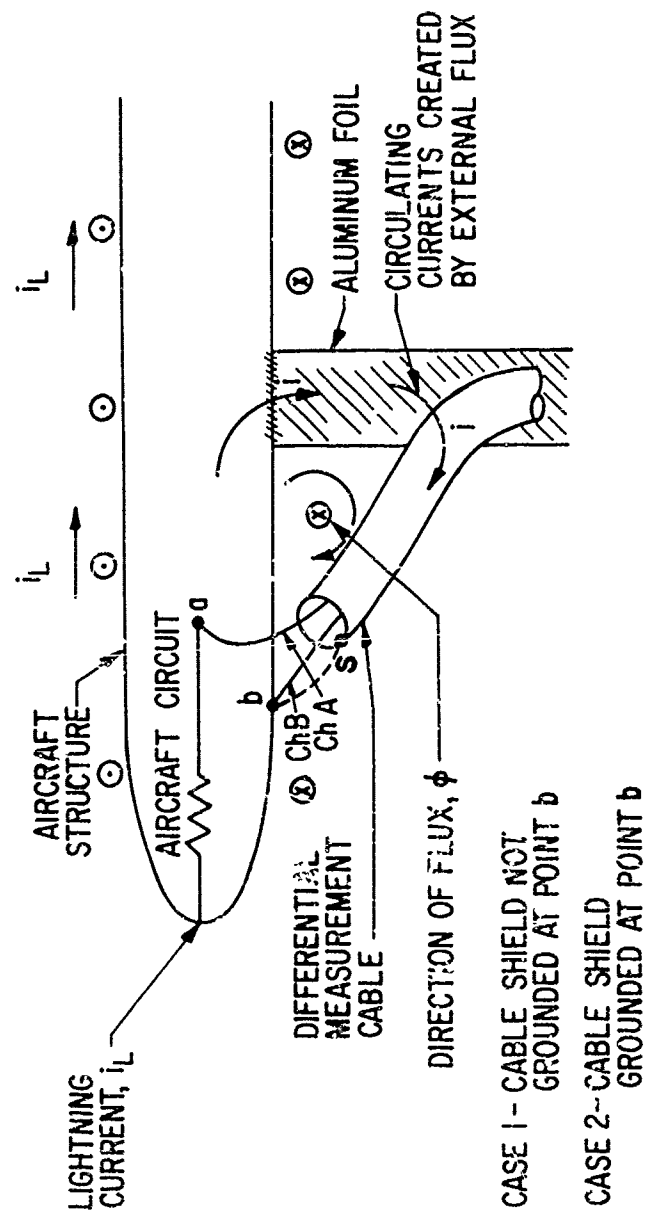


FIGURE 9- DESCRIPTION OF CONNECTIONS THAT CAUSE MEASUREMENT ERRORS ON DIFFERENTIAL MEASUREMENT SYSTEM USED WITH AIRCRAFT TRANSIENT ANALYZER TEST TECHNIQUE.

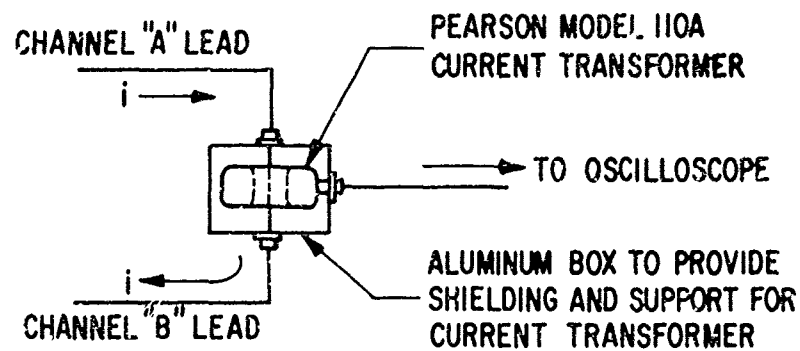


FIGURE 10 - DESCRIPTION OF MEASUREMENT OF SHORT CIRCUIT INDUCED CURRENTS ON AIRCRAFT ELECTRICAL CIRCUITS



FIGURE 11 - CURRENT TRANSFORMER IN RETURN CONNECTION TO AIRCRAFT TRANSIENT ANALYZER USED FOR MEASURING SIMULATED LIGHTNING CURRENT

Naval Weapons Center was to try the test technique in a realistic application and compare results obtained in the High Voltage Laboratory on the F89-J wing with results obtained on a complete F89-J aircraft. The test setup at China Lake is shown in Figure 12.

**COMPARISON OF RESULTS** - For comparison tests the simulated lightning current was injected onto the right wing of the F89-J aircraft at points similar to those used on the F89-J wing at the High Voltage Laboratory. The current was taken off the aircraft at the root end of the wing of the F89-J aircraft at China Lake.

Figure 13 shows oscillograms of simulated lightning currents applied to the forward end of the right wing tip tank of the F89-J wing in the High Voltage Laboratory outdoor area and the F89-J aircraft at China Lake Naval Weapons Center. The current was produced in both cases by the aircraft transient analyzer. It flowed off the aircraft at the root of the wing in both cases.

The maximum current injected in the wing at the High Voltage Laboratory was 1832 amperes. The maximum current applied to the F89-J aircraft at China Lake was 1033 amperes. In terms of a proportionality, the High Voltage Laboratory current was 1.77 times greater than the China Lake current.

Figure 14 is composed of resultant open circuit voltages and short circuit currents measured on Position Light Circuit L.050, conductor 2L10E18, in the F89-J wing at the High Voltage Laboratory and at China Lake.

The maximum open circuit voltages measured are 6 volts on the wing at High Voltage Laboratory and 3 volts on the aircraft at China Lake. This gives a ratio of 2 to 1. The maximum short circuit currents measured are 0.8 amperes on the wing at High Voltage Laboratory and .45 amperes on the aircraft at China Lake. This gives a ratio of 1.78 to 1.

Comparing the induced voltage and current ratios to the ratio of applied lightning currents, a nearly linear relationship was observed between induced voltage amplitudes and applied current amplitudes.

The polarity change observed between the oscillograms of the High Voltage Laboratory results and the China Lake results was due to reversed connections of the measurement leads into the oscilloscopes. The positive deflections are the correct polarity.

**LIGHTNING CURRENT FLOW PATH** - Figure 15 shows various lightning current flow paths used on the F89-J aircraft at China Lake. It is noted that the current injection point is the same in all three cases, Position #1, the forward end of the tip tank. The flow path with the lightning current passing through the right wing, Figure 15a, repeats the flow path used on the F89-J wing at the High Voltage Laboratory. A more realistic flow path is with the lightning current passing from wing tip to wing tip as shown in Figure 15b.

Figure 15c is another possible flow path. The simulated lightning current used for these flow path tests had a  $6.7 \times 18.2$  microsecond wave shape with a peak current of 1000 amperes.

Figures 16 and 17 show induced voltages and currents measured on the Position Light Circuit, L.050, conductor 2L10E18, using the three different lightning current flow paths. This data illustrates voltages induced in the light circuit in the right wing is solely a function of the current flow through that wing and is not measurably influenced by the current flow situation in other parts of the airframe where this circuit does not exist. The subsequent lightning current flow paths through the rest of the airframe and external return path have no measurable effect on the voltage induced in the right wing light circuit, as can be seen in Figures 16 and 17.

Only current flowing in the portion of the aircraft enclosing the circuit in question is effective in causing an induced voltage in that circuit. The factors that influence the magnitude and wave shape of the induced voltages are listed in Table 3.

**POSITION OF A CIRCUIT IN RELATION TO APPLIED CURRENT ATTACHMENT POINT** - To illustrate some of the factors that influence the magnitude of voltage induced on a circuit, Figure 18 shows induced voltages on the Position Light circuit, L.050, conductor 2L10E18, with the lightning current being injected at points shown on Figure 19. An applied current waveshape of  $7.4 \times 20.5$  microseconds at a maximum value of 1033 amperes was used.

For Position 1, a maximum induced voltage of 3 volts was measured. This waveshape can be seen on Figure 14. Positions 2 to 5 are shown on Figure 18. The induced voltage is drastically reduced when the lightning current is injected in the wing instead of the wing tip fuel tank. Current flowing down the fuel tank, plus wing-to-tank bonding resistance, influences the induced voltage on the light circuit. Injecting the current at Positions 2 & 3 creates a lower induced voltage due to the location of the circuit run and the shielding afforded by the wing structure. Currents injected at Positions 4 and 5 provide less influence on the circuit due to location, shielding and length of circuit influenced by the lightning current.

#### INDUCED VOLTAGE SCALING RELATIONSHIP

On comparing induced measurements made at the High Voltage Laboratory with measurements made at China Lake, a nearly linear relationship was found between lightning current amplitude and induced voltage amplitude. However, complete linearity when comparing measured results was not observed. The basis for a discrepancy was investigated.

One possible cause of measurement disagreement was test configuration variation. The measurements being compared were always made on the same F89-J wing circuit (L.050)

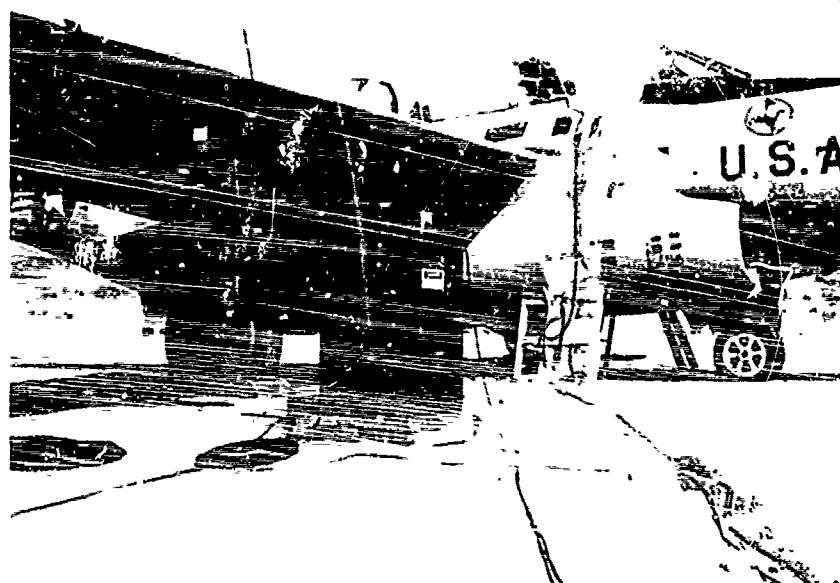
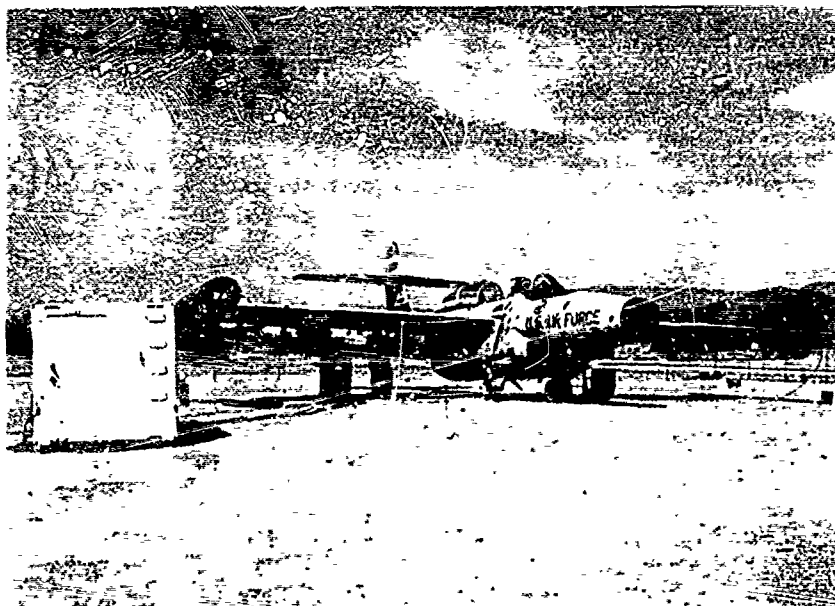
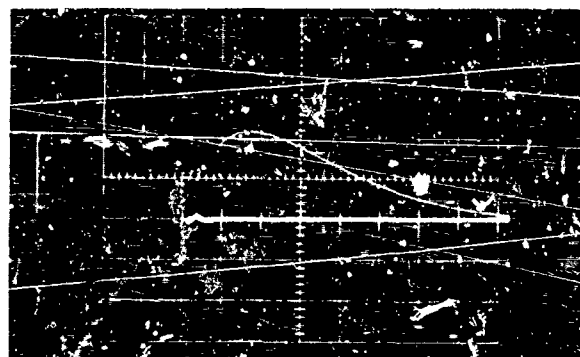


FIGURE 12 - INDUCED VOLTAGE TEST SET-UP AT CHINA LAKE NAVAL WEAPONS CENTER SHOWING POSITION OF AIRCRAFT TRANSIENT ANALYZER AND MEASUREMENT ENCLOSURE

SIMULATED LIGHTNING CURRENT APPLIED TO F89-J WING  
AT HIGH VOLTAGE LABORATORY

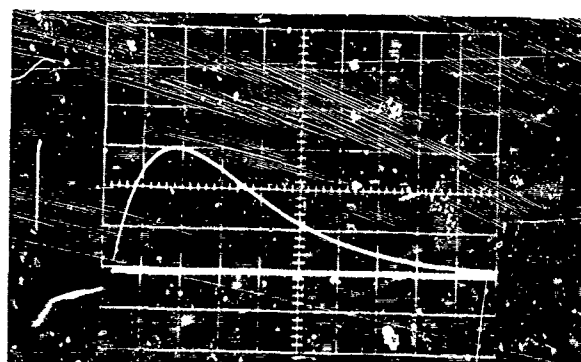


1832 AMPS MAX

833 AMPERES/DIV

5  $\mu$  SEC/DIV

SIMULATED LIGHTNING CURRENT APPLIED TO F89-J  
WING AT CHINA LAKE



1033 AMPS MAX

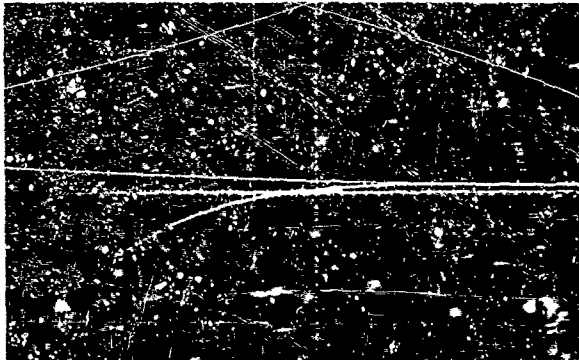
333 AMPERES/DIV

5  $\mu$  SEC/DIV

FIGURE 13-SIMULATED LIGHTNING CURRENT APPLIED TO THE RIGHT WING TIP  
TANK OF THE F89-J WING IN THE HIGH VOLTAGE LABORATORY  
OUTDOOR AREA AND THE F89-J AIRCRAFT AT CHINA LAKE

MEASURED ON WING AT HIGH VOLTAGE LABORATORY

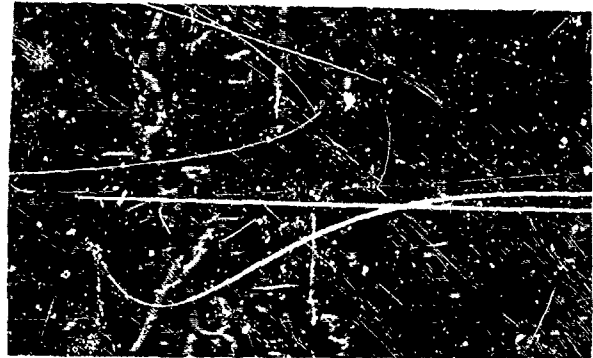
OPEN CIRCUIT VOLTAGE,  $e_{oc}$



5 VOLTS/DIV

5  $\mu$  SEC/DIV

SHORT CIRCUIT CURRENT,  $i_{sc}$

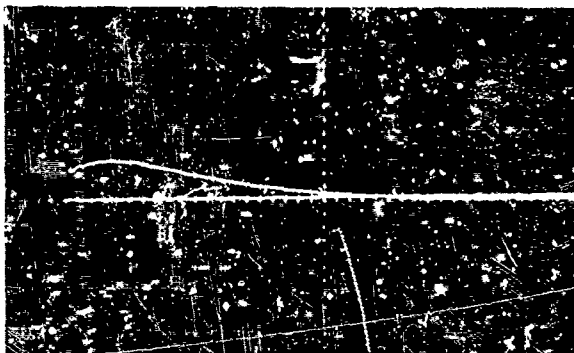


0.5 AMPERES/DIV

5  $\mu$  SEC/DIV

MEASURED ON F89-J AT CHINA LAKE

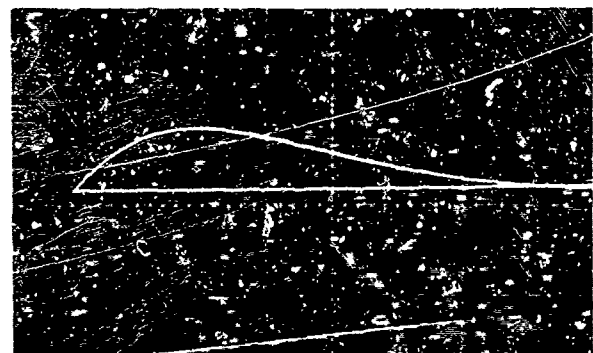
OPEN CIRCUIT VOLTAGE,  $e_{oc}$



5 VOLTS/DIV

5  $\mu$  SEC/DIV

SHORT CIRCUIT CURRENT,  $i_{sc}$



0.5 AMPERES/DIV

5  $\mu$  SEC/DIV

FIGURE 14 - COMPARISON OF OPEN CIRCUIT VOLTAGES AND SHORT CIRCUIT CURRENTS MEASURED ON CIRCUIT L.050, CONDUCTOR 2L10F18, IN THE F89-J WING AT THE HIGH VOLTAGE LABORATORY AND AT CHINA LAKE NAVAL WEAPONS CENTER

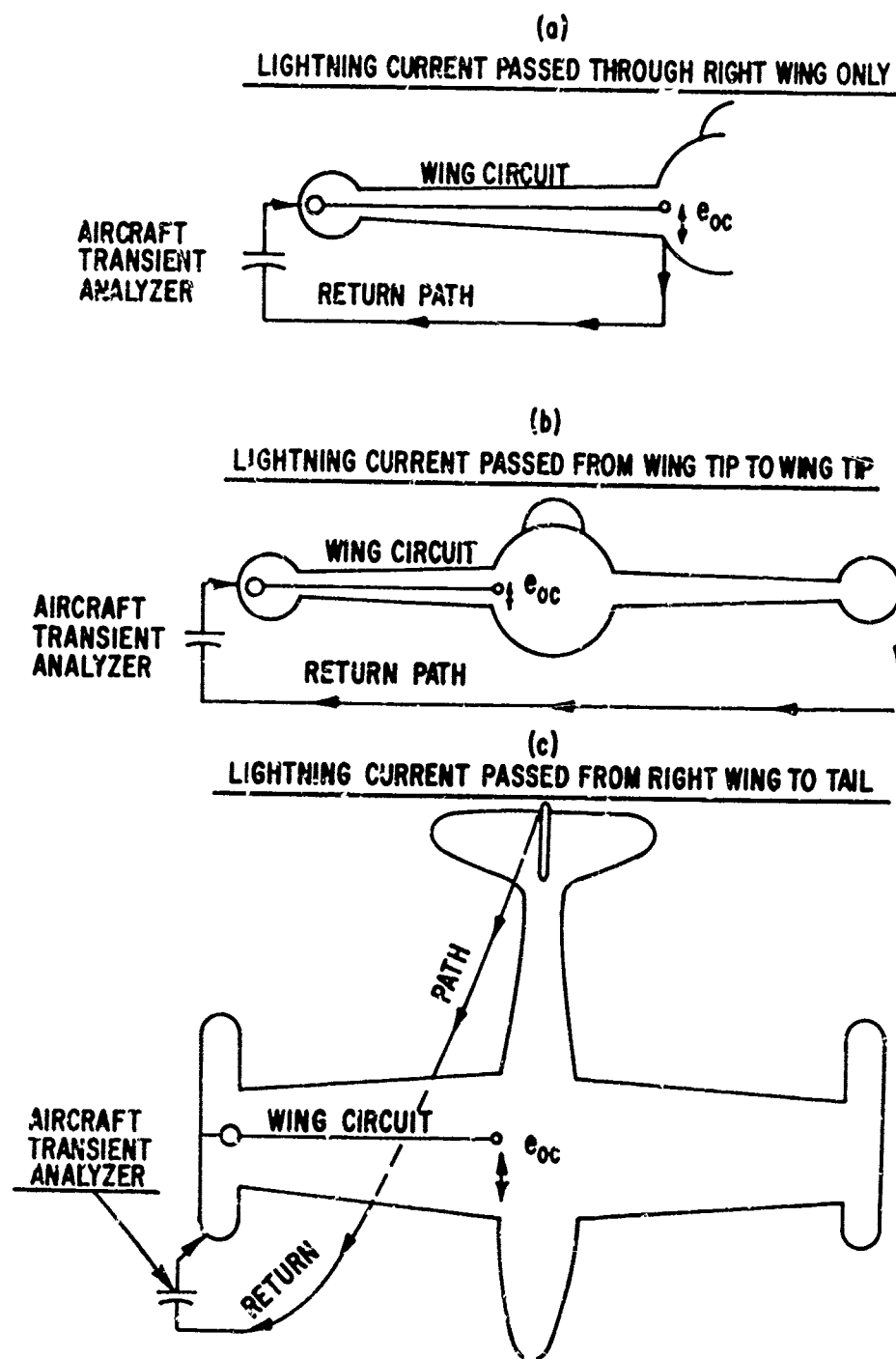
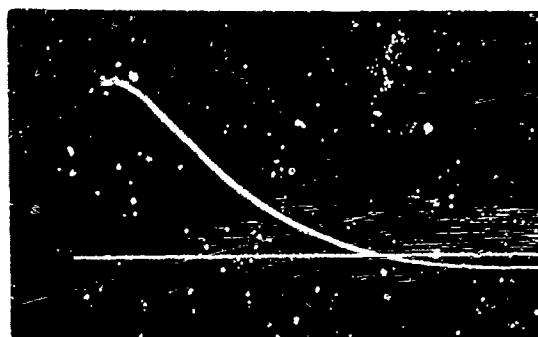


FIGURE 15-VARIOUS LIGHTNING CURRENT FLOW PATHS USED ON F89-J AIRCRAFT  
AT CHINA LAKE

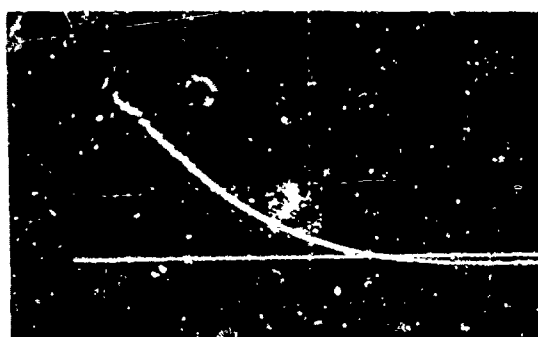
**LIGHTNING CURRENT PASSED THROUGH RIGHT WING ONLY**



**1 VOLT/DIV**

**5 $\mu$ SEC/DIV**

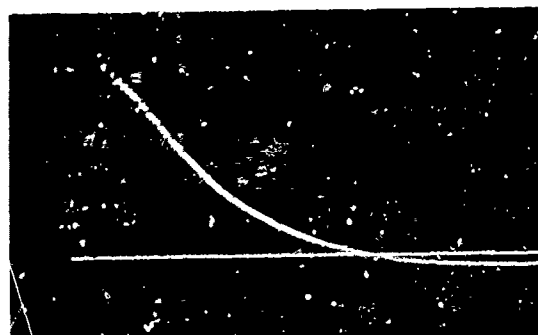
**LIGHTNING CURRENT PASSED FROM WING TIP TO WING TIP**



**1 VOLT/DIV**

**5 $\mu$ SEC/DIV**

**LIGHTNING CURRENT PASSED FROM RIGHT WING TO TAIL**



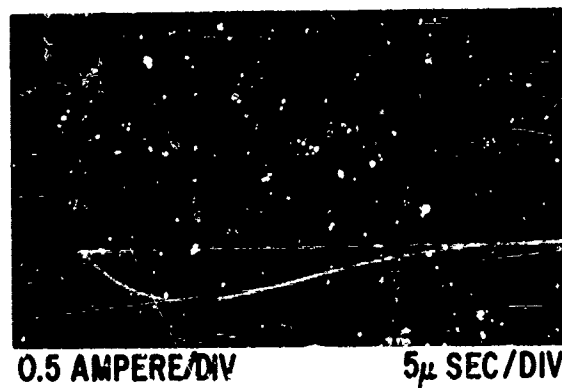
**1 VOLT/DIV**

**5 $\mu$  SEC/DIV**

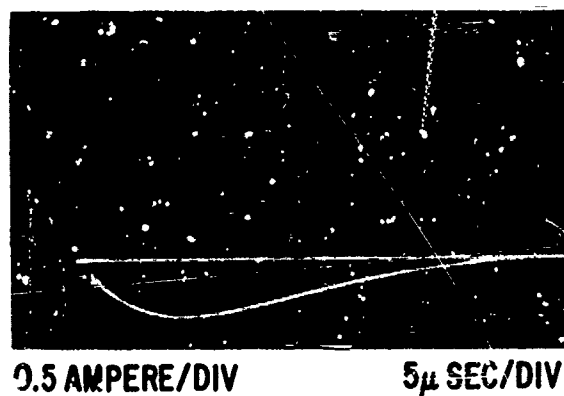
**FIGURE 16 - COMPARISON OF INDUCED VOLTAGES ASSOCIATED WITH VARIOUS LIGHTNING CURRENT PATHS. CIRCUIT L050 POSITION LIGHTS CONDUCTOR 2L10E18**



**LIGHTNING CURRENT PASSED THROUGH RIGHT WING ONLY**



**LIGHTNING CURRENT PASSED FROM WING TIP TO WING TIP**



**LIGHTNING CURRENT PASSED FROM RIGHT WING TO TAIL**

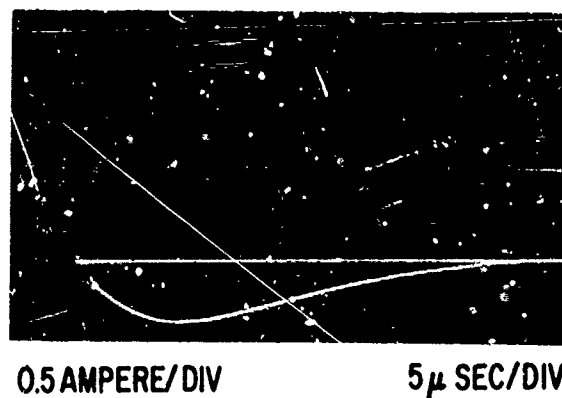
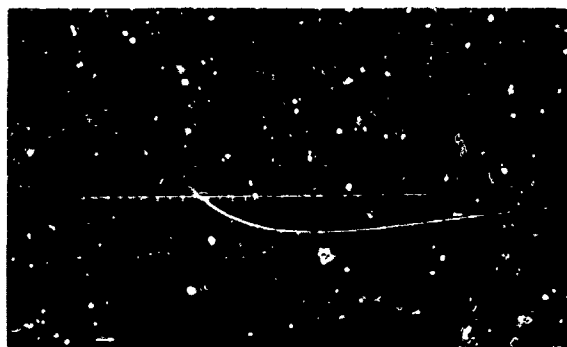


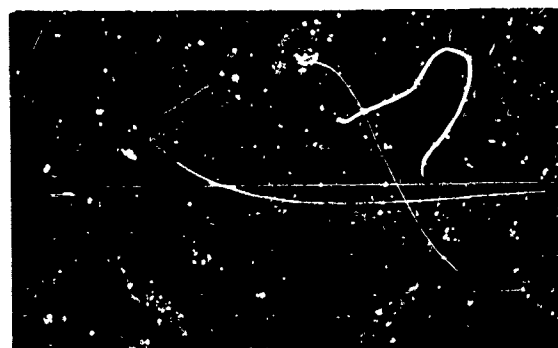
**FIGURE 17 - COMPARISON OF INDUCED CURRENTS ASSOCIATED WITH VARIOUS LIGHTNING CURRENT PATHS. CIRCUIT L.050 POSITION LIGHTS CONDUCTOR 2L10F18**

POSITION #2  
OUTBOARD LEADING EDGE



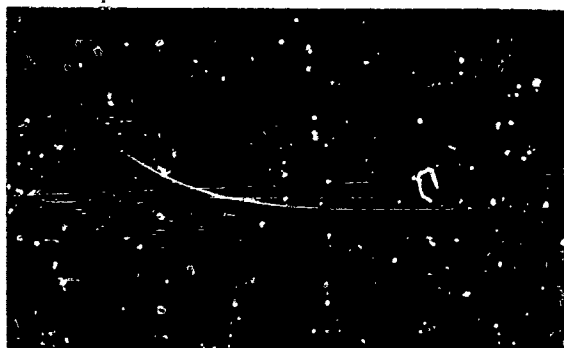
0.2 V/DIV. 0.54 VOLTS MAX.  $5\mu\text{s/DIV.}$

POSITION #3  
TRAILING EDGE OF AILERON



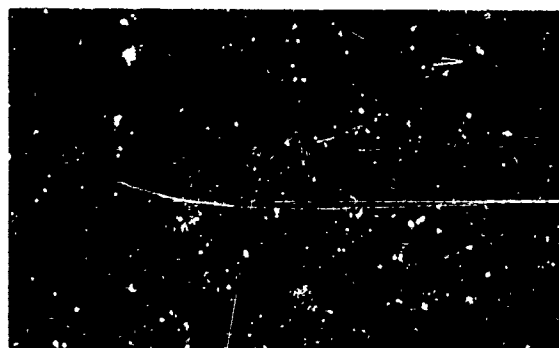
0.2V/DIV. 0.28 VOLTS MAX.  $5\mu\text{s/DIV.}$

POSITION #4  
CENTER OF WING SURFACE



0.2V/DIV. 0.22 VOLTS MAX  $5\mu\text{s/DIV.}$

POSITION #5  
INBOARD LEADING EDGE



0.2 V/DIV. 0.1 VOLTS MAX.  $5\mu\text{s/DIV.}$

FIGURE 18- OPEN CIRCUIT INDUCED VOLTAGES MEASURED ON CIRCUIT L.050 POSITION LIGHTS CONDUCTOR 2LICEI3 USING FAST SIMULATED LIGHTNING CURRENT WAVE ( $7.4 \times 20.5 \mu\text{SEC}$ ) INJECTED AT POINTS DESIGNATED ABOVE.

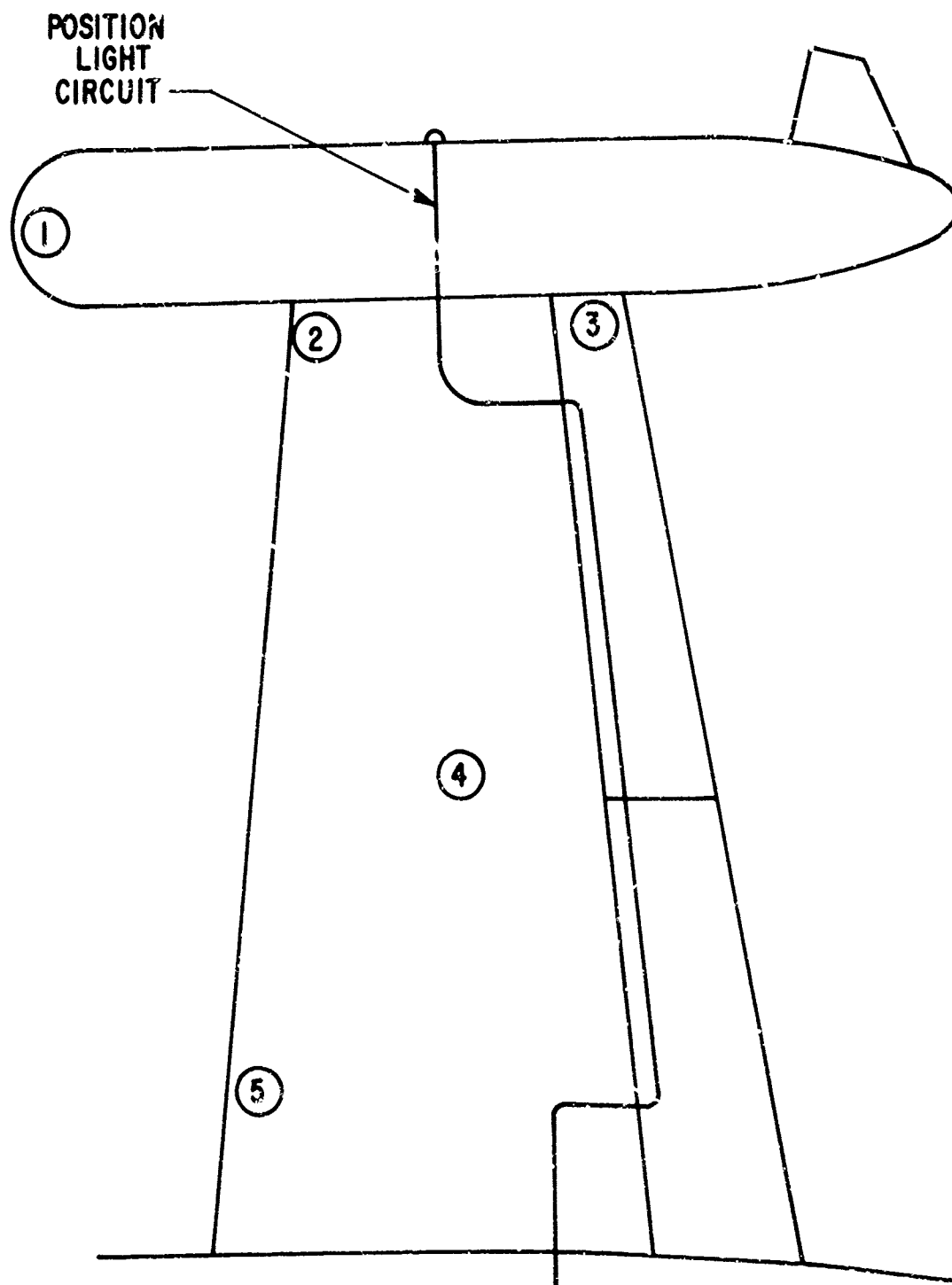


**FIGURE 19 - SIMULATED LIGHTNING STROKE LOCATIONS ON F89-J  
AIRCRAFT-CIRCLED NUMBERS INDICATE LOCATIONS  
SELECTED.**

Table 3 - Factors That Influence the Magnitude and Wave Shape of Induced Voltages	
Influencing Factors	Influencing Characteristics
length of circuit	A longer length circuit can have a larger voltage induced on it due to an increase in the effect of lightning current on the circuit.
position of circuit	Although this factor can have many characteristics, the main one is the amount of exposure to the electromagnetic fields that the circuit would have in its position in the aircraft.
shielding of circuit	Adequate circuit shielding can be accomplished by utilizing the metallic structure (position of circuit) or placing the circuit conductors in conduit or metal sheath, such as coaxial cable.
thickness of aircraft skin	The shielding afforded by the aircraft skin and also the rate of diffusion of the current through the skin (skin effect).
composition of aircraft skin	All aluminum structures provide more shielding of electrical circuits than nonmetallic or semi-metallic structures.
wave shape of lightning current impulse	Risetime and total duration of the lightning current are the main factors. Faster risetimes can induce larger voltages in circuits.
amplitude of lightning current impulse	The larger the applied lightning current, the larger the induced voltage.
lightning attachment point relative to circuit position	If an electrical circuit is positioned close to the point where a lightning stroke attaches itself to an aircraft structure, the influence of the lightning current on that circuit is greater than if the lightning stroke is further away from the circuit.

but there were two test circuit configurations.

(1) F89-J wing outside in the High Voltage Laboratory's outdoor test area with the root end covered by copper screen and a separate shielded measurement enclosure.

(2) Wing attached to F89-J fuselage in complete aircraft test at China Lake with a separate shielded measurement enclosure.

In each case above, the major variation is the shielding configuration at the root end and becomes a significant part of the magnetic circuit and could cause the difference observed in the induced-voltage measurements measured on the same wing circuit under the different test configuration.

For example, measurements made in the High Voltage Laboratory on the wing on the position lamp circuit, L.050, were made at the circuit terminating connector within the wing root, whereas the China Lake measurements on the same circuit were made at a bulkhead connector in the cockpit, thus including an additional segment of the cable in the circuit.

On the other hand, when measurements were made at different lightning current amplitudes on the same test configuration, a linear scaling relationship is much more evident. This is shown in Figure 20. The F89-J wing at this time was positioned in the outdoor area.

In each test configuration mentioned above care was taken to obtain low noise measurements. The efforts to eliminate extraneous noise resulted in induced-voltage measurements that were accurate.

## CONCLUSIONS

This program is based on the development of a technique to be used for investigating the effect of lightning currents on aircraft electrical circuits.

This test technique can be used on any aircraft now flying today. Due to the low currents used to induce voltages in the aircraft circuitry there is no deterioration, either electrical or mechanical, of the aircraft under test.

The portability of the technique allows the convenience of choosing the location where the aircraft will be tested. All commercial and military airports can adequately provide the support facilities needed for this type of testing. 110 volts AC is the only power required for this test technique. No special step-up transformers or rectifiers are required to provide power to the aircraft transient analyzer and the measurement equipment, which are commercially available oscilloscopes.

The size of the test site is governed only by the size of the aircraft to be tested. Additional space is needed only for the enclosure housing the measurement instrumentation. The test site area would be completely enclosed by rope and warning signs to insure personnel safety.

The time from arrival on the test site to actual data acquisition is very short.

Depending on the accessibility of the circuitry to be tested a day of set-up time is all that is needed. This involves no modifications, either electrical or mechanical to the aircraft. All measurement leads are clip-on type and, if needed, require only the use of masking tape to keep the leads in position.

During all testing the structure of the aircraft is solidly grounded. If need be, this permits personnel to be in contact with the aircraft and stay seated in the cockpit during the time that the lightning current is being applied to the aircraft.

The compactness of this test technique allows the use of only two people to run the tests. This includes the operation of the transient analyzer and the measurement oscilloscopes. This economy of use of personnel is reflected in savings in total costs.

The test technique allows for data that can be accumulated and analyzed immediately for significant problem areas and areas for further study.

## REFERENCES

1. K.J. Lloyd, J.A. Plumer and L.C. Walko, "Measurements and Analysis of Lightning Induced Voltages in Aircraft Electrical Systems", Final Report, NASA Contract NAS3-12019, March 1, 1970, G.E. High Voltage Laboratory Report No. 69-161.
2. E.C. Jordan, "Electromagnetic Waves and Radiating Systems", Prentice-Hall, Inc., 1950.

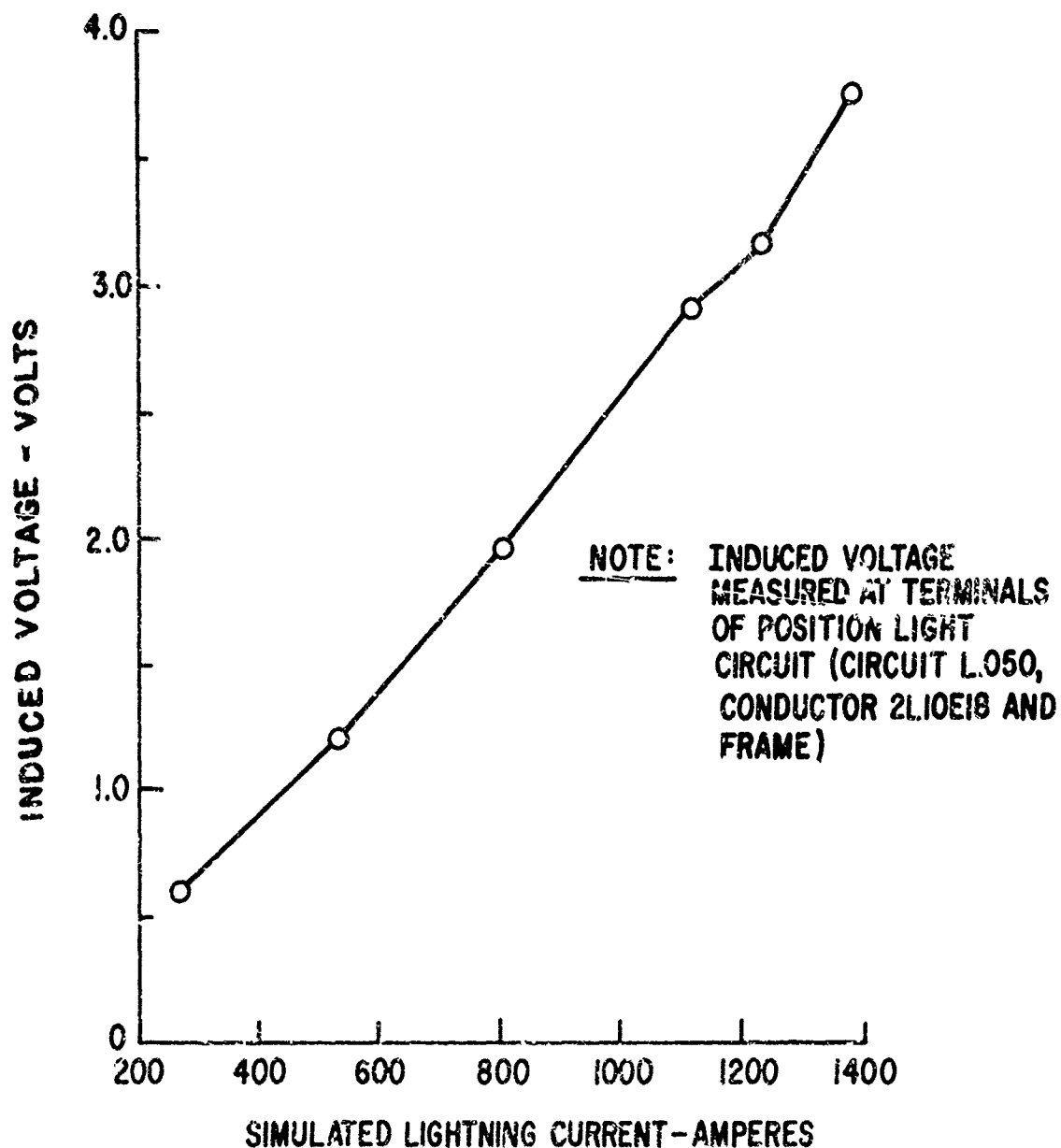


FIGURE 20 - AMPLITUDE OF INDUCED VOLTAGE VERSUS AMPLITUDE OF SIMULATED  $9 \times 18 \mu\text{SEC}$  LIGHTNING CURRENT DISCHARGED TO LOCATION NO. 1 (FWD. END OF WING TIP FUEL TANK) OF F89-J WING AT HIGH VOLTAGE LABORATORY OUTDOOR TEST AREA USING AIRCRAFT TRANSIENT ANALYZER.

## Lightning Protection Approaches For Helicopters

J. D. Robb and J. R. Stahmann  
Lightning & Transients Research Institute

### ABSTRACT

With the greater use of helicopters under instrument conditions, the probability of lightning strikes considerably increases. Although very little protection development has been carried out to date, initial protection approaches have been developed based on damage analysis from in-flight strikes and laboratory testing. Special consideration must be given to the problems unique to helicopters. These include:

- a. greater inherent structural vulnerability because of the necessarily light weight blade construction,
- b. greater shock hazards to pilots because of the larger window areas, and
- c. greater exposure of the electrical/electronic circuitry to thunderstorm electromagnetic field effects because of the more open construction.

The most critical problem is probably blade protection because of their light weight and high relative probability of being struck.

The two major approaches for blade protection include:

- a. protection provisions to keep the lightning strike energies on the blade exterior and
- b. if the stroke can pass through the blade interior, provision of sufficient conductor cross sectional area so that no major internal sparking results. Techniques for accomplishing this are suggested.

A VERY LIMITED AMOUNT of lightning protection development has been carried out for helicopters. Early helicopters have been relatively simple vehicles intended for VFR operations. However, with the greatly extended use of modern helicopters for both commercial and military operations, they tend to be used more and more under increasingly adverse weather conditions and lightning strikes become much more probable.

Many years of experience with lightning strikes to fixed wing aircraft have indicated that it is not possible to predict a large percentage of lightning strikes unless operations are limited to nearly clear sky conditions. A significant proportion of strikes do occur in other than known thunderstorm conditions, for example, below or between stratus layers. Pilots report being aware of no lightning, other than the strike that hit the aircraft.

Commercial airline jet aircraft are struck quite often. This averages about one strike per 3,000 flight hours which requires repair. Thus, in spite of a rather extensive amount of lightning protection effort and

development, there still remains approximately one damaging lightning strike per year for each commercial aircraft. It should be noted that most lightning damage to commercial jet aircraft does not involve safety of flight and is accepted as cheaper to repair than protect, for example, a hole in the wingtip. With long-range jet operations, this decreases somewhat because of the greater percentage of time at high altitude, but it is also probable that many lightning strikes are not reported because the strike did not produce sufficient disturbance to justify a thorough investigation of the vehicle for evidence of damage. However, it should be noted that these low magnitude strikes such as occur in the upper cloud regions and which are probably not presently reported could be serious with newer types of materials, such as the fiberglass and boron or graphite epoxy composite materials.

With increasing helicopter flight operations under adverse weather conditions, the need for some lightning protection becomes necessary, particularly in view of the great importance in helicopter design attached to weight reduction and the resulting tendency for much greater use of non-metallic structure. Analysis of a recent helicopter accident has resulted in increased lightning testing of helicopter blades and the development of some lightning protection methods for helicopters.

As noted, relatively little lightning protection development has been carried out for helicopters to date with the exception of some earlier work by LTRI done for a few companies. Therefore, the following material represents essentially a brief summary of both the limited development carried out to date, specifically on helicopters, with suggested lightning protection approaches based on all lightning damage experience for fixed and rotary wing aircraft, as the damage is a function primarily of the type of construction, not the type of vehicle.

### LIGHTNING STROKE DEVELOPMENT AND CONTACT MECHANISMS

In considering the mechanisms of possible lightning stroke damage to helicopters, it is useful to review the basic mechanisms of stroke contact. A natural lightning discharge initiates from a charge region in a cloud in the form of a step leader which advances in approximately 50 meter steps toward another charged region or toward the earth as illustrated in Figure 1. In some cases, the helicopter triggers a lightning discharge which would not have occurred otherwise, and in some cases it merely diverts the discharge slightly out of its normal path so that the stroke passes through the vehicle.

When the step leader contacts the earth or another charge region, the existence of an ionized conducting path between the earth and the charge region (or two oppositely charged

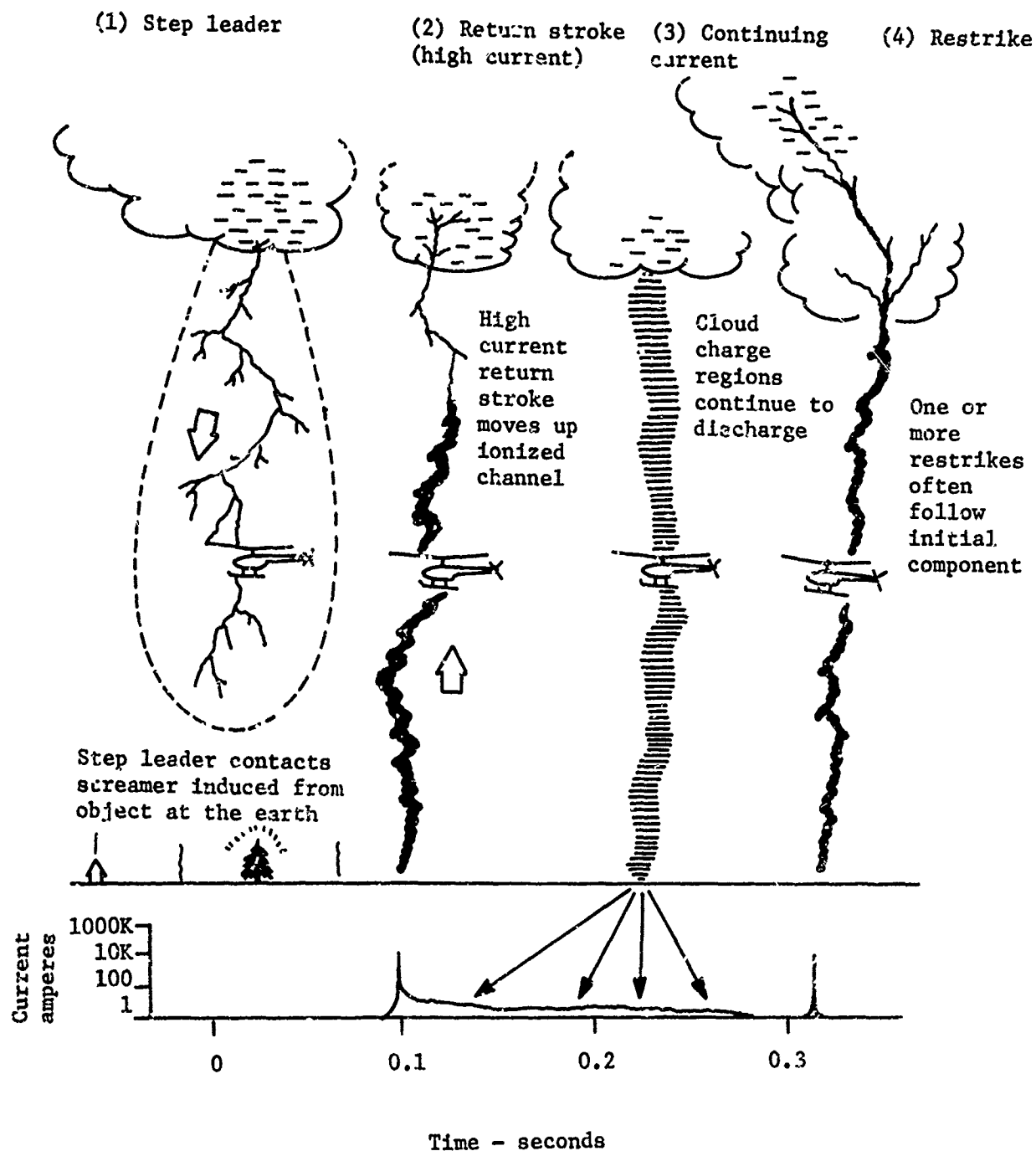


**Figure 1.** Mechanism of stroke contact and passage through helicopter.



regions in the cloud to cloud strokes) results in a current pulse in the form of an ionization wave which travels back up the step leader path to the initiating charge region in the cloud. The high current ionizing wave is referred to as the "return stroke" and consists of a fast-rising high-current surge. This is often followed by continuing currents of 100 to 1000 amperes which may last up to one second followed sometimes by high current restrikes.

As a step leader approaches the vehicle, the intense voltage existing between its tip and the aircraft induces streamers and intense ionization off all the aircraft external surfaces, particularly from the extremities. Figure 2 shows the streamering off a model helicopter subjected to intense electric fields in the laboratory. When the step leader contacts one of the vehicle extremities through the streamer, the vehicle's potential is immediately raised to the extreme potential of the lightning discharge and additional streamering takes place from the opposite extremities of the vehicle to form the step leader for the continuation of the stroke path to another charge region or to the earth. The several phases in the propagation mechanisms of the natural lightning stroke to and through the helicopter are illustrated in Figure 3.

It should be noted that in any case of significant damage to a helicopter the discharge passed through the vehicle, and did not initiate from it or terminate on it as may be shown by energy and charge calculations, Appendix I. The different phases of the discharge are illustrated in the photograph of Figure 4, which shows a triggered natural lightning discharge to the LTRI Research Vessel Thunderbolt taken from a distance of 10 meters. The typical current waveform is illustrated below.

As the vehicle moves past the relatively stationary ionized stroke channel, the stroke sweeps over the helicopter permitting contact at nearly any point behind the forward strike points. The effect is complicated by the complex motion of the blades and the helicopter; however, this means, in effect, that nearly any type of lightning stroke component may be expected at a midchord midspan blade region or any area of the fuselage. The speed of the step leader is such that the blades are relatively stationary during the formative stages but as the continuing components of the stroke may last for most of a second, several blade revolutions are possible during a single stroke.

#### LIGHTNING DAMAGE MECHANISMS TO MATERIALS

**METAL SKINS** - Lightning effects on metal skins are of primary concern in fuel tank areas. Lightning damage occurs because the skin at the lightning strike point is unable to carry the discharge current without heating the metal to

the melting or vaporization temperatures. The skin may be heated by thermal contact with the arc temperature of 25,000°C or by resistance heating of the skin by the lightning current flow.

For aircraft aluminum, the low melting temperature, 1100°F, acts as a thermal reservoir to limit the temperature of the phase boundary between the molten and solid aluminum. This liquid surface, in effect, limits the heat transfer into the skin, i.e., the heat converted into the heat of fusion and heat of vaporization. The ability of the skin to withstand the high thermal arc temperatures (which at 25,000°C far exceed the melting temperature of the skin materials) is therefore determined by the ease with which it can transfer the heat away from the arc contact point; this, in turn, is a function of the skin thickness at the contact point. Because of good conductivity of aluminum, aircraft skins have seldom shown evidence of heating except at the arc point. The total current-carrying capability of various metal skin materials is a function of the resistivity, specific heat, heats of fusion and vaporization, ambient conditions and many other factors.

**DIELECTRIC COMPOSITES** - For dielectric composites, (conventional fiberglass materials used in blades and general structures), the resistivity is so high that lightning potentials will generally flash over the external surface unless guided into the interior of plastic structures by metallic end fittings, buried conductors, or by poor construction of the plastic boundaries (poor from a lightning point of view) as illustrated in Figure 5a. The arc produces vaporization of the resins along the path and intense gas pressures, particularly when confined. In providing lightning protection for plastic surfaces, therefore, the principal problem is to ensure that the lightning is discharged over the outside surface of the vehicle. Lightning discharge arcs inside a vehicle can produce serious structural damage.

**CONDUCTING COMPOSITES** - Unprotected conducting composite skins, such as boron and graphite epoxy, are inherently more vulnerable to lightning damage than dielectric composites, such as fiberglass honeycomb, because heat energy is developed in the conducting layers to add to the total energy and the quantity of vaporized resin which produces the overpressure as illustrated in Figure 5b.

Pressures from discharges to dielectric materials (or metals) fall off rapidly with distance from the penetration point by virtue of the increasing frontal area of the wave (the energy is distributed over a greater area). However, the directionally oriented filaments of the conducting composites channel the energy along the filamentary direction to produce relatively much greater areas of damage. This effect depends of course on the type of composite and layer orientations. Considerable efforts have been directed toward protection



Figure 2. Streamering off model in laboratory illustrates induced streamers in flight which lead approaching lightning stroke into helicopter.

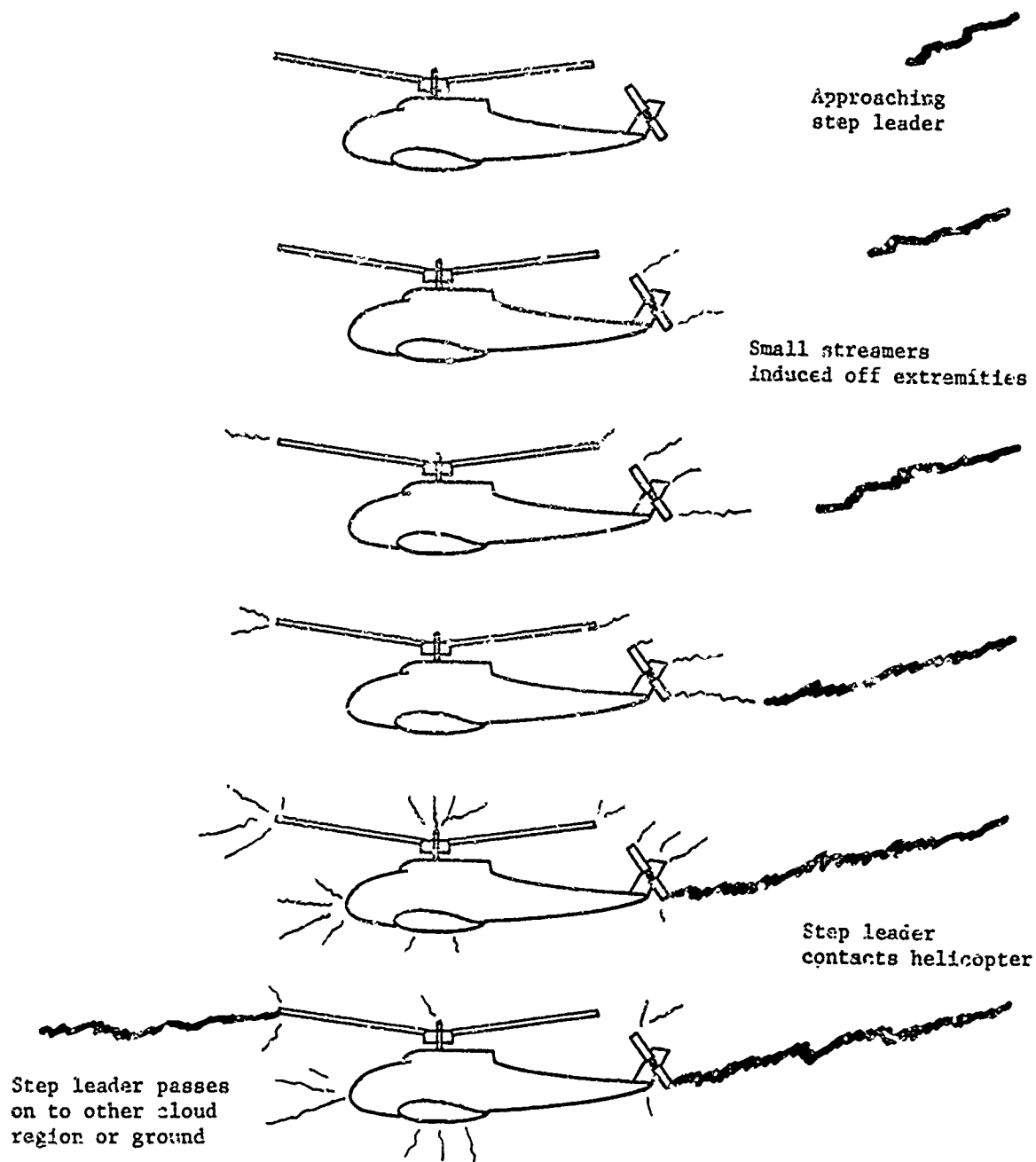


Figure 3. Illustration of stroke contact mechanism with helicopter.

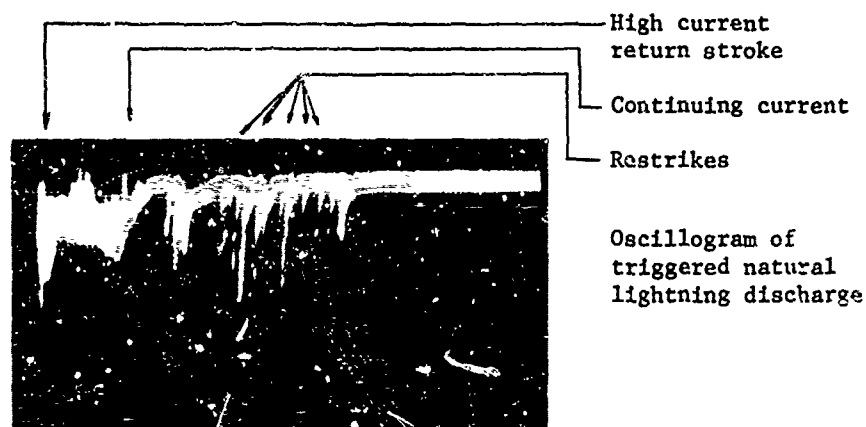
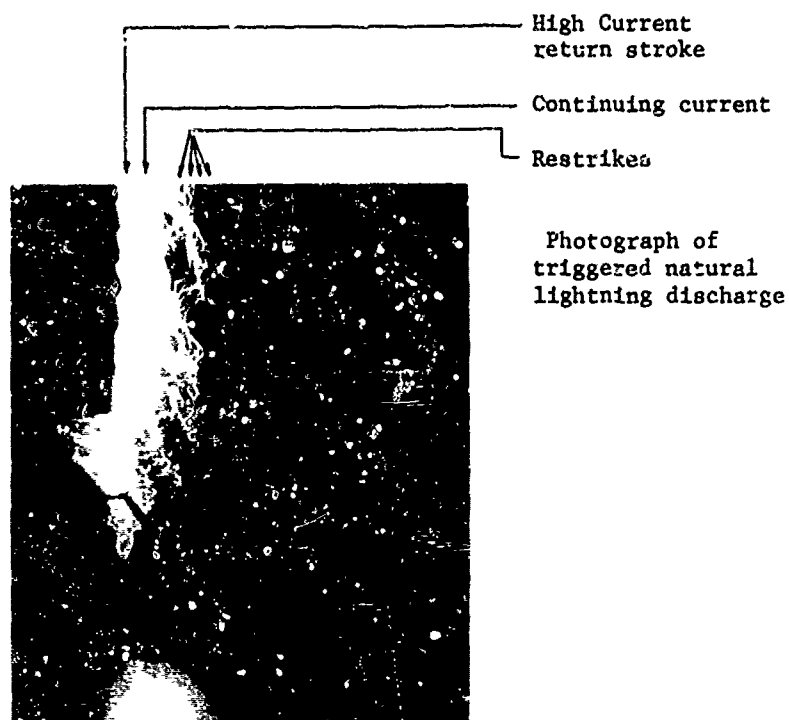
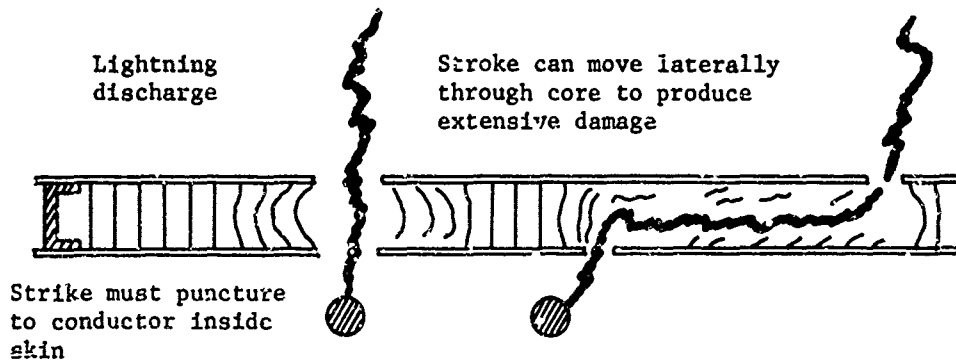
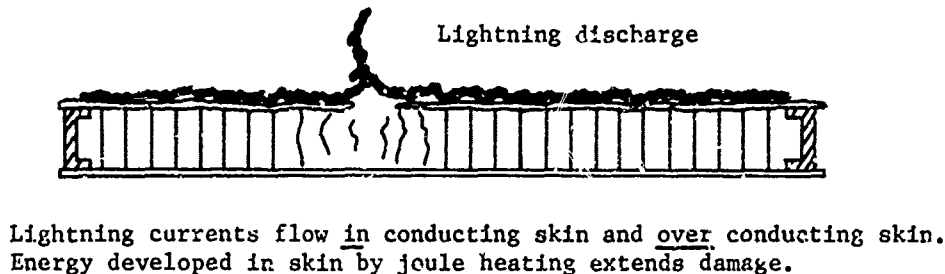


Figure 4. Photograph and oscillogram of triggered natural lightning discharge illustrating typical high current return stroke, continuing currents and multiple restrikes.

a. Dielectric composite skin and core (fiberglass)



b. Conducting composite skin (boron or graphite epoxy) dielectric core



c. Dielectric or conducting composite skin, metal honeycomb core

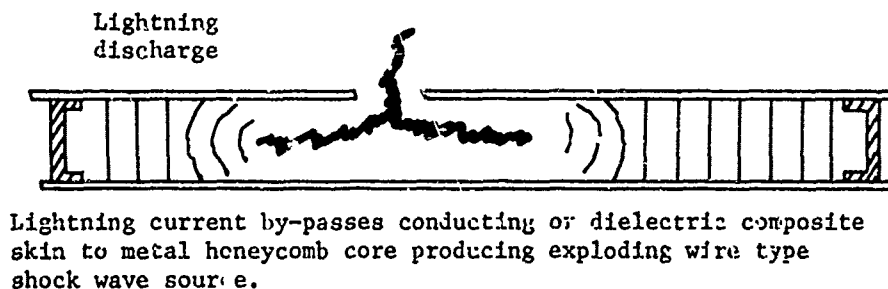


**Figure 5** Lightning damage mechanisms for unprotected dielectric and conducting composites (fiberglass and boron or graphite epoxy).

and a variety of effective protection schemes have been developed.

Also of importance in evaluating possible damage is the way in which the material is used. For example, either conducting or dielectric composite material over aluminum honeycomb core can result in puncture of the composite material, with principal current conduction through the aluminum honeycomb core producing aluminum vapor and an "exploding foil" shock wave inside the structure as shown in Figure 5c. The exploding foil is similar to the exploding wires used to drive hypersonic shock tubes. Because the resistance inside the section through the aluminum honeycomb core is much lower than through the skin, most of the current flow through the aluminum foil will vaporize it and produce extensive damage.

Calculated values for energy developed in various materials by a moderately severe lightning stroke current are presented in Table I for a section of material approximately 6 inches square by 0.040 inch thick, with the current applied across the two opposite edges. The lightning current waveform used in the examples represents a moderately severe natural lightning discharge and reaches a crest of 100,000 amperes in 10 microseconds and decays to half value in about 25 microseconds. As may be seen, the energy developed in the metals is relatively low compared to that developed in the boron and graphite epoxy materials.

Also of importance is the location where composite materials are to be used. Where they are not used for primary structures, as in leading or trailing edges, loss of extensive sections may not always introduce hazards to flight. The cost of protection in terms of weight and expense can then be traded against the cost of occasional repair. Where the materials are used for primary structures and safety of flight is involved, some type of protection should be provided.

Unfortunately, methods used for protecting plastic sections such as radomes are not totally effective for conductive composite materials because of conductivity. Conducting strips are used on radomes and other plastic sections to attract lightning discharges to the diverter strips so that the discharges do not puncture the plastic surfaces. This diverter effect is produced because intense momentary electrical gradients exist on the strips because of the lack of conductivity of the adjacent radome material (even with antistatic conducting coatings as indicated in Figure 6.) The electric field is similar to that which would occur with the protection strips in free space but with no dielectric as illustrated in Figure 6. Some composite materials have sufficient low resistance that streamers nearly equivalent to those from the metallic strips will be produced, with little diverting action from the strips. If the strips are sufficiently close together, a few inches

for example, the discharge will surface flash to the protection strip from the contact point on the composite thus doing little damage.

In contrast to the external skin which is contacted directly by lightning stroke arcs, metal conductors inside an aircraft may be required to carry the stroke currents but do not have to withstand the arc temperatures. However, other effects such as inductively coupled potentials and magnetic force effects must still be considered. For example, a lightning discharge to a metallic conductor connected to the inside of a plastic section can still couple large voltages into wiring because of the huge magnetic fields present about the conductor. Also, the currents can produce large magnetic forces which can tear lightning conductors loose.

The potentially most damaging type of effect other than sparking in fuel systems is the internal lightning stroke arc. Metallic conductors such as bonding wires from external lightning protection strips or across floating sections of the vehicle to the main airframe, although they may not need to withstand arc temperatures, are still required to withstand the huge magnetic force effect which to a large extent is a function of geometry. Any right angle bends in the conductor can produce forces as great as two tons to pull the bonding jumper loose from the solderless connector to which it is attached.

The massive damage which has been observed on large aircraft vertical fin antenna systems with fiberglass insulation gaps is due to mechanisms of this type which, because of inadequately installed bonding, develop internal lightning arcs to produce explosive pressures.

The effects of lightning on materials may be summarized as pitting, melting and hole puncture of generally limited degree in metal skins, moderate size holes in dielectric composite materials, slightly greater areas of damage in conducting composite materials and in explosive structural effects where the arcs are permitted to develop for any substantial distances inside structures of either metal or plastic.

#### DAMAGE TO HELICOPTERS FROM LABORATORY AND NATURAL LIGHTNING DISCHARGES

Natural lightning strikes and laboratory test discharges have demonstrated nearly total destruction of some fiberglass blade designs indicating the need for at least minimum artificial lightning discharge tests of all helicopter blades.

As indicated in previous sections, of particular concern is the development of internal arcs which can produce the explosive or catastrophic effects on the blades. With metallic components such as control rods or wing tip lights, which can lead the stroke inside, there exists the possibility of developing internal arcs. Other areas of

TABLE I  
Calculated Energy in Various Materials  
from 100 Kiloampere Current \*\*

Material	Energy-W
Plastics	$W_p = 0$ damage from external arc energy and pressures
Metals $R = 3 \times 10^{-6}$ ohms	$W_m = \int I^2 R dt$ $= 3 \times 10^{-6} \times 1.71 \times 10^{+5}$ $= 0.51$ joules
Boron Epoxy $R = 8.5 \times 10^3$ ohms	$W_b = 8.5 \times 10^3 \times 1.71 \times 10^5$ $= 1.45 \times 10^9$ $= 1450$ megajoules*
Graphite $R = 0.025$ ohms	$W_g = 0.025 \times 1.71 \times 10^5$ $= 4280$ joules

\* Most of the current will flashover the surface, after destruction of the material, thus greatly reducing the effective energy developed in the material.

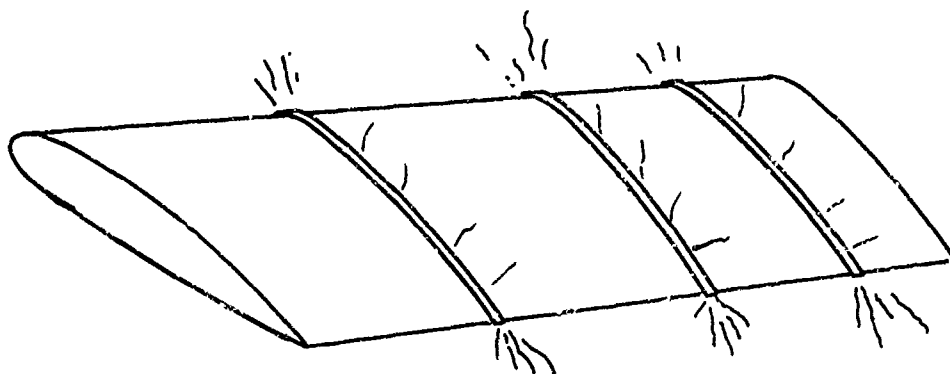
\*\* Assuming a typical lightning waveform with a rise to a crest of 100,000 amperes in 5 microseconds and a decay to half value in 25 microseconds, the current wave form may be expressed mathematically as the difference of two exponentials.

$$i(t) = i_0 \left\{ \exp(-\alpha t) - \exp(-\beta t) \right\}$$

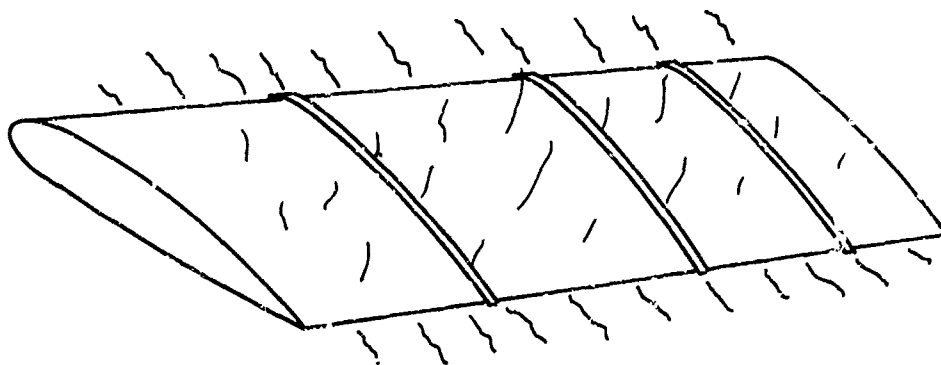
where  $i_0 = 142$  KA,  $\alpha = 4.4 \times 10^4$  /sec.  $\beta = 4.6 \times 10^5$   
and where R = the resistance across two edges of a sample of the material 6 inches square by 0.040 inches thick. The energy is then:

$$W = \int_0^\infty R I^2 dt$$

$$= R \times 1.71 \times 10^5 \text{ joules.}$$



a. Strip diverting action dielectric composites



b. Reduced strip diverting action, conducting composites also supply streamer.

Figure 6. With conducting composites, metal diverting strip effectiveness is reduced because composites also feed streamers.



concern include the metal conducting paths and particularly metal to metal joints such as bearings where lightning arcs can produce a variety of effects from total welding of small ball bearings in the races to pit marks on larger bearings which can possibly result in subsequent fatigue or corrosion induced failure.

The use of a metal spar is preferable from a lightning point of view as it provides a continuous lightning path from the blade extremity to the hub, but it does not necessarily provide complete lightning protection. Adhesively bonded skin on blade boxes may be separated from the spar to produce unbalance and possible subsequent blade failure from air flow and inertial effects.

In summary, lightning stroke currents to helicopter blades can produce explosive damage from internal arcs whether channeled into the blade interior through blade tip lights, anti-erosion cuffs, trim tabs, control rods or other metallic components and severe damage can be produced in either metal or plastic blades. In general the use of a continuous metal spar for the blade tip to the rotor is preferred. Lightning damage to bearings is of more concern with small bearings; however, pitting of larger bearings can result in possible subsequent fatigue and corrosion problems.

Little evidence exists of natural stroke damage to helicopter fuel systems; however, it is reasonable to assume that helicopters are not immune to the lightning effects on fuel systems which have been observed on commercial, military and general aviation aircraft. It is also reasonable to assume that helicopters in which the shielding of the metal skin is much less effective because of the large open areas should be susceptible to greater pulse coupling than fixed wing aircraft and substantial pulse coupling can occur into electrical circuitry even on commercial airliners.

#### PROTECTION APPROACHES

Probably the most serious aspects of the lightning protection problem are: (1) the fuel systems, and (2) damage to structural plastic sections in which huge energies can be developed, producing in some cases nearly total destruction. For the fuel systems, a complete checkoff approach should be considered in which only lightning tested components are used including plastic fuel tank access doors and all fuel tank components which are mounted in the outer tank walls, such as fuel probes, fuel filler caps, fuel pumps, dip sticks, and fuel drain valves. Experience with commercial and military aircraft through the years indicates that fuel systems can be exploded and that one military fuel, JP-4, is probably the worst from a lightning strike point of view as it is flammable (explosive) in the temperature range at which most lightning

strikes occur. Thus all lightning induced sparking should be suppressed within the tank area. Techniques have been developed for nearly all of the above problems for fixed wing aircraft which indicate at least initial possible approaches for helicopter protection. As an illustration, both fiberglass and graphite composites can utilize external conducting strips or continuous coatings of aluminum foil, flame spray or mesh. Shielding wires can be utilized for pilot canopies and for electrical circuit boards covered by plastic sections. Engine controls and aircraft electrical circuits can be effectively protected against induced surges with protection devices and as mentioned a variety of techniques are available for protection of fuel systems, including lightning proof fuel filler caps and new access door designs. The general approaches are discussed in more detail in the following section.

Plastic fuel tanks present a possible hazard from lightning strike puncture and also from induced streamering inside the fuel tank from nearby lightning strokes or lightning discharges which contact extremities of the aircraft not even necessarily near the tank area as illustrated in Figures 2 and 3. The induced streamering which can be produced inside the tank and the possible skin punctures can present a possible hazard as evidenced in ignition of plastic fuel tanks on both military and civilian aircraft. Streamer formation inside fuel tanks is illustrated in Figure 7. Although this remains an area requiring further development at least an initial approach would appear to be the utilization of an external conducting coat of flame spray aluminum, aluminum foil or possibly wire mesh. Also the use of external metallic strips is not entirely ruled out as the electric field penetration in between the strips should be relatively low unless metallic components within the tank are quite close to the internal plastic fuel tank wall in an area unprotected by the strips.

One other area of concern in regard to all fuel tanks but particularly plastic tanks is the problem of magnetic flux coupling into wiring loops within the tank to produce magnetically induced voltages as illustrated in Figure 8. This is a much more difficult problem to solve and depends upon a variety of factors such as geometries of the wiring within the tank and the location of the tank. The use of wiring configurations or metal structure in which loops are not formed within the tank should reduce the effects of magnetic flux coupling. This also applies, of course, to metallic plumbing used in the tank; again no loops should be used and in any event some type of lightning tests should be carried out on the tank system.

The most important general rule for lightning protection development of all aircraft and all types of fuel tank components

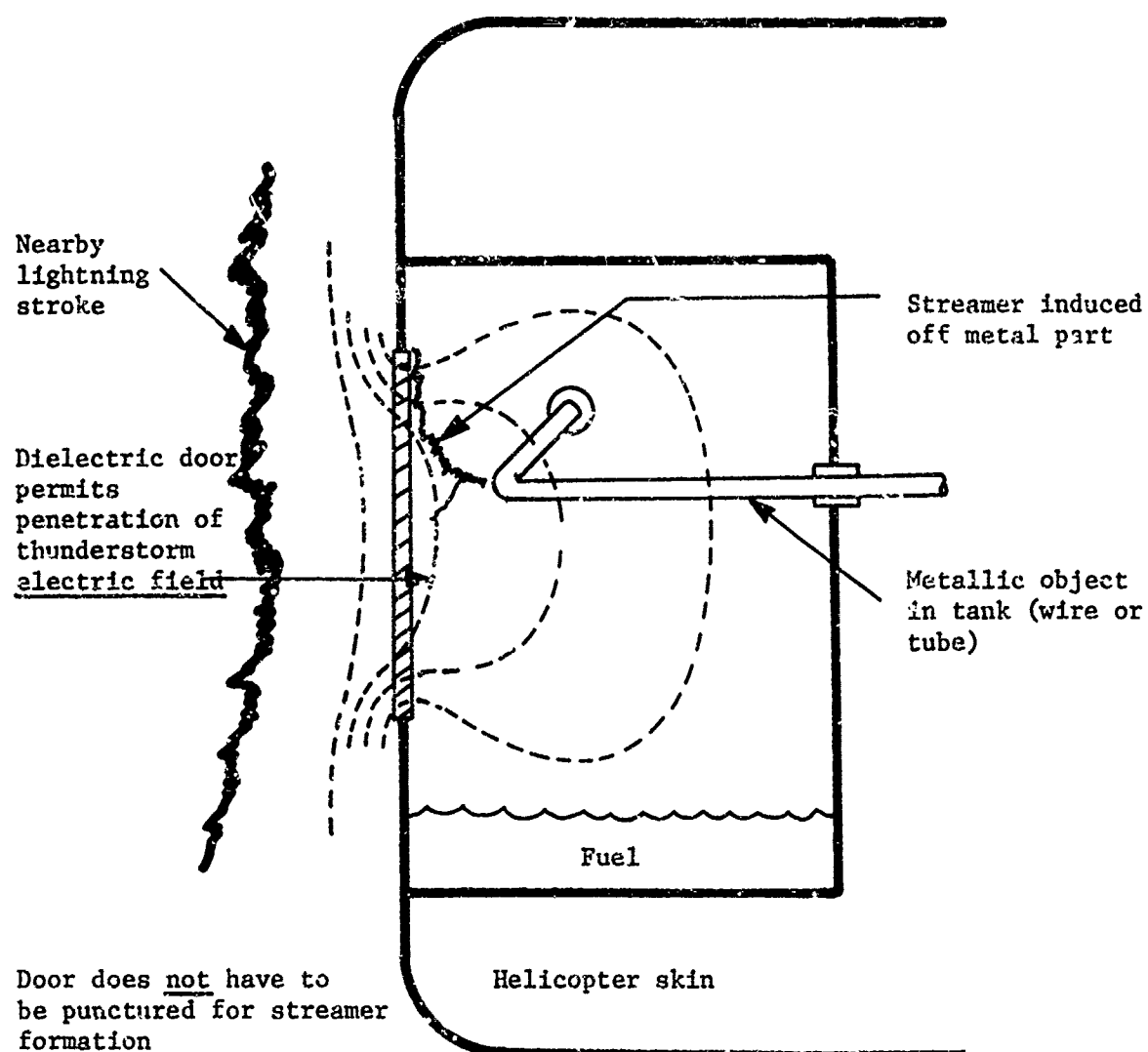


**Figure 7.** Possible sparking sources inside fuel tanks with dielectric walls from incident electric field.

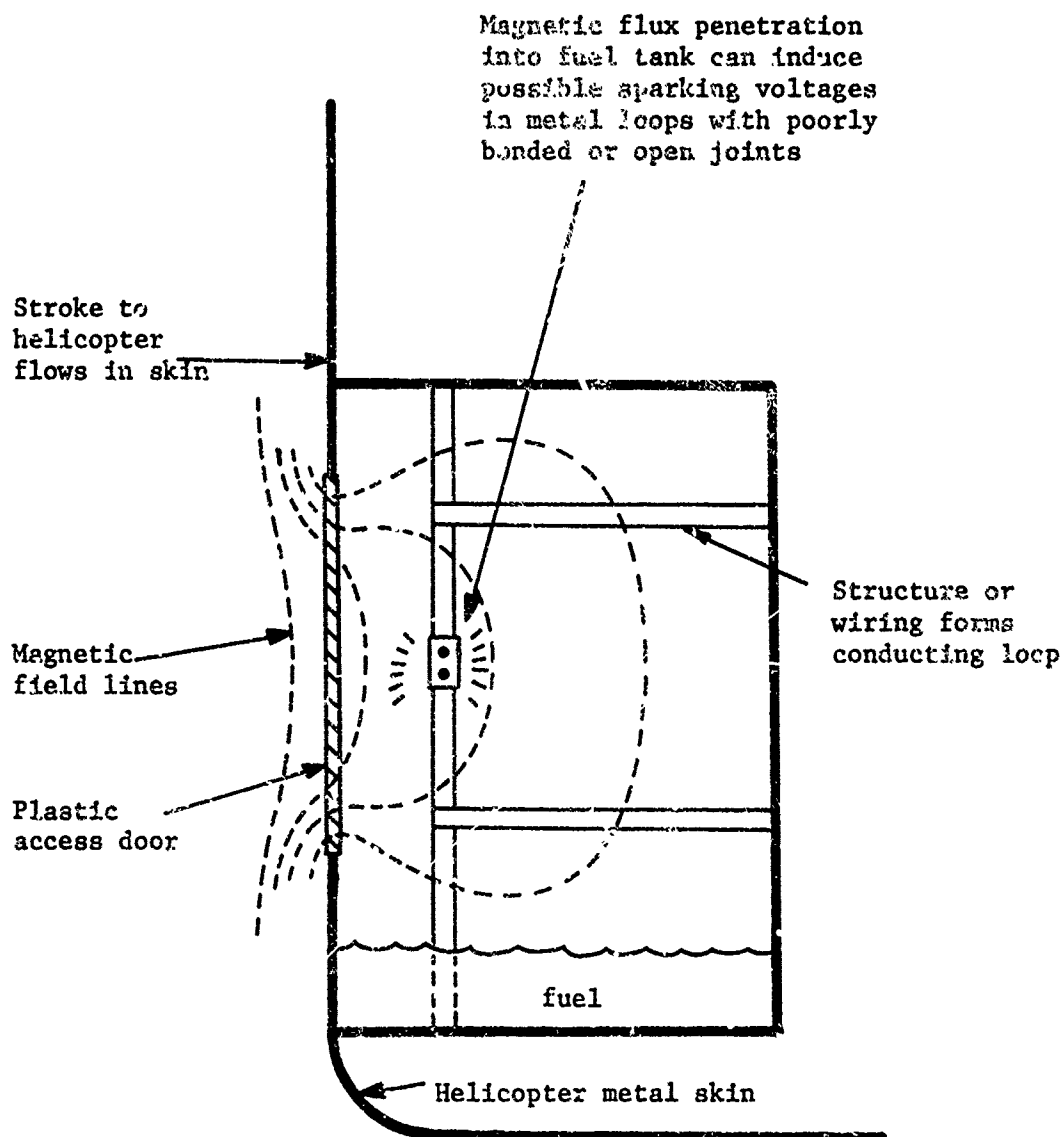


Figure 8. Possible sparking sources inside fuel tanks from magnetic field penetration.

is that lightning tests should be carried out for confidence in the design because of the variety of lightning current waveshapes and the variety of effects on various materials and components. Because of this complexity, only the use of severe artificial lightning discharge testing can give confidence that the system can withstand moderately severe natural lightning discharges.

Helicopter blades represent one of the most probable strike points on a helicopter and as such require the careful consideration of the need for lightning protection. Considerations can generally be broken up into the two major types of blades, those of essentially all metal construction and those using total or partial dielectric or conducting composite materials. The important criteria in plastic blade design from a lightning point of view is to keep the lightning discharge currents on the outside of the blades where they can do little damage as illustrated in Figure 9. If currents do pass through the blade interior one must assure that they can carry maximum lightning currents without serious damage or hazard to the blade. This means that the use of adhesive bonding for joining metallic skins to blade spars or trailing edges must be carefully checked.

Also specific protection must be provided to prevent lightning discharge currents from peeling the metal skin away at these points where the windstream can possibly amplify the damage to catastrophic proportions. For direct or swept natural lightning discharges, however, the all metal blade theoretically approaches the optimum solution of complete electromagnetic shielding providing electrical bonding can be maintained between the various blade elements. It should also be noted that one of the worst sources of precipitation-static type radio interference is caused by electrically floating metallic sections on a helicopter, particularly if they are in areas directly contacted by atmospheric particles, such as snow or dust, thus bonding of metallic components on the helicopter blade is also important for reduction of radio interference.

For blades with partial or total composite materials of either dielectric or conducting fibers, provision must be made to keep the lightning stroke energies on the outside of the blade or to provide adequate current paths through the interior as discharges through inadequate conductors can produce explosive damage. Metal structure should be electrically bonded to a main spar if one is used or to other metal parts to provide a continuous path for the lightning stroke currents. Composite external skins if of sufficient area will require external protection to prevent swept strokes from puncturing into the blade interior.

The general criteria for dielectric composites has been derived from aircraft radome development and utilizes the parameter

of surface flashover versus puncture distance. For a dielectric skin with a given dielectric puncture strength, a specific distance between external conductors may be used in which no puncture will occur almost independent of the distance from which external electrical discharges approach the central area of the panel. The higher the dielectric strength the larger the panel may be without danger of puncture. The specific exception occurs when metal parts are located very close to the inside surface. For the average fiberglass skins, because the glass fibers to resin boundaries are somewhat porous, the dielectric strengths are not in general very high and relatively small panels must be used, of the order of a few feet square. With conducting composites such as the boron or graphite epoxies, damage can also be done to smaller segments and therefore protection must be provided in either continuous outer metallic coatings or with separated strips. It should be noted that this is based on preliminary data on protection of conducting composite materials and that current research may provide better coatings for this purpose.

#### CONCLUDING COMMENTS

A survey of lightning hazards and protection for helicopters has indicated that increasing lightning strikes and lightning damage may be expected on helicopters because of the increasing use of plastics and conducting composite materials which are much more vulnerable to lightning damage and because of the increasing exposure of helicopters to instrument weather. Thus, at least fuel systems and rotor blade assemblies should be checked with artificial lightning discharge currents to assure that neither control systems nor critical structures will be dangerously affected.

#### REFERENCES

1. Proceedings, Lightning and Static Electricity Conference, 3-5 Dec. 1968, Technical Report, AFAL-TR-68-290, Part II, AD-693135, 570 pp, 1969.
2. B.J. Solak, (1966), "The Influence of Lightning and Static Electricity on Helicopter Design," Journal of the American Helicopter Society, Vol. 11, No. 1, p 10.
3. M.M. Newman, J.D. Robb, and J.R. Stahmann (1968), "Lightning Electrical Hazards to Flight Vehicles," AFAL-TR-68-163, p. 27-30.
4. M.M. Newman, J.D. Robb, and J.R. Stahmann (1965) Lightning Electromagnetic Environment and Laboratory Reproduction Techniques, AFAL-TR-64-341, LTRI Nr. 425, 129 pp.
5. Advisory Circular AC 20-53, "Protection of Aircraft Fuel Systems Against Lightning," Federal Aviation Agency, October 1967.

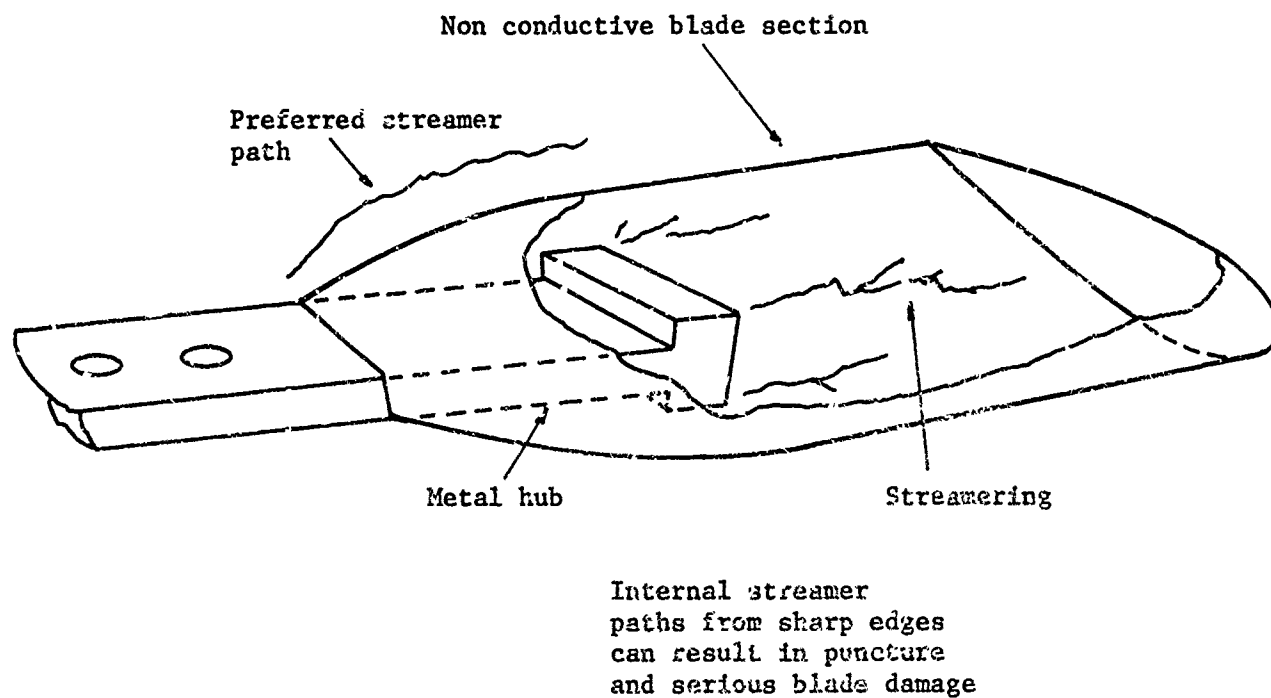


**Figure 9.** Metal hub of all plastic blade can streamer inside plastic along joint lines to initiate lightning penetration for full length of blade.

# APPENDIX I

## CALCULATIONS OF FRICTION CHARGE ENERGY STORAGE ON HELICOPTER

The energy storage is equal to

$$W = \frac{1}{2} CE^2$$

where W = energy in joules  
C = capacity in farads  
E = voltage in volts

Energy storage for typical voltages and capacities is shown below:

TABLE OF ENERGIES

Helicopter Capacity picofarads	Helicopter voltage in kilovolts			
	50	100	200	400
50	.125	.5	2.	4.0
100	.250	1.0	4.	8
200	.50	2.0	9.	16
400	1.0	4.0	16.	32*
800	2.0	8.0	32.	64

\*comparable to vacuum tube hi fi amplifier filter capacitor - 500 pF @ 400 volts

The above table indicates that static electrification energies are equal to a few tens of joules maximum, which is far below the levels required to produce structural damage of significant pitting.

## Helicopter Cargo Handling - Electrostatic Considerations

B. J. Solak  
The Boeing Company, Vertol Division

J. E. Nanevich  
Stanford Research Institute

G. J. Wilson  
The Boeing Company, Vertol Division

C. H. King  
The Boeing Company, Commercial Aircraft Group

### ABSTRACT

Application of active and passive systems for static electricity dissipation of the Heavy Lift Helicopter during cargo hook operations is discussed in light of the recent flight tests at Yuma Proving Ground.

Active dissipation of the required current into the surrounding atmosphere appears feasible, whereas accurate sensing of the helicopter voltage falls short of the design objective.

The feasibility of passive dissipation is briefly discussed based on resistance measurements of the Yuma Desert.

WITH THE CONTRACT AWARD to develop advanced technology components for the Heavy Lift Helicopter (HLH), The Boeing Company with Stanford Research Institute (SRI) as subcontractor got the assignment to solve the most troublesome static electricity problem, affecting a helicopter, namely:

1. Potential equalization between the helicopter cargo hook or cargo at one potential and the ground or the cargo handler on the ground at another potential.

The design objective is to limit energy transfer on contact to 1 millijoule. For a heavy lift helicopter of 120,000 lbs gross weight and the electric capacity of the order of 2,000 picofarads this is equivalent to no more than about 1,000 volts potential difference.

2. All previous tests have indicated that the natural charging rates are of the order of 300 microamperes for a 40,000 lb helicopter gross weight. For the 120,000 lb heavy lift helicopter an

estimated charging rate of 600 microamperes was set as the design objective for dissipating capability.

The design objective for an active automatic system can be stated therefore as follows: Not more than 1 millijoule discharge (potential difference less than 1,000 to 2,000 volts) under 600 microamperes natural charging conditions. The laboratory tests at SRI, ground tests at Vertol and flight tests at Yuma are described in detail in the paper "Experimental Investigation of Problems Associated with Discharging Hovering Helicopter" (Reference 1). In this paper the impact of the test results on the solution of the HLH cargo hook operation is presented.

### ACTIVE VERSUS PASSIVE SYSTEM

There are two basic approaches to solution of the large hovering helicopter problem, namely:

1. Actively dissipating proper polarity and amperage charges into the surrounding air to counteract the natural charging of the helicopter. This method is commonly called an active system since a high voltage power supply is used to produce the discharge.

2. Reducing the helicopter voltage by means of passive corona points and grounding the helicopter by means of droplines (passive system).

At the first glance the passive system seems more attractive since it is by far simpler, safer, less expensive and more reliable than the active system. On closer inspection the passive system has drawbacks. Corona dischargers alone will not reduce the maximum voltage to the desired 1,000 to 2,000 volts. The conducting ropes dropped from the helicopter may spark, present a danger of entanglement with trees, etc., and are subject to loss, when cargo gets deposited on them. To top it all, the ground may be loose dust or loose dry snow with a relatively high resistance.

FOR THE ABOVE REASONS, an active system may be more desirable if technically feasible and if acceptable with respect to complexity, cost, reliability, fail safety, etc. The passive grounding system was therefore considered the

alternate in the Boeing Heavy Lift Helicopter program, and would be developed in case the active system met with insurmountable obstacles.

#### ACTIVE DISSIPATION - DESIGN PARAMETERS

The following design parameters have been surveyed and investigated:

1. Maximum triboelectric charging currents for a medium lift helicopter.
2. Dissipating of charges into two different air streams, associated with the helicopter (rotor downwash and engine exhaust).
3. Ability to sense the correct voltage difference between the helicopter and the ground (without ground contact).
4. Ion cloud over the ground surface below the hovering helicopter.
5. Resistance of the ground surface under dry desert conditions.

In subsequent paragraphs the above design parameters are given a closer look, with emphasis on the feasibility of the active system.

#### TRIBOELECTRIC CHARGING

IN THE TESTS CONDUCTED AT YUMA Proving Ground an area of sand was plowed up (disced) to loosen up the desert dust, then the helicopter was flown into this area. A wire was lowered from the helicopter and connected to a grounding stake, driven into the desert. The current flowing to ground through the grounding wire was recorded in the helicopter. Figure 1 shows a photograph of this test and a time history of the triboelectric current, while the helicopter gradually blew the loose dust away.

As can be seen, a 28,000 lb helicopter, hovering in a heavy dust cloud can produce 200 to 300 microamperes peak charging currents. The high charging was encountered on three successive flights. On subsequent flights, since the loose dust had been blown away the observed currents were on the order of 40 to 80 microamperes.

Helicopters in Alaska and the CH-54 in commercial application in moderate climate, have apparently encountered higher currents. Sparks three feet long have been reported in dry snow clouds. Under thunderheads and drizzle, sparks up to six feet long have

been reported in the CH-54.

The above data amply justifies the requirement of 600 microamperes maximum dissipating capability for a helicopter of 120,000 lbs gross weight. Under the worst condition, charging currents on the order of 1,000 to 1,500 microamperes may be possible.

#### DISCHARGING

IT IS KNOWN FROM ALL PREVIOUS TESTS that there are two important parameters, which determine the amperage of the corona current, leaving the helicopter ( $I_g$  = the net discharge current) namely:

1. E field around the corona point, which returns the ions to the helicopter, which for a given geometric configuration, is directly related to the voltage difference between the helicopter and the power supply.
2. Velocity of the air mass which carries the ions away. Figure 2 gives the basic idea and the nomenclature used in this paper.

Several probe configurations were tried and the experimental results have indicated that very little can be gained by probe configuration, e.g. a ring of corona points and single corona point produce basically the same net  $I_g$  current. The reason for this is that the current which leaves the helicopter is determined by the ion mobility in the air velocity field and the E field. Since  $I_g$  is directly proportional to the air velocity, we have three design choices:

1. Discharging into the slipstream of the rotors (air velocity of the order of 80 ft/sec).
2. Discharging into the turbine exhaust (gas velocity of the order of 200 to 300 ft/sec, but the temperature of the order of 500 to 600°C, partially nullifying the gain of high velocity due to higher ion mobility).
3. Discharging from the blade tips (air velocity of the order of 700 ft/sec).

Let's discuss all these alternatives.



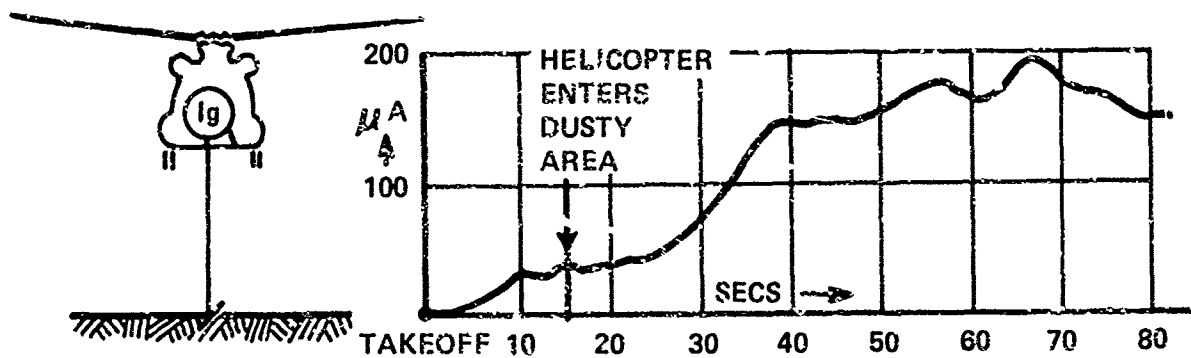
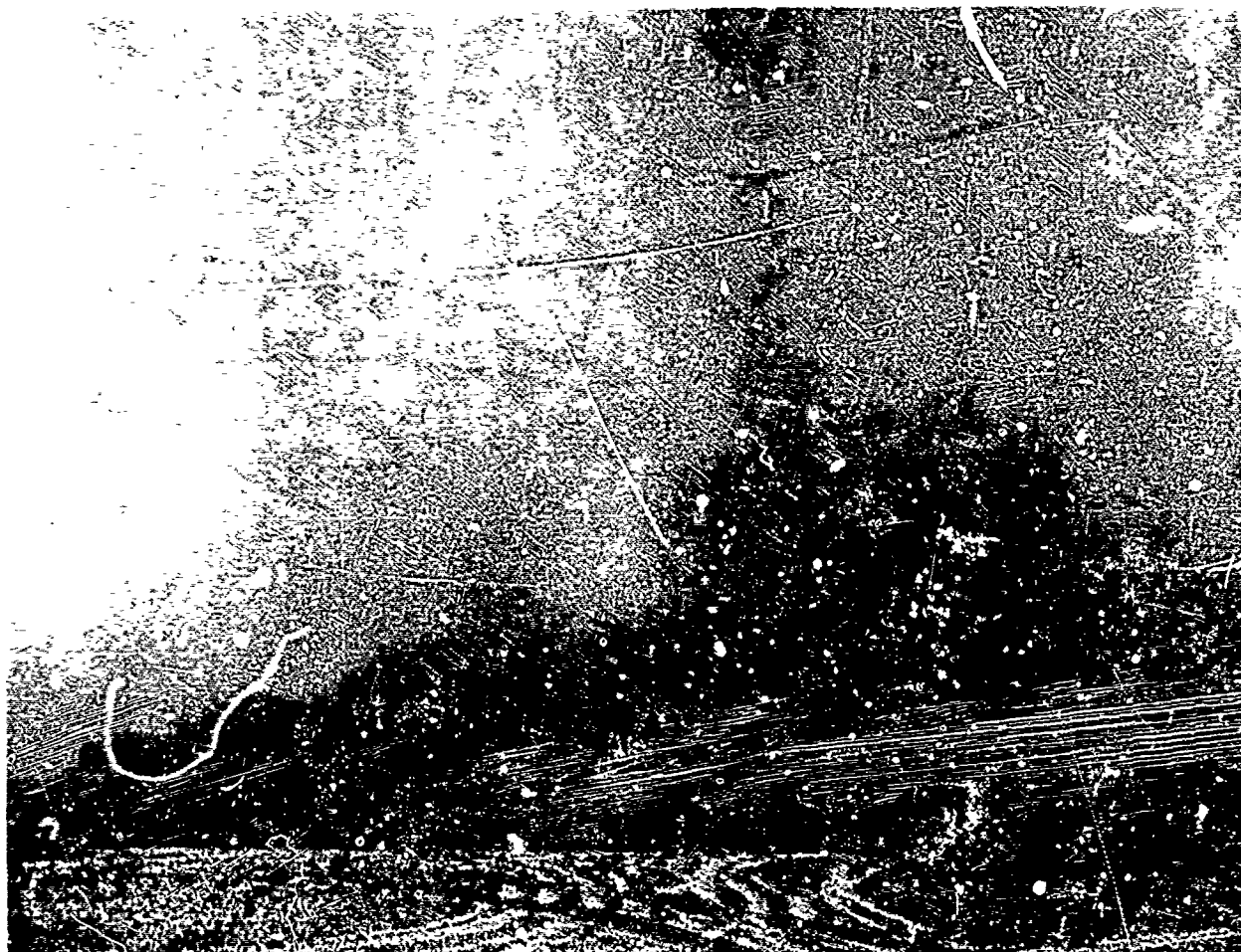


Fig. 1 - TRIBOELECTRIC CHARGING TEST OF A HOVERING HELICOPTER

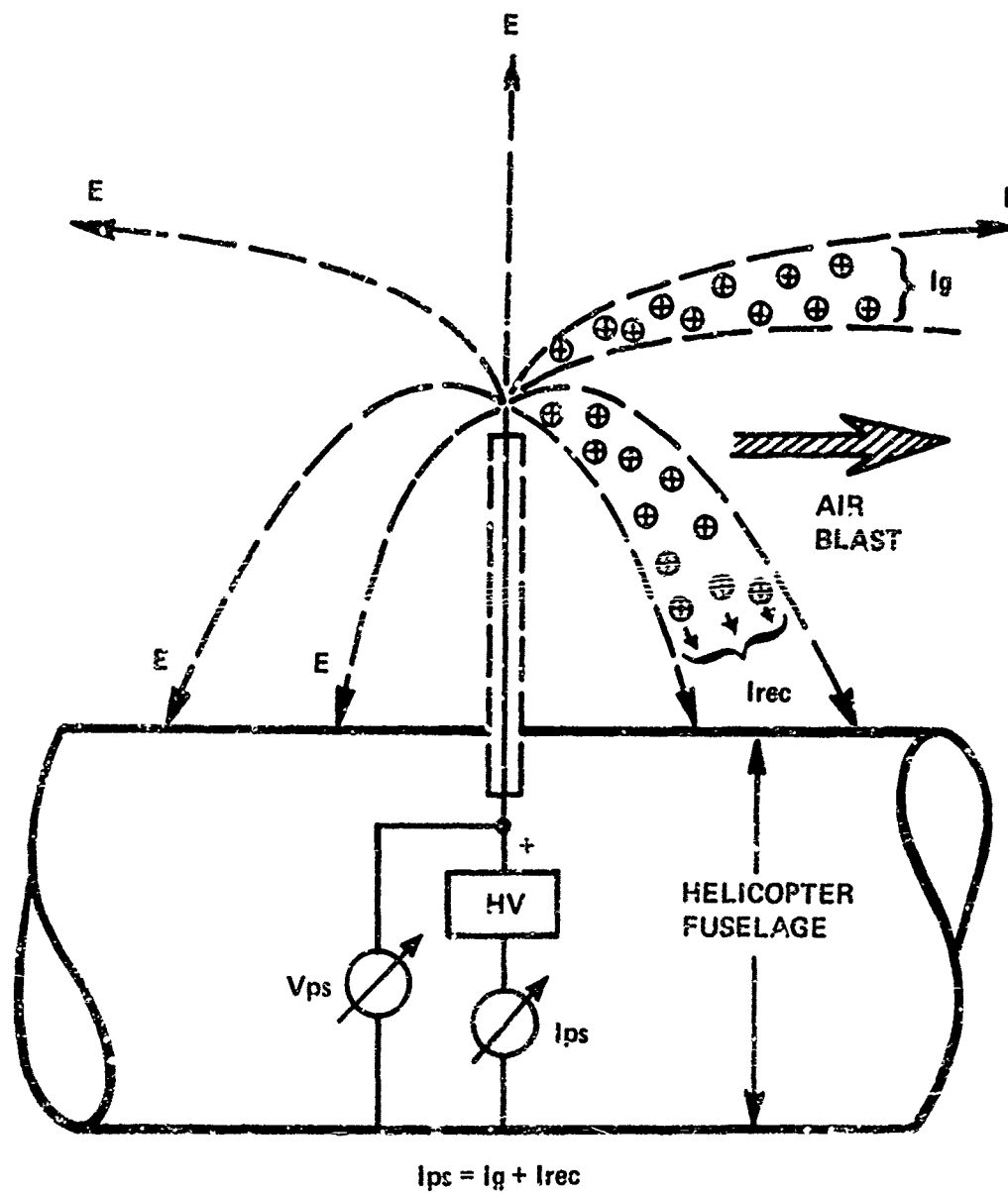


Fig. 2 - DISCHARGING NOMENCLATURE

## DISCHARGING INTO THE HELICOPTER SLIP-STREAM

This was the method pursued by the Dynasciences Corporation, who for the last decade have marketed active discharge systems. Figure 3 shows the experimental results (quoted from Reference 2). In our effort to produce sufficient ions for heavy lift helicopter sensing fidelity tests (reported in Reference 1), we have extended this method almost to the design limits (long outriggers and high power supply voltage) as shown in Figure 4. By decreasing the E field (increasing the distance of the probes to the skin), we did obtain substantial  $I_g$  increases. However we got only 200  $\mu A$  from 4 corona points using approximately 200 KV. Increasing the insulator length between the corona points and the fuselage to a full 6 feet would probably increase the current to 300  $\mu A$ . To obtain the required 600  $\mu A$ , the helicopter would therefore have to be fitted with approximately 8 corona points, sticking out from the fuselage or 6 ft. insulators - a difficult and cumbersome solution to say the least.

## DISCHARGING INTO THE TURBINE EXHAUST

The lure of the high gas velocity has produced several attempts to discharge into the turbine exhaust, both in this country and in the United Kingdom (References 3 and 4). The results of laboratory, ground and air tests of various dissipator geometrics located in the exhaust plume of the CH-47 helicopter turbines are fully discussed in Reference 1. Figure 5 shows flight test result of dissipator test at Yuma. A ring dissipator was located in the turbine exhaust, five turbine exhaust diameters aft of the tailpipe exit plane. Superimposed are test results of tests run in 1963 and the ground tests at Vertol in 1972. Discharge currents of the order of 160  $\mu A$  were obtained. The larger turbine exhausts of the HLH and exhaust directions which do not pass over any fuselage skin should easily allow discharges of 200  $\mu A$  per engine at dissipator voltages of 200 to 250 KV. With three turbines, the design objective of 600  $\mu A$  can be met. If however, field experience shows much larger dissipation current

requirements, the necessary voltage increase and the dissipator distance increase may make this solution cumbersome.

## DISCHARGING FROM THE BLADE TIPS

Based on extrapolation of the influence of air velocity on the discharge current it appears feasible to discharge approximately 100 microamperes from a blade tip at 50 KV probe voltage. It also appears feasible to locate the high voltage source on the rotor hub and to supply the blade tips through coaxial cables of approximately 0.5 inch diameter. Such a cable could be submerged inside the blade trailing edge. Due to lack of funds for blade modifications, no tests were conducted and the above figures are based on extrapolations. If future blades include an integrated blade tip design, incorporating lightning protection and passive dissipation, the active dissipation could probably share the corona points on an either/or basis with passive dissipation.

IN AN EFFORT TO INCREASE the dissipated current, the following additional approaches have been investigated:

1. Dissipating by charged water droplets - this approach is being explored by Dr. Buser of the U. S. Army ECOM Laboratory and is the subject of a separate paper.

2. Corona point dissipation using pulsed high voltage supply - this method was explored by Dr. M. Mulcahy of ION Physics, Inc., under a subcontract to Boeing-Vertol. The pulsing has decreased the recirculation significantly (80%) but the net discharge current increased only 17%. It is not known how much the pulsing will increase radio interference.

3. Narrow high velocity blast over the coronapoints - the results of this experiment, using a small diameter nozzle, indicated that very little could be gained by this method over the use of a single corona point in the turbine exhaust. The reason for this is the fact that the narrow blast of air very quickly became turbulent and mixed with the surrounding air, allowing recirculation to the

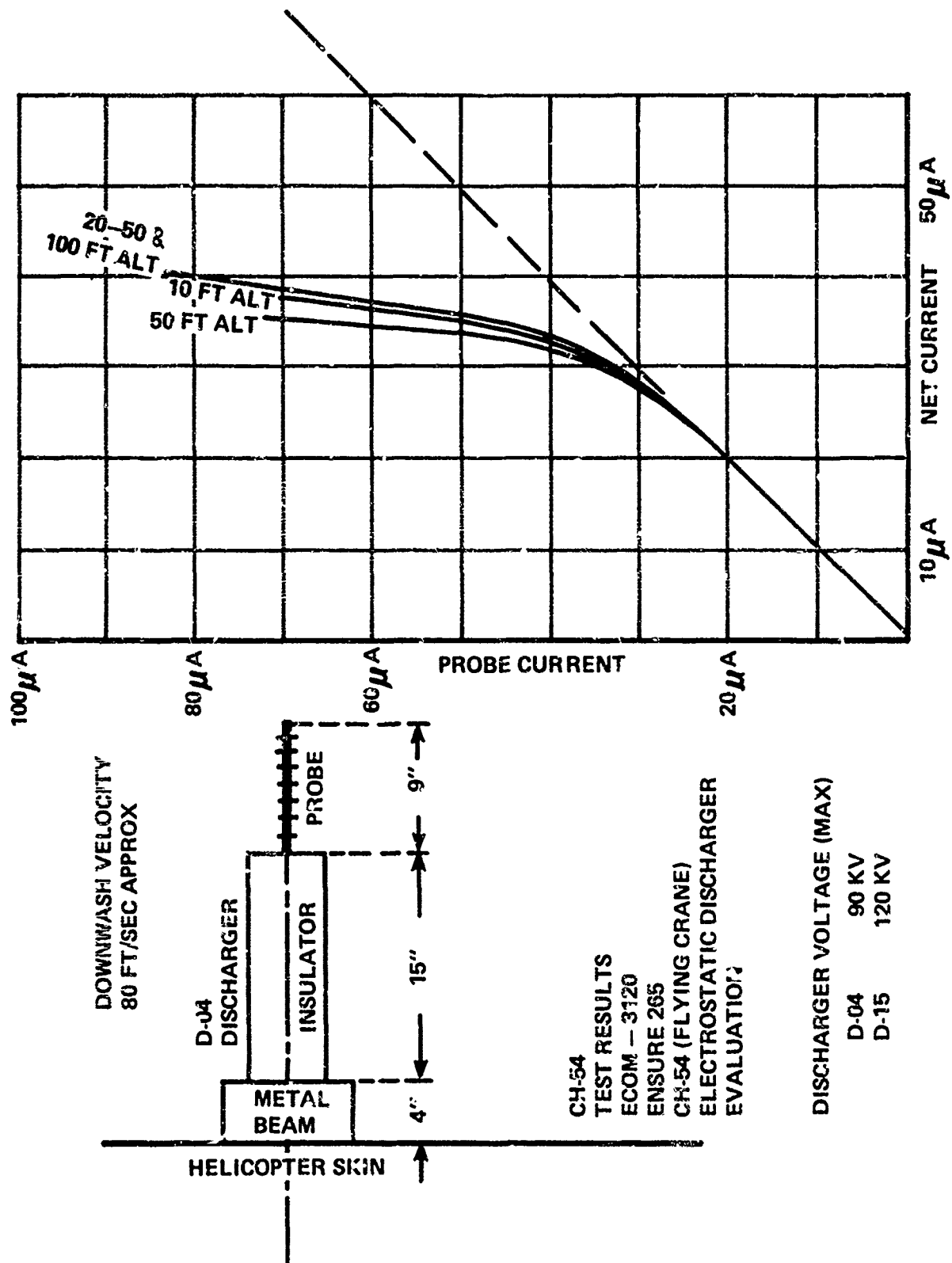


Fig. 3 - EXPERIMENTAL RESULTS

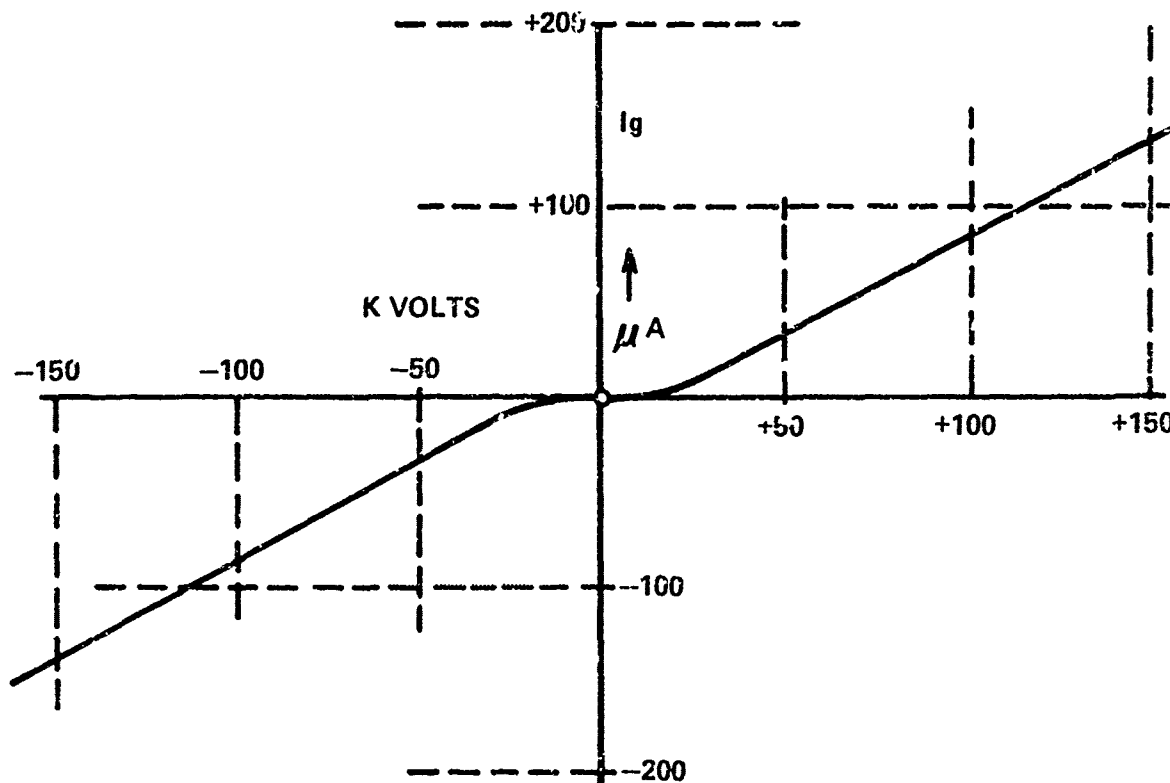
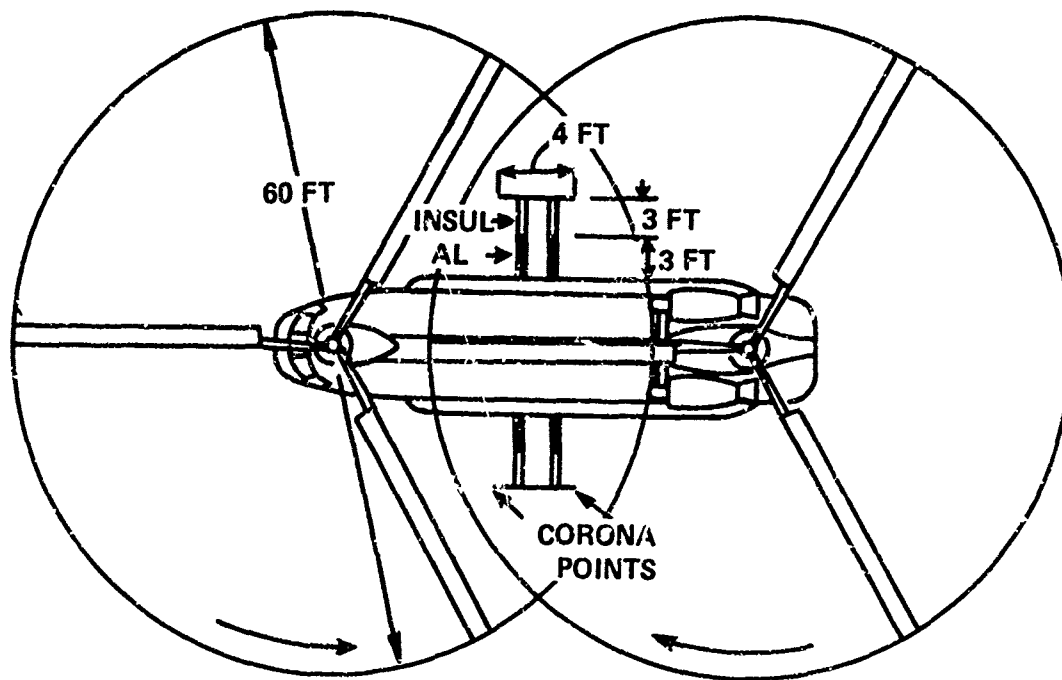


Fig. 4 - DISCHARGING TEST LIMITS

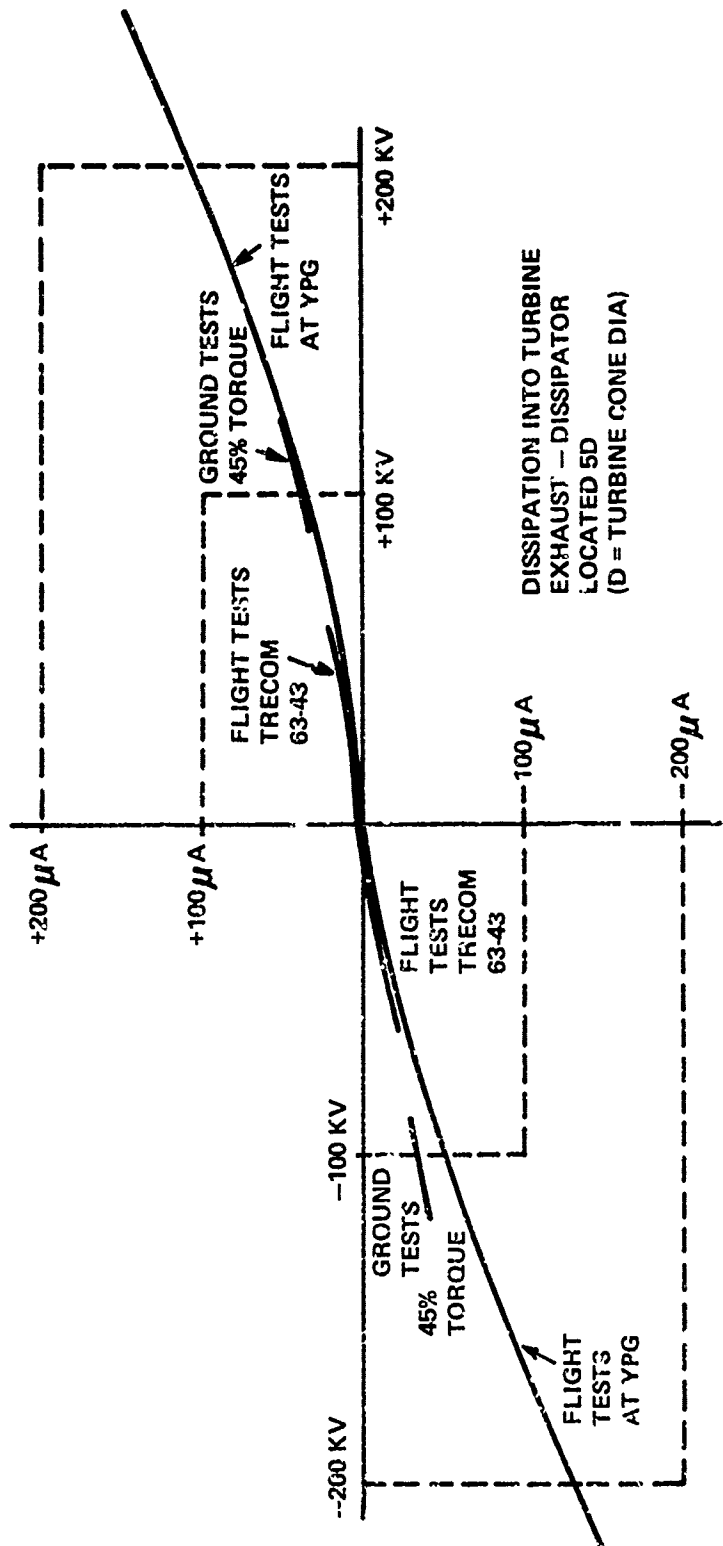
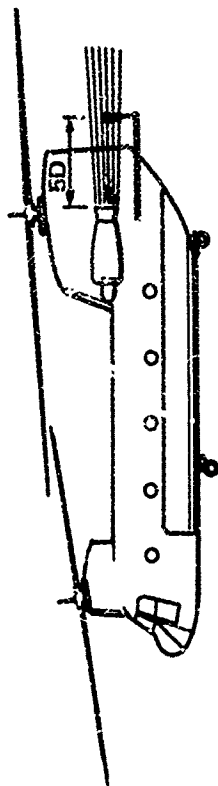


Fig. 5 - FLIGHT TEST RESULT OF DISSIPATOR TEST

fuselage.

It is sufficient to report here that the above approaches have not as yet materially improved the active dissipation picture, presented in preceding paragraphs.

#### SENSING

A practical solution of the active dissipation system depends on accurate measurement of the E vector due solely to the voltage difference between the helicopter and the ground. The measurement accuracy should be such that no more than 1,000 V remain on the helicopter. An error of e.g. 3,000 V would increase the energy of the discharge to 10 millijoule. The sources of measurement errors are shown in Figure 6. Let's discuss them.

When we manually bring the  $I_q$  to zero (by increasing the dissipation) the conditions represent the design objective, namely no voltage between the helicopter and the ground. The  $E_h$  vector which we are solely interested in, has been reduced to zero. Under these conditions, any value other than zero indicated by the field meters represents an error, which when nulled by some form of an automatic feedback control loop would leave some voltage on the helicopter. These errors in reading of field sensors are due to:

- Ed - due to voltage of the dissipator
- Ei(+)-due to dissipated ions by discharger and electrification of the desert surface
- Ei(-)-due to negative ions generated triboelectrically on the blades striking the dust particles (or snow, with reversed polarities)

An elaborate series of experiments conducted at Yuma and aimed at evaluating  $E_h$ , Ed, Ei and Ei are reported in Reference 1. In this paper it is sufficient to tabulate the results as shown in Figure 6. When  $I_q$  was nulled manually, the readings of field meters E1, E2, E3 and E4 did not go to zero, but were indicating some values of E related to the ion influences (Ed can be neglected). Knowing field meter calibrations, i.e. the ratio of E in-

dicated to the voltage on the helicopter for each field meter, it is possible to calculate the helicopter voltage value which would correspond to the indicated E and then the discharge energy, stored in the helicopter. The following conclusions can be drawn:

1. Residual energies due to sensing errors of the E field are far in excess of the design objective of 1 millijoule.

2. Readings of E2 show polarity reversals, which most probably are due to the electrification of the plexiglas cockpit enclosure located in the vicinity of the field mill. This points to the fact that plastic covers over the cargo or plastic cargo enclosures could completely falsify the readings of a field meter located on the cargo hook.

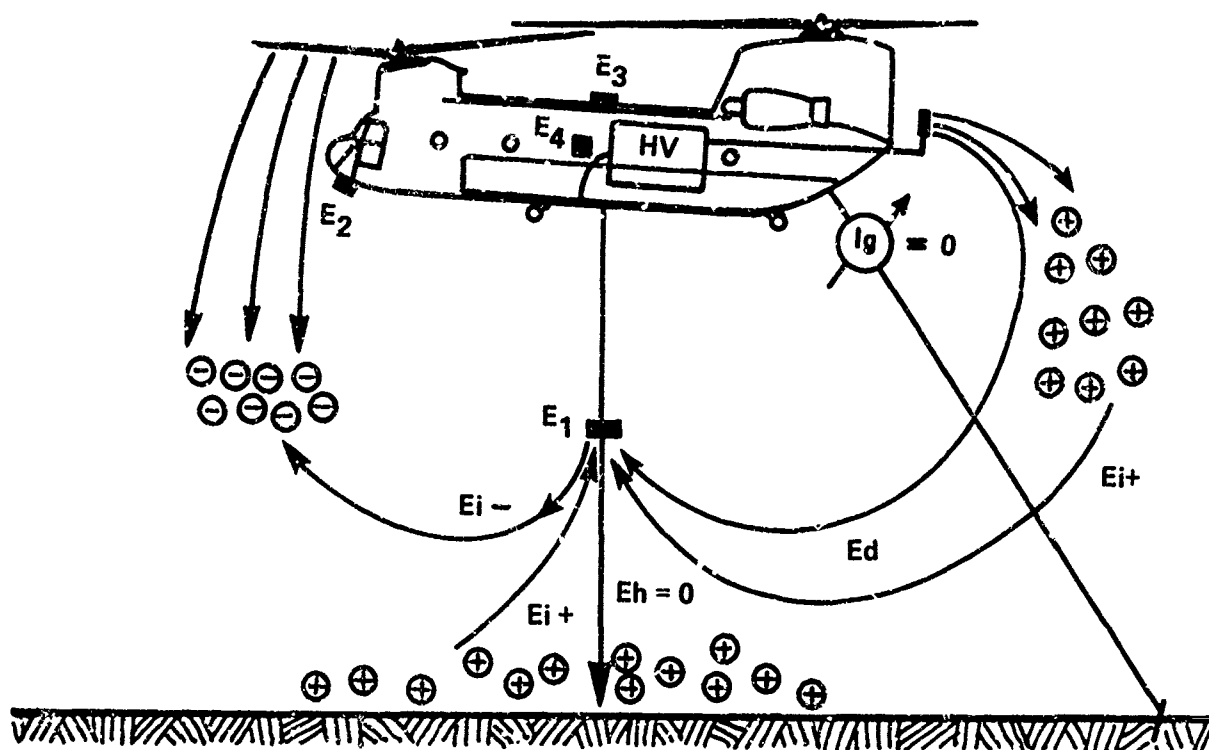
3. The above described series of experiments apply to the conditions over the desert. It can only be speculated that similar conditions (with sign reversal) will prevail over dry snow. No field measurements during charging by rain are known to the writer. This is probably due to practical experimental difficulties of encountering a drizzle under a thunderhead with an instrumented helicopter and an array of field meters on the ground.

4. Measurement errors when under a thunderhead, in a heavy earth gradient, are not known and will be as difficult to acquire as 3. above.

#### SENSING DIRECTLY BY A VOLTMETER

The obvious solution for accurate sensing of the voltage between the cargo hook and the cargo handler appears to be by means of a "infinite impedance" voltmeter and a resistive link to the ground. One such scheme is shown in Figure 7.

This would eliminate the sensor error problems caused by the ion cloud around the helicopter. Since the helicopter could be at a voltage level of  $10^6$  volts, the resistive link would have to be of the order of  $10^9 \Omega$  in order to limit the current flowing through the cargo handler to less than one milliamper, (a level considered acceptable based on experiments by Durbin and Born, see Reference 5).



HOVER ALT	SENSOR	LIGHT WIND HEAD ON			35 KNOTS ABEAM		
		E KV/m	KV	JOULES	E KV/m	KV	JOULES
25 ft	$E_2$ (NOSE)	26	45	2.0	27	47	2.2
25 ft	$E_3$ (TOP)	5	22	.5	6	27	.8
25 ft	$E_4$ (SIDE)	5	45	2.0	6	55	3.0
	$E_1$ (CARGO HOOK OVER DESERT)						
25 ft	25 ft	14	20	.4	—	—	—
25 ft	15 ft	19	8	.06	46	17	.3
25 ft	5 ft	33	7	.05	48	8	.06
50 ft	25 ft	58	32	1.0	—	—	—

Fig. 6 - SOURCES OF MEASUREMENT ERROR



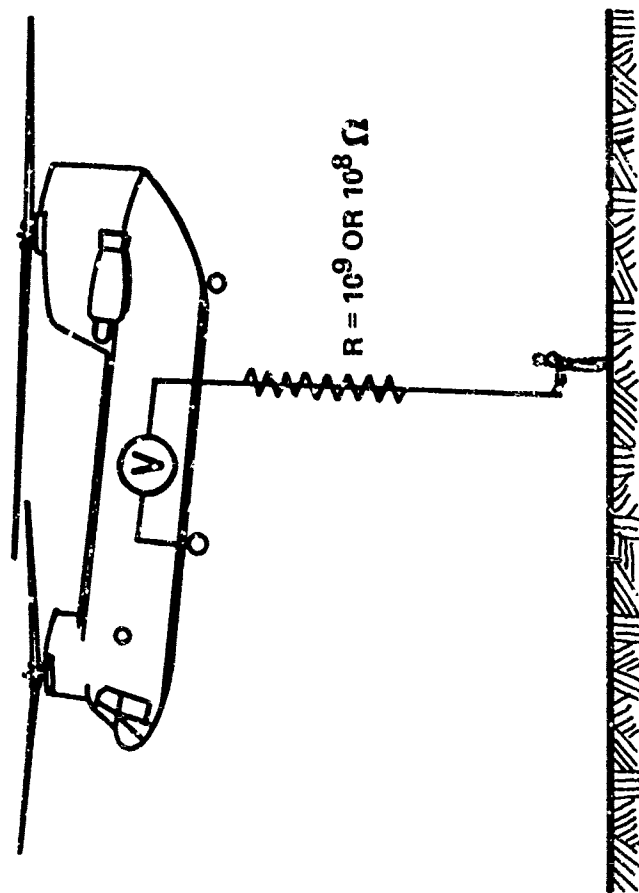


Fig. 7 - INFINITE IMPEDANCE VOLT-METER AND RESISTIVE LINK METHOD  
OF SENSING VOLTAGE BETWEEN CARGO HOOK AND CARGO HANDLER

Durbin and Born point out that by limiting the maximum voltage of the helicopter by passive dischargers, the resistance of the link could be decreased, thus presenting a lesser problem to maintain this resistance under all conditions, e.g. drizzle, dirt on the dropline or insulators. If for example, the passive dischargers would limit the maximum voltage on the helicopter to  $10^5$  volts the resistive link could be of the order of  $10^8 \Omega$ , a value much more readily maintained under field conditions. The length of the required insulator would decrease and the whole problem would become amenable to a good mechanical solution.

#### PASSIVE DISSIPATION

If we give up voltage sensing by field mills and use a dropline - why not give up the expensive active dissipation system, which when failed - can charge the helicopter to a million volt in less than one second? The answer to this question depends on the grounding technology - dropweights, arrows trailing wire, etc. In the last paragraph the measurements of the ground conductivity will be presented. It is advisable to point out here that grounding of the helicopter cannot be by a high resistance link, like the voltmeter link, discussed above. A  $10^8 \Omega$  resistance in presence of 100 microamperes charging current would maintain the helicopter at 10,000 volt and at 600 microamperes at 60,000 volt. Either we accept a low resistance path and sparking on grounding contact or we have to accept programmed resistance starting with a high resistance at ground contact followed by decreased resistance after the contact is made.

Figure 8 gives a schematic example of a purely passive grounding system for a helicopter. It consists of a warning system, a grounding system (dropweight) and a standby grounding system (an arrow trailing steel thread) to be used when the dropweight either cannot be used or the high resistance of the surface must be pierced to achieve good grounding. The success of a passive system design will depend on:

1. How low can we limit the helicopter voltage by means of passive corona dischargers? If this voltage can be kept below 100 KV under heavy

charging conditions, the sparking on grounding can be greatly reduced.

2. Successful mechanical design of the required corona warning, dropweight, arrow discharger, etc.

3. Acceptance of dropline by the military customer.

#### GROUND RESISTANCE

As part of the Yuma flight test program, the desert resistance was measured. A resistance below  $10^6 \Omega$  was measured between a dropweight and a conductive layer of the ground. With a suitable dropweight design it appears that the desert is an acceptable grounding surface. The resistance of dry frosty snow in the Arctic is not known to the writers and will have to be investigated.

#### REFERENCES

1. "Experimental Investigation of Problems Associated with Discharging Hovering Helicopters", J. Nanevich, D. Douglas, S. Blair Poteate, B. J. Solak
2. ECOM 3120 ENSURE 265, CH-54 Electrostatic Discharger Evaluation, by Inslerman, Creed, Barr and Spicer, April 1969
3. RAE Report 71219 November 1971 "Evaluation of an Active Electrostatic Discharger Mounted on the Engine Exhaust of a Helicopter", by T.R. Andrews and R. H. Forrest
4. TRECOM Technical Report 63-43 "A High-Performance Electrostatic Discharger for Helicopters" December 1963, by Dynascience Corporation
5. A Passive Discharge System for the Electrically Charged Hovering Helicopter, G. J. Born and E. G. Durbin

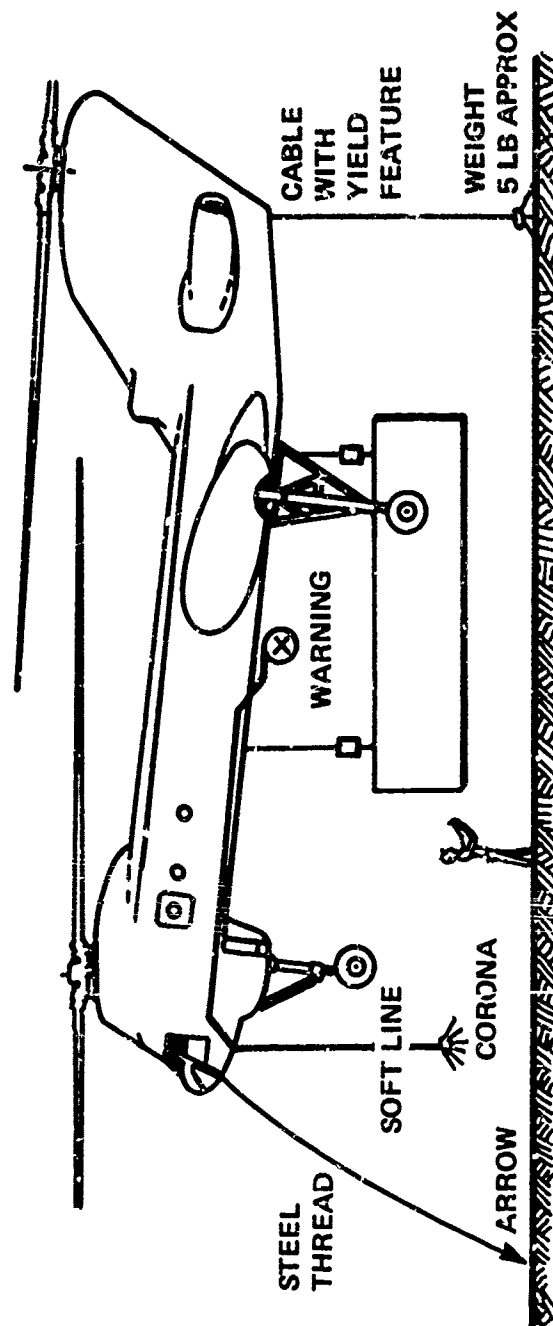


Fig. 8 - EXAMPLE OF A PURELY PASSIVE GROUNDING SYSTEM FOR A HELICOPTER

SESSION IX

WORKSHOP: LIGHTNING SIMULATION, TESTING, AND MIL-B-5087B

J.A. FLUMER, CO-CHAIRMAN & ORGANIZER

GENERAL ELECTRIC HIGH VOLTAGE LABORATORY

and

J.D. ROBB, CO-CHAIRMAN & ORGANIZER

LIGHTNING AND TRANSIENTS RESEARCH INSTITUTE

Introduction to Workshop: Lightning  
Simulation, Testing, and MIL-B-5087B

J.D. Robb  
Lightning & Transients Research Institute

J.A. Plumer  
General Electric Company  
Corporate Research and Development

LIGHTNING EFFECTS on aerospace vehicles are complex because of the variety of components in the natural lightning discharge, the variety of materials and construction techniques used in modern aerospace vehicles and the sensitivity and complexity of their electrical and electronic systems. This is compounded by greater exposure of these systems to lightning by virtue of increased use of titanium or reinforced plastic external skins. These trends also increase the importance of dynamic effects such as the sweeping of lightning discharges over the aircraft surface.

The original lightning bonding specification from which the present MIL-B-5087B has evolved was derived at the first symposium on lightning effects on aircraft (1)\*. Because of the recognized complexity of effects a simplified approach was taken in which a single severe test discharge or combination of test discharges was used to assure satisfactory lightning protection. This was based on the concept that because of its severity, anything that passed this severe test even on a marginal basis should be quite adequate for use in aircraft.

The original maximum test current was 100,000 amperes and was later increased to 200,000 amperes as in the present specification. For the past generation of aircraft, compliance with this severe specification did not substantially penalize the aircraft designs. Also in the early form there was no firm requirement for lightning testing, resulting in incomplete enforcement of the specification requirements. Presently MIL-B-5087B spells out unequivocally that tests must be performed with 200,000 ampere currents to demonstrate protection and, whereas this was considered to be oversevere when first specified, there is some discussion at the present time that 200 kiloamperes may not even be severe enough for a single test stroke concept.

The use, however, of the more sensitive electronic systems and the greater exposure and structural vulnerability of the proposed future aircraft designs requires that a more careful look be taken at the standards such as MIL-B-5087B in order to provide a specification which more carefully matches the actual lightning protection requirements of any particular part of a vehicle to what it will actually be subjected to in flight. For example, it may be oversevere to require 200 kA tests of areas which in all probability will never receive a

single stroke as they are located in what is designated by the FAA as a zone #3 area where neither swept nor direct strokes are probable.

Other tests, to establish adequate lightning protection for electrical or avionics systems, for example, are absent from present specifications, and perhaps should be considered if protection of these critical systems is to be assured. These effects are interrelated with others such as structural materials vulnerability, and it is obvious that a completely detailed specification of tests to assure complete protection of the aircraft may be exceedingly detailed and difficult to define, if only because the design of each new aircraft is unique. Thus, a systems analysis approach may be worth consideration, in which the specification sets protection requirements and gives overall guidance but does not attempt to prescribe the details of each and every test required along the way.

Some greater detailing of the protection requirements is certainly suggested, particularly in view of the increasing use of more vulnerable materials which are more sensitive to over specification. Perhaps a criteria for the degree of detailing needed for such lightning tests as are required can be defined as that degree sufficient to assure identical results from the tests when performed by different laboratories on identical test objects. The resulting consistency in test application would increase confidence and assurance that specified test criteria are being met. At present, for example, MIL-B-5087B alludes to the necessity for high voltage or dielectric breakdown requirements, but fails to define the necessary tests. Laboratories are left to their own judgment in selecting test parameters, and results obtained by one laboratory may not agree with those obtained at another, even though the test objectives may be the same.

There exist some contradictions in the present specifications which are generally recognized as typical problems in any specification for modern complex aerospace vehicles. One of these is the bonding requirement for conductivity between all adjacent metal sections, which contradicts the corrosion requirements of complete insulation between metal sections. An additional example is in the strict interpretation of the bonding requirements which would require bonding between

\*Numbers in parentheses designate References at end of paper.

helicopter rotors and the fuselage. Whereas this might be possible, it would be extremely difficult and there is no evidence yet to indicate that it is necessary in view of the massiveness of the bearings required to carry the flight loads. Thus, some additional detailing of the present MIL-B-5087B specification with respect to these contradictions is certainly suggested.

The Session panel has been selected specifically to represent knowledgeable engineers who are actively involved in lightning design and testing of aircraft, and familiar with recent research and development advances in this field. It is hoped that from this meeting new suggestions may be brought out for improvement of the specification and for better lightning simulation for aerospace vehicle testing, from which a reasonably balanced approach can be developed between extremes of a single very oversevere discharge, or a multiple number of detailed test current waveforms applied for each particular vehicle or component being tested. The improved specifications, to which we hope these discussions will contribute, can lead to an overall increase in the economy, efficiency and reliability with which lightning protection is provided for modern aircraft.

#### REFERENCE

1. L&T Report No. 100, Proceedings, 1948 Symposium on Lightning Protection for Aircraft, November, 1948.

British Civil Airworthiness Requirements for  
Electrical Bonding and Lightning Discharge  
Protection in Relation to Specification  
MIL-8-5087

B L Perry  
UK Civil Aviation Authority  
(Airworthiness Division.)

ABSTRACT

A revision to the bonding and lightning discharge protection standards of the British Civil Airworthiness Requirements (BCAR's), has recently been proposed in order to update these in relation to the latest knowledge and experience on aircraft and equipment. The changes made relative to current British and Anglo French requirements are discussed and it is suggested that this document could, in conjunction with a revision of specification MIL-8-5087, form the basis of a common international standard.

A REVIEW HAS BEEN UNDERTAKEN of the existing bonding requirements as detailed in BCAR's Chapter D4-6, in the light of current UK and US experience. This has shown the need to revise the current standards to match the increased system complexity, and possible vulnerability, of modern aircraft, including powered-lift machines and to take into account the use of new materials and construction techniques. The proposed changes are discussed in detail below and include the experience gained from recent FAR's and the Anglo French supersonic transport standard TSS 8-6.

SUMMARY OF PROPOSED CHANGES

**AIRCRAFT SHAPE** - It has been found convenient to define three zones on the external surface of the aircraft, each having different lightning strike probabilities. For aircraft of conventional shape, flight experience has confirmed the validity of the zones defined in TSS 8-6 and FAA Advisory Circular AC 20-53. However, for an aircraft of non conventional shape these zones may require redefining and the proposed amendment takes account of this and suggests the use of model testing as a guide to zone definition. It is also proposed that the scope of the zoning be widened to take account not only of the effects of lightning on fuel systems but other effects such as those on structural materials, or equipment and wiring located in these zones.

**AIRCRAFT ALTITUDE** - it is possible that powered-lift aircraft in particular may operate for longer periods at altitudes where the probability of a lightning strike is at its highest i.e. approx. 80% of strikes occur between 2000 ft. and 12,000 ft. No changes are proposed to cover specifically this case, since it should be covered within the basic requirements or taken into account for any probability arguments.

**ENGINE ARRANGEMENTS** - on conventional aircraft there is little evidence to suggest that the jet efflux, which may be ionized, increases the risk of air to air lightning strikes. Nevertheless it is possible that, on an aircraft using a multiplicity of engines in the lift mode, the risk of air to ground strikes could be appreciably increased (cf Apollo 12). While not directly covered, this aspect is emphasized under the section dealing with system effects, particularly as regards the possible effects on engine control systems and autoland systems in the critical, near the ground, regimes. It is also possible that the use of multiple lift engines, with an increase in (possibly) ionised jet efflux, may increase the static charging of the aircraft with resultant interference problems. This effect is also emphasized in the applicable sections of the requirements.

**MATERIALS** - With the increasing use of modern materials and construction techniques the text and appendix has been re-written, as appropriate, to emphasize the hazards. Among the most important materials and effects are the following:-

a) Non conducting materials such as fibre glass or all plastic honeycomb. Mechanical damage may be caused to such materials by the passage through them of a lightning strike with possible resultant effects on the airframe or other systems. Loss of the intrinsic screening of airframe mounted systems or equipment must also be considered, see also para on Systems below.

b) Composite materials such as metal skinned plastic honeycomb or plastic skinned metal honeycomb.

Effects similar to those listed above depending on the materials used and their construction.

c) Carbon (or boron) fibre reinforced plastics.

Effects similar to those listed above with, in addition, possible severe degradation of the mechanical strength of the material if it is used in such a way as to make it possible for the conducting fibres to carry lightning currents. Present evidence in the USA (and to a lesser extent recent UK testing) indicates that in such cases the material must be protected by a conducting cage which prevents such current flow.

d) Modern paint finishes.

Such paints as epoxy, acrylic or polyurethane are particularly good electrical insulators and experience has shown that on some aircraft an appreciable static build up can occur with resultant interference with aircraft systems. There are also some indications that such paint finishes can affect the path and restrike locations of swept lightning strokes.

SYSTEMS - There is an increasing tendency for aircraft to use more complex electrical control systems operating at low signal levels. This will be particularly true of powered-lift machines in such areas as engine or lift device control, stability augmentation systems and automatic landing systems.

Such modern systems are not only more vulnerable to interference effects from lightning or static but also the effect of such system interference on the aircraft itself could be more serious. The increased use of non-metallic structure can also decrease the screening effect of the airframe on the circuits involved. The relevant sections of the requirements have therefore been amended to emphasize these dangers.

CHARACTERISTICS OF LIGHTNING DISCHARGES - In the light of more recent information, the lightning stroke, and suggested test current characteristics, are revised in line with TSS 8-6. It is accepted that these test current characteristics are not the optimum and a UK research programme is under way, one object of which is to provide the data on which a final review can be made. At this stage however, the best data available is considered to be that given in TSS 8-6.

RESISTANCE AND CONTINUITY - This section has been rewritten in a similar manner to TSS 8-6 and the table of resistance values included as appendix guidance material rather than in the main text. This change is based upon the results of an investigation carried out among UK constructors and operators at the time of writing TSS 8-6 and is felt to represent more nearly the current position.

#### PROPOSED REQUIREMENTS FOR ELECTRICAL BONDING AND LIGHTNING DISCHARGE PROTECTION

1. INTRODUCTION - This Chapter prescribes requirements and its Appendices give recommended practices relating to the following subjects:-

1.1 The protection of the aircraft against lightning discharges.

1.2 The electrical bonding of the aircraft structure, components and equipment in order:-

(a) to prevent dangerous accumulation of electrostatic charges,

(b) to minimize the possibility of electric shock from the electricity supply and distribution system,

(c) to provide an adequate electrical

return path on aircraft having earthed electrical systems,

(d) to prevent interference with the functioning of essential services (e.g. radio communications and navigational aids), and

(e) to prevent deterioration of structural strength or deformation, particularly of composite material structures (see App. No. 1, para. 8)

2. PRIMARY AND SECONDARY CONDUCTORS - (see App. No. 1, para. 6) For the purposes of this Chapter Primary Conductors shall be those conductors which are required to carry lightning discharge currents, and Secondary Conductors shall be those conductors provided for other forms of bonding.

2.1 The cross sectional area of Primary Conductors made from copper shall be not less than 3 mm<sup>2</sup> (approx. 0.0045 sq. ins., i.e. 0.25 in. by 26 SWG) except that where a single conductor is likely to carry the whole discharge from an isolated section, the cross sectional area shall be not less than 6 mm<sup>2</sup> (approx. 0.009 sq. in., i.e. 0.5 in. by 26 SWG). Aluminium Primary Conductors shall have a cross sectional area giving an equivalent surge carrying capacity.

2.2 Primary Conductors shall be used for:-

(a) Connecting together the main earths of separable major components which may carry lightning discharges.

(b) Connecting engines to the main earth (see para. 5).

(c) Connecting to the main earth all metal parts presenting a surface on or outside of the external surface of the aircraft (see para. 3.1.2).

2.3 The electrical impedance of Primary Conductors to a lightning discharge shall be as low as is practicable.

2.4 The cross sectional area of Secondary Conductors made from copper shall be not less than 1 mm<sup>2</sup> (approx. 0.001 sq. in.). Where a single wire is used its size shall be not less than 1.2 mm dia (18 SWG).

3. PROTECTION AGAINST LIGHTNING DISCHARGES - (see App. No. 1, para. 8). -

3.1 The aircraft shall be effectively provided with means to conduct lightning strikes, the characteristics of which are described in App. 1, so that the aircraft or its occupants will not be endangered. Account shall be taken of the Lightning Strike Zones detailed in Appendix No. 1, para. 3. The means provided shall be such as to:-

(a) Minimise damage to the aircraft structure or components.

(b) Prevent the passage of such electrical currents as will cause dangerous malfunctioning of the aircraft or its equipment.

(c) Prevent the occurrence of high potential differences within the aircraft.

3.1.1 Compliance with para 3.1 shall be established by the provision of an electrically conducting cage in accordance with para. 3.1.4(a), (b) or (c) as applicable.



This cage shall either constitute or be electrically connected to the main earth system.

### 3.1.2 External Metal Parts

External metal parts shall either be:-

(a) electrically bonded to the main earth system by primary bonding, or

(b) so designed and/or protected that a lightning discharge to the part (e.g. a radio aerial) will cause only local damage which will not endanger the aeroplane or its occupants.

3.1.2.1 In addition, where internal linkages are connected to external parts (e.g. control surfaces), the linkages shall be bonded by primary bonding as close to the external part as possible.

3.1.2.2 Where a primary bond is fitted across an operating jack (e.g. on control surfaces or nose droop) it shall be of such an impedance and so designed as to limit to a safe value the passage of current through the jack.

NOTE: In considering external metal parts, consideration should be given to all flight configurations (e.g. lowering of undercarriage and wing-flaps) and also the possibility of damage to the aeroplane electrical system due to surges caused by strikes to protuberances (such as pitot heads) which have connections into the electrical system.

3.1.3 External Non-metallic Parts. (see also Appendix No. 1, para 8).

External non-metallic parts shall be so designed and installed that:-

(a) they are provided with effective lightning diverters which will safely carry the lightning discharges described in Appendix 1, or

(b) damage to them by lightning discharges will not endanger the aeroplane or its occupants, or

(c) a lightning strike on the insulated portion is improbable because of the shielding afforded by other portions of the aeroplane.

3.1.3.1 Where lightning diverters are used the surge carrying capacity and mechanical robustness of associated conductors shall be at least equal to that required for Primary Conductors.

### 3.1.4 Electrically Conducting Cage

(a) Aircraft of Metallic Construction.

In general the skin of an all-metal aircraft will be accepted as adequate to meet the requirements of 3.1.1 provided that the method of construction is such that it produces satisfactory electrical contact at joints.

NOTE: An electrical contact with a resistance less than 0.05 ohm will be considered as satisfactory.

(b) Aircraft of Non-metallic Construction (see App. No. 1, para 5). The cage shall consist of metallic conductors the surge carrying capacity and mechanical robustness of which are at least equal to that required for Primary Conductors. The conductors shall be as straight as practicable, and where changes

of direction are unavoidable, sharp curves shall be avoided.

All metal parts shall be bonded to the cage with Primary Conductors as appropriate. Guidance on the probability of a lightning strike, and hence the need to bond, is given in Appendix No. 1, para. 3.

(c) Aircraft of Composite Construction. Where component parts of an aircraft are of non-metallic construction, protection shall be provided, as appropriate. If in the form of a cage this shall meet the relevant parts of (b). When designing such protection the possible effects outlined in Appendix No. 1 para. 8 shall be taken into account.

## 4. PROTECTION OF FUEL SYSTEM - (see also Appendix No. 1, para. 4)

4.1 The fuel storage system of the aeroplane shall either be so:-

4.1.1 situated that it is improbable that it will be struck by lightning, or

4.1.2 protected that in the event of it being struck by lightning a catastrophe is not likely to occur.

4.2 The outlets of venting and jettisoning systems shall be so located and designed that:-

4.2.1 it is improbable that they will be struck by lightning,

4.2.2 they will not under any atmospheric conditions which the aeroplane may encounter experience electrical discharges of such magnitudes as will ignite any fuel/air mixtures of the ratios likely to be present, and

4.2.3 the fuel and its vapours in flammable concentrations will not pass close to parts of the aeroplane which will produce electrical discharges capable of igniting fuel/air mixtures.

NOTE: Electrical discharges may, in addition to direct lightning strikes, be caused by corona and streamer formation in the vicinity of thunderstorms.

4.3 The fuel system of the aeroplane shall be so designed that the passage of lightning discharges through the main aeroplane structure will not produce, by the processes of conduction or induction, such potential differences as will cause electrical sparking through areas where there may be flammable vapours.

4.4 Consideration shall be given, during the design of the system, to the effect of the accumulation of static charges (see paras. 6.4 and 6.5).

5. ENGINES AND ENGINE MOUNTINGS - Where the engine is not in direct electrical contact with its mounting the engine shall be electrically connected to the main earth system by at least two removable Primary Conductors, one on each side of the engine.

## 6. PROTECTION AGAINST THE ACCUMULATION OF STATIC CHARGES - (see also Appendix No. 1 para. 8)

6.1 General. All items, which by the accumulation and discharge of static charges

may cause a danger of electric shock, ignition of inflammable vapours, or interference with essential equipment, e.g. radio communications, navigational aids, or other vital control systems, shall be adequately bonded to the main earth systems.

Account shall be taken, in the design and location of systems or equipment, of the possibility of electrostatic charging from the jet efflux of the engines.

NOTE: See para. 8 for resistance values appropriate to various forms of bonding.

6.2 Intermittent Contact. The design shall be such as to ensure that no fortuitous intermittent contact can occur between metallic and/or metallized parts.

6.3 Grounding of Main Earth System. The main earth system shall be connected to ground automatically when the aircraft is on the ground. The resistance between the main earth system and the ground, when the aircraft is at rest, shall not exceed 10 megohms.

NOTE: The resistance should be measured between the main earth system and a metal plate on which the earthing means, e.g. tyre, is resting.

6.4 Filling Points. It shall readily be possible to bond refuelling equipment, including the refuelling nozzle, to the aeroplane and to make the bonding connection before the filler cap is removed. The efficiency of the connection shall be independent of the particular type of refuelling equipment being used.

6.5 High Pressure Refuelling and Fuel Transfer. (see also Appendix No. 1, para. 7) Where provision is made for high pressure refuelling and/or for high rates of fuel transfer it shall be established, by test, or by consultation with the appropriate fuel manufacturers, that dangerously high voltages will not be induced within the fuel system. If compliance with this requirement involves any restriction on the types of fuel to be used or the use of additives, this shall be stated in the Flight Manual and placarded at the refuelling point.

7. MANDATORY RADIO EQUIPMENT - The requirements of this paragraph 7 are applicable to the installation of mandatory radio equipment in aircraft.

NOTES: (1) In the case of aircraft fitted with mandatory radio receiving or transmitting apparatus an additional reason for bonding is to provide an earth system of low resistance and maximum self capacity for the efficient operation of the radio equipment.

(2) See also Section R "Radio".

7.1 The metal frame and mounting structure carrying each radio unit shall be bonded to the main earth by at least one Primary Conductor or its equivalent.

7.2 Within a radius of 2.4 metres (8 feet) of any unscreened radio and radio transmitting equipment or its aerial lead, any long electrically conducting parts (including metallic pipe lines and metal braiding and conduit)

which are not insulated from earth, shall be electrically bonded to the main earth system.

7.3 Provision shall be made for the bonding of all radio transmitting and receiving apparatus to the main earth by means of one or more Primary Conductors, or their equivalent. In the case of aircraft of non-metallic or composite construction, the main bonding strips shall be connected together near these points with Primary Conductors.

8. RESISTANCE AND CONTINUITY MEASUREMENTS - (see also Appendix No. 2) The aeroplane constructor shall prepare and submit to the Certification Authorities a schedule for resistance and continuity measurements, which shall contain, as a minimum the data prescribed in para. 8.1 to para. 8.3. The measurements shall also be made on all series aeroplanes.

8.1 A description of the measuring apparatus to be used with a statement of the accuracy which is claimed for the equipment.

8.2 A description of the method, or methods, to be employed for the attachment of the test apparatus to the aeroplanes and its equipment.

NOTE: Where the type of apparatus employed and/or its method of attachment produces test values in excess of those given in Appendix No. 2, the background evidence to show the acceptability of such methods should be detailed.

8.3 A detailed list of all points on the aeroplane, including its equipment, for which measurements are required and for each set of measurements the maximum acceptable resistance. Measurements are required to determine the efficacy of bonding and connection between, at least, the following:-

8.3.1 Primary Bonding

(a) the extremities of the fixed portions of the aeroplane and such fixed external panels and components where the method of construction and/or assembly leads to doubt as to the repeatability of the bond, e.g. removable panels,

(b) the engines and the main aeroplane earth,

(c) external movable metal surfaces or components and the main aeroplane earth,

(d) the bonding conductors of external non-metallic parts and the main aeroplane earth, and

(e) internal components for which a Primary Bond is specified and the main aeroplane earth.

8.3.2 Secondary Bonding

(a) metallic parts, normally in contact with flammable fluids, and the main aeroplane earth,

(b) isolated conducting parts subject to appreciable electrostatic charging and the main aeroplane earth,

(c) electrical panels and other equipment accessible to the occupants of the aeroplane and the main aeroplane earth, to avoid the danger of electrical shock from

circuits of 50 volts (RMS or DC) or more.

(d) earth connections, which normally carry the main electrical supply and the main aeroplane earth. The test on these connections shall be such as to ensure that the connections can carry, without risk of fire or damage to the bond, or excessive volt drop, such continuous normal currents and intermittent fault currents as are applicable.

(e) electrical and electronic equipment and the aeroplane main earth, where applicable, and as specified by the aeroplane constructor,

(f) static discharger wicks and the main aeroplane structure, and

(g) the main aeroplane earth system and ground, measured when the aeroplane is at rest.

#### APPENDIX NO. 1

1. ELECTRICAL CHARACTERISTICS OF LIGHTNING DISCHARGES - In the absence of better information the data contained in this Paragraph 1 should be used for the purpose of assessing the adequacy of lightning discharge protection of aeroplanes. Table 1 shows typical lightning characteristics.

NOTES: (1) The duration of flash may be made up of a number of discharges.

(2) For the purposes of test or assessment, a discharge current having two components (as in Table 2, Appendix No. 1) may be taken as being equivalent to a lightning strike from the aspects of heating and disruptive forces.

#### 2. THE PROTECTION OF EXTERNAL NON-METALLIC PARTS -

2.1 Where non-metallic parts are fitted externally to the aeroplane in situations where they may be exposed to lightning discharges (e.g. radomes) the risks include the following:-

2.1.1 the disruption of the materials because of rapid expansion of gases within them (e.g. water vapour),

2.1.2 the rapid build up of pressure in the enclosures provided by the parts resulting in mechanical disruption of the parts themselves or of the structure enclosed by them,

2.1.3 fire caused by the ignition of the materials themselves or of the materials contained within the enclosures, and

2.1.4 holes in the non-metallic part which may present a hazard at high speeds.

2.2 The materials used should not absorb water or occlude gases, and should be of high dielectric strength in order to encourage surface flash-over rather than puncture. Laminates made entirely from solid material are preferable to those incorporating laminations of cellular material.

2.3 Those external non-metallic parts which are classified as Primary Structure should be protected by Primary Conductors.

2.4 Where damage to an external non-metallic part which is not classified as Primary Structure may endanger the aeroplane, the part should be protected by adequate

lightning diverters.

2.5 In some cases (e.g. radomes) confirmatory tests may be required to check the adequacy of the lightning protection provided.

#### 3. LIGHTNING STRIKE ZONES -

3.1 Lightning Strike Zones. It is convenient to define three zones on the external surface of the aeroplane, each having a different lightning strike probability. (but see para. 3.1.4 for aircraft of non-conventional shape).

3.1.1 Zone 1. Surfaces of the aeroplane for which there is a high probability of direct stroke attachment. These areas are:-

(a) within 0.5 metre (18 inches) of any trailing edge or tail extremity,

(b) within 0.5 metre (18 inches) of wing tip measured parallel to the tip,

(c) within 0.5 metre (18 inches) of any sharp leading edge which is likely to form a point of attachment for lightning strikes,

(d) forward unprotected projections (e.g. nose of aircraft, engine nacelle forward of wing), and

(e) any other projecting part may constitute a point of attachment.

3.1.2 Zone 2. Surfaces for which there is a probability of strokes being swept rearward from a Zone 1 point of direct stroke attachment (e.g. fuselage nose). Zone 2 extends 0.5 metre (18 inches) laterally to each side of fore and aft lines passing through Zone 1 forward projection points of stroke attachment. All fuselage surfaces and surfaces of nacelles not defined as Zone 1 are included in Zone 2 unless it can be shown, for example, that certain nacelle surfaces are adequately protected by their position relative to the wing.

3.1.3 Zone 3. Surfaces for which there is only an Extremely Remote probability of direct or swept strokes. Ignition sources in these are as would exist only in the event of streamer. This zone includes all surfaces of the aeroplane not coming under the definitions for Zones 1 and 2.

3.1.4 General. Guidance on the Zones for a particular aeroplane configuration may be obtained by simulated lightning strike tests on a model aeroplane. Such testing is particularly desirable for aircraft of non-conventional shape.

4.1 Available data indicates that effective fuel system lightning protection is obtained if:-

(a) in Zone 1, the protection takes account of all fuel system parts, direct strokes, the attendant blast effects, and possible penetration, vent outlets are protected against the effects of direct stroke attachment and semi-insulated fuel system parts are designed to prevent sparking when flammable vapours can exist.

(b) in Zone 2, vent outlets and semi-insulated fuel system parts are protected

TABLE 1 (APPENDIX NO. 1)

Charge transfer	maximum normal	600 coulombs 50 to 200 coulombs
Peak current	maximum normal	500 kA about 50 kA
Duration of flash	maximum	2 seconds
Duration of peak current	about 25 micro seconds to half peak value, critically damped	

TABLE 2 (APPENDIX NO. 1)

Component	Peak current	Duration	Charge transfer
1	200 kA	To crest value in 15 micro seconds decaying to 50000 amperes in 30 micro seconds from initiation	4 coulombs
2	500 amperes	1 second rectangular wave	500 coulombs

TABLE 3 (APPENDIX NO. 1)

FUEL SYSTEM PART	ZONE 1	ZONE 2	ZONE 3
Tank skin	Aluminium alloy thicker than 2 mm (0.080 in) or equivalent	-  * See Note	-
Flush or recessed fuel vent outlets	Protect against direct strokes and streamering	Protect against direct strokes and streamering	-
Protruding types of fuel vent outlets	Protect against direct strokes and streamering	Protect against direct strokes and streamering	Protect against streamering
Access doors, filler caps and other semi- insulated parts	Protect against direct stroke attachments	Protect against direct stroke attachments	-

\*NOTE: Protection may be required for those tank surfaces which are exposed to swept strokes.

in the same manner as for Zone 1.

(c) in Zone 3, vent outlets having a protruding configuration are protected to avoid ignition of fuel vapours by streamering.

4.2 A tabular description of Zones and protection guidelines is given in Table 3 (Appendix No. 1).

4.3 General Guidelines for Detailed Design Features

4.3.1 Access Doors and Filler Caps

(a) Positive measures should be taken to prevent internal arcing and sparking such as:-

(i) the provision of a continuous and good electrical contact around the entire periphery of the part, and

(ii) to design the part in such a way that any arcing or sparking which might occur would take place on the outside of the fuel tank rather than on the inside.

(b) At present the only satisfactory method of evaluating the efficacy of the precautions described in para. 3.3.1(a) has been found to be by testing using discharges equivalent to those given in Table 2 (Appendix No. 1) for component's 1 and 2.

NOTE: A suitable test method is described in FAA Advisory Circular AC 20-53, which cancels and replaces AC 25-3A.

4.3.2 Vent Outlet Designs. Vent outlet configurations can usually be described in three general classes as described in para. 3.3.2(a) to (c).

NOTE: Lockheed Report, Document NASA TN D-2240 'Investigation of Mechanisms of Potential Aircraft Fuel Tank Vent Fires and Explosions caused by Atmospheric Electricity', includes a description of typical designs.

(a) Class 1. A mast type vent which discharges into the outlet wake with mixing taking place downstream (e.g. Figure 8(a) of Lockheed Report).

(b) Class 2. A mast type vent discharging into the free stream. In this case the vent outlet is separated from the external surface sufficiently to discharge the fuel vapours away from the boundary layer (e.g. Figure 8(b) of Lockheed Report).

(c) Class 3. Flush type vent designs discharging into the boundary layer (e.g. Figures 8(a), (d), (e) and (f) of Lockheed Report).

(d) Class 1 and 2 vents are considered likely points for streamer formations whereas Class 3 vents are not.

(e) The evaluation of venting systems having outlets located in Zones 1 and 2, regardless of the class of outlet configuration, involves consideration of all conditions resulting from a lightning strike at or near the outlet (including blast pressures). Various means of preventing ignition or arresting flame propagation are considered feasible; however the actual performance of the protective means is not usually predictable without suitable testing. Some examples of protective means are:-

(i) dilution of vented vapours with free air to keep the mixtures in the 'too lean' range,

(ii) acceleration of the vented vapours by ram air to an exit speed above the flame propagation speed,

(iii) flame arresters,

(iv) fire and explosion suppression devices, and

(v) use of an inert atmosphere in the venting system.

(f) For vent outlets which are located in Zone 3, the flush designs (Class 3) are considered relatively immune from streamer formations, whereas the protruding types (Classes 1 and 2), are considered to be likely points for streamer formations and protection of the vent against flame propagation is important. A flame arrester could furnish this protection; however the design conditions for the flame arrester would not be as severe as in the case of vents located in Zones 1 and 2 because of the absence of blast pressure effects. Tests conducted to show the flame propagation characteristics through vent outlets located in Zone 3 can be conducted with a low energy source for ignition (e.g. a spark plug).

4.3.3 Flame Arresters. The only reliable method for determining the capability of a flame arrester design is to test it under pressure characteristics likely to be encountered from a natural lightning stroke and with a reasonably accurate reproduction of the actual vent design including tuoling bends, obstructions and outlet shape. Evaluation of the flame arrester also includes the determination that no hazards (e.g. icing) are introduced by the addition of the flame arrester.

4.3.4 The Protection of Fuel Tanks. In order to avoid the risk of lightning discharge to fuel tanks the surfaces of which are effectively part of the external surface of an aircraft the following precautions should be observed:-

(a) Fuel should not be stored in the leading or trailing edges of wings, tailplanes, fins, etc., or in the extremities of the fuselage.

(b) Fuel should not be stored within 0.5 metre (18 inches) of the tips of wings, etc.

(c) The exposed external surfaces of the tanks should be free of sharp projections, edges or small radii.

Where it is not possible to situate tanks which are effectively part of the external surface of the aircraft as described in para. 4.3.4 (a) and (b) (e.g. in the case of wing tip tanks) precautions as detailed in para. 4.3.4.1 or 4.3.4.2, as appropriate, should be taken.

4.3.4.1 Metal Tanks

(a) Measures should be taken to prevent explosive mixtures from occurring within the tank, or

(b) It should be established that an explosion occurring within the tank would not cause a catastrophe, or

(c) Where exposed to lightning strikes, the tank wall thickness should not be less than 0.08 in. Additionally, the exposed extremities of tip and pod tanks should not contain fuel. The exposed external surfaces of the tanks should be smooth, or

(d) The exposed ends of the tank should not contain fuel and the tanks should be fitted with adequate lightning diverters. In such cases the walls of the tank should not be less than 0.04 in. thick.

4.3.4.2 Non-metallic Tanks. The exposed ends of the tank should not contain fuel and the external surfaces of the tank should be protected by lightning diverters at least to the standard required for non-metallic aircraft. The inside of the tank should be kept as free as possible of metal work and such metal work should be bonded by primary conductors to the main earth system of the aircraft at the root of the tank. The internal bonding system should be so designed and arranged in relation to the lightning diverters that it will not constitute a path for the discharge in the case of the tank being struck by lightning.

#### 5. MAIN EARTH SYSTEMS FOR AIRCRAFT OF NON-METALLIC CONSTRUCTION -

##### 5.1 Fuselage

5.1.1 Four or more conductors, extending the whole length of the fuselage, should be provided. The number and disposition of these conductors should be such that they are not more than 2 metres (6 feet) apart as measured round the periphery of the fuselage at the position of greatest cross sectional area. The conductors should be placed on or near the outer skin at approximately equal intervals and joined together at their ends in the manner described in para. 5.6.

5.1.2 The conductors described in para. 5.1.1 should be inter-connected by similar conductors at positions corresponding to the terminals provided for inter-connecting the wing and fuselage main earth systems and intermediately at intervals not exceeding 6 metres (20 feet).

5.2 Wings and Tailplanes. Conductors, extending from root to tip, should be provided in accordance with Table 4 (App. No. 1). The wing or tailplane root end of each conductor should be connected to the fuselage main earth system, and the outboard ends should be connected in the manner described in para. 5.6. The strips should be transverseley interconnected by similar strips at intervals not exceeding 6 metres (20 feet).

5.3 Fin and Rudder. A conductor should be disposed at the leading edge of the fin and down the rudder post. A further conductor should be provided at the trailing edge of the rudder. These conductors should be connected to at least each end hinge and to the fuselage main earth.

5.4 Elevators. A conductor should be provided at the trailing edge of each elevator. The conductors should be connected to at least each end hinge and to the fuselage main earth.

5.5 Ailerons and Wing-Flaps. All aileron and wing-flap hinges should be connected to the wing main earth, and a conductor on or near the trailing edge of each aileron and wing-flap should be connected to each end hinge and to the wing main earth.

5.6 Lightning Strike Plates. Lightning strike plates, extending round the edge of each extremity of each wing and tailplane, and round the nose and tail of the fuselage, should be provided on the exterior of the aircraft structure except where existing metallic structure can serve the same purpose. The strike plates may be covered with dope, fabric, paint, etc., if desired. Each strike plate should consist of a strip of copper of not less than 2.5 mm width x 0.45 mm (1 in. width x 26 SWG) thickness, or other material of equivalent surge current capacity and mechanical robustness; the plate should be of sufficient length to extend on both sides to a distance of 600 mm (24 in.) as measured from the outer extremity, and should form the means of joining together the ends of the main earth conductors at these extremities.

#### 6. PRIMARY CONDUCTORS -

6.1 The joints detailed in this paragraph 6.1 are acceptable as parts of the Primary Conductors:-

6.1.1 Provided that all insulating finishes are removed from the contact area before assembly, metal-to-metal joints held together by threaded devices, riveted joints, structural wires under appreciable tension, and bolted and clamped fittings.

NOTE: A surface anodised in accordance with Specification DTD.910B is an almost perfect insulator for a potential difference of less than 130 volts, but the surface is readily broken by the rotation of a bolt head or the forming of a rivet. In these latter cases it is unnecessary to remove the anodic finish. However, when two anodised parts are clamped together without any relative motion being involved, the anodised surface should be removed over an area strictly limited to that necessary to ensure efficient electrical contact, and the assembly coated with a suitable protective material such as a jointing compound containing barium chromate.

6.1.2 Most cowl fasteners and locking and latching mechanisms, provided that the current path is of sufficiently low impedance.

6.1.3 Metal-to-metal hinges for doors and panels and metal-to-metal bearings (including ball bearings). In the case of bearings in control surface hinges either it should be demonstrated by test or by reference to relevant experience that the bearings will withstand a lightning discharge without dangerous seizure or the bearings should be bonded across by a jumper. In the latter case,

TABLE 4 (APPENDIX NO. 1)

Wing or Tailplane Root Chord (metres)	Minimum Number of Conductors	Approximate position
Less than 2.5	2	At leading edge and trailing edge.
2.5 - 4.5	3	At leading edge, trailing edge and mid chord.
4.5 or more	4	At leading edge, trailing edge, $1/3$ chord and $2/3$ chord.

NOTE: "Trailing edge" in Table 4 (App. No. 1) refers to that of the fixed wing or tailplane structure only. "Wing root chord" excludes fillets, but includes wing-flaps in the retracted position.

bonding jumpers should be as flexible and as short and of as low an impedance as is practicable and should not be tinned. Great care should be taken to avoid any possibility of the jumper jamming the controls even when the jumper is disconnected.

#### 7. ELECTROSTATIC VOLTAGE INDUCED DURING HIGH PRESSURE REFUELLING -

7.1 With standard refuelling equipment and standard aircraft turbine fuels, voltages high enough to cause sparking may be induced between the surface of the fuel and the metal parts of the tank at refuelling rates above 250 gal/min. These induced voltages may be increased by the presence of additives and contaminations (e.g. anti-corrosion inhibitors, lubricating oil, free water), and by splashing or spraying of the fuel in the tank.

7.2 The static charge can be reduced in the following ways:-

(a) By measures taken in the refuelling equipment such as increasing the diameter of refuelling lines and designing filters to give the minimum of electrostatic charging.

(b) By changing the electrical properties of the fuel by the use of anti-static additives and thus reducing the accumulation of static charge in the tank to a negligible amount.

(c) Floor-filling of each compartment.

7.3 The critical refuelling rates are related to the aircraft refuelling installations, and the designer should seek the advice of fuel suppliers on this problem.

#### 8. THE USE OF NON-METALLIC MATERIALS RELATIVE TO ATMOSPHERIC ELECTRICAL HAZARDS -

8.1 Some of the materials used and possible effects upon the aircraft and its systems are considered below.

(a) Non conducting materials such as fibre glass or all plastic honeycomb.

Mechanical damage may be caused to such materials by the passage through them of a lightning strike, with possible resultant effects upon the airframe on other systems (see also App. No. 1 para. 2). Loss of the intrinsic screening provided by a metal airframe must also be considered and the possible interference, by lightning strikes or static discharges, with critical control systems, taken into account.

(b) Composite materials such as metal skinned plastic honeycomb or plastic skinned metal honeycomb.

Effects similar to those in (a) above depending upon the materials used and their location.

(c) Carbon (or Boron) fibre reinforced plastics.

Effects similar to those listed in (a) above with, in addition, possible severe degradation of the mechanical strength of the material if it is used in such a way as to make it possible for the conducting fibres to carry lightning currents. Present evidence indicates that, in such cases, the material must be protected by a suitable conducting

cage.

(d) Paint finishes.

Certain paints are particularly good electrical insulators and experience has shown that an appreciable static build up can occur with resultant interference with aircraft systems. There are also indications that such paint finishes can affect the path and restrike locations of swept lightning strokes.

8.2 In general, some form of high voltage/current tests will be required to give confidence that structure will not be damaged in such a way as to hazard the aircraft. Close attention will be required both in the design of the airframe and of the systems to ensure that electrical interference effects are minimised. Where appropriate, tests will be required to ensure that these design aims have been satisfied.

#### APPENDIX NO. 2

##### 1. MEASUREMENT OF ELECTRICAL RESISTANCE AND BONDING -

1.1 Several methods of measuring low values of resistance are available, but it has been determined that, in general, three methods are normally used on aircraft, viz:-

1.1.1 A Bonding Tester with integral battery and indicator with voltage and current coils.

NOTE: This instrument is normally supplied with connection leads and prods.

1.1.2 A double bridge milliohm meter method using a current of not less than 10 amperes in the bond.

NOTE: Joints should be made using bolted connections.

1.1.3 Ammeter-Voltmeter method using calibrated ammeter and voltmeter and bolted connections or a combination of bolted connections and prods.

1.2 Large variations, up to approximately an order of difference, in measured results can be obtained, when measuring the same resistance, depending on the test equipment and connections used. The values quoted in Table 1 (Appendix No. 2) are based on the use of bolted connections. Where other methods of attachment are used, which produce higher resistance values, these may be acceptable subject to satisfactory evidence in their use.

1.3 Table 1 (Appendix No. 2) gives guidance on the acceptable maximum values of resistance which experience has shown to give satisfactory results. As described in Para. 1, these are based on the use of bolted connections and higher values may be acceptable.

#### SUMMARY

The preceding section of the paper provides a detailed proposal for the airworthiness requirements for bonding and lightning protection for modern aircraft. It is felt that this proposal should provide adequate guidance



TABLE 1 (APPENDIX NO. 2)

Paragraph No. PRIMARY	Condition	Maximum resistance in Milliohms using Bolted Connections
8.3.1(a)	Between extremities of the fixed portions of the aeroplane and between fixed panels and components as specified.	1 for light alloy 10 for stainless steel
8.3.1(b)	Between engines and aeroplane earth.	1 for light alloy 10 for stainless steel
8.3.1(c)	Between external components and aeroplane earth.	5 for light alloy 10 for stainless steel
8.3.1(d)	Between conductors on external non metallic parts and aeroplane earth.	5
8.3.1(e)	Between internally mounted primary bonded components and aeroplane earth.	2

Paragraph No. SECONDARY	Condition	Maximum Resistance in Milliohms (unless otherwise stated) Using Suitable Test Equipment
8.3.2(a)	Between metallic parts normally in contact with flammable fluids and aeroplane earth.	10 for light alloy 100 for stainless steel
8.3.2(b)	Between isolated conducting parts subject to appreciable electrostatic charging and aeroplane earth.	0.5 Megohm or not exceeding $10^5$ Ohm/square surface resistivity for non conducting surfaces in contact with the metal air-frame.
8.3.2(c)	For the avoidance of electrical shock from equipment which carries 50 volt (RMC or DC) or more.	500
8.3.2(d)	Main electrical ear connections.	50mV drop for normal currents.
8.3.2(e)	Between electrical and electronic equipment and aeroplane earth.	Where applicable to be specified by the aeroplane constructor
8.3.2(f)	Between static discharger wicks and structure.	1000
8.3.2(g)	Between aeroplane earth and ground	10 Megohms

as well as regulatory material, to cover, at least, the next generation of civil aircraft. While the format of this proposal differs from that of the U.S. Specification MIL-B-5087, it is suggested that the proposed revisions to the MIL specification should take into account the material of this (U.K.) proposal both to ensure adequate safety of the aircraft and as a basis for ensuring a common international approach to the problem areas.

#### ACKNOWLEDGEMENTS

The author wishes to thank his colleagues and members of the British aircraft industry for their help and guidance in the compilation of data and preparation of this paper and the Civil Aviation Authority for permission to publish.

## Factors Affecting Puncture of Aluminium Alloy by Simulated Lightning

John Phillpott  
UKAEA, Culham Laboratory, Abingdon,  
Berks, U.K.

### ABSTRACT

Aircraft flying close to or through a thunderstorm active area are likely to be subjected to a lightning strike. The outer skin of an aircraft usually comprises thin metallic sheets and consequently there is a finite risk that the skin will be punctured. Laboratory tests are performed to investigate the vulnerability of panels in critical areas. Existing airworthiness specifications dictate the current waveform to be used, but do not identify the electrode conditions and configurations. It will be shown that the latter are of great significance, and this suggests that for all future airworthiness requirements the electrode geometry should be specified.

THE OBJECTIVES of this experimental work were to determine the minimum number of coulombs required to puncture Aluminium Alloy (HE 15) sheets as a function of peak current, polarity, waveshape, arc length and electrode diameter. Airworthiness authorities consider that 0.080" (2 mm) of the Al alloy is sufficient to give adequate lightning protection, and this thickness was chosen for this investigation.

### EQUIPMENT

The test equipment comprised:-

- (a) 200 kJ, 20 kV capacitor bank capable of being crowbarred to give a unidirectional waveform.
- (b) Photodiode detection unit.
- (c) Range of inductors 0.41-12.6 mH.
- (d) Electrode diameter of 14.7 mm and 9.5 mm.

The capacitor current was measured using a coaxial shunt with an L/R time of about 20  $\mu$ s. A filter was placed in front of the photodiode which completely blocked out the infrared, but was transparent to the blue end of the spectrum. Puncture could therefore be determined within 50  $\mu$ s. The general arrangement is shown in Figure 1. The current waveform and the signal from the photodiode were displayed on the same oscilloscope, so that the number of coulombs to produce puncture could easily be evaluated. The current rise

time was between 1 ms and 5 ms with the decay of current mainly dominated by the arc voltage which was about 150 V for 3 mm electrode/sheet spacing. Consequently the waveshape was approximately triangular, with puncture occurring before 50% of the current decay in the majority of cases.

The electrode/sheet spacing was varied between 3 mm and 300 mm and at all spacings, except where indicated, a 38 SWG copper fuse wire was used to produce the initial breakdown. Two rod electrodes of Copper-Tungsten sintered material of 9.5 mm and 14.7 mm diameter were used in order to investigate the effects of changes of electrode size.

### RESULTS

Figure 2 shows a graph of the number of coulombs required to puncture the 2 mm of Al alloy against puncture time for 14.7 mm and 9.5 mm electrodes with 3 mm spacing for positive and negative polarities. Figure 3 shows a similar graph where the peak current has been plotted as a function of puncture time.

With the sheet as an anode, there was a wide scatter in the experimental results, particularly for the low current, long time shots. For the 14.7 mm diameter electrode the coulombs required to give a time of 25 ms varied between 29 and 72 C and for the 9.5 mm diameter between 15 and 29 C. The curve drawn for this condition shows a trend rather than an accurate graph. These results which are of the opposite polarity to previous work (1, 2)\* are in reasonable experimental agreement with those obtained by Brick (3) using a 400 V battery system.

With the sheet as a cathode, the scatter was relatively small, and the result reproducible. The curve through these points was lower but of the same shape as those previously described (1, 2) for a 9.5 mm electrode without a fuse wire initiation.

\*Numbers in parentheses designate References at end of paper.

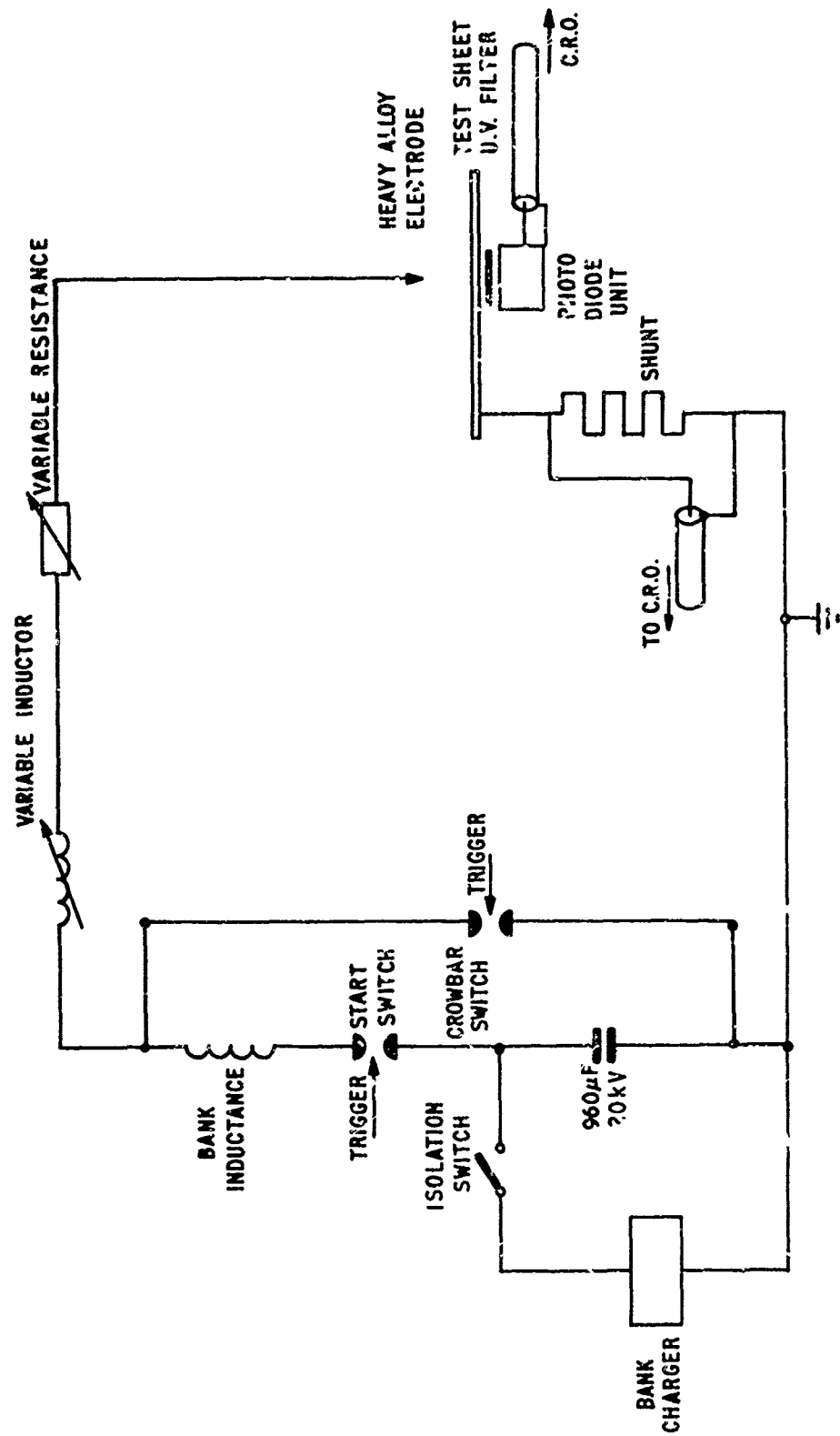


FIG.1 CIRCUIT DIAGRAM FOR EXPERIMENTAL WORK

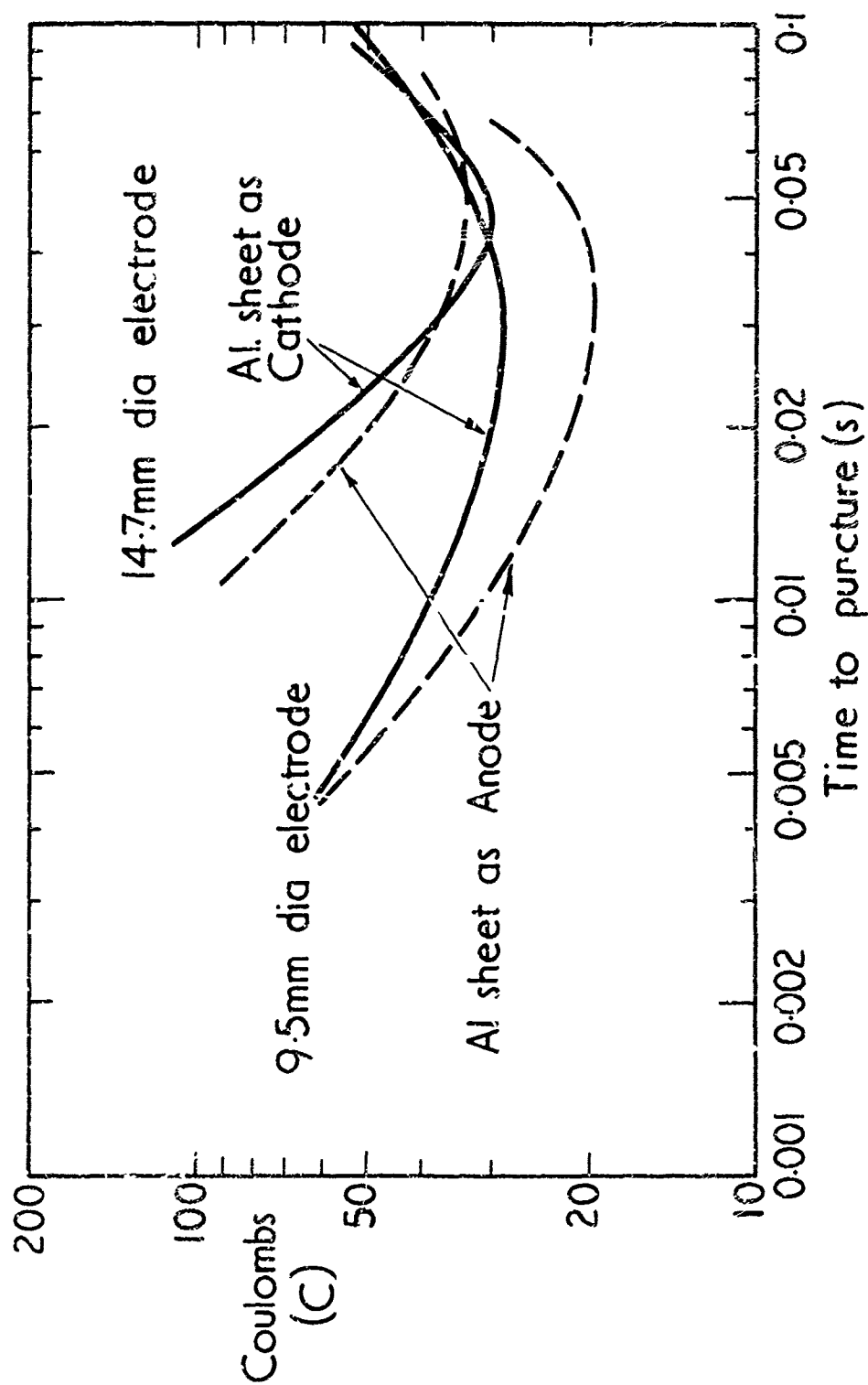


Fig 2. Graph of number of Coulombs required to puncture 2mm of Al. alloy against puncture time for 14.7 mm and 9.5 mm electrodes with 3mm arc length.

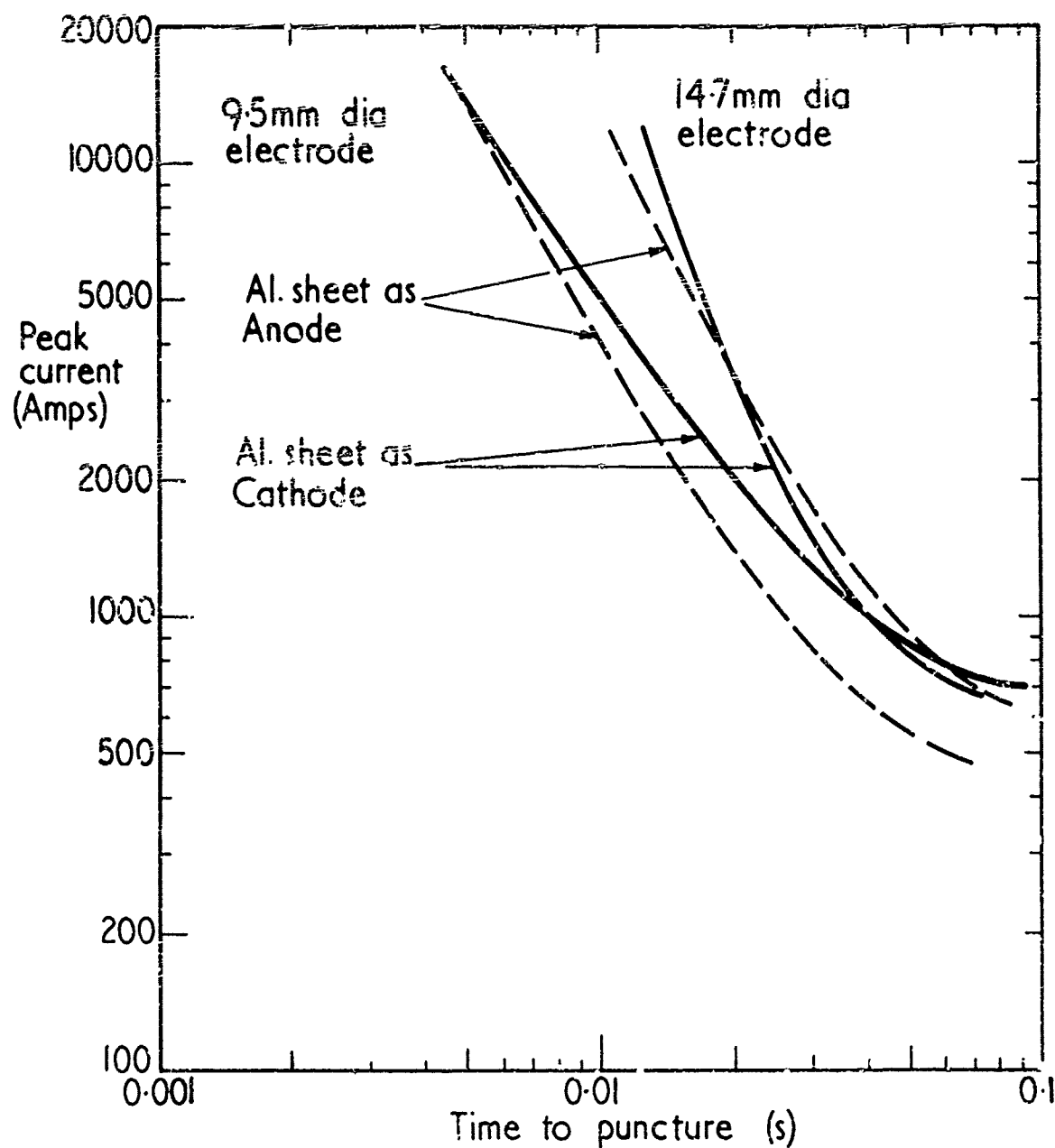


Fig. 3. Graph of Peak current required to puncture 2 mm of Al. alloy. against puncture time for 14.7mm and 9.5mm electrodes with 3mm. arc length.

An investigation into the effects of omitting the fuse wire initiation with the 9.5 mm electrode showed that at about 15 kA and a 3 mm arc, the number of coulombs required to puncture were reduced by about 20% compared with the coulombs under air breakdown conditions. At this particular current level the results, both with and without the fuse wire, happen to be independent of polarity.

It should be noted that there is a minimum in the coulomb curves (Figure 2) which occurs at about 1,000 amps. Thus, it is possible for the required coulombs to be produced by either high current, short-time (5 kA, 10 ms) or low current long-time pulses (700 amps, 70 ms).

Figure 4 shows the variation in the number of coulombs required to puncture as a function of arc length for both polarities and an electrode diameter of 9.5 mm. This shows that there is a significant variation in the number of coulombs and that, with the longer arc, more energy can be absorbed by the sheet before puncture occurs. For instance, with the sheet as a cathode, the number of coulombs under short arc conditions is about 60, whereas for long arcs up to about 250 C are required. This effect is probably due to limited movement of the arc root on the sheet. In the case of an epoxy painted surface, where the paint probably reduces the arc root movement, twice the coulombs can be absorbed with a 300 mm arc compared with a 10 mm arc length.

The results also indicate that the effect of arc length is even greater with the (unpainted) alloy sheet as an anode, and with arc lengths of greater than a few cm, more coulombs can be absorbed than as a cathode. This is against the trend of the short arc results.

#### CONCLUSIONS

It has been shown that the electrode conditions and configurations can be responsible for producing wide variations in the number of coulombs required to puncture 2 mm of Al alloy. It is important that any future airworthiness specifications should detail the electrode configuration to be used to ensure that all components are tested to the same standard, and if possible to give a better approximation to in-flight conditions.

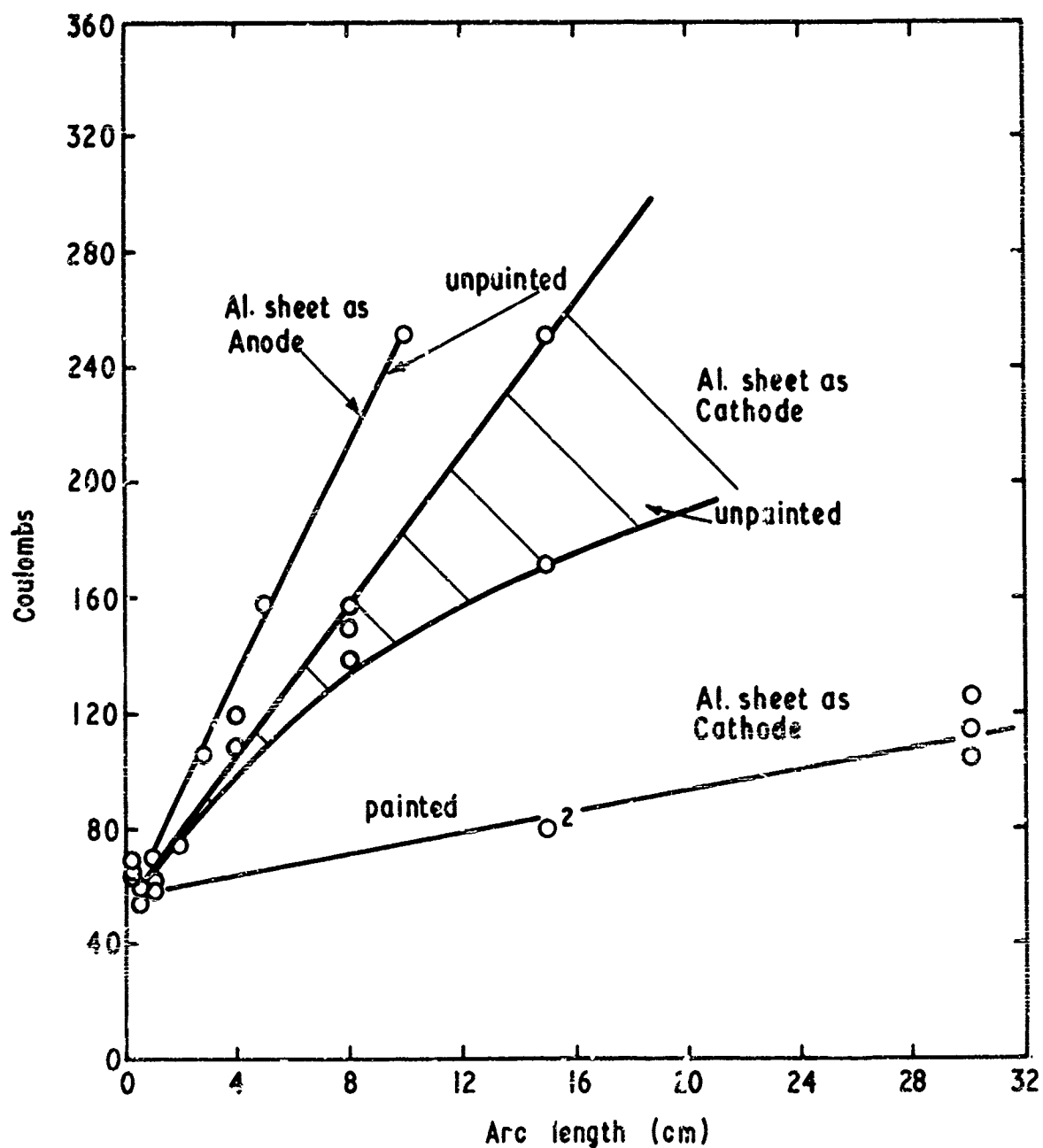
#### ACKNOWLEDGEMENTS

The author acknowledges the support given by the Procurement Executive U.K. Ministry of Defence for this work.

Messrs J L Browning and J G Talboys were responsible for the experimental work and analysis of the results.

#### REFERENCES

1. T E James and J Phillpott, "Lightning Strikes to Aircraft". Culham Laboratory Report CLM-R.111, May 1971.
2. J Phillpott, "Puncture of Metallic Skins by Simulated Lightning". IEE Gas Discharges Conf. London, 1972.
3. R O Brick, "A Method of Establishing Lightning-Resistance/Skin Thickness Requirements for Aircraft". Lightning and Static Elec. Conf. AFAL-TR-68-290, 1968.



Coulombs required to puncture 0.080 ins of Al. alloy  
against arc length for currents  $\approx 10\text{kA}$

Fig. 4



Comments on MIL-B-5087B(2), Bonding, Electrical,  
and Lightning Protection, for Aerospace  
Systems

Floyd P. Holder  
Lockheed-Georgia Company

1. In paragraph 3.3.4 the term, "lightning entry" needs clarifying. Some tend to understand this to mean literally a flash going through an electromagnetic opening, such as a windshield or radome. This is much too narrow a view, so an improvement would be "lightning or lightning-effects entry." The object would be to cover such considerations as:  
Lightning-caused internal hot spots in fuel tanks, even if burn-through does not occur.  
Lightning-caused air-breakdown or conductive-contact sparking at fuel tank closures, joints, fasteners, etc.  
Lightning-energy in electrical form, (i.e., without accompanying heat, light, pressure, and sound, along antenna leads, wiring, control cables, ducting, screw jacks, etc. Entry may be by conduction or induction.  
Lightning-caused personnel hazards due both to IZ drops along structure and interfaces and to induced effects resulting from personnel exposure to intense electric and/or magnetic fields or flux changes.
2. Paragraph 3.3.4 as revised by Amendment 2 states, "Lightning protection shall be provided at all possible points of entry into the aircraft and shall be proven by test." The intent here was probably that it shall be proven by test that lightning protection is provided at all possible points of entry. But the statement can be construed to mean virtually that lightning protection at every possible point of entry must be proven by test. There is a subtle but vast difference in the two interpretations. Depending on who is doing the construing, the second interpretation could lead to a fantastic and unnecessarily expensive lightning-test program. This would be a "swing of the pendulum" too far in the opposite direction to the test applicability prior to Amendment 2, which is discussed in item 3, below.
3. Paragraph 3.3.4.5 states, "Laboratory tests of lightning protection provisions for external sections, such as radomes and canopies, shall be performed ....." Before the amendments this was the only statement of lightning-test applicability. It raises wide-open questions as to what all is meant by "external sections," especially since the lightning-oriented reader may well not associate "external sections," with such things as fuel-tank closures. He

knows that such closures are usually most needful of lightning-integrity testing; yet the limited reference only to radomes and canopies tends to steer away from any such requirement. As a result, conscientious military-aircraft manufacturers have tended either to set their own requirements (with 3.3.4.5, as a lower boundary) or to be guided by FAA Advisory Circular AC 20-53, or both.

4. In both paragraphs 3.3.4 and 3.3.4.5 the test-waveform description is unnecessarily restrictive for most high-current-test purposes. A damped oscillatory wave is usually entirely adequate and much easier to obtain than the unipolar pulse described--especially with the included 90-percent-point description given. Commonly the peak current is stipulated, then the rise time from  $t = 0$  (the beginning of the current transient) to  $t = t_{\text{peak}}$ , and then the total time from  $t = 0$  to  $t = 50$  percent--i.e., from  $t = 0$  to that instant at which the current becomes one-half its (maximum) peak after having just passed that peak. Thus, a test strike that rose to a peak of 200,000 amperes in 10 microseconds, then dropped through 100,000 amperes in a total time of 20 microseconds would be called a 200,000 ampere, 10/20 strike. The Lightning and Transients Research Institute (LTRI) has often contended that a 15/30 strike is appropriate. Others favor other waveforms. For example, Dr. Martin A. Uman in his McGraw-Hill book Lightning (page 4) shows 2/40 as representative of (widely variable) measurements made at the ground. MIL-A-9094D, Arrester, Lightning, General Specification for, calls for both 100,000-ampere, 5/10 and 200,000-ampere, 10/20 strikes. In any event, liberal time tolerances in MIL-B-5087 (not presently given there) should be justifiable on the basis of the wide divergence of values given in the literature. And allowing the trail-off oscillations for practical testing should be justifiable on the premise that for hardware-test purposes those oscillations merely increase the stringency of the test slightly again in the face of the wide variability of data on the severity of natural lightning. If high-rate-of-current-rise testing is to be performed separately--as later comment will support--the larger numbers, such as 15/30, give a more stringent high-current test than the smaller, such as 5/10, because the energy spent at the test specimen is greater. Thus,

$$\text{Energy} = R \int i^2 dt,$$

where  $R$ , in simple terms, is the effective resistance of the energy-dissipating portion of the test specimen and is assumed to be  $e$

- fixed-shape function of t.
5. Paragraphs 3.3.4 and 3.3.4.5, and the amendments, link the high-rate-of rise component directly to the high-current component. Not only does this make for a waveform that for most hardware-test purposes is unnecessarily hard and expensive to obtain, it tends to obscure what are best kept as two separate effects: viz, induced voltage transients (from the high-rate-of-rise component) and blast/ metallic-sparking/ electromechanical effects (from the high-current component). It is hereby suggested that these and other components, and various limits of each where applicable (e.g., 200 coulombs as one "high-coulomb" limit and 500 coulombs as another), be enumerated separately. The preparer of a given subsystem or system purchasing specification could then easily assemble for lightning protection merely by reference to the proper item identifiers in MIL-B-5087 (Rev.). Similarly, appropriate composite strikes (test strikes combining two or more components) could also be readily called out, where desirable.
  6. Some clarification accompanying the last sentence of paragraph 3.3.4.5. is needed. That sentence probably alludes to such testing as high-current or composite "shots" that simulate natural lightning tracking along a radome's dielectric surface and approaching a diverter strip from the side. There are other comparable possibilities. But it is not difficult to miss that point completely and misunderstand the sentence to be referring to high-voltage, long spark model tests. By their nature these tests are made by firing at the test sample from all reasonable angles expected from lightning strikes. Actually, however, no long-spark testing of radomes, models, or whatever is mentioned in MIL-B-5087, though it probably should be.
  7. Also not yet mentioned in MIL-B-5087B(2) are intermediate strikes (for maximum pitting effects), high-coulomb strikes (for maximum heating or burning damage), and swept strikes (for minimum-penalty, realistic operational evaluation of the other two). Examples of the first of these appear in MIL-A-9094D, paragraphs 4.6.11 (b) and 4.6.11.1 (b). Examples of the second are given in subparagraphs (c) of those same two paragraphs and also in FAA Advisory Circular AC20-53. The third (swept strikes) have been studied by industry for several years and are discussed in the literature but are not known to appear as yet in a Government specification or standard. Investigation in this last case probably should not be considered exhaustive at this time.
  8. Paragraph 3.1.2 states, "Bonding jumpers (see 6.2.3.) shall conform to MS25083 for thermal environments less than 300 F." Paragraph 3.3.4.2. states, "Control surfaces and flaps shall have a bonding jumper across each hinge, except for installations having a single hinge in which case a minimum of two jumpers are required." Paragraph 3.3.4.2 is a subparagraph of paragraph 3.3.4, "Class L bonding lightning protection) (except for antenna systems." Thus, MIL-B-5087B bonding-jumper requirements are represented as being adequately covered by MS25083, so long as two jumpers are used. It is recalled that MS25083 jumpers designated for lightning-current handling were high-current tested some years ago and found to break at 60,000 amperes, each. This testing was done probably during the life span of MIL-B-5087A which had a high-current requirement of only 100,000 amperes instead of the present 200,000 of MIL-B-5087B. If the only two hinges of a given control surface were widely separated and a "worst-case" strike made contact near one of the two (each having one MS25083 jumper), that jumper could be expected to carry more-- possibly considerably more-- than half the current, which, exceeding 60,000 amperes, would snap the jumper. Only with that strike near the electrical center between the two jumpers in this case could both jumpers be expected to survive the 100,000-jumper strike. The 200,000 amperes of MIL-B-5087B would snap both jumpers if applied at the electrical center. Thus, it appears that MS25083 lightning-current jumpers have not kept pace with the updating of MIL-B-5087. Until this is corrected it is probably wise, in those cases where maximum-current protection by jumpers is a "must," to double up on the number of MS25083 jumpers required or to take some equivalent step. It should be realized, however, that a great majority of strikes reach far lower than 100,000 amperes. It should also be realized that in many cases a jumper becomes virtually useless, anyway. If a steep-fronted strike produces enough inductive drop in the protective jumpers to initiate an arc breakdown across the hinge or other hardware being protected, the arc may well become the path of least impedance and cause essentially as much damage as if the jumper had not existed. So there is an increasing trend toward "designing around" a need for lightning protection by jumpers (e.g., intentional spark paths, etc). Even then, however, other requirements, such as precipitation charge dissipation, must not be overlooked.
  9. Time and again the question is raised as to what d-c resistance value must be stipulated to assure an adequate lightning-current path. There is no pat answer. As noted in the previous item, a properly configured open circuit may be best. In many cases, on the other hand, the path

(usually an interface is the path of concern) inherently trends toward a dead short. Metallic fuel-area closures are common examples. If various resistances are measured and recorded on a specimen that subsequently passes lightning-integrity qualification tests, the recorded values can later be used as manufacturing controls to assure that production items supposedly like the tested item are in fact like it and therefore safe. Otherwise no particularly useful lightning-integrity-to-resistance correlation is believed to have been found.

Lightning Simulation and Testing in  
Relation to Specification MIL-B-5087

R H Evans  
UK Ministry of Defence  
and  
J Phillpott  
UK Atomic Energy Authority

ABSTRACT

Discussions are in progress on possible revisions to aircraft lightning protection specifications, particularly with reference to the waveform of the lightning test current. Fundamental requirements for a test waveform are suggested and then the waveforms of both natural and test specification strokes are analysed into three fundamental components. It is concluded that present specifications are inadequate in certain respects and a revised waveform is proposed. Some brief details are given of a UK Applied Research Programme intended as a contribution to knowledge upon which further refinements of test specifications may be based.

SPECIFICATION MIL-B-5087 is a US Military specification dealing with electrical bonding and lightning protection for aerospace systems. The present issue is dated 1964. An amendment in 1970 reduced the recommended test current for instances when flight safety is not a factor and made some other detailed changes. During the last few years considerable extra knowledge has been gained as a result of both laboratory tests and operational experience, and therefore a discussion on possible updating of the specification is to be welcomed. This is particularly so because various international bodies are attempting international standardisation, often using MIL-B-5087 as a basis for discussion.

SUGGESTED REQUIREMENTS FOR A TEST WAVEFORM

It is suggested that a revised specification should meet the following requirements as far as possible.

1. It should simulate the characteristics of natural lightning as closely as possible so that structures passing the test are ensured of safety, but it must not incorporate excessive safety factors, which would of course incur weight and other penalties.

2. Consideration should be given to the particular part of the aircraft involved, both because the probable severity of the stroke varies with location on the aircraft (in the case of swept strokes) and because damage can more readily be tolerated in some parts than others. Various civil specifi-

cations (1) (2) (3)\* divide the aircraft surface into three zones defined as follows:

Zone 1 comprises those areas for which there is a high probability of a direct strike. Zone 2 comprises those areas for which there is a probability of strikes being swept rearward from a point of attachment in Zone 1. Zone 3 comprises the remainder of the aircraft.

It is suggested that the same system should be adopted for Military aircraft. The zones could be fairly exactly defined for conventional aircraft shapes, but for newer designs it might be necessary to establish the zones by strike point location tests on models.

3. Since lightning strikes have various effects such as heating, sparking, magnetic forces and induced voltages in electrical circuits, consideration should be given to the employment of a particular waveform appropriate to each effect or group of effects being investigated, rather than a universal waveform for all effects. In other words the test waveform would represent the fundamental characteristics of the lightning discharge relevant to a given failure mechanism.

4. All relevant parameters should be specified, in order to simulate accurately the actual operational conditions; for example some hitherto unspecified parameters such as arc length may have an important effect on the damage inflicted and a combination of maximum current with a short arc might be an excessively severe test. Specification of all parameters is also important to ensure that results are reproducible and that valid comparisons can be made between the results reported from different test facilities.

5. The test specified should not be so complex that the test facilities become too elaborate and expensive to build and operate. However, too much emphasis should not be placed on this consideration, since it is often possible for comparatively simple local facilities to be employed for preliminary work, with a final check at a more elaborate national facility.

\*Numbers in parentheses designate References at end of paper.

## COMPONENTS OF CURRENT WAVEFORM

The current flowing in a lightning stroke varies widely from stroke to stroke and also depends among other factors on whether it is a cloud/cloud or a cloud/ground discharge. In the latter case there is a considerable difference in waveform between a negative stroke (conveying a negative charge to ground) and a positive stroke. Thus a test waveform attempts to simulate the significant characteristics of a wide variety of natural waveforms. The main parameters of interest are duration, peak current, rate of rise of current ( $di/dt$ ), charge transferred (coulombs) and  $\int i^2 dt$ , which is a measure of the energy dissipated in a fixed resistance and will be referred to as the  $i^2t$  content of the discharge. The  $i^2t$  content is also a measure of the stress due to magnetic forces in structures whose natural period is considerably greater than the time-constant of decay of the current waveform. In general, lightning flashes consist of one or more of the following components and existing test waveforms also consist of combinations of these components.

A. A "fast" component or impulse having a peak of say 200 kA and a rise time of up to about 15  $\mu s$ . The initial rate of rise could be as high as 100 kA/ $\mu s$ . This represents the impulses present in a negative ground flash, and transfers very little charge.

B. An "intermediate" component, having a peak of up to 50 kA and a duration of a few ms. This represents the "tail" of a positive ground flash and has substantial charge and  $i^2t$  content.

C. A continuing current of a few hundred amp (say up to 1 kA) for one or two seconds. This represents the current flowing between strokes in a negative flash and may also be considered to correspond to a cloud/cloud discharge. The charge transferred is high but the  $i^2t$  content is low.

Specification MIL-B-5087 contains only component A, the specifications listed as References 1, 2 and 3 contain A and C, and Reference 4 contains all three components. It is considered that although existing specifications are often adequate in respect of peak current and rate of rise, and also the charge transfer in itself is adequate, they are inadequate in respect of total  $i^2t$  content and charge transfer at intermediate currents. In other words the intermediate component is inadequately represented. It is true that this component is mainly associated with positive discharges, which probably occur with only about one quarter of the frequency of negative discharges, but nevertheless it is necessary to represent it if safety is to be assured.

## APPLIED RESEARCH PROGRAMME

Although we consider that present

knowledge is sufficient for a useful revision of lightning test specifications, it is realised that there are still many points on which additional investigation is needed and this may well result in further revisions. As a contribution towards improved methods of simulation as well as better means of lightning protection, studies (5) (6) to formulate the problems and to outline a research programme were sponsored by the UK Ministry of Defence, and these were followed by a four-year Applied Research contract on the Culham Laboratory of the Atomic Energy Authority. The programme (5) includes strike point location studies and also high current investigations, the latter being divided into the following broad subjects.

1. The Effects of Stationary Arcs
  - a. Burn through times and hot spot temperatures for various metals, surface coatings, arc lengths and configurations.
  - b. Magnetic forces and stresses with representative wave-forms and configurations. Calculation and tests.
  - c. Composite materials including carbon fibre reinforced plastic. Protection methods.
  - d. Externally mounted components, for example antennas and pitot probes. Review problems and methods of protection.
2. The Effects of Swept Strokes
  - a. Dwell time, burn-through times and hot spot temperatures for arc length of up to 40 cm with swept strokes.
  - b. The effect of stress concentrations around projections.
  - c. Effects of various surfaces.
  - d. Effect of relative air velocity. Aerodynamic effects near surface (boundary layers).
  - e. Effect of repeated strokes.
  - f. Any special effects relevant to composite materials.
  - g. Possible methods of diverting swept strokes from particular vulnerable areas.
3. Sparking Phenomena
  - a. Configuration of joints relevant to fuel ignition by sparking.
  - b. Damage to structures due to sparking.
4. Induced Voltages in Electrical Systems
  - a. Relation between lightning current in airframe and induced voltage in wiring for various configurations.
  - b. Feasibility of testing complete aircraft at reduced currents using portable equipment and scaling the results.
  - c. Probable effects on equipment and cables.
  - d. Shielding and protection methods.
  - e. Injected or induced voltages into internal wiring due to strikes to terminal equipment.

The equipment set up for the high current studies includes the following:

1. Fast Bank (80 kJ 100 kV) - This bank will produce 200 kA with a rise time of

about 15  $\mu$ s into a 4  $\mu$ H load (about 6 metre component length) and simulates a severe first stroke of a lightning discharge, as well as providing the first component of the waveform of references 1, 2 and 3.

2. Intermediate Bank (250 kJ 20 kV)

- This bank will produce a unidirectional current pulse of amplitude variable between 50 kA and 100 amps and a charge transfer of up to 500 coulombs. Therefore it is suitable for simulating the "intermediate" current of a lightning discharge and for performing the 500 coulomb continuing current test of references 1, 2 and 3.

3. High di/dt Generator (40 kJ 1 MV)

- This generator will be capable of producing 100 kA 100 kA/ $\mu$ s into a 4  $\mu$ H load (6 metre component) and thus providing the high di/dt associated with Group 2 and 3 tests.

4. Swept Stroke Equipment - A method has been developed of simulating the movement of an arc root along an aircraft by driving the arc electromagnetically with a transverse magnetic field. The magnetic field can be reduced near the surface of the test component to simulate the presence of a boundary layer.

#### PROPOSED TEST WAVEFORM

In order to represent severe strokes in respect of all significant parameters and at the same time to adapt the tests both to the particular effect being investigated and to the zone of the aircraft concerned, the waveforms described in Table 1 are suggested. The tests are specified for zone 1 and zone 2 of the aircraft, sub-divided into three groups representing the type of test, that is, the particular failure mechanism being investigated.

It will be noted that the "fast" A component has been omitted from Group 1 since the significant effects in this group are believed to be represented by the charge transfer and  $i^2t$  content of the "intermediate" B component. The "continuing" C current which is called for in some specifications has been omitted in all tests, since it is considered that the necessary charge transfer and  $i^2t$  content can be more realistically contained in the intermediate B current with a peak value of 30 kA. The charge transfer for the intermediate current in zone 1 has been specified as 500 coulombs; this may be considered rather high since the figure for natural lightning is believed to be about 350 coulombs maximum but it is recommended in order to represent a margin of safety and the uncertainty of simulating the damage due to a multiple stroke flash with a single component waveform. Further experimental data may justify a decrease in the figure.

The intermediate B currents for zone 2 have been relaxed by a factor of 5 compared with zone 1 in respect of charge transfer and  $i^2t$ , based on a swept stroke dwell time of

about 5 ms. This again is subject to amendment when further data has been obtained from swept stroke investigations.

The rate of rise for the fast A component has been maintained at 100 kA/ $\mu$ s for a peak current of 200 kA in zone 1. For zone 2 it is suggested that the peak may be reduced to 100 kA but maintaining the same value of rate of rise. For Group 3 (induced voltages in electrical systems), only the fast A component is significant, and component B has therefore been omitted. The exact waveform of the current pulse is important because the induced voltages depend on the time characteristics in a complex manner. For example, the voltage induced in a cable might be due to a combination of two effects. First the magnetic flux may link the cable directly by an air path (or other non-metallic path) inducing a voltage proportional to di/dt. Secondly the flux can penetrate the metallic skin or screens, and the internal field which induces the voltage would be subjected to both attenuation and time delay depending on the nature of the waveform. It is suggested in Table 1 that the pulse shape be provisionally defined as having a ratio of pulse length to rise time of 5. Once the waveform has been decided it may be possible in view of the work (7) carried out on scaling the effects to test with a wave having the correct timing but at a much lower current level and then to calculate the full-scale injected voltage by proportion. However, this method does not in itself determine the damage which would be inflicted by the full-scale injected voltage, and it does not allow for the further induced effects that might follow from sparking or other non-linear occurrences in a full-scale test.

The recommended waveforms for Group 2, incorporating both the fast A component and the intermediate B component, are illustrated for aircraft zones 1 and 2 in Figure 1.

#### REFERENCES

1. Federal Aviation Agency "Protection of Aircraft Fuel Systems Against Lightning" Advisory Circular AC 40-53 June 1967.
2. UK Air Registration Board "Provisional Air Worthiness Requirements for Civil Powered-Lift Aircraft. Chapter P4-6, electrical bonding and lightning discharge protection" 1972.
3. Anglo-French TSS Standard 8-6 "Electrical Bonding and Lightning Discharge Protection" July 1969.
4. Specification MIL-A-9094 "General Specification for Lightning Arresters" March 1969.
5. T E James and J Phillpott "Simulation of Lightning Strikes to Aircraft" UK Atomic Energy Authority, Culham Laboratory Report CLM-R111. May 1971.

6. R H Golde, A A Hudson, J D Ibbott and E L White "An Aircraft Lightning Strike Test Facility - A Study of Requirements" Electrical Research Association, Leatherhead, England, Report ERA 71-167. December 1971.

7. P T Hacker and J A Plumer "Measurements and Analysis of Lightning Induced Voltages in Aircraft Electrical Circuits" Proceedings of Lightning and Static Electricity Conference, December 1970.

Table 1 - Proposed Lightning Test Currents

Type of Test	Component A Fast	Component B Intermediate
<u>Group 1</u>  Resistive heating Skin hot spots Skin puncture Mechanical strength	Zone 1	
		50 kA 500 coulomb $7.5 \cdot 10^6 \text{ A}^2\text{s}$
	Zone 2	
		30 kA 100 coulomb $1.5 \cdot 10^6 \text{ A}^2\text{s}$
<u>Group 2</u>  Internal sparking - fuel ignition Sparking damage at joints Induced and direct voltage flashover	Zone 1	
	200 kA 100 kA/ $\mu\text{s}$	30 kA 500 coulomb $7.5 \cdot 10^6 \text{ A}^2\text{s}$
	Zone 2	
	100 kA 100 kA/ $\mu\text{s}$	30 kA 100 coulomb $1.5 \cdot 10^6 \text{ A}^2\text{s}$
<u>Group 3</u>  Induced voltages in electrical systems	200 kA 100 kA/ $\mu\text{s}$ Pulse length to be about 5 times the rise time	

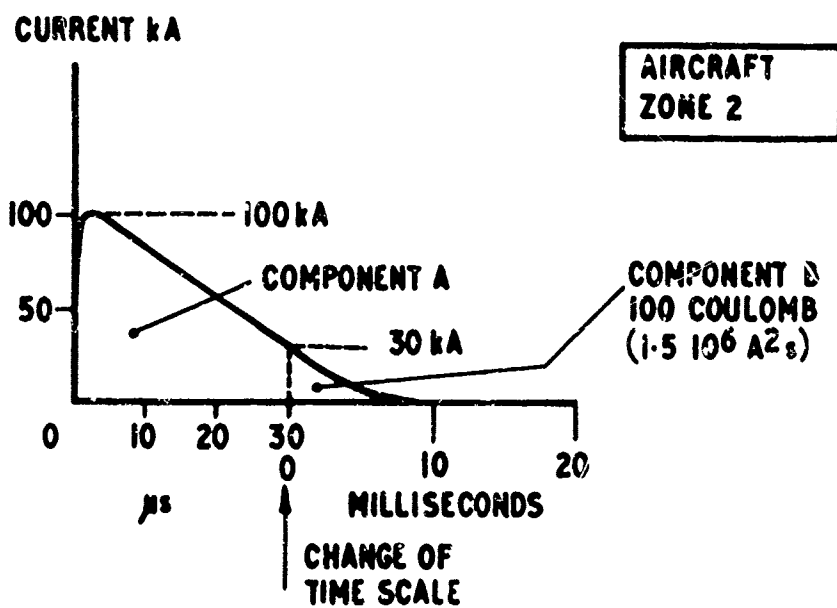
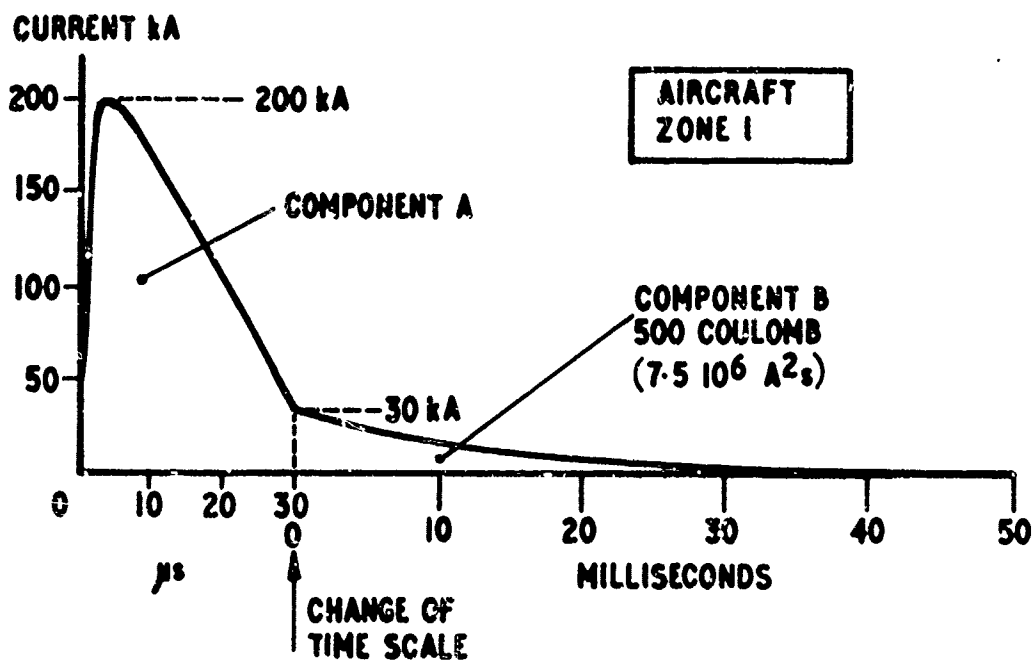


**FIGURE 1**



SESSION X

SUPPLEMENTARY PAPERS

## Aerosol Discharge System for Heavy Lift Helicopters

Rudolf G. Buser, Helmut H. Kaunzinger and  
Hans E. Inslerman  
US Army Electronics Command, Fort Monmouth,  
New Jersey

### ABSTRACT

A new concept for an electronically controllable discharge of surface charges which may accumulate on helicopters and present a considerable hazard to personnel is explored. It uses mechanical transport of charges by liquid droplets. Theory of nozzle produced sprays operating in electric field gradients is developed and criteria for efficient charge transport are established. Experimental results for single nozzles and multiple nozzle clusters are presented, and the application of these results to the Army's ongoing Heavy Lift Helicopter design study given. Nozzle clusters with a current capacity up to 100  $\mu$ A have been tested, with linear additive properties for higher current capabilities. Recently concluded flight tests indicate the feasibility of meeting the discharge current objectives of heavy cargo helicopters without use of excessively high voltages. Desirable system characteristics are minimal ion recirculation and elimination of sensor instabilities. Design refinement is expected to result in a simple, low-cost system with the minimum use of expendables, air, and water.

ACCUMULATION of charges on metallic and dielectric bodies due to surface contact effects (tribo-electric charging) is found in a variety of military and commercial operations (hazardous electro-static charges affect operations in paper and textile industry, printing plants, mills, mines, and oil tankers). For helicopters, this process, together with inductive charging due to large scale atmospheric electrical fields, and chemical charging due to the specific chemistry of the combustion process, presents a problem of long standing, involving hazards to personnel and possible ignition of fuel air mixtures and activation of explosives; several attempts have been made to develop a technically and operationally acceptable solution to this problem (1),(2),(3). For new large size transport helicopters now in the planning stage, the probability for hazardous incidents is considerably increased. An automatic system which permits a reliable controlled discharge of the helicopter to zero potential during typical loading or unloading conditions seems highly desirable. In the proposed conceptual approach, helicopter discharge is only attempted when the location for loading or unloading is reached. At this point, a field sensor, located on or clipped to the cargo hook (load), is activated, determines strength and polarity of the field, and transfers this information to a receiver-processor unit, which in turn

operates an indicator and discharger. The field sensor controls the discharger such that the potential of the cargo hook for the duration of the operation is kept close to the local ground potential. Field sensor, receiver-processor unit, discharger and indicator represent the overall helicopter discharge system concept as shown in Figure 1. In the following, one specific element of the system, namely, a discharger which uses the controlled emission of charge carrying liquid droplets is discussed in detail and its operational performance presented. It will be shown that the selected technique permits realization of the required discharger specifications, namely, short term discharge capability of 500  $\mu$ A or more for both polarities, a response time in the order of 10 ms sufficient to follow rapidly changing sensor indications, low power consumption (50W) and weight (10kgf excluding discharge fluid).

It is recognized that other elements of this system, specifically the problem of field sensing under extreme environmental conditions (such as found in the desert or arctic) are equally important in the operational analysis of the total system, however, they will not be pursued in this context.

### PRINCIPLE OF OPERATION; SINGLE NOZZLE RESULTS

If a conductive liquid is moving into an electrical field, generally two effects take place: The material becomes polarized by induction due to the acting coulomb forces; induced changes in surface tension will influence surface properties of the substance. In Figure 2, this principle is applied to an all or partially metallic nozzle structure. A conductive liquid which is kept on nozzle potential by wall contact leaves the nozzle under pressure through a center hole and enters into a field originally defined by the nozzle body and grid electrode several millimeters away (the grid electrode is kept at a constant potential against the nozzle by means of a power supply). In this process, electrostatic forces induce charges to flow to the surface of the liquid to keep nozzle and liquid at a fixed common potential, and the surface layer becomes charged opposite to the charge of the grid (field lines shown are obtained from two dimensional field plots). Fast streaming air leaves the nozzle under high pressure from an annular orifice surrounding the liquid, interacts with the liquid, and charged droplets are formed. The charged droplets leave the nozzle system

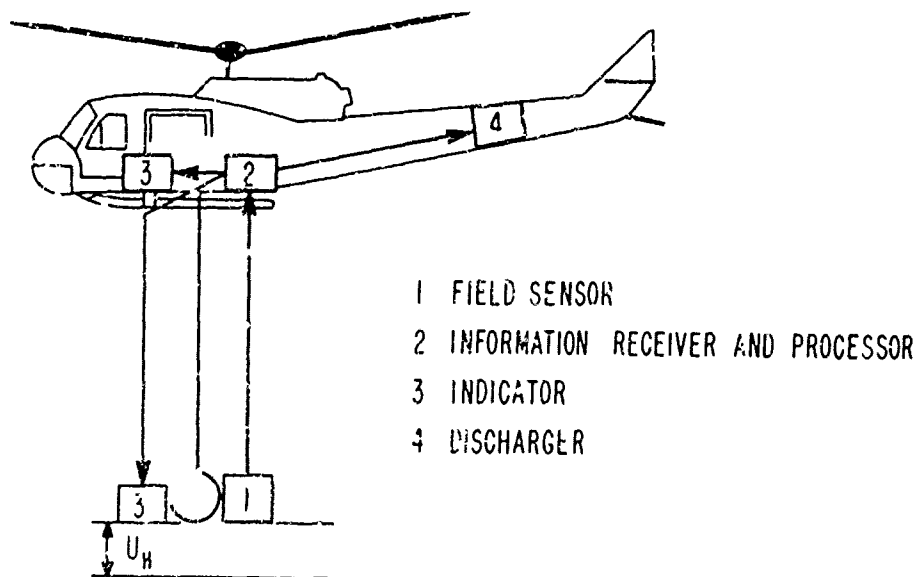


Fig. 1 - Fundamental elements of the helicopter discharge system.

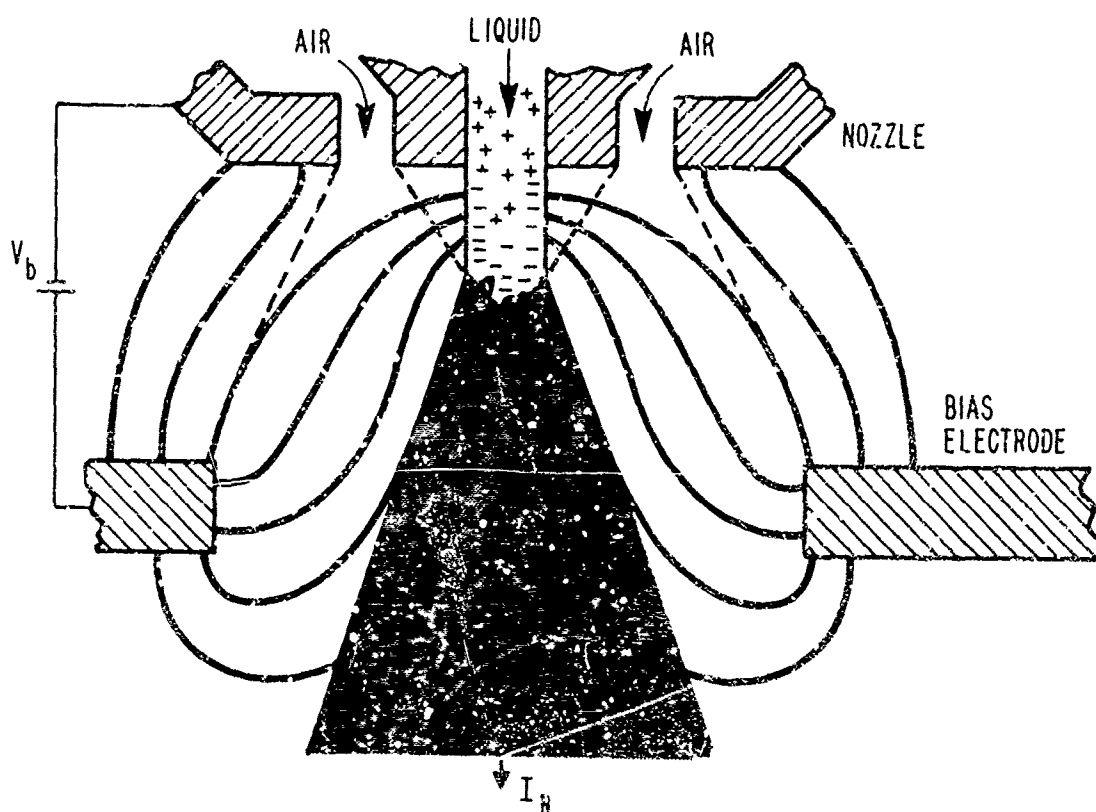


Fig. 2 - Principle of operation of the discharger.

through a grid opening. It is this process which permits a mechanical transport of charges away from the nozzle structure and from the body to which the nozzle is connected, producing the actual nozzle discharge current.

A quantitative theoretical analysis of the various processes discussed in the previous paragraph is difficult and only in part feasible (4). For an optimized system, there are the following considerations: Droplets should be in the one micron regime and stable, such that the low mobility (Stoke's law) prevents significant recirculation to the helicopter body; maximum charge  $q$  should be transferred to the droplet (Reynolds criterion), a process which may be air breakdown limited. Details of the selected nozzle geometry, and other operational parameters (liquid and air feed pressure) will have a significant effect. As an example in Figure 3, the resulting  $I_N$  for different water orifices of a circular nozzle design is shown together with optimum voltage and pressure settings.

From an engineering point of view, the system may be considered as a capacitor. To optimize the system, the capacitance between the liquid column and the biasing grid should be as high as possible, that is, for a given bias voltage the distance between both should be chosen so that most field lines end at the liquid column and that the surface interaction layer be maximized. For a given nozzle geometry and mode of operation, the capacitor model predicts a linear current bias voltage relationship up to the corona or breakdown voltage limit, with response times in the order of milliseconds. In Figure 4, representative results for the dependence of nozzle current upon bias voltage, together with the leakage current observed between nozzle and bias electrode, are shown.

An important parameter in the operation of the system is the choice of the liquid itself. Without further specifications, a "sufficiently" conductive liquid has been assumed, conductivity being aside from the surface tension the only material quantity entering the analysis. If the conductivity were to be substantially reduced, the observed discharge current will become resistance limited and an unwanted voltage drop between liquid column and nozzle structure develops. In the extreme of perfect metallic conduction, penetration of the field lines into the inner part of the interaction layer becomes impossible and the effective interaction area is reduced. This may be seen from Figure 5 where the dependence of the nozzle current upon conductivity of water (adjusted by the addition of NaCl) is shown. Experiments with other inorganic or organic liquids with low conductivity support this model further.

The effect of surface tension upon the droplet size distribution is shown in Figure 6 where the experimentally determined droplet size distribution is presented for two nozzle geometries (760 and 800 nozzle series). The peak near 0.5 micron without electric field

(solid line) changes drastically with application of the field (dashed line). Since the liquid consumption in both tests stays constant, most droplets with the field applied must be produced with a radius smaller than 0.5 micron. In contrast, nozzle 701, which also peaks without field near 0.5 micron, changes less with applied bias voltage and produces a small current. Similar is the effect of small amounts of liquid additives in modifying the surface tension properties. In Figure 7 the change in recirculation current  $I_R$  (as measured in an electric field perpendicular to the direction of the nozzle discharge current below the nozzle structure) is shown; as the amount of glycerin is increased,  $I_R$  at constant nozzle current  $I_N$  is significantly reduced, indicating concomitant changes in the particle size-charge distribution.

#### MULTIPLE NOZZLE DESIGN; LABORATORY AND FIELD PERFORMANCE

After theoretical analysis and experiments with a single nozzle with annular bias electrodes, it was concluded that a single nozzle could be expected to produce a current typically between 10 and 20  $\mu A$  (\*). In order to approach the required discharge currents with the present design, clusters of biased spray nozzles had to be considered. For external mounting on the helicopter fuselage, either within the exhaust stream or in the rotor down stream, such a cluster must be compact and rigid. Under these conditions, the nozzles operate close to one another and their mutual interference may not be ignored. In all nozzle performance tests, a circular cluster with one nozzle in the center and 6 nozzles 2.5 cm apart on a 5.0 cm circle was chosen. The internal water and air distribution channels with low pressure drop characteristics and the associated seals limited the overall diameter of the nozzle cluster to 10 cm. A close-up picture of the 7 nozzle cluster is shown in Figure 8. The common electrode for all 7 nozzles of the cluster is a flat disk mounted concentric with the cluster body and has seven apertures in register with the seven nozzles. This common bias electrode is mounted with two sheets and four posts of insulating material, properly spaced against the nozzles. This configuration eliminates surface leakage currents greatly. Figure 9 is a photograph of the cluster assembly, with bias electrode and support, and metal shield to prevent deposition of mist on the bias electrode support.

Two configurations of this nozzle cluster were mounted outside the fuselage of an CH47C Helicopter extending 2.5 feet out into the airstream under the blade overlap region, with airfoils covering the exterior structure over their entire length to reduce the turbulent air. With a water consumption of 5  $cm^3/\mu A$  min, and air consumption of 0.05  $m^3/\mu A$  min with the geometries so far investigated. (It seems probable that these values may be significantly improved and the air consumption be considerably reduced.)

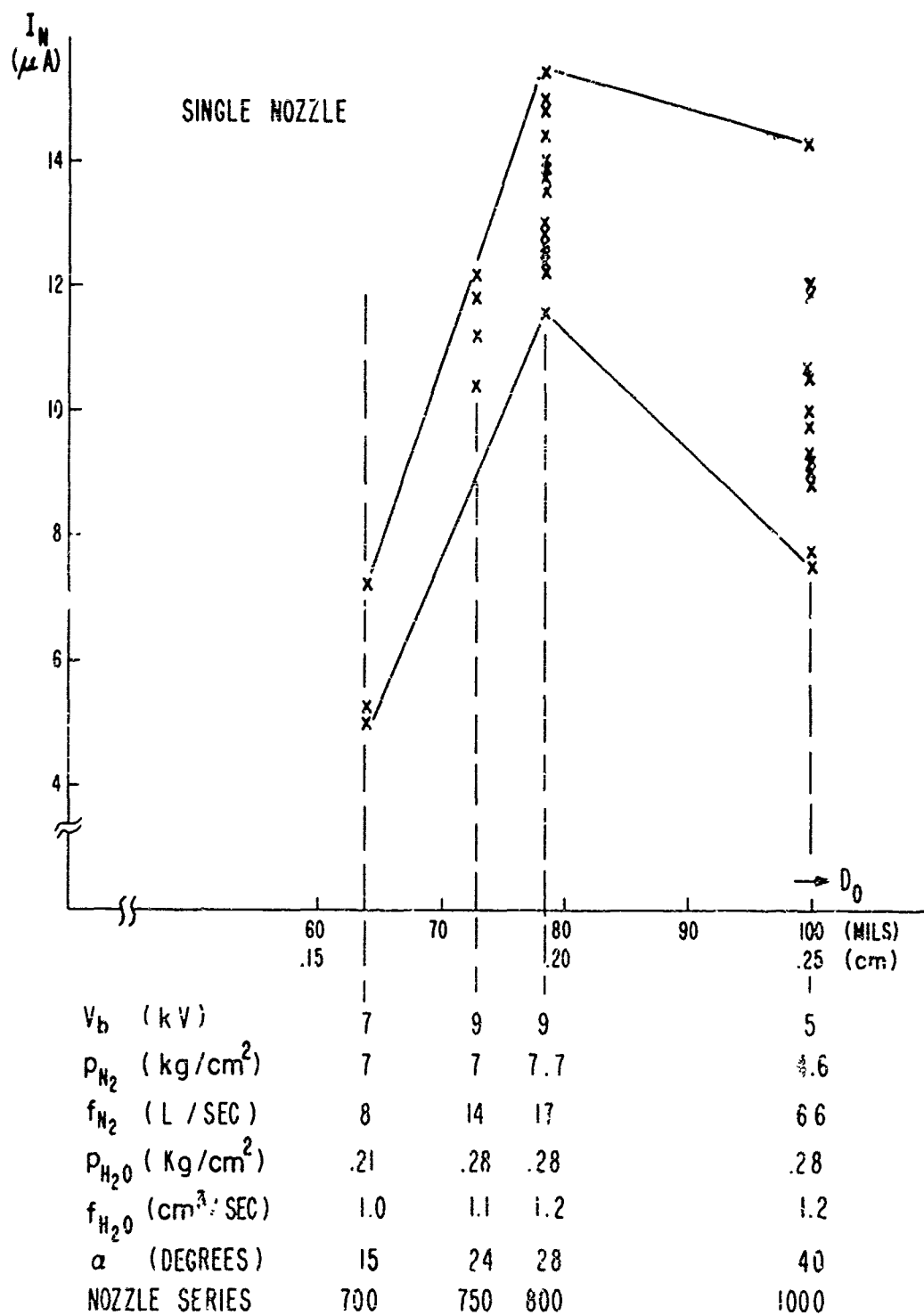


Fig. 3 - Distribution of nozzle current for different air orifices. Below the graph is a list of the optimum voltage and pressure settings, resulting flow rates and spray cone angles.

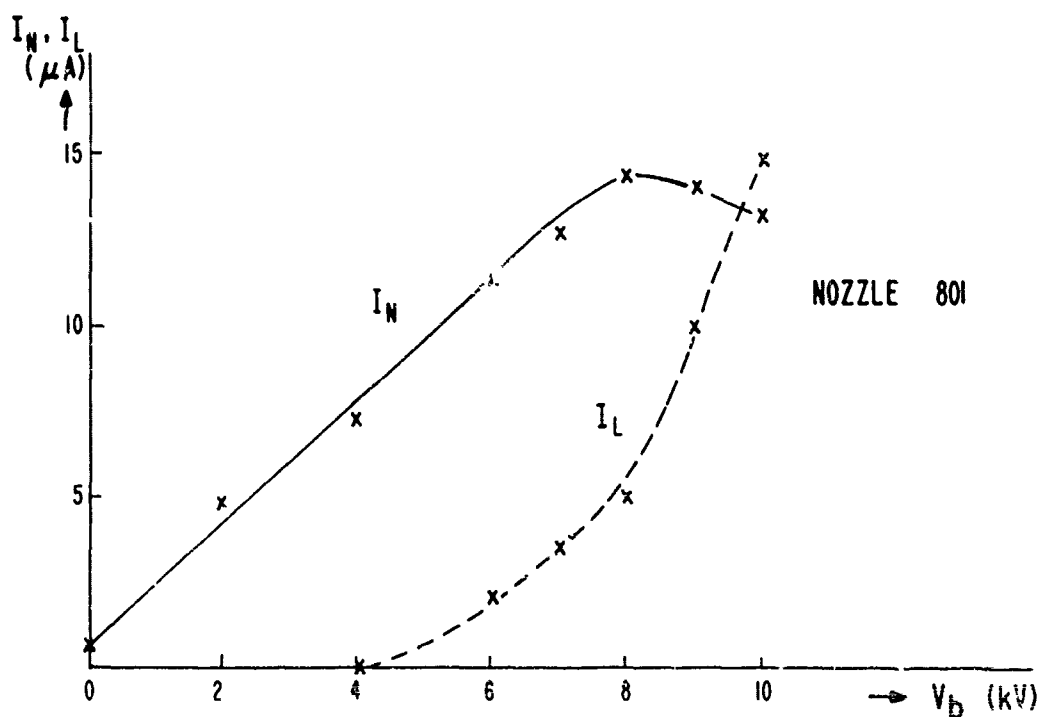


Fig. 4 - Nozzle current and leakage current variation with bias voltage. Dashed line shows the leakage current  $I_L$ .

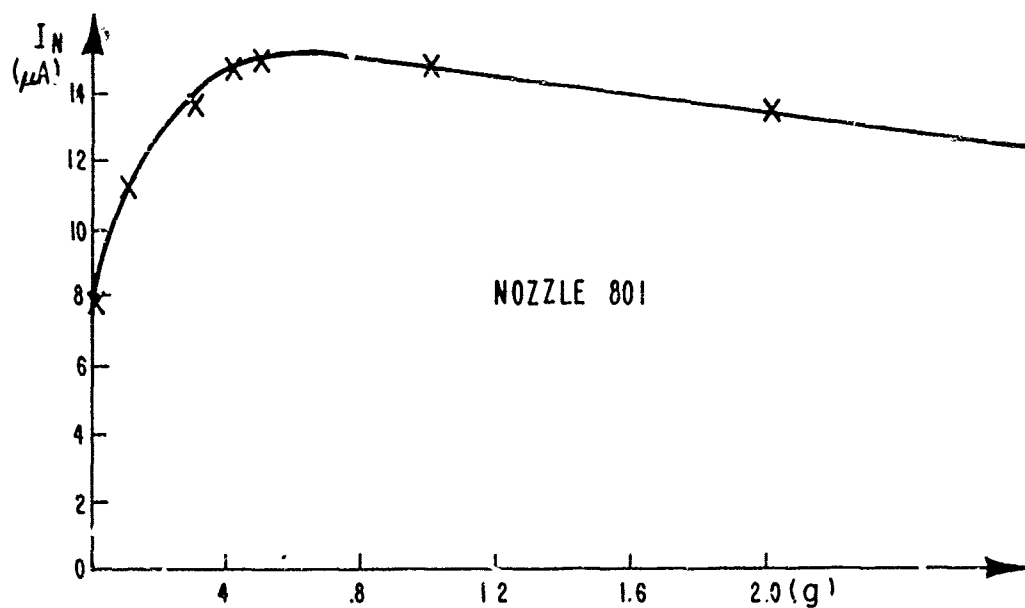


Fig. 5 - Nozzle current variation with salinity. The horizontal scale indicates the weight of table salt (NaCl) added to 8 liter distilled water.

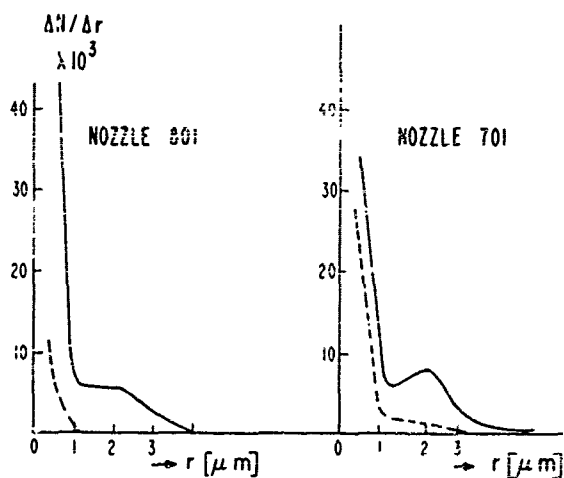


Fig. 6 - Droplet count as a function of droplet radius. The droplet count of 8 droplet size groups was determined with a Royco 4000 particle counter for the 700 and 600 nozzle series. Solid lines are for zero bias voltage, dotted lines for bias voltages of 4.6 kV and 9.2 kV, and for nozzle currents of 6 and 15  $\mu A$ , respectively.

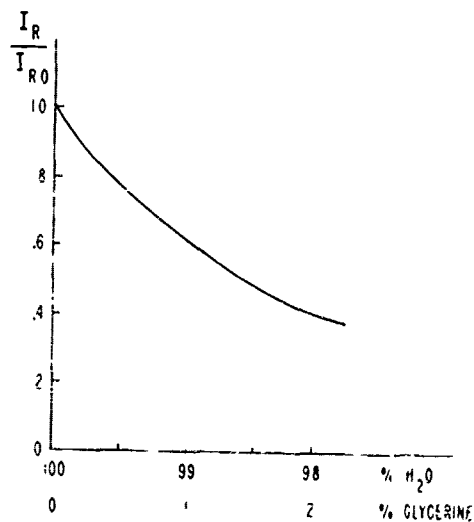


Fig. 7 - Reduction of recirculation effects with chemical additives increasing surface tension and particle size.

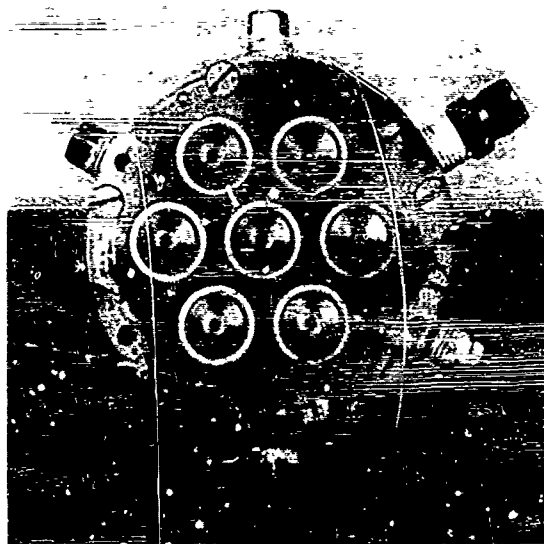


Fig. 8 - Front view of a compact seven-nozzle cluster.

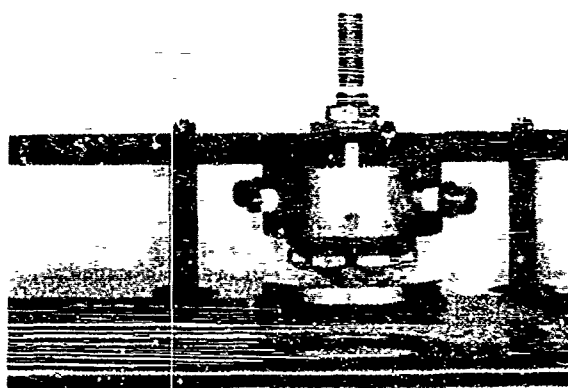


Fig. 9 - Side view of the discharger used in laboratory tests.

flow experienced by an open structure. Figure 10 presents the sideview of the installation of one cluster.

Two sets of tests were conducted to obtain static and dynamic data of the effective discharge current: In one set, the helicopter was connected (via 400 ft cable) to a low impedance power supply on ground adjustable from 0 to 20 kV in order to make a static determination of the effective discharge current in comparison to the actual nozzle current. In the other set, the helicopter was floating while charged particles emitted from the nozzles charged the aircraft to the corona equilibrium. A sudden change in particle polarity initiated the discharge and subsequent charge to opposite polarity. In this dynamic method, the effective discharge current is determined from the calibrated helicopter voltage readings which are proportional to the field mill indications at a constant altitude. Figure 11 depicts the aircraft instrumentation package consisting of: a high voltage power supply ( $V_b$ ) for the bias electrode with provision for rapid polarity switching at the high voltage output, compressed nitrogen with regulators ( $N_2$ ) in lieu of compressed air, fluid storage tanks ( $H_2O$ ) pressurized by nitrogen through a separate regulator, magnetic valves (MV) and pressure gages (PM) in the feed lines to the nozzle clusters, and recorders determining nozzle currents, leakage currents, and cable current or field mill indication.

In Figure 12, the various elements of the instrumentation package are shown as they are mounted inside the helicopter. Figure 13 shows the helicopter in flight with one discharger operational hovering at 25 feet.

Experimental results of the static and dynamic tests, resulting from 25 test runs, are summarized in Figure 14. While there was no difficulty in duplicating the original nozzle currents, as determined in the laboratory under flight conditions, the effective discharge current, with the helicopter connected to ground (static test), was only 30-40% of the nozzle current and indicates a considerable degree of recirculation.

If the helicopter is put on a potential above ground (by energizing the low impedance high voltage source in series with the ground cable), the recirculation current is reduced as is expected. On the other hand, evaluation of dynamic measurements leads to somewhat different, though not inconsistent results, indicating reduced particle recirculation effects. These data were derived from recorded charts taken during each test as shown in Figure 15. Here, the effective particle current  $i_{eff}$ , between helicopter and ground, has been determined as the difference between the total helicopter to ground current and the atmospheric discharge current at the humidity and temperature conditions of the test site. The total discharge current  $i_t$  has been derived from the helicopter voltage using the relation

$$i_t = C_H \cdot dU_H/dt \quad (1)$$

( $C_H \approx 500$  pF at 25 feet altitude;  $U_H$  is obtained from the calibrated field mill indication). For equal helicopter voltages, the corresponding atmospheric discharge current values were derived from the observed exponential voltage decay following termination of particle emission.

A comparison of the static and dynamic test results at zero helicopter voltage in Figure 14 shows that the particle recirculation to the aircraft varies from 65% to 40% of the emitted particle current  $i_H$  with the described (not optimized) nozzle configuration discussed previously. The dynamic data are taken with the aircraft floating (equivalent resistance  $R_{eq} \approx 109$  ohms), which is a close representation of the true electric environment of the helicopter. The variation between the static and dynamic measurements probably indicates the influence of the ground cable used in the static tests in changing the charge distribution on the helicopter and the concomitant distortion of the field between helicopter and ground. It is this deviation from a relatively uniform capacitor field which may cause unreliable indications on field meters located on the fuselage.

Figure 14 also clearly indicates that recirculation at high electrical fields, between aircraft and ground, is rapidly reduced to low values as the aircraft potential increased to 100 kV. This is in contrast to the corona discharge approach, where the recirculation becomes a maximum at high potential. Additional tests were conducted at aircraft potentials above 150 kV using two additive nozzle clusters. The data lead to the conclusion that the particle recirculation will approach zero as the aircraft potential rises near the corona limit.

## CONCLUSIONS

1. Controlled emission of charge carrying liquid droplets has been successfully demonstrated. Single circular nozzle currents, up to 16  $\mu A$  with acceptable operational efficiency, have been achieved, and a compact seven nozzle cluster array with currents up to 80  $\mu A$  have been developed; prospects for further improvements in performance look promising.

2. The flight tests indicate that the droplet discharge principle does work. Additional efforts changing the droplet size-charge distribution are required to reduce the recirculation for near zero potential operation. Sensor measurements and previously obtained systems results indicate overall feasibility of an automatic helicopter discharge system.



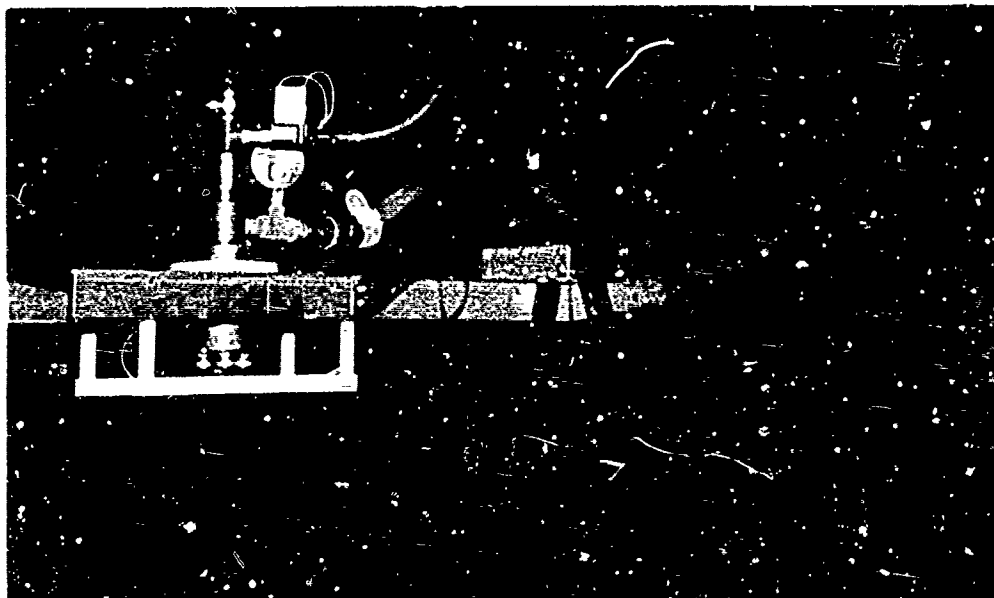


Fig. 10 - Starboard side discharger without airfoil.

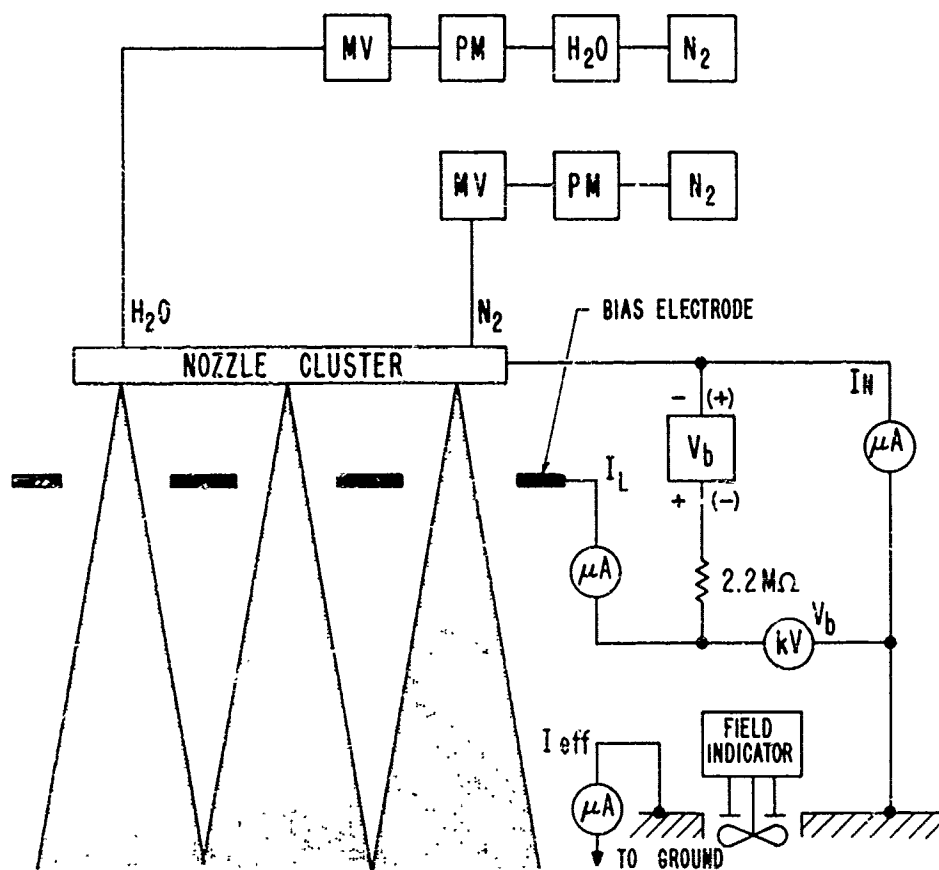


Fig. 11 - Flight test instrumentation for one discharger unit.

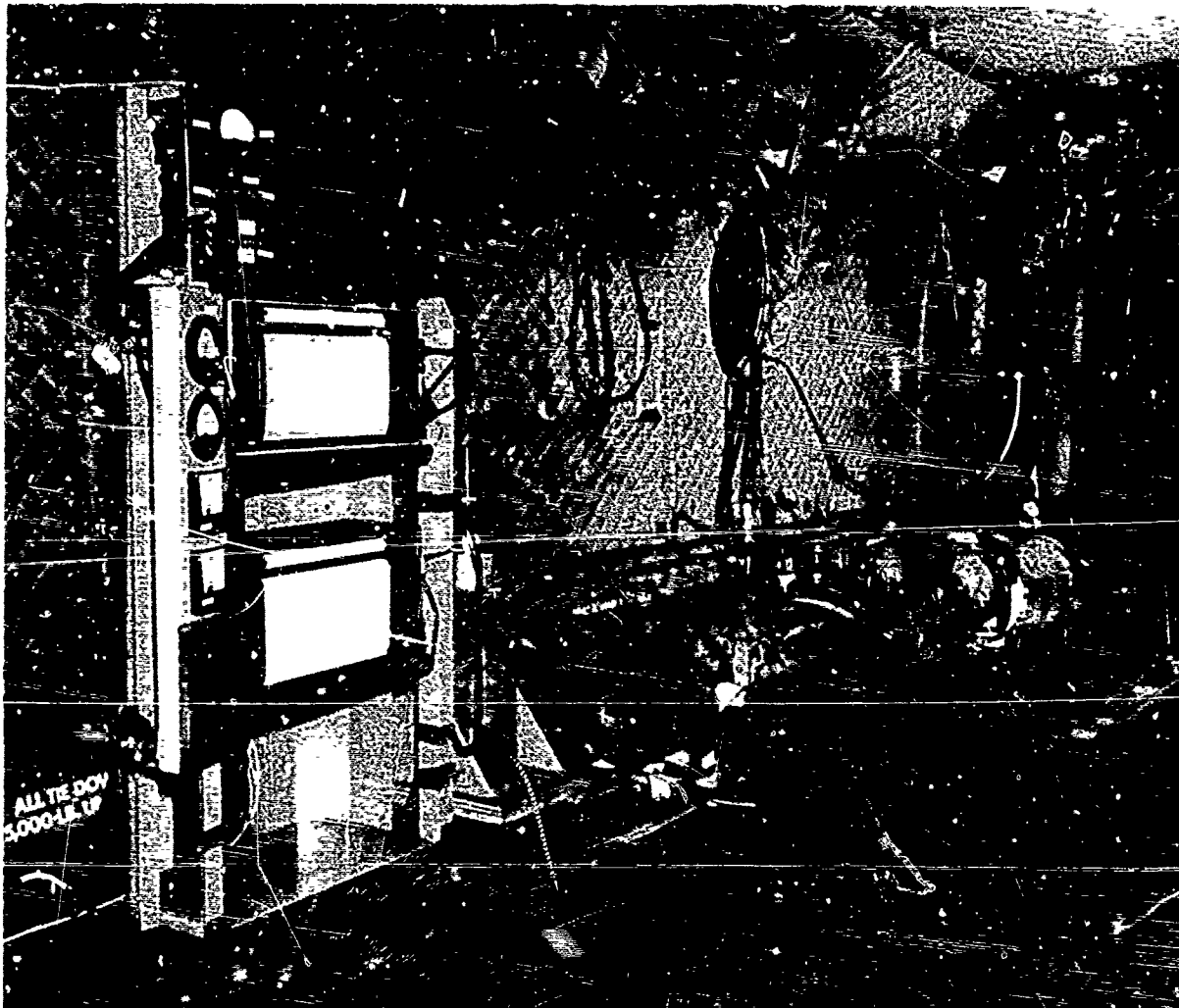


Fig. 12 - Internal instrumentation for flight tests.

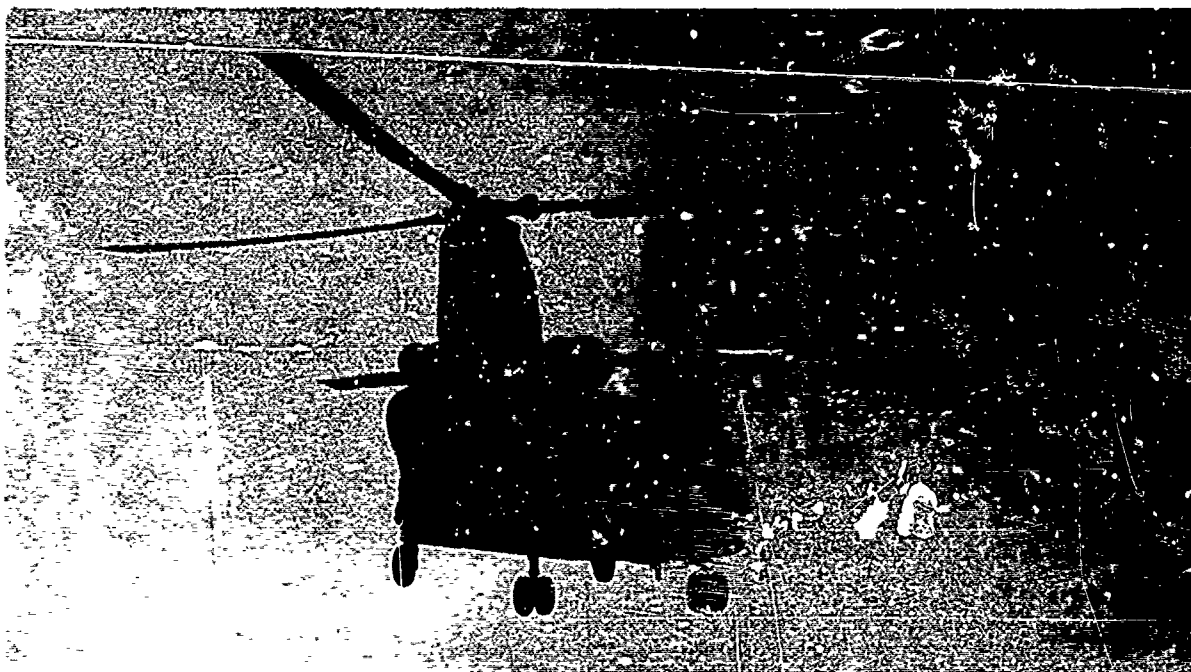


Fig. 13 - CH47C helicopter in test flight showing operation of starboard discharger.

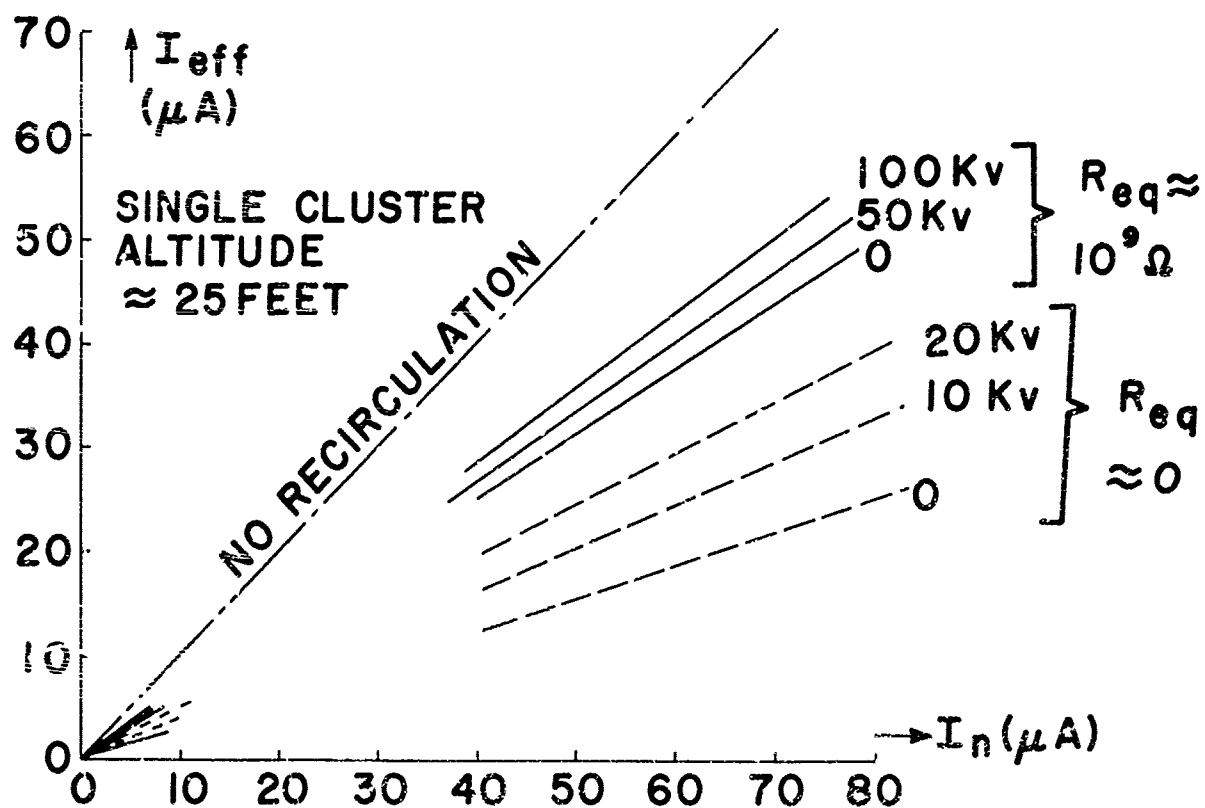


Fig. 14 - Effective discharge current versus emitted current, data normalized to single cluster from static ( $R_{eq} \approx 0$ ) and dynamic ( $R_{eq} \approx 10^9 \Omega$ ) tests.

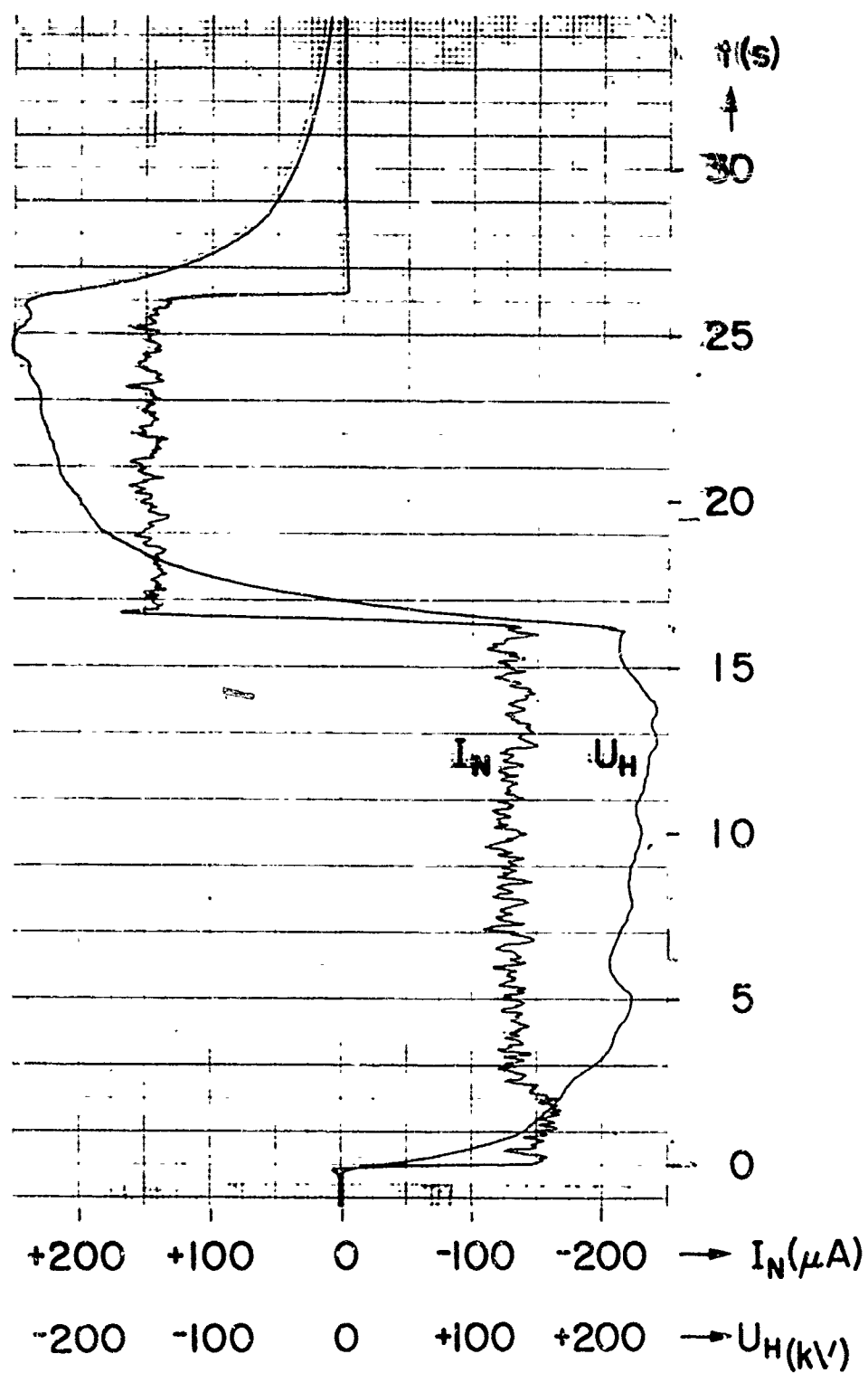


Fig. 15 - Sample recording of helicopter potential  $U_H$  and total emitted current  $I_N$  as functions of time.

#### REFERENCES

1. H. E. Inslerman, et al., ENSURE 265 C-54 (Flying Crane) Electrostatic Discharge Evaluation, ECOM TR-3120.
2. Resistive Link Portions of "Safe Cargo Hook-Up System," ECOM TR 02412-6, PPAR Contract DA 28-043-AMC-02412(E). Sept 1970.
3. T. R. Andrews and R. H. Forrest, "Evaluation of an Active Electrostatic Discharge Mounted on an Engine Exhaust of a Helicopter," TR-71219, Royal Aircraft Establishment (UK), Nov 1971.
4. R. G. Buser, H. M. Kaunzinger and H. E. Inslerman, "Discharge of Helicopters by Electronically Controlled Emission of Charge Carrying Liquid Droplets," 1972 US Army Science Conference.

# A Passive Discharge System for the Electrically Charged Hovering Helicopter

G.J. Born and E.J. Durbin  
Instrumentation and Control Laboratory  
Department of Aerospace & Mechanical Sciences  
Princeton University, Princeton, New Jersey

## ABSTRACT

The charging and discharging processes of a helicopter in flight are discussed. Emphasis is placed upon obtaining approximations for estimating the magnitude of the problem for given environmental conditions. The problems of electrostatic charging and discharging of helicopters with regard to safety of personnel, cargo and radio frequency interference are stated. Acceptable safety limits for personnel protection and safe cargo handling are presented.

A solution to the discharge problems of the electrically charged hovering helicopters is proposed, using current technology. The construction and test results of this "safe-cargo system" (SAFCAR) are described.

THE ELECTROSTATIC CHARGING AND DISCHARGING phenomena experienced by helicopters in flight leads to many operational problems. In forward flight, the presence of static charges on the airframe may cause some radio and navigational equipment interference to be experienced during natural corona discharge. Passive dischargers can often diminish these effects.

A cargo helicopter may be required to hover in the vicinity of ground personnel and equipment during loading and unloading operations under various environmental conditions. Under certain adverse conditions, large electrostatic potentials on the airframe can present a serious hazard.

The hazards can be divided into three basic areas: first, injury to ground handling personnel performing the cargo hook-up; second, possible damage to the cargo itself as a result of discharge current passing through it; third, ignition of fuel-air mixtures in the vicinity of arcs occurring when ground contact is made.

A reasonable solution to the discharge of an electrically charged hovering cargo helicopter must provide:

1. a discharge capability that discharges the helicopter from several hundred kilovolts to approximately earth potential, and/or limits the discharge current, at the point of contact, to a safe level;

2. a steady discharge current capability of at least several hundred micro amperes

under all environmental conditions (corona discharge currents are strongly influenced by environmental effects);

3. a discharge time constant of the order of a second (tentative, subject to results of further investigation);

4. a solution reasonable in cost and weight.

In an earlier paper, [1\*], it was stated that the best helicopter discharge method to date, under all conditions, is a proper grounding technique. All aircraft should be grounded and continuously held at ground potential when fuel, explosives, or similar dangerous cargoes are loaded or unloaded. If the operation takes place where fuel-air mixtures are present, it is advisable that the first earth contact be made via a resistive link of the order of  $10^8$  ohms to reduce the danger of fuel-air ignition (e.g. ground contact be made by a resistive link hanging from the helicopter).

In this paper the background of the problem will be examined. This leads to a specific grounding configuration. The test results of such a configuration are then presented.

## ELECTROSTATIC CHARGING AND DISCHARGING PHENOMENA OF AIRBORNE HELICOPTERS

The main elements involved in the electrical charging and discharging phenomena of airborne helicopters are:

- A. The electrical properties of the helicopter in the atmosphere;

- B. The charging and discharging processes of the helicopter;

- C. The electrical potential of a helicopter in flight.

\* Numbers in brackets designate References at the end of the paper.

A. The Electrical Properties of the Helicopter in the Atmosphere - The capacitance of a helicopter at high altitudes depends only on the helicopter's shape and dimensions. In ground proximity, the helicopter capacitance is increased. Figure 1 presents measured helicopter capacitance values,  $C_H$ , which are approximately proportional to the helicopter body dimensions.

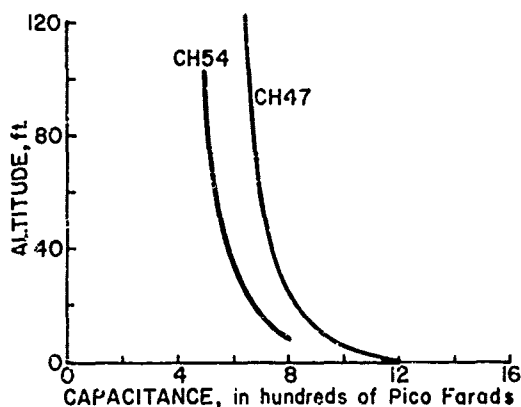


Fig. 1 - Helicopter capacitance as a function of altitude.

The resistance of the air is inversely proportional to the concentration of charge carriers (electrons, whether or not attached to molecules, and ions), the charge on them, and their mobility. The mobility of the charge carriers is inversely proportional to the air density. Under certain atmospheric conditions such as smoke and fog, charge carriers attach themselves to impurities thereby forming "large ions" with reduced mobility. In the lower atmosphere the mobility and the ion concentration depend upon the purity of the air; this explains the large variation in measured air resistance. At sea level, the atmospheric resistivity is in the order of  $10^{13}$  to  $10^{14}$  ohms/meter. The resistivity of the air in the vicinity of a propeller or rotor is decreased over that of still air because the propeller or rotor imparts velocity to the air, and the effective mobility of the ions is increased. Since the resistivity is a function of the number of ions and of their mobility, the effect of this velocity is to reduce the resistivity.

The effective helicopter resistance is defined as the electrical resistance in ohms or the airborne helicopter to ground. The effective resistance of a helicopter, with the engine running, is in the order of  $5 \times 10^9$  ohms. Figure 2 shows the measurements of the effective helicopter resistance as a function of altitude and corona discharge current.

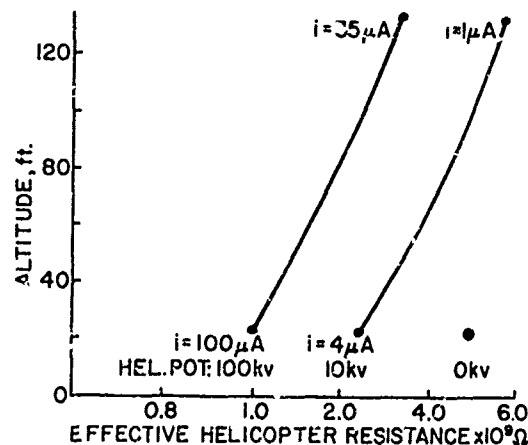


Fig. 2 - Measured effective helicopter resistance vs. altitude (CH47).

The combined effect of helicopter capacitance and effective resistance determines the helicopter charging and discharging time constant, usually in the order of 10 seconds. Measured values of a few seconds to 30 seconds have been recorded, depending on helicopter size, hover height and atmospheric conditions.

B. The Charging and Discharging Processes of a Helicopter - When the processes described below increase or decrease the absolute potential of the helicopter with respect to the earth's potential, they are called charging or discharging processes, respectively.

1. Charging due to Atmospheric Electric Field  
In the absence of any charging process a helicopter flying in the atmosphere would assume a steady state potential equal to the atmospheric potential which exists at that altitude. The atmospheric potential near the ground at an altitude  $h$  is the integral of the potential gradient from the ground to that altitude; that is approximately equal to the product of helicopter altitude times potential

gradient. In fair weather the potential gradient is usually positive and can be several hundred volts per meter. In electrically disturbed weather, fog or rain for example, the potential gradient is usually negative and can be several kilovolts per meter. Under conditions of an approaching thunderstorm, much higher potential gradients have been measured, in the order of a thousand kilovolts per meter prior to lightning strikes. Figure 3 shows expected field strengths under various atmospheric conditions.

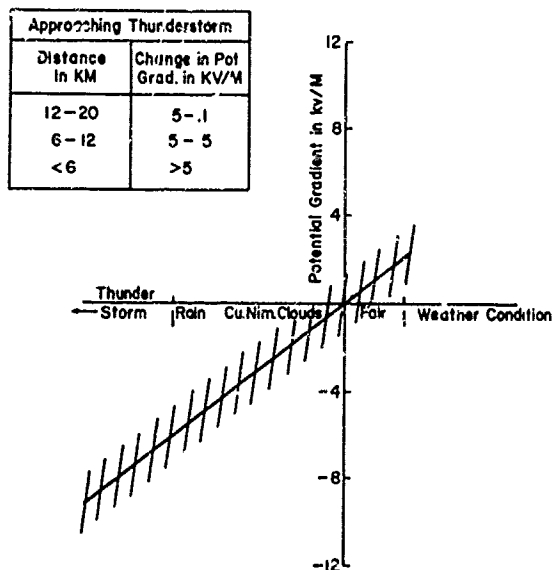


Fig. 3 - Measured potential gradient in KV/M near ground level as a function of weather condition.

## 2. Nonatmospheric Field Charging Processes -

A number of such effects have been described and measured. The most important ones that yield high charging currents are described below.

**Triboelectric Charging** - Triboelectric or frictional charging results when dissimilar materials come in contact with one another. When particles normally found in a helicopter environment, such as dust, sand, snow, rain, etc., strike the aircraft, charging occurs. The charge rate or current depends upon the material, mass, total surface area of the particles intercepted. Usually these currents are less than 50 microamperes, but under extreme conditions currents of several times this number have been reported [2,3]. Some evidence exists that the effective helicopter resistance is lowered in conditions of high triboelectric charging (in the order of  $5 \times 10^8$  ohms).

**Precipitation** - Heavy rain, especially from cumulonimbus clouds, snow, etc., can be

electrically charged and can produce positive or negative charging currents in the order of 100 microamperes, although maximum currents reported in heavy rainstorms near Singapore have been as high as 0.5 mA.

The nonatmospheric charging processes are functions of the amount of particles intercepted, which is a function of the mass flow through the rotor. This depends on the helicopter weight, density of the particles in the air and type of particles. In Figure 4, a monogram shows the charging current as a function of environment and helicopter weight. This graph can be used to estimate the charging current for a given helicopter weight and environment; examples are given for the UH1 and the CH47 helicopters.

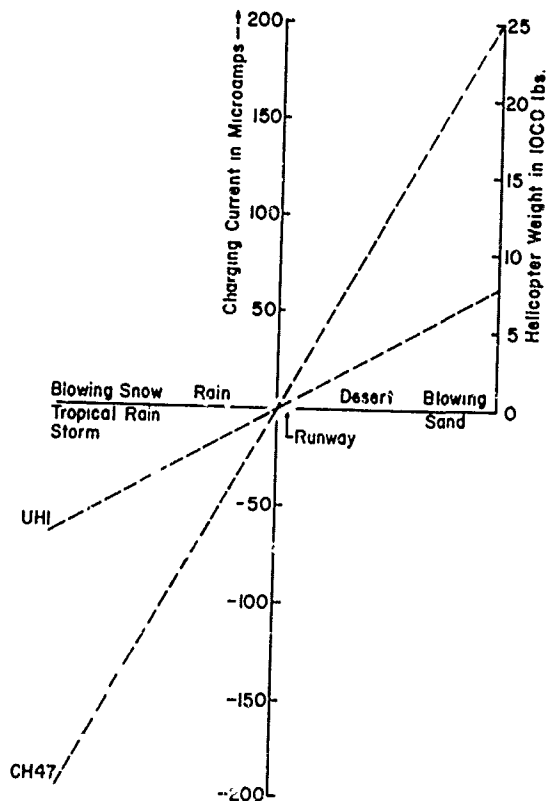


Fig. 4 - Estimated charging current as a function of environment and helicopter weight, (based on experimental data).

## The Ion-generating Charging Process -

The main source reported for the ion-generating charging process is the engine, which can produce ions of one dominant polarity. The generated ion current is also a function of fuel and air composition, as well as engine condition. The aircraft is charged to the opposite of the ion polarity. The order of magnitude of current reported for engine exhaust is in the order of a few microamperes [3], although current levels



in excess of 10 microamperes have been reported.

3. Corona Discharge Process - The basic mechanism of a corona discharge consists of electrons accelerated by the strong electric field near any sharp point. The field strength at the sharp point is directly proportional to the potential at the point and inversely proportional to the square root of the radius of curvature of the point. Thus, when the radius is very small the field strength can be quite large. Locally accelerated electrons ionize the air; these ions are removed from the vicinity of the point by the motion of the air or by the electrical field.

At high currents the magnitude of the corona current from a point is proportional to the voltage squared and is strongly dependent upon geometry and atmospheric conditions and the corona current increases with increasing air velocity. With corona currents in the vicinity of the helicopter, the effective helicopter resistance to ground decreases.

C. The Electrical Potential of a Helicopter in Flight - The airborne helicopter can become charged by any of the charging processes. In principle, these charging processes can be divided into two groups:

1. Electric Field Charging Effects - Assume that an uncharged helicopter becomes airborne. The uncharged helicopter has a capacitance  $C_H$  with respect to earth. The value of the helicopter capacitance is a function of altitude. When the atmospheric potential that exists at the helicopter altitude is not equal to ground potential, then the helicopter is getting charged to the atmospheric potential. In the absence of all other charging processes, the helicopter potential  $V_H$  will become equal to the atmospheric potential  $V_A$ . The time constant of this atmospheric charging process is equal to the product of  $R_H \times C_H$  (in the order of 10 to 30 seconds).

2. Current Generation Effects - When only a charging current is present in absence of an electric field charging process, the potential of the helicopter rises in a time,  $T$ , seconds to a value given by

$$V_H = \frac{Q}{C_H} = \frac{1}{C_H} \int_0^T I_C dt \quad (1)$$

where  $V_H$  is the incremental helicopter voltage in volts

$Q$  is the net charge in coulombs

$C_H$  is the capacitance of the aircraft in farads

$I_C$  is the charging current in amperes

There is a limit to the helicopter potential  $V_H$ . When the helicopter potential rises sufficiently above or below the atmospheric potential ( $V_A$ ) that exists at the helicopter altitude, the corona discharge process starts. This is mainly corona current from areas of high radius of curvature or sharp points. The helicopter discharge current increases as the potential rises, until a state of equilibrium is reached such that the charging current equals the discharging current. Figure 5 shows measured discharge current of the helicopter under natural conditions at 25 ft. hover altitude.

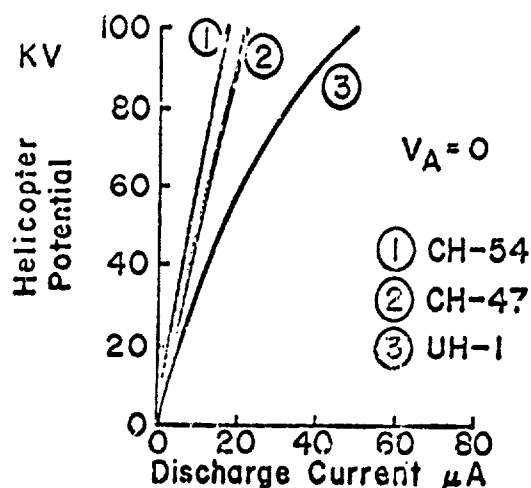


Fig. 5 - Helicopter discharge current as a function of helicopter potential natural conditions at 25 feet hover altitude.

The effectiveness of the corona points determines the effective resistance  $R_H$  of the helicopter. Properly designed passive dischargers (corona points) reduce the effective helicopter resistance. In Figure 6, curves 1, 2, and 3 represent passive dischargers on the rotor blades of the CH47. Curve 4 is obtained by placing a passive dissipator (braiding) 100 feet below the helicopter. NOTE: 40 microamperes discharge current, with 26 kilovolts on the helicopter corresponds to a resistance of  $6.5 \times 10^8$  ohms.

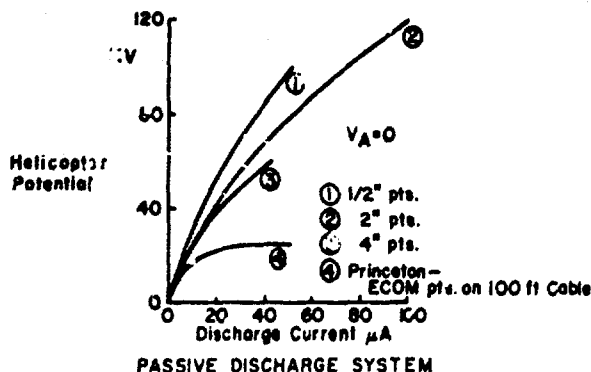


Fig. 6 - Helicopter discharge current from passive dischargers on the rotor blades of a CH47 (25 foot hover), and from a passive discharger (braiding) on a 100 ft. cable, below the helicopter.

For the CH54 helicopter or any other helicopter which has a cargo hook, one can use a passive dissipator on the cargo hook. This can reduce the electrostatic problems considerably. There is evidence that when the surface of helicopter rotor blades is electrically conductive and electrical contact is made with the helicopter fuselage, the effective helicopter resistance  $R_H$  is reduced. (For example, compare Figure 5, curve 3 and Figure 6, curve 1) Measurements indicate that the current to voltage ratio increases with increasing voltage. It is estimated that properly designed passive dissipators can keep the helicopter potential well below 300 kilovolts for 1 milliamperes current, (at 25 ft. hover).

When the helicopter has reached its charged equilibrium, the increase in helicopter potential above the atmospheric potential, due to the charging current is equal to the product of the charging current  $I_C$ , and the effective helicopter resistance,  $R_H$ .

The total helicopter potential  $V_H$  with respect to ground is the sum of the atmospheric potential  $V_A$  and the voltage due to the charging current  $R_H I_C$ .

The helicopter potential is thus dependent on:

- The helicopter capacitance  $C_H$  (in the order of  $10^{-9}$  F).
- The effective helicopter air resistance  $R_H$  (in the order of  $5 \times 10^9$  ohms).
- The atmospheric potential  $V_A$  (the product of estimated potential gradient and helicopter height).
- The charging current  $I_C$  (estimated from helicopter weight and environmental conditions).

A simple useful model of the helicopter charging process is given by the equivalent circuit shown in Figure 7.

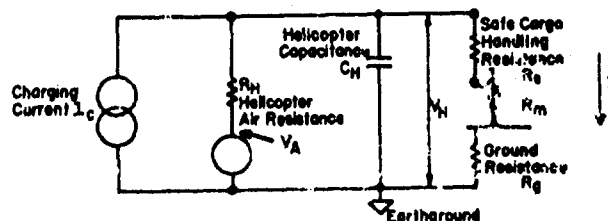
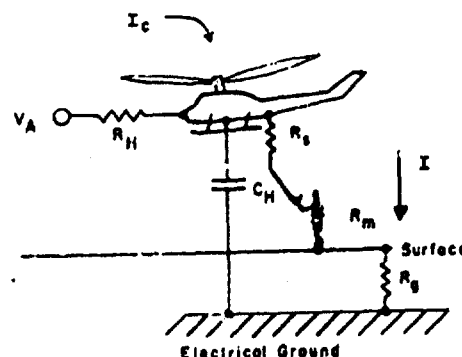


Fig. 7 - Charging and discharging processes of a hovering helicopter.

$V_A$  is a voltage source or generator representing the atmospheric potential,  $I_C$  is the charging current of a current source or generator representing charging mechanisms such as precipitation or blowing sand and dust.  $C_H$  is the capacitance between the helicopter and ground, and  $R_H$  is the resistance between the helicopter and ground. It should

be noted that  $R_H$  in series with the voltage source  $V_A$  determines the charging current of the earth's electric field and therefore  $R_H$  can be considered as the internal resistance of this atmospheric voltage generator.  $V_H$  is the resultant voltage between the helicopter and ground due to the various sources. The helicopter resistance  $R_H$  is actually a function of the current flowing through it, but for simplicity, it is considered to be constant.

#### SAFETY LIMITS OF A CHARGED HELICOPTER

The helicopter capacitance charged to a high voltage is hazardous to personnel or cargo. A large number of "safe" limits for discharges have been determined and reported in the literature which deals with three problem areas, personnel safety, cargo safety, and radio frequency interference.

**A. Personnel Safety** - For a capacitor type of discharge through the human body (resistance of a hundred to several thousand ohms), the sensation threshold level is an energy of the order of one (1) millijoule. (Note: 1 millijoule in  $1 \times 10^{-9}$  F, the helicopter capacity, corresponds to about 1400 volts). Experience has shown that a 10 millijoule discharge under most circumstances causes no great discomfort. Note that the level of energy discharged after a person scuffs across a rug in winter and touches some grounded object is typically 10 to 25 millijoules. It is felt that the sensation associated with a 10 millijoule discharge during a concentrated effort would be insignificant under most circumstances. A significant discharge is that which would cause a person to move involuntarily as a reaction to the shock in such a manner that a loading operation would be aborted. On this basis, the 10 millijoule level was established as reasonable operating level for loading and unloading operations. This is far below the lethal levels (References 7 and 8).

For a constant current type discharge through the human body, the sensation threshold is about 1 milliamperere. Reference 7 indicates that a safe "let go" is possible at a current of 9 milliampereres. This is also far below the lethal DC current level (References 7 and 8).

The sensation threshold for a short transient discharge is a peak current which exceeds the continuous current level. Thus the continuous current level is a conservative standard.

**B. Cargo Safety** - Some examples of published safety limits of a capacitive type dis-

charge for cargo operations are as follows:

1. Explosives (igniters):  $10^{-3}$  millijoule
2. Explosives: several millijoules to 0.5 joule
3. Ignition of stoichiometric fuel-air-gas mixtures:

Energy limits: 0.5 - 1 millijoule.  
Electric current limits

- (a) 180-200  $\mu$ a for constant current,
- (b) 1 milliamperere for a duration of 100 millisec,
- (c) 100 milliampereres for a duration of 0.01 millisec.

b and c represent the same discharge energy.

Normally in open air, the probability of having a stoichiometric mixture appears to be small. Under these circumstances, larger energies are required to ignite the fuel-air mixture. In all the helicopter loading and unloading operations to date, there have been few, if any, cases where ammunition or fuel has been ignited or exploded due to static electricity discharges. On this basis alone, the probability for discharge of significant amounts of energy through sensitive portions of ammunition appear to be small, and the probability of igniting fuel is equally small. This experience has been with helicopters unprotected from the electrostatic charge accumulation. Any reduction in the charge would certainly reduce the probability of ignition.

**C. Radio Frequency Interference** - When the helicopter is charged to a high potential, erratic corona discharges occur which produce RFI. This electrical noise source can severely hinder and even saturate some communication and navigation equipment.

#### THE SAFE CARGO HOOK-UP SYSTEM

**A. Observations** - In reducing the hazards of electrically charged helicopters during cargo hook-up procedures, the following observations should be made:

1. Properly grounding the helicopter (by an electrical conductor) and keeping the helicopter grounded eliminates the hazard.
2. Almost any continuous contact between a conductor and ground surface (sand, asphalt, grass) is sufficient to bring the helicopter's potentials to safe levels.

3. During the grounding procedures before ground contact is made, personnel on the ground may come in contact with the grounding conductor.

4. Upon making ground contact, under certain conditions, the discharge energy can ignite fuel-air mixtures and explosives.

5. The continuous direct current level threshold of sensation is in the order of one milliamperere. The effects of short durations of direct current, such as capacitance-resistance discharges, are less severe than the effects of continuous direct currents of the peak level.

6. When the discharge occurs via a resistive path, the current in the discharge path is determined by the helicopter potential and the resistance of the path.

7. Passive dissipators on the rotor blades diminish the potential build-up on the helicopter.

### B. Conclusions

1. The best method to date, to discharge a hovering cargo helicopter under all conditions, is a proper grounding technique.

2. The aircraft should be grounded and continuously held at ground potential when fuel, explosives, or similar dangerous cargoes are loaded or unloaded.

3. For ground personnel safety and when fuel-air mixtures are present, it is advisable that the first earth contact be made via a resistive path, in order to limit the current to a safe level.

4. Passive dissipators, on the rotor blades and/or cargo hook should be used to diminish the helicopter potential build up.

C. System Analysis - In Figure 7 the resistive grounding path for discharging consists of

$R_s$  the safe cargo handling resistance approximately (100 megohms).

$R_g$  the ground resistance, or the resistance from the ground contact to earth ground (< 10 megohms).

$R_m$  the resistance of the man (< 3 kilo ohm).

When electrical contact is not made through the resistances  $R_s$ ,  $R_m$  and  $R_g$ , then the helicopter voltage is determined by:

$$C_H \frac{dV_H}{dt} + \frac{V_H - V_A}{R_H} - I_c = 0 \quad (2)$$

With the initial condition  $V_H = 0$  at  $t = 0$  this yields:

$$V_H = (V_A + R_H I_c) (1 - e^{-\frac{t}{R_H C_H}}) \quad (3)$$

The charging time constant is:

$$T = R_H C_H \quad (4)$$

and the final helicopter potential at equilibrium is:

$$V_H = V_A + R_H I_c \quad (5)$$

Note that if the helicopter air resistance  $R_H$  can be made zero (or small) then the helicopter potential  $V_H$  equals (or approximates) the atmospheric potential  $V_A$ .

When electrical contact is made and an electrical grounding path is established through the resistances  $R_s$ ,  $R_m$  and  $R_g$ , then the helicopter potential is determined by:

$$C_H \frac{dV_H}{dt} + \frac{V_H - V_A}{R_H} + \frac{V_H}{R_s + R_m + R_g} - I_c = 0 \quad (6)$$

With an initial helicopter potential  $V_{H0}$  at  $t = 0$ , this yields for the helicopter voltage  $V_H$ :

$$V_H = \frac{(R_s + R_m + R_g)}{R_H + (R_s + R_m + R_g)} (V_A + I_c R_H) (1 - e^{-\frac{t}{C_H R}}) + V_{H0} e^{-\frac{t}{C_H R}} \quad (7)$$

where:  $R$  is the parallel combination of  $R_H$  and the grounding path

$$R = \frac{R_H (R_s + R_m + R_g)}{R_H + (R_s + R_m + R_g)}$$

The final helicopter potential at equilibrium is:

$$V_{H\infty} = \frac{(R_s + R_m + R_g)}{R_H + (R_s + R_m + R_g)} (V_A + I_c R_H) \quad (8)$$

The discharging time constant is

$$T_d = C_H R \quad (9)$$

The current through the resistive grounding path is:

$$I = \frac{V_H}{R_s + R_m + R_g} \quad (10)$$

### D. Examples

1. No Ground Resistance ( $R_g = 0$ ) and No Safe Cargo Resistance ( $R_s = 0$ ). This is the case of the unprotected helicopter and a man with resistance  $R_m$  making the electrical

conductive path between helicopter and ground. Under normal operational conditions, the electrical resistance  $R_m$  is much smaller than the helicopter air resistance  $R_H$ .

Substitution of  $R_s = 0$ ,  $R_g = 0$  and  $R_m \ll R_H$  yields:

$$R = \frac{R_m R_H}{R_H + R_m} \approx R_m$$

$$V_H \approx (V_A + R_H I_C) e^{-\frac{t}{R_m C}}$$

The current  $I$  through the conduction path is.

$$I = \frac{V_H}{R_m} \quad (10a)$$

This current given by Equation (10a) will pass through the man touching the charged helicopter and under normal operating conditions exceeds by far the "safe current level". By placing the safe cargo resistance  $R_s$  in series with the man's resistance ( $R_m$ ), the current level can be kept within "safe current levels".

If a helicopter of 1,000  $\mu\text{F}$  is charged to 100 kilovolts and the resistance  $R_m$  is 500 ohms, the peak current equals 200 amperes in the impulse energy discharge of 5 joules.

2. No Ground Resistance ( $R_g = 0$ ) and a Safe Cargo Resistance ( $R_s \approx 10^8$  ohms) - When making ground contact, such a discharge system should have the following characteristics:

- The peak current should be about 1 milliamperes. This level occurs when a helicopter is charged to 100 kilovolts,

$$\frac{100 \times 10^3 \text{ volts}}{100 \times 10^5 \text{ ohms}} = 1 \times 10^{-3} \text{ ampere}$$

- The time constant should be less than a second. The discharge time constant equals the helicopter capacitance times the total resistance to ground. The latter is always less than the lowest resistance path to ground. For a helicopter of  $10^{-3}$  farads the time constant is

$$T = C_H (R_s + R_m) \approx C_H R_s = 10^{-3} \times 10^8 = 10^{-1} \text{ sec.}$$

$$(R_m \ll R_s)$$

In this example the final helicopter potential at equilibrium will be

$$V_{H\infty} = \frac{R_s + R_m}{R_H + R_s + R_m} (V_A + I_C R_H) \approx \frac{R_s}{R_H + R_s} (V_A + I_C R_H)$$

Assume this helicopter operates in rain hovering at 30 feet, in an atmospheric potential gradient of  $-4\text{kv/m}$  and a triboelectrical charging current of  $-30 \mu\text{A}$ , and the effective air resistance is  $2 \times 10^8$  ohms.

The helicopter potential is before ground contact is made:

$$V_H = (V_A + I_C R_H) = (-40 + -60) = -100 \text{ kilovolts}$$

The final helicopter potential after ground contact is:

$$V_{H\infty} \approx \frac{R_s}{R_H + R_s} (V_A + I_C R_H) = \frac{10^8}{2.1 \times 10^8 + 10^8} 10^5 = -4.8 \text{ kilovolts}$$

This voltage on a helicopter of 1,000 picofarads can produce an energy discharge equal to  $1 \times 10^{-9} \times (4.8 \times 10^3)^2 = 22 \text{ millijoules}$ .

3. A Large Ground Resistance  $R_g$  and a Safe Cargo Resistance  $R_s$  - Under most operating conditions, such as over clay, sand, runway surfaces, the measured ground resistance  $R_g$  is less than the safe cargo resistance  $R_s$  ( $10^8$  ohms) and the effect of the ground resistance is small. However, there can exist situations where the ground resistance  $R_g$  is large. This might occur over a thick layer of fresh snow.

When the safe cargo hook-up system is used, and no other contact with the helicopter is made then the current through the conduction path is less than with no ground resistance. Hence: when the safe cargo resistance is placed in series with the hook and only hook contact is made, electrical current limiting is effective and a ground resistance  $R_g$  has no deleterious effects on the safe cargo hook-up system.

However, the final helicopter potential is after the ground contact is made:

$$V_{H\infty} = \frac{R_s + R_g}{R_H + R_s + R_g} (V_A + I_C R_H)$$

When a helicopter is charged to  $-100 \text{ kv}$ , with ground resistance  $R_g = 5 \times 10^8$  ohms, the final helicopter voltage becomes

$$V_{H\infty} = \frac{10^8 + 5 \times 10^8}{2 \times 10^8 + 10^8 + 5 \times 10^8} 10^5 = -23 \text{ kilovolts}$$

In this case two situations can occur:

- Personnel standing on a large ground resistance. Under this condition the energy discharge is equal to

$$\frac{1}{2} C_{\text{man}} V_H^2 = \frac{1}{2} 50 \times 10^{-12} \times (23 \times 10^3)^2 = 13 \text{ millijoules}$$

- b. Personnel standing on a large load with a capacitance to ground when making contact with the helicopter. The safe cargo hook up resistance is short circuited. This short circuit provides a discharge path for charge equalization between the charged helicopter capacitance and the uncharged load capacitance.

If the load capacitance was also 1,000 pf, the energy transfer through the short circuit can be  $\frac{1}{2} \frac{1}{2} C_H V_{H\infty}^2 = 130$  millijoules, which causes severe shock.

Hence, when in extreme cases the ground resistance is large, personnel should not come in contact with the helicopter directly only through a safe cargo handling resistor.

E. System Description - The proposed SAFCAR system consists of two elements

1. Passive dissipators on the blades and/or hook for limitation of the electrical potential on the helicopter.

2. A resistive element in the discharge path to limit the electrical current to "safe" levels.

A resistive element can be placed between the cargo hook and the airframe or can be placed in the grounding path (resistive grounding link). Both methods are described below:

1. An Electrical Resistive Element Between Cargo Hook and Airframe - This element performs two functions: it diminishes the electrical current through the cargo hook (The electrical current is determined by the ratio of the potential difference and electrical resistance in the path), and after ground contact has been made, it reduces the helicopter potential with respect to ground.

The construction method for an insulated hook can be one of the following:

- a. An insulated beam or cargo hook (resistance between airframe or cargo hook). This approach is operationally very desirable as cargo loading procedures are not affected. To use this method, a change in existing aircraft construction must be made.
- b. Insulated cargo link. In this case, the resistance is placed between a new hook and the original cargo hook on the aircraft. In this approach, a "doughnut" type device with a hook can be hung on the original cargo hook of the helicopter.

In the implementation of these methods, the cargo hook capacitance should be minimized because the cargo hook capacitance can cause an electrical charge transfer when hook contact is made. (Typical measured capacitance values of a CH47 cargo hook, < 30 pF)

2. An Electrical Resistive Element in the Grounding Path (grounding link) - The grounding link is a device that can be attached to the cargo hook or cargo and provides grounding with resistance in the grounding path. The purpose of a resistive grounding link is to reduce the electrical potential of the helicopter and/or cargo to ground potential. The resistance diminishes the electrical current in the ground path when the grounding link comes in contact with ground, personnel or cargo.

Essentially, a ground link is a conductor of 8 feet or more in length with a resistance on the order of  $10^6$  ohms. This length insures ground contact is made before personnel can make contact with the hook. The grounding link reduces the helicopter potential to a value given by Equation (8).

In order to provide safety under all conditions, it is essential that a good ground contact ( $R_g < 10^7$  ohms) is made and that the helicopter and load are grounded and kept grounded during cargo operations.

This method is quite inexpensive and can solve the personnel safety problem but requires changes in operational hook-up procedures.

If desirable, as for flammable cargo, the grounding link can also be used for discharging the cargo prior to release. A "ground link" is then connected to the cargo so as to make ground contact before cargo release.

F. System Tests and Evaluation - Laboratory tests were performed to confirm the current threshold levels with high voltages using resistors and capacitances for simulating the helicopter and the hook capacitance to ground. It was assumed that passive dissipators in a helicopter would limit the helicopter voltage to the order of 100 kilovolts.

Several resistive grounding links were designed and tested in the laboratory. The test results were promising and a safe cargo hook up system was designed to insulate the cargo hook from the airframe of the CH47 helicopter.

The insulated cargo hook was tested electrically up to 100 kV and the resistance was measured to be  $10^6$  ohms. The touch test was performed. A ground strap was wrapped around the little finger and touch was made at 10 kV steps up to 70 kV. A mild sensation was

detected from 30 kV on up to 70 kV. A second touch test was made up to 100 kV with the same results except that at 85 to 100 kV no sensation was experienced. In both tests a faint snap was heard just prior to touch.

The safe cargo hook-up system (SAFCAR) was installed in a CH47 helicopter. The latter was artificially charged to 70 kV (limit of the voltage generator). The cargo hook was touched by personnel. The worst sensation detected, caused by the unprotected hook capacitance, corresponded to the mild shock one gets from a carpet. Similar experiments were conducted with resistive grounding links on a CH54 helicopter. A summary of the results is given in Figure 8.

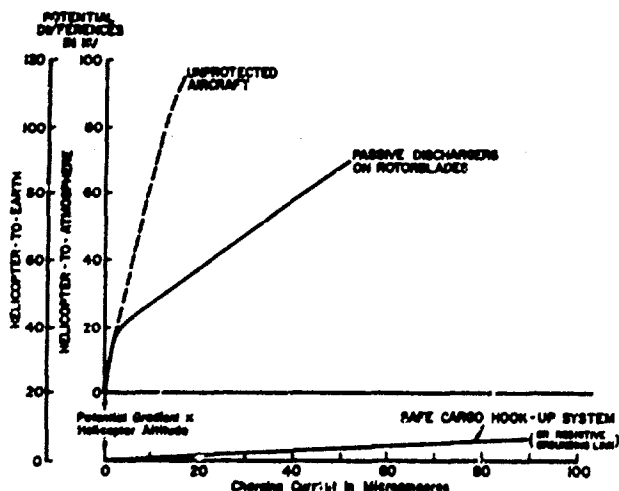


Fig. 8 - Safe cargo hook-up system evaluation (for an atmospheric potential of 20 kV)

The left ordinate axis gives the helicopter potential with respect to ground; the right ordinate axis gives the helicopter potential with respect to the atmosphere at the helicopter altitude. The difference between the two ordinates is the atmospheric potential which is approximately equal to potential gradient times helicopter altitude. In Figure 8, this atmospheric potential is 20 kilovolts. The passive dischargers on the rotor blades reduces the electrical helicopter potential with respect to the atmospheric potential.

The curve marked "safe cargo hook up system" (SAFCAR), or resistive grounding link, indicates the potential on the helicopter with respect to ground after electrical ground is made. With the safe cargo hook up system, the current is greatly reduced whenever electrical contact is made with the hook. When electrical

ground contact is made and maintained, the helicopter cargo and hook potential become as indicated in Figure 8.

In the case of a resistive grounding link, Figure 8 indicates a lowering of the electrical potential (with respect to ground) of the helicopter and cargo hook when electrical ground contact is made and maintained.

The evaluation of the proposed systems can be summarized as follows:

1. Laboratory models of the "safe cargo hook up system" (SAFCAR) have been successfully tested in the laboratory and with artificially charged airborne helicopters.
2. The method is reasonable in cost and weight. Depending upon the system version chosen, no changes or only small changes need to be made in the operational cargo loading procedures.
3. If desirable, as for flammable cargo, a "grounding link" can also be used for discharging the cargo prior to release.

G. Recommendations - A simple solution to the electrostatic problems connected with the loading of a hovering helicopter is proposed. The "safe cargo hook up system" provides reasonable personnel and cargo safety during cargo hook-up operations.

Some engineering problems should be further investigated and complete prototypes should be made to be tested in the field under all operational conditions.

In the development or design of new cargo helicopters, emphasis should be placed upon the possible solutions of electrostatic problems.

The "safe cargo hook up system", if implemented in the basic helicopter design, could be incorporated with relatively small penalties in cost and weight.

#### ACKNOWLEDGEMENT

The work reported here is part of a study which was originally supported by the Aviation Laboratory of the U.S. Army, and support was continued by the U.S. Army Avionics Laboratory, ECOM. The development, testing and evaluation of the passive discharge system is the result of cooperative effort, at various times, with the following persons: E.G. Sharkoff (U.S. Army Picatinny Arsenal), R. Creed, M.M. Chrepta, and H.E. Inslerman (U.S. Army Avionics Laboratory, ECOM).

# REFERENCES

1. Born, G., Creed, R., Durbin, E.J. and Sharkoff, E. "The Electrostatic Charging and Discharging Phenomena of Helicopters in Flight", Lightning and Static Electricity Conference, 3-5 December 1968.
2. Seibert, J. "Helicopter Static Electricity Measurement", TRCOMTR, AD No. 282 087.
3. Rogers, M.E. and Miniham, E.B. "Interim Report on Investigation of Static Build-Up on Helicopters with Particular References to Whirlwind MK10.s." Royal Aircraft Establishment Technical Report No. 66152.
4. "CH47 Cargo Helicopter, Cargo Beam Insulator Design and Evolution", Avionics Laboratory, November 1968.
5. Sharkoff, F.G. "Electrostatic Research", The Princeton Pennsylvania Army Avionics Research Program, 1969 3rd Annual Report, ECOM-02412-5, pp. 43-58.
6. Born, G.J. and Durbin, E.J., "A Fundamental Study of Static Electric Phenomena", The Princeton Pennsylvania Army Avionics Research Program, 1970 4th Annual Report, ECOM-02412-6, pp. 27-53.
7. Balziel, C.F. and Lee, W.R., "Zethal Electric Currents", IEEE Spectrum, February, 1969.
8. Susskind, C., "The Encyclopedia of Electronics", Reinhold Publishing Corporation, New York. Chapman & Hall LTD., London, pp. 205-208.



## COMPARATIVE EVALUATION OF A NEW RADOME LIGHTNING PROTECTION SYSTEM

BY

L. C. Hoots, Technical Products Division, Brunswick Corporation

and

M. P. Amason & G. J. Cassell, Douglas Aircraft Co., McDonnell-Douglas Corporation

Previous aircraft radome lightning protection systems have included several types of metallic strip diverters. A more recent innovation has been to replace such strips with a series of metal segments connected with resistance material. Comparative antenna testing is described, in which a radome was alternately fitted with the two types of diverters. For the ogive nose cone and enclosed low sidelobe test antenna, sidelobes created by diverters are noted to decrease from ten (10) db for solid metal to one (1) db with the segmented strips. In addition to the radar antenna tests, results showing the protective capability of segmented diverters for lightning are summarized. Plans for additional work tasks relative to segmented diverter strips, to be conducted as a part of a current Air Force sponsored project, are related.

IN A GREAT MANY AIRCRAFT, the metal radar antenna installation housed within the nose cone or radome provides metallic objects with edges and protrusions. These are the main source of ionized streamers created at the aircraft nose by high stress fields. These streamers can pass through an unprotected radome creating the path for main lightning stroke attachment. Although strike incidence in this area may be low in comparison to some other aircraft features, the risk factor is of enough significance that metallic diverters are often used to intercept the strike and transfer the associated charge to the aircraft fuselage.

### PAST PRACTICE

Configurations to provide radome lightning protection have varied considerably in the past. Typical installations have included conductors orientated lengthwise and spaced radially around the radome to provide a cage or shield of protection for the enclosed antenna system. A nose radome with radial lightning strip diverters used is shown in Figure 1. Such an electrostatic shield reduces streamers from the antennas and provides a new source of streamers outside the radome. Lightning can then attach to these external streamers and travel down the strips to the fuselage without damaging the radome or antennas. Specific layouts for such an installation generally depend upon factors such as the antenna location, proximity of the antenna to the radome wall, and the dielectric breakdown strength of the plastic structure. Such designs are ordinarily subjected to simulated lightning testing and are dimensionally dependent upon the specific

enclosed objects and the degree of protection desired.

Diverter strips have comprised three main types, namely:

- (1) Thin, foil-like, conductors for single stroke protection,
- (2) Rectangular cross-sectional diverters about 1/2" wide and 1/8" thick to provide permanent protection, and
- (3) Circular cross-section rods on the radome interior with metal buttons protruding through the wall to maintain a flush exterior profile.

These three diverter types are illustrated in Figure 2, and all may be arranged as previously illustrated. The foil strip vaporizes upon being struck by lightning. The strip with rectangular cross-section provides permanent protection at the sacrifice of increased drag. The internal rod with through-protrusions is also permanent and eliminates the drag penalty, but involves considerable detailed design and test of mechanical fasteners. This difficulty in design arises as a result of the considerable magnetic ( $L di/dt$ ) forces developed at the rod-button junctures. All three of the diverters described influence the radiation patterns of enclosed radar antennas. The lightning protection/radar degradation trade-offs thus caused have been acceptable compromises in some past systems; however, the degree of distortion of antenna patterns from such obstructions can be considerable.

### SEGMENTED DIVERTER STRIPS

A more recent development has been the use of diverters comprising a series of small, button-like, metal segments connected with resistance material. These items, illustrated in Figure 3, have been previously reported and are patented by Douglas (U.S. Patent No. 3,416,027 granted in 1968). Upon intercept of lightning, an ionized channel is formed whereby the stroke travels above the segmented strips, exterior to the radome wall, to the aircraft fuselage. The resistance material is useful both in initiating this ionized channel and in providing a bleed-off path for precipitation static. One of the primary reasons for the use of this diverter type is that the metal segments may be 1/10th wavelength or smaller at X-band, and hence minimal antenna pattern distortion is incurred.

Evolving airborne radar systems of the pulse doppler type rely upon extremely low sidelobes to permit detection of targets and prevent "clutter" in the direction of the ground. With the solid metallic diverters previously discussed, sidelobes may be raised (typically) 10 db above the levels associated with the modern antennas used with such radar. In a current program sponsored by the Air Force Materials Laboratory, a task was implemented to define an appropriate lightning protection system and demonstrate pattern performance with such an antenna.\* Prior to fabrication of required demonstration radomes, extensive pattern testing was accomplished at Brunswick with an already available nose cone. In addition to measuring the effects of segmented diverter strips in detail, direct comparison between these and the solid types was incorporated by means of alternately fitting the radome with the two types of protective devices.

#### ANTENNA TEST RESULTS

The radome utilized was a filament wound half-wave wall construction with an approximate ogive shape. The wall thickness was tapered in the radome longitudinal direction to effect minimum wall reflections for the particular test antenna and X-band operational frequency. As a means of highlighting diverter effects, these were installed temporarily using thin tape, and patterns were compared to baseline antenna/radome composite system patterns. The segmented diverters were fabricated on a thin reinforced epoxy laminate approximately 0.010 inches thick, and therefore the effects of the carrier laminate were not separable from the effects of the metal segments or resistance material. Metal foil strips were used for convenience to reasonably represent any of the three solid metallic diverter types.

A photograph of the test radome is shown in Figure 4, and a close-up of the segmented diverter strip is shown in Figure 5. Eight strips each 42 inches long were employed, the surface spacing varying from about seventeen (17) inches at the radome base to eleven (11) inches at the forward extent of the diverters.

Transmission loss testing was accomplished with the radome in its normal (0°) roll position and rolled 30°, 45°, 60°, 75°, and 90°. The radome was then scanned  $\pm 60^\circ$  in azimuth about the stationary antenna, simulating in-flight antenna scans. Transmission changes, in percent, are shown in Figure 6. The losses with diverter strips were about 6% maximum and 3% average more than for the radome alone.

\*Contract No. F33615-71-C-1380.

"Manufacturing Methods for High Temperature Reinforced Plastic Aircraft Radomes".

Boresight or pointing error values were simultaneously measured, and changes are shown in Figure 7. These were increased as much as 1.2 milliradians for one particular radome roll position; however, the maximum measured error for all scans was only 0.5 milliradians higher with the segmented diverter strips than for the radome only.

Radiation pattern testing was accomplished for a number of conditions. The solid metallic diverter strips induced sidelobes at several angular positions. These induced lobes were particularly prominent for antenna pointing positions of twenty (20) degrees or more from the radome nose. Figure 8 illustrates this problem, a portion of the sidelobe region of the radiation pattern with diverters being overlayed with the same scan for the radome only. For the illustrated pattern, the magnitude of the induced sidelobe is seven (7) db greater with strip than for the radome alone. At other angles, magnitudes of increase of as much as ten (10) db were observed, for angular widths up to fifteen (15) degrees. Reducing the number or diverter strips from seven (7) to one (1) did not significantly alter the magnitude of this strip induced lobe, although its angular width was only about one-third (1/3) as much. Sidelobes of this magnitude and width are not acceptable for the intended application.

Comparable patterns using the segmented metal style of diverters showed only minor induced sidelobes. Figure 9 is the same pattern angle previously illustrated, and shows results with segmented diverters in comparison to radome only tests. At this particular scan angle, the maximum magnitude of the sidelobe with diverters does not exceed that applicable for the radome only. Other patterns in comparable angular areas showed increases on the order of one (1) db. Further, a study of data for the complete number of patterns made indicate that these diverters did not increase the average sidelobe level by more than about one (1) db. At the critical angular regions illustrated, this amounts to an improvement factor of nine (9) db in the magnitude of sidelobe increase. Overall, the pattern results for segmented diverters indicate a significant achievement as compared to previous strip types. For most applications, the segmented strips largely eliminates previous compatibility problems between lightning protection design and microwave considerations.

#### LIGHTNING PROTECTION TEST RESULTS

The lightning protection capability of solid diverter types have been previously reported, and will not be repeated here. For example, an overview is given in reference 1, and specific designs are reported in references 2 and 3. Testing of the segmented

strips has been accomplished during several programs.

**TEST CRITERIA** - Measured data indicate that the lightning strike phenomena generally consists of three significant phases: the prestrike phase, the high peak current phase, and a heavy coulomb phase.

It is during the relatively low current prestrike phase when the lightning stepped leader approaches the aircraft that an ionized channel is created in the air above the segmented strips. This ionized channel above the strip provides the path for the high peak currents and heavy coulomb transfers.

The peak current in a lightning stroke will generally be 10 to 20 kiloamperes, but in some instances has been as high as 200 kiloamperes. The peak current has an average rate of rise of 10 kiloamperes per microsecond and a maximum rate of 100 kiloamperes per microsecond. During the peak current phase of a lightning strike, high vaporization pressures and strong mechanical forces can be created.

The heavy coulomb phase follows the peak current phase. In the heavy coulomb phase 100 to 200 amperes may flow for a period of up to one second, transferring a total charge of 30 to 200 coulombs. This phase of the lightning strike can produce burning and eroding of the metal transfer points.

The segmented lightning strips have been tested to determine their shielding characteristics and ability to withstand the peak currents and heavy coulomb transfers associated with lightning strokes.

**ELECTROSTATIC SHIELDING MEASUREMENTS** - High voltage tests have been performed by Douglas at Lightning and Transients Research Institute, Miami, Florida, to establish the electrostatic shielding characteristics of the segmented strips. Flat panel measurements were made to determine the approximate spacing required between the strips to provide the necessary protection for a particular antenna/radome installation. Final measurements were made on the actual radome.

A typical test set-up for high voltage measurements on a flat panel is shown in Figure 10. A photograph of a high voltage test on a flat panel with segmented strips installed is shown in Figure 11. The simulated lightning stroke can be seen traveling above the four foot long segmented strips to ground. The spacing between the strips is twenty-one inches. The high gradient point under the panel and midway between the two strips was 2.4 inches from the panel. The exact spacing required between the strips to

provide the necessary shielding is a function of the length of the strips, the dielectric strength of the radome wall, and the shape and location of metal objects within the radome. The spacing is normally seventeen to twenty-one inches.

**HIGH PEAK CURRENT MEASUREMENTS** - High peak current tests were made at Douglas and L.T.R.I. to determine damage to the strips caused by vaporization pressures and mechanical forces. A block diagram of the test set-up used at L.T.R.I. is shown in Figure 12. A photograph of the location of the probes with respect to the lightning strips is shown in Figure 13. The high voltage probe was attached to the ungrounded end of the segmented strip using metal foil. The voltage potential between the high current probe and ground was 25 kilovolts. When the high voltage generator was discharged across the segmented strip the high current discharge was triggered as shown in Figure 14. Figure 15 shows the waveform as it appeared on the oscillograph. The peak current was 160 kiloamperes. The rate of rise to peak was approximately 6.5 kiloamperes per microsecond.

No damage occurred to the panel or the two lightning strips. A photograph of the test panel after test is shown in Figure 16. A close-up photograph of the segmented strip in the high current probe area is shown in Figure 17. There are no significant burns on the strip because the lightning does not attach to it. The segmented strips simply guide the stroke to ground.

A photograph of the grounded bolt at the end of the segmented strip to which the simulated lightning attached is shown in Figure 18. The strip is butted against the bolt. No intimate contact is required if a bleeder resistor is used. A photograph of the bleeder resistor is shown in Figure 19. The resistor is connected to the strip as illustrated in Figure 20. This bleeder resistor in conjunction with the resistance material joining the segments prevents the strip from creating an RF noise source during certain charging conditions on the aircraft. No bleed resistor is required if the strips are connected to the grounding bolt.

**HEAVY COULOMB TRANSFERS** - The most difficult part of the lightning stroke to simulate when testing the segmented strips is the heavy coulomb transfer that occurs during the last phase of the stroke. For this test it is necessary that the ionized channel established over the strip during the high voltage discharge be maintained long enough that 200 amperes of current can be discharged through the same channel, from a DC voltage source, for a period of one second.

Douglas has performed tests on the segmented strips where eight coulombs was transferred over a 16-inch length, approximately 40 coulombs over a 4-inch length and over 200 coulombs over a one-half inch length. These tests indicated that the segmented strips will withstand the burning and eroding caused by charge transfers in excess of 200 coulombs.

#### STRIP AVAILABILITY AND CURRENT FURTHER WORK

Convenient strips incorporating the metal segments and resistance material on a thin (approximately 0.010 inch) laminate carrier are now available from Communications Components Corporation, Costa Mesa, California, a licensee of McDonnell-Douglas Corporation. The one tenth inch diameter segments presently available are adequate for most applications up to and including Ku-band. If necessary, the segment size can be further reduced to facilitate use in the higher frequency ranges. Additionally, in particular radome designs where the laminate carrier degradation effects must be avoided, fabrication techniques making these an integral part of the radome may be implemented. An example of such a situation would be an "A" sandwich radome with thin skins (facings), operating at a relatively high frequency.

As a part of the earlier referenced Air Force sponsored project, further work tasks for the segmented diverters are being implemented. Included in these tasks are the necessary items to define manufacturing methods for applying a high temperature version of the strips to a polyimide foam core radome, and the standard type to representative filament wound radomes in a retrofit fashion. Additionally, the temperature up-grading of the segmented strips is to be accomplished with a goal of service to 600°F. Additional antenna testing with primary emphasis on sidelobes will be accomplished at Ku-band. Simulated lightning testing of a polyimide foam core radome incorporating the higher temperature segmented diverter strips will be conducted, as well as electrical, structural, and environmental tests.

#### REFERENCES

M. P. Amason, G. J. Cassell, "Radome Lightning Protection Techniques", Douglas Aircraft Company, Technical Paper No. 5839. Published in the 20th Annual Symposium Proceedings, United States Air Force Antenna Research and Development, October 1970.

J. D. Robb, R. Genz, "Development of Lightning Protection, C-141 Nose Radome", L and T Report No. 416, September 1963.

J. D. Robb, J. R. Stahmann, J. A. Bochland, and D. Bohne, "Lightning Protection Development, C5-A Nose Radome", L and T Report No. 467, January 1968.

M. P. Amason, G. J. Cassell, J. T. Kung, and W. W. McCloud, "Aircraft Lightning Protection Design Considerations". Douglas Aircraft Company, Technical Paper No. 6043. Published in 1972 Lightning and Static Electricity Conference, December 1972.

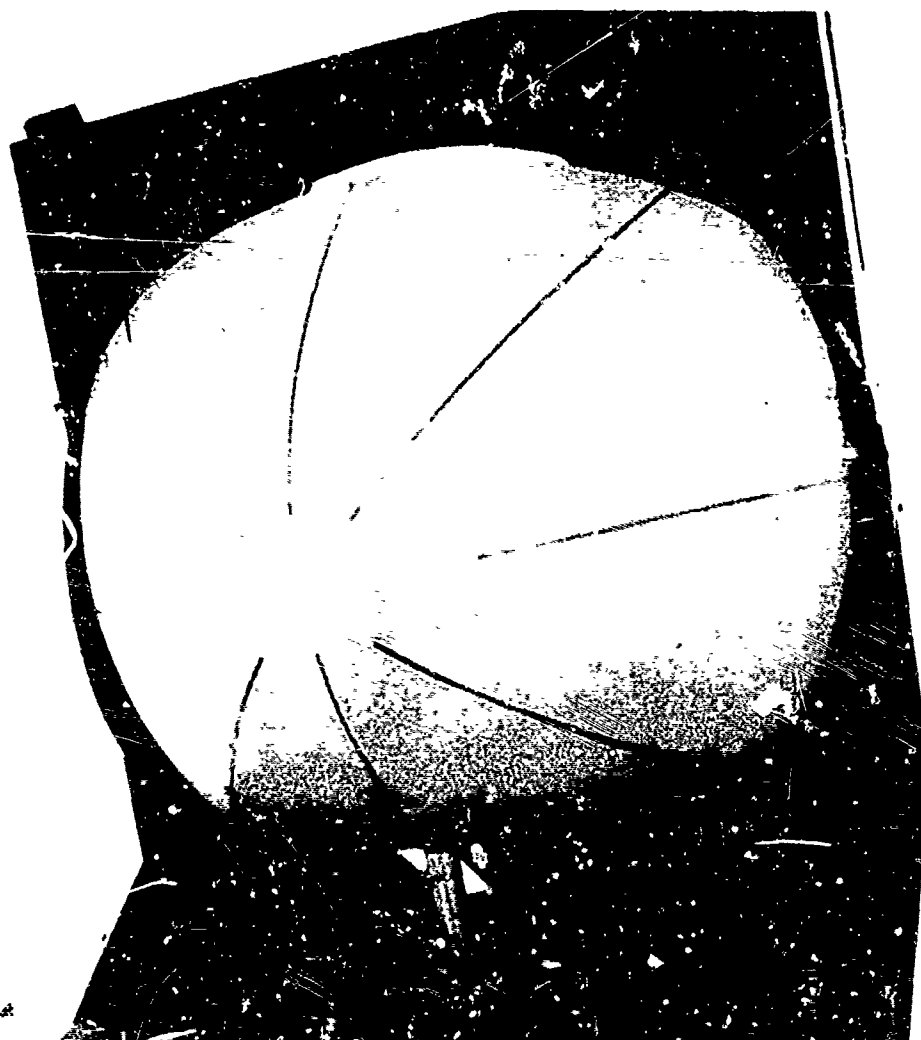


FIGURE 1: NOSE RADOME WITH RADIAL STRIPS  
INSTALLED

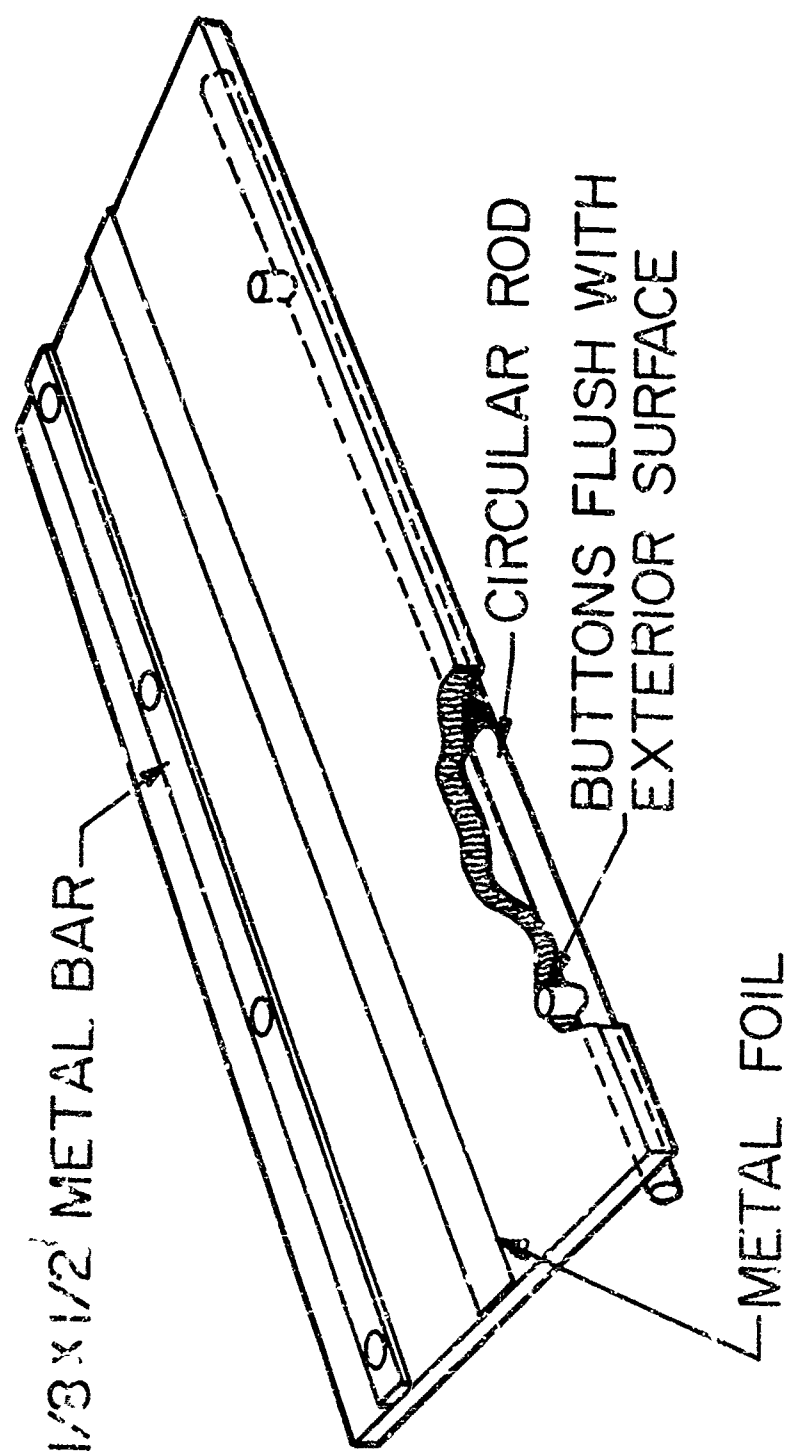


FIGURE 2: THREE SOLID METAL DIVERTERS  
ON SUBSTRATE

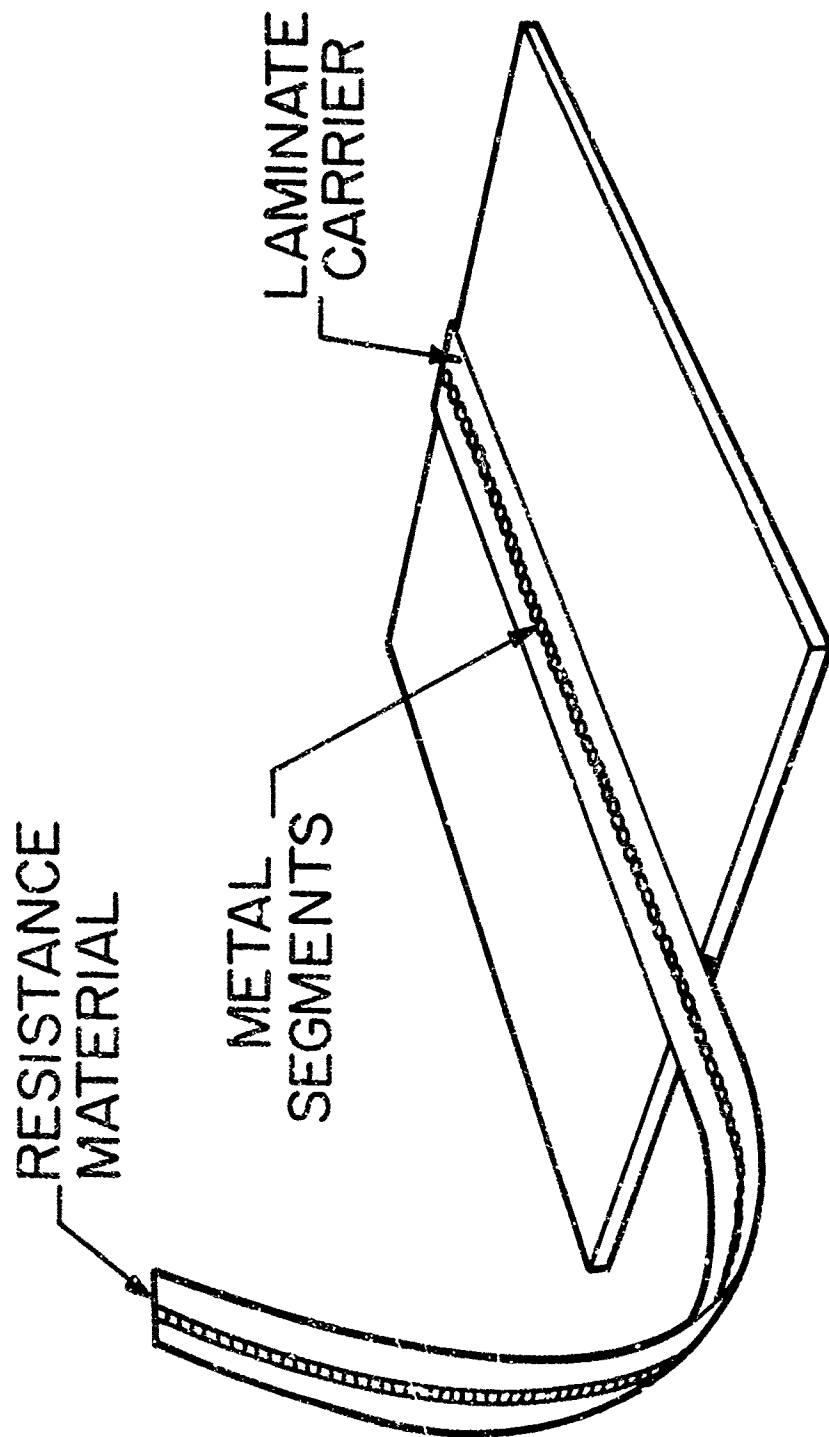


FIGURE 3: SEGMENTED DIVERTER STRIP  
(PARTIALLY ON SUBSTRATE)



FIGURE 4: RADOME USED FOR ANTENNA TESTS



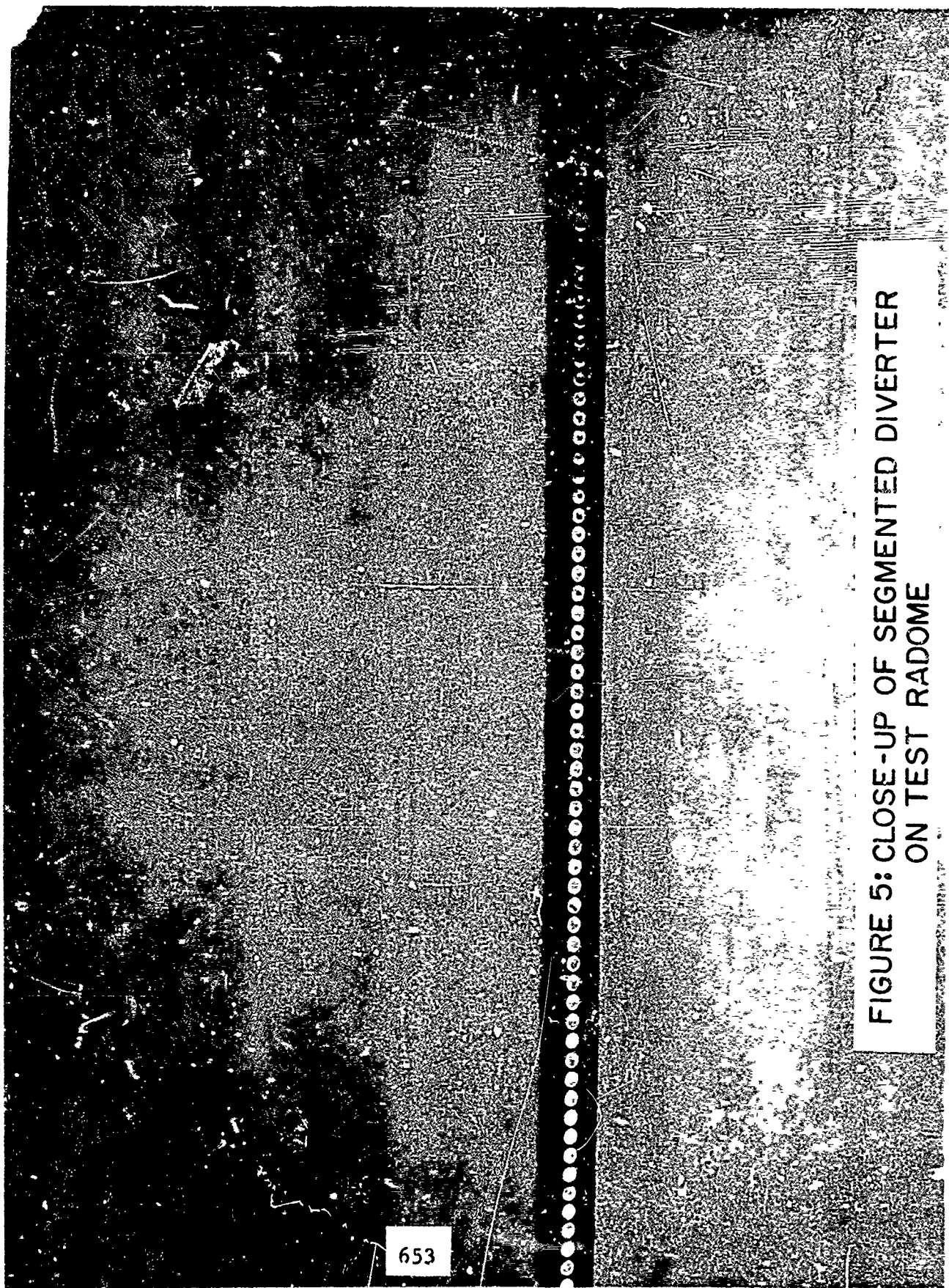


FIGURE 5: CLOSE-UP OF SEGMENTED DIVERTER  
ON TEST RADOME

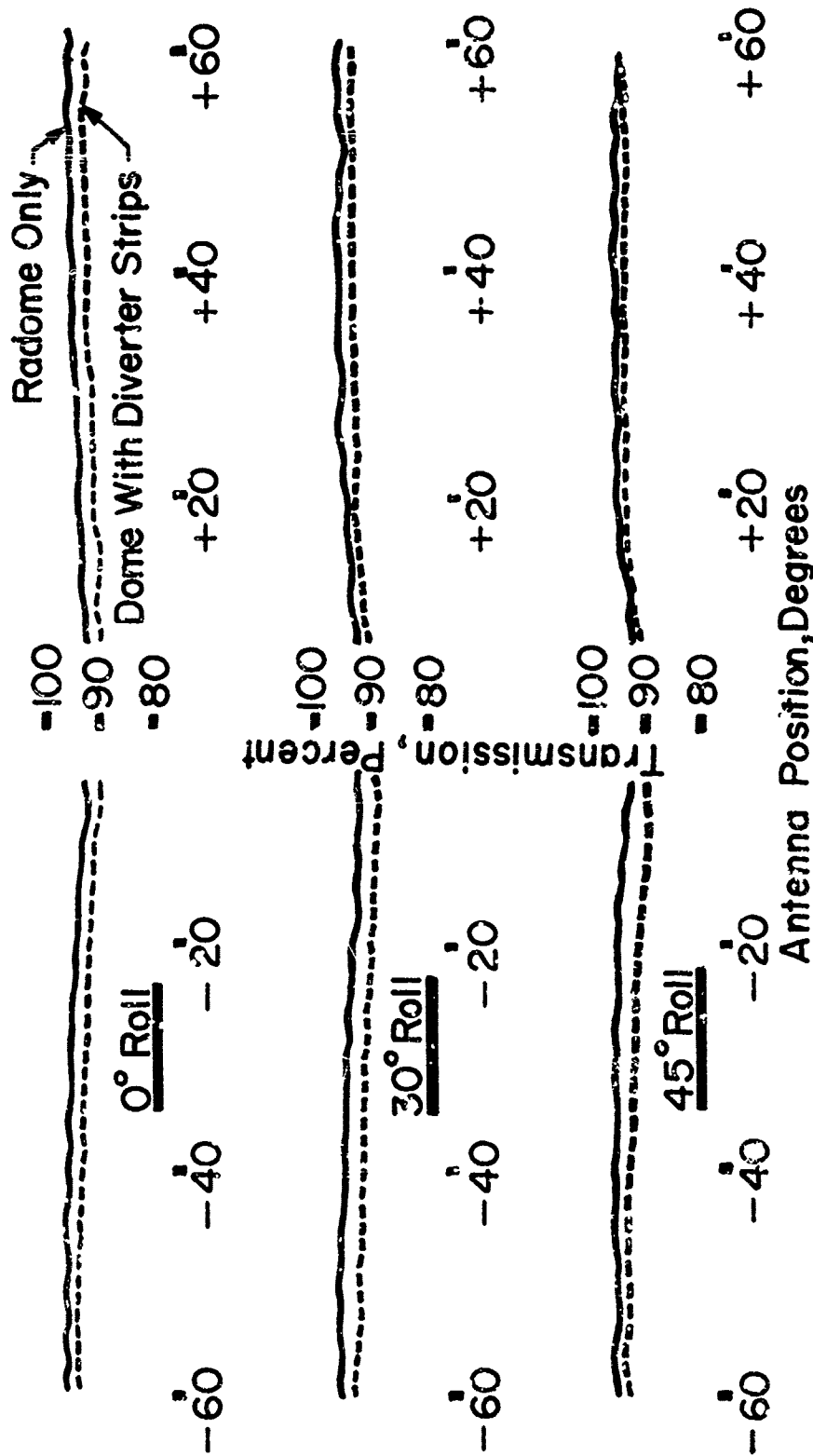


FIGURE 6: COMPARATIVE TRANSMISSION PERFORMANCE  
RADOME ALONE VS. DOME WITH SEGMENTED  
DIVERTER STRIPS

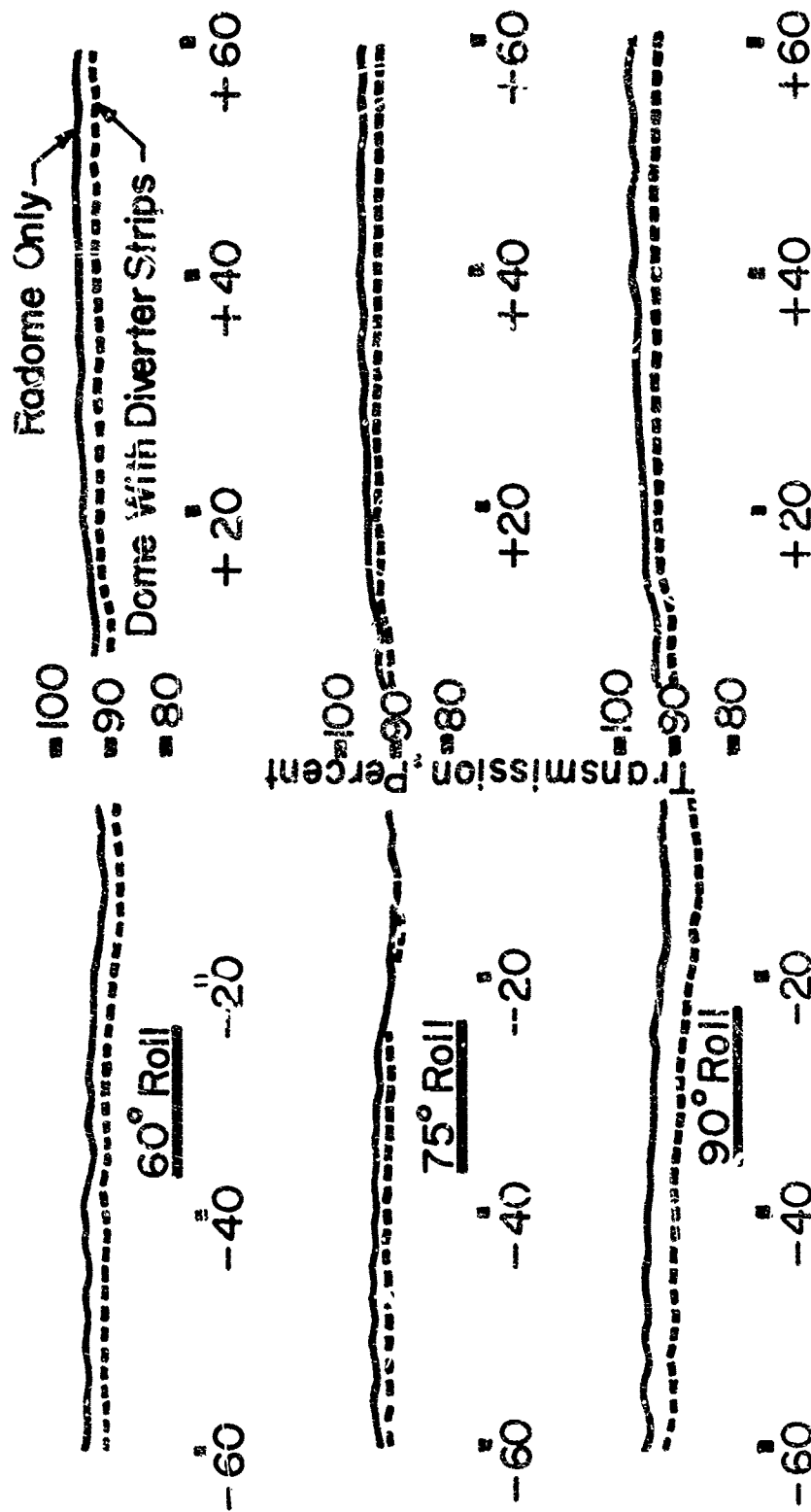


FIGURE 6(Cont.): COMPARATIVE TRANSMISSION PERFORMANCE  
RADOME ALONE VS. DOME WITH SEGMENTED  
DIVERTER STRIPS

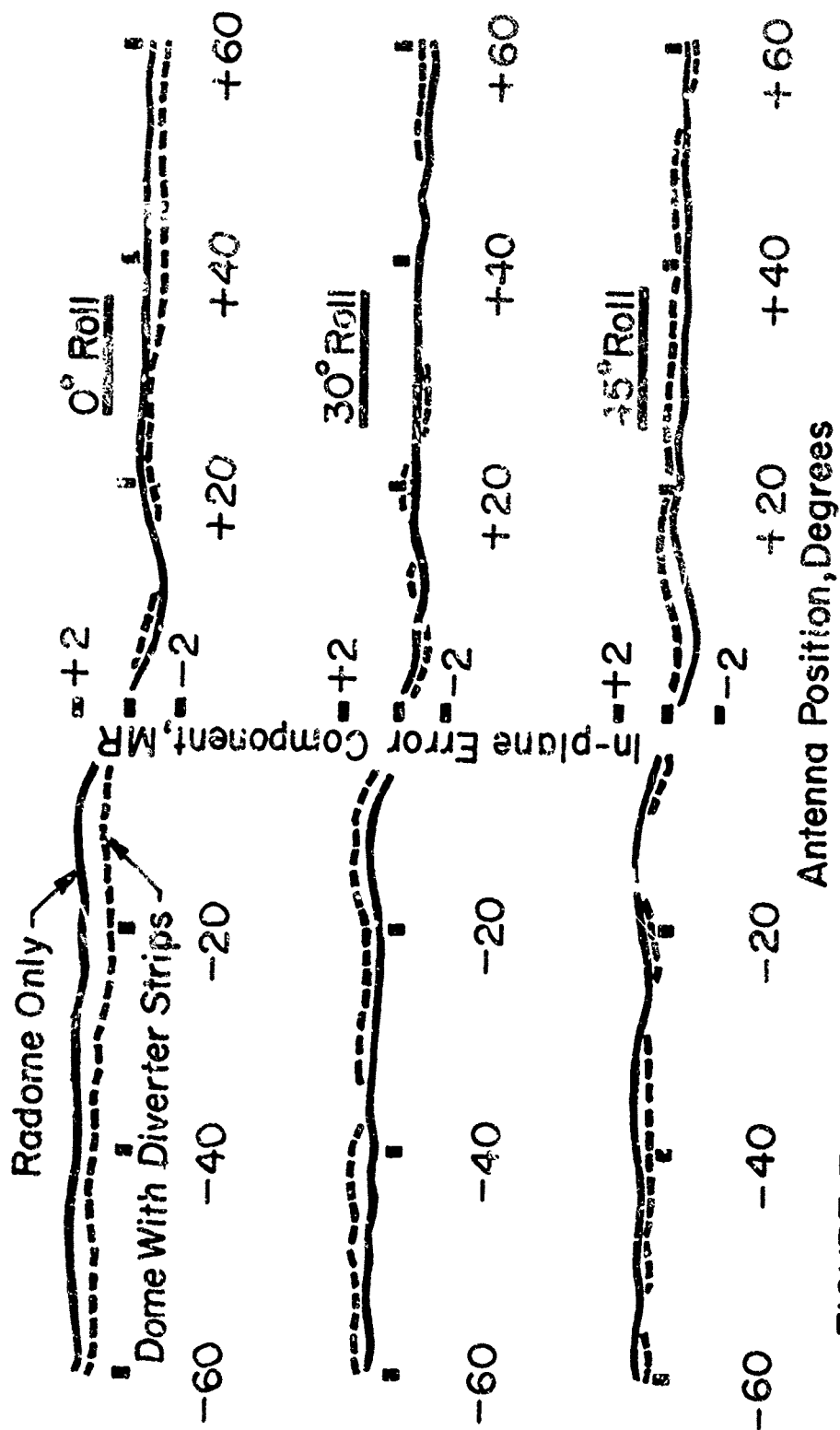


FIGURE 7: COMPARATIVE BORESIGHT ERROR PERFORMANCE  
RADOME ALONE VS. DOME WITH SEGMENTED  
DIVERTER STRIPS

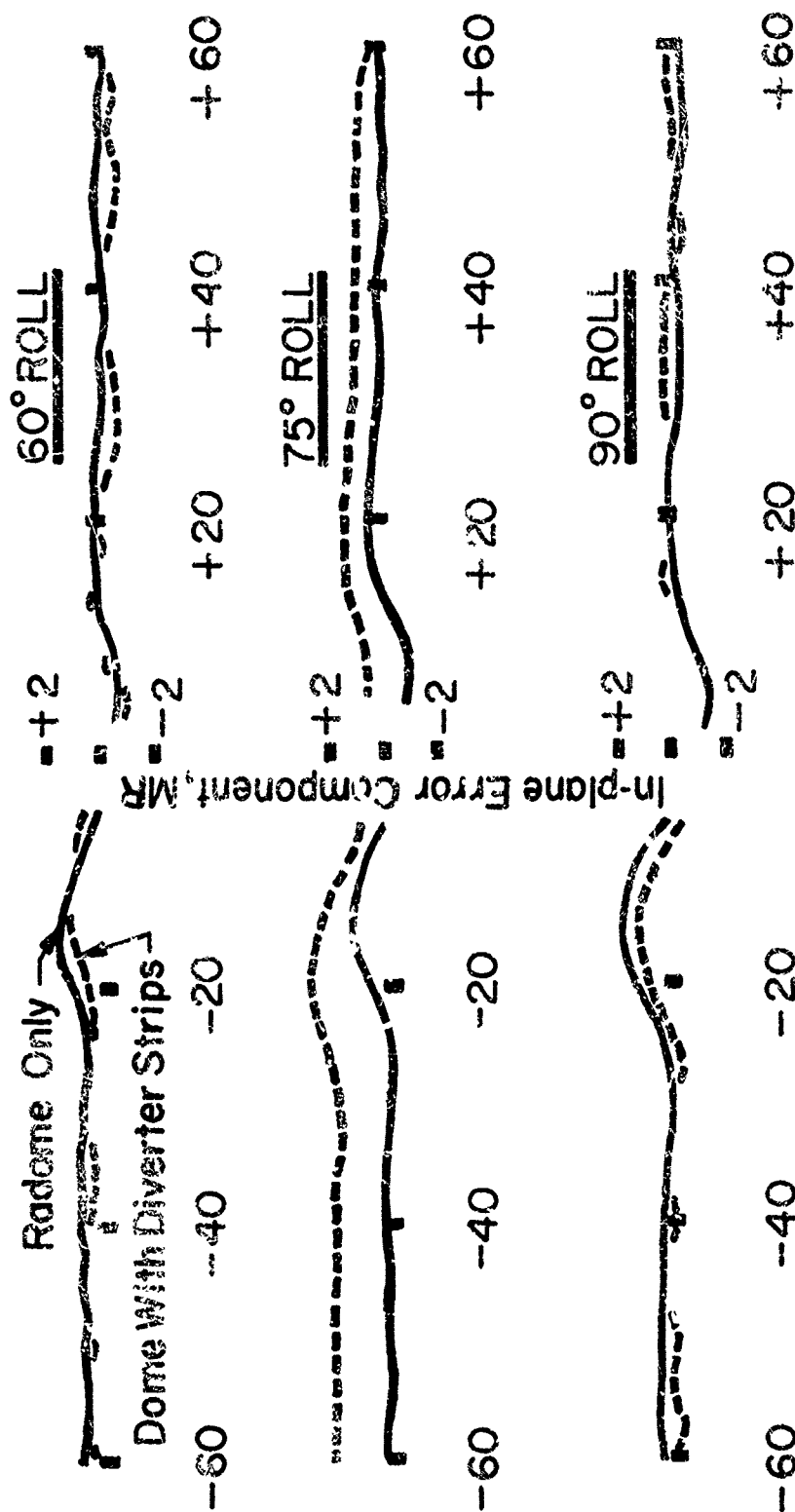


FIGURE 7(Cont.): COMPARATIVE BORESIGHT ERROR PERFORMANCE  
RADOME ALONE VS. DOME WITH SEGMENTED  
DIVERTER STRIPS

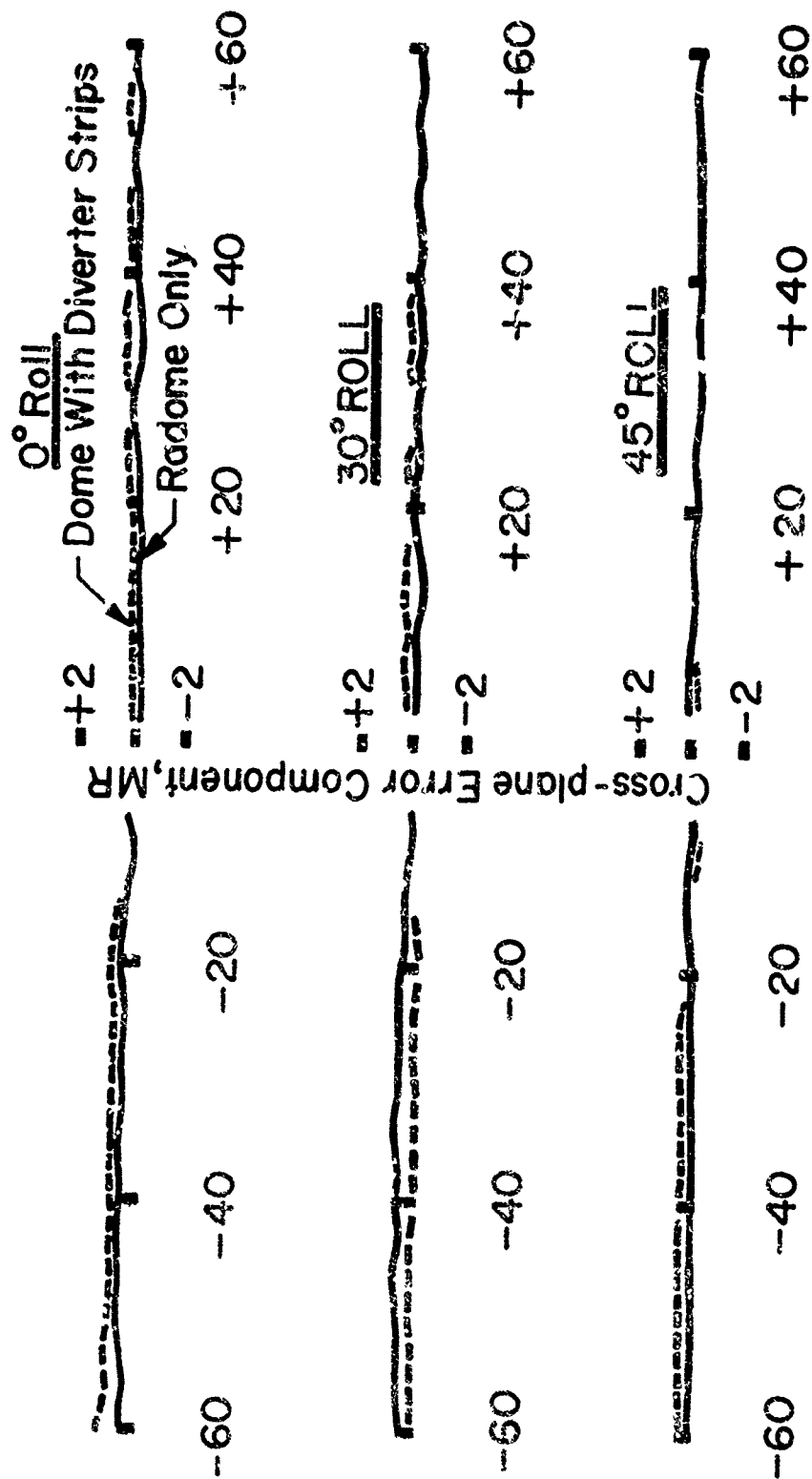


FIGURE 7(Cont.): COMPARATIVE BORESIGHT ERROR PERFORMANCE  
 RADOME ALONE VS. DOME WITH SEGMENTED  
 DIVERTER STRIPS

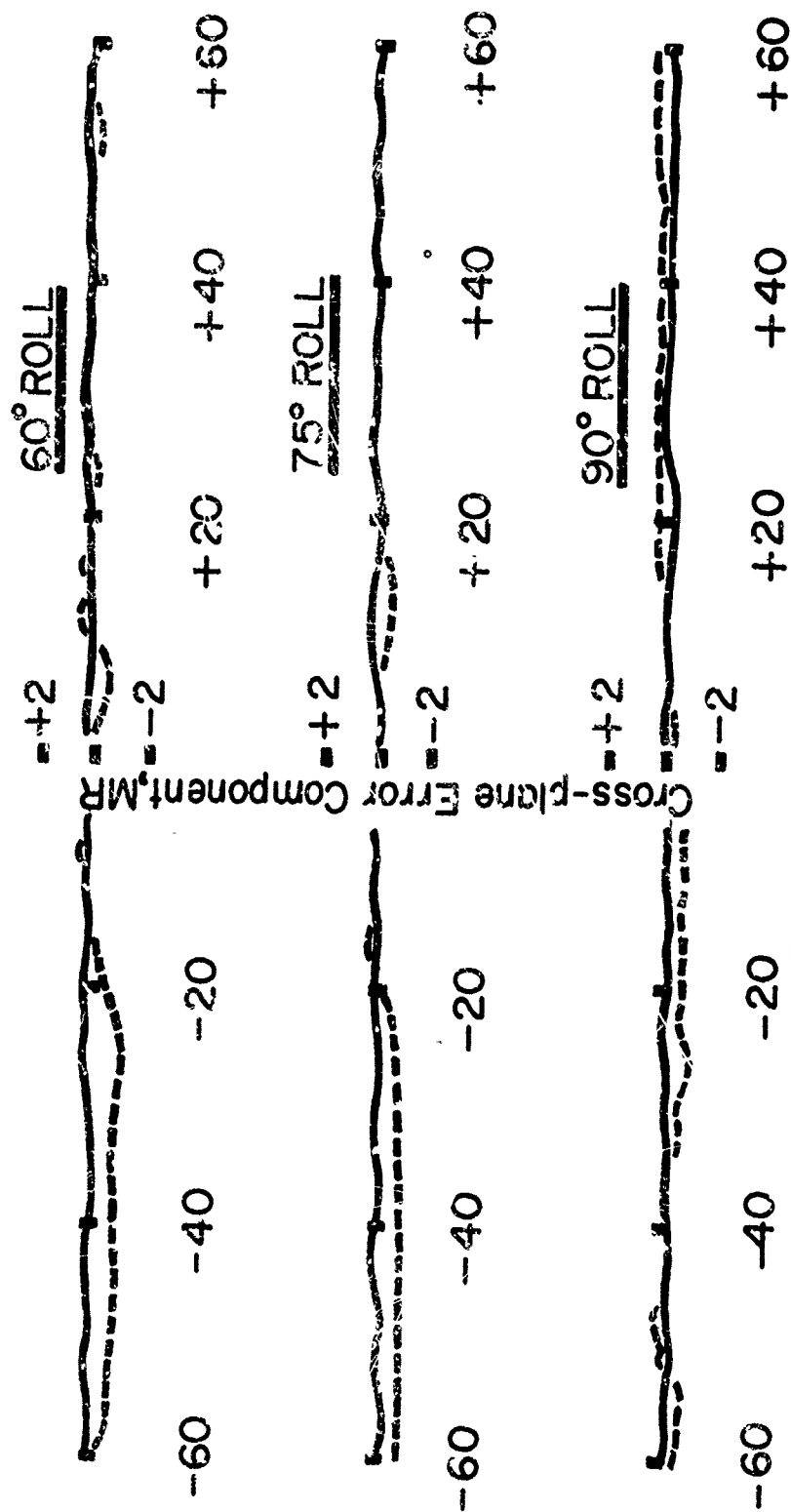


FIGURE 7(Cont.): COMPARATIVE BORESIGHT ERROR PERFORMANCE  
RADOME ALONE VS. DOME WITH SEGMENTED  
DIVERTER STRIPS

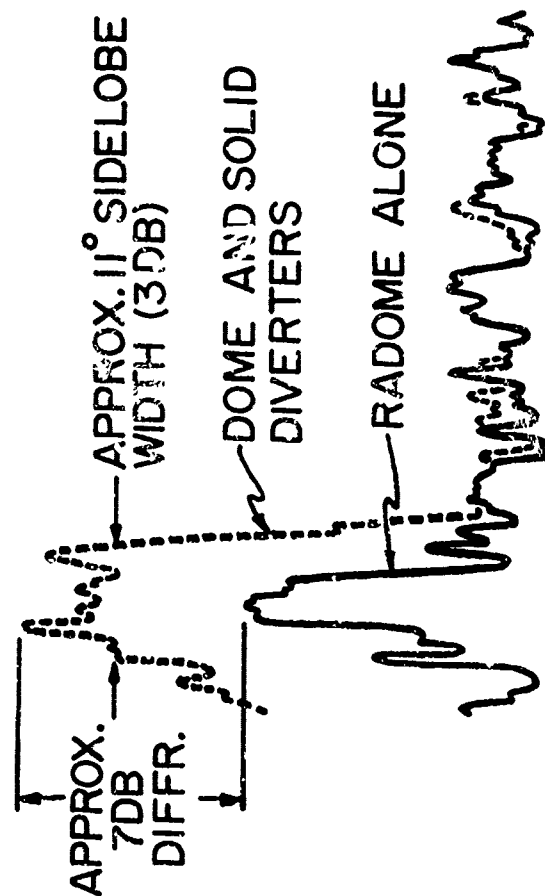
■ + 20 DB

■ + 10 DB

■ 0

■ -10 DB

Power Relative To Arbitrary Reference, DB



ELEVATION PLANE PATTERN

- Antenna Position in Dome 20° From Nose
- Great Circle Cut, Tilted 5° From Main Beam Center

ELEVATION ANGLE, DEGREES

FIGURE 8: COMPARATIVE PARTIAL ANTENNA PATTERN, SIDELOBE REGION - RADOME ALONE VS. DOME WITH SOLID DIVERTER STRIPS



— + 20 DB

— + 10 DB

— 0

— -10 DB

Power Relative To Arbitrary Reference, DB

# ELEVATION PLANE PATTERN

- Antenna Position  
in Dome 20°  
From Nose
- Great Circle Cut,  
Tilted 5° From  
Main Beam Center

— DOME AND SEGMENTED  
DIVERTERS

— RADOME ALONE



-84° -72° -60° -48° -36° -24° -12°  
ELEVATION ANGLE, DEGREES

FIGURE 9: COMPARATIVE PARTIAL ANTENNA PATTERN, SIDELOBE  
REGION-RADOME ALONE VS. DOME WITH SEGMENTED  
DIVERTER STRIPS

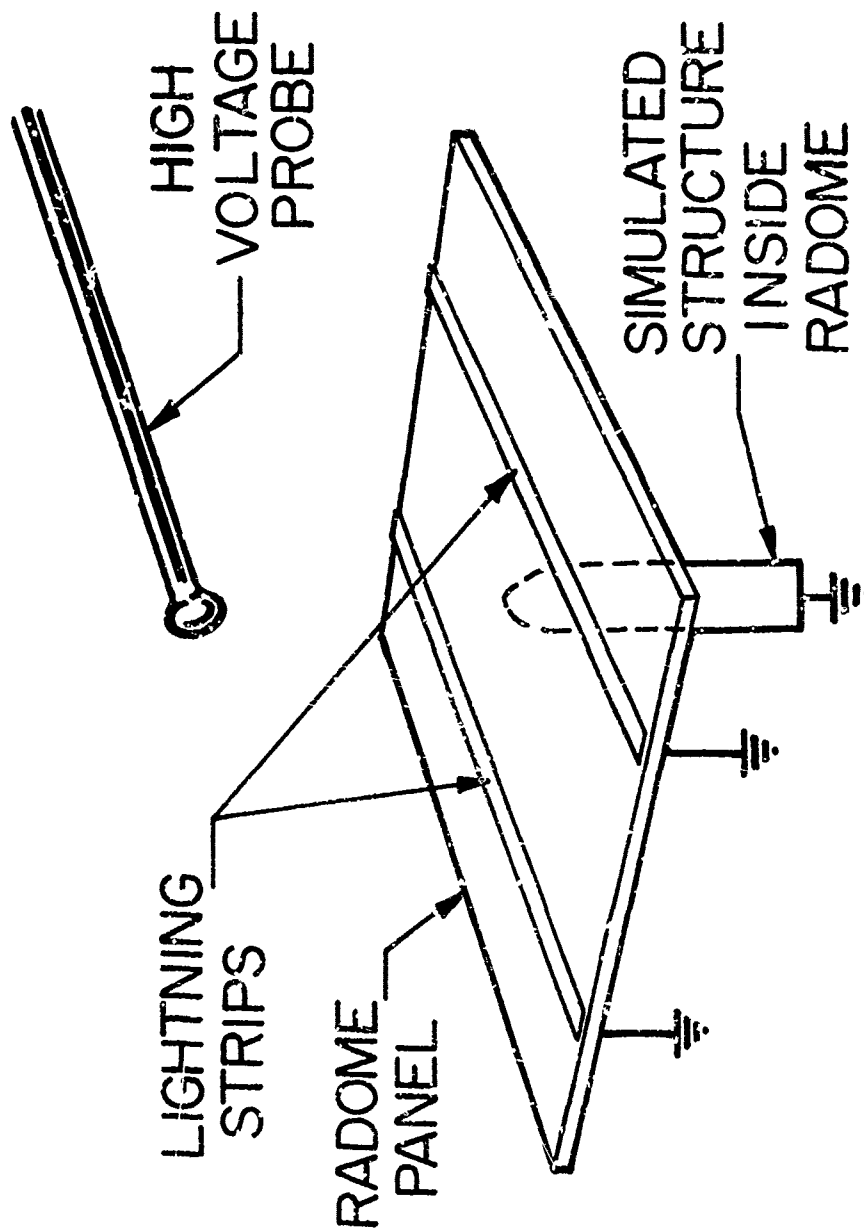


FIGURE 10: TYPICAL TEST ARRANGEMENT,  
HIGH VOLTAGE (SHIELDING)  
STUDIES ON FLAT PANEL



FIGURE II: SIMULATED LIGHTNING STRIKE TO DIELECTRIC  
PANEL, SEGMENTED STRIPS INSTALLED AT  
21" SPACING

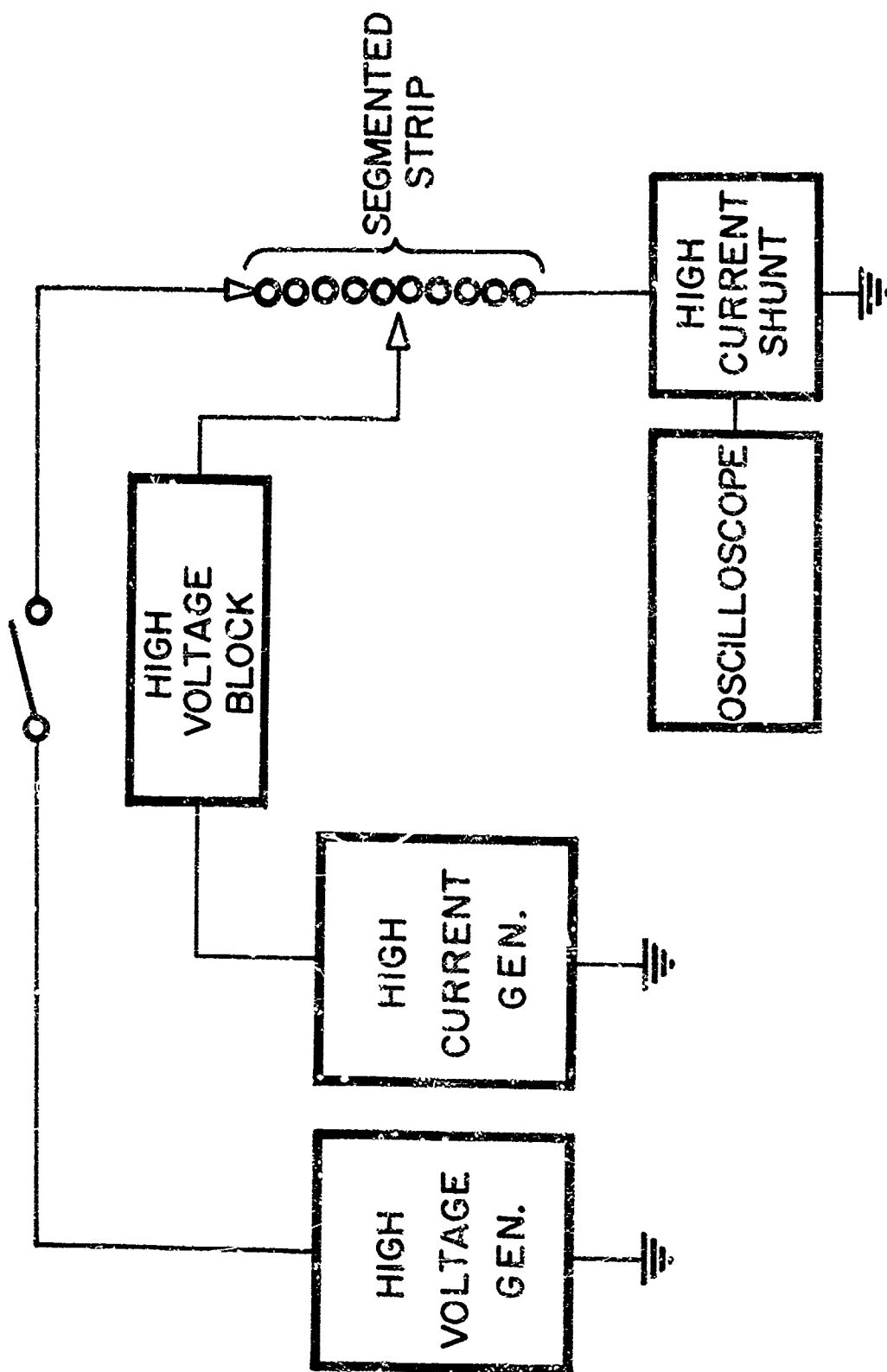


FIGURE 12: TEST SET-UP DIAGRAM,  
HIGH PEAK CURRENT TESTS

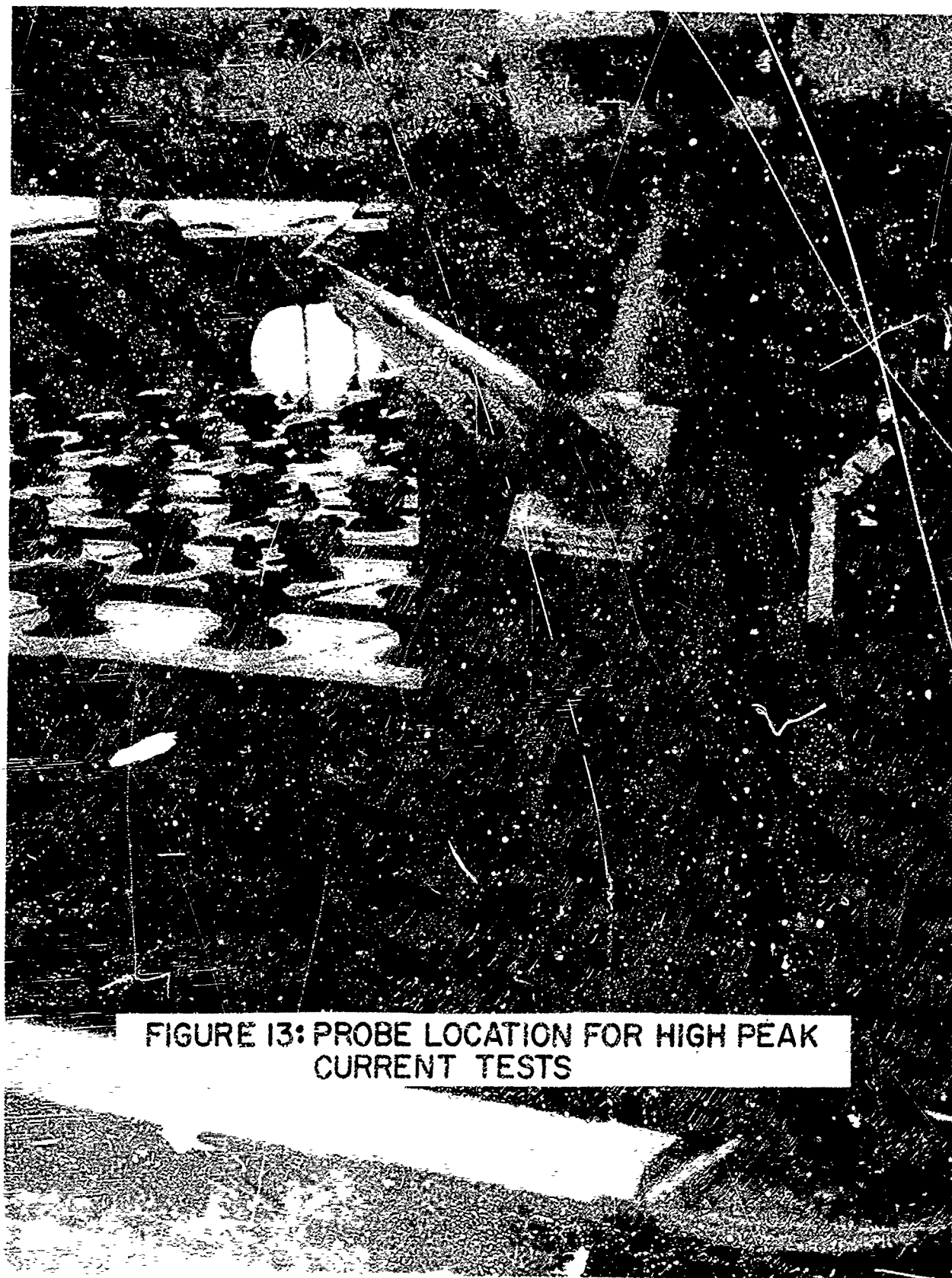


FIGURE 13: PROBE LOCATION FOR HIGH PEAK  
CURRENT TESTS

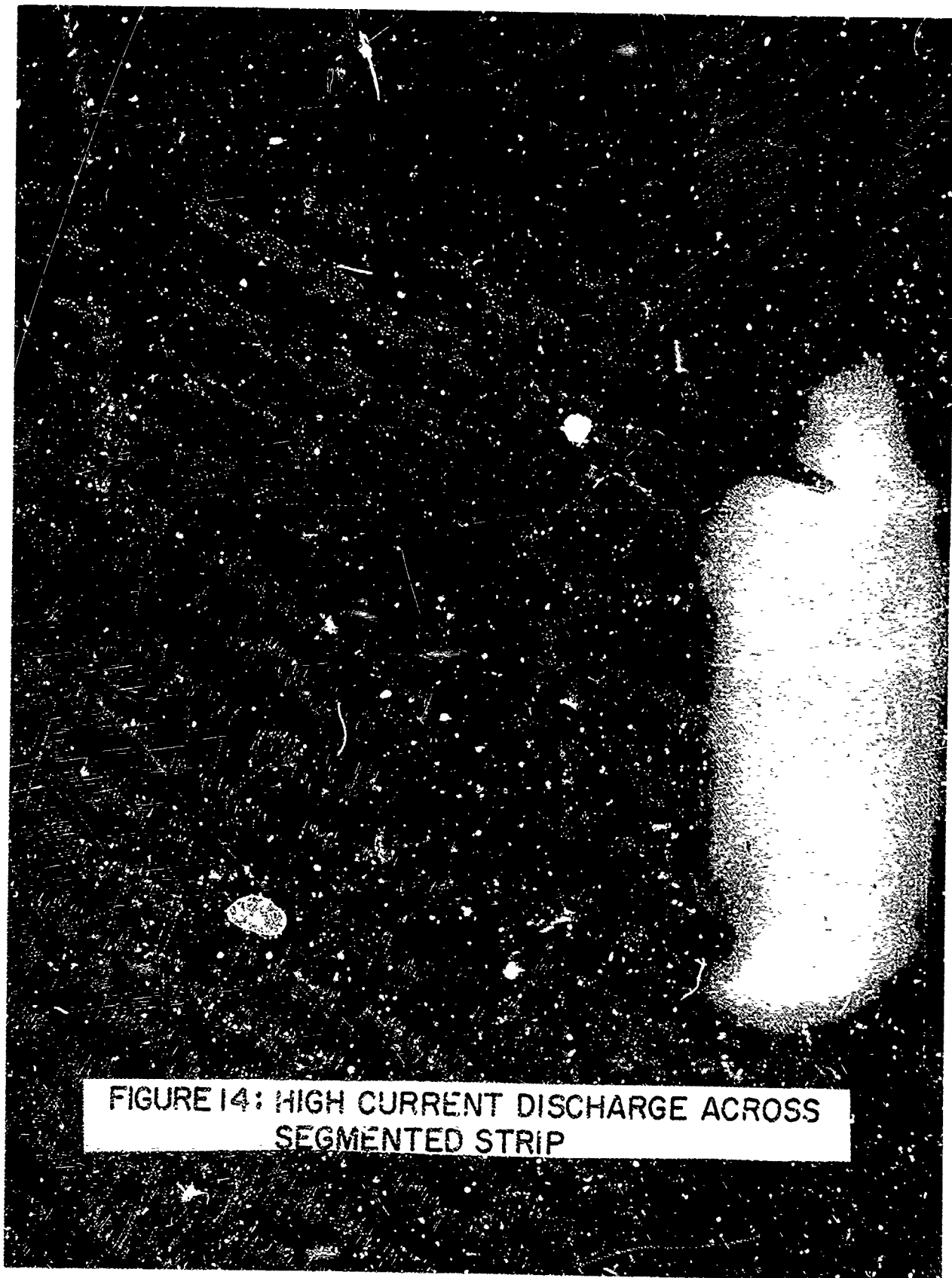


FIGURE 14: HIGH CURRENT DISCHARGE ACROSS  
SEGMENTED STRIP



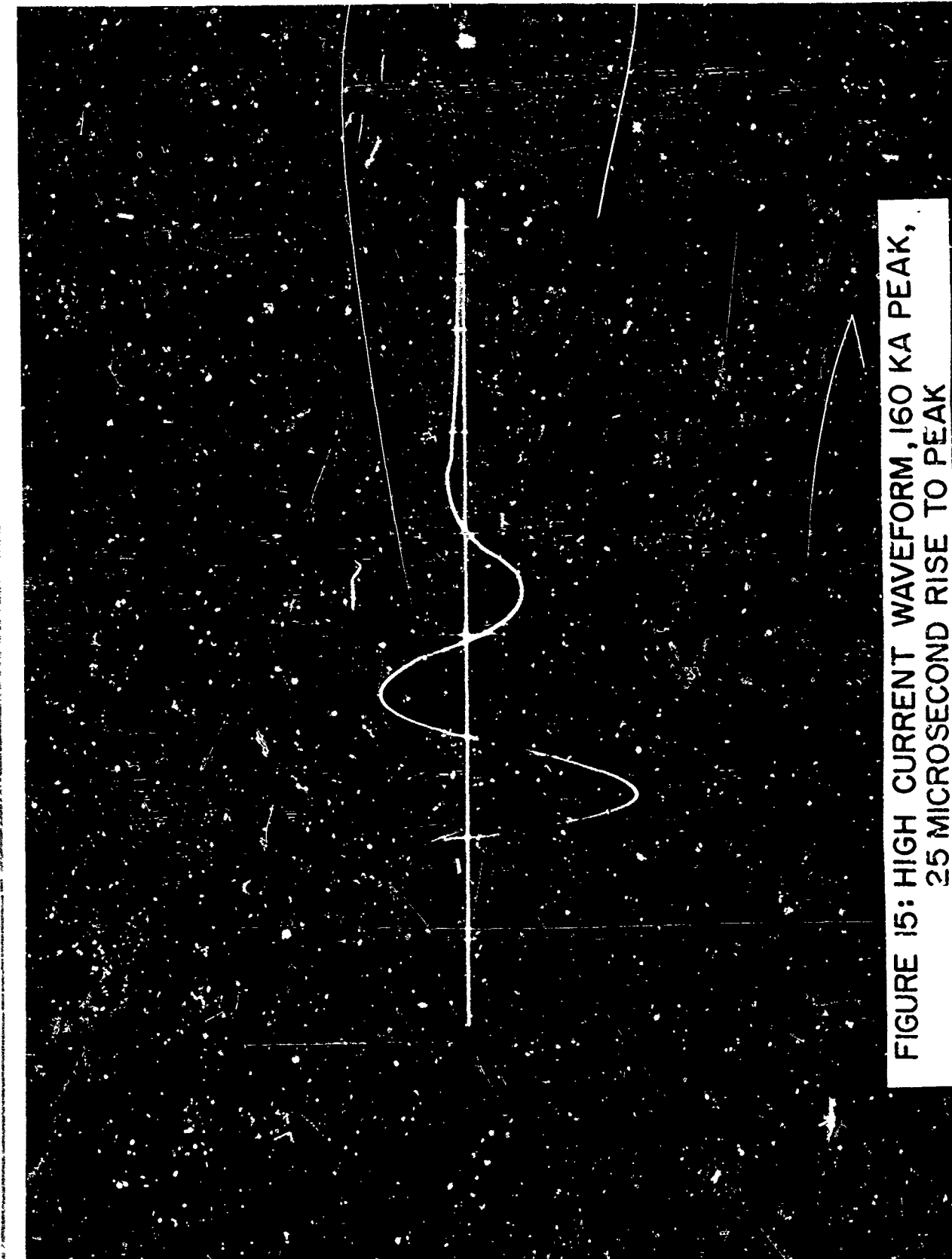


FIGURE 15: HIGH CURRENT WAVEFORM, 160 KA PEAK,  
25 MICROSECOND RISE TO PEAK



FIGURE 16: PANEL AFTER HIGH CURRENT TESTS



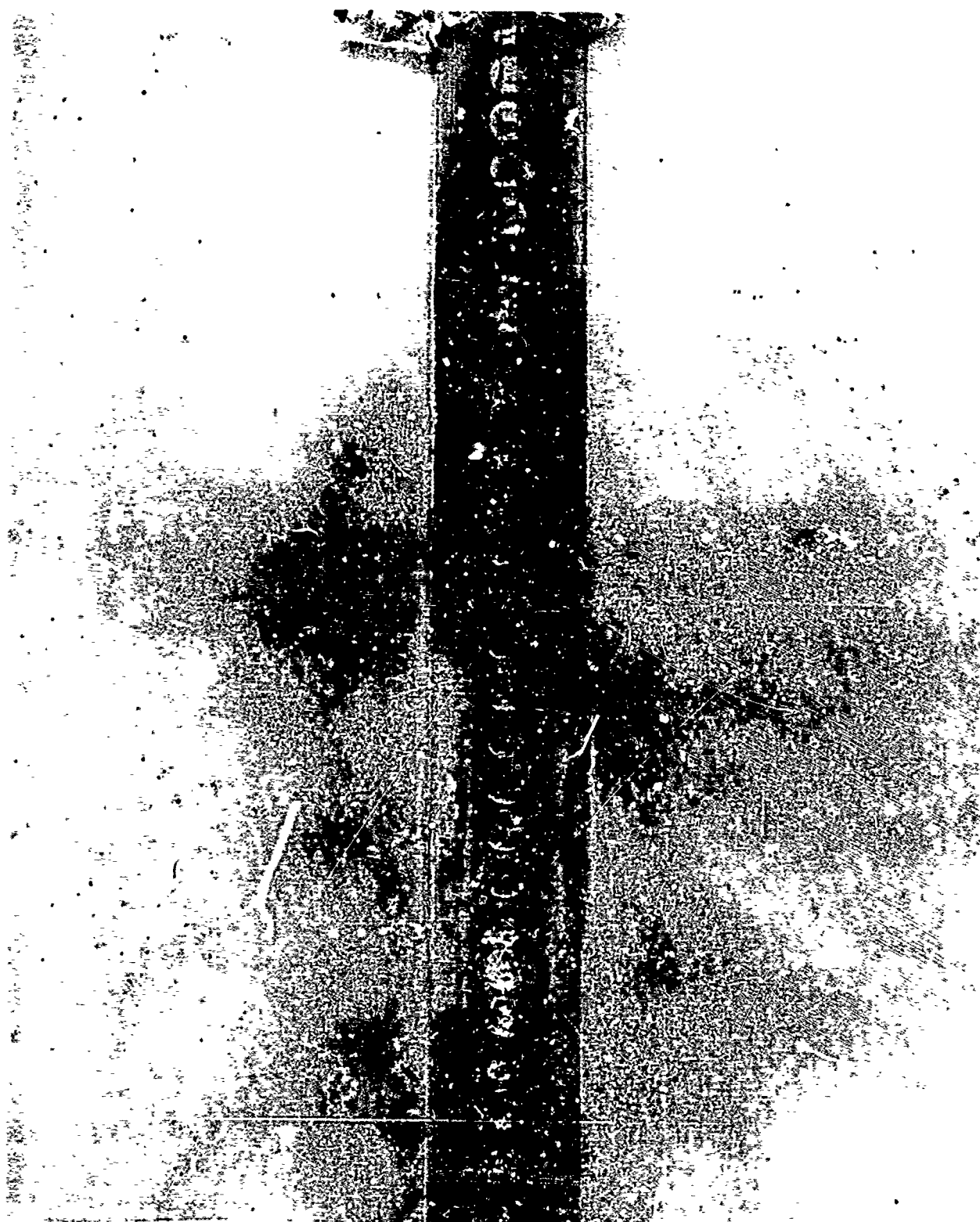


FIGURE 17: CLOSE-UP OF SEGMENTED STRIP IN  
PROBE AREA AFTER HIGH CURRENT TESTS

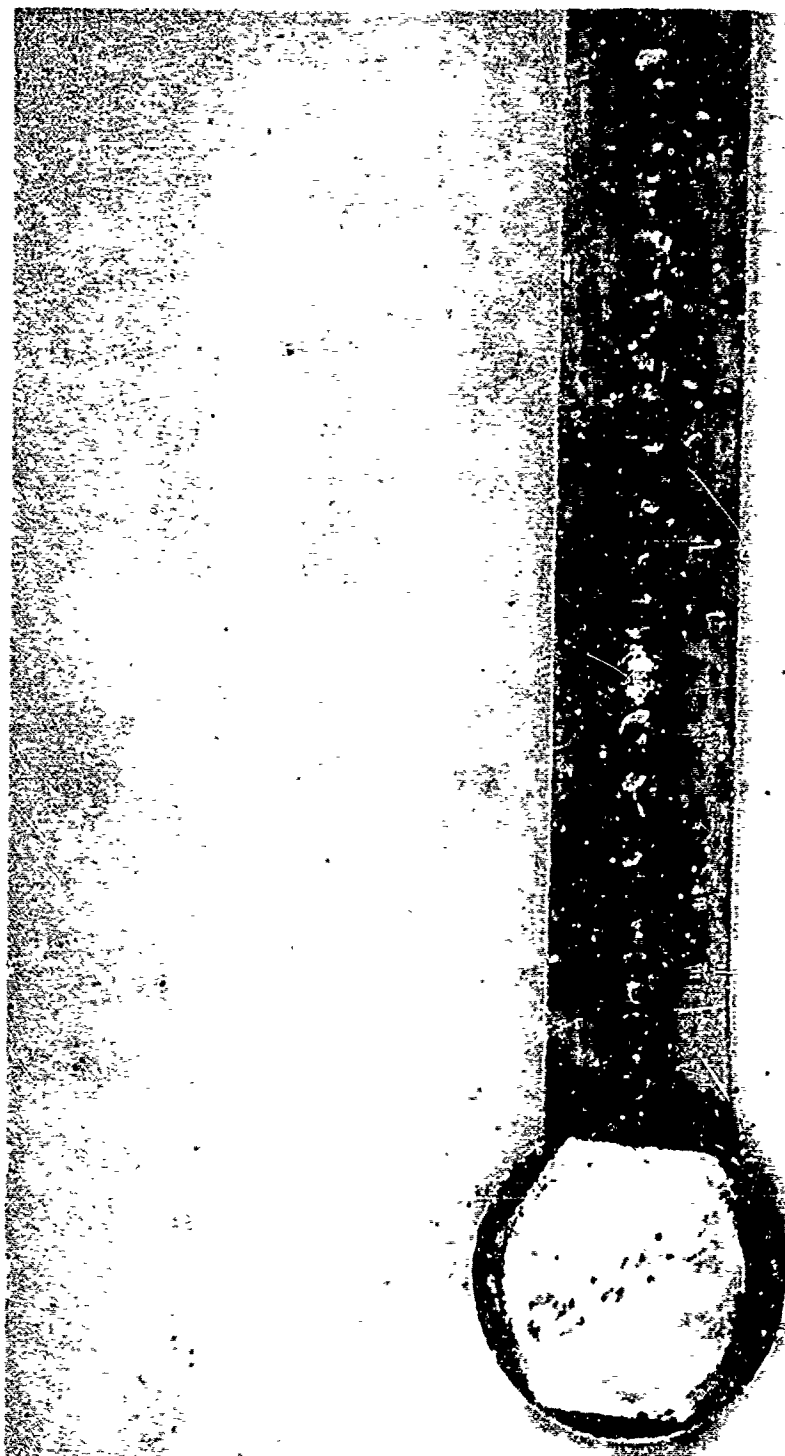


FIGURE 18: CLOSE-UP OF GROUNDED BOLT AFTER TEST

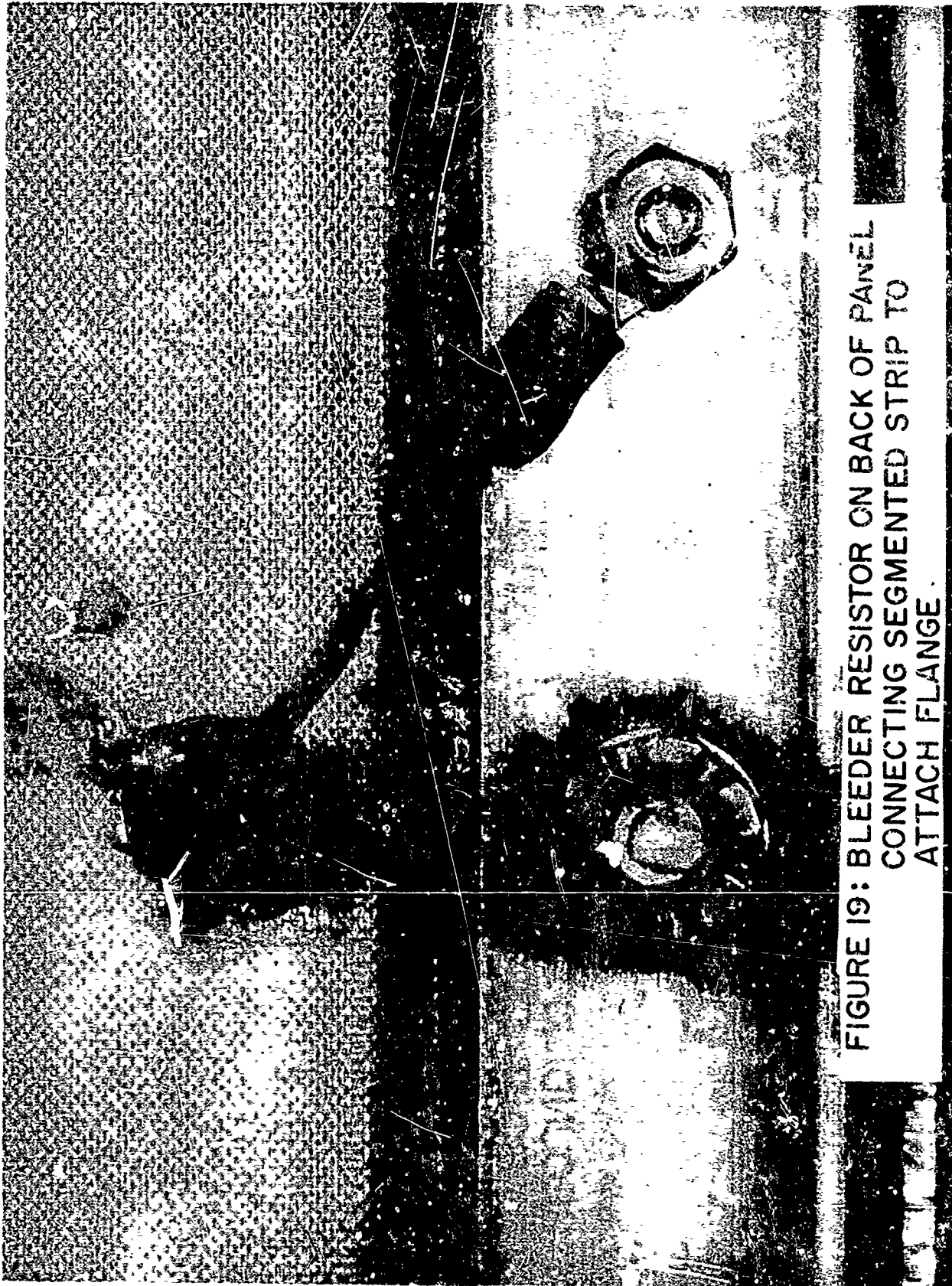


FIGURE 19: BLEEDER RESISTOR ON BACK OF PANEL  
CONNECTING SEGMENTED STRIP TO  
ATTACH FLANGE.

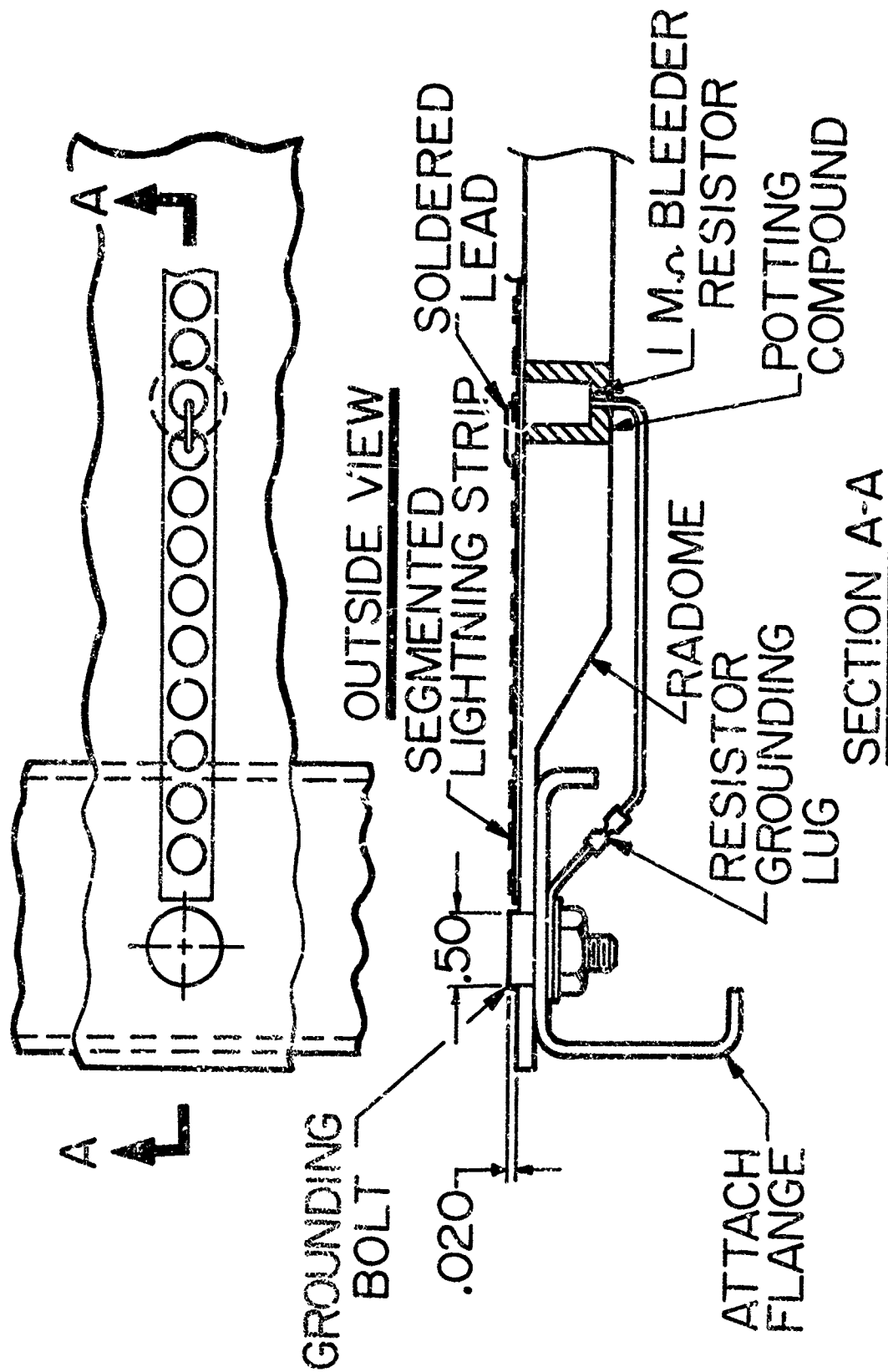


FIGURE 20: METHOD OF ATTACHING AND GROUNDING  
SEGMENTED STRIP TO RADOME